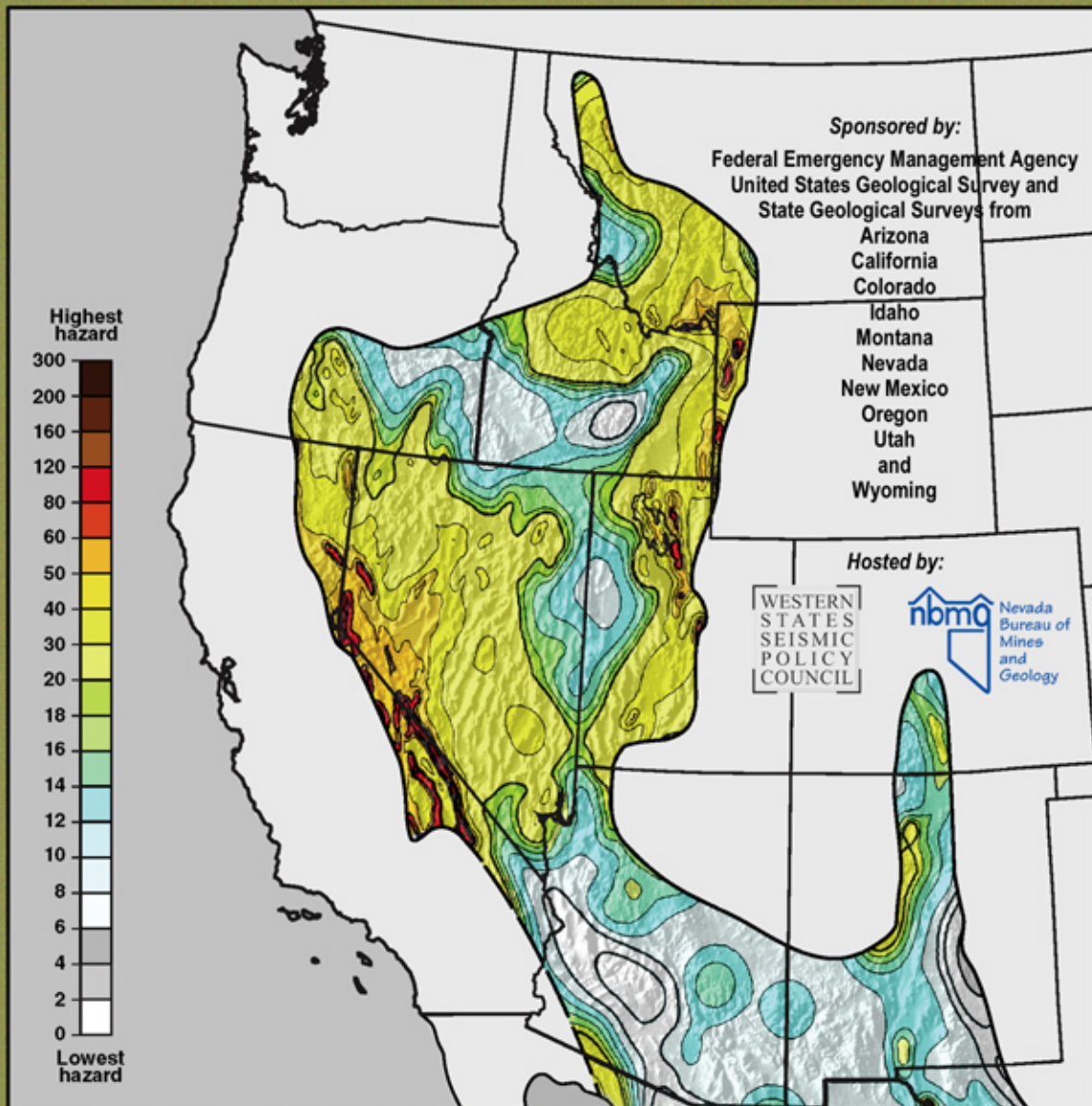


# WESTERN STATES SEISMIC POLICY COUNCIL

## PROCEEDINGS VOLUME BASIN AND RANGE PROVINCE SEISMIC HAZARDS SUMMIT II

EDITED BY WILLIAM R. LUND



Peak accelerations (%g) with 2% probability of exceedence in 50 years

2005



MISCELLANEOUS PUBLICATION 05-2  
UTAH GEOLOGICAL SURVEY  
A DIVISION OF  
UTAH DEPARTMENT OF NATURAL RESOURCES



# STATE OF UTAH

Jon Huntsman, Jr., Governor

## DEPARTMENT OF NATURAL RESOURCES

Michael Styler, Executive Director

### UTAH GEOLOGICAL SURVEY

Richard G. Allis, Director

#### PUBLICATIONS

contact

Natural Resources Map/Bookstore

1594 W. North Temple

telephone: 801-537-3320

toll-free: 1-888-UTAH MAP

website: <http://mapstore.utah.gov>

email: [geostore@utah.gov](mailto:geostore@utah.gov)

#### THE UTAH GEOLOGICAL SURVEY

contact

1594 W. North Temple, Suite 3110

Salt Lake City, UT 84116

telephone: 801-537-3300

website: <http://geology.utah.gov>

ISBN 1-55791-725-6

Although this product represents the work of professional scientists, the Utah Department of Natural Resources, Utah Geological Survey, makes no warranty, expressed or implied, regarding its suitability for any particular use. The Utah Department of Natural Resources, Utah Geological Survey, shall not be liable under any circumstances for any direct, indirect, special, incidental, or consequential damages with respect to claims by users of this product.

*The Utah Department of Natural Resources receives federal aid and prohibits discrimination on the basis of race, color, sex, age, national origin, or disability. For information or complaints regarding discrimination, contact Executive Director, Utah Department of Natural Resources, 1594 West North Temple #3710, Box 145610, Salt Lake City, UT 84116-5610 or Equal Employment Opportunity Commission, 1801 L. Street, NW, Washington DC 20507.*



# WESTERN STATES SEISMIC POLICY COUNCIL

## ***PROCEEDINGS VOLUME BASIN AND RANGE PROVINCE SEISMIC HAZARDS SUMMIT II***

Evaluating Approaches, Techniques, and Policies for  
Seismic Hazard Characterization in Extensional Regions  
*Reno-Sparks, Nevada, on May 16-19, 2004*

*Edited by  
William R. Lund  
Utah Geological Survey*

*Sponsored by  
Federal Emergency Management Agency  
United States Geological Survey  
And state geological surveys from  
Arizona  
California  
Colorado  
Idaho  
Montana  
Nevada  
New Mexico  
Oregon  
Utah  
and  
Wyoming*

*Hosted by:*



The Miscellaneous Publication series of publications from the Utah Geological Survey provides non-UGS authors with a high-quality format for publishing the results of their research. Reviews have been incorporated in this document; however, this publication does not necessarily conform to UGS technical, policy, or editorial standards. Although this work represents the work of professional scientists, the Utah Department of Natural Resources, Utah Geological Survey, makes no warranty, expressed or implied, regarding its suitability for a particular use. The Utah Department of Natural Resources, Utah Geological Survey, shall not be liable under any circumstance for any direct, indirect, special, incidental, or consequential damages with respect to claims by users of this product.



**MISCELLANEOUS PUBLICATION 05-2**      **2005**  
**UTAH GEOLOGICAL SURVEY**  
*a division of*  
**UTAH DEPARTMENT OF NATURAL RESOURCES**



## PREFACE

This Proceedings Volume documents the results of the second Basin and Range Province Seismic Hazards Summit held in Reno-Sparks, Nevada on May 16-19, 2004. Included are abstracts of the 26 oral presentations made at the summit, which were grouped into the following categories: (1) Earthquake Hazards of the Basin and Range Province, (2) Estimating Earthquake Size and Hazard From Faults, (3) Determining Fault Activity, (4) Earthquake Recurrence Intervals, and (5) Ground Motion for the Basin and Range Province. Thirty-eight poster presentations were also made at the summit, on topics as diverse as establishing guidelines for evaluating surface fault rupture, digital trench wall logging, and using ShakeMap as a tool for understanding earthquake hazards. The abstracts for the poster presentations are likewise included in this volume. Twenty presenters agreed to prepare papers or expanded abstracts of their talks or posters for inclusion in this volume, and an additional 10 posters are included here in their entirety.

As Proceedings Volume Editor, I express my appreciation to the speakers and poster presenters who so willingly shared of their expertise, experience, and not least of all their time to make the second Basin and Range Province Seismic Hazards Summit a success. The accumulated knowledge and wisdom contained in this volume regarding seismic-hazard characterization, analysis, and policy makes an important contribution to our understanding of earthquake hazards in the Basin and Range Province, and will serve as a technical and policy benchmark for the region for years to come.

William R. Lund  
Proceedings Volume Editor

# CONTENTS

INTRODUCTION

PROGRAM AGENDA

ABSTRACTS

    PRESENTER ABSTRACTS

    POSTER ABSTRACTS

PAPERS

CHALLENGES IN DETERMINING THE EARTHQUAKE HAZARDS FROM ACTIVE FAULTS IN THE BASIN AND RANGE PROVINCE *by D. Burton Slemmons, Professor Emeritus, Center for Neotectonic Studies, University of Nevada, Reno, and Craig M. dePolo, Nevada Bureau of Mines and Geology*

SUMMARY OF LATE QUATERNARY TECTONICS OF THE BASIN AND RANGE PROVINCE IN NEVADA, EASTERN CALIFORNIA, AND UTAH *by Michael Machette, U.S. Geological Survey*

CHALLENGES IN ASSESSING SEISMIC HAZARD ACROSS THE INTERMOUNTAIN WEST *by Mark D. Petersen, Arthur D. Frankel, Chris H. Cramer, Stephen C. Harmsen, Kathleen Haller, and Harley M. Benz, U.S. Geological Survey*

IDENTIFICATION AND CHARACTERIZATION OF ACTIVE (HOLOCENE) EXTENSIONAL FAULTS IN SOUTHEASTERN IDAHO, NORTHEAST UTAH, AND SOUTHWEST WYOMING – IMPLICATIONS FOR PIPELINE CROSSING DESIGN *by Donald O. West and Graeme Major, Golder Associates, Inc., and Suzanne R. Hickham, The Williams Companies, Inc.*

ESTIMATING PREHISTORIC EARTHQUAKE MAGNITUDE FROM POINT MEASUREMENTS OF SURFACE RUPTURE *by Mark A. Hemphill-Haley, Department of Geology, Humboldt State University, and Ray J. Weldon, II, Department of Geological Sciences, University of Oregon*

PROBABILISTIC FAULT-DISPLACEMENT HAZARD ANALYSIS: A CASE STUDY FROM SKULL VALLEY, UTAH *by Kathryn L. Hanson and Robert R. Youngs, Geomatrix Consultants, Inc., and Frank F. Swan, Consulting Geologist*

PALEOSEISMIC INVESTIGATIONS OF THE STANSBURY AND MID-VALLEY FAULTS, SKULL VALLEY, UTAH *by Frank F. Swan, Consulting Geologist, Kathryn L. Hanson and Robert R. Youngs, Geomatrix Consultants, Inc., and Michael M. Angell, William Lettis & Associates*

PATTERN AND TIMING OF FAULTING IN THE CENTRAL NEVADA SEISMIC BELT AND IMPLICATIONS FOR SEISMIC HAZARDS OF THE

WESTERN BASIN AND RANGE PROVINCE by *John W. Bell, Nevada Bureau of Mines and Geology; S. John Caskey, Department of Geosciences, San Francisco State University; and Alan R. Ramelli, Nevada Bureau of Mines and Geology*

SEPARATION AND IDENTIFICATION OF CHARCOAL AND ORGANICS FROM BULK SEDIMENT SAMPLES FOR IMPROVED RADIOCARBON DATING AND STRATIGRAPHIC CORRECTIONS by *Kathryn Puseman and Linda Scott Cummings, Paleo Research Institute*

PRELIMINARY PALEOSEISMIC INVESTIGATION OF THE CANYON FERRY FAULT, WEST-CENTRAL MONTANA by *Larry W. Anderson and Lucille A. Piety, U.S. Bureau of Reclamation, Seismotectonics and Geophysics Group; Susan S. Olig, URS Corporation; and Steven L. Forman, Department of Earth and Environmental Sciences, University of Illinois*

SHAKEMAP AS A TOOL FOR UNDERSTANDING EARTHQUAKE HAZARD IN NEVADA by *Glen Biasi, Nevada Seismological Laboratory, and Kent Lindquist, Lindquist Consulting*

ACTIVE TECTONICS OF THE NEPHI SEGMENT, WASATCH FAULT, UTAH by *Christopher DuRoss and Ronald L. Bruhn, Department of Geology and Geophysics, University of Utah*

BASIN AND RANGE SEISMICITY: DISTRIBUTION, OCCURRENCE RATES, MOMENT RELEASE, AND COMPARISON WITH GEODESY by *Aasha Pancha and John G. Anderson, Seismological Laboratory and Department of Geological Sciences, University of Nevada, Reno*

DETERMINATION OF LOW-STRAIN SITE-AMPLIFICATION FACTORS IN THE SALT LAKE VALLEY, UTAH, USING ANSS DATA by *Kris Pankow and James C. Pechmann, University of Utah Seismograph Stations*

A MULTIDISCIPLINARY APPROACH TO SEISMIC HAZARD IN THE RENO-CARSON METROPOLITAN REGION by *Feng Su, John G. Anderson, and Aasha Pancha, Seismological Laboratory, University of Nevada, Reno*

ISSUES IN EVALUATING GROUND-MOTION HAZARD IN THE BASIN AND RANGE PROVINCE by *Ivan G. Wong, Seismic Hazards Group, URS Corporation*

UTAH QUATERNARY FAULT PARAMETERS WORKING GROUP: CRITICAL REVIEW OF UTAH PALEOSEISMIC-TRENCHING DATA AND CONSENSUS RECURRENCE-INTERVAL AND VERTICAL SLIP-RATE ESTIMATES FOR UTAH'S QUATERNARY FAULTS by *William R. Lund, Utah Geological Survey*

A STRAIGHTFORWARD WAY OF NAMING PALEOEARTHQUAKES *by*  
*Craig M. dePolo, Nevada Bureau of Mines and Geology*

PROBABILISTIC EARTHQUAKE GROUND-MOTION HAZARD MAPS FOR  
MONTANA *by* *Ivan Wong, Susan Olig, Mark Dober, Doug Wright, and Eliza*  
*Nemser, Seismic Hazards Group, URS Corporation; David Lageson, Department of*  
*Earth Sciences, Montana State University; Walter Silva, Pacific Engineering &*  
*Analysis; Michael Stickney, Montana Bureau of Mines & Geology; Michele*  
*Lemieux, Montana Department of Natural Resources and Conservation; and Larry*  
*Anderson, U.S. Bureau of Reclamation, Seismotectonics and Geophysics Group*

## POSTERS

MAGNITUDE AND RUPTURE LENGTH ESTIMATES FROM POINT  
MEASUREMENTS OF DISPLACEMENT *by* *Glenn Biasi, University of Nevada,*  
*Reno Seismological Laboratory, and Ray J. Weldon II, University of Oregon*  
*Department of Geological Sciences*

MIOCENE AND YOUNGER FAULTS IN IDAHO *compiled by* *Roy M.*  
*Breckenridge, Reed S. Lewis, Guy W. Adema, and Daniel W. Weisz*

MIOCENE AND YOUNGER FAULTS IN IDAHO AND EARTHQUAKES IN  
IDAHO 1872—2000 *compiled by* *Roy M. Breckenridge, Reed S. Lewis, Guy W.*  
*Adema, and Daniel W. Weisz, Idaho Geological Survey*

GUIDELINES FOR EVALUATING SURFACE-FAULT-RUPTURE HAZARDS  
IN UTAH *by* *Gary E. Christenson, Utah Geological Survey; L. Darlene Batatian,*  
*Salt Lake County Geologist; Craig V Nelson, Western GeoLogic*

INTEGRATION OF GEOLOGIC AND GEODETIC DATA INTO KINEMATIC  
MODELS OF CONTEMPORARY STRAIN IN THE PACIFIC NORTHWEST  
AND ACROSS THE CASCADIA SUBDUCTION ZONE *by* *Mark Hemphill-*  
*Haley, Department of Geology, Humboldt State University, and Gene Humphreys,*  
*Department of Geological Sciences, University of Oregon*

QUATERNARY FAULT AND FOLD DATABASE AND MAP OF UTAH *by*  
*Michael D. Hylland, Utah Geological Survey*

CRITIQUE AND USE OF HISTORICAL METHODOLOGY IN SEISMIC  
HAZARDS ANALYSIS OF EARTHQUAKES IN THE BASIN AND RANGE:  
EXPANDING THE HISTORICAL CATALOG AND THE SEARCH FOR  
TRIGGERED (?) EVENTS FROM THE SAN ANDREAS FAULT *by* *Dawn C.*  
*Martindale, Department of History, Utah State University, and James P. Evans,*  
*Department of Geology, Utah State University*

HORSTS AND GRABENS OF COLORADO'S HIGH PLAINS *by* *Vince Matthews*  
*and Matthew L. Morgan, Colorado Geological Survey*

ACTIVE TECTONIC STRAIN PARTITIONING IN THE NORTHERN INTERMOUNTAIN SEISMIC BELTS *by Michael C. Stickney, Montana Bureau of Mines and Geology, and David R. Lageson, Department of Earth Sciences, Montana State University*

DIGITAL TRENCH WALL LOGGING: APPLYING MORPHOLOGICAL IMAGE PROCESSING TECHNIQUES TO TRENCH WALL STRATIGRAPHY – WASATCH FAULT 2003 AT MAPLETON, UTAH *by Julie B. Willis, Chaiwoot Boonyasiriwat, Gerald T. Schuster, and Christopher B. DuRoss, University of Utah*

#### EXTENDED ABSTRACTS

SEGMENTATION AND HOLOCENE DISPLACEMENT HISTORY OF THE GREAT SALT LAKE FAULT, UTAH *by David A. Dinter and James C. Pechmann, University of Utah Department of Geology and Geophysics*

DIGITAL TRENCH WALL LOGGING: APPLYING MORPHOLOGICAL IMAGE PROCESSING TECHNIQUES TO TRENCH WALL STRATIGRAPHY *by Julie B. Willis<sup>1</sup>, Chaiwoot Boonyasiriwat<sup>2</sup>, Gerard T. Schuster<sup>1</sup>, and Christopher B. DuRoss<sup>1</sup>*

*(<sup>1</sup>University of Utah, Department of Geology and Geophysics, <sup>2</sup>University of Utah, Department of Computational Engineering and Science)*

## **INTRODUCTION**

The Western States Seismic Policy Council (WSSPC), U.S. Geological Survey, Federal Emergency Management Agency, and western states geological surveys sponsored the second Basin and Range Province Seismic Hazards Summit (BRPSHSII) in Reno-Sparks, Nevada, on May 16-19, 2004. The meeting successfully highlighted technical issues important to understanding earthquake hazards in the Basin and Range Province (BRP), and in developing policy recommendations to aid BRP states in reducing earthquake losses. BRPSHSII built on the results of BRPSHSI held in May 1997, also in Reno and sponsored by the same groups.

BRPSHSII brought together geoscientists, engineers, emergency managers, and policy makers to present and discuss the latest earthquake-hazards research, and to evaluate research implications for hazard reduction and public policy. Sessions addressed: (1) general earthquake hazards issues, (2) estimating earthquake size and hazards from faults, (3) determining fault activity, (4) earthquake recurrence intervals, and (5) earthquake ground motions. The agenda included 26 invited speakers and 38 poster presentations; nearly 100 individuals attended the meeting.

Specific BRP earthquake issues identified and discussed at the BRPSHSII included: (1) using time-dependent, Poisson, and clustering models in characterizing fault behavior, (2) using displacements to estimate earthquake magnitudes, (3) the need for developing both short- and long-term paleoseismic records for faults, (4) reconciling modern geodetic extension rates and geologic slip rates, and (5) determining appropriate attenuation relations and stress drops for modeling earthquake ground motions, including consideration of evidence from precarious rock studies. The final session addressed near-fault ground motions, and site and basin effects on ground shaking levels in the BRP.

BRPSHSII provided a vehicle to advocate for improved seismic-hazard analyses, and for a firm scientific foundation for seismic policy in the BRP.

WSSPC defines “seismic policy” as related to the concept of “government policy,” which is the philosophical basis for laws, regulations, and practices adopted by government. Thus “seismic policy” is government policy that relates to earthquake hazards and earthquake hazard mitigation. The National Seismic Hazard Maps are a fulcrum of seismic policy, bringing together state-of-the-art techniques and data to reduce seismic risk. Other important policy considerations include developing guidelines for inclusion of faults as earthquake sources, and guidelines for mitigating earthquake risks and developing earthquake-resistant structures. The characteristics of earthquakes in the BRP may not be unique, but they have distinctions that warrant seismic-policy considerations specific to the BRP. The Basin and Range Province Committee reviewed the policy issues raised at BRPSHSII and drafted four policy recommendations, which they then forwarded to WSSPC. After review and discussion by the WSSPC Board, three of the recommendations were adopted at the September 2004 WSSPC Annual Meeting in St. Louis. The fourth policy was deferred for future consideration. The three approved policies are:

### **WSSPC PR 04-5: Basin and Range Province Earthquake Working Group(s)**

WSSPC recommends convening a technical Basin and Range Province Earthquake Working Group(s) (BRPEWG) to develop scientific consensus regarding fault behavior, ground-shaking and ground-failure modeling and research priorities relevant to seismic policy and the U.S. Geological Survey National Seismic Hazard Maps in the Basin and Range Province. The BRPEWG would be convened under the auspices of the USGS NSHM project.

### **WSSPC PR 04-6: Priorities for Applied Research on Earthquake Hazards**

Projects supported by the National Earthquake Hazards Reduction Program through the U.S.

Geological Survey should focus on work that has significant impact on the reduction of earthquake risks in the near- to mid-term.

**WSSPC PR 04-7: Supporting Non-technical Explanation of USGS Uncertainty Maps to Accompany Probabilistic Seismic Hazard Maps**

WSSPC encourages the USGS to provide, in addition to the uncertainty maps, a narrative that characterizes the uncertainties, explains non-technically how that uncertainty affects interpretation of the probabilistic hazard map, and explains why maps change from version to version.

**ACKNOWLEDGMENTS**

The second Western States Seismic Policy Council Basin and Range Province Seismic Hazard Summit (BRPSHSII) was convened through the efforts of a many individuals. They cannot all be mentioned here, but the success of BRPSHSII is a direct result of their hard work and they are all greatly appreciated. However, special thanks are in order to the members of the Basin and Range Province Committee, which organized the summit

under the able chairmanship of Craig dePolo Nevada Bureau of Mines and Geology). The Summit Steering Committee, Gary Christenson, William Lund, Ivan Wong, Tom Sawyer, Phil Pearthree, Roy Breckenridge, and Steve Weiser were instrumental in organizing the summit agenda. Terri Garside (Nevada Bureau of Mines and Geology) provided the administrative skills and know-how to keep the summit planning moving forward, on budget, and on time.

The Basin and Range Province Committee extends its thanks to the WSSPC Board, U.S. Geological Survey, and the Federal Emergency Management Agency without whose support and encouragement the summit could never have taken place. And of course, thanks to the many technical experts who made presentations, there likewise would have been no summit without them.

Finally, thank you to the authors who prepared papers or provided a digital copy of their posters for this proceedings volume, to Cheryl Gustin (Utah Geological Survey) for her skill in formatting many of those papers for publication, to William Lund (Utah Geological Survey) for editing this volume, and to the Utah Geological Survey for publishing it.

## DEDICATION

### Dr. Jonathan G. Price

The Western States Seismic Policy Council's Basin and Range Province Committee is pleased to dedicate this volume to Dr. Jonathan G. Price in recognition of his leadership in the WSSPC, his participation and support of BRPSHS I and II, and his support of basic and applied seismic-hazard-reduction research in the Basin and Range Province.

Jon received a Bachelor of Arts in Geology and German at Lehigh University in 1972, a Master of Arts in Geology at the University of California, Berkeley in 1975, and a Doctorate in Geology at the University of California, Berkeley in 1977. Jon's early career was as a geologist with the Anaconda Company working at the Yerington copper mine in Nevada where he mapped deposits and logged core. After a brief stint as an Adjunct Assistant Professor teaching economic and physical geology at Bucknell University, Jon joined United States Steel Corporation as an exploration geologist mapping uranium deposits in south Texas. In 1981, Jon went to work for the Texas Bureau of Economic Geology and worked his way up from Research Associate to Program Director of Mineral Resources and Director of the Texas Mining and Mineral Resources Research Institute. Since 1988 Jon has served as Nevada State Geologist and Director of the Nevada Bureau of Mines and Geology. He has steadily enhanced the Bureau and encouraged a broadening of its activities, including a recently added geodetic component. Jon is an extremely dedicated and hard worker. His current position requires a wide range of management, technical, and political skills, and he is extremely apt at all. Jon's areas of personal research include igneous petrology, geochemistry of ores and unmineralized rocks, mineral resource assessment, aqueous geochemistry, and geologic hazards.



Jon served as WSSPC Chairman from 1998 to 2002. These were critical years for the WSSPC, and Jon contributed much energy and many hours to keep the Council running smoothly and to help it grow and become more effective. Jon has participated in all major activities of the Basin and Range Province Committee, including various symposia and committee meetings at the Council's annual meetings, the Post-Earthquake Technical Information Clearinghouse Workshop, and most importantly, the two Basin and Range Province Seismic Hazard Summits. Jon was an active participant at both Summits leading the policy discussions conducted each afternoon. In addition, Jon has steadily promoted research on seismic hazards in the Basin and Range Province through participation in national organizations and committees, such as the Association of American State Geologists, the U.S. Geological Survey's Scientific Earthquake Studies Advisory Committee, the U.S. Geological Survey's Advisory Committee for the National Cooperative Geologic Mapping Program, and the National Science Foundation's EarthScope Science and Education Committee.

In appreciation of his outstanding support and enthusiasm, the WSSPC Basin and Range Province Committee dedicates this volume to Jon Price.

## Basin and Range Province Seismic Hazard Summit II

### AGENDA

#### Sunday (May 16)

3:00 Registration/Poster Set Up

6:00 Poster Display Icebreaker/no-host bar

#### Monday (May 17)

7:00 Registration/continental breakfast

8:00 Summit Opening

8:30-12:00 First Session (Earthquake Hazards of the Basin and Range Province)

8:30 **Slemmons, Burt** - Challenges in Determining the Earthquake Hazards From Active Faults in the Basin and Range Province

9:00 **Machette, Michael** - Summary of the Late Quaternary Tectonics of the Basin and Range Province in Nevada and Utah

9:30 **Peterson, Mark** - Seismic Hazard Mapping in the Intermountain-West Region

10:00 - BREAK -

10:30 **Lund, Bill** - Utah Quaternary Fault Parameters Working Group: Critical Review of Paleoseismic-Trenching Data and Consensus Recurrence-Interval and Slip-Rate Estimates for Utah's Quaternary Faults

11:00 **Haller, Kathleen** - Fault Segmentation Models in Probabilistic Seismic Hazard Assessment

11:30 **West, Donald** - Identification and Characterization of Active (Holocene) Extensional Faults in Southeast Idaho, Northeast Utah, and Southwest Wyoming - Implications for Pipeline Crossing Design

12:00 - LUNCH - (served on site)

1:15-4:15 Second Session (Estimating Earthquake Size and Hazards from Faults)

1:15 **Wells, Don** - Approaches and Issues in Estimating Maximum Magnitudes for Fault Sources in Seismic Hazard Analyses

1:45 **Hemphill-Haley, Mark** - Estimating Prehistoric Earthquake Magnitude From Point Measurements of Surface Rupture

2:15 **Hecker, Suzanne** - Low Slip-at-a-Point Variability: Implications for Earthquake-Size Distribution, Fault-Rupture Hazard, and Ground-Motion Modeling

-BREAK -

3:15 **Hanson, Kathryn** - Probabilistic Fault Displacement Hazard Analysis: A Case Study from Skull Valley, Utah

3:45 **Olig, Susan** - Top 10 Reasons (or Problems) for Using Displacements in Probabilistic Seismic Hazard Analyses

4:15 Technical Discussion with Speakers (panel discussion)

4:40 Policy Discussion (led by Jon Price)

5:30 Poster Session/Social/no-host bar

#### Tuesday (May 18)

7:00 Registration/continental breakfast

8:15 Days Overview

8:30-12:00 Third Session (Determining Fault Activity)

8:30 **Thatcher, Wayne** - Present Day Deformation of the Great Basin and its Implications for Seismic Hazard Assessment

9:00 **Unruh, Jeff** - Neotectonics of the Walker Lane Belt, California and Nevada, and Implications for Seismic Hazard Assessment

9:30 **Bell, John** - Pattern and Timing of Faulting in the Central Nevada Seismic Belt and Implications for Seismic Hazards in the Western Basin and Range Province

10:00 - BREAK -

10:30 **Puseman, Kathy** - Separation of Charcoal and Organics from Bulk Soil Samples Prior to Radiocarbon Analysis

11:00 **Seitz, Gordon** - Closing the Gap Between On and Offshore Paleoseismic Records in the Lake Tahoe Basin

11:30 **McCalpin, James** - Estimating Slip Rates and Recurrence Intervals for Quaternary Faults in the Basin and Range Province, Using Geologic Data  
12:00 - LUNCH - (served on site)  
1:30-3:00 Fourth Session (Earthquake Recurrence Intervals)  
1:30 **Schwartz, David** - Hebgen Lake Revisited: Implications for the Behavior and Paleoseismology of Normal Faults  
2:00 **Olig, Susan** - Time-Dependent Probabilistic Seismic Hazard Analyses along the Wasatch Front, Utah and the Need for Longer Paleoseismic Records  
2:30 **Bruhn, Ron** - High-Resolution Seismic Tomography and Coring of Quaternary Deposits to Explore the-'Pulse of the Earthquake Engine'  
3:00 - BREAK -  
3:30 Technical Discussion with Speakers (panel discussion)  
4:00 Policy Discussion (led by Jon Price)  
5:00 End of sessions  
7:00 Optional discussion on prioritization of post-earthquake scientific studies (probably at local brewery across the street)  
9:00 end of day (no later than)

### **Wednesday (May 19)**

8:00 Registration/continental breakfast  
8:45 Days overview  
9:00-1:45 Fifth Session (Ground Motion in the Basin and Range Province)  
9:00 **Wong, Ivan** - Issues in Evaluating Ground Motion Hazard in the Basin and Range Province  
9:30 **Campbell, Ken** - Perspective on Attenuation Relationships for the Basin and Range Province  
10:00 **Somerville, Paul** - Characterization of Near Fault Ground Motions for Design  
10:30 - BREAK -  
11:00 **Graves, Robert** - Basin Effects on Ground Motions  
11:30 **Silva, Wait** - Site Characterization and Site Effects on Ground Motions  
12:00 - LUNCH - (on own)  
1:15 **Brune, Jim** - Precarious Rock Constraints on Ground Motion: Comparisons with Predictions from Foam Rubber Models  
1:45 Technical Discussion with Speakers (panel discussion)  
2:00 Policy Discussion (led by Jon Price)  
3:00 Summit Adjournment/poster breakdown  
3:10 Short Basin and Range Province Committee meeting

## **PRESENTER'S ABSTRACTS**

(in chronological order by presentation time)

*(click on links below)*

CHALLENGES IN DETERMINING THE EARTHQUAKE HAZARDS FROM ACTIVE FAULTS IN THE BASIN AND RANGE PROVINCE, D. Burton Slemmons and Craig M. dePolo

SUMMARY OF THE LATE QUATERNARY TECTONICS OF THE BASIN AND RANGE PROVINCE IN NEVADA AND UTAH, Michael N. Machette

SEISMIC HAZARD MAPPING IN THE INTERMOUNTAIN-WEST REGION, Mark D. Petersen, Arthur D. Frankel, and Chris H. Cramer

UTAH QUATERNARY FAULT PARAMETERS WORKING GROUP: CRITICAL REVIEW OF PALEOSEISMIC-TRENCHING DATA AND CONSENSUS RECURRENCE-INTERVAL AND SLIP-RATE ESTIMATES FOR UTAH'S QUATERNARY FAULTS, William R. Lund

FAULT SEGMENTATION MODELS IN PROBABILISTIC SEISMIC HAZARD ASSESSMENT, Kathleen M Haller

IDENTIFICATION AND CHARACTERIZATION OF ACTIVE (HOLOCENE) EXTENSIONAL FAULTS IN SOUTHEAST IDAHO, NORTHEAST UTAH AND SOUTHWEST WYOMING—IMPLICATIONS FOR PIPELINE CROSSING DESIGN, Donald O. West, Graeme Major, and Suzanne R. Hickham

APPROACHES AND ISSUES IN ESTIMATING MAXIMUM MAGNITUDES FOR FAULT SOURCES IN SEISMIC HAZARD ANALYSES, Donald L. Wells

ESTIMATING PREHISTORIC EARTHQUAKE MAGNITUDE FROM POINT MEASUREMENTS OF SURFACE RUPTURE, Mark A. Hemphill-Haley and Ray J. Weldon II

LOW SLIP-AT-A-POINT VARIABILITY: IMPLICATIONS FOR EARTHQUAKE-SIZE DISTRIBUTION, FAULT RUPTURE HAZARD, AND GROUND-MOTION MODELING, Suzanne Hecker and Norman A. Abrahamson

PROBABILISTIC FAULT DISPLACEMENT HAZARD ANALYSIS: A CASE STUDY FROM SKULL VALLEY, UTAH, K. L. Hanson, R. R. Youngs, and F. H. Swan

PRESENT DAY DEFORMATION OF THE GREAT BASIN AND ITS IMPLICATIONS FOR SEISMIC HAZARD ASSESSMENT, Wayne Thatcher and Bill Hammond

NEOTECTONICS OF THE WALKER LANE BELT, CALIFORNIA AND NEVADA, AND IMPLICATIONS FOR SEISMIC HAZARD ASSESSMENT, Jeffrey Unruh

PATTERN AND TIMING OF FAULTING IN THE CENTRAL NEVADA SEISMIC BELT AND IMPLICATIONS FOR SEISMIC HAZARDS OF THE WESTERN BASIN AND RANGE PROVINCE, John W. Bell, S. John Caskey, and Alan R. Ramelli

SEPARATION OF CHARCOAL AND ORGANICS FROM BULK SOIL SAMPLES PRIOR TO RADIOCARBON ANALYSIS, Kathryn Puseman and Linda Scott Cummings

CLOSING THE GAP BETWEEN ON AND OFFSHORE PALEOSEISMIC RECORDS IN THE LAKE TAHOE BASIN, Gordon Seitz and Graham Kent

ESTIMATING SLIP RATES AND RECURRENCE INTERVALS FOR QUATERNARY FAULTS IN THE BASIN AND RANGE PROVINCE, USING GEOLOGIC DATA, James P. McCalpin

HEBGEN LAKE REVISITED: IMPLICATIONS FOR THE BEHAVIOR AND PALEOSEISMOLOGY OF NORMAL FAULTS, D.P. Schwartz, S. Hecker, H.D. Stenner

TIME-DEPENDENT PROBABILISTIC SEISMIC HAZARD ANALYSES ALONG THE WASATCH FRONT, UTAH AND THE NEED FOR LONGER PALEOSEISMIC RECORDS, Susan S. Olig, Patricia A. Thomas, and Ivan G. Wong

HIGH-RESOLUTION SEISMIC TOMOGRAPHY AND CORING OF QUATERNARY DEPOSITS TO EXPLORE THE 'PULSE OF THE EARTHQUAKE ENGINE,' Ronald Bruhn, Gerard Schuster, Ann Mattson, Maike Buddensiek, Christopher DuRoss, and Travis Crosby

ISSUES IN EVALUATING GROUND MOTION HAZARD IN THE BASIN AND RANGE PROVINCE, Ivan G. Wong

PERSPECTIVE ON ATTENUATION RELATIONSHIPS FOR THE BASIN AND RANGE PROVINCE, Kenneth W. Campbell

CHARACTERIZATION OF NEAR FAULT GROUND MOTIONS FOR DESIGN, Paul Somerville

BASIN EFFECTS ON GROUND MOTIONS, Robert Graves

PRECARIOUS ROCK CONSTRAINTS ON GROUND MOTION: COMPARISONS WITH PREDICTIONS FROM FOAM RUBBER MODELS, James N. Brune

# CHALLENGES IN DETERMINING THE EARTHQUAKE HAZARDS FROM ACTIVE FAULTS IN THE BASIN AND RANGE PROVINCE

D. Burton Slemmons, Professor Emeritus, Center for Neotectonic Studies, Univ. of Nevada, Reno, NV 89557  
(PO Box 81050, Las Vegas, NV 89180), bslemmons@aol.com

Craig M. dePolo, Nevada Bureau of Mines and Geology, Univ. of Nevada, Reno, NV 89557.

## Introduction

The determination of seismic sources and earthquake hazards in the complex Basin and Range Province (BAR) is challenging. There are hundreds to thousands of Quaternary faults in the province, and most do not have adequate paleoseismologic studies. Faults commonly have distributed patterns, indistinct end points, moderate to low slip rates that may change with time, and may be buried by young basin fill. This makes the definition of potential earthquake rupture parameters difficult to determine. The western part of the BAR is especially influenced by the right-lateral faulting transform motion along the Pacific-North American Plate boundary, which has a branch (Eastern California Shear Zone) extending northeast into the BAR and accommodates about 25 percent (12 mm/yr) of the total plate boundary motion. The narrow Walker Lane belt (8 mm/yr) has most of this deformation with mainly right-lateral faults with subordinate normal-slip faulting, and normal-slip faults dominate along Wasatch and Sierra Nevada boundary zones and the central and eastern BAR.

## Historical Record

Earthquakes during the brief historical record provide a key to interpreting paleoseismology. At least 25 historical surface faulting events in the BAR and Eastern California shear zone are listed in Table 1. These events range in magnitude from 5.6 to ~7.6. Earthquakes over magnitude 6.5, generally had primary surface fault ruptures in patterns that range from narrowly focused to widely distributed, and had endpoints that were distinct fault discontinuities in only about half of the cases. The number of structural and/or geometric segments involved during historical events range from single segment ruptures to multiple segments ruptures (up to 5 segments). Although some large events were widely distributed, or had unusually short surface rupture lengths, maximum surface displacement is usually proportional to earthquake magnitude, and accordingly is a key parameter to consider in earthquake size estimation. The historical earthquakes occurred in a wide variety of geologic settings, including range-front, piedmont, basin, and bedrock settings, and occurred in portions of the BAR that have different levels of tectonic activity (e.g., the active transtensional Walker Lane belt versus the tectonically less active southern BAR). All primary surface-faulting events ruptured Quaternary faults, but nearly half of these ruptures occurred along faults lacking Holocene activity, and the age of the penultimate rupture for some events varied from place to place within the rupture zone. These events indicate that potential BAR earthquakes can occur in all geologic and tectonic settings, and with a fairly large range in fault characteristic and parameters for a given magnitude. Realizing and dealing with these uncertainties is a challenge and current limitation for estimating earthquake hazards in the BAR.

## Challenges in Determining the Earthquake Hazards from Faults

**State-of-the-Art Factors:** These factors include unidentified earthquake faults, important faults that have not been studied or are inadequately studied, uncertainties in determining fault activity and fault rupture parameters, the small historical earthquake and well-studied fault databases, uncertainties in fault behavior, uncertainty in direct application of geodesy to faults, uncertainty in assigning scaling parameters, and distinction of rupture modes.

**Geologic Factors:** These factors include the large number of Quaternary faults to be studied, variable and wide-ranging earthquake recurrence intervals and fault slip rates, complexity of fault interactions, and indistinct fault terminations.

**Historical Earthquake Faults:** These factors include indistinct rupture discontinuities (e.g. 1932), multiple structural and geometric segments (e.g. 1915, 1954), distributed fault traces (e.g. 1932), large events with relatively short fault lengths

**Table 1. Historical surface faulting in the Basin and Range Province and the Eastern California shear zone.**

NO	DATE	FAULT LOCATION	M <sub>w</sub> MAG	ZONE LENGTH (km)	ZONE WIDTH (km)	MAX. DISPL (m)	AGE OF PREVIOUS ACTIVITY; NUMBER OF SEGMENTS
1	1869?	Olinghouse, NV	6.7±	~20	<1?	3.7	Holocene (Holo), 1 segment?
2	1872	Owens V, CA	~7.6	~108	Var. 3-16; Avg 8	RL 9, V 4.4	>8,000 yrs (Holo); 3 or 4 segs.
3	1887	Sonora, Mex	7.3	101.4	1-3, Avg ~2	V 4.87	100 ka to 200 ka; 2-3.
4	1903?	Wonder, NV	~6.5±	11?	~1	V ~1	L. Quat; 1?
5	1915	Pleasant V, NV	7.2-7.6	>62	V 2-5, Avg >2	V 5.8	Holo or L. Quat.; 4-5.
6	1932	Cedar Mtn, NV	7.1	75	3-15, Avg 8	SS 2.7	Holo and L. Quat; ~3.
7	1934	Excelsior Mtn, NV	6.3	>1.7	<1	V 0.13, LL 0.	L. Quat; 1.
8	1934	Hansel V, UT	6.6	11	~2.5	V 0.5, LL 0.2	L. Quat.
9	1947	Manix, CA*	6.2	1.6?	?	LL 0.076	1?
10	1948	Ft. Sage Mtn, CA	5.6	~9	<1	V 0.6,	Holo; 1.
11	1954a	Rainbow Mtn, NV	~6.5	18	12	V 0.7, RL~1.0	Holo; 1?
12	1954b	Fourmile Flat, NV	6.4	~6	~1	~1.5	Late Holo; 1.
13	1954c	Stillwater, NV	6.8-7.0	31-	>3, Avg 2	V 0.8	2?
14	1954d	Fairview Pk, NV	7.2	46	<13-19	4.8	L. Quat. (>35 ky); 3-4+.
15	1954e	Dixie V, NV	~7.0	42	5	3.8	Variable, Holo and L. Quat; 2.
16	1959	Hebgen L, MT	7.3	26.5	15	6.1	Holo; 2-3.
17	1975	Galway L, CA*	5.2	6.8		0.015	Holo; 1.
18	1979	Homestead V, CA*	5.2	3.25		RL 0.1, V .04	Holo and L. Quat; 1.
19	1980	Mammoth, CA	6.0-6.5	20	V 0.3,	?	Triggered? Larger Holo event.
20	1983	Borah Pk., ID	6.9	34	1-7, Avg 2	2.7	Holo, and L. Quat; 2-3.
21	1986	Chalfant V, CA	6.2	13-15.5	RL 7-11	0.05v	Holo; triggered slip?
22	1993	Eureka V, CA	5.8	>4	?	0.02	Triggered slip?
23	1992	Landers, CA*	7.3	~80	RL ~6, Avg 5	~6.7	Holo and L. Quat; 3-4.
24	1994	Double Spgs Fl, NV	5.8	~6.5	2	~0.1?	Holo and L. Quat; triggered slip.
25	1999	Hector Mine, CA*	7.1	41	1	RL 5.2	L. Quat (and older?)

\* Faulting event is within the Eastern California shear zone in the Mojave Desert.

(1959), wide range in fault parameters for a given magnitude 1986), faults with repeated historical rupture events (1903 and 1954d, 1932 and 1954d, and 1954a and 1954c), clustering of events in time (1954 sequence).

Historical Faulting Studies Indicate that Earthquake Hazard Studies Need to Consider:

1. Surface fault ruptures commonly are in broad zones with many distributed or triggered fault offsets several km away from the main rupture (1915, 1932, 1954a, 1954c, 1954d, 1954e, 1959, 1980, 1983, 1993).
2. Several surface fault ruptures activated late Quaternary to Holocene faults with different penultimate ages for various parts of the rupture zones (1954d, 1954e, 1992, 1999).
3. In addition to range-front faulting, surface ruptures commonly branch into or are within valleys, and less commonly rupture within horst blocks (1872, 1903, 1934, 1954d). Faults in the valley floors are in zones where alluvial processes rapidly conceal, or partly conceal, paleoseismologic evidence of ancient past events that may be difficult to detect or resolve. Ruptures from at least three historical events overlap, and reactivate known historical faulting: 1903 Wonder, 1932 Cedar Mountain, and 1954 Fairview Peak earthquakes.
4. Segmentation and segmentation lengths are subjectively determined from geological or geophysical evidence. The analyses of dePolo et al. (1989) and Slemmons (1995) suggest for earthquake magnitudes above 6.5 that the ruptures that break two to five segments with surface rupture lengths from less than 10 km to more than 40 km.
5. More than one half the larger events have occurred in the relatively small area in or near Walker Lane belt and Eastern California shear zone of the BAR. Here, the translational plate boundary influence, and connection to the San Andreas fault system may cause many faults to have higher fault slip rates, shorter recurrence intervals, and a greater prevalence of strike-slip fault systems than is typical for the province.

## SUMMARY OF THE LATE QUATERNARY TECTONICS OF THE BASIN AND RANGE PROVINCE IN NEVADA AND UTAH

Michael N. Machette, U.S. Geological Survey, MS 966, Box 25046, Denver, CO 80225-0046 (machette@usgs.gov)

This paper focuses on the highly extended Basin and Range Province of Utah and Nevada, which is the type locality of active extensional tectonics in the United States. As such, it should be a robust source of information on fault mechanics and geometry, and earthquake timing and recurrence, but it is not. The region is larger than Europe, contains almost 1000 faults, and is relatively remote. In the course of compiling information on potential earthquake source areas in the western U.S., it has become apparent that there are several problems that limit our understanding of the characteristics of active faulting of the Basin and Range Province. On one hand is the sheer abundance of Quaternary faults in the province; conversely, only limited paleoseismic studies have been conducted, and radiocarbon-datable materials are very rare owing to the province's arid to semi-arid climate and sparse vegetation. Recent advances in luminescence (TL and OSL) and cosmogenic-nuclide dating techniques help address the latter problem, but these methods are expensive and time consuming. The large number of faults for which data are needed is a real limitation that will be addressed only by increasing the number of paleoseismic studies or the application of regional reconnaissance tools that give geologically realistic estimates of paleoseismic parameters (slip rates, recurrence intervals, and times of most recent movement). Thus, truly characterizing the seismogenic potential of Basin and Range faults is a task that will require a considerable amount of time and manpower.

Most Quaternary faults in the province trend north, have normal-slip displacement, and bound strongly uplifted or tilted ranges. Although the uplifted ranges are geomorphically spectacular, the associated Quaternary fault slip rates are relatively slow (ca. 0.1 mm/yr), and the recurrence interval for M 6.5+ earthquakes is relatively long (ca. 104 yr). Some faults are considerably more active, especially those at the eastern and western margins of the province, such as the Genoa (2-3 mm/yr), Death Valley (4-5 mm/yr), and Wasatch (1-1.5 mm/yr) faults. Hundreds of more typical Basin and Range faults appear to be less active, but their behavior remains poorly characterized. Recent paleoseismic studies show that some of these faults have average slip rates of 0.05-0.15 mm/yr and recurrence intervals of tens to hundreds of thousands of years. The relatively low hazard posed by single faults is contrasted by the hundreds of Quaternary faults that riddle the province and therefore increases the average rate of earthquake recurrence in any particular region.

The USGS's new compilation of faults in the Basin and Range Province (see Machette and others, this volume) shows 741 reported Quaternary structures in Nevada and Utah. About 150 of these faults (20%) have been active in the past 15,000 years (15 k.y.), whereas 320 (43%) have been active in the past 130 k.y. (i.e., since the penultimate glacial cycle). One result of recent paleoseismic investigations is that, in many cases, dating faulted deposits shows that the most recent movement is younger than the age inferred from geomorphologic analyses, such as fault-scarp morphology, or from detailed surficial mapping. There are many ways to make a fault-scarp appear older than its actual age, such as by burial by eolian, colluvial, or alluvial deposits. In contrast, there are only few ways to make a scarp look younger (fluvial trimming is the most likely). Thus, many of the estimates of the time of most recent movement shown in the fault database probably err on the old side. In addition, we used inclusive time categories, such as <130 ka, to bracket the times of faulting; thus, each category must include some younger faults. We suspect that the above cited number and percentages of faults with <15 ka and <130 ka movement are minimum values that will increase as more faults are studied in detail. One positive result of this analysis is that the <130-ka time window captures almost half of the Quaternary faults and mimics their distribution well. This window is long enough to include one or more typical earthquake cycle (at least two events, one recurrence interval) on most faults, whereas the <15 ka window is geologically inadequate for sampling potential earthquake sources. This was also demonstrated by dePolo and Slemmons (1998) when they pointed out that only about half of the eleven historical ruptures in the Basin and Range Province had occurred on mapped Holocene faults.

Except for aftershock activity on some of the historical ruptures in the province, there is little spatial association between faulting and recorded seismicity and virtually no examples of foreshock activity for large earthquakes. For example, the Wasatch fault zone is poorly expressed on Utah seismicity maps, and the Thousand Springs segment of the Lost River fault (northern Basin and Range in Idaho) was virtually aseismic before 1983 Borah Peak earthquake. Similar examples are common in the Basin and Range, especially in its southern half. For the most part, the normal faults of the Basin and Range Province seem to be aseismic and locked, but may be loaded to near the point of failure as in the case with the 1954 Fairview Peak and Dixie Valley earthquakes.

In contrast, the Central Nevada Seismic Belt (CNSB) has been the preferred area for historic earthquakes larger than M 6.5 in the Basin and Range Province. From 1872 to 1954, seven large earthquakes caused surface ruptures along this NNE-

trending belt-an average of one rupture every 14 years. A recent summary of paleoseismic investigations of the CNSB (Bell and Caskey, in press) has shown that this rate and spatial pattern of activity is anomalous. There is no compelling evidence for similar precursory activity in the past 50 k.y. on this belt, and there has been almost 50 years of quiescence since the last large earthquake. So, two of the most perplexing questions about the CNSB are “why here and where next?”

With the advent of GPS monitoring we are starting to better characterize the distribution and rate of extension associated with active faults of the Basin and Range Province. However, even for campaign-style GPS networks, there are typically two to four Quaternary faults between measurement stations. This spacing problem leaves open the question of which of the many Quaternary faults are really active. Hopefully, our new fault database, continuing paleoseismic investigations in the Intermountain West, and targeted GPS surveys will help pinpoint those Quaternary faults with the most potential for future large magnitude earthquakes and surface rupturing. Ultimately, the scientific challenge is to compare geologically determined rates and styles of deformation to contemporary strain fields determined by GPS and see if the regions of accelerated extension are relicts of the recent past activity or precursors of future activity.

## Seismic Hazard Mapping in the Intermountain-West Region

Mark D. Petersen, Arthur D. Frankel, and Chris H. Cramer

The Intermountain-West region contains hundreds of seismically active faults. Most of these earthquake sources have low to moderate slip rates, and only rupture in large earthquakes every few thousand to tens of thousands of years. In spite of these low activity rates, several faults have generated large earthquakes: ten earthquakes have ruptured the surface during the past two centuries, and several of those ruptures are attributable to faults that did not have evidence of Holocene displacement. The large number and vast extent of these faults cause a significant hazard that must be considered in engineering, emergency response planning, and other public policy applications. We recently updated the USGS National Seismic Hazard Maps, and the 2002 version maps are now available on the USGS website (<http://geohazards.cr.usgs.gov/eq/>). This update involved reassessment of fault slip rates, magnitudes, magnitude-frequency distributions, geodetic data, and attenuation relations. Several issues are being evaluated for future versions of these maps:

- (1) Alternative source models: We compare the hazard calculated using an alternative multi-segment rupture model for the Wasatch fault with the individual segment rupture models that were used in the 2002 update.
- (2) Alternative recurrence models: Time-dependent hazard at sites along the Wasatch front have been calculated using the Brownian Passage Time recurrence distribution. This distribution is characterized by mean recurrence and aperiodicity that are computed from the paleoseismic data. Geodetic data were evaluated to analyze strain rates across the Great Basin, and those data influenced modeling of the Central Nevada Seismic Zone.
- (3) Updated attenuation relations: Current studies are focusing on the attenuation properties of the crust across the Basin and Range province.
- (4) Monte Carlo uncertainty analysis: We have calculated uncertainty for the hazard at several sites by varying the characteristic magnitude, fault slip rate or recurrence rate, fault length, magnitude-frequency distributions, and attenuation relations. This uncertainty is about +/- 50% of the mean value at one standard deviation.
- (5) Urban hazard maps: We have begun collecting data along the Wasatch fault to develop a community 3-D velocity model and ground deformation models. These data are critical for assessing site response in the shallow and deep sediments. In addition, we are collaborating with state surveys, academia, and industry to establish working groups that will evaluate earthquake hazards on a regional scale.

Evaluation of these important issues by working groups from the Earth-science, engineering, and decision-making communities will lead to products that incorporate the best science available and that are useful for public policy applications.

## **Utah Quaternary Fault Parameters Working Group: Critical Review of Paleoseismic-Trenching Data and Consensus Recurrence-Interval and Slip-Rate Estimates for Utah's Quaternary Faults**

Lund, William R., Utah Geological Survey, SUU Box 9053, Cedar City, Utah 84720, lund@suu.edu

The Utah Geological Survey convened a Utah Quaternary Fault Parameters Working Group comprised of experts in paleoseismology and seismology to review Utah's Quaternary fault paleoseismic-trenching data, and to determine consensus mean recurrence and slip-rate estimates when the data permitted. Utah has 212 Quaternary faults or fault sections; paleoseismic trenching data are available for 31 (15%) of them. Available data come from nearly 60 sources representing the work of more than 40 researchers over the past 30-plus years. Used extensively by researchers and geologic and engineering practitioners, Utah's paleoseismic trenching data have not been critically reviewed to establish consensus fault parameter values and appropriate uncertainty limits. Consensus paleoseismic data are critical in four areas related to reducing earthquake losses in Utah: (1) updating the National Seismic Hazard Maps, (2) providing consensus paleoseismic data and uncertainty limits for use by other researchers, (3) characterizing seismic sources, and (4) preparing PSHAs.

The Working Group evaluated both geologic and laboratory uncertainties associated with the data, recalibrated radiometric ages as necessary, incorporated an updated Lake Bonneville chronology in relative age estimates as appropriate, and reinterpreted some previous study results. The review showed that only the six central segments of the Wasatch fault zone and a few other faults close to the Wasatch Front or near critical facilities have received detailed study, and even for those faults, reliable paleoseismic data seldom extend beyond the middle Holocene. Information for other faults typically consists of a single study, often of reconnaissance nature, and often on only one section of a probable multi-section fault. Consequently, the Working Group's recurrence and slip-rate estimates typically have high associated uncertainty.

## Fault segmentation models in probabilistic seismic hazard assessment

Kathleen M Haller, U.S. Geological Survey, P.O. Box 25046 MS 966, Denver, CO 80225, haller@usgs.gov

Historic ruptures and paleoseismic investigations demonstrate that only part of a long fault (>50-60 km) typically ruptures during a surface-faulting earthquake. This behavior, which is believed to repeat through several to many seismic cycles, is generally referred to as fault segmentation. Models of fault segmentation are common aspects of geological studies of active faults, and incorporating these models will clearly influence how the seismic hazard of a fault is characterized. Therefore, the question is raised: Are we ready to incorporate fault segmentation into probabilistic seismic hazard assessments given our current knowledge of fault behavior?

In many ways, our confidence in the location (or existence) of segment boundaries reflects the level of understanding of a particular fault. Plate-boundary faults in California are some of the best-studied structures in the United States, yet for most of these faults, few investigators agree on a single fault-segmentation model. With the possible exception of the Wasatch fault, no fault in the intermountain west has been studied nearly as well as many of those in California, and, consequently, we usually rely on a single model, if there is one at all. How confident are we in that single, uncontested model?

Most segmentation models are based primarily on paleoseismic and/or geomorphic information and the two-dimensional geometry of the fault. Trenching investigations can provide valuable information about the recent events at a single point on the fault. At best, the data might include the age of one or more events and determine the amount and style of displacement. To identify a fault segment from trenching alone would require multiple, closely spaced trenches, which is neither feasible nor practical. Instead, the site-specific data are generalized to characterize the behavior of a segment whose lateral extent is based on geomorphic similarities and other geologic criteria. Most faults in the intermountain west have recurrence intervals of thousands to tens of thousands of years, which allows us to discriminate between scarps of different age from one segment to the next. However, in cases where the age of the most recent event on adjacent segments is closely spaced, neither trenching nor geomorphic studies alone are capable of defining a model.

Geophysical and geologic studies can also provide additional evidence about the location of possible/probable segment boundaries for some faults in the intermountain west. Gravity data provide a generalized picture of the basement topography beneath the nearly flat, low-density valley fill. Commonly, the central parts of segments coincide with closed gravity lows, and the ends coincide with gravity highs. Geologic mapping can identify favorably oriented geologic structures that might arrest seismogenic rupture. The presence of major cross faults in the footwall at a segment boundary, by itself, is not sufficient evidence to identify the potential for rupture termination. However, a cross fault can play an important role in rupture arrest if it extends to and intersects the active fault at hypocentral depths at the segment boundary. Recent geologic mapping suggests that segment boundaries can coincide with structurally complex zones in the footwall that are up to tens of kilometers in length. Can we make generalizations from these examples to infer the locations of segment boundary for the hundreds of unstudied faults in the intermountain west that may pose a hazard?

Identifying fault segments that rupture independently is important for probabilistic seismic hazard assessments; however, if one incorporates the many published models without caution, the results may be very misleading. In most analyses conducted today, fault (or segment) length is the sole parameter used to determine a characteristic magnitude. If the rupture segment is misidentified, then the assigned magnitude and the calculated hazard will be inaccurate. Therefore, rigorous criteria are needed and should be uniformly applied when fault-segmentation models are used in seismic hazard analyses.

# Identification and Characterization of Active (Holocene) Extensional Faults in Southeast Idaho, Northeast Utah and Southwest Wyoming —Implications for Pipeline Crossing Design

Donald O. West, Golder Associates Inc., Redmond, WA  
Graeme Major, Golder Associates Inc., Reno, NV  
Suzanne R. Hickham, Williams Gas Pipelines, Houston, TX

The region of southeast Idaho, northeast Utah and southwest Wyoming straddles the Northeast Basin and Range and Middle Rocky Mountains tectonic provinces. The Basin and Range is characterized by active (historic and Holocene), mountain front extensional fault tectonics and historical seismicity, while the Middle Rocky Mountains has a comparatively low level of tectonic activity. The region includes several mapped active extensional faults (e.g., Rock Creek fault, West and East Bear Lake faults, Bear River fault, West and East Cache faults, Wasatch fault zone), and a number of mapped late Cenozoic (pre-Holocene) faults. The historical seismicity, which should reflect the active fault tectonics, is concentrated to the north of the region in the Star Valley, Wyoming area, to the west in the Cache Valley, Utah area, and to the south along the Wasatch Front in Utah (Figure 1). The eastern part of the region, and the area farther to the east (the transition from the Basin and Range to the Middle Rocky Mountains), is relatively aseismic (Figure 1). However, this area also includes extensional faults, such as the Rock Creek fault, that have geomorphic and geologic evidence of significant Holocene displacement (Figure 2).

For linear facilities in the region such as buried pipelines, the presence of active extensional faults means that if they cross the faults, they may be subject to the effects of sudden, episodic normal-slip surface displacement events. The potential impact of fault rupture on a pipeline depends on the nature, orientation, geometry, width, and magnitude of the displacement, and on the orientation of the pipeline relative to the strike of the fault. It is also dependent on the depth and width of pipe burial and the nature of the backfill material.

Williams Gas Pipelines' Rockies Displacement Expansion Project, located in southeast Idaho and southwest Wyoming, addressed the potential fault displacement hazard through a program to identify and characterize the active faults, and mitigate the displacement effects through pipeline design. The Rockies Project included about 91 miles of new pipeline, distributed among six loop segments. Based on an office evaluation of available literature and data, as well as the geomorphic interpretation of stereoscopic aerial photographs, and field (aerial and ground) geomorphic and geologic mapping, four active Holocene normal-slip faults were identified crossing three of the loop segments. The four extensional faults included the Rock Creek, Bennetts Spring, East Bear Lake, and East Gem Valley faults. The Bennetts Spring fault had not been previously identified or mapped as a fault. Based on mapped and estimated fault geometric and geologic characteristics, the maximum calculated normal-slip displacement/event among the four faults ranged from 0.55 to 4.8 m, while average displacement ranged from 0.3 to 2.1 m. Estimated maximum widths of the four fault zones ranged from 80 to 230 m. Estimated average slip rates among the four faults ranged from 0.1 to 1.7 mm/yr.

For the Rockies Project pipeline mitigation design, the fault rupture parameters that were considered included the components of maximum displacement along the axis of the pipeline ( $x$ ), the maximum lateral displacement perpendicular to the axis ( $y$ ), and the maximum vertical displacement in the plane of the pipe axis ( $z$ ). For all the faults, maximum  $x$  values ranged from 0.27 to 1.76 m, maximum  $y$  values from -1.64 to 0.17 m, and maximum  $z$  values from -0.45 to -2.18 m. For all the fault crossings, future displacement would primarily put the pipeline into axial tensional stresses as well as vertical shear. For three of the fault crossings, the planned pipeline design (e.g., pipe wall thickness, trench geometry) was adequate to mitigate the effects of fault displacement. For the East Bear Lake fault, which had essentially the largest potential design displacements ( $x$ ,  $y$ ,  $z$ ), the pipeline design was enhanced through the width of the fault zone to mitigate the effects of the displacement.

# Seismicity of Utah 1990 - 2001



**Figure 1. Historical Seismicity of Utah.** The region of interest in southeast Idaho is at the “T” intersection of the boundaries between Idaho, Utah and Wyoming. Note the concentration of seismicity to the north, west and south of this region, and the relatively sparse seismicity to the east and southeast.



**Figure 2.** Rock Creek Fault, Wyoming. Aerial view to the east of the topographic scarp of the Rock Creek fault west of Kemmerer, WY. The normal-slip fault is north-striking, with the west side down along a fault plane dipping about 60 degrees to the west. The topographic scarp is about 3-9 m high, and cuts bedrock and Holocene alluvium (and possibly landslide deposits) along its more than 16 km length. The geomorphically fresh nature of the scarp, and its height, suggest more than one Holocene displacement event.

## Approaches and Issues in Estimating Maximum Magnitudes for Fault Sources in Seismic Hazard Analyses

Donald L. Wells, Geomatrix Consultants, Inc., 2101 Webster Street, 12th Floor, Oakland, CA,  
dwells@geomatrix.com

One of the basic steps in performing seismic hazard analyses is estimating the earthquake magnitude, the length or area of rupture, or the displacement that may occur on a fault during a future earthquake. Traditionally, these source parameters have been estimated from empirical regressions that relate these parameters (magnitude, rupture length, rupture area, and maximum and average displacement) to each other. Alternatively, estimates for source parameters may be derived from observed/measured parameters of historical events or from the relationship between seismic moment and rupture dimensions. Each of these approaches has strengths and weaknesses. Although large historical earthquakes, such as the 1915 Pleasant Valley, 1932 Cedar Mountain, 1954 Fairview Peak-Dixie Valley, 1959 Hebgen Lake, and 1983 Borah Peak earthquakes, may provide suitable estimates of source parameters for future earthquakes on the causative faults, such historical data is available for relatively few of the known seismogenic faults. Use of the relationships between magnitude, earthquake size (seismic moment), and rupture dimensions requires information about three parameters (e.g., rupture length, width, and average displacement) to determine the fourth parameter (seismic moment and magnitude). Because the average displacement cannot be independently estimated from observational data, this approach cannot be applied for most seismic sources. Therefore, seismic hazard evaluations typically use regression relationships among source parameters to estimate magnitude or rupture dimensions for seismic sources. This study will focus on concerns in the application of empirical regression relationships.

A first concern for an empirical relationship is the type and extent of data available to assess potential relationships. A second concern is the form of the regression used to develop the relationship, e.g., linear, multi-linear or non-linear, and weighting of data. Recent studies (e.g., Shaw and Scholz [2001], and Hanks and Bakun [2002]) have confirmed that earthquake source parameters do not scale uniformly, and that fault area scales uniformly with magnitude to the maximum rupture width (corresponding to  $M \sim 6.3/4$ ), and for larger earthquakes, fault length and displacement scale uniformly with magnitude, except perhaps for the largest earthquakes with width to length ratio greater than  $\sim 10$ . Because most of the observational data is in the range of  $M$  6 to 7, with few data for  $M \sim 8$ , the traditional linear regressions typically are well fit to the data for earthquakes of  $M$  6 to 7, and show an increasing misfit for larger earthquakes. This misfit has significant consequences for developing seismic moment-balanced earthquake probabilities for a specified time period. Ongoing work will assess various forms of regression models that may provide a better fit over the entire range of the empirical data.

Additional issues for development of empirical regressions include the limited data for large magnitude historical normal and reverse faulting earthquakes, difficulty in measuring coseismic surface displacement for dipping faults, approach to calculating average fault displacement from limited surface measurements, difficulty in interpreting surface lengths of complex ruptures, and difficulty in measuring the coseismic rupture area. Given a series of regression relationships, further concerns include selection of appropriate relationships for specific tectonic environments, and techniques for estimation/measurement of a dependent source parameter (such as rupture length, rupture area, maximum or average displacement) for use in evaluating an independent source parameter (typically magnitude). Some issues of application of empirical regressions include the use of source parameters near the limits of, or outside the range of observational data used to develop the relationships, estimation of parameters that cannot be directly measured such as rupture width or average fault displacement, and use of uncertainty in source parameters.

## **Estimating Prehistoric Earthquake Magnitude From Point Measurements of Surface Rupture**

Mark A. Hemphill-Haley, Department of Geology, Humboldt State University, Arcata, CA 95521  
mark@humboldt.edu

Ray J. Weldon II, 1272 Department of Geological Sciences, University of Oregon, Eugene, OR 97403

We have developed a method for estimating the magnitude of prehistoric earthquakes using displacement data that usually can be collected from paleoseismic investigations. This method is necessary because essentially all current magnitude estimates for prehistoric events rely upon determining the total length of coseismic surface rupture, which is rarely measurable, or rely on segmentation scenarios, for which uncertainties cannot be quantified. While, surface rupture length is a better predictor of magnitude than displacement for historic earthquakes, paleoseismic investigations are better at providing measurements of the amount of displacement at a site along a fault. The key to our method is to incorporate the variability in displacement observed in 14 modern events, which allows a formal uncertainty in magnitude to be assigned to prehistoric ruptures. We show how multiple measurements along a preserved fraction of a rupture can be combined to reduce the uncertainty in the estimate of magnitude. Our analysis shows that uncertainty asymptotically approaches the natural variability of ruptures so 5 to 10 displacement measurements are sufficient to characterize paleomagnitude. We conclude that sampling of scarps with lengths of even 10% of the original rupture can provide magnitude values that reasonably estimate the earthquake. Tests of the method, using randomly sampled data from the 1992 Mw 7.3 Landers and 1954 Ms 6.8 Dixie Valley earthquakes, provide close approximations of the actual magnitudes.

## Low Slip-at-a-Point Variability: Implications for Earthquake-Size Distribution, Fault Rupture Hazard, and Ground-Motion Modeling

Suzanne Hecker, U.S. Geological Survey , shecker@usgs.gov  
Norman A. Abrahamson , Pacific Gas & Electric Company

Analysis of a composite geologic data set (521 observations from 180 sites) shows that event-to-event variability in slip at a point on a fault is less than expected from a Gutenberg-Richter (G-R) distribution of earthquake sizes and less than assumed in fault rupture hazard evaluations. The narrow range in slip at a point implies that slip patterns repeat and thus distributions of rupture asperities, which govern ground motions, also repeat.

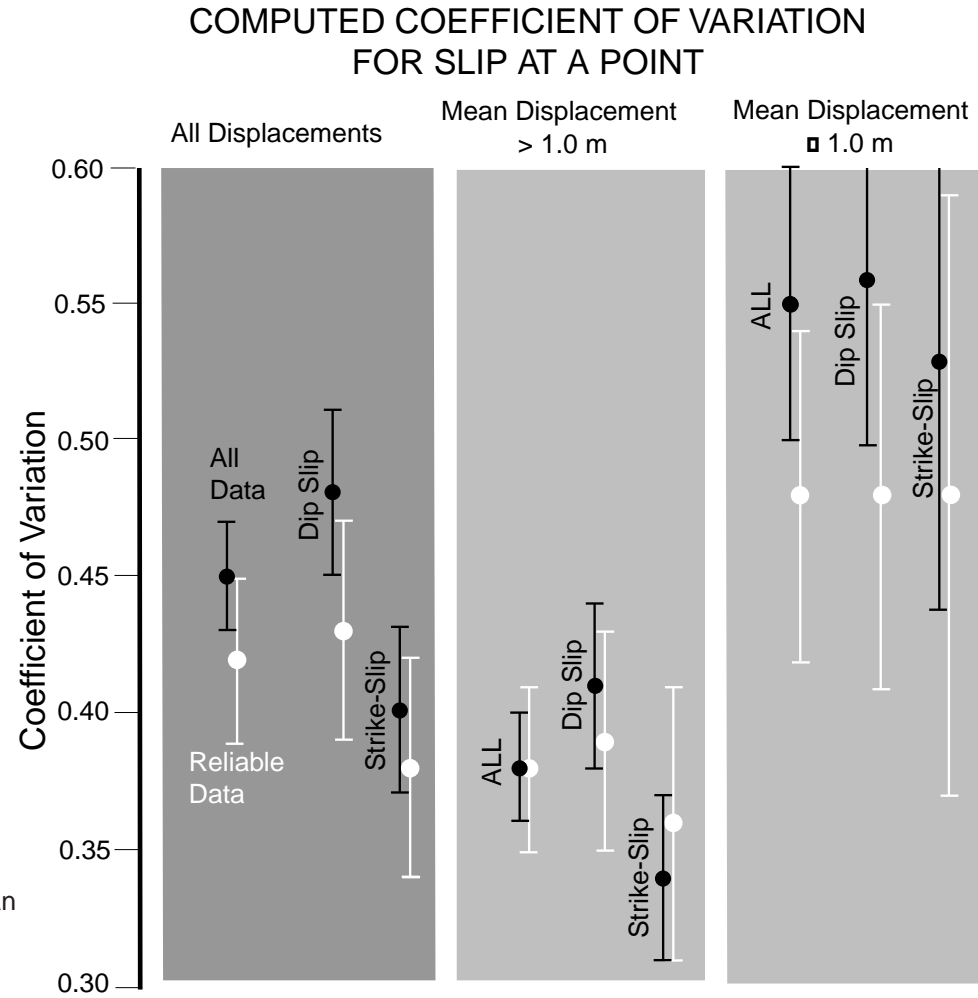
We estimate the coefficient of variation (CV, the standard deviation divided by the mean) of slip at a point by assuming that the CV is constant for all sites or a subset of sites to allow for statistical analysis. Direct calculation of the CV for all sites yields a value of 0.45(0.02) (figure 1). We can show that this estimate is unbiased, even given the small number of observations per site. We compare this result to expected values for the Characteristic and G-R models of earthquake occurrence. We use a forward modeling approach- in which we consider the effect of sampling slip at a point instead of having direct measurements of earthquake magnitudes on a fault. Two factors that could produce variability in slip at a point that is less than the actual variability in earthquake size are: 1) moderate-size earthquakes are less likely than large earthquakes to rupture through a particular site; 2) small-slip ruptures that pass through a site are less likely than large-slip ruptures to be detected as discrete events. A factor that could produce variability in slip at a point that is greater than the variability in earthquake size is variability in slip pattern (that is, variability in the distribution of slip from event to event). The modeling results are most sensitive to: 1) variability in slip pattern, 2) variability in slip as a function of magnitude, and 3) the threshold of event detection. To produce CV values consistent with the data requires that the slip-magnitude relation have a standard deviation much smaller than that commonly assumed from global earthquake data and that the slip pattern have much less variability than the variation along strike in a single earthquake. Small standard deviations imply that slip at a point and rupture pattern are repeatable for a given magnitude. Because each of the exponentially distributed magnitudes would have to have characteristic slip and characteristic slip pattern, we conclude that the G-R model can be rejected as a model for the occurrence of earthquakes on individual faults.

$$C.V. = \frac{\sigma_i}{\bar{D}_i} = \alpha$$

$$C.V. = \sqrt{\frac{\sum_{i=1}^{N_{site}} \sum_{j=1}^{N_i} \left( \frac{D_{ij} - \bar{D}_i}{\bar{D}_i} \right)^2}{(N_{displ} - N_{site})}}$$

$$S.E.[C.V.] = \sqrt{\frac{2(N_{displ} - N_{site})}{N_{displ}^2}} \cdot C.V.$$

Figure 1. Direct computation of C.V. for the entire data set and data subsets. The error bars represent the standard error (S.E.). The sensitivity of C.V. to mean displacement accounts for why the C.V. of dip-slip faults is larger than that of strike-slip faults.



## Probabilistic Fault Displacement Hazard Analysis: A Case Study from Skull Valley, Utah

K. L. Hanson<sup>1</sup>, R. R. Youngs<sup>1</sup>, and F. H. Swan<sup>2</sup>

<sup>1</sup> Geomatrix Consultants, Inc. Oakland, CA, khanson@geomatrix.com

<sup>2</sup> Consulting Geologist, San Francisco, CA

Probabilistic fault displacement hazard analysis (PFDHA) relates annual frequency of recurrence of surface faulting events to the size of the event. In support of siting investigations for a proposed interim storage facility for radioactive waste, seismic hazard and fault evaluation studies were conducted in Skull Valley, Utah (Fig. 1). These studies provide new data on the location, geometry, and slip rate of the Quaternary active Stansbury fault and two previously unrecognized active faults within the basin (referred to as the East and West faults) (see Swan and others, this volume). Proprietary industry data, both gravity and seismic reflection data, were used to constrain the locations of major faults. High-resolution seismic S-wave reflection surveys and detailed surface and subsurface Quaternary studies provide data to evaluate the style, location, geometry, and slip rate of primary, and secondary distributed faulting (Fig. 2).

The proposed site straddles a zone of secondary faulting in the hanging wall of the East fault. To quantify the hazard associated with coseismic fault displacement expected to occur within this zone of distributed faulting, a PFDHA was conducted. Two approaches, referred to as the earthquake and displacement approaches as defined by Youngs and others (2003), were used to estimate the frequency and size of events. For the earthquake approach source characterization parameters developed for the ground motion hazard assessment were used (Fig. 3). For the displacement approach displacement and slip rate data at specific locations were interpreted from high resolution seismic reflection data calibrated with drilling information. Based on these data, slip-rate and slip-per-event distributions were developed that characterize the overall uncertainty in these parameters. In addition to uncertainties related to the age of the displaced datum and the amount of cumulative displacement, the slip-rate distributions also include uncertainties related to the limited sample size and the relation between the measured values at specific locations to the average value along the section of fault of concern.

Figure 4 shows the fault displacement hazard results for three sites representing different categories of locations within the proposed storage area. The uncertainty in the hazard results are represented by the percentile curves. The distribution is skewed, with the mean hazard lying near the 75th percentile distributions. The design probability level of interest for the proposed storage facility is  $5 \times 10^{-4}$  per year, which corresponds to a 2,000-year return period. The hazard curves at the three sites all fall below this level, even for the smallest displacement considered. Thus, the 2000-yr return period displacement due to faulting at the three locations is less than 0.1 cm, which is much lower than settlement displacements considered in the design. Therefore, despite the presence of recently active faults at the site, surface rupture hazard was not considered to pose a significant risk to the proposed facility.

Youngs, R. R. and others, 2003, Probabilistic fault displacement hazard analysis (PFDHA): Earthquake Spectra, v. 19, p. 191-219.

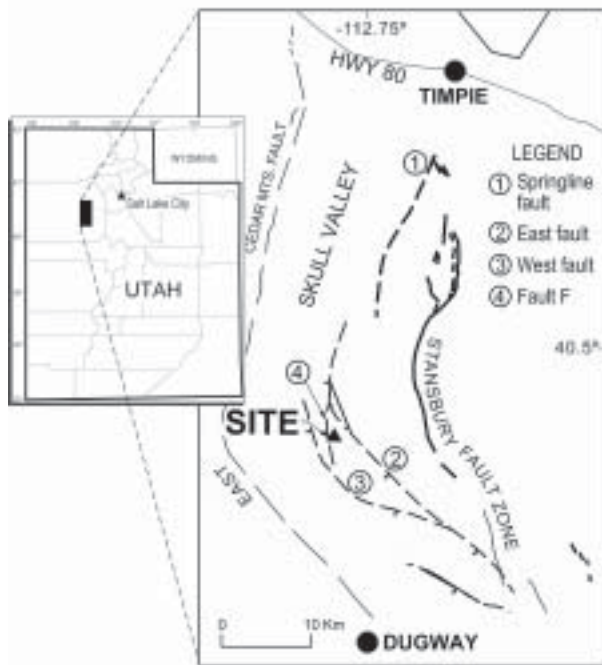


Figure 1. Location of faults, Skull Valley, Utah.

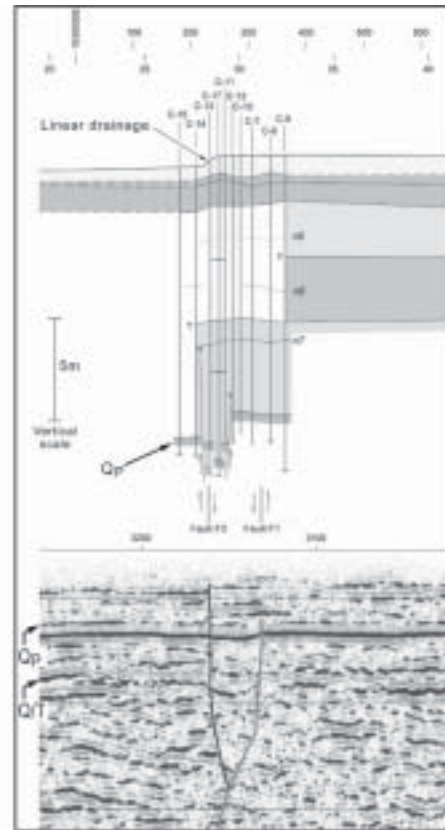


Figure 2. Examples of drilling and high-resolution s-wave seismic reflection data used to identify and characterize Quaternary faults.

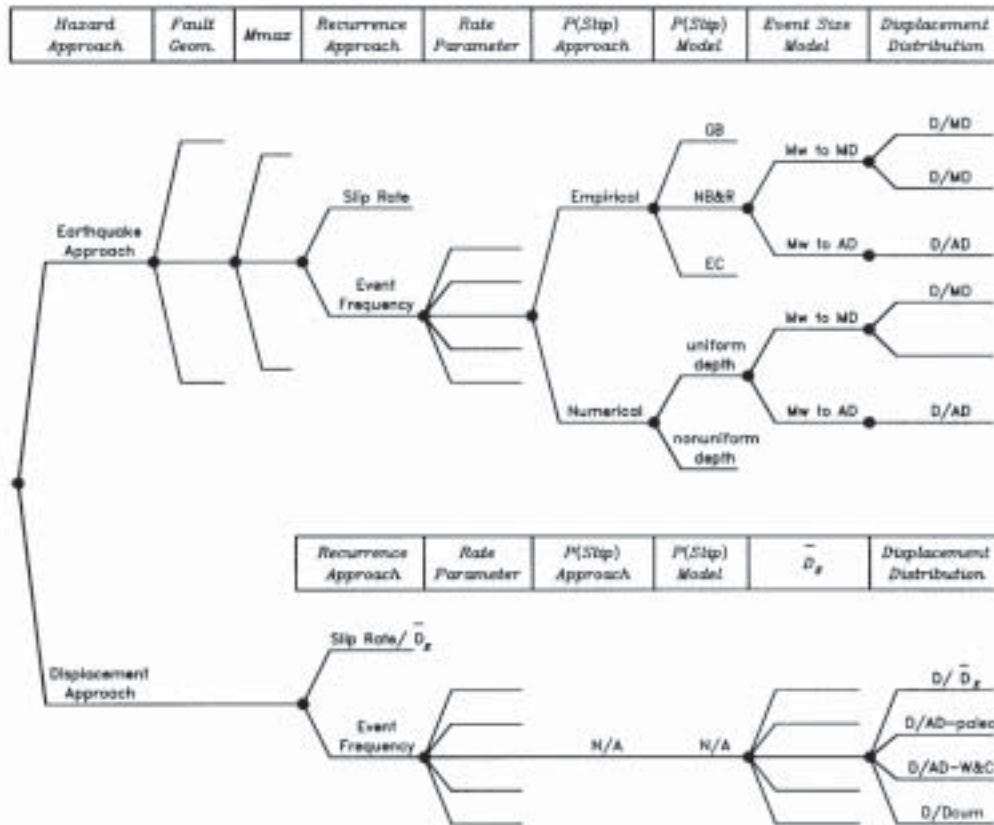


Figure 3. General PFDHA logic tree showing alternative parameters required for the *earthquake* and *displacement* approaches. (Modified from Youngs and others, 2003)

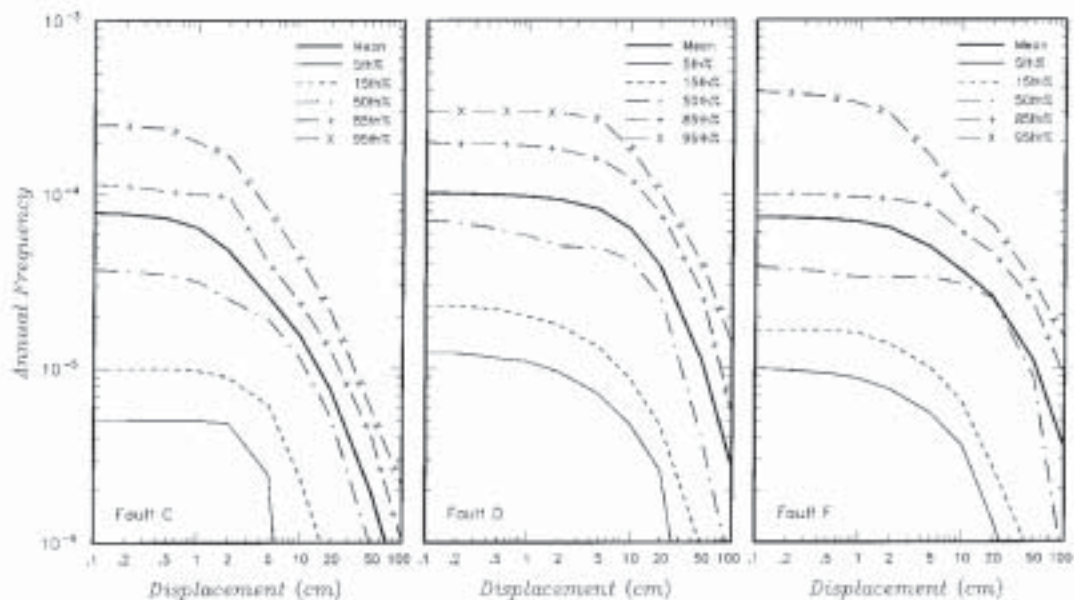


Figure 4. Computed total mean and 5<sup>th</sup> - to - 95<sup>th</sup> -percentile displacement hazard curves for representative faults in the hanging wall of the East fault.

## **Present Day Deformation of the Great Basin and its Implications for Seismic Hazard Assessment**

Wayne Thatcher and Bill Hammond  
U.S. Geological Survey, MS/977, Menlo Park, CA 94025, USA

Geodetic measurements made with the Global Positioning System (GPS) in the interior western U. S. during the past decade are defining the spatial distribution and rates of current deformation over broad regions with unprecedented detail. These results are just now beginning to be used in seismic hazard analysis and loss estimation.

Current deformation is concentrated in narrow zones at or near the margins of the Great Basin in areas with the highest densities of active Holocene faulting. These areas include: the Eastern California Shear Zone (ECSZ), the Walker Lane Fault Zone (WLFZ) of eastern California and western Nevada; the central Nevada Seismic Zone (CNSZ); the Wasatch Fault Zone (WFZ) of Utah; and the Cascade Graben of Oregon. Large intervening regions of the Great Basin are characterized by low or undetectable rates of present-day deformation, even in areas of demonstrable late Quaternary or Holocene faulting and minor seismic activity. However, areal coverage remains incomplete. Results from new campaign GPS networks to be resurveyed in the next 5 years and permanent sites to be installed in the Plate Boundary Observatory (PBO) project will considerably expand and refine estimates of crustal deformation rates.

GPS results will play an important and growing role in seismic hazard analysis. In particular, GPS estimates of fault slip rate will be incorporated into the next update of USGS National probabilistic strong ground motion maps. These maps in turn form the basis for FEMA's HAZUS methodology for estimating site-specific annualized earthquake loss.

GPS estimates of slip rate obtained to date do not always agree with those independently obtained from paleoseismic studies, and more research is needed to understand the sources of these differences. Meanwhile, from the standpoint of seismic hazard analysis it is important to reconcile these differences in an interim way, perhaps by a consensus-seeking process involving both knowledgeable scientists and pragmatic decision makers.

# USGS - NASA Interior Western US 'Pre-EarthScope' Campaign GPS Networks



FIGURE 1: GPS station map

Black sites surveyed 1992-2002 and results published or submitted for publication  
 Blue sites surveyed in 1999 & 2003 and results are being prepared for publication  
 Magenta sites surveyed once in 2000, expecting resurvey in 2004  
 Cyan sites surveyed once in 2001, expecting resurvey in 2005  
 Red sites have been surveyed in September 2003, expecting resurvey in 2007

# Neotectonics of the Walker Lane Belt, California and Nevada, and Implications for Seismic Hazard Assessment

Jeffrey Unruh

William Lettis & Associates, Inc., 1777 Botelho Drive, Suite 262, Walnut Creek, CA 94596

unruh@lettis.com

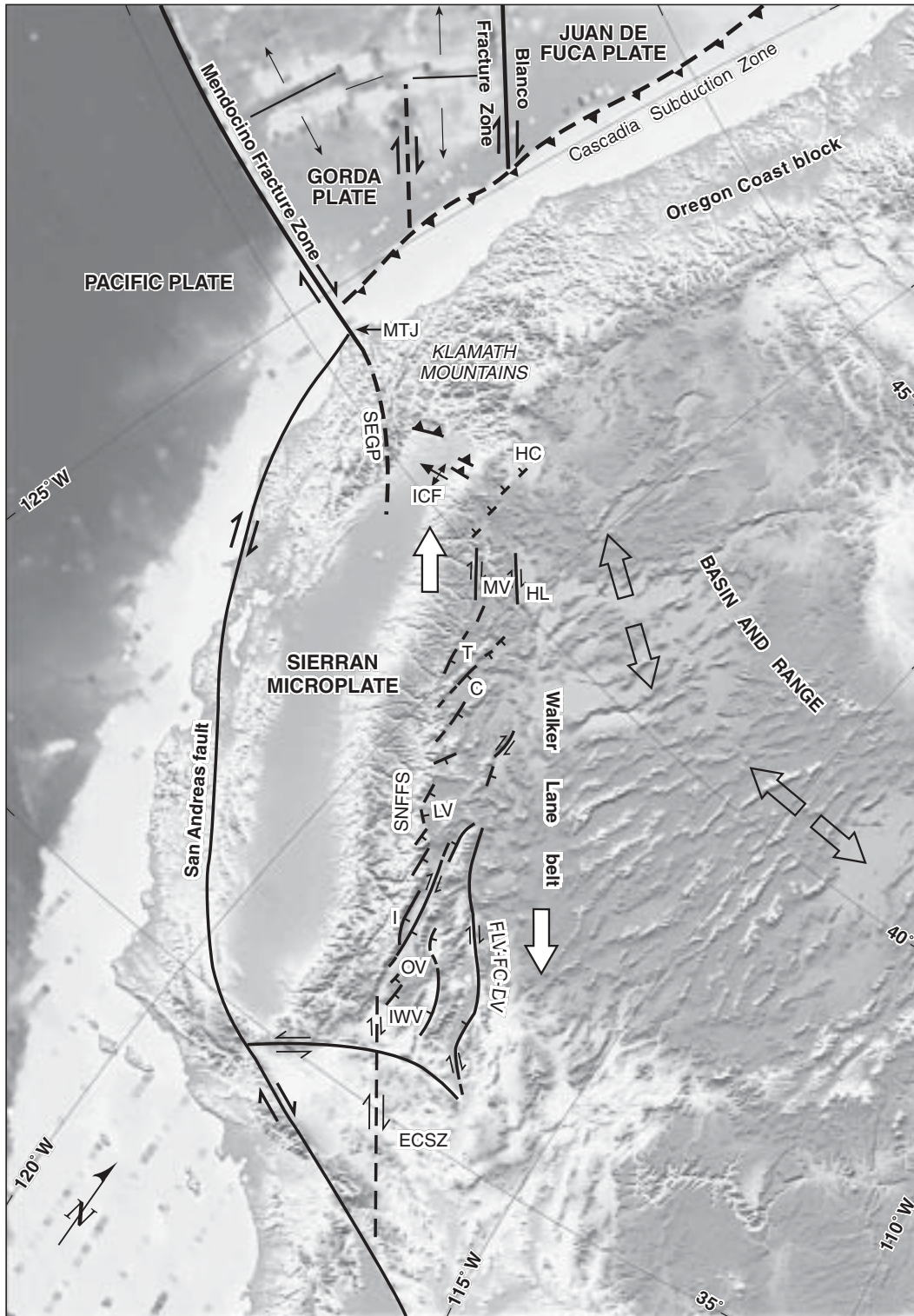
## Abstract

The Walker Lane belt (WLB) is an approximately 100-km-wide zone of Quaternary strike-slip and normal faulting that borders the eastern Sierra Nevada range in California and Nevada (Stewart, 1988). Although many workers consider the WLB part of the Basin and Range province, it is a distinct seismotectonic and structural domain primarily related to the northwest translation of the Sierra Nevada—Central Valley (i.e., Sierran) microplate with respect to stable North America. The kinematics of mixed strike-slip and normal faulting in the WLB are most simply and directly interpreted in the context of Sierran–North American (S–NA) motion. Active right lateral strike-slip faults in the WLB are subparallel to small circles about the S–NA Euler pole; right-normal oblique faults (e.g., the Owens Valley fault) typically strike slightly clockwise of S–NA motion. Dextral faults progressively assume more westerly orientations from south to north in the WLB, consistent with geodetically documented south-to-north variations in the azimuth of S–NA motion (Argus and Gordon, 2001). Normal faults in the WLB strike ~45° clockwise of the S–NA small circle trajectories and exhibit well-defined, left-stepping en echelon patterns (e.g., the Sierra Nevada frontal fault system), typical of dextral transtensional tectonics. Major graben (e.g., Lake Tahoe basin; Carson Valley) are located in regions where the locus of deformation steps eastward in a releasing geometry relative to S–NA motion.

The southern WLB is a direct continuation of the eastern California shear zone, a belt of distributed NW dextral shear and strike-slip faulting in the eastern Mojave block that transfers about ~20% to 25% of total Pacific–North American motion to the interior of the western US east of the Sierran microplate. At the latitude of southern Owens Valley, geodetic data indicate the WLB accommodates about 11 mm/yr of NW dextral shear (Gan et al., 2000; Dixon et al., 2000). The zone of NW dextral shear east of the Sierran microplate broadens northward, extending 200 km east of the WLB into the western Great Basin at the latitude of Reno (Bennett et al., 2003). Integrated NW dextral shear across the northern WLB at the latitude of Mohawk Valley and Honey Lake (about 5–6 mm/yr) is about 50% of that of the southern WLB. At least some NW dextral shear in the northern WLB is transferred in a left-restraining step across the northern Sacramento Valley and southern Klamath Mountains to the southern Cascadia subduction zone.

The first-order kinematics of the WLB have implications for regional seismic hazard assessment in eastern California and western Nevada. One consequence of the left-stepping, en echelon pattern of normal faults in the WLB is that individual structural segments generally range up to about 25 km in length, implying maximum earthquake magnitudes of about Mw 6.9 for single-segment ruptures (e.g., dePolo et al., 1993). In contrast, strike-slip and normal-oblique faults commonly exceed 40 km in length and potentially are capable of generating M7+ earthquakes (e.g., the M7.5+ 1872 earthquake on the dextral-oblique Owens Valley fault). The integrated rate of dextral shear across the southern WLB is about twice that of the northern WLB: all things being equal, we expect large earthquakes to occur more frequently in the southern WLB than in the north. Although this implies that the total earthquake hazard may be higher in the southern WLB, the higher population and on-going urbanization of the Tahoe–Reno–Carson area imply greater earthquake risk in the northern WLB.

**Figure 1.** Oblique Mercator projection of the western Cordillera about the Sierra Nevada—North American Euler pole (Argus and Gordon, 2001). The direction of instantaneous Sierra Nevada—North American (S–NA) motion is vertical everywhere in the projection. Strike-slip faults of the Walker Lane belt are subparallel to S–NA motion; normal faults strike ~45° clockwise of that motion; and major graben and zones of extension are located in areas where the locus of deformation along the eastern Sierra is steps eastward in a releasing geometry (Quaternary faults modified from Jennings, 1994). MTJ Mendocino triple junction; SEGP subducted southern edge of the Gorda plate; CB Cape Blanco; ICF Inks Creek fold belt; HC Hat Creek graben; A Lake Almanor structural basin; MV Mohawk Valley; HL Honey Lake fault; T Lake Tahoe basin; C Carson Valley; LV Long Valley; SNFFS Sierra Nevada frontal fault system; I Independence fault; OV Owens Valley; IWV Indian Wells Valley; ECSZ Eastern California Shear Zone.



# Pattern and timing of faulting in the central Nevada seismic belt and implications for seismic hazards of the western Basin and Range province

John W. Bell<sup>1</sup>, S. John Caskey<sup>2</sup>, and Alan R. Ramelli<sup>1</sup>

<sup>1</sup> Nevada Bureau of Mines and Geology, University of Nevada, Reno NV 89557

<sup>2</sup> Department of Geosciences, San Francisco State University, San Francisco, CA 94132

The central Nevada seismic belt (CNSB) is a concentration of historical (1915-1932-1954) surface faulting in the western Basin and Range province, forming a linear, nearly continuous 300-km-long rupture zone (Fig. 1). We have integrated previous results with new paleoseismic and exploratory trenching data from the historical zones in order to look for evidence of older, similar belt-like patterns or elevated slip rates that could indicate whether the CNSB is a zone of focused, long-term crustal strain, and hence a persistent zone of elevated seismic hazard. Conversely, the lack of evidence for long-term belt-like behavior in the CNSB would have implications bearing on the seismic hazard presented by other late Quaternary faults in the western Nevada region.

The data show that the continuous rupture belt produced by the seven earthquakes occurring between 1915 and 1954 is unique in the available paleoseismic record. At the 1954 Fairview Peak fault, the lack of prehistorical faulting in deposits containing the Wilson Creek bed 19 tephra eliminates the possibility of an identical seismic belt in the last 35.4 ka. Our studies also show that the faults have net slip rates ranging from a low of 0.09 mm/yr on the Fairview Peak fault to a high of 0.7 mm/yr on the 1932 Cedar Mountain fault. These are considered moderate- to low rates similar to most late Quaternary faults in the western Basin and Range province which have slip rates between 0.1-1.0 mm/yr. In contrast, it is significant to note that the highest slip-rate faults (>1 mm/yr) known in the region—the Genoa, Honey Lake, and Pyramid Lake faults (Fig. 1)—have not ruptured historically. Such faults illustrate that high slip rate cannot be the sole determining factor in forecasting seismic hazard.

Based on these results we reach several conclusions regarding the longer-term (~Holocene) behavior of the CNSB and the western Nevada region. Although paleoseismic data preclude an older identical rupture belt among the historical zones, consideration of associated Holocene faults within the greater CNSB region indicates that several similar, but not identical, belt-like rupture patterns are plausible during the last 13 ka. Although long-term strain (represented by density of young faults) does appear to increase from east to west into the CNSB, the slip-rate data demonstrate that the CNSB is not a belt of concentrated or elevated crustal strain compared with areas that extend west to the Sierra Nevada. The increase in the distribution of Holocene fault activity from east to west into the CNSB is consistent with a marked increase in the 1992-2002 GPS velocity field at the latitude of the 1954 rupture sequence. The contemporary strain measured by GPS across the CNSB (2.20-3.13 mm/yr) is significantly greater than the long-term geologic extension rate (0.57-1.10 mm/yr), indicating that the CNSB may continue to be a zone of elevated near-term seismic hazard.

We further conclude that the results of our study of fault behavior in the CNSB best support the belt migration model proposed by Wallace (1987) for the western Basin and Range province in which temporal tectonic pulses are believed to migrate regionally, activating different belt-like combinations of late Quaternary faults in an as yet unknown pattern of migration. Together with the evidence indicating that the highest slip-rate faults in the region have not been historically active, the migration model introduces uncertainties into estimating seismic hazard and suggests that probabilistic seismic hazard models that utilize moment rate as a determining hazard factor may need to incorporate these variables.

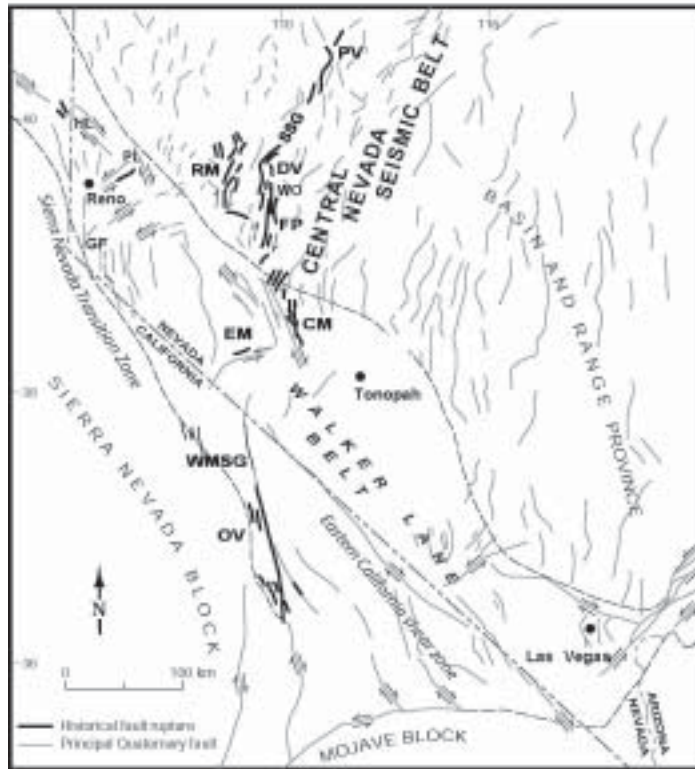


**Figure 1.** Principal structural-tectonic features of the western Basin and Range region showing major Quaternary fault traces (light black lines), historical surface fault traces (heavy black lines), and the location of the central Nevada seismic belt. The historical events include: 1872 Owens Valley (OV), 1903 Wonder (WO), 1915 Pleasant Valley (PV), 1932 Cedar Mountain (CM), 1934 Excelsior Mountain (EM), 1954 Rainbow Mountain-Stillwater (RM), 1954 Fairview Peak (FP), and 1954 Dixie Valley (DV). The only two sections in the sequence of faulting between Owens Valley and Pleasant Valley that have not historically ruptured are the White Mountains seismic gap (WMSG) and the Stillwater seismic gap (SSG). Other principal faults include: Genoa fault (GF), Pyramid Lake fault (PL), and the Honey Lake fault (HL). The Walker Lane belt is delineated by the dashed line.

# SEPARATION OF CHARCOAL AND ORGANICS FROM BULK SOIL SAMPLES PRIOR TO RADIOCARBON ANALYSIS

Kathryn Puseman and Linda Scott Cummings

Paleo Research Institute  
2675 Youngfield Street  
Golden, CO 80401  
pri2004@comcast.net

One of the standard tools used in paleoflood studies, paleoseismology, paleoclimatology, and archaeology is radiocarbon dating. Often, bulk soil samples are sent for dating; however, bulk soil has the potential for containing large amounts of modern carbon. Using a flotation process commonly employed for separating charcoal and other macrofloral remains in archaeological samples, bulk soil samples can be floated and examined to recover and separate charcoal and other charred organic remains suitable for radiocarbon analysis. Identification of charcoal or other carbon prior to radiocarbon dating provides an opportunity to date specific materials, resulting in more accurate dates, while concomitantly providing paleoenvironmental data. This paper will discuss the issues involved in selecting the best remains recovered after flotation to submit for dating. Occasionally deposits are noted that must be identified, such as those representing a cienega, marsh or bosque, because they facilitate correlation across the fault zone. Pollen analysis adds another dimension in the identification of these deposits, making possible such correlations across fault zones.

Bulk soil samples are commonly used for radiocarbon analysis for several reasons. Often, no apparent charcoal or other charred organic material is observed. A bulk soil sample charred at a conventional radiocarbon analysis rate is less expensive than a date obtained using AMS (accelerator mass spectrometry) radiocarbon analysis on a small amount of charred material. However, several problems exist in using bulk soil for radiocarbon analysis. These include 1) uncertainties surrounding the time between the formation of the material being analyzed and the point at which it was deposited, 2) determining the exact relationship between the datable material and the stratigraphy from which it was recovered, and 3) post-depositional contamination. It is better to submit a specific type of material for radiocarbon analysis (i.e. bone, charcoal, other charred organic material, shell, etc.) rather than a bulk soil sample.

Not only is it important to recover a specific type of material for dating, it is important to identify the material being dated. The separation and identification process must be performed under strict conditions of cleanliness to prevent contamination. Identification of charcoal and other charred plant material prior to radiocarbon analysis provides the opportunity to choose the material that would yield the best date possible. For example, a mixed charcoal sample might not yield as good a date as a single identified species. Identification of material is a recommended pretreatment strategy.

## **Closing the Gap between On and Offshore Paleoseismic Records in the Lake Tahoe Basin**

Gordon Seitz, San Diego State University, Dept. Geological Sciences, MC-1020  
5500 Campanile Dr., San Diego State University  
San Diego, CA 92182-1020  
seitz3@mail.earthlink.net

Graham Kent, 9500 Gilman Drive, IGPP-0225, University of San Diego,  
San Diego, CA 92093

### **Abstract**

The severity of seismic hazard within the Lake Tahoe basin has been largely under-appreciated, due in large part to lake coverage. The water and forest coverage resulting in reduced onshore geomorphic expression has delayed the recognition of active faults. Current seismicity and geodetic studies are consistent with typical active faults of the Basin and Range region. Our recent geologic studies clearly show significant Holocene activity on three major faults. However, what is not known is the recurrence behavior of these faults, the associated magnitude and the timing of the most recent event.

The deformation across three active faults, within the Lake Tahoe basin (Figure 1), totaling 80 km in length, has been characterized using a novel combination of swath bathymetry, high resolution seismic CHIRP, airborne laser altimetry imagery, deep-water (~500m) and shallow-water (~25m) AMS C-14 and OSL dated sediment cores. This has resulted in the most robust slip rate estimates for Lake Tahoe faults.

Vertical separation rates across the lake basin from down dropping from the west to the east encompassing either the Stateline/North Tahoe fault or all three faults, including the West Tahoe and Incline Village faults, were estimated by correlating three strainmarkers (Figure 2): 1) an approximately 22 m displacement of a clearly imaged stratigraphic horizon, the McKinney Bay slide deposits, across the Stateline/North Tahoe fault, 2) the 9-15 m of displacement and northward tilt across the entire lake, of a submerged abrasion platform, and 3.) the approximately 30 m vertical displacement of two shoreline caves on the west and east side of Lake Tahoe, which formed during a Tahoe-age lake stand, with an estimated age of approximately 60 ka by correlation to a Tahoe-age moraine (cosmogenic surface exposure date).

The consistency of these three independent vertical separation rate estimates is compelling evidence of significant active faulting. Additionally, the single fault rate is slightly lower as one would expect. We have collected a striking sub-meter resolution seismic image of the Stateline fault expressed as a 10 m high surface scarp, located at a water depth of 500 m (Figure 3). Extrapolating sedimentation rates from a C-14 dated sediment core has allowed an age estimate of the McKinney Bay slide deposit. The shallow submerged abrasion platform is displaced about half the amount of the single-fault displacement McKinney Bay slide deposit. C-14 and OSL dated shallow-water cores of the submerged abrasion platform along the east shore further constrain the age to approximately 20 ka. We have surveyed the base elevations of Eagle Rock and Cave Rock caves and the difference is 30 m, down on the east side. These caves both show evidence of wave-cut notches. Best estimates of vertical separation rates range from 0.4 to 0.55 mm/yr, which corresponds to an east west extension rates ranging from 0.32 to 0.23 mm/yr. Given the dimensions of the Lake Tahoe faults and typical displacements on comparable Basin and Range faults, this strain is most likely released in large seiche producing M7 range earthquakes with a recurrence time on the order of a few thousand years.

Most of the active Lake Tahoe faults are located in the deeper portions of the lake, however our 2004 field target, the Incline Village fault clearly extends onshore. Of the three major faults that we have identified as active, the easternmost Incline Village fault creates a spectacular on and offshore scarp in late Pleistocene to early Holocene age deposits. This presents a unique opportunity to conduct an onshore trenching study in close proximity to a detailed offshore high-resolution seismic 3d grid with associated sediment coring. Conducting this study in for Lake Tahoe relatively shallow water (15-25m) will also help develop the methodology for offshore paleoseismic investigations in other locations. We anticipate that results from this study may provide the first onfault evidence of past earthquake occurrence and associated earthquake magnitude for the Lake Tahoe Basin. Additionally, these results may provide a test for the increasingly cited "earthquake induced turbidite model" being applied here and elsewhere.

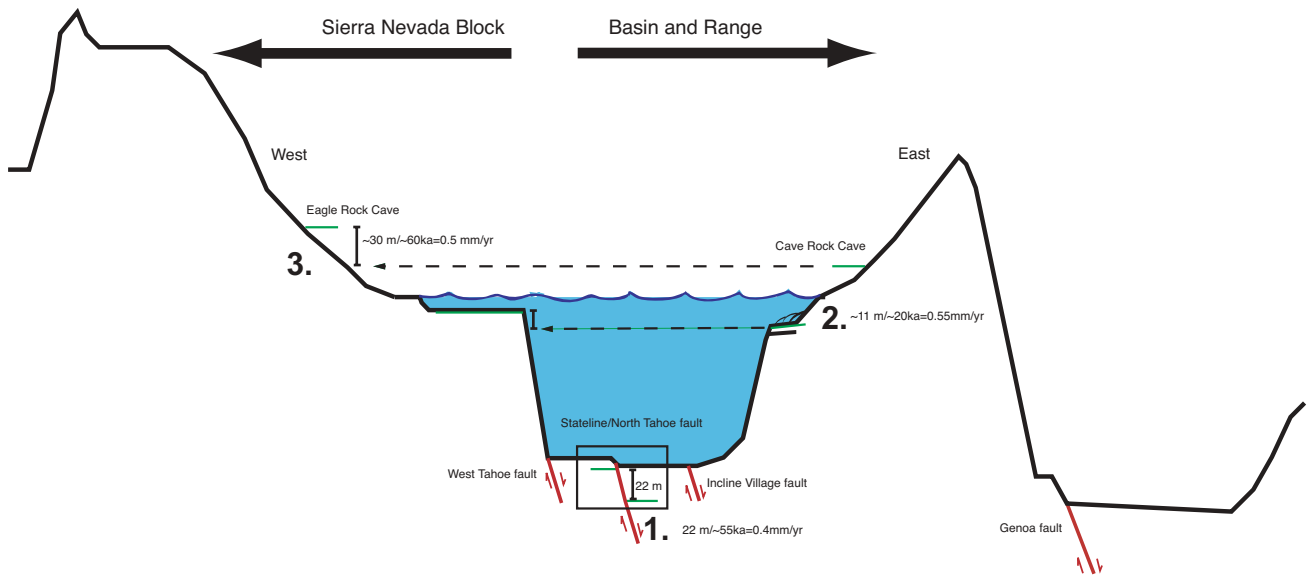


**Figure 1.** Map of Lake Tahoe bathymetry and active faults.

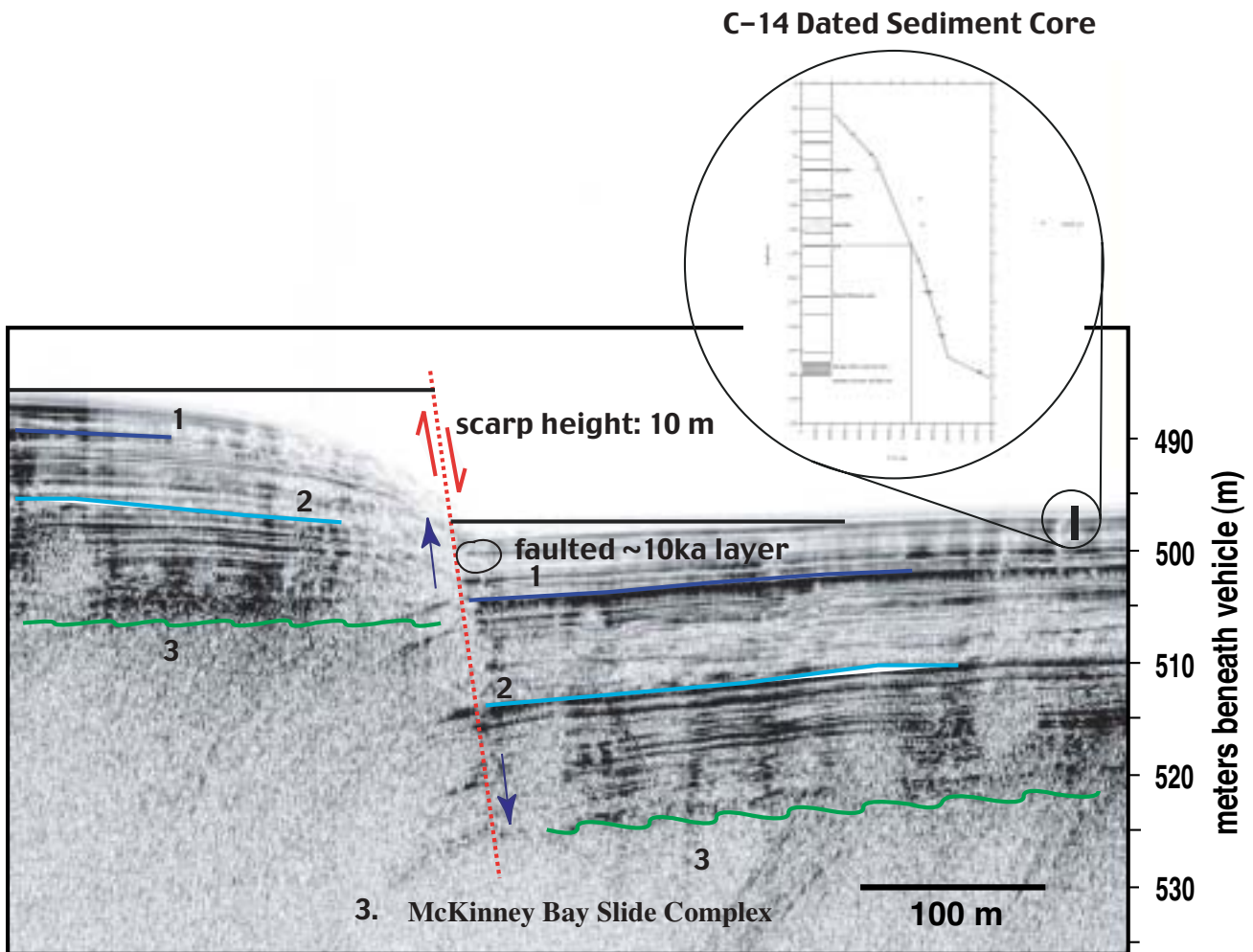


**Figure 2.** Schematic Lake Tahoe basin west to east cross-section. Three strainmarkers, and their corresponding vertical separation rates are indicated.

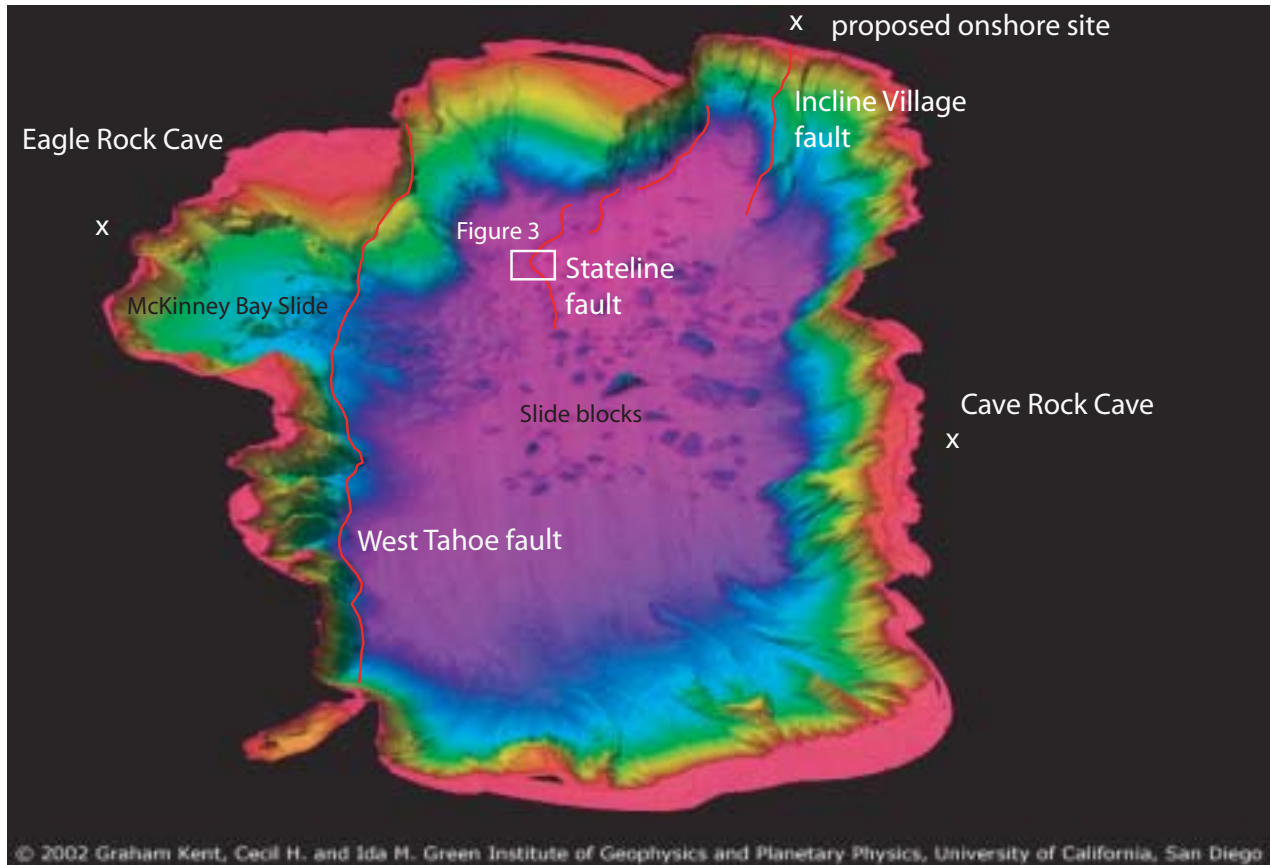


**Figure 3.** Seismic CHIRP profile across the Stateline fault showing that 20 to 25 m of vertical displacement has occurred, since the McKinney Bay slide deposits first blanketed the lake-floor. Our age estimate of this marker is based on extrapolating sedimentation rates derived from the AMS C-14 dated sediment core and speculative correlations of seismic stratigraphy to Pleistocene glacial periods.

## ESTIMATING SLIP RATES AND RECURRENCE INTERVALS FOR QUATERNARY FAULTS IN THE BASIN AND RANGE PROVINCE, USING GEOLOGIC DATA

McCalpin, James P., GEO-HAZ Consulting, Inc., P.O. Box 837, Crestone, CO 81131 mccalpin@geohaz.com

Slip rates and recurrence intervals for Quaternary faults can be estimated from either geomorphic data or from subsurface (trench) data, but the data must be treated differently to produce meaningful estimates of the mean and variance. Total uncertainty in these paleoseismic parameters is the product of both the uncertainty in measuring fault displacement and age (measurement uncertainty) and fault rupture variability between one seismic cycle and the next in time and space (intrinsic variability).

When using geomorphic data such as fault scarp heights, we know the following:

### KNOWN

1. total (vertical) displacement at a point
2. vertical displacement along strike
3. age of displaced landform

### UNKNOWN

1. number of displacement events
2. exact timing of displacement events

An advantage of geomorphic data is its along-strike continuity, thus we can measure an “average” fault scarp height on each of the faulted datums along the fault’s length. For representing the seismic moment of paleoearthquakes, this average displacement is a robust measurement. A disadvantage is that any slip rate calculated as total displacement/age of landform is a minimum slip rate, because the slip may have accumulated/been released in only part of the cited time span. In general, uncertainty in timing will be larger than uncertainty in displacement. Without knowing the number and timing of paleoearthquakes, no interval recurrence intervals can be estimated. However, a maximum estimate of long-term average recurrence interval can be made, given some assumptions.

When using subsurface data such as trench data, we typically know the following:

### KNOWN

1. number of displacement events
2. displacement of each event at a point
3. exact timing of displacement events at that point

### UNKNOWN

1. vertical displacement along strike

An advantage of trench data is that we know the age and displacement of individual paleoearthquakes, thus we can compute “interval slip rates” that cover discrete seismic cycles. Using a slip history diagram, we can graphically portray slip rates from closed and open seismic cycles. A disadvantage is that any slip rate calculated is only valid for that one point on the fault, and is difficult to relate to the average slip rate of the entire fault. In general, uncertainty in displacement will be larger than uncertainty in timing. Recurrence intervals can be dated directly, and given a long enough record (10 paleoearthquakes), may be sufficient to extract the intrinsic variability component out of the total uncertainty.

# Hebgen Lake Revisited: Implications for the Behavior and Paleoseismology of Normal Faults

D.P. Schwartz, S. Hecker, H.D. Stenner  
USGS, Menlo Park, CA  
[dschwartz@usgs.gov](mailto:dschwartz@usgs.gov)

The 1959 Mw 7.3 Hebgen Lake, Montana normal-faulting earthquake was one of the largest in the US during the 20<sup>th</sup> century. Surface rupture occurred primarily on two faults, the Hebgen and Red Canyon, with rupture lengths of 13km and 18km, and surface displacements of 1-3m and 1-5.5m, respectively. The complexity of the surface rupture, the variability in earthquake repeat time and slip rate, and rapid changes to the morphology of the penultimate event scarp present issues for quantifying seismic hazard on normal faults in the Basin and Range.

Recent multi-site investigations on these faults (Hebgen Lake Paleoseismology Working Group, 2000) include: 1) trenching and radiocarbon dating on the Hebgen fault at Cabin Creek (Pierce et al., 2000) and Section 31 (Hecker et al., 2000, 2002) and on the Red Canyon fault at Grayling Creek (Haller et al., 2000) and 2) cosmogenic isotope dating (<sup>26</sup>Al and <sup>10</sup>Be) of quartz-rich cobbles on displaced fan and terrace surfaces at these sites (Van der Woerd et al., 2000). These investigations found evidence of three late Pleistocene- Holocene surface-rupturing earthquakes (including 1959) on the Hebgen and Red Canyon faults (Figure 1). Radiocarbon dates indicate that the penultimate event on each occurred 1-3 ka. Geomorphic relations and cosmogenic dating show the pre-penultimate event on the Hebgen fault occurred 10-14.5 ka; evidence of this event is suggested in the Red Canyon trenches but it is undated. The two recurrence intervals for the past three large events are very different, 1-3ka between the penultimate and 1959 events and 7-13.5ka between the pre-penultimate and penultimate events. Similarly, the vertical slip rate on these faults has varied through time. The rate is  $\sim 0.8$  mm/yr for the past  $\sim 14.5$  ka and  $\sim 1.5$  mm/yr for the past  $\sim 3$ ka.

One interesting observation is that the scarp associated with the penultimate earthquake has been severely eroded, and in some locations completely removed, by upslope retreat of the 1959 free face. This is particularly evident where the fault crosses steeper slopes and where the 1959 free face was large. At Section 31 remnants of the penultimate event bevel can be seen on photographs taken shortly after the earthquake Figure (2A). By 1978, when follow-up photography was taken at the site, the penultimate scarp had been largely eroded (Figure 2B). By the time we trenched in 2000 it was gone (Figure 2C). Similar scarp retreat and removal of a penultimate event bevel is observed as well on the 1983 Borah Peak, Idaho rupture. The rapid disappearance of the prior-event scarp cautions against assuming that a morphologically simple scarp represents a single paleoearthquake.

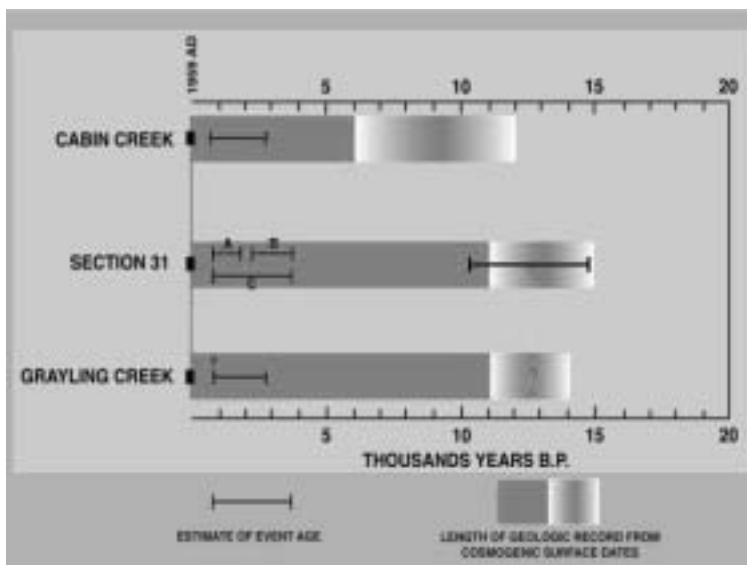


**Figure 1.** Summary of earthquake dates and length of the geologic record at sites on the Hebgen (Cabin Creek, Section 31) and Red Canyon (Grayling Creek) faults. Three interpretations of dates at Section 31 are shown by A, B, and C.



**Figure 2.** Sequence of progressive morphologic changes along the 1959 surface rupture at the Cabin Creek site. Note the complete removal of the bevel from the penultimate event. Photos show scarp in A) 1959, B) 1978, and C) 2000.

# TIME-DEPENDENT PROBABILISTIC SEISMIC HAZARD ANALYSES ALONG THE WASATCH FRONT, UTAH AND THE NEED FOR LONGER PALEOSEISMIC RECORDS

Susan S. Olig, Patricia A. Thomas, and Ivan G. Wong  
Seismic Hazards Group,  
URS Corporation, Oakland, CA  
susan\_olig@urscorp.com

Most earth scientists believe that earthquakes occur more periodically than randomly in time. Therefore, using time-dependent rather than Poisson models in probabilistic seismic hazard analyses should provide better estimates. The Wasatch Front, astride the Wasatch fault, is the first place in the Basin and Range Province where time-dependent models were used in probabilistic hazard analyses. Even though the paleoseismic record for the Wasatch fault has become much more complete over the past three decades, debate continues over apparent variations in patterns of earthquake recurrence and their causes. As part of a microzonation study of the urbanized Salt Lake Valley (Wong et al., 2002), we revisited the issue of time-dependent models in probabilistic hazard analysis using the most recent paleoseismic data for the Wasatch fault to extend the record back 17,000 years. Applying the approach of the Working Group on California Earthquake Probabilities (1999), we calculated conditional probabilities and time-dependent (equivalent Poisson) recurrence intervals (TDRIs) for surface-faulting earthquakes on the Brigham City and Salt Lake City segments of the Wasatch fault. We assumed a lognormal renewal model to calculate conditional probabilities for the next 50 years. Coefficients of variation (COV) are poorly constrained and so we used a broad range from 0.3 to 0.7. Resulting TDRIs vary by more than an order of magnitude, depending on: 1) the value of the COV; 2) whether the short-term (<6-9 ka) or long-term (<17 ka) paleoseismic record is used; and 3) the elapsed time since the youngest surface-faulting event (Table 1).

For the Salt Lake City segment, the elapsed time is less than mean recurrence, and TDRIs range from 450 to 9,600 years depending primarily on the length of the paleoseismic record used (Table 1). Using these TDRIs can either increase the hazard by over 50% (using the shorter paleoseismic record) or decrease it by 20% (using the longer paleoseismic record). In contrast, for the Brigham segment, the elapsed time exceeds or is close to the mean recurrence, resulting in TDRIs that range from 300 to 1,500 years (Table 1), which are consistently much shorter than the mean recurrence used. Thus, using a time-dependent model for this segment consistently increases the hazard, with ground motions about 1/3 higher on average at the 2,500-year return period. Results from these analyses highlight the importance of extending the paleoseismic record elsewhere in the Basin and Range Province where rates of activity may be relatively low, but have varied through late Quaternary time. Such longer paleoseismic records are vital to better understanding the large variations in rates of activity that are observed on many faults, and how these variations should be incorporated into hazard analyses. Longer records are also needed to better determine COVs and just how periodic earthquakes are occurring on faults. This information is absolutely necessary if time-dependent models are to become the standard of practice in future probabilistic seismic hazard analyses.

**Table 1**  
**Time-Dependent Recurrence Parameters**

	Salt Lake City Segment:						Brigham City Segment:					
	Shorter Record (past 6 ka)			Longer Record (past 17 ka)			Shorter Record (past 9 ka)			Longer Record (past 17 ka)		
<b>Mean Recurrence</b>	1,333 years <sup>1</sup>			2,617 years <sup>2</sup>			1,279 years <sup>3</sup>			2,396 years <sup>4</sup>		
<b>Elapsed Time</b>	1,300 years <sup>1</sup>			1,300 years <sup>1</sup>			2,125 years <sup>3</sup>			2,125 years <sup>3</sup>		
<b>Coefficient of Variation</b>	0.3	0.5	0.7	0.3	0.5	0.7	0.3	0.5	0.7	0.3	0.5	0.7
<b>Conditional Probabilities (%)<sup>5</sup></b>	11	7	6	< 1	< 2	2	16	9	6	5	4	3
<b>Time-Dependent (Equivalent Poisson) Recurrence Intervals<sup>6</sup></b>	450 yrs	650 yrs	850 yrs	9,600 yrs	2,900 yrs	2,200 yrs	300 yrs	550 yrs	800 yrs	950 yrs	1,250 yrs	1,500 yrs
<b>UQFPWG Recurrence Interval Distribution<sup>7</sup></b>	1,350 (500 – 2,400) yrs						1,300 (500 – 2,800) yrs					

<sup>1</sup> Based on data from Black *et al.* (1996) that Event W occurred  $5,300 \pm 750$  cal yr B.P. and Event Z occurred  $1,300 \pm 650$  cal yr B.P.

<sup>2</sup> Calculated assuming that Event T occurred about 17 ka (McCalpin, 2002) and that Event Z occurred  $1,300 \pm 650$  cal yr B.P. (Black *et al.*, 1996).

<sup>3</sup> Calculated assuming that Event U occurred  $8,518 \pm 340$  cal yr B.P. and Event Z occurred  $2,125 \pm 104$  cal yr B.P. (McCalpin and Forman, 2002).

<sup>4</sup> Calculated assuming Event T occurred about 16.5 ka and Event Z occurred  $2,125 \pm 104$  cal yr B.P. (McCalpin and Forman, 2002, p. 41).

<sup>5</sup> For the next 50 years and assuming a lognormal renewal model

<sup>6</sup> Rounded to the nearest 50 years.

<sup>7</sup> Preferred (minimum and maximum) values recommended by the Utah Quaternary Fault Parameter Working Group (Lund, this volume) are shown for comparison.

## REFERENCES

- Black, B.D., Lund, W.R., Schwartz, D.P., Gill, H.E., and Mayes, G.H., 1996, Paleoseismology of Utah, Volume 7 - Paleoseismic investigation on the Salt Lake City segment of the Wasatch fault zone at the South Fork Dry Creek and Dry Gulch sites, Salt Lake County, Utah: Utah Geological Survey Special Study 92, 22 p.
- McCalpin, J.P., 2002, Post-Bonneville paleoearthquake chronology of the Salt Lake City segment, Wasatch fault zone, from the 1999 "Megatrench" site: Utah Geological Survey Miscellaneous Publication 02-7, 37 p.
- McCalpin, J.P. and Forman, S.L., 2002, Post-Provo paleoearthquakes chronology of the Brigham City segment, Wasatch fault zone, Utah: Utah Geological Survey Miscellaneous Publication 02-9, 46 p.
- Wong, I., Silva, W., Olig, S., Thomas, P., Wright, D., Ashland, F., Gregor, N., Pechmann, J., Dober, M., Christenson, G., and Gerth, R., 2002, Earthquake scenario and probabilistic ground shaking maps for the Salt Lake City, Utah, metropolitan area, Utah Geological Survey Miscellaneous Publication MP-02-05, 50 p. with CD ROM.
- Working Group on California Earthquake Probabilities (WGCEP), 1999, Earthquake probabilities in the San Francisco Bay Region: 2000 to 2030 ( A summary of findings: U.S. Geological Survey Open-File Report 99-517, 34 p.

# HIGH-RESOLUTION SEISMIC TOMOGRAPHY AND CORING OF QUATERNARY DEPOSITS TO EXPLORE THE 'PULSE OF THE EARTHQUAKE ENGINE'

Ronald Bruhn, Gerard Schuster, Ann Mattson,  
Maïke Buddensiek, Christopher Duross, and Travis Crosby

Department of Geology and Geophysics  
University of Utah  
Salt Lake City, UT 84112

Our research group is studying the 'pulse of the earthquake engine' to determine recurrence patterns of normal faulting in the eastern Basin and Range Province over a period of several hundred thousand years. The work is motivated by the need to refine statistical models of earthquake recurrence, and also to further develop mechanical models of faulting by constraining temporal parameters. Important aspects of the research include determining the existence or absence of temporal clustering of earthquakes, and the significance of such temporal behavior for fault mechanics. We have selected several sites along normal faults in the Eastern Basin and Range Province including the Provo and Nephi segments of the Wasatch fault, and normal faults along the western flanks of the Oquirrh, Stansbury, and Tintic Mountains. To date, work is almost completed on the Mercur fault in the Oquirrh Mountains, we have done both tomographic surveying and coring in the Provo segment of the Wasatch fault, and completed mapping and analysis of fault scarps in the Nephi segment in preparation for seismic surveying and coring.

High-resolution seismic tomographic surveying is conducted to detect or 'image' low-velocity colluvial wedge deposits that lie beneath and adjacent to Quaternary fault scarps. These deposits are then cored with a percussion-hammer drill to depths of several tens of meters. The cored material is used to verify the tomographic imaging, identify sedimentary facies, and collect material for dating. Loess deposited at the base of buried fault scarps is dated by stimulated luminescence methods in the laboratory of Dr. S.L. Forman, University of Illinois at Chicago. We anticipate applying cosmogenic isotope and U-series dating to supplement the stimulated luminescence dating in the near future. The tomographic method is verified by comparing the seismic data with paleoseismic trench logs where possible. Further effort is needed to resolve problems associated with imaging in different types of sedimentary and structural environments – the site on the Provo segment of the Wasatch fault is especially challenging.

The study of the Mercur fault illustrates the potential of the research. Seismic imaging showed two vertically stacked wedge-shaped bodies of low-velocity colluvium that were separated by higher-velocity sedimentary deposits. Drilling and coring of these deposits verified the seismic interpretation and stimulated luminescence dating of several loess horizons provided information on faulting extending back to 300 ka with cumulative vertical displacement up to 30 m. Fault slip-rates during this interval of time were between 0.09 and 0.12 m/kyr. We will be able to constrain the long-term pattern of earthquake recurrence once dating of the loess samples is completed.

## ISSUES IN EVALUATING GROUND MOTION HAZARD IN THE BASIN AND RANGE PROVINCE

Ivan G. Wong  
Seismic Hazards Group  
URS Corporation  
1333 Broadway, Suite 800  
Oakland, CA 94612  
ivan\_wong@urscorp.com

Assessing earthquake ground motion hazard in the Basin and Range Province has relied largely on the assumption that ground shaking in the province behaves in the same manner as it does in California. This situation is a result of the lack of strong motion data in the Basin and Range Province where the few records that exist are primarily for  $M < 6$  earthquakes. No large Basin and Range earthquake ( $M > 6.5$ ) has been recorded at distances less than 80 km. This poses a challenge for performing seismic hazard evaluations in the Basin and Range Province because large ground motions are of greatest engineering relevance.

In the past decade, efforts to characterize ground shaking in the Basin and Range Province have benefited from seismic hazard studies at DOE facilities including the Idaho National Engineering and Environmental Laboratory in eastern Idaho, Los Alamos National Laboratory in northern New Mexico, and Yucca Mountain, Nevada. As part of these efforts, the first attenuation relationships developed for the Basin and Range Province and other extensional environments were based largely on strong motion data from outside the province (Spudich *et al.*, 1997; 1999) or numerical ground motion modeling (Wong *et al.*, 1996; 2001). These relationships suggest that for a given magnitude and distance, ground motions are about 20% lower in extensional regimes compared to California. Though this is an extremely significant observation, it has yet to be confirmed by large magnitude Basin and Range strong motion data. A key question is what is the cause of these lower ground motions, e.g., lower stress drops for earthquakes in the Basin and Range Province or greater crustal attenuation (lower  $Q$ ). Limited studies, to date, indicate that  $Q$  in the Basin and Range Province is higher than in California but not as high as in the central and eastern U.S.

Because the large population centers in the Basin and Range Province (e.g., Salt Lake City, Las Vegas, Albuquerque, and Reno) are located in fault-bounded sedimentary basins, near-fault effects and near-surface and basin site amplification are also critical factors that need to be considered in estimating ground motions. Potential near-field effects such as hanging wall/footwall effects and rupture directivity on normal faults need to be evaluated. Although theoretically these effects are expected to occur, strong motion data to corroborate their existence in extensional regimes are almost nonexistent.

In the recent development of scenario and probabilistic ground shaking hazard maps for the Salt Lake City area and central Wasatch Front, Utah, and Albuquerque-Santa Fe, New Mexico, corridor (Wong *et al.*, 2001; 2002; 2004), we have relied extensively on stochastic numerical ground motion modeling to address the above issues. For example, we have used point-source and finite-fault simulations combined with empirical attenuation relationships to estimate scenario and probabilistic ground motions. The normal faulting finite-fault simulations include rupture directivity, hanging wall/footwall effects, region-specific  $Q$ , and  $\kappa$ . However, the inputs required for the numerical modeling are not well constrained, again substantiating the need for empirical data. The scenario ground motions are reduced by 20% to accommodate the difference between extensional and compressional ground motions.

Near-surface site amplification is estimated through the calculation of amplification factors based on *in situ* shear-wave velocity ( $V_s$ ) data, nonlinear dynamic material properties, and depth to a reference rock datum. Based on the  $V_s$  data and surficial geology, site response categories can be defined and strain- and depth-dependent amplification factors calculated. However, with the possible exception of portions of the Salt Lake City area, adequate local and regional databases of  $V_s$  are lacking even in the urban areas of the Basin and Range Province. Current shear modulus reduction and damping curves are for generic soil types and may not be representative of some deposits found in the province such as glacial till.

There is a significant need for models that characterize the basin geometry and depth and distribution of unconsolidated and semi-consolidated sediments in the Basin and Range Province. Because of this need, insufficient studies have been performed along the Wasatch Front, in the Rio Grande rift, and elsewhere, to estimate long-period basin effects on ground

motions. Efforts along the Wasatch Front by the Utah Ground Shaking Working Group are underway to fill in this data gap. Similar U.S. Geological Survey, state, and university-coordinated efforts to address earthquake ground shaking hazard need to be undertaken in other populated areas of the Basin and Range Province.

## REFERENCES

- Spudich, P., Fletcher, J.B., Hellweg, M., Boatwright, J., Sullivan, C., Joyner, W.B., Hanks, T.C., Boore, D.M., McGarr, A., Baker, L.M., and Lindh, A.G., 1997, SEA96 - A new predictive relation for earthquake ground motions in extensional tectonic regimes: *Seismological Research Letters*, v. 68, p. 190-198.
- Spudich, P., Joyner, W.B., Lindh, A.G., Boore, D.M., Margaris, B.M., and Fletcher, J.B., 1999, SEA99 – A revised ground motion prediction relation for use in extensional tectonic regimes: *Bulletin of the Seismological Society of America*, v. 89, p. 1156-1170.
- Stepp, J.C., Wong, I., Whitney, J., Quittmeyer, R., Abrahamson, N., Coppersmith, K., Toro, G., Youngs, R., Savy, J., Sullivan, T., and Yucca Mountain PSHA Project Members, 2001, Probabilistic seismic hazard analyses for ground motions and fault displacement at Yucca Mountain, Nevada: *Earthquake Spectra*, v. 17, p.113-151.
- Wong, I., Olig, S., Dober, M., Silva, W., Wright, D., Thomas, P., Gregor, N., Sanford, A., Lin, K-W., and Love, D., 2004, Earthquake scenario and probabilistic ground shaking hazard maps for the Albuquerque-Belen-Santa Fe, New Mexico corridor, *New Mexico Geology*, v. 26, p. 3-33.
- Wong, I., Silva, W., Gregor, N., Wright, D., Ashland, F., McDonald, G., Olig, S., Christenson, G., and Solomon, B., 2002, Earthquake scenario ground shaking maps for the central Wasatch Front, Utah, 7th U.S. National Conference on Earthquake Engineering Proceedings (CD ROM).
- Wong, I., Silva, W., Olig, S., Thomas, P., Wright, D., Dober, M., Gregor, N., Ashland, F., Christenson, G., and Pechmann, J., 2001, Earthquake scenario and probabilistic ground shaking maps for the Salt Lake City metropolitan area, Utah, Utah Geological Survey Miscellaneous Publication MP-02-05, 50 p.
- Wong, I.G., Silva, W.J., Youngs, R.R., and Stark, C.L., 1996, Numerical earthquake ground motion modeling and its use in microzonation, Proceedings, 11th World Conference on Earthquake Engineering: Pergamon (CD-ROM).

## PERSPECTIVE ON ATTENUATION RELATIONSHIPS FOR THE BASIN AND RANGE PROVINCE

Kenneth W. Campbell, *EQECAT, Inc.*, [kcampbell@absconsulting.com](mailto:kcampbell@absconsulting.com)

In its 2002 update of the US seismic hazard maps, the USGS recognized that there might be a difference in the character of ground motion between extensional (e.g., Basin and Range Province) and non-extensional tectonic regimes. This recognition came about largely from a study conducted by Spudich et al. (1999) (SEA99), who developed a strong-motion attenuation relationship based specifically on strong-motion recordings from worldwide extensional regimes. By comparing predicted ground motions from this relationship with that predicted by the Boore et al. (1997) relationship, SEA99 concluded that ground motions from extensional regimes were on average 10-20% lower than those from strike-slip faults in non-extensional regimes. However, because of the dependence on largely non-US earthquakes and the concern raised by SEA99 that there might be a systematic difference in the stiffness of generic rock sites between the two regimes, the USGS supplemented this relationship with four attenuation relationships from non-extensional regimes: Abrahamson and Silva (1997) (AS97), Boore et al. (1977) (BJF97), Sadigh et al. (1997), and Campbell and Bozorgnia (2003) (Fig. 1). These four relationships were evaluated for strike-slip faulting and based primarily on recordings from coastal California. The result was that SEA99 was given 20% weight in the USGS analysis, which corresponds to an overall reduction of 2-4% in ground motions in extensional regimes compared to those from strike-slip earthquakes in non-extensional regimes.

A recent study by Pankow and Pechmann (2004) suggests that the average value of  $V_{s30}$  for SEA99 generic rock is actually closer to 910 m/s rather than the value of 620 m/s assumed by SEA99, after they corrected for the bias in the rock predictions noted by the authors. This difference in  $V_{s30}$  can easily explain the 10-20% difference in ground motion noted by SEA99 when compared with BJF97 (Fig. 2). The comparison with BJF97 is most appropriate because of the similar functional forms and magnitude scaling parameters between SEA99 and BJF97. In an independent study, Abrahamson and Becker (1997) incorporated the SEA99 extensional recordings into AS97 and found that they were on average 20% lower, apparently supporting the SEA99 results. However, Walt Silva (personal comm., 2003), co-author of AS97, believes that the generic rock sites used in AS97 have a relatively low average  $V_{s30}$  of around 520 m/s. Using the  $V_{s30}$ -based site factors given in BJF97, this difference in  $V_{s30}$  would result in an average decrease in AS97 spectral predictions for periods of 0.02 to 2.0 s of 23%, almost exactly the same decrease predicted by AS97 for extensional regimes when the SEA99 extensional recordings are included. A comparison of the SEA99 and BJF97 spectra for soil sites ( $V_{s30} = 310$  m/s) shows some difference in ground motion, but over a limited range of periods (Fig. 3).

The main conclusion from this discussion is that there is a great deal of uncertainty in the estimation of ground motion in extensional regimes, especially in the US, and that one should not necessarily accept the SEA99 and modified AS97 attenuation relationships at face value. Until this issue is better understood, the approach taken by the USGS in developing the 2002 update to the US seismic hazard maps might be a reasonable way of incorporating this uncertainty in deterministic and probabilistic seismic hazard analyses for the Basin and Range Province.

- Abrahamson, N.A., and Becker, A.M., 1997, Ground motion characterization at Yucca Mountain, Nevada, a report to the U.S. Geological Survey that fulfills Level 4 Milestone SPG28EM4, WBS No. 1.2.3.2.8.3.6.
- Abrahamson, N.A., and Silva, W.J., 1997, Empirical response spectral attenuation relations for shallow crustal earthquakes: *Seismological Research Letters*, v. 68, p. 94–127.
- Boore, D.M., Joyner, W.B., and Fumal, T.E., 1997, Equations for estimating horizontal response spectra and peak acceleration from western North American earthquakes: a summary of recent work: *Seismological Research Letters*, v. 68, p. 128–153.
- Campbell, K.W., and Bozorgnia, Y., 2003, Updated near-source ground motion (attenuation) relations for the horizontal and vertical components of peak ground acceleration and acceleration response spectra: *Bulletin of the Seismological Society of America*, v. 93, p. 314–331.
- Sadigh, K., Chang, C.Y., Egan, J.A., Makdisi, F., and Youngs, R.R., 1997, Attenuation relationships for shallow crustal earthquakes based on California strong motion data: *Seismological Research Letters*, v. 68, p. 180–189.
- Spudich, P., Joyner, W.B., Lindh, A.G., Boore, D.M., Margaris, B.M., and Fletcher, J.B., 1999, SEA99: a revised ground motion prediction relation for use in extensional tectonic regimes: *Bulletin of the Seismological Society of America*, v. 89, p. 1156–1170.
- Pankow, K.L., and Pechmann, J.C., 2004, The SEA99 ground-motion predictive relations for extensional tectonic regimes: revisions and a new peak ground velocity relation: *Bulletin of the Seismological Society of America*, v. 94, p. 341–348.

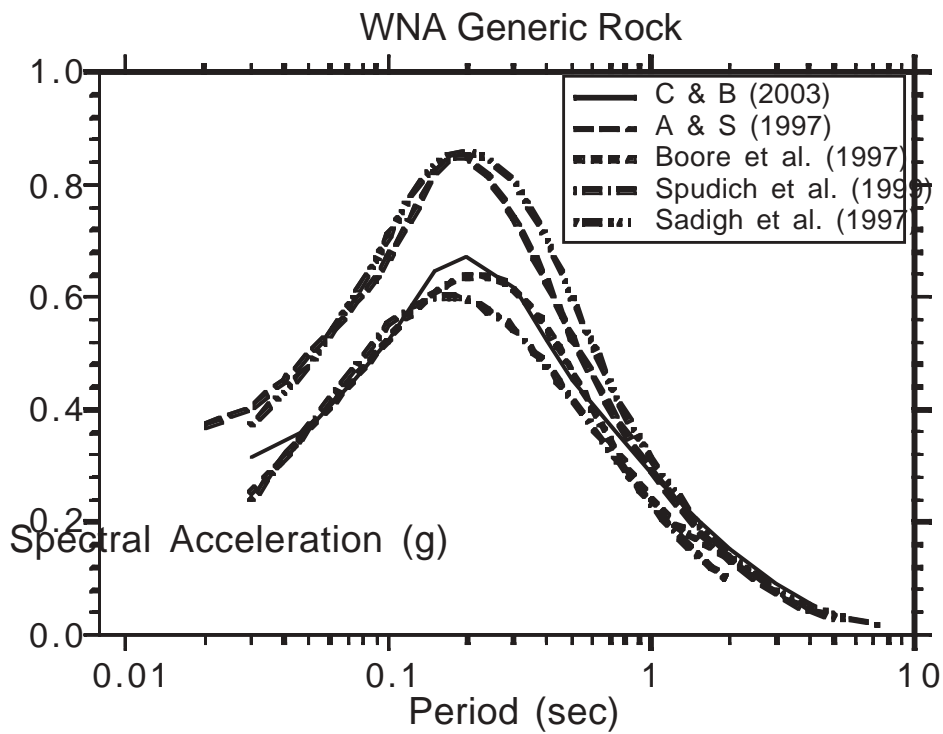


**Figure 1.** Comparison of spectra for generic rock,  $M=7$ ,  $R=10$  km, and strike-slip faulting.

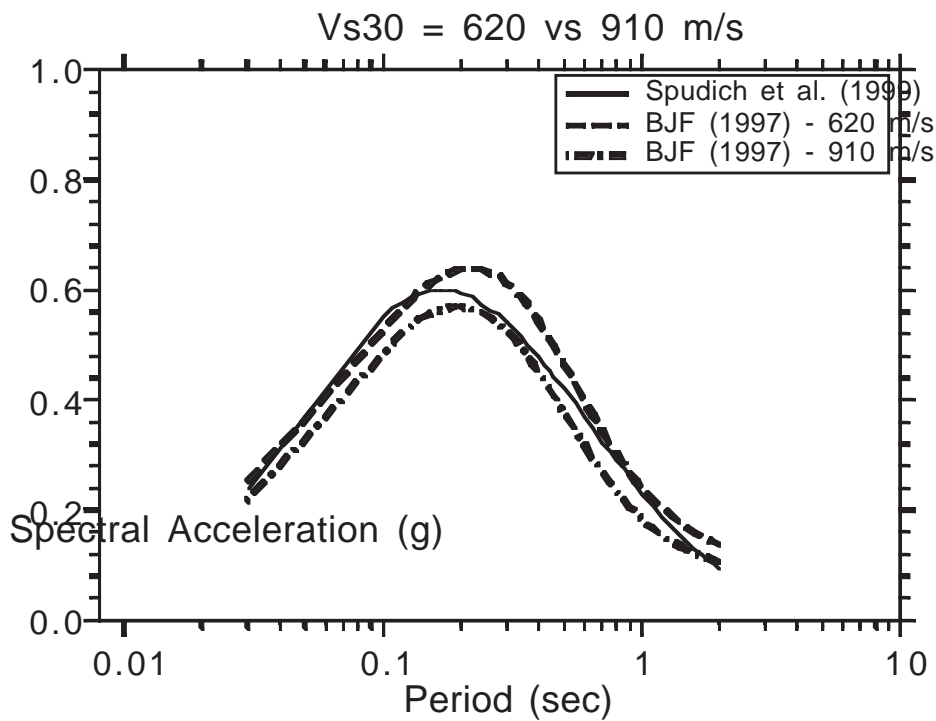


**Figure 2.** Comparison of spectra for  $V_{s30} = 620$  and  $910$  m/s,  $M=7$ ,  $R=10$  km, and strike-slip faulting.

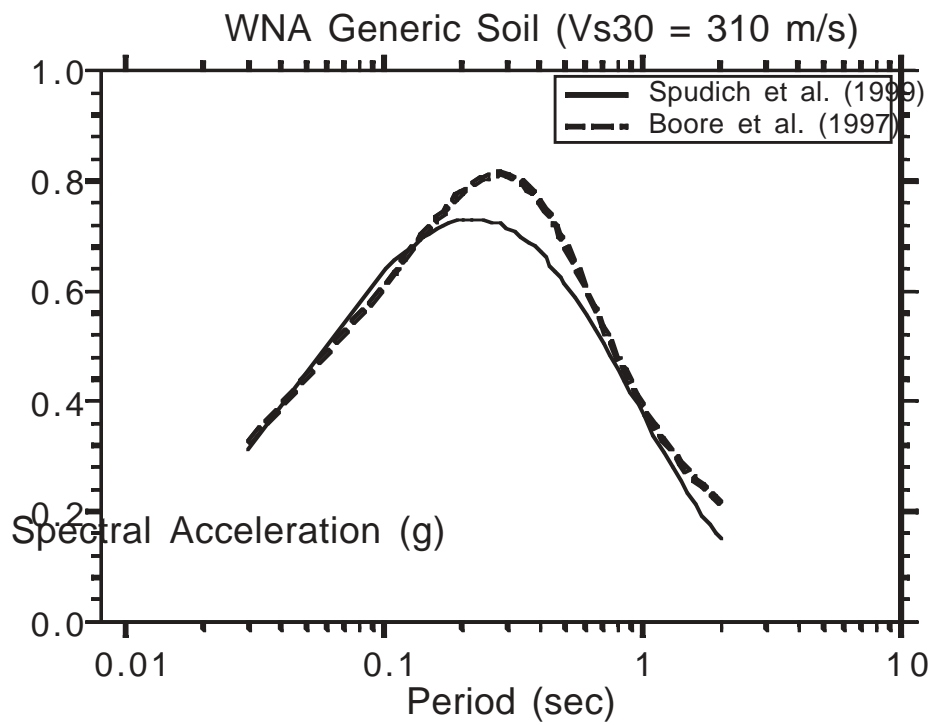


**Figure 3.** Comparison of spectra for generic soil,  $M=7$ ,  $R=10$  km, and strike-slip faulting.

## CHARACTERIZATION OF NEAR FAULT GROUND MOTIONS FOR DESIGN

Paul Somerville  
URS Corporation  
566 El Dorado Street, Pasadena, CA 91101

Ground motion recordings from recent earthquakes confirm that near-fault ground motions are different from ordinary ground motions in that they often contain strong coherent dynamic long period pulses and permanent ground displacements, as expected from seismological theory (Figure 1). The dynamic motions are dominated by a large long period pulse of motion that occurs on the horizontal component perpendicular to the strike of the fault, caused by rupture directivity effects. The permanent ground displacements occur at about the same time as the large dynamic motions, indicating that the permanent and dynamic displacements need to be treated as coincident loads.

Forward rupture directivity causes the horizontal strike-normal component of ground motion to be systematically larger than the strike-parallel component at periods longer than about 0.5 seconds (Figure 2). To accurately characterize near fault ground motions, it is therefore necessary to specify separate response spectra and time histories for the strike-normal and strike-parallel components of ground motion.

An empirical model for dynamic near-fault ground motions that assumes monotonically increasing spectral amplitude at all periods with increasing magnitude, representing directivity as a broadband effect at long periods, was developed by Somerville et al. (1997) and modified by Abrahamson (2000) (Figure 3, center panel). However, near fault recordings from recent earthquakes indicate that the directivity pulse is a narrow band pulse whose period increases with magnitude (Figure 2). Preliminary equations for the magnitude dependence of the period of the pulse have been developed for rock and soil site conditions. This magnitude dependence of the pulse period causes the response spectrum to have a peak whose period increases with magnitude, such that the near-fault ground motions from moderate magnitude earthquakes may exceed those of larger earthquakes at intermediate periods (around 1 second). A response spectral model has been developed to incorporate the magnitude dependent shape of the response spectrum of the forward rupture directivity pulse (Somerville, 2003) (Figure 3, bottom panel).

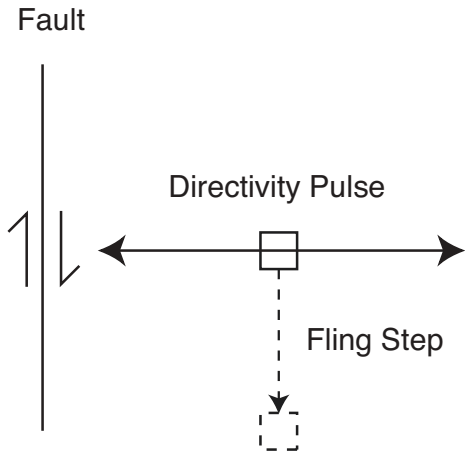
To augment these response spectral models of near fault ground motions, time domain models of the forward rupture directivity pulse have been developed that describe the amplitude and period of the rupture directivity pulse as a function of earthquake magnitude and fault distance. The directivity pulse can be combined with the permanent fault displacement to provide a complete description of the near-fault ground motion time history.

Abrahamson, N.A., 2000. Effects of rupture directivity on probabilistic seismic hazard analysis. Proceedings of the 6<sup>th</sup> International Conference on Seismic Zonation, Palm Springs, Earthquake Engineering Research Institute.

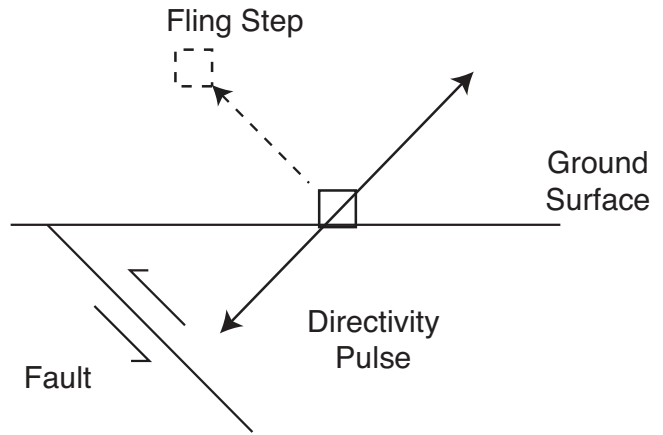
Somerville, P.G., N.F. Smith, R.W. Graves, and N.A. Abrahamson (1997). Modification of empirical strong ground motion attenuation relations to include the amplitude and duration effects of rupture directivity, *Seismological Research Letters* 68, 199-222.

Somerville, P.G. (2003). Magnitude scaling of the near fault rupture directivity pulse. *Physics of the Earth and Planetary Interiors*, 137, 201-212.

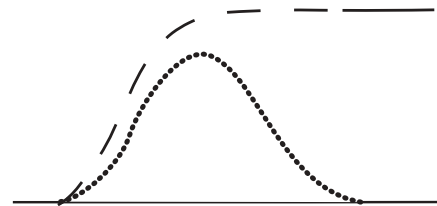
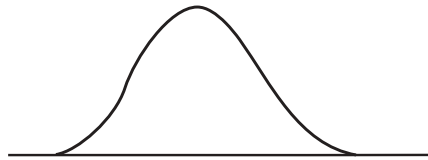
## STRIKE SLIP (Map View)



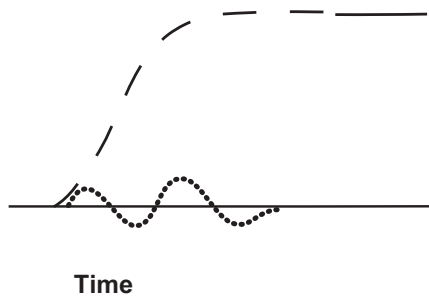
## DIP SLIP (Cross Section)



Strike Normal  
Component of  
Displacement



Strike Parallel  
Component of  
Displacement



Time



Time

Figure 1. Top: Schematic orientation of the rupture directivity pulse and fault displacement ("fling step") for strike-slip (left) and dip-slip (right) faulting. Bottom: Schematic partition of the rupture directivity pulse and fault displacement between the strike normal and strike parallel components of ground displacement. Waveforms containing static ground displacement are shown as dashed lines; versions of these waveforms with the static displacement removed are shown as dotted lines.

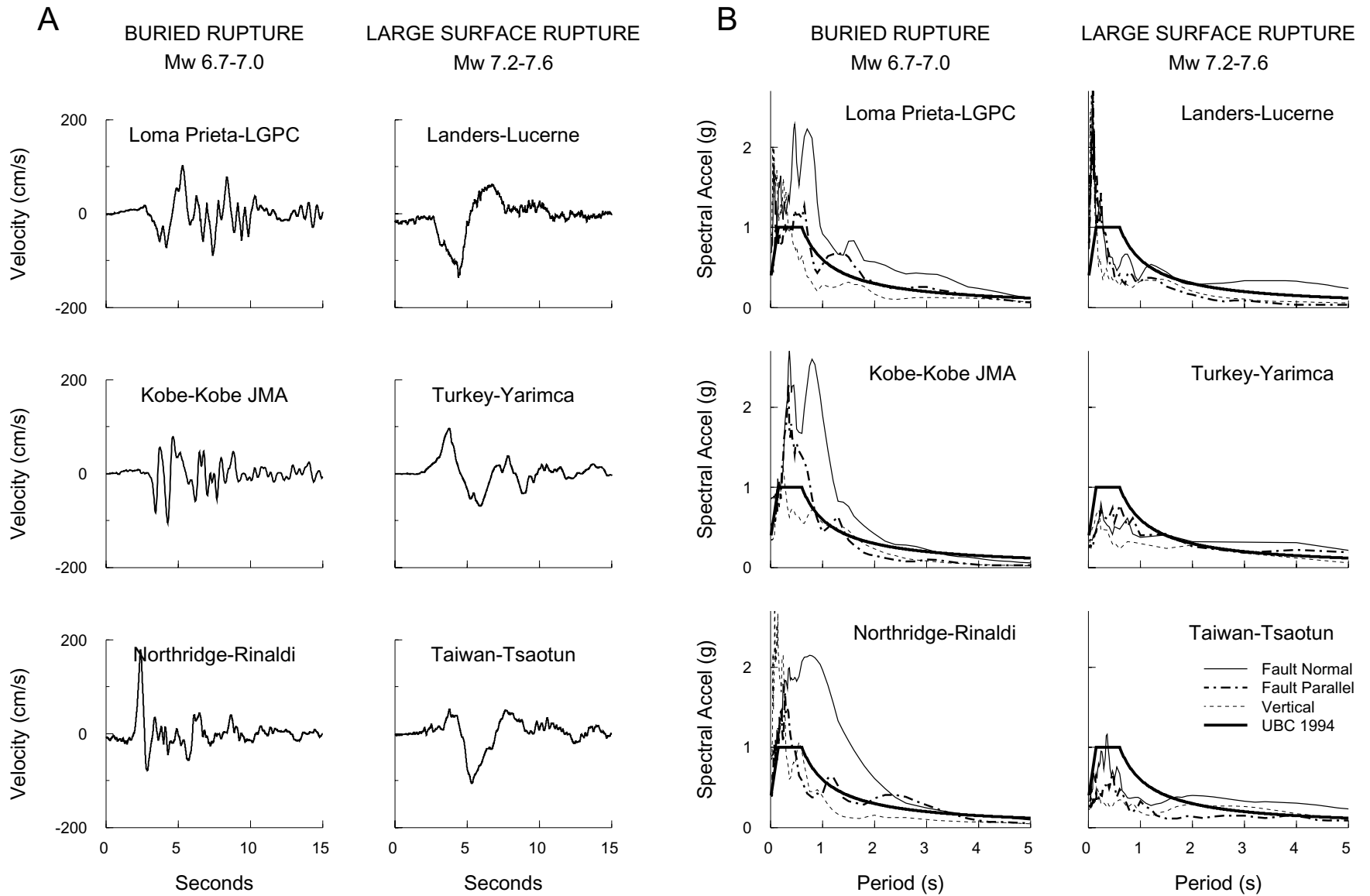


Figure 2. A: Fault-normal velocity pulses recorded near three moderate magnitude earthquakes (left column) and three large magnitude earthquakes (right column), shown on the same scales. B: Corresponding acceleration response spectra, with 1994 UBC code spectrum shown for reference.

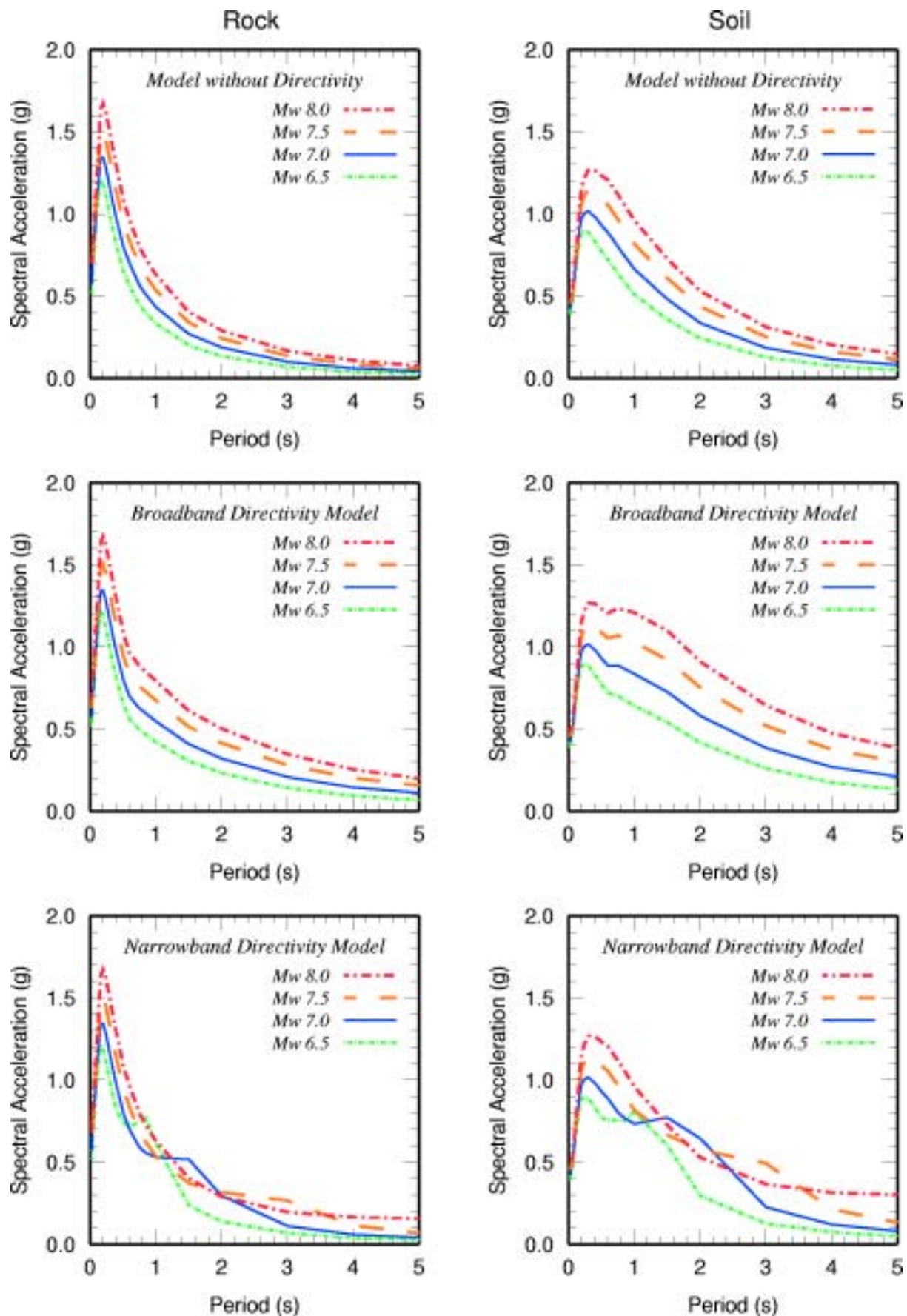


Figure 3. Near fault response spectral model, strike-slip, 5km for rock sites (left) and soil sites (right). Top: model without directivity (Abrahamson and Silva, 1997). Middle: Broadband directivity model (Somerville et al., 1997). Bottom: Narrow band directivity model (Somerville, 2003).

## Basin Effects on Ground Motions

Robert Graves  
URS Group, Inc.  
Pasadena, CA, USA  
robert\_graves@urscorp.com

I present a methodology for generating broadband (0 - 10 Hz) ground motion time histories for moderate and larger crustal earthquakes ( $M_w > 5.5$ ), including the effects of basin response. The hybrid technique combines a stochastic approach at high frequencies with a deterministic approach at low frequencies. The broadband response is obtained by summing the separate responses in the time domain using matched butterworth filters centered at 1 Hz. I use a kinematic description of fault rupture, incorporating spatial heterogeneity in slip, rupture velocity and rise time by discretizing an extended finite-fault into a number of smaller subfaults. The stochastic approach sums the response for each subfault assuming a random phase, an omega-squared source spectrum and generic ray-path Green's functions. Gross impedance effects are incorporated using quarter wavelength theory to bring the response to a reference baserock level. The deterministic approach sums the response for many point sources distributed across each subfault. Wave propagation is modeled using a 3D viscoelastic finite difference algorithm with the minimum shear wave velocity set at 620 m/s. Short- and mid-period amplification factors provided by Borchardt (1994) are used to develop frequency-dependent non-linear site amplification functions.

I have tested the methodology by modeling the recorded ground motion time histories from the 1994 Northridge earthquake. The simulation model incorporates the complex 3D velocity structure of the Los Angeles and San Fernando basins, as well as a detailed representation of heterogeneous rupture across a finite-fault plane. The rupture model is based on a smoothed version of the Hartzell et al (1996) slip distribution. In order to retain the predictive capability of the approach, rupture velocity and slip function are determined using simple scaling formulae. The simulation does well at reproducing the general character (amplitude, duration and waveform) of the recorded motions across a broad frequency band (0.1 – 10 Hz).

An application of a similar broadband modeling approach involves estimation of ground motions expected in the vicinity of the Jackson Lake Dam (JLD) for possible ruptures of the Teton fault (O'Connell et al., 2003). The Jackson Lake Dam is situated on a shallow basin with very low seismic velocities (Figure 3). This setting is typical of many sedimentary environments in the Basin and Range. Small event ground motions recorded at JLD show strong amplification as well as significant basin-edge-generated secondary S-waves. The ground motion modeling using a 3D velocity structure reproduces these observed effects. Simulations of scenario events on the Teton fault indicate that basin effects will produce significant amplification of motions.

O'Connell, D. R. H., C. K. Wood, D. A. Ostenaar, L. V. Block, and R. C. LaForge (2003). Ground motion evaluation for Jackson Lake Dam, Minidoka Project, Wyoming, *U. S. Bureau Reclamation., Report 2003-2*, Denver, CO, 493pp.

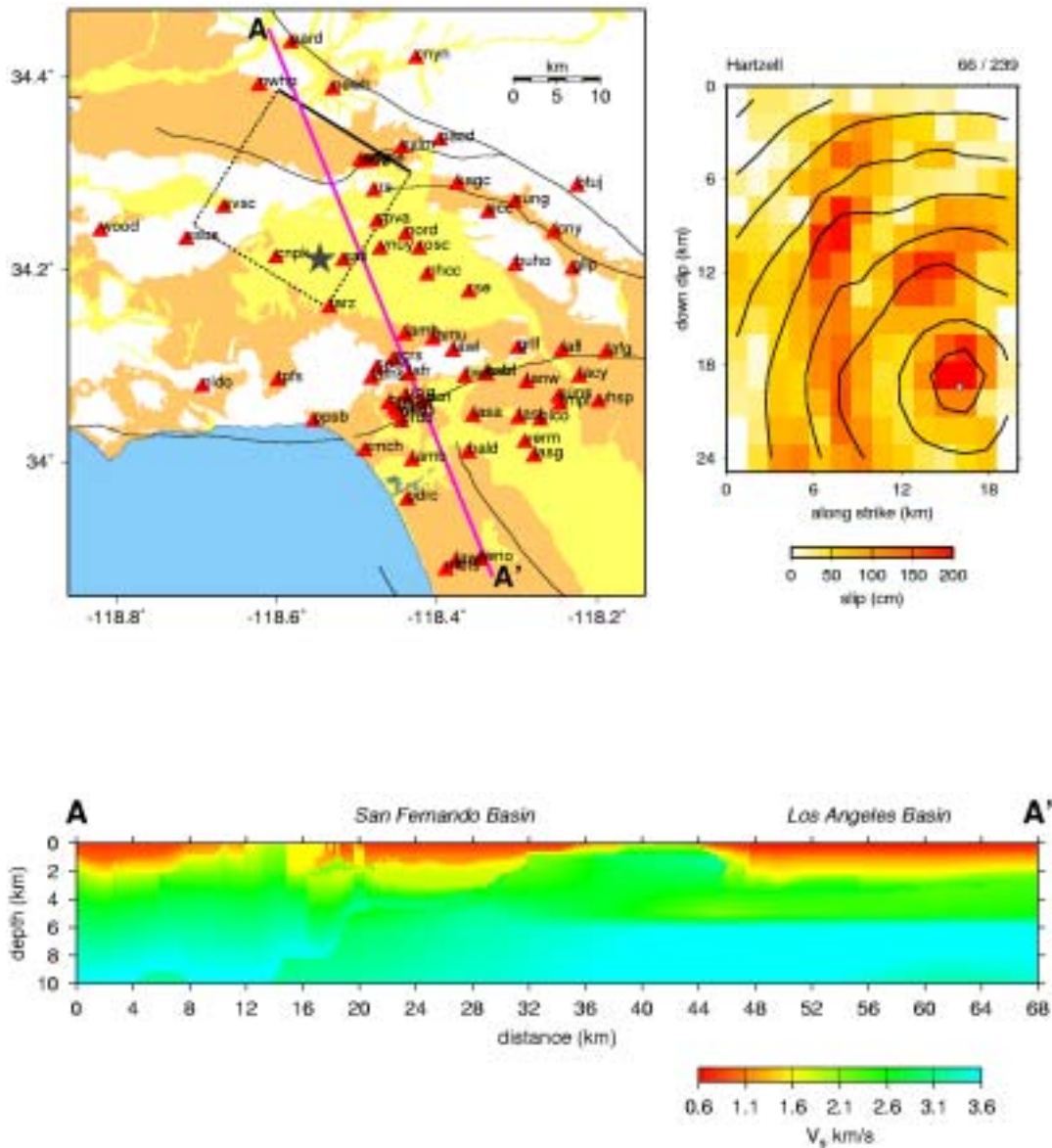


**Figure 1.** Simulation model for the 1994 Northridge earthquake. Top left shows strong motion instrument locations in the near fault region. Dashed lines indicate surface projection of the fault plane. Top right shows slip distribution from Hartzell et al. (1996). Contours show rupture front at 1 sec intervals determined from scaling relation. Bottom shows shear wave velocity along profile A—A'. Low velocity regions of the San Fernando and Los Angeles basins are indicated.

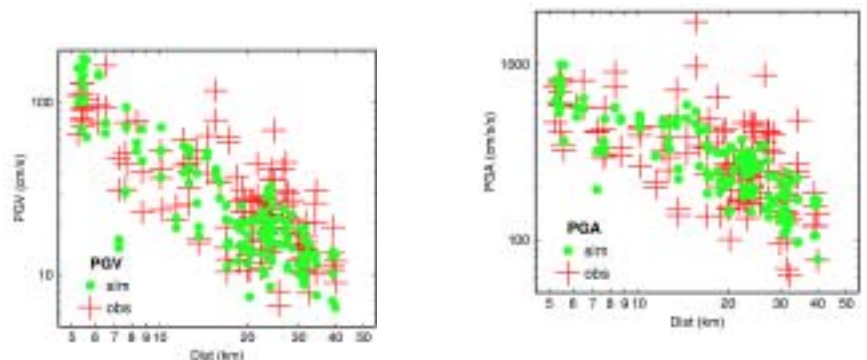
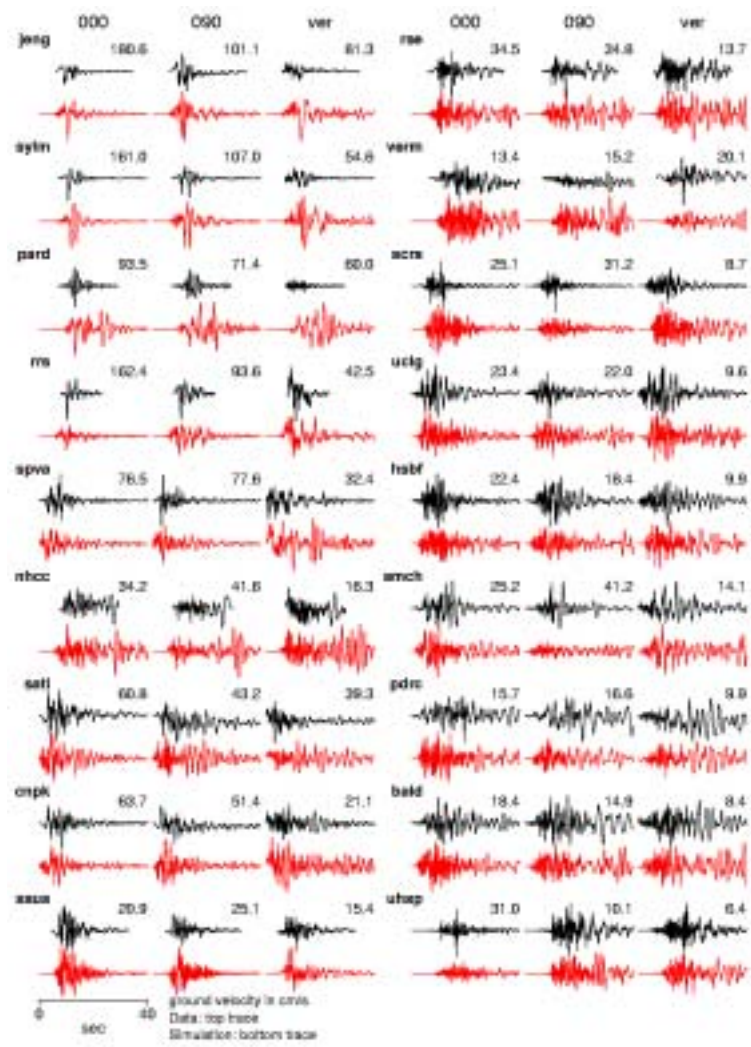


**Figure 2.** Top shows comparison of observed (black) and simulated (red) three-component ground velocities at 18 selected sites for the Northridge earthquake. For each station and component the traces are scaled to the maximum amplitude of the observed or simulated time history. Bottom compares observed (red crosses) and simulated (green circles) for PGA (left) and PGV (right) plotted as a function of closest distance to fault rupture at 69 sites. PGA and PGV are measured from the observed and simulated time histories.

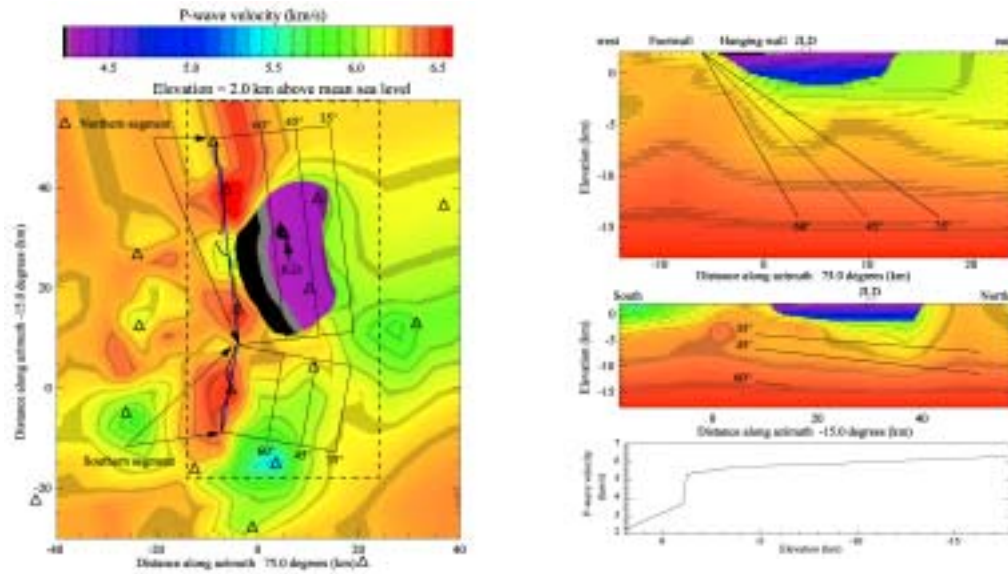


**Figure 3.** Top left shows plan view of 3D P-wave velocity model in vicinity of Jackson Lake Dam (JLD). Solid rectangles show surface projections of hypothetical Teton fault scenarios. Top right shows vertical cross-sections through 3D model with velocity vs. depth profile beneath JLD. Bottom panels show simulated fault normal and fault parallel ground velocities for full rupture of 35° dipping Teton fault. Seismograms span a 19 km profile extending from just west of the Teton fault (TF) through JLD (Dam). Western edge of low velocity basin (LVB) generates strong secondary S-waves indicated by dashed line. Peak velocity is plotted above each trace. Source: O’Connell et al (2003).

# PRECARIOUS ROCK CONSTRAINTS ON GROUND MOTION: COMPARISONS WITH PREDICTIONS FROM FOAM RUBBER MODELS

James N. Brune  
Seismological Laboratory, University of Nevada, Reno  
[brune@seismo.unr.edu](mailto:brune@seismo.unr.edu)

Preliminary studies of the distribution of precarious rocks in extensional regions have suggested the following conclusions for ground motions, compared with ground motions from trans-pressure strike-slip faults: (1) ground motions on the foot wall of normal faults is markedly lower, and (2) ground motions near trans-tensional strike-slip faults or trans-tensional sections of strike-slip faults (e.g., trans-tensional step-overs) are relatively low. For the hanging wall of normal faults precarious rock evidence is relatively limited, but preliminary estimates indicate ground motions significantly larger than for the foot-wall. Overall the data indicate that average ground motions in extensional areas are considerably lower than for ordinary or trans-pressure strike slip fault regimes. The difference is considerably larger than suggested by recent ground motion regressions for extensional areas.

Foam-rubber physical models and lattice numerical models of normal faulting also indicate low foot-wall ground motions.

Physical foam rubber models may be used to illustrate partitioning between aleatory and epistemic uncertainties, as well as the statistical effects of the ergodic assumption, as compared with the other extreme model, the “characteristic ground motion earthquake” model. Many repeated unilateral ruptures in the foam rubber model correspond closely to the “characteristic ground motion earthquake” model. Relatively narrow Gaussian statistical distributions are observed at specific sites relative to the nucleation points and direction of rupture. This is because fixing the relative position on the radiation pattern eliminates some sources of epistemic uncertainty, -namely radiation pattern uncertainty and directivity uncertainty. However if we had erroneously attributed these variations as due to random aleatory effects, and had fit a Gaussian to the whole data set, we would have obtained a much broader (erroneous) Gaussian. At low probabilities (maximum values for thousands of repeats of the “characteristic ground motion earthquakes”), we would then predict unrealistically large ground motions as compared to the actual observations. This “ergodic” error may apply to real earth cases where the very-low-probability hazard is controlled by large numbers of earthquakes on the same fault, e.g., some sites near the San Andreas fault.

## POSTER ABSTRACTS

(in alphabetical order by main author)

*(click on links below)*

The Late Quaternary Canyon Ferry Fault, West-central Montana, Larry W. Anderson, Lucille A. Piety, Susan S. Olig, and Steven L. Forman

Holocene and Latest Pleistocene Faulting on the Southern Inyo Mountain Fault, Southern Owens Valley, Eastern California: a Previously Unrecognized Active Fault in Owens Valley, Steven N. Bacon and Angela S. Jayko

ShakeMap as a Tool for Understanding Earthquake Hazard in Nevada, Glenn Biasi, Kent Lindquist, and Kenneth Smith

Magnitude and Rupture Length Estimates From Point Measurements of Displacement, Glenn Biasi and Ray J. Weldon II

Map of Miocene and Younger Faults and Earthquakes in Idaho, Roy M. Breckenridge and Loudon R. Stanford

Slip Rate and Paleoseismic Studies on Northern Walker Lane and Basin and Range Fault Zones in the Context of Geodesy, R.W. Briggs, S.G. Wesnousky, F.J. Ryerson, R.C. Finkel, and A.S. Meriaux

HAZUS-MH: Benefits of Census Block Level Analysis for Earthquakes, James C. Case, Seth J. Wittke, Matthew L. Bowen, and Justin T. Carreno

Integrated Earthquake Hazard of the Wasatch Front from GPS Measurements and Elastic-Viscoelastic Fault Modeling, Wu-Lung Chang and Robert B. Smith

Guidelines for Evaluating Surface-fault-rupture Hazards in Utah, Gary E. Christenson, L. Darlene Batatian, and Craig V Nelson

A Straightforward Way of Naming Paleoearthquakes, Craig M. dePolo

Quaternary Structure and Geomorphic Expression of the Warm Springs Valley Fault System, Western Nevada, Craig M. dePolo, Alan R. Ramelli, Christopher D. Henry, James E. Faulds, and Thomas L. Sawyer

Holocene Segmentation and Displacement History of the East Great Salt Lake Fault, Utah, David A. Dinter and James C. Pechmann

Active Tectonics of the Nephi Segment, Wasatch Fault Zone, Utah, Revisited, Christopher B. DuRoss and Ronald L. Bruhn

Improving Hazard Estimates in the Reno-Carson Metropolitan Region, Feng Su, John G. Anderson and Aasha Pancha

The Method of Information Location of the Center Zone of Expected Earthquake: Direct and

Inverse Tasks of Forecasting, H.H. Asadov and Sh.H. Mammadov

Recognizing Postseismic Transients with GPS at the Central Nevada Seismic Belt, William C. Hammond

Quaternary Fault and Fold Database and Map of Utah, M.D. Hylland

Dating Sinter Deposits in Dixie Valley, Nevada: a Record of Hot Spring-fault Interaction in the Great Basin, Susan Juch Lutz and S. John Caskey

Quaternary Fault Database for the Basin and Range Province of Nevada and Utah, Michael N. Machette, Kathleen M. Haller, B. Susan Rhea, and Richard L. Dart

Critique and Use of Historical Methodology in Seismic Hazards Analyses of Earthquakes in the Basin and Range; Expanding the Historical Catalog and the Search for Triggered Events from the San Andreas Fault, Dawn C. Martindale and James P. Evans

Horsts and Grabens of Colorado's High Plains, Vince Matthews and Matthew Morgan

Estimating Slip Rates and Recurrence Intervals for Quaternary Faults in the Basin and Range Province, Using Geologic Data, James McCalpin

Prehistoric Earthquakes on the Hubbell Spring Fault: Evidence for Coseismic Noncharacteristic Rupture of Intrabasin Faults in the Rio Grande Rift, Susan S. Olig, Martha C. Eppes, Steven L. Forman, David W. Love, and Bruce D. Allen

Basin and Range Seismicity: Distribution, Regional and Local Occurrence Rates, Moment Release and Comparison with Geodesy, Aasha Pancha and John G. Anderson

Determination of Low-Strain Site Amplification Factors in the Salt Lake Valley, Utah, Using ANSS Data, Kris L. Pankow and James C. Pechmann

Preliminary Paleoseismology of the Southern Steens Fault Zone, Bog Hot Valley, Nevada, Stephen F. Personius, Anthony J. Crone, Michael N. Machette, Jai Bok Kyung, Hector Cisneros, and David J. Lidke

Peavine Peak fault: Another Piece of the Walker Lane Puzzle, Alan R. Ramelli, John W. Bell, and Craig M. dePolo

Evaluation of an Earthquake Hazard Mapping Model for Reno, Nevada, James B. Scott, Matthew Clark, Thomas Rennie, Aasha Pancha, Hyunmee Park, Matthew Purvance, Glenn Biasi, Abdulrasool Anooshehpour, and John N. Louie

Quaternary Fault Map of Owens Valley, Eastern California, D. Burton Slemmons, Eutizio Vittori, A.S. Jayko, Gary Carver, and Charles E. Glass

Historic and Instrumental Seismicity in the Reno-Carson City-Lake Tahoe Area: Local Tectonics and Seismic Hazard, Ken Smith

A Record of the Past Three Surface-Rupturing Earthquakes Along the Central Hurricane Fault,

Rock Canyon, Arizona, H.D. Stenner, C.J. Crosby, T.E. Dawson, L. Amoroso, P.A. Pearthree, and W.R. Lund

Active Tectonics and Strain Partitioning in the Northern Intermountain Seismic Belt, Michael C. Stickney and David R. Lageson

Paleoseismic Investigations of the Stansbury and Mid-Valley Faults, Skull Valley, Utah, F.H. Swan, K.L. Hanson, and M.M. Angell

Spatial Relations among Young Faults, Basin Fill and vs in Las Vegas Basin: Implications for Ground Shaking, Wanda J. Taylor, Barbara Luke, Catherine Snelson, Ying Liu, Jeff Wagoner, Arthur Rodgers, Dave McCallen, Tiana Rasmussen, and John Louie

Seismic Hazard at the Designated Repository for High-Level Nuclear Waste, Yucca Mountain, Nevada, from 25 Years of Seismic Monitoring, David von Seggern

Digital Trench Wall Logging: Applying Morphological Image Processing Techniques to Trench Wall Stratigraphy, Julie B. Willis, Chaiwoot Boonyasirawat, Gerald T. Schuster, and Christopher B. DuRoss

Probabilistic Earthquake Ground Motion Hazard Maps for Montana, Ivan Wong, Susan Olig, Mark Dober, Doug Wright, Eliza Nemser, David Lageson, Walter Silva, Michael Stickne, Michele Lemieux, and Larry Anderson

Long Term Seismic Hazard Assessment for Boise, Idaho: Moderate Risk Arising from a Large Number of Low Recurrence Rate Sources, James E. Zollwe

# THE LATE QUATERNARY CANYON FERRY FAULT, WEST-CENTRAL MONTANA

Larry W. Anderson (landerson@do.usbr.gov)

Lucille A. Piety

U.S. Bureau of Reclamation, Seismotectonics and Geophysics Group, Box 25007,  
D-8330, Denver, CO 80225

Susan S. Olig

URS Corporation, 500 12<sup>th</sup> St., Suite 200, Oakland, CA 94607

Steven L. Forman

Department of Earth and Environmental Sciences, University of Illinois, 845 W. Taylor St., Chicago, IL 60607

## ABSTRACT

The 48-km-long Canyon Ferry fault bounds the west side of the Big Belt Mountains, approximately 30 km east of Helena, Montana. The fault is a major, down-to-the-west structure bounding the northern Townsend Basin. Although the fault has significant late Cenozoic displacement, like many faults in Montana and the northern Basin and Range, the late Quaternary activity of the fault is poorly documented. Based on aerial photograph interpretation, reconnaissance surficial geologic mapping, and scarp profiling, the late Quaternary Canyon Ferry fault can be characterized by rupture lengths of at least 40 km. The possibility also exists that the Toston fault, located immediately south of the Canyon Ferry fault, may be part of this system which would indicate that total rupture lengths of over 60 km may be possible.

A paleoseismic trench excavated at the G/T Ranch near the central portion of the Canyon Ferry fault provides important information on the slip rate, recurrence, and slip per event for the fault. Age data are from eleven infrared stimulated luminescence (IRSL) analyses on fine-grained deposits (primarily loess) collected from the trench. At the trench site, total dip-slip displacement of approximately 9 m occurred over a 55 kyr period between about 68 ka and 13 ka. These data indicate a long term late Quaternary slip rate of 0.16 mm/yr (0.13-0.2 mm/yr) for the fault. Interestingly, based on about 5 m of dip slip in the last 21 kyr, the rate is 0.24 mm/yr (0.2-0.29 mm/yr). More importantly, stratigraphic relationships and the numerical ages provide strong evidence for seismic clustering of events. At least two, and probably three, surface-rupturing events occurred between about 21 ka and 13 ka indicating short term rates of 0.54 mm/yr (0.35-0.91 mm/yr). No surface rupturing events have occurred since about 13 ka. Thus, recurrence intervals for the Canyon Ferry fault could be as long or longer than 13 kyr or as short as a few thousand years.

# **Holocene and latest Pleistocene faulting on the southern Inyo Mountain fault, southern Owens Valley, eastern California: A previously unrecognized active fault in Owens Valley**

Steven N. Bacon, Piedmont GeoSciences Inc., 10235 Blackhawk Drive, Reno, NV 89506  
steve@piedmontgeosciences.com, and  
Angela S. Jayko, U.S. Geological Survey, 3000 East Line Street, Bishop, CA 93514

The Inyo Mountain fault (IMF) is discontinuous and locally cuts alluvial deposits at the base of the Inyo's between Mazourka Canyon and Hwy 190. The southern section of the IMF trends ~310–340° for at least 12 km near Keeler along Owens Dry Lake (Fig. 1). Shutter ridges with deflected interfluvial alluvium of late Mio(?)–Pleistocene age suggests long-term dextral motion along prominent northeast facing scarps. Based on inferred ages of fan deposits cut by multiple- and single-event normal fault scarps and subsurface evidence from a natural exposure, at least 2 events occurred during the last 20 ka, with the youngest event in the last 10 ka. Fault scarps are generally mountain-side down, northeast-facing and composed of bedrock and alluvium. Many bedrock scarps display antecedent channels and strath terraces on the footwall. Late Quaternary alluvial scarps range in height from 0.5–1.75 m in the northern part of the section, 0.5–3.0 m in the central part to 1.0 m in the south (Fig. 1). Along the southern part of the fault zone, two exposures in ~3–4 m deep washes incised into alluvial (Q2b/Q3b) fans reveal a ~0.75 m wide fault zone with strikes of 340° and 346°, dips of 78°W and 81°E, and slickensides with rakes of 11°SE. In addition, offsets at two other sites have ~2.0–2.5 m apparent dextral offset of active wash channels (Fig. 1).

Evidence of the most recent event (MRE) is from a ~0.5 m northeast facing single-event scarp and depressions on a <10 ka fan surface at the 'slate' canyon paleoseismic site (Figs. 1 and 2). A channel nearly normal to the trace of the MRE scarp on the fan surface is dextrally displaced  $2.2 \pm 0.8$  m. A 10 ka or younger remnant fan surface mapped as (Q2b/c) is preserved along the east, downthrown side of the IMF, whereas a 20–10 ka alluvial fan surface mapped as (Q3b/a) is on the westside (Fig. 2). At the site, an ~4–5 m high channel north of the faulted surface exposes an ~30 m wide zone of steeply northeast dipping faults and fractures, as well as a shear zone with vertically aligned clasts (Fig. 3). Lateral motion is indicated by variation in thicknesses of offset units and the presence of an ~20–40 cm wide vertical shear zone with vertically aligned pebbles and cobbles separating dissimilar horizontally imbricated gravels and sands. The logged exposure is ~30 m west of the 0.5 m MRE fault scarp that separates the (Q3b/a) and (Q2b/c) surfaces. The (Q3b/a) surface appears to show warping in the near-field, based on bedding defined by pebble imbrications and surface profiling (Profile A–A'; Fig. 4). Based on morpho-stratigraphic position, the scarp and faults of the (Q3b/a) surface are younger than a remnant fluvial gravel terrace lying ~8 m higher on the flanks of the wash. We infer the fluvial gravel is the maximum aggradation surface from the last glacial maximum (~20 ka).

Based on the magnitude of displacement and minimum 12 km fault length, the MRE on the southern IMF may have a longer rupture length than has yet been recognized. Thus, further work is required to determine the full seismic hazard, and to integrate the results with kinematic models of strain distribution in southern Owens Valley.

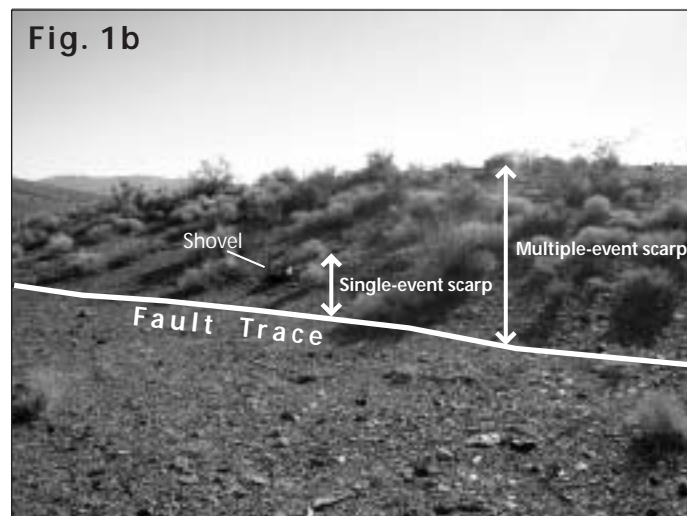
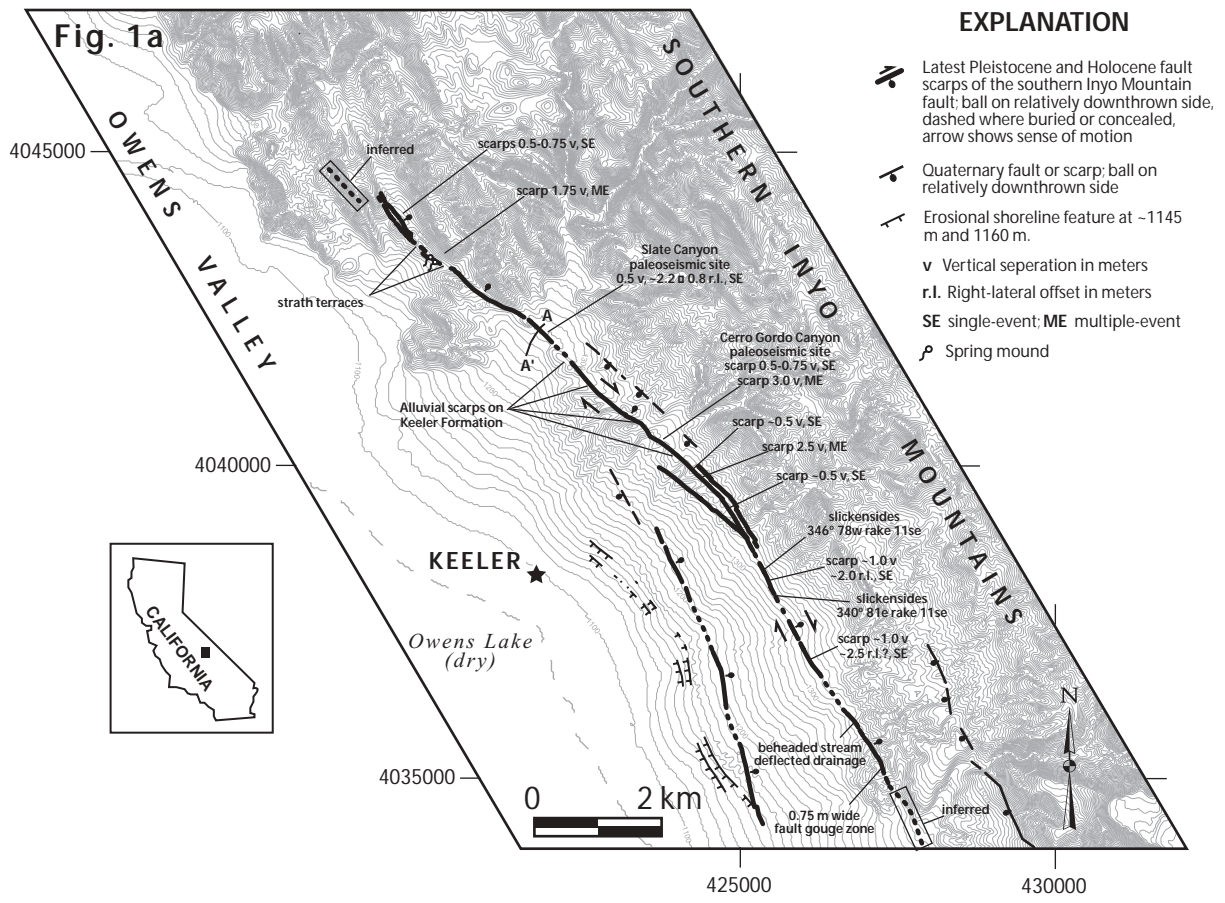


**Fig. 1.** Fault map showing the location of Holocene and latest Pleistocene fault scarps on the southern Inyo Mountain fault and other Quaternary faults in Owens Lake basin, in addition to scarp heights and the location of paleoseismic sites discussed in text (Fig. 1a). Photograph (Fig. 1b) looking to the south-southeast of ~3.0 m multiple-event and 0.5-0.75 m high single-event normal scarps at the Cerro Gordo paleoseismic site (see Fig. 1a for location of site). The scarps are on a ~20-10 ka (Q3b/a) remnant fan surface. Note shovel for scale.

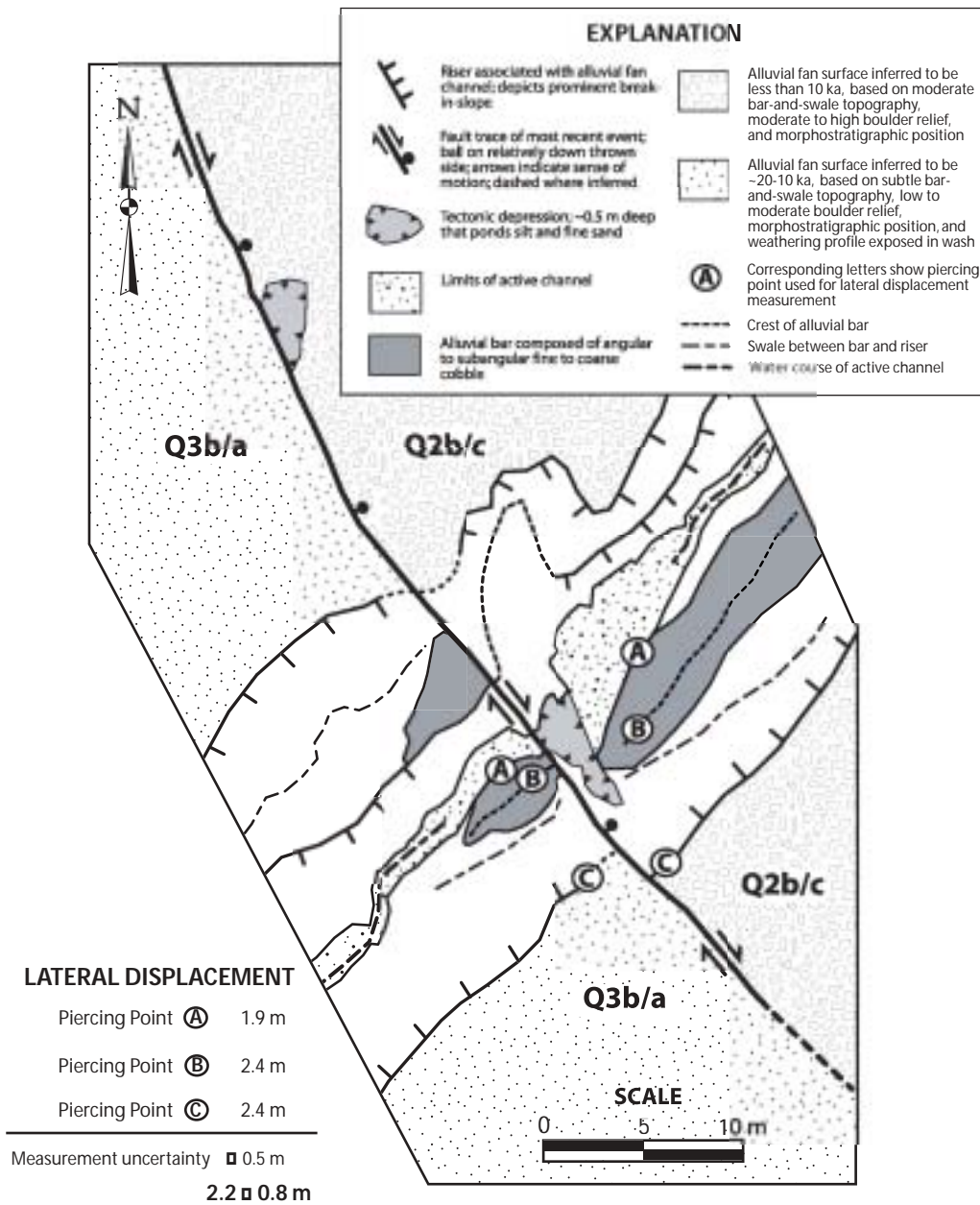


**Fig. 2.** Geomorphic map at the Slate Canyon paleoseismic site showing channel features and the trace of the most recent event on the southern Inyo Mountain fault that formed 0.5 m northeast facing normal fault scarp, 0.5 m deep depressions, and dextrally displaced <10 ka channel features  $2.2 \pm 0.8$  m. The trace of the MRE separates ~20-10 ka (Q3b/a) and <10 ka (Q2b/c) fan surfaces.

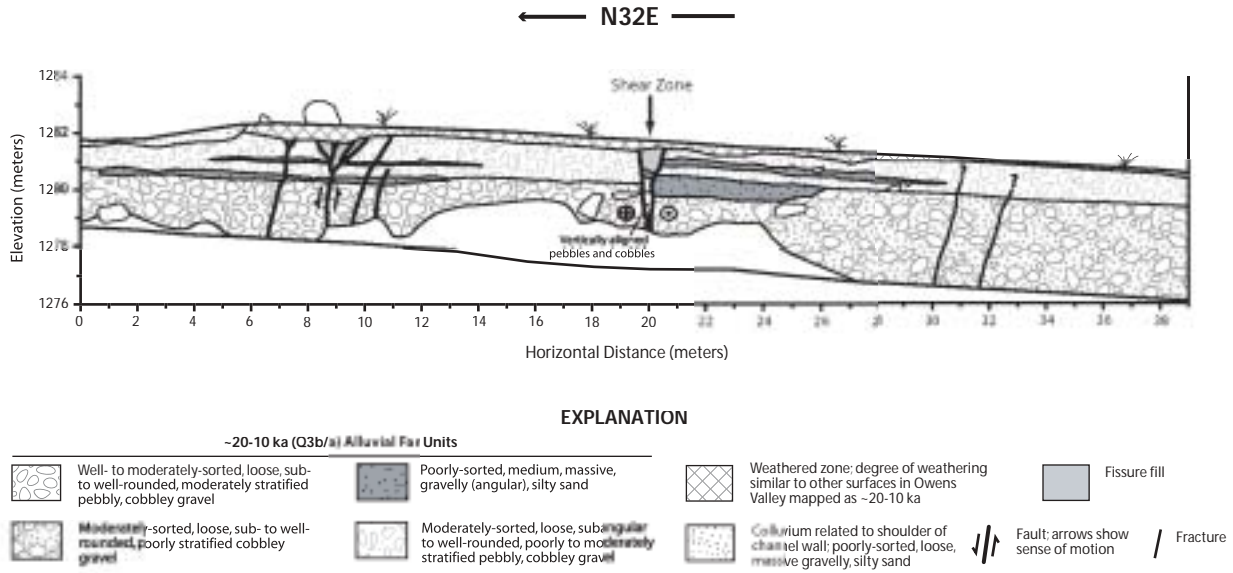


**Fig. 3.** Logged natural wash exposure at the Slate Canyon paleoseismic site showing ~20-10 ka alluvial gravels and silty sands displaced by northeast dipping faults and fractures, a fissure feature, and a vertical shear zone that separates dissimilar alluvial sediments. Both the silty sand units have apparent normal offsets across the shear zone of ~1.0 m down to the northeast. Faults and fractures are truncated by a weathered zone. One paleoearthquake is identified in the exposure between 20 and 10 ka.

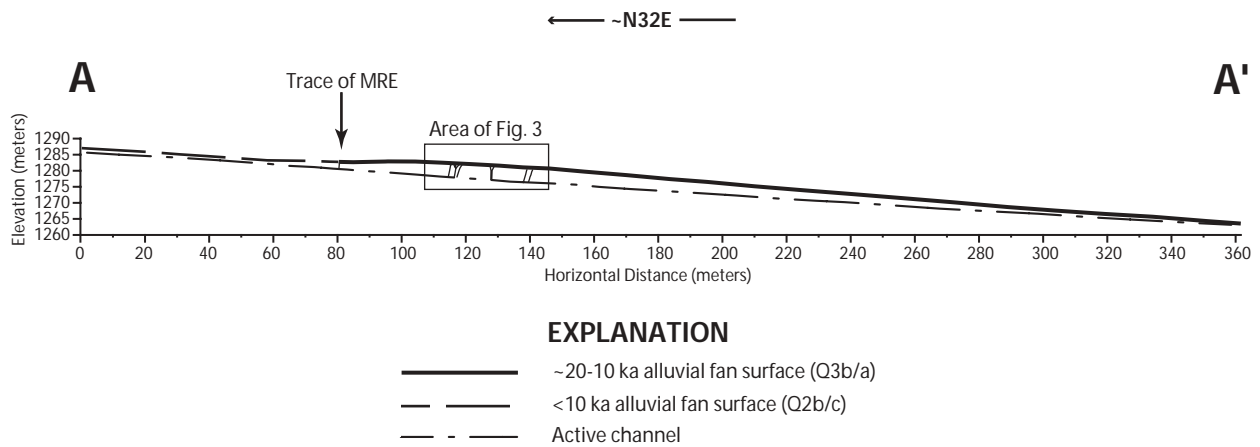


**Fig. 4.** Geomorphic profile of A-A' at the Slate Canyon paleoseismic site illustrating warping of the Q3b/a surface in the near-field, based on ~4-5 m of incision of the active channel at the fault zone compared to ~0.5 m of incision of the same surface ~220 m to the west. The location of profile A-A' is shown on Figure 1. The logged area of Figure 3 is shown in relation to the trace of the most recent event.

## ShakeMap as a Tool for Understanding Earthquake Hazard in Nevada

Glenn Biasi (Nevada Seismological Lab, MS-174, University of Nevada, Reno, NV 89557, glenn@seismo.unr.edu), Kent Lindquist (Lindquist Consulting, Fairbanks, AK), and Kenneth Smith (Nevada Seismological Lab, UNR).

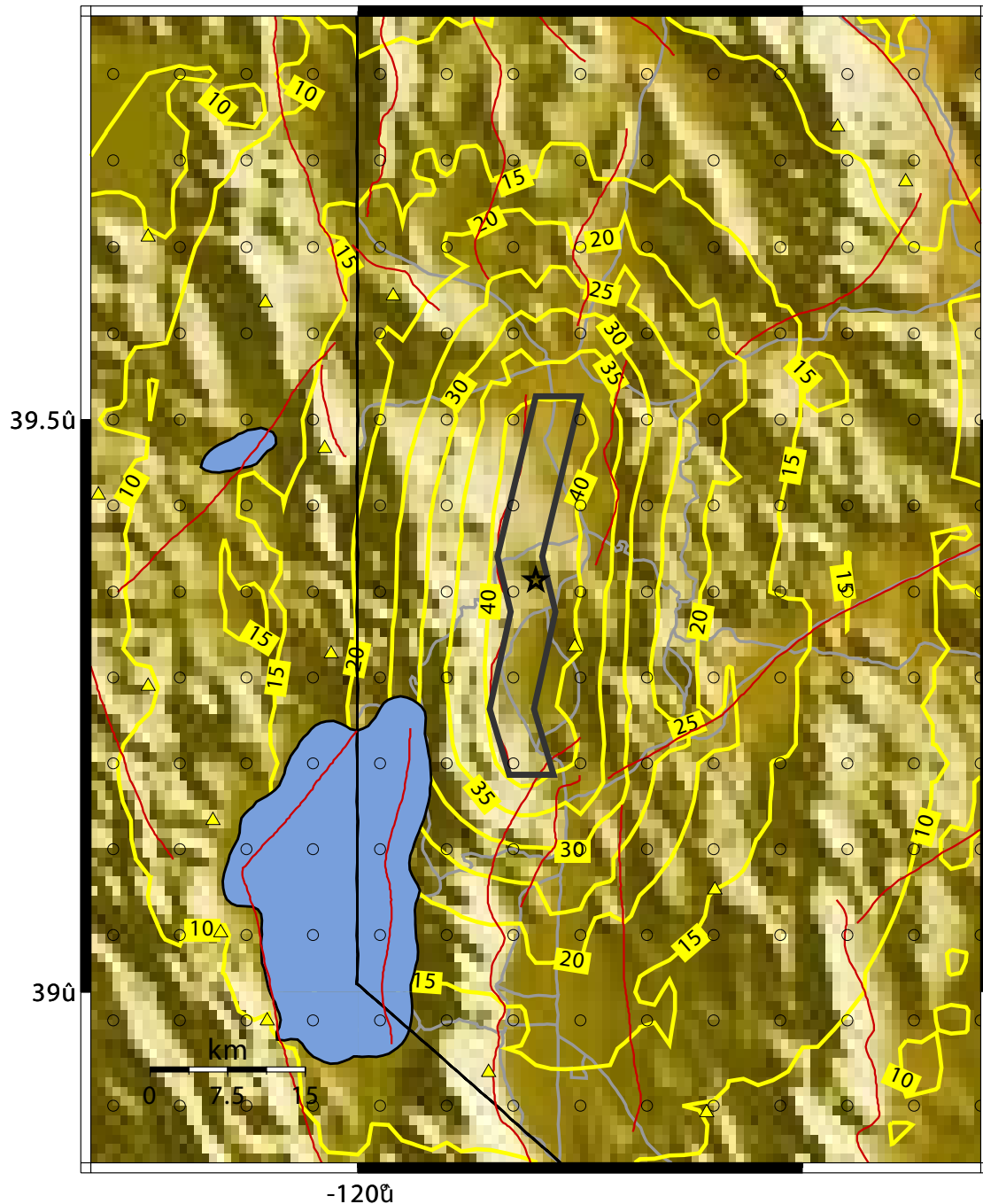
ShakeMap is being developed by the U.S. Geological Survey as a tool to synthesize instrumental recordings of strong ground motion and present them in map views useful for emergency response, loss evaluation, and public information. New strong-motion instrumentation provided under the Advanced National Seismic System (ANSS) initiative has significantly improved urban monitoring in western U.S. regional seismic networks (RSN's). ShakeMaps are being made by RSNs in California, Utah, and the Pacific Northwest, typically within minutes after  $M \sim 4.0$  and larger earthquakes. The Nevada Seismological Laboratory (NSL) has recently added over 30 new ANSS strong-motion instruments, and now has the capability to make ShakeMaps in near real time.

ShakeMap can also be used to predict ground motions given an earthquake location and size. To predict ground motions in un-instrumented areas, ShakeMap uses empirical regression relations. One can construct scenario earthquakes from known or suspected faults and use ShakeMap to predict and display the spatial extent of expected strong shaking. Maps can be used to assess risk and plan responses. Seismic hazards maps built using ShakeMap can be related by this scenario capability to U.S.G.S. maps of seismic hazard for a region of interest. We illustrate this process using the seismic hazard of downtown Reno, Nevada.

Individual faults contributing most to the seismic hazard in Reno were identified using data from the U.S.G.S. National Seismic Hazards Mapping Project. We used the 2002 version to deaggregate the 2% in 50 year hazard into contributing faults, then ran scenarios for the discrete faults contributing 1% or more to the total. Specific faults listed include the Mount Rose fault zone, the North Peavine Mountain fault, and the Spanish Springs fault. Of these, the Mount Rose fault zone is the greatest contributor to strong ground motions in the Reno/Sparks area. This fault is approximately 38 km in length and thought capable of an  $M_{6.7}$  earthquake. Using the finite fault prediction capabilities in ShakeMap, the approximate geometry of the fault can be incorporated. Scenario predictions (Figure 1) indicate that ground shaking of over 40% g can be expected across much of the valley. Amplification by soft sediments is only coarsely accounted in this estimate, so locally higher accelerations might be expected. Spectral accelerations at 3, 1, and 0.3 second periods are predicted to be 21%, 63%, and 110 %g in the central part of the valley. The North Peavine Mountain and Spanish Springs faults are greater hazards for communities north and northeast of Reno but still contribute predicted accelerations near downtown Reno of about 0.25 g.

Results highlight the need for more detailed site characterization in the valley. Probabilities of ground motion depend strongly on limited field estimates of recurrence and likely magnitude and highlight the value of continued efforts in paleoseismology and geologic mapping.

-- Earthquake Planning Scenario --  
 Peak Accel. Map (in %g) for 2004 Mtrose Scenario  
 Scenario Date: Sun May 16, 2004 12:00:00 PM GST M 6.7 N39.36 W119.80 Depth: 10.0km



PLANNING SCENARIO ONLY -- PROCESSED: Wed Mar 31, 2004 10:55:53 PM GST

Figure 1: Example ShakeMap of peak ground acceleration for a Scenario earthquake on the Mount Rose fault system. A characteristic magnitude of 6.7 and a fault length of 38 km were used. The Reno/Sparks metropolitan area is centered on the leg of the fault north of the hypothetical epicenter (star). Contours are in percent  $g$ . The heavy lined polygon is the map projection of the fault including an eastward dip. ShakeMap uses the minimum distance from the fault, but relies on regression relationships to predict ground motion. Parameters such as stress drop are not used. A pseudo-geology has been used here that scales  $V_{s30}$  from local topographic slope.

## Magnitude and Rupture Length Estimates From Point Measurements of Displacement

Glenn Biasi (Nevada Seismological Lab, MS-174, University of Nevada, Reno, NV 89557, glenn@seismo.unr.edu) and Ray J. Weldon II (Department of Geological Sciences, University of Oregon, Eugene, OR 97403, ray@newberry.uoregon.edu).

Measured surface displacements from surface ruptures vary along the rupture to such a degree that a measurement at a single point, such as is made at a paleoseismic trenching site, only loosely constrains paleomagnitude or rupture length. Using a new method we show that slip variability can be inverted quantitatively to give probability density functions of magnitude and rupture length given a point measurement of rupture displacement. The inversion begins by noting that rupture displacement variability can be summarized in the form of a histogram. Common features of individual rupture profiles emerge when they are normalized by length and average displacement. Figure 1 shows the result for the 13 ruptures considered in Hemphill-Haley and Weldon (1999, *BSSA*). Note that the average histogram captures rupture variability without constraining any rupture shape per se. Extremes are also preserved, so that excursions are allowed up to three times the average. Note also that these measurements are from real ruptures, so the result is data based.

Once the histogram in Figure 1 is rescaled by an average displacement-magnitude relationship, it may be interpreted as the probability distribution of rupture displacements given the earthquake magnitude. We developed a Bayesian inverse probability relationship that converts displacement given magnitude to the desired relationships of magnitude and rupture length given a paleoseismic displacement observation. Figure 2 shows this inversion for the case where ruptures of any magnitude are considered equally likely in the interval from  $M6.6$  to  $8.1$  (the range of data in the Wells and Coppersmith (1994, *BSSA*) regression). Individual plots show discrete probability distribution functions for magnitude and rupture length,  $p(M|d_{obs})$  and  $p(L|d_{obs})$ , respectively. Qualitatively,  $p(M|d_{obs})$  conforms to expectations. For example, given a rupture displacement of about 2 meters, one would expect an  $M7.2$  to  $7.4$  event, but would have to recognize the possibility that the measurement was at an exceptionally large displacement point on a  $M6.8$  event, or a small displacement point of a larger earthquake. The Bayesian inverse allows quantitative probabilities to be assigned to these possibilities. Thus present results should be useful for estimating earthquake magnitude and rupture length in probabilistic seismic hazard analyses when some point observation of rupture displacement is available.

The Bayesian framework can incorporate other sources of constraint or information. While we used the Wells and Coppersmith magnitude-average displacement ( $M-AD$ ) regression, other regressions or even a tabular  $M-AD$  relationship would work. More precise magnitude and rupture length estimates may be made if the distribution of earthquake magnitudes is known for the fault under study. The Gutenberg-Richter magnitude-frequency relationship yields shorter rupture length and smaller magnitude estimates for a given observed displacement than a model where any magnitude earthquake is considered equally likely. However, at least on the southern San Andreas fault, the Gutenberg-Richter model over-predicts the number of ground ruptures compared to paleoseismic rupture chronologies. An ad hoc magnitude distribution model that enforces average (but not individual) per-event

displacement from recurrence interval and fault geodetic rate is shown to be capable of matching both displacement and recurrence rate in paleoseismic data. For the San Andreas fault this model predicts larger earthquakes and longer ruptures than a model in which earthquakes of any size are considered equally likely. Extensions of the method are in progress to incorporate the probability of ground rupture given magnitude and an inversion when the observed displacement cannot be considered a random sample from the rupture histogram.

Figure 1. Histogram of rupture measurements for 13 events from Hemphill-Haley and Weldon (1999). Original rupture profiles were resampled at 1% intervals and binned, so over 1300 rupture displacement estimates are here summarized

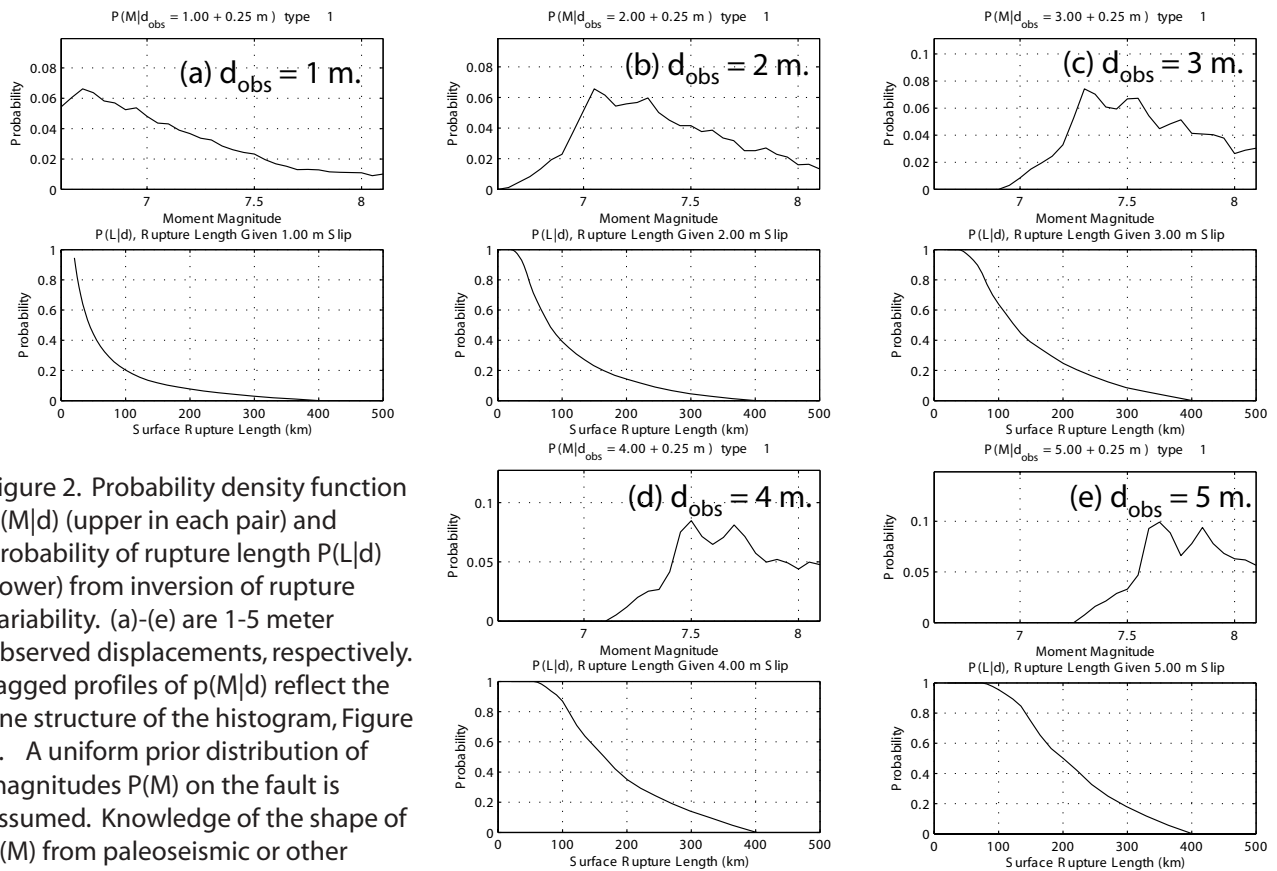
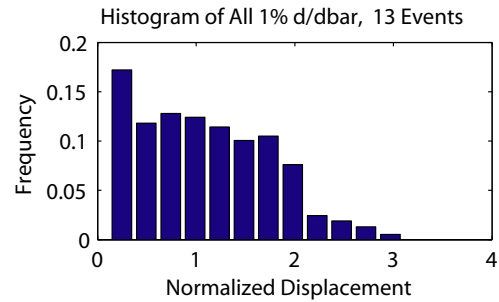


Figure 2. Probability density function  $p(M|d)$  (upper in each pair) and probability of rupture length  $P(L|d)$  (lower) from inversion of rupture variability. (a)-(e) are 1-5 meter observed displacements, respectively. Jagged profiles of  $p(M|d)$  reflect the fine structure of the histogram, Figure 1. A uniform prior distribution of magnitudes  $P(M)$  on the fault is assumed. Knowledge of the shape of  $P(M)$  from paleoseismic or other considerations can be used to refine  $p(M|d)$  and  $P(L|d)$ .

## Map of Miocene and Younger Faults and Earthquakes in Idaho

Roy M. Breckenridge and Loudon R. Stanford  
Idaho Geological Survey  
University of Idaho  
Moscow, ID 83844-3014  
roybreck@uidaho.edu

Faults shown on this map offset Miocene or younger rocks and deposits, or they have geomorphic expression as an escarpment. The Tertiary faults represent planes of weakness and zones of stress transfer between tectonic provinces, and thus they provide a record of the temporal and spatial development of the Basin and Range in Idaho. The data used to compile the map were taken from numerous reports on regional faults, seismotectonics, and geology. Details and source information have been compiled for each fault. We acknowledge the assistance of K.S. Sprenke, K.L. Othberg, Bill Bonnicksen, Rick Neir, B.K. Peterson, A.P. Hilt, and Mike McConnell. The map has also benefitted greatly from reviews and information provided by S.U. Janecke, J.P. McCalpin, and K.M. Haller.

Epicenters of earthquakes with magnitude 3 and greater are shown for Idaho and the surrounding area. The fault classification scheme is modified from the Western States Seismic Policy Council's Recommendation 02-3, *Active Fault Definition for the Basin and Range Province* (see under WSSPC Programs at Internet site [www.wsspc.org](http://www.wsspc.org)) and from K.L. Pierce and L.A. Morgan, 1992, *The Track of the Yellowstone Hot Spot: Volcanism, Faulting, and Uplift*, in P.K. Link, M.A. Kuntz, and L.B. Platt, eds., *Regional Geology of Eastern Idaho and Western Wyoming*: Geological Society of America Memoir 179, p. 1-53.

Reference: *Miocene and Younger Faults in Idaho and Earthquakes in Idaho 1872-2000*, compiled by Roy M. Breckenridge, Reed S. Lewis, Guy W. Adema, and Daniel W. Weisz, Idaho Geological Survey, version 9-11-2003, scale 1:1,000,000.

# Slip Rate and Paleoseismic Studies on Northern Walker Lane and Basin and Range Fault Zones in the Context of Geodesy

R.W. Briggs<sup>1</sup>, S.G. Wesnousky<sup>1</sup>, F.J. Ryerson<sup>2</sup>, R.C. Finkel<sup>2</sup>, and A.S. Meriaux<sup>2</sup>

<sup>1</sup>Center for Neotectonic Studies, University of Nevada, Reno

<sup>2</sup>Lawrence Livermore National Laboratory

Continuous and campaign GPS geodetic surveys (e.g. Bennett et al., 1998, 2003; Thatcher et al., 1999) have generally shown low rates of roughly E-W extension across the eastern and central Basin and Range and a significant component of NW-directed, right-lateral shear beginning near the Central Nevada Seismic Belt and continuing across the northern Walker Lane. The geodetic data provide the basis for our work on the Pyramid Lake fault zone, a right-lateral, strike-slip fault of the northern Walker Lane near Reno, for which we estimate a post-Lahontan (~15.5 ka) slip rate of  $2.6 \pm 0.3$  mm/year. This rate accounts for 25- 70% of the ~4-8 mm/year of right-lateral shear (Thatcher et al., 1999) measured geodetically across the region at ~39° 45' N latitude. Trenches excavated along the Olinghouse fault, a NE-trending, left-lateral strike-slip fault conjugate in orientation to the Pyramid Lake fault zone, indicate that the fault has been the source of multiple Holocene earthquakes and may rupture more frequently near its intersection with the Pyramid Lake fault. This may indicate interaction between the Pyramid Lake and Olinghouse fault zones in a style similar to numerous historical conjugate earthquakes (e.g. 1987 Superstition Hills/Elmore Ranch earthquakes, 1994/1995 Double Springs Flat earthquakes) and may be important for seismic hazard models of the region. While the Pyramid Lake fault zone appears to accommodate the majority of right lateral shear at its latitude, the fate of the remaining shear measured geodetically across the northern Walker Lane not yet clear due to only a first-order understanding of northern Walker Lane active fault locations, geometries, and paleoseismic histories. In contrast to the northern Walker Lane, the locations of active Basin and Range faults are relatively well known, but few geologic slip rates have been obtained using absolute dating methods. We are using cosmogenic surface dating techniques (<sup>10</sup>Be and <sup>36</sup>Cl) to quantify normal fault slip rates along the Ruby Mountains fault zone in eastern Nevada and the Dixie Valley fault zone in the Central Nevada Seismic Belt and we will discuss our results in the context of geodetic measurements. Preliminary results on the Ruby Mountains range front fault indicate that the late Pleistocene slip rate may be similar to that inferred from range front geomorphology (~0.3-0.5 mm/year) and thus the characterization of the Central Basin and Range as a geodetic microplate should be applied cautiously to seismic hazard models.

## HAZUS-MH: BENEFITS OF CENSUS BLOCK LEVEL ANALYSIS FOR EARTHQUAKES

CASE, James C.; WITTKE, Seth J.; BOWEN, Matthew L.; and CARRENO, Justin T.; Wyoming State Geological Survey, Box 1347, Laramie, WY 82073. jcase@uwyo.edu

HAZUS (Hazards U.S.) is a nationally standardized, GIS-based, risk assessment and loss estimation computer program that was originally designed in 1997 to provide the user with an estimate of the type, extent, and cost of damages and losses that may occur during and following an earthquake. It was developed for the FEMA by the National Institute of Building Sciences (NIBS). There have been a number of versions of HAZUS generated by FEMA, with HAZUS-MH (HAZUS – MultiHazard) being the most recent release. HAZUS-MH incorporates a flood and wind module with the previously existing earthquake module.

HAZUS was originally designed to generate damage assessments and associated ground motions based largely upon analysis at the census-tract level. HAZUS calculated a ground motion value for the centroid of a census tract, and applied that value to the entire tract. In many of the western states, census tracts are very large, and parts of the tracts may be subjected to ground shaking that is considerably different than the value at the centroid. FEMA Region VIII and their subcontractor on HAZUS, PBS&J from Atlanta, have worked closely with the Wyoming State Geological Survey (WSGS) to develop a census-block-based analysis for HAZUS-MH in Wyoming. The block-level analysis is a significant improvement. Ground motion values for Wyoming are now calculated at the centroid of census blocks. In Teton County, Wyoming, there are 3 census tracts and 1,062 census blocks, resulting in a significant larger number of ground acceleration values that will be used in all Teton County analyses.

HAZUS is packaged with default data for infrastructure, homes, businesses, and roads from national non-proprietary data sources. The default data needs to be refined at the State and local level, which the WSGS has been doing for almost two years. In addition, HAZUS can incorporate a “soils” layer, a landslide layer, and a liquefaction layer. Once those layers are incorporated and default datasets in HAZUS are updated or corrected, the HAZUS analysis is much more defensible.

A 2,500-year probabilistic earthquake scenario was run for Teton County, Wyoming in both HAZUS 99, using default data with census-tract analyses, and in HAZUS-MH using default data with census-block analyses. Casualty and building-related economic loss estimates for each method of analysis are presented in Tables 1-4.

The changes in casualties and business losses from HAZUS 99 to HAZUS- MH are significant. Casualty estimates (Tables 1 and 3) have significantly increased from HAZUS 99 to HAZUS-MH at 2 AM, significantly decreased from HAZUS 99 to HAZUS-MH at 2PM, and slightly increased from HAZUS 99 to HAZUS-MH at 5 PM. A dramatic increase can be seen in estimated building-related losses (Tables 2 and 4) from HAZUS 99 to HAZUS-MH. Total estimated damage of \$325,600,000 was calculated for HAZUS 99. Total estimated damage of \$567,060,000 was calculated for HAZUS-MH. The HAZUS-MH casualty and building-loss estimates will be affected even more with the inclusion of “soils”, landslide, and liquefaction data.

Table 1: Teton County, Wyoming Casualty Estimates — HAZUS 99-SR2 Tract-Level Analysis, Default Data (2500-year probabilistic)

		Level 1	Level 2	Level 3	Level 4
<b>2 AM</b>	<b>Residential</b>	87	21	3	5
	<b>Non-Residential</b>	15	4	1	1
	<b>Commute</b>	0	0	0	0
	<b>TOTAL</b>	102	26	3	7
<b>2 PM</b>	<b>Residential</b>	22	5	1	1
	<b>Non-Residential</b>	332	102	17	34
	<b>Commute</b>	0	0	0	0
	<b>TOTAL</b>	354	107	18	35
<b>5PM</b>	<b>Residential</b>	26	6	1	2
	<b>Non-Residential</b>	148	45	8	15
	<b>Commute</b>	0	0	1	0
	<b>TOTAL</b>	174	52	9	17

**Table 2: Teton County, Wyoming Building-Related Economic Loss Estimates — HAZUS 99-SR2 Tract-Level Analysis,**  
**Default Data (2500-year probabilistic)**  
(Millions of dollars)

Category	Area	Residential	Commercial	Industrial	Others	Total
<b>Building Loss</b>	Structural	19.0	12.4	3.0	1.0	35.3
	Non-Structural	84.3	35.5	7.0	2.8	129.7
	Content	25.0	15.8	4.4	1.3	46.5
	Inventory	N/A	0.4	1.0	0.0	1.4
	SUBTOTAL	128.3	64.0	15.4	5.1	212.9
<b>Business Interruption Loss</b>	Wage	7.5	23.3	0.6	0.4	31.9
	Income	3.2	22.9	0.4	0.1	26.6
	Rental	14.8	7.0	0.3	0.2	22.3
	Relocation	18.9	10.0	1.4	1.6	31.9
	SUBTOTAL	44.3	63.3	2.8	2.3	112.7
	TOTAL	172.6	127.3	18.2	7.5	325.6

Table 3: Teton County, Wyoming Casualty Estimates — HAZUS-MH Block-Level Analysis, Default Data (2500-year probabilistic)

		Level 1	Level 2	Level 3	Level 4
<b>2 AM</b>	<b>Commercial</b>	3	1	0	0
	<b>Commuting</b>	0	0	0	0
	<b>Educational</b>	0	0	0	0
	<b>Hotels</b>	25	7	1	2
	<b>Industrial</b>	3	1	0	0
	<b>Other-Residential</b>	50	13	1	3
	<b>Single Family</b>	77	18	2	4
	<b>TOTAL</b>	159	40	5	10
<b>2 PM</b>	<b>Commercial</b>	201	61	10	20
	<b>Commuting</b>	0	0	0	0
	<b>Educational</b>	1	0	0	0
	<b>Hotels</b>	5	1	0	0
	<b>Industrial</b>	26	8	1	2
	<b>Other-Residential</b>	9	2	0	0
	<b>Single Family</b>	14	3	0	1
	<b>TOTAL</b>	256	76	12	24
<b>5 PM</b>	<b>Commercial</b>	127	39	6	13
	<b>Commuting</b>	0	0	0	0
	<b>Educational</b>	0	0	0	0
	<b>Hotels</b>	7	2	0	1
	<b>Industrial</b>	16	5	1	1
	<b>Other-Residential</b>	19	5	1	1
	<b>Single Family</b>	31	7	1	2
	<b>TOTAL</b>	200	57	9	17

Table 4: Teton County, Wyoming Building-Related Economic Loss Estimates — HAZUS-MH Block-Level Analysis,

Default Data (2500-year probabilistic)

(Millions of dollars)

Category	Area	Single Family	Other Residential	Commercial	Industrial	Others	Total
<b>Income Losses</b>							
	Wage	0.00	7.59	31.79	0.54	0.63	40.54
	Capital- Related	0.00	3.24	30.91	0.30	0.12	34.58
	Rental	6.81	12.37	9.21	0.06	0.28	28.72
	Relocation	0.77	0.21	0.54	0.01	0.07	1.61
	<b>SUBTOTAL</b>	<b>7.58</b>	<b>23.41</b>	<b>72.45</b>	<b>0.91</b>	<b>1.10</b>	<b>105.45</b>
<b>Capital Stock Losses</b>							
	Structural	37.73	11.29	22.18	2.66	2.40	76.24
	Non-Structural	141.50	60.78	76.49	9.43	6.31	294.50
	Content	34.04	12.58	34.11	5.13	2.91	88.77
	Inventory	0.00	0.00	0.86	1.14	0.09	2.10
	<b>SUBTOTAL</b>	<b>213.27</b>	<b>84.64</b>	<b>133.63</b>	<b>18.36</b>	<b>11.71</b>	<b>461.61</b>
	<b>TOTAL</b>	<b>220.85</b>	<b>108.05</b>	<b>206.08</b>	<b>19.27</b>	<b>12.81</b>	<b>567.06</b>

# Integrated Earthquake Hazard of the Wasatch Front from GPS Measurements and Elastic-Viscoelastic Fault Modeling

Wu-Lung Chang and Robert B. Smith  
Department of Geology and Geophysics, University of Utah  
Salt Lake City, UT 84112  
(wchang@mines.utah.edu)

Contemporary crustal deformation along the 370 km-long Wasatch fault, Utah, has been measured by GPS and modeled for elastic and viscoelastic mechanisms. The Wasatch Front GPS network, including 90+ campaign sites surveyed in 1992-1995, 1999, and 2001 and 11 permanent stations operating continuously from as early as mid-1996, spans a 100-km wide area across the fault. Combining data from these sites revealed surface velocities with horizontal components of  $1.8 \pm 0.5$  mm/yr and  $2.2 \pm 1.0$  mm/yr across the northern and southern part of the Wasatch fault, respectively, with directions nearly perpendicular to the fault (Figure 1). Analysis of the spatial variation of the velocity field found a local strain concentration at a 30-km zone across the Salt Lake City segment of the Wasatch fault that may be produced by the interseismic fault loading.

We first examined the viscoelastic postseismic responses caused by the most recent paleoearthquakes on the Wasatch and the East Great Salt Lake faults and large ( $M > 5.5$ ) historic earthquakes in the Wasatch Front area. Rheological models of the lithosphere implied by the change of surface deformation following the 1959  $M_s=7.5$  Hebgen Lake, Montana, earthquake and the long-term deformation of the lacustrine shoreline caused by the Lake Bonneville rebound were applied. Results suggested that postseismic signals contribute insignificantly to the current surface deformation in the Wasatch Front area. A nonlinear optimization algorithm for dislocation fault-modeling was then implemented to investigate the geometry and loading rate of the Wasatch fault zone that best fit the horizontal velocity field observed by GPS. A dislocation dipping  $27^\circ$  and creeping at 7 mm/yr from depths of 9-20 km, which corresponds to the interseismic loading part of the Wasatch fault, is our favorite model based on the current GPS data (Figure 2). A dual-dislocation model that reflects the changes in strikes of the surface trace of the Wasatch fault, moreover, better explains the variations of the velocity field near the fault.

The ground-shaking hazard of a site in Salt Lake Valley was also evaluated by integrating various types of earthquake sources including fault slip rates, historic seismicity, and geodetic data, for probabilistic analyses of the annual exceedance of horizontal peak ground acceleration (Figure 3). The upper-bound scenarios considering geodetic earthquake moment rate, for example, increase the annual frequency of  $PGA \geq 0.7g$  by a factor of about 3.0 compared with the result including the historic seismicity.

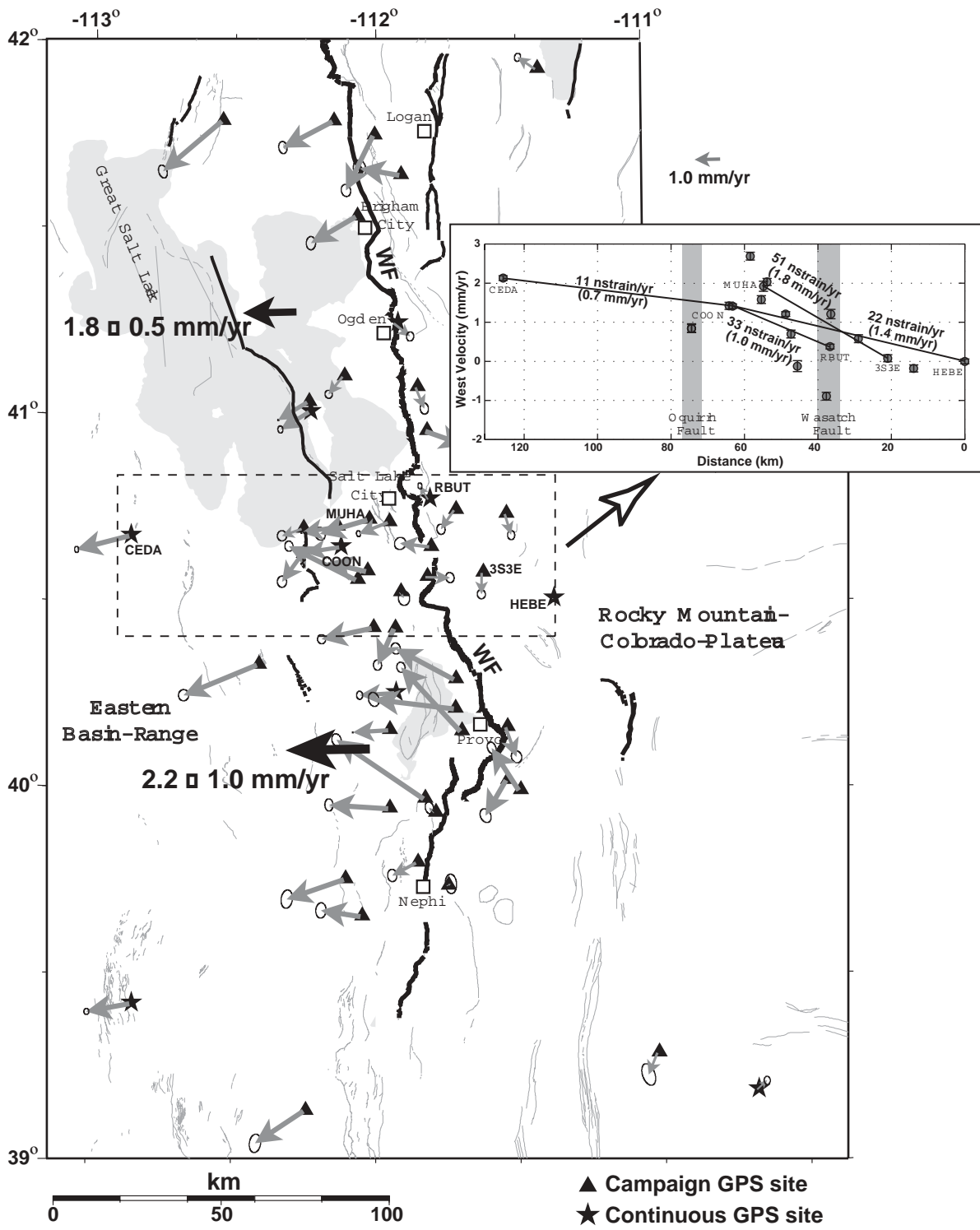


Figure 1. The Wasatch Front GPS network and horizontal velocity field (error ellipses in 2- $\sigma$ ). Thin lines delineate late-Quaternary fault scarps, and thick lines highlight the Holocene-active faults including the Wasatch fault (WF). Insert figure shows high west velocity gradients (strain rates) across a narrow zone of about 40 km (3S3E to COON) spanning the central Wasatch fault.

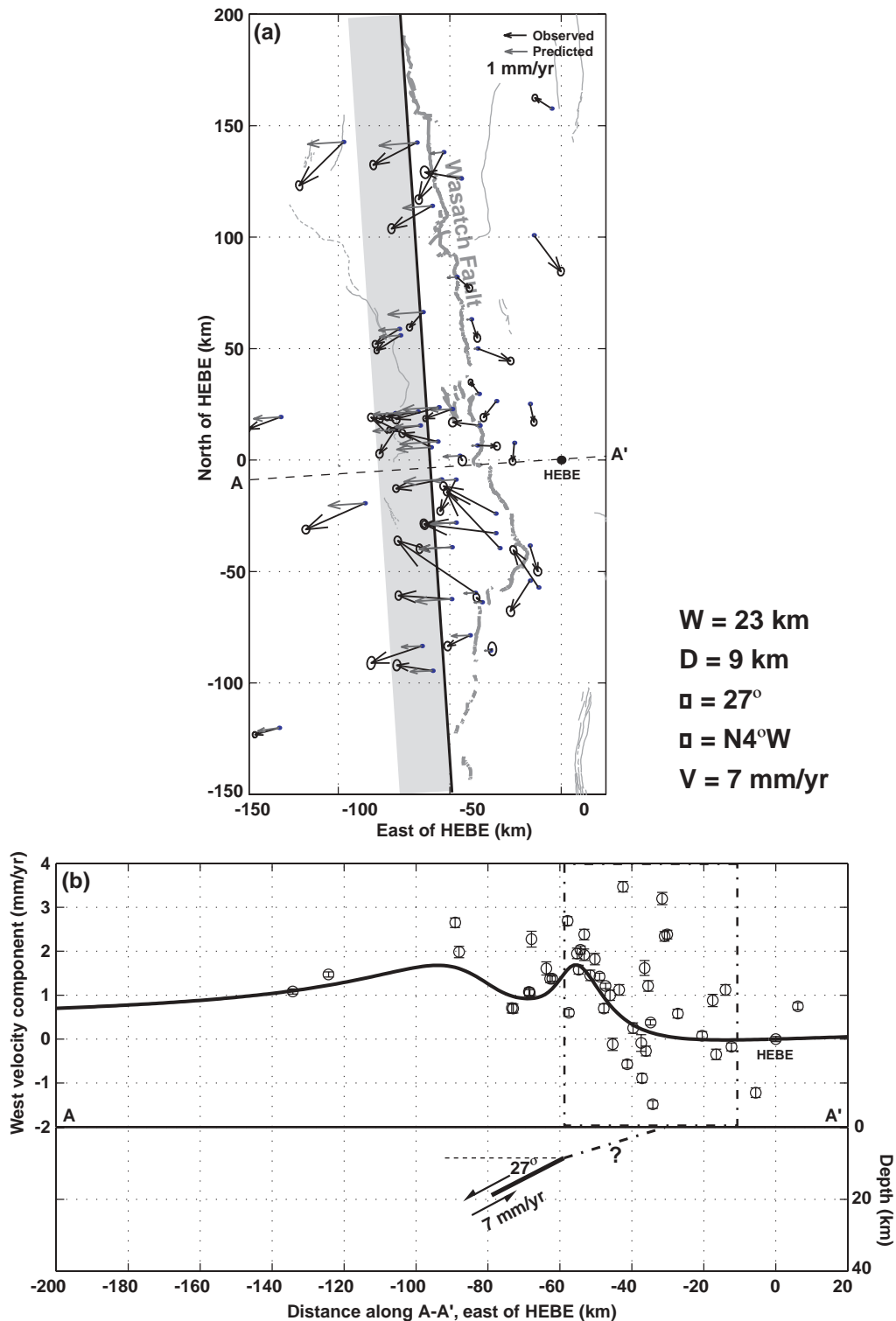


Figure 2. An optimal dislocation model for the Wasatch fault. (a) Map-view of the dislocation (gray area), corresponding to the loaded part of the fault at depth. The observed and predicted horizontal velocity vectors (fixed to HEBE) are also shown. (b) Vertical profile (A-A') of the dislocation and the predicted curve of the west velocities. The box with dash-dot outline marks the locations of observed fault scarps (thick gray lines in (a)), and the dash-dot line (with ?) shows a hypothetical extension of the dislocation to the surface straight. The parameters of the dislocation are:  $W$ =the width;  $D$ =the locking depth;  $\theta$ =the dip angle,  $\phi$ =the strike;  $V$ =the loading rate.

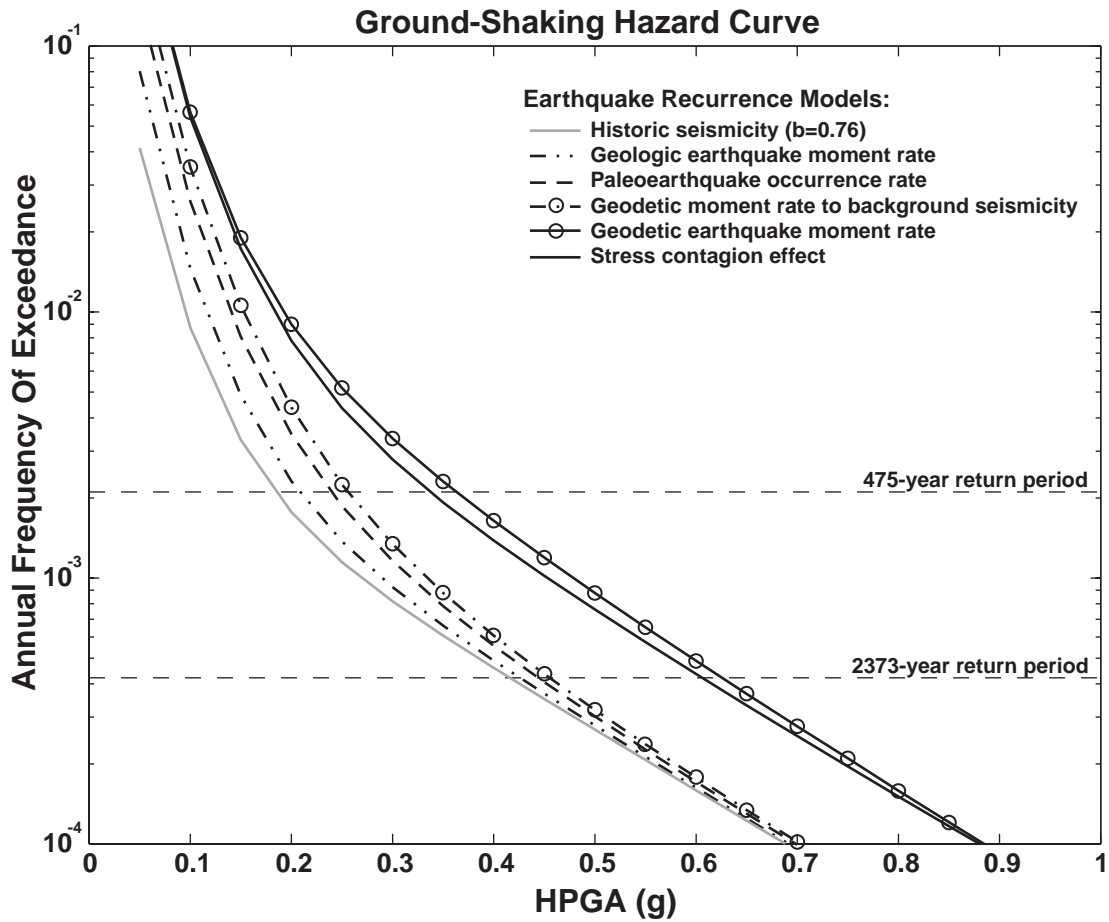


Figure 3. Earthquake ground-shaking hazard curves. The estimations present the annual frequency of exceedance of horizontal peak ground acceleration (HPGA) for a soil site near Salt Lake City, Utah (111.9°W, 40.7°N). The stress-contagion effect assumes 15-km induced-ruptures on adjacent segments (see text for details). The HPGA attenuation is based on *Spudich et al.* [1999] for extensional regimes.

# **GUIDELINES FOR EVALUATING SURFACE-FAULT-RUPTURE HAZARDS IN UTAH**

by

Gary E. Christenson, Utah Geological Survey, L. Darlene Batatian, Salt Lake County Geologist, and Craig V Nelson, Western GeoLogic  
garychristenson@utah.gov

The purpose of the *Guidelines for evaluating surface fault rupture hazards in Utah* is to outline appropriate surface-fault-rupture-hazard investigation techniques and report content to ensure adequate studies to protect the public, aid in land-use regulation, and facilitate risk reduction. Surface-fault-rupture hazard studies use the characteristics of past surface faulting as a scientific basis for reducing the hazard from future, presumably similar, faulting.

Faults are grouped into Holocene (<10,000 years), Late Quaternary (<130,000 years), or Quaternary (<1.6 million years) activity classes to determine the need for site-specific study and setbacks. The Utah Geological Survey (UGS) recommends site-specific studies for all critical facilities and structures for human occupancy along Holocene faults, and for critical facilities along Late Quaternary faults (table 1). For well-defined faults, we recommend a special-study area 500 feet wide on the downthrown side and 250 feet wide on the upthrown side. For buried or approximately located faults, we recommend a special-study area 1000 feet on either side of the mapped fault where at least surficial geologic studies are conducted to identify possible faults for further study.

A site-specific surface-fault-rupture-hazard evaluation typically includes a literature review, aerial photograph analysis, and field investigation, usually including surficial geologic mapping and trenching to determine the age, displacement, and dip of faults. Setbacks are then determined based on these factors, footing depths, and the criticality of the facility (table 1, figure 1). Reports should include site-specific maps showing faults, geology (if necessary), locations of subsurface investigations, and “non-buildable” setback areas. Risk-reduction measures in addition to setbacks include foundation reinforcement and disclosure. Surface-fault-rupture-hazard studies must be signed and stamped by the licensed Utah Professional Geologist performing the study.

Table 1. Study and setback recommendations and criticality factors (U) for IBC building occupancy class (International Code Council, 2000).

IBC building occupancy class	Study and setback recommendations <sup>1</sup>			Criticality <sup>3</sup>	U <sup>3</sup>	Minimum setback <sup>4</sup>
	Fault activity class					
	H	LQ	Q			
A. Assembly	R	P	O	2	2.5	25 feet
B. Business	R	P	O	3	2.0	20 feet
E. Educational	R	R	R <sup>2</sup>	1	3.0	50 feet
F. Factory/industrial	R	P	O	3	2.0	20 feet
H. High hazard	R	R	R <sup>2</sup>	1	3.0	50 feet
I. Institutional	R	R	R <sup>2</sup>	1	3.0	50 feet
M. Mercantile	R	P	O	3	2.0	20 feet
R. Residential (R-1, R-2, R-3 [ $>10$ dwelling units], R-4)	R	P	O	3	2.0	20 feet
R-3. Residential (R-3 [ $\leq 10$ dwelling units])	R	P	O	4	1.5	15 feet
S. Storage	O	O	O	-	-	-
U. Utility and misc.	O	O	O	-	-	-

<sup>1</sup> Fault activity class (H-Holocene, LQ-Late Quaternary, Q-Quaternary); study and setback or other risk-reduction measure: R — recommended; P - considered prudent but decision should be based on risk assessment; or O — optional but need not be required by local government based on the low likelihood of surface rupture. Appropriate disclosure is recommended in all cases.

<sup>2</sup> Study recommended; setback or other risk-reduction measure considered prudent but decision should be based on risk assessment; appropriate disclosure is recommended.

<sup>3</sup> Criticality is a factor based on relative importance and risk posed by a building; lower numbers indicate more critical facilities. Criticality is included in setback equations by the factor U. U is inversely proportional to criticality to increase setbacks for more critical facilities.

<sup>4</sup> Use the greater of this minimum or the calculated setback.

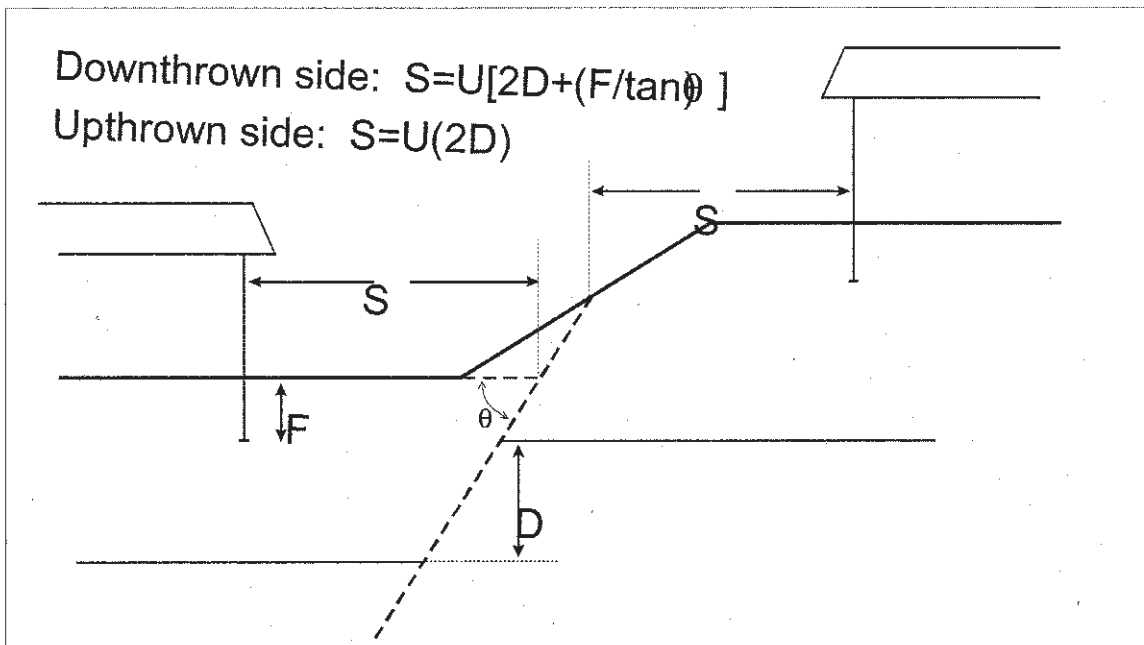


Figure 1. Formulas and schematic diagram showing variables used to determine setbacks.  $S$ , setback within which buildings are not permitted;  $U$ , criticality factor, based on the IBC building occupancy class (table 1);  $D$ , expected fault displacement per event (use the maximum vertical displacement measured for past events or, if not measurable, estimated based on paleoseismic data)-along main traces where displacement is not measurable, a maximum estimated single-event displacement should be used;  $F$ , maximum depth of footing or subgrade portion of the building; and  $\theta$ , dip of the fault (degrees).

## A Straightforward Way of Naming Paleoearthquakes

Craig M. dePolo

Nevada Bureau of Mines and Geology, University of Nevada, Reno, NV, 89557

The current approaches to identify paleoearthquakes are cumbersome, non-intuitive, and difficult to communicate, especially to non-earthquake scientists and lay people. A simpler method that numbers the events is more straightforward, more easily communicated, and commonly is used by default anyway in discussions and presentations. The most common ways to name paleoearthquakes, such as those identified in trenching studies, are to assign them letters starting with the end of the alphabet, or to give most recent three events some specific terms. In the first approach, the “z” event is the most recent paleoevent, “y” is the next oldest, and so forth. Not having learned the alphabet backwards, I find this confusing, especially knowing the order of events several earthquakes into a chronology. The second approach starts clearly with the term “the most recent event,” although it occasionally has to be referenced to the prehistorical record to clarify with the most recent historical event. The second event back is termed the “penultimate” event, a Latin word that means “second last” or the “last but one,” and is intended to mean the earthquake that came before the most recent event. Although there is a bit of a ramp-up period for newcomers, paleoearthquake geologists smoothly use these terms as lingo. The third event back is given the name the “antepenultimate” event, or the “last but two.” This system breaks down seriously at the fourth-event back, the “pre-antepenultimate” event, and the fifth-event back, the “pre-pre-antepenultimate event,” or perhaps we should substitute “the last but four.” Earthquake geologists commonly refer to these terms as their acronyms, MRE, PE, APE, and pre-APE in conversation. The terms penultimate and antepenultimate are perceived as quintessential scientific jargon by non-earthquake scientists and they are commonly surprised we have such complicated jargon for such a simple notion.

A straightforward way to name paleoearthquakes is to number them backwards, using the same reference frame that we naturally refer to these events. The first event back would be Paleoearthquake 1 (PE1), the second event back would be Paleoearthquake 2 (PE2), and so forth. Sweet! This approach is intuitively easy to use, and can readily be communicated with others, including those not familiar with paleearthquake jargon. For example, PE6 is the sixth event back. The terms are efficient and effective to use, especially their acronyms; for example, the scarp generated by PE2, or scarp-derived colluvium from PE2 overlying PE3 fractures. The datum for this approach is the beginning of the historical record. It expands open ended back in time, in the direction of new discoveries. Thus, paleoearthquake chronologies using this system are easily built on when older events are identified. Historical events are usually given site names, so there is not a large need for a parallel naming system; if there was, however, the same datum would be advocated, the beginning of the historical record, and the event numbers would increase with time into the open ended future.

The term “most recent event” is simple, eloquent, and is easily communicated, and I do not advocate abandoning it. The most recent event is synonymous with Paleoearthquake 1. I do advocate, however, that this simpler, numbered approach to naming paleoearthquakes is superior to approaches currently used, and should replace them.

## Quaternary Structure and Geomorphic Expression of the Warm Springs Valley Fault System, Western Nevada

Craig M. dePolo, Alan R. Ramelli, Christopher D. Henry, James E. Faulds,  
Nevada Bureau of Mines and Geology, Univ. of Nevada, Reno, NV, 98557, cdepolo@unr.edu  
Thomas L. Sawyer  
Piedmont GeoSciences, 10235 Blackhawk Drive, Reno, NV, 89506-8527

The Warm Springs Valley fault system (WSVFS) is a major, northwest-striking, right-lateral member of the northern Walker Lane belt in western Nevada. This large, well-exposed strike-slip fault system consists of multiple parallel and anastomosing fault traces that exhibit different geomorphic expression in different geologic settings. The southern 54 km of the system has well-developed late Quaternary tectonic geomorphology and is the focus of this study. The system extends to the north into Honey Lake Valley, California, however, and may have a total length of up to 96 km. The WSVFS appears to have two overall orientations. The southern half of the system has an overall strike of  $\sim N40^{\circ}EW$ . The northern half has a strike of  $\sim N55^{\circ}EW$ , although more mapping of the system in California is needed to confirm this.

The structure of the WSVFS is complex and commonly includes two or more parallel and anastomosing fault traces. Although the system is fairly continuous, right and left steps, with their associated extension and contraction, are common. Right steps dominate the system at both large and small scales, however, likely caused by the overall transtensional nature of the fault.

The WSVFS creates large- to small-scale linear valleys, linear depressions, and a series of aligned linear ridges immediately north of Warm Springs Valley. The local geomorphic expression of the WSVFS is related to geologic setting. Three distinct settings are present, alluvial basins, piedmonts, and bedrock areas. Based on these settings, five geomorphic sections of the WSVFS are proposed (south to north): Pah Rah Range section, Warm Springs Valley section, Winnemucca Valley section, Virginia Mountains section, Honey Lake Valley section. The Pah Rah Range section is characterized by a bedrock fault and, outboard of the range front, a buried fault. The 12-km-long section has sidehill benches and swales, and ends to the south in a small, intermountain pull-apart basin; expression is subtler because the slip rate is likely lower than the rest of the system. Faults in the Warm Springs Valley section cross the floor of northern Warm Springs Valley, which was inundated during the high stand of latest Pleistocene Lake Lahontan. The 9-km-long section has discontinuous small fault scarps, vegetation lineaments, and push-up mounds in latest Pleistocene and Holocene deposits. This subtle expression was likely created from the last few events. For much of this section, geomorphic expression is buried and/or modified by Holocene fluvial erosion and burial, and fault traces are indistinct. In the 12-km-long Winnemucca Valley section faults cross Quaternary alluvial fans and Tertiary volcanic deposits. Spectacular, aligned linear ridges along this section are cored by older alluvium and bedrock and are up to 1.5 km long. Geomorphic expression is nearly continuous, but erosion and burial tends to obscure expression of the most recent events. The Virginia Mountains section is a bedrock setting and is about 21 km long. Geomorphic expression includes side-hill benches and swales, linear valleys, saddles in ridges, and small fault facets. The northern portion of the section includes a pull-apart basin, with a central closed depression that is about  $5\frac{1}{2}$  km long and 1 km wide. We did not study the Honey Lake section, but it exhibits linear faults in a deep basin alluvial and lacustrine setting.

# Holocene segmentation and displacement history of the East Great Salt Lake fault, Utah

David A. Dinter and James C. Pechmann  
University of Utah Department of Geology and Geophysics  
E-mail: dadinter@mines.utah.edu

The East Great Salt Lake fault (EGSLF) is an active, segmented, west-dipping normal fault submerged beneath the Great Salt Lake 10-30 km west of the Ogden-Salt Lake City metropolitan area and 30-65 km west of the Wasatch fault (Fig. 1). A discontinuous topographic high defined, from north to south, by the Promontory Mountains and Fremont and Antelope Islands, marks the footwall of the EGSLF. The north and south main basins of the Great Salt Lake, which contain up to 4000 meters of Neogene sediment, lie to the west in its hanging wall. Using Geopulse and Chirp high-resolution seismic reflection profiling, we mapped the active traces of the EGSLF and auxiliary faults south of Promontory Point and imaged hanging-wall tectonostratigraphic geometries indicative of six Holocene surface-rupturing earthquakes. We cored the seismic event horizons, dated them by radiocarbon methods, and calculated the average recurrence interval of large earthquakes from the dates obtained.

A neotectonic map constructed from 40 seismic profiles crossing the EGSLF and some 20 additional lines crossing the basin to the west delineates two major normal fault segments south of Promontory Point, separated by a 1-2-km left step west of northern Antelope Island (Fig. 1). The southern (Antelope) segment is 35 km long (straight line, tip-to-tip) and has a prominent lakebed scarp with up to 3.6 m relief. It bends sharply to the southwest near its southern terminus, where displacement is apparently transferred to the Oquirrh fault zone. The Fremont segment is 30 km long and has no lakebed scarp along most of its length. Active traces of one or more additional segments to the north, submerged beneath the north arm of the lake west of the Promontory Peninsula, have not yet been fully profiled or mapped. Normal fault empirical relationships for both rupture length and rupture area predict maximum event magnitudes ( $M_w$ ) of 6.9 for the Antelope segment and 6.8 for the Fremont segment (Wells and Coppersmith, 1994, BSSA, v. 84, 974-1002). The maximum net vertical tectonic displacement associated with the most recent Antelope segment earthquake is consistent with a magnitude ( $M_w$ ) as great as 7.2.

Surface ruptures of EGSLF segments produce tectonic event horizons in hanging-wall deposits within ~1 km of the main fault trace that are recognizable on high-resolution seismic reflection profiles. Tectonostratigraphic geometries imaged in post-Bonneville (post-13.5 ka) hanging-wall deposits include coseismic bedding rotations and stratigraphically limited subsidiary faults, and displacement-related onlap surfaces and angular unconformities (Figs. 2 and 3). These features delineate event horizons associated with the three most recent earthquakes each on the Antelope and Fremont segments.

To obtain material for radiocarbon dating, continuous cores were collected from hanging wall deposits near the center of each fault segment using a hydraulic-assisted piston corer deployed from a barge. Five of the six recognized event horizons occur within Holocene clastic lacustrine sediment, from which was separated nonwood charcoal presumed to derive primarily from grass and brush fires on slopes and in valleys surrounding the Great Salt Lake. The sixth horizon, representing the earliest event imaged on the Fremont segment, falls within a 12-meter-thick pre-Holocene salt and sapropel unit. A maximum date for this event was obtained from charcoal contained in clastic deposits immediately beneath the salt interval. The radiocarbon dates are summarized in Table 1. Our results indicate single-segment recurrence intervals ranging from 3260 (+150/-180) to 5580 (+220/-170) years on the Antelope and Fremont segments of the East Great Salt Lake fault, with a mean single-segment recurrence interval of 4200 years.

Table 1. Earthquake Recurrence Intervals, East Great Salt Lake Fault

Earthquake pairs	Dates of occurrence (terrestrially calibrated <sup>1</sup> , residence- corrected <sup>2</sup> calendar yr BP <sup>3</sup> ) <sup>4</sup>	Recurrence interval (yr) <sup>4</sup>
<b>Antelope Island segment (<math>M_w[\text{max}] \leq 7.2 \pm 0.4</math>)</b>		
EH-A3	586 +201/-241	5584 +219/-172
EH-A2	6170 +236/-234	
EH-A2	6170 +236/-234	3728 +204/-351
EH-A1	9898 +247/-302	
<b>Fremont Island segment (<math>M_w[\text{max}] = 6.8 \pm 0.3</math>)</b>		
EH-F3	3150 +235/-211	3262 +151/-184
EH-F2	6412 +209/-211	
EH-F2	6412 +209/-211	< 5015 +587/-424
EH-F1	< 11,427 +605/-449	
<b>Average single-segment recurrence interval = 4200 years</b>		

1 - Raw <sup>14</sup>C years were converted to calendar years using Stuiver et al. (1998) terrestrial calibration (CALIB v. 4.3).

2 - Correction for carbon residence time in provenance area prior to deposition = -321 +191/-171 cal yr, the difference between the terrestrially calibrated <sup>14</sup>C date of Mazama ash interval at Site GSL00-3 (= 7994 +170/-128 cal yr BP) and terrestrial calibration (= 7673 +113/-86 cal yr BP) of published Mazama <sup>14</sup>C age (= 6845 ± 50 <sup>14</sup>C yr BP; Bacon, 1983, JVGR, v. 18, 57-115).

3 - Calendar years before 1950.

4 - Errors shown are 2 sigma.

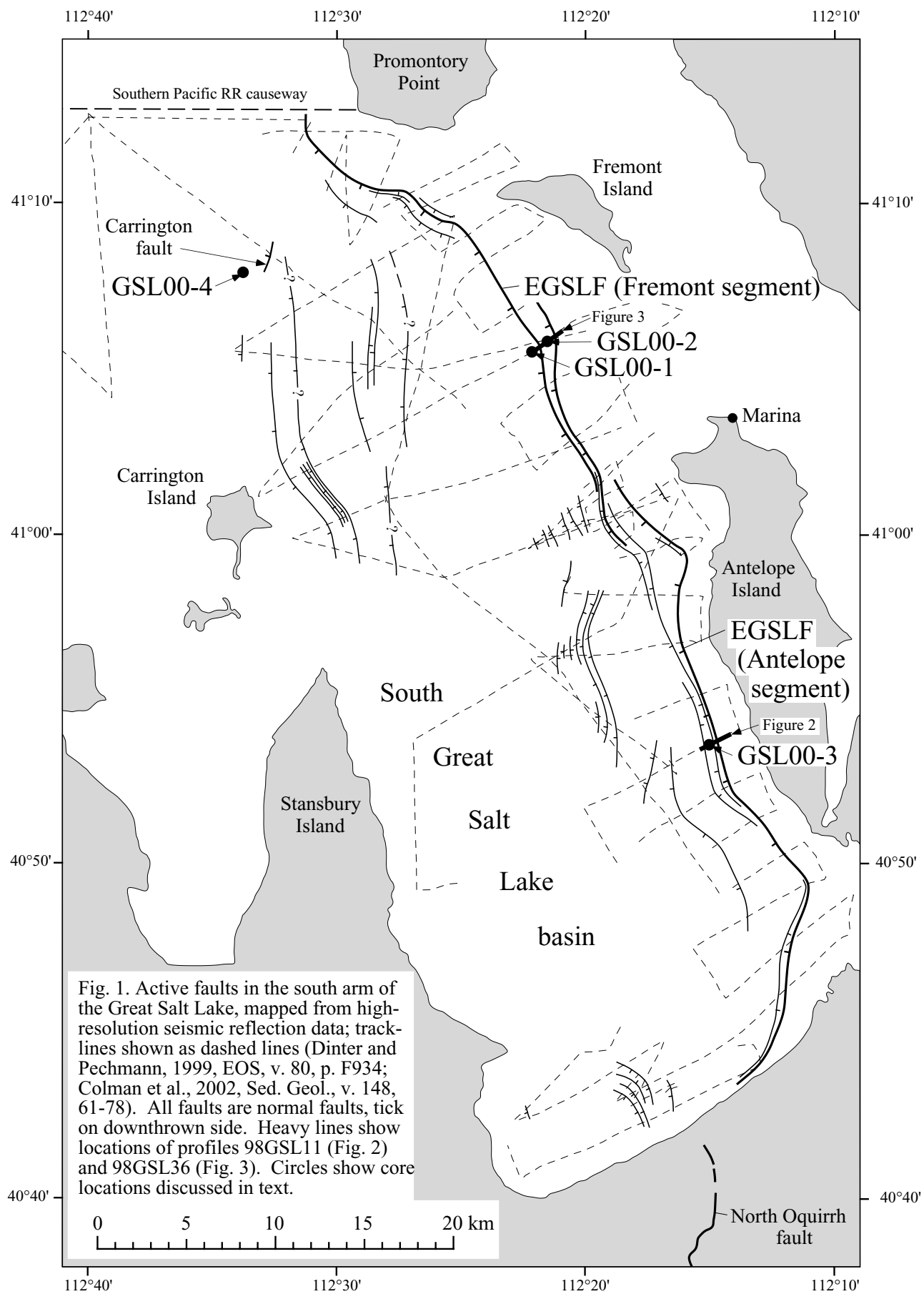


Fig. 1. Active faults in the south arm of the Great Salt Lake, mapped from high-resolution seismic reflection data; track-lines shown as dashed lines (Dinter and Pechmann, 1999, EOS, v. 80, p. F934; Colman et al., 2002, Sed. Geol., v. 148, 61-78). All faults are normal faults, tick on downthrown side. Heavy lines show locations of profiles 98GSL11 (Fig. 2) and 98GSL36 (Fig. 3). Circles show core locations discussed in text.

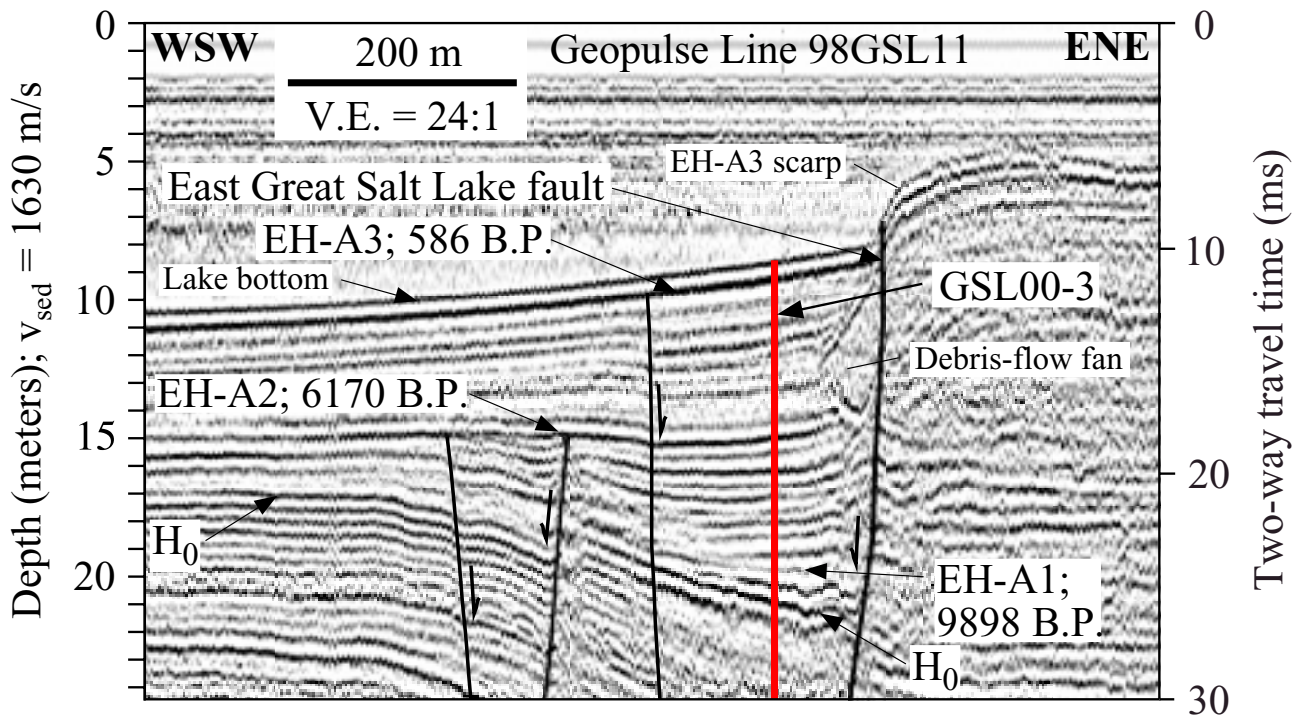


Fig. 2. Geopulse Line 98GSL11, showing earthquake event horizons for the three most recent surface-rupturing events on Antelope Island segment of East Great Salt Lake fault, and location of core site GSL00-3. Event ages shown are terrestrial-calibration calendar years B.P. (before 1950), corrected for carbon residence time in depositional provenance. (See Table 1 footnotes). See Fig. 1 for location of profile.

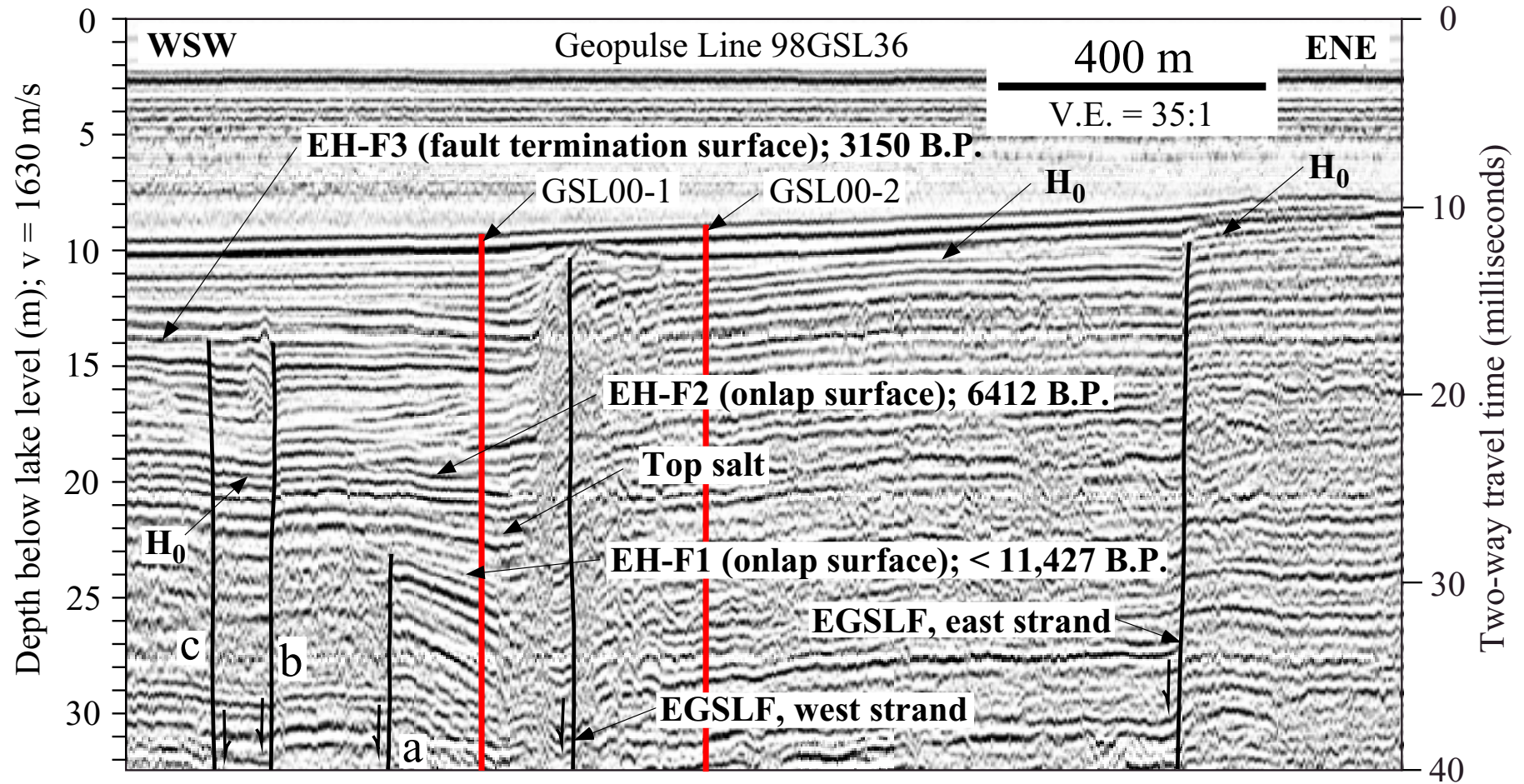


Fig. 3. Geopulse Line 98GSL36, showing earthquake event horizons for the three most recent surface-rupturing events on Fremont Island segment of East Great Salt Lake fault, and locations of core sites GSL00-1 and GSL00-2. Event ages shown are terrestrial-calibration calendar years B.P. (before 1950), corrected for carbon residence time in depositional provenance. (See Table 1 footnotes). See Fig. 1 for location of profile.

# Active Tectonics of the Nephi Segment, Wasatch Fault Zone, Utah, Revisited

Christopher B. DuRoss and Ronald L. Bruhn, University of Utah Department of Geology and Geophysics,  
cduross@mines.utah.edu

The Nephi segment is the southernmost segment of the Wasatch fault to rupture multiple times in the Holocene. The segment is divided into two fault strands that are separated by a connecting fault in bedrock; 1) the 25 km long Nephi and 2) the 17 km long Santaquin strands. In this study we have refined the Holocene to latest Pleistocene history of paleoearthquakes, and constrained the short-term (Holocene) and long-term (Late Pleistocene to present) fault slip rates based on Quaternary fault mapping and the numerical analysis of fault scarps. The Nephi segment ruptured with paleoearthquake magnitudes of 6.5 – 7.1 every 1.2 +/- 0.3 ka since the mid-Holocene and every 4.2 +/- 1.7 ka during the mid-Holocene to latest Pleistocene (~12 ka). The average recurrence interval is 9.5 ka from the latest Pleistocene to ~53 ka, using a mean vertical displacement per event of 1.9 m. The increased frequency of paleoearthquakes in the Holocene may indicate the temporal clustering of earthquakes and is important for assessing the seismic hazard potential of the Wasatch fault. This study has also resolved the timing of surface ruptures on the Nephi segment, contributing to an understanding of the Late Pleistocene to present spatial and temporal variability of paleoearthquakes on the Wasatch fault.

The Nephi segment ruptured a minimum of 6 times since the latest Pleistocene. Two paleoearthquakes with an average displacement of 2.0 – 2.3 m each ruptured the entire segment at 12.4 +/- 2.5 ka and 7.0 +/- 1.4 ka. Parts of the Nephi segment ruptured 4 times during the Holocene. The Nephi strand ruptured at 4.0 +/- 1.5 ka and 1.4 +/- 0.5 ka, with a mean vertical offset per event of 1.9 +/- 0.2 m, and the Santaquin strand ruptured at 2.6 +/- 0.7 ka and 0.5 +/- 0.1 ka, with 1.5 +/- 0.7 m of offset per event. The vertical slip rate for the Nephi segment is 1.4 mm/yr for the Holocene (since 7 ka) and 0.7 mm/yr since the latest Pleistocene (since 12 ka). In contrast, the Late Pleistocene (since 53 ka) rate is 0.3 mm/yr. The two most recent ruptures on the Santaquin strand may have been triggered by faulting along the Provo segment to the north, evidenced by the similar timing of events and the limited 6.5 km long Santaquin strand ruptures with 1 – 2 m of vertical offset. Rupture contagion between the Nephi and Provo segments partially explains the decreased recurrence time between moderate (M 6.5 – 6.7) paleoearthquakes on the Nephi segment in the Holocene.

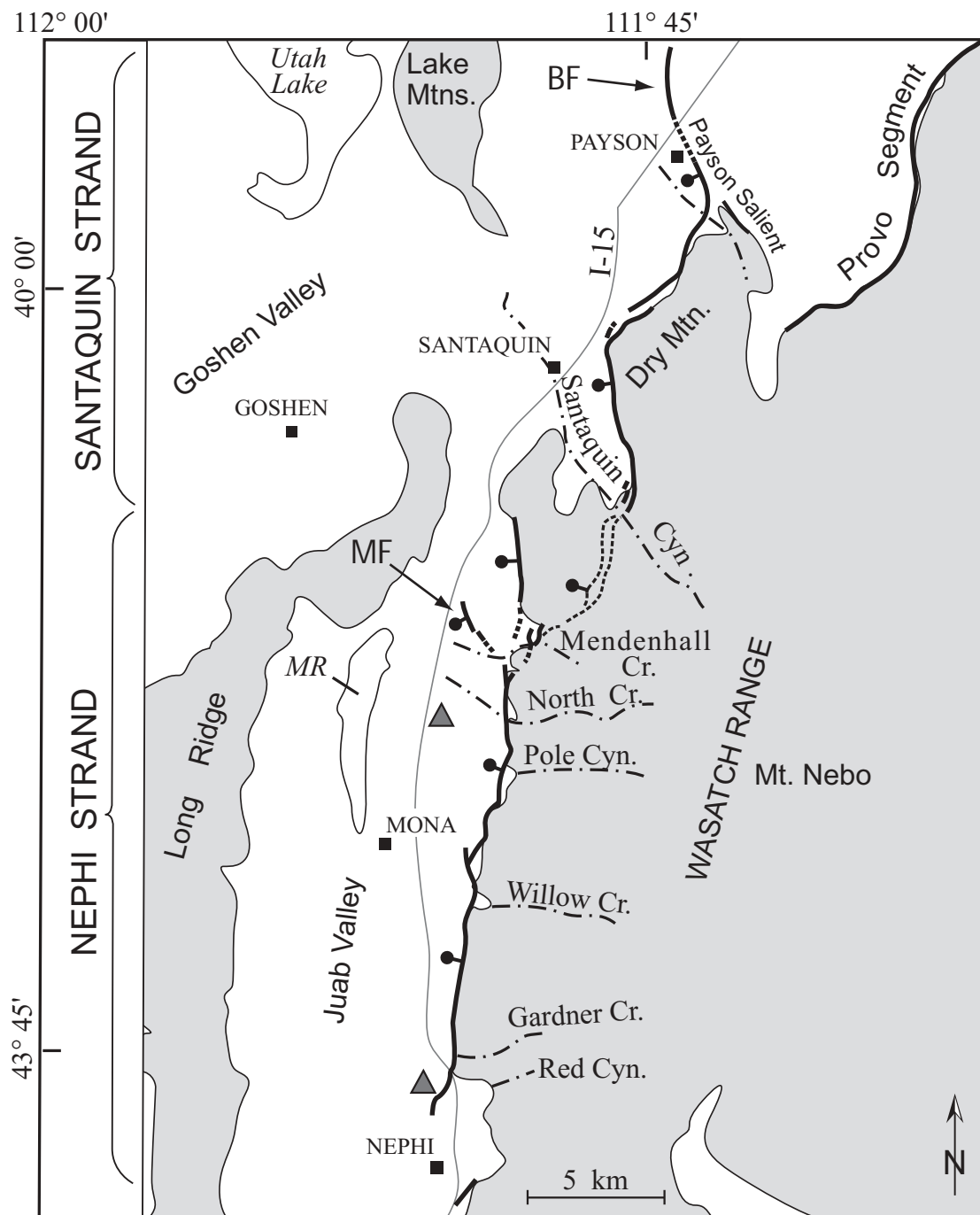
**Table 1. Preferred rupture scenario for the Nephi segment**

<b>Rupture event<sup>a</sup></b>	<b>Vertical offset<sup>b</sup> (m)</b>	<b>Preferred event age<sup>c</sup> (ka)</b>
Event Z <sup>S</sup>	1.0	0.5 +/- 0.1
Event Y <sup>N</sup>	1.7	1.4 +/- 0.5
Event X <sup>S</sup>	2.0	2.6 +/- 0.7
Event W <sup>N</sup>	2.0	4.0 +/- 1.5
Event V <sup>N,S</sup>	2.0	7.0 +/- 1.4
Event U <sup>N,S</sup>	2.3	12.4 +/- 2.5
oldest event <sup>N,S</sup>	-	53.2 +/- 5.6

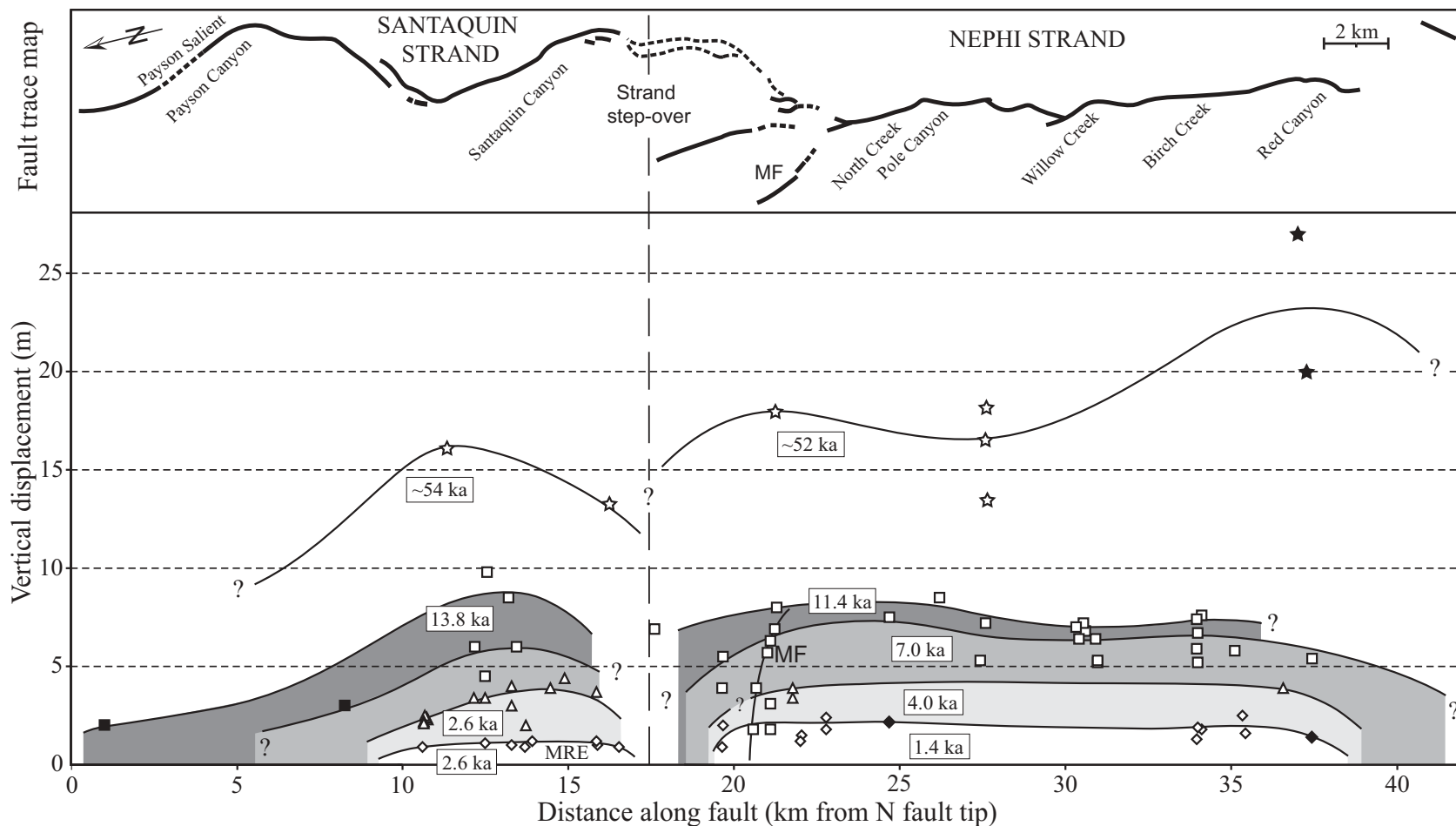
  

<b>Rupture events<sup>d</sup></b>	<b>Slip rate<sup>e</sup> (mm/yr)</b>	<b>Time range<sup>f</sup> (ka)</b>
Z – Y	1.5	0.5 – 1.4
Z – X	1.5	0.5 – 2.6
Z – W	1.4	0.5 – 4.0
Z – V	1.1	0.5 – 7.0
Z – U	0.7	0.5 – 12.4
Z – oldest	0.3	0.5 – 53.2
U – oldest	0.2	12.4 – 53.2

<sup>a</sup> Preferred rupture scenario for the Nephi segment, <sup>N</sup> = rupture on the Nephi strand, <sup>S</sup> = rupture on the Santaquin strand. <sup>b</sup> Average vertical slip per rupture event based on scarp profile data. <sup>c</sup> Preferred event ages are based on mean scarp initiation ages from diffusion modeling. <sup>d</sup> Rupture events used for slip rate calculation. <sup>e</sup> Slip rate is determined by dividing the mean slip per event by the mean recurrence interval. <sup>f</sup> Time range for slip rate calculation.



**Figure 1.** Nephi segment of the Wasatch fault, divided into the Nephi and Santaquin strands. Shaded areas represent mountainous regions, with major drainages (dashed and dotted lines). Heavy black line is the Wasatch fault, with ball and bar on downthrown side. BF ñ Benjamin fault, MF ñ Mendenhall fault. Dark gray triangles indicate locations of fault trench studies. MR ñ Mona Reservoir. Modified from Harty et al. (1994).



**Figure 2.** Distribution of vertical slip along the Nephi segment. Ages are mean scarp initiation ages from scarp diffusion modeling. Diamonds ñ youngest event scarps, triangles ñ second event, squares ñ third and fourth events, stars ñ oldest event. Black diamonds from Hanson et al. (1981, 1982) and Jackson (1991), black squares from Machette (1992), black stars from Mattson and Bruhn (2001). MF is the Mendenhall fault, vertical dashed line indicates location of strand step-over.

## **Improving Hazard Estimates in the Reno-Carson Metropolitan Region**

Feng Su, John G. Anderson and Aasha Pancha, Seismological Laboratory, University of Nevada-Reno,  
Reno, Nevada 89557, feng@seismo.unr.edu

The Reno-Carson metropolitan area is the second most populated region in Nevada. It lies in one of the most seismically active parts of the state. Thirteen earthquakes of magnitude 6 or greater have occurred in this region since 1850 (dePolo et al., 1997). Probabilities of potentially damaging earthquakes within the region are relatively high, as demonstrated by DePolo et al (1997) and more recently by the USGS hazard maps (1996, 2002).

We attempt to investigate the impact of alternative seismicity models on the probabilistic seismic hazard estimates for the Reno-Carson Metropolitan Region. Our new model employs a new, comprehensive catalog of earthquakes developed for the Basin and Range province that is substantially more complete than the catalog used by the USGS (1996, 2002). This new catalog, intended to be complete for magnitude  $M > 5$ , is obtained through compilation of 15 existing catalogs and supplemented by the review of 42 published journal articles. A different methodology used in seismicity smoothing is investigated. Also, much more of GPS data is available for this area, increasing our understanding of the shear zones dramatically. Other newly developed information on faults and slip rates from this region are also used. Based on these new inputs, a set of alternative probabilistic seismic hazard source models were developed as perturbations to the USGS hazard model (1996,2002). Moment rates from these alternative models are computed as a check. The probabilistic seismic hazard from each of these inputs have been calculated and compared with the result from USGS.

**THE METHOD OF INFORMATION LOCATION OF THE  
CENTER ZONE OF EXPECTED EARTHQUAKE.  
DIRECT AND INVERSE TASKS OF FORECASTING**

**Asadov H.H., Mammadov Sh.H.**

**Azerbaijan National Aerospace Agency**

**hasadzade [2001@yahoo.com](mailto:2001@yahoo.com)**

It is well – known that non – elastic earthquakes are preceded by low – frequency electromagnetic radiation. At the same time the common opinion is that absolutely valid forerunners are unknown. Taking into consideration above, we should acknowledge, that each prognosis always consists of elements of “near miss” and “fault alarm” probabilities. But such a situation cannot prohibit using of optimization methods in studying of problems related with earthquakes prediction. Guided by above provisions we have proposed that the problem of the earthquakes’ prediction should be studied from two positions. These positions are formulated by us as two tasks of earthquake’s prediction: direct and inverse tasks. Now we describe the direct task of the earthquake prediction.

1. *Direct task of the earthquakes prediction:* Gathering of maximal information using electromagnetic radiation from center zone of earthquakes.

We assume, that there are  $n$  number of sensors – receivers of electromagnetic radiation at the homogenous seismic active area, which are placed at the various distance from center zone of the earthquake. Center zone of the earthquake is to be predicted using other type precursor, for example ionospheric airglow. We should find out optimal function

$$L_i = f(T_i), \quad (1)$$

where  $L_i$  - distance between sensor numbered as  $i$  and center zone;  $T_i$  - time of retrieval of information from sensor number  $i$ .

Following functional is chosen as criterion of optimization

$$F = \sum_{i=1}^n \left[ \frac{T_i}{\Delta T} \log_2 (\psi_0 + \psi'_L + 1) + \lambda (\psi_0 + \psi'_L + 1) \right], \quad (2)$$

where  $\Delta T$  - step of sampling;  $\psi_0$  - signal / noise ratio at  $L=0$ ;  $\psi'_L = \frac{d\psi}{dL}$ ;  $\lambda$  - multiplier of Lagrange.

It should be noted, that functional (2) is composed taking into consideration following limitation condition

$$\sum_{i=1}^n L_i = \text{const}_1 \quad (3)$$

or

$$\sum_{i=1}^n (\psi_0 + \psi'_L L_i + 1) = \text{const}_2. \quad (4)$$

The limitation conditions (3) and (4) mean, that the network of sensons is fixed relative to predicted center zone of earthquake. Solution of above optimization task using formula of Euler gives us following type of function

$$L_i = \frac{\psi_0 + 1}{|\psi'_L|} - \frac{T_i \cdot \psi_0}{T_{max} |\psi'_L|}. \quad (5)$$

The formula (5) can be commented as follows. The sensor placed near to center zone of earthquake should be retrieved during the long time period, and vice – versa.

Above result will be used in solution second task of earthquake prediction which is formulated below.

2. *Inverse task of the earthquakes prediction*: Determination of the center zone of earthquakes using condition of receive of the maximal information.

First of all, we should stress out, that the intensity of electromagnetic radiation depends on two factors:

1. Distance between the receiver and center zone of earthquake -  $L$ .
2. Frequency of electromagnetic radiation -  $F$ .

Above dependences in both case expressed by fading of intensity of electromagnetic radiation.

Taking into account of above, we can find the signal/noise ratio  $\psi$  of the received signal as

$$\psi = (L, F) = \psi_0 + \frac{\partial \psi}{\partial L} \cdot \Delta L + \frac{\partial \psi}{\partial F} \cdot \Delta F, \quad (6)$$

where  $\psi_0 = \psi(L=L_0; F=F_0)$ .

Now considering the whole net of seismosensors consisting of  $n$  ones, and taking into account, that optimal system of processing is designed in such a manner, that it receives signals of duration  $T_i$ ,  $i=\overline{1, n}$ , where value of  $T_i$  increases depending on  $i$ . In this case, the amount of information, which is gathered from all  $n$  sensors can be assessed as follows

$$\Phi = \sum_{i=1}^n \frac{T_i}{\Delta T} l o g_2 \left[ \psi_0 + \frac{\partial \psi}{\partial L} \Delta L + \frac{\partial \psi}{\partial F} \Delta F + 1 \right]. \quad (7)$$

Using formula (7) we can solve two type of optimization task, which allow us to form two methods for prediction of earthquakes center using maximal informational criteria.

1. Receive of electromagnetic radiation at the same frequency.
2. Receive of electromagnetic radiation at the same distance used for confirmation of found center of earthquake on the first method.

The first method is described below. During the whole period of information retrieval, total amount of gained information can be found as

$$M_0 = \sum_{i=1}^n M_i = \sum_{i=1}^n \frac{T_i}{\Delta t} l o g_2 (\psi_0 + \psi L_i + 1),$$

where  $T_i$  - duration of information retrieval from the sensor numbered as  $i$ .

Taking into account formula (4) above, the functional of effectiveness can be formed in the integral form as

$$\Phi = \int_0^{T_{max}} \left[ \frac{T}{\Delta t} l o g_2 (\psi_0 + \psi' L + 1) + \lambda (\psi_0 + \psi' L + 1) \right] dT.$$

According to the principle of optimal lowering of dimensionality [2], we should find such type of optimal function  $L = \varphi(T)$  which would lead the functional of effectiveness to its maximal value.

Solution of above maximization task using Euler's formula gives us following type of said function

$$L = \frac{\psi_0 + 1}{|\psi'|} - \frac{T \psi_0}{T_{max} |\psi'|}. \quad (8)$$

As a result, we have possibility to carry out an adaptive control of seismosensors, i.e. all system of gathering and processing of seismic information.

On the basis of above result we can propose a new method of informational forecasting of place of expected earthquakes. We assume that seismosensors are placed on the territory with high seismic risk (figure 1). In order to forecast the place of earthquake we should designate set of values  $\{L_i\}$ , and set of values  $\{T_i\}$ , where dependence between  $L_i$  and  $T_i$  should be in line with formula (8), which guarantee maximum value of total information gathered from seismosensors. Selected three seismosensors  $S_1, S_2, S_3$  will be commutated during time period  $T_i$  determined by formula (8). Under above conditions computer should detect maximum amount of information, if the point  $A$  is actually the center of expected earthquake. Selected set of sensors should be moved along the territory in order to detect maximum of gathered information. More strictly no sensors, but selector contour of three sensors should be moved over the territory via fixed set of sensors and movement of this contour should be stopped if maximal amount of information is reached. Then using known set of  $L_i$ , we can find needed center place of earthquake by redistribution of  $T_i$  on  $S_i = \overline{1, n}$ .

Receive of electromagnetic radiation at the same distance used for confirmation of found center of the earthquake on first method.

In this case, the ratio signal/noise  $\psi$  in the channel of propagation of low – frequency electromagnetic radiation from the source of these signals as far as receiver in the first approximation can be found as

$$\psi = \psi_0 + \psi'_F \cdot F, \quad (9)$$

where  $\psi'_F = \frac{\partial \psi}{\partial F}$ ;  $F$  - frequency of electromagnetic radiation.

During the whole period of information retrieval total amount of gathered information can be found as

$$M_0 = \sum_{i=1}^n M_i = \sum_{i=1}^n \frac{T_i}{\Delta t} \log_2 (\psi_{01} + \psi'_F \cdot F + 1), \quad (10)$$

where  $T_i$  - duration of information retrieval from the sensor numbered as  $i$ .

Then we use a limitation condition

$$\sum_{i=1}^n (\psi_{01} + \psi'_F \cdot F_i + 1) = \text{const}$$

or

$$\sum_{i=1}^n F_i = \text{const}. \quad (11)$$

A limitation condition (11) means, that band of reasonably received frequencies is limited.

Taking into account of (10) and (11) we can form the functional of effectiveness as follows:

$$\Phi = \int_0^{T_{\max}} \left[ \frac{T}{\Delta T} \log_2 (\psi_{01} + \psi'_F \cdot F + 1) + \lambda (\psi_{01} + \psi'_F \cdot F + 1) \right] dT, \quad (12)$$

where  $T$  - time of information retrieval;  $\lambda$  - multiplier of L' Agrange.

According to the principle of optimal lowering of dimensionality [2], we should find such type of optimal function  $F = \varphi(T)$  which would lead the functional of effectiveness (7) to its maximal value.

Solution of above optimization task using Euler's formula gives us following type of said function

$$F = \varphi(T) = \frac{\psi_0 + 1}{|\psi'_F|} - \frac{T \cdot \psi_0}{T_{\max} |\psi'_F|} \quad (13)$$

As a result we obtain the possibility to carry out an adaptive control of seismosensors, i.e. whole system of gathering and processing of seismic information. This does mean, that sensor with lowest frequency of received signal should be examined during uppermost time period in order to reach maximal efficiency of the system.

On the basis of above result we can propose a new second method for informational forecasting of center of expected earthquakes. We assume that seismosensors are placed on the territory with high seismic risk, forming a rectangular Net (figure 2).

In order to forecast the place of earthquake we should designate a set of values  $\{F_i\}; i=\overline{1, n}$ , and set of values  $\{T_i\}; i=\overline{1, n}$ , where dependence between  $F_i$  and  $T_i$  should be in line with formula (13), which guarantees reaching of maximum value of total information, gathered from seismosensors. Here we should note, that each sensor consists of  $n$  receiver with fixed frequency  $\{F_i\}; i=\overline{1, n}$ .

Hence, each sensor is compound on  $n$  number of receiver and makes it possible to receive in the frequency band  $\{F_1, F_2, \dots, F_n\}$ .

Selected contour of four seismosensors (in figure 3 they are  $S_1, S_2, S_4, S_5$ ) will be moved across the high rise territory – area of placement of sensors, and the movement of the contour should be stopped in the point, where the estimated value of functional of effectiveness reaches a maximal value. Such assessment can be realized using computer, which should also control movement of the contour of sensors.

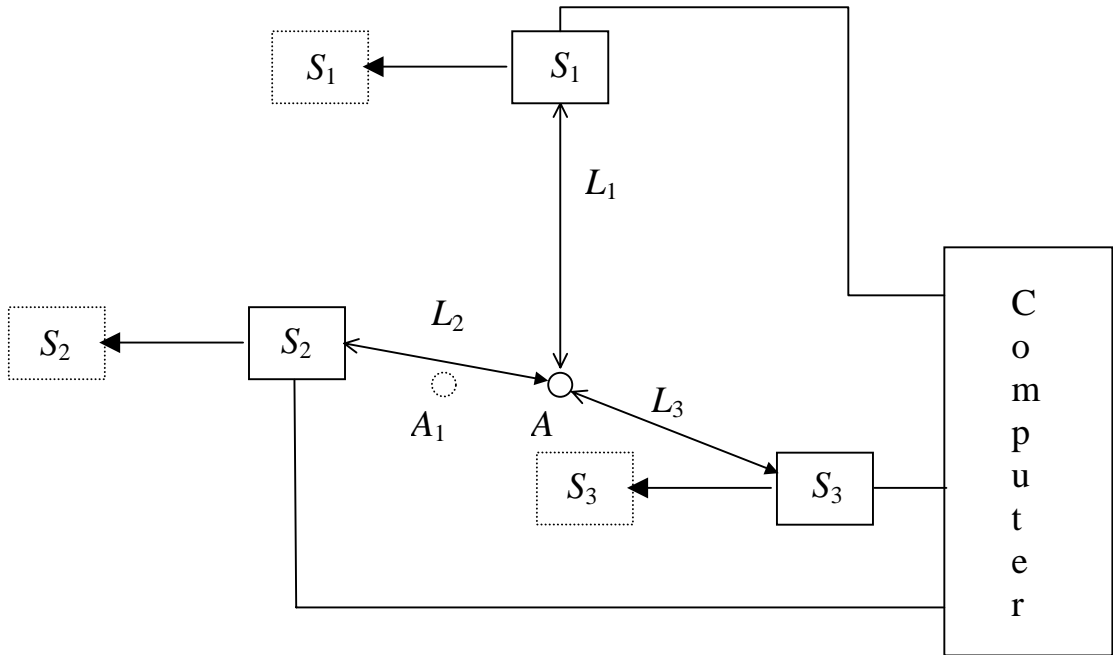


Figure 1: Explanation of method of forecasting.

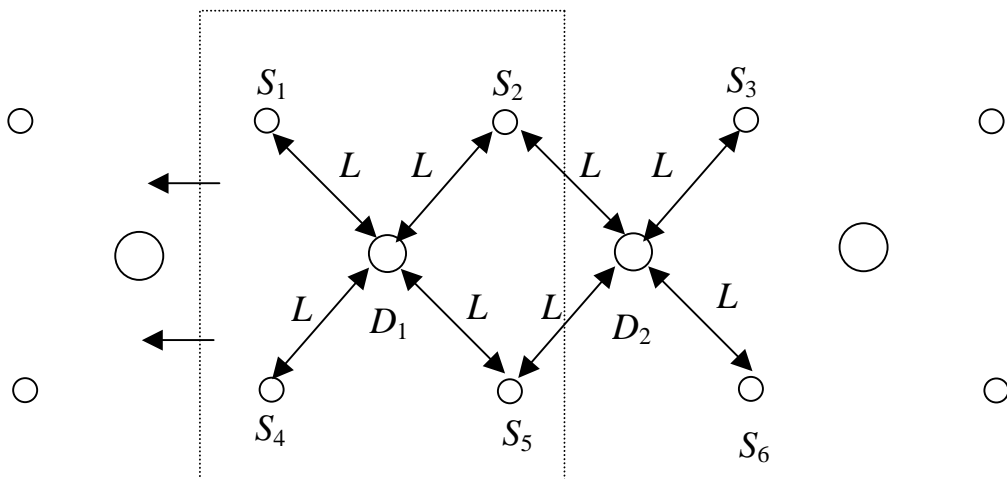


Figure 2: Movement of the contour across the net of sensors.

## Recognizing postseismic transients with GPS at the Central Nevada Seismic Belt

William C. Hammond  
NASA Postdoctoral Fellow  
*Earthquake Hazards Team*  
U.S. Geological Survey MS/977  
Menlo Park, CA 94025  
bhammond@usgs.gov

In the 20<sup>th</sup> century, at least six  $M > 6$  earthquakes occurred in central Nevada, organized in a quasi-linear roughly north-south sequence. The region of these ruptures has become known as the Central Nevada Seismic Belt (CNSB), and today experiences elevated levels of crustal seismicity and geodetically measured deformation compared to the rest of the Basin and Range province. Whether the elevated rates of activity imply ongoing elevated seismic hazard depends on the physical mechanism that causes this deformation. For example, interseismic strain accumulation will tend to increase seismic hazard with time, while postseismic stress relaxation processes generally will not. Thus, distinguishing the effects of interseismic strain from relaxation at the Central Nevada Seismic Belt is crucial for evaluating seismic hazard.

Our group has made geodetic measurements with the Global Positioning System (GPS) between 1992 and 2003 across the entire Basin and Range province, including the vicinity of the CNSB. I present a synthesis of horizontal GPS velocities obtained from a combination of data from campaign-mode measurements and continuously recording sites, as well as a strain rate model that is derived from these velocities. The geodetic transect suggests that the east-west extension rate has a pronounced maximum at the CNSB. One of a few possible interpretations of this anomaly is that viscoelastic relaxation following the 20<sup>th</sup> century events contributes to the modern geodetic deformation field. This hypothesis is supported by a recently published modeling study predicting a similar east-west extension rate from viscoelastic relaxation of the lower crust and upper mantle (*Hetland and Hagar, 2003*), and by measurements made with Interferometric Synthetic Aperture Radar, (InSAR) (*Gourmelen and Amelung, 2003*). A constraint on the relative contributions from viscoelastic relaxation and interseismic strain accumulation can be made by assuming that relaxation explains the factor of ~2 discrepancy between geodetically and paleoseismologically inferred slip rates. In this way I evaluate the limit to which postseismic relaxation contributes to the geodetically observed deformation field, and improve understanding of seismic hazard as inferred from geodesy.

Gourmelen, N., and F. Amelung (2003), Anomalous crustal deformation in the Central Nevada Seismic Belt detected by InSAR, *Eos Trans. AGU*, 84(46).  
Hetland, E.A., and B.H. Hagar (2003), Postseismic relaxation across the Central Nevada Seismic Belt, *J. Geophys. Res.*, 108(B8), doi:10.1029/2002JB002257.

## Quaternary Fault and Fold Database and Map of Utah

Hylland, M.D., Utah Geological Survey, P.O. Box 146100, Salt Lake City, Utah 84114-6100,  
mikehylland@utah.gov.

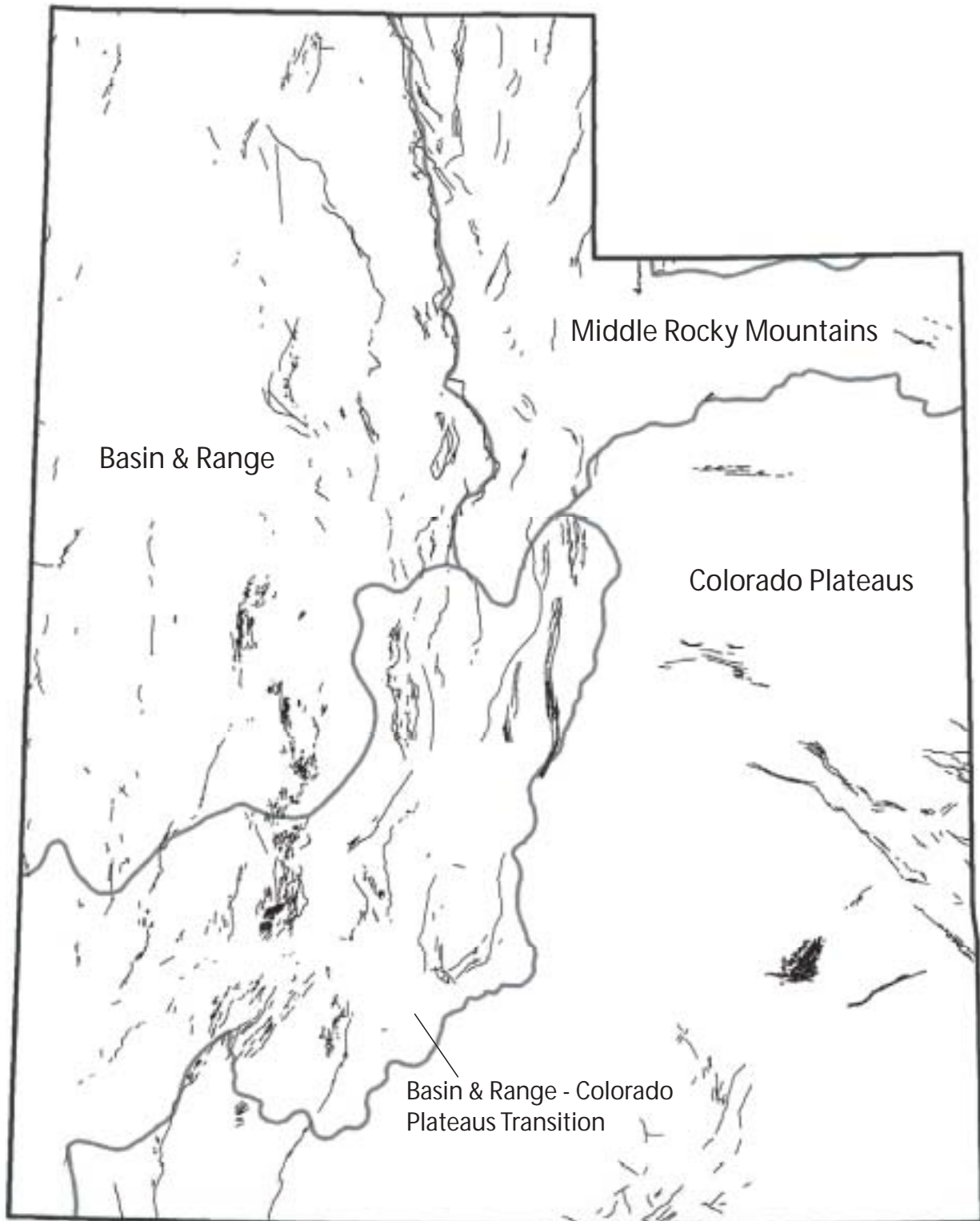
The *Quaternary Fault and Fold Database and Map of Utah* is the most up-to-date and comprehensive source of information on Quaternary faults and folds in Utah. This compilation by Utah Geological Survey (UGS) and U.S. Geological Survey (USGS) authors is the result of a cooperative effort to provide data for the USGS national database of active faults. The Utah database contains entries for 212 faults, fault sections, and fault-related folds. Data include location and mapping information; geologic and geomorphic descriptions; physical characteristics including length, average strike, sense of movement, and dip; and information pertinent to earthquake-hazard studies including timing of most recent paleoevent, recurrence interval, and slip rate. The database also includes summaries of paleoseismology (largely trenching) studies; such studies have been conducted on 33 faults in Utah.

The database has three structural categories of faults and fault-related folds: (1) simple (faults having synchronous rupture and a single structural style), (2) sectioned (related faults and fault sections that may or may not be synchronous or of a single structural style, and segmented faults that have well-defined seismic or structural segments acting independently of one another), and (3) suspected (faults of uncertain seismogenic potential). Most faults in Utah are simple faults having normal displacement, uncertain or low slip rates (<0.2 mm/yr), and unknown or long recurrence intervals (>1000 yr), and generally conform to characteristic regional faulting patterns. In the Basin and Range Province, east-west late Cenozoic extension formed many north-south-trending range-front normal faults. In the Colorado Plateaus, the sense of faulting includes normal slip, strike slip, and oblique slip. In the Middle Rocky Mountains, normal faults bounding intermontane grabens are common. Suspected faults are generally in the Colorado Plateaus, mostly associated with collapse due to salt dissolution, and in the Basin and Range, associated with Quaternary volcanism and other non-tectonic causes. Other Basin and Range faults may sole into shallow, low-angle detachments and may not be capable of generating strong ground motions. Long sectioned faults are mainly in the Basin and Range and Middle Rocky Mountains provinces. The Wasatch fault zone is the longest sectioned (segmented) fault, and the most active fault, in Utah; central segments show evidence for repeated Holocene activity and have slip rates approaching 2 mm/yr. Other faults active in the Holocene are mostly in the Wasatch Front area of northern Utah and generally have slip rates of 0.2-1 mm/yr.

The map and database are available on compact disc, as well as on the UGS Web site ([geology.utah.gov](http://geology.utah.gov)). Updates are incorporated into the database on a regular basis. The database is presently being updated with consensus slip rates and recurrence intervals developed by a panel of experts for Utah's 33 relatively well-studied faults. The full reference citation for the map and database is as follows:

Black, B.D., Hecker, S., Hylland, M.D., Christenson, G.E., and McDonald, G.N., 2003, Quaternary fault and fold database and map of Utah: Utah Geological Survey Map 193DM, compact disc.

# Quaternary Fault and Fold Map of Utah



# Dating sinter deposits in Dixie Valley, Nevada: A record of hot spring-fault interaction in the great basin

Susan Juch Lutz<sup>1</sup>, and S. John Caskey<sup>2</sup>

1. Energy & Geoscience Institute, Univ. of Utah, Salt Lake City, UT; sjlutz@egi.utah.edu

2. Department of Geosciences, San Francisco State Univ., San Francisco, CA; caskey@sfsu.edu

## ABSTRACT

The Dixie Valley geothermal field occurs in an area known as the “Stillwater seismic gap”, a 45 km-long section of the Dixie Valley fault that lies between the 1915 ( $M_s$  7.7) Pleasant Valley and 1954 ( $M_s$  6.8) Dixie Valley fault rupture zones to the north and south, respectively (Figs. 1 and 2). Fossil hot spring deposits are exposed at the Stillwater range front just south of the producing geothermal field, at the northern extent of a late Holocene rupture zone along the Dixie Valley fault. These deposits are composed of both travertine and siliceous sinter that have trapped pollen and other organic materials during their formation. Radiocarbon dates on the organic material indicate that the youngest hot spring deposits in the Section 10/15 sinter area are between 3.4 and 2.5 ka. Clasts of quartz sinter in diatomite at the Dixie Comstock hot-spring gold mine yielded a  $^{14}\text{C}$  age of 10,722  $\pm$  70 years BP, approximately coeval with pluvial Lake Dixie that filled Dixie Valley at 11-12 ka. The mineralogy and texture of the siliceous sinters are consistent with their age. The youngest deposit consists of hyaline “geyserite” that likely formed from actively spouting eruptions of boiling fluids along the fault zone at about 2.5 ka. X-ray diffraction analyses (Fig. 3) indicate that the sinter is composed of original opal-A which has not undergone the transition to the more crystalline opal-CT or cristobalite (opal-C). Slightly older (2.2 to 3.4 ka) sinters appear to be admixtures of opal-CT, and microcrystalline quartz. Sinter clasts at the Dixie Comstock mine have completely transformed to quartz. The process of maturation or “aging” of the sinter (the transformation from juvenile opal-A to crystalline quartz) appears to occur within 11,000 years.

There are three parts of the geyserite-sinter deposit: the upper geyserite, steeply-dipping outflow channels that mantle the range front, and a shallowly-dipping apron terrace where the sinter is interbedded with marsh deposits at the base of the slope. The lower sinter terrace is broken by a fault that has vertically displaced the footwall from the hanging wall by about 3 meters (Fig. 4). Radiocarbon dating of sinter samples from both sides of the fault yielded ages of about 2.5 ka, indicating a maximum age for the surface-rupturing earthquake. Trench studies previously bracketed the age of the earthquake (“The Gap”  $M_w$  7 event) between 3.7 and 2.0 ka. This portion of the Dixie Valley fault, just a few kms southwest of the producing geothermal field, appears to have been actively discharging geothermal fluids until about 2.5 ka when fault rupture and associated stress changes related to The Gap earthquake effectively put an end to the hot spring activity. The 3.4-2.5 ka spring activity may have been related to a period of increasing tectonic stress and fracture dilatancy *preceding* The Gap event.

Steam now emanates from the fault zone and small fumaroles occur locally along The Gap surface rupture. The transition from hot spring activity before the earthquake to fumarole activity after the earthquake suggests deeper boiling at a lowered water table within the fault zone, and fluid pressure reduction and stress drop as a result of the surface rupture (Caskey and Wesnousky, 2000). The present-day stress regime based on borehole studies in nearby well 66-21 (Hickman et al., 1997; Barton et al., 1998), indicate that fractures and faults near the well are not critically stressed for frictional failure. Even though the faults and fractures in well 66-21 were found to be optimally oriented for normal faulting, a high ratio of  $S_{hmin}$  to  $S_v$  appears to have a great effect on the fracture permeability in this nonproductive well. The observed sequence of hot spring and faulting activity at Dixie Valley is consistent with modern earthquake theory and fracturing dynamics in normal fault zones (Sibson, 1986; Parry and Bruhn, 1990; Bruhn et al, 1994) which predict a period of dilatancy before frictional failure and earthquake rupture. This period of dilatancy may relate to periods of high permeability and hot spring activity along the Dixie Valley fault. The episodic nature of the hot spring activity is revealed by the range of ages of the thermal spring deposits in the area, as well as the variation in silica mineralogies and maturation.

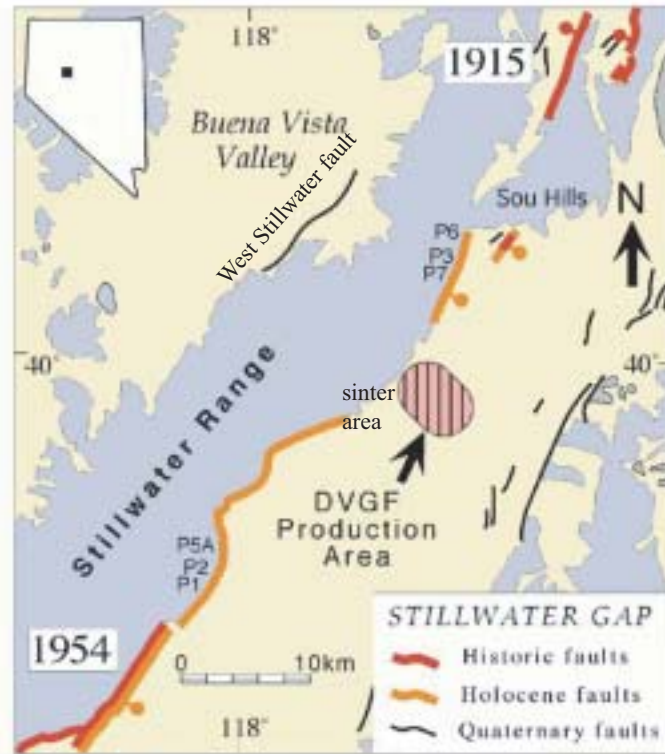


Fig. 1. Generalized fault map of the Stillwater Gap area showing the distribution of the historic 1915 M7.7 Pleasant Valley and 1954 M6.8 Dixie Valley fault ruptures (bold dark lines), Holocene ruptures (bold light lines) and Quaternary faults (thin black lines). The Dixie Valley geothermal field (DVGf) occurs in an area where recent fault scarps are not recognized (Caskey and Wesnousky, 2000). Fossil hot spring sinters occur at the northern endpoint of surface ruptures that are Holocene in age, just south of the Dixie Valley production area.

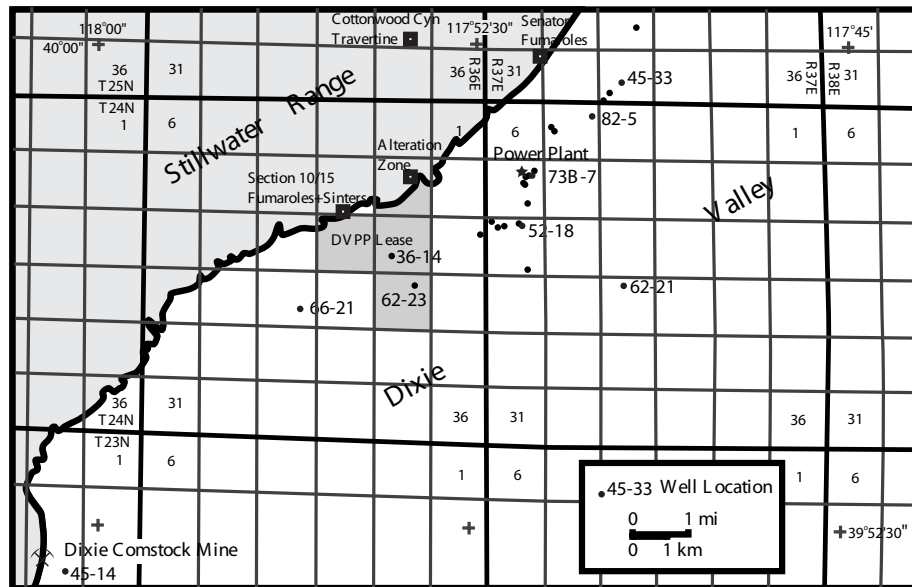
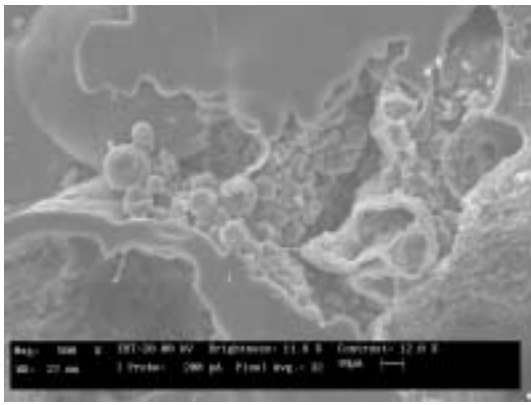
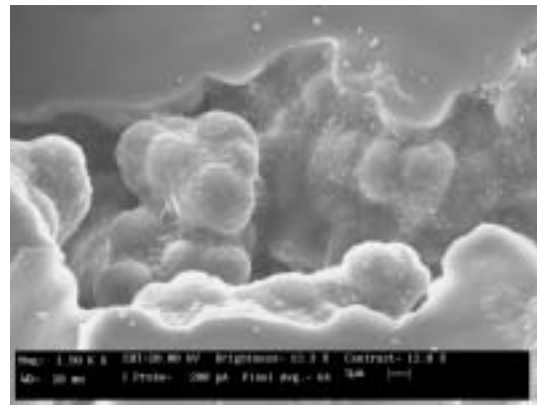


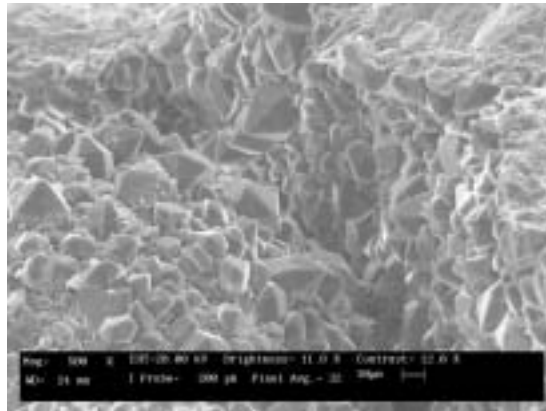
Fig. 2. Location of selected wells in the Dixie Valley geothermal field, and travertine and sinter sample localities along the eastern Stillwater range front in northern Dixie Valley, Nevada. Fossil hot spring sinter deposits occur along the surface trace of the Dixie Valley fault in Sections 10, 11 and 15 of R36E T24N in Churchill County.



Opal-A



Opal-A to Opal-CT



Microcrystalline Quartz

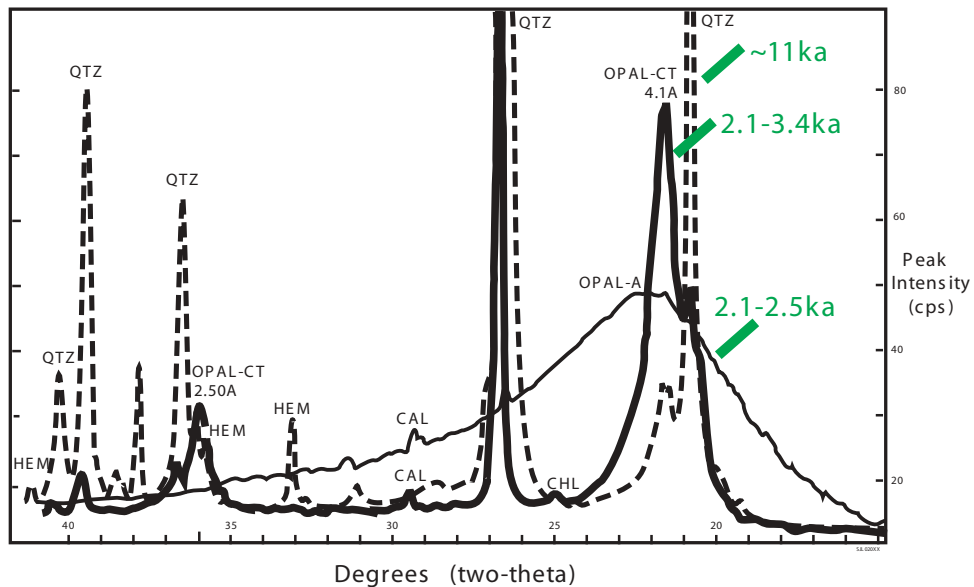


Fig. 3. Scanning electron microscopy (SEM) images and X-ray diffraction (XRD) patterns of three sinter samples, illustrating characteristic silica mineralogies and the general age of each deposit. The thin black line is the XRD pattern of a young geyserite sample that is composed of noncrystalline opal-A with traces of calcite (CAL). The thick black line represents a sinter sample from Section 11 that contains paracrystalline opal-CT, crystalline quartz (QTZ), and traces of chlorite (CHL) and calcite (CAL). The lower sinter terrace in Section 11 (dashed line) is predominantly composed of crystalline quartz with minor amounts of opal-CT and hematite (HEM).



Fig.4a. The Section 15 sinter deposit is composed of steeply-dipping "geyserite" proximal to the hot spring vent (see light-colored area at the right of the person), and a shallowly-dipping outflow apron (in foreground). The Section 10/15 geyserite-outflow apron sinter drapes steeply over Jurassic footwall rocks near its vent and dips more gently as an outflow apron towards the valley, cementing fluvial and alluvial gravels at the mouths of small gullies.

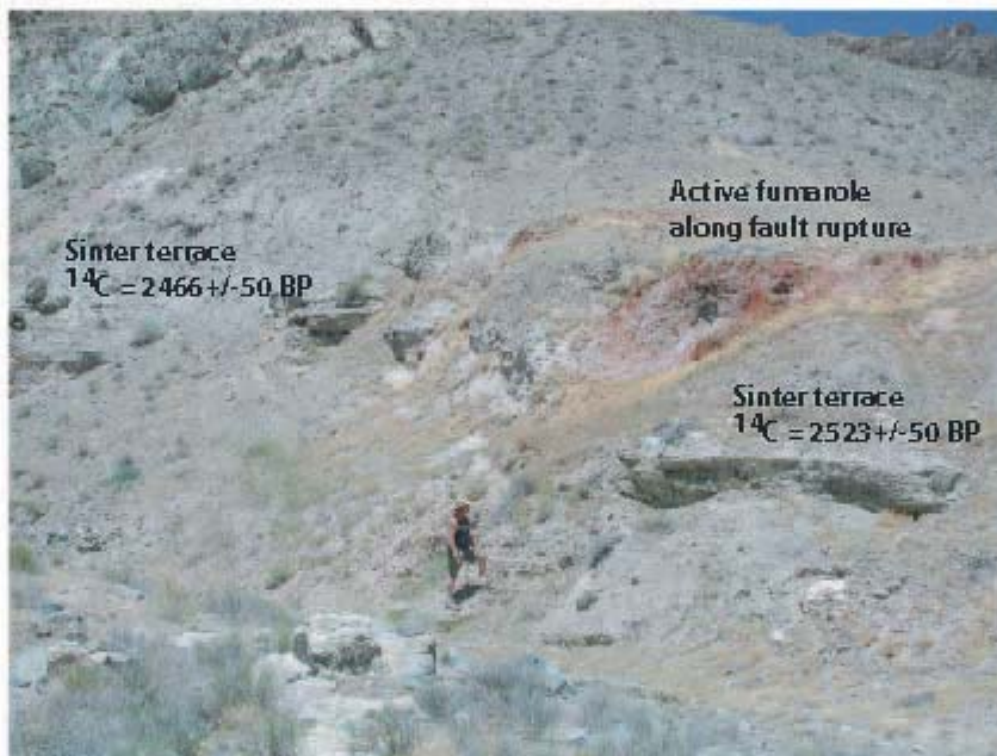


Fig.4b. Faulted sinter terrace in Section 10. The sinter terrace is vertically offset by 3 meters. The fault here represents surface rupturing at the range front-valley interface related to "The Gap" M7.1 earthquake. The age of the terrace at about 2.5 ka constrains the age of the The Gap earthquake to between 2.5 and 2.0 ka (previous trench dates had bracketed the age of this event between 3.7 and 2.0 ka; Caskey, 2002).

# QUATERNARY FAULT DATABASE FOR THE BASIN AND RANGE PROVINCE OF NEVADA AND UTAH

Michael N. Machette, Kathleen M. Haller, B. Susan Rhea, and Richard L. Dart; U.S. Geological Survey, MS 966, Box 25046, Denver, CO 80225-0046 (machette@usgs.gov)

The USGS has completed a comprehensive compilation of data related to Quaternary faults and folds that are potential seismic sources for large surface-rupturing earthquakes throughout the U.S. The compilation consists of an extensive database (i.e., ca. 10,000 p.) and accompanying maps of Quaternary faults and folds that are accessible via the Internet (see <http://Qfaults.cr.usgs.gov/>). The data for the Basin and Range (B&R) Province will be very useful to compare Quaternary geologic deformation rates with GPS-derived geodetic strain rates (e.g., NSF's Earthscope Plate Boundary Observatory).

This poster features a new map of Quaternary faults and folds of the B&R Province in Nevada and Utah, as well as global positioning satellite (GPS) stations (USGS, Cal Tech, and Univ. of Utah) and paleoseismic study sites. Current campaign-style and continuous GPS stations are now widely distributed across the northern B&R Province, whereas paleoseismic studies have been concentrated mainly along the Utah part of the Intermountain Seismic Belt, the Central Nevada Seismic Belt, and the Yucca Mountain area of southern Nevada.

The Quaternary fault and fold map shows the time of most recent faulting or folding, sense of fault movement, slip- or uplift-rate category, and a numeric identifier that links to the text database. The GIS map data are maintained in ArcInfo on a Unix server and linked to a File Maker Pro web database that contains comprehensive written descriptions of the features, several examples of which are displayed on this poster. More than 1,000 Quaternary faults are shown on the map, most of which are in the highly extended B&R Province of Nevada and western Utah.

To visually distinguish potential earthquake sources, we categorized the time of most recent surface rupture on the faults as <1.6 Ma, (Quaternary, colored black on poster), <750 ka (middle and late Quaternary, blue), <130 ka (late Quaternary, green), <15 ka (latest Quaternary, orange), and historic (<200 yrs, red). The late Quaternary time frame is probably the most relevant for seismic-hazards assessments because it spans multiple earthquake cycles on most Basin and Range extensional faults. The slip-rate categories (mm/yr) are binned to distinguish between relatively inactive faults (<0.2, thin lines) and active normal faults (0.2-1, medium lines), and between moderately active (0.2-1) and quite active (>1, thick lines) normal, oblique and strike-slip faults. With few exceptions, the only faults having slip rates that exceed 2 mm/yr are the Holocene strike- or oblique-slip faults in the western part of the B&R Province.

The data used to make this poster are available from our website, which utilizes two map interfaces tailored to a different users. The static-map interface is based on states (e.g., Nevada) or regions (e.g., Eastern U.S). Clicking on a state brings up the state map showing all of the 1°x 2° sheets for the state. Each of these sheets covers an area about 120 miles wide (E-W) and 60 miles high (N-S). Clicking on a sheet brings up a shaded relief map of the area showing all of its Quaternary faults. Each fault is numbered and linked to a text description via a look-up table that is shown below the map. The static map images are small (typically 30 kb), so they load and refresh quickly using a standard dial-up modem, which is still the typical method of connecting to the Internet.

The second map interface is dynamic and utilizes ArcInfo's Interactive Map Server (IMS) software to link the GIS data to our fault and fold database. The interface loads a shaded-relief base map of the U.S. and a series of user-controlled layers, such as streams, roads, and towns, as well as the trace of the Quaternary faults and folds. The IMS tools allow users to zoom, pan, query, and link to the database. This powerful interface loads large images and requires high-speed Internet access. Clicking on individual faults or folds with the information tool leads one to the text descriptions, which are running on the independent FileMaker Pro database described previously.

Much of the information in the database is based on paleoseismology, which is the geologic study of prehistoric earthquakes. Paleoseismology combines geologic tools such as trenching with archeological-style analysis to determine the times and sizes of ancient earthquakes of the Quaternary period. This extended record of earthquakes is extremely helpful in assessing the potential hazard posed by the thousands of Quaternary faults in the United States.

The web site is designed to fulfill the needs of a broad group of users ranging from the science community to the general public. The database is the primary source for USGS seismic-hazards information on faults and fault-related folds in the United States, providing geologic information on the probable sources of past, current and possible future surface-rupturing or surface-deforming earthquakes of magnitude 6 or greater.

Note: The data for Nevada were mainly compiled by employees of the USGS and Piedmont Geosciences (Reno, Nevada), whereas the data for Utah were compiled by the Utah Geological Survey. This work was funded by the National Earthquake Hazards Reduction Program, either internally (USGS) or as part of the externals grants program. Cooperators for this effort, which are too numerous to list herein, are shown on the website. The authors of this poster managed the larger National effort, and facilitated and reviewed the compilations.

## **“Critique and Use of Historical Methodology in Seismic Hazards Analyses of Earthquakes in the Basin and Range; Expanding the Historical Catalog and the Search for Triggered Events from the San Andreas Fault.”**

Dawn C. Martindale, Department of History, Utah State University, Logan, Utah, dcmartindale@yahoo.com  
James P. Evans, Department of Geology, Utah State University, Logan, Utah.

In recent years the use of historical methodology introduced and integrated into seismic studies of the Basin and Range has resulted in two outcomes. The first consists primarily of crucial analytical updates of moderate large earthquakes leading to increased understanding in the nature of shaking. The second result includes the location of new earthquakes previously not listed in earthquake catalogs and scholarly publications, with possible reference to triggered events from the San Andreas Fault.

We examine single event records that convey information addressing displacement, damage and other distinct attributes of shaking for large Western United States earthquakes. A prime example of the use of this methodology is our reexamination of the 1884 Bear Lake, Utah earthquake. Original estimates stated the 1884 event to encompass roughly 15,600 km<sup>2</sup> and an MMI intensity range between four and eight. Utilizing historical research methods, including examining additional newspapers, personal journals, local photographs, archival collections, and historical-society documents new estimates of the initial and subsequent shocks surfaced. Intensity range increased to between two and ten and the felt area expanded to encompass roughly 44,200 km<sup>2</sup>. A more intriguing result included the relocation of the inferred epicenter from the southeast location of Bear Lake to the northwest side near Paris and Liberty, Idaho. This places the earthquake on an antithetic normal fault in the hanging wall of the east-dipping Bear Lake fault. Other interesting data included direction, length and time of the initial and subsequent shocks.

During the reanalysis of the Bear Lake earthquake primary sources also led to the discovery of six additional earthquakes in Utah not previously listed in catalogs. Application of similar methodology is currently being utilized to update the nineteenth-century earthquake catalogs and further understand the seismic hazard threat in Utah.

We use similar methodology to reexamine the 1857 Fort Tejon, California earthquake. We have found 150 additional felt reports beyond the ones listed by previous scholars. Similar results to those of Bear Lake are anticipated as initial analysis is being processed. We also infer that earthquakes in Beaver, Utah, February 1857 and Western Nevada, September 1857 may be related to large aftershocks or the main rupture of the Ft. Tejon event. Both shocks are currently under review, using historical methodology, to further understand the relationship and relevance to the 1857 event and the nature of triggered events in the Basin and Range area.

Methods and techniques used by historians, specifically an extensive review of archival and historical society materials, along with a historiography of previous work, serve a crucial role in assisting seismologists in further understanding the significance and implications of seismic events in the pre-instrument era.

Summary of Felt Reports

Location	Intensity	Time of 1st Quake	Length of 1st Quake	Direction 1st Quake Felt	Heard Noise Prior	# of Aftershocks (Nov 10)	# of Aftershocks (Nov 11-13)
<b>Wyoming</b>							
Evanston	—	—	—	—	—	—	—
Fort Bridger	III-IV	2:00 AM	5-10 Sec	W to E	—	—	—
<b>Utah</b>							
Brigham City	III	1:40 AM (T)	10 Sec	N to S	—	—	(1)*
Laketown	IV	2:00 AM	10 Sec	—	—	—	—
Lewiston	IV	Abt 2 AM	—	—	—	—	—
Logan	IV	Bf 2 AM	Few Mins.	—	—	2	(1)*
Ogden	IV	—	—	Follow Mts	—	—	—
Randolph	III-IV	—	—	—	—	—	—
Richmond	IV--VII	1:55 AM	—	—	yes	—	—
Salt Lake	IV	1:55/ 2 AM	30 Sec 10-15 Sec	E to W N to S	yes	—	—
<b>Idaho</b>							
Battle Creek/ (Franklin)	IV-V	—	—	—	—	—	—
Blain/ Little	IV	—	—	—	—	(Several)	—
Wood Valley	—	—	—	—	—	—	—
Bloomington	IV	1:58 AM	—	E to W N to S	yes	2 (in AM)	—
Gentile Valley	V	AFT 1:30AM	—	—	yes	3--5	1- Wen (am)
Georgetown	V	2AM	12-15 SEC/ (1-7 MINS)	—	yes	3	—
Liberty	VI-VII	1:52 AM	—	NW to SE	yes	21 (in AM)	2+ (Tue PM)
Montpelier	IV	1:56/7 AM	10-15 SEC	—	yes	2 (In AM)	—
Paris	VII-X	1:50/1:53 AM	30+ SEC	NW to SE	yes	6 (in AM)	2-tue (am) 3 Wen (-) 2- Thur (am)
Pocatello	IV	—	—	—	—	—	—
St. Charles	IV	1:55 AM	30 SEC	N to S	—	—	—
Soda Springs	IV	—	—	—	—	—	—

Figure 1. Summary of Felt Reports, 1884 Bear Lake, Utah Earthquake

Location	Intensity (MMI)	Time of 1st Shock	Length of 1st Shock
<b>Nevada</b>			
Las Vegas	II,III	9 A.M	30 seconds
Potsi Lead Mines	I	in morning	---
<b>California</b>			
Benicia	---	---	---
Benson's Ferry	V, VI, VII, X	---	---
Fort Tejon	III, VII, VIII, X, XI, XII	8:30 AM	3 to 5 mins
- 1 mi N	VIII	---	---
- betn Fort and Lake Elizabeth	XII	---	---
Fort Miller	Felt	---	---
Fort Tejon Mill	VII, VIII	---	---
Iowa Hill	---	---	---
Kern Lake	X	---	---
Kern River	VII, X, XII	---	---
Lake Hughes/Mill Potrero	IX+	---	---
Los Angeles	III, V, VI, X	8:25 am; 8:30 am	2 mins
Millerton	II	---	---
Marysville	Felt	---	---
The Mohave	III+	---	---
Mohave River	III, VII	bwtn 8-9 am	30-40 sec
Mokelumne Hill	IV, V	---	---
Monte	VII, VIII	---	---
Monterey	III+	7:00 AM	---
Mouth of Colorado River	V?	---	---
Reed's Rancho	X-XI	---	---
Sacramento	II, V, VI	7:45, 8:05, 8:15, 8:19	2-3 mins, few sec, under 4 min
Salinas River	VI	---	---
San Benito Ranch	VI-VII?	---	---
San Benito and River	VI-VII	---	---
San Bernardino	II, III, V, VI, VII, X	8:08 am, 8:25 am	almost 3 mins
San Buenaventura	VII+	---	---
- 30 miles SE (canyon)	IV-V	8:24 AM	2 mins
San Diego	III, VI, VIII	8:30 am, 8:45 am	several mins
San Fernando	VII	---	---
San Francisco	IV-VIII	8, 8:14, 8:15 am	---
SF Cont			
San Gabriel River	VII	---	---
San Jose	IV-V	8:05, 8:30 am	1 min
San Juan	---	---	---
San Pedro	VIII	---	---

**Figure 2.** Summary of Felt Report, 1857 Fort Tejon, California Earthquake (Condensed version)

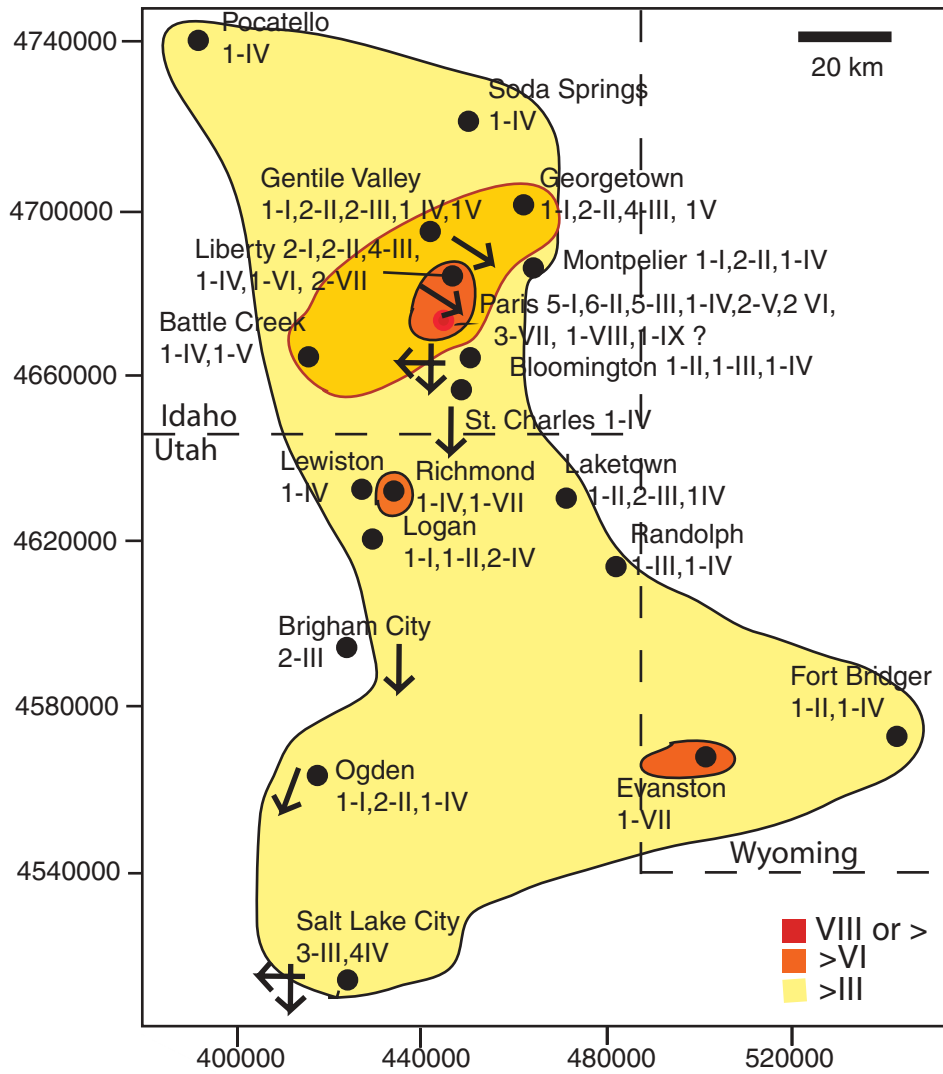


**Figure 3.** Kreiged Contour Map of Mercalli Intensities based on Individual Felt Areas from the 1884 Bear Lake, Utah earthquake.

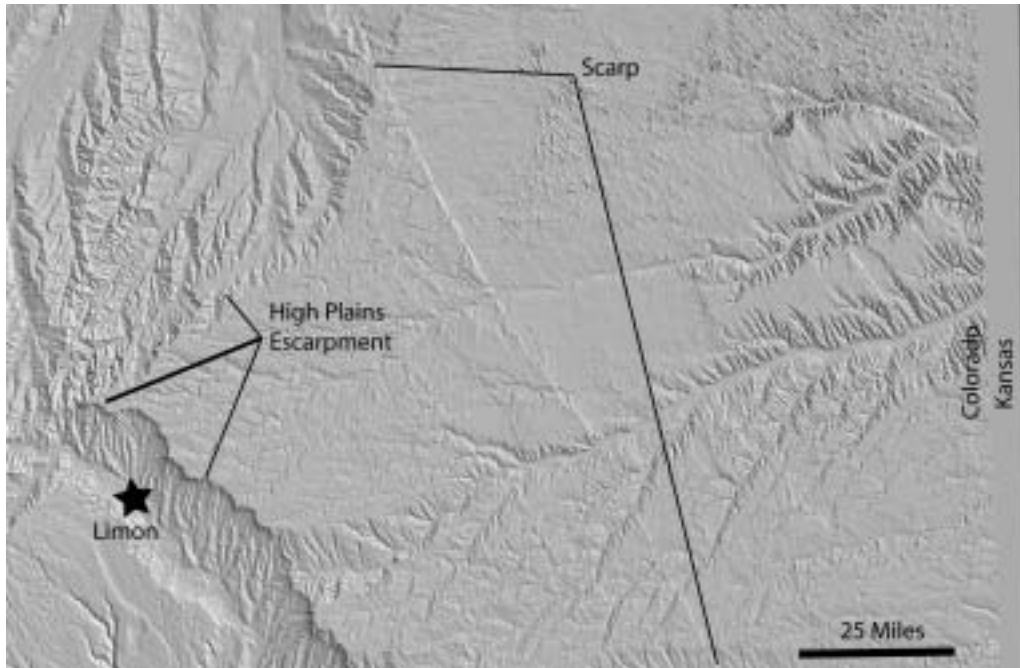
## **Horsts and Grabens of Colorado's High Plains**

Vince Matthews, Colorado Geological Survey, Denver, Colorado  
Matthew Morgan, Colorado Geological Survey, Denver, Colorado

The prevalent view of Neogene deformation in the Great Plains contends that it is limited to gentle, eastward tilting during uplift of the Southern Rocky Mountains. This deformation is commonly characterized as part of nothing more than a broad up-warping of the whole region. Faulting was thought to play only a minor role in the deformation— either within the mountains or the plains. However, experimental and theoretical rock mechanics suggest that deformation such as this should be accomplished by brittle, rather than ductile, deformation in the upper crust.

Documentation of brittle, Neogene and Quaternary deformation in the Colorado Rockies, on discrete faults with displacements of thousands of meters, raised the question of whether the accompanying deformation in the Great Plains was also accomplished by faulting. Several lines of evidence indicate that Neogene and Quaternary faulting are an important deformational component in the Great Plains.

A digital elevation model reveals a major graben 25 miles wide. The eastern scarp is 95 miles long and 70 to 100 feet high. Geomorphologic and geologic analysis of the High Plains reveals smaller horst and graben structures occurring over large areas. These features have significance for groundwater, earthquake hazard, and hydrocarbon accumulation.



Digital elevation model (V.E. 8X) of Colorado's eastern High Plains. The High Plains surface dips gently toward the east and roughly approximates the top of the Miocene Ogallala formation. The town of Limon is 70 miles east of the mountain front. The noted scarp is 70–100 feet high and at least 95 miles long.



First order trend surface residual map made from the above DEM. This map highlights a major graben that is about 25 miles wide. The following images show eastern and western scarps forming this graben.



View of 80-foot-high scarp on western edge of graben.



View of 70-foot-high scarp on eastern edge of graben.

## ESTIMATING SLIP RATES AND RECURRENCE INTERVALS FOR QUATERNARY FAULTS IN THE BASIN AND RANGE PROVINCE, USING GEOLOGIC DATA

McCalpin, James P., GEO-HAZ Consulting, Inc., P.O. Box 837, Crestone, CO 81131 mccalpin@geohaz.com

Slip rates and recurrence intervals for Quaternary faults can be estimated from either geomorphic data or from subsurface (trench) data, but the data must be treated differently to produce meaningful estimates of the mean and variance. Total uncertainty in these paleoseismic parameters is the product of both the uncertainty in measuring fault displacement and age (measurement uncertainty) and fault rupture variability between one seismic cycle and the next in time and space (intrinsic variability).

When using geomorphic data such as fault scarp heights, we know the following:

KNOWN

1. total (vertical) displacement at a point
2. vertical displacement along strike
3. age of displaced landform

UNKNOWN

1. number of displacement events
2. exact timing of displacement events

An advantage of geomorphic data is its along-strike continuity, thus we can measure an “average” fault scarp height on each of the faulted datums along the fault’s length. For representing the seismic moment of paleoearthquakes, this average displacement is a robust measurement. A disadvantage is that any slip rate calculated as total displacement/age of landform is a minimum slip rate, because the slip may have accumulated/been released in only part of the cited time span. In general, uncertainty in timing will be larger than uncertainty in displacement. Without knowing the number and timing of paleoearthquakes, no interval recurrence intervals can be estimated. However, a maximum estimate of long-term average recurrence interval can be made, given some assumptions.

When using subsurface data such as trench data, we typically know the following:

KNOWN

1. number of displacement events
2. displacement of each event at a point
3. exact timing of displacement events at that point

UNKNOWN

1. vertical displacement along strike

An advantage of trench data is that we know the age and displacement of individual paleoearthquakes, thus we can compute “interval slip rates” that cover discrete seismic cycles. Using a slip history diagram, we can graphically portray slip rates from closed and open seismic cycles. A disadvantage is that any slip rate calculated is only valid for that one point on the fault, and is difficult to relate to the average slip rate of the entire fault. In general, uncertainty in displacement will be larger than uncertainty in timing. Recurrence intervals can be dated directly, and given a long enough record (10 paleoearthquakes), may be sufficient to extract the intrinsic variability component out of the total uncertainty.

# PREHISTORIC EARTHQUAKES ON THE HUBBELL SPRING FAULT: EVIDENCE FOR COSEISMIC NONCHARACTERISTIC RUPTURE OF INTRABASIN FAULTS IN THE RIO GRANDE RIFT

Susan S. Olig<sup>1</sup>, Martha C. Eppes<sup>2</sup>, Steven L. Forman<sup>3</sup>,  
David W. Love<sup>4</sup>, and Bruce D. Allen<sup>5</sup>

The Hubbell Spring fault (HSF) is an intrabasin fault near the eastern margin of the Albuquerque-Belen basin in the central Rio Grande rift, and is one of the most active faults in the region. Recent mapping and geophysical studies indicate that the fault geometry is more complex and longer than previously thought, with two dominant subparallel west-dipping splays (western and central) extending for over 40 km south of Albuquerque (Figure 1). An enigmatic eastern splay appears buried along its southern 2/3 and may be older than late Quaternary, with possibly a much longer history of deformation than the rest of the HSF. We conducted a paleoseismic investigation at the Carrizo Spring trench site on the central HSF (Figure 1) that included mapping, trenching drilling and luminescence analyses (Olig *et al.*, 2004). We found structural, stratigraphic, and pedologic evidence for the occurrence of at least 4, and probably 5, large earthquakes that occurred since deposition of piedmont deposits on the Llano de Manzano surface about  $83.6 \pm 6.0$  ka. All of these events included warping across a broad deformation zone, whereas the 3 largest events also included discrete slip across five fault zones. The total down-to-the-west throw of piedmont deposits is  $7.3 \pm 0.5$  m. Behavior appears non-characteristic, with preferred vertical displacements per event ranging from 0.4 to 3.7 m. Fault-related deposition was dominated by eolian rather than colluvial sedimentation, similar to previous trench studies of other faults in the region (e.g., Personius and Mahan, 2003). Luminescence ages indicate that the timing of the 4 largest surface-deforming events on the central HSF overlaps with the timing of the four youngest faulting events on the western HSF (Figure 2), suggesting coseismic rupture of the central and western HSF. Displacement data and correlation between sites of buried soils on event horizons also supports coseismic rupture. The smallest warping event on the central HSF does not appear to correlate to any events on the western HSF, indicating that independent rupture of the central HSF also does occasionally occur. However, we estimate that over 96% of the late Quaternary strain on the HSF occurred as coseismic rupture of the western and central splays. The average recurrence interval for coseismic rupture over the past 3 complete seismic cycles is 19 (+5, -4) ky, consistent with recurrence intervals estimated for individual cycles, which are 17 ky, 27 ky, and 14 ky (Figure 2). Assuming the eastern splay is no longer active, we estimate a cumulative average vertical slip rate for the past 4 complete seismic cycles on the HSF of about 0.2 mm/yr, one of the highest late Quaternary rates in the region. In comparison, slip rates for individual complete seismic cycles vary by an order of magnitude, ranging from 0.044 mm/yr to 0.46 mm/yr (Figure 3). This is due to noncharacteristic behavior, a finding that may have significant implications for

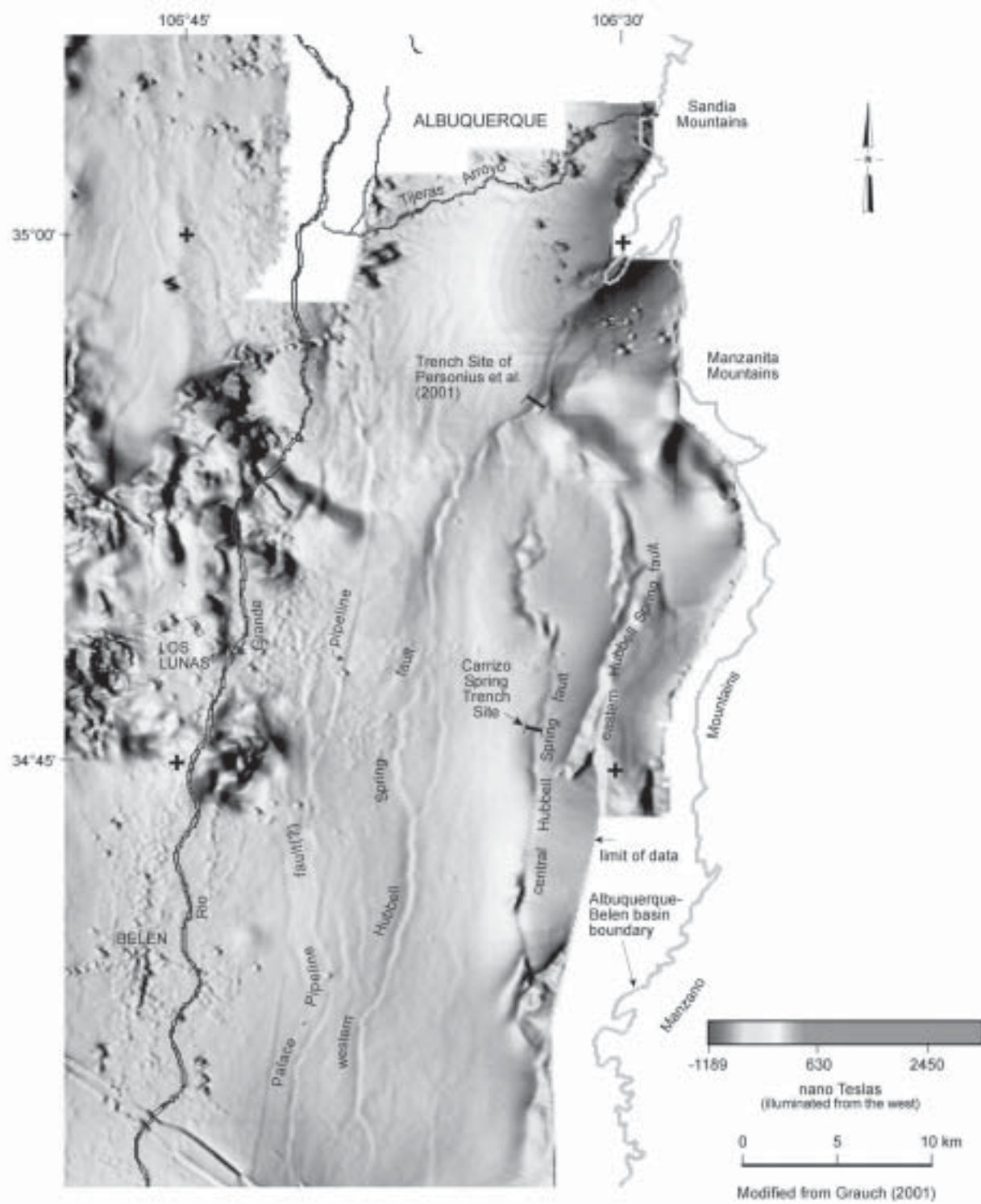


**Figure 1.** Shaded-relief aeromagnetic map (from Grauch, 2001) showing trench sites on the Hubbell Spring Fault.

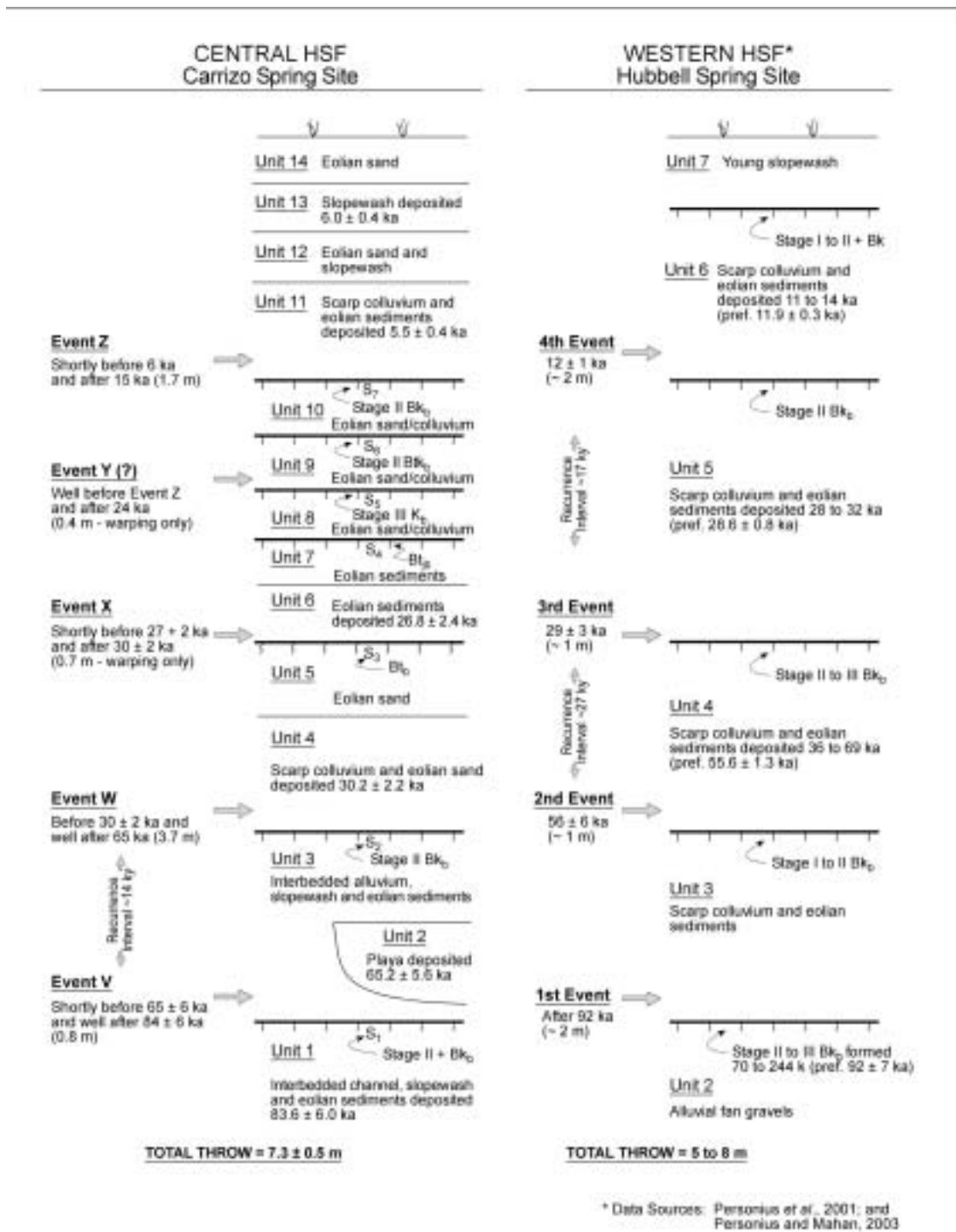
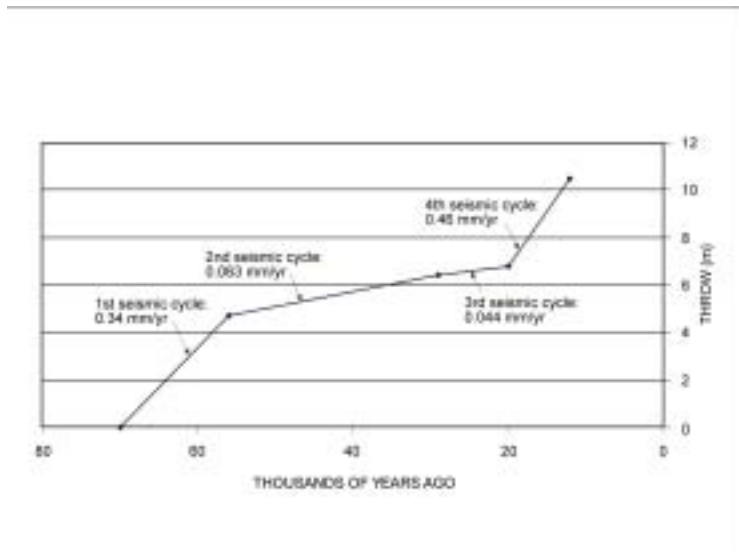


Figure 2. Comparison of the paleoseismic records of the central and western Hubbell Spring faults.



**Figure 3.** Plot of cumulative vertical slip rates for the Hubbell Spring fault.

seismic hazards elsewhere in the rift. Additional investigation is needed to determine how activity on the HSF may relate to nearby faults along the eastern rift margin, including the Palace-Pipeline to the west, the Manzano fault to the east, and unnamed faults on the Llano de Manzano to the south.

## REFERENCES

- Grauch, V.J.S., 2001, High-resolution aeromagnetic data, a new tool for mapping intrabasinal faults: Example from the Albuquerque basin, New Mexico: *Geology*, v. 29, no. 4, p. 367-370.
- Olig, Susan S., Eppes, Martha C., Forman, Steven L., Love, David, W., and Allen, Bruce D., 2004, Paleoseismic investigation of the central Hubbell Spring fault, central New Mexico, Unpublished Final Technical Report to the U.S. Geological Survey, NEHRP Award No. 99HQGR0089, variously paginated.
- Personius, S.F., Eppes, M.C., Mahan, S.A., Love, D.W., Mitchell, D.K., and Murphy, A., 2001, Log and data from a trench across the Hubbell Spring fault zone, Bernalillo County, New Mexico: U.S. Geological Survey Miscellaneous Field Studies Map MF-2348, v. 1.1.
- Personius, S.F. and Mahan, S.A., 2003, Paleearthquakes and eolian-dominated fault sedimentation along the Hubbell Spring fault zone near Albuquerque, New Mexico: *Bulletin of the Seismological Society of America*, v. 93, no. 3, p. 1,355-1,369.

## ACKNOWLEDGEMENTS

We thank Sean Connell (NMBGMR), Anne Tillery (formerly UNM, now URS), and Nicole Bailey (UNM) for assistance, and the Cordova family for permission to conduct this study on their ranch. This study was funded by U.S. Geological Survey Award No. 99HQGR0089 with additional support from NMBGMR and URS Corporation. The views and conclusions contained in this article are those of the authors and should not be interpreted as necessarily representing the official policies, either expressed or implied, of the U.S. government.

## (Footnotes)

- <sup>1</sup> Seismic Hazards Group, URS Corporation, Oakland, CA, susan\_olig@urscorp.com
- <sup>2</sup> Formerly Earth & Planetary Science, University of New Mexico, Albuquerque, NM; Presently Department of Geography and Earth Sciences, University of North Carolina at Charlotte
- <sup>3</sup> Department of Geological Sciences, University of Illinois at Chicago, Chicago, IL
- <sup>4</sup> New Mexico Bureau of Geology and Mineral Resources, Socorro, NM
- <sup>5</sup> New Mexico Bureau of Geology and Mineral Resources, Albuquerque, NM

## **Basin and Range Seismicity: Distribution, regional and local occurrence rates, moment release and comparison with geodesy.**

Aasha Pancha and John G. Anderson  
Seismological Laboratory and Department of Geological Sciences,  
University of Nevada Reno  
pancha@seismo.unr.edu

Scalar moment rates estimated from a 146-year seismicity catalog are compared with deformation rates of the Basin and Range province determined using space geodesy. The southwestern boundary of the study area (Figure 1) runs down the crest of the rigid Sierra Nevada Range, California, and extends on the same trend to include regions in the Mojave Desert where deformation is more related to the northward motion of the Sierra Nevada Mountains than to the main motion of the San Andreas Fault. Seismic moment rates have been estimated from a new catalog of earthquakes intended to be complete for  $M \geq 5$ . The catalog was compiled from 15 preexisting catalogs, supplemented by the review of 42 published journal articles. Throughout the catalog compilation, care was taken to obtain the moment magnitude or a reasonable, and not inflated, equivalent. 80% of the moment release occurred during 10 earthquakes of magnitude  $M_W \geq 6.79$ .

Figures 2 and 3 show the spatial distribution of earthquake numbers, of moment release, and the magnitude of crustal deformation in the direction of motion of the Sierra Nevada block relative to stable North America. Within the scatter of the data, the spatial patterns of seismic activity, seismic moment, and geodetic deformation are the same. The spatial pattern of earthquakes matches the geodetic pattern of deformation. About 50% of the earthquakes in the catalog, 75% of the seismic moment release, and 70% of the geodetic deformation, has been released within a strip of about 200 km zone along the western edge of the province, coinciding with the Northern Walker Lane (Figure 2). Activity along the eastern half of the Great Basin is significantly smaller than in the west (Figure 3). The greatest increase on all three rates in Figure 3 occurs at the very eastern edge of the Basin and Range.

Several techniques, ultimately traceable to Kostrov and Brune, are used to translate the geodetic strain rates into rates of seismic moment release. Rates determined from seismicity, of  $4.5 \times 10^{25}$  to  $10.8 \times 10^{25}$  dyne-cm/year, substantially overlap the range determined from the geodetic data,  $6.0 \times 10^{25}$  to  $13.0 \times 10^{25}$  dyne-cm/year. This agreement suggests that within uncertainties, the rate of historic earthquakes within the Basin and Range province, taken as a whole, provides a reasonable estimate for the future rate of seismicity. These results support the hypothesis that even a few years of detailed geodetic monitoring can provide a good constraint on seismic hazard estimates.

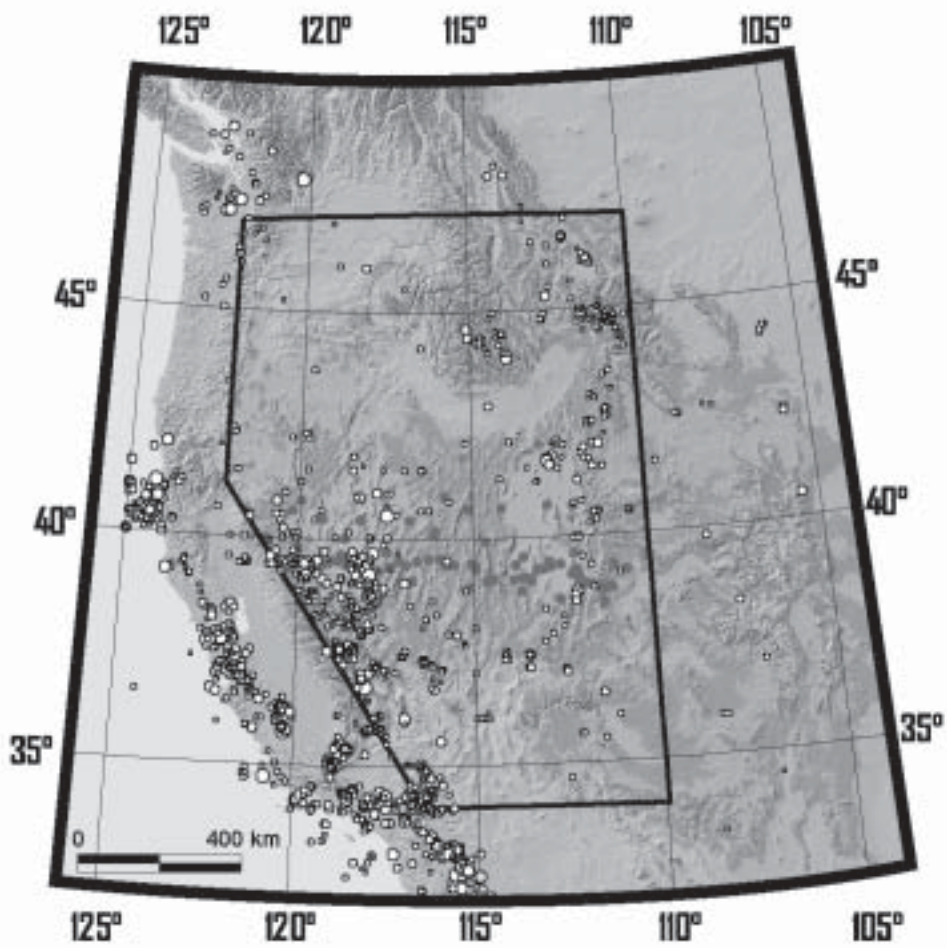


**Figure 1.** Map of the western United States, showing topography, earthquakes with  $M_e \geq 4.8$  (white circles with radius proportional to magnitude) and Global Positioning System stations providing data for this study (gray circles). The study area, outlined with a bold polygon, encloses all major earthquakes that can be associated with deformation of the Basin and Range province.

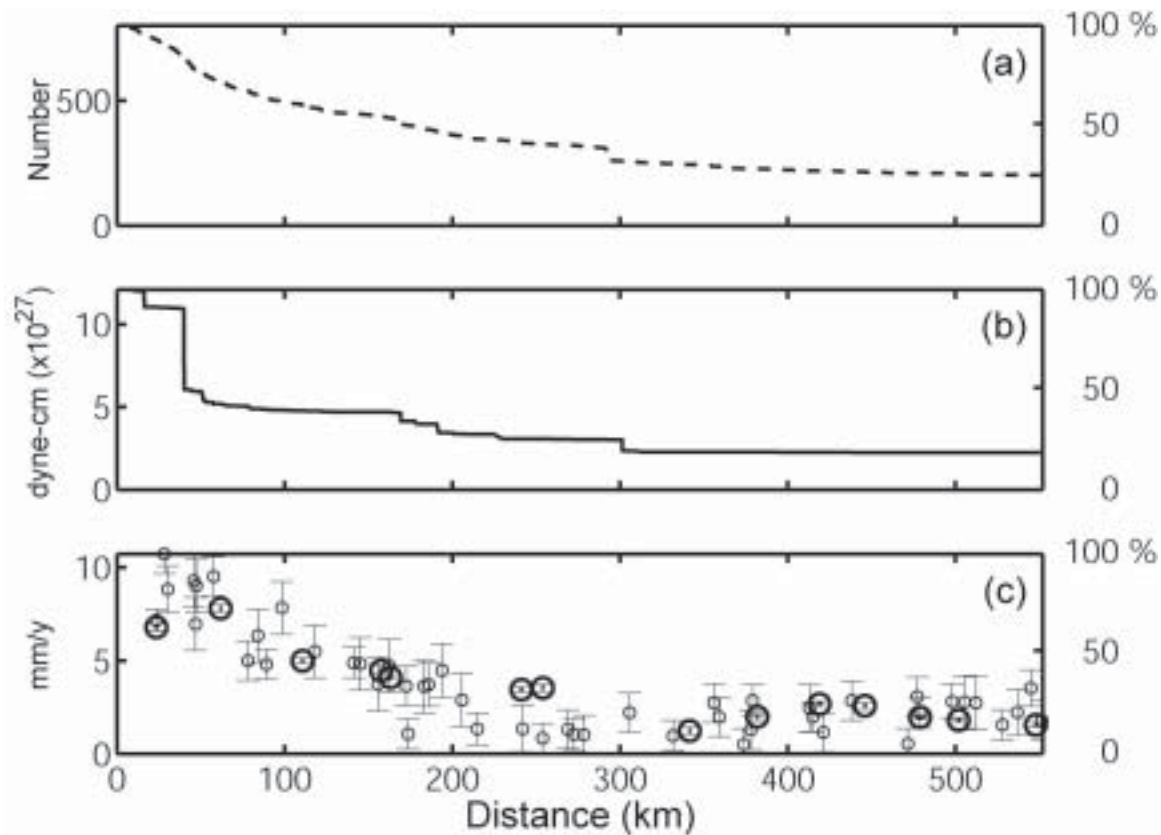


**Figure 2.** Cumulative number of earthquake events (a) and cumulative seismic moment release (b), as a function of the perpendicular distance from the southwestern boundary of the study region (Figure 1). Velocity rates (c) determined from geodesy (Wernicke *et al*, 2000 [bold circles]; Thatcher *et al*, 1999 [circles]) are shown for comparison. The magnitude of the velocity field parallel to the direction of motion of the Sierra Nevada block relative to stable North America is plotted. Uncertainties for the GPS data are also shown. Percentages shown on the right hand side of each plot are values normalized by the total number of earthquakes (800), total moment ( $1.24 \times 10^{28}$  dyne-cm), and maximum geodetic rate (16.69 mm/yr).

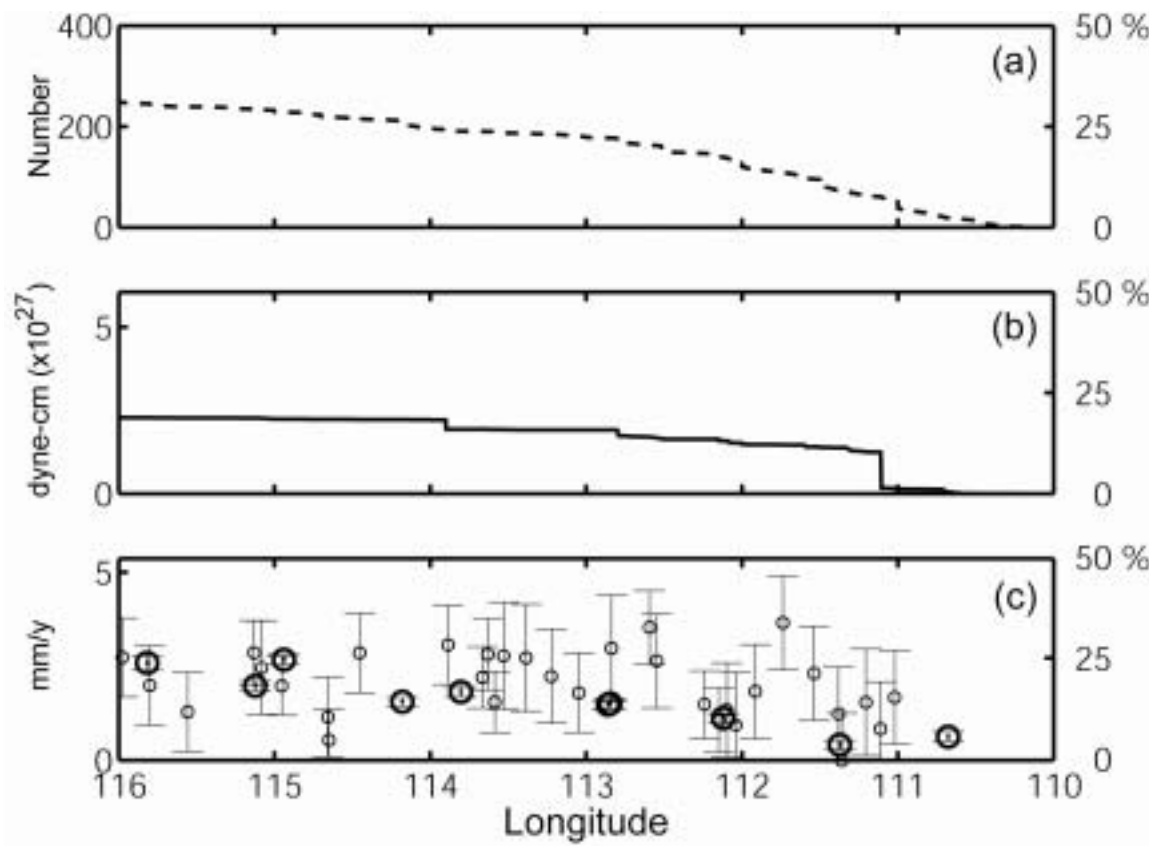


**Figure 3.** Cumulative number of earthquake events (a), cumulative seismic moment release (b), and geodetic velocity rates (c) (see Figure 2), as a function of the perpendicular distance from the eastern boundary of the study region (Figure 1), simply approximated by longitude of the observations. Uncertainties for the GPS data are also shown.

## Determination of Low-Strain Site Amplification Factors in the Salt Lake Valley, Utah, Using ANSS Data

Kris L. Pankow and James C. Pechmann, University of Utah Seismograph Stations, ([pankow@seis.utah.edu](mailto:pankow@seis.utah.edu))

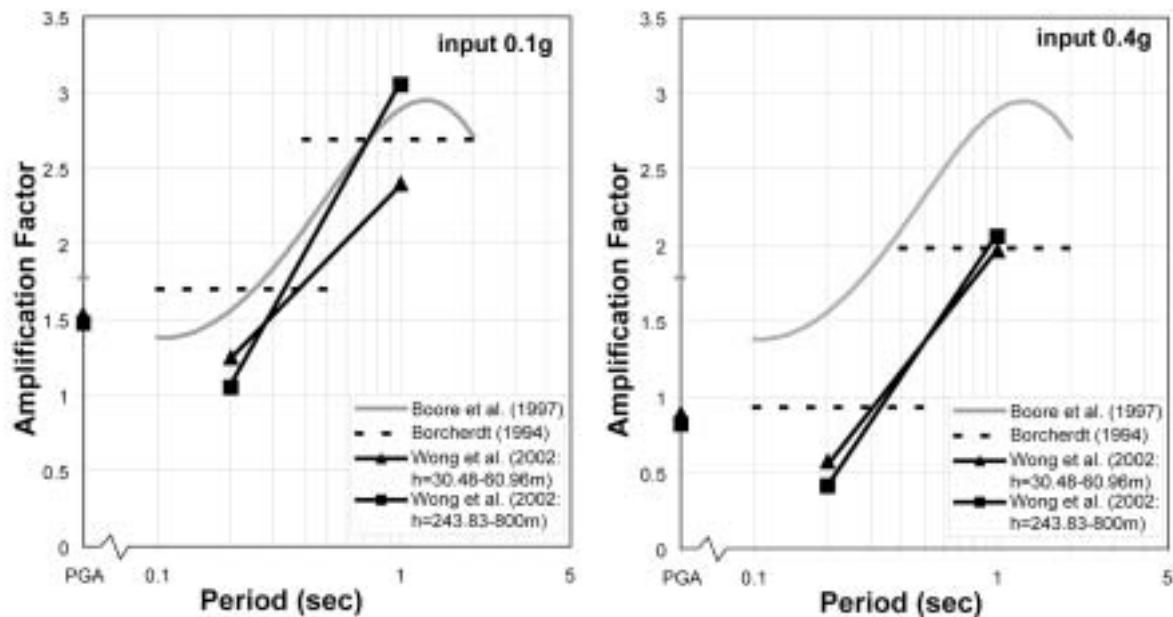
Using data from the Advanced National Seismic System (ANSS) network in and near the Salt Lake Valley (SLV), Utah, we are measuring average, frequency-dependent, low-strain site amplification factors for geologically-based site response units defined by Ashland (2001). Site amplification factors are used extensively in probabilistic and deterministic seismic hazard analyses and for creating near-real-time maps of ground shaking (ShakeMaps). These factors can be grouped into three types based on how they are determined: (1) empirical methods, which are often applied in conjunction with determining empirical ground motion predictive relations (e.g., Boore et al., 1997); (2) theoretical methods, such as the well-known equivalent-linear soil response modeling program SHAKE and similar codes (e.g., Wong et al., 2002); and (3) a combination of empirical and theoretical methods (e.g., Borchardt, 1994). These three different methods for determining site amplification factors can lead to significantly different results. Figure 1 compares site amplification factors from the three studies cited above for two different SLV site response units: (a) lacustrine-alluvial silts and clays (average S-wave velocity in the uppermost 30 m ( $V_{s30}$ ) = 199 m/sec) and (b) lacustrine-alluvial gravel ( $V_{s30}$  = 387 m/sec). The Borchardt (1994) and Boore et al. (1997) amplification factors on Figure 1 were calculated assuming a reference rock site  $V_{s30}$  of 910 m/sec (Pankow and Pechmann, 2004). Of particular note on Figure 1 are the large discrepancies in the factors at 0.2 sec period, for both site response units, at both low-strain and high-strain. Also of note are the differences at 1-sec period between the amplification factors determined by Wong et al. (2002) for different unconsolidated sediment depths. At low strain, the differences among predicted site amplification factors are large enough that we should be able to select the factors that best fit the weak motion data for the SLV. We assume that if a set of site amplification factors cannot predict low-strain amplification, then predicted amplifications for high-strain are also incorrect. Furthermore, we note that even low-strain site amplification factors are relevant to seismic hazard analyses because they are applicable to ground motions up to at least ~0.15 g (Borchardt, 1994; Wong et al., 2002; Beresnev and Wen, 1996) and the threshold of damage to weak construction is about 0.1 g (Richter, 1958, p. 26).

To measure the site amplification factors, we compute horizontal-component spectral ratios of local earthquake recordings from ~30 SLV strong motion stations on soil and 5 nearby strong motion and broadband stations on rock. We use these spectral ratios to compute, tabulate, and map average site amplification factors for the instrument sites in the short-period (0.1-0.5 sec) and mid-period (0.4-2.0 sec) bands defined by Borchardt (1994). These amplification factors will be averaged by site response unit and compared to the three published sets of site amplification factors mentioned above. We will also look for a correlation between the amplification factors and unconsolidated sediment depths, as predicted by the Wong et al. (2002) amplification factors shown on Figure 1. This work should lead to improved estimates of ground shaking from future large earthquakes in Utah.

### References Cited

- Ashland, F. X. (2001). Site-response characterization for implementing SHAKEMAP in northern Utah, *Utah Geol. Surv., Report of Investigation 248*, 10 pp., 2 pl.
- Beresnev, I. A. and K. Wen (1996). Nonlinear soil response—A reality? *Bull. Seism. Soc. Am.* **86**, 1964-1978.
- Boore, D. M., W. B. Joyner, and T. E. Fumal (1997). Equations for estimating horizontal response spectra and peak acceleration from western North American earthquakes: A summary of recent work, *Seism. Res. Lett.* **68**, 128-153.
- Borchardt, R. D. (1994). Estimates of site-dependent response spectra for design (methodology and justification), *Earthquake Spectra* **10**, 617-653.
- Pankow, K. L. and J. C. Pechmann (2004). The SEA99 ground-motion predictive relations for extensional tectonic regimes: Revisions and a new peak ground velocity relation, *Bull. Seism. Soc. Am.* **94**, 341-348.
- Richter, C.F. (1958). *Elementary Seismology*, W.H. Freeman and Co., San Francisco, CA, 768 pp.
- Wong, I., W. Silva, S. Olig, P. Thomas, D. Wright, F. Ashland, N. Gregor, J. Pechmann, M. Dober, G. Christenson, and R. Gerth (2002a). Earthquake scenario and probabilistic ground shaking maps for the Salt Lake City, Utah, metropolitan area, *Utah Geol. Surv., Misc. Publ. MP-02-5*, 50 pp., 9 plates.

**a) Lacustrine - alluvial silts and clays**



**b) Lacustrine - alluvial gravel**

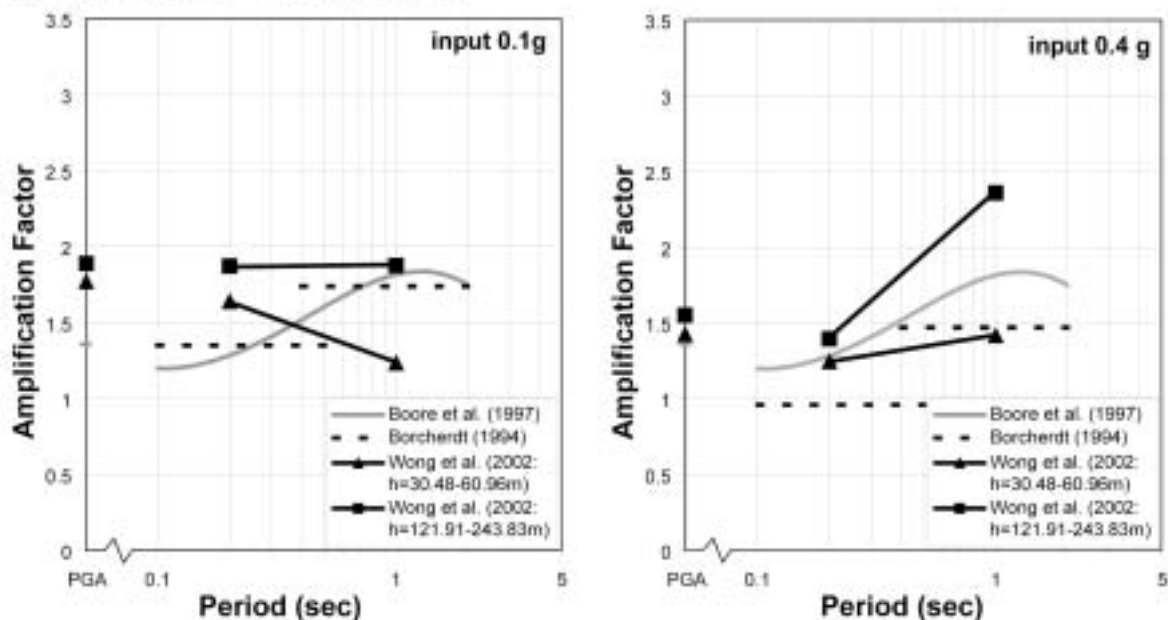


Figure 1. Site amplification factors as a function of period predicted for two SLV site response units -- a) soft lacustrine alluvial silts and clays and b) stiff lacustrine alluvial gravels -- from three different studies: Borchardt (1994), dashed lines; Boore et al. (1997), gray lines; Wong et al. (2002), black symbols connected by solid lines. The latter are shown for two different ranges of unconsolidated sediment depth as triangles (thin deposits) and squares (maximum thicknesses of deposits appropriate for the units). The amplification factors are shown for two levels of input ground motion: weak motion, 0.1g, and maximum ground motions on rock for an M 7.0 earthquake as predicted by Pankow and Pechmann (2004), 0.4g.

## **Preliminary paleoseismology of the southern Steens fault zone, Bog Hot Valley, Nevada**

Stephen F. Personius<sup>1</sup> (personius@usgs.gov), Anthony J. Crone<sup>1</sup>, Michael N. Machette<sup>1</sup>, Jai Bok Kyung<sup>2</sup>,  
Hector Cisneros<sup>3</sup>, and David J. Lidke<sup>1</sup>

<sup>1</sup>U.S. Geological Survey, Denver, CO 80225; <sup>2</sup>Korea National University of Education, Chongwon-Gun, South Korea; <sup>3</sup>Universidad Nacional de San Luis, San Luis, Argentina

The 200-km-long Steens fault zone forms the longest, most topographically prominent fault-bounded escarpment in the Basin and Range of eastern Oregon and northernmost Nevada. The down-to-the-east normal fault is marked by Holocene fault scarps along nearly half its length, including the southern one-third of the fault from the vicinity of Pueblo Mountain to the southern margin of Bog Hot Valley southwest of Denio, Nevada. We studied this section of the fault to better constrain late Quaternary slip rates, which we hope to compare to deformation rates derived from a recently established geodetic network in the region. We excavated a trench across one of a series of right-stepping fault scarps that extend south from the southern end of the Pueblo Mountains and traverse the floor of Bog Hot Valley, about 4 km south of Nevada State Highway 140 (fig. 1). This site was chosen because of the presence of well-preserved fault scarps, their development on lacustrine deposits thought to be suitable for luminescence dating, and the proximity of two nearby geodetic stations that straddle the fault zone.

The trench was located at an elevation of 1292 m and revealed an east-dipping fault zone and an adjacent graben in well-stratified lacustrine silt, sand, and gravel. The site is about midway between two paleo-shorelines (1310 m and 1280 m) of pluvial Lake Alvord, which during the last-glacial maximum extended 120 km from the northern end of the Alvord Desert to the southern end of Bog Hot Valley. The late Quaternary history of Lake Alvord is poorly known and is complicated by the occurrence of at least one overflow event in the Lake Alvord basin that may have lowered the lake level from the 1310 m shoreline to the 1280 m shoreline sometime in the late Quaternary. In Bog Hot Valley, neither the 1310-m nor 1280-m shoreline is well preserved, which could be a reflection of their age, the amount of time the lake spent at their respective levels, or geomorphic factors such as lack of significant fetch or shallow water depth. Luminescence ages are pending, but our limited soils data (maximum stage I-II Bk horizon development) are more consistent with a latest Quaternary (Lahontan Seho-equivalent) age for the deposits exposed at the trench site than with correlation to an older lacustrine cycle. We hope our luminescence ages will help determine the ages of the faulted deposits and thus the relative ages of the Lake Alvord shorelines.

The trench exposed distinct fault-scarp colluvial wedges and intervening soils that are clear stratigraphic and structural evidence of three post-lake surface-faulting events. We found additional evidence of an earlier event that probably occurred while the site was still covered by the waters of Lake Alvord. Prominent liquefaction features record this earlier event, which may have been caused by a large-magnitude earthquake on either the Bog Hot Valley strand of the Steens fault zone or on some other nearby fault. Total vertical offset across the trenched scarp as measured with fault-scarp profiles and offsets of distinctive stratigraphic units in the trench is  $4.3 \pm 0.2$  m.

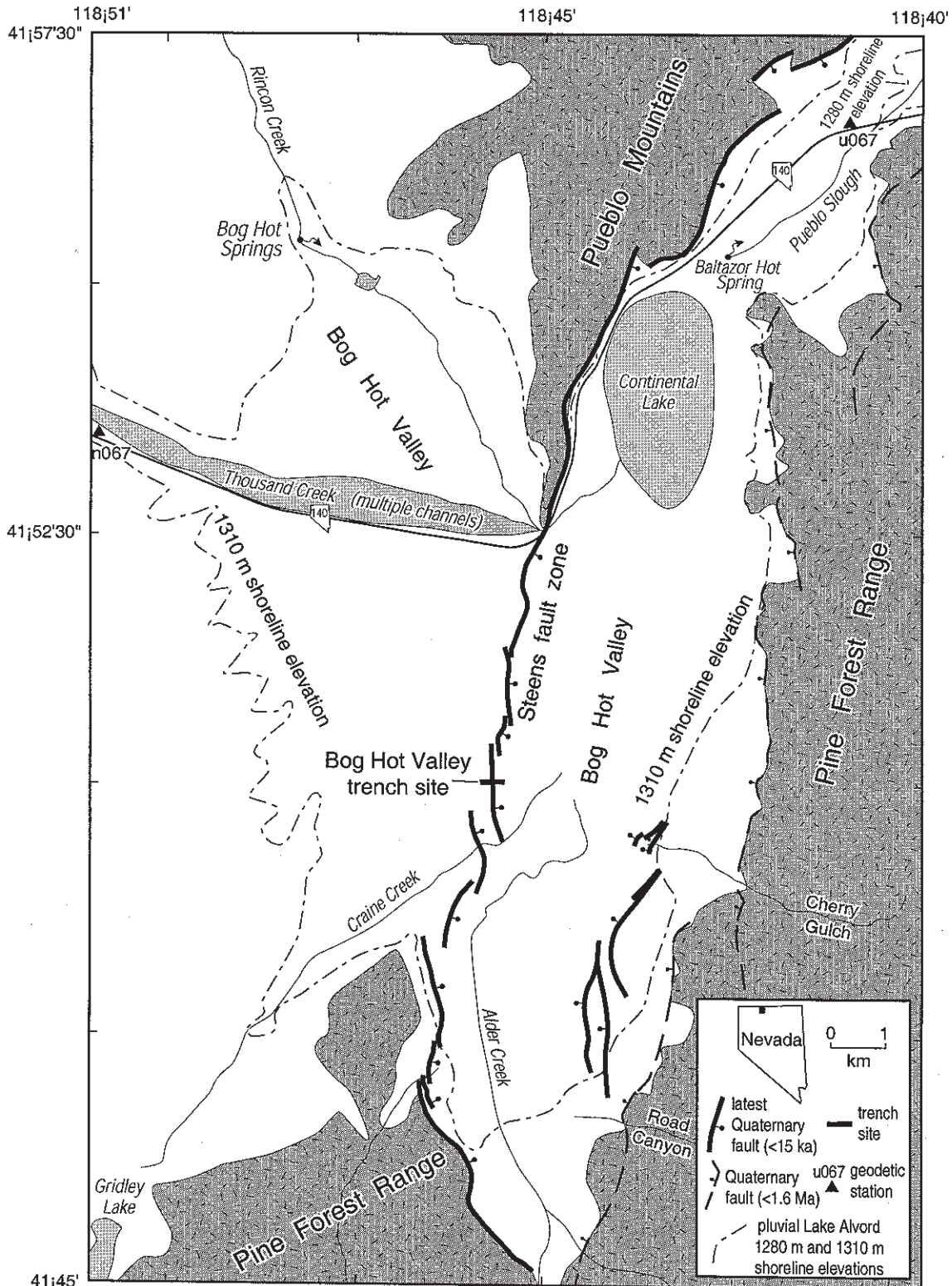


Figure 1. Map of southern Steens fault zone, northern Nevada. Trench site is located on the floor of Bog Hot Valley at an elevation midway between the 1310 m and 1280 m (northeast corner of figure) paleo-shorelines of pluvial Lake Alvord.

## Peavine Peak fault: Another Piece of the Walker Lane Puzzle

Alan R. Ramelli, John W. Bell, and Craig M. dePolo: Nevada Bureau of Mines and Geology, University of Nevada, Reno, Nevada 89557, ramelli@unr.edu

The Peavine Peak fault (PPF) bounds the steep northeastern flank of Peavine Peak, the prominent mountain located just northwest of Reno (fig. 1). The PPF poses a significant seismic hazard, because it forms the southern boundary of several basins in the north Reno area that are undergoing rapid suburban development (i.e., Cold Spring, Lemmon, and Golden Valleys), and the southeastern end of the fault is located 5 km or less from downtown Reno.

The PPF has a northwest strike, paralleling the major right-lateral faults of the northern Walker Lane (i.e., Pyramid Lake, Warm Springs Valley, Honey Lake Valley, and Mohawk Valley faults). However, the PPF differs from these faults in that it has a much shorter length (20 km vs.  $\geq 40$  km), it has a consistent (and possibly dominant) vertical component of displacement, and trench results indicate more frequent earthquake recurrence.

We excavated two trenches across the section of the PPF having the most prominent geomorphic expression and the largest fault scarps. Six bulk soil samples from one of the Peavine trenches yielded mid- to late Holocene radiocarbon ages. These ages are consistent with soil development, but are not in stratigraphic order, so we infer that the older ages approximate the age of faulted fan deposits and that anomalously old ages result from reworked material. Based on the trench relations, we interpret that four or five surface-rupturing events occurred over the past 6000-8000 years, indicating a recurrence interval on the PPF that is similar to the Carson Range fault system (e.g., Genoa fault). In contrast, the major right-lateral faults in the northern Walker Lane are generally characterized by only two or three Holocene earthquakes, which probably involve significantly larger displacements than the PPF events.

Sense of slip on the PPF remains problematic. Vertical offsets average 1.5 to 2 m per event at the trench site. Several lines of evidence indicate the PPF also has a component of right-lateral slip: 1) the fault's strike is parallel to major strike-slip faults in the region; 2) the fault has a left-stepping *en echelon* pattern; 3) there is an apparent pull-apart basin at the fault's north end (fig. 2); and 4) the fault zone exposed in the trenches has a subvertical dip and "flower-structure" appearance. None of these lines of evidence require that strike-slip displacement is dominant, and based on the fault's geomorphology, we believe that the vertical displacement is equal to or greater than the lateral.

Assuming approximately equal components of normal and right-lateral offset, we estimate the cumulative net displacement at the trench site to be ~10 m. We therefore estimate a Holocene slip rate of ~1 mm/yr, indicating the Peavine Peak fault is one of the most active faults in the region.

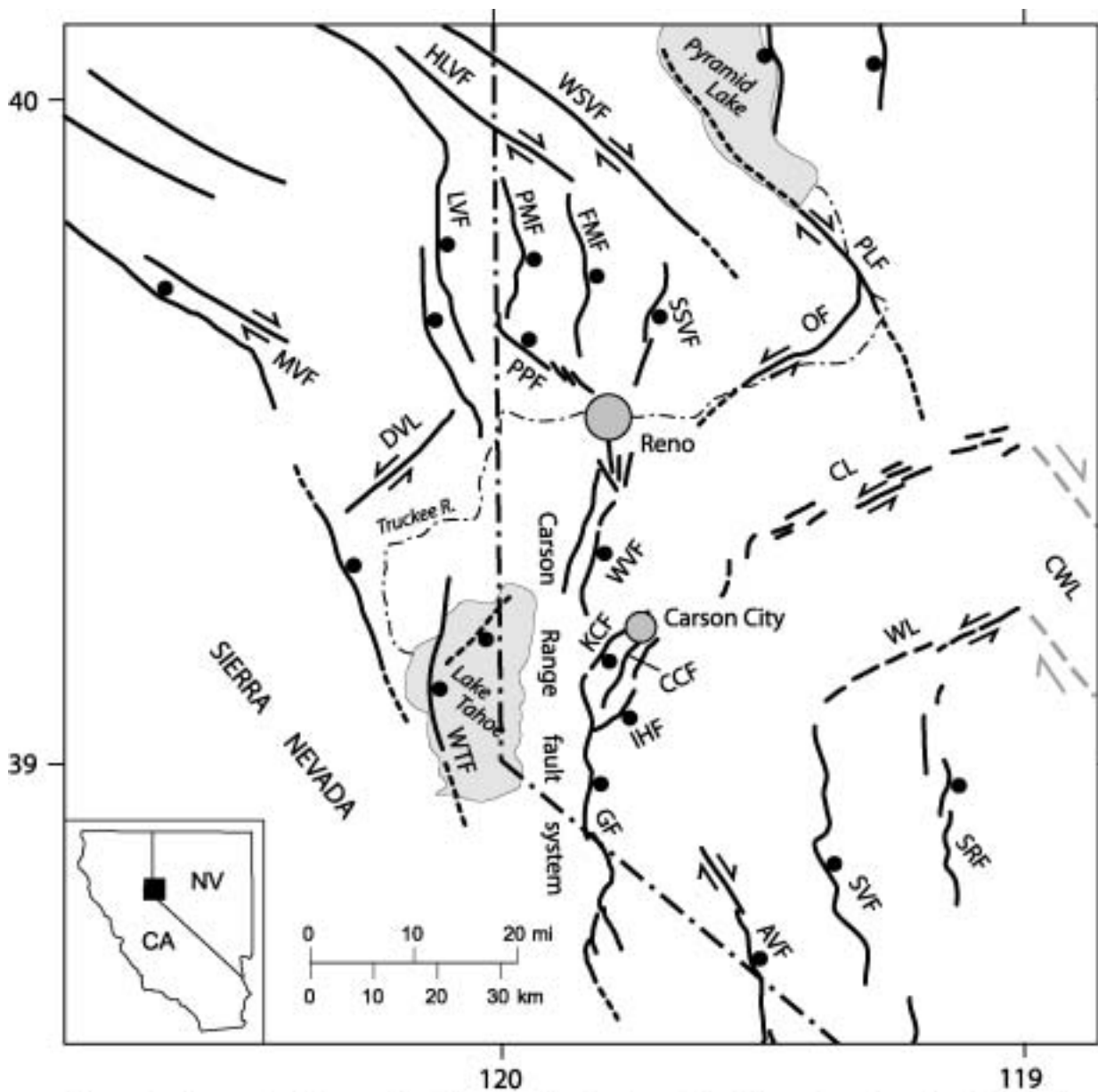


Figure 1. Generalized map of Quaternary faults in western Nevada and eastern California.

- |                                       |                                   |
|---------------------------------------|-----------------------------------|
| AVF-Antelope Valley fault             | MVF-Mohawk Valley fault           |
| CCF-Carson City fault                 | OF-Olinghouse fault               |
| CL-Carson lineament                   | PLF-Pyramid Lake fault            |
| CWL-projection of Central Walker Lane | PMF-Peterson Mountain fault       |
| DVL- Dog Valley lineament             | PPF-Peavine Peak fault            |
| FMF-Freds Mountain fault              | SRF-Singatse Range fault          |
| GF- Genoa fault                       | SSVF-Spanish Springs Valley fault |
| HLVF-Honey Lake fault                 | SVF-Smith Valley fault            |
| IHF-Indian Hill fault                 | WL-Wabuska lineament              |
| KCF-Kings Canyon fault                | WSVF-Warm Springs Valley fault    |
| LVF-Long Valley fault                 | WTF-West Tahoe fault              |
|                                       | WVF-Washoe Valley fault           |

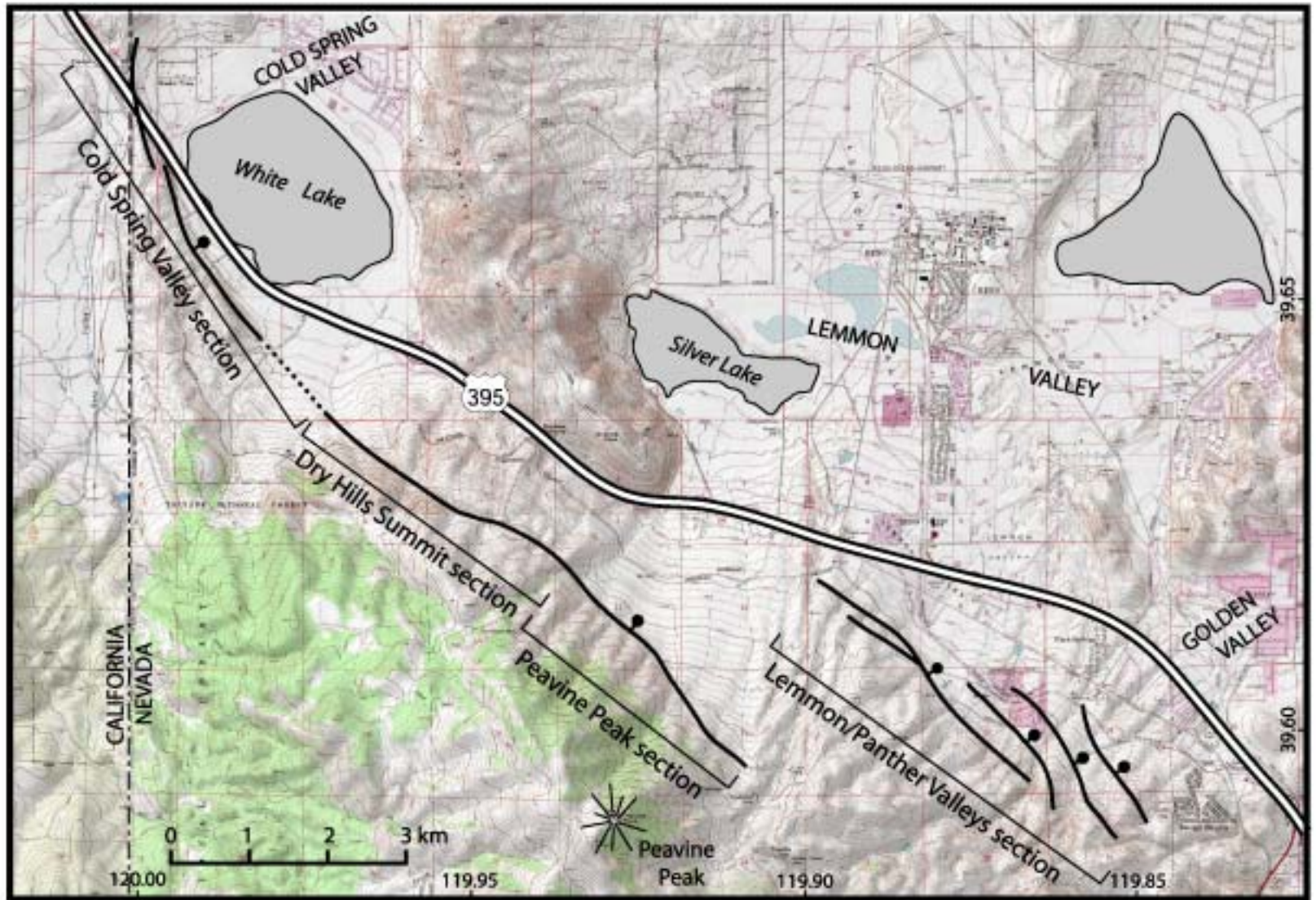


Figure 2. Geomorphic sections of the Peavine Peak fault

## Evaluation of an earthquake hazard mapping model for Reno, Nevada

James B. Scott\*, Matthew Clark, Thomas Rennie, Aasha Pancha, Hyunmee Park, Matthew Purvance, Glenn Biasi, Abdulrasool Anoshehpour, and John N. Louie.

Seismological Laboratory, University of Nevada, Mail Stop 174, Reno, NV 89557

\*jscott@seismo.unr.edu

We combined the results of a shallow shear-velocity ( $V_{30}$ ) transect (Fig. 2) across 16 km of the Reno, Nevada basin (Fig. 1) performed in October and November, 2001 with a gravity-depth modeling study reported in 2000 to produce a shear-velocity model applicable to the shallow basin (Fig. 3). We used the model to extrapolate earthquake ground-motion amplifications from the 2000 Truckee, California earthquake for ANSS stations in the Reno area. We evaluate the predicted amplification against the strong-motion records of the earthquake recorded at four ANSS stations within the mapped area. Shallow shear velocity predicts earthquake ground motion amplification and potential hazard in similar alluvium-filled basins, and is the basis of site hazard classification under NEHRP-UBC provisions (BSSC, 1998). A geologic map-based classification of nearly the entire Reno basin would be NEHRP-D. Our transect of  $V_{30}$  revealed that, in fact, most (82%) of the transect length is classified NEHRP-C. There is no correlation of  $V_{30}$  with most mapped surface geology or agricultural soil type (Fig. 4). A precarious rock site on the northwestern side of the basin placed a 0.6 g limit on historic shaking. We conclude that: 1) The Reno basin has stiff Tertiary sediments underlying the surface at shallower depths than do other urban basins such as the Los Angeles basin. Weaker soils appear to occur east of downtown Reno in the broad floodplain of the Truckee River. 2) Surface geology is a poor predictor of  $V_{30}$  in the Reno basin. 3) Very large earthquakes have probably not occurred in the Reno area in geologically recent times.

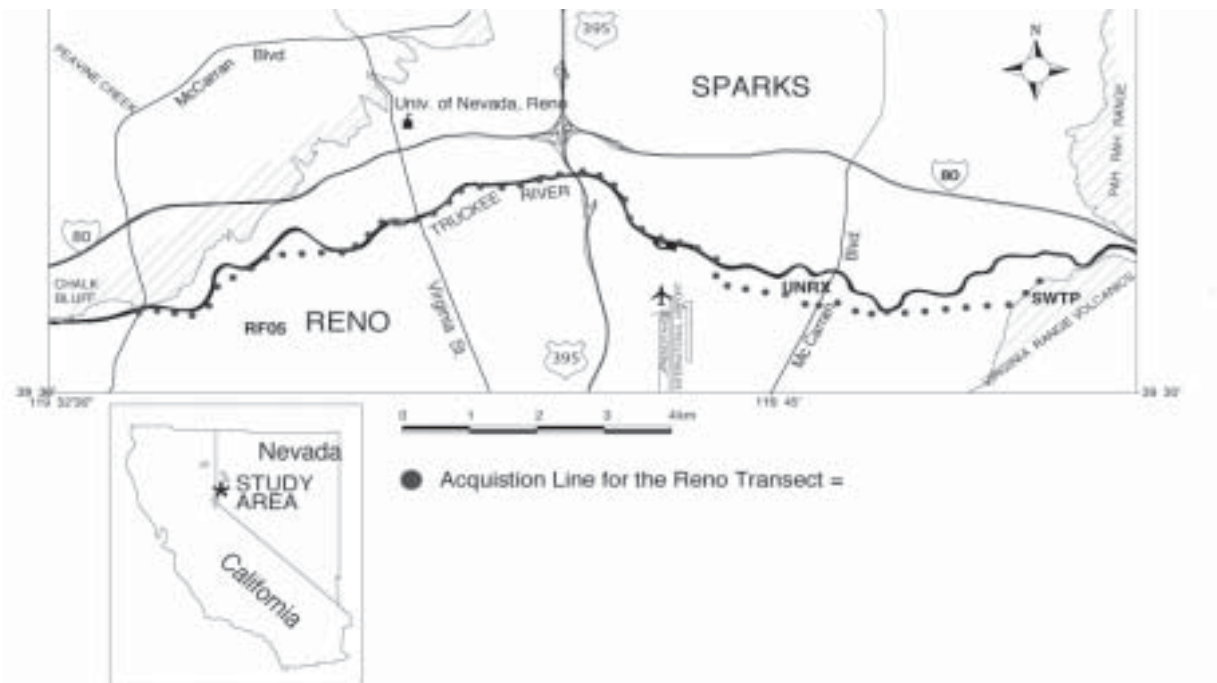


Figure 1. Reno transect route

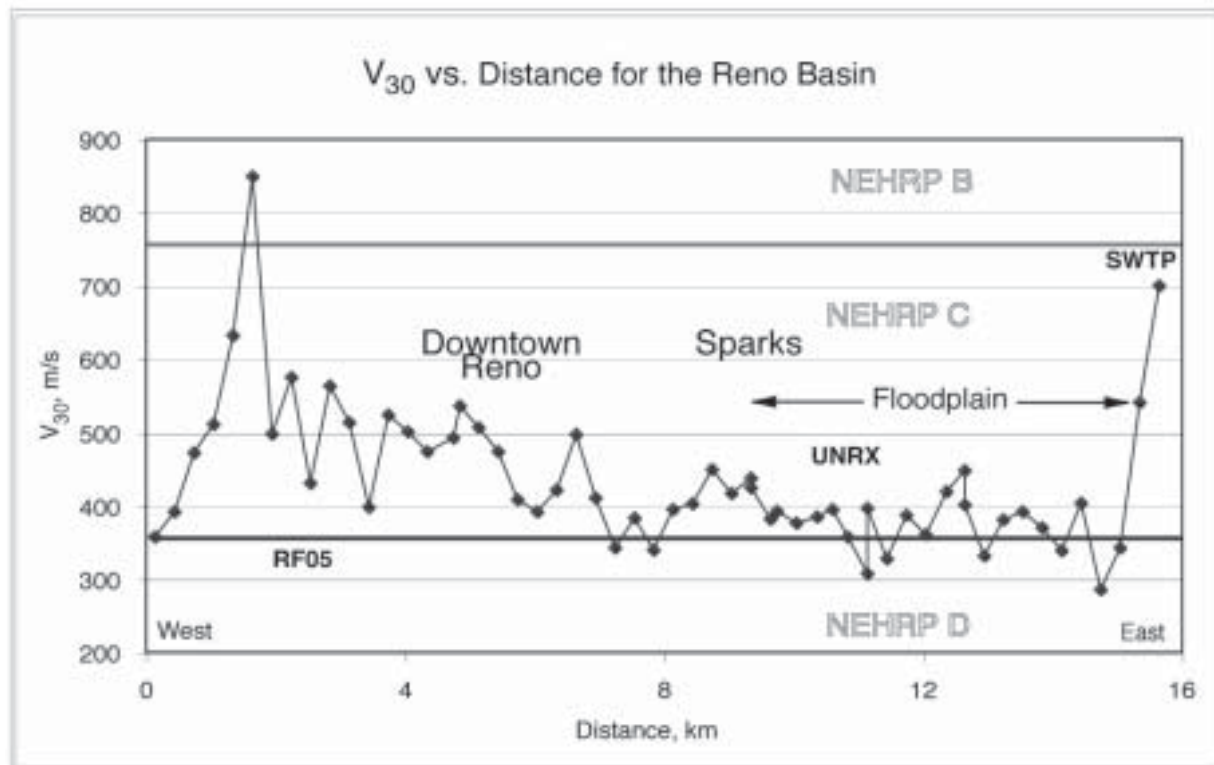


Figure 2.  $V_{30}$  vs. distance along transect

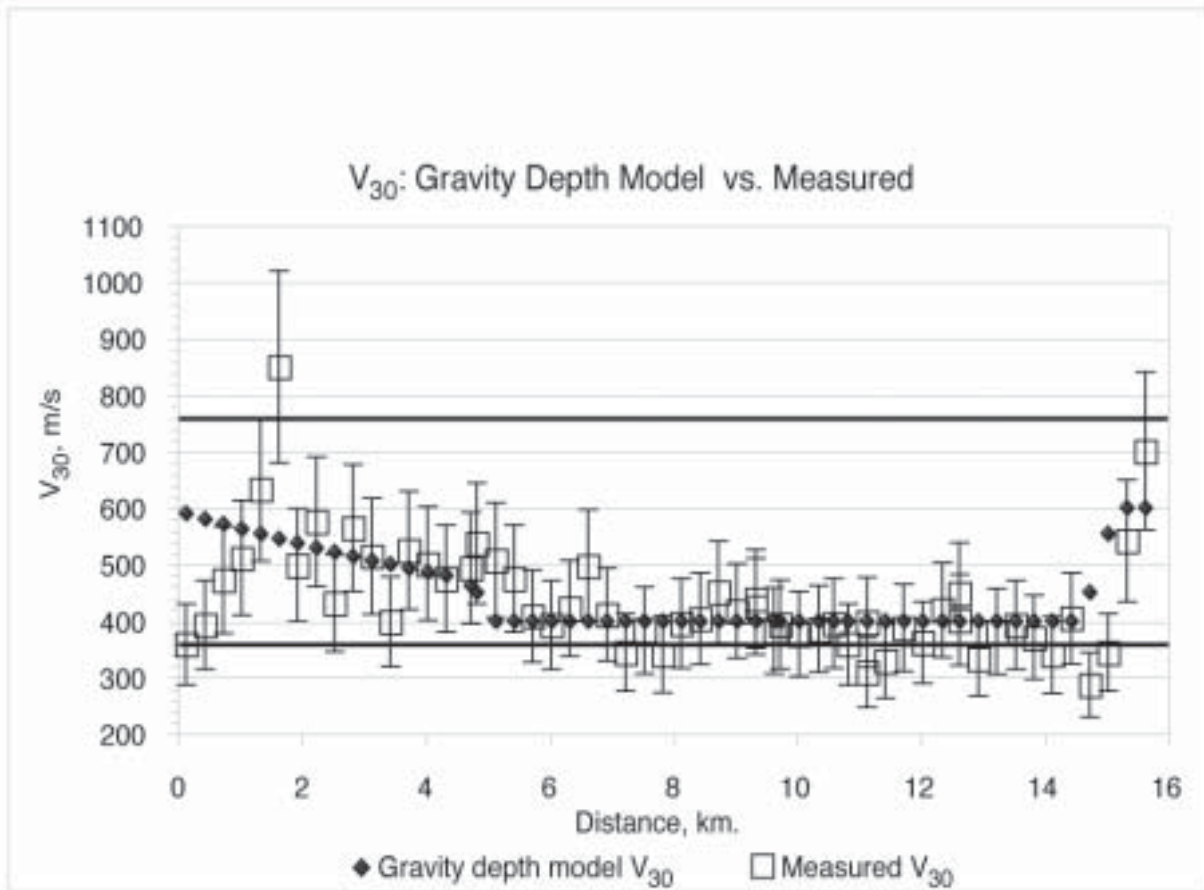


Figure 3. Gravity depth model for V30

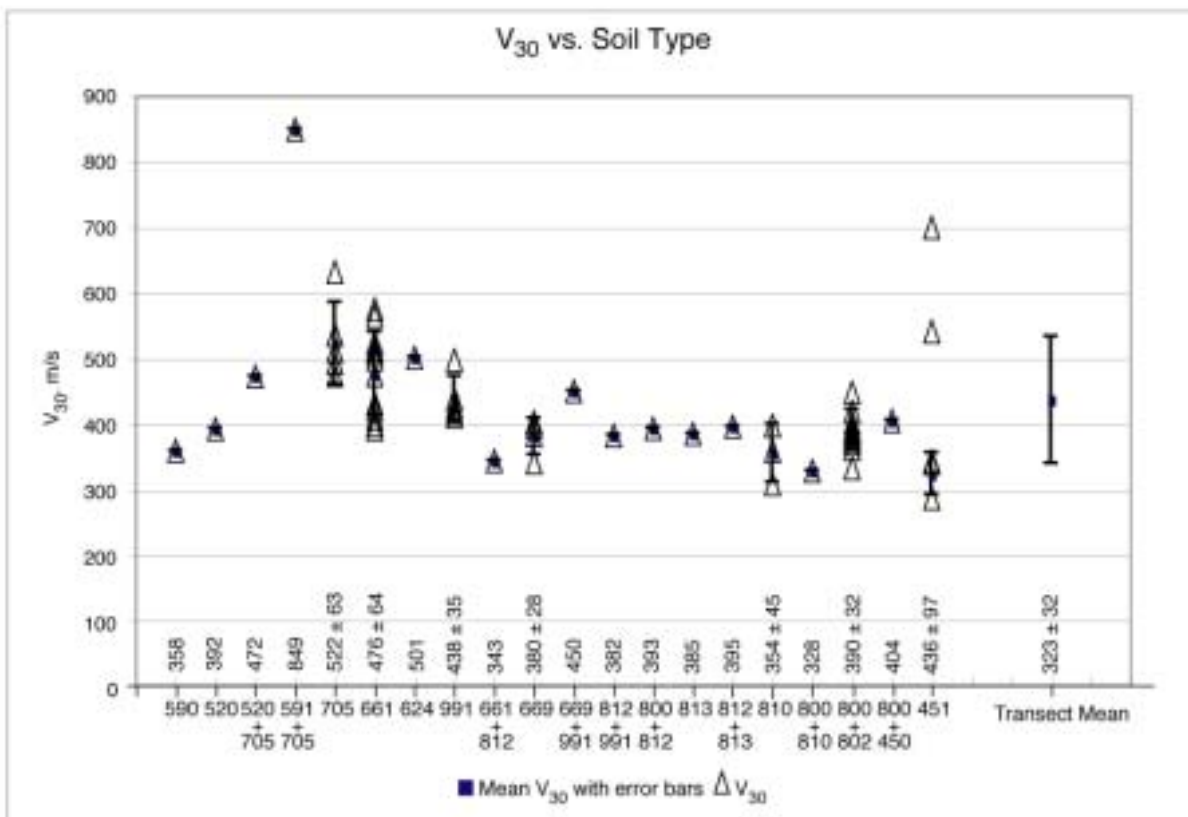
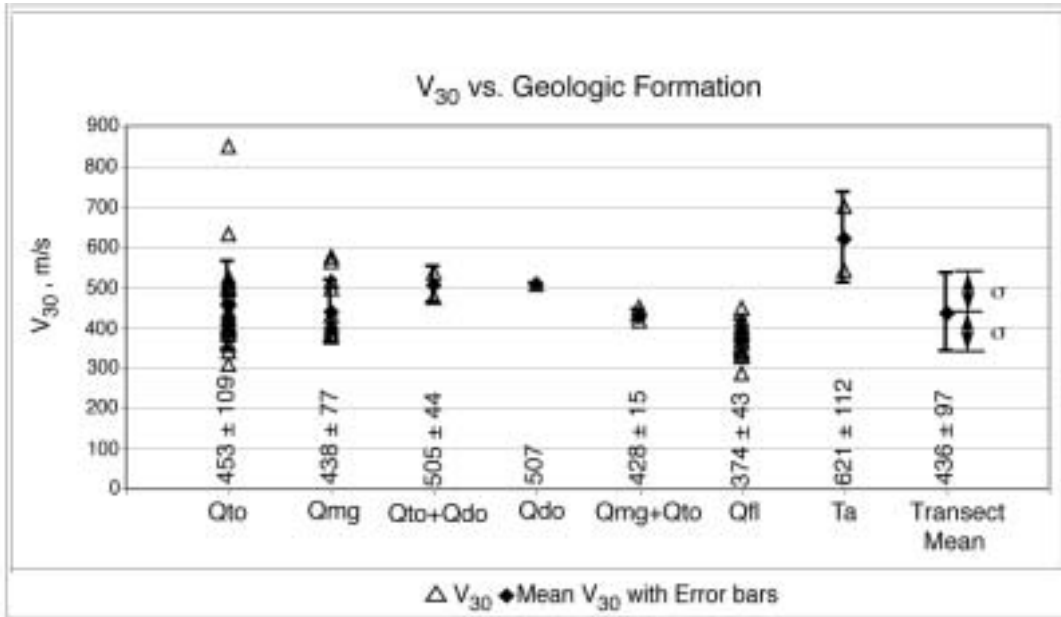


Figure 4. V<sub>30</sub> correlations to geology (from Reno folio and Vista quadrangle geologic maps; NBMG) and soil type (from USDA -SCS Soil survey of Washoe County, Nevada)

## Quaternary Fault Map of Owens Valley, Eastern California

Slemmons, D. Burton., Professor Emeritus, Center for Neotectonic Studies, University of Nevada, Reno, bslemmons@aol.com; Vittori, Eutizio, Italian Agency for the Protection of the Environment; Jayko, A. S., U. S. Geological Survey; Carver, Gary, Professor Emeritus, Humboldt State University; and Glass, Charles E., Professor Emeritus, University of Arizona, Tuscon

Owens Valley is a 170 km long late Cenozoic graben that lies along the southwest edge of the Basin Range Province extending southward from the Long Valley caldera to the northern and western flanks of the Coso Range. It lays within the Eastern California Shear Zone, a segment of the larger Walker Lane deformation belt. The zone accommodates geodetic strain rates of ~11 mm/yr (cf. Bennett et al.,1999). Field and low-sun angle aerial photograph studies (1967-1993), with additional field mapping (2002-2004), augments Gilbert (1884) and Beanland and Clark's work on the 1872 rupture by showing the broader Quaternary fault activity flanking the valley floor adjacent to the active Owens Valley fault zone(OVFZ). Low-sun angle aerial photographs at 1:12,000 scale cover nearly all the range fronts and valley floor permitting detailed mapping of the 1872 ruptures within the central part of the valley and the older Quaternary fault scarps that control the larger graben geometry. Fault scarps are classified based on their aerial photo and field appearance into four age groups: 1) 1872, 2) Holocene, 3) Late Pleistocene, and 4) Pleistocene or older. In addition, the Pleistocene lake shorelines are shown.

The 1872, M 7.4-7.6 earthquake ruptured a 116 km segment of the OVFZ with displacements of up to 10 m dextral-slip (Slemmons et. al., 1969; Beanland and Clark, 1992). The rupture terminates at right-steps in the OVFZ which splays into the late Quaternary basaltic Big Pine volcanic field to the north and bimodal Coso field to the south. This interpretation of the 1872 scarp shows a somewhat longer length than previous maps, with the rupture terminating southwest of Dirty Socks Spring near Red Ridge. In several places, especially where the 1872 rupture deviates from the main 340° strike, the associated scarps display significant vertical components with beveled scarp profiles, making identification of reactivation events more evident. Sections of the 1872 rupture of 34 km, 11, 10.5, and 10 km lengths show pure transcurrent displacement. Four east-stepping restraining bends link the right lateral sections. The pattern of faulting around and inside Owens lake indicates that the lake basin is a pull-apart, controlled by a right-step of the main NNW right-slip fault zone consistent with transtension.

Beanland, S., and Clark, M.,1994, The Owens Valley fault zone, eastern California, and surface rupture associated with the 1872 earthquake: U.S. Geological Survey Bulletin 1982, 29 p.

Bennett, R. A., J. L. Davis, and B. P. Wernicke,1999, Present-day pattern of Cordilleran deformation in the western United States, *Geology*, v. 27, 371-374.

Slemmons, David B; Carver, Gary A; Cluff, Lloyd S, 1969, Historic faulting in Owens Valley, California: Special Paper, Geological Society of America, pp.559-560.

*Table 1. Historical surface faulting in the Basin and Range Province and the Eastern California shear zone.*

NO	DATE	FAULT LOCATION	M <sub>w</sub> MAG	ZONE LENGTH (km)	ZONE WIDTH (km)	MAX. DISPL (m)	AGE OF PREVIOUS ACTIVITY; NUMBER OF SEGMENTS
1	1869?	Olinghouse, NV	6.7±	~20	<1?	3.7	Holocene (Holo), 1 segment?
2	1872	Owens V, CA	~7.6	~108	Var. 3-16; Avg 8	RL 9, V 4.4	>8,000 yrs (Holo); 3 or 4 segs.
3	1887	Sonora, Mex	7.3	101.4	1-3, Avg ~2	V 4.87	100 ka to 200 ka; 2-3.
4	1903?	Wonder, NV	~6.5±	11?	~1	V ~1	L. Quat; 1?
5	1915	Pleasant V, NV	7.2-7.6	>62	V 2-5, Avg >2	V 5.8	Holo or L. Quat.; 4-5.
6	1932	Cedar Mtn, NV	7.1	75	3-15, Avg 8	SS 2.7	Holo and L. Quat; ~3.
7	1934	Excelsior Mtn, NV	6.3	>1.7	<1	V 0.13, LL 0.	L. Quat; 1.
8	1934	Hansel V, UT	6.6	11	~2.5	V 0.5, LL 0.2	L. Quat.
9	1947	Manix, CA*	6.2	1.6?	?	LL 0.076	1?
10	1948	Ft. Sage Mtn, CA	5.6	~9	<1	V 0.6,	Holo; 1.
11	1954a	Rainbow Mtn, NV	~6.5	18	12	V 0.7, RL~1.0	Holo; 1?
12	1954b	Fourmile Flat, NV	6.4	~6	~1	~1.5	Late Holo; 1.
13	1954c	Stillwater, NV	6.8-7.0	31-	>3, Avg 2	V 0.8	2?
14	1954d	Fairview Pk, NV	7.2	46	<13-19	4.8	L. Quat. (>35 ky); 3-4+.
15	1954e	Dixie V, NV	~7.0	42	5	3.8	Variable, Holo and L. Quat; 2.
16	1959	Hebgen L, MT	7.3	26.5	15	6.1	Holo; 2-3.
17	1975	Galway L, CA*	5.2	6.8		0.015	Holo; 1.
18	1979	Homestead V, CA*	5.2	3.25		RL 0.1, V .04	Holo and L. Quat; 1.
19	1980	Mammoth, CA	6.0-6.5	20	V 0.3,	?	Triggered? Larger Holo event.
20	1983	Borah Pk., ID	6.9	34	1-7, Avg 2	2.7	Holo, and L. Quat; 2-3.
21	1986	Chalfant V, CA	6.2	13-15.5	RL 7-11	0.05v	Holo; triggered slip?
22	1993	Eureka V, CA	5.8	>4	?	0.02	Triggered slip?
23	1992	Landers, CA*	7.3	~80	RL ~6, Avg 5	~6.7	Holo and L. Quat; 3-4.
24	1994	Double Spgs Fl, NV	5.8	~6.5	2	~0.1?	Holo and L. Quat; triggered slip.
25	1999	Hector Mine, CA*	7.1	41	1	RL 5.2	L. Quat (and older?)

\* Faulting event is within the Eastern California shear zone in the Mojave Desert.

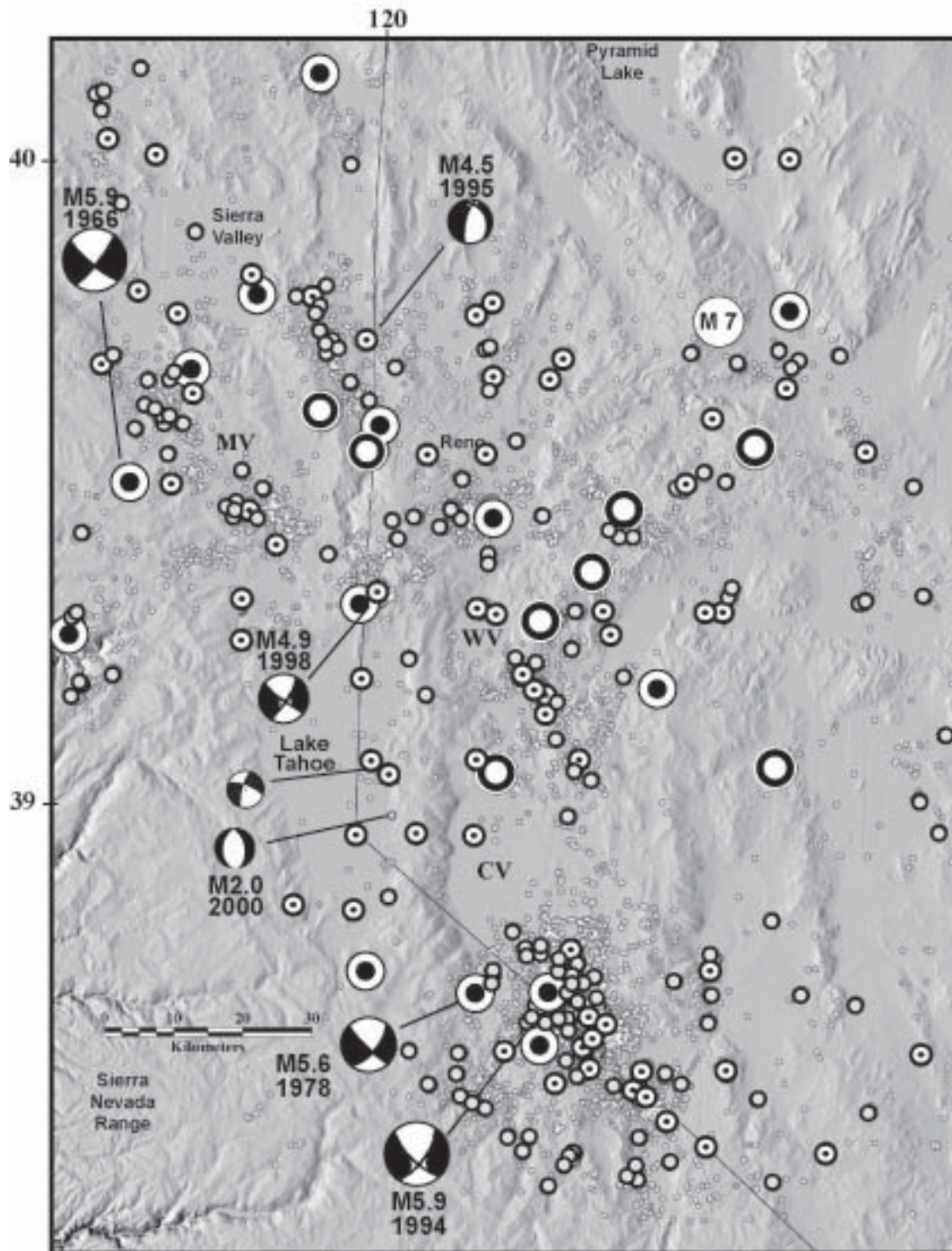
# Historic and Instrumental Seismicity in the Reno-Carson City-Lake Tahoe Area: Local Tectonics and Seismic Hazard

*Ken Smith*

University of Nevada Reno  
Nevada Seismological Laboratory

Geodetic data indicate that the Sierra Nevada block is moving at about 14 mm/yr N40-45W relative to stable North America. This motion accounts for about 20-25% of the western North American plate motion budget and is generally oblique to active faults along the Sierra Nevada-Great Basin Boundary Zone (SNGBBZ) and Walker Lane belt in the Central Western Great Basin. Through-going strike-slip faulting is concentrated east of the Sierran Range front through the Central Walker Lane belt. Active normal faulting, on the other hand, is primarily concentrated along a series of north-south striking left-stepping range bounding faults along the SNGBBZ from Long Valley through the Reno-Lake Tahoe area. Also, a series of NS striking down to east normal faults, younging westward, extend from the Wassuk Range NNW to the Sierran front, in a zone that is generally free small magnitude earthquake activity. Locally, strike-slip faulting, primarily recognized from earthquake focal mechanisms, is observed throughout the SNGBBZ and in the Reno-Lake Tahoe area, although it would appear, based on surface faulting, to account for significantly less of the Quaternary moment rate than normal faulting. However, the moment release from strike-slip faulting in the instrumental period exceeds that of normal faulting in the Reno-Lake Tahoe area. Instrumental seismicity in the Lake Tahoe region is primarily concentrated in transitions between left-stepping normal faults in predominantly high-angle strike-slip faulting that in some cases exhibits a conjugate faulting geometry. These zones have been the source regions of recent moderate sized earthquakes. Normal and strike-slip regimes, in the upper crust along the Sierran front, operate under a consistent E-W directed T-axis, with the P-axis rotating locally to reflect normal or strike-slip faulting. Also, these slip transition zones of concentrated seismicity and strike-slip faulting appear to exhibit a different recurrence behavior than the adjacent primary normal fault systems. They are characterized by a lower maximum magnitude and recurrence relation with a b-value of near 1, whereas the normal fault zones are generally free of background seismicity suggesting a characteristic recurrence behavior. Considering that the Quaternary moment release and displacements are dominated by the normal fault systems, one important kinematic problem is how to reconcile extension directions and slip vectors with Sierran motions. We should note an unusual sequence of earthquakes that continued from August 2003 through early 2004 that does not fit any of these preconceived notions of the Reno-Lake Tahoe area seismotectonics. About 1500 earthquakes were located at a depth of between 25-30 km beneath north Lake Tahoe, exhibiting a high b-value (~2), more characteristic of volcanic swarms than of tectonic earthquakes, and that was also dominated by reverse faulting mechanisms.

# Historical Seismicity Late 1800's to Present



- M < 3
- ⊙ M 4.0-4.9
- ⦿ M 6.0-6.9
- M 3.0-3.9
- ⦿ M 5.0-5.9

## A Record of the Past Three Surface-Rupturing Earthquakes Along the Central Hurricane Fault, Rock Canyon, Arizona

Stenner, H.D., Crosby, C.J., Dawson, T.E., Amoroso, L., *USGS, Menlo Park, CA*; Pearthree, P.A., *Arizona Geological Survey, Tucson, AZ*; and Lund, W.R., *Utah Geological Survey, Cedar City, UT*.

The Hurricane fault is a long, active normal fault in northwestern Arizona and southwestern Utah that helps to accommodate the transition from Basin and Range extension to the relatively stable Colorado Plateau (Fig.1). Long-term slip rates along the fault decrease from north to south. The north-central 'Anderson Junction' section of the fault has slipped at a rate of ~0.2mm/yr for the past 70-210k.y. (Stenner *et al.*, 1999). The most recent surface-rupturing earthquake (MRE) along the southern Anderson Junction section was ~M6.5-6.8 (average displacement ~0.6m) and occurred ~5-15ka, as interpreted from work at Cottonwood Canyon (Stenner *et al.*, 1999). Large, 18-20m displacements of older, ~70-125ka alluvial surfaces at Cottonwood Canyon require either larger offsets per event than the MRE or frequent events (~0.6m displacement) occurring every ~3-4k.y.

The Cottonwood Canyon site is ~4km south of the Rock Canyon site and ~6.5km south of the Honeymoon Trail site, both the focus of current study. Trenching at Rock Canyon reveals evidence for three late Quaternary surface-rupturing events (Fig.2). The MRE accommodated 0.3-0.4m of net vertical slip. The displacement for the penultimate event is poorly constrained but the penultimate and pre-penultimate events together accommodated 2.6-3.7m. If the two events were equal in size, then they were both larger than the MRE. Alternatively, the penultimate event may have resulted in a displacement of <1m, roughly similar in size to the MRE. If so, the pre-penultimate event was considerably larger, resulting in ~2-3m of net displacement.

A trench excavated at the Honeymoon Trail site reveals a relatively small slip of 0.4-0.7m, similar to both Rock Canyon and Cottonwood Canyon's MRE (Fig.1). They are likely the same event.

The variable displacements at Rock Canyon and the confirmation of a small MRE for this section of fault may indicate: 1) that the fault does not behave characteristically (and variably sized earthquakes occur), 2) that the tails of larger ruptures have overlapped from different originating sections, or 3) that the fault's slip rate has decreased during the past one or two seismic cycles and small earthquakes are now more likely to occur than >M7 events.

Stenner, H. D., W. R. Lund, P. A. Pearthree, and B. L. Everitt (1999). Paleoseismologic investigations of the Hurricane fault in northwestern Arizona and southwestern Utah, Arizona Geological Survey Open-File Report 99-8, 138p.

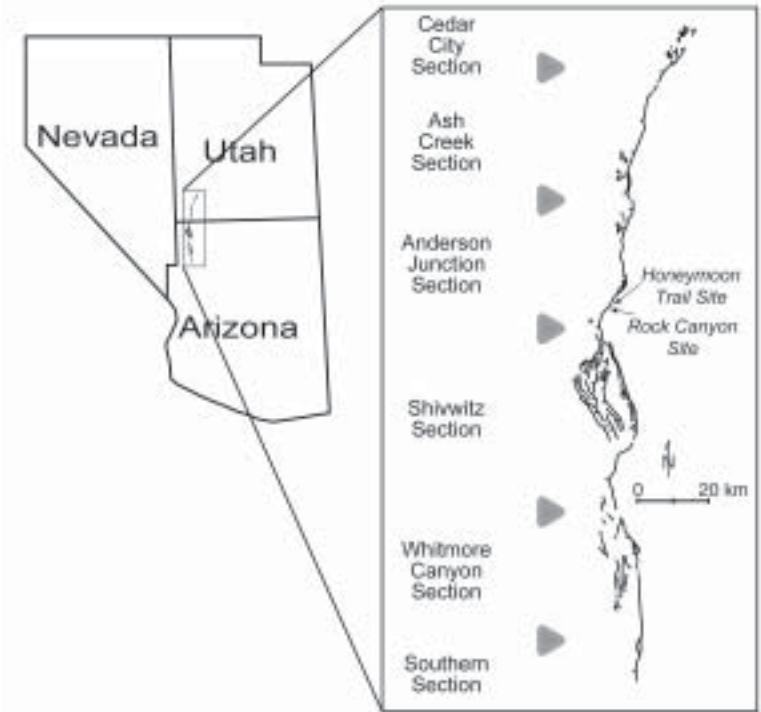


Fig. 1. Location map for the Hurricane fault with close up of fault detail. The six named sections of the fault are shown, including the Anderson Junction section, the focus of this study. Also shown is the log of a trench at the Honeymoon Trail site. The trench revealed that the MRE displaced the latest Pleistocene or early Holocene alluvial terrace deposits 0.4-0.7m across a small graben. Unit 1 is a colluvial deposit derived from the fault scarp, units 1a and 1b are subsequent slope-wash deposits that filled in the topographic low formed by the graben.

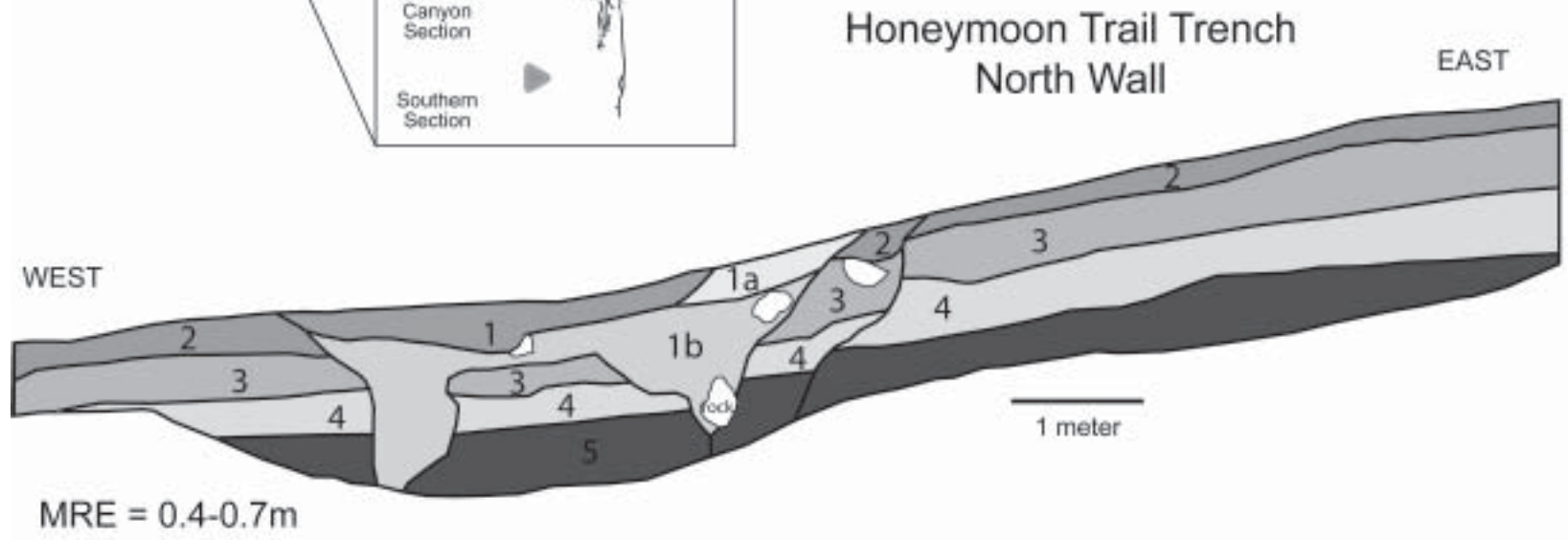
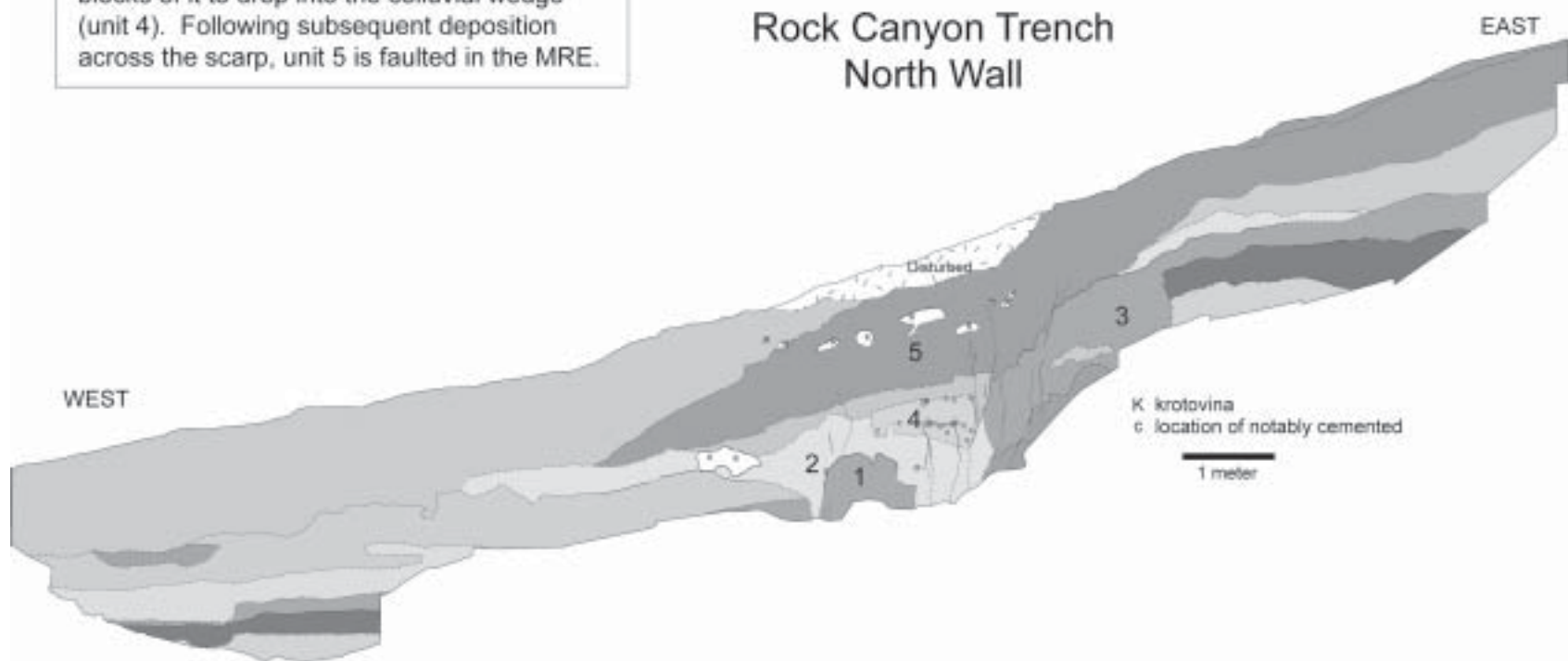


Fig. 2. Log of the north wall of the trench at the Rock Canyon site. Three events are recorded in the alluvium. The earliest event formed the fissures observed in unit 1. This event occurred prior to the soil development of unit 3, and unit 2 is part of the colluvial wedge from the earliest event. The penultimate event then occurred, faulting unit 3 and allowing blocks of it to drop into the colluvial wedge (unit 4). Following subsequent deposition across the scarp, unit 5 is faulted in the MRE.



## Active Tectonics and Strain Partitioning in the Northern Intermountain Seismic Belt

Michael C. Stickney  
Montana Bureau of Mines and Geology  
Montana Tech of the University of Montana  
Butte, MT 59701  
Email:  
[mstickney@mtech.edu](mailto:mstickney@mtech.edu)

David R. Lageson  
Department of Earth Sciences  
Montana State University  
Bozeman, MT 59717  
Email: [Lageson@montana.edu](mailto:Lageson@montana.edu)

We determined fault plane solutions for 82 earthquakes that have occurred since 1982 in northwest and west-central Montana using P-wave first motions recorded by the Montana seismograph network. We included four older fault plane solutions in our analysis. Thirty-six percent of the focal mechanisms showed strike-slip offset, 34 percent showed normal offset, and 29 percent showed oblique offset. A single event in northern Idaho showed reverse slip.

All but four normal-faulting earthquakes (Figure 1) occurred north of the Lewis and Clark zone (LCZ) in the vicinity of the Mission and Swan faults, and near the southern tip of the South Fork Flathead fault. They also occurred well away from mapped Quaternary faults. North of the LCZ, the preponderance of normal mechanisms have northerly trending nodal planes subparallel to mapped Quaternary faults. However, hypocenter positions and nodal plane orientations suggest that only two normal mechanism events are consistent with slip on the Mission and Swan faults. Strike-slip earthquakes (Figure 2) are widely distributed throughout the northernmost Intermountain Seismic Belt; many are near mapped Quaternary normal faults. A linear cluster of epicenters trending ESE from the southern tip of the Ovando fault includes four strike-slip mechanisms having nodal planes subparallel to the trend, indicating right-lateral slip at depth along this LCZ fault. The westerly trending nodal planes from strike-slip events within the LCZ consistently indicate right-lateral slip.

T-axis orientations (Figure 3) for 50 percent of the fault plane solutions trend east-west  $\pm 15^\circ$ ; another 30 percent trend N45 E-S45 W  $\pm 15^\circ$ , which is the average Basin and Range extension direction observed in SW Montana. Seventy-seven percent of the P-axes trend N15 W-S15 E  $\pm 30^\circ$ . Normal and strike-slip fault plane solutions with east-west to NE-SW T-axes indicate that the regional stress field is favorably oriented to produce slip on normal faults in NW Montana. Where these faults terminate southward into the LCZ, right-lateral slip on older WNW-trending faults is expected. We believe that low-slip-rate, right-lateral strike-slip faults exist in the LCZ but surface expressions have not yet been identified in forested regions with glacial cover.

Our model of regional extension places the northern limit of the Basin and Range province at the north end of the Flathead Valley. Southward, the northern Rockies are extending westward in five quasi-coherent crustal domains bounded by right-lateral, strike-slip, and oblique-slip accommodation and transfer zones, with each south-side domain translating further west than those to the north. The LCZ represents the northernmost accommodation zone. This model predicts a horizontal velocity field (westward extension accompanied by clockwise rotation) for the region between the Snake River Plain and northwest Montana.

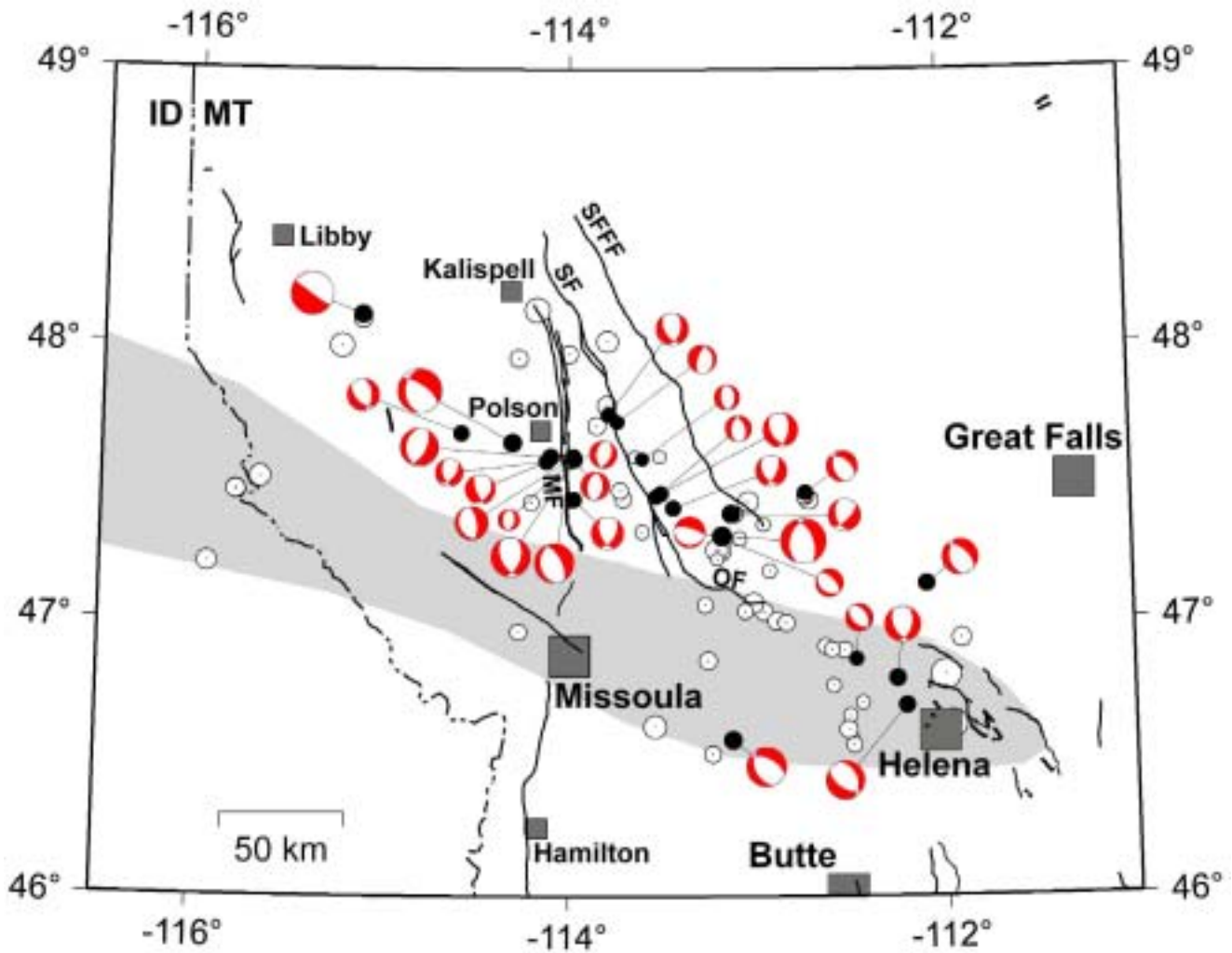


**Figure 1.** Earthquakes with normal slip mechanisms (black circles); open circles are epicenters with other mechanisms. Fault plane solutions are lower-hemisphere projections scaled to earthquake magnitude with compressional quadrants shaded. Light gray shading shows the extent of the Lewis and Clark zone. Line segments show Quaternary faults; bold segments (near Helena and southern Mission Fault) show faults with latest Quaternary offset. OF, Ovando Fault; MF, Mission Fault; SF, Swan Fault; SFFF, South Fork Flathead Fault.

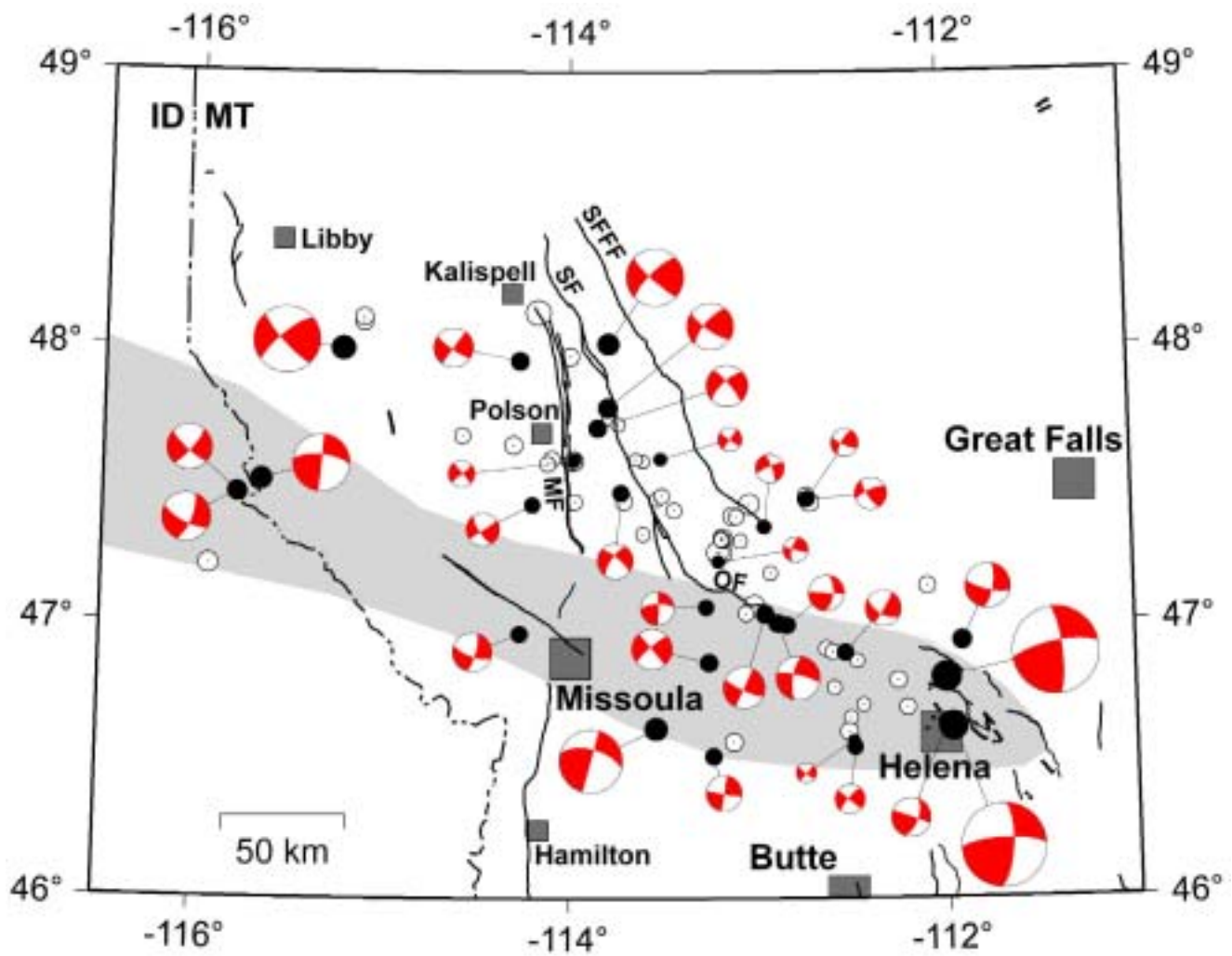
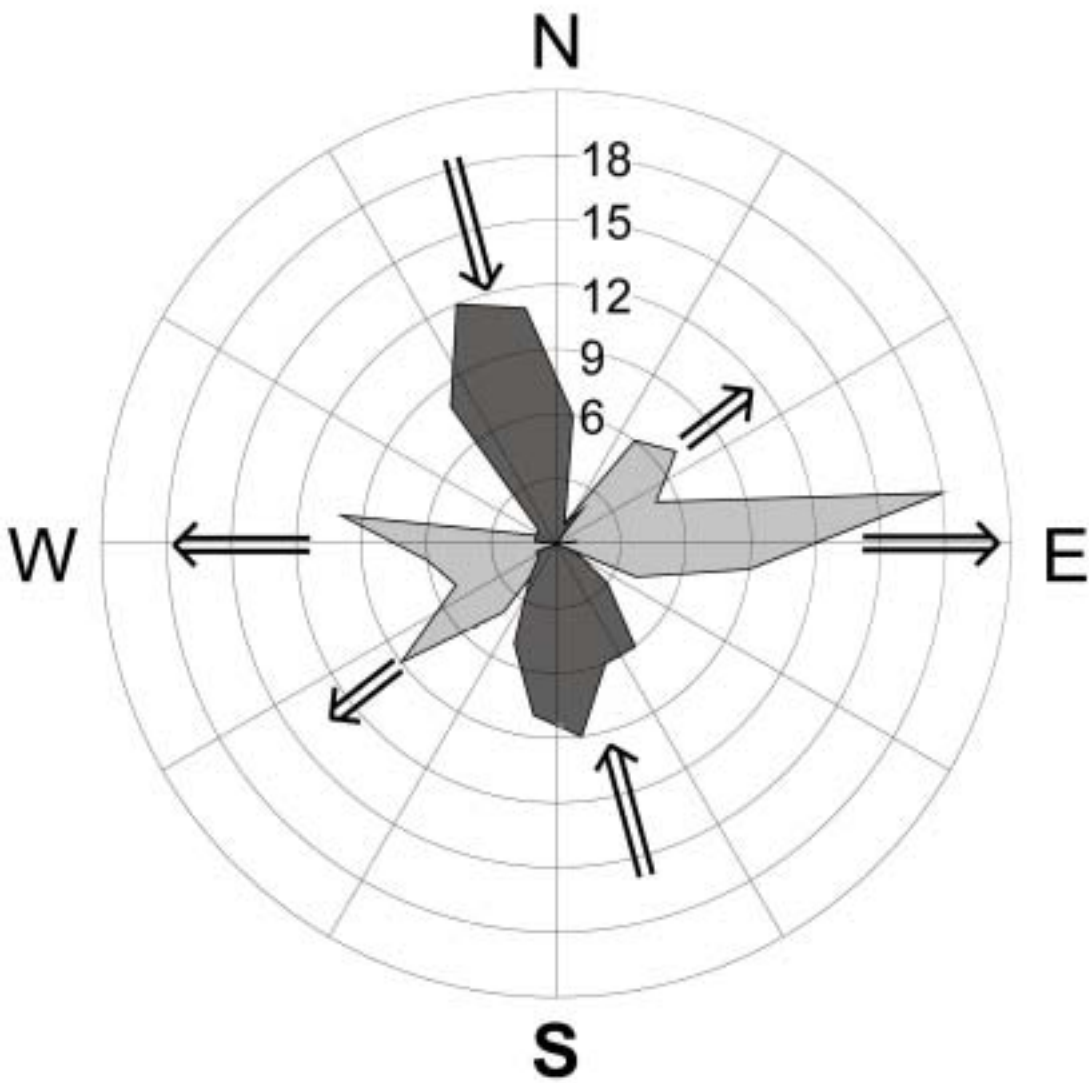


Figure 2. Earthquakes with strike-slip mechanisms. Other features are the same as in Figure 1.



**Figure 3.** T-axis (light gray) and P-axis (dark gray) orientations for 86 fault plane solutions in northwestern and west-central Montana. Radial units are the number of T- or P-axis orientations per 15° interval. Arrows signify dominant extension and compression directions.

## Paleoseismic Investigations of the Stansbury and Mid-Valley Faults, Skull Valley, Utah

F. H. Swan<sup>1</sup>, K.L. Hanson<sup>2</sup> and M.M. Angell<sup>3</sup>

<sup>1</sup> Consulting Geologist, San Francisco, CA, [bertswan3@aol.com](mailto:bertswan3@aol.com)

<sup>2</sup> Geomatrix Consultants, Inc., Oakland, CA

<sup>3</sup> William Lettis and Associates, San Rafael, CA

Recent studies in the Skull Valley, Utah provide new data on the location, geometry, and slip rate of the Quaternary active Stansbury fault and two previously unrecognized active faults within the basin (Fig. 1). Proprietary industry data, both gravity and seismic reflection data, were used to constrain the locations of major faults. High-resolution seismic S-wave reflection surveys and detailed surface and subsurface Quaternary studies provided data to evaluate the style, location, geometry, and slip rate of both primary, secondary, and distributed faulting.

The Stansbury fault is the major west-dipping normal fault that forms the structural boundary between the valley (half graben) on the west and the uplifted Stansbury Mountains to the east (Fig. 2). Near Antelope Canyon, the late Quaternary slip rate on the Stansbury fault is estimated to be  $3.9 \pm 0.04$  mm/yr (i.e., the cumulative rate across the main trace and two secondary traces in the hanging wall) (Fig. 3; Table 1). This slip rate is faster than previously reported estimates, primarily because displacement across the secondary traces was not included in the earlier estimates.

In the southern part of Skull Valley, two west-dipping mid-valley normal faults are informally named the East fault and the West fault. In the northern part of the basin, the postulated Springline fault occupies a similar structural position. The preferred slip rate on the East fault is  $0.2 \pm 0.1$  mm/yr based on measured displacements on three stratigraphic datums that range in age from 12 ka to  $\geq 160$  ka. A slip rate on the West fault of 0.05 to 0.07 mm/yr is based on the displacement of a single datum, the Stansbury bar, which is estimated to be 20 ka.

The probable maximum magnitude for the Stansbury, East and West faults are calculated based on empirical relations that relate magnitude to fault-rupture dimensions. The maximum earthquake magnitude distribution includes alternative maximum rupture scenarios for each fault. Alternative models treat the West fault as a primary independent fault or as a secondary fault in the hanging wall of the East fault. The mean maximum magnitudes for the three faults are: **M** 7.0 for the Stansbury fault, **M** 6.5 for the East fault and **M** 6.4 for the West fault in the independent fault model.

---

<sup>1</sup> Consulting Geologist, San Francisco, CA; [bertswan3@aol.com](mailto:bertswan3@aol.com)

<sup>2</sup> Geomatrix Consultants, Inc., Oakland, CA

<sup>3</sup> William R. Lettis and Assoc., Walnut Creek, CA

**Table 1**  
**Fault Slip Rate Data – Stansbury Fault Zone**  
**Skull Valley, Utah**

Location	Displaced Datum	Age (ka)	Cumulative Vertical Displacement (m)	Slip Rate (mm/year)	Comments	
<b>Stansbury Fault – Main Trace:</b>						
a)	Profile SF-1a - Antelope Canyon	Late Pinedale (?) alluvial fan surface	35 ±5	4.6 ±0.4	0.13 ±0.03	Long term rate on primary trace based on multiple events.
b)	Profile SF-1b - Antelope Canyon	Holocene stream terrace	8 ±2	1.9 ±0.2	0.36 +0.16/-0.09	Same trace as above; rate is probably based on a single event and is, therefore, unreliable.
<b>Stansbury Fault – Secondary Traces:</b>						
c)	Profile SF-2 - Indian-Hickman alluvial fan	Post-Stansbury Pre-Bonneville shorelines	18 ±2	2.7	0.15±0.02	Inflection in scarp profile and geomorphic relations indicate displacement is due to two events.
d)	Profile SF-3 - Indian-Hickman alluvial fan	Post-Stansbury Pre-Bonneville shorelines	18 ±2	1.9 ±0.1	0.11 ±0.02	Inflection in scarp profile and geomorphic relations indicate displacement is due to two events.
<b>Cumulative Slip Rate Across Zone:</b>						
g)	Transect west of Indian Hickman Canyon	--	--	--	0.39 ±0.04	Sum of slip rates a, c and d

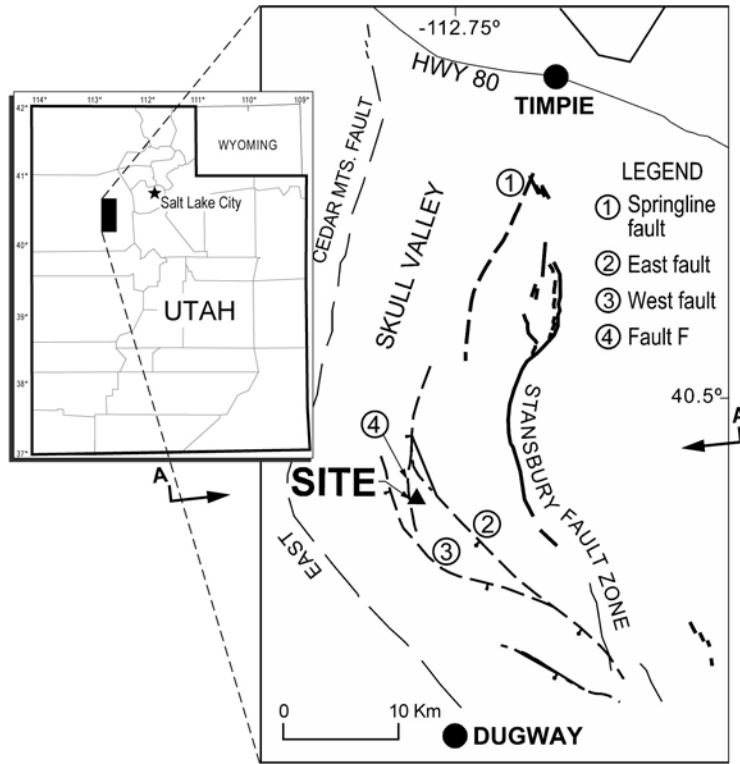


Figure 1. Location of faults, Skull Valley, Utah.

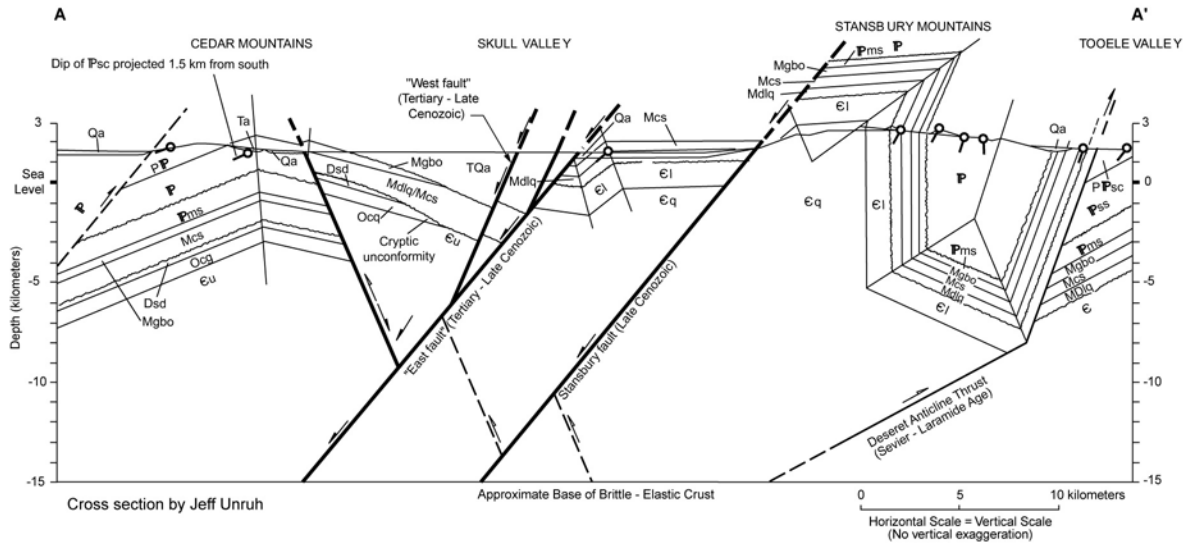
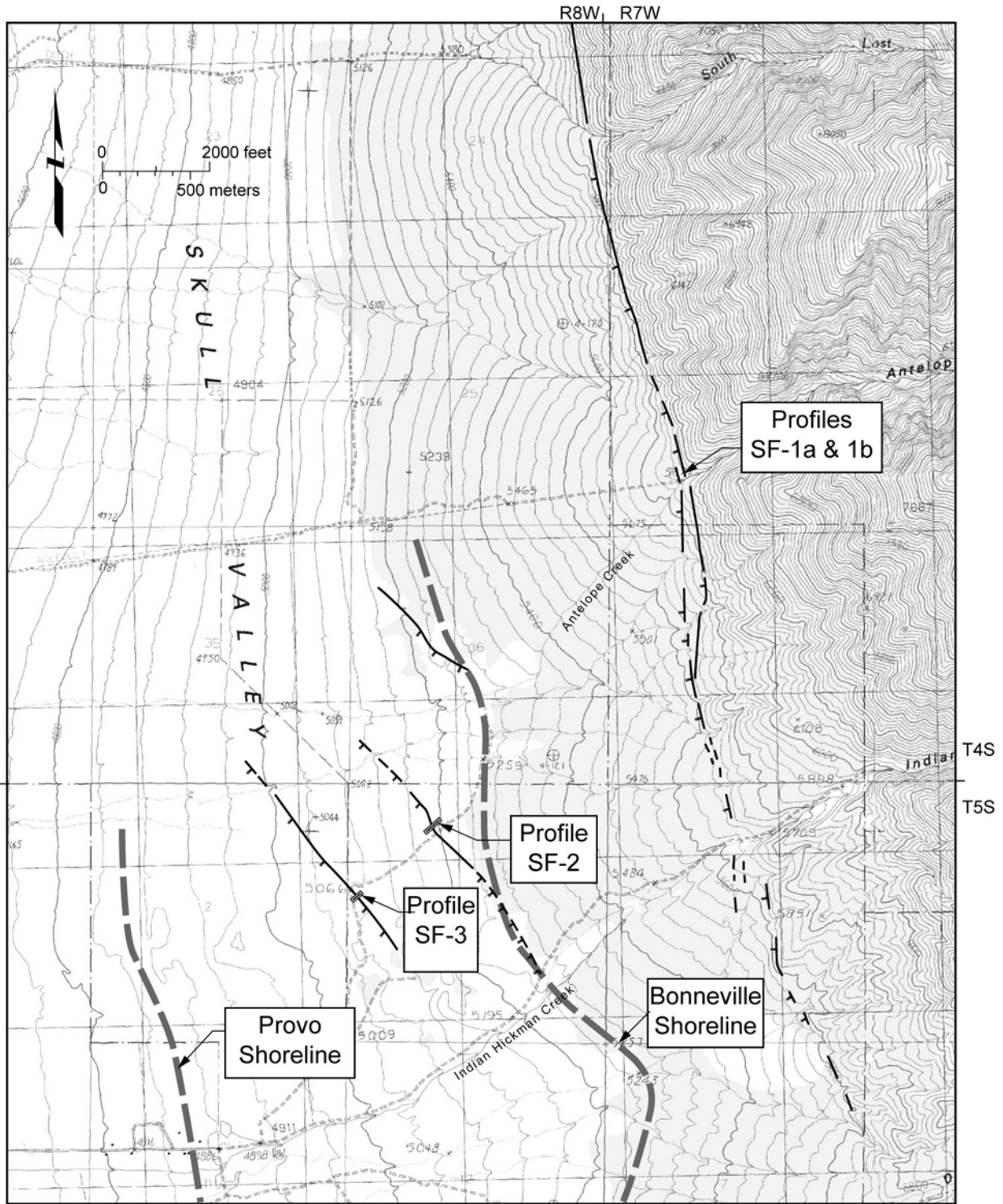


Figure 2. Structural geologic cross-section, Tooele Valley to Great Salt Lake Desert, Utah.



Base map from U.S.G.S Deseret Peak, Utah 7.5' topographic quadrangle, 1985.

Figure 3. Location of measured profiles across traces of the Stansbury fault east of the site.

## Spatial relations among young faults, basin fill and $V_s$ in Las Vegas basin: Implications for ground shaking

Taylor, Wanda J.<sup>1</sup>; Luke, Barbara<sup>2</sup>; Snelson, Catherine<sup>1</sup>; Liu, Ying<sup>2</sup>;  
Wagoner, Jeff  
<sup>3</sup>; Rodgers, Arthur<sup>4</sup>; McCallen, Dave<sup>4</sup>; Rasmussen, Tiana<sup>5</sup>; and  
Louie, John<sup>5</sup>

<sup>1</sup>Department of Geoscience, University of Nevada Las Vegas, 4505 Maryland Parkway, 4010, Las Vegas, NV 89154-4010

<sup>2</sup>Department of Civil & Environmental Engineering, University of Nevada Las Vegas, 4505 Maryland Parkway, Las Vegas, NV 89154-4015

<sup>3</sup>Lawrence Livermore National Laboratory, Earth Science Division, P.O. Box 808 L-221, Livermore, CA 94551

<sup>4</sup>Lawrence Livermore National Laboratory, Earth Science Division, P.O. Box 808, L-206, 8000 East Avenue, Livermore, CA 94551

<sup>5</sup>Nevada Seismological Laboratory and Department of Geological Sciences, Mail Stop 174, University of Nevada, Reno, NV 89557

*Las Vegas basin, southern Nevada contains as much as 4.5 km of basin fill that unconformably overlies Mesozoic and Paleozoic bedrock. The basin is bounded on the north by NW-striking Las Vegas*

*Valley shear zone and on the east by the N-striking Frenchman and NNW-striking River Mountains faults. Those three faults had significant motion in Miocene time (Fig. 1). The west-central part of the basin is cut by a series of E-dipping Quaternary faults including the Cashman, Valley View and Decatur-Eglington faults (Fig. 1). In this study we examine the spatial relations among young faults, basin-fill lithologies and  $V_s$  to aid in assessing the ground shaking hazard.*

The quality of the characterization of the subsurface lithologies beneath a basin is a common source of uncertainty in estimating the ground shaking hazard. Here, to reduce that uncertainty, we use lithologic data from ~1200 wells, < 640 m deep and 6 deep wells to characterize the lithologies under Las Vegas Valley. The lithologies fall into three spatial categories: western, central – Las Vegas Wash, and eastern. The western region is wide. The subsurface lithologies are dominantly coarse-grained (gravel to boulder) and mixed-size (clay to boulder) deposits that we interpret as alluvial fan deposits (Fig. 2). Near the center of the basin these fan deposits interfinger with clay-dominated deposits, which to the east, interfinger with a narrow zone of coarse-grained (gravel to boulder) and mixed size (clay to boulder) alluvial fan deposits. The central clay-rich zone, lies below and is wider than, but generally parallels Las Vegas Wash (Fig. 1). The clay-rich deposits are weaker than the coarse and mixed-grain size sediments, and thus, present a greater ground shaking hazard.

The greatest structural control on the basin-fill sediments appears to be from the Frenchman River Mountains fault, on the E side and the Las Vegas Valley shear zone on the N side. These faults appear to have had significant offset in the Miocene, therefore, the Las Vegas basin began to form at least as early as Miocene time. A Miocene age of basin initiation is confirmed by the presence of Miocene-age sediments of the Horse Spring and Muddy Creek Formations, or their equivalents, in some of the deeper wells.

Our SASW (Spectral Analysis of Surface Waves) studies of  $V_s$  at ~20 different sites within the region indicate that  $V_s$  generally increases with depth, but is lowest for the clay and clay-rich deposits (400-600 m/s). These relatively low values indicate that the ground shaking hazard is likely to be greatest above the clay-rich central zone.

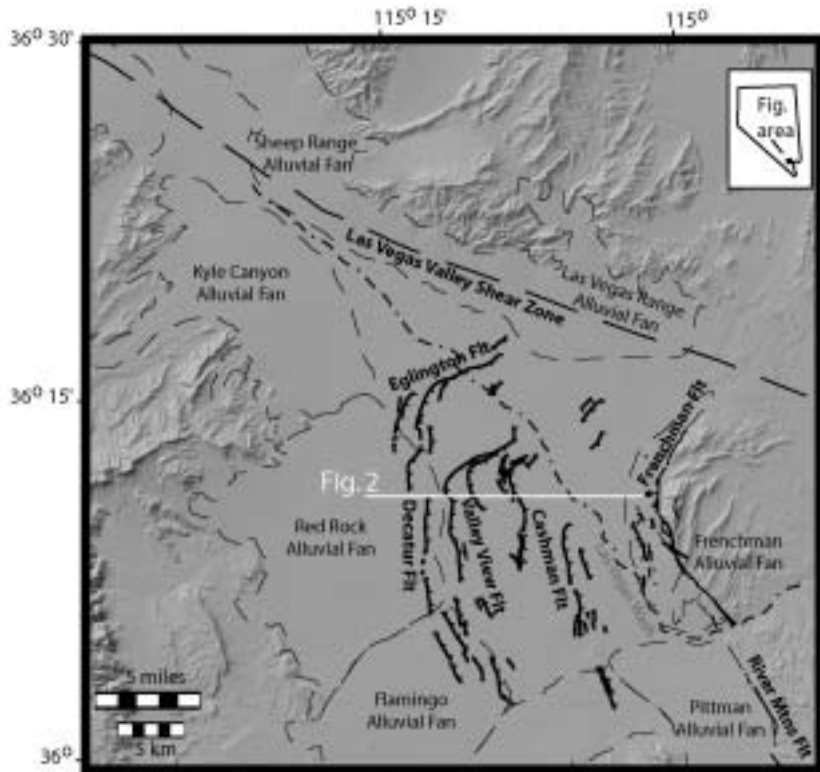


Figure 1. Location of significant Cenozoic faults and alluvial fans in the Las Vegas basin. Clay deposits are depth tend to be located in the general vicinity of Las Vegas Wash.

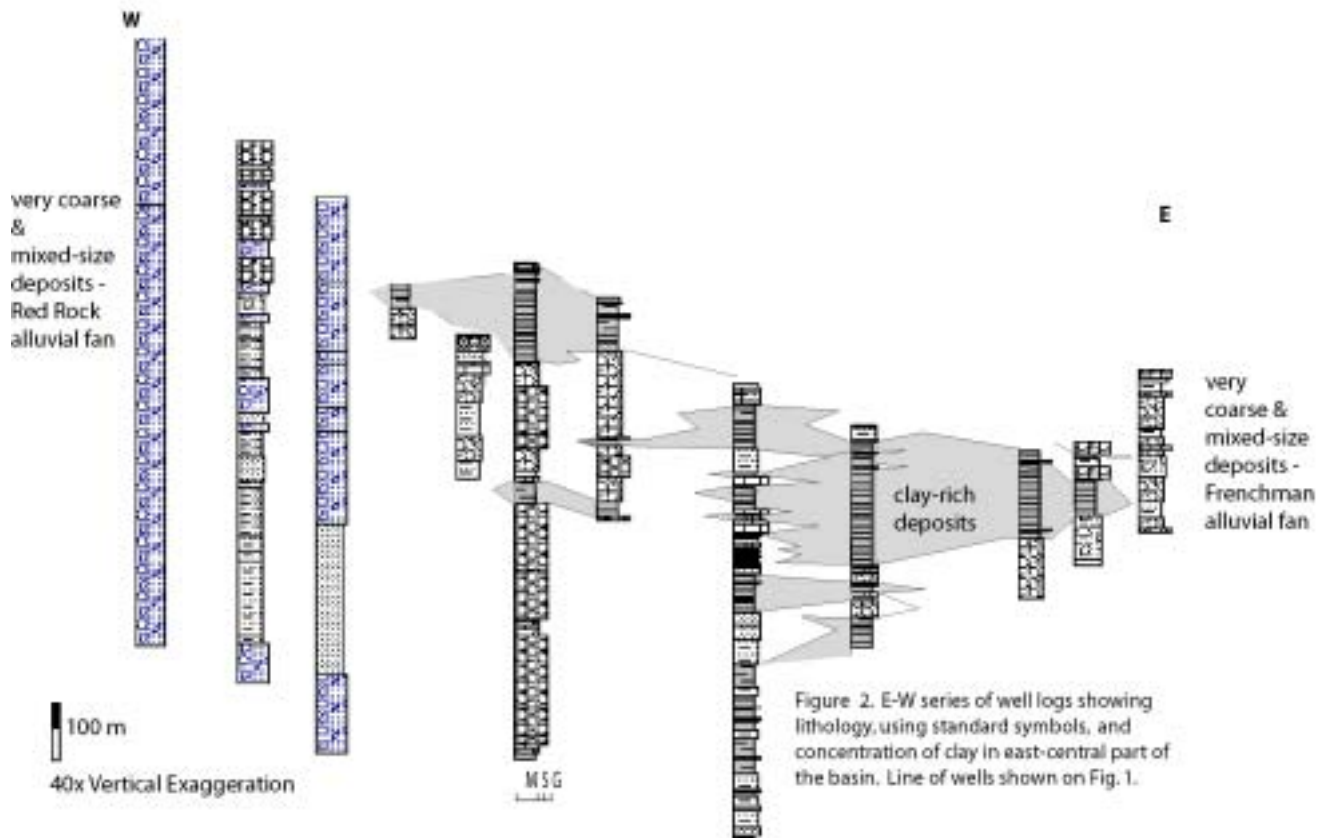


Figure 2. E-W series of well logs showing lithology, using standard symbols, and concentration of clay in east-central part of the basin. Line of wells shown on Fig. 1.

## Seismic Hazard at the Designated Repository for High-Level Nuclear Waste, Yucca Mountain, Nevada, from 25 Years of Seismic Monitoring

David von Seggern (vonseg@seismo.unr.edu)  
Nevada Seismological Laboratory, U. Nevada

The instrumental monitoring of seismic activity around Yucca Mountain (YM), Nevada, began in 1978 with the installation of a network of analog stations with mostly vertical components. This network monitored activity out to roughly 125 km from YM. In 1995 a network of three-component, 24-bit digital stations was installed to replace the analog network. Although smaller in extent (~ 50 km radius around YM), this network is far more capable of detecting and characterizing earthquakes in the region. Today, the digital network comprises 30 digital weak-motion stations; in addition, there are 17 strong-motion sites in the inner part of the network close to YM.

Figure 1 shows the seismic activity above M 2 and within 65 km of YM recorded from 1978 through 2003. The cutoff at 65 km was made in order that results from both networks could be used. The largest event recorded within this region was the M 5.6 Little Skull Mountain (LSM) earthquake on 29 June 1992, almost surely triggered by the M 7.1 Landers, California, earthquake that occurred a day prior. This one incident demonstrates that accumulated stress near YM is subject to release due to an energy pulse of a relatively distant earthquake. The LSM earthquake was followed by a vigorous aftershock sequence of over 15,000 located events, continuing even now. The 2nd-largest event in the area shown was the M 4.7 Frenchman Flats earthquake on 27 January 1999. The 3rd-largest was the surprising M 4.4 event on 14 June 2002 in the aftershock zone of the LSM earthquake; this event is so late in the aftershock sequence and of such relatively large magnitude that it fails the conventional definitions of aftershocks.

Using all the data shown in Figure 1 plus all the  $M < 2$  activity not shown, the cumulative recurrence curve is shown in Figure 2 for the 25 years. In this figure the contribution of the 1978-1995 analog network and 1995-2003 digital networks are also shown separately. This clearly shows that the digital network is achieving a reporting threshold at least 0.5 unit lower than that of the analog network. Within the 10-km circle surrounding YM, the digital threshold is below M 0. Through 2003 the largest earthquake recorded within this area by the digital network is only M 0.6 and the total number is 27, indicating a very low rate of seismic moment release in the immediate vicinity of YM itself. This observation agrees well with the low slip rates inferred from geologic evidence at known faults in the same vicinity and with the observations of numerous precarious rocks in the YM block.

A large number of focal mechanisms have been determined for earthquakes reported by the analog and digital networks. These mechanisms can be presented succinctly as a graphical mapping of the P (pressure) and T (tension) axes computed from the focal mechanisms as in Figure 3. The overwhelming evidence is that the mean T axis is directed along the WNW-ESE direction at relatively low angle, indicating regional tensional strain along this direction. The P axes are less concentrated, and their relatively broad range of dips indicates a mixture of dip-slip to strike-slip mechanisms. Thus the minimum stress rotates between vertical and horizontal, a common feature of tensional zones.

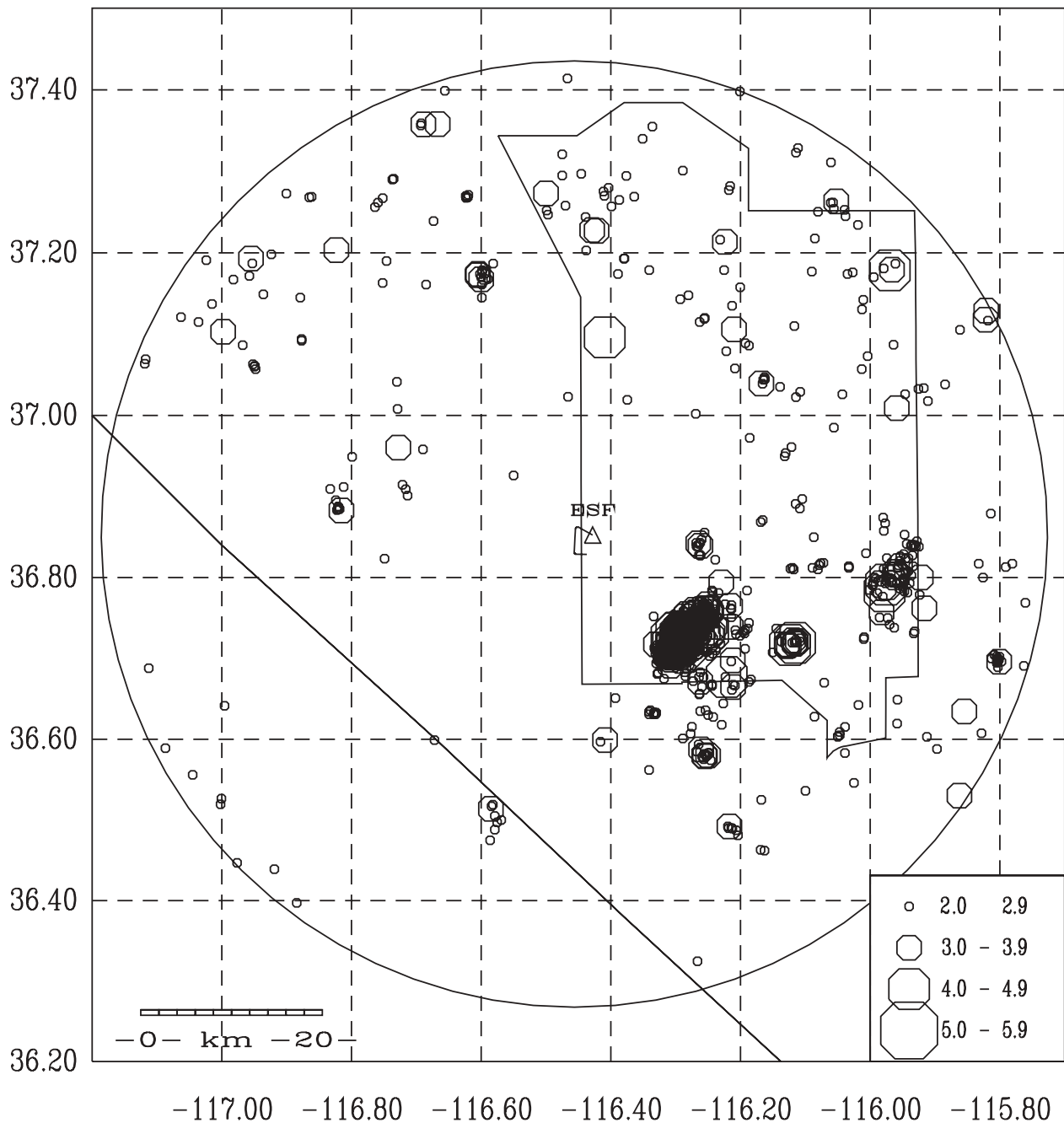


Figure 1. All earthquakes with  $M > 2$  during 1978-2003 in the vicinity of Yucca Mountain, Nevada. The ring is a 65-km radius from station RPY above the designated repository, and it indicates the approximate reporting area of the current digital network. "ESF" is the Exploratory Surface Facility, a 5-km tunnel excavated in Yucca Mountain. The large cluster of events to the southeast of Yucca Mountain is the aftershock zone of the 1992 Little Skull Mountain earthquake of  $M$  5.6. The symbol for this event is obscured by those of the numerous aftershocks.

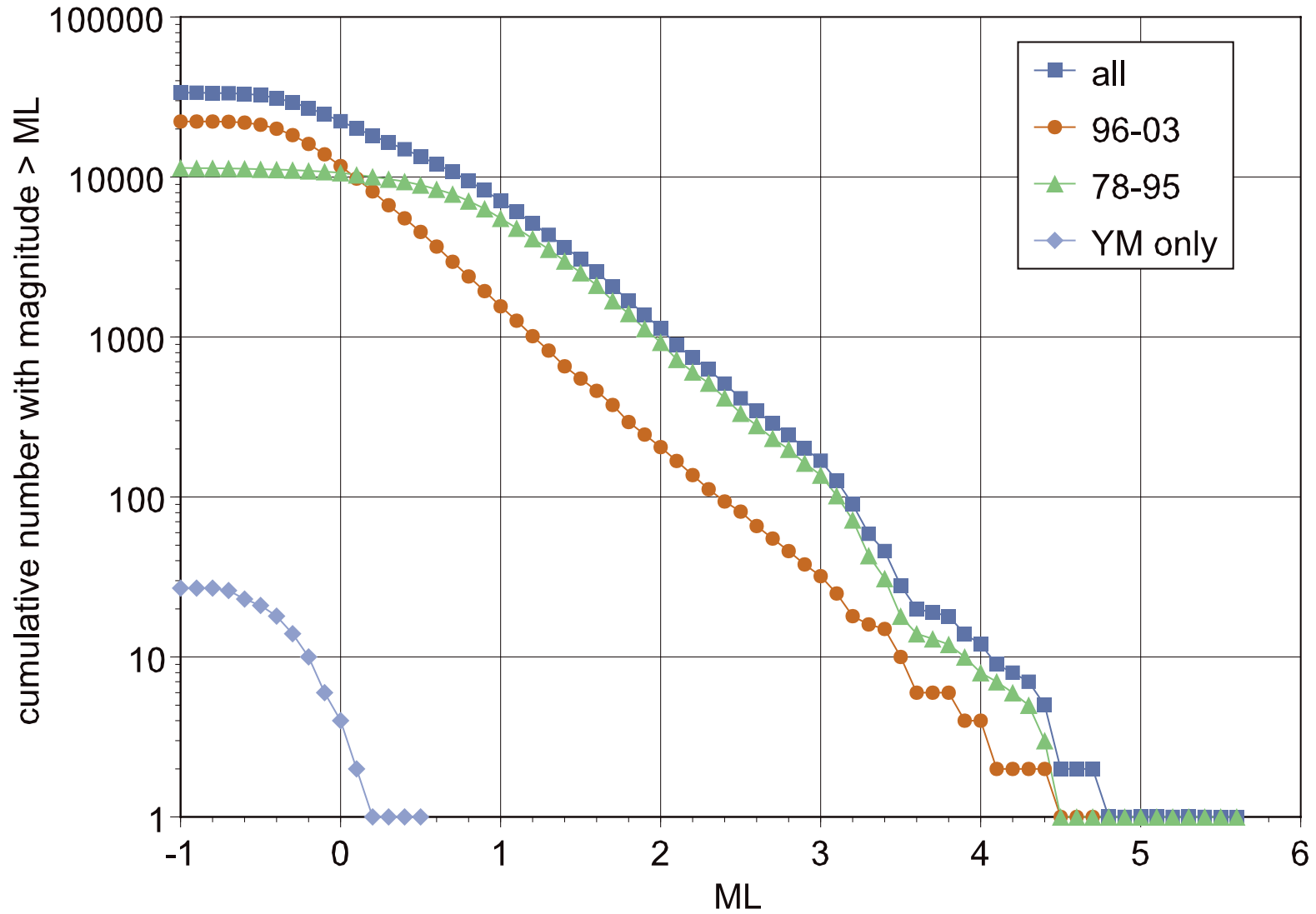


Figure 2. Earthquake recurrence curves for 4 datasets comprising events within 65 km of Yucca Mountain. "all" comprises the entire time period; "78-95" comprises the period of the analog network; "96-03" comprises the period of the digital network; and "YM only" uses only events < 10 km from Yucca Mt. in 96-03.

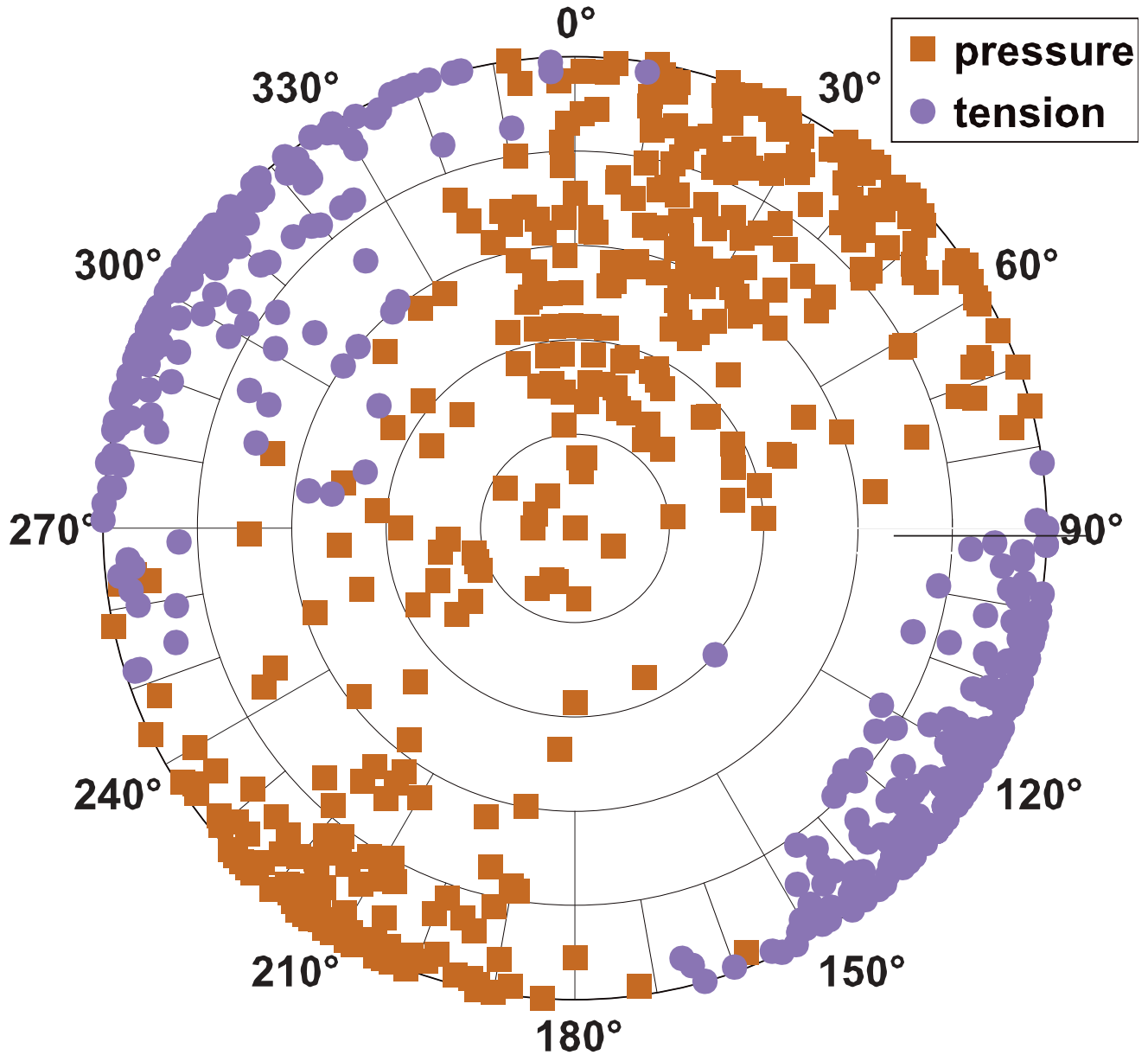


Figure 3. Orientations of the pressure (P) and tension (T) axes from focal mechanisms determined by the NSL (1993-2003) in the vicinity of Yucca Mountain (65-km radius). The point at which the P or T axis intercepts the lower focal sphere is projected vertically to the equatorial plane to give the point shown here. T axes are directed generally WNW to ESE and fall at shallow dip angles (horizontal tension) while the P axes are directed orthogonally but generally at higher angles.

## Digital trench wall logging: applying morphological image processing techniques to trench wall stratigraphy

Julie B. Willis<sup>1</sup>, Chaiwoot Boonyasirawat<sup>2</sup>, Gerald T. Schuster<sup>1</sup>, Christopher B. DuRoss<sup>1</sup>

<sup>1</sup>University of Utah, Department of Geology and Geophysics

<sup>2</sup>University of Utah, Department of Computational Engineering and Science

E-mail: jwillis@mines.utah.edu

Traditionally, the walls of trenches dug across active faults are hand logged to separate clasts exposed in the trench walls from the matrix fill. Such logging is subject to human error and does not lend itself readily to statistical analyses of the sedimentary packages identified in the trench walls. Here we propose an algorithm to produce a digital log of trench wall sediments that autonomously separates clasts from the matrix and generates dimensional and orientation statistics for the separated clasts. The algorithm was developed and tested using digital photos of a section of the upper level of the Mapleton, Utah 'mega-trench,' which was cut across the Wasatch fault in 2003 (Figure 1).

The algorithm consists of a linked sequence of fundamental image processing techniques: histogram normalization, thresholding, edge detection, edge linking, watershed transform, opening, and dilation (Figure 2). The algorithm successfully segmented 2900 clasts from each other and from the matrix in a colluvial wedge, a debris flow and a channel deposit previously identified in the trench wall. Accuracy varied between 70% and 95%, depending on the contrast between the clasts and between the clasts and the matrix in the digital photo. The algorithm was also applied to a higher contrast and less complex image of a Mars surface with 100% accuracy (Figure 3). Further optimization of the algorithm can be achieved with minimal user-controlled reclassification prior to the final labeling step.

After executing the algorithm, each classified clast is a labeled watershed region from which the eccentricity, area, perimeter, axes lengths, and orientation among other parameters quickly can be calculated. Statistical comparisons of our minimal data set (4 m<sup>2</sup>) indicate that three measures, the clast-to-matrix ratio, clast eccentricity, and clast orientation potentially may be used to statistically differentiate colluvial wedges, debris flows and channel deposits exposed in trench walls (Figure 4). For the data set, the clast to matrix ratio is 9 to 18 % greater in the colluvial wedge than in the debris flow and channel deposit respectively. Clasts in the channel deposit have a slightly greater tendency towards roundness than clasts in the colluvial wedge and debris flow. In the colluvial wedge 73% of clasts have a planar preferred orientation greater than  $\pm 20^\circ$  (with 24% of these clasts oriented coincident with a fault dip of  $\sim 60^\circ$ ), while only  $60 \pm 3\%$  of clasts in the debris flow and channel deposit have a planar preferred orientation greater than  $\pm 20^\circ$ . These latter clasts also have no preferred orientation coincident with the dip of the fault. Future work on additional trench wall images will help determine whether measurements of clast eccentricity, clast orientation and the clast-to-matrix ratio can be used to definitively categorize trench wall stratigraphy.

The proposed algorithm is not restricted to clast segmentation and trench wall stratigraphy. Other suggested applications include analyzing landslides, stream braiding patterns, downhole digital images of boreholes, joint patterns, and planetary surfaces (Figure 3).

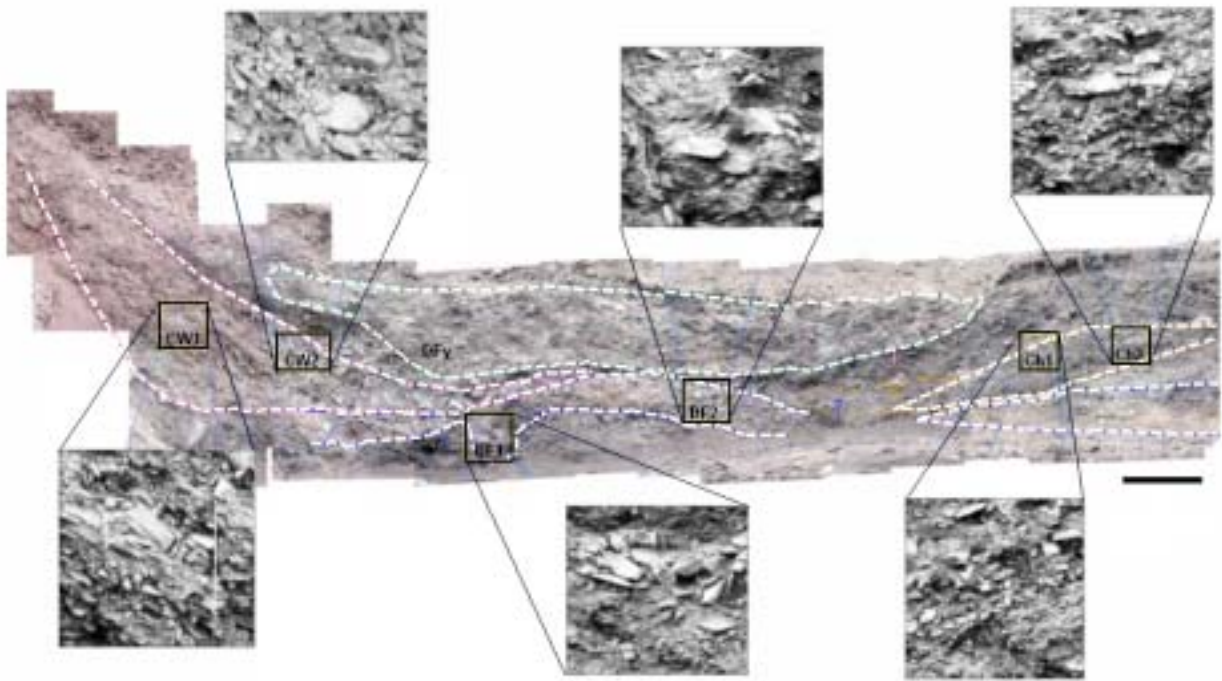


**Figure 1.** Digital photo mosaic of a section of the upper level of the 2003 Mapleton trench wall. An optimized sequence of morphological image processing techniques was used to separate clasts from matrix in each enlarged image. The resulting digital log of the enlarged image could then be statistically analyzed. Dashed lines separate previously determined stratigraphic units: CW = colluvial wedge; DF = debris flow; DFy = younger debris flow; Ch = channel deposits. Bar represents 1 m on the mosaic and 10 cm on the enlarged images. Photos courtesy Utah Geological Survey.

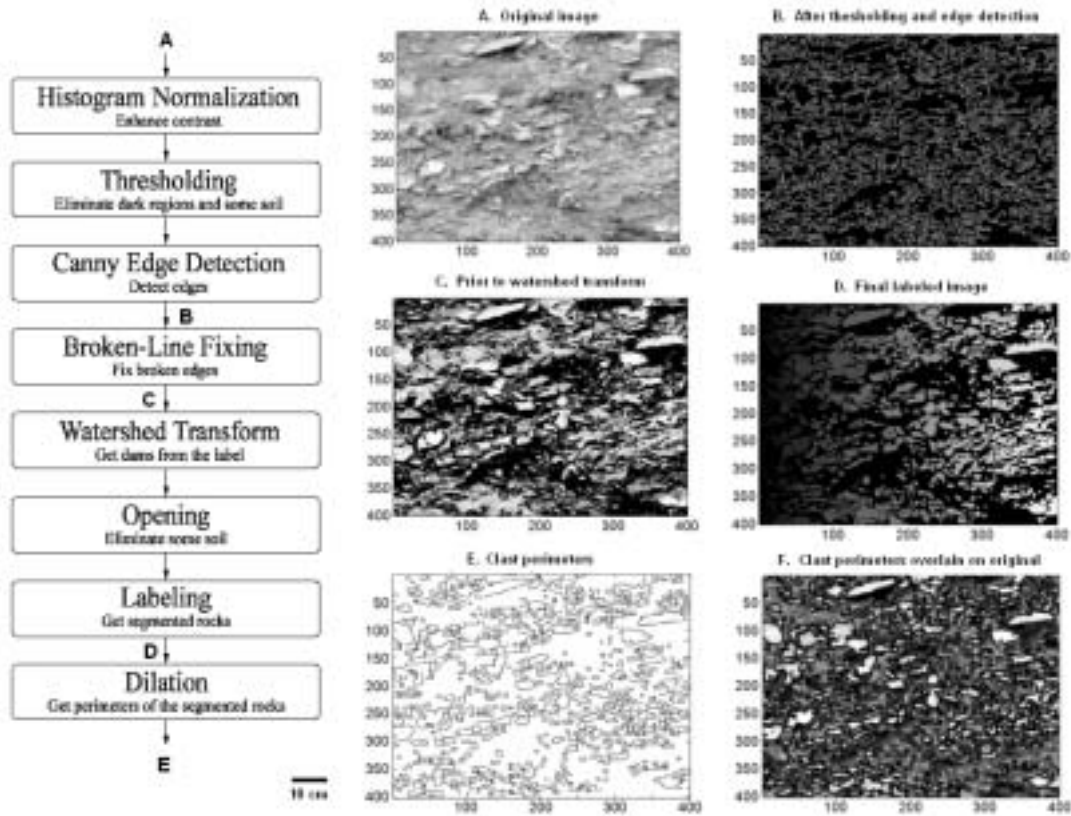


**Figure 2.** Flowchart and selected images illustrating the morphological clast segmentation algorithm. The original image is Ch1 from Figure 1. Letters on algorithm refer to images. The algorithm correctly separated 90% of the clasts from each other and from the background matrix. About 10% of the clasts were oversegmented. About 20% of the matrix was classified as small clasts (<0.3 cm<sup>2</sup>), which were eliminated in the statistical analysis. Figure E is the digital log.

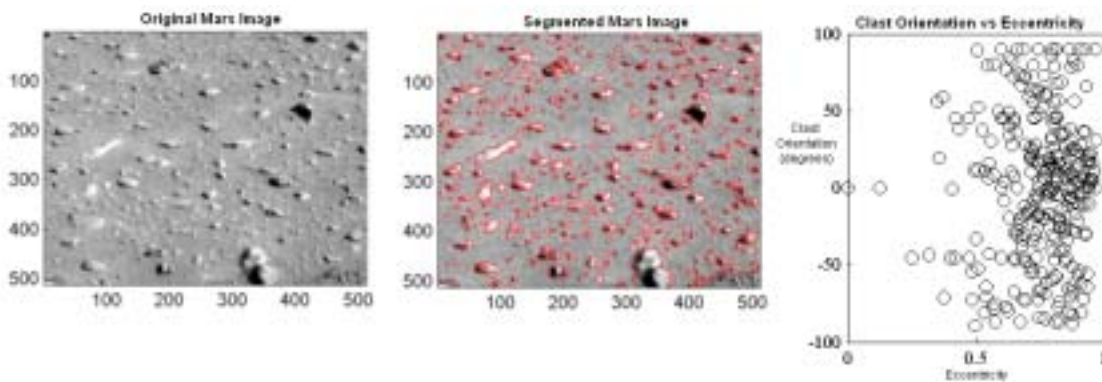


**Figure 3.** Segmentation of rocks exposed on a Mars surface. Plot shows example statistics that quickly can be calculated for each segmented and labeled rock. Other statistics that can be calculated include centroid, perimeter, area, and lengths of major and minor axes.

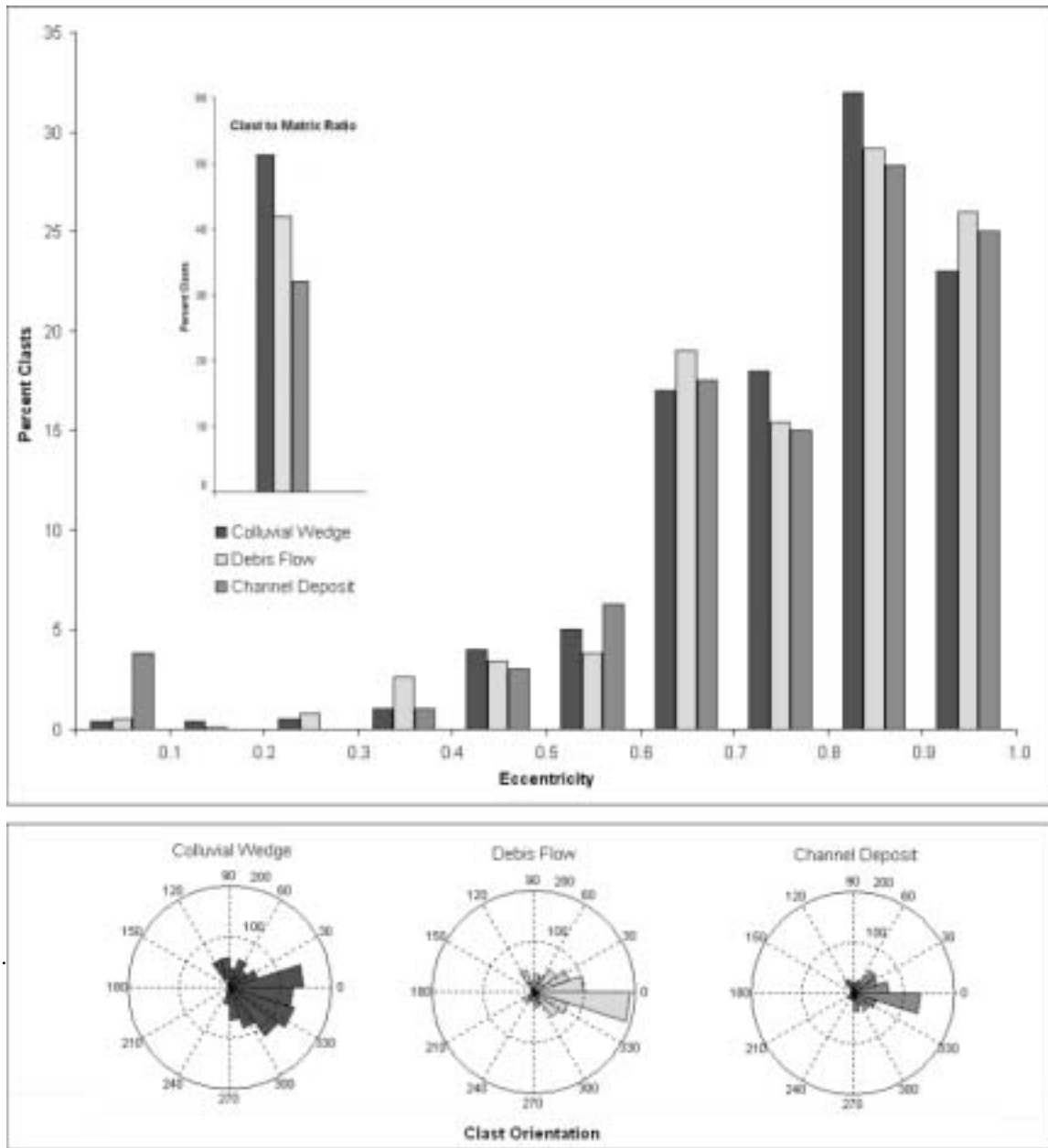


**Figure 4.** Comparison of data generated using 4 m<sup>2</sup> of segmented images from the 2003 Mapleton, Utah trench walls. The images were previously identified as colluvial wedge, debris flow or channel deposit. Noticeable differences between the percent clasts, the eccentricity, and the clast orientation may prove to be statistically important if they persist after processing additional trench wall images. Clasts less than 0.3 cm<sup>2</sup> were considered oversegmented matrix and were eliminated from the analyses. Standard deviation eccentricity: 0.16 (colluvial wedge), 0.15 (debris flow), 0.20 (channel deposit). Standard deviation orientation: 48.6 (colluvial wedge), 39.0 (debris flow), 40.2 (channel deposit). Standard deviation area: 14.3 (colluvial wedge), 17.3 (debris flow), 28.4 (channel deposit).

# PROBABILISTIC EARTHQUAKE GROUND MOTION HAZARD MAPS FOR MONTANA

Ivan Wong, Susan Olig, Mark Dober, Doug Wright, and Eliza Nemser  
Seismic Hazards Group  
URS Corporation, 1333 Broadway  
Oakland, CA 94612  
ivan\_wong@urscorp.com

David Lageson  
Montana State University, Department of Earth Sciences  
Bozeman, MT

Walter Silva  
Pacific Engineering & Analysis, El Cerrito, CA

Michael Stickney  
Montana Bureau of Mines & Geology, Butte, MT

Michele Lemieux  
Montana Department of Natural Resources and Conservation, Helena, MT

Larry Anderson  
U.S. Bureau of Reclamation, Denver, CO

## ABSTRACT

Western Montana is characterized by abundant late-Quaternary Basin and Range normal faulting and historical seismicity. It includes the Intermountain Seismic Belt (ISB), a zone of elevated seismicity, and the seismically and volcanically-active Yellowstone region. Paralleling the southwestern border of the state is the Centennial Tectonic Belt (CTB), also a zone of significant seismicity. The largest historical event has been the 1959 moment magnitude (**M**) 7.3 Hebgen Lake earthquake located just west of Yellowstone National Park. In contrast, eastern Montana, similar to other portions of the Great Plains in the central U.S., has only two known faults of possible late-Quaternary age. Seismicity is also at a relatively low level although the largest event has been about **M** 5.5.

Because of the potential earthquake threat to dams in the state, we have developed a set of probabilistic earthquake ground motion maps for the Montana Department of Natural Resources and Conservation (DNRC) Dam Safety Program. The statewide maps display peak horizontal acceleration and 0.2 and 1.0 sec spectral acceleration for 10%, 2%, and 1% in 50 years exceedance probabilities (return periods of 500, 2500, and 5000 years, respectively). This range of exceedance probabilities was selected to consider the range of hazard categories of Montana dams based on downstream risk. Ground motions are calculated for a rock site condition and at the ground surface; the latter includes site response effects for the areas underlain by unconsolidated sediments. A total of 18 maps were developed for the three exceedance probabilities, three spectral accelerations, and two site conditions (Wong *et al.*, 2004).

There were five principal tasks in this study: (1) seismic source characterization; (2) definition and characterization of geologic site response categories and assignment of amplification factors; (3) seismic attenuation characterization; (4) probabilistic ground motion calculations; and (5) map development. Our seismic source characterization model for this analysis included 92 potential fault sources and relied heavily on recent compilations by Haller *et al.* (2000) and Stickney *et al.* (2000). We included all known faults longer than 5 km with evidence for repeated Quaternary movement within Montana and extending out to 50 km beyond the border. We also considered more significant faults out to 100 km, including longer, more active faults (e.g., Teton, Lemhi, and Lost River faults). Unfortunately, most of the Quaternary faults in Montana (> 85%) have not been studied in any detail and very few data are available to develop rupture models and constrain slip rates.

To address the hazard from background seismicity, we defined eight regional source zones: the northern and central ISB, CTB, Yellowstone region, Northern and Middle Rocky Mountains, Northern Great Plains, and the eastern Snake River Plain. We adopt values of

$M 6$  to  $6\Omega \pm \sigma$  depending on the seismotectonic setting. In addition to the traditional approach of using areal source zones (assuming uniformly distributed seismicity), Gaussian smoothing was also used to address the hazard from background earthquakes in the probabilistic analysis. In this approach, we smoothed the historical background seismicity to incorporate a degree of stationarity, using a spatial window of 15 km.

An important consideration in the selection of attenuation relationships is that western Montana is located in the extensional Basin and Range Province where normal faulting dominates and eastern Montana lies within the compressional Midcontinent. To characterize the attenuation of ground motions, we used attenuation relationships appropriate for soft rock sites in the western U.S. and hard rock sites in the Midcontinent, and a stochastic numerical ground motion modeling technique. It has been increasingly recognized that earthquakes in extensional tectonic regimes produce lower ground motions than events in compressional/strike-slip regimes for the same magnitude and distance (e.g., Spudich *et al.*, 1999).

To compensate for the lack of region-specific attenuation relationships, the stochastic ground motion modeling approach was used to develop such relationships for both western and eastern Montana. The point-source version of the stochastic methodology was used to model earthquakes of  $M$  5.5, 6.5, and 7.5 in the distance range of 1 to 400 km. Uncertainties in stress drop, magnitude-dependent focal depths, the crustal attenuation parameters  $Q_0$  and  $h$ , the near-surface attenuation parameter ( $\kappa$ ), and the rock profile atop the crustal model were included in the computations of the attenuation relationships through parametric variations.

Amplification factors were used to modify the rock motions, consequently incorporating site response into the hazard maps. These factors were based on five generalized geologic site response categories (hard rock, soft rock, Quaternary alluvium, Quaternary lacustrine deposits, and Quaternary glacial till). Subsurface geologic and geotechnical data are significantly inadequate for Montana and so we adopted amplification factors from correlative categories developed in studies for Salt Lake Valley and California. Depth-dependent site amplification factors were used for the basins in western Montana.

The resulting hazard maps for an uniform site condition of soft rock show the highest hazard is concentrated along the most active faults (Figure 1). For example, at a return period of 5000 years, the highest peak horizontal accelerations reach upwards of 1 g in the vicinity of the active Centennial fault near the Montana-Idaho border. Other relatively moderate hazard areas occur in the vicinities of the Mission, Canyon Ferry, Madison, Emigrant, and Red Rock faults. Areas away from the more active faults in western Montana are characterized by values of 0.10 to 0.30 g. Eastern Montana is characterized by peak horizontal accelerations of less than 0.10 g at a return period of 5000 years due to the lack of active faults and a low-level of seismicity.

#### Reference

- Haller, K.M., Stickney, M.C., and Machette, M.N., 2000, Quaternary faults and seismicity in western Montana: Montana Bureau of Mines and Geology Open-File Report 114, 241 p.
- Spudich, P., Joyner, W.B., Lindh, A.G., Boore, D.M., Margaris, B.M., and Fletcher, J.B., 1999, SEA99 – A revised ground motion prediction relation for use in extensional tectonic regimes: Bulletin of the Seismological Society of America, v. 89, p. 1156-1170.
- Stickney, M.C., Haller, K.M., and Machette, M.N., 2000, Quaternary faults and seismicity in western Montana: Montana Bureau of Mines and Geology Special Publication 114.
- Wong, I., Olig, S., Dober, M.,
- Wright, D., Nemser, E., Lageson, D., Silva, W., Stickney, M., Lemieux, M., and Anderson, L., 2004, Probabilistic earthquake hazard maps for the State of Montana, Montana Bureau of Mines and Geology (in press).

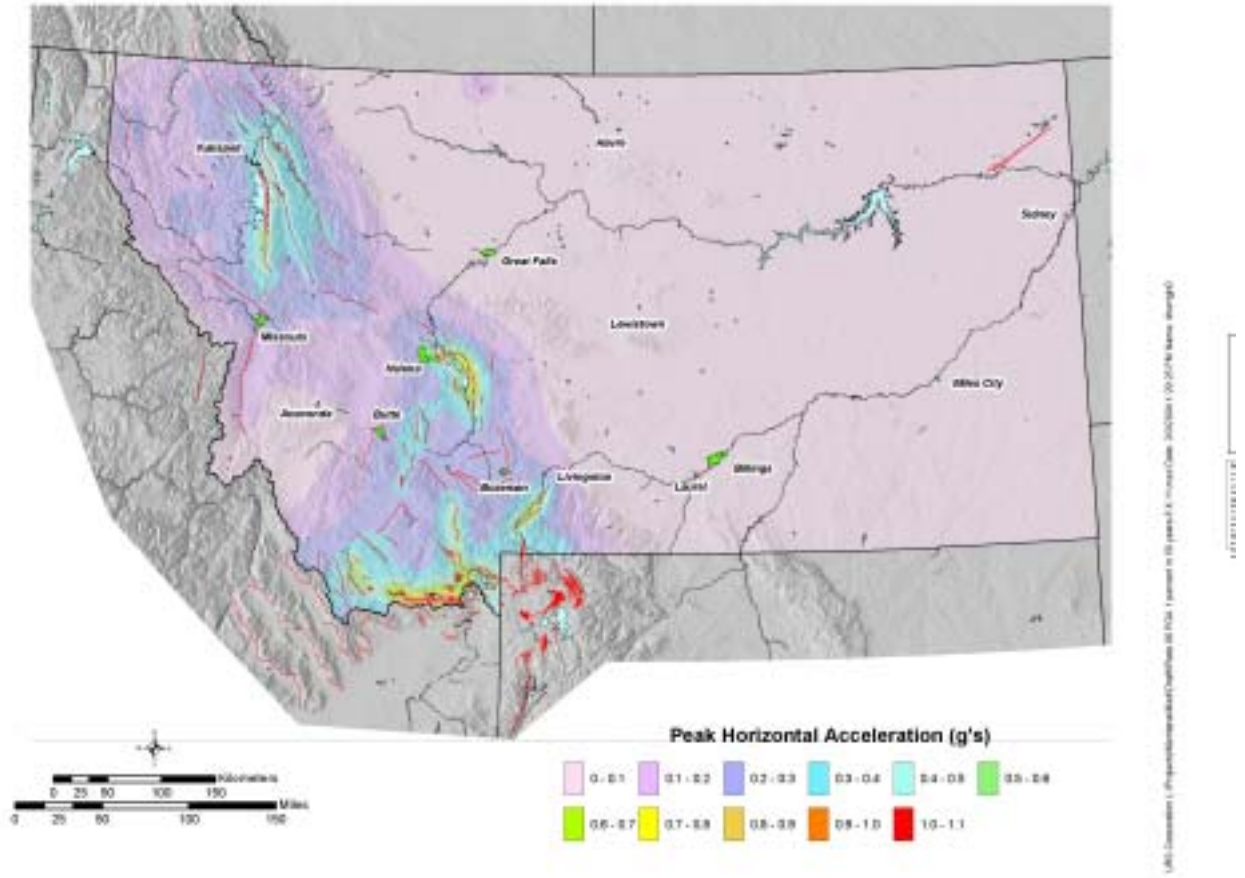


**Figure 1.** Peak horizontal acceleration (g) on rock for a 5000-year return period. Quaternary faults modified from Stickney et al. (2002).

# Long Term Seismic Hazard Assessment for Boise, Idaho: Moderate Risk Arising from a Large Number of Low Recurrence Rate Sources

James E. Zollweg (jzollweg@hotmail.com)  
Northwest Geosensing, P. O. Box 8742 Boise, ID 83707

## Abstract

The Boise area has not historically experienced a serious earthquake. Nearly all earthquakes reported felt are relatively large events occurring some distance from the city. The strongest city-wide average intensity on record is VI (light structural damage), which has been reported for three different earthquakes. The 1983 Borah Peak earthquake (distance 200 km) caused several cases of structural damage to multistory buildings, but most buildings experienced no damage. This suggests that the average level of shaking in Boise on that occasion was at the threshold between no and slight structural damage.

Several Quaternary faults are known near Boise. Detailed studies of most faults have never been performed. It is believed that additional active and potentially active faults remain to be discovered if systematic investigations are undertaken. For this evaluation, a set of 16 probable Quaternary active faults plus a random earthquake was chosen (Table 1). Most of these sources are at distances greater than 50 km. Faults were included on basis of geological or geomorphic evidence, possibly related seismicity, or favorable orientation for slip under the present NE-SW extensional regional stress field. Slip rates in most cases are very uncertain, but in most cases are  $<0.01$  mm/yr. Other than the inclusion decision itself, no attempt was made to define a fault's status as "active" or "inactive", since the slip rate (in combination with distance and maximum magnitude) ultimately decides the fault's influence on the city's seismic hazard.

The SEA99 relationships (Spudich et al., 1999) and the intensity/acceleration results of Wald et al. (1999) were used estimate average intensities at Boise for each source at a distance of 50 km or less. There are no historical or instrumental data to verify the accuracy of these estimates. Ground motions at greater distances were estimated from Joyner and Boore (1981). This relationship underestimates ground motions derived from historical intensity data by a factor of roughly ten. It is hypothesized that both a low attenuation rate and a large site factor are responsible for the discrepancy. Correcting predicted intensities to match the observed historical ones leads to an estimate of about 800 years for the return time of an average intensity of VII at Boise, and about 9000 years for intensity VIII. These estimates are fairly robust since they depend little on the uncertainties for any particular fault. The major uncertainty in the evaluation is the combined effect of site factor and regional attenuation. The results are in qualitative agreement with the lack of an average intensity VII event in the roughly 140 year historical record.

Table 1. Quaternary and Possible Quaternary Faults Included in Boise Seismic Hazard Evaluation

	Length (km)	Vertical Slip Rate (mm/yr)	Maximum Credible Earthquake $M_w$	Distance from Boise (km)	Expected Intensity in Boise
Boise Front Fault System	~90	0.005	6.5	0	VIII
"Emmett" Fault	~70	0.005	6.5	0	VIII
Random Earthquake	---	---	6.0	25	VII
Squaw Creek	48	0.1	7.0	40	VIII
Big Flat	32	0.03	6.8	50	VII
Willow Creek	~70	0.003	6.5	50	VII
Deer Park	(30)	0.005	6.8	70	VII
Deadwood-Reeves Creek	(30)	0.02	6.7	70	VII
Shirt Creek	13	0.02	6.6	85	VII
Long Valley, south segment	29	0.05	6.5	90	VI
Parker Ranch	(10)	0.2	6.9	90	VII
Halfway Gulch	~90	~0.5	7.2	100	VII
Cottonwood Mountain	36	0.15	6.9	100	VII
Council	(30)	0.03	6.9	115	VI
Long Valley, north segment	37	0.05	6.9	115	VI
Sawtooth	70	0.05	7.0	115	VI
Juniper Mountain	15	0.05	6.5	135	V

**Table 1.**

**Quaternary and Possible Quaternary Faults Included in Boise Seismic Hazard Evaluation**

Fault	Length (km)	Vertical Slip Rate (mm/yr)	Maximum Credible Earthquake $M_w$	Distance from Boise (km)	Expected Intensity in Boise
Boise Front Fault System	~90	0.005	6.5	0	VIII
"Emmett" Fault	~70	0.005	6.5	0	VIII
Random Earthquake			6.0	25	VII
Squaw Creek	48	0.1	7.0	40	VIII
Big Flat	32	0.03	6.8	50	VII
Willow Creek	~70	0.003	6.5	50	VII
Deer Park	(30)	0.005	6.8	70	VII
Deadwood-Reeves Creek	(30)	0.02	6.7	70	VII
Shirt Creek	13	0.02	6.6	85	VII
Long Valley, south segment	29	0.05	6.5	90	VI
Parker Ranch	(10)	0.2	6.9	90	VII
Halfway Gulch	~90	~0.5	7.2	100	VII
Cottonwood Mountain	36	0.15	6.9	100	VII
Council	(30)	0.03	6.9	115	VI
Long Valley, north segment	37	0.05	6.9	115	VI
Sawtooth	70	0.05	7.0	115	VI
Juniper Mountain	15	0.05	6.5	135	V

## PAPERS

*(Click on links to view each paper)*

CHALLENGES IN DETERMINING THE EARTHQUAKE HAZARDS FROM ACTIVE FAULTS IN THE BASIN AND RANGE PROVINCE by *D. Burton Stemmons, Professor Emeritus, Center for Neotectonic Studies, University of Nevada, Reno, and Craig M. dePolo, Nevada Bureau of Mines and Geology*

SUMMARY OF LATE QUATERNARY TECTONICS OF THE BASIN AND RANGE PROVINCE IN NEVADA, EASTERN CALIFORNIA, AND UTAH by *Michael Machette, U.S. Geological Survey*

CHALLENGES IN ASSESSING SEISMIC HAZARD ACROSS THE INTERMOUNTAIN WEST by *Mark D. Petersen, Arthur D. Frankel, Chris H. Cramer, Stephen C. Harmsen, Kathleen Haller, and Harley M. Benz, U.S. Geological Survey*

IDENTIFICATION AND CHARACTERIZATION OF ACTIVE (HOLOCENE) EXTENSIONAL FAULTS IN SOUTHEASTERN IDAHO, NORTHEAST UTAH, AND SOUTHWEST WYOMING – IMPLICATIONS FOR PIPELINE CROSSING DESIGN by *Donald O. West and Graeme Major, Golder Associates, Inc., and Suzanne R. Hickham, The Williams Companies, Inc.*

ESTIMATING PREHISTORIC EARTHQUAKE MAGNITUDE FROM POINT MEASUREMENTS OF SURFACE RUPTURE by *Mark A. Hemphill-Haley, Department of Geology, Humboldt State University, and Ray J. Weldon, II, Department of Geological Sciences, University of Oregon*

PROBABILISTIC FAULT-DISPLACEMENT HAZARD ANALYSIS: A CASE STUDY FROM SKULL VALLEY, UTAH by *Kathryn L. Hanson and Robert R. Youngs, Geomatrix Consultants, Inc., and Frank F. Swan, Consulting Geologist*

PALEOSEISMIC INVESTIGATIONS OF THE STANSBURY AND MID-VALLEY FAULTS, SKULL VALLEY, UTAH by *Frank F. Swan, Consulting Geologist, Kathryn L. Hanson and Robert R. Youngs, Geomatrix Consultants, Inc., and Michael M. Angell, William Lettis & Associates*

PATTERN AND TIMING OF FAULTING IN THE CENTRAL NEVADA SEISMIC BELT AND IMPLICATIONS FOR SEISMIC HAZARDS OF THE WESTERN BASIN AND RANGE PROVINCE by *John W. Bell, Nevada Bureau of Mines and Geology; S. John Caskey, Department of Geosciences, San Francisco State University; and Alan R. Ramelli, Nevada Bureau of Mines and Geology*

SEPARATION AND IDENTIFICATION OF CHARCOAL AND ORGANICS FROM BULK SEDIMENT SAMPLES FOR IMPROVED RADIOCARBON DATING AND STRATIGRAPHIC CORRECTIONS by *Kathryn Puseman and Linda Scott Cummings, Paleo Research Institute*

PRELIMINARY PALEOSEISMIC INVESTIGATION OF THE CANYON FERRY FAULT, WEST-CENTRAL MONTANA by *Larry W. Anderson and Lucille A. Piety, U.S. Bureau of Reclamation, Seismotectonics and Geophysics Group; Susan S. Olig, URS Corporation; and Steven L. Forman, Department of Earth and Environmental Sciences, University of Illinois*

SHAKEMAP AS A TOOL FOR UNDERSTANDING EARTHQUAKE HAZARD IN NEVADA by *Glen Biasi, Nevada Seismological Laboratory, and Kent Lindquist, Lindquist Consulting*

ACTIVE TECTONICS OF THE NEPHI SEGMENT, WASATCH FAULT, UTAH by *Christopher DuRoss and Ronald L. Bruhn, Department of Geology and Geophysics, University of Utah*

BASIN AND RANGE SEISMICITY: DISTRIBUTION, OCCURRENCE RATES, MOMENT RELEASE, AND COMPARISON WITH GEODESY by *Aasha Pancha and John G. Anderson, Seismological Laboratory and Department of Geological Sciences, University of Nevada, Reno*

DETERMINATION OF LOW-STRAIN SITE-AMPLIFICATION FACTORS IN THE SALT LAKE VALLEY, UTAH, USING ANSS DATA by *Kris Pankow and James C. Pechmann, University of Utah Seismograph Stations*

A MULTIDISCIPLINARY APPROACH TO SEISMIC HAZARD IN THE RENO-CARSON METROPOLITAN REGION by *Feng Su, John G. Anderson, and Aasha Pancha, Seismological Laboratory, University of Nevada, Reno*

ISSUES IN EVALUATING GROUND-MOTION HAZARD IN THE BASIN AND RANGE PROVINCE by *Ivan G. Wong, Seismic Hazards Group, URS Corporation*

UTAH QUATERNARY FAULT PARAMETERS WORKING GROUP: CRITICAL REVIEW OF UTAH PALEOSEISMIC-TRENCHING DATA AND CONSENSUS RECURRENCE-INTERVAL AND VERTICAL SLIP-RATE ESTIMATES FOR UTAH'S QUATERNARY FAULTS by *William R. Lund, Utah Geological Survey*

A STRAIGHTFORWARD WAY OF NAMING PALEOEARTHQUAKES by *Craig M. dePolo, Nevada Bureau of Mines and Geology*

PROBABILISTIC EARTHQUAKE GROUND-MOTION HAZARD MAPS FOR MONTANA by *Ivan Wong, Susan Olig, Mark Dober, Doug Wright, and Eliza Nemser, Seismic Hazards Group, URS Corporation; David Lageson, Department of Earth Sciences, Montana State University; Walter Silva, Pacific Engineering & Analysis; Michael Stickney, Montana Bureau of Mines & Geology; Michele Lemieux, Montana Department of Natural Resources and Conservation; and Larry Anderson, U.S. Bureau of Reclamation, Seismotectonics and Geophysics Group*

# **PROBABILISTIC EARTHQUAKE GROUND MOTION HAZARD MAPS FOR MONTANA**

Ivan Wong, Susan Olig, Mark Dober, Doug Wright, and Eliza Nemser  
Seismic Hazards Group, URS Corporation, 1333 Broadway, Oakland, CA 94612

David Lageson  
Montana State University, Department of Earth Sciences, Bozeman, MT 59717

Walter Silva  
Pacific Engineering & Analysis, El Cerrito, CA 94530

Michael Stickney  
Montana Bureau of Mines & Geology, Butte, MT 59701

Michele Lemieux  
Montana Department of Natural Resources and Conservation, Helena, MT 59620

Larry Anderson  
U.S. Bureau of Reclamation, Denver, CO 80225

## **ABSTRACT**

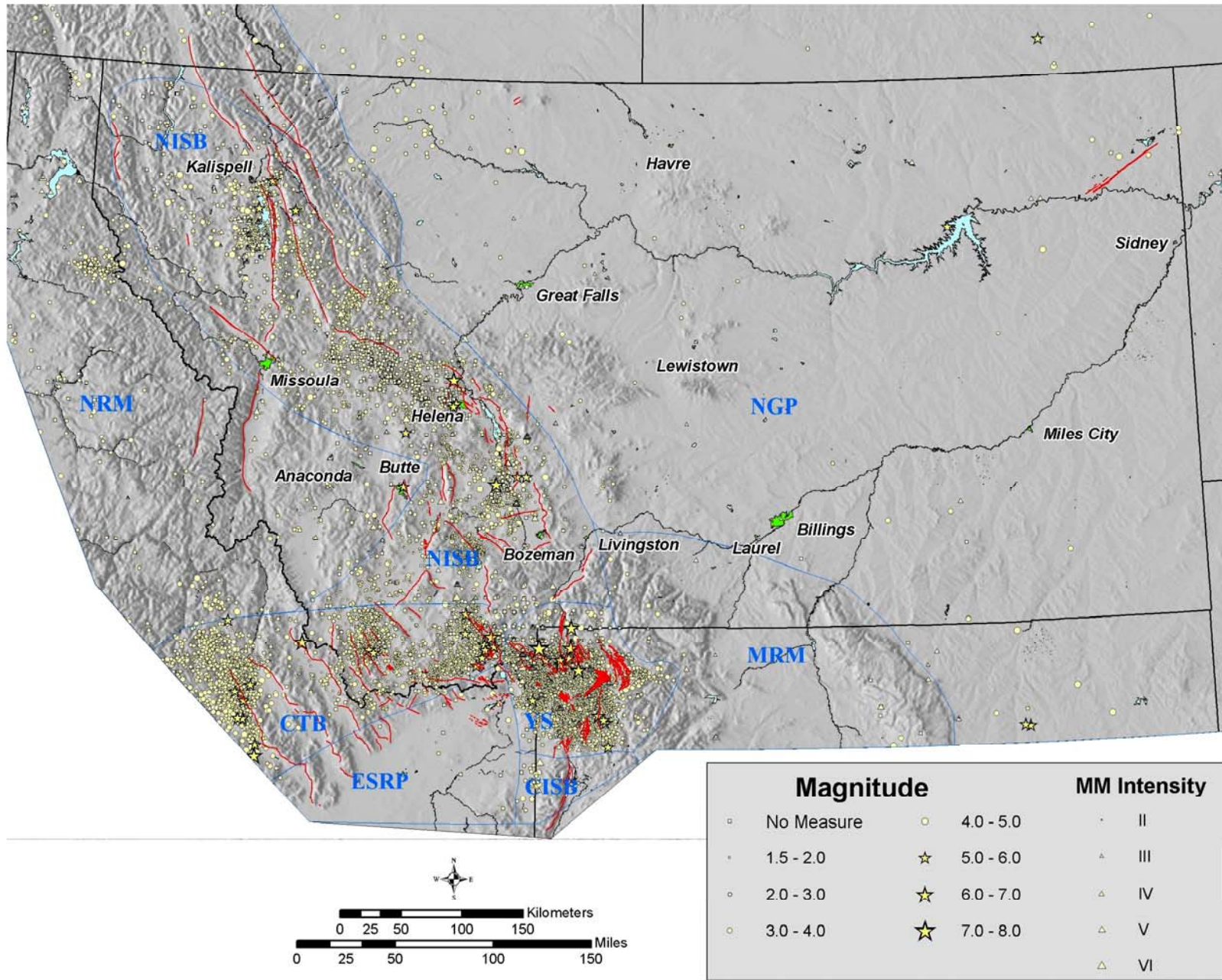
A set of probabilistic earthquake ground motion maps have been developed for the Montana Department of Natural Resources and Conservation Dam Safety Program. The 18 statewide maps display peak horizontal acceleration and 0.2 and 1.0 sec (5 Hz and 1 Hz, respectively) horizontal spectral acceleration for approximate return periods of 500, 2500, and 5000 years (exceedance probabilities of 10%, 2%, and 1% in 50 years, respectively). The maps display ground motions for two site conditions: soft rock and the ground surface.

## **INTRODUCTION**

Western Montana is characterized by abundant late-Quaternary Basin and Range normal faulting and historical seismicity (Figure 1). It includes the Intermountain seismic belt (ISB), a zone of elevated seismicity, and the seismically and volcanically active Yellowstone region. Paralleling the southwestern border of the state is the Centennial Tectonic Belt (CTB), also a zone of significant seismicity (Figure 1). The largest historical event is the 1959 moment magnitude (**M**) 7.3 Hebgen Lake earthquake just west of Yellowstone National Park. In contrast, eastern

Montana, similar to other portions of the Great Plains in the central U.S., has only two known faults of possible late-Quaternary age. Seismicity is also at a relatively low level, although the largest event has been about **M** 5.5 (Figure 1).

Because of the potential earthquake threat to dams in the state, we developed a set of probabilistic earthquake ground motion maps for the Montana Department of Natural Resources and Conservation (DNRC) Dam Safety Program (Wong and others, 2004). The statewide maps display peak horizontal acceleration and 0.2 and 1.0 sec spectral acceleration for 10%, 2%, and 1% in 50 years exceedance



I.G. Wong and others

Figure 1. Historical seismicity (1809 to 2001), Quaternary faults (red lines), and regional seismic source zones in Montana.

probabilities (return periods of 500, 2500, and 5000 years, respectively). This range of return periods was selected to consider the range of hazard categories of Montana dams based on downstream risk. The maps are for both a soft rock site condition and at the ground surface; the latter includes site response effects for the areas underlain by unconsolidated sediments. We developed a total of 18 maps for the three return periods, three spectral accelerations, and two site conditions (Wong and others, 2004). Three additional maps were developed that display the dominant magnitudes that control peak acceleration hazard for the three return periods.

### **APPROACH**

This study involved five principal tasks: (1) seismic source characterization; (2) definition and characterization of geologic site-response categories and assignment of amplification factors; (3) seismic attenuation characterization; (4) probabilistic ground-motion calculations using logic trees; and (5) map development. Our seismic source characterization model for this analysis included 92 potential fault sources and relied heavily on recent compilations by Haller and others (2000) and Stickney and others (2000). We included all known faults longer than 5 km with evidence for repeated Quaternary movement within Montana and extending to 50 km beyond the state border. Prominent faults in the state by virtue of their length and/or slip rate include the Centennial, Mission, Canyon Ferry, Madison, Emigrant, and Red Rock faults. We also considered longer more active faults to 100 km beyond the state's borders, including the Teton, Lemhi, and Lost River faults. Unfortunately, most of the Quaternary faults in Montana (> 85%) have not been studied in any detail and very few data are available to develop rupture models and constrain slip rates.

To address the hazard from background seismicity, we defined eight regional source zones: the northern and central ISB (NISB and CISB), CTB, Yellowstone region, Northern and Middle Rocky Mountains (NRM and MRM), Northern Great Plains (NGP), and the eastern Snake River Plain (ESRP) (Figure 1). We adopted a value of  $M 6.5 \pm 0.3$  for the

maximum background earthquake for western Montana and  $M 6.0 \pm 0.5$  for eastern Montana. In addition to the traditional approach of using regional seismic source zones (assuming uniformly distributed seismicity), Gaussian smoothing (Frankel, 1995) was also used to address the hazard from background earthquakes in the probabilistic analysis. In this approach, we smoothed the historical background seismicity to incorporate a degree of stationarity, using a spatial window of 15 km. We weighted the two approaches equally.

Amplification factors were used to modify the rock motions, both soft and hard rock, to incorporate site response into the hazard maps. These factors were based on five generalized geologic site-response categories (hard rock, soft rock, Quaternary alluvium, Quaternary lacustrine deposits, and Quaternary glacial till). Subsurface geologic and geotechnical data are inadequate for Montana, so we adopted amplification factors from correlative categories developed in studies for Salt Lake Valley (Wong and others, 2002), California (Silva and others, 1999) as well as a set of California-derived NEHRP factors for site categories A and B/C (Silva and others, 2000).

An important consideration in the selection of attenuation relationships is western Montana's location in the extensional Basin and Range Province where normal faulting dominates. Conversely, eastern Montana lies within the compressional Midcontinent. To characterize the attenuation of ground motions, we used multiple empirical attenuation relationships appropriate for soft rock sites in the western U.S. and hard rock sites in the Midcontinent, and a stochastic numerical ground-motion modeling technique. It is increasingly recognized that earthquakes in extensional tectonic regimes produce lower ground motions than events in compressional/strike-slip regimes for the same magnitude and distance, so we assigned higher weights to extensional attenuation relationships such as Spudich and others (1999) and a modified Abrahamson and Silva (1997) for the empirical relationships.

To compensate for the lack of region-specific attenuation relationships, we used the stochastic ground motion modeling approach (Silva and others, 1997) to develop relationships for both western and

eastern Montana. The point-source version of the stochastic methodology was used to model earthquakes of  $M$  5.5, 6.5, and 7.5 in the distance range of 1 to 400 km. Uncertainties in stress drop, magnitude-dependent focal depths, the crustal attenuation parameters  $Q_0$  and  $\eta$ , the near-surface attenuation parameter ( $\kappa$ ), and the rock profile atop the crustal model were included in the computations of the attenuation relationships through parametric variations. We assigned the stochastic attenuation relationships a weight of 0.6 and the empirical relationships 0.4 in the probabilistic hazard analysis.

### HAZARD MAPS

The resulting hazard maps for a uniform site condition of soft rock and ground surface show that the probabilistic hazard in Montana ranges from very low to very high depending on the proximity to active faults (e.g., Figure 2). The highest hazard is concentrated along the most active faults. For example, at a return period of 5000 years, the highest surficial peak horizontal accelerations reach upwards of 1 g in the vicinity of the active Centennial fault along the Montana-Idaho border (Figure 2). At a 2500-year return period, the peak acceleration still exceeds 0.7 g. Other relatively moderate to high hazard ( $> 0.3$  g) areas occur in the vicinities of the Mission, Canyon Ferry, Madison, Emigrant, and Red Rock faults. Areas away from the more active faults in western Montana are characterized by surficial values of 0.1 to 0.3 g (Figure 2). Eastern Montana is characterized by peak horizontal accelerations of less than 0.1 g at a return period of 5000 years due to the absence of active faults and a low-level of seismicity (Figure 2). The exception are areas located along rivers and streams where peak accelerations are amplified due to the accumulated fluvial deposits (e.g., Billings). The ground motions at the return period of 2500 years reflect a similar pattern to that of the 5000-year return period maps. The 500-year return period maps exhibit low ground motions except along the Centennial fault. In general, site amplification has a significant impact on ground shaking in the Quaternary basins in Montana where

several cities/towns are located (Figure 2).

### ACKNOWLEDGMENTS

This study was funded by the Montana Department of Natural Resources Dam Safety Program and FEMA through the National Dam Safety Act. Financial support was also provided by URS Corporation and the Montana Bureau of Mines and Geology. Our thanks to Melinda Lee and Fabia Terra for assisting in the preparation of this paper and to Bob Green and Bill Lund for their reviews.

### REFERENCES

- Abrahamson, N.A. and Silva, W.J., 1997, Empirical response spectral attenuation relations for shallow crustal earthquakes: *Seismological Research Letters*, v. 68, p. 94-127.
- Frankel, A., 1995, Mapping seismic hazard in the central and eastern United States: *Seismological Research Letters*, v. 66, p. 8-21.
- Haller, K.M., Stickney, M.C., and Machette, M.N., 2000, Quaternary faults and seismicity in western Montana: Montana Bureau of Mines and Geology Open-File Report 411, 241 p.
- Silva, W.J., Abrahamson, N.A., Toro, G., and Constantino, C., 1997, Description and validation of the stochastic ground motion model: unpublished report prepared for the Brookhaven National Laboratory.
- Silva, W.J., Li, S., Darragh, R., and Gregor, N., 1999, Surface geology based strong motion amplification factors for the San Francisco and Los Angeles area: unpublished report prepared for PEARL by Pacific Engineering & Analysis.
- Silva, W., Martin, G., Abrahamson, N., and Kircher, C., 2000, Reassessment of site coefficients and near-fault factors for building code provisions: unpublished report prepared for U.S. Geological Survey, NEHRP Award 98-HQ-GR-1010, 211 p.
- Spudich, P., Joyner, W.B., Lindh, A.G., Boore, D.M.,

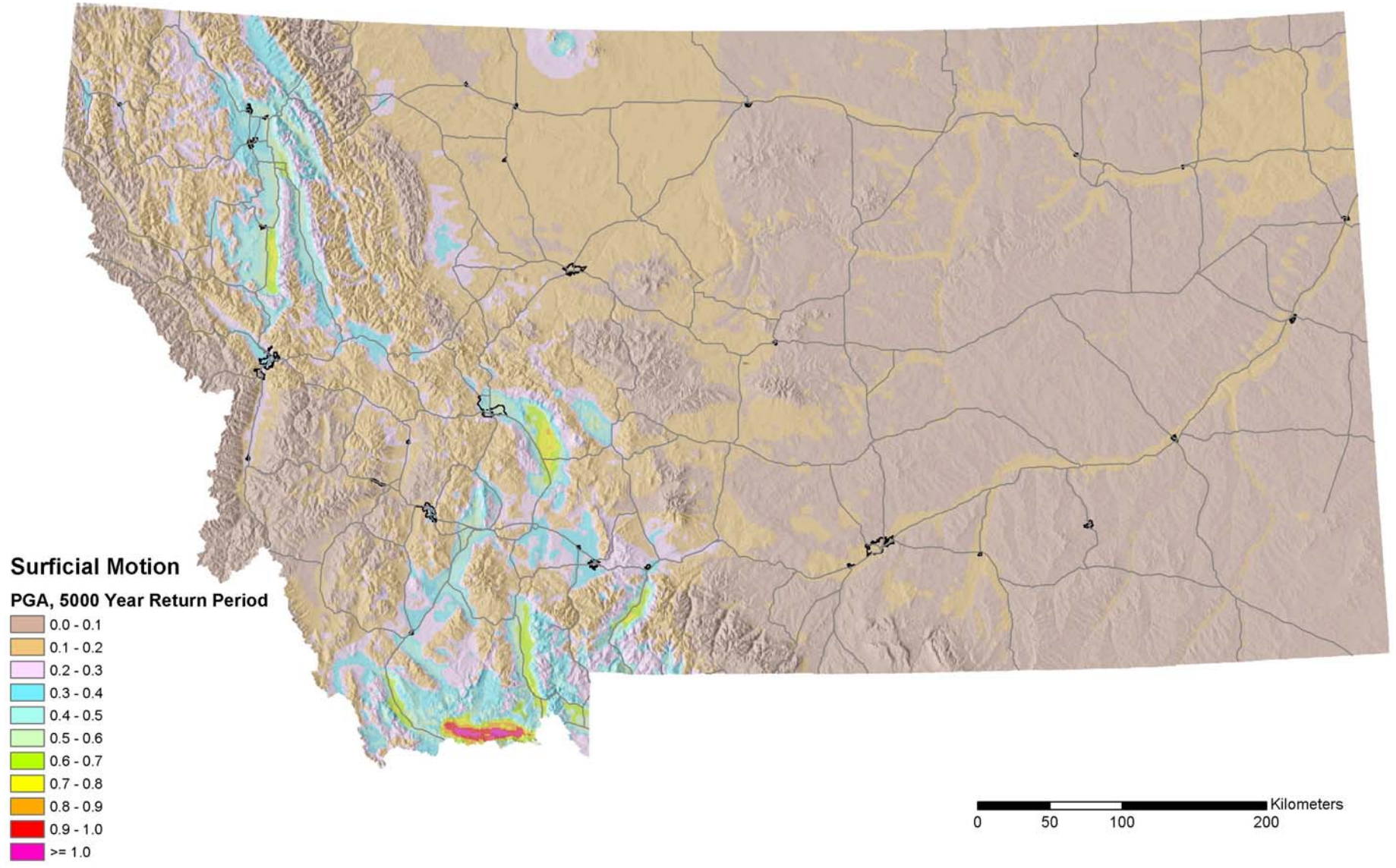


Figure 2. Peak horizontal acceleration (g) at the ground surface for a 5000-year return period.

- Margaris, B.M., and Fletcher, J.B., 1999, SEA99 – A revised ground motion prediction relation for use in extensional tectonic regimes: *Bulletin of the Seismological Society of America*, v. 89, p. 1156-1170.
- Stickney, M.C., Haller, K.M., and Machette, M.N., 2000, Quaternary faults and seismicity in western Montana: Montana Bureau of Mines and Geology Special Publication 114.
- Wong, I., Olig, S., Dober, M., Wright, D., Nemser, E., Lageson, D., Silva, W., Stickney, M., Lemieux, M., and Anderson, L., 2004, Probabilistic earthquake hazard maps for the State of Montana: Montana Bureau of Mines and Geology (in preparation).
- Wong, I., Silva, W., Olig, S., Thomas, P., Wright, D., Ashland, F., Gregor, N., Pechmann, J., Dober, M., Christenson, G., and Gerth, R., 2002, Earthquake scenario and probabilistic ground shaking maps for the Salt Lake City, Utah, metropolitan area: Utah Geological Survey Miscellaneous Publication MP-02-05, 50 p. with CD ROM.

***IDENTIFICATION AND CHARACTERIZATION OF ACTIVE  
(HOLOCENE) EXTENSIONAL FAULTS IN SOUTHEAST IDAHO,  
NORTHEAST UTAH, AND SOUTHWEST WYOMING –  
IMPLICATIONS FOR PIPELINE CROSSING DESIGN***

Donald O. West, Golder Associates Inc., Redmond, WA  
Graeme Major, Golder Associates Inc., Reno, NV  
Suzanne R. Hickham, The Williams Companies, Inc., Houston, TX

**ABSTRACT**

The region of southeast Idaho, northeast Utah, and southwest Wyoming straddles the northeast Basin and Range and Middle Rocky Mountains geomorphic/tectonic provinces. The Basin and Range is characterized by active (historic and Holocene), mountain-front extensional fault tectonics and significant historical seismicity, while the Middle Rocky Mountains has a comparatively low level of tectonic activity. The region, and nearby areas of the Basin and Range, include a number of active extensional faults (e.g., Rock Creek fault, West and East Bear Lake faults, Bear River fault, West and East Cache faults, Wasatch fault zone, Lost River Range fault), which exhibit historic surface rupture and/or Holocene surface displacement. The region also includes a number of late Cenozoic (pre-Holocene) faults. Historical seismicity, which should reflect active fault tectonics, is concentrated to the north of the region in the Star Valley, Wyoming area; to the west and southwest in the Cache Valley, Utah area; and to the south along the Wasatch Front in Utah. The eastern part of the region, and the area farther to the east (the transition from the Basin and Range to the Middle Rocky Mountains), is relatively aseismic based on the historical earthquake record. However, this area also includes extensional faults, such as the Rock Creek fault, that have geomorphic and geologic evidence of significant Holocene displacement.

Linear facilities such as buried pipelines, which cross active extensional faults, may be subject to the effects of sudden, episodic normal-slip surface displacement earthquakes. The impact of fault rupture on a pipeline depends on the nature, orientation, geometry, width, and magnitude of the displacement, and on the orientation of the pipeline relative to the strike of the fault. It also depends on the depth of pipe burial, the geometry of the pipe trench, the nature of the trench backfill material, and the pipe characteristics.

The Williams Companies' (Williams) Rockies Displacement Expansion Project (Expansion Project) is in southeast Idaho and southwest Wyoming and traverses the Basin and Range Province, as well as the transition zone with the Middle Rocky Mountains. The Expansion Project addressed the potential for surface-fault displacement across the pipeline through a program to identify and characterize active faults along the pipeline right-of-way, and mitigate the displacement effects through pipeline design. The Expansion Project included about 148 km of new pipeline, distributed among six loop segments.

Based on an evaluation of available literature and data, we identified 12 Holocene and Pleistocene faults that cross, or were projected to cross four of the six Expansion Project loop segments. Based on geomorphic interpretation of stereoscopic aerial photographs, aerial reconnaissance, and ground-based geomorphic and geologic mapping of the 12 mapped faults, we identified four active Holocene normal-slip faults crossing three of the Expansion Project

loop segments. The four faults included the Rock Creek, Bennetts Spring, East Bear Lake, and East Gem Valley faults. The Bennetts Spring fault was not previously identified or mapped as a fault. Each of the four faults is well expressed geomorphically with well-defined linear scarps, truncated and faceted ridge spurs, and vegetation lineaments.

Based on mapped and estimated fault geometric and geologic characteristics, the maximum calculated normal-slip displacement per surface-faulting event among the four faults ranged from 0.55 to 4.8 m. Average displacement per event ranged from 0.3 to 2.1 m. Estimated maximum widths of the four fault zones ranged from about 10 to 670 m. Estimated average late Quaternary slip rates among the four faults ranged from 0.1 to 1.7 mm/yr.

For the Expansion Project pipeline mitigation design, and following the methodology used for active fault crossing mitigation design for the Kern River Pipeline in 1990 (e.g., the Wasatch fault), the fault-rupture parameters considered included the components of maximum displacement along the axis of the pipeline (x), the maximum lateral displacement perpendicular to the axis (y), and the maximum vertical displacement in the plane of the pipe axis (z). For the four active faults, maximum x values ranged from 0.27 to 1.76 m, maximum y values from -1.64 to 0.17 m, and maximum z values from -0.45 to -2.18 m.

For all four fault crossings, future displacement would primarily put the pipeline into axial tensional stress as well as vertical shear. For three of the fault crossings, the planned pipeline design (e.g., pipe-wall thickness, trench geometry, pipe orientation with respect to the fault) was adequate to mitigate the effects of fault displacement. For the East Bear Lake fault crossing, which had the largest potential design displacements (x, y, z), thicker wall pipe was installed through the width of the fault zone to mitigate the effects of displacement.

## INTRODUCTION

### Background

There are over 68,000 km of buried natural gas pipelines, and over 164,000 km of buried crude and refined oil pipelines in the conterminous United States (O'Rourke and Liu, 1999). These energy pipelines include both transmission and distribution systems that cover large geographic areas, and are often exposed to a variety of geologic hazards, including seismic hazards (Braun and others, 1996; O'Rourke and Liu, 1999). Seismic hazards that have the potential to adversely affect buried pipelines include wave-propagation and permanent-ground-deformation hazards. Wave-propagation hazards include the effects of strong earthquake shaking and the associated transient strain and curvature of the ground resulting from the passage earthquake waves. Wave-propagation hazard is characterized primarily by peak ground acceleration and

peak ground velocity (O'Rourke and Liu, 1999). Permanent ground deformation, resulting from primary or secondary earthquake processes, arises from the permanent differential translation or displacement of the volume of ground (soil or rock) that contains the pipeline. Permanent-ground-deformation hazards include surface-fault displacement, earthquake-induced landslide movement, soil liquefaction and lateral spreading, and soil settlement (O'Rourke and Liu, 1999). Surface-fault displacement across a buried energy pipeline can severely damage or rupture the pipeline, resulting in release of natural gas, liquid crude oil, or other products.

With respect to surface-fault displacement, the Basin and Range Province of the western United States contains numerous late Quaternary (Pleistocene and Holocene) normal-slip faults, as well as numerous, buried

energy transmission and distribution pipelines (natural gas and liquid). The Williams Companies (Williams) own and operate Northwest Pipeline, a 6,500-km natural gas transmission system that extends from Ignacio in southwest Colorado to Sumas in northwest Washington, on the border with British Columbia, Canada. The existing pipeline system consists of a mainline, loop line, and a number of laterals. The mainline was constructed in the mid-1950s, and the existing loop lines and laterals were constructed at various times during the 1970s through 1990s to increase capacity and reach new customers.

In 2000, Williams began development of the Rockies Displacement Expansion Project (Expansion Project) to substantially replace pipeline displacement capacity with physical capacity in the project corridor. Williams completed construction of the Expansion Project in 2003. Investigation of active faults that could affect the Expansion Project was part of the overall identification and evaluation of geologic hazards required for Federal Energy Regulatory Commission (FERC) approval and permitting of the project, and specifically for pipeline-fault-displacement-hazard mitigation design.

For the Expansion Project design, and to address FERC's regulatory requirements, we defined an active fault as one that has had historic displacement (e.g., surface displacement), or geomorphic or geologic evidence of displacement during the Holocene (generally the past 10 kyr). This is a common fault activity criterion for typical engineered facilities, and is used in California to delineate fault-rupture-hazard zones (Reiter, 1990; California Division of Mines and Geology, 1992; Jennings, 1994). A potentially active fault is one that exhibits no evidence of Holocene displacement, but has geomorphic or geologic evidence of Pleistocene (10 ka to 1.6 Ma) displacement.

## **Objectives, Approach, and Methodology**

The primary objectives of this fault investigation were to identify active faults that could impact the design of the Expansion Project, and to develop fault-rupture-design parameters for pipeline crossing design. To meet these objectives we conducted an office-based review and evaluation of available data regarding the location, extent, and nature of active and potentially active faults in the region of the Expansion Project; and made a field reconnaissance of the geomorphic and geologic nature of the faults. The primary tasks undertaken to implement the approach included:

- Compilation, review, and evaluation of available literature, data, and mapping regarding the geology, geomorphology, tectonics, seismicity, and geologic and seismic hazards in the region of the Expansion Project. The purpose of this task was to develop general information and data on the presence, location, nature, and characteristics of active and potentially active faults in the region of the Expansion Project.
- Geomorphic analysis and evaluation using 1:24,000-scale stereoscopic aerial photographs along the Expansion Project pipeline right-of-way to identify and describe linear geomorphic features that may be indicative of active faulting.
- Helicopter aerial reconnaissance of active and potentially active fault crossings identified from the previous tasks to identify geomorphic features that may indicate active faulting to confirm preliminary conclusions regarding fault location with respect to the pipeline right-of-way, and to confirm conclusions regarding fault activity.
- Field geomorphic and geologic reconnaissance mapping of target fault

locations to confirm: (1) the level of activity of the fault, (2) the fault location with respect to the pipeline, (3) the fault orientation and geometry with respect to the pipeline, and (4) develop fault-specific displacement data from the nature of observed displacements of geomorphic features along the fault.

- Analysis and evaluation of the data collected to estimate fault-rupture characteristics at the fault/pipeline crossings for pipeline design purposes, particularly the maximum and average displacement per surface rupture event, and the geometry of such displacement relative to the orientation of the pipeline.
- Identification of site-specific fault-displacement-design parameters to develop pipeline/fault crossing design alternatives.

### Expansion Project Description

The Expansion Project is in southeast Idaho and southwest Wyoming, and consists of six loop segments of the existing 56-cm diameter, high-pressure natural gas transmission pipeline. The six loop segments combine for a total length of about 148 km along a pipeline length of about 325 km. Individual loop segment lengths vary from about 8 to 50 km. Table 1 summarizes the physical characteristics of the various loop segments, and Figure 1 shows their locations.

The new steel pipeline for four of the six loop segments was 61 cm in diameter, and had a nominal wall thickness of 6.35 mm or 7.92 mm. The remaining two loops were 76 cm in diameter, and had a nominal wall thickness of 7.2 mm or 7.92 mm. The grade of the pipe steel was X70. Concrete-coated pipe at selected locations provides stream erosion (scour) mitigation and mitigates for positive buoyancy in shallow ground-water areas.

*Table 1. Characteristics of loop segments*

<b>Loop Name</b>	<b>Location/Province</b>	<b>Loop Length (km)</b>
Muddy Creek	Southwest Wyoming/ Wyoming Basin of the Middle Rocky Mountains	49.5
Kemmerer	Southwest Wyoming/ Wyoming Basin and Wyoming Ranges of the Middle Rocky Mountains	25.2
Pegram	Southwest Wyoming/ Wyoming Ranges of the Middle Rocky Mountains and Basin and Range	18.0
Soda Springs	Southeast Idaho/Basin and Range	31.8
Lava	Southeast Idaho/Basin and Range	15.3
Pocatello	Southeast Idaho/Basin and Range	7.7

*Identification and Characterization of Active  
(Holocene) Extensional Faults in Southeast Idaho,  
Northeast Utah, and Southwest Wyoming – Implications for Pipeline Crossing Design*

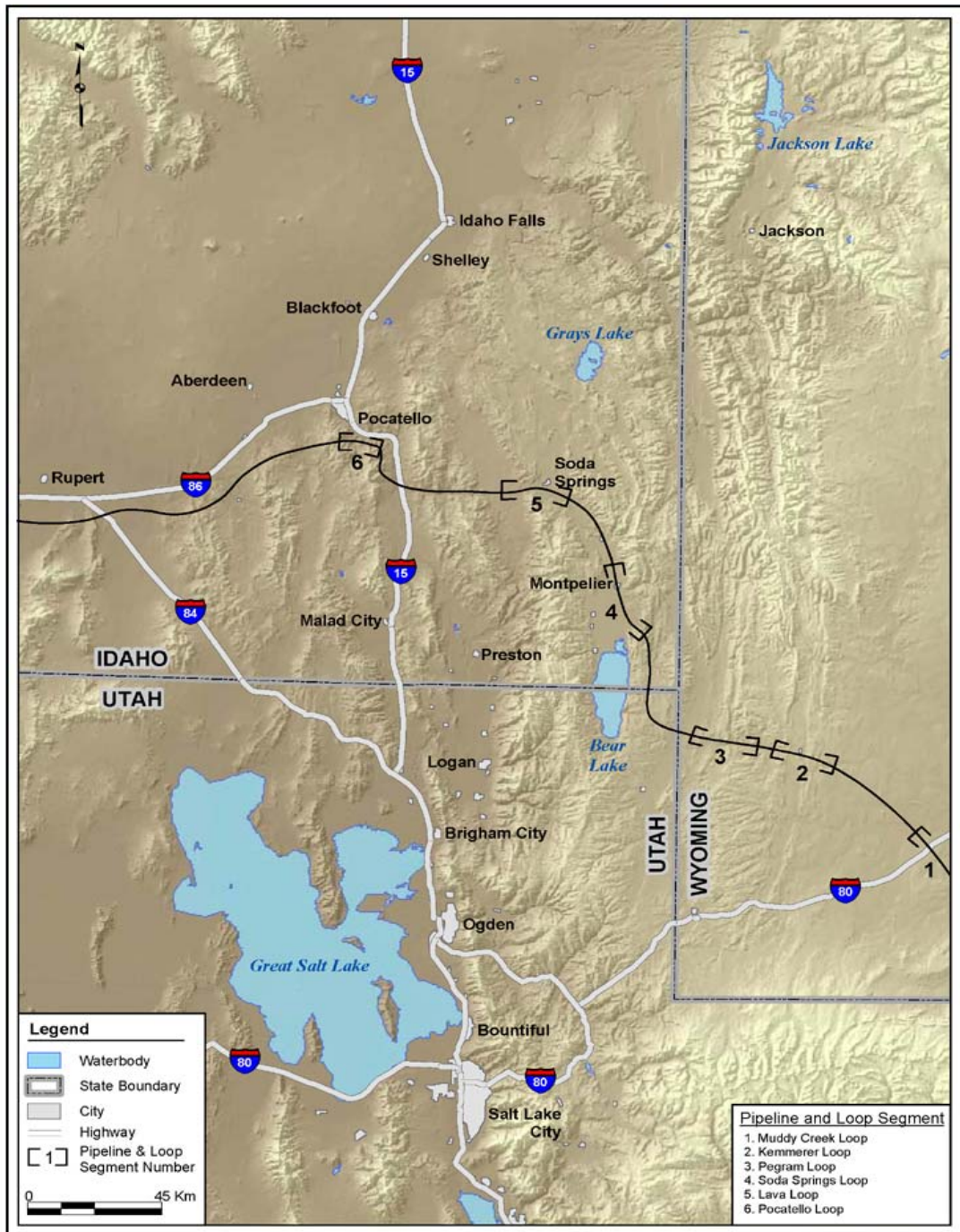


*Figure 1. Regional location map*

## TECTONIC/SEISMIC SETTING

The region of the Expansion Project includes both areas that have undergone intense folding and faulting, and areas that have remained relatively undeformed over geologic time. The Wyoming Basin of the Middle Rocky Mountains, within which the Muddy Creek Loop and much of the Kemmerer Loop are located, is characterized by gently dipping and sparsely faulted Cretaceous rocks. The relative stability of this area over geologic time is evident in the low level, or lack of Quaternary and historic tectonic activity, such as active (i.e., Holocene) faulting and historical seismicity (Machette and others, 2001; Figure 2).

The western part of the Kemmerer Loop, and all of the Pegram Loop are in the Wyoming Ranges of the Middle Rocky Mountains, while the Soda Springs, Lava, and Pocatello loops are in the Basin and Range. The Wyoming Ranges and the Basin and Range have intensely folded and faulted bedrock. There are numerous Holocene- and Pleistocene-age faults mapped in southwestern Wyoming and southeastern Idaho (Witkind, 1975a, 1975b; Othberg and Breckenridge, 1981; Arabasz and Julander, 1986; Smith and Arabasz, 1991; West, 1993; Yeats and others, 1997; Idaho Geological Survey, 2000; Machette and others, 2001; Laabs and others, 2001). Most of these faults are generally north-striking, normal-slip, basin-and-range, mountain front faults. Several of the normal-slip faults are within the Wyoming Ranges of the Middle Rocky Mountains, suggesting that the extensional tectonics of the Basin and Range extend eastward in a relatively broad transition zone. West (1993) suggests that the activity in the transition zone may be related to reactivation of older thrust faults. Figure 2 shows the location of Holocene-age and

Pleistocene-age faults in proximity to the six loop segments of the Expansion Project.

The region of the Expansion Project has had a low to moderately high level of activity in terms of the frequency and magnitude of historical earthquakes. Historical seismicity is concentrated in the Intermountain seismic belt (ISB) that extends about 1,500 km from southern Nevada and northern Arizona to northwest Montana (Smith and Sbar, 1974; Smith and Arabasz, 1991). The ISB is characterized by a prominent north-trending, curvi-linear zone of mostly shallow focus earthquakes (< 20 km deep) that is about 100-200 km wide (Smith and Arabasz, 1991). The part of the ISB that includes the Expansion Project coincides with the northeastern Basin and Range Province and the tectonic transition zone between the Basin and Range and the Middle Rocky Mountains.

Historical seismicity in the region of the Expansion Project, with magnitudes greater than M 4.0, is concentrated to the north and north-northeast near Afton, Wyoming, and to the south and southwest, along the Wasatch Front of Utah and around the northern part of the Great Salt Lake (Figure 2). Significant historical surface-faulting earthquakes in the ISB include the 1934, surface wave magnitude ( $M_S$ ) 6.6 Hansel Valley, Utah earthquake; the 1959, moment magnitude ( $M_W$ ) 7.3 Hegben Lake, Montana earthquake; and the 1983,  $M_W$  6.9 Borah Peak, Idaho earthquake (Smith and Arabasz, 1991). The 1934 Hansel Valley earthquake was the closest of these earthquakes to the Expansion Project. Its epicenter was about 140 km southwest of Montpelier, Idaho, beneath the north shore of Great Salt Lake (Figure 2). The Hansel Valley earthquake produced 11 km of total normal-slip surface rupture along strike, and a maximum normal-slip vertical displacement of 0.5 m (Black, 1999).

*Identification and Characterization of Active  
(Holocene) Extensional Faults in Southeast Idaho,  
Northeast Utah, and Southwest Wyoming – Implications for Pipeline Crossing Design*

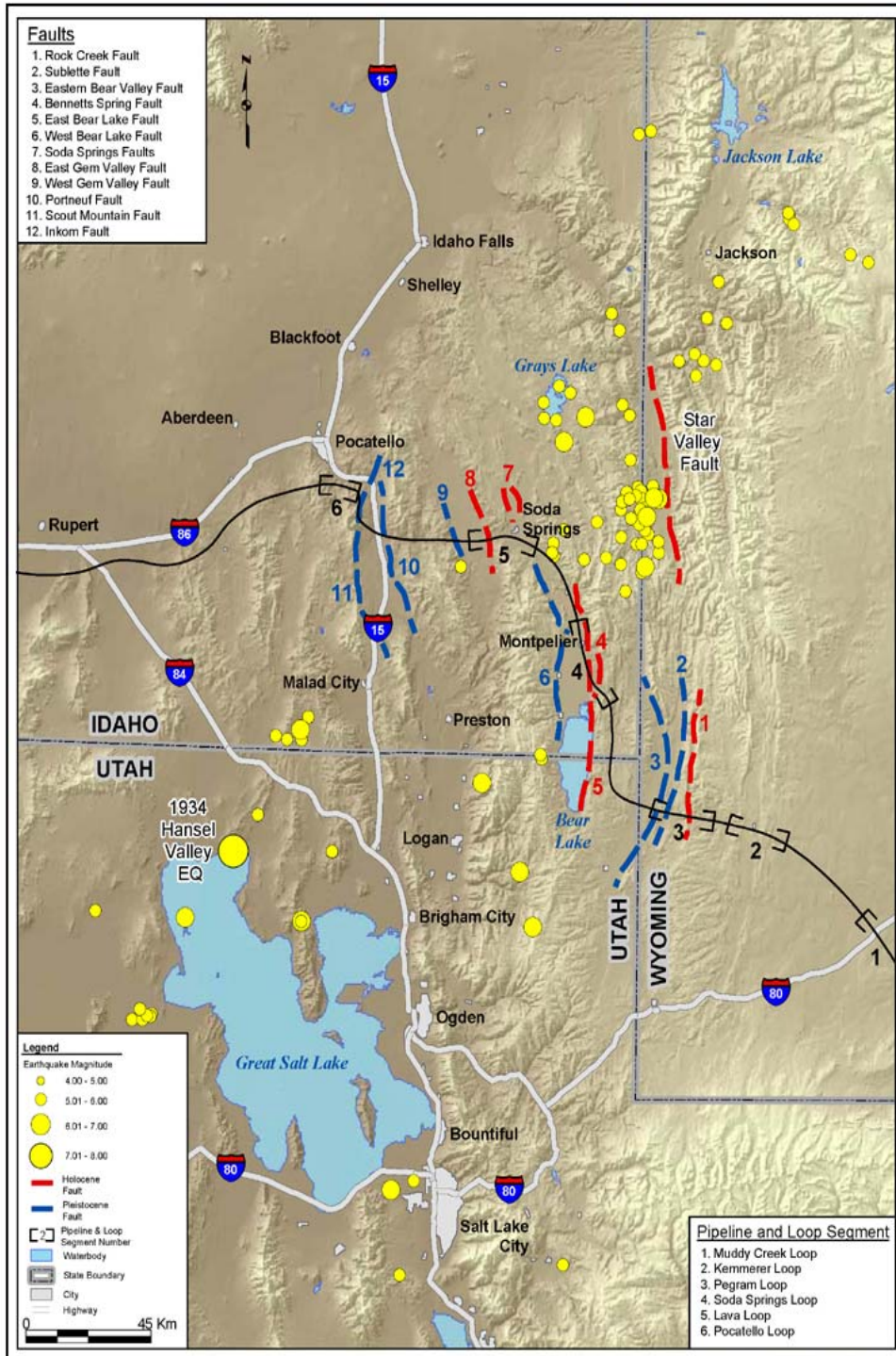


**Figure 2. Regional tectonic and seismic setting of the Expansion Project**

## **DESCRIPTION OF ACTIVE (HOLOCENE) FAULTS CROSSED BY THE EXPANSION PROJECT**

### **General**

Based on a review of available literature, data, and mapping, as well as the aerial and field reconnaissance conducted for this study, we identified 12 active (Holocene) or potentially active (Pleistocene) Basin and Range normal-slip faults that could affect the Expansion Project. These faults either cross the pipeline, or are projected to cross it along the Pegram, Soda Springs, and Lava loops. Figure 2 shows the 12 faults with respect to the Expansion Project loop segments.

Eleven of the active or potentially active faults were identified from the literature review. We discovered one previously unmapped fault based on the results of this investigation. Of the 12 faults, five are active, while seven are potentially active. The active faults exhibit geomorphic and/or geologic evidence of Holocene-age displacement, while the potentially active faults do not.

The five active faults are the Rock Creek, Bennetts Spring, East Bear Lake, Soda Springs, and East Gem Valley faults. This investigation demonstrated that the Soda Springs faults, a series of parallel and slightly en echelon, north-northwest-striking, normal-slip faults, die out before crossing the Expansion Project alignment at Soda Springs, Idaho. Therefore, the Soda Springs faults did not affect development of fault-displacement parameters for pipeline design.

### **Rock Creek Fault**

The Rock Creek fault is the easternmost of the active faults that affect the Expansion Project (Figure 2). It crosses the Pegram Loop segment at approximate pipeline milepost (MP) 464.5 (Figure 3). Witkind (1975a) first identified the Rock Creek fault as an active tectonic feature, and it has subsequently been

listed as such by McCalpin (1994), the U.S. Geological Survey (1996), and Machette and others (2001).

The Rock Creek fault is about 41 km long, and is a normal-slip fault with the west side down-dropped (McCalpin, 1994). The fault has an overall strike azimuth of about 005 degrees (N5E), and an estimated westerly dip of about 60 degrees. The fault is at the base of north-trending Dempsey Ridge in the area of the pipeline crossing, but it cuts across the mid-slope area to the north of the crossing (Figure 3). The fault locally displays graben-like features in the hanging wall (Figure 3), and based on our interpretation of the stereoscopic aerial photographs, the width of the fault zone could be as much as 400 m.

Witkind (1975a) indicated that scarps along the Rock Creek fault in Holocene alluvium are as much as 15-18 m high. McCalpin (1994) reported scarps as high as 25 m, with isolated scarps in alluviated drainages ranging from 6-8 m high. McCalpin (1994) further reported at least two Holocene displacement events with the most recent displacement about 3.3 ka.

Our investigation shows that the Rock Creek fault scarp varies from about 3-9 m high, and displaces both bedrock and alluvium. It is traceable for more than 16 km north of the pipeline crossing. The scarp is higher where underlain by bedrock, and lower where it is formed on alluvium. At the pipeline crossing, the scarp is not visible in an apparent late Holocene alluvial fan, although the fault is well expressed just to the north of the crossing by a high fault-line scarp in bedrock (Figure 3).

The strike of the Rock Creek fault at the pipeline crossing is about 350 degrees (N10W), and the pipeline is oriented about 270 degrees (Figure 3). Thus the Rock Creek fault crosses the Expansion Project pipeline with a crossing angle of 80 degrees.

Identification and Characterization of Active  
(Holocene) Extensional Faults in Southeast Idaho,  
Northeast Utah, and Southwest Wyoming – Implications for Pipeline Crossing Design

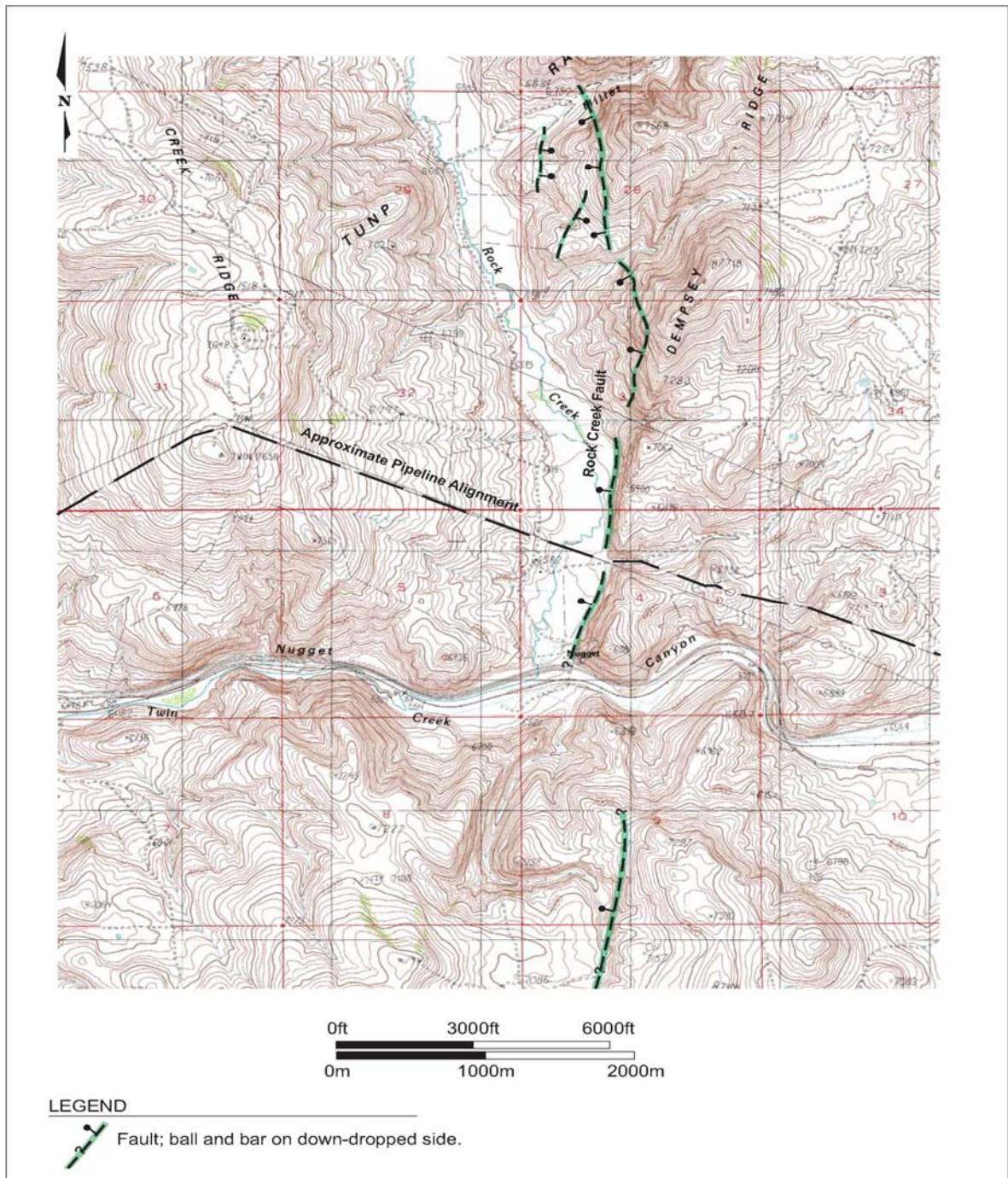


Figure 3. Rock Creek fault map

## **Bennetts Spring Fault**

The Bennetts Spring fault is a slightly curvi-linear, west-dipping, normal-slip fault that crosses the Soda Springs Loop in the Bear River Valley at MP 504.57 (Figures 2 and 4). The Bennetts Spring fault was not previously identified in the literature as an active or potentially active fault. We identified it during the Expansion Project investigation from our ground-based geomorphic and geologic reconnaissance, and further characterized it from our geomorphic evaluation of stereoscopic aerial photographs and during our aerial reconnaissance.

The strike of the Bennetts Spring fault is about 020 degrees (N20E), and it has a westerly dip estimated to be 60 degrees. It is at the base of the Sheep Creek Hills, and extends northward for about 11.5 km from just south of the Bear River to about Montpelier Canyon. The fault is defined by a linear series of west-facing faceted ridge spurs, and a west-facing scarp. The scarp ranges from about 6 to 12 m high. On the south side of the Bear River Valley, the scarp is also associated with a prominent spring (Bennetts Spring; Figure 4).

Along the west base of the Sheep Creek Hills, the Bennetts Spring fault is overlain by undisturbed late Holocene alluvial fans, because the scarp does not continue across the fans (Figure 4). The fault is also concealed beneath the alluvium of the Bear River Valley, (Figure 4). These geomorphic relations suggest that the most recent displacement of the Bennetts Spring fault is pre-latest Holocene (i.e., more than 2 to 3 ka).

The strike of the Bennetts Spring fault at the pipeline crossing is about 034 degrees (N34E), and the pipeline orientation is 315 degrees (Figure 4). Thus, the Bennetts Spring fault crosses the pipeline with a crossing angle of 79 degrees.

## **East Bear Lake Fault**

Witkind (1975b) first identified the East Bear Lake fault and subsequent workers have also considered it active (Arabasz and Julander, 1986; Smith and Arabasz, 1991; U.S. Geological Survey, 1996; Haller and Lewis, 1999; Idaho Geological Survey, 2000; and Laabs and others, 2001). The fault is about 80 km long, and forms the eastern boundary of the Bear Lake Valley graben (Figure 2).

Haller and Lewis (1999) identify three segments of the East Bear Lake fault; northern, central, and southern. The pipeline crosses the central segment at MP 511.21 on the Soda Springs Loop, just south of Montpelier, Idaho (Figure 5).

The East Bear Lake fault is generally north striking, with an estimated westerly dip of about 60 degrees. The fault trends along the west base of the Aspen Range north of Bear Lake, crosses the Bear Lake/Bear River Valley south of Montpelier, Idaho, and continues south along the east side of Bear Lake into northern Utah (Figure 2).

North of Montpelier, Idaho, the East Bear Lake fault is expressed as a linear, west-facing scarp superimposed on west-facing faceted ridge spurs at the base of the Aspen Range. The scarp along this section is about 6 to 9 m high. In the Bear Lake/Bear River Valley south of Montpelier, the fault is defined by a low, west-facing linear scarp in valley alluvium (Figure 5). There the scarp ranges from about 2 to 4 m high, and ponds water on the west side of the scarp to form extensive marshes (Figure 5). Haller and Lewis (1999) indicate that scarps formed in late Pleistocene and Holocene Valley alluvium range from 1.5 to 6 m high.

Paleoseismic trench investigations on the southern segment suggest that the most recent displacement of the East Bear Lake fault may have been about 2.6 to 4.6 ka, and there may

Identification and Characterization of Active  
(Holocene) Extensional Faults in Southeast Idaho,  
Northeast Utah, and Southwest Wyoming – Implications for Pipeline Crossing Design

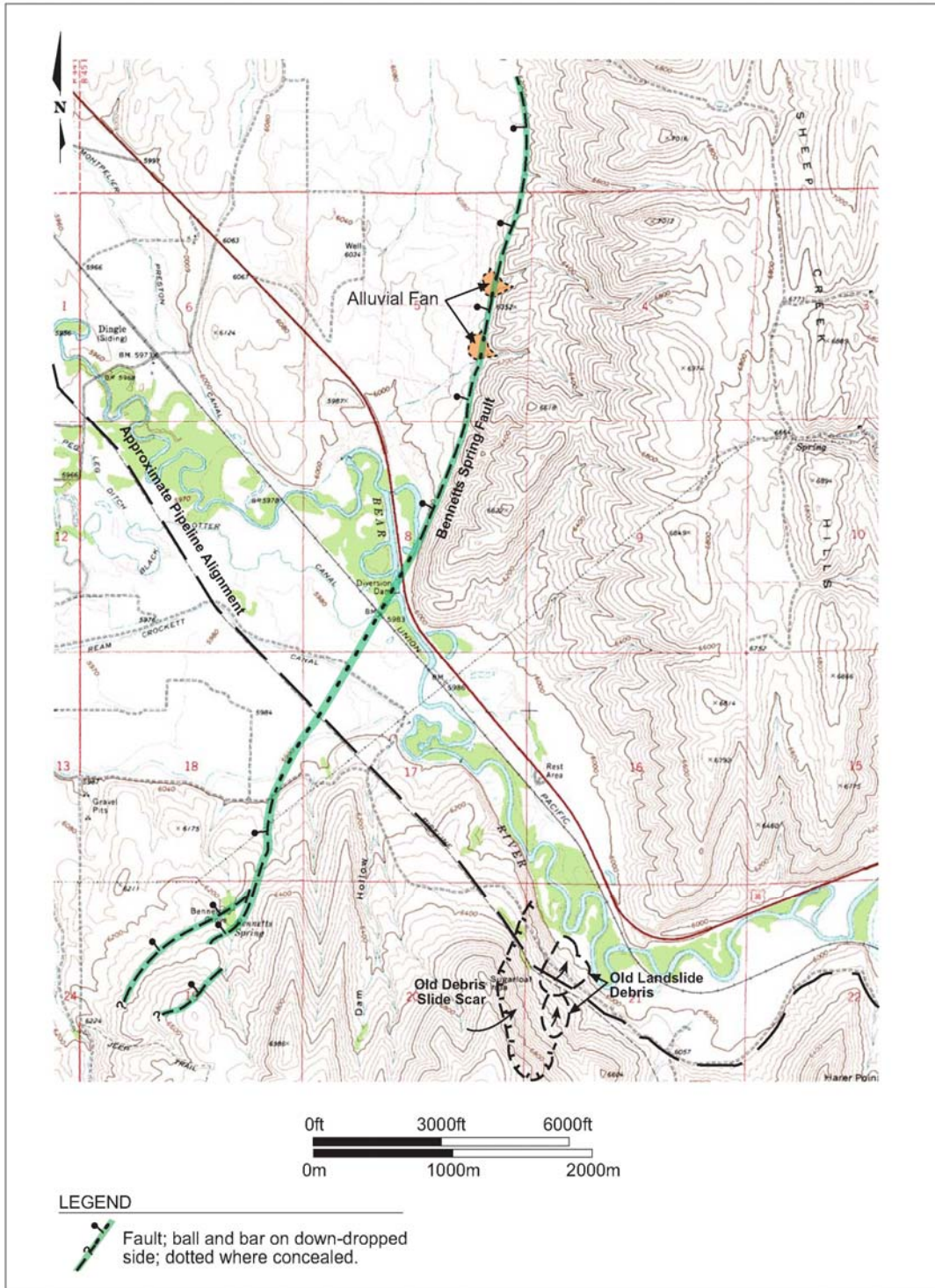


Figure 4. Bennetts Spring fault map

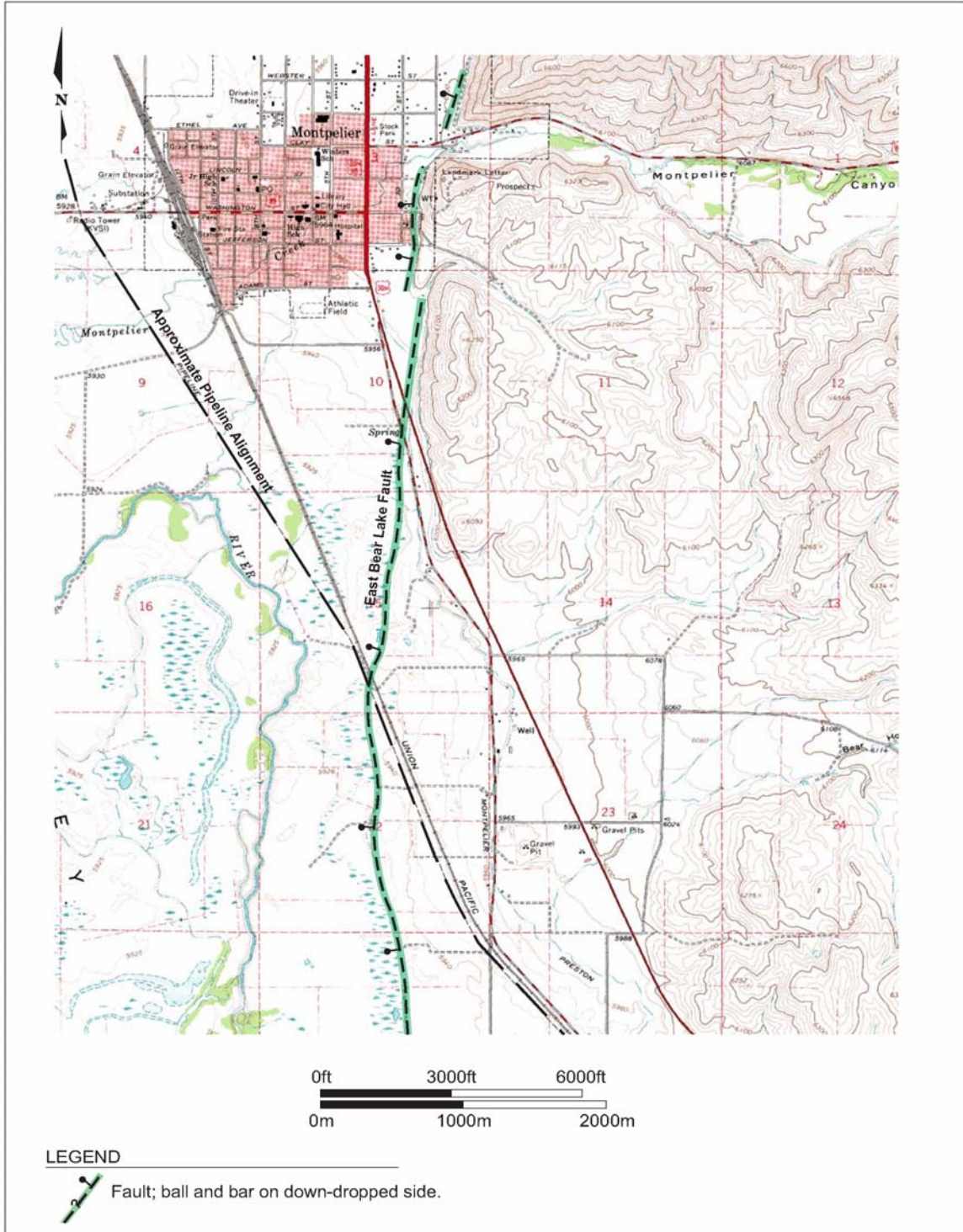


Figure 5. East Bear Lake fault map

have been from two to four Holocene displacement events (Black and others, 1999). The amount of displacement per faulting event, at the fault trench sites, ranged from about 2.6 to 5.6 m (Black and others, 1999). The strike of the East Bear Lake fault at the pipeline crossing is about 013 degrees (N13E), and the orientation of the pipeline is about 330 degrees (Figure 5). Thus, the East Bear Lake fault crosses the pipeline with a crossing angle of 43 degrees.

### **East Gem Valley Fault**

Armstrong (1969) mapped the East Gem Valley fault as cutting mid-Pleistocene basalt flows. We interpreted the basalt flows to be the 140 ka Blackfoot lavas of the Gem Valley volcanic field (Link and others, 1999). The East Gem Valley fault has also been mapped by Witkind (1975b), Smith and Arabasz (1991) and the Idaho Geological Survey (2000) as Quaternary, or late Quaternary.

The East Gem Valley fault is a north-striking, west-dipping normal-slip fault that extends about 65 km along the western base of the Bear River Range and the Chesterfield Range east of Soda Springs, Idaho (Figure 2). The East Gem Valley fault crosses the Lava Loop at MP 547.67 (Figure 6).

The East Gem Valley fault displaces the Blackfoot lavas for more than 20 km. The fault is expressed as a prominent, sinuous, fresh-looking, west-facing scarp, with local graben features that have less prominent east-facing scarps (Figure 6). The west-facing scarp ranges from 2 to 21 m high, while the local, east-facing scarps range from 2 to 12 m high. The highest scarps are observed about 760 m north of the pipeline, and about 5 km south, at the Last Chance Tunnel near Grace, Idaho. At the pipeline crossing, the west-facing scarp is about 2 to

3 m high. There is a parallel, low, subtle scarp about 200 m west of the main, west-facing scarp at the pipeline crossing, which suggests that the fault zone may be at least 200 m wide at this location.

The strike of the East Gem Valley fault at the pipeline crossing is about 013 degrees (N13E), and the orientation of the pipeline is about 264 degrees (Figure 6). Thus, the East Gem Valley fault crosses the pipeline with a crossing angle of 71 degrees.

### **Development and Summary of Active (Holocene) Fault Characteristics**

We compiled geomorphic and geologic characteristics of each of the active faults that cross the Expansion Project loop segments from the available literature, and/or from the results of our field reconnaissance. Of particular importance were data related to total fault length, fault segment length, fault dip, down-dip rupture width, slip rate, and displacement per event. In some cases, these data were available from the literature while in other cases; we estimated the parameters based on our own investigation. These data were compiled for each active fault-crossing site. Using the site-specific fault characteristics data, and the fault rupture-earthquake magnitude relations of Wells and Coppersmith (1994) and Anderson and others (1996), we derived the maximum earthquake for each active fault, and back calculated the maximum and average fault displacements per event from the earthquake magnitude. We then developed fault-displacement-design parameters for each crossing. Table 2 summarizes the input fault characteristic-data, and the resulting displacement per event data for each active fault crossing.

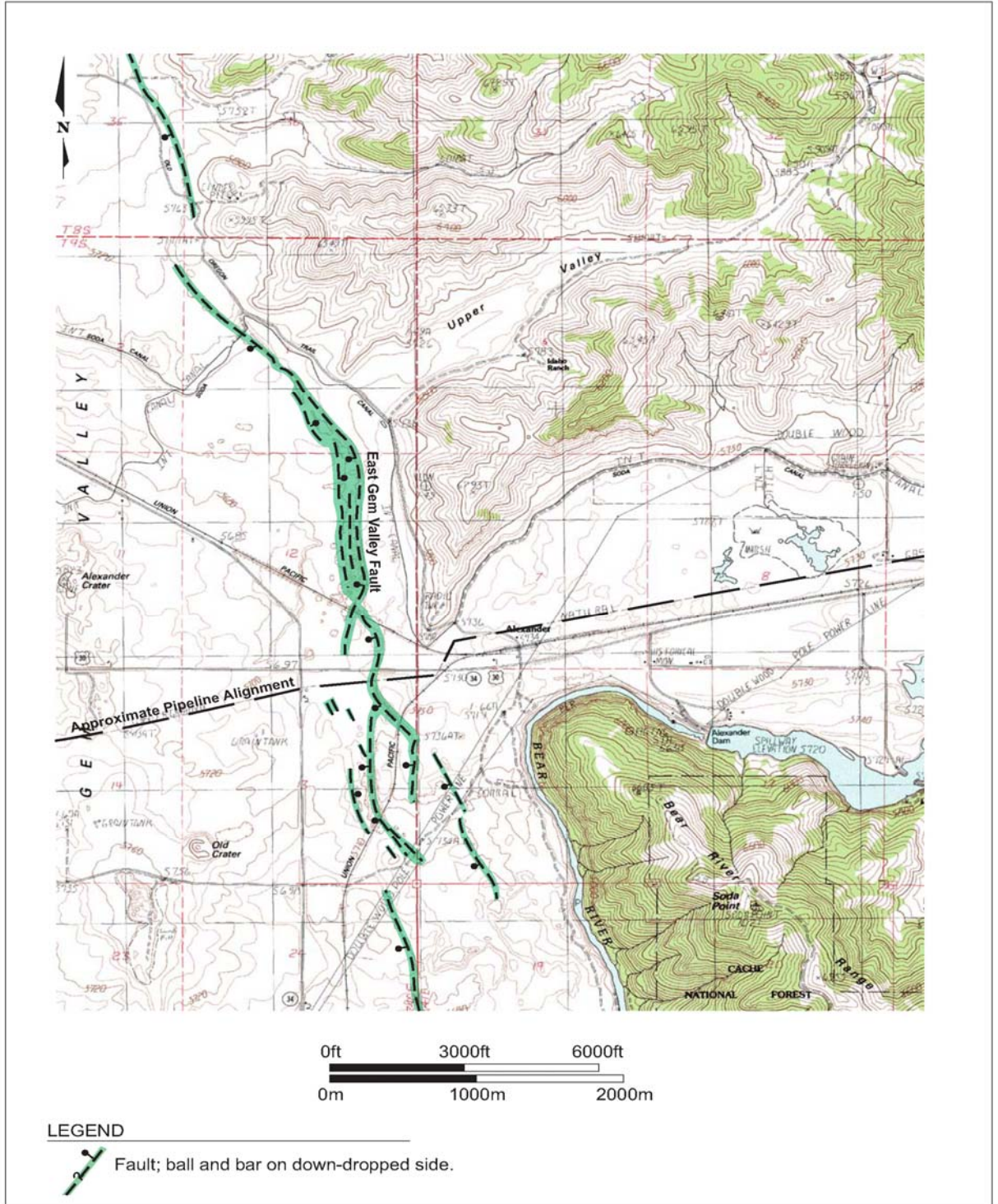


Figure 6. East Gem Valley fault map

**Table 2. Estimated geologic and geometric characteristics of active faults affecting the Expansion Project**

<b>Fault</b>	<b>Total Length (km)</b>	<b>Segment Length (km)</b>	<b>Rupture Width (km)</b>	<b>Rupture Area (km<sup>2</sup>)<sup>1</sup></b>	<b>Slip Rate (mm/yr)</b>	<b>Max. Earthquake (M<sub>w</sub>)<sup>2</sup></b>	<b>Displ. (m)<sup>3</sup></b>
Rock Creek	41	41	17	697	1.7	7.0	2.62 (1.22)
Bennetts Spring	11.5	11.5	17	196	< 0.2	6.5	0.55 (0.30)
East Bear Lake	80	39	17	663	0.86	7.2	4.8 (2.1)
East Gem Valley	65	20	17	340	0.1	6.7	1.03 (0.52)

**Notes:**

- <sup>1</sup> Rupture area is the product of segment length and rupture width.
- <sup>2</sup> M<sub>w</sub> is the moment magnitude.
- <sup>3</sup> Maximum displacement; average displacement in parentheses.

**DEVELOPMENT OF FAULT  
DISPLACEMENT PARAMETERS FOR  
PIPELINE CROSSING DESIGN**

Surface rupture along an active fault results in permanent ground displacement and deformation that may rupture or damage a pipeline that crosses the fault. Whether a pipeline is adversely affected by surface rupture, or the degree to which it is affected, depends primarily on the type of fault, its orientation and dip relative to the orientation of the pipeline, the amount and sense of fault displacement, the spatial distribution of the displacement in the width of the fault zone, the pipe characteristics, and the nature of the backfill material in the pipeline trench (Kennedy and others, 1977; Sergent, Hauskins and Beckwith, 1990a, 1990b; O’Rourke and Liu, 1999).

Williams previously addressed the effects of active fault rupture in the design of the Kern River Pipeline in 1990 that crossed the Wasatch fault zone in Utah, as well as other active and potentially active faults in the Basin and Range between the Wasatch Front and Bakersfield, California (Sergent, Hauskins and Beckwith, 1990a, 1990b). We utilized the same methodology to develop fault-displace-

ment-design parameters for the Expansion Project.

We developed site-specific fault data and displacement-design parameters for each of the active fault crossings. The fault data included the fault location, its orientation and dip, the amount of displacement per faulting event, and the pipeline orientation. The fault-displacement-design parameters included the amount of displacement expected in three geometric axes keyed to the orientation of the pipe. With the exception of the location data, the fault data and displacement-design parameters are summarized in Table 3, and discussed below.

We identified the precise location of the fault crossing for the Expansion Project in terms of the milepost and the surveyed stationing along the pipeline. The location was the point along the pipeline where the fault plane crossed the loop pipeline. The width of the fault zone was measured from this location. Fault orientation at the pipeline crossing was provided in terms of the fault dip and dip direction. The estimated maximum and average fault displacements per event at the pipeline crossing provide the range of reasonably expected displacements that should be considered for pipeline design. The fault

zone width is the distance along the pipeline over which displacement could occur. The fault zone width is expressed as a distance up-station and down-station from the fault plane crossing. The widths given in Table 3 are commonly asymmetric about the fault location station reflecting the presence of graben structures in the fault hanging wall. The pipe orientation at the fault crossing, combined with the fault strike, establish the crossing angle. Depending on the type of fault (i.e., strike-slip, normal-slip or reverse-slip), the crossing angle determines to a large degree whether the expected displacement puts the pipeline into tensional or compressive stress.

The fault-displacement-design parameters (Table 3) provide the estimated maximum and average displacement in the three axes about the pipeline. The values were calculated from the estimated maximum and average displacement data for each fault, at the pipeline crossing (Table 2), following the methodology used by Williams for the Kern River Pipeline (Sergent, Hauskins and Beckwith, 1990a, 1990b). Figure 7 presents the methodology schematically.

The “x” direction is the expected horizontal component of fault displacement along the pipeline axis with positive values in the up-station direction. Displacement in the “x” direction is a function of the amount of normal-slip, dip-slip displacement, the fault dip, and the intersection (crossing) angle between the fault strike and the pipe orientation (Figure 7).

The “y” direction is the expected horizontal lateral component of fault displacement perpendicular to the pipe axis, with positive values to the right of the pipe axis facing up-station. Displacement in the “y” direction is also a function of the amount of normal-slip, dip-slip displacement, the fault dip, and the intersection angle between the fault and the pipeline (Figure 7).

The “z” direction is the expected vertical component of fault displacement in the plane of the pipe axis, with negative values in the downward direction. Displacement in the “z” direction is a function of the normal-slip, dip-slip displacement, and the fault dip angle in the plane of the pipe axis (Figure 7).

**Table 3. Estimated active fault data and fault displacement design parameters for Expansion Project pipeline crossings**

Fault (Loop)	Dip/Dip Direction (degrees)	Displ. (m) <sup>1</sup>	Fault Zone Width (m) <sup>2</sup>	Pipe Orientation (degrees)	Fault Displacement Design Parameters <sup>3</sup>		
					x (m)	y (m)	z (m)
Rock Creek (Pegram)	60/260	2.62 (1.22)	50/30	270	1.29 (0.60)	-0.23 (-0.11)	-2.18 (-1.02)
Bennetts Spring (Soda Springs)	60/304	0.55 (0.30)	100/100	315	0.27 (0.15)	-0.05 (-0.03)	-0.45 (-0.25)
East Bear Lake (Soda Springs)	60/283	4.80 (2.10)	35/20	330	1.76 (0.77)	-1.64 (-0.72)	-2.10 (-0.92)
East Gem Valley (Lava)	60/283	1.03 (0.52)	200/30	264	0.49 (0.25)	0.17 (0.08)	-0.80 (-0.41)

**Notes:**

- <sup>1</sup> Estimated maximum dip-slip fault displacement given the maximum magnitude earthquake (Table 2). Value in parentheses is average displacement.
- <sup>2</sup> Estimated width of fault zone along pipe axis at fault crossing. Value to the left of slash is the width up-station of the fault crossing while the value to right is the width down-station.
- <sup>3</sup> Fault-displacement-design parameters derived following methodology of Sergent, Hauskins and Beckwith (1990a, 1990b). The “x” direction value refers to the calculated component of maximum displacement along the axis of the pipeline, and is positive in the up-station direction. The “y” direction value is the component of maximum lateral (horizontal) displacement perpendicular to the pipe axis, and is positive to the right of the pipe when facing up-station. The “z” direction value is the component of maximum vertical displacement in the plane of the axis of the pipe, and is negative in the downward direction. Values in parentheses indicate the average displacement.

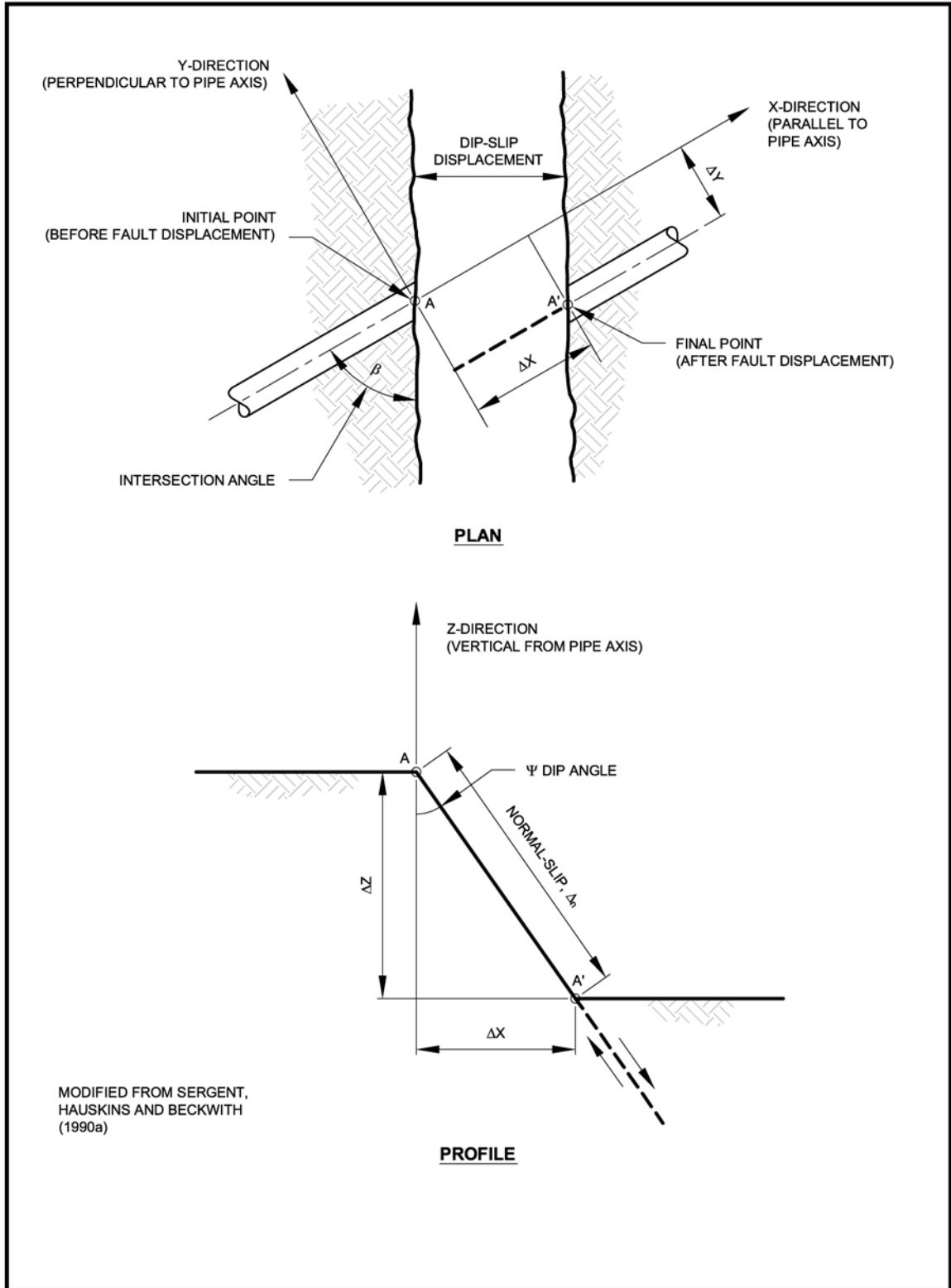


Figure 7. Definition of normal-slip fault displacement design parameters

## DISCUSSION AND CONCLUSIONS

The expected displacement from future fault-rupture events on the active faults that cross the Pegram, Soda Springs, and Lava loops of the Expansion Project would, in general, tend to put the pipeline into axial tensional stress, as well as vertical shearing stress. The largest calculated displacements are for the East Bear Lake fault crossing of the pipeline, and this crossing also has the lowest crossing angle (43°). This low crossing angle results in the largest “y” direction displacement (e.g., -1.64 m) compared to the other active faults (Table 3). The Rock Creek fault crossing angle is 80 degrees, and the calculated displacements for the fault are slightly less than for the East Bear Lake fault in the “x” and “z” directions. The calculated displacements for the Bennetts Spring and East Gem Valley faults are the smallest of the active faults (e.g., less than about 0.8 m in the “x,” “y,” and “z” directions), and the crossing angles are 79 and 71 degrees, respectively.

Several possible fault-displacement-mitigation options are available to pipeline designers. If it is a new pipeline, avoidance (e.g., route selection around the fault) may be a viable mitigation option. However, if the route is already established, such as was the case for the Expansion Project, avoidance may not be an available option. The length of the fault, or land ownership considerations may also preclude avoidance as an option. Where avoidance is not possible, typical mitigation options include:

- Varying the orientation of the pipeline to induce or enhance tensile stress on the pipeline, and to reduce compressive stress. Modern, ductile steel pipelines are generally more resistant to the effects of tensile stress compared to compressive stress.
- Increasing the pipe wall thickness, and specifying favorable steel characteristics for the area of the fault

crossing. This provides an increased capacity to withstand ground displacement and deformation through zones of fault displacement.

- Installing automatic shutoff valves on either side of the fault crossing to isolate the area in the event of rupture or damage to the pipeline caused by fault displacement.
- Employing above ground construction over the fault crossing to separate the pipeline from the effects of surface fault rupture in the ground.
- Minimizing the burial depth of the pipeline, and/or use of select trench backfill materials to enhance the unanchored length of the pipeline, thereby increasing the tolerance of the pipeline to fault displacement. The geometry of the excavated trench, its width and depth are based on site-specific conditions. The select backfill is generally a granular material placed in a loose to medium-dense condition.
- Installing multiple-layered geotextile around the pipe to reduce pipe-soil friction and enhance the unanchored length of the pipeline.

Based on the fault-displacement-design parameters (Table 3), as well as pipe-stress analyses (AMEC Earth and Environmental, 2002), only the East Bear Lake fault crossing required special fault-displacement mitigation. The mitigation consisted of the installation of thicker (i.e., 12.7 mm) wall steel pipe through the width of the fault zone (i.e., 150 m to the west of the crossing, and 180 m to the east). For the Rock Creek, Bennetts Spring, and East Gem Valley fault crossings, the initial design characteristics of the pipe planned for the project exceeded the structural demand created by the calculated fault displacements (Table 3), and thus, no special fault displacement mitigation design was required for these crossings (AMEC Earth and Environmental, 2002).

## ACKNOWLEDGMENTS

Golder Associates Inc., through the efforts of technical teams from the Redmond, Washington and Reno, Nevada offices, conducted the investigation of active faults for the Expansion Project. The work was completed under contract to The Williams Companies, Inc., Houston, Texas. Williams granted permission to present to, and publish the results of the investigation in the Proceedings Volume for Western States Seismic Policy Council, Basin and Range Province Seismic Hazards Summit II Conference, which is greatly appreciated by the authors.

## REFERENCES

- AMEC Earth and Environmental, 2002, Report of fault-rupture design services, four fault crossings, Rockies Displacement Expansion Project, Lincoln County, Wyoming and Caribou and Bear Lake Counties, Idaho: letter to Williams, Houston, TX, November 14, 2002.
- Anderson, J.G., Wesnousky, S.G., and Stirling, M.W., 1996, Earthquake size as a function of fault slip rate: Bulletin of the Seismological Society of America, v. 86, n. 3, p. 683-690.
- Arabasz, W.J., and Julander, D.R., 1986, Geometry of seismically active faults and crustal deformation within the Basin and Range-Colorado Plateau transition in Utah: Geological Society of America Special Paper 208, p. 43-74.
- Armstrong, F.C., 1969, Geologic map of the Soda Springs quadrangle, southeastern Idaho: U.S. Geological Survey Miscellaneous Geologic Investigations Map I-557, scale 1:48,000.
- Black, B.D., 1999, 1934 Hansel Valley Earthquake: Utah Geological Survey, <http://www.ugs.state.ut.us/maps/geohazmap/qfaults/image2/maptext/HanselValley>.
- Black, B.D., Hylland, M., Hecker, S., and Lewis, R.S., compilers, 1999, Fault number 2364c, Eastern Bear Lake fault, southern section, in Quaternary fault and fold database of the United States, ver 1.0: U.S. Geological Survey Open-File Report 03-417, <http://qfaults.cr.usgs.gov>.
- Braun, J., Major, G., West, D.O., and Bukovansky, M., 1998, Geologic hazards evaluation boosts risk-management program for western U.S. pipeline: Oil and Gas Journal, November 9, 1998, p. 73-79.
- California Division of Mines and Geology, 1992, Fault-rupture hazard zones in California, Alquist-Priolo Special Studies Zones Act of 1972 with index to special studies zones maps: Special Publication 42, revised 1992, 32p.
- Haller, K.M., and Lewis, R.S., compilers, 1999, Fault number 2364b, Eastern Bear Lake fault, central section, in Quaternary fold and fault database of the United States, ver 1.0: U.S. Geological Survey Open-File Report 03-417, <http://qfaults.cr.usgs.gov>.
- Idaho Geological Survey, 2000, Quaternary and Active Faults Map of Idaho., scale 1:3,350,000.
- Jennings, C.W., 1994, Fault activity map of California and adjacent areas with locations and ages of recent volcanic eruptions: California Division of Mines and Geology Geologic Data Map No. 6, scale 1:750,000..
- Kennedy, R.P, Chow, A.W., and Williamson, R.A., 1977, Fault movement effects on buried oil pipeline: Transportation Engineering Journal of ASCE, v. 103, n. TE5, p. 617-633.
- Laabs, B.J., Kaufman, D.S., and Umhoefer, P.J., 2001, Tectonic geomorphology and late-Quaternary uplift in Bear Lake Valley, Utah and Idaho: Geological Society of America Abstracts with Programs, Annual Meeting, November 5-8, 2001.

- Link, P.K., Kaufman, D.S., and Thackray, G.D., 1999, Field guide to Pleistocene Lakes Thatcher and Bonneville and the Bonneville Flood, southeastern Idaho *in* Hughes, S.S. and Thackray, G.D., eds., Guidebook to the Geology of Eastern Idaho: Idaho Museum of Natural History, p. 251-266.
- Machette, M.N., Pierce, K.L., McCalpin, J.P., Haller, K.M., and Dart, R.L., 2001, Map and data for Quaternary faults and folds in Wyoming: U.S. Geological Survey Open-File Report 01-461, scale 1:750,000.
- McCalpin, J.P., compiler, 1994, Fault number 729, Rock Creek fault, in Quaternary fault and fold database of the United States, ver 1.0: U.S. Geological Survey Open-File Report 03-417, <http://qfaults.cr.usgs.gov>.
- Othberg, K.L., and Breckenridge, R.M., 1981, Interpreting geologic hazards in Idaho from remotely sensed imagery: Idaho Bureau of Mines and Geology Open-File Report 81-6.
- O'Rourke, M.J., and Liu, X., 1999, Response of buried pipelines subject to earthquake effects: (New York, NY), Multi-disciplinary Center for Earthquake Engineering Research, 247 p.
- Reiter, L., 1990, Earthquake hazard analysis: Columbia University Press, New York, NY, 254 p.
- Sergent, Hauskins and Beckwith, 1990a, Report for evaluation and treatment at fault crossings and related design methodology, spreads 5, 6, 7 and 8: prepared for Kern River Gas Transmission Company, Salt Lake City, UT, Communication No. 7, May 18, 1990.
- Sergent, Hauskins and Beckwith, 1990b, Report for fault crossing design memorandum, Spreads 1, 2, 3, and 4, Kern River gas Transmission Pipeline: prepared for Kern River Gas Transmission Company, Salt Lake City, UT, Communication No. 25, December 21, 1990.
- Smith, R.B., and Arabasz, W.J., 1991, Chapter 11, Seismicity of the Intermountain Seismic Belt *in* Slemmons, D.B., Engdahl, E.R., Zoback, M.D., and Blackwell, D.D., eds., Neotectonics of North America: Geological Society of America, Decade Map Volume 1, p. 185-228.
- Smith, R.B., and Sbar, M.L., 1974, Contemporary tectonics and seismicity of the western United States with emphasis on the Intermountain seismic belt: Geological Society of America Bulletin, v. 85, p. 1205-1218.
- U.S. Geological Survey, 1996, National seismic hazard maps: Documentation June 1996, Open-File Report 96-532.
- Wells, D.L., and Coppersmith, K.J., 1994, New empirical relationships among earthquake magnitude, rupture length, rupture width, rupture area, and surface displacement: Bulletin of the Seismological Society of America, v. 84, n. 4, p. 974-1002.
- West, M.W., 1993, Extensional reactivation of thrust faults accompanied by coseismic surface rupture, southwestern Wyoming and north-central Utah: Geological Society of America Bulletin, v. 105, p. 1137-1150.
- Witkind, I.J., 1975a, Preliminary map showing known and suspected active faults in Wyoming: U.S. Geological Survey Open-File Report 75-279, scale 1:500,000.
- Witkind, I.J., 1975b, Preliminary map showing known and suspected active faults in Idaho: U.S. Geological Survey Open-File Report 75-278, scale 1:500,000.
- Yeats, R.S., Sieh, K., and Allen, C.R., 1997, The geology of earthquakes: (New York, NY), Oxford University Press, 568 p.

***PALEOSEISMIC INVESTIGATIONS  
OF THE STANSBURY AND MID-VALLEY FAULTS,  
SKULL VALLEY, UTAH***

Frank H. Swan  
Consulting Geologist  
240 Laidley Street, San Francisco, California 94131

Kathryn L. Hanson and Robert R. Youngs  
Geomatrix Consultants, Inc.,  
2101 Webster, 12<sup>th</sup> Floor, Oakland, California; 94612

Michael M. Angell  
William Lettis & Associates  
999 Andersen Drive, Suite 120, San Rafael, California; 94901

**ABSTRACT**

Geological and geophysical investigations in Skull Valley, Utah provide new data on the location, geometry, and late Quaternary slip rate of the Stansbury fault and two previously unrecognized mid-valley faults within the basin. Proprietary gravity and seismic reflection data were used to constrain the locations of major faults. High-resolution seismic S-wave reflection surveys and detailed surface and subsurface Quaternary studies provided data to evaluate the style, location, geometry, and slip rate of both primary and secondary distributed faulting.

The Stansbury fault is the major west-dipping normal fault that forms the structural boundary between the valley (half graben) on the west and the uplifted Stansbury Mountains to the east. Near Antelope Canyon, the late Quaternary slip rate on the Stansbury fault is estimated to be  $0.39 \pm 0.04$  mm/yr (i.e., the cumulative rate across the main trace and two secondary traces in the hanging wall). This slip rate is faster than previously reported estimates, primarily because displacement across the secondary traces was not included in the earlier estimates.

In the southern part of Skull Valley, two west-dipping mid-valley normal faults are informally named the East fault and the West fault. In the northern part of the basin, the postulated Springline fault occupies a similar structural position. The preferred slip rate on the East fault is  $0.2 \pm 0.1$  mm/yr based on measured displacements on three stratigraphic datums that range in age from 12 ka to  $\geq 160$  ka. A slip rate on the West fault of 0.05 to 0.07 mm/yr is based on the displacement of a single datum, the Stansbury bar, that is estimated to be 20 ka.

The probable maximum magnitude for the Stansbury, East and West faults are calculated based on empirical relations that relate magnitude to fault-rupture dimensions. The maximum earthquake magnitude distribution includes alternative maximum rupture scenarios for each fault. Alternative models treat the West fault as a primary independent fault or as a secondary fault in the hanging wall of the East fault. The mean maximum magnitudes (moment magnitudes) for the three faults are: **M** 7.0 for the Stansbury fault, **M** 6.5 for the East fault and **M** 6.4 for the West fault in the independent fault model.

## INTRODUCTION

Studies conducted for a proposed Private Fuel Storage Facility (Geomatrix Consultants, 1999) provide new data for assessing the potential earthquake hazards associated with the Stansbury fault and related mid-valley faults in Skull Valley, Utah (Figure 1).

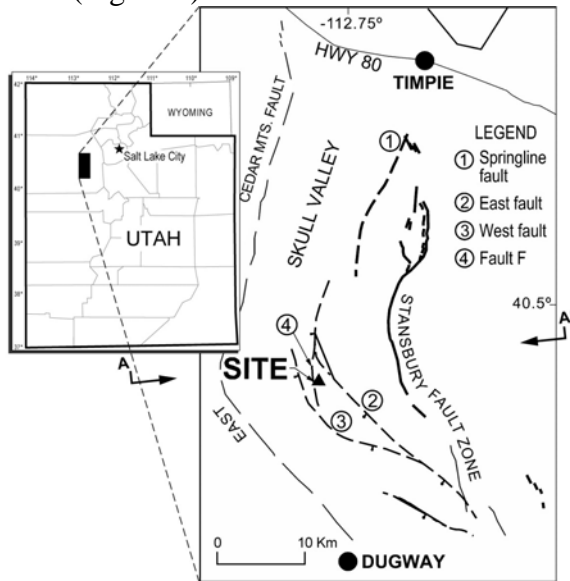


*Figure 1 Map showing location of known (solid lines) and inferred (dashed lines) active faults in the Skull Valley, Utah study area..*

In addition to review of existing data, extensive surface and subsurface investigations were completed for this study. Proprietary industry data, both gravity and seismic reflection data, were obtained and analyzed to constrain the locations of major faults in Skull Valley. Six kilometers of high-resolution seismic S-wave reflection data were collected to image reflectors in the upper part of the Tertiary and the overlying Quaternary section in the vicinity of the proposed storage area. Borings and trenches provided confirmation of the location and activity of faults identified from the seismic survey data. Geologic mapping and

surveying of Quaternary deposits and landforms in the site area and along the Stansbury fault zone to the east of the site provided new data to evaluate the nature and timing of late Quaternary deformation in the site region.

## GEOLOGIC SETTING

Skull Valley is a structural half graben within the Basin and Range province that is bounded on the west by the Cedar Mountains and on the east by the Stansbury Mountains (Figure 2).

The stratigraphy in the vicinity of the proposed storage facility consists of an approximately 150 to 250 m-thick section of Quaternary and Tertiary basin fill overlying Paleozoic bedrock. The Quaternary section consists of a sequence of primarily lacustrine deposits representing a series of pluvial lake cycles that interfinger with subaerial sediments along the margins of the basin. Correlation of these deposits to a well established regional pluvial chronostratigraphy provides well-constrained age estimates for late Quaternary deposits at the site (Table 1). At the proposed storage area, Quaternary deposits are approximately 26 m thick. The Quaternary sediments overlie Tertiary basin fill deposits that consist of an interbedded sequence of siltstone, claystone, and tuffaceous sediments. The upper part of the Tertiary basin fill is middle to late Miocene. Elsewhere in the region, the upper part of the Tertiary basin fill is Pliocene in age.

Interpretations of four high-resolution seismic shear wave survey lines collected for this study were used to identify the location of faults in proximity to the proposed storage area site (Geomatrix Consultants, 1999; Bay Geophysical Associates, 1999). Two prominent reflectors that can be traced across the entire

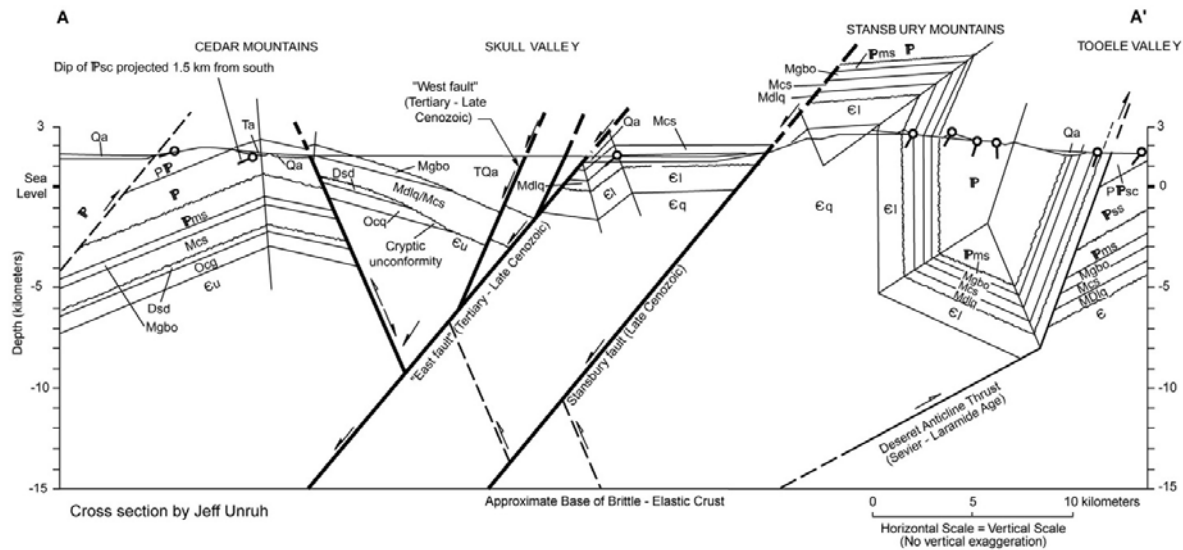


Figure 2 Structural east-west geologic cross section from Tooele Valley to Great Salt Lake Desert, Utah.

site represent unconformities at the base of the Bonneville alloformation (reflector Qp) and the Quaternary/Tertiary contact (reflector Q/T). The Qp unconformity represents the subaerial period of erosion, deposition, and soil formation that occurred between the Little Valley lake cycle, which ended about 130 ka, and the Bonneville lake cycle. The oldest Bonneville lake sediments at the site are about 28 ka. The Q/T reflector likely represents an unconformity at the top of the Salt Lake Group.

The time represented by the Q/T unconformity is not well constrained. Detailed sampling of one borehole showed a relatively uniform section of lacustrine deposits below the Qp unconformity/pre-Bonneville deposits and the top of the Salt Lake Group (Q/T reflector) that correlates to the Little Valley alloformation (~130 to 160 ka). These data suggest a minimum upper constraining age for the Q/T boundary at this location of > 160 ka. A maximum age of approximately 4 Ma is based on the estimated age of the underlying Salt Lake Group.

The major structures in the region (Plate 1 and Figure 2) consist of pre-mid-Tertiary

contractional structures that are no longer active, and which have been faulted and offset by younger post-mid-Tertiary normal faults and related extensional deformation. The faults most significant to the fault evaluation study include:

- The Stansbury fault zone, which lies 9 km east of the site and is the main structural boundary between the Skull Valley half graben and the uplifted Stansbury Mountains to the east;
- two mid-valley faults, the East fault and the West fault, which lie about 0.9 km east and 2 km west of the site respectively; and
- a broad zone of distributed faulting on the down-thrown side of the East fault that is bounded by the two mid-valley faults.

### STANSBURY FAULT ZONE

The Stansbury fault zone forms the border between the western margin of the Stansbury Mountains and piedmont slopes that border the eastern margin of Skull Valley. It is a west-dipping normal fault that displaces the late Quaternary alluvial fans. The length of fault that is reported to have had late Quaternary displacement is

**Table 1**  
*Summary of Ages of Major Stratigraphic Units*

Unit/Associated Geomorphic Surfaces	Estimated Age (ka)	Climatic Condition	Marine Oxygen Isotope Stage <sup>1</sup>
Post-Provo Deposits	≤ 12 ka	Interpluvial	Stage 1
Bonneville Alloformation	28 ka to 12 ka	Pluvial	Stage 2
Provo Shoreline	~14.3 ka <sup>2</sup> to ~12 ka		
Bonneville Shoreline	~16 ka to ~14.5 ka		
Stansbury Shoreline	~22 ka to ~20 ka		
Stansbury Deep-water facies	~24 ka to 22 ka		
End of Late Pinedale Alluvial Fan Deposition	35 ± 5 ka	Glacial/ Interglacial Transition	Stage 2/3
Cutler Dam Alloformation (not observed at PFSF site)	~ 60 ka	Pluvial	Stage 4
Early Pinedale Alluvial Fan	~60 to 70 ka	Glacial/ Interglacial Transition	Stage 4/5
Qp Unconformity	130 ka to 28 ka	Interpluvial	Stage 5
Promontory Soil formed in pre-Bonneville subaerial deposits			
Little Valley Alloformation	~150 ka to 130 ka	Pluvial	Stage 6
Bull Lake Alluvial Fan	~160 ka	Glacial/ Interglacial Transition	Stage 6/7
Pre-Little Valley Subaerial Deposits	≥160 ka	Interpluvial	Stage 7 and older
Q/T Unconformity	> 4 Ma to 160 ka	N/A	N/A

<sup>1</sup> Shackleton and Opdyke (1973)

<sup>2</sup> Light and Kaufman (1997)

approximately 40 to 45 km (Hecker, 1993; Helm, 1995) extending from the northern end of the Stansbury Mountains at the village of Timpie, to Johnson Pass near the village of Willow Springs. Helm (1995) notes that the fault consists of two distinct sections, separated by a west-trending cross fault coincident with Pass Canyon and the southern margin of Salt Mountain. She postulates that the fault sections are rupture segments that may, or may not, rupture independently.

All workers agree that there has been late Quaternary movement on the Stansbury fault, but there is some uncertainty concerning the timing of the most-recent displacement. On the basis of fault-scarp morphology, Barnhard and Dodge (1988) and Helm (1995) suggest that the most recent movement on the Stansbury fault occurred prior to the Lake Bonneville highstand (more than 15,000 years ago). In contrast, on the basis of stream nickpoints located a short distance upstream of the scarps, Everitt and Kaliser (1980) concluded that the most recent movement on the fault occurred during the Holocene. Barnhard and Dodge (1988) addressed this possibility by visiting two stream channels that have prominent nickpoints, and concluded that resistant bedrock influenced upstream migration of the nickpoints, and thus that the fault has not had Holocene displacement.

Aerial photographs (1:20,000 scale) were analyzed and a field reconnaissance was conducted along traces of the Stansbury fault east of the site (Figure 3) to evaluate the timing and amount of the most recent Quaternary displacements. Scarp profiles were measured across the main fault trace at the mouth of Antelope Canyon (Figure 4) and across two secondary traces that lie 1½ to 2 km west of the range front (Figure 5).

### **Main Fault Trace**

East of the site the main fault scarp is generally between elevation 1710 m and 1770 m (5600 and 5800 feet) (i.e., about 120 m to 150 m) higher than the Bonneville shoreline (the apexes of the alluvial fans are displaced across small graben that are evident at the mouths of Indian Hickman and Antelope Canyons. North of Indian Hickman Canyon, the main fault scarp is readily apparent on the aerial photographs. South of Indian Hickman Canyon, the scarp is more subdued and appears to be eroded and buried by young alluvial fan deposits.

At the mouth of Antelope Canyon, a young stream terrace that is inset below the alluvial fan can be seen on the aerial photographs on the east (upthrown) side of the fault appears to be truncated by the fault.

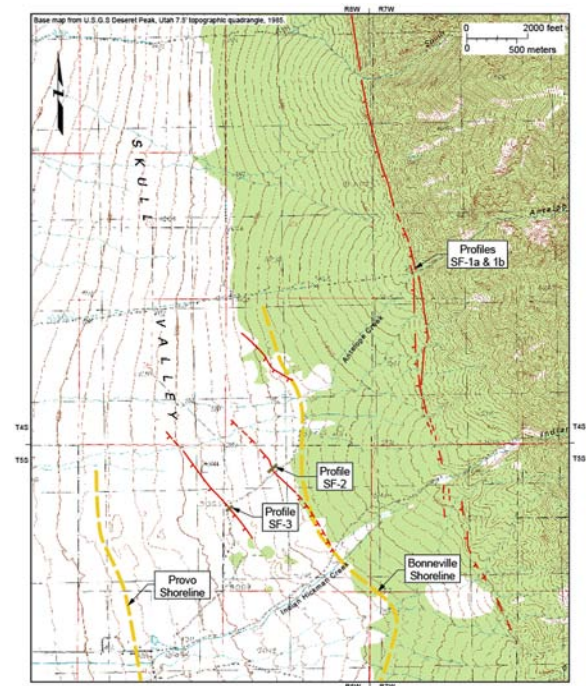


**Figure 3** Map showing traces of the Stansbury fault east of the site and locations of scarp profiles.

At the mouth of Indian Hickman Canyon the young alluvial deposits do not appear to be displaced.

The modern stream is incised more than 15 m below the apex of the fan. There is an approximately 1- to 4-m high terrace that is inset below the fan surface along the north side of the creek. This terrace is displaced across a 2.9-m-high scarp and the vertical displacement of the terrace surface is  $1.9 \pm 0.2$  m. The age of this terrace is not well constrained. Based on the geomorphic position of the terrace and the relatively subdued character of the scarp along this segment of the fault compared to Basin and Range faults that have had late Holocene displacement, the scarp is inferred to have formed during the early to middle Holocene.

It probably represents a single displacement event.

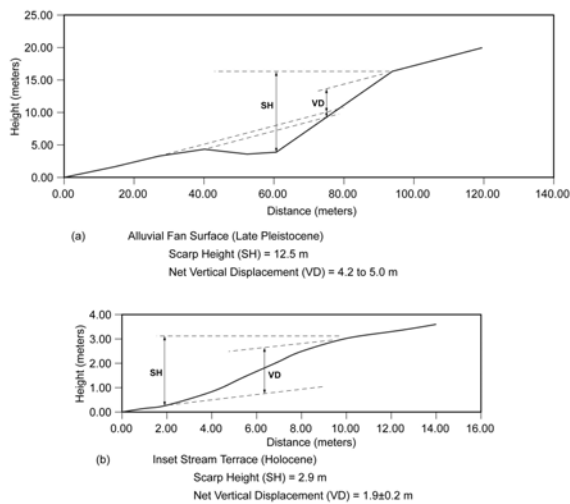


**Figure 4** Profiles SF-1A and SF-1B across fault scarp along the main trace of the Stansbury fault at Antelope Canyon, Utah.

### Secondary Fault Traces

Sack (1993) maps three secondary fault traces that appear to be northwest-trending splays off of the main fault trace. These fault traces are well expressed on the aerial

photographs as 0.8- to 2-km long linear scarps that traverse an alluvial fan surface. The fan surface has been modified by wave erosion during transgression of the Pleistocene lake to the Bonneville shoreline. The alluvial fan at profiles SF-2 and SF-3 (Figures 3 and 5) is significantly older than the fan gravel at profile SF-1a. The fan surface is much more dissected. Quartzite boulders and cobbles commonly have thick weathering rinds that consist of a dark red rind up to 1 mm thick over a more diffuse zone of weathering up to 1 cm thick. Boulders having thick rinds that are spalling off are common on the fan surface. These weathering characteristics are characteristic of Bull Lake and older alluvial fans in the Basin and Range. Correlation with the Bull Lake glaciation suggests the fan gravel is at least 160 ka. Shorelines eroded into the fan surface are clearly truncated along the fault. These shorelines lie above the Provo shoreline and had to have formed prior to, or during, the transgression of the lake to the Bonneville shoreline. Recessional shorelines would not have formed during the rapid draw down of the lake from the Bonneville to the Provo level.

Assuming they formed during the most recent transgression, they are younger than the Stansbury shoreline (about 20 ka) and older than the Bonneville shoreline (about 15 ka). Based on their elevation, they are inferred to be about  $18 \pm 2$  ka. The scarp heights at profiles SF-2 and SF-3 are 3.6 m and  $2.8 \pm 0.1$  m respectively, and the vertical displacements are 2.7 m and 1.9 m (Figure 5).

Inflections in the scarp profiles (changes in slope angle in the face of the scarps) indicate the cumulative displacement probably was produced by multiple events.

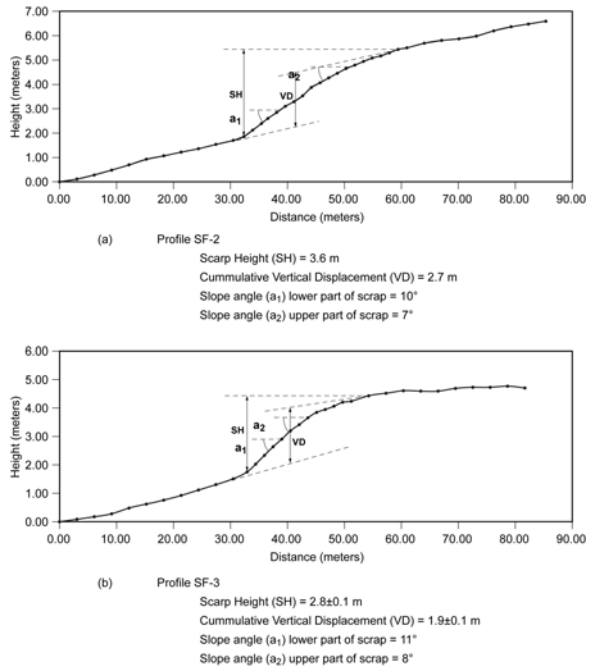


**Figure 5** Profiles SF-2 and SF-3 across two western traces in the hanging wall of the Stansbury fault southwest of Antelope Canyon, Utah.

Geomorphic relations along the scarps indicate the cumulative displacement at SF-2 and SF-3 is the result of at least two events on each of these traces.

Southeast of profile SF-2 the scarp intersects a gravel bar (elevation 1598 m /5240 feet) associated with the Bonneville shoreline (Figure 3). A discontinuous lineament can be traced across the bar that suggests there has been post-Bonneville displacement along this trace. The scarp across the bar is lower than the scarp to the northwest and it has been obscured in most places by Holocene alluvial fans that grade out across the Bonneville shoreline. These relations suggest there was at least one pre-Bonneville event (i.e., prior to ~15 ka) followed by an early to middle Holocene event (i.e., post Bonneville but older than the alluvial fans that bury the Bonneville shoreline). These relations are consistent with the inferred early- to middle-Holocene age for the most recent event on the main

trace at Antelope Canyon. Assuming two events, the average displacement per event was 1.4 m.

The timing of the most recent events along the scarp at profile SF-3 are not as well constrained, but the geomorphic relations suggest their ages are similar to those along the scarp at SF-2. The southeast end of the scarp cuts a gravel bar at elevation 1550 m (5080 feet), which formed during the transgression to the Bonneville shoreline. The bar is younger than the Stansbury shoreline (~20 ka) and older than the Bonneville shoreline (~ 15 ka). Near the northwest end of this feature (0.75 km northwest of profile SF-3), the scarp is breached by a gully and a small debris-flow fan has formed west of (on the down-thrown side of) the scarp. The fan buries the lower half of the scarp face. The presence of the scarp across the apex of this small fan, a sharp vegetation lineament across the fan and the fact that the fan has subsequently been incised suggest this young (middle Holocene ?) fan has been displaced by the fault. Assuming the scarp along profile SF-3 was formed by at least two events indicates an average vertical displacement per event of  $\leq 1$ m.

### Slip Rate

Table 2 is a summary of the displacement data on the Stansbury fault east of the site and the calculated slip rates. The value of 0.36 mm/yr for the Holocene stream terrace (line b on Table 2) is based on a single event displacement. Therefore, it is not a reliable average late Quaternary slip rate, which should represent the average behavior during successive events. The late Quaternary rates on the individual traces range between  $0.11 \pm 0.02$  and  $0.15 \pm 0.02$  mm/yr. These rates are somewhat higher than the late Cenozoic rate of  $0.07 \pm 0.02$

mm/yr calculated by Helm (1995) for the northern section of the Stansbury fault, and are generally consistent with published rates of other Basin and Range faults that lie west of the Wasatch, which typically have late Quaternary slip rates in the range of 0.1 to 0.2 mm/yr.

Summing the slip rates on the faults that intersect a transect extending west of Indian Hickman Canyon indicates a cumulative late Quaternary slip rate across the Stansbury fault zone of  $0.39 \pm 0.04$  mm/yr. This value is faster than previously reported estimates, primarily because displacement across secondary traces was not included in the previous estimates. Helm (1995) concludes that the southern section of the fault, which lies west of the highest part of the range, is probably characterized by faster Quaternary slip rates than the northern section of the Stansbury fault. Considering this, and taking into account the uncertainties in the displacement data, the average slip rate along the length of the Stansbury fault is probably in the range of  $0.4 \pm 0.1$  mm/yr.

### **Average Slip Per Event**

From the scarp profiles described above, the single-event displacements are estimated to be about 1.9 m on the main trace of the Stansbury fault zone (profile SF-1b) and 1.4 m and  $\leq 1$  m on the secondary fault traces (profiles SF-2 and SF-3 respectively). This indicates a possible range of single event displacements of about 1 m, assuming the fault traces ruptured independently, to about 4 ½ m, if the primary and secondary traces all ruptured simultaneously. The Holocene faulting on the main trace appears to die out between Antelope and Indian Hickman canyons at about the latitude as the northern limit of the secondary traces. This suggests the most likely vertical displacement during the most recent event is about 2 m to 2 ½ m.

The 2-m value corresponds to the displacement from profile SF-1b ( $1.9 \pm m$ ). The 2 ½-m value corresponds to the sum of profiles SF-2 and SF-3 divided by two events. The displacement measurements along this section of the fault are likely to be somewhat higher than the average for the entire length of the Stansbury fault. Scarp heights tend to be higher and the height of the range to the east is higher than the sections of the fault to north and south.

## **MID-VALLEY FAULTS (SKULL VALLEY)**

Two west-dipping normal faults are mapped along the center of the basin in the southern part of Skull Valley (Figures 1 and 2; Plate 1). The faults bound Hickman Knolls, which is a bedrock outlier in the southern part of Skull Valley. The two principal mid-valley faults are informally referred to as the East fault and the West fault. These faults are probably truncated by the east-west trending Pass Canyon fault (Plate 1), but the East fault might be a continuation of the postulated Springline fault, a previously inferred fault in the northern part of Skull Valley (Rigby, 1958; Hood and Wadell, 1968; Helm, 1995). Small faults identified in the area between the East fault and the West fault are interpreted to be due to secondary deformation in the hanging wall of the East fault. The structural data suggest that the site is in the stepover area between the East and West faults.

### **East Fault**

The East fault consists of a zone of west-dipping normal faults that was imaged on both deep seismic reflection data (i.e., proprietary oil company data) and the shallow high-resolution seismic survey

conducted for this study (Geomatrix Consultants, 1999; Bay Geophysical Associates, 1999). The easternmost trace coincides with a topographic escarpment along the western flank of Castle Rock Knoll that truncates a Bull Lake or older age alluvial fan.

Late Pleistocene/Holocene activity is indicated for the East fault based on: (1) discrete displacements of the Qp reflector imaged in the seismic data (Bay Geophysical Associates, 1999), (2) the Bull Lake or older age alluvial fan appears to be truncated by the fault, and (3) the Provo shoreline appears to be at a higher elevation east of the fault relative to the corresponding shoreline on Hickman Knolls west of the fault.

Estimated displacements and slip rates calculated for the East fault are summarized in Table 3. The slip rate estimates are based on displaced datums ranging in age from  $\geq 160$  ka to 12 ka, and thus are considered to be representative of the late Pleistocene slip rate for this fault. Based on these data, the preferred estimate for the late Quaternary slip rate on the East fault is  $0.2 \pm 0.1$  mm/yr.

### **West Fault**

The West fault is a west-dipping normal fault that was imaged in deep seismic reflection data (i.e., proprietary oil company data). This fault, which lies west of Hickman Knolls, projects beyond the western extent of the shear-wave seismic survey lines acquired for this study. The projected trace of the fault coincides with possible vertical displacements of the Stansbury cross-valley bar suggesting late Pleistocene activity.

A prominent gravel bar associated with the Stansbury shoreline (Table 1) extends from the northern end of Hickman Knolls westwards across the valley floor for more

than 6 km. Based on test pits and a detailed topographic survey of the surface of the bar, the vertical separation of the Stansbury age deposits ( $\sim 20$  ka) is 1 to 1.5 m across the West fault (Table 3). The fault zone aligns with linear drainages and tonal lineaments identified on aerial photographs along the western boundary of the Hickman Knolls bedrock outcrop. It may be associated with a series of northwest-trending lineaments identified by Sack (1993) in Sections 23 and 26, T5S, R8W (near "North Basin" on Plate 1). Most of the lineaments in this zone appear to be related to shoreline processes, but one of the lineaments consists of a sharp tonal contrast that appears to cut across the topographic contours. This suggests it is not due to wave erosion and might be tectonic in origin. Based on the net vertical separation of the Stansbury Bar across the projected trace of the West fault, the late Quaternary slip rate is 0.05 to 0.07 mm/yr (Table 3). This slip rate, which is based on apparent displacement of a single datum, may have occurred during a single event. This estimate, therefore, is not considered very reliable. The cumulative displacement of Tertiary strata across the West fault compared to the more significant displacements across the East fault suggest that the West fault at the latitude of the proposed storage facility is a less significant fault, which is consistent with the lower calculated slip rate on the West fault.

### **Zone of Distributed Faulting**

A broad zone of distributed faulting is present in the area between the East and West faults. This 2700-m to 3700-m wide zone contains numerous small west-dipping and east-dipping normal faults. Several of the faults imaged on the high-resolution seismic reflection lines do not appear to extend above the Q/T reflector, suggesting

**Table 2**  
*Fault slip rate data – Stansbury fault zone*

Location	Displaced Datum	Age (ka)	Cumulative Vertical Displacement (m)	Slip Rate (mm/year)	Comments	
<b>Stansbury Fault – Main Trace:</b>						
a)	Profile SF-1a - Antelope Canyon	Late Pinedale (?) alluvial fan surface	35 ±5	4.6 ±0.4	0.13 ±0.03	Long term rate on primary trace based on multiple events.
b)	Profile SF-1b - Antelope Canyon	Holocene stream terrace	8 ±2	1.9 ±0.2	0.36 +0.16/-0.09	Same trace as above; rate is probably based on a single event and is, therefore, unreliable.
<b>Stansbury Fault – Secondary Traces:</b>						
c)	Profile SF-2 - Indian-Hickman alluvial fan	Post-Stansbury Pre-Bonneville shorelines	18 ±2	2.7	0.15±0.02	Inflection in scarp profile and geomorphic relations indicate displacement is due to two events.
d)	Profile SF-3 - Indian-Hickman alluvial fan	Post-Stansbury Pre-Bonneville shorelines	18 ±2	1.9 ±0.1	0.11 ±0.02	Inflection in scarp profile and geomorphic relations indicate displacement is due to two events.
<b>Cumulative Slip Rate Across Zone:</b>						
g)	Transect west of Indian Hickman Canyon	--	--	--	0.39 ±0.04	Sum of slip rates a, c and d

**Table 3**

*Fault slip rate data – East fault and West Fault*

Location	Displaced Datum	Age (ka)	Vertical Separation			Slip Rate (mm/year)	Comments	
			Seismic Survey		Offset Geomorphic Features (m)			
			Calculated Based on Seismic Profile (m) <sup>1</sup>	Adjusted Value (m) <sup>2</sup>				
<b>1) East Fault:</b>								
a)	Fault A-1 – Seismic Line A	Qp <sup>3</sup>	50 to 60 <sup>4</sup>	1.6	4.8	--	0.088 ±0.008	Down-to-the-west.
b)	Fault A-4 – Seismic Line A	Qp	50 to 60	0.4	1.2	--	0.022 ±0.002	Down-to-the-west.
c)	Fault A-2 – Seismic Line A	Qp	50 to 60	0.3	0.9	--	0.018 ±0.002	Down-to-the-east.
d)	Fault A-3 – Seismic Line A	Qp	50 to 60	1.3	3.9	--	0.71 ±0.007	Down-to-the-west.
e)	Net Displacement Across Faults A-1, A-4, A-2, and A-3.			3.0	9.0	--	<b>0.165 ±0.015</b>	Net displacement is down-to-the-west.
f)	Cumulative across East Fault and secondary traces. (Between Hickman Knolls and Goshute Village)	Provo Shoreline	14.3	--	--	3 ±1 <sup>5</sup>	<b>0.2 ±0.1</b>	Net displacement across zone is approximately 10 ft. down-to-the-west.
g)	Truncated edge of alluvium Sec. 32, T4S, R8W	Qf <sub>bl</sub> (?) <sup>6</sup>	>160 ka	--	--	-30 to -50 <sup>7</sup>	<b>&lt; 0.2 to 0.3</b>	
<b>2) West Fault:</b>								
a)	Between TP-14 and drainage that breaches Stansbury bar in SW ¼ Sec. 12, T5S, R8W	Stansbury Bar	~20 ka	--	--	1 to 1.5	0.05 to 0.07	Down-to-the-west. Distributed on multiple fault traces.

<sup>1</sup> Source: Bay Geophysical Associates, 1999, Table 1.

<sup>2</sup> Adjusted value is 3 times the calculated value based on locations where offsets observed on seismic lines were also measured between borings.

<sup>3</sup> Unconformity between Promontory soil and base of Bonneville alloformation.

<sup>4</sup> Minimum age of Promontory soil based on age of ~28 ka age of the base Bonneville alloformation at the site and estimated minimum interval of 20 ka to 30 ka needed to form a Stage 2+ carbonate soil.

<sup>5</sup> Based on interpretation of 1:20,000-scale aerial photographs and USGS 7.5' topographic maps, the Provo shoreline at the village is at an elevation of 4860 ft.; at Hickman Knolls, it is at an elevation of 4850 ft.

<sup>6</sup> Based on the weathering rinds on quartzite boulders, the alluvial fan is inferred to correlate to Bull Lake or older Basin and Range fans (Oxygen Isotope Stage 6 or older), which suggest a minimum age ~160 ka.

<sup>7</sup> Based on height of the scarp (100 ft) and depth of Bonneville alloformation to the west in boring C-5 (47').

that there has been no late Quaternary movement on these traces. Approximately fifteen of the identified fault traces displace the Q/T reflector. The displacement of the Q/T unconformity across individual faults is very small; ranging from  $\leq 0.6$  m, (i.e., the threshold of detection) to a maximum of about two and a half meters (Bay Geophysical Associates, 1999; Geomatrix Consultants, 1999).

Approximately ten of the identified fault traces appear to displace or deform the Qp reflector and extend into the overlying Bonneville sediments, suggesting late Pleistocene (post-28 ka) activity on these traces. Drilling, trenching, and mapping data were used to further constraint the location and amount of late Pleistocene deformation across individual fault traces in the vicinity of the proposed storage facility (See companion paper by Hanson and others in this volume). Based on the amount of vertical separation on the Qp reflector, calculated slip rates on the individual fault traces within the zone of distributed faulting range from  $< 0.005$  mm/yr to almost 0.04 mm/yr. However, because the faults occur in zones with both west- and east-dipping normal faults, the net displacement on the Qp unconformity across individual graben indicate slip rates ranging from 0 mm/yr (i.e., no detectable net offset) to 0.02 to 0.03 mm/yr.

This broad zone of distributed faulting lies in the stepover area between the East and West faults (Plate 1). The small faults in this zone are interpreted to be secondary deformation related to the stepover and/or secondary faulting in the hanging wall of the East fault. The faults are not interpreted to be independent seismogenic sources.

## **MAXIMUM EARTHQUAKE MAGNITUDES**

The probable maximum earthquake magnitudes for the Stansbury, East and West faults were calculated based on empirical relationships between magnitude and rupture length, magnitude and rupture area, magnitude and single event displacement (Wells and Coppersmith, 1994); the relationship of Anderson and others (1996) between magnitude, rupture length, and slip rate; and the relationship between magnitude, rupture length, and maximum displacement (Mason, 1996). The individual techniques were assigned relative weights that reflect the combined weights of expert panel members who characterized the seismic source parameters for the Yucca Mountain PSHA (CRWMS, 1998). The weights assigned to the various empirical methods varied among the different experts. However, when viewed collectively, the judgements of the eighteen panel members indicate that the most weight is given to relationships based on rupture length and/or rupture area. These two methods received about equal weight with the rupture length relationship being favored slightly over the rupture area relationship. The relationship based on rupture length plus slip rate received the lowest weight. Assigned weights for this method ranged from 0 to 0.4 with the collective weight being less than or about equal to 0.1. Relationships based on displacement (either maximum displacement or average displacement) were considered less stable than those based on rupture length and area and also were assigned a low weight that was only a little higher than the weight assigned to the relationship based on rupture length plus slip rate. For the Stansbury fault, which has displacement data available, the relative weights assigned to the methods for

estimating maximum magnitude are: magnitude versus rupture length [0.4]; magnitude versus rupture area [0.35]; magnitude versus displacement [0.15]; magnitude versus rupture length and maximum displacement [0.05]; and magnitude versus rupture length and slip rate [0.05]. When using displacement to estimate magnitude, average displacement is considered to be a more stable indicator of the size of the earthquake than maximum displacement, which only occurs along a very short length of the total rupture. Given the displacement method, the relation based on average displacement is assigned a weight of 0.7 and the one based on maximum displacement is assigned a weight of 0.3. There are no single-event displacement data for the mid-valley faults. For these faults the method relating magnitude to rupture length and slip rate is assigned a weight of 0.1 and the remaining weight is assigned equally between the other methods.

The maximum magnitude distribution includes alternative rupture scenarios as described for each fault source and reflects the postulated maximum rupture dimensions based on combinations of rupture length and width. The maximum rupture length depends on the total fault length and on the length of the longest part of the fault that is expected to rupture during a single event. Geometric and other geologic constraints also are considered in assigning weights to various possible rupture scenarios. Down-dip width is computed from fault dip, thickness of the seismogenic zone, and limitations imposed by fault geometries where two faults intersect.

Seismicity data indicate that the largest historical earthquakes in the Basin and Range province occurred on 45 to 65 degree dipping normal faults that nucleated

at depths of about 15 km (Smith and others, 1985). The uncertainty in the fault dip is represented by considering three equally likely values of 45, 55, and 65 degrees.

Depth to the base of the seismogenic zone was based on depth distributions of seismicity in the region, which indicate that most of the earthquakes occur shallower than about 18 km, with some as deep as 25 km. We consider the thickness of the seismogenic crust to be uncertain within the range of 15 to 20 km. The discrete probability distribution of 15 km [0.4], 18 km [0.4], and 20 km [0.2] is used to express this uncertainty. The depths of 15 and 18 km are favored because of the typical depth of large Basin and Range earthquakes and nearly all of the seismicity occurs shallower than 18 km.

### **Maximum Magnitude Stansbury Fault Zone**

The Stansbury fault zone has a total length of 73 km. The fault sections identified by Helm (1995) are used with minor modifications to define possible rupture segments (Plate 1 and Table 4). The fault sections include a 24-km-long section from Timpie south to Pass Canyon (Section "A"), and a 23-km-long section from Pass Canyon to Johnson Pass (Section "B"). In addition, we consider the possibility of additional fault sections south of Johnson Pass. The mapped fault trace and linear range front between Johnson Pass and The Dell, the substantial relief of the Onaqui Mountains, and the fault trace at the southern end of the range mapped by Sack (1993) all suggest the fault may continue to the south. We identify fault section "C", which extends from Johnson Pass to The Dell and is 9 km long. We also consider fault section "D", which extends

**Table 4***Rupture-length Scenarios used to calculate maximum magnitudes*

Fault Source	Rupture Scenario <sup>1</sup>	Length (km)	
Stansbury Fault	Pass Canyon to Johnson Pass (Section B)	23	
	Timpie to Johnson Pass (Sections A + B)	47	
	Pass Canyon to the Dell (Sections B + C)	32	
	Timpie to the Dell (Sections A + B + C)	56	
	Timpie to Lookout Pass (Sections A + B + C + D)	73	
Mid-Valley Faults East Fault/ Springline Fault (EF/SpF)	Gravity Low	12	
	South tip to Castle Rock	18	
	South tip to Pass Canyon	28	
	South tip to Burnt Spring	46	
	Springline Fault (SpF)	Pass Canyon –Burnt Spring	18
	East Fault (EF)	Gravity Low	12
		South tip–Castle Rock	18
		South tip–Pass Canyon	28
	West Fault (WF) Model A	Gravity Low	12
		South tip (East fault) – North basin	23
	Model B	Gravity Low	12
		South tip (East fault)–North basin	21
		South tip (West fault)–Pass Canyon west	36

<sup>1</sup> See Plate 1 for locations of postulated rupture-segment boundaries.

from The Dell to Lookout Pass and is 17 km long.

We consider five rupture scenarios for the maximum-magnitude earthquake that incorporate various combinations of the four fault sections noted above (Tables 4 and 5). Because of the prominence of fault scarps across late Quaternary alluvial deposits along the Stansbury fault between Pass Canyon and Johnson Pass, as well as the proximity of this section, each of the

scenarios includes rupture of section "B". The relatively short rupture of 23 km, in which section "B" ruptures alone, is given a low weight [0.1], because it is likely that the maximum earthquake includes rupture along at least one other section. Scenarios that include rupture of section "B" and an adjacent section are given higher probabilities, including a weight of 0.2 for the 47 km-long rupture of sections "A" and "B", and a weight of 0.3 for the 32-km-long

rupture of sections "B" and "C". The 56-km-long scenario in which all three of the northern sections ("A", "B", and "C") rupture is weighted 0.3, based on the presence of evidence of recurrent displacement along all three sections. Lastly, the longest scenario, in which rupture occurs along all four sections of the entire 73-km-long fault, is weighted low [0.1] because of the discontinuity of the fault between The Dell and Lookout Pass.

The maximum magnitude distribution for the Stansbury fault includes all five of the rupture scenarios and reflects the postulated rupture dimensions based on combinations of rupture lengths and widths. In addition, data for average displacement during a single event were included in the assessment. These data suggest that the average displacement during a single event on the segment of the Stansbury fault that lies closest to the site is between 2 to 3 m. The following distribution for average single event displacement was used in this analysis: 1 m [0.1], 2 m [0.4], 3 m [0.4], 4.5 m [0.1]. The estimated late Pleistocene slip rate of the Stansbury fault is in the range of  $0.4 \pm 0.1$  mm/yr. We represent the uncertainty in slip rate with the discrete distribution of 0.3 mm/yr [0.2], 0.4 mm/yr [0.6], and 0.5 mm/yr [0.2]. Figure 6 presents the maximum earthquake magnitude distribution based on these seismic source characteristics. The expected (mean) maximum magnitude for the Stansbury fault is **M 7.0**.

### Maximum Magnitude Mid-Valley Faults (Skull Valley)

Quaternary activity has been documented on a zone of faults within the southern Skull Valley that includes the East fault and the West fault. A similar fault, the postulated Springline fault has been inferred

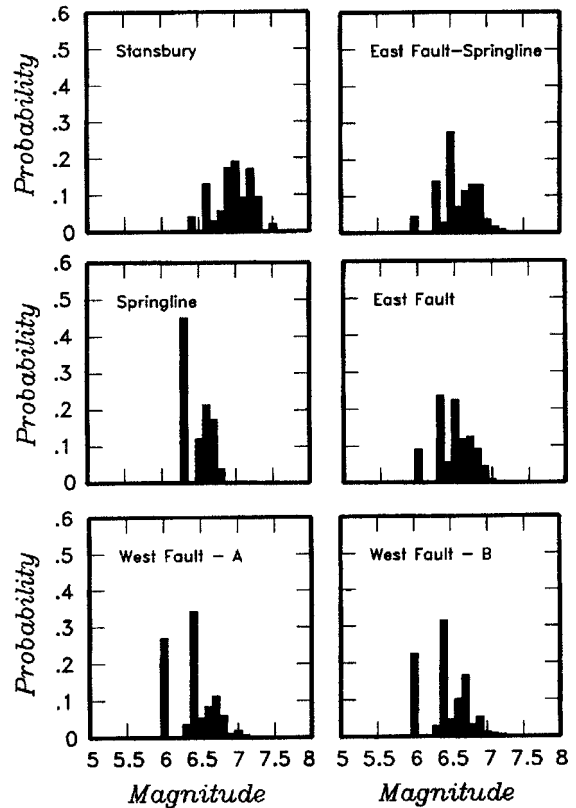
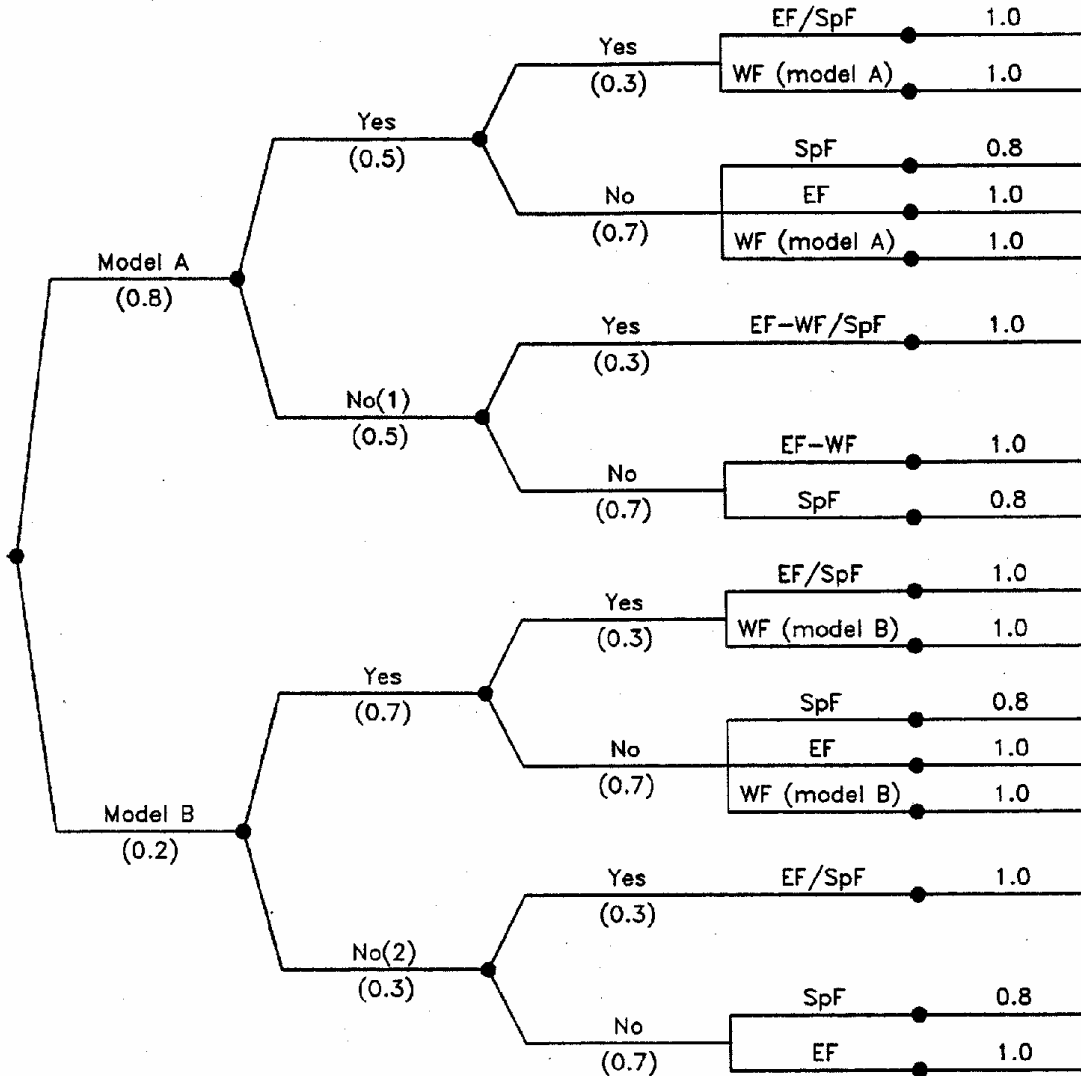


Figure 6 Maximum earthquake magnitude distributions for the Stansbury and Mid Valley faults in Skull Valley, Utah.

in the northern part of Skull Valley (Rigby, 1958; Hood and Wadell, 1968; Helm, 1995). Quaternary activity has not been documented for this fault, but based on analogy to the mid-valley faults in the southern part of the valley, the postulated Springline fault may also be active. Alternative structural models (Plate 1) that allow the possibility that some of these faults are linked or coalesce at depth, and could rupture together during individual earthquakes are considered for these fault sources. A logic tree summarizing the fault sources implied for each of these models is given in Figure 7.

The first node of the logic tree addresses the preference for the two alternative structural models. These models

<i>Structural Model (Section 2.0)</i>	<i>West Fault (WF) Independent Seismic Source</i>	<i>Linked East Fault and Springline Fault</i>	<i>Fault Sources</i>	<i>Probability of Activity</i>
---------------------------------------	---	---	----------------------	--------------------------------



1. WF merges with EF above seismogenic depth. Slip rate estimate is based on combined slip rates indicated for both faults.
2. Deformation along WF is treated as secondary rupture in the hanging wall of EF.

Figure 7 Logic tree for alternative structural models for the mid-valley fault sources in Skull Valley, Utah

chiefly reflect a difference in the assessment of the geometry and seismogenic capability of the West fault. In both models the East fault is included as active fault source that may, in some scenarios be linked along strike with the postulated Springline fault. Structural model A, in which the West fault splays from the East fault in the vicinity of Johnson Pass, best fits the available geologic and gravity data and thus, is given significantly more weight [0.8]. The alternative model B, which is given a weight of 0.2, allows for a longer West fault and captures the uncertainty in the southern extent of this fault.

Assessments of the seismogenic capability of the West fault are dependent on the structural model. In model A, the West fault may or may not be an independent seismic source depending on the geometry of the fault and possible intersection with the East fault at depth. Given the uncertainty in the geometries of these faults at depth, the probability of the West fault being an independent seismic source (i.e., it does not coalesce with the East fault above seismogenic depth) is assigned a weight of 0.5. In model B, the West fault is judged to be an independent fault source with a probability of 0.7. The higher weight given to the likelihood the fault is a seismic source is based on the structural relationships that require a fault between elevated bedrock in Hickman Knolls and the deep part of the basin, and evidence for late Pleistocene activity on the West fault. Lower weight [0.3] is given to the possibility that Hickman Knolls is a detached bedrock slide (i.e., is rootless), thus, obviating the need for a block-bounding fault to the west.

The second node of the logic tree addresses the likelihood that the East fault and the postulated Springline fault are linked along strike. A possible structural boundary between the northern and southern parts of

Skull Valley is suggested by structural and gravity data. Helm (1995) noted that the Pass Canyon cross fault and a fault segment boundary along the Stansbury fault coincide with a regional alignment of tectonic features in the Oquirrh, Wasatch, and Uinta Mountains. The apparent truncation of Salt Mountain along this trend combined with gravity data that indicate the formation of two distinct depocenters in the northern and southern parts of the basin suggest that this structural trend persists across Skull Valley. This, in addition to the lack of geomorphic expression of continuity between the East and postulated Springline faults, is the basis for giving low weight [0.3] to the possibility the two faults are linked and higher weight [0.7] to the possibility they are independent fault sources.

Maximum rupture length scenarios for each of the proposed fault sources are summarized in Table 4. Postulated rupture segment boundaries are shown on Plate 1. Weights were assigned to maximum rupture lengths to reflect our judgment of the validity of the alternative segmentation models. The assessment of maximum magnitude distributions for the alternate fault sources are shown on Figure 6. These distributions reflect the postulated rupture dimensions based on combinations of rupture lengths and widths.

The slip rate distributions used for the individual fault sources (Table 5) vary depending on the structural model. Slip rate estimates for the East and West faults derived from paleoseismic data provide the basis for estimating the slip rate values used for the mid-valley faults. Generally, the highest weight is given to the central estimates, with less weight given to the end member values that capture the uncertainties in paleoseismic estimates.

**Table 5**

*Fault parameters and assigned probability weights used to assess maximum earthquake magnitudes.*

Fault	Probability of Activity	Total Length (km)	Downdip Geometry	Maximum Rupture Lengths (km)	Slip Rate (mm/yr) [wt]	Average Single Event Displacement (m)
<b>Stansbury Fault Zone</b>						
	1.0	73	45°W [0.33] 55°W [0.34] 65°W [0.33]	23 [0.1] 47 [0.2] 32 [0.3] 56 [0.3] 7.3 [0.1]	0.3 [0.2] 0.4 [0.6] 0.5 [0.2]	1 [0.1] 2 [0.4] 3 [0.4] 4.5 [0.1]
<b>Mid-Valley Faults</b>						
East fault (EF), West fault (WF), and Springline fault (SpF)	EF [1.0] WF [1.0] SpF [0.8]	EF 28 [1.0] SpF 18 [1.0] EF/SpF 46 [1.0] WF-Model A 23 [1.0] WF-Model B 36 [1.0]	45°W [0.33] 55°W [0.34] 65°W [0.33]  In cases where the West fault is treated as an independent fault source, the dips of the East and West faults are modeled to be parallel to preclude intersections or truncations of the faults at depth.	EF 12 [0.2] 18 [0.5] 28 [0.3]  SpF 18 [1.0]  EF/SpF 12 [0.1] 18 [0.3] 28 [0.5] 46 [0.1]  <u>WF-Model A</u> 12 [0.6] 23 [0.4]  WF-Model B 12 [0.5] 21 [0.4] 36 [0.1]	EF 0.05 [0.1] 0.1 [0.3] 0.2 [0.4] 0.3 [0.19] 0.45 [0.01]  WF 0.01 [0.2] 0.04 [0.5] 0.07 [0.2] 0.1 [0.1]  EF-WF 0.05 [0.1] 0.1 [0.28] 0.2 [0.29] 0.3 [0.28] 0.45 [0.05]  SpF 0.05 [0.2] 0.1 [0.2] 0.2 [0.35] 0.3 [0.2] 0.45 [0.05]	

There is no independent slip rate data for the postulated Springline fault. In cases where the Springline fault is modeled as a separate source, it is given a slip rate distribution comparable to the East fault with weights more evenly distributed to reflect greater uncertainty. Slightly higher weight is given to higher slip rates in models in which the West fault coalesces with the East fault at depth and is treated as a single fault source (with or without linkage to the Springline fault).

The probable maximum magnitude distributions for selected rupture scenarios for the mid-valley faults are shown in Figure 6. If the East and West faults are considered to be independent seismogenic sources, the mean maximum magnitudes are **-M** 6.5 for the East fault and **M** 6.4 for the West fault.

## CONCLUSIONS

The results of this study provide new information on the location and activity of previously unrecognized faults within the central Skull Valley basin (i.e., the Mid-Valley faults) as well as a better constrained late Pleistocene slip rate for the Stansbury fault. These data have implications for the assessment of seismic hazards on both a local as well as regional basis.

The combined slip rates estimated for the Stansbury fault and the Mid-Valley faults is higher than previously considered in regional slip rate budgets (Thatcher and others, 1999). Skull Valley lies along the proposed transect for a regional geodetic survey across the entire Basin and Range province that will be conducted as part of the NSF Plate Boundary Observatory research initiative (PBO 1999). The results of this study better constrain the geologic slip rate that can be compared with shorter term geodetic rates that will result from the

PBO survey. In addition, the results of this study suggest that additional slip may also be occurring on other mid-valley faults within the Basin and Range that have not been recognized or adequately characterized.

## ACKNOWLEDGMENTS

The study for Private Fuel Storage, LLC was conducted by Geomatrix Consultants Inc., while under contract to Stone & Webster Engineering Corporation. The fault evaluation studies were directed by John Donnell (Program Manager for Stone and Webster) and Kevin Coppersmith. Without the permission and cooperation of Chairman Leon Bear and the Skull Valley Band of the Goshute Indians, this study would not have been possible.

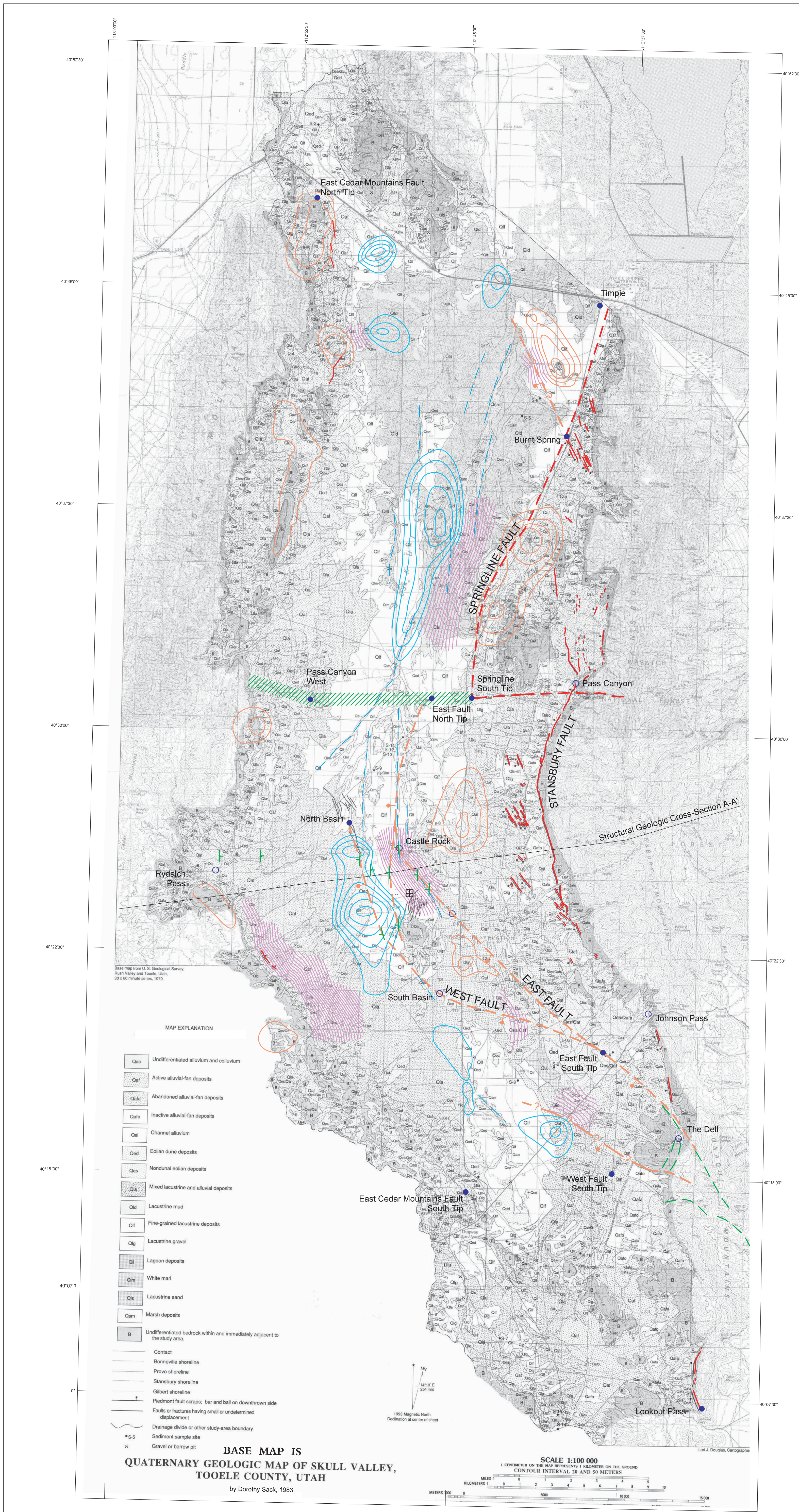
In addition to the authors, the following Geomatrix personnel participated in the study; Robert R. Youngs, John Luttinger, David Lapp, Brian Thompson, and Fred Chandler. Personnel from William Lettis & Associates provided additional support for the project. Jeff Unruh developed the regional structural cross sections and gravity modeling. Chris Hitchcock assisted in the drilling program. Richard P. Gillespie (Stone & Webster Engineering Corporation) provided logistical support and assisted in the field investigations. John C. Clark (Bay Geophysical Associates, Inc.) directed the high resolution seismic shear wave survey and provided preliminary interpretations of the survey results. Dr. Donald Currey (Limnотectonics Laboratory, University of Utah) participated in the Quaternary stratigraphic studies and provided review of the Quaternary mapping investigations. Dr. Ronald Bruhn, and Anne Mattson (Department of Geology and Geophysics, University of Utah) participated in a review

of preliminary trenching and seismic profile structural interpretations. Dr. Michael Perkins (Department of Geology and Geophysics, University of Utah) conducted tephrochronology investigations. Ronald L. Bruhn and William R. Lund provided independent technical reviews of this paper.

## REFERENCES

- Anderson, J.G., Wesnousky, S.G., and Stirling, M.W., 1996, Earthquake size as a function of fault slip rate, *Bulletin of the Seismological Society of America*, v. 86, no. 3, p 683-690.
- Barnhard, T.P., and Dodge, R.L., 1988, Map of fault scarps formed on unconsolidated sediments, Tooele 1° x 2° quadrangle, northwestern Utah: U. S. Geological Survey Miscellaneous Field Studies Map MF-1990, scale 1:250,000.
- Bay Geophysical Associates, 1999, High resolution seismic shear wave reflection profiling for the identification of faults at the Private Fuel Storage Facility Skull Valley, Utah: Report prepared for Stone & Webster Engineering Corporation, Englewood, Colorado, Bay Geophysical Project No. 98-024.
- Civilian Radioactive Waste Management System Management and Operating Contractor (CRWMS M&O), 1998, Probabilistic seismic hazard analyses for fault displacement and vibratory ground motion at Yucca Mountain, Nevada: U.S. Department of Energy DE-AC04-94AL85000, Prepared for the U.S. Geological Survey, February 23.
- Cook, K.L., Bankey, V., Mabey, D.R., and DePangher, M., 1989, Complete Bouguer gravity anomaly map of Utah: Utah Geological and Mineral Survey Map 122, scale 1:500,000.
- Everitt, B.L., and Kaliser, B.N., 1980, Geology for assessment of seismic risk in the Tooele and Rush Valleys, Tooele County, Utah: Utah Geological Survey Special Studies 51, 33 p.
- Geomatrix Consultants, Inc., 1999, Fault evaluation study and seismic hazard assessment, Private Fuel Storage Facility, Skull Valley, Utah: San Francisco, California, prepared for Stone and Webster Engineering Corporation, Project No. 4790, 118 p.
- Hecker, S., 1993, Quaternary tectonics of Utah with emphasis on earthquake-hazard characterization: Utah Geological Survey Bulletin 127, 157 p., 2 plates.
- Helm, J.M., 1995, Quaternary faulting in the Stansbury fault zone, Tooele County, Utah, *in* Lund, W.R., (ed.), *Environmental and Engineering Geology of the Wasatch Front Region: Utah Geological Association Publication 24*, p. 31-44.
- Hood, J.W., and Waddell, K.M., 1968, Hydrologic reconnaissance of Skull Valley, Tooele County, Utah: Utah Department of Natural Resources, Technical Publication No. 18, 57 p.
- Light, A., and Kaufman, D., 1997, Amino acid paleotemperature reconstruction and radiocarbon shoreline chronology of the Lake Bonneville Basin, USA: *Geological Society of America Abstracts with Programs*, v. 29, no. 6, p. A-253.
- Mason, D.B., 1996, Earthquake magnitude potential of the Intermountain seismic belt, USA, from surface-parameter scaling of late Quaternary faults: *Bulletin of the Seismological Society of America*, v. 86, p. 1487-1506.
- Maurer, R.E., 1970, Geology of the Cedar Mountains, Tooele County, Utah: Ph.D. dissertation, University of Utah, Salt Lake City, 184 p., plus maps.
- Moore, W.J., and Sorenson, M.L., 1979, Geologic map of the Tooele 1; by 2; Quadrangle, Utah: U.S. Geological

- Survey Miscellaneous Investigations Series Map I-1132, scale 1:100,000.
- PBO Steering Committee to the National Science Foundation, 1999, The Plate Boundary Observatory, Creating a four-dimensional image of the deformation of Western North America, white paper based on input from the PBO Workshop held October 3-5, 1999:  
<http://www.ciw.edu/PBO/PBOWhitepaper.pdf>.
- Rigby, J.K., 1958, Geology of the Stansbury Mountains, Toole County, Utah, *in* Guidebook to the Geology of Utah: Utah Geological Society, no. 13, 175 p.
- Sack, D., 1993, Quaternary geologic map of Skull Valley, Tooele County, Utah: Utah Geological Survey Map 150, Scale 1:100,000.
- Shackleton, N.J., and Opdyke, N.D., 1973, Oxygen isotope and paleomagnetic stratigraphy of equatorial Pacific core V28-238—Oxygen isotope temperatures and ice volumes on a  $10^5$  year and  $10^6$  year scale: *Quaternary Research*, v. 3, p. 39-55.
- Smith, R.B., Richins, W.D., and Doser, D.I., 1985, The 1983 Borah Peak, Idaho earthquake - regional seismicity, kinematics of faulting, and tectonic mechanism: *Proceedings of Workshop XXVIII on the Borah Peak, Idaho, Earthquake*, v. A, U.S. Geological Survey Open-File Report 85-290, p. 236-263.
- Thatcher, W., Foulger, G. R., Julian, B. R., Svarc, J., Quilty, E., and Bawden, G. W., 1999, Present-day deformation across the Basin and Range province, Western United States: *Science*, v. 283, p. 1714-1718.
- Wells, D.W., and Coppersmith, K.J., 1994, New empirical relationships among magnitude, rupture length, rupture width, rupture area, and surface displacement, *Bulletin of the Seismological Society of America*, v. 84, p. 974-1000.

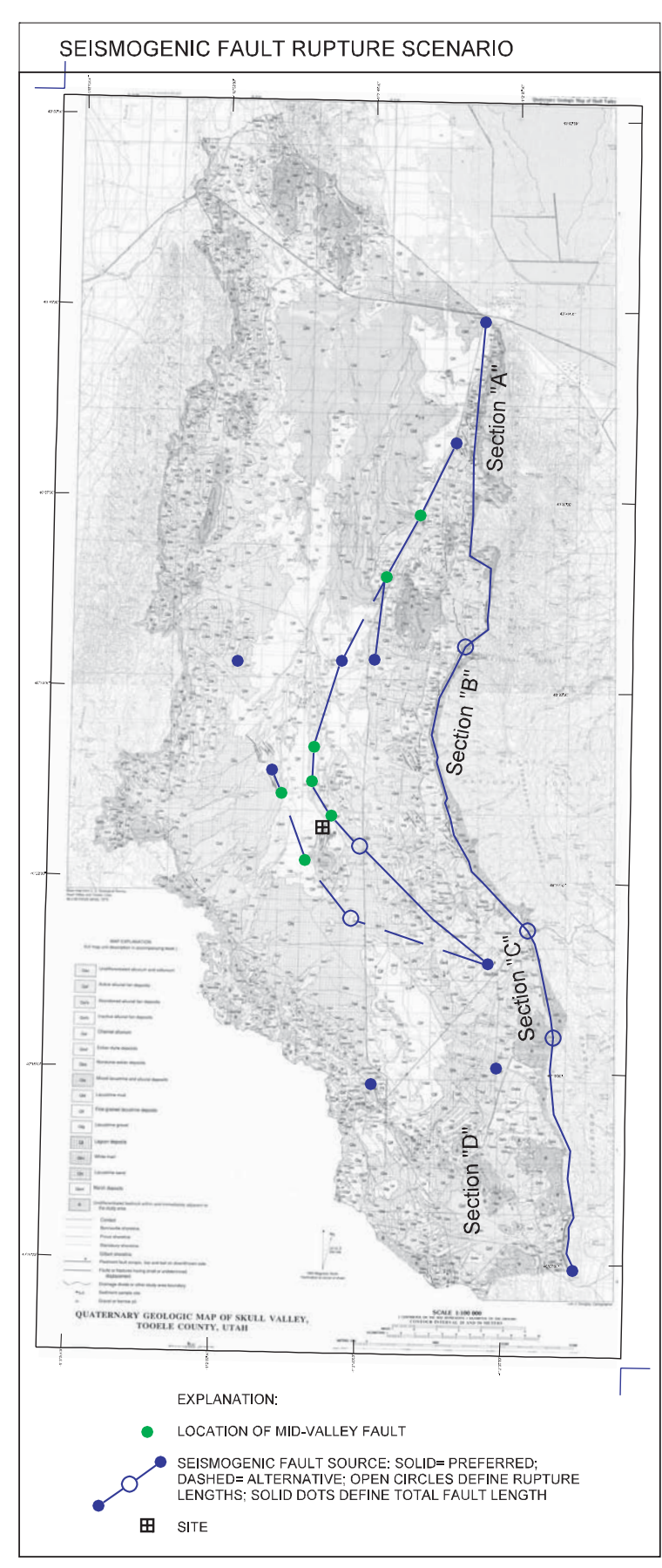
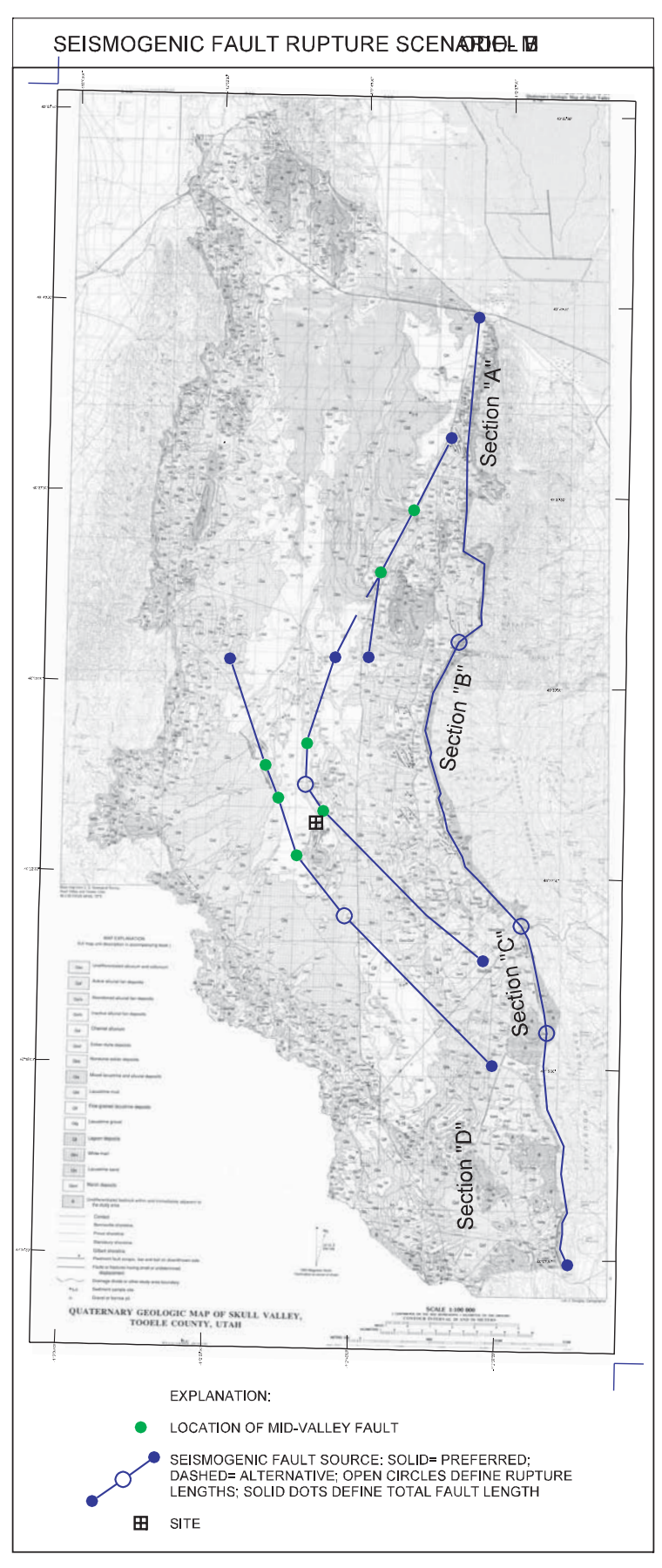


**MAP EXPLANATION**

- Qac Undifferentiated alluvium and colluvium
- Qaf Active alluvial-fan deposits
- Qais Abandoned alluvial-fan deposits
- Qafo Inactive alluvial-fan deposits
- Qal Channel alluvium
- Qed Eolian dune deposits
- Qes Nondunal eolian deposits
- Qla Mixed lacustrine and alluvial deposits
- Qld Lacustrine mud
- Qlg Lacustrine gravel
- Qli Lagoon deposits
- Qlm White marl
- Qls Lacustrine sand
- Qsm Marsh deposits
- B Undifferentiated bedrock within and immediately adjacent to the study area.
- Contact
- Bonneville shoreline
- Provo shoreline
- Stansbury shoreline
- Gilbert shoreline
- Piedmont fault scarp; bar and ball on downthrown side
- Faults or fractures having small or undetermined displacement
- Drainage divide or other study-area boundary
- Sediment sample site
- Gravel or borrow pit

**BASE MAP IS  
QUATERNARY GEOLOGIC MAP OF SKULL VALLEY,  
TOOELE COUNTY, UTAH**  
by Dorothy Sack, 1983

**SCALE 1:100,000**  
1 CENTIMETER ON THE MAP REPRESENTS 1 KILOMETER ON THE GROUND  
CONTOUR INTERVAL 20 AND 50 METERS



- EXPLANATION:**
- QUATERNARY FAULT BASED ON PREVIOUS GEOLOGIC MAPPING; DASHED WHERE INFERRED
  - QUATERNARY FAULT BASED ON INTERPRETATIONS MADE DURING THIS STUDY; QUERIED WHERE UNCERTAIN
  - LOCATION OF BEDROCK FAULT PICK FROM SEISMIC REFLECTION AND/OR GEOLOGIC DATA
  - BEDROCK FAULT BASED ON PREVIOUS GEOLOGIC MAPPING
  - PASS CANYON STRUCTURE: EXTENSION TO WEST FROM PASS CANYON FAULT (HELM, 1995) BASED ON GRAVITY DATA
  - LINEAR DRAINAGE
  - ANOMALOUS GRAVITY HIGH
  - ANOMALOUS GRAVITY LOW
  - GRAVITY GRADIENT EXCEEDS 0.01 mgals
  - LOCATION OF FAULT SOURCE SEGMENT BOUNDARY (DEFINES RUPTURE LENGTH)
  - LOCATION OF FAULT SOURCE (TOTAL FAULT LENGTH)

**PLATE 1  
FAULT SEGMENTATION MODELS – SKULL VALLEY, UTAH**

*F. H. Swan and others: Paleoseismic Investigations of the Stansbury and Mid-Valley Faults, Skull Valley, Utah Basin and Range Province Seismic Hazards Summit II, 2004*

# ***CHALLENGES IN DETERMINING EARTHQUAKE HAZARDS FROM ACTIVE FAULTS IN THE BASIN AND RANGE PROVINCE***

D. Burton Slemmons, Professor Emeritus, Center for Neotectonic Studies, University of Nevada, Reno, NV 89557 (P.O. Box 81050, Las Vegas, NV 89180), bslemmons@aol.com

Craig M. dePolo, Nevada Bureau of Mines and Geology, University of Nevada, Reno, NV 89557, cdepolo@unr.edu

## **ABSTRACT**

At least 25 historical surface-faulting earthquakes occurred in the Basin and Range Province, the Mojave Desert, and the Southern Basin and Range regions between 1868 and 1999. These earthquakes provide the paleoseismologic basis for evaluation of earthquake hazards in the province, but show a complexity that needs to be resolved for making hazard analyses. Complications and challenges for making earthquake hazard studies are discussed in this paper.

## **INTRODUCTION**

Recent paleoseismologic studies in Utah, southern Nevada, and Arizona show that determination of seismic sources and earthquake hazards in the complex Basin and Range Province (BRP) is challenging (Hecker, 1993; Slemmons, 1995). There are hundreds to thousands of Quaternary faults in the BRP, and most lack adequate paleoseismologic studies. Faults commonly have distributed patterns, indistinct end points, and moderate to low slip rates that may change with time, and may be buried by young basin fill. Moreover, from earthquake to earthquake, different sets of faults in a zone may rupture, and each individual fault strand has a rupture history that is different from nearby faults in the zone. This makes the definition of potential earthquake rupture parameters and fault segmentation difficult to predict and analyze (dePolo and others, 1989; dePolo and others, 1991; Slemmons, 1995) and make it important to have analyses by experts using recent paleoseismologic principles and methods (McCalpin, 1996; Yeats and others, 1997).

The western part of the BRP is influenced by right-lateral deformation along the Pacific-North American Plate boundary and the Eastern California shear zone that branches from the boundary and extends northeastward into the BRP with ~25 percent (12 mm/yr) of the total plate boundary motion, which is unevenly distributed across the province. The Walker Lane belt (~8 mm/yr) at the western edge of the BRP accommodates most of this deformation with right-lateral faults, and subordinate normal-slip faults. The less active (~3mm/yr total), eastern two-thirds of the BRP exhibits mostly normal faulting. The historical record of large earthquakes and surface faulting in the BRP (Table 1) shows that although there is a higher rate (3 of 8 surface-faulting earthquakes) of seismic and tectonic activity in the western part in the province (Eastern California shear zone and Walker Lane belt), over one-half the historic  $M > 7$  earthquakes (5 of 8 earthquakes) occurred in the eastern two-thirds of the province. The historical record and active fault compilations both indicate that the seismic hazard, although unevenly distributed, is pervasive near active faults in all parts of the BRP.

Recent paleoseismologic studies in Utah, southern Nevada, and Arizona show that several geological processes can mask, exaggerate, or modify interpretations of the seismic potential of many Quaternary faults (Hecker, 1993; Slemmons, 1995). In Las Vegas and Pahrump Valleys early studies attributed the complex distributed ruptures found there to aseismic compaction faulting, but recent studies in Las Vegas and Pahrump Valleys (Bell, 1981; Slemmons and others, 2001; dePolo and others, 2002) indicate that the main contribution to active fault scarps is tectonic and seismogenic, and compaction or ground water produce minor modifications. In North Las Vegas, Nevada one of the main “compaction faults” was shown in deep exploratory trenches to be a major tectonic fault that had two large faulting events since late Pleistocene, with the younger earthquake dated by  $^{14}\text{C}$  at 14,690 cal yr B.P. (dePolo and others, 2002).

## **HISTORICAL RECORD**

Surface-rupturing earthquakes during the brief BRP historical record provide a key for interpreting the much longer paleoseismologic record using regressions between earthquake magnitude, surface rupture length, and fault displacement (Wells and Coppersmith, 1994). At least 25 historical surface faulting earthquakes have occurred in the BRP, and Eastern California shear zone between about 1869 and 1999 (Table 1). These earthquakes range in magnitude from 5.6 to ~7.6. Earthquakes over magnitude 6.5 generally had primary surface fault ruptures in patterns that range from narrowly focused to widely distributed, and had endpoints that produced distinct fault discontinuities in only about half of the cases. The number of structural and/or geometric segments involved during the historical earthquakes includes both single-segment and multiple-segment ruptures (up to 5 segments). Although some large earthquakes were widely distributed, or had unusually short surface rupture lengths, maximum surface displacement is usually proportional to earthquake magnitude, and accordingly displacement is a key parameter for

earthquake size estimation. The historical earthquakes occurred in a wide variety of geologic settings, including range-front, piedmont, basin, and bedrock settings, and are in portions of the BRP that have different levels of tectonic activity. All primary surface-faulting earthquakes ruptured Quaternary faults, but nearly half of the ruptures occurred along faults with no Holocene activity, and the age of the penultimate events vary from place to place within each rupture zone. These historical earthquakes indicate that future BRP earthquakes can occur in all geologic and tectonic settings, and with a fairly large range in fault characteristics and parameters for a given magnitude. Realizing and dealing with these uncertainties is a challenge and limitation for estimating earthquake hazards in the BRP.

## **CHALLENGES IN DETERMINING EARTHQUAKE HAZARDS FROM FAULTS**

### **State-of-the-Art Factors**

These factors include unidentified earthquake faults, important faults that have not been studied or are inadequately studied, uncertainties in determining fault activity and fault rupture parameters, the limited historical earthquake and well-studied fault databases, uncertainties in fault behavior, uncertainty in direct application of geodesy to faults, uncertainty in assigning scaling parameters, and distinction of rupture modes.

### **Geologic Factors**

These factors include the large number of Quaternary faults yet to be studied, variable and wide-ranging earthquake recurrence intervals and fault slip rates, complexity of fault interactions, and indistinct fault terminations.

### **Historical Earthquake Faults**

These factors include indistinct rupture discontinuities (1932 in Table 1), multiple structural and geometric segments (1915, 1954 in Table 1),

distributed fault traces (1932 in Table 1), large events with relatively short fault lengths (1959 in Table 1), wide range in fault parameters for a given magnitude (1986 in Table 1), faults with repeated historical surface-rupture earthquakes (1903 and 1954d, 1932 and 1954d, and 1954a and 1954c in Table 1), and clustering of earthquakes in time (1954 sequence in Table 1).

### CONSIDERATIONS FOR EARTHQUAKE HAZARD STUDIES

1. Surface fault ruptures commonly are in broad zones with many distributed or triggered fault displacements several kilometers away from the main rupture (1932, 1954a, 1954c, 1954d, 1954e, 1959, 1980, 1983, 1993 in Table 1).
2. Several surface faulting ruptures activated late Quaternary to Holocene faults with different penultimate ages for various parts of the rupture zones (1954d, 1954e, 1992, 1999 in Table 1).
3. In addition to range-front faulting, surface ruptures commonly branch into or are within valleys, and less commonly rupture within horst blocks (1872, 1903, 1934, 1954d in Table 1). Faults in valley floors are in zones where alluvial processes rapidly conceal, or partly conceal, paleoseismologic evidence of ancient past earthquakes making them difficult to detect or resolve. Ruptures from at least three historical earthquakes overlap, and reactivate known zones of historical faulting (1903, 1932, 1954 in Table 1).
4. Segmentation and segmentation lengths are subjectively determined from geological or geophysical evidence. The analyses of dePolo and others (1989, 1991), and Slemmons (1995) suggest for earthquake magnitudes above 6.5 that ruptures typically break two to five segments with surface-rupture lengths from less than 10 km to more than 40 km.

5. Less than one half the larger historical earthquakes are in the comparatively high-slip Walker Lane belt. Here, the translational plate boundary influence and connection to the San Andreas fault system may cause many faults to have higher slip rates, shorter recurrence intervals, and a greater prevalence of strike-slip faulting than is typical for the BRP as a whole. The eastern and northern parts of the BRP have more than one-half the larger historical events, with widely distributed large earthquakes and surface faulting. This indicates that the seismic hazard is pervasive near active faults throughout the BRP.

### REFERENCES

- Bell, J. W., 1981, Subsidence in Las Vegas Valley: Nevada Bureau of Mines and Geology, Bulletin 95, 84 p, 1 plate, scale 1:62,500.
- dePolo, C.M., Clark, D.G. Slemmons, D. B., and Aymard, W. H., 1989, Historical Basin and Range Province surface faulting and fault segmentation, *in* Schwartz, D. P., and Sibson, R.H., editors, Fault segmentation and controls of rupture initiation and termination: U. S. Geological Survey Open-File Report 89-315, p. 131-162.
- dePolo, C.M., Clark, D.G. Slemmons D.B., and Ramelli, A. R., 1991, Historical surface faulting Basin and Range Province, western North America: implications for fault segmentation: *Journal of Structural Geology*, v. 13, p. 123-136.
- dePolo, C.M., Borron, S., Bell, J., and Slemmons D.B., 2002, Evidence for earthquakes along the Las Vegas Valley fault system [abs.]: *Geological Society of America Rocky Mountain Section, Abstracts with Programs*, v. 34, no. 4, p. 35.
- Hecker, S., 1993, Quaternary tectonics of Utah with emphasis on earthquake-hazard characterization: *Utah Geological Survey Bulletin* 127, 157 p., scale 1:500,000.

- McCalpin, J. P., 1996, *Paleoseismology*: San Diego, Academic Press, 588 p.
- Slemmons, D. B., 1995, Complications in making paleoseismic evaluations in the Basin and Range Province, western United States, *in* Serva, L., and Slemmons, D. B. editors, *Perspectives in paleoseismology: Association of Engineering Geology Special Publication 6*, p. 19-33.
- Slemmons, D.B., Bell, J.W., dePolo, C.M., Ramelli, A.R., Rasmussen, G.S., Langenheim, V.E., Jachens, R.C., Smith, K., O'Donnell, J., 2001, Earthquake hazard in Las Vegas, Nevada, *in* Luke, B., Jacobson, E., and Werle, J. editors, *Proceedings 36th Annual Symposium on Engineering Geology and Geotechnical Engineering*, March 28-30, 2001: University of Nevada, Las Vegas, p. 447-459.
- Wells, D. L., and Coppersmith, K. J., 1995, New empirical relationships among magnitude, rupture width, rupture area, and surface displacement: *Seismological Society of America Bulletin*, v. 84, p. 974-1002.
- Yeats, R.S., Sieh, K., Allen, C. R., 1997, *The Geology of Earthquakes*: New York, Oxford University Press, 568 p.

**Table 1. Historical surface faulting in the Basin and Range Province and the Eastern California shear zone (including the southern Basin and Range).**

NO	DATE	FAULT LOCATION	M <sub>w</sub>	ZONE LENGTH (km)	ZONE WIDTH (km)	MAX. DISPL (m)	AGE OF PREVIOUS ACTIVITY; NUMBER OF SEGMENTS
1	1869?	Olinghouse, NV	6.7±	~20	<1?	3.7	Holocene, 1 segment?
2	1872	Owens Valley, CA	~7.6	~108	Var. 3-16; avg. 8	RL 9, V 4.4	>8,000 yrs; 3 or 4 segments.
3	1887	Sonora, Mexico	7.3	101.4	1-3, avg. ~2	V 4.87	100 ka to 200 ka; 2-3.
4	1903?	Wonder, NV	~6.5±	11?	~1	V ~1	Late Quaternary; 1?
5	1915	Pleasant Valley, NV	7.2-7.6	>62	V <sup>2</sup> 2-5, avg. >2	V 5.8	Holocene or Late Quaternary; 4-5.
6	1932	Cedar Mountain, NV	7.1	75	3-15, avg. 8	SS <sup>4</sup> 2.7	Holocene and Late Quaternary; ~3.
7	1934	Excelsior Mountain, NV	6.3	>1.7	<1	V 0.13, LL <sup>5</sup> 0	Late Quaternary; 1.
8	1934	Hansel Valley, UT	6.6	11	~2.5	V 0.5, LL 0.2	Late Quaternary
9	1947	Manix, CA <sup>1</sup>	6.2	1.6?	?	LL 0.076	1?
10	1948	Ft. Sage Mountain, CA	5.6	~9	<1	V 0.6	Holocene; 1.
11	1954a	Rainbow Mountain, NV	~6.5	18	12	V 0.7, RL~1.0	Holocene; 1?
12	1954b	Fourmile Flat, NV	6.4	~6	~1	~1.5	Late Holocene; 1.
13	1954c	Stillwater, NV	6.8-7.0	31-	>3, avg. 2	V 0.8	2?
14	1954d	Fairview Peak, NV	7.2	46	<13-19	4.8	Late Quaternary (>35 ky); 3-4+.
15	1954e	Dixie Valley, NV	~7.0	42	5	3.8	Variable, Holocene and Late Quaternary; 2.
16	1959	Hebgen Lake, MT	7.3	26.5	15	6.1	Holocene; 2-3.
17	1975	Galway Lake, CA <sup>1</sup>	5.2	6.8		0.015	Holocene; 1.
18	1979	Homestead Valley, CA <sup>1</sup>	5.2	3.25		RL 0.1, V 0.04	Holocene and Late Quaternary; 1.
19	1980	Mammoth, CA	6.0-6.5	20	V 0.3,	?	Triggered? Larger Holocene event.
20	1983	Borah Peak, ID	6.9	34	1-7, avg. 2	2.7	Holocene, and Late Quaternary; 2-3.
21	1986	Chalfant Valley, CA	6.2	13-15.5	RL <sup>3</sup> 7-11	V 0.05	Holocene; triggered slip?
22	1993	Eureka Valley, CA	5.8	>4	?	0.02	Triggered slip?
23	1992	Landers, CA <sup>1</sup>	7.3	~80	RL ~6, avg. 5	~6.7	Holocene and Late Quaternary; 3-4.
24	1994	Double Springs Flat, NV	5.8	~6.5	2	~0.1?	Holocene and Late Quaternary; triggered slip.
25	1999	Hector Mine, CA <sup>1</sup>	7.1	41	1	RL 5.2	Late Quaternary (and older?)

<sup>1</sup>Faulting event is within the Eastern California shear zone in the Mojave Desert. <sup>2</sup>Vertical. <sup>3</sup>Right lateral. <sup>4</sup>Strike slip. <sup>5</sup>Left lateral.

***SEPARATION AND IDENTIFICATION OF CHARCOAL AND  
ORGANICS FROM BULK SEDIMENT SAMPLES FOR  
IMPROVED RADIOCARBON DATING AND STRATIGRAPHIC  
CORRELATIONS***

Kathryn Puseman  
and  
Linda Scott Cummings

Paleo Research Institute  
2675 Youngfield Street  
Golden, CO 80401  
[pri2004@comcast.net](mailto:pri2004@comcast.net)

**ABSTRACT**

One of the standard tools used in paleoflood studies, paleoseismology, paleoclimatology, and archaeology is radiocarbon dating. Often, bulk sediment samples are submitted for dating; however, bulk sediment has the potential for containing large amounts of modern carbon and/or reworked older carbon. Using a flotation process commonly employed for separating charcoal and other macrofloral remains in archaeological samples, bulk sediment samples can be floated and examined to recover and separate charcoal and other charred organic remains suitable for radiocarbon dating. Identification of charcoal or other carbon prior to radiocarbon dating provides an opportunity to date specific materials, resulting in more accurate dates, while concomitantly providing paleoenvironmental data. Occasionally deposits are noted that must be identified, such as those representing a cienega, marsh, or bosque, because they represent specific environments or depositional conditions that can facilitate correlation across the fault zone. Pollen analysis adds another dimension in the identification of these deposits.

**INTRODUCTION**

Although archaeologists and other researchers commonly use bulk sediment samples for radiocarbon dating, such samples are very low in the "recommended sample material for radiocarbon dating" order (Taylor, 1987). It is preferential to submit a specific type of material for

radiocarbon dating whenever possible (i.e. charcoal, other charred organic material, bone, shell, etc.), rather than a bulk sediment sample.

Not only is it important to recover a specific type of material for dating, it is important to identify the material being dated. The separation and identification process must be performed under strict

conditions of cleanliness to prevent contamination. Identification of charcoal and other charred plant material prior to radiocarbon dating provides the opportunity to choose the material that will yield the best age possible. Identification of material is a recommended pretreatment strategy (Taylor, 1987). Paleoenvironmental interpretations also can be made using the identified charcoal and other charred plant material. Pollen analysis of bulk sediments can yield even greater paleoenvironmental data.

## **DISCUSSION**

Bulk sediment samples are commonly used for radiocarbon dating in several areas of research including paleoflood studies, paleoseismology, paleoclimatology, archaeology, and others. There are several reasons why bulk samples are used. Often, no apparent charcoal or other charred organic material is observed. A bulk sediment sample charged at a conventional radiocarbon rate is less expensive than an Accelerator Mass Spectrometry (AMS) date on a small amount of charred material. Some researchers are concerned about turn around time and believe it will take a long time to send the soil sample in to have specific material separated and identified for dating. Others are unaware of possible alternatives.

However, several problems exist in using bulk sediment for radiocarbon dating (Matthews 1980). These include uncertainties surrounding the time between the formation of the material being analyzed and the point at which it was deposited, determining the exact relationship between the datable material and the stratigraphy

from which it was recovered, and post-depositional contamination.

Taylor (1987:62) notes that "radiocarbon activity of soil organic fractions is extremely variable and the usefulness of using such values to infer age ... is generally quite limited except under special conditions." Some researchers believe that using bulk samples collected from buried soils that are beyond the range of bioturbation limits the input of organic material and restrict the potential for contamination. However, unless deposition was very rapid, these sediments were within the range of bioturbation at some time in the past, meaning that they may well be bioturbated.

Bulk sediment samples are not recommended for radiocarbon dating because a sample may incorporate either old or modern carbon depending on environmental conditions, the type of material, and the degree to which the sample is closed to contamination. Older material can be eroded, reworked, and incorporated into younger deposits. Sediments also receive continual input of new carbon (Hsieh 1992, 1993; Birkeland 1999). Younger material is commonly introduced through bioturbation such as insect, earthworm, or burrowing animal activity. Seeds, leaves, and grasses often are carried into the subsurface for food and bedding. Burrowing creatures also may introduce fecal material into the sediment.

To illustrate that a bulk sediment sample often consists of a variety of materials, a bulk sample collected during a paleoflood study from a stream terrace along Lost Creek in northeast Utah was submitted to a "bucket float" process used to examine archaeological macrofloral samples

(Puseman 1997). The floated sample was examined to determine the material present after removing the sediment smaller than 0.25 mm in size. From the original 2.3 L of sediment present, a light fraction weighing 24.52 g was recovered. Of this amount, less than gram was charcoal or other charred plant material (Table 1). The sample contained charred and uncharred seeds, numerous uncharred rootlets from modern plants, four identified charcoal types, a piece of animal tooth, a few uncharred bone fragments, insect chitin fragments, mollusk and snail shells, and sclerotia. Sclerotia are the resting structures of mycorrhizae fungi, such as *Cenococcum graniforme*, that have a mutualistic relationship with tree roots. They are found with a variety of coniferous and deciduous trees including *Abies* (fir), *Juniperus communis* (common juniper), *Larix* (larch), *Picea* (spruce), *Pinus* (pine), *Pseudotsuga* (Douglas fir), *Acer pseudoplatanus* (sycamore maple), *Alnus* (alder), *Betula* (birch), *Carpinus caroliniana* (American hornbeam), *Carya* (hickory), *Castanea dentata* (American chestnut), *Corylus* (hazelnut), *Crataegus monogyna* (hawthorn), *Fagus* (beech), *Populus* (poplar, cottonwood, aspen), *Quercus* (oak), *Rhamnus fragula* (alder bush), *Salix* (willow), and *Tilia* (linden) (McWeeney 1989:229-130; Trappe 1962).

Because the organic matter in sediments is a mixture of materials of different ages and because the proportions of old and modern carbon incorporated into subsurface deposits are unknown, radiocarbon ages obtained from bulk sediment samples represent a composite age for all of the organics in the sample. Depending on the number of factors that

control the accumulation and decay of organic matter in a given deposit, the proportions of young to old carbon can be highly variable and result in large uncertainties in the measured ages. Because of these large uncertainties, bulk ages are questionable at best and may not accurately represent the true age of a deposit. Contamination of a bulk sample with younger carbon has a greater effect on the resulting age than does contamination with older carbon (Polach and others, 1981, Rosholt and others, 1991). Studies by Andrews and Miller (1980) demonstrate that addition of only 5 percent modern carbon into a sample can give a true age of 20,000 years an apparent age of 16,500 years, and give a true age of 5,000 years an apparent age of 4,650 years. When 20 percent modern carbon is introduced, a true age of 10,000 years gives an apparent age of about 7,000 years (Figure 1).

### **Sample Processing Method**

Bulk sediment samples submitted to Paleo Research Institute for separation and identification of charcoal or other charred organic material prior to radiocarbon dating are processed by a “bucket float” method used to examine archaeological macrofloral samples, with a few adjustments. Each sample is measured and added one liter at a time to approximately 10 liters of water. The sample is stirred to create a vortex, which helps the charcoal and other organic material float to the surface of the water. The sample is poured through a 150 micron mesh sieve, and floating material (“light fraction”) is collected in the sieve. Additional water is added and the process

Table 1. Contents of a bulk sediment sample from along Lost Creek, Utah (Puseman 1997)

Sample No.	Identification	Part	Charred		Uncharred		Weights/ Comments
			W	F	W	F	
LC1-3-4	Liters Floated						2.30 L
86-97 cmbs	Light Fraction Weight						24.52 g
	FLORAL REMAINS:						
	Poaceae (Grass family)	Caryopsis	2				
	<i>Rosa</i> (Wild rose)	Seed	5	2			
	Fruity tissue			1			
	Unidentified	Seed	2				
	<i>Chenopodium</i> (Goosefoot)	Seed			3	6	
	<i>Taraxacum</i> (Dandelion)	Seed			2		
	Modern rootlets					X	Numerous
	Sclerotia				X		Few
	CHARCOAL/WOOD:						
	<i>Alnus</i> (Alder)	Charcoal		19			0.13 g
	<i>Artemisia</i> (Sagebrush)	Charcoal		1			0.01 g
	<i>Rosa</i> (Wild rose)	Charcoal		4			0.02 g
	<i>Salix</i> (Willow)	Charcoal		11			0.07 g
	Unidentified $\geq 2$ mm	Charcoal		X			0.13 g
	NON-FLORAL REMAINS:						
	Animal tooth enamel					1	
	Bone					6	
	Insect chitin					13	
Mollusk shell $\geq 1$ mm				1	116	0.24 g	
Rock/Gravel					X	Present	

W = Whole

F = Fragment

X = Presence noted in sample

g = grams

cmbs = centimeters below ground surface

mm = millimeters

L = Liter

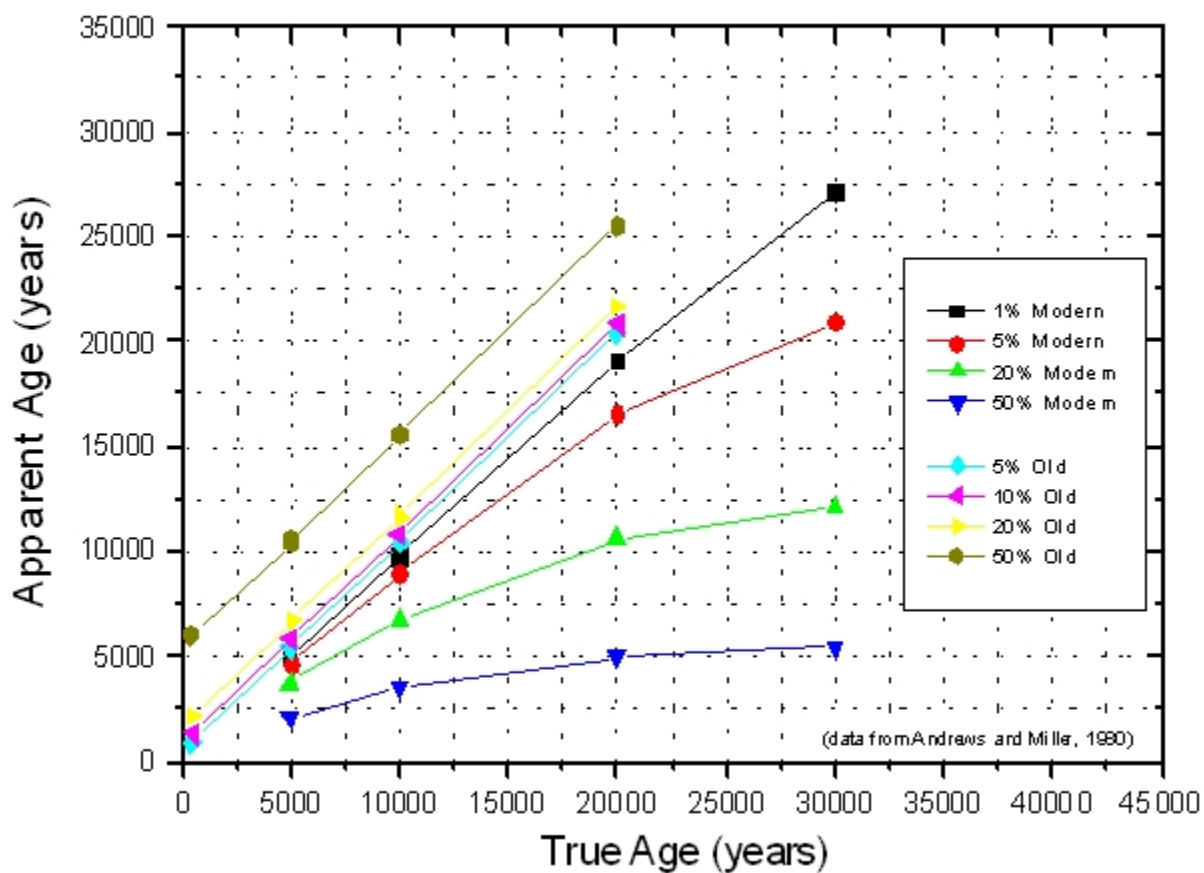


Figure 1. Effect of carbon contamination on radiocarbon ages.

repeated until all floating material is removed from the sample (a minimum of 5 times). The light fraction is dried on plastic wrap. The material that remains in the bottom the bucket (heavy fraction) consists of rock/gravel, shell, and bone. This material is separated using a 0.5 mm mesh screen. The material remaining in the 0.5 mm screen is dried on newspaper.

The dried light and heavy fractions are poured through a series of graduated screens (U S Standard Sieves with 2 mm, 1 mm, 0.5 mm, and 0.25 mm openings) to separate the material into different size fractions for easier viewing through a microscope. The material from each screen size is examined under a binocular microscope at a magnification of 10x. Charcoal and other charred organic remains are separated. Most charcoal and some seeds are identified at a magnification of 70x. Charcoal and other material also can be examined at magnifications of up to 800x.

### **Determining the Best Material for Dating**

Charcoal and charred organic material are the most reliable types of material for radiocarbon dating. Charcoal fragments exhibiting sharp, straight edges and “normal” charcoal characteristics are preferentially pulled for radiocarbon dating. These charcoal fragments are identified to family or genus, the number of fragments and weights of each type are recorded, and the individual types are bagged separately. The minimum requirement of charcoal for standard AMS radiocarbon dating reported by Beta Analytic, Inc., is about 3 mg or 0.003 g, so that at least 300 micrograms of final carbon is available for dating. The

“Micro-Sample AMS Counting Service” is now available for samples containing only 100-300 micrograms of final carbon; therefore, it is now possible to date charcoal weighing only 1 mg or 0.001 g.

Smoothed, rounded edges indicate that charcoal was transported prior to deposition and therefore is not the best charcoal for dating the deposit. Vitrified charcoal exhibits a shiny, glassy appearance due to fusion by heat. It is possible that vitrified charcoal reflects wood that burned when it was fresh and green and had a higher moisture content. Vitrified pieces of charcoal are usually not identifiable to genus or species; however, accurate radiocarbon ages have been obtained by researchers submitting this type of charcoal for dating (Ralph Klinger, personal communication, June 28, 2004). These charcoal types also are separated, weighed, and packaged individually; however, they are labeled as exhibiting “rounded edges” or “vitrified.”

Other charred organic remains, such as charred seeds, fruits or monocot stem fragments, also can be dated. Monocots include grasses, sedges, and members of the lily family such as yucca. These remains are pulled from the sample, identified, weighed, and bagged separately.

When an insufficient amount of charcoal or charred organic material is available for dating, bone and mollusk shell also have been used.

The identification of specific carbon-bearing materials is particularly advantageous, and allows the researcher to know precisely what material to submit for radiocarbon dating. Charcoal and other charred plant remains that have been specifically identified can help resolve issues concerning stratigraphic relations

between the sample and the stratum from which it was collected. For example, in fluvial deposits, the identification of local riparian flora versus distant or exotic species can be particularly helpful in interpreting the depositional context. More accurate ages also can be obtained by submitting only specific types of charcoal or other charred plant material for dating. It is preferential to date a local species rather than a foreign one, to date a single species rather than a mixture of several types, and to date the plant type with the shortest life span, such as dating charcoal from a shorter-lived shrub rather than a longer-lived tree. Taylor (1987:41) notes that "whenever possible, the proper scientific nomenclature for species of plant and animal sample material should be obtained even if the fragmentary nature of the sample permits only genus or even family level designations."

### **Paleoenvironmental Research Questions**

Identification of charcoal and other charred organic material prior to submission for radiocarbon dating also can provide paleoenvironmental data and/or information concerning use of individual plants. Assuming that subsurface disturbance is not too great, charred organic material from non-cultural deposits most likely represents plants growing in the area that were burned in a past fire.

Paleoenvironmental questions sometimes are more completely answered by pollen analysis of the bulk sediment. One such example involved a bulk sediment sample from a suspected cienega or marsh deposit from a paleoseismic trench across the East Franklin Mountains Fault in El

Paso, Texas. The carbonate-rich sediment comprising this deposit yielded a conventional radiocarbon date of  $29,520 \pm 260$  yr B.P. The researcher was hoping to find macro or micro remains that would confirm a cienega or marsh origin of the deposit. The macrofloral record consisted only of a few uncharred rootlets from modern plants. Pollen analysis was recommended for the soil sample. The pollen record from the deposit revealed a very different vegetation community from the sparse cactus cover currently noted in the area. Further, it suggested more of a bosque plant community, rather than a cienega. Bosque communities are typically dense stands of mesquite and acacia with oaks well-represented in the higher elevations. High frequencies of *Acacia* (acacia), *Prosopis* (mesquite), and *Quercus* (oak) pollen (Figure 2) indicate growth of these trees. The presence of Lamiaceae (mint family) and *Typha* (cattail) pollen indicate that not only was subsurface water available, but that there was open water or perennially marshy conditions in the area. *Larrea* (creosote bush) pollen also was present. Creosote pollen is produced in very small quantities and does not travel far, indicating that the creosote bushes grew nearby. This collection of pollen types suggests that the area supported a narrow band of riparian plants, probably along a slow moving stream. The types of vegetation changed spatially very rapidly from the riparian plants immediately adjacent to the stream, through the oak and mesquite bosque, to a creosote desert scrub community (Varney, 2004).

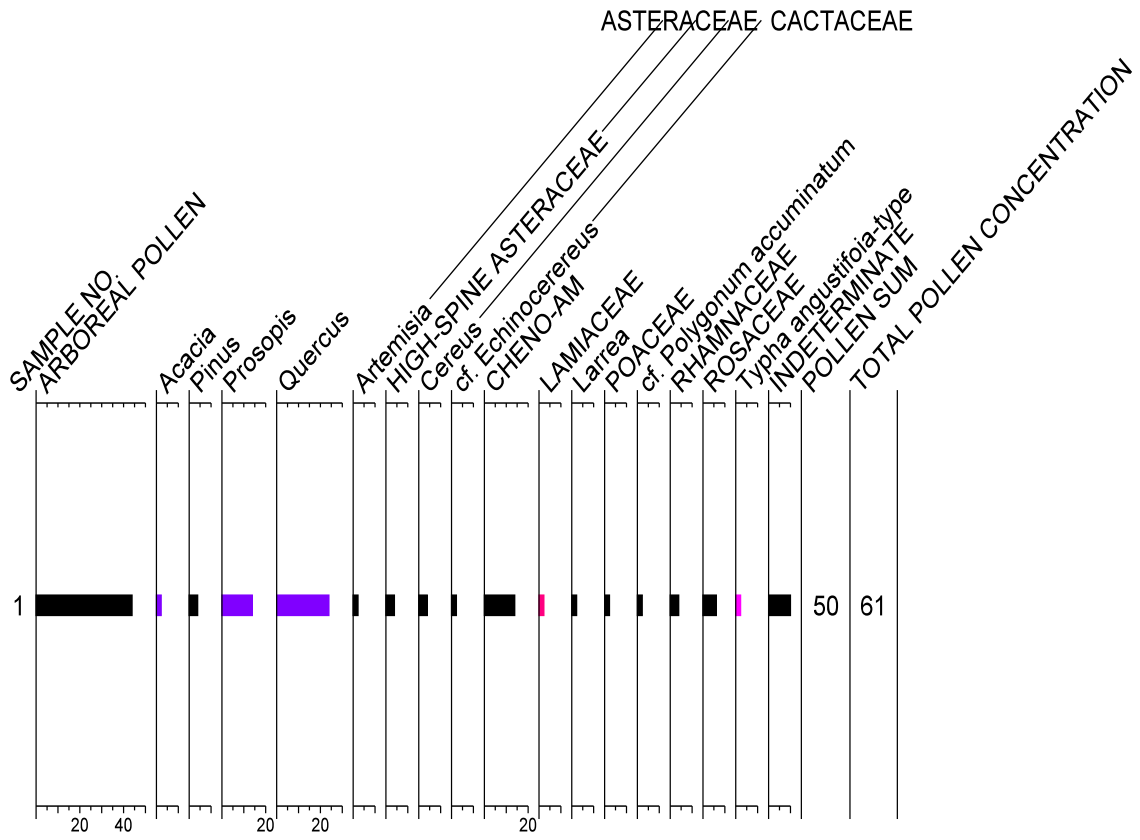


Figure 2. Pollen diagram for the East Franklin Mountains Fault

## SUMMARY

When submitting material for radiocarbon dating, it is best to submit identified material, especially charcoal and other charred organic material, rather than bulk sediment samples whenever possible. Bulk sediment samples can contain reworked older material and/or introduced younger material; therefore, ages derived from bulk sediment samples might not accurately characterize the true age of the deposit. Wood charcoal and charred organic material are believed to be the most reliable types of samples for radiocarbon dating. The material to be dated should be identified prior to radiocarbon dating to determine the best material for dating. Prior identification also can provide information concerning plants present in the past environment. When paleoenvironmental issues are a main concern, pollen analysis provides more comprehensive paleoenvironmental data.

## ACKNOWLEDGMENTS

The authors would like to thank Ralph Klinger at the Bureau of Reclamation in Denver, Colorado, for providing technical advice, access to articles, and Figure 1, and to both Larry Anderson and Ralph Klinger for their review of this manuscript.

## REFERENCES

- Andrews, J. T. and G. H. Miller, 1980, Dating Quaternary deposits more than 10,000 years old. Chapter 18 in *Timescales in Geomorphology*, edited by R. A. Cullingford, D. A. Davidson, and J. Lewin. John Wiley & Sons, Ltd.
- Birkeland, P. W., 1999, *Soils and Geomorphology*. Oxford University Press, New York.
- Hsieh, Y. P., 1992, Pool size and mean age of stable soils organic carbon in cropland. *Soil Science Society of America Journal* 56:460-464.
- 1993, Radiocarbon signatures of turnover rates in active soil organic carbon pools. *Soil Science Society of America Journal* 57:1020-1022.
- Matthews, J. A., 1980, Some problems and implication of  $^{14}\text{C}$  dates from a podzol buried beneath an end moraine at Haugabreen, southern Norway. *Geografiska Annaler* 62A:185-208.
- McWeeney, Lucinda, 1989, What lies lurking below the soil: Beyond the archaeobotanical view of flotation samples. *North American Archaeologist* 10(3):227-230.
- Polach, H., J. Golson, and J. Head, 1981, Radiocarbon Dating: A guide for archaeologists on the collection and submission of samples and age-reporting practices. In *Australian Field Archaeology: A Guide to Techniques*. Australian Institute of Aboriginal Studies, Canberra, Australia, p. 145-152.

- Puseman, Kathryn, 1997, Examination of bulk sediment and detrital charcoal from along Lost Creek, northeast Utah. Ms. on file with the U.S. Bureau of Reclamation, Denver Federal Center, Denver, Colorado.
- Rosholt, J. N., S. M. Colman, M. Stuiver, P. E. Damon, C. W. Naeser, N. D. Naeser, B. J. Szabo, D. J. Muhs, J. C. Liddicoat, S. L. Forman, M. N. Machette, and K. L. Pierce, 1991, Dating methods applicable to the Quaternary. In *Dating Methods Applicable to the Quaternary*, edited by R. B. Morrison, pp. 45-74. The Geology of North America, vol. K-2, Geological Society of America, Boulder, Colorado.
- Taylor, R. E., 1987, *Radiocarbon Dating, An Archaeological Perspective*. Academic Press, Inc., Orlando.
- Trappe, James M., 1962, Fungus associates of ectotrophic mycorrhizae. In *The Botanical Review*. U.S. Department of Agriculture, Washington, D.C.
- Trumbore, Susan E, 2000, Radiocarbon Geochronology. In *Quaternary Geochronology Methods and Applications*, edited by J. S. Noller, J. M. Sowers, and W. R. Lettis, pp. 41-60. AGU Reference Shelf 4, American Geophysical Union, Washington, D.C.
- Varney, R. A., 2004, Pollen and macrofossil analysis of sediments from a buried paleosol associated with the East Franklin Mountain fault, west Texas. Ms. on file with GEO-HAZ Consulting, Inc., Crestone, Colorado.

Peer Reviewers:

Larry W. Anderson  
Geologist  
U.S. Bureau of Reclamation  
Box 25007, D-8330, Federal Center  
Building 67, Room 1080  
Denver, CO 80225-0007  
303-445-3170

Ralph E. Klinger, Ph.D.  
Geomorphologist  
U.S. Bureau of Reclamation  
P.O. Box 25007, D-8530  
Denver, CO 80225-0007  
303-445-3173

## ***CHALLENGES IN ASSESSING SEISMIC HAZARD ACROSS THE INTERMOUNTAIN WEST***

Mark D. Petersen, Arthur D. Frankel, Chris H. Cramer, Stephen C. Harmsen,  
Kathleen Haller, and Harley M. Benz

U.S. Geological Survey  
Denver Federal Center, MS 966, Box 25046  
Denver, CO 80225

### **ABSTRACT**

We present the 2002 National Seismic Hazard map and discuss four challenges for future updates of the map. These challenges include:

1. Developing better ground-motion prediction models specific for the Intermountain West
2. Collecting and interpreting additional geological and geophysical information to produce better source models
3. Conducting tests and modeling uncertainties of the hazard maps
4. Communicating the seismic hazard information more effectively to the end-user communities.

### **INTRODUCTION**

In 2002 the U.S. Geological Survey released updated U.S. National Seismic Hazard Maps that incorporate new ground shaking information, updated fault parameters, and alternative source models (Figure 1, see <http://eqhazmaps.usgs.gov/>, Frankel et al., 2002). These maps are currently being implemented in national building codes, insurance rate structures, and public-policy decisions. The models and parameters used to develop the maps for the Intermountain West were discussed at science and user workshops in Salt Lake City, Utah. In addition, the hazard maps and fault parameters were reviewed by several state geological surveys, a technical review committee, and other interested scientists and engineers. Implementation of the review and workshop comments resulted in a significant reduction in the level of seismic hazard across the Intermountain West; the 2002 probabilistic ground motions are generally 10% to 15% lower than the 1996 hazard estimates for the risk levels applied to the building codes (2% probability of exceedance in 50 years).

This decrease was primarily caused by recent modifications to ground-motion-prediction equations. In future updates of the U.S. National Seismic Hazard Maps and construction of complementary urban hazard maps, we must improve our understanding of these general ground-shaking characteristics and, in particular, how shallow soils and basin structure amplify or de-amplify ground shaking. In addition to ground-motion studies, we need to better define seismic sources and shallow soil properties, to assess uncertainties in the hazard maps, and to improve our communication of earthquake hazard and risk to non-engineers.

The internal and external components of the USGS National Earthquake Hazards Reduction Program (NEHRP) collect geologic and geophysical information across the Intermountain West that are needed for developing the U.S. National Seismic Hazard Maps and for developing other hazard products that communicate hazard to end-user communities. The USGS

**Peak Acceleration (%g) with 2% Probability of Exceedance in 50 Years  
USGS Map, Oct. 2002rev**

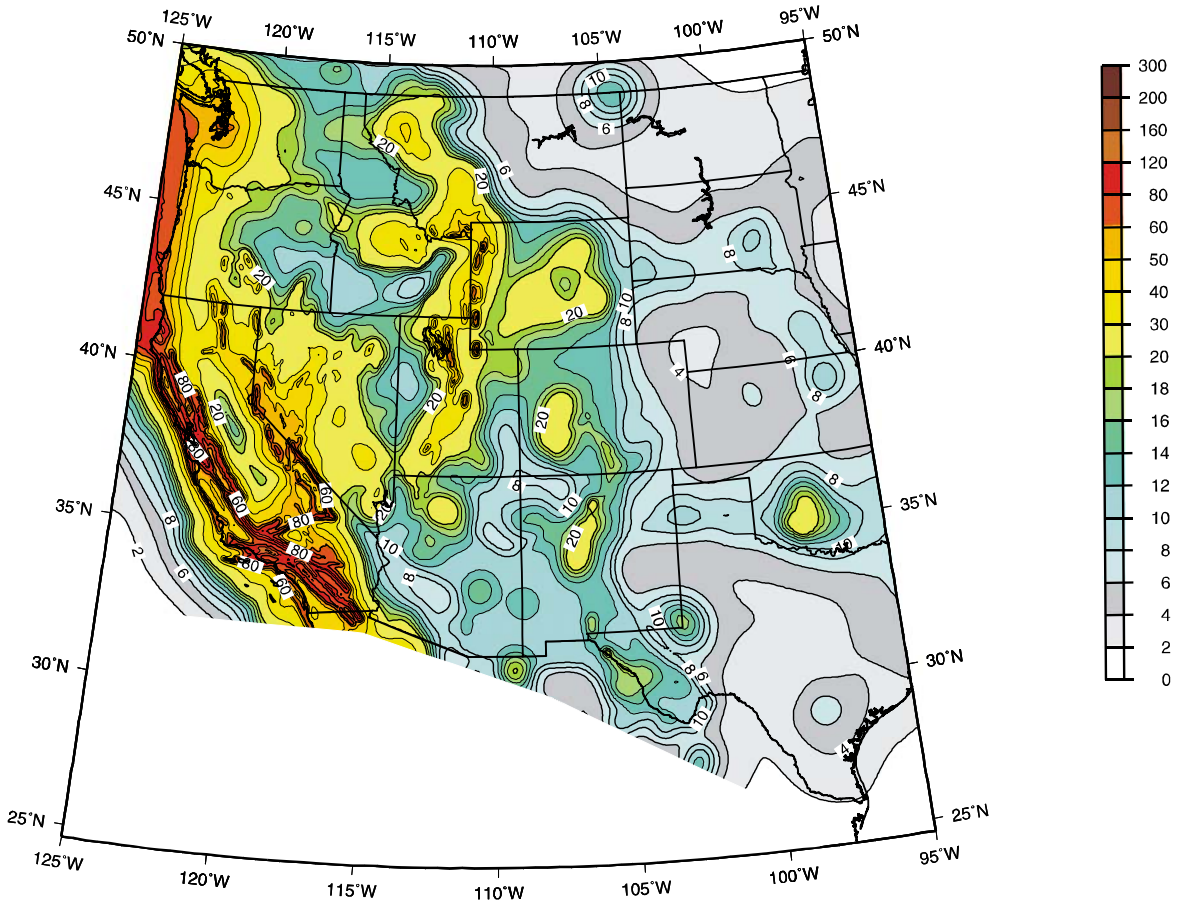


Figure 1. 2002 hazard map for the western U.S. for peak horizontal acceleration on firm rock site condition for risk level used in building codes (2% probability of exceedance in 50 years).

collects earthquake data (Advanced National Seismic System - ANSS) and develops maps of ground shaking (SHAKEMAP) in near real time, collects strain data using GPS technology, acquires shear-wave velocity data using reflection and refraction techniques for shallow sediments, and explores the prehistoric recurrence intervals of earthquakes through paleoseismic studies. These studies are closely coordinated with state and local geological surveys, and depend on external investigations by government, academia, and consultants.

In this paper, we will discuss four specific challenges in updating the U.S. National Seismic Hazard Maps. Improving our understanding of the uncertainties and parametric sensitivity in earthquake ground-shaking hazard will also guide the science community in delineating future research directions that may have important public-policy implications.

## CHALLENGES

### **Challenge 1: Need for better estimates of ground shaking in the Intermountain West region**

Probably the largest uncertainty in regional hazard estimates pertains to characterization of ground shaking. We need to develop better ground motion prediction equations that include estimates of uncertainty in ground shaking for different sizes of earthquakes and soil characteristics. The USGS has funded several internal and external projects to study these attenuation relations and the site response in the Intermountain West. In addition, we are coordinating with the Pacific Engineering Research Center to develop the next generation of attenuation relations. These relations are primarily being developed using California data, but they may also be useful in predicting ground shaking for normal faults commonly observed in the Intermountain West. In the future, we hope to develop attenuation relations that are specific for the earthquake ruptures and geologic characteristics inherent to the Intermountain West.

Once we develop regional information on soils and basin structure, we can construct urban hazard maps that are useful for regional risk assessments. The USGS is cooperating with the Utah Geological Survey to build a “*community soil velocity model*” that will archive all soil velocity data from the Salt Lake Valley. This basin model will enable development of 3-D synthetic simulations of strong ground shaking. These urban hazard maps and associated ground motion simulations will be helpful for engineering projects and urban planning. We eventually hope to develop urban hazard maps for several populated high-risk areas across the Intermountain West region.

Few moderate to large Intermountain West earthquakes have been recorded and, therefore, uncertainties associated with ground shaking in the region are high. However, we can collect seismic information that will help reduce these uncertainties in the future. We can deploy instruments to record future large earthquakes, and we can record and analyze smaller earthquakes scattered across the region. These smaller earthquake records may be used to extrapolate ground motions for large earthquakes. For example, the Advanced National Seismic System (ANSS) stations are currently recording the shaking from many small earthquakes across the Intermountain West (Figure 2). These shaking records contain information specific to the Intermountain West regarding stress drops, frequency dependent Q attenuation properties, basin structure, and crustal properties. In addition, these records provide information about ground motions from normal-fault earthquakes that are not as well understood as ground motions for earthquakes with other fault mechanisms. The ANSS data will be a critical component of the information used to develop future relations that will predict earthquake ground shaking distributions for the Intermountain West.

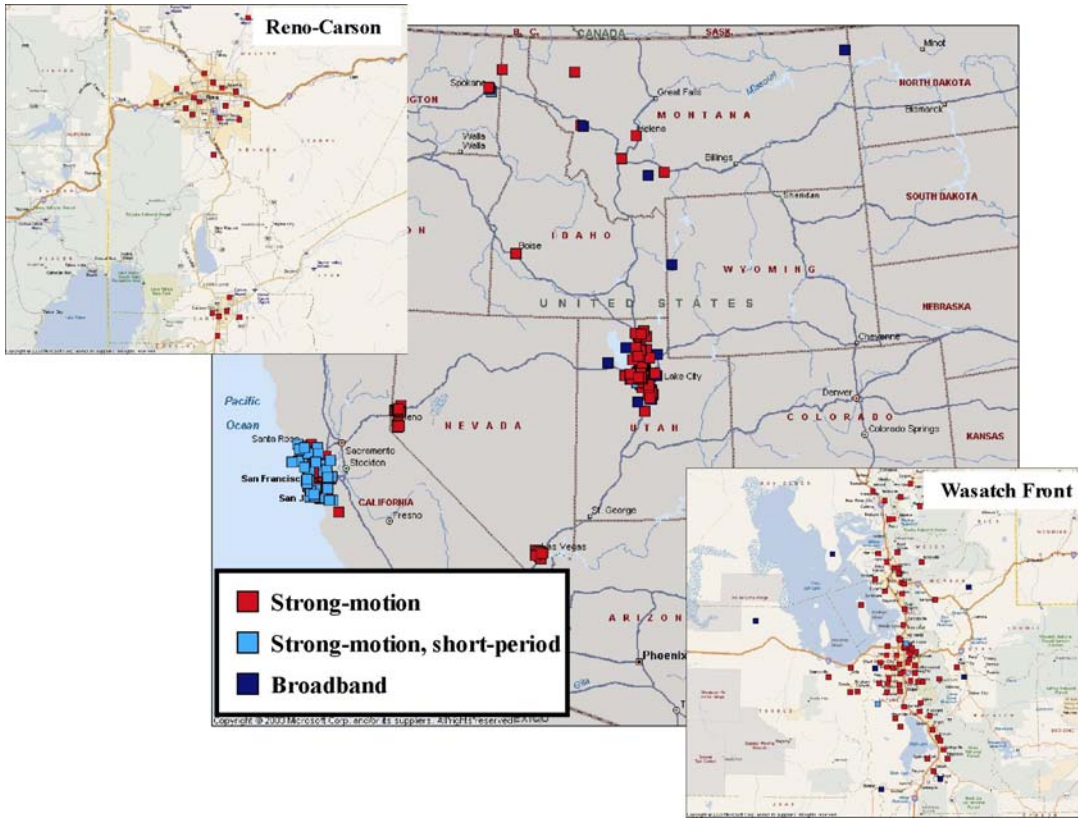


Figure 2. Advanced National Seismic System seismic station distribution across the Intermountain West region.

## **Challenge 2: Need for more geologic and geophysical data to define earthquake source parameters and recurrence models.**

Over the next few years the USGS plans to establish working groups in the Intermountain West that will be tasked with developing input information for urban and regional hazard maps, constructing community velocity models, acquiring geotechnical information relevant to liquefaction- and landslide-hazard mapping, interpreting ground-motion data for improvement of current attenuation relations, and considering newly published fault information. For example, the Utah Geological Survey and USGS established three topical working groups including a Utah Quaternary Fault Working Group that reviews information related to mean fault slip rates, paleoseismic recurrence intervals, and the uncertainties associated with each of these parameters (Lund, this volume). This working group has been very successful in interpreting the published data, recommending research priorities, and establishing consensus within the community for the parameters used in developing the National Seismic Hazard Maps.

The working groups will provide advice to the USGS on geological and seismological issues related to the National Seismic Hazard Maps. For example, during the development of the 2002 maps an issue arose pertaining to the recurrence of moderate to large size earthquakes on the Wasatch fault. The USGS developed several scenarios that incorporated different ratios of Gutenberg-Richter and characteristic distributed earthquakes (Figure 3). The Utah Geological Survey and academic institutions in the State of Utah discussed these issues with the USGS and submitted a recommendation that was implemented in the hazard maps. Another example of how these working groups can assist in the National map development is in providing advice on recurrence intervals for large earthquakes. Chang and Smith (2002) examined the combined effect of different large earthquake

sources along the Wasatch fault using paleoseismic data from the Wasatch fault. Modeling various multi-segment ruptures along a fault involves correlations of many paleoseismic studies, and is best coordinated through a working group. In addition, Figure 4 shows the correlation of the paleoseismical recurrence intervals and the calculated recurrence intervals for large earthquakes across the Intermountain West. The observed paleoseismic recurrence intervals are based on dating of offset soil horizons observed in trenches, while the calculated recurrence intervals are based on an expected characteristic magnitude and measured long-term slip rate. The correlation between these data sets is quite high, but the calculated rates are generally biased toward shorter recurrence intervals than the recurrence periods observed from trench data. In the future these working groups, made up of experts on Utah fault paleoseismology, can provide technical recommendations on how to assess these recurrence intervals and multiple-segment ruptures when considering disparate sources of information.

## **Challenge 3: Need to test models and model uncertainties in hazard estimates**

Testing is an important component in developing any public-policy model with financial and social application. However, testing of the National Seismic Hazard Maps is difficult because they are defined by low return periods (e.g., 2500 years) that will not be testable for millennia. Tests that we can perform directly use the 100 to 150 year record of historical earthquakes and their effects within the Intermountain West. For example, we can compare the rate of earthquakes in the National Seismic Hazard Model with the rate of earthquakes observed during the past century. Another test is to compare the intensities observed from historic earthquakes with the ground motions predicted in the National Seismic Hazard Maps for short return periods.

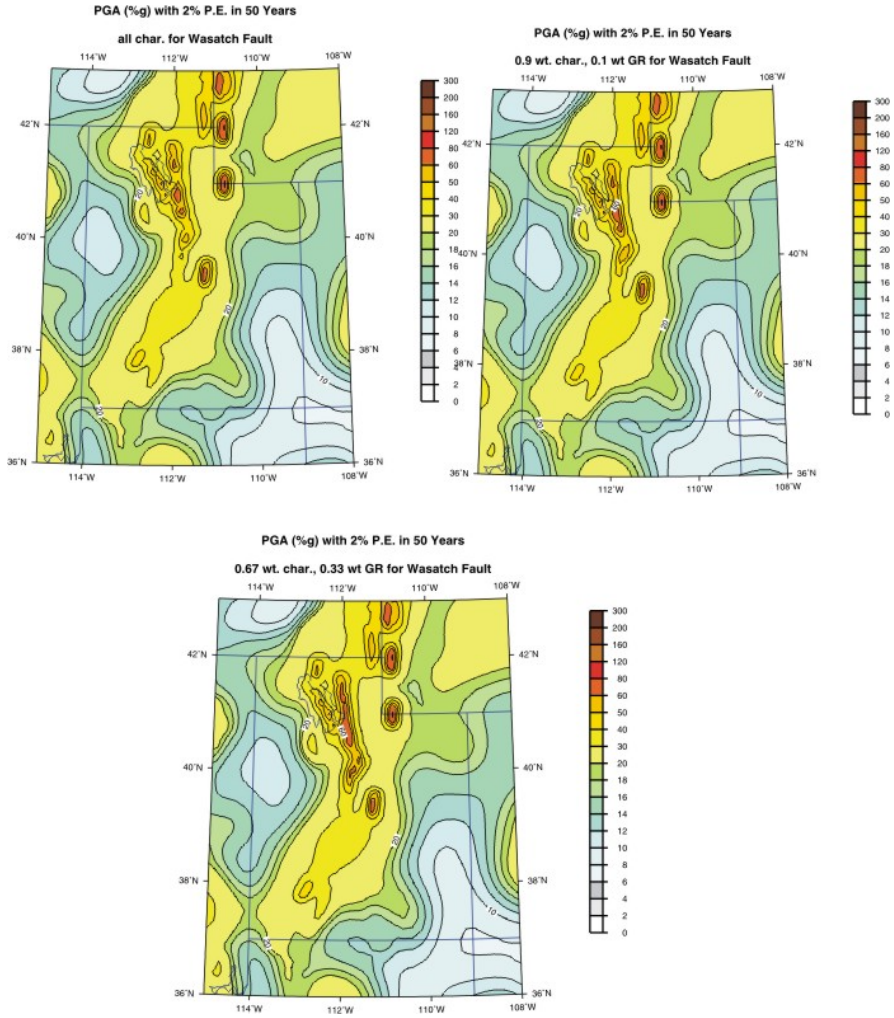


Figure 3. Comparison of hazard for different ratios of characteristic and Gutenberg Richter distributed earthquakes along the Wasatch fault.

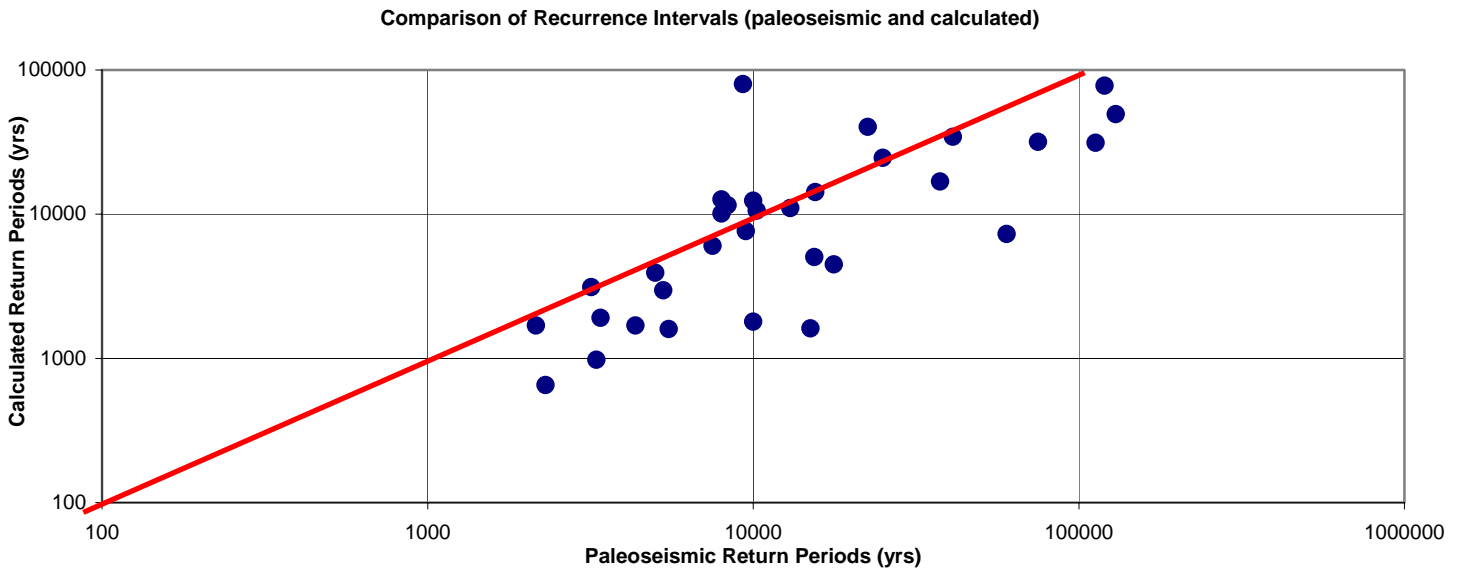


Figure 4. Comparison of paleoseismic and calculated return periods for large earthquakes in the Intermountain West region

The USGS is commencing work to develop both of these types of tests for this region.

The National Seismic Hazard Maps are based on parameters that have high associated uncertainties, making it difficult for geologists or seismologists to specify earthquake parameters with a single value. Therefore, it is more useful when these scientists develop probability density functions that describe the variability in these input parameters. The inputs can be then be varied in the hazard calculations to study the uncertainty and sensitivity in the hazard and risk estimates. Uncertainty studies focus on how much the hazard estimates vary whereas the sensitivity studies focus on quantifying how much the input parameters contribute to the hazard. Figure 5 shows a preliminary uncertainty map for the Salt Lake Valley that was prepared using data from the Utah Fault Working Group. The uncertainty measure used in the map is the coefficient of variation (defined as the sample standard deviation divided by the sample mean). The uncertainties for ground shaking along the Wasatch fault are lower than for many other nearby faults, generally lower than 0.4. This relatively low uncertainty results from the many paleoseismic studies that have constrained recurrence rates along this fault. In contrast, the Eastern Great Salt Lake Valley Fault has slip rates and corresponding recurrence rates with high uncertainties. The COV's associated with ground shaking are generally greater than 0.6 near these faults. Improving our understanding of the slip rates for faults in the Salt Lake Valley could directly improve the hazard estimates used in the building codes and our confidence in those estimates. Uncertainty analyses indicate which faults and functions are most important to study for reducing the hazard uncertainties across the region.

#### **Challenge 4: Need to communicate with engineers and other decision makers**

The U.S. National Seismic Hazard Mapping Project has established an effective line of

communication with the building code communities through the Building Seismic Safety Council. Building code development groups have applied the USGS National Seismic Hazard Maps to building codes in 1997 (Federal Emergency Management Agency, 1998) and 2000 (International Code Council, Inc., 2000). Earth-scientists now provide engineers with technical information that will be used for designing buildings capable of withstanding future earthquake shaking.

The hazard maps are not easy to understand, so an important challenge is to find ways to communicate more effectively with both engineering and non-engineering communities so that this important information is correctly transmitted to decision makers. The USGS is currently developing maps and other products that display different representations of the seismic hazard across a region that, hopefully, will communicate this information better to the non-engineering community. One example of this type of product, is a map that shows the probability of having one or more earthquakes within a 50 km distance during a 50-year interval using the USGS source model. Figure 6 shows an 80% chance of having one or more earthquakes between magnitude 5 and 6, and a 40% chance of having one or more earthquakes greater than magnitude 6 earthquakes during any 50-year period within 50 km of Reno, Nevada. These probabilities are high, and earthquake probability maps may be easier to interpret for some users than the ground-motion probability representations currently defined for design. We have also begun to develop maps that show the expected intensities (damage states) and the intensities that have a 10% probability of being exceeded in a 50-year period. Intensity is a parameter that is more easily understood by public-policy decision makers.

Another product that is useful for the insurance industry and potentially for other decision makers as well, is a time-dependent map of earthquake hazard that considers the timing of the last earthquake and the interactions

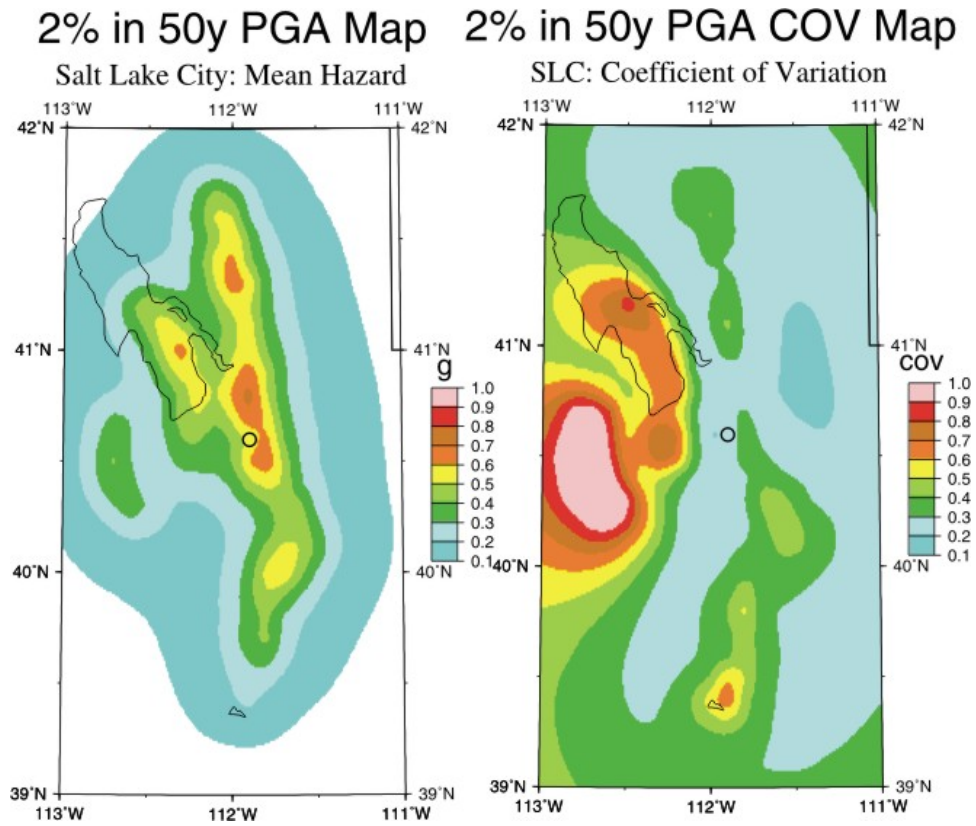


Figure 5. Seismic hazard and related Monte Carlo uncertainty maps for the Salt Lake Valley for a risk level of 2 % probability of exceedance in 50 years.

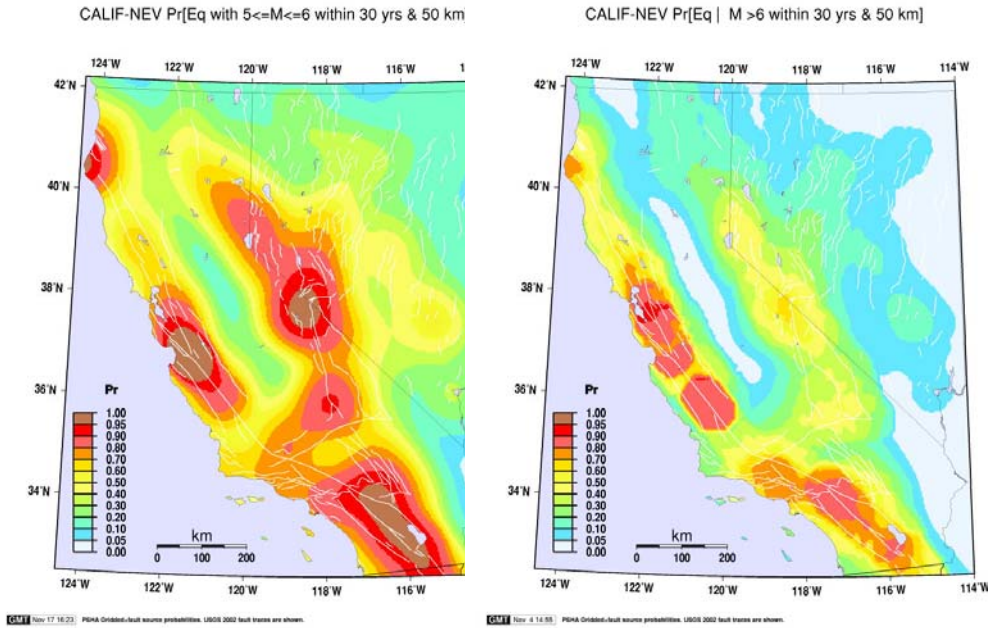


Figure 6. Probability maps for the 2002 hazard model showing probability of having earthquake between ( $M5$  to  $6$  and  $M >6$ ) for California and Nevada.

	Med. Rec.	Elapsed time	50-year prob
Brigham City:	1230	2175	8%
Weber:	1674	1066	3%
Salt Lake:	1367	1280	6%
Provo:	2413	668	0.1%
Nephi:	2706	1198	0.8%

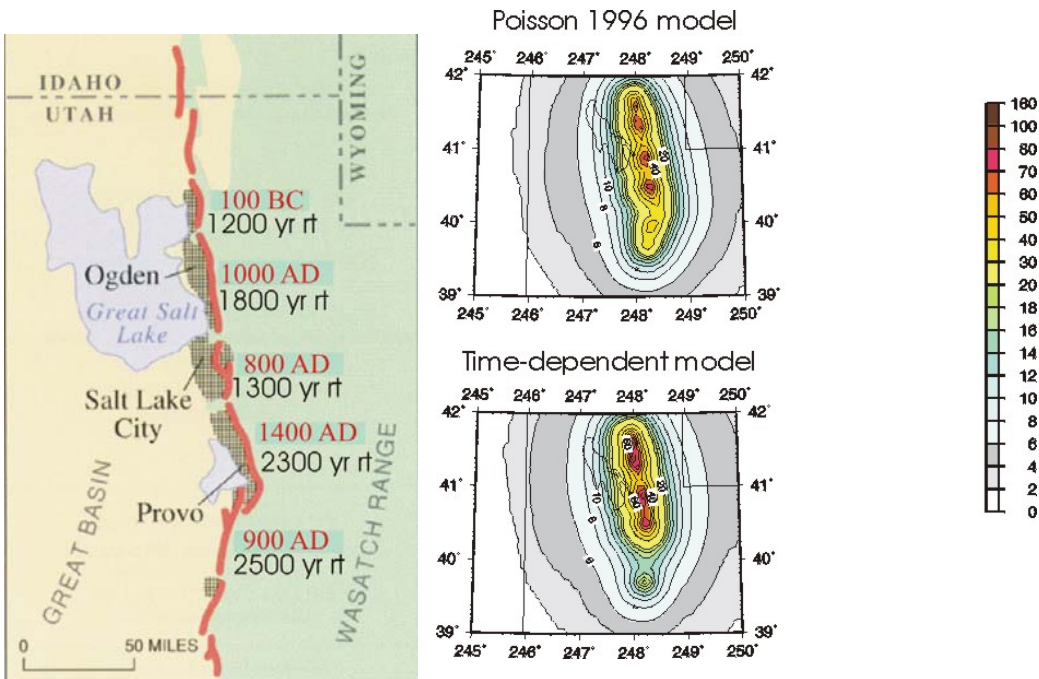


Figure 7. Comparison of time-dependent and time-independent (Poisson) hazard for the Wasatch fault. The numbers in the fault map are generalized. Poisson and time-dependent models are based on 1996 USGS National Seismic Hazard Maps.

of fault segments. Geologists and seismologists are currently collecting data and constructing fault rupture models that are essential for calculating these hazard estimates. This information can drive the hazard either up or down compared to time-independent hazard estimates depending on the recurrence interval and the time since the last earthquake. For example, Figure 7 shows estimated recurrence intervals and the time since the last earthquake along segments of the Wasatch fault. In order to calculate a time-dependent uncertainty we use mean recurrence intervals and the timing of the last earthquake defined by McCalpin and Nishenko (1996) and apply other parameters that describe the shape of the distribution from the Working Group on California Earthquake Probabilities (2003). The time-dependent hazard model is higher near the northern segments of the Wasatch fault by as much as 50%, but is lower near the southern segments compared with a time-independent (Poisson) model (Figure 7). This is because the elapsed time since the last earthquake along the Salt Lake and Brigham City segments of the Wasatch fault is quite long compared to the average earthquake recurrence interval whereas the time since the last earthquake on the Provo and Nephi segments of the fault is relatively short compared to the average recurrence time on those fault segments. These time-dependent maps may be important for some users of the hazard information, in particular if the science community agrees that the earthquake has not occurred for a significant amount of time. The USGS is beginning to develop these types of maps to communicate with some decision makers. However, we must continue to think of new ways and products to communicate this hazard information to all potential users of the data.

## CONCLUSIONS

The USGS has worked in cooperation with other federal agencies, state and local

governments, academia, and the consulting industry to update the hazard maps for the Intermountain West. For future updates of the hazard models it is critical that we maintain these partnerships and reach out to the broader user communities, both engineering and non-engineering, to communicate this information more effectively. Directed and collaborative research on issues of ground shaking, earthquake sources, and hazard uncertainty characterization will help us develop a stronger foundation for the National Seismic Hazard Maps.

## REFERENCES

- Chang, W. and Smith, R.B., 2002, Integrated seismic-hazard analysis of the Wasatch Front, Utah, *Bulletin of the Seismological Society of America* **92**, p. 1904-1922.
- Federal Emergency Management Agency, 1998, NEHRP recommended provisions for seismic regulations for new buildings and other structures 1997 Edition, Part 1- Provisions: FEMA **302** February 1998.
- Frankel, A.D., Petersen, M.D., Mueller, C.S., Haller, K.M., Wheeler, R.L., Leyendecker, E.V., Wesson, R.L., Harmsen, S.C., Cramer, C.H., Perkins, D.M., Rukstales, K.S., 2002, Documentation for the 2002 update of the National Seismic Hazard Maps: U. S. Geological Survey Open-File Report **02-420**.
- International Code Council, Inc., 2000, International Building Code and International Residential Code, published March 2000 by the International Conference of Building Officials (ICBO).
- McCalpin, J.P., and Nishenko, S.P., 1996, Holocene paleoseismicity, temporal clustering, and probabilities of future large ( $M > 7$ ) earthquakes on the Wasatch fault

zone, Utah: *Journal of Geophysical Research*  
**101**, p. 6233-6253.

Working Group on California Earthquake  
Probabilities, 2003, Earthquake probabilities  
in the San Francisco Bay Region: 2002-2031:  
U.S. Geological Survey Open-File Report  
**03-214**.

### **ACKNOWLEDGMENTS**

We would like to thank David Perkins and Charles Mueller for helpful reviews. We also appreciate the editing advice provided by William Lund and Cheryl Gustin.

## ***Determination of Low-Strain Site-Amplification Factors in the Salt Lake Valley, Utah, Using ANSS Data***

Kris L. Pankow and James C. Pechmann, University of Utah Seismograph Stations,  
135 South 1460 East, Room 705 WBB, Salt Lake City, UT 84112-0111  
([pankow@seis.utah.edu](mailto:pankow@seis.utah.edu) and [pechmann@seis.utah.edu](mailto:pechmann@seis.utah.edu))

### **ABSTRACT**

Using data from the Advanced National Seismic System network in and near the Salt Lake Valley (SLV), Utah, we measured average, frequency-dependent, low-strain site-amplification factors for site-response units mapped by others on the basis of geology and near-surface shear-wave velocity. The site-amplification factors were determined using distance-corrected spectral ratios between horizontal-component ground-motion recordings from soil sites and reference rock sites. To test various models for the distance correction terms, we measured spectral ratios between recordings at 12 Paleozoic rock sites. These spectral ratios indicate that the ground motions decrease with hypocentral distance,  $r$ , at rates of  $r^{-1.5}$  in the period range 0.4 to 2.0 sec and  $r^{-2.0}$  in the period range 0.1 to 0.5 sec. We calculated the soil/rock spectral ratios using two different reference stations on Paleozoic rock. Geometric mean site-amplification terms for three SLV site response units were obtained by combining data from both reference stations. Comparing the resultant site-amplification factors to those of previous studies indicates that empirically based predictions better fit the observed data. Specifically, the empirically based site-amplification factors of Borchardt (1994) and Boore and others (1997) fit the data better than the theoretically based factors of Wong and others (2002a, b), even though the latter were developed specifically for the SLV site-response units.

### **INTRODUCTION**

It has long been recognized that ground motions in sedimentary basins can be greatly affected by soil properties and by the 2- and 3-D basin structure (e.g., Anderson and others, 1986; Singh and others, 1988; U.S. Geological Survey Staff, 1990; Kramer, 1996; Davis and others, 2000; Field and others, 2000; Joyner, 2000). Thus, in characterizing and preparing for earthquake ground shaking in sedimentary basins, an understanding of these properties is a prerequisite. In this paper, we analyze data from the Advanced National Seismic System (ANSS; U. S. Geological Survey, 1999) network in and near the sedimentary basin of the Salt Lake Valley (SLV), Utah, to determine average levels of ground-motion amplification on previously mapped soil site-response units in the basin relative to nearby Paleozoic bedrock sites (Figures 1 and 2).

Earthquake hazards in the SLV are a serious

concern because the valley is a major urban center with a population of approximately 900,000 people (40% of the population of Utah). The most obvious source of seismic hazard is the Salt Lake City segment of the Wasatch fault, a major normal fault that separates the Salt Lake Basin from the Wasatch Range to the east (Machette and others, 1991). Paleoseismological studies of the Salt Lake City segment show that large,  $M \sim 7$ , surface-faulting earthquakes have occurred on average once every  $1,350 \pm 200$  yrs during the past 6,000 yrs, with the last one occurring  $1,230 \pm 60$  yrs ago (Black and others, 1995; McCalpin and Nishenko, 1996; McCalpin and Nelson, 2000). Based on this information, McCalpin and Nelson (2000) have estimated the probability of such an event occurring during the next 100 years to be about 16%, and Wong and others (2002a) have estimated the probability during the next 50 years to be 6% to 9%. Other active faults located in and near the SLV also

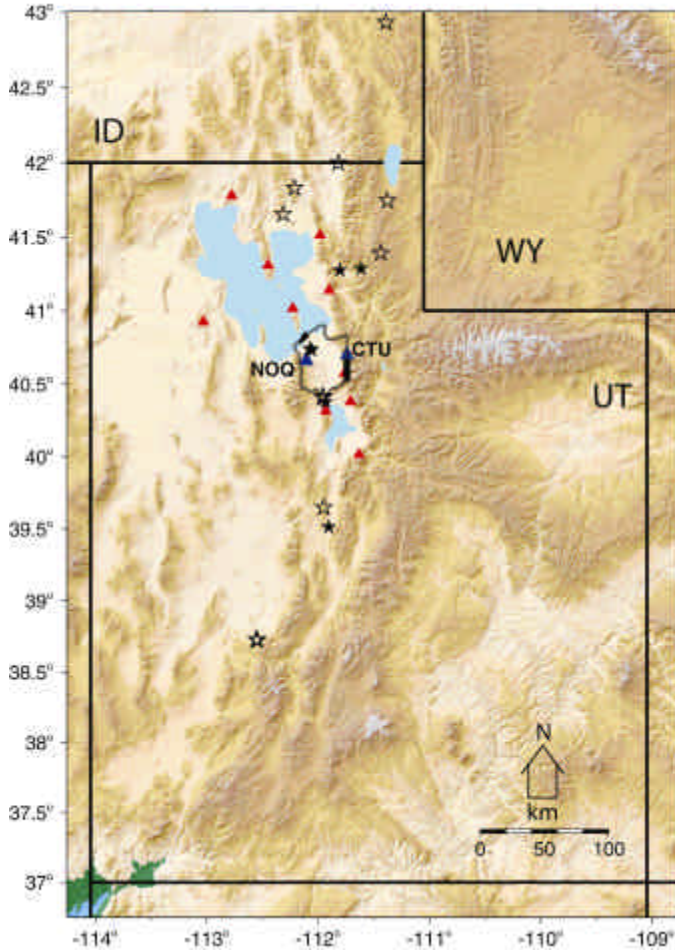


**Figure 1.** Map of Utah and the surrounding region showing broadband and strong-motion stations on Paleozoic rock, which we used to test the distance corrections (triangles), the two reference rock stations used to calculate the site-amplification factors (blue triangles), earthquakes used for testing the distance corrections (stars), and earthquakes used to calculate the site-amplification factors (solid stars). The gray polygon outlines the region shown in Figure 2.

pose a significant seismic hazard (Arabasz and others, 1992; Wong and others, 2002a).

Ground-motion amplification in sedimentary basins is commonly characterized by site-amplification factors, which are multiplicative corrections for the effects of “near-surface” materials on ground motions. Site-amplification factors are used extensively in probabilistic and deterministic seismic-hazard analyses and for creating near-real-time maps of ground shaking (ShakeMaps). Site-amplification factors currently used in ground-motion studies are typically functions of both frequency and average shear-wave

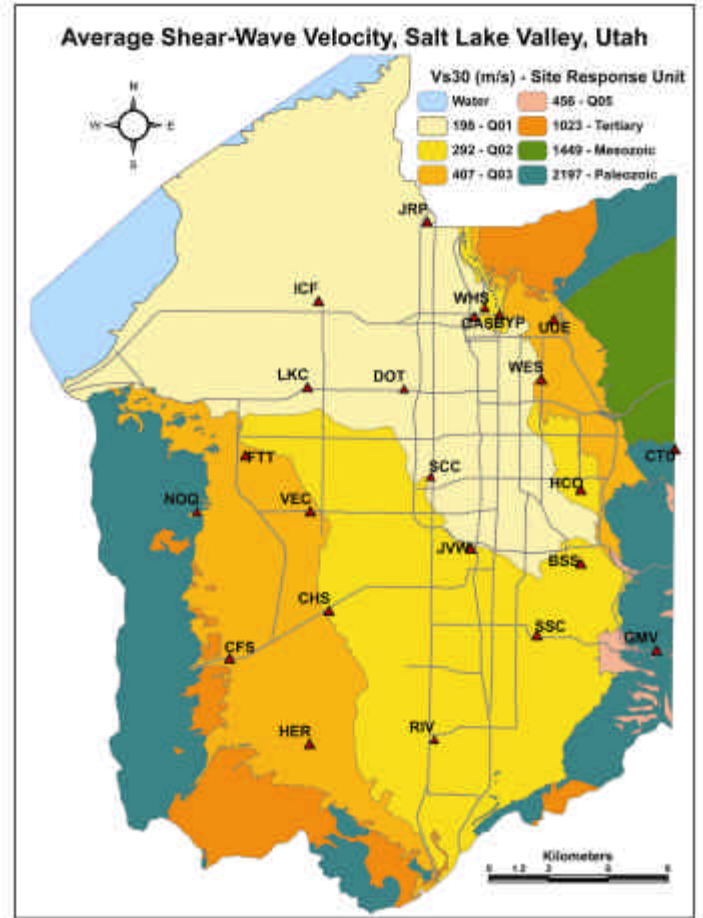


**Figure 2.** Map of the Salt Lake Valley, Utah, showing locations of Advanced National Seismic System strong-motion and broadband stations used in this study and geologically based site-response units, which are grouped according to average shear-wave velocity in the uppermost 30 m (Ashland 2001; personal communication 2004).

velocity in the uppermost 30-meters ( $V_{s30}$ ). Some of them are also functions of other parameters, such as sediment thickness and the horizontal peak ground acceleration (PGA) of the rock at the base of the sediments.

Site-amplification factors can be grouped into three types based on how they are determined. The first type consists of site-amplification factors that are derived empirically, usually in studies of ground motion predictive relations. A particularly relevant example for Utah is the set of amplification factors determined by Boore and others (1994, 1997), which was subsequently used in the predictive relations for extensional regimes developed by Spudich and others (1999) and

Pankow and Pechmann (2004). The Boore and others (1994, 1997) amplification factors are independent of amplitude and have been used for seismic-hazard analyses in Utah in conjunction with the predictive relations of Boore and others (1994, 1995, 1997) and Spudich and others (1999). The second type of site-amplification factor consists of those which are derived from theoretical methods, such as the well-known equivalent-linear soil response modeling program SHAKE. Examples of such factors include those determined by Wong and others (2002a, b; see also Solomon and others, 2004) for SLV soil site-response units, which they used to create probabilistic and deterministic seismic-hazard maps for the SLV. The Wong and others (2002a, b) site-amplification factors are functions of input rock motion PGA and unconsolidated sediment thickness as well as frequency and  $V_{s30}$ . The third type of site-amplification factor consists of those derived using both empirical and theoretical methods, such as those of Borchardt (1994). His factors are based on empirical data at low strains and "laboratory and numerical modeling results" at high strains, and are functions of input rock motion PGA, frequency, and  $V_{s30}$ . In Utah, the Borchardt (1994) amplification factors are used to create ShakeMaps and ShakeMap scenarios (Pankow and others, 2001; Pankow, 2003).

The three different studies cited above predict disparate site-amplification factors for SLV sites at both high and low strain. Even at low strain the differences are large enough that by using weak motion data collected by ANSS instruments throughout the valley, we can select the factors that best fit the weak-motion data. Knowing which, if any, of these sets of site-amplification factors is appropriate for the SLV is crucial for hazard mapping. Use of incorrect site-amplification factors could lead to overestimation or underestimation of predicted ground motions in this area.

In this paper, we apply the spectral-ratio method to weak-motion data collected at ANSS stations to measure frequency-dependent, low-strain site-amplification factors for SLV soil sites. In this method, the ratio between spectra of seismic data

from the same event recorded at a soil site and a nearby rock site is interpreted to represent the ground-motion amplification at the soil site relative to the rock site—after applying a distance correction (e.g., Borchardt, 1970). The measured low-strain site-amplification factors are then averaged over SLV site-response units, which were defined by Ashland (2001 and personal communication, 2004; Figure 2) on the basis of geology and  $V_{s30}$  measurements, and compared to the three sets of published site-amplification factors discussed above. Although we only have low-strain data, this analysis is important for three reasons. First, at low strain the amplification should be a linear process. If a given set of site-amplification factors cannot predict low-strain, linear amplification then predicted amplifications at higher strain, where non-linear effects are expected, would be questionable. Second, even low-strain site-amplification factors are relevant to seismic-hazard analyses because they are applicable to ground motions up to at least  $\sim 0.15$  g (Borchardt, 1994; Beresnev and Wen, 1996; Wong and others, 2002a), and the threshold of damage to weak construction is about 0.1 g (Richter, 1958, p. 26). Finally, our study in the linear soil-response domain will provide a baseline for studying non-linear effects when future large earthquakes occur in the SLV.

## DATA

Eighteen local earthquakes recorded at ANSS strong-motion and broadband stations make up the dataset for this study (Table 1 and Figure 1). These earthquakes range in local magnitude ( $M_L$ ) from 2.0 to 5.3 and are at epicentral distances of 10 to 260 km from the primary rock reference station, NOQ (see Figure 2). All 18 events were used to test possible distance correction methods for the spectral ratios. Six events that were well-recorded by stations located on soil in the SLV were used to determine site amplification. The epicentral distances from these six events to the soil sites used to determine site-amplification factors range from

**Table 1. Earthquakes used in this study<sup>†</sup>**

<b>DATE</b> <b>(YEAR MO DY)</b>	<b>ORIGIN TIME</b> <b>(UTC)</b>	<b>LATITUDE</b>	<b>LONGITUDE</b>	<b>DEPTH</b> <b>(KM)</b>	<b>MAG.</b> <b>(M<sub>L</sub>)</b>	<b>DIST TO</b> <b>NOQ</b> <b>(KM)</b>
20010223	21:43:50.82	38.7270	-112.555	1.10	4.0	217
20010224	10:54:40.75	38.7265	-112.544	2.02	3.6	217
20010228	04:09:46.14	38.7217	-112.546	0.16	3.6	218
20010421	17:18:56.28	42.9320	-111.391	1.04	5.3	260
20010524*	02:40:40.89	40.3762	-111.933	6.44	3.3	35
20010708*	13:55:51.33	40.7418	-112.073	10.81	3.3	11
20020614	07:45:46.38	41.3917	-111.436	7.39	3.0	100
20020728	19:38:40.03	41.7453	-111.379	9.39	3.6	136
20020921	20:14:15.02	40.4177	-111.958	11.53	2.7	29
20021004	12:30:56.98	41.6548	-112.312	0.06	2.4	112
20021010	06:52:43.82	40.4073	-111.953	6.34	2.0	31
20030103*	05:02:12.16	41.2747	-111.802	11.86	3.6	74
20030201	20:37:31.24	41.8285	-112.212	0.17	3.2	131
20030417*	01:04:19.07	39.5130	-111.905	0.88	4.3	128
20030712*	01:54:40.04	41.2857	-111.615	9.23	3.5	82
20031227	00:39:24.37	39.6485	-111.950	1.85	3.6	112
20040225	00:41:03.64	41.9970	-111.818	2.46	3.4	151
20040318*	21:22:37.49	40.7302	-112.056	7.93	2.4	10

<sup>†</sup> locations and magnitudes are from the University of Utah earthquake catalog (<http://www.quake.utah.edu>)

\* denotes events used to calculate soil/rock spectral-amplitude ratios; all events were used to evaluate the distance corrections

2 to 146 km, with a median of 60 km. The earthquakes occurred both north and south of the valley, providing some azimuthal variation in the ray paths (Figure 1). There were also two events located beneath the valley itself.

The dataset used for the distance correction tests was recorded at 12 stations located on Paleozoic rock in northern Utah (Figure 1). We selected this group of stations in order to obtain a widespread distribution with minimal differences in site response. We calculated the site-amplification factors using 20 stations located on soil and two reference rock stations located on Paleozoic rock near the SLV: NOQ and CTU. NOQ is west of the valley on Permian limestone. CTU is east of the valley on Pennsylvanian quartzite. Seismic refraction data indicate that the near-surface *P*-wave velocity of the quartzite is 1745 m/sec (G. T. Schuster, written communication, 1993) which, assuming a near-surface *P*-to-*S* velocity ratio of 2.0,

suggests an *S*-wave velocity of ~870 m/sec. Both reference stations have GURALP broadband velocity sensors and REF-TEK digital recorders operating at sample rates of 100 samples/sec. The soil sites where amplification factors were measured are well-distributed throughout the valley on the three main *V*<sub>s30</sub> units (Figure 2). The instruments at these sites are either Kinometrics Model K2 recorders with episensor accelerometers or REF-TEK Model ANSS-130 recorders with MEMS accelerometers. These data are also recorded digitally at 100 samples/sec.

## METHODOLOGY

### Interpretation of Spectral Ratios

The theoretical basis of the spectral-ratio method is the following simple, but widely used, frequency-domain model for ground motion:

$$A_{ij}(r_{ij}, f) = E_i(r_{ref}, f) S_j(f) D(r_{ref}, r_{ij}, f) \quad (1)$$

where  $A_{ij}$  is the spectral amplitude of ground motion from earthquake  $i$  recorded at station  $j$ ,  $r_{ij}$  is the hypocentral distance from earthquake  $i$  to station  $j$ ,  $f$  is frequency,  $E_i(r_{ref}, f)$  is a source excitation term, assumed to be isotropic, which gives the spectral amplitude of ground motion from earthquake  $i$  at reference distance  $r_{ref}$ ,  $S_j(f)$  is the site-amplification factor, and  $D(r_{ref}, r_{ij}, f)$  is a function describing the distance dependence of the ground motion. To the extent that the assumption of an isotropic source is valid, the source term can be removed by computing the ratio between the spectral amplitudes of ground motion from the same earthquake recorded at two stations, station  $j$  and reference station  $o$ . Computing this ratio and solving for the ratio of the site-amplification factors for the two stations gives

$$\frac{S_j(f)}{S_o(f)} = \frac{A_{ij}(r_{ij}, f) D(r_{ref}, r_{io}, f)}{A_{io}(r_{io}, f) D(r_{ref}, r_{ij}, f)} \quad (2)$$

Thus, the site-amplification factor of station  $j$  relative to that of reference station  $o$ ,  $S_j(f)/S_o(f)$ , can be determined from the observed spectral ratio,  $A_{ij}(r_{ij}, f)/A_{io}(r_{io}, f)$ , provided that the distance correction  $D(r_{ref}, r_{io}, f)/D(r_{ref}, r_{ij}, f)$  is known.

### Data Processing

We applied the following processing procedure to all of the raw waveform data for this study to obtain velocity traces in the passband 0.4 to 40 Hz: (1) removal of the DC offset, (2) tapering with a 5% Hanning taper, (3) deconvolution of the instrument velocity response by spectral division, and (4) highpass filtering with a frequency domain cosine taper between 0.2 and 0.4 Hz. We then calculated the Fourier spectra of both horizontal components for a 50-sec data window beginning 5 seconds before the  $P$ -wave arrival and for a 25-sec noise window immediately prior to the  $P$ -wave window. Before computing the spectra, a 10% Hanning taper was applied to the windows and they

were padded with zeros to twice their original length. Finally, we computed average horizontal spectral ratios over the mid-period (0.5 to 2.5 Hz) and short-period (2 to 10 Hz) bands of Borchardt (1994), using only records for which the spectral signal-to-noise ratio was greater than 3 over the entire band. For the purposes of this study, the average horizontal spectral ratio is defined as

$$\frac{A_{ij}(r_{ij}, f)}{A_{io}(r_{io}, f)} = \frac{A_{iJE}(f) + A_{iJN}(f)}{A_{ioE}(f) + A_{ioN}(f)} \quad (3)$$

where  $A_{iJE}(f)$  and  $A_{iJN}(f)$  are the Fourier amplitude spectra of earthquake  $i$  recorded on the east and north components, respectively, of station  $j$ . The spectrum of each component was smoothed separately with a moving average of  $\pm 16$  points ( $\pm 0.1$  Hz) before computing the spectral ratio. Figures 3 and 4 show examples of processed data in the time and frequency domains, respectively.

### Distance Corrections

The distance function  $D$  in (1) is generally assumed to have the form

$$D(r_{ref}, r_{ij}, f) = \frac{g(r_{ij})}{g(r_{ref})} e^{-P f (r_{ij} - r_{ref}) / b Q(f)} \quad (4)$$

where  $g(r_{ij})$  is the geometrical spreading function,  $\beta$  is the average shear-wave velocity along the raypaths, and  $Q(f)$  is a frequency-dependent quality factor  $Q_0 f^\eta$ , where  $Q_0$  and  $\eta$  are constants. From (4), the distance correction factor in (2) takes the form

$$\frac{D(r_{ref}, r_{io}, f)}{D(r_{ref}, r_{ij}, f)} = \frac{g(r_{io})}{g(r_{ij})} e^{-P f (r_{io} - r_{ij}) / b Q(f)} \quad (5)$$

which is independent of  $r_{ref}$  (e.g., Hartzell and others, 1996; Harmsen, 1997).

Brockman and Bollinger (1992) and Jeon and Herrmann (in press) have modeled the distance dependence of  $S_g/L_g$  ground motion spectral

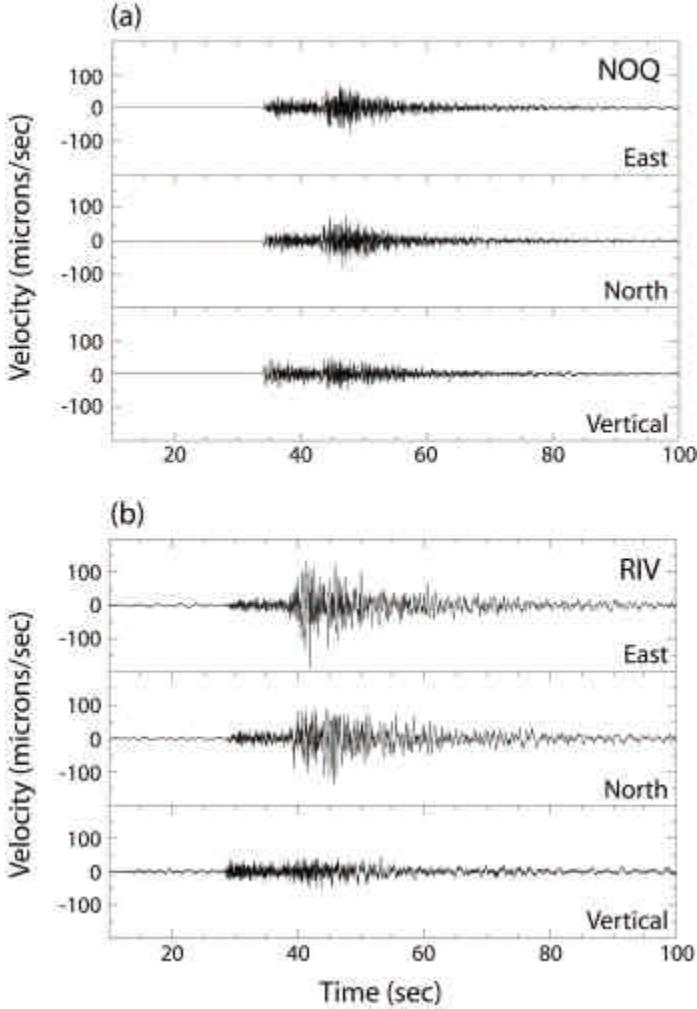


**Figure 3.** Velocity records (filter bandpass 0.4 – 40 Hz) from the soil site RIV (hypocentral distance 85.5 km) and the rock reference station NOQ (hypocentral distance 75.0 km) for an ML 3.6 earthquake on Jan. 3, 2003.

amplitudes in Utah by inverting for the parameters in (1) and (4) using data from the Utah regional seismic network. In order to test the accuracy of spectral ratio distance corrections based on their models and another model discussed below, we used records of 18 local earthquakes from 12 northern Utah stations located on Paleozoic rock—including the two stations which we selected as reference rock stations for our study (Figure 1, Table 1). We calculated ratios between average horizontal-component Fourier spectra of the records from all of the possible pairs of stations which recorded each earthquake. For these spectral ratios, if it is assumed that all of the Paleozoic rock sites

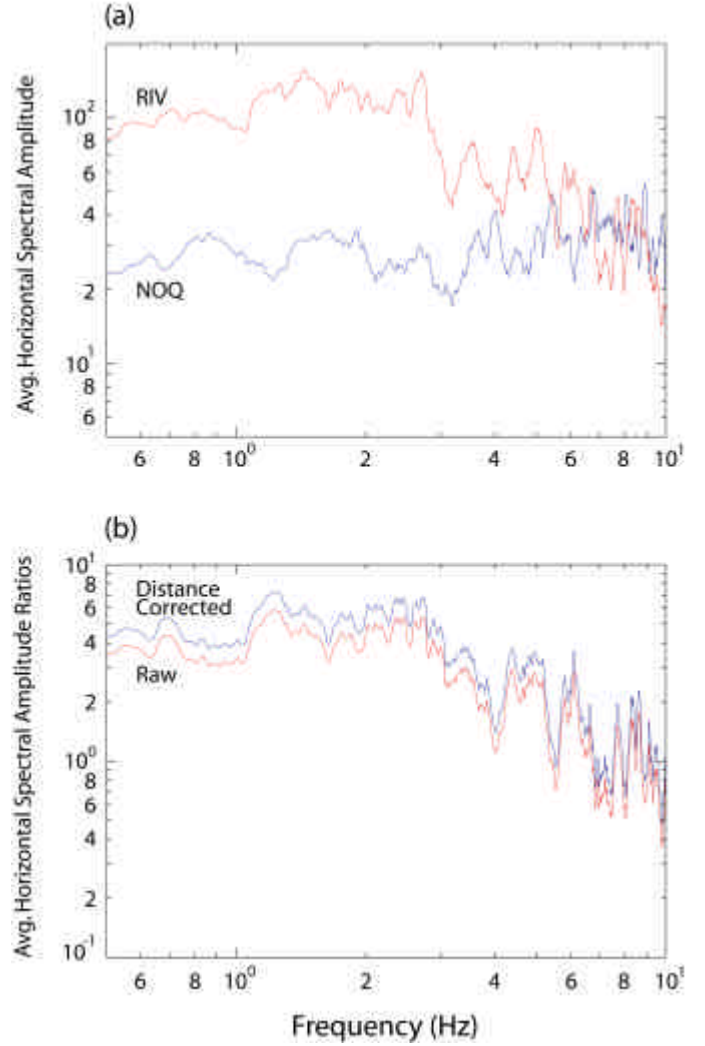


**Figure 4.** (a) Average horizontal-component spectra for the velocity records in Figure 3: NOQ (blue) and RIV (red). (b) The average horizontal component spectral-amplitude ratios—distance corrected (blue) and uncorrected (red)—for the two stations in (a).

have similar site-amplification factors, then  $S_j(f)/S_o(f) \approx 1$  and (2) simplifies to

$$\frac{A_{ij}(r_{ij}, f)}{A_{io}(r_{io}, f)} = \frac{D(r_{ref}, r_{ij}, f)}{D(r_{ref}, r_{io}, f)}. \quad (6)$$

Thus, with this data set, the accuracy of the distance corrections can be evaluated by comparing the observed and predicted spectral ratios on the left - and right-hand sides of equation (6), respectively. We made such comparisons using average values of

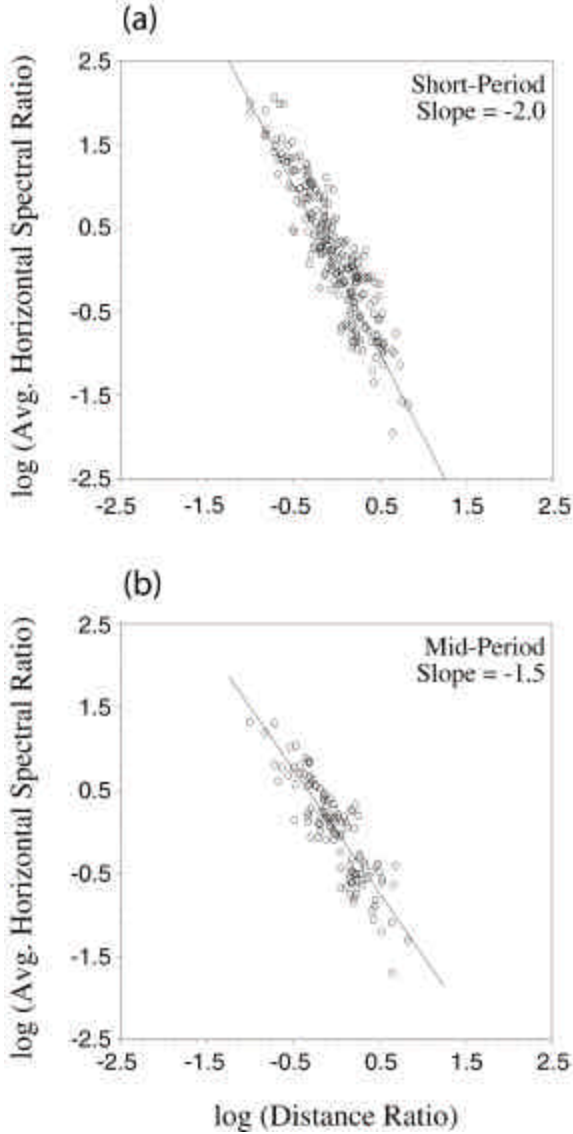


**Figure 5.** Observed spectral ratios plotted versus  $\log_{10}(\text{Distance Ratio})$ , where the distance ratio is the ratio between the hypocentral distances of the two stations. (a) short-period band (0.1 to 0.5 sec) and (b) mid-period band (0.4 to 2.0 sec). The lines indicate fits to the data for an exponential model (see text).

the observed spectral ratios over the mid-period (0.5 to 2.5 Hz) and short-period (2 to 10 Hz) bands. The predicted values were calculated for the frequencies at the mid points of these period bands: 1.5 and 6.0 Hz, respectively.

Figure 5 shows the logarithms of the observed spectral ratios plotted versus  $\log_{10}(r_{ij}/r_{io})$ . The lines on the plots show linear regression fits to the data for the simple exponential model

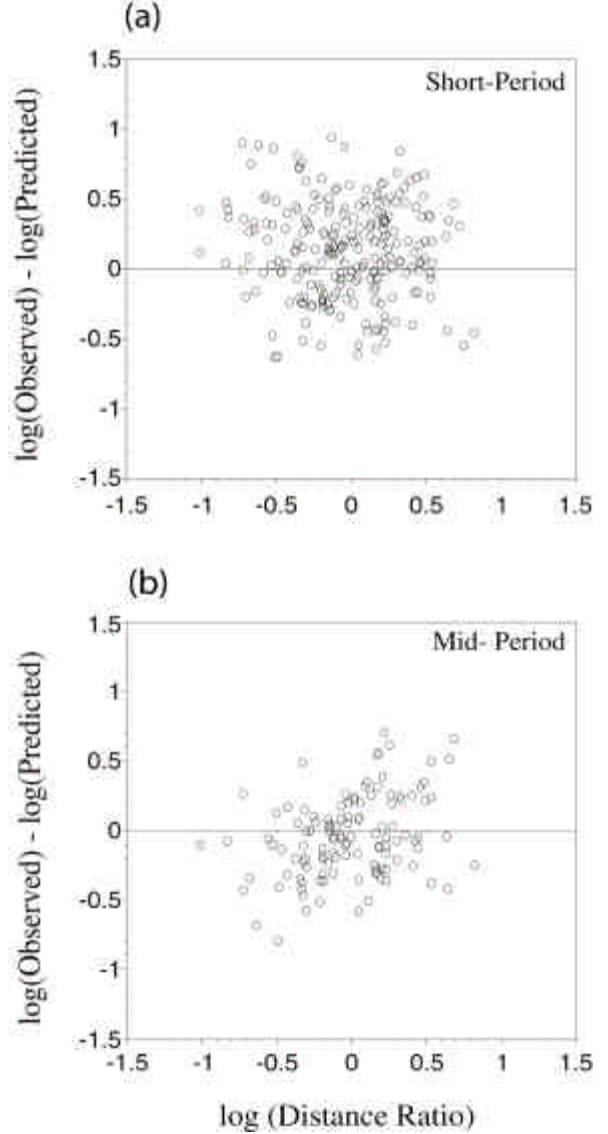


**Figure 6.** Spectral-ratio residuals, defined as  $\log_{10}(\text{Observed Ratio}) - \log_{10}(\text{Predicted Ratio})$ , versus  $\log_{10}(\text{Distance Ratio})$ , where the distance ratio is the ratio between the hypocentral distances of the two stations. The observed ratios are between average horizontal-component Fourier amplitude spectra of recordings from the same event at two different Paleozoic rock sites (see Figure 1), averaged over the short-period band (0.1 to 0.5 sec) in (a) and the mid-period band (0.4 to 2.0 sec) in (b). The predicted ratios are based on the Brockman and Bollinger (1992) model for Sg/Lg geometrical spreading and attenuation in Utah, and assume that the effects of site amplification and the source are similar at both recording sites. The plots demonstrate that there is no significant bias in the spectral-ratio residuals.

$$\frac{A_{ij}(r_{ij}, f)}{A_{io}(r_{io}, f)} = \left( \frac{r_{ij}}{r_{io}} \right)^{-p} \quad (7)$$

where  $p$  is a constant. The best-fit  $p$  values and their 95% confidence limits are  $1.5 \pm 0.2$  and  $2.0 \pm 0.1$  for the mid-period and short-period bands, respectively. It is worth noting that both of these  $p$  values are much higher than 1.0, the value which is often assumed for exponential distance-correction functions based on geometrical spreading for body waves in a homogeneous half space (e.g., Borchardt and Glasmoyer, 1992; Borchardt, 1994).

Overall, the Brockman and Bollinger (1992) model provides a better fit to the data in Figure 5 than the exponential model shown on this figure or the Jeon and Herrman (in press) model. Figure 6 shows plots of spectral ratio residuals,

$$\log_{10}(\text{Observed}) - \log_{10}(\text{Predicted}) = \log_{10} \frac{A_{ij}(r_{ij}, f)}{A_{io}(r_{io}, f)} - \log_{10} \frac{D(r_{ref}, r_{ij}, f)}{D(r_{ref}, r_{io}, f)} \quad (8)$$

versus  $\log_{10}(r_{ij}/r_{io})$  for the Brockman and Bollinger (1992) model. These plots and similar plots versus  $r_{io}$  show that there is no significant distance bias in the spectral ratio residuals, although the mid-period residuals show a slight tendency to increase with the distance ratio  $r_{ij}/r_{io}$ . It is surprising that the Brockman and Bollinger (1992) model fits our horizontal-component spectral ratios better than the Jeon and Herrmann (in press) model. The data set for the former study was five times smaller and consisted of vertical-component records only, whereas Jeon and Herrmann used both horizontal- and vertical-component data. However, Jeon and Herrmann did not find much difference in the distance dependence of ground motion spectral amplitudes on horizontal and vertical components and recommended a single model for both components. Based on our tests, we decided to correct our soil/rock spectral ratios at each frequency point using equation (5) with the parameters from the Brockman and Bollinger (1992) model:  $g(r_{ij}) = r_{ij}^{-0.9}$ ,  $\mathbf{b} = 3.5$  km/sec, and  $Q(f) = 97f^{0.80 \pm 0.08}$ .

## Determination of Average Site-Amplification Factors

To obtain the best possible estimate of the average site-amplification factors for each SLV site-response unit, we calculated the geometric mean of the distance-corrected spectral ratios for all of the stations located on that unit. Initially, these geometric means were calculated separately for the spectral ratios relative to each of the two reference rock sites, NOQ and CTU (Figure 2). It is desirable to combine the spectral ratios for both reference rock sites because of the limited amount of data and the need to average out source effects. However, NOQ/CTU spectral ratios indicate that ground motions at NOQ are amplified significantly relative to those at CTU, with average geometric mean amplification factors of 1.45 and 1.93 for the mid-period and short-period bands, respectively (Figure 7c). Therefore, it is necessary to correct the soil/rock spectral ratios for the differences in site amplification at the two reference rock sites. We chose to adjust the geometric mean CTU-referenced spectral ratios to NOQ site conditions and then compute the geometric mean of this result and the geometric mean NOQ-referenced spectral ratios. Let  $\bar{S}_{k/NOQ}(f)$  and  $\bar{S}_{k/CTU}(f)$  be the geometric means of the distance-corrected spectral ratios for stations on site-response unit  $k$  relative to NOQ and CTU, respectively. Let  $\bar{S}_{NOQ/CTU}(f)$  be the geometric mean of the distance-corrected spectral ratios for NOQ relative to CTU. Finally, let  $\bar{S}_k(f)$  be the combined NOQ-CTU geometric mean of the distance-corrected spectral ratios for stations on site-response unit  $k$ , relative to NOQ rock site conditions.  $\bar{S}_k(f)$ , as defined by the equation

$$\log \bar{S}_k(f) = \frac{1}{2} \left[ \log \bar{S}_{k/NOQ}(f) + \log(\bar{S}_{k/CTU} / \bar{S}_{NOQ/CTU}) \right] \quad (9)$$

is our preferred estimate of the average site-amplification factors for site-response unit  $k$ . Note

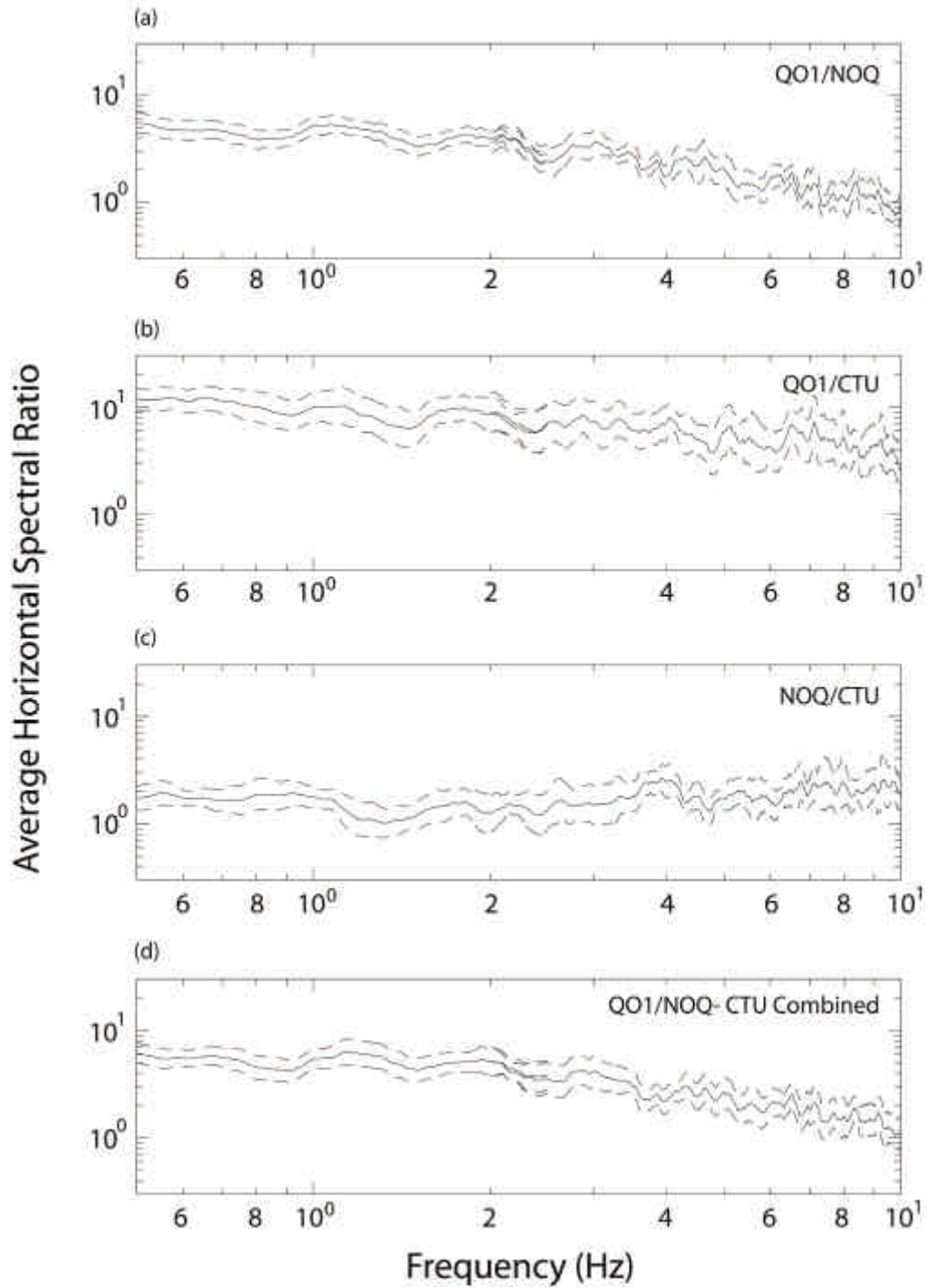


**Figure 7.** Steps involved in calculating the average site-amplification factors for site-response unit Q01. The geometric means (solid lines) of the distance-corrected spectral ratios for stations on site-response unit Q01 relative to NOQ [(a);  $\bar{S}_{k/NOQ}(f)$ ] and CTU [(b);  $\bar{S}_{k/CTU}(f)$ ]. (c) The distance-corrected spectral ratios for station NOQ relative to CTU [ $\bar{S}_{NOQ/CTU}(f)$ ].

(d) The combined NOQ-CTU geometric mean of the distance-corrected spectral ratios for stations on site-response unit Q01 relative to NOQ rock site conditions,  $\bar{S}_k(f)$ . The dashed lines show the 95% confidence limits on the geometric means.

that  $\bar{S}_{k/NOQ}(f)$  and  $\bar{S}_{k/CTU}(f)$  are given equal weight in calculating  $\bar{S}_k(f)$ . Weighting  $\bar{S}_{k/NOQ}(f)$  and  $\bar{S}_{k/CTU}(f)$  by the number of spectral ratios used to determine each would not have a large effect on the result because the numbers of spectral ratios relative to NOQ and CTU are comparable. If the 95% confidence limits on  $\log \bar{S}_{k/NOQ}(f)$ ,  $\log \bar{S}_{k/CTU}(f)$ , and  $\log \bar{S}_{NOQ/CTU}(f)$  are designated by  $2\mathbf{s}(\log \bar{S}_{k/NOQ}(f))$ ,  $2\mathbf{s}(\log \bar{S}_{k/CTU}(f))$ , and  $2\mathbf{s}(\log \bar{S}_{NOQ/CTU}(f))$ , respectively, then if we assume that all three of these quantities can be treated as independent random variables, the 95% confidence limits on  $\log \bar{S}_k(f)$  are given by

$$2\mathbf{s}(\log \bar{S}_k(f)) = \frac{1}{2} \left[ \left( 2\mathbf{s}(\log \bar{S}_{k/NOQ}(f)) \right)^2 + \left( 2\mathbf{s}(\log \bar{S}_{k/CTU}(f)) \right)^2 + \left( 2\mathbf{s}(\log \bar{S}_{NOQ/CTU}(f)) \right)^2 \right]^{1/2} \quad (10)$$

To illustrate the steps involved in calculating the average site-amplification factors, Figure 7 shows  $\bar{S}_{k/NOQ}(f)$ ,  $\bar{S}_{k/CTU}(f)$ ,  $\bar{S}_{NOQ/CTU}(f)$ , and  $\bar{S}_k(f)$  for site-response unit Q01. Note that the data sets for the mid-period (0.5 to 2.5 Hz) and short-period (2 to 10 Hz) bands are not exactly the same because some records had adequate signal-to-noise ratios in only one of these two bands. Nevertheless, the two sets of functions agree very well in the frequency range 2.0 to 2.5 Hz where the mid-period and short-period bands overlap.

## RESULTS

Figure 8 shows the combined geometric mean spectral ratios relative to reference station NOQ for the three largest  $V_{S30}$  units in the SLV (Figure 2). The geometric mean spectral ratio for site-response unit Q01 is significantly higher than

that of Q03 over nearly the entire frequency range examined, 0.5 to 10 Hz. The geometric mean spectral ratios for Q02 generally lie between those of Q01 and Q03 for the frequency range of 0.5 to 4 Hz and are comparable to those of Q03 at higher frequencies. The 95% confidence limits for Q02 and Q03 overlap over the whole frequency range shown. Relative to NOQ rock-site conditions, we find mean mid-period amplification factors ranging from 2.1 on Q03 to 4.9 on Q01 and mean short-period amplification factors ranging from 1.1 on Q03 to 2.3 on Q01 (Table 2).

Figure 9 shows the comparison of our results with the three previously mentioned sets of site-amplification factors, which can be used to predict ground motion differences among the SLV site-response units. Wong and others (2002a, b) calculated their site-amplification factors relative to ground motions at the surface of a generic western U.S. soft rock profile for which we computed a  $V_{S30}$  of 530 m/s. We calculated the site-amplification factors of Borchardt (1994) and Boore and others (1997) shown in Figure 9 assuming a reference rock  $V_{S30}$  of 910 m/sec (Pankow and Pechmann, 2004)—similar to our estimate of the near-surface shear-wave velocity at reference station CTU (~870 m/sec). If we had used a reference  $V_{S30}$  of 530 m/sec instead of 910 m/sec for our calculations, then on Figure 9 these two sets of amplification factors would be ~20% lower in the short-period band and ~30% lower in the mid-period band.

For Q01 we observe higher amplification factors than predicted by any of the three models. For Q02 and Q03 the data more closely match the predictions of Borchardt (1994) and Boore and others (1997), than those of Wong and others (2002a, b). The observed mid-period site-amplification factors are higher than the observed short-period amplification factors for all three site-response units. The empirically based amplification factors of Boore and others (1997) and Borchardt (1994) are also higher in the mid-period band than in the short-period band, but the differences are smaller than we observe.

We observe, consistent with the predictions

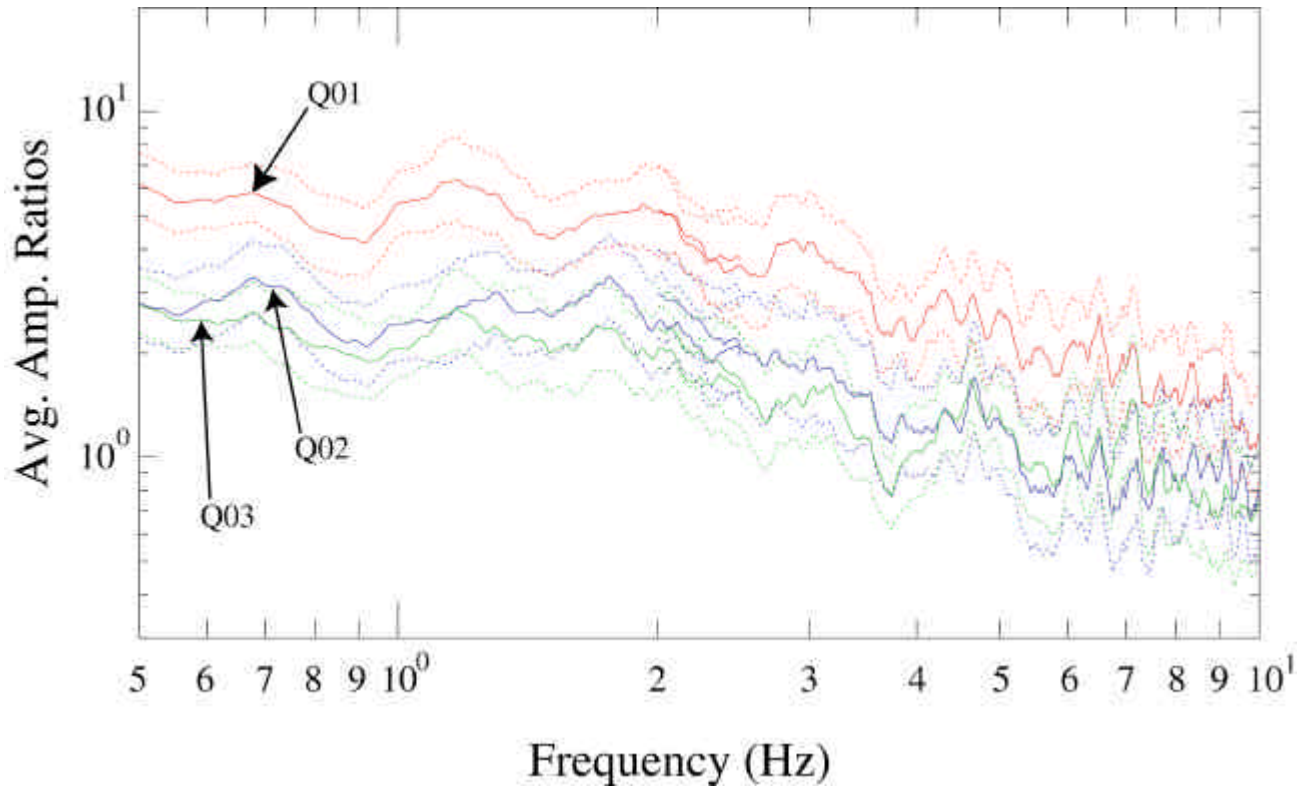


**Figure 8.** Combined NOQ-CTU spectral ratios relative to station NOQ (Figure 2) over the frequency range 0.5 to 10.0 Hz for three different SLV site-response units (Figure 2): Q01 (red), Q02 (blue), and Q03 (green). Shown are the geometric mean spectral ratios (solid lines) and their 95% confidence limits (dotted lines).

**TABLE 2. Empirical low-strain site-amplification factors\***

SALT LAKE VALLEY SITE-RESPONSE UNIT	SHORT-PERIOD FACTOR 0.1-0.5 SEC	MID-PERIOD FACTOR 0.4-2.0 SEC
Q01—Lacustrine and alluvial silt, clay, and fine sand	2.27 (3.08, 1.67)	4.92 (6.28, 3.85)
Q02—Lacustrine sand and gravel; interbedded lacustrine silt, clay, and sand	1.18 (1.68, 0.831)	2.57 (3.39, 1.96)
Q03—Lacustrine and alluvial gravel and sand	1.10 (1.51, 0.800)	2.12 (2.76, 1.63)

\*Values in parentheses are upper- and lower-bound 95% confidence limits

of Borchardt (1994) and Boore and others (1997), that the short-period amplification factors are higher on the deep soft soils of Q01 than on the thin stiff soils of Q03. This result disagrees with the predictions of Wong and others (2002a, b), which show lower short-period site-amplification factors on Q01 than on Q03. The theoretical amplification factors of Wong and others (2002a, b), which

depend on sediment thickness, show a general increase in amplification factors with increasing period from 0.1 to between 0.4 and 0.8 sec.

However, at ~0.6 sec the site-amplification factors begin to decrease with period. The decrease is more pronounced for shallow sediment thickness than for the deeper columns of sediment. We do not observe this decrease in our data.

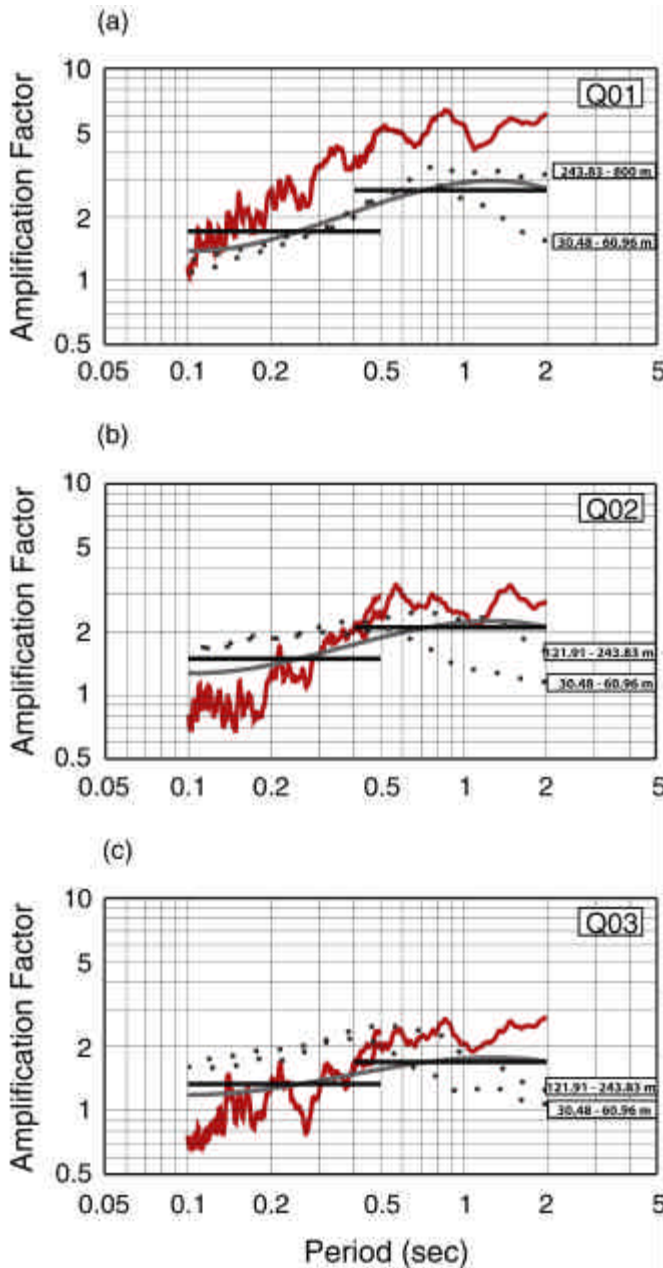


**Figure 9.** Observed (red) and predicted (black and gray) site-amplification factors as a function of period for three different SLV site-response units. The observed amplification factors are geometric means (solid red lines) from this study, relative to NOQ site conditions. The predicted amplification factors from Borchardt (1994, solid black lines), for rock peak acceleration 0.1 g, and Boore and others (1997, solid gray lines) were calculated assuming a reference rock site  $V_{s30}$  of 910 m/sec (Pankow and Pechmann, 2004). The predicted amplification factors from Wong and others (2002a, b; dotted black lines), for rock peak acceleration of 0.05 g, are shown for two different ranges of unconsolidated sediment depth as labeled on the plots. (a) Q01, (b) Q02, and (c) Q03.

## CONCLUSIONS

In this study, we set out to determine if any of three sets of site-amplification factors, which have been applied to the SLV, match observed low-strain data. Overall, the data for the three most widespread  $V_{s30}$  units in the SLV (Figure 2) are best matched by the site-amplification factors of Borchardt (1994) and Boore and others (1997). However, their predicted amplification factors show less variability with period and with  $V_{s30}$  unit than we observe (Figure 9). One limitation of our study is that we do not have the data to fully account for sediment thickness as was done in Wong and others (2000a, b), and thus our site-amplification factors are averaged values. However, the ranges of sediment thickness plotted for Wong and others (2002a, b) on Figure 9 span the thickness ranges of Arnow and others (1970) for each unit in the SLV. If the site-amplification factors of Wong and others (2000a, b) are correct, we would expect the general shapes of the curves to mimic those of the measured amplification factors. But this is not the case. The Wong and others (2002a, b) factors show decreases in site amplification at periods above  $\sim 0.6$  sec. This decrease is not observed in our geometrical mean site-amplification factors, nor was it observed in the processing of the individual spectral ratios. Given this discrepancy, the unknowns associated with sediment thickness, and the higher short-period amplification factors on the thin stiff soil (Q03) compared to the thick soft soil (Q01) incorrectly predicted by Wong and others (2002a, b), we conclude that, at least with the present state of knowledge, the empirically based site-amplification factors of Borchardt (1994) and Boore and others (1997) provide the best alternatives for estimating site amplification in the SLV.

## ACKNOWLEDGMENTS

We are grateful to Ivan Wong for providing digital files of the Wong and others (2002a, b) reference rock model and site-amplification factors

and to Francis Ashland for providing the revised Salt Lake Valley site-response unit map. Constructive reviews by Relu Burlacu, Walter Arabasz, and editor Bill Lund led to improvements of this article. This research was supported by the U. S. Geological Survey, Department of the Interior, under USGS Award Number 03HQGR0134.

## REFERENCES

- Anderson, J.G., Bodin, P., Brune, J.N., Prince, J., Singh, S.K., Quaas, R. and Onate, M., 1986, Strong ground motion from the Michoacan, Mexico, earthquake: *Science*, v. 233, p. 1043-1049.
- Arnow, T., Van Horn, R., and LaPray, R., 1970, The pre-Quaternary surface in the Jordan Valley, Utah: U.S. Geological Survey Professional Paper. 700-D, p. D257-D261.
- Arabasz, W.J., Pechmann, J.C., and Brown, E.D., 1992, Observational seismology and the evaluation of earthquake hazards and risk in the Wasatch front area, Utah, *in* Gori, P.L. and Hays W.W., editors, *Assessment of Regional Earthquake Hazards and Risk Along the Wasatch Front*, Utah: U.S. Geological Survey Professional Paper. 1500-A-J, D1-D36.
- Ashland, F.X., 2001, Site-response characterization for implementing SHAKEMAP in northern Utah. Utah Geological Survey Report of Investigation 248, 10 p., 2 pl.
- Beresnev, I.A., and Wen, K.L., 1996, Nonlinear soil response; a reality?: *Bulletin of the Seismological Society of America*, v 86, p. 1964-1978.
- Black, B.D., Lund, W.R., and Mayes, B.H., 1995, Large earthquakes on the Salt Lake City segment of the Wasatch fault zone-summary of new information from the South Fork Dry Creek site, Salt Lake County, Utah, *in* Lund, W.R., editor, *Environmental and Engineering Geology of the Wasatch Front Region: 1995 Symposium and Field Conference*, Utah Geological Association Publication, v. 24, p. 11-30.
- Boore, D.M., Joyner, W.B., and Fumal, T.E., 1994, Estimation of response spectra and peak accelerations from western North American earthquakes: An interim report, Part 2: U.S. Geological Survey, Open-File Report. 94-127, 40 p.
- Boore, D.M., Joyner, W.B., and Fumal, T.E., 1995, Ground motion estimates for strike- and reverse-slip faults: Letter to colleagues, 4 p.
- Boore, D.M., Joyner, W.B., and Fumal, T.E., 1997. Equations for estimating horizontal response spectra and peak acceleration from western North American earthquakes: A summary of recent work: *Seismological Research Letters*. v. 68, p. 128-153.
- Borcherdt, R.D, 1970, Effects of local geology on ground motion near San Francisco Bay: *Bulletin of the Seismological Society of America*, v. 60, p. 29-61.
- Borcherdt, R. D., 1994, Estimates of site-dependent response spectra for design (methodology and justification): *Earthquake Spectra*, v. 10, p. 617-653.
- Borcherdt, R. D., and Glassmoyer, G., 1992, On the characteristics of local geology and their influence on ground motions generated by the Loma Prieta earthquake in the San Francisco Bay region, California: *Bulletin of the Seismological Society of America*, v. 82, p. 603-641.
- Brockman, S. R., and Bollinger, G. A., 1992, Q estimates along the Wasatch Front in Utah derived from Sg and Lg wave amplitudes: *Bulletin of the Seismological Society of America*, v. 82, p. 135-147.
- Davis, P.M., Rubinstein, J.L., Liu, K.H., Gao, S.S., and Knopoff, L., 2000, Northridge earthquake damage caused by geologic focusing of seismic waves: *Science*, v. 289, p. 1746-1750.
- Field, E.H., and the SCEC Phase III Working Group, 2000. Accounting for site effects in probabilistic seismic hazard analyses of southern California: Overview of the SCEC Phase III report: *Bulletin of the Seismological Society of America*, v. 90, p. S1-S31.
- Hartzell, S. H, Leeds, A., Frankel, A. D., and

- Michael, J. A., 1996, Site response for urban Los Angeles using aftershocks of the Northridge earthquake: *Bulletin of the Seismological Society of America*, v.86, Part B Suppl., p.S168-S192.
- Harmsen, S. C., 1997, Estimating the diminution of shear-wave amplitude with distance; application to the Los Angeles, California, urban area: *Bulletin of the Seismological Society of America*, v.87, p.888-903.
- Jeon, Y., and Hermann, R. B., in press, High frequency earthquake ground motion scaling in Utah and Yellowstone: *Bulletin of the Seismological Society of America*.
- Joyner, W.B., 2000, Strong motion from surface waves in deep sedimentary basins: *Bulletin of the Seismological Society of America*, v. 90, p. S95-S112.
- Kramer, S.L., 1996, *Geotechnical earthquake engineering: Upper Saddle River, New Jersey*, Prentice Hall, 653 p.
- Machette, M.N., Personius, S.F., Nelson, A.R., Schwartz, D.P., and Lund, W.R., 1991, The Wasatch fault zone, Utah-segmentation and history of Holocene earthquakes: *Journal of Structural Geology*, v. 13, p. 137-149.
- McCalpin, J.P., and Nishenko, S.P., 1996, Holocene paleoseismicity, temporal clustering, and probabilities of future large ( $M > 7$ ) earthquakes on the Wasatch fault zone, Utah: *Journal of Geophysical Research*, v. 101, p. 6233-6253.
- McCalpin, J.P. and Nelson, C.V., 2000, Long recurrence records from the Wasatch fault zone, Utah: Final Technical Report, Contract 99HQGR0058, National Earthquake Hazards Reduction Program, U.S. Geological Survey, 61 p.
- Pankow, K. L., Pechmann, J. C., Nava, S. J., and Arabasz, W. J., 2001, Implementing ShakeMap in Utah before the 2002 Winter Olympics: *Seismological Research Letters*, v. 72, pp. 232.
- Pankow, K.L., 2003, The anatomy of an earthquake scenario: M7 on the Salt Lake City segment of the Wasatch fault, Utah: *Geophysical Research Abstracts 5*, EGS-AGU-EUG Joint Assembly, Compact Disk, ISSN No. 1029-7006.
- Pankow, K. L., and Pechmann, J. C., 2004, The SEA99 ground-motion predictive relations for extensional tectonic regimes: Revisions and a new peak ground velocity relation: *Bulletin of the Seismological Society of America*, v. 94, p. 341-348.
- Richter, C.F., 1958, *Elementary seismology: San Francisco, CA*, W.H. Freeman and Co., 768 p.
- Solomon, B.J., Storey, N., Wong, I., Siva, W., Gregor, N., Wright, D., and McDonald, G., 2004, Earthquake-hazards scenario for a M7 earthquake on the Salt Lake City segment of the Wasatch fault zone, Utah: *Utah Geological Survey Special Study 111 DM*, 59 p., 6 plates (compact disk).
- Singh, S.K, Mena, E., and Castro, R., 1988, Some aspects of source characteristics of the 19 September, 1985 Michoacan earthquake and ground motion amplification in and near Mexico City from strong ground motion data: *Bulletin of the Seismological Society of America*, v. 78, p. 451-477.
- Spudich, P., Joyner, W. B., Lindh, A. G., Boore, D. M., Margaris, B. M., and Fletcher, J. B., 1999, SEA99: A revised ground motion prediction relation for use in extensional tectonic regimes: *Bulletin of the Seismological Society of America*, v. 89, p. 1156-1170.
- U.S. Geological Survey Staff, 1990, The Loma Prieta, California, earthquake: An anticipated event: *Science*, v. 247, p. 286-293.
- U.S. Geological Survey, 1999, An assessment of seismic monitoring in the United States: Requirements for an Advanced National Seismic System: U. S. Geological Survey Circular 1188, 55 p.
- Wong, I., Silva, W., Olig, S., Thomas, P., Wright, D., Ashland, F., Gregor, N., Pechmann, J., Dober, M., Christenson, G., and Gerth, R., 2002a, Earthquake scenario and probabilistic ground shaking maps for the Salt Lake City, Utah, metropolitan area: *Utah Geological Survey Miscellaneous Publication MP-02-5*, 50 p., 9 plates.
- Wong, I., Silva, W., Gregor, N., Wright, D., Ashland, F., McDonald, G., Olig, S.,

Christenson, G., and Solomon, B., 2002b,  
Earthquake scenario ground shaking maps for  
the central Wasatch Front, Utah: Proceedings of

the 7<sup>th</sup> U.S. National Conference on Earthquake  
Engineering, Boston, Mass., July 21-25, 2002,  
(compact disk).

# ***BASIN AND RANGE SEISMICITY: DISTRIBUTION, OCCURRENCE RATES, MOMENT RELEASE, AND COMPARISON WITH GEODESY***

Aasha Pancha and John G. Anderson  
Seismological Laboratory and Department of Geological Sciences  
Mail Stop 174  
University of Nevada  
Reno, Nevada, 89557.  
Phone: 775-784-4975  
Fax: 775-784-4165  
Email: [pancha@seismo.unr.edu](mailto:pancha@seismo.unr.edu), [jga@unr.edu](mailto:jga@unr.edu)

## **ABSTRACT**

Scalar moment rates estimated from a 146-year seismicity catalog agree, within uncertainties, with the deformation rate of the Basin and Range Province determined using space geodesy. Seismic moment rates have been estimated from a new catalog of earthquakes intended to be complete for  $M \geq 5$ . The catalog was compiled from 15 preexisting catalogs, supplemented by the review of 42 published journal articles. Throughout the catalog compilation, care was taken to obtain the moment magnitude or a reasonable, and not inflated, equivalent. Eighty percent of the moment release occurred during 10 earthquakes of magnitude  $M_w \geq 6.76$ . The spatial distribution of earthquakes and their moment release matches the geodetic pattern of deformation. All three are concentrated in a  $\sim 200$  km zone along the western boundary of the study region, which widens to the north. Several techniques, ultimately traceable to Kostrov (1974) and Brune (1968), are used to translate the geodetic strain rates into rates of seismic moment release. Rates determined from seismicity, of  $4.5 \times 10^{25}$  to  $10.8 \times 10^{25}$  dyne-cm/year, overlap the range determined from the geodetic data,  $5.87 \times 10^{25}$  to  $13.0 \times 10^{25}$  dyne-cm/year. This agreement suggests that within uncertainties, the rate of historic earthquakes within the Basin and Range Province, taken as a whole, provides a reasonable estimate for the future rate of seismicity. These results support the hypothesis that even a few years of detailed geodetic monitoring can provide a good constraint on seismic-hazard estimates.

## **INTRODUCTION**

Earthquake occurrence rates are essential for seismic-hazard analysis. The adequacy of seismic catalogues for seismic-hazard analysis is governed by the product of the area of interest, catalogue duration (Smith, 1976), and regional strain rate (Ward, 1998a); the catalogue duration is almost always insufficient. Fault slip rates and crustal deformation rates may be used to compensate for inadequate catalogs. Geological data on fault slip rates are labor intensive and difficult to obtain, as the appropriate fault exposures are often not

available. Geodetic data on crustal deformation rates, in contrast, are relatively easily obtained with just a few years of observations using the Global Positioning System (GPS). It seems reasonable that these contemporary strain rates should also correlate with earthquake rates (e.g. Shen-Tu and others, 1998; Ward, 1998a, b; Shen-Tu and others, 1999), but the hypothesis has not been widely tested.

The Basin and Range Province extends from the rigid Sierra Nevada block in the west to the Colorado Plateau in the east (Figure 1). The province is an actively deforming region of Cenozoic extension, characterized by north trending

ranges of relatively uniform spacing and elevation, which are bounded by normal faults and separated by basins. Early extension may be related to buoyancy forces within the lithosphere (Wernicke, 1992), while present day extension may be related to high gravitational potential energy of the elevated western United States moderated by forces exerted by bounding plates and low-density magmatic contributions to the lithosphere (Lachenbruch and Morgan, 1990; Jones and others, 1996; Humphreys, 1998; Thatcher and others, 1999).

The orientation of normal faults within the Basin and Range is consistent with the orientation of stresses needed to produce right-lateral slip along the San Andreas fault system. A portion of the Pacific–North American relative plate motion is taken up by displacement and deformation in the Basin and Range Province, with relative motion between the Sierra Nevada – Great Valley microplate and the central Great Basin, indistinguishable from the Pacific – North American plate motion (Bennett and others, 2003). Motion west of about  $118^\circ$  W is in agreement with Pacific Plate motion (Thatcher and others, 1999; Hammond and Thatcher, in press), suggesting coupling of the plate motion.

Geodetic measurements show concentrated deformation at the eastern (~50 km) and western (~200 km) edges of the region, coinciding with regions of modern seismicity, and with little deformation in between (Thatcher and others, 1999; Bennett and others, 2003; Hammond and Thatcher, in press). The style of Basin and Range deformation varies across six tectonic domains delimited by strain transitions. The greatest deformation takes place across a zone of conjugate strike-slip and normal faults, at a rate of  $12.5 \pm 0.15$  mm/year between  $119.1^\circ$ W and  $120.2^\circ$ W. More recent data confirm this observation, with velocities west of  $117.7^\circ$ W increasing from ~1 mm/yr to ~12 mm/yr (Bennett and others, 2003; Hammond and Thatcher, in press). Strain rates increase from north to south along this western boundary of the region (Bennett and others, 2003). These high velocity gradients imply high seismic risk, increasing the potential for more frequent damaging earthquakes.

We studied the relation between the spatial pattern of seismicity and geodetic strain in the Basin and Range Province. We also compare historical earthquake occurrence rates with those inferred from geodetic strain rates. The rate comparison is quantified as a comparison of seismic-moment rates, as seismic moment is related to both the amount of deformation and the consequent character of ground motions measured on seismograms.

## ANALYSIS AND RESULTS

Figure 1 outlines the study area. The southwestern boundary of the study area runs down the crest of the rigid Sierra Nevada Range, California, and extends on the same trend to include regions in the Mojave Desert where deformation is more related to the northward motion of the Sierra Nevada mountains than to the main motion of the San Andreas fault.

We estimated seismic-moment rates from a new catalog of earthquakes intended to be complete for magnitude  $M \geq 5$  (Figure 1). Earthquakes within the study region with  $M \geq 4.8$  in any of 15 preexisting catalogs were supplemented by the results of 42 journal articles. The final catalog has 800 earthquakes, and 487 earthquakes with  $M \geq 5.0$  since 1855. Several of the catalogs and individual studies include an earthquake in 1852 in western Nevada, with  $M=7.3$ . The anecdotal evidence for this earthquake is not sufficient to assign a magnitude and location that is reliable enough for this study.

For most earthquakes, we estimated seismic moment from magnitude, but moment -magnitude ( $M_w$ ) estimates were selected when available. For the most significant events, where many  $M_w$  estimates are available, we established criteria to select the most favored  $M_w$  value. The Harvard long period surface-wave estimates of the seismic moment have been consistent for the past 27 years and hence we gave them primary preference. Other surface-wave estimates, followed by body-wave, geological, and geodetic estimates were then

considered. For the other earthquakes, care was taken to avoid inflated magnitude estimates, usually by using the smallest magnitude from any catalog. This yields a lower-bound estimate for the occurrence rate of moderate-sized earthquakes.

The magnitudes were then treated as moment magnitude. We estimated the seismic moment of each event using the relation (Hanks and Kanamori, 1978)

$$M_o = 10^{\frac{3}{2}M_w + 16.05} \quad (1).$$

We confirmed this relation for moderate-magnitude earthquakes in Nevada.

Considering completeness intervals for various magnitudes, the discrete Gutenberg–Richter relation for the number of earthquakes,  $n$ , equal to magnitude  $M \pm 0.5$  is  $\log n = 5.83 - 1.01M$ . Using cumulative rates of occurrence over appropriate catalog durations, we obtained a relation of  $\log N = 6.27 - 1.09M$ , predicting 4.4 earthquakes per century with  $M_w \geq 7.0$ , 0.53 earthquakes per year with  $M_w \geq 6.0$ , and 6.6 earthquakes per year with  $M_w \geq 5.0$ . The  $b$ -value for either relation is typical. Of the total moment, 80% was released during 10 earthquakes of magnitude  $M_w \geq 6.79$ , and 90% was released in the 29 events of  $M_w \geq 6.3$ . Thus small events do not significantly release accumulating strain.

Figures 2.1, 2.2 and 2.3 show the spatial distribution of earthquake numbers, of moment release, and of crustal deformation as a function of perpendicular distance from the southwestern boundary of the study region. Three domains, each 300 km wide as illustrated in Figure 1, are shown, a southern ( $\sim 35^\circ\text{N}$ ), a central ( $\sim 37^\circ\text{N}$ ) and a northern zone ( $\sim 40^\circ\text{N}$ ). The geodetic profile utilizes averaged geodetic rates (Blewitt and others, 2002). Deformation is concentrated within a zone about 200 km wide along the southwestern edge of the Province, coinciding with the northern Walker Lane Belt (Stewart, 1988). The plots show that the spatial patterns of seismic activity, seismic moment, and geodetic deformation are similar along all of the profiles. They all clearly show a northward

widening of the deformation zone along the western edge of the Province. Within the southern domain (Figure 2.1), deformation is concentrated within a 50 km zone, accommodating about 60% of the geodetic deformation, 60% of the seismic-moment rate, and 70% of the earthquakes. Across the central domain, the earthquake count and geodetic deformation follow the same trend with 85% of the earthquakes and 85% to 95% of the geodetic deformation occurring within a 200 km zone. This is in contrast to the seismic-moment rate, 95% of which is released within 30 km of the western edge, the moment release being dominated by the 1872 Owens Valley event (Table 2), the largest event in the catalog. The greatest deformation rate evident from the geodetic data occurs across a 100 km zone. The northern domain has 90% of its earthquakes, 60% of the moment release, and 70% to 90% of the geodetic deformation occurring across a 200 km zone. Deformation is dominated by seismic activity in 1954, which includes four of the largest events in the region, and the Cedar Mountain earthquake (Table 2), along with associated aftershocks.

Figure 2.4 shows that activity along the eastern half of the Great Basin is significantly less than in the west. The greatest increase on all three rates in Figure 2.4 occurs at the very eastern edge of the Basin and Range. About 25% of the earthquakes and 18% of the seismic moment are concentrated east of  $113^\circ\text{W}$ . Less than about 8% of the deformation measured with GPS occurs there.

Some uncertainties affect Figure 2. The earthquake count lacks aftershocks of the 1872 Owens Valley (southwestern domain) and the 1915 Pleasant Valley (Table 2) (northwestern domain) earthquakes, the 1872 earthquake being the largest in the catalog. If those aftershocks were included, the earthquake rate might also become as concentrated as the seismic moment in the western part of the profile. In general, all curves within the scatter of the data, the spatial patterns of seismic activity, seismic moment, and geodetic deformation are the same.

We estimate the historical seismic-moment rate from Figure 3a using a statistical approach. Seismic moment is a tensor. Here we use the magnitude of

the maximum eigenvalue. Although tensor information is available for the ten largest earthquakes, which release 80% of the total seismic moment, use of tensors increases the number of degrees of freedom, and therefore requires a longer observation time to obtain a reliable comparison. A fit to the end points of the cumulative-rate curve with time gives an average rate of  $9.02 \times 10^{25}$  dyne-cm/year. Figure 3a shows a non-unique, but plausible rationale for moment rates as low as  $6.05 \times 10^{25}$ , or as high as  $10.06 \times 10^{25}$  dyne-cm/year. A least-squares fit to the points in Figure 3a (1 point for each year with an earthquake) has a slope of  $7.28 \pm 0.5 \times 10^{25}$  dyne-cm/yr. Note that the lower bound on the cumulative moment corresponds to the upper bound on the moment-rate estimate from historical earthquakes. To quantify and assess uncertainties associated with these seismic-moment rates, we repeated the procedure shown in Figure 3a, using (1) upper-bound estimates of the smaller events, and (2) Monte Carlo realizations.

We repeated the earthquake magnitude selection for the smaller events without  $M_w$  estimates, with the largest magnitude of any listed catalog selected as the favored magnitude instead of the smallest. This yields a catalog representing an upper bound estimate for the occurrence rate. Figure 3b shows the results of using this upper bound catalog. A fit to the end points of the cumulative-rate curve gives an average rate of  $10.07 \times 10^{25}$  dyne-cm/year. Figure 3b shows moment rates as low as  $6.56 \times 10^{25}$ , or as high as  $10.83 \times 10^{25}$  dyne-cm/year, while a least-squares fit to the points give a slope of  $7.93 \pm 0.5 \times 10^{25}$  dyne-cm/yr.

The procedure in Figure 3a was automated and repeated for randomly chosen moments of the ten largest earthquakes, which control the total moment release. We selected the moment release for each of these events randomly assuming a constant probability density between minimum and maximum  $M_w$  estimates. The maximum and minimum  $M_w$  values were selected based on the most reliable and appropriate estimates of  $M_w$  from the literature (Table 2). We held the moment release for all other earthquakes constant at the

favored values based on lower bound estimates. Data points corresponding to those used to calculate rates shown in Figure 3a were applied. We generated a total of 50,000 Monte Carlo realizations. From these realizations, distribution of the minimum, average, and maximum rates are shown in Figure 4 and summarized in Table 3 along with results from Figure 3. A least-squares fit to each realization was also calculated. Considering one standard deviation about the mean values, the moment rate ranges from  $5.07 \times 10^{25}$  to  $8.67 \times 10^{25}$  dyne-cm/yr (Table 3). Extremes selected by the visual approach (Figure 3) are outside the two-standard-deviation limits of the least-squares fit. The absolute range of moment rates determined via the Monte Carlo method range from  $4.17 \times 10^{25}$  to  $10.09 \times 10^{25}$  dyne-cm/year (Table 3). Thus limits on the moment rate from historical seismicity are  $4.2 \times 10^{25}$  to  $10.8 \times 10^{25}$  dyne-cm/year.

The range of moment rates, determined above, can be compared with moment rates that can be estimated from the geodetic deformation rates. To do this we need models that relate the deformation rates to moment rates. Methods to estimate moment rates from the crustal deformation rates are available in the literature, assuming all deformation occurs seismically. For a fault with average geological slip rate  $\dot{s}$ , the moment rate is predicted to be

$$\dot{M}_o = \mu A \dot{s} \quad (2).$$

where  $\mu$  is the shear modulus, and  $A$  is the total area of fault that ruptures seismogenically (Brune, 1968). As this equation is independent of the width of the zone, it can be extended for a volume subjected to a uniform stress field, in which all faults are parallel to the margin. Where crustal deformation is expressed as a broad zone of deformation, with numerous faults of variable orientation and importance, it is appropriate to use regional strain rates instead of the slip rate. Techniques have been proposed to translate the tensor geodetic strain rate into rates of scalar seismic moment release. Kostrov (1974) and Ward (1998a) relate the average strain rate over a volume and the sum of earthquake moment tensors. The moment rate is reduced to a scalar quantity by replacing the tensor strain rate by

its largest eigenvalue and the tensor -moment rate by a scalar quantity. An assumption is made that the average surface strain is representative of the volume strain at depth. Methods to estimate moment rates from the crustal-strain rates are available in the literature; however, there is variation in the literature over the best scalar representation of surficial strain.

Anderson (1979) modeled a volume extending or contracting in one direction, (say  $x_2$ ), presenting a best estimate solution to the problem as

$$\dot{M}_o = 2\mu L_1 L_2 W \dot{\epsilon}_2 / k \quad (3).$$

where  $L_1$  is the length of the region,  $L_2$  is the width of the region in the direction that it is straining,  $W$  is the seismogenic thickness, and  $\dot{\epsilon}_2$  is the strain rate. The strain rate in turn is given by  $\dot{\epsilon}_2 = V_2 / L_2$  where  $V_2$  is the relative extension or convergence velocity of the opposite sides of the region. Parameter  $k$  is a dimensionless constant that adjusts for the inefficiency of randomly oriented faults to accommodate strain.

Ward (1994, 1998a, b) proposes a minimum rate, which incorporates the maximum eigenvalue i.e., the principle surficial extension and contraction rates with

$$\dot{M}_o = 2\mu W \Sigma \text{Max}(|\dot{\epsilon}_1|, |\dot{\epsilon}_2|) \quad (4).$$

where  $\dot{\epsilon}_1$  and  $\dot{\epsilon}_2$  are the principle surficial extension and contraction rates, and  $\Sigma$  is the surface area of the region. The Working Group on California Earthquake Probabilities (1995) also uses a minimal approach to represent the moment-rate tensor, utilizing the difference between the principal strain rates as expressed by equation 5.

$$\dot{M}_o = 2\mu W \Sigma (\dot{\epsilon}_1 - \dot{\epsilon}_2) \quad (5).$$

Correspondence of the scalar moment rate with a given surface strain accumulation is non-unique. Savage and Simpson (1997) emphasize that the moment tensor is resolved into the superposition of two or more double-couple mechanisms, and this resolution can be done in many ways. Savage and Simpson (1997) therefore suggest the preferred estimate is that which produces the smallest scalar-moment rate, equivalent to the principal surface-strain rates acting over a region, given by:

$$\dot{M}_o^{(\min)} = 2\mu W \Sigma \text{Max}(|\dot{\epsilon}_1|, |\dot{\epsilon}_2|, |\dot{\epsilon}_1 + \dot{\epsilon}_2|) \quad (6).$$

Recognizing the area  $\Sigma$  in Equations (4), (5), and (6) to be equivalent to  $L_1 L_2$  in Equation (3), these equations are similar. Equation (6) accommodates strain in multiple directions but if strain is only in the  $x_2$  direction the strain rate terms are identical. Equation (3) converges to Equation (6) when  $k=1$ . Savage and Simpson (1997) noting that their method gives similar results to Ward (1994, 1998a, b) and only differs if  $\dot{\epsilon}_1$  and  $\dot{\epsilon}_2$  have the same sign, while the Working Group representation is much less.

Acknowledging the non-uniqueness and uncertainty involved with converting surface strain to a scalar-moment rate, this study utilizes all four methods discussed above to help quantify the moment rate from geodesy and its associated errors. We take the shear modulus to be  $\mu=3 \times 10^{11}$  dyne/cm<sup>2</sup> (Anderson, 1979) and assume all deformation occurs seismically above a brittle-ductile transition depth of  $W=15$  km, determined from the depth distribution of earthquakes. For a particular assumption about a random distribution of fault orientation, Anderson (1979) found  $k=0.64$ , probably giving a lower limit to this parameter. Total scalar moment and deformation rates for central Asia and southern California are consistent with  $k=0.75$  (Anderson, 1979; Chen and Molnar, 1979), and therefore we applied that value in this study.

We predict the moment rate for the Basin and Range Province from geodetic, Satellite Laser Ranging, and Very Long Baseline Interferometry data obtained across the Basin and Range from more than 42 studies and inverted for strain-rate-tensor components (Blewitt and others, 2002). While the bi-cubic Bessel interpolation of the data smoothes the data to a degree, additional smoothing is applied to account for the distribution of geodetic data. We used both the unsmoothed data (underdamped), and smoothed data (damped) in separated calculations to estimate the moment release from the geodetic deformation rates. Table 4 summarizes the results. Resulting moments from

geodesy are in the range from  $5.87 \times 10^{25}$  to  $21.41 \times 10^{25}$  dyne-cm/year.

We utilized fault parameters used as input to the 1996 and 2002 USGS seismic hazard maps (Frankel and others, 1996, 2000) to determine the moment rate from geology from Equation (2). Data for California come from the 1996 model, while all other data for the study region come from the 2002 model. We assume  $\mu=3 \times 10^{11}$  dyne/cm<sup>2</sup>. Resultant geological-moment rates for the region are much lower than both the seismicity and geodetic rates (Table 5, Figure 5). This is not surprising considering the limited paleoseismic data. Uncertainties associated with the measurement of the fault parameters, would reflect in uncertainties in the moment rate presented here. Although beyond the scope of this study, inclusion of these uncertainties may result in the geological-moment rate being of the same order of magnitude as the seismicity rate.

Rates determined from seismicity, of  $4.5 \times 10^{25}$  to  $10.8 \times 10^{25}$  dyne-cm/year, substantially overlap the range determined from the geodetic data,  $5.87 \times 10^{25}$  to  $21.41 \times 10^{25}$  dyne-cm/year (Figure 5). This suggests that the rate of historic earthquakes within the Basin and Range Province, taken as a whole, is within a factor of two of the rate that should be expected in the future. Following from the suggestion of Smith (1976) and Ward (1998a), we define  $Z = T\Sigma\bar{\epsilon}$ , the product of the duration of the earthquake record ( $T$ ), the area of the region, and the average strain rate,  $\bar{\epsilon}$ . For  $T=146$  years,  $\Sigma=1.28 \times 10^6$  km<sup>2</sup>, and  $\bar{\epsilon}=1.2 \times 10^{-8}$ /yr,  $Z \approx 2.2$  km<sup>2</sup>. Based on these Basin and Range results, it is reasonable to expect that in other regions with  $Z \geq 2$  km<sup>2</sup>, historical seismicity and geodesy will agree within uncertainties of about a factor of two.

## CONCLUSIONS

The most important conclusion of this study is that the geodetic spatial distribution is consistent with the spatial distribution of the seismic-moment release, and that the rate of earthquakes implied by geodesy is consistent with the historical estimate.

Assuming this is confirmed elsewhere, this result has worldwide implications. The adequacy of seismic catalogs for seismic-hazard analysis is governed by the product of the area of interest, catalog duration (Smith, 1976), and regional strain rate (Ward, 1998a); the catalog duration is almost always insufficient. Geological data on fault slip rates are quite difficult to obtain, as the appropriate fault exposures necessary to obtain slip rates and magnitudes of past earthquakes are often not available. Geodetic data, in contrast, are relatively easily obtained with just a few years of observations. With deformation rates from space geodesy, seismic-hazard and recurrence estimates can become much more reliable on a global scale.

## ACKNOWLEDGMENTS

We thank Feng Su for a helpful review and Steven Wesnousky, Bob Wallace, and anonymous reviewers for their helpful comments and suggestions. This research was supported by the U.S. Geological Survey National Earthquake Hazards Reduction Program under award number 01HQGR0012.

## BIBLIOGRAPHY

Pancha A., and Anderson J. G., 2004, Comparison of seismic and geodetic scalar moment rates across the Basin and Range province: Bulletin of the Seismological Society of America, in preparation.

## REFERENCES

- Anderson, J. G., 1979, Estimating the seismicity from geological structure for seismic-risk studies: Bulletin of the Seismological Society of America, v. 69, no. 1, p. 135-158.
- Anderson, J. G., and Brune, J. N., 1999, Methodology for using precarious rocks in Nevada to test seismic hazard models: Bulletin

- of the Seismological Society of America, v. 89, no. 2, p. 456-467.
- Barker, M. R., and Doser, D. I., 1988, Joint inversion of regional and teleseismic earthquake waveforms: *Journal of Geophysical Research*, v. 93, no. B3, p. 2,037-2,045.
- Beanland, S., and Clarke, M. M., 1993 Late Quaternary history of the Owens Valley fault zone, eastern California and surface rupture associated with the 1872 earthquakes: *Geological Society of America, Abstracts with Programs*, v. 25, no. 5, p. 7.
- Bennett, R. A., Wernicke, B. P., Niemi, N. A., Friedrich, A. M., and Davis, J. L., 2003, Contemporary strain rates in the northern Basin and Range Province from GPS data: *Tectonics*, v. 22, no. 2, p. 3-1 – 3-31, doi:10.1029/2001TC1355.
- Blewitt, G., Coolbaugh, M., Holt, W., Kreemer, C., Davis, J., and Bennett, R., 2002, Targeting of potential geothermal resources in the Great Basin from regional relationships between geodetic strain and geological structures: *Transactions Geothermal Resources Council*, v. 26, p. 523-526.
- Brune, J. N., 1968, Seismic moment, seismicity, and slip rate along major fault zones: *Journal of Geophysical Research*, v. 73, no. 2, p. 777-784.
- Chen, W.-P., and Molnar, P., 1977, Seismic moments of major earthquakes and the average rate of slip in central Asia: *Journal of Geophysical Research*, v. 82, no. p. 20, 2945-2969.
- Doser, D. I., 1985, Source parameters and faulting processes of the 1959 Hebgen Lake, Montana, earthquake sequence: *Journal of Geophysical Research*, v. 90, no. B6, p. 4537-4555.
- Doser, D. I., 1986, Earthquake processes in the Rainbow Mountain-Fairview Peak-Dixie Valley, Nevada, region 1954-1959: *Journal of Geophysical Research*, v. 91, no. B12, p. 12,572-12,586.
- Doser, D. I., 1988, Source parameters of earthquakes in the Nevada seismic zone, 1915-1943: *Journal of Geophysical Research*, v. 93, no. B12, p. 15,001-15,015.
- Doser, D. I., and Kanamori, H., 1987, Long-period surface waves of four western United States earthquakes recorded by the Pasadena strainmeter: *Bulletin of the Seismological Society of America*, v. 77, no. 1, p. 236-243.
- Doser, D. I., and Smith, R. B., 1985, Source parameters of the 28 October 1983 Borah Peak, Idaho, earthquake from body wave analysis: *Bulletin of the Seismological Society of America*, v. 75, no. 4, p. 1041-1051.
- Doser, D. I., and Smith, R. B., 1989, An assessment of source parameters of earthquakes in the Cordillera of the western United States: *Bulletin of the Seismological Society of America*, v. 79, no. 5, p. 1383-1409.
- Frankel, A., Mueller, C., Barnhard, T., Perkins, D., Leyendecker, E., Dickman, N., Hanson, S., and Hopper, M., 1996, National seismic-hazard maps: Documentation June 1996: U.S. Geological Survey, Open-File Report 96-532, 110 p.
- Frankel, A. D., Petersen, M. D., Mueller, C. S., Haller, K. M., Wheeler, R. L., Leyendecker, E. V., Wesson, R. L., Harmsen, S. C., Cramer, C. H., Perkins, D. M., and Rukstales, K. S., 2002, Documentation for the 2002 Update of the National Seismic Hazard Maps: U.S. Geological Survey Open-File Report 02-420, 33 p.
- Hammond, W. C., and Thatcher, W., 2004, Contemporary tectonic deformation of the Basin and Range Province, western United States - 10 years of observation with the Global Positioning System: *Journal of Geophysical Research*, in press.
- Hanks, T. C., and Kanamori, H., 1978, A moment magnitude scale: *Journal of Geophysical Research*, v. 84, no. B5, p. 2348-2350.
- Hanks, T. C., Hileman, J. A., and Thatcher, W., 1975, Seismic moments of the larger earthquakes of the Southern California region: *Geological Society of America Bulletin*, v. 86, no. 8, p. 1131-1139.
- Humphreys, E. D., Hemphill-Haley, M. A., and Coblenz, D. D., 1998, Processes of ongoing deformation in the western United States: *American Geophysical Union, EOS Transactions*, v. 79, F558
- Jones, C. H., Unruh, J. R., and Sonder, L. J., 1996, The role of gravitational potential energy in active deformation in the southwestern United States: *Nature*, v. 381, no. 6577, p. 37-41.

- Kostrov, V. V., 1974, Seismic moment and energy of earthquakes, and seismic flow of rock: *Earth Physics*, v. 1, p. 23-40.
- Lachenburch, A. H., and Morgan, P., 1990, Continental extension, magmatism and elevation-formal relations and rules of thumb: *Tectonophysics*, v. 174, no. 1-2, p. 39-62.
- Mason, D. B., 1996, Earthquake magnitude potential of the Intermountain seismic belt, USA, from surface-parameter scaling of late Quaternary faults: *Bulletin of the Seismological Society of America*, v. 86, no. 5, p. 1487-1506.
- Savage, J. C., and Hastie, L. M., 1969, A dislocation model for the Fairview Peak, Nevada, earthquake: *Bulletin of the Seismological Society of America*, v. 59, no. 5, p. 1937-1948.
- Savage, J. C., and Simpson, R. W., 1997, Surface strain accumulation and the seismic moment tensor: *Bulletin of the Seismological Society of America*, v. 87, no. 5, p. 1345-1353.
- Shen-Tu, B., Holt, W. E., and Haines, A. J., 1998, Contemporary kinematics of the western United States determined from earthquake moment tensors, very long baseline interferometry, and GPS observations: *Journal of Geophysical Research*, v. 103, no. B8, p. 18,087-18,117.
- Shen-Tu, B., Holt, W. E., and Haines, A. J., 1999, Deformation kinematics in the western United States determined from Quaternary fault slip rates and geodetic data: *Journal of Geophysical Research*, v. 104, no. B12, p. 28,927-28,955.
- Sieh, K. E., Jones, L. M., Hauksson, E., Hudnut, K. W., Eberhart-Phillips, D., Heaton, T. H., Hough, S. E., Hutton, L. K., Kanamori, H., Lilje, A., Lindvall, S. C., McGill, S. F., Mori, J. J., Rubin, C. M., Spotila, J. A., Stock, J. M., Thio, H. K., Treiman, J. A., Wernicke, B. P., and Zachariassen, J., 1993, Near-field investigations of the Landers earthquake sequence, April to July 1992: *Science*, v. 260, no. 1505, p. 171-176.
- Smith, S. W., 1976, Determination of maximum earthquake magnitude: *Geophysical Research Letters*, v. 3, no. 6, p. 351-354.
- Stewart, J. H., 1988, Tectonics of the Walker Lane Belt, western Great Basin; Mesozoic and Cenozoic deformation in a shear zone, *in* Ernst, W. G., editor, *Metamorphism and crustal evolution of the Western United States*, v. 7. Englewood Cliffs, New Jersey, Prentice-Hall, p. 683-713.
- Thatcher, W., Foulger, G. R., Julian, B. R., Svarc, J., Quilty, E., and Bawden, G. W., 1999 Present-day deformation across the Basin and Range Province, western United States: *Science*, v. 283, no. 5408, p. 1714-1718.
- Ward, S. N., 1994, A multidisciplinary approach to seismic hazard in Southern California: *Bulletin of the Seismological Society of America*, v. 84, no. 5, p. 1293-1309.
- Ward, S. N., 1998a, On the consistency of earthquake moment rates, geological fault data, and space geodetic strain - the United States: *Geophysical Journal International*, v. 134, no. 1, p. 172-186.
- Ward, S. N., 1998b, On the consistency of earthquake moment rates, geological fault data, and space geodetic strain - Europe: *Geophysical Journal International*, v. 135, no. 3, p. 1011-1018.
- Wells, D. L., and Coppersmith, K. J., 1994, New empirical relationships among magnitude, rupture length, rupture width, rupture area, and surface displacement: *Bulletin of the Seismological Society of America*, v. 84, no. 4, p. 974-1002.
- Wernicke, B., 1992, Cenozoic extensional tectonics of the U.S. Cordillera, *in* Lipman, P. W., Burchfiel, B. C., and Zoback, M. L., editors, *The Cordilleran Orogen- Conterminous U.S.:* Geological Society of America, *The Geology of North America*, v. G-3, p. 553-581.
- Working Group on California Earthquake Probabilities (1995), *Seismic hazards in southern California: probable earthquakes, 1994-2024*, *Bull. Seism. Soc. Am.*, 85, 379-439.

**Table 1: Catalogs included in the compiled earthquake database.**

Catalogs Searched	Abbreviation	Web Address
Historical and Preliminary Data	PDE	<a href="http://www.neic.cr.usgs.gov/neis/epic/epic.html">http://www.neic.cr.usgs.gov/neis/epic/epic.html</a>
Significant Earthquakes Worldwide	NOAA	<a href="http://www.neic.cr.usgs.gov/neis/epic/epic.html">http://www.neic.cr.usgs.gov/neis/epic/epic.html</a>
Significant US Earthquakes	USHIS	<a href="http://www.neic.cr.usgs.gov/neis/epic/epic.html">http://www.neic.cr.usgs.gov/neis/epic/epic.html</a>
California	CDMG	<a href="http://www.neic.cr.usgs.gov/neis/epic/epic.html">http://www.neic.cr.usgs.gov/neis/epic/epic.html</a>
Canada	EPB	<a href="http://www.neic.cr.usgs.gov/neis/epic/epic.html">http://www.neic.cr.usgs.gov/neis/epic/epic.html</a>
Mexico, Central America, Caribbean	NGDC	<a href="http://www.neic.cr.usgs.gov/neis/epic/epic.html">http://www.neic.cr.usgs.gov/neis/epic/epic.html</a>
Eastern, Central and Mountain States	SRA	<a href="http://www.neic.cr.usgs.gov/neis/epic/epic.html">http://www.neic.cr.usgs.gov/neis/epic/epic.html</a>
Nevada Seismological Laboratory, University of Nevada, Reno	UNR1852	<a href="http://www.seismo.unr.edu/Catalog/catalog-search.html">www.seismo.unr.edu/Catalog/catalog-search.html</a>
University of California, Berkeley	BK	<a href="http://quake.geo.berkeley.edu/ncedc/catalog-search.html">http://quake.geo.berkeley.edu/ncedc/catalog-search.html</a>
Council of the National Seismic System	CNSS	<a href="http://quake.geo.berkeley.edu/cnss-catalog.html">http://quake.geo.berkeley.edu/cnss-catalog.html</a>
Pasadena	SCSN	<a href="http://www.scecdc.scec.org/catalogs.html">www.scecdc.scec.org/catalogs.html</a>
Northern California Earthquake Data Center	NCSN	<a href="http://quake.geo.berkeley.edu/cnss/catalog-search.html">http://quake.geo.berkeley.edu/cnss/catalog-search.html</a>
Utah (regional and historic)		<a href="http://www.quake.utah.edu/catalog/catalog.shtml">www.quake.utah.edu/catalog/catalog.shtml</a>
Yellowstone		<a href="http://www.quake.utah.edu/catalog/ynp.shtml">http://www.quake.utah.edu/catalog/ynp.shtml</a>
Harvard		<a href="http://www.seismology.harvard.edu/CMTsearch.html">http://www.seismology.harvard.edu/CMTsearch.html</a>

Table 2: Ten largest events in the compiled catalog.

Year	Month	Day	Hour	Minute	Latitude	Longitude	Preferred Magnitude $M_w$	Minimum Magnitude $M_w$	Maximum Magnitude $M_w$	Earthquake Name
1872 <sup>1</sup>	3	26	10	30	36.70	-118.10	7.74	7.44	7.74	Owens Valley
1915 <sup>2</sup>	10	3	6	53	40.50	-117.50	7.18	6.82	7.18	Pleasant Valley
1932 <sup>3</sup>	12	21	6	10	38.80	-117.98	7.10	6.80	7.10	Cedar Mountain
1954 <sup>4</sup>	8	24	5	51	39.60	-118.50	6.76	6.27	6.76	Stillwater
1954 <sup>5</sup>	12	16	11	7	39.20	-118.00	7.12	6.91	7.35	Fairview Peak
1954 <sup>6</sup>	12	16	11	11	39.67	-117.90	6.92	6.60	7.15	Dixie Valley
1959 <sup>7</sup>	8	18	6	37	44.88	-111.10	7.32	7.25	7.42	Hebgen Lake
1983 <sup>8</sup>	10	28	14	6	44.96	-113.90	6.93	6.70	7.20	Borah Peak
1992 <sup>9</sup>	6	28	11	57	34.20	-116.44	7.29	7.22	7.30	Landers
1999 <sup>10</sup>	10	16	9	46	34.59	-116.27	7.12	7.10	7.12	Hector Mine

<sup>1</sup> The preferred and maximum magnitude is from Hanks and others (1975), the minimum is from Beanland and Clarke (1993).

<sup>2</sup> The preferred and maximum magnitude is from Wells and Coppersmith (1994), the minimum is from Doser (1988).

<sup>3</sup> The preferred and maximum magnitude is from Wells and Coppersmith (1994), the minimum is from Doser (1986) and Doser and Smith (1989).

<sup>4</sup> The preferred and maximum magnitude is from Mason (1996), the minimum is from Barker and Doser (1988).

<sup>5</sup> The preferred magnitude is from Doser and Smith (1989), the maximum and minimum are from Doser and Kanamori (1987) and Doser (1986) respectively.

<sup>6</sup> The preferred magnitude is from Doser and Kanamori (1987), the maximum and minimum are from Doser and Kanamori (1987) and Doser and Smith (1989) respectively.

<sup>7</sup> The preferred magnitude is from Doser and Smith (1989), the maximum is from Savage and Hastie (1969) and minimum is from Doser (1985) and from Doser and Smith (1989).

<sup>8</sup> The preferred magnitude is from the Harvard catalog, the maximum and minimum are from Mason (1996) and Doser and Smith (1985) respectively.

<sup>9</sup> The preferred magnitude is from the Harvard catalog, the maximum and minimum are from Seih and others (1993) and Wells and Coppersmith (1994) respectively.

<sup>10</sup> The preferred and maximum magnitude is from the Harvard catalog, the minimum is from UC Berkeley and the Council of the National Seismic System catalogs.

Table 3: Statistical distribution of seismic moment rates determined from 5000 Monte Carlo simulations.

Seismic Moment Rate dyne-cm/year	Preferred	Upper Bound	Minimum	Maximum	Mean	Standard Deviation
Visual Lower Bound	$6.05 \times 10^{25}$	$6.56 \times 10^{25}$	$4.17 \times 10^{25}$	$6.64 \times 10^{25}$	$5.42 \times 10^{25}$	$0.35 \times 10^{25}$
Visual Upper Bound	$10.06 \times 10^{25}$	$10.83 \times 10^{25}$	$5.72 \times 10^{25}$	$10.09 \times 10^{25}$	$7.92 \times 10^{25}$	$0.75 \times 10^{25}$
End Points	$9.02 \times 10^{25}$	$10.07 \times 10^{25}$	$5.16 \times 10^{25}$	$9.04 \times 10^{25}$	$7.11 \times 10^{25}$	$0.67 \times 10^{25}$
Least Squares	$7.28 \times 10^{25}$	$7.93 \times 10^{25}$	$4.45 \times 10^{25}$	$7.78 \times 10^{25}$	$6.15 \times 10^{25}$	$0.47 \times 10^{25}$

Table 4. Moment rates from Geodesy

Citation	Equation *	Moment Rate dyne-cm/yr	
		Damped	Underdamped
Anderson (1979)	$\dot{M}_o = 2\mu L_1 L_2 W \dot{\epsilon}_2 / k$	$10.31 \times 10^{25}$	$21.41 \times 10^{25}$
Ward (1994, 1998a, b)	$\dot{M}_o = 2\mu W \Sigma \text{Max}( \dot{\epsilon}_1 ,  \dot{\epsilon}_2 )$	$7.73 \times 10^{25}$	$16.06 \times 10^{25}$
Working Group (1995)	$\dot{M}_o = 2\mu W \Sigma (\dot{\epsilon}_1 - \dot{\epsilon}_2)$	$5.87 \times 10^{25}$	$11.47 \times 10^{25}$
Savage and Simpson (1997)	$\dot{M}_o^{(\text{min})} = 2\mu W \Sigma \text{Max}( \dot{\epsilon}_1 ,  \dot{\epsilon}_2 ,  \dot{\epsilon}_1 + \dot{\epsilon}_2 )$	$7.89 \times 10^{25}$	$16.55 \times 10^{25}$

\* Where  $L_1$  is the length of the region,  $L_2$  is the width of the region in the direction that it is straining,  $W$  is the seismogenic thickness,  $\dot{\epsilon}_2 = V_2 / L_2$  where  $V_2$  is the relative extension or convergence velocity of the opposite sides of the region,  $\dot{\epsilon}_1$  and  $\dot{\epsilon}_2$  are the principle surficial extension and contraction rates, and  $\Sigma$  is the surface area of the region,  $k$  is a dimensionless constant that adjusts for the inefficiency of randomly oriented faults to accommodate strain.

*Table 5: Comparison of moment rates for the Basin and Range province.*

<b>Data/Method*</b>		<b>Moment Rate (dyne-cm/yr)</b>
<b>1. Seismicity</b>		4.17 to 10.09 $\times 10^{25}$
<b>2. Geodesy</b>		5.87 to 21.41 $\times 10^{25}$
<b>3. Geology</b>	<b>USGS 2002/1996 data <math>\dot{M}_o = \mu A \dot{s}</math></b>	2.54 $\times 10^{25}$

\* Assuming  $\mu=3 \times 10^{11}$  dyne/cm<sup>2</sup> for geodesy and geology.

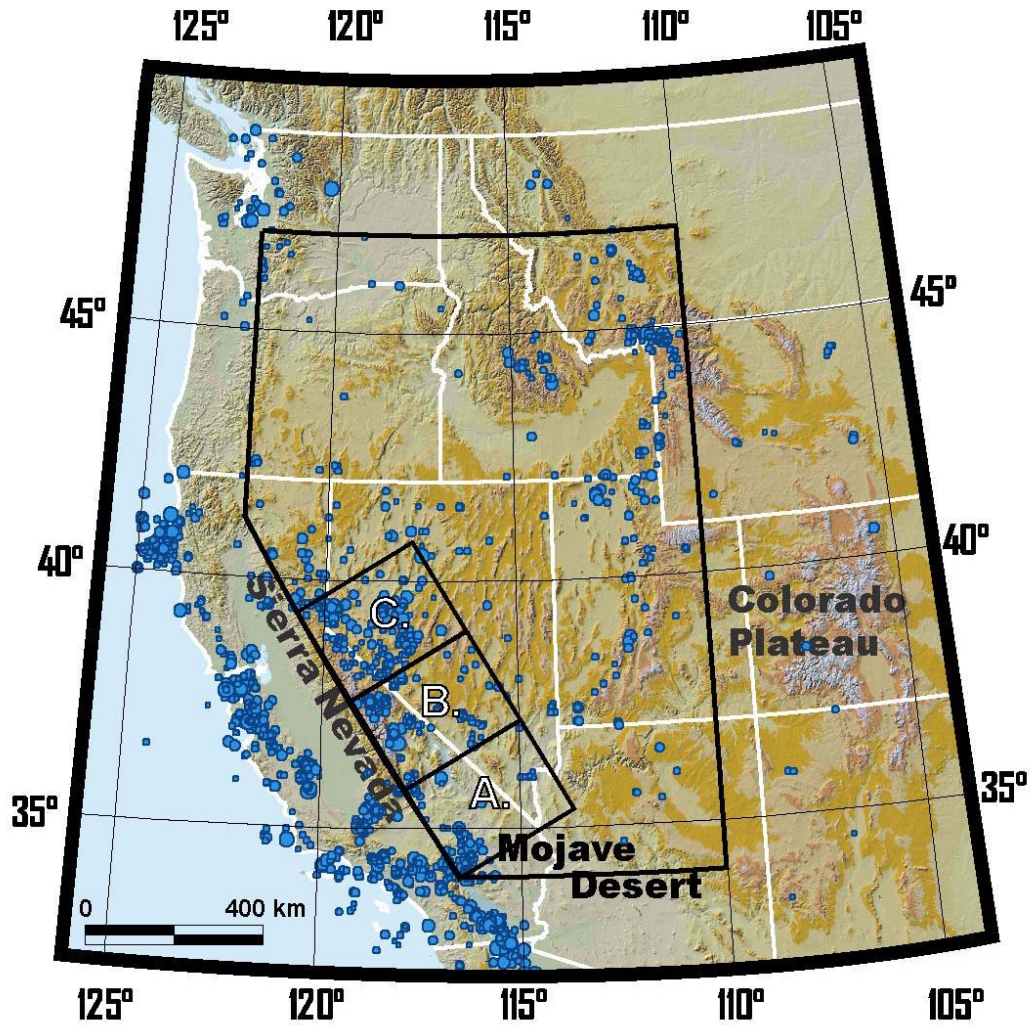


**Figure 1:** Map of the western United States, showing topography, earthquakes with  $M \geq 4.8$  (blue circles with radius proportional to magnitude). The study area, outlined with a bold polygon, encloses all major earthquakes that can be associated with deformation of the Basin and Range Province. Regions A, B and C refer to the Southwestern, Central and Northwestern sub regions shown in Figure 2.

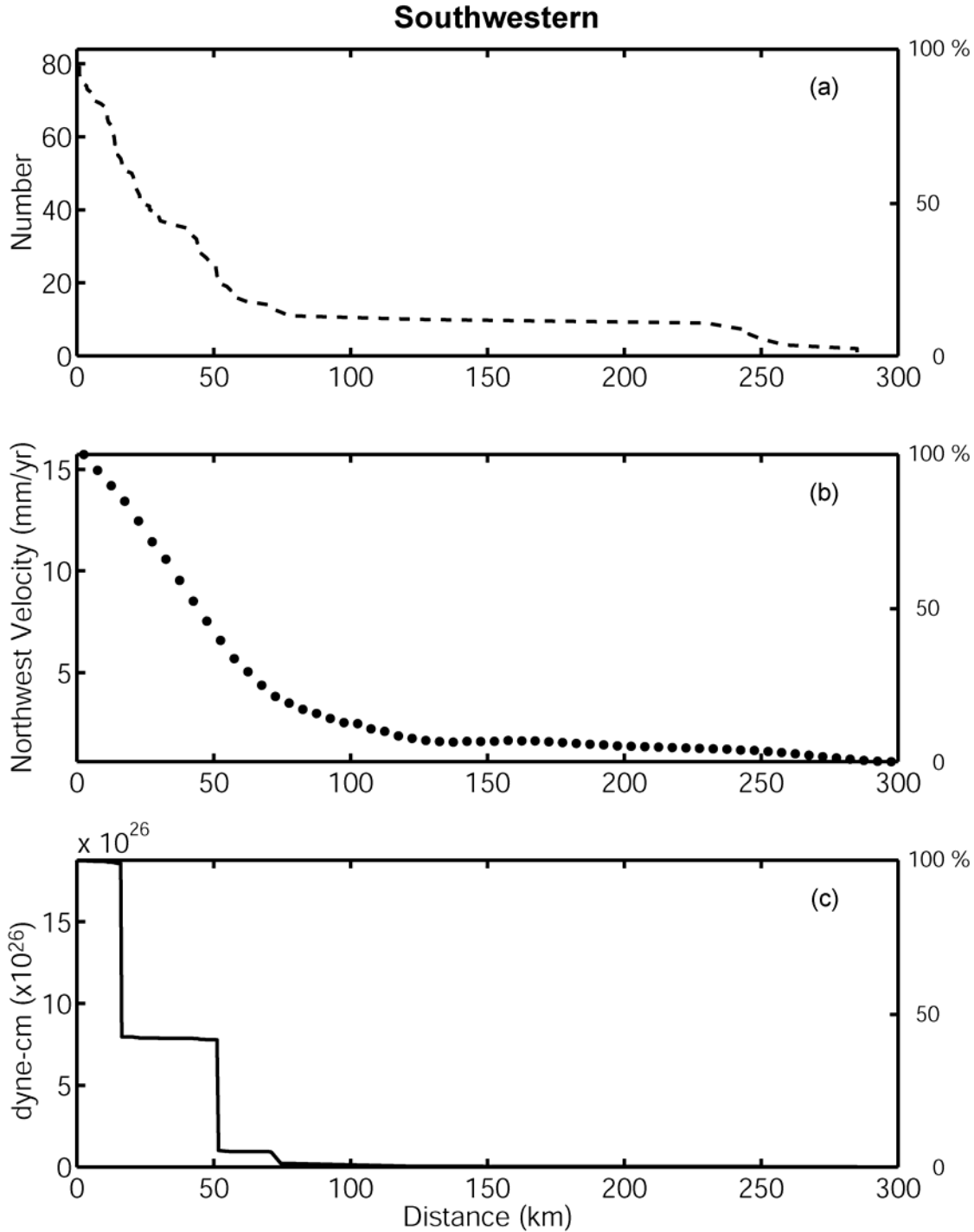


**Figure 2.1** Profiles through domain A. (a) Cumulative number of earthquake events, (b) averaged N37°W components of velocity determined from inversion of geodetic data (Blewitt and others, 2002,) and (c) cumulative seismic-moment release, as a function of the perpendicular distance from the southwestern boundary of the study region (Figure 1).

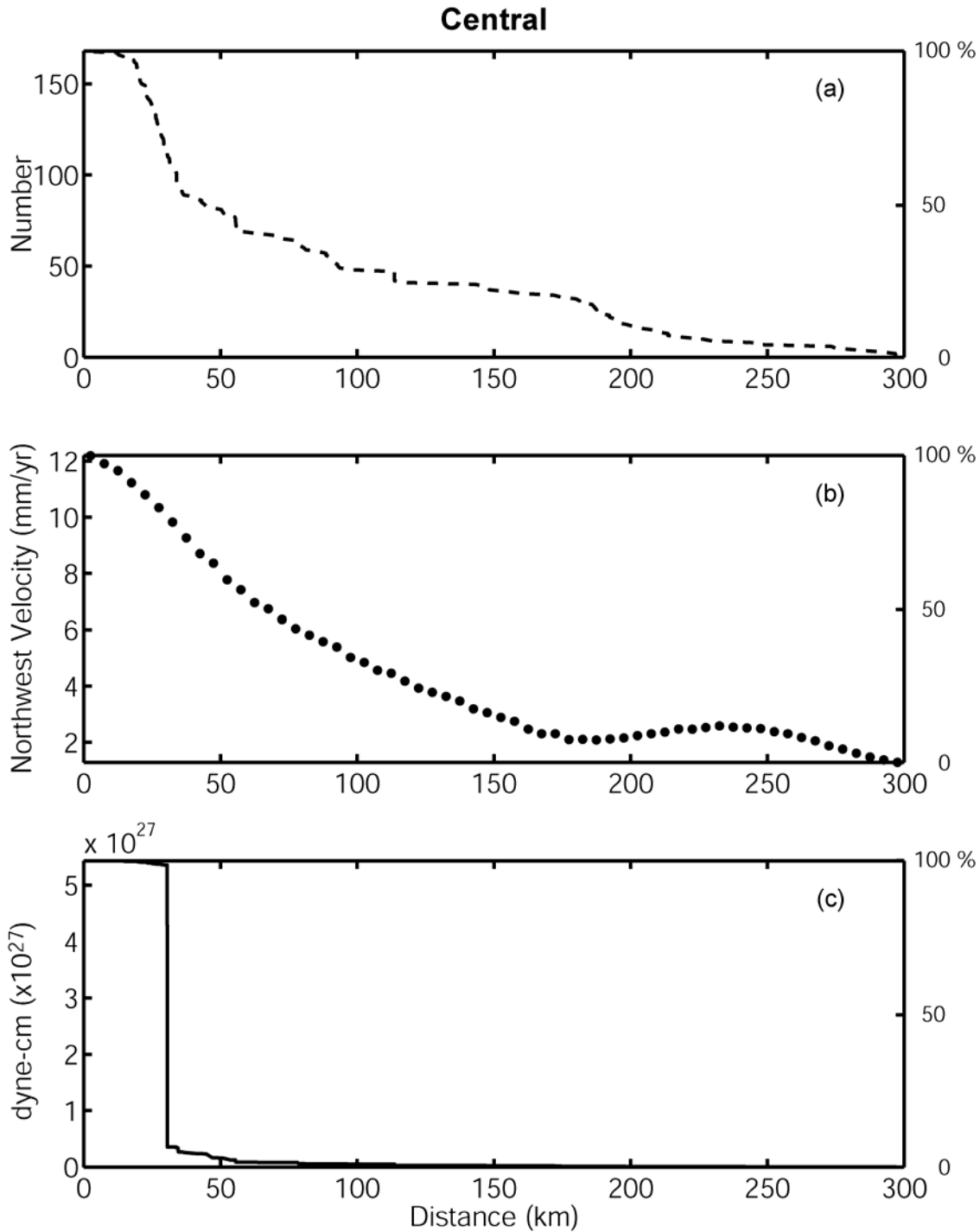


**Figure 2.2** Profiles through domain B. (a) Cumulative number of earthquake events, (b) averaged N37°W components of velocity determined from inversion of geodetic data (Blewitt and others, 2002), and (c) cumulative seismic-moment release, as a function of the perpendicular distance from the southwestern boundary of the study region (Figure 1).

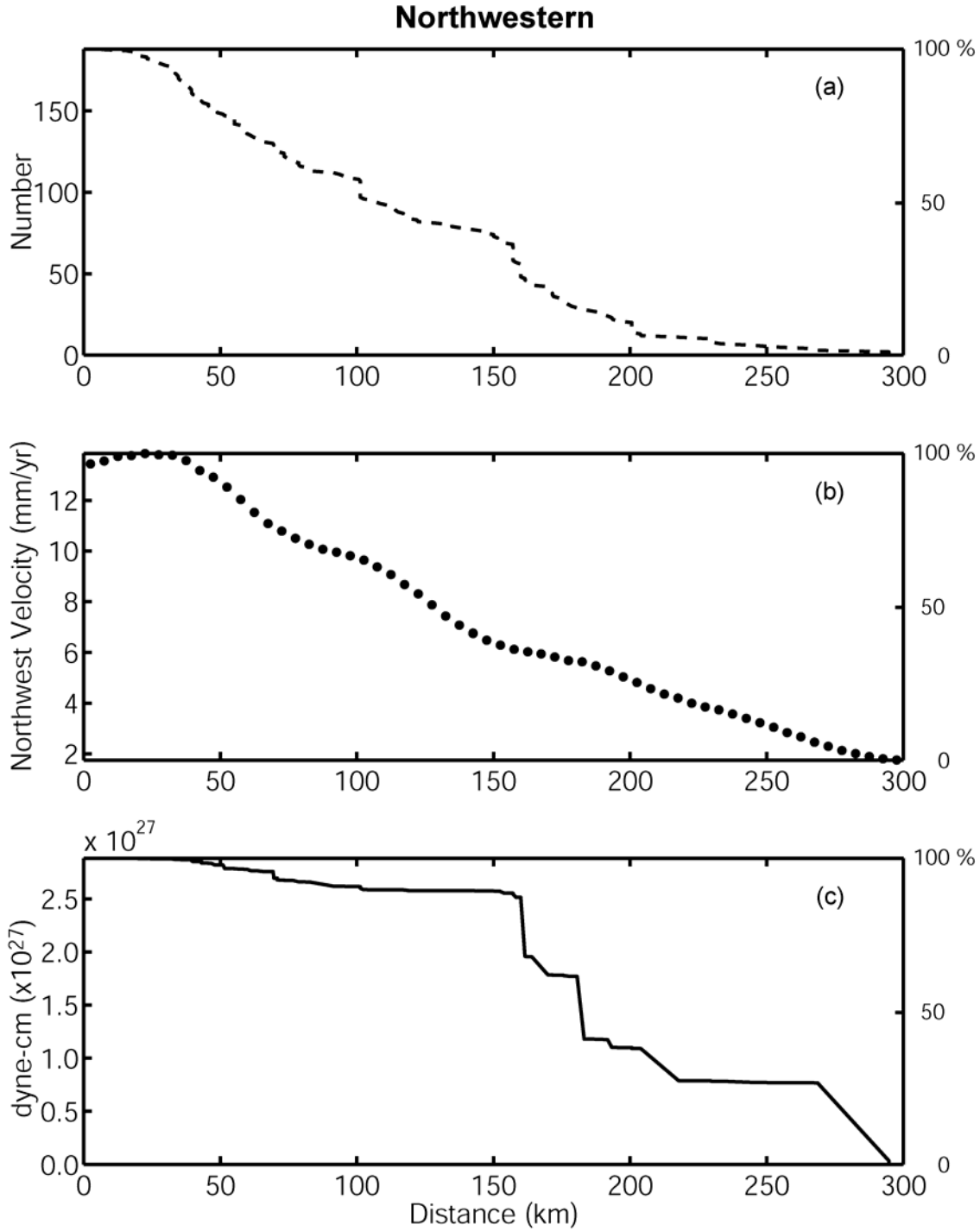


**Figure 2.3** Profiles through domain C. (a) Cumulative number of earthquake events, (b) averaged N37°W components of velocity determined from inversion of geodetic data (Blewitt and others, 2002), and (c) cumulative seismic-moment release, as a function of the perpendicular distance from the southwestern boundary of the study region (Figure 1).

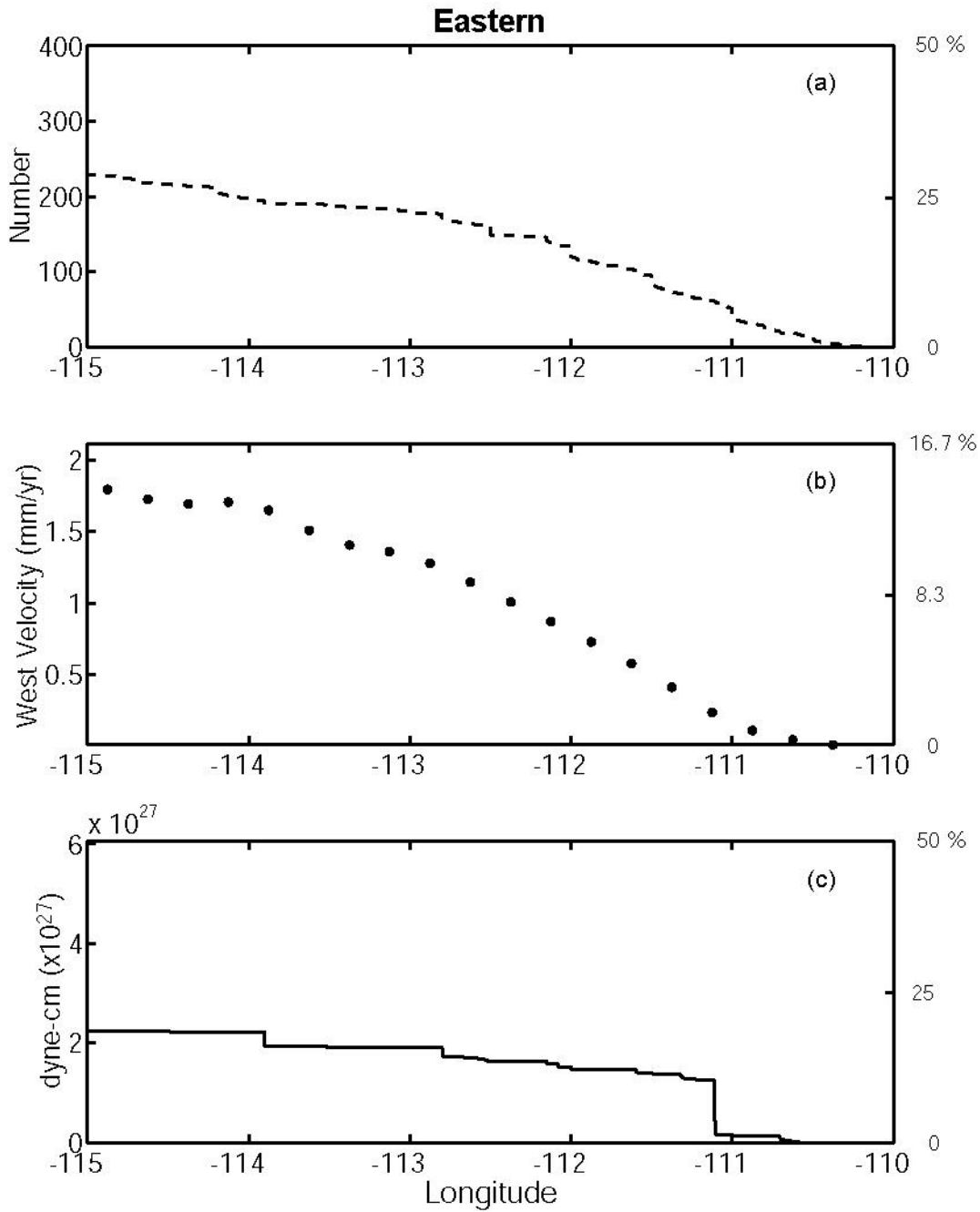


**Figure 2.4** (a) Cumulative number of earthquake events, (b) east-west components of velocity determined from inversion of geodetic data (Blewitt and others, 2002), and (c) cumulative seismic-moment release, as a function of the east-west distance.

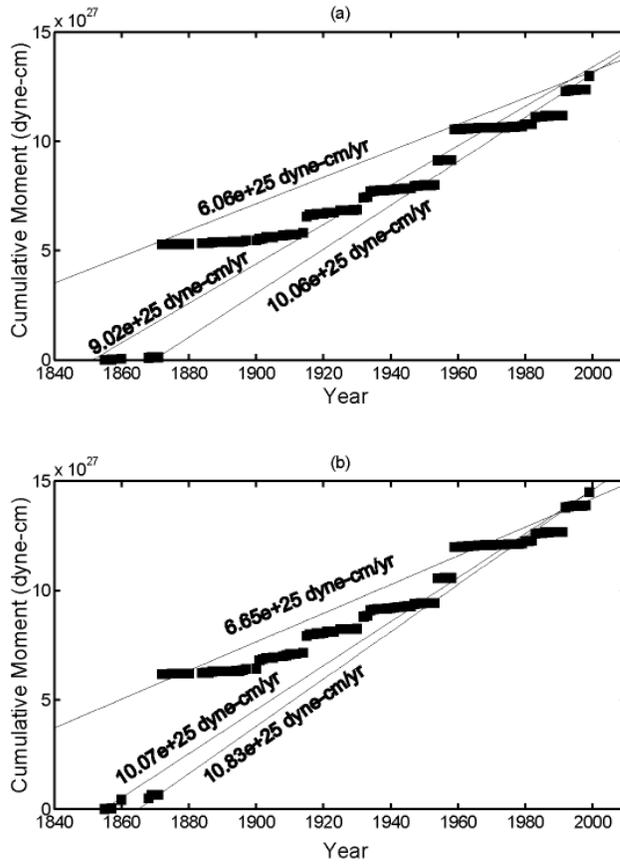


**Figure 3:** (a) Plot of cumulative seismic-moment release with time over the study region, based on preferred moment estimates for each earthquake. The lines show the average, and plausible lower and upper bounds, for the seismic-moment rate for the region. (b) Same as (a) but based on upper bound moment estimates for moderate sized earthquakes.

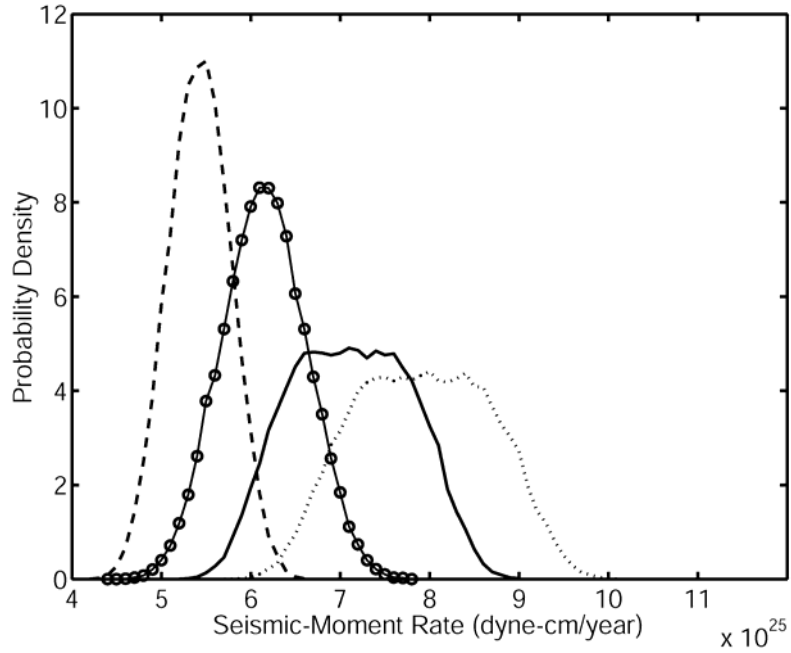


**Figure 4:** Distribution of the average (solid line) and upper (dotted) and lower (dashed) bounds of the seismic moment rates determined from 50,000 Monte Carlo simulations. The distribution due to a least-squares fit to the points is also shown (solid line with circles overlaid). The bin width is  $0.1 \times 10^{25}$  dyne-cm/yr.

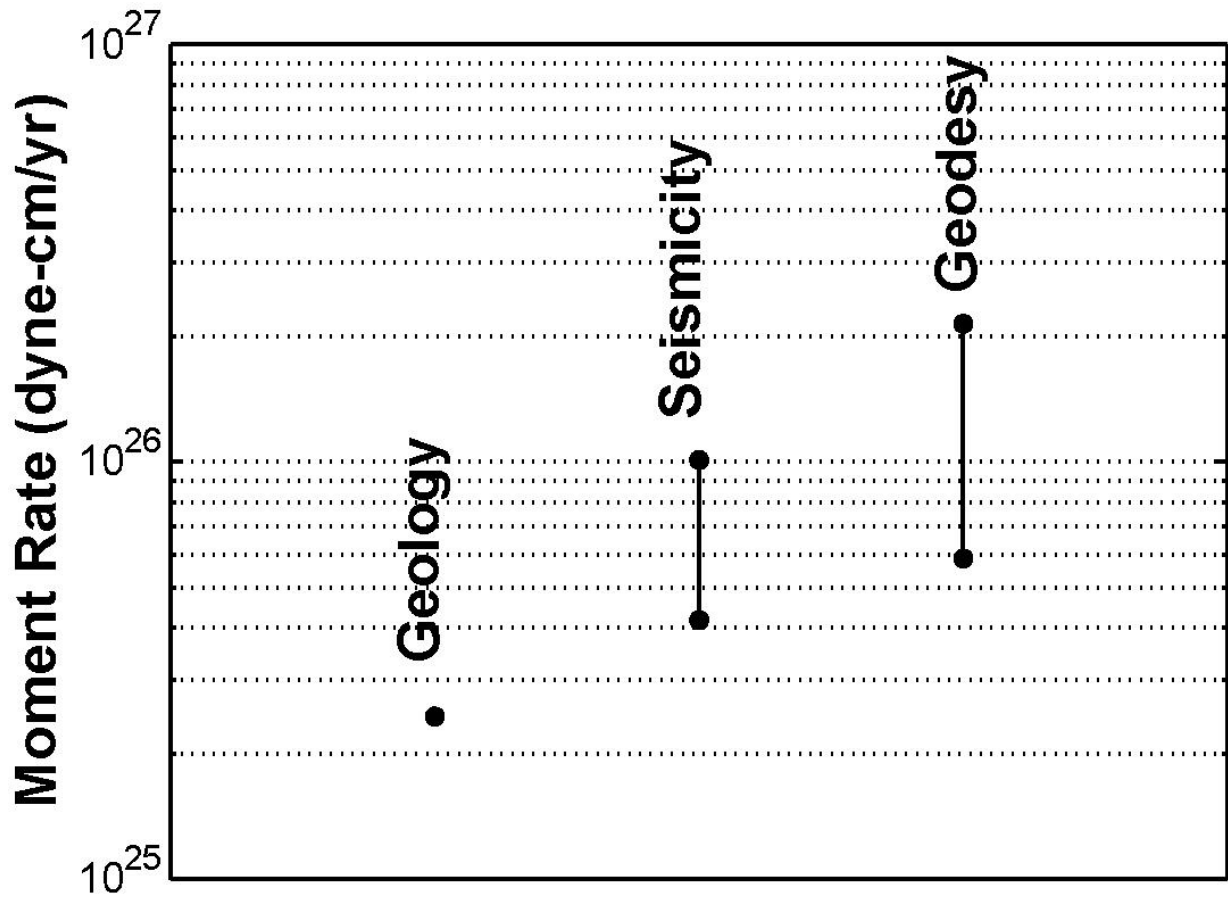


**Figure 5:** Plot showing comparison of the range of moment rates determined from the historical seismicity to those determined from geodesy.

## ***SUMMARY OF THE LATE QUATERNARY TECTONICS OF THE BASIN AND RANGE PROVINCE IN NEVADA, EASTERN CALIFORNIA, AND UTAH***

Michael N. Machette  
<machette@usgs.gov>  
U.S. Geological Survey  
Central Region Geologic Hazard Team  
MS 966, PO Box 25046  
Denver, Colorado 80225-0046

### **ABSTRACT**

Most Quaternary faults in the Great Basin portion of the Basin and Range Province trend northerly, have normal-slip displacement, and bound uplifted or tilted ranges. Although the uplifted ranges are spectacular geomorphic features, the associated Quaternary faults' relatively low slip rates have relatively long recurrence intervals between M 6.5+ earthquakes. A small percentage of the faults are quite active, especially those at the eastern and western margins of the province, including the Genoa (2-3 mm/yr), Death Valley (4-5 mm/yr), and Wasatch (1-1.5 mm/yr) faults. Hundreds of more typical Basin and Range faults are clearly less active, but their long-term behavior remains poorly characterized. Recent paleoseismic studies show that some of these faults have average slip rates of 0.05-0.15 mm/yr and recurrence intervals of tens to hundreds of thousands of years for surface-faulting earthquakes. Although individual faults pose relatively low hazard, the net results is amplified because hundreds of Quaternary faults riddle the province and, therefore, increase the average rate of earthquake recurrence in any particular region.

The USGS's new compilation of faults in the Basin and Range Province (see Machette and others, in this volume; <http://Qfaults.cr.usgs.gov/>) includes about 750 reported Quaternary structures in the Great Basin. Roughly 150 of these faults (20 percent) have evidence of surface rupture in the past 15,000 years, whereas 320 (43 percent) have similar evidence in the past 130,000 years. (i.e., since the penultimate glacial cycle). One result of recent paleoseismic investigations is that, in many cases, dating faulted deposits shows that the most recent movement is younger than the age that would be inferred on the basis of geomorphologic analyses, such as fault-scarp morphology, or from detailed surficial mapping. Many surficial processes can make a fault-scarp appear older than its true age, such as by burial by eolian, colluvial, or alluvial deposits. In contrast, there are only few ways to make a scarp look morphologically younger (fluvial trimming is the most likely). Thus, many estimates of the time of most recent movement shown in the fault database probably err on the old side. In addition, we used inclusive time categories, such as <130,000 years, to bracket the times of faulting; thus, each category includes some younger faults. We suspect that the above cited number and percentages of faults with <15,000 years and <130,000 years movement are minimum values that will increase as more faults are studied in detail. One result of our analysis of the time/space patterns for faulting in the province is that the <130,000-year time window captures almost one-half of the Quaternary faults and reflects their distribution well. This window is long enough to span at least one typical earthquake cycle (two events define one recurrence interval) on most faults, whereas the <15,000 years window is geologically too short to adequately sample all potential earthquake sources. This characteristic was also demonstrated by de Polo and Slemmons (1998) who pointed out that only about half of the 11 historical ruptures in the Basin and Range Province occurred on mapped Holocene faults.

Except for aftershock activity associated with some historical ruptures in the province, there is little spatial association between specific faults and recorded seismicity and virtually no examples of foreshock activity preceding large earthquakes. For example, the Wasatch fault zone is poorly defined by earthquakes on Utah seismicity maps, and the Thousand Springs segment of the Lost River fault (northern Basin and Range Province in Idaho) was virtually aseismic at  $M > 3.5$  for at least two decades before the 1983 Borah Peak earthquake (Dewey, 1987). Similar examples are common in the Great Basin, especially in its southern half. For the most part, normal faults of the Great Basin seem to be aseismic and locked, but may be loaded to near the point of failure as was the case with the 1954 Fairview Peak and Dixie Valley earthquakes.

The global positioning system (GPS) data shows some close associations with the fault data in the Great Basin. Recent analyses show a simple pattern of extension that is concentrated in three belts: 1) along the Wasatch Front in the Intermountain seismic belt (ISB), 2) in the Central Nevada seismic belt (CNSB), and 3) along the Eastern California seismic belt (ECSB). Generally speaking, the central part of the Great Basin (eastern Nevada and western Utah) show little evidence for contemporary extension and the timing most of the surface rupturing on faults in this area is late Quaternary ( $< 130,000$  years) or older. One conclusion from the pattern of fault slip rates is that most of the gross topography of the interior Great Basin is probably a relict of the late Miocene (15-5 Ma) and Pliocene (5-1.6 Ma) normal faulting, with minor rejuvenation during the Pleistocene.

The CNSB and ECSB have been the preferred areas for historic earthquakes larger than  $M 6.5$  in the Basin and Range Province. From 1872 to 1954, seven large earthquakes caused surface ruptures along this NNE-trending belt—an average of one rupture every 14 years. Recent summaries of paleoseismic investigations of the CNSB (Bell and others, 2004; Bell and others, in this volume) have shown that this rate and spatial pattern of activity is anomalous. There is no compelling evidence for similar precursory activity in the past 50,000 years on this belt, and there has been almost 50 years of quiescence since the last large earthquake. So, two of the most pertinent questions about the CNSB are “why here and where next?” Ultimately, the broader scientific challenge in the Basin and Range Province is to compare geologically determined rates and styles of deformation to contemporary strain fields determined by GPS to see if regions of accelerated extension are relicts of geologically recent activity or precursors of future activity. Hopefully, the new compilation of faults in the Basin and Range Province (see Machette and others, in this volume) will provide an ever-growing archive of paleoseismic information for such comparisons.

## INTRODUCTION

This paper focuses on the highly extended portion of the Basin and Range Province in Nevada, eastern California, and Utah, which could be considered the type locality of active extensional tectonics in the United States. This portion of the Basin and Range (a geologic province) encompasses most of the Great Basin (a physiographic province), and although I will be speaking in geologic terms, the specific area of interest is the Great Basin. The Great Basin contains at least 100 aligned basins and ranges that form north-trending chains (Figure 1). The deep basins are typically filled with Neogene sediment, and one or both margins are marked by

Quaternary or Neogene faults. Structurally, the basins are generally one-sided half grabens that alternate geometry from deep-on-the-east to deep-on-the-west, but also from north to south across transverse, NW-trending zones of accommodation (see Stewart, 1980; Thenhaus and Barnhard, 1989) that are influenced by crustal structures. The region is larger than Europe and contains almost 1000 mapped Quaternary faults. Three metropolitan areas (Ogden-Weber, Salt Lake City, and Provo in Utah, and Reno-Carson City and Las Vegas in Nevada) in the region contain more than 90 percent of its total population, and are all on the margins of the province (Figure 1). The Great Basin is roughly 750 km wide at 40° N latitude (W-E between Reno and Provo) and 600 km long at 105° longitude (N-S through Las Vegas). It is traversed by a network of two-lane highways, but the major Interstate highways (I-80 E-W and I-15 N-SW) provide the main transportation and growth corridors. U.S. Highway 50 (America's Loneliest Highway) traverses the northern Great Basin from east to west between latitudes 39° and 40°N, and provides a convenient baseline for ongoing global positioning system (GPS) studies. The intervening portions of the Great Basin are relatively remote and sparsely populated (cattle and sheep outnumber humans by several orders of magnitude). In spite of seemingly unlimited opportunities to decipher the history of Quaternary faulting in the province, detailed paleoseismic investigations are limited. Thus,

although, one might think that the province would be a robust source of information on fault mechanics and geometry, and on earthquake timing and recurrence, it is not.

In the course of compiling information on potential earthquake source areas in the western United States, it has become apparent that several aspects conspire to limit our understanding of the characteristics of active faulting of the Basin and Range Province. On one hand is the sheer number of Quaternary faults in the province to be studied. Conversely, until recently only a few detailed paleoseismic studies had been conducted and, because radiocarbon-datable materials are very rare owing to the province's arid to semi-arid climate and sparse vegetation, it has been difficult to constrain the timing of prehistoric earthquakes. However, with the advent of GPS monitoring of extension across the region (see following discussion), there has been an acceleration of efforts to study the paleoseismic history of faults in the region, primarily by the Nevada Bureau of Mines, University of Nevada, USGS, and Utah Geological Survey. For example just this year paleoseismologists have submitted or published ten new papers on the paleoseismicity of faults in the Great Basin (see Bell and others, 2004; Briggs and Wesnousky, 2004, in this volume; Caskey and others, 2004; Crone and others, in press; Lund, in press; Friedrich and others, 2004; Machette and others, in press; Personius and Mahan, 2005; Wesnousky, 2004a; and Wesnousky and others, 2004b). This rapidly expanding database of paleoseismic data has greatly increased our knowledge of selected faults, primarily in central and northern Nevada.

In addition, recent advances in luminescence (TL and OSL) and cosmogenic-nuclide dating help address the problem of dating specific faulting events, but these methods are expensive and time consuming. However, now have the tools to determine the key paleoseismic parameters necessary to characterize active faults: event timing and displacement amounts (which lead to recurrence interval and slip rate), and rupture length. The large number of faults for which data are needed remains a real limitation that can be addressed only by con-

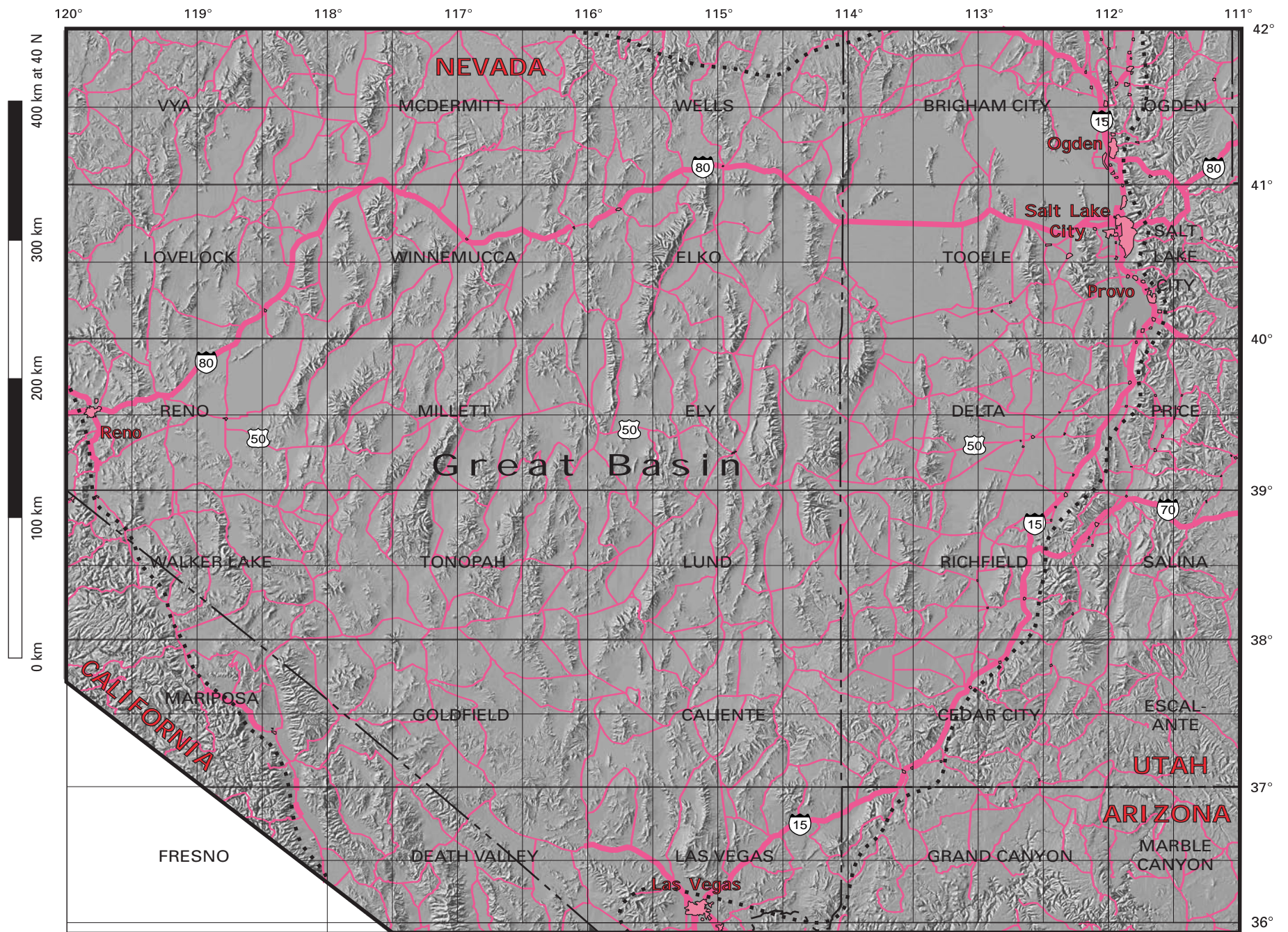


Figure 1. Index map to the Nevada, eastern California, and Utah portions of the Basin and Range Province (hereafter referred to as Great Basin). Shaded relief map shows typical pattern of basins and ranges. Major transportation routes and towns are shown in pink, along with the names and location of 1:250,000-scale topographic maps. Boundary of Great Basin shown by dotted lines.

tinuing the newly accelerated pace of paleoseismic studies or by applying regional reconnaissance tools that give geologically realistic estimates of paleoseismic parameters (slip rates, recurrence intervals, and times of most recent movement). Thus, truly characterizing the seismogenic potential of Basin and Range faults is a task that will require considerable time and manpower.

### **PURPOSE OF THE PAPER**

This paper is a summary of the late Quaternary tectonics of the Great Basin portion of the Basin and Range Province as revealed by the spatial and temporal patterns of faulting. The basic data source is the USGS's new fault compilation (see following discussion of sources of data). As such, this summary is only current as of May 2004 because the fault database is a dynamic source. Nevertheless, the basic patterns deciphered from this data will probably not change radically in the near future, just the details.

This paper has the five main objectives:

- 1) Review the Quaternary history of Basin and Range faults in the Great Basin;
- 2) Identify general spatial and temporal patterns of faulting;
- 3) Review existing data on fault slip rates;
- 4) Discuss prehistoric analogs of and future activity in the Central Nevada seismic belt; and
- 5) Provide a framework for papers in this volume.

### **SOURCES OF DATA**

The illustrations showing fault timing and distribution, which are the core of this paper, were built from the USGS' new compilation of Quaternary faults in the United States. Currently, this database includes about 1775 faults and fault sections (portions of faults that may represent various types of segments). Data from the Basin and Range Province (see Machette and others, in this volume) comprises about 58 percent (1025 faults and sections) of the entire National dataset, whereas data for the Great Basin comprise about 46 percent (813 faults and sections) of the National dataset. The Basin and Range data were compiled by geolo-

gists from State geological surveys (Arizona, Colorado, and Utah), from the USGS (mainly Denver personnel), and from the consulting community (mainly Piedmont Geosciences). Our effort to compile a National fault database has been ongoing for nearly a decade, with most of the compilations for the Intermountain states having been published by the USGS or by State geological surveys (i.e., Montana, Utah, and Colorado). An earlier map by Thenhaus and Wentworth (1982) showed general zones or areas having similar ages [*sic*, times] of surface faulting, but the original data were not included nor was the timing database very refined.

Haller and others (1993) established the fault database criteria for the entire United States over a decade ago; they defined the time intervals and slip-rate categories, as well as terminology in order to construct a systematic and geologically based National fault compilation. This effort was modified from a similar scheme developed by Trifonov and Machette (1993) for the International Lithosphere Programs World Map of Active Faults. The database is described in moderate detail in the accompanying paper by Machette and others () and is available on the internet at <http://Qfaults.cr.usgs.gov>, so I do not describe it here in detail.

### **TEMPORAL AND SPATIAL PATTERNS OF FAULTING**

In the database, the times of fault activity are grouped into five categories: 1) historic (ca. <150 years), 2) <15 ka, 3) <130 ka, 4) <750 ka, and 5) Quaternary (<1.6 Ma). You should note that each increasingly long time interval includes all the faults in younger intervals; for example, the <130-ka time interval includes all the historic, <15 ka, and <130 ka faults. Table 1 lists time abbreviations and geologic time intervals used in this report.

The current compilation contains about 810 reported Quaternary structures (faults and fault sections) in eastern California, Nevada, and Utah. Faults in the Mojave region, including the Garlock, were excluded from the tabulation. About 200 (25 percent) of these 810 structures have been active in the past 15,000 years (15 kyr), whereas 380 (47

percent) have been active in the past 130 kyr (i.e., since the penultimate glacial cycle related to marine oxygen isotope stage VI). One positive result of this analysis is that the <130 ka time window captures almost half of the Quaternary faults and reflects their distribution well. This time window is long enough to span at least one earthquake cycle (two events and one recurrence interval) on most faults, whereas the <15 ka window is geologically too short to adequately sample all potential earthquake sources. This aspect of fault-timing sampling was also demonstrated by de Polo and Slemmons (1998) who recognized that only about one-half of the 11 historical ruptures in the Basin and Range Province had occurred on mapped Holocene faults. Conversely, in more actively deforming region, such as the transpressive domains of coastal California, recurrence intervals are short enough (hundreds to thousand years) and slip rates are high enough (typically > 1mm/yr) that the 10,000 years of the Holocene epoch will capture multiple faulting events. Thus, depending on the rate of tectonic activity in different regions, the time window needed to capture one or more earthquake cycles varies widely (see Machette, 2000).

Table 1. Time terms used in this report

Time abbreviations	Geologic time intervals (informal)
Ma: millions of years ago (a point in time).	<15 ka: Post glacial and Holocene (<10 ka)
kyr: thousands of years (an interval of time).	<130 ka: Late Quaternary
myr: millions of years (an interval of time).	<750 ka: Late and middle Quaternary
Ma: millions of years ago (a point in time).	<1.6 Ma: Quaternary (late, middle and early)

Recent paleoseismic investigations have, in many cases, found that dating faulted deposits often shows the most recent fault movement to be younger than the age inferred from geomorphologic analyses, such as fault-scarp morphology, or from detailed surficial mapping. From a geologist's perspective, there are many ways to make a fault-scarp appear older than its actual age, such as by burial by eolian, colluvial, or alluvial deposits. In contrast, there are few ways to make a scarp look younger

than it actually is (fluvial trimming is the most likely). Thus, many of the estimates of the time of most recent movement that are shown in the fault database and are based on geomorphic parameters probably err on the old side. In addition, our use of inclusive time categories, such as <130 ka, to bracket times of faulting surely causes some categories to include some younger faults (i.e., <15 ka in this case). We suspect that the above cited number and percentages of faults with <15 ka and <130 ka movement are minimum values and these numbers will probably increase as more faults are studied in detail.

### Historical surface faulting

The vast majority of historical surface faulting in the Great Basin has occurred in the CNSB and ECSB (see following discussions), with only one surface-rupturing earthquake in Utah (Hansel Valley, 1934) (Figure 2). In the western Great Basin, there have been 15 surface-faulting earthquakes in the past 150 years, including an early but questionably located event near Reno in 1860 or 1869 (Table 2). Most of these earthquakes caused surface rupturing on preexisting Quaternary faults although only about one-half of the earthquakes occurred on faults that have demonstrable Holocene activity (see discussion of de Polo and Slemmons, 1998). Three additional historical earthquakes have occurred in the province, but are outside of the study area: 1) the 1959 Hebgen Lake, Montana earthquake and 2) the 1983 Borah Peak, Idaho, earthquake, both near the northeastern margin of the province, and 3) the 1887 Bavispe (Sonora) earthquake in northern Sonora, Mexico, 40 km southeast of Douglas, Arizona in the southernmost part of the province. The Bavispe earthquake produced the longest normal-slip rupture of all of the historical faults in the province. A recent investigation by Suter (2001) has documented 101 km of surface rupture (end to end length), which they equate to a moment magnitude of about  $7.4 \pm 0.3$ . This earthquake occurred on the Pitaychachi fault, whose previous surface rupturing occurred >100 ka (Bull and Pearthree, 1984).

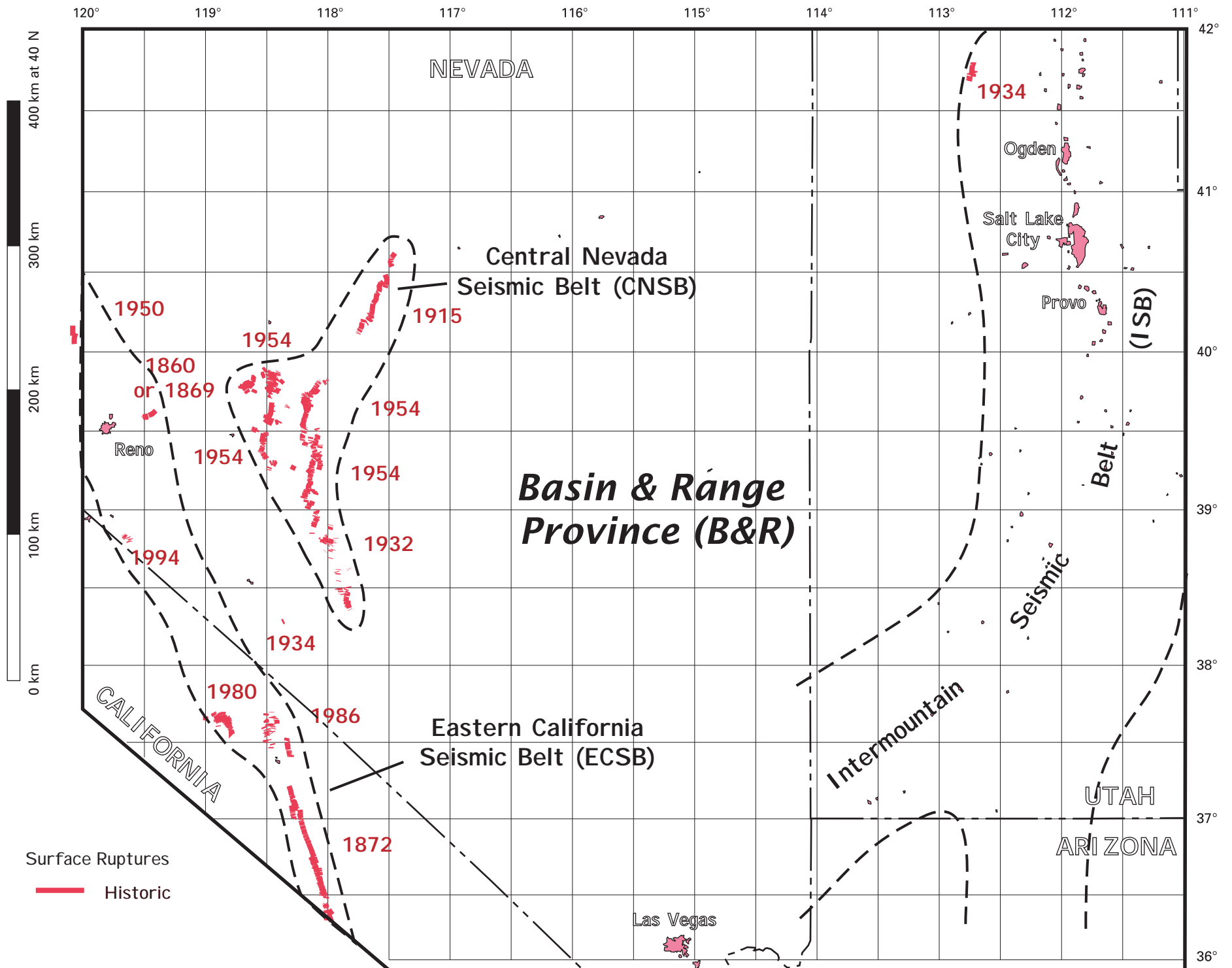


Figure 2. Faults with historic (<150 years) surface rupture in the Great Basin. Year of earthquake shown.

*Table 2. Historic earthquakes with surface rupture on faults in the Great Basin*

[Data from USGS database as of May 2004 (see <http://Ofaults.cr.usgs.gov/> for current listing). General location is by indexed to Army Map Service 1:250,000-scale sheet and state. Does not include the Garlock fault (no. 69) or other faults of the Mohave Desert region of southern California]

Historical earthquakes	Fault No.	Name of fault and/or fault section	General location
1860 Pyramid Lake (NV) or 1869 Olinghouse (NV)	1668	Olinghouse fault (not proven)	Reno, NV
1872 Owens Valley (CA)	51b	Owens Valley fault zone, 1872 rupture section	Mariposa, CA/NV
1903 Wonder (NV)	1691	Gold King fault	Reno, NV
1915 Pleasant Valley (NV)	1136 1136a 1136b 1136d	Pleasant Valley fault zone: China Mountain section (N) Tobin section Pierce section Sou Hills section (S)	Winnemucca, NV
1932 Cedar Mountain (NV)	1322 1324 1325	Gabbs Valley fault zone Unnamed faults flanking Cedar Mtn. Monte Cristo fault zone	Tonopah, NV
1934 Hansel Valley (UT)	2358	Hansel Valley fault	Brigham City, UT
1934 Excelsior Mountain (NV)	1316	Unnamed faults in Excelsior Mtn.	Walker Lake, NV
1950 Fort Sage (CA)	24	Fort Sage fault	Susanville, CA
1954 Rainbow Mtn (NV)	1679	Rainbow Mountain fault zone	Reno, NV
1954 Stillwater (NV)	1680	Unnamed faults in Fourmile Flat	Reno, NV
1954 Fairview Peak (NV) (Probably from Fairview Peak earthquake):	1690 1312 1689 1688 1691 1692	Fairview fault zone Also: Hot Springs fault zone Louderback Mountains fault Unnamed fault in eastern Dixie Valley Gold King fault West Gate fault	Reno, NV
1954 Dixie Valley (NV)	1687b	Dixie Valley fault zone, 1954 section	Reno, NV
1980 Mammoth Lakes (CA)	44	Hilton Creek fault	Mariposa, CA/NV
1986 Chalfant Valley (CA)	48	Fish Slough fault zone	Mariposa, CA/NV
1994 Double Springs Flat (NV)	1286	East Carson Valley fault zone	Walker Lake, NV/CA

The CNBS is a NNE-trending zone of historical faults that extends from the Monte Cristo Valley (near Gabbs, Nevada) on the south to the northern end of Pleasant Valley (about 50 km south of Winnemucca, Nevada) on the north. Large surface-faulting earthquakes in this belt occurred in 1915 (Pleasant Valley; Wallace, 1984) and 1932 (Cedar Mountain; Gianella and Callaghan, 1934a, b), but culminated with a sequence of four earthquakes in 1954 (Table 2), the two largest and latest occurring

in December just four minutes apart (Fairview Peak and Dixie Valley; de Polo and others, 1991; Caskey, 1996). The Central Nevada seismic belt has been tectonically stable and relatively aseismic for the past 50 years although GPS data indicates that this belt continuous to experience geologically fast rates of extension (see later discussion of “General patterns from GPS data”).

The ECSB is a NNW-trending zone of historical faults that extends from Owens Valley on the south

to Surprise Valley in northeastern California on the north. It includes a tectonically interesting region called the Walker Lane, which contains a mixture of NNE- and NNW-trending faults (see Wesnousky, 2004a) that typically have had a large component of lateral and or normal slip (de Polo and others, 1991), depending on their orientation. The oldest historical faulting in this belt started possibly with the 1869 Olinghouse earthquake (see Briggs and Wesnousky, 2004) (or an earthquake in 1860) but was followed four years later by the province's first really large historical earthquake—the 1872 Owens Valley earthquake. This earthquake, which was studied by Gilbert (1884), is probably the first well-documented surface-rupturing earthquake in the United States. The remaining historical earthquakes in the belt have been of lesser magnitude, with relatively short surface ruptures forming in 1903 (Wonder), 1934 (Excelsior Mountain), 1950 (Fort Sage), 1980 (Mammoth Lakes, volcano-event?), 1986 (Chalfant Valley) and 1994 (Double Springs Flat) (visit <http://Qfaults.cr.usgs.gov> for information on these faults). Although these events were of  $M6\pm0.5$  and thus smaller than the major surface-rupturing earthquakes, they show that the ECSB continues to release strain. Conversely, the adjacent CNSB has remained locked for the past 50 years or has released all of its accumulated strain.

Interestingly, the Intermountain seismic belt (ISB), which lies at the eastern margin of the province in Utah, is not marked by abundant surface faulting that characterizes the western side of the province (Figure 2). One obvious problem with seismicity catalogs is the relatively short time period for historical recordings. For example, the first Mormon settlers arrived in the Salt Lake area in 1849—only 155 years ago. Similarly, the first pioneers crossed Death Valley that same year, although the valley wasn't permanently settled until the 1870s with the discovery of borax (see Nelson *in* Machette and others, 2001). In Death Valley, the youngest movement on the Death Valley fault system is not yet dated, but it may have occurred soon before settlement based on the youthful character of the fault scarps along the Black Mountains and Grapevine Mountains. Thus, if the

province had been settled for a longer time, say 300 to 500 years earlier, then the pattern of historical faulting might better match the seismic belts that are based strictly on felt and instrumental seismicity for the past one and one-half centuries.

### **Latest Quaternary (<15 ka) faulting**

Faults with evidence for surface rupturing in the past 15 kyr are unevenly distributed across the Great Basin and are preferentially concentrated along the province's eastern and western margins, and in west-central Nevada. About 200 (25 percent) of the 810 Great Basin structures have been active in the past 15,000 years (15 kyr). There are few young faults in southwestern Nevada and along the northern Utah-Nevada border region. In Utah, most of the province boundary is marked by active young faults such as the Wasatch, Great Salt Lake, and Hurricane fault zones, including some faults that bound intra-province ranges and basins west of the Wasatch Front. The presence of latest Pleistocene lakes across a large part of the northern Great Basin has had little affect on the fault distribution shown in Figure 3, since the <15 ka faults generally cut the lacustrine deposits (generally older than 12-15 ka as discussed later). The main reason that we selected 15 kyr for our first geologic time slice was that this datum has widespread stratigraphic signature; it is generally considered to be near the maximum extent of glaciers and pluvial lakes, which are common in the region. The more traditional Holocene (10 ka) break has less distinct geologic signature in the Great Basin; instead it is more firmly linked to archeological studies. Likewise, the 130-kyr-time window (discussed below) is related to the end of the penultimate glaciation and pluvial episode associated with marine oxygen-isotope stage VI, and therefore also has a widespread stratigraphic signature.

A long, fairly continuous band of young NNW-striking faults is present in southeastern California, east of the Sierra Nevada, and includes the ECSB. The longer structures that have had prehistoric surface rupture include the Death Valley fault system (with three fault zones), the Panamint Valley and Hunter Mountain-Saline Valley fault zones, and associated linking structures—all typically have

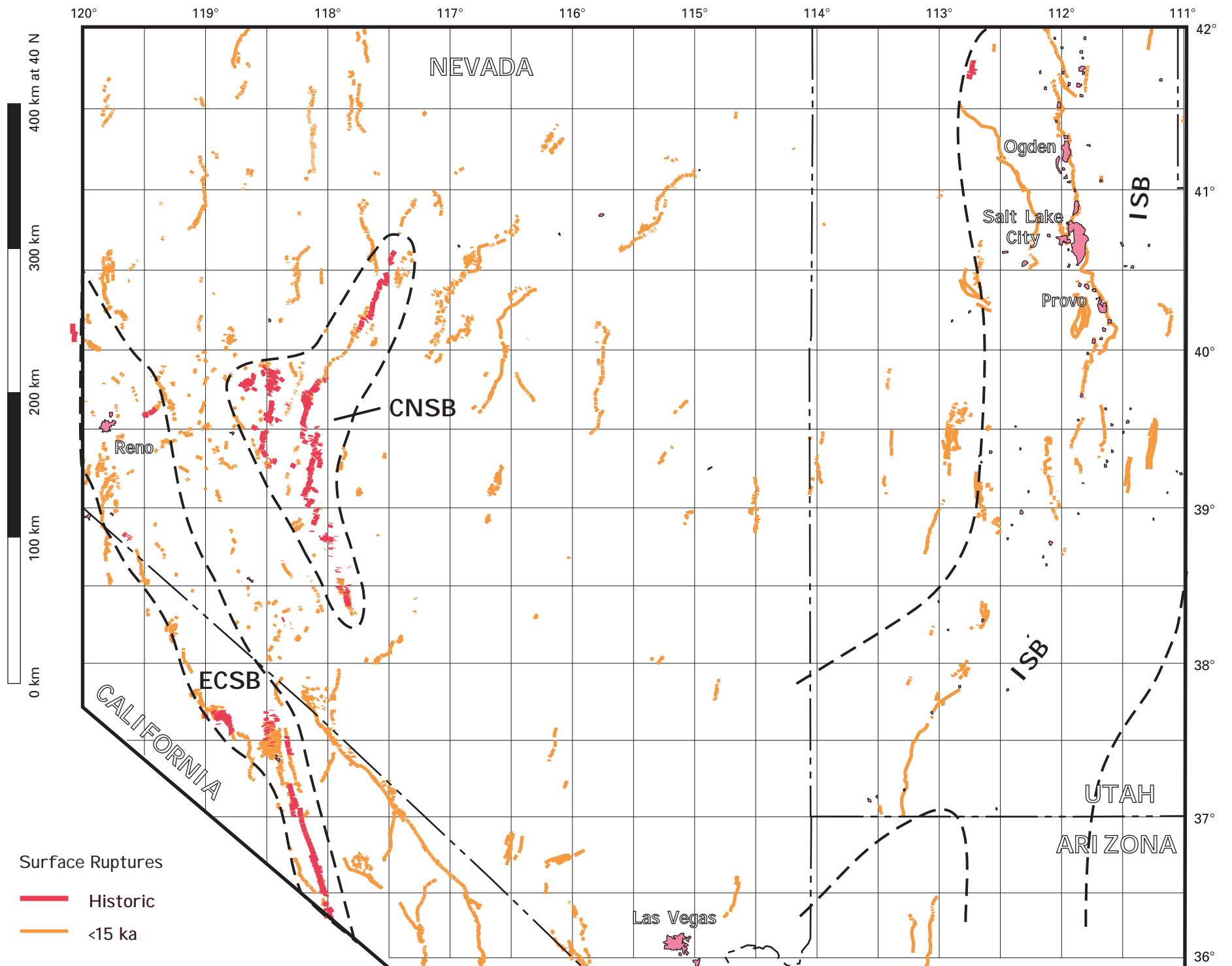


Figure 3. Map showing faults that had surface rupture in the past 15 kyr (latest Pleistocene and Holocene) in the Great Basin.

relatively high slip rates and geologically young activity. This belt of faulting marks the southern part of the ECSB (see Figure 2), which forms the active, northwestward-moving margin of the province. This belt and the adjacent Walker Lane are characterized by NNW-striking faults that have predominantly right-lateral strike-slip movement and NE-striking (linking) normal faults that have down to the northwest motion. Although beyond the map area of Figure 2, this belt of faults continues beyond Reno into northeastern California and southeastern Oregon where the youngest structures include the Honey Lake, Hat Creek, and Surprise Lake faults (see Table 3). As a result, the eastern Sierra Nevada forms an active margin for the northwesterly expansion of the Basin and Range Province.

The young faults in the interior of the Great Basin are concentrated mainly in northwestern half Nevada and along ranges west of the Wasatch Front in west-central Utah. There are relatively few young faults in the western part of Utah, along the Nevada/Utah border, and in southern Nevada. In virtually all cases, the young faults are along only one margin of a basin, and the other margin is passive (but not necessarily dead, see following discussion of Quaternary faulting and Figure 6). The concentration of young faults in the northwestern portion of the province suggests that most of the WNW- to NW-directed extension in the interior of the province is being accommodated at its leading (NW) edge. This inference is supported further by the general distribution of young faults on the latest Pleistocene pluvial basin floors that define a widespread time datum: the Lahontan basin is displaced by tens of young faults in northwestern Nevada, whereas the Bonneville basin is displaced by fewer than ten faults in northwestern Utah.

#### **Late Quaternary (<130 ka) faulting**

As one expands the time frame the late Quaternary (<130 ka), the pattern of faulting becomes more complete across the province (Figure 4A). Nearly one-half (380 or 47 percent) of the faults in the Great Basin have evidence of movement in the past 130 kyr. Most range-bounding faults have been active in this time interval with obvious gaps mainly in northernmost central Nevada, in the

northwest corner of Utah, and in the intersection area of Arizona, Nevada, and Utah. With the exception of the previously discussed areas of <15 ka faulting, the greatest concentration of <130 ka faults is in the central Great Basin where the basin elevations are the highest. Within this time frame, many basins have active faults on both margins. This pattern is probably the result of a long sampling interval that includes several to many earthquake cycles: in 130 kyr, there is time to have accumulated enough strain for surface rupturing on relatively slow moving (<0.2 mm/yr) faults along the less active (more passive) margins of basins.

One major problem of evaluating faulting in the 130-ka time frame is the widespread occurrence of the lakes throughout the Great Basin. These lakes have come and gone repeatedly throughout the Pleistocene, although only last few lake cycles are the best documented (see Reheis, 1999). The basin floors in northwest Utah are underlain by deposits of the last cycle of Lake Bonneville, which culminated about 14,500 radiocarbon years ago (estimated at about 17,500 calendar years ago using new correction factors; see Cerling and Craig, 1994), by 60-70 ka deposits of the Jordan Valley cycle (also known as the Hansel Valley cycle), and by the pre-130 ka Little Valley lake cycle. A similar relation exists within the Lake Lahontan basin in northwest Nevada, although those lakes appear to have reached its maximum extent a bit later in the latest Pleistocene (perhaps 13,000-13,600 radiocarbon years ago; Adams and Wesnousky, 1998), and previous lake cycles are not well dated. Lacustrine deposits from late Pleistocene Lake Bonneville and Lake Lahontan (and smaller pluvial lakes) have obscured or buried many preexisting fault scarps (Figure 4B). The scarcity of <15 ka faults on the floor of Lake Bonneville suggests that the northwestern part of Utah is not as active as the equivalent Lake Lahontan part of Nevada, which is riddled with young faults. Overall, pluvial lake deposits have obscured the true distribution of faulting in the Great Basin over the past 130 kyr.

*Table 3. Faults with >1 mm/yr slip in the Great Basin*

[All of these faults were active in the past 15 kyr. Data from USGS database (<http://Ofaults.cr.usgs.gov/>) of May 2004. General location is by Army Map Service 1:250,000-scale sheet. Does not include the Panamint Valley fault zone (no. 67), which is not yet described, nor Garlock fault (no. 69) or other faults of the Mohave Desert region]

Fault No.	Fault name	Slip rate (mm/yr)	General location
4	Surprise Valley fault	1-5	Alturas, CA
6	Mayfield fault zone	1-5	Alturas, CA
9	Hat Creek fault	1-5	Alturas, CA
22	Honey Lake fault zone	1-5	Susanville, CA
41	Mono Lake fault	1-5	Walker Lake, NV/CA
44	Hilton Creek fault	1-5	Mariposa, CA/NV
45	Round Valley fault	1-5	Mariposa, CA/NV
49	Fish Lake Valley fault zone		
49a	Leidy Creek section	1-5	Mariposa, CA/NV
49b	Wildhorse Creek section	1-5	Mariposa, CA/NV
49c	Oasis section	>5	Mariposa, CA/NV
49d	Cucomongo section	1-5	Goldfield, NV/CA
51	Owens Valley fault zone		
51a	Keough Hot Springs section	1-5	Mariposa, CA/NV
51b	1872 Rupture section	1-5	Mariposa, CA/NV
66	Hunter Mountain-Saline Valley fault zone		
66a	Saline Valley section	1-5	Death Valley, CA/NV
66b	Hunter Mountain section	1-5	Death Valley, CA/NV
70	Owl Lake fault	1-5	Trona, CA
141	Northern Death Valley fault zone		
141a	Grapevine Mountains section	1-5	Death Valley, CA/NV
141b	Mesquite Flat-Screwbean Spring section	1-5	Death Valley, CA/NV
141c	Kit Fox Hills section	1-5	Death Valley, CA/NV
142	Black Mountains fault zone		
142b	Artists Drive section	1-5	Death Valley, CA/NV
142c	Copper Mtn. section	1-5	Death Valley, CA/NV
142d	Smith Mountain section	1-5	Trona, CA
143	Southern Death Valley fault zone		
143a	Confidence Hills section	1-5	Trona, CA
143b	Nobel Hills section	1-5	Trona, CA
1285	Genoa fault	1-5	Reno, NV
1647	Mount Rose fault zone	1-5	Reno, NV
1669	Pyramid Lake fault zone	1-5	Reno, NV
2351	Wasatch fault zone		
2351d	Brigham City section	1-5	Brigham City, UT
2351e	Weber section	1-5	Ogden, UT
2351f	Salt Lake City section	1-5	Salt Lake City, UT
2351g	Provo section	1-5	Salt Lake City, UT
2351h	Nephi section	1-5	Price, UT

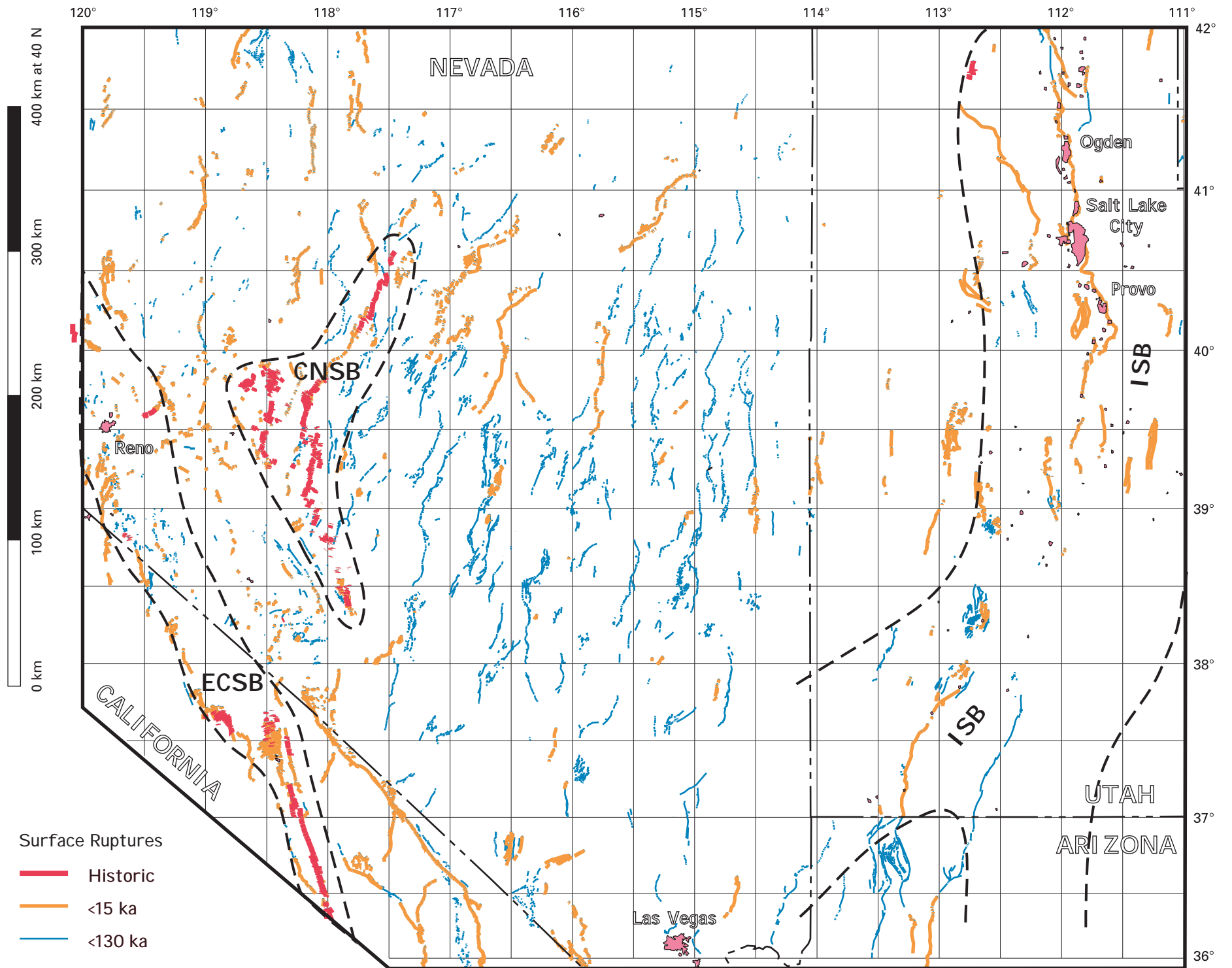


Figure 4A. Map showing late Quaternary (<130 ka) faults that had surface rupture in the Great Basin.

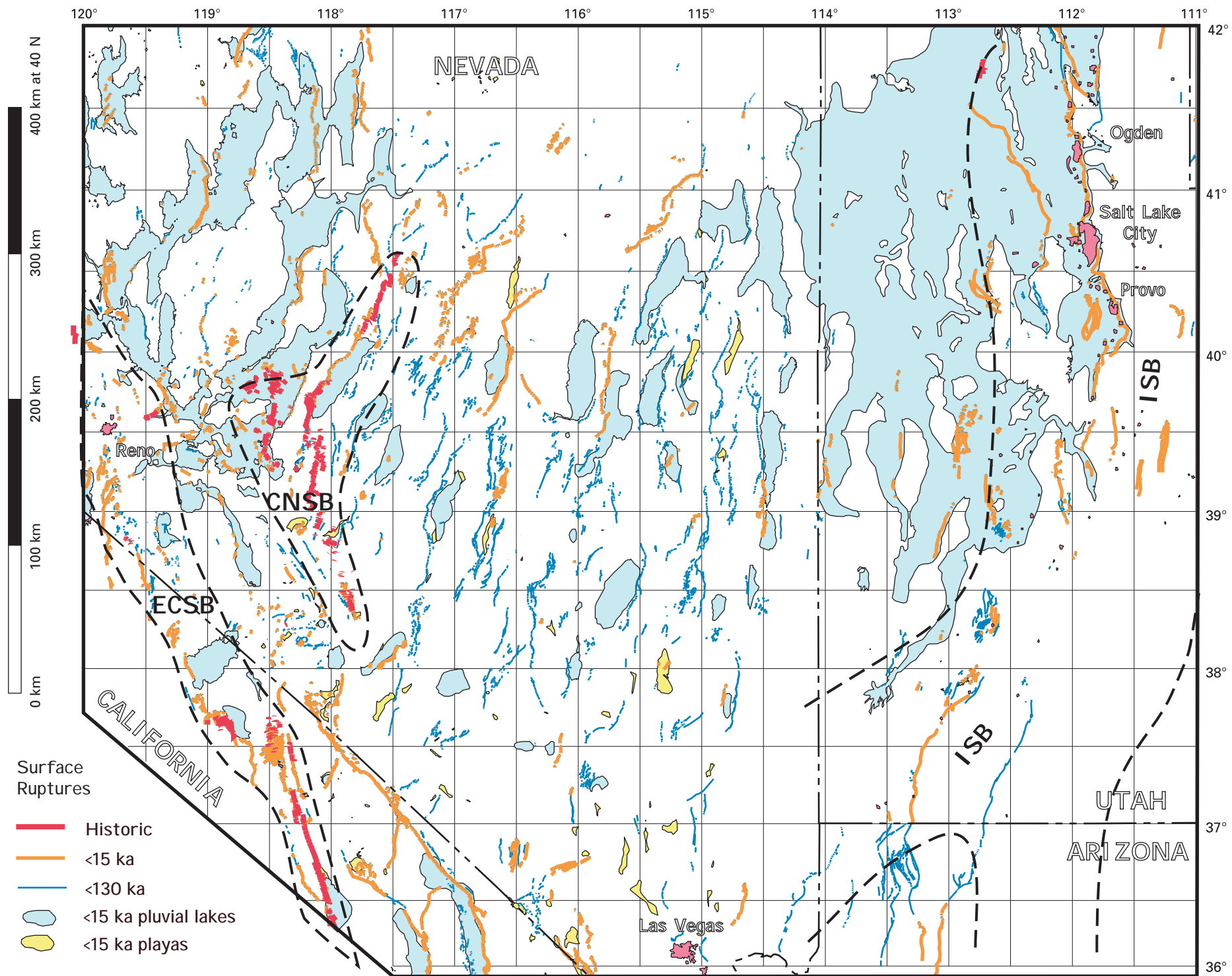


Figure 4B. Map showing late Quaternary (<130 ka) faults, and pluvial lakes and playas in the Great Basin.

### **Late and middle Quaternary (<750 ka) faulting**

The next older time interval for categorizing faulting is the entire late and middle Quaternary, which we defined as starting at about 750 ka (see Haller and others, 1993). This time frame marks the youngest major change in the Earth's magnetic field, from the Matuyama reverse epoch (2.5-0.78 Ma) to the Bruhnes normal epoch (780 ka to present), which is an important and recognizable geologic time datum. In addition, in the Great Basin at least two major volcanic ashes were deposited near this time interval, namely the 770 ka Bishop ash and the 640 ka Lava Creek Ash, each of which provide age control for differentiating early and middle Quaternary deposits.

Adding middle Quaternary faults (130 ka-750 ka, Figure 5) to the post-130 ka faults (see Figure 4) results in few substantial changes in the pattern of faulting, but it does highlight the faults within the ISB (Figure 1) and along some ranges in relatively inactive portions of Nevada.

### **Quaternary (<1.6 Ma) faulting**

The Quaternary time frame (Figure 6) shows a pattern of faults that is fairly uniform faulting across the Great Basin, with obvious exceptions in eastern Nevada and northwestern Utah where Lake Bonneville was prevalent. New (Quaternary) faults show up prominently in southern Utah and northern Arizona, particularly in the Grand Canyon region where early Quaternary basalts are displaced. Some of Quaternary-age faults concentrated along the California/Nevada border region south of Lake Tahoe are probably misclassified (late Tertiary rather than Quaternary), and abrupt terminations of faults along lines of latitude or longitude are the result of incomplete mapping (see for example, the northeastern corner of the Mariposa 1° x 2° sheet, Figure 1). Many of the Quaternary faults on Figure 5 are short or discontinuous, which is result of the ample time for streams to remove evidence of movement on those faults. In fact, ruptures on these faults are probably more continuous than shown, so estimates of the length of Quaternary faults are probably minimum values.

In summary, the new fault database shows progressively longer time slices that reveal interesting

patterns in the temporal and spatial distribution of faulting in the Great Basin. The province margin fault systems are those that have moved most recently, whereas the historically active CNCB is a geological anomaly. If one considers only the <15 ka faults, you get a skewed picture of potential faulting in the province. The longer <130-ka time window captures almost half of the Quaternary faults and reflects their distribution well. This window is long enough to span one or more typical earthquake cycles (two events yield one recurrence interval) on most faults, whereas the <15 ka window is geologically too short to adequately sample all potential earthquake sources. One additional point should be made here. That is, the relatively low hazard posed by a single Quaternary fault is compounded by the presence of hundreds of them in the Great Basin: the net result is an increase in the average rate of surface faulting in any particular region. In the past, I've referred to this compounding affect as the composite recurrence of faulting. For example, on the Wasatch fault zone, single fault segments have individual recurrence intervals that range from 500 to as much as 2,500 years (Lund, in press); however, the Holocene portion of this long fault has a composite recurrence interval of about 400 years (see Machette and others, 1992).

### **SLIP-RATE PATTERNS FOR FAULTING**

The patterns shown by fault slip rates define domains of varying activity. The following discussion will focus on fault activity as monitored by reported slip rates. We defined four slip-rate categories for the database: >5, 1-5, 0.2-1, and <0.2 mm/yr (very fast, fast, moderate, and slow) in the database. We used these rather broad categories because few faults in the region have good geologically determined slip rates, but nevertheless a fault's general level of activity can be characterized from studies of displacement versus age of deposits or from morphometric parameters (scarp morphology or range-front facets). In the Great Basin virtually all the faults have slip rates of <5 mm/yr, so only the three lower categories are discussed herein. Using slip rate categories allowed us to characterize all the faults irregardless of whether or not they had

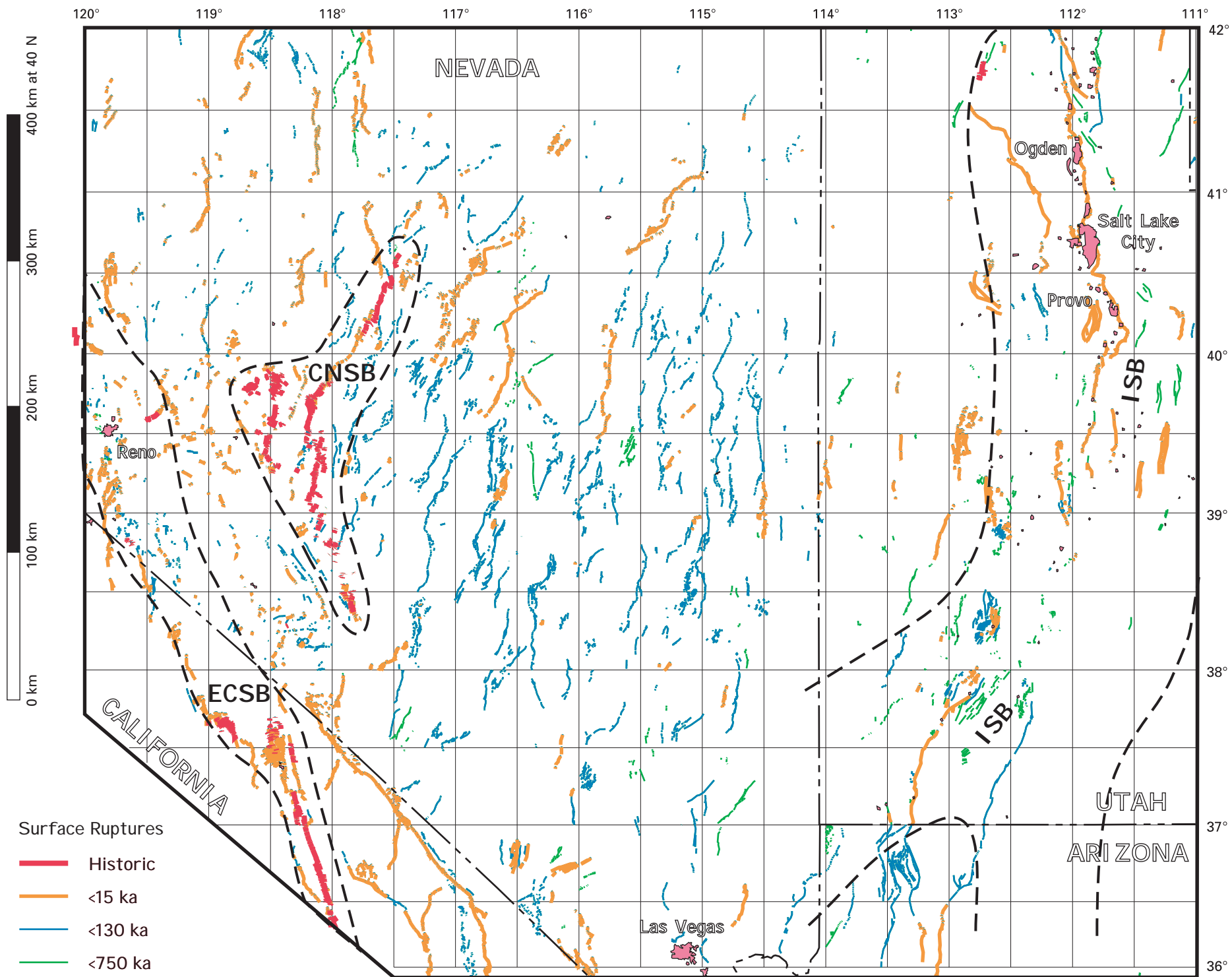


Figure 5. Map showing faults that had surface rupture in the past 750 k.y. (late and middle Quaternary) in the Great Basin.

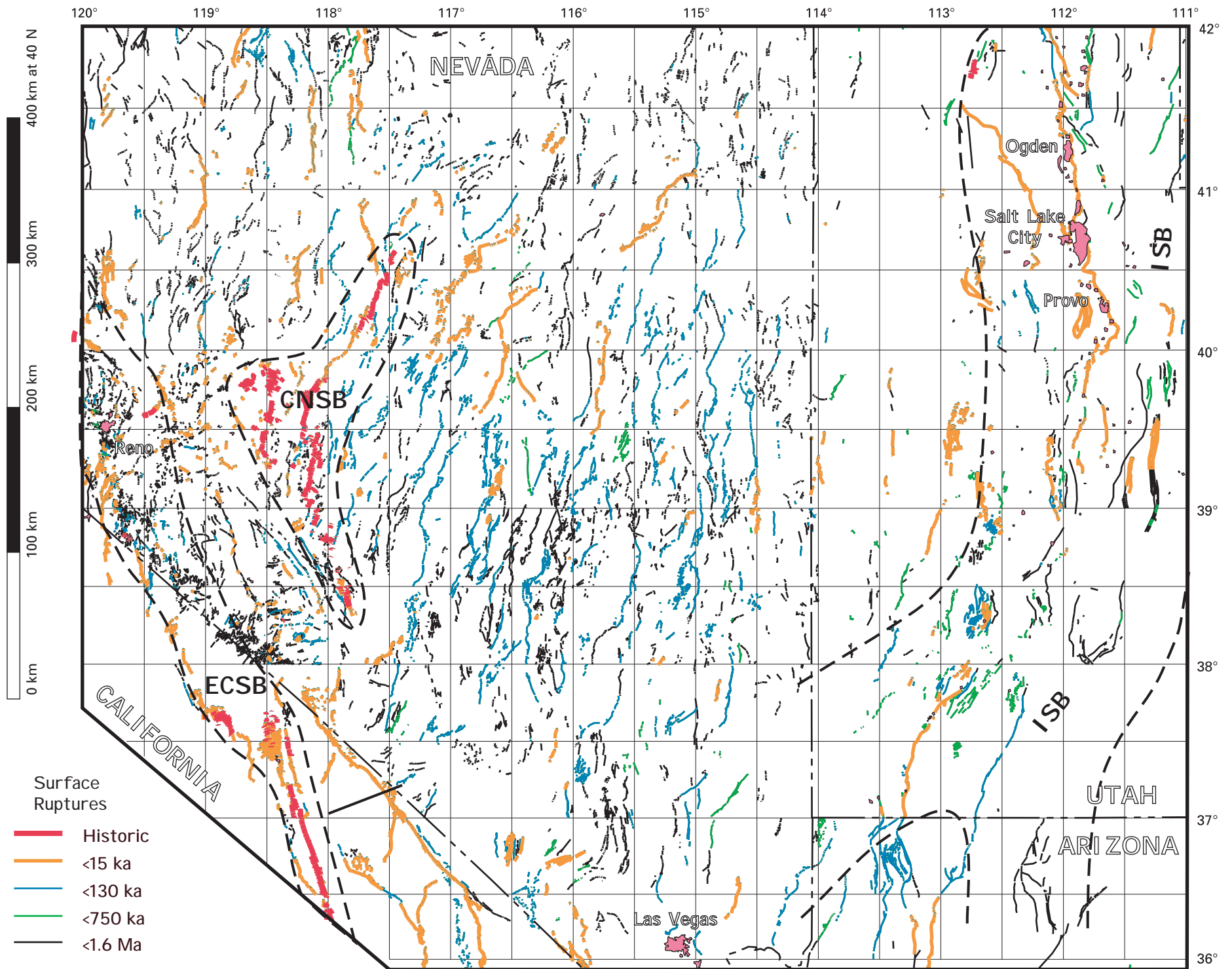


Figure 6. Map showing faults that had surface rupture in the past 1,600,000 yr (1.6 Ma, Quaternary) in the Great Basin.

a reported slip rate or data from which a slip rate could be calculated. In addition, there are many ways that slip rates have been reported both correctly (slip between dated events) and incorrectly (i.e., net slip in some time interval).

Even though many uplifted ranges in the province are geomorphically spectacular, about 90 percent of the associated Quaternary faults (Figure 6) are slipping at relatively slow rates (ca. 0.2 mm/yr or less) and have long recurrence intervals for M 6.5+ earthquakes (ca.  $10^4$ - $10^5$ yr). From the following figures (7, 8, and 9) it will be obvious that some faults are considerably more active than others (as defined by slip rate), especially along the eastern and western margins of the province. These include the Genoa (2-3 mm/yr), Death Valley (4-5 mm/yr), and Wasatch (1-1.5 mm/yr) faults. Interestingly, there are only about one and one-half as many faults (50) moving at intermediate rates (0.2-1.0 mm/yr) as the fast ones (>1 mm/yr). This leaves about 730 typical Basin and Range faults that are clearly less active (<0.2 mm/yr), but their behavior remains poorly characterized. Recent paleoseismic studies show that some of these faults have average slip rates of 0.05-0.15 mm/yr, and recurrence intervals of tens of thousands to perhaps a hundred thousand years (see for example, Bell and others, 2004; Caskey and others, 2004; Crone and others, in press; Machette and others, in press; Personius and Mahan, 2005; Wesnousky and others, 2004b).

### High slip faults (>1 mm/yr)

Thirty two Quaternary faults or fault sections (4.0 percent of the population) that have apparent slip rates of >1 mm/yr (see Table 3) are concentrated in two belts in the Great Basin. The western belt (Figure 7) is largely coincident with the ECSB, but also includes prominent strike-slip faults in Death Valley (#141-143), Fish Lake Valley (#49), Hunter Mountain-Saline Valley (#66), Panamint Valley (#67, not included in Table 3), and Owens Valley (#51). As mentioned above, the Genoa fault (#1285) has a reported net slip rate of 2-3 mm/yr, making it the highest-slip normal fault in the province. The northern part of this belt includes the Mt. Rose (#1647), Pyramid Lake (#1669), Honey Lake (#22), Hat Creek (#9), Mayfield (#6), and Surprise

Valley (#4) faults (all north of Lake Tahoe), and the Mono Lake (#41), Hilton Creek (#44), and Round Valley (#45) faults, which mark the western province boundary south of Lake Tahoe. The >1 mm/yr faults in the western belt are typically right-lateral, strike-slip faults, but the latter three (southern) faults have dominantly normal slip.

The only faults on the eastern margin of the province that exceed 1 mm/yr are the five active central segments of the Wasatch fault zone (#2351, Table 3; see also Lund, in press), which are in the ISB. These fault segments extend from Brigham City on the north to Nephi on the south. They typically have average Holocene slip rates of 1-1.5 mm/yr, but there is strong evidence that slip rates have changed substantially through time (Machette and others, 1992). With the exception of Wasatch fault in Utah and the Teton fault (#768) in western Wyoming (east of the Great Basin), no other faults in the ISB have well-documented slip rates that exceed 1 mm/yr.

Interestingly, recent paleoseismic studies show no evidence for high long-term slip rates in the CNSB (see review by Bell and others, 2004), which suggests that the sequence of historical faulting in the belt is anomalous rather than characteristic (see following discussion of ancient analogs to the CNSB).

All faults that have high slip rates are either historic movement or young (<15 ka) because for high slip-rate faults, 15 kyr is long enough to span one or more full seismic cycles. For example, a fault with a nominal slip rate of 1 mm/yr will accumulate enough strain in the Holocene (ca. 10 kyr) to produce 10 m of displacement. Normal faults typically have an upper bound of about 3 m for vertical slip per event, whereas lateral-slip faults might produce as much as 5-8 m of slip in a very large earthquake. Thus, by picking a slip rate bound of 1 mm/yr for one of our database categories, we established a filter that naturally identifies young and highly active faults.

We have two high-slip-rate categories in the database (1-5 mm/yr and >5 mm/yr), but the Oasis section of the Fish Lake Valley fault (#49c) is the only documented fault that has a slip rate of >5

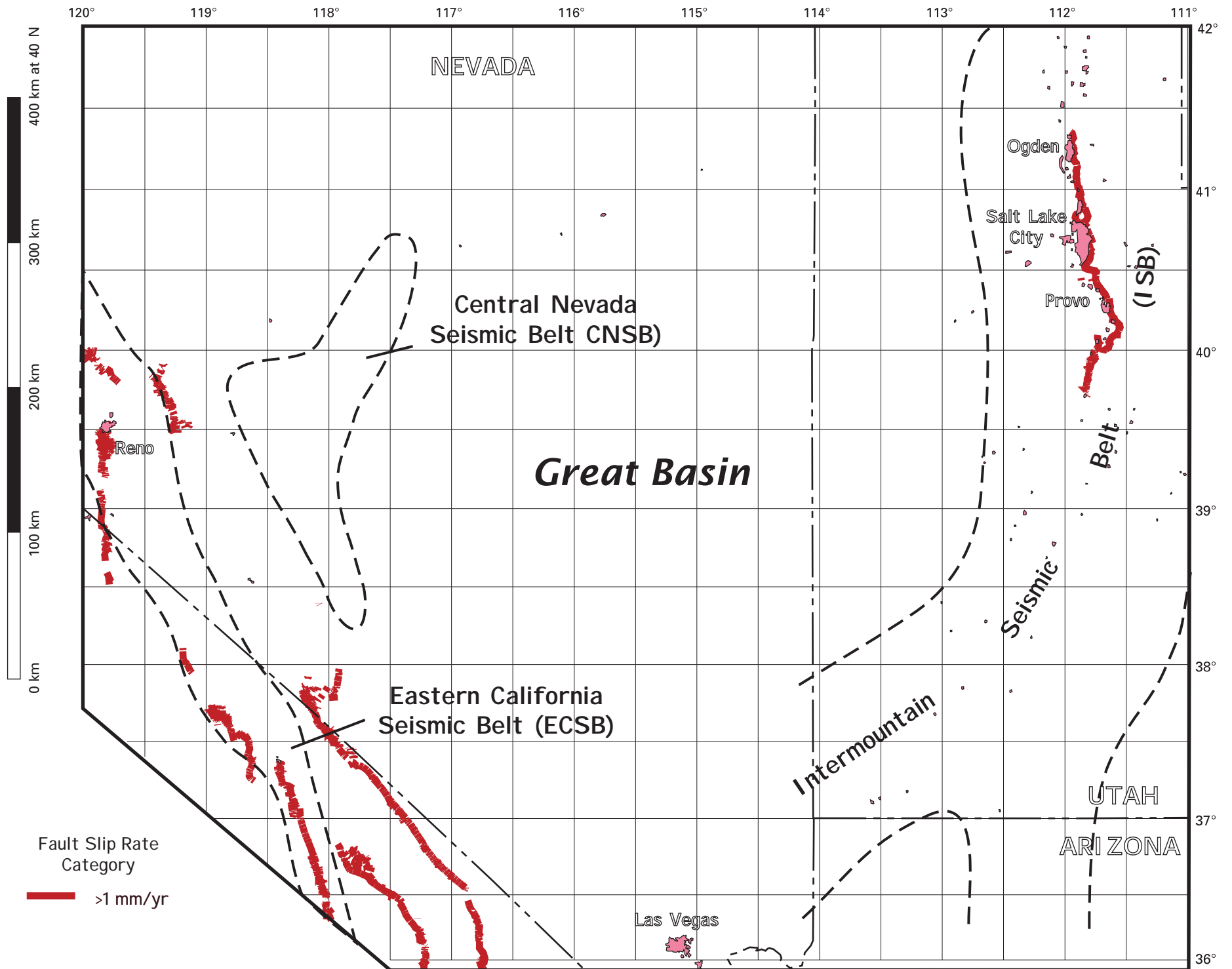


Figure 7. Map showing Quaternary faults in the Great Basin that have high slip rates.

mm/yr in the Great Basin (Table 3). All other  $>5$  mm/yr faults in the United States are in compressional or transpressional domains associated with the interaction of the North American, Pacific, and San Juan de Fuca plates (i.e., San Andreas fault system and Cascadia subduction zone).

#### **Moderate slip faults (1-0.2 mm/yr)**

The fault database contains roughly 1.5 times as many Great Basin faults that are moving at intermediate rates (0.2-1.0 mm/yr) than at fast rates ( $>1$  mm/yr). Still, this number (50) is only about 6.2 percent of the 810 faults in the Great Basin portion of the Basin and Range Province.

The 0.2-1 mm/yr faults are generally within the ISB belt, or are in or along the ECSB and CNSB (Figure 8). The single obvious outlier in this pattern is the relatively continuous zone of faulting that extends north-northeast along the eastern and western margins of the Toiyabe Range (faults #1337 and #1336c, respectively) and north along the western margin of the Simpson Park Mountains (fault #1178). This belt of intermediate-rate faulting is roughly 200 km long and, although poorly dated, may be an ancient analog to the contemporary CNSB.

Most of the interior of the Great Basin lacks intermediate slip-rate faults, as is clearly shown in Figure 8. None of the perhaps 100 ranges and basins in northern or eastern Nevada nor those in western Utah appear to be uplifting (or downdropping) at regionally anomalous rates of  $>0.2$  mm/yr, which can form mountain ranges in Quaternary time (i.e., roughly 2 km of structural relief in 1 myr). Thus, one conclusion from this pattern of fault slip rates is that most of the gross topography of the interior Great Basin is probably a relict of the late Miocene (15-5 Ma) and Pliocene (5-1.6 Ma) normal faulting, with minor rejuvenation during the Pleistocene.

#### **Low slip faults ( $<0.2$ mm/yr)**

The remainder of the roughly 730 faults (90 percent of total) in the Great Basin appear to be moving rates less than 0.2 mm/yr (Figure 9). However, the well controlled slip-rate data for the region is so sparse, some of these slow slip faults

might be moving faster, whereas many might have insignificantly small slip rates (ca. 0 mm/yr), especially those that are classified as Quaternary. In the database there are many examples of faults that displace early Pleistocene deposits (750 ka to 1.6 Ma) tens of meters (or less), which suggests long-term slip rates of 0.003 (5 m in 1.6 myr) to 0.03 mm/y (30 m in 750 kyr). These rates are nearly one to almost two orders of magnitude lower than our lowest slip-rate category threshold of 0.2 mm/yr.

### **CONTEMPORARY EXTENSION IN THE NORTHERN GREAT BASIN**

The focus of this paper is not to review the methods or results of research on contemporary extension rates in the Northern Great Basin, but instead to highlight the variety and quantity of geological data on fault activity that has become available in the past 10-15 years. Posters at this meeting described recent results of GPS measurements and several recent papers have presented the latest thinking on contemporary strain rates and the geologic forces driving extension in the region (i.e., Hammond and Thatcher, 2004).

With the advent of GPS monitoring, we now are able to measure the direction, rate, and general distribution of strain release across the Great Basin. Prior to establishing GPS networks (early 1990s), the only modern system for detecting earth deformation was Very Long Baseline Interferometry (VLBI). VLBI measurements indicated about 12 mm/yr of west-directed extension across the Great Basin (Minster and Jordan, 1984; Dixon and others, 1995), although these measurements were considered to be preliminary and were determined from long base lines with very widely separated stations. Nevertheless, they showed a rate of extension that is comparable with those determined from a cross-basin, continuously monitoring GPS network (see Bennett and others, 1998, 2003) and from campaign-style networks (see Thatcher and others, 1999; Thatcher, 2003; Hammond and Thatcher, 2004). The main difference in these two types of GPS networks are their continuity and spatial density: the continuous GPS sites collect a

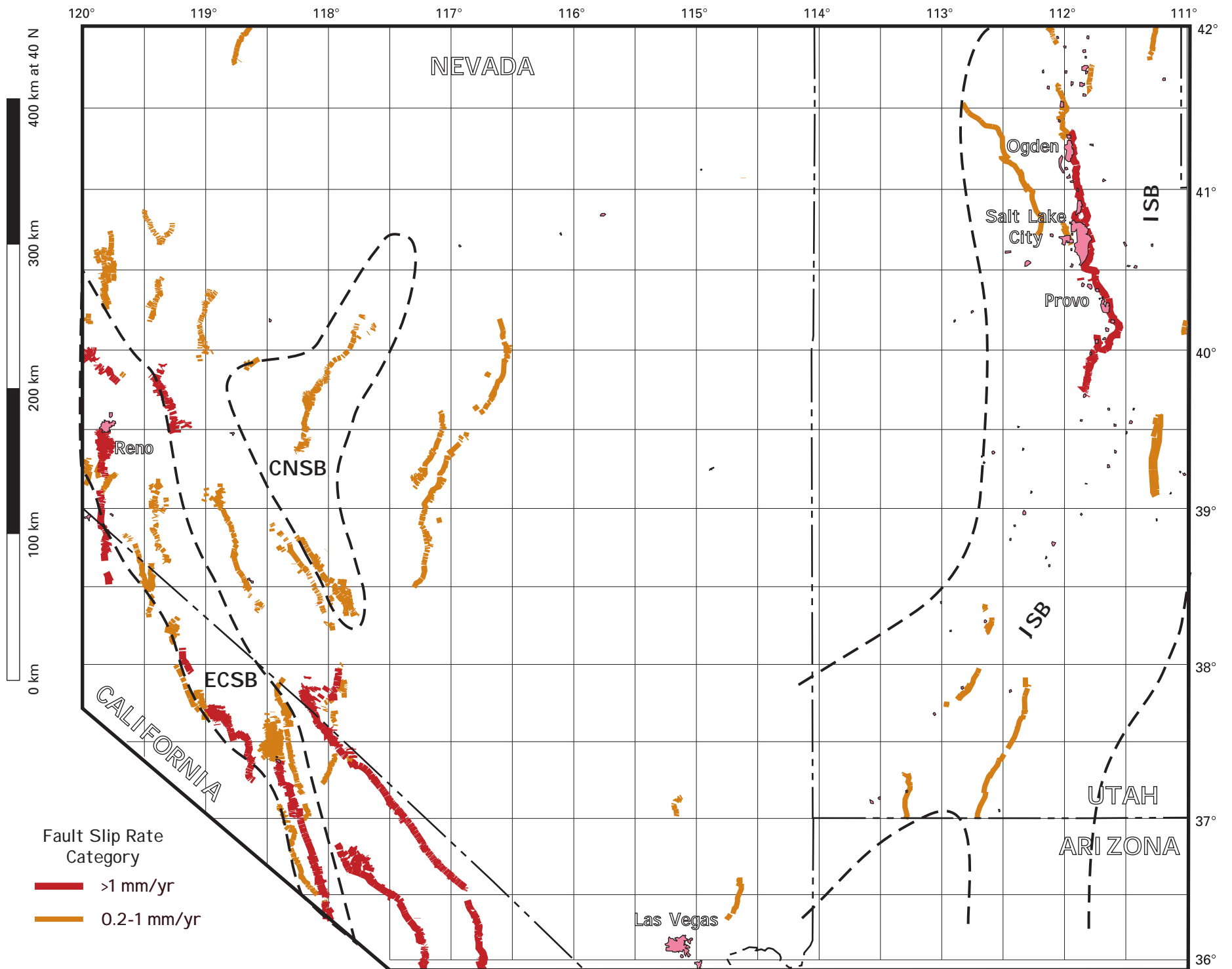


Figure 8. Map showing Quaternary faults in the Great Basin that have high and moderate slip rates.



measurement every 30 seconds (Bennett and others, 1998) but over relatively long station spacing (100 km), whereas the campaign-style networks re-occupy stations 15-25 km apart on an annual (or multi-year) basis and collect data for only 6-24 hours. Used together, the two GPS data sets provide a powerful tool for analyzing contemporary deformation, both in terms of magnitude and direction, across broad regions. These data define an end member (multi-decade long time frame) for comparing extension rates with geologic data (pre-historic, geologically short time frame). However, even for campaign-style GPS networks in the Great Basin, the station spacing can span be several Quaternary faults which leaves the question of which of several Quaternary faults are really active and which ones are inactive. Conversely, the GPS data clearly show concentrated zones or areas of strain accumulation across the Great Basin (see following discussion and Figure 10).

Remotely sensed 3-D positioning data are now becoming available using Interferometric Synthetic Aperture Radar (InSAR) technology, which uses radar satellite images to provide region-wide measurements of deformation. The satellite constantly sends radar waves toward the earth and records the reflected waves off the Earth's surface. Every point in a satellite image (pixel) contains two types of information: intensity and phase. Intensity can be used to characterize the surface material and its orientation with respect to the satellite. The phase is of primary interest to geodesists. If the radar data resamples the exact same portion of the Earth, then the phase images should be identical. Conversely, if the phase on successive images is different, then something has moved. By merging two images and plotting the differences in phase, one can map the location and amount of ground deformation.

InSAR data has been used commonly in studies of large-surface rupturing earthquakes, such as the 1992 Landers (California), 1999 Izmit (Turkey), and 2002 Denali (Alaska) earthquakes. More recently, geoscientists have been using new INSAR data to look for aseismic deformation, such as creep along the San Andreas fault. Unpublished analyses of multi-year images for the west-central Great

Basin show large-magnitude shifts in landscape position within the CNSB (John Bell, oral commun., 2004).

Hopefully, our fault database, continuing paleoseismic investigations in the Intermountain West, new InSAR data, and targeted GPS surveys will help pinpoint those Quaternary faults that are directly associated with contemporary strain accumulation, and thus will identify those that might potentially rupture in future large-magnitude earthquakes. Ultimately, the scientific challenge is to compare geologically determined rates and styles of deformation to contemporary strain fields determined from GPS and InSAR data and see if the regions of accelerated modern extension are relicts of recent past activity or are precursors of future activity.

### **General patterns from GPS data**

During the past decade, GPS data have revealed a variety of similar patterns of extension across the northern Great Basin. From the very beginning, there was clear evidence for 10-12 mm of WNW-directed extension as first indicated by the VBLI data and over the years, details have changed and patterns refined. In the late 1990s, Bennett and others (2003; see also Friedrich and others, 2004) proposed a belt of compression southeast of Battle Mountain, Nevada, that was based primarily on the anomalous behavior of a single continuous GPS station (LEWI). Their explanation of the compression involved an eastward, slowly propagating wave of deformation related to the 1954 faulting events in the CNSB. However, the newest GPS paper dealing with the Great Basin (Hammond and Thatcher, 2004) shows a simple pattern of extension (Figure 10B) that is concentrated in three belts: 1) along the Wasatch Front, 2) in the CNSB, and 3) along the ECSB.

Hammond and Thatcher's (2004) GPS data is from a transect centered on U.S. Highway 50 (popularly billed as America's Loneliest Highway). Their campaign data and nearby continuous station data were used to construct a velocity profile (Hammond and Thatcher, 2004, Figure 2c) across the Basin and Range that is roughly centered on 39.5°N latitude (Figure 10B). For comparison, I

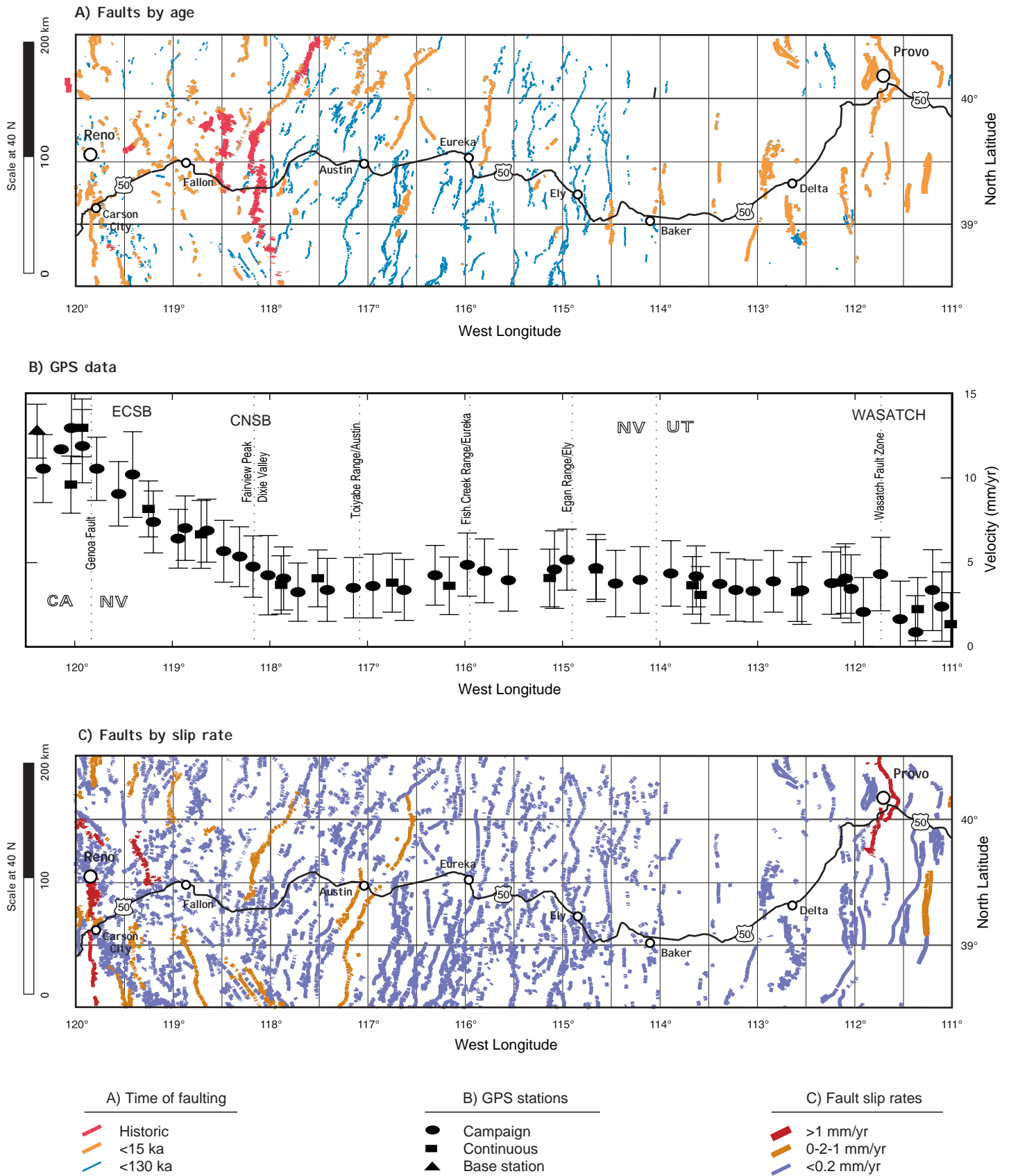


Figure 10. Comparison of time of faulting (A), GPS velocity data (B), and fault slip rates (C) for the area adjacent to U.S. Highway 50 (track of GPS network). Modern velocities across the Great Basin (B) show significant changes at eastern margin (WASATCH), across the CNSB, and at western margin (ECSB). Most of the 11-12 mm/yr of extension is at and west of the CNSB.

plotted the faults in the same area according to time of most recent surface rupture (historic, <15 ka, and <130 ka; Figure 10A) and according to slip rate (>1, 0.2-1, and <0.2 mm/yr; Figure 10C).

The GPS data shows some close associations with the fault data, as noted by Hammond and Thatcher (2004), who used a preliminary version of our Great Basin fault data. Generally speaking, the central part of the Great Basin (eastern Nevada and western Utah) shows little evidence for contemporary extension (Figure 10B), and most faulting in this area is late Quaternary (<130 ka) or older (Figure 6). Faults that lack young (<130 ka) movement generally have low slip rates (see Figure 10C). This generalization is not perfect because, for example, the Toiyabe fault is classified as a late Quaternary (<130 ka) fault, whereas its reported slip rate is 0.2-1 mm/yr. In this case, the faulting may be younger than reported because the fault has neither been studied in terms of geomorphology and surficial geology nor has it been trenched for to determine the timing of its latest surface rupture. Conversely, very young (historic or <15 ka) faults may or may not have reported slip rates of >0.2 mm/yr; the reported rate (or category) depends largely on where the fault is in its individual seismic cycle. This was well illustrated by de Polo and others (1991) who found that more than half of the historic faulting in the Basin and Range Province occurred on pre-Holocene faults.

The two regions of greatest contemporary extension in the Great Basin, its western and eastern margins (Figure 10B), have a high concentration of faults that are <15 ka, but they are not necessarily historic in age. Only faults in the CNSB and ECSB have had historic surface rupturing, whereas structures from near Austin, Nevada (117.5°W) east to the Wasatch fault have not ruptured in historic time. This may just be an artifact of the short period of historic monitoring through felt and recorded seismicity not giving a true indication of which faults are accumulating and releasing strain at depth. The historic earthquake record for the Wasatch Front region is only about 150 years long—the length of time the region has been populated by European settlers. By comparison, recurrence intervals on

individual segments of the Wasatch fault zone are commonly >500 years to as much as 2,500 years long (Lund, in press).

The plot of faults by slip rate (Figure 10C) shows a stronger correlation to the GPS data (Figure 10B) than do the fault ages (Figure 10A). Slip rate is a direct geologic measure of strain rate, and the two previously mentioned regions of extension have faults categorized as slipping at average rates of 0.2-1 mm/yr (orange lines) and > 1 mm/yr (red lines). The one obvious exception is a belt of moderate slip-rate faults (0.2-1 mm/yr) between Austin and Eureka, Nevada (Figure 8). These include the Toiyabe Range fault zone (#1137) and Western Toiyabe Range fault zone (#1136), respectively, and the Simpson Park Mountains fault zone (#1178). The Simpson Park Mountains fault zone may continue northeastward as the Cortez Mountains fault zone (#1157). Recent paleoseismic studies of the Cortez Mountains fault zone (also known as the Crescent fault) have indicated movement as young as 3 ka (Friedrich and others, 2004), but no slip rates have been determined for the fault zone. These faults form a wide zone of extension that extends at least 200 km in a NNE direction, a length that is almost as long as the CNSB. However, not all of these faults have not been studied in detail, so some times of movement may be misclassified.

In summary, the times of faulting and slip rates for structures along the Highway 50 GPS transect (Figure 10) show compatible and even correlative patterns. The short record of felt and recorded seismicity in the Great Basin and the lack of detailed studies for most faults in the transect limit the one-to-one association of faults and velocity changes reported by Hammond and Thatcher (2004). Nevertheless, continued refinement of the GPS and InSAR data, additional paleoseismic studies of major faults across the transect, and improvements in Quaternary dating techniques applicable to fault studies will eventually help us identify which of the hundreds of relatively young (<130 ka) faults in the Great Basin are contributing to the 11-12 mm/yr of net NNW-directed extension across the region.

## **CENTRAL NEVADA SEISMIC BELT**

### **Historic surface ruptures and prehistoric faults**

Except for aftershock activity associated with some of the faults with historical ruptures in the province, there is little spatial association between faulting and recorded seismicity and virtually no examples of foreshock activity for large earthquakes. For example, the Wasatch fault zone is poorly expressed on Utah seismicity maps, and the Thousand Springs segment of the Lost River fault (northern Basin and Range Province in Idaho) was virtually aseismic before it ruptured during the 1983 Borah Peak earthquake (Dewey, 1987). Similar examples of a lack of correlation between contemporary  $M < 6$  seismicity and faulting are common in the Great Basin, especially in its southern half. For the most part, the normal faults in the Great Basin seem to be aseismic and locked, but may be near the point of failure as was the case in the 1954 Fairview Peak and Dixie Valley earthquake sequence.

In contrast, the ECSB and CNSB have been the preferred areas for historic earthquakes larger than  $M 6.5$  in the Basin and Range Province (Figure 2). From 1872 to 1954, seven large earthquakes caused surface ruptures along these NNW- and NNE-trending belts—an average of one rupture every 14 years. A recent summary of paleoseismic investigations of the CNSB (Bell and others, 2004) has shown that this rate and spatial pattern of activity is geologically anomalous. There is no compelling evidence for similar precursory activity in the past 50 kyr on this belt, and there has been almost 50 years of quiescence since the last large earthquake. So, two perplexing questions about the CNSB are “why here have the earthquakes clustered here and where will the next surface ruptures occur?”

### **Late Quaternary faulting along the CNSB**

The CNSB is remarkable mainly for of its historical activity. This NNE-trending zone of historical surface-rupturing faults extends from the Monte Cristo Valley on the south to the northern end of Pleasant Valley on the north. Although largest magnitude earthquakes in this belt occurred in 1915 (Pleasant Valley) and 1932 (Cedar Mountain), historical activity culminated with a sequence of

four earthquakes in 1954 (Table 2), the two largest (Fairview Peak and Dixie Valley), occurring in December 1954, just four minutes apart.

Within this 250-km-long belt, the historical faults are interspersed with faults that are prehistoric in terms of most recent movement. For example, in 1954 the Dixie Valley fault ruptured, but its southward extension—the Sand Springs fault—has no historic ruptures. Similarly, the 1915 Pleasant Valley fault zone ruptured, but its northward extension—the Sonora Range fault—has no historic ruptures. Similarly, between the Dixie Valley and Pleasant Valley faults there is an approximately 35-km-long section of range-front fault that is referred to as the Stillwater (Range) gap. Any of these prehistoric faults could be the focus of future surface-rupturing earthquakes that would restart the 40-year-long cluster (1915-1954) of earthquake activity in the CNSB.

One of the most important questions concerning the CNSB is whether or not it has acted similarly (temporal clustering) in the past. Recent studies by John Caskey, John Bell, Alan Ramelli, and Steve Wesnousky (and their colleagues), as well as those by USGS geologists (mainly Tony Crone, Kathy Haller, myself, and Stephen Personius) has helped assemble the paleoseismic history of the CNSB. These results are elucidated in a new paper by Bell and others (2004), and, thus is just briefly reviewed herein.

Basically, the time sequence for large fault-rupturing earthquakes in the CNSB region is one of irregularly spaced events that do not show the temporal clustering that defines the modern CNSB (Figure 11). For example, the faults that were activated in the 1932 Cedar Mountain earthquake show short repeat times (1-3 kyr) within clusters and longer (4-6 kyr) intercluster repeat times. On average, the Cedar Mountain faults have short recurrences (4 kyr, 6 events in ca. 20 ka) compared to other faults in the CNSB. Conversely, faults to the north typically have one or two prehistoric (penultimate) faulting events, with some recurrence intervals exceeding 15 kyr (Pleasant Valley) to 35 kyr (Fairview Peak). Most of the events are only broadly constrained by radiocarbon dates or lumi-

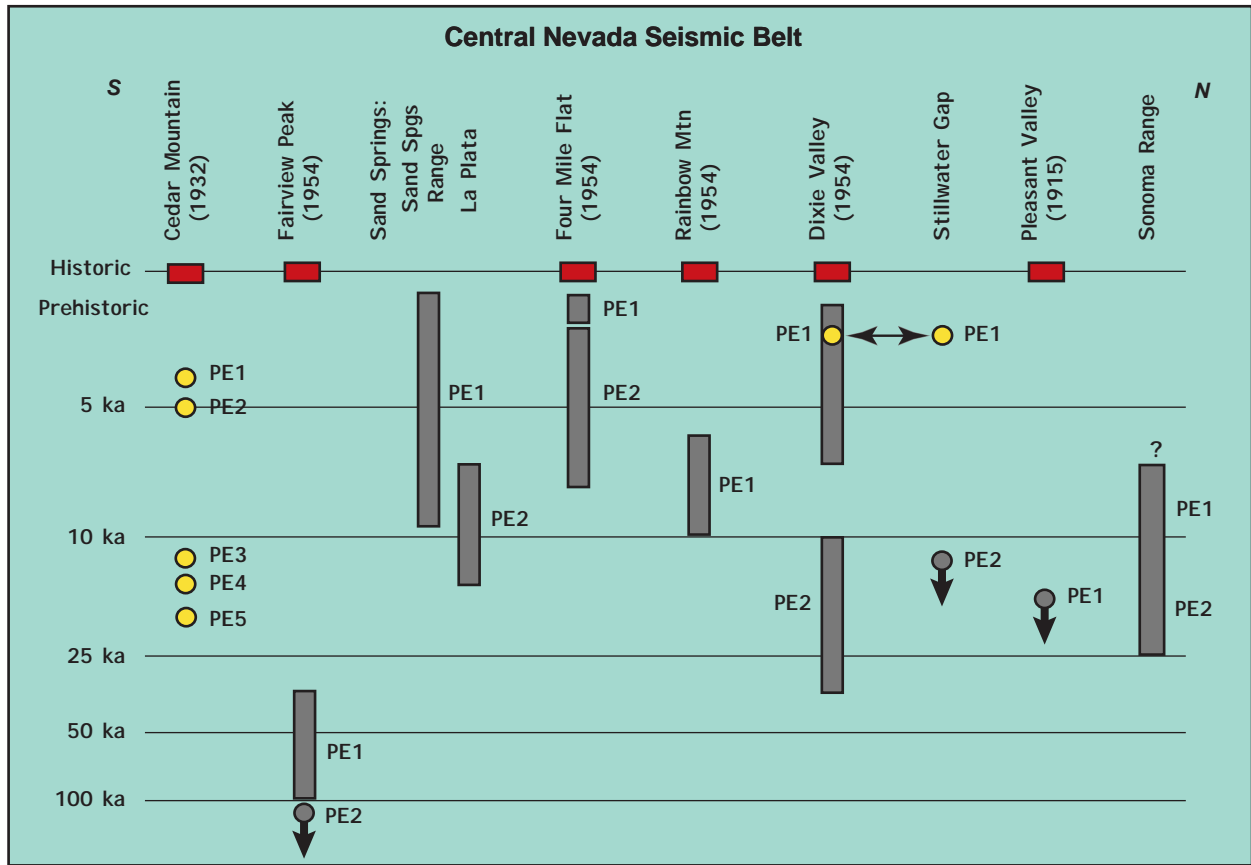


Figure 11. Schematic diagram showing times of surface rupture on Quaternary faults in part of the Central Nevada seismic belt. Information is based on new synthesis by Bell and others (2004). Gray boxes show permissible times of fault rupture; yellow dots indicate more specific time limits. Arrows indicate minimum possible time of earthquake. Timing of penultimate event (PE1, 2.0-2.5 ka) in Dixie Valley is inferred from studies along the Stillwater Gap.

nescence age estimates on faulted or unfaulted deposits. For the Stillwater Gap, Bell and others (2004) have a well-controlled time of about 2.0-2.5 kyr for the penultimate event (PE1, Figure 11) that they also attribute to the Dixie Valley fault.

Bell and others (2004) do not make a case for prehistoric analogs on the CNSB, but consider that some multi-fault rupture patterns (laterally smaller temporal clusters) may have occurred in the past. Nevertheless, at this time the conclusion seems to be that there have not been similar belt-long ruptures in the past 35 kyr to perhaps 100 kyr on the CNSB. One possible prehistoric analog to this belt might be the faults along the Toiyabe-Simpson Park Mountains, as mentioned previously. They show evidence of a belt-like rupture pattern, but the times of individual fault ruptures in the belt are unknown at this time. As for recurrence intervals in the CNSB, the general pattern seems to be two to three events in the Holocene, but there are two faults with no Holocene events: the Fairview Peak and Pleasant Valley faults, which ruptured in 1954 but had been stable for tens of thousands of years before their recent activity (Figure 11).

### SUMMARY

Information culled from the USGS's new National Quaternary fault and fold database (<http://Qfaults.cr.usgs.gov>) and from new paleoseismic studies that are either published or in press help decipher broader spatial and temporal patterns of late Quaternary faulting in the Great Basin of eastern California, Nevada, and Utah. Several key points from this summary review are listed below.

Late Quaternary faulting is concentrated in three distinct areas along the margins of the Great Basin, specifically the ECSB and CNSB in Nevada and the ISB in Utah. The central part of the Great Basin, specifically in western Utah and eastern to southern Nevada, appears to be least active in terms of fault recency and has slow fault-slip rates.

Using a time window for the past 130 kyr captures most of the faults that are known to have Quaternary activity in the Great Basin, and thus provides a restricted but reliable window for probabilistic seismic-hazards analysis at low probability

levels (i.e., 2 percent in 1,000 years).

The presence of extensive late Pleistocene pluvial lakes obscures or buries evidence of pre-15 ka faulting, and older lakes (i.e., 130-150 ka) obscure evidence of middle to early Quaternary faulting. These gaps in the record of faulting are particularly noticeable in the Lake Bonneville basin, which mainly flooded low-lying areas of northwestern Utah.

Over most of the Great Basin, fault slip rates and recurrence intervals are slow (<0.2 mm/yr) and long (tens of thousands of years), except in the Walker Lane and along the Wasatch Front. Here faults have slip rates that approach and exceed 1-5 mm/yr and appear to rupture on intervals of hundreds of years (strike-slip faults) to thousands (normal faults) years. The pattern of fault slip rates suggest that most of the gross topography of the interior Great Basin is probably a relict of the late Miocene (15-5 Ma) and Pliocene (5-1.6 Ma) normal faulting, with minor rejuvenation during the Pleistocene.

The concentration of historical surface ruptures in the CNSB appears to be a geological anomaly—this seismic belt has had no similar precursory activity in the late Quaternary. Other faults in the Great Basin may have previously ruptured in a belt-like pattern although dating or paleoseismic studies have not been conducted to determine if such belts are present in the region. For example, the relatively continuous zone of faulting that extends north-northeast along the eastern and western margins of the Toiyabe Range may have had a belt-like pattern of rupture.

Although any one single fault poses a relatively low hazard, the presence of numerous late Quaternary faults in any particular region increases the average rate of earthquake recurrence in the Great Basin. The fact that virtually all of these faults are seismically inactive gives one the impression that the hazard posed by faulting in the Great Basin is relatively low. Conversely, the presence of active fault belts, such as the CNSB and ECSB, and new GPS data show that the region is experiencing modest extension which can be accommodated by earthquakes of moment magnitude 7.

## ACKNOWLEDGMENTS

This paper was derived from data compiled by a team of geologists at the USGS, at State geological surveys, private consulting firms, and in academia. In alphabetical order, they include Kenneth D. Adams, R. Ernest Anderson, Bill D. Black, Gary E. Christenson, Craig dePolo, Kathleen M. Haller, Suzanne Hecker, Michael D. Hylland, David J. Lidke, myself, James P. McCalpin, Greg N. McDonald, John A. Oswald, Margaret Hiza Redsteer, Marith C. Reheis, Peter C. Rowley, Janet E. Sawyer, Thomas L. Sawyer, and Barry J. Solomon. (See USGS fault database for affiliations and addresses of the compilers). The fault trace data were supplied by Richard Dart (USGS), who graciously transformed the Arcshape files into post-script files for my use in Adobe Illustrator. However, any errors in visualization or analysis of the data are solely my responsibility. This paper is the outgrowth of oral presentation at the 2003 AGU meeting (San Francisco, CA), which I was invited to give by Ivan Wong of URS Corporation (Oakland, CA).

## REFERENCES

- Adams, K.D., and Wesnousky, S.G., 1998, Shoreline processes and the age of Lake Lahontan highstand in the Jessup embayment, Nevada: Geological Society of America Bulletin, v. 110, p. 1318-1332
- Bell, J.W., Caskey, S.J., Ramelli, A.R., and Guerrieri, L., 2004, Pattern and Rates of Faulting in the Central Nevada Seismic Belt and Paleoseismic Evidence for Prior Beltlike Behavior: Bulletin of the Seismological Society of America, v. 94, no. 4, p. 1229-1254.
- Bell, J.W., Caskey, S.J., and Ramelli, A.R., this volume, Pattern and timing of faulting in the central Nevada seismic belt and implications for seismic hazards of the western Basin and Range Province, *in* Lund, W.R., editor, Proceedings of the Basin and Range Province Seismic Hazards Summit II, Western States Seismic Policy Council meeting, Reno, Nevada, May 16-91, 2004: Utah Geological Survey Special Miscellaneous Publication, compact disk.
- Bull, W.B., and Pearthree, P.A., 1984, Frequency and size of Quaternary surface ruptures of the Pitaycachi fault, northeastern Sonora, Mexico: Bulletin of the Seismological Society of America, v. 78, p. 956-978.
- Bennett, R.A., Wernicke, B.P., and Davis, J.L., 1998, Continuous GPS measurements of contemporary deformation across the northern Basin and Range Province: Geophysical Research Letters, v. 25, no. 4, p. 563-566.
- Bennett, R.A., Wernicke, B.P., Niemi, N.A., Friedrich, A.M., Davis, J.L., 2003, Contemporary strain rates in the northern Basin and Range Province from GPS data: Tectonics, v. 22, no. 2, 1008, doi: 10.1029/2001TC001355 (31 p.).
- Briggs, R.W., and Wesnousky, S.G., 2004, Late Pleistocene fault slip rate, earthquake recurrence, and recency of slip along the Pyramid Lake fault zone, Nevada: Journal of Geophysical Research, v. 109, no. B08402, doi: 10.1029/2003JB002717.
- this volume, Late Pleistocene paleoearthquake activity of the Olinghouse fault zone, Nevada, *in* Lund, W.R., editor, Proceedings of the Basin and Range Province Seismic Hazards Summit II, Western States Seismic Policy Council meeting, Reno, Nevada, May 16-91, 2004: Utah Geological Survey Special Miscellaneous Publication, compact disk.
- Caskey, S.J., 1996, Surface faulting, static stress changes, and earthquake triggering during the 1954 Fairview Peak (Ms 7.2) and Dixie Valley (Ms 6.8) earthquakes, central Nevada: Reno, University of Nevada—Mackay School of Mines, unpublished Ph. D. thesis, 144 p.
- Caskey, S.J., Bell, J.W., Ramelli, A.R., and Wesnousky, S.G., 2004, Historic Surface Faulting and Paleoseismicity in the Area of the 1954 Rainbow Mountain and Stillwater Earthquake Sequence, Central Nevada: Bulletin of the Seismological Society of America, v.94, no. 4, p. 1255-1275
- Cerling, T.E., and Craig, H., 1994, Cosmogenic <sup>3</sup>He production rates from 39 degrees N to 46 degrees N latitude, western USA and France:

- Geochimica et Cosmochimica Acta, v. 58, no.1, p. 249-255
- Crone, A.J., Kyung, J.-B., Machette, M.N., Lidke, D.J., Okumura, K., and Mahan, S.A., in press, Data related to late Quaternary surface faulting on the Eastgate fault, Churchill County, Nevada: U.S. Geological Survey Scientific Investigations Map.
- de Polo C.M., and Slemmons, D.B., 1998, Age criteria for active faults in the Basin and Range Province, in Lund, W.E., ed., Proceeding volume, Basin and Range Seismic-Hazards Summit: Utah Geological Survey Miscellaneous Publication 98-2, p. 74-83
- de Polo, C.M., Clark, D.G., Slemmons, D.B., and Ramelli, A.R., 1991, Historical surface faulting in the Basin and Range Province, western North America—Implications for fault segmentation: *Journal of Structural Geology*, v. 13, no. 2, p. 123-136
- Dewey, J.W., 1987, Instrumental seismicity of central Idaho: *Bulletin of the Seismological Society of America*, v. 77, no. 3, p. 819-836
- Dixon, T.R., Stefano, R., Lee, J., and Reheis, M.C., 1995, Constraints on present-day Basin and Range deformation from space geodesy: *Tectonics*, v. 14, p. 755-772.
- Friedrich, A.M., Lee, J., Wernicke, B.P., and Sieh, K., 2004, Geologic context of geodetic data across a Basin and Range normal fault, Crescent Valley, Nevada: *Tectonics*, v. 23, TC2015, doi: 10.1029/2003TC001528 (24 p.).
- Gianella, V.P., and Callaghan, E., 1934a, The Cedar Mountain, Nevada, earthquake of December 20, 1932: *Bulletin of the Seismological Society of America*, v. 24, p. 345- 377.
- 1934b, The earthquake of December 20, 1932, at Cedar Mountain, Nevada, and its bearing on the genesis of Basin Range structure: *Journal of Geology*, v. 42, p. 1-22.
- Gilbert, G.K., 1884, A theory of the earthquakes of the Great Basin, with a practical application: *American Journal of Science*, Third Series, v. XXVII, no. 157, p. 49-54
- Haller, K.M., Machette, M.N., and Dart, R.L., 1993, Maps of major active faults, Western Hemisphere; International Lithosphere Program (ILP) Project II-2: Guidelines for U.S. database and map: U.S. Geological Survey Open-File Report 93-338, 45 p.
- Hammond, W.C., and Thatcher, W., 2004, Contemporary tectonic deformation of the Basin and Range Province, western United States—10 years of observation with the Global Positioning System: *Journal of Geophysical Research*, v. 109, doi: 10.1029/2003JB002746.
- Lund, W.R., in press, Utah Quaternary Fault Parameters Working Group—Review of Utah paleoseismic-trenching data and determination of consensus recurrence-interval and vertical slip-rate estimates: *Utah Geological Survey Bulletin*, variously paginated (see also this volume).
- Machette, M.N., 2000, Active, Capable, and Potentially Active Faults—A paleoseismic perspective, in G. Cello, D. Giovanni, C. Invernizzi, and E. Tondi, eds., *The Resolution of Geological Analysis and Models for Earthquake Faulting Studies: Journal of Geodynamics*, v. 29, p. 387-392.
- Machette, M.N., Johnson, M.L., and Slate, J.L., (eds.), 2001, Quaternary and Late Pliocene geology of the Death Valley region—Recent observations on tectonics, stratigraphy, and lake cycles (Guidebook for the 2001 Pacific Cell: Friends of the Pleistocene field trip): U.S. Geological Survey Open-File Report 01-51, 246 p.
- Machette, M.N., Personius, S.F., and Nelson, A.R., 1992, Paleoseismology of the Wasatch fault zone—A summary of recent investigations, conclusions, and interpretations, in Gori, P.A., and Hays, W.W., eds., *Assessing Regional Earthquake Hazards and Risk along the Wasatch Front, Utah*; U.S. Geological Survey Professional Paper 1500, Chapter A, p. A1-A72.
- Machette, M.N., Haller, K.M., Rhea, B.S., and Dart, R.L., this volume, Quaternary fault database for the Basin and Range province of Nevada and Utah, Lund, W.R., in press, Utah Quaternary Fault Parameters Working Group—Review of Utah paleoseismic-trenching data and determination of consensus recurrence-interval and

- vertical slip-rate estimates: *Utah Geological Survey Bulletin*, variously paginated (see also this volume).
- Machette, M.N., Haller, K.M., Ruleman, C.A., Mahan, S., and Okumura, K., in press, Evidence for late Quaternary movement on the Clan Alpine fault, west-central Nevada—Trench logs, location maps, and sample and soil descriptions: *U.S. Geological Survey Scientific Investigations Map*.
- Minster, J.B., and Jordan, T.H., 1984, Vector constraints on Quaternary deformation of the western United States east and west of the San Andreas fault, in J.K. Crouch, and S.B. Bachman, eds., *Tectonics and Sedimentation along the California margin: Pacific Section, Society of Economic Paleontologists and Mineralogists*, v. 38, p. 1-16, Los Angeles.
- Personius, S.F., and Mahan, S.A., 2005, Paleoearthquakes on the Santa Rosa Range fault zone, northern Nevada, and potential for future extension of the Central Nevada seismic belt: *Bulletin of the Seismological Society of America*, v. 95, no. 1 (in press).
- Reheis, M., 1999, Extent of Pleistocene lakes in the western Great Basin: *U.S. Geological Survey Miscellaneous Field Studies Map MF-2323*, scale 1:800,000
- Stewart, J.H., 1971, Basin and Range structure—A system of horsts and grabens produced by deep-seated extension: *Geological Society of America Bulletin*, v. 82, p. 1019-1044.
- 1980, Regional tilt patterns of late Cenozoic basin-range blocks in western United States: *Geological Society of America Bulletin*, v. 91, p. 460-464
- Suter, Max, 2001, The historical seismicity of northeastern Sonora and northwestern Chihuahua, Mexico (28-32°N, 106-111°W): *Journal of South American Earth Sciences*, v. 14, p. 521-532.
- Thatcher, W., 2003, GPS constraints on the kinematics of continental deformation: *International Geology Review*, v. 45, no. 3, p. 191-212.
- Thatcher, W., Foulger, G.R., Julian, B.R., Svarc, J.L., Quity, E., and Bawden, G.W., 1999, Present day deformation across the Basin and Range Province, Western United States: *Science*, v. 283, no. 5408, p. 1714-1718.
- Thenhaus, P.C., and Barnhard, T.P., 1989, Regional termination and segmentation of Quaternary fault belts in the Great Basin, Nevada and Utah: *Bulletin of the Seismological Society of America*, v. 79, no. 5, p. 1426-1438.
- Thenhaus, P.C., and Wentworth, C.M., 1982, Map showing zones of similar ages of surface faulting and estimated maximum earthquake size in the Basin and Range Province and selected adjacent areas: *U.S. Geological Survey Open-File Report 82-742*, 16 p., 1 plate, scale 1:2,500,000.
- Trifonov, V.G., and Machette, M.N., 1993, The World Map of Major Active Faults Project, in D. Giardini and P. Basham, eds., *Special Issue—Technical Planning Volume for the ILP's Global Seismic Hazards Assessment Program for the UN/IDNDR: Istituto Nazionale di Geofisica Annali di Geofisica*, v. XXXVI, no. 3-4, p. 225-236, June-July, 1993.
- Wallace, R.E., 1984, Fault scarps formed during the earthquakes of October 2, 1915, in Pleasant Valley, Nevada, and some tectonic implications, in *Faulting related to the 1915 earthquakes in Pleasant Valley, Nevada: U.S. Geological Survey Professional Paper 1274-A*, p. A1-A33, 1 pl., scale 1:62,500
- Wesnousky, S.G., 2004a, written communication (Active faulting in the Walker Lane: Manuscript submitted to *Tectonics*).
- Wesnousky, S.G., Barron, A.D., Briggs, R.W., and Kumar, S.C., 2004b, written communication (Paleoseismic transect across the northern Great Basin, USA: Manuscript submitted to *Journal of Geophysical Research*).

# **UTAH QUATERNARY FAULT PARAMETERS WORKING GROUP: CRITICAL REVIEW OF UTAH PALEOSEISMIC-TRENCHING DATA AND CONSENSUS RECURRENCE-INTERVAL AND VERTICAL SLIP- RATE ESTIMATES FOR UTAH'S QUATERNARY FAULTS**

William R. Lund  
Utah Geological Survey  
SUU Box 9053  
Cedar City, UT 84720  
[WilliamLund@utah.gov](mailto:WilliamLund@utah.gov)

*The Utah Geological Survey published a more comprehensive version of this paper as UGS Bulletin 2005-134*

## **ABSTRACT**

The Utah Quaternary Fault Parameters Working Group, a panel of experts convened in 2003-04, has completed a comprehensive evaluation of paleoseismic-trenching data available for Utah's Quaternary faults, and where the data permit have assigned consensus preferred recurrence-interval (RI) and vertical slip-rate (VSR) estimates for the faults/fault sections under review. Trenching data are available for 33 (16%) of Utah's 212 Quaternary faults/fault sections and related structures. The available paleoseismic-trenching data are most abundant on the six central, active segments of the Wasatch fault zone coincident with the populous Wasatch Front, and typically are much less abundant for faults elsewhere in Utah.

The general paucity of paleoseismic-trenching data, combined with large uncertainties associated with some of the data, prevented using rigorous statistical techniques to determine RI and VSR values. Consequently, the Working Group relied on the broad experience and best professional judgment of its members to assign preferred RI and VSR estimates to the faults/fault sections under review. For some faults/fault sections, the trenching data were insufficient for the Working Group to make RI and VSR estimates. The Working Group also determined "best estimate" confidence limits for the RI and VSR estimates that reflect both epistemic and aleatory uncertainties associated with each fault/fault section. Until superseded by information from new paleoseismic investigations, the Working Group's preferred RI and VSR estimates and associated confidence limits represent the best available information regarding surface-faulting activity for the faults/fault sections reviewed, and can be considered as approximating average RI and VSR values and 2-sigma variability about those mean values.

## **INTRODUCTION**

This report presents the results of the Utah Quaternary Fault Parameters Working Group (hereafter referred to as the Working Group) review and evaluation of Utah's Quaternary fault paleoseismic-trenching data. The purpose of the review was to (1) critically evaluate the accuracy

and completeness of the paleoseismic-trenching data, particularly regarding earthquake timing and displacement, (2) where the data permit, assign consensus, preferred recurrence-interval (RI) and vertical slip-rate (VSR) estimates with appropriate confidence limits to the faults/fault sections under review, and (3) identify critical gaps in the paleoseismic data and recommend where and what

kinds of additional paleoseismic studies should be performed to ensure that Utah’s earthquake hazard is adequately documented and understood. It is important to note that, with the exception of the Great Salt Lake fault zone, the Working Group’s review was limited to faults/fault sections having paleoseismic-trenching data. Most Quaternary faults/fault sections in Utah have not been trenched, but many have RI and VSR estimates based on tectonic geomorphology or other non-trench-derived studies. Black and others (2003) compiled the RI and VSR data for Utah’s Quaternary faults, both those with and without trenches.

Although used extensively by researchers and geologic and engineering practitioners, prior to this review, Utah’s Quaternary fault paleoseismic-trenching data had not been critically evaluated to establish consensus fault parameter values and confidence limits. Consequently, users unfamiliar with the database and unaware of important caveats often did not recognize variations in the quality and

completeness of the data. Consensus RI and VSR estimates are a critical component in four areas directly related to reducing losses from earthquakes in Utah: (1) updating the National Seismic-Hazard Maps, (2) characterizing seismic sources, (3) performing probabilistic seismic-hazard analyses, and (4) providing consensus paleoseismic data for research into other earthquake topics. With a widely distributed consensus dataset, all users can have access to expert-reviewed paleoseismic-trenching data that are qualified with appropriate caveats, and from which they can make informed judgments regarding their own research and projects.

Table 1 presents a summary of the Working Group’s results. An expanded table in the appendix contains additional critical background information regarding the paleoseismic data considered in the Working Group review.

**Table 1. Summary of Working Group consensus values for timing of most recent surface faulting and preferred recurrence-interval and vertical slip-rate estimates.**

<b>Fault Fault Section/Segment<sup>1</sup></b>	<b>Timing of Most Recent Earthquake</b>	<b>Preferred Recurrence Interval (kyr)<sup>2,3</sup></b>	<b>Preferred Vertical Slip Rate (mm/yr)<sup>2</sup></b>
Wasatch fault zone Brigham City segment	2100±800 cal yr B.P. <sup>4</sup>	0.5-1.3-2.8	0.6-1.4-4.5
Weber segment	0.5±0.3 ka <sup>5</sup> /950±450 cal yr B.P. <sup>6</sup>	0.5-1.4-2.4	0.6-1.2-4.3
Salt Lake City segment	1300±650 cal yr B.P.	0.5-1.3-2.4	0.6-1.2-4.0
Provo segment	600±350 cal yr B.P.	1.2-2.4-3.2	0.6-1.2-3.0
Nephi segment	≤1.0±0.4 ka <sup>7</sup>	1.2-2.5-4.8	0.5-1.1-3.0
Levan segment	≤1000±150 cal yr B.P.	>3, <12 <sup>8</sup>	0.1-0.6 <sup>8</sup>
Joes Valley fault zone <sup>9</sup>	Not constrained	5-10-50	No estimate
West Valley fault zone	1.3-1.7 ka	No estimate	0.1-0.4-0.6
West Cache fault zone Clarkston fault	3600-4000 cal yr B.P.	5-20 <sup>8</sup>	0.1-0.4-0.7
Junction Hills fault	8250-8650 cal yr B.P.	10-25 <sup>8</sup>	0.05-0.1-0.2
Wellsville fault	4400-4800 cal yr B.P.	10-25 <sup>8</sup>	0.05-0.1-0.2
East Cache fault zone central section	4.3-4.6 ka	4-10-15	0.04-0.2-0.4
Hurricane fault zone Anderson Junction section	5-10 ka	5-50 <sup>8</sup>	0.05-0.2-0.4
Great Salt Lake fault zone <sup>10</sup> Fremont Island segment	3150+235/-211 cal yr B.P.	1.8-4.2-6.6	0.3-0.6-1.6

Antelope Island segment	586+201/-241 cal yr B.P.	1.8- <b>4.2</b> -6.6	0.3- <b>0.6</b> -1.6
Oquirrh fault zone	4.8-7.9 cal yr B.P.	5- <b>20</b> -50	0.05- <b>0.2</b> -0.4
Southern Oquirrh Mountains fault zone Mercur fault	Shortly after 4.6±0.2 ka	5- <b>20</b> -50	0.05- <b>0.2</b> -0.4
Eastern Bear Lake fault southern section	<2.1±0.2 ka, but >0.6±0.08 ka	3- <b>8</b> -15	0.2- <b>0.6</b> -1.6
Bear River fault zone	2370±1050 yr B.P. <sup>11</sup>	1-100 <sup>8</sup>	0.05- <b>1.5</b> -2.5
Morgan fault zone central section	<8320±100 <sup>14</sup> C yr B.P. <sup>12</sup>	25-100 <sup>8</sup>	0.01- <b>0.02</b> -0.04
James Peak fault	>30-70 ka	10- <b>50</b> -100	0.01- <b>0.03</b> -0.07
Towanta Flat graben <sup>9</sup>	>130-150 ka	25- <b>50</b> -200	No estimate
Bald Mountain fault	>130 ka	No estimate	No estimate
Strawberry fault	≥1.5 ka	5- <b>15</b> -25	0.03- <b>0.1</b> -0.3
Hansel Valley fault	C.E. 1934 <sup>13</sup>	15- <b>25</b> -50	0.06- <b>0.12</b> -0.24
Hogsback fault southern section	Not constrained	No estimate	No estimate
North Promontory fault	Latest Pleistocene/Holocene	No estimate	0.1- <b>0.2</b> -0.5
Sugarville area faults	Not constrained	No estimate	No estimate
Washington fault zone northern section	Not constrained	No estimate	No estimate
Fish Springs fault	<2280±70 <sup>14</sup> C yr B.P.	No estimate	No estimate

<sup>1</sup> "Section" refers to a portion of a fault defined on the basis of static geologic criteria (geomorphic or structural), but for which no evidence presently exists to show that its history of surface faulting is different from adjacent parts of the fault. "Segment" refers to a portion of a fault, typically also defined on the basis of geomorphic or structural criteria, but for which historical surface ruptures or paleoseismic data show that the history of surface faulting is different from adjacent portions of the fault, and therefore that the seismogenic behavior of the segment is independent from that of the remainder of the fault.

<sup>2</sup> Consensus preferred recurrence-interval and vertical slip-rate estimates (**bold**) with approximate 2-sigma confidence limits; see section on Consensus Process for a discussion of the process used to determine these values.

<sup>3</sup> kyr = thousand years.

<sup>4</sup> cal. yr. B.P. = calendar years before present; designates <sup>14</sup>C ages that have been calibrated to calendric years according to one of several available data sets used to correct <sup>14</sup>C ages for the uneven production of <sup>14</sup>C in the atmosphere over time. Present, by convention, is taken as A.D. 1950.

<sup>5</sup> ka = kilo-annum: thousand years before present.

<sup>6</sup> Two most recent earthquakes are reported for Weber segment; no consensus among investigators regarding the 0.5 ka event.

<sup>7</sup> Most recent surface-faulting earthquake may be as young as 0.4 ka.

<sup>8</sup> Due to limited data, parameter is reported as a range rather than as a central value with approximate 2-sigma confidence limits.

<sup>9</sup> Seismogenic origin of structure is uncertain.

<sup>10</sup> Information is derived from high-resolution geophysics and drilling information; there are no trench data.

<sup>11</sup> Calendar calibrated but no mean residence correction applied.

<sup>12</sup> <sup>14</sup>C yr B.P. = radiocarbon years before present; designates the age of a sample in <sup>14</sup>C years prior to calibration to correct for the uneven production of <sup>14</sup>C in the atmosphere over time. Present, by convention, is taken as A.D. 1950.

<sup>13</sup> Historical surface-faulting earthquake; C.E. = Current Era.

## UTAH QUATERNARY FAULT PARAMETERS WORKING GROUP

Various seismic-hazard-evaluation initiatives in California (Working Group on California Earthquake Probabilities, 1988, 1990, 1999) have successfully employed the concept of working groups composed of technical experts in a field of interest to critically evaluate various datasets and arrive at consensus decisions regarding data values and reliability. The UGS employed a similar strategy and convened the Utah Quaternary Fault Parameters Working Group composed of experts in

the fields of paleoseismology and seismology in 2003-04. The paleoseismologists on the Working Group collectively represent many decades of experience in conducting paleoseismic investigations in Utah as well as throughout the United States and around the world. Likewise, the seismologists on the Working Group are familiar with Utah tectonics, and have worked directly with Utah's paleoseismic data.

The Working Group included two categories of experts, all serving in a volunteer capacity. The first category consists of paleoseismologists having direct knowledge of Utah's Quaternary fault

dataset. These individuals have investigated one or more of Utah’s Quaternary faults, and are responsible for much of the paleoseismic-trenching data reviewed by the Working Group. The second category consists of knowledgeable experts capable of providing critical analysis of the paleoseismic

data, but who have not conducted paleoseismic studies in Utah and therefore have no vested interest in the Utah data; this group includes both paleoseismologists and seismologists. Table 2 lists the members of the Utah Quaternary Fault Parameters Working Group and their affiliations.

**Table 2. Members of the Utah Quaternary Fault Parameters Working Group.**

**Category 1: Paleoseismologists who have conducted paleoseismic investigations in Utah.**

- Suzanne Hecker – U.S. Geological Survey; Menlo Park, California
- Michael Hylland – Utah Geological Survey; Salt Lake City, Utah
- William Lund – Utah Geological Survey; Cedar City, Utah
- Michael Machette – U.S. Geological Survey; Denver, Colorado
- James McCalpin – GEO-HAZ Consulting; Crestone, Colorado
- Alan Nelson – U.S. Geological Survey; Denver, Colorado
- Susan Olig – URS Corporation; Oakland, California
- Dean Ostenaar – U.S. Bureau of Reclamation; Denver, Colorado
- Stephen Personius – U.S. Geological Survey; Denver, Colorado
- David Schwartz – U.S. Geological Survey; Menlo Park, California

**Category 2: Subject-matter experts who have not conducted paleoseismic investigations in Utah.**

- Craig dePolo – Nevada Bureau of Mines and Geology; Reno, Nevada
- Kathleen Haller – U.S. Geological Survey; Denver, Colorado
- Philip Pearthree – Arizona Geological Survey; Tucson, Arizona
- James Pechmann – University of Utah Seismograph Stations; Salt Lake City, Utah
- Mark Petersen – U.S. Geological Survey; Denver, Colorado
- Robert Smith – University of Utah Dept. of Geology and Geophysics; Salt Lake City, Utah
- Ivan Wong – URS Corporation; Oakland, California

**PALEOSEISMIC-TRENCHING DATABASE**

**Utah Quaternary Faults**

There are 212 Quaternary faults, fault sections, and fault-related folds in Utah (Hecker, 1993; Black and others, 2003). They are chiefly normal-slip faults or are related to normal-slip deformation. Utah includes parts of three physiographic provinces: the Basin and Range, Colorado Plateau, and Middle Rocky Mountains. Quaternary faults are present in all three provinces; however, the greatest number of faults is in the Basin and Range

Province, which comprises roughly the western half of Utah. Over the past approximately 30 years, a time span encompassing the entire history of paleoseismic investigations on normal-slip faults worldwide, investigators have conducted paleoseismic-trenching studies on 33 (16%) of Utah’s Quaternary faults or fault sections. Much of that effort was directed at the six central segments of the Wasatch fault zone (WFZ) that have evidence of Holocene surface faulting. Table 3 lists the Quaternary faults in Utah that have paleoseismic-trenching information and Figure 1 shows their locations.

**Table 3. Utah Quaternary faults/fault sections that have paleoseismic-trenching data.**

Wasatch fault zone	Great Salt Lake fault zone*
Brigham City segment	Fremont Island segment
Weber segment	Antelope Island segment
Salt Lake City segment	Oquirrh fault zone

Provo segment	Southern Oquirrh Mountains fault zone
Nephi segment	Mercur fault
Levan segment	Eastern Bear Lake fault
Joes Valley fault zone	southern section
East Joes Valley fault	Bear River fault zone
West Joes Valley fault	Morgan fault zone
Intragraben faults	James Peak fault
West Valley fault zone	Towanta Flat graben
Taylorsville fault	Bald Mountain fault
Granger fault	Strawberry fault
West Cache fault zone	Hansel Valley fault
Clarkston fault	Hogsback fault
Junction Hills fault	southern section
Wellsville fault	North Promontory fault
East Cache fault zone	Sugarville area faults
central section	Washington fault zone
Hurricane fault zone	northern section
Anderson Junction section	Fish Springs fault

\* Paleoequake information is from detailed seismic reflection surveys and drilling.

## **Paleoseismic-Trenching Investigations**

Paleoseismic-trenching investigations in Utah fall into one of five categories: (1) U.S. Geological Survey (USGS)-funded studies performed by Woodward-Clyde Consultants (WCC), (2) studies performed during the “Wasatch Front Regional Earthquake Hazards Assessment,” cosponsored by the USGS and the UGS, (3) other USGS-funded studies under NEHRP, (4) U.S. Bureau of Reclamation (USBR) studies related to water impoundment or conveyance structures, and (5) other studies performed chiefly by universities and geotechnical consultants. Black and others (2003) show the location of all paleoseismic-trenching studies conducted on Utah’s Quaternary faults.

### **Woodward-Clyde Consultants**

Beginning in the 1970s and extending to the mid-1980s with funding from the USGS, WCC pioneered the paleoseismic study of normal-slip faults by first mapping and then trenching young scarps on the WFZ. The WCC investigations (Swan and others, 1980, 1981a, 1981b; Hanson and others, 1981, 1982; Schwartz and others, 1983; Schwartz and Coppersmith, 1984) were the first performed on normal-slip faults anywhere, and much of what is now known regarding the study of

normal faults in trenches was first developed on the WFZ by WCC. Conducted early in the history of normal-fault paleoseismology, the WCC studies predate more recent advancements in paleoseismology and geochronology.

### **Wasatch Front Regional Earthquake Hazards Assessment**

Beginning in 1983 and continuing until 1989, the USGS targeted the Wasatch Front region for intense study under the auspices of the Regional Earthquake Hazards Assessment element of NEHRP. The “Wasatch Front Regional Earthquake Hazard Assessment” conducted in cooperation with the UGS resulted in the first detailed (1:50,000-scale) geologic maps of the Brigham City (BCS), Weber (WS), Salt Lake City (SLCS), and Provo segments (PS) of the WFZ (Personius, 1990; Personius and Scott, 1992; Machette, 1992; Nelson and Personius, 1993), as well as the East Cache fault zone (ECFZ; McCalpin, 1989). Additionally, both USGS and other investigators performed paleoseismic-trenching studies, chiefly on the WFZ and other faults in northern Utah (McCalpin, 1985; Keaton and others, 1987; Machette and Lund, 1987; Nelson and others, 1987; Schwartz and Lund, 1988; Keaton and Currey, 1989; Forman and others, 1991; McCalpin, 1990, 1994, 2003; Jackson, 1991; Lund

and others, 1991; McCalpin and Forman, 1991; Personius, 1991; Machette and others, 1992; McCalpin and others, 1992).

### **USGS National Earthquake Hazards Reduction Program**

Following the end of the Wasatch Front Regional Earthquake Hazard Assessment in 1989, the USGS funded additional paleoseismic-trenching studies in Utah through the External Research Program of NEHRP. While performed chiefly on the WFZ and other nearby faults (McCalpin and Forman, 1993, 2002; McCalpin and others, 1994; Black and others, 1996; Lund and Black, 1998; McCalpin and Nelson, 2000; McCalpin, 2002; Olig and others, 2004), NEHRP-funded trenching studies expanded to other areas of Utah as well (Olig and others, 1996; Stenner and others, 1999; Black and others, 2000; Lund and others, 2001; Olig and others, 2001). NEHRP also funded the detailed mapping (1:50,000 scale) of the Nephi segment (NS) of the WFZ (Harty and others, 1997), the West Cache fault zone (WCFZ; Solomon, 1999), and the Levan segment (LS) of the WFZ (Hylland and Machette, 2004). NEHRP is presently supporting mapping of the Fayette segment (FS) of the WFZ by the UGS, trenching on the PS of the WFZ (Olig and others, 2004), and a geophysical and drilling investigation of the Great Salt Lake fault zone (GSLFZ) beneath Great Salt Lake (Dinter and Pechmann, 2004a, 2004b).

### **U.S. Bureau of Reclamation**

Between 1982 and 1992, the USBR conducted both regional and project-specific paleoseismic-trenching investigations in support of construction and operation of USBR dams, reservoirs, and water-conveyance structures in Utah (Nelson and Martin, 1982; Martin and others, 1985; Nelson and Weisser, 1985; Foley and others, 1986; Nelson and VanArsdale, 1986; Sullivan and others, 1988a, 1988b; Ostenaar, 1990; Nelson and Sullivan, 1992; Sullivan and Nelson, 1992). These studies constitute the bulk of the paleoseismic-trenching

investigations performed in the Middle Rocky Mountains and Colorado Plateau in Utah.

### **Other Studies**

Universities and geotechnical consulting firms have also conducted fault-trenching studies in Utah. West (1994) trenched the Bear River fault zone (BRFZ) and Hogsback fault (HF) as part of his Ph.D. studies at the Colorado School of Mines (project originally initiated as a USBR investigation). As recognition of earthquake hazards in Utah has increased, some local jurisdictions have adopted ordinances requiring earthquake-hazard evaluations. This is particularly true in Salt Lake County, where geotechnical consultants have trenched the SLCS of the WFZ (Robison and Burr, 1991; Korbay and McCormick, 1999; Simon and Shlemon, 1999). Other faults investigated by geotechnical firms include the Washington fault zone (WaFZ) and Hurricane fault zone (HFZ; Earth Sciences Associates, 1982) in southwestern Utah and the Sugarville area faults (SAFs; Dames and Moore, 1978) in Utah's Sevier Desert.

### **WORKING GROUP REVIEW PROCESS**

Although the Utah paleoseismic-trenching database is small compared to California's, where similar evaluations of paleoseismic data have been conducted, it was neither reasonable nor practical to expect Working Group members serving in a volunteer capacity to review each of the more than 60 paleoseismic source documents available for Utah's Quaternary faults. To expedite the process, the Working Group Coordinator summarized the available paleoseismic-trenching data and forwarded the summary information to Working Group members for their review. The Working Group convened three times to evaluate the data, and to come to consensus decisions regarding preferred RI and VSR estimates for the faults under review. The Working Group Coordinator then summarized the paleoseismic data and the results of the Working Group's deliberations on a "Consensus

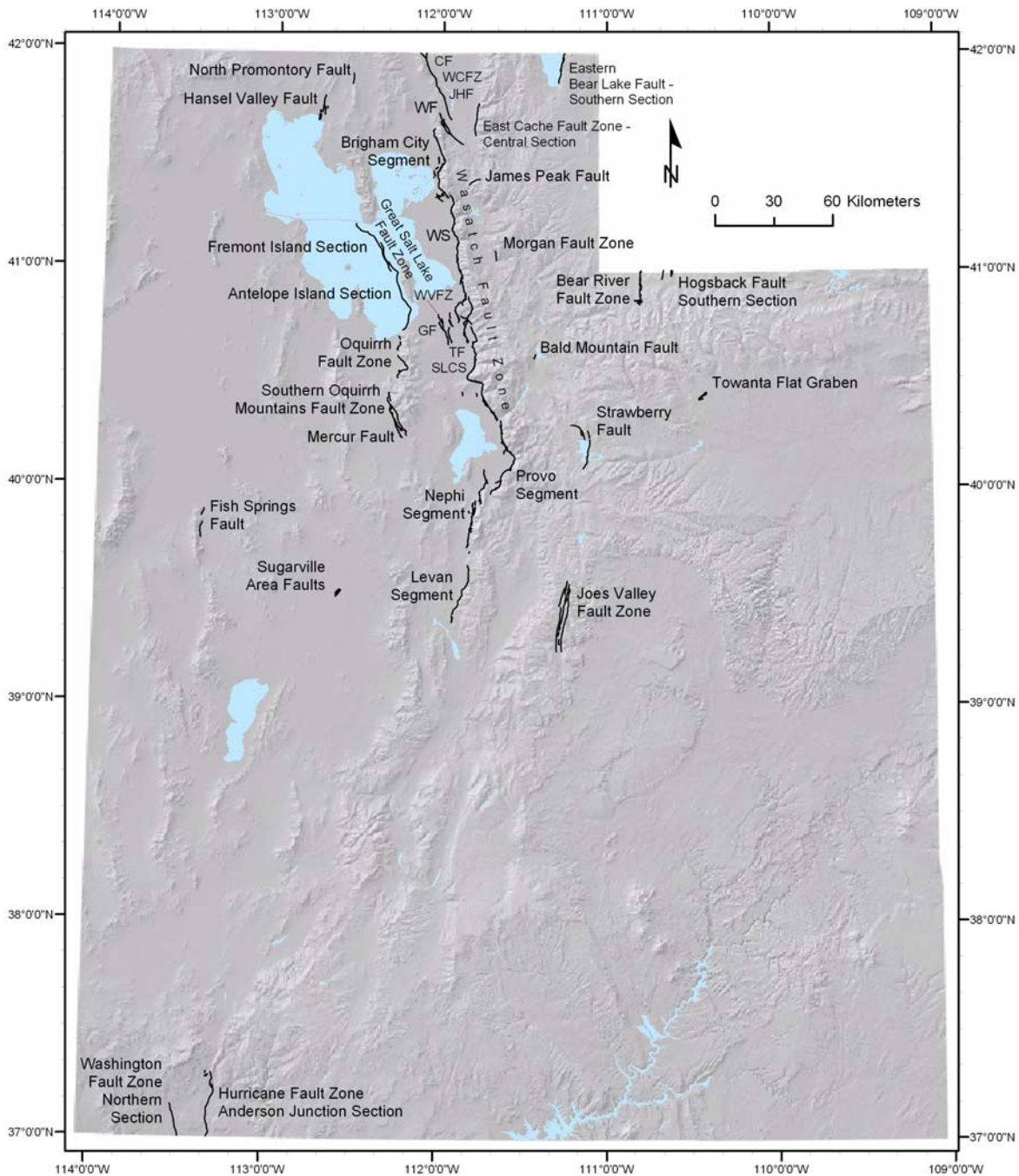


**Figure 1. Locations of Quaternary faults/fault sections for which paleoseismic-trenching or geophysical and drilling data are available: WVFZ = West Valley fault zone, GF = Granger fault, TF = Taylorsville fault, WCFZ = West Cache fault zone, CF = Clarkston fault, JHF = Junction Hills fault, WF = Wellsville fault, WS = Weber segment of the Wasatch fault zone, SLCS = Salt Lake City segment of the Wasatch fault zone.**

Recurrence-Interval and Vertical Slip-Rate Estimate” form for each fault/fault section. The consensus forms represent the principal result of the Working Group review, and should be consulted for details of each fault/fault section and of the review process.

### Review Process Tasks

The Working Group review consisted of the following principal tasks:

1. Preliminary Working Group meeting to establish review parameters and process. Due to delays in approval of the federal FY 2003 budget, this initial meeting was replaced by e-mail and telephone contacts to facilitate project start-up.
2. Detailed review by the Working Group Coordinator of published and unpublished paleoseismic-trenching data available for the six central segments (BCS, WS, SLCS, PS, NS, LS) of the WFZ; preparation of summary data forms for each paleoseismic source document, and of a synthesis form for each segment as a whole.
3. Distribution of completed summary and synthesis forms to the Working Group for their review.
4. First Working Group meeting in Salt Lake City, Utah, on June 4 and 5, 2003, to evaluate the paleoseismic-trenching data for the six central WFZ segments.
5. Detailed review of published and unpublished paleoseismic-trenching data pertaining to the remaining Quaternary faults/fault sections in Utah that have paleoseismic-trenching data; preparation of data forms summarizing the information in each paleoseismic source document, and of a synthesis form for each Quaternary fault/fault section.
6. Distribution of completed data and synthesis forms to the Working Group for their review.
7. Second Working Group meeting in Salt Lake City, Utah, on September 4 and 5, 2003, to evaluate the paleoseismic-trenching data available for Quaternary faults/fault sections, exclusive of the WFZ.
8. Incorporation of the Working Group’s recommendations regarding earthquake timing, RI, and VSR into Consensus Recurrence-Interval and Vertical Slip-Rate Estimate forms for the WFZ segments and other Quaternary faults/fault sections.
9. Distribution of the draft consensus forms to Working Group members for review and comment.
10. Third Working Group meeting in Salt Lake City, Utah, on February 27, 2004, to finalize RI and VSR estimates.
11. Presentation of the Working Group’s results and recommendations at professional society meetings, and to geological and engineering groups in Utah.
12. Preparation of a USGS Final Technical Report contract deliverable and a UGS Bulletin presenting the Working Group’s results and recommendations.
13. Update of the *Quaternary Fault and Fold Database and Map of Utah* (Black and others, 2003) with the new consensus RI and VSR values.

### Consensus Process

The Working Group review showed that the paleoseismic-trenching data for Utah’s Quaternary faults are generally not adequate to permit rigorous statistical analysis of the data, or to constrain RI and VSR values within rigidly quantifiable bounds. Therefore, the Working Group relied on the expertise and collective judgment of its members to assign preferred RI and VSR estimates to the faults/fault sections under review. The preferred values represent the Working Group’s best collective judgment regarding a “mean” RI and VSR for the fault/fault section, based on paleoseismic-trenching data available at the time of the review.

The Working Group also assigned confidence limits to the RI and VSR estimates. Although much of the trenching data are not amenable to statistical

analysis, the Working Group kept in mind the concept of 2-sigma variability (5<sup>th</sup> and 95<sup>th</sup> percentiles) about the preferred RI and VSR estimates as they assigned upper and lower bounds to their confidence limits (table 1, appendix). The goal was to capture both the uncertainty associated with incomplete knowledge of the fault/fault section (epistemic uncertainty – for example, data available from only a single trench site along a many kilometer-long fault) and natural variation in the seismogenic process through time (aleatory uncertainty – for example, variations in the length of interevent intervals). The confidence-limit distribution around the preferred RI and VSR estimates is in some cases skewed to capture apparent variability in fault/fault section behavior.

Establishing preferred RI and VSR estimates and associated confidence limits often generated spirited discussion among Working Group members, and in several instances considerably stretched their comfort levels. Although individual members of the Working Group may retain reservations regarding some RI and VSR estimates or associated confidence limits, the reported values represent the final consensus of the Working Group. Therefore, until superseded by information from new paleoseismic investigations, the Working Group's preferred RI and VSR estimates and confidence limits represent the best available fault activity information for those faults/fault sections, and can be considered as approximating mean RI and VSR values and 2-sigma variability about those mean values.

## **ISSUES RELEVANT TO THE WORKING GROUP REVIEW**

### **Sources of Uncertainty**

#### **Epistemic Uncertainty**

A key component of the Working Group review was identification of “sources of uncertainty” within Utah's paleoseismic-trenching data. Hecker and others (1998) compiled possible sources of

uncertainty in fault-activity studies for the Long Beach, California 30'x60' quadrangle fault map and database. A modified form of that list was used to evaluate epistemic uncertainty resulting from incomplete or imperfect knowledge regarding Utah's paleoseismic-trenching data.

Principal sources of epistemic uncertainty for the six central, active segments of the WFZ include the following:

- Investigators identified two different most recent surface-faulting earthquakes (MRE) at the two trench sites on the BCS, even though the two sites are within a few kilometers of each other.
- Timing of older earthquakes on the BCS have  $\pm$  uncertainties that equal or exceed the interevent intervals between the earthquakes.
- Multiple investigators differ in their interpretation of the timing of the MRE on the WS, raising the possibility of partial segment rupture or rupture overlap from adjacent segments.
- Latest Pleistocene and early Holocene surface-faulting earthquakes on the SLCS are identified on the basis of a retrodeformation analysis of a trench exposure; the earthquakes lack direct stratigraphic and structural evidence of their occurrence.
- Differences in the number and timing of surface-faulting earthquakes near the southern end of the PS (Water Canyon), when compared to the timing of earthquakes farther north on the segment, indicate either partial segment rupture of the PS, or rupture overlap from surface faulting on the NS to the south. Conversely, recent scarp mapping and diffusion modeling on the NS indicates that surface rupture may propagate from the PS to the NS during some large earthquakes.
- Both paleoseismic-trenching investigations performed on the NS produced conflicting sets of numerical ages on samples from the same geologic units resulting in significant

uncertainty regarding paleoearthquake timing; as a result, the surface-faulting chronology for the NS can vary depending on which ages are selected to constrain earthquake timing.

- Over 300 numerical age determinations, chiefly  $^{14}\text{C}$  and TL accumulated over 30-plus years, constrain the timing of surface faulting on the WFZ; the  $^{14}\text{C}$  ages represent a wide variety of sampling, dating, and calibration techniques, thus injecting variability into the absolute-age dataset.
- The Working Group considers many of the confidence limits originally reported with the timing of surface-faulting earthquakes as too narrow, and as not fully accounting for the geologic (aleatory) uncertainty associated with earthquake timing.

For Utah's other Quaternary faults, sources of epistemic uncertainty include the following:

- Seismogenic capability of fault uncertain.
- Zone of deformation wider than the zone of study – not all scarps trenched.
- Time period too long or too short to represent contemporary conditions.
- Studies limited to a single strand or section of a complex fault zone.
- Number of surface-faulting earthquakes uncertain.
- Surface-faulting earthquake timing only broadly constrained (thousands to tens of thousands of years) or unknown.
- Vertical displacement per earthquake and/or cumulative vertical displacement poorly constrained or unknown.
- Interevent intervals open at one or both ends.
- Number of interevent intervals may be too few to yield representative mean recurrence.
- Earthquake recognition based on indirect stratigraphic or structural evidence.
- Selected paleoseismic parameter conflicts with other data at the site.

- Uncertain correlation of earthquakes between fault strands.

### **Aleatory Uncertainty**

Uncertainty due to inherent variability of the seismogenic process is largely unknown for the faults/fault sections reviewed by the Working Group. All of the faults/fault sections lack the definitively complete and sufficiently long paleoseismic records required to illustrate the full range of variability in the seismogenic process. This is true even for the five central segments of the WFZ (BCS, WS, SLCS, PS, NS), which are the most studied faults in Utah, but where McCalpin and Nishenko (1996) note that “The small number of observed recurrence intervals from individual fault segments (1 to 3) during the past 5.6 kyr [thousand years] precludes the unequivocal demonstration of a particular type of recurrence behavior (i.e., random versus periodic).” The coefficient of variation (COV; ratio of the standard deviation to the mean) provides a measure of the periodicity of earthquake recurrence intervals (Norman Abrahamson, Pacific Gas and Electric Company, written communication to Susan Olig, Working Group member, 2000). The smaller the COV (<0.3) the more periodic is earthquake recurrence, while a large COV (>1) indicates earthquakes are not periodic. The limited long-term recurrence information available for Utah faults/fault sections (BCS, SLCS, West Valley fault zone [WVFZ], Southern Oquirrh Mountain fault zone [SOMFZ], Hansel Valley fault [HVF]; appendix) indicates that large variations in earthquake repeat times and size are possible, likely representing large COV values.

The Working Group recognized the potential effect of aleatory uncertainty on their RI and VSR estimates, and attempted to incorporate the effects of that variability when assigning confidence limits to their preferred RI and VSR values. However, the Working Group acknowledges that due to a lack of data, they may have underestimated the effects of process variability for some faults/fault sections.

## **Data Adequacy**

Closely associated with data uncertainty is the issue of data adequacy – are the available paleoseismic-trenching data sufficiently abundant to make reliable RI and VSR estimates for the faults or fault sections under review? Utah's paleoseismic-trenching data divide naturally into two groups: (1) data for the WFZ, Utah's longest, most active, and most studied fault, and (2) data for Utah's other Quaternary faults that have been studied in trenches or natural exposures.

### **Wasatch Fault Zone**

The WFZ, by virtue of its collocation with the populous Wasatch Front and abundant geomorphic evidence of geologically recent surface faulting, is the most studied and best understood Quaternary fault in Utah. Investigators have performed multiple paleoseismic investigations on the six active central segments of the WFZ, and although significant questions remain unanswered (see above) the surface-faulting histories of most segments are generally well understood to at least the middle Holocene. Two segments, BCS and SLCS, also have information on surface faulting extending to the latest Pleistocene; however, the timing of the older earthquakes is not as well constrained, and in some instances direct physical evidence of surface faulting (colluvial wedges, fault terminations, fissures and fissure-fill deposits) is lacking. A NEHRP-funded paleoseismic-trenching investigation conducted cooperatively between URS Corporation and the UGS in 2003 (Olig and others, 2004) is designed to extend the surface-faulting record on the PS to the latest Pleistocene; however, final results of that investigation are not yet available.

### **Other Quaternary Faults**

Paleoseismic-trenching data for Utah's other Quaternary faults are more limited than for the WFZ. Data limitations are related to four principal causes: (1) reduced fault activity, (2) remote fault

locations away from large population centers, (3) typically shorter fault lengths, and (4) difficulty identifying older earthquakes. Less active faults produce fewer earthquakes over a given time period; consequently, unless the deposits being trenched are old, a typical 3- or 4-meter-deep paleoseismic trench exposes evidence for fewer earthquakes. The remote location of many faults equates to lower earthquake risk and consequently to less intensive study. Off the Wasatch Front, most faults have only a single trenching investigation, even on faults with evidence of possible segmentation or other complexities. Short faults typically produce smaller earthquakes with smaller displacements, which can make recognizing the geologic record of their occurrence more difficult. Finally, where trenches expose evidence for early to middle Quaternary surface faulting, recognition of individual surface-faulting earthquakes has proven difficult; investigators typically report evidence of surface faulting, but are unsure of the exact number of earthquakes. This problem becomes more acute for older earthquakes that were also small.

## **Constraining Age Estimates**

### **Numerical Ages**

**Radiocarbon ages:** Paleoseismic-trenching studies in Utah have resulted in more than 300 numerical ages. The majority are  $^{14}\text{C}$  ages, which are of two principal types: (1) ages from charcoal obtained by standard gas proportional counting techniques, or ages obtained using an accelerator mass spectrometer for samples too small for conventional counting methods, and (2) apparent mean residence time (AMRT) ages on bulk organic samples, usually collected from buried soils, tectonic crack-fill material, or colluvial-wedge deposits. Bulk organic samples contain carbon of different ages, and the  $^{14}\text{C}$  ages obtained from them must be corrected to account for this "carbon-reservoir" effect. Machette and others (1992) and McCalpin and Nishenko (1996) include discussions of AMRT ages and their proper correction for carbon age spans and carbon mean residence time.

Production of  $^{14}\text{C}$  in the upper atmosphere has varied through time due to fluxes in the Earth's magnetic field, and more recently due to open-air nuclear weapons testing. The variable rate of production means that  $^{14}\text{C}$  has been incorporated into living organisms (plant and animal) in different proportions to  $^{12}\text{C}$  at different times in the past. Therefore,  $^{14}\text{C}$  ages ( $^{14}\text{C}$  yr B.P.) must be calibrated to adjust for the different production rates. Correction of  $^{14}\text{C}$  years to calendar years (cal yr B.P.) relies chiefly on the radiometric dating of tree rings and marine coral of otherwise known age, and comparing the ages of those materials to the resulting  $^{14}\text{C}$  ages. Calibrating  $^{14}\text{C}$  ages beyond about 20,000 years ago (ka) remains difficult. Once a properly corrected and calibrated calendar age is obtained, it remains for the paleoseismic investigator to interpret the age within the sample's geologic context and determine how closely the age constrains the timing of surface faulting.

Since the inception of paleoseismic-trenching studies in Utah, significant advances have been made in methodologies for calendar-calibrating  $^{14}\text{C}$  ages, and in our understanding of how to properly sample for, correct, and interpret AMRT ages on bulk organic samples. The science of paleoseismology also has advanced over that same time period, and our understanding of how to conduct paleoseismic-trenching investigations and interpret their results has also improved. The result is a dataset of  $^{14}\text{C}$  ages that are calibrated to a variety of standards, if at all; sampled by a variety of techniques; analyzed by different laboratories; and interpreted by investigators having varying levels of experience and expertise.

**Luminescence ages:** Investigators have employed a variety of luminescence dating techniques in paleoseismic-trenching investigations in Utah. Thermoluminescence dating is the most common. Most TL ages were obtained during the 1980s on the central segments of the WFZ. There is no recognized need or procedure to calibrate TL or other luminescence ages and they are assumed to be calendar ages.

## Relative Ages

**Lake Bonneville chronology:** Much of the WFZ and many other Quaternary faults in northern and western Utah lie below the highstand of Lake Bonneville, a late Pleistocene pluvial lake (Gilbert, 1890) that occupied the Bonneville basin from about 32.5 to 13.9 ka (Donald Currey, University of Utah Geography Department, written communication to the UGS, 1996; verbal communication to Working Group, 2004). At its highest elevation (Bonneville shoreline, 1551 m [5090 ft]), Lake Bonneville had a surface area in excess of 50,000 km<sup>2</sup> (20,000 mi<sup>2</sup>) and a maximum depth of more than 305 m (1000 ft). Lake Bonneville lacustrine deposits and post-Bonneville alluvium and colluvium dominate the Quaternary geology of the Bonneville basin.

Four prominent shorelines, two transgressive (Stansbury and Bonneville), one regressive (Provo), and one related to the post-Bonneville highstand of Great Salt Lake (Gilbert), provide well-documented time lines against which the timing of surface faulting can be compared. However, Lake Bonneville deposits also bury older Quaternary deposits in the basin, making it difficult to decipher the history of older surface faulting. The details of Lake Bonneville chronology continue to evolve through time (Oviatt and Thompson, 2002; Donald Currey, University of Utah Geography Department, verbal communication to Working Group, 2004), and many early paleoseismic studies relied on age estimates of Bonneville deposits and shorelines that were subsequently revised. Additionally, early paleoseismic-trenching investigations used Lake Bonneville age estimates reported in  $^{14}\text{C}$  years. Donald Currey (University of Utah Geography Department, written communication to UGS, 1996; verbal communication to Working Group, 2004) calendar-calibrated key Lake Bonneville ages, and showed that Lake Bonneville events and features are as much as 4.5 kyr older than indicated by  $^{14}\text{C}$  ages. Table 4 presents Currey's Lake Bonneville chronology.

**Table 4. Timing of events related to the transgression and regression of Lake Bonneville (modified from Donald Currey, University of Utah, written communication to the UGS, 1996; verbal communication to Working Group, 2004).**

Lake Stage	Radiocarbon Years ( <sup>14</sup> C yr B.P.)	Calendar Years (cal yr B.P.)
Start of Lake Bonneville	28,000	~32,500
Stansbury shoreline	21,000 – 20,000	24,400 – 23,200
Bonneville shoreline	15,500 – 14,500	18,000 – 16,800
Start/end Bonneville flood	14,500	16,800
Provo shoreline	14,500 – 14,000	16,800 – 16,200
Gilbert shoreline	11,000 – 10,000	12,800 – 11,600

When possible, the Working Group used the calendar-calibrated ages in table 4 to revise RI and VSR estimates for paleoseismic-trenching investigations that relied on <sup>14</sup>C years for the ages of Lake Bonneville features and events.

**Soil-profile development:** Relative age estimates based on soil-profile development play an important part in many paleoseismic-trenching investigations in Utah, particularly reconnaissance investigations off the Wasatch Front. Information presented in paleoseismic source documents seldom permits an independent evaluation of relative soil age. Therefore, unless there was a compelling reason to do otherwise, the Working Group accepted relative age estimates based on soil development as reported by original investigators, while recognizing that uncertainties associated with soil-profile age estimates may be thousands to tens of thousands of years.

### Net Vertical-Displacement Data

Net vertical-displacement data for Utah's Quaternary faults come from two principal sources: (1) topographic profiles measured across scarps, with or without an accompanying trench, and (2) measurements made in trenches. Uncertainties in net vertical-displacement data are of three principal types: (1) measurement uncertainty, (2) sparse data, and (3) incomplete documentation.

### Measurement Uncertainty

**Scarp profiles:** Scarp profiles are commonly used to determine scarp height and net vertical displacement across fault scarps. Profiling techniques range from highly accurate, computer-assisted surveying, to sequential measurements of slope angle along a profile line using a meter stick lying on the ground and an Abney level resting on the stick to measure slope angles. Both methods, and others, produce accurate profiles; uncertainty with the resulting net displacement data relates chiefly to issues of erosion and deposition on and adjacent to the scarp, effects of near-field deformation (for example – graben formation, back-tilting, and warping), failure to profile all scarps at a site, and difficult site conditions. Where unmodified pre-faulting surfaces on both sides of a scarp can be accurately projected to the fault, topographic profiles provide a reliable measurement of cumulative net vertical displacement. However, where complicating factors are present, uncertainty enters into the measurements, and considerable experience is required to interpret profile results and arrive at reliable net vertical-displacement estimates.

**Measurements in trenches:** Correlative stratigraphy displaced across a fault zone and exposed in a trench can provide a direct measure of fault displacement. However, many trenches lack correlative stratigraphy, and net vertical-displacement measurements from trenches are often estimates based on secondary stratigraphic and structural relations, thickness of colluvial-wedge deposits, retrodeformation reconstructions, and trench depth. As is the case with scarp profiles, in the absence of a best-case scenario, experience is required to obtain reliable net vertical-displacement estimates from trench exposures.

### Sparse Data

Net vertical-displacement measurements are point values made at individual locations along a

fault. Slip distribution during a surface-faulting earthquake varies along strike, rising to a maximum at one or more points and decreasing to zero at the ends of the rupture (Crone and others, 1985). Characterizing slip distribution along a fault requires careful geologic mapping and the making of numerous displacement measurements along the fault trace. With the possible exception of the WS of the WFZ, no Quaternary faults/fault sections in Utah have sufficient displacement data to fully characterize their slip distribution.

Net vertical-displacement information is most abundant for the BCS, WS, SLCS, and PS of the WFZ. These data represent a combination of measurements made during paleoseismic-trenching investigations from both scarps and trenches, and scarp-profile measurements made as the USGS mapped these segments. With few exceptions, the net vertical-displacement data are sparsely distributed along the segments, and their interpretation is complicated by complex rupture patterns, poorly constrained deposit ages, and the presence of non-correlative geologic units on either side of many scarps. The exception is the WS, where the USGS measured 375 scarp profiles (77 in the field and 298 using a photogrammetric plotter and aerial photographs); however, only about 30 of those measurements are included on the geologic map of the WS (Nelson and Personius, 1993).

Off the WFZ, net vertical-displacement information is commonly limited to one or two points along a fault, and represents “best available” data for the fault/fault section. Where the measurements lie within the slip-distribution curve for the faults is almost always unknown.

### **Incomplete Documentation**

Incomplete documentation of net vertical-displacement measurements is common in many paleoseismic source documents. As discussed above, measurements of net vertical displacement, whether from scarp profiles or trenches, frequently include important caveats that require explanation. The net vertical-displacement data reviewed by the Working Group ranged from detailed explanations

of how displacement was measured and associated uncertainty evaluated, to cursory statements of displacement values, commonly reported to the nearest meter, with no accompanying explanatory information. The Working Group review showed that for some investigations not all scarps were trenched or profiled, so reported net vertical-displacement values are minima, while at other sites antithetic scarps, even when recognized, were not included in the net displacement budget, and the resulting net vertical-displacement measurements are too large. Consequently, where explanatory details are lacking, the accuracy of the net vertical-displacement information for Utah’s Quaternary faults is often questionable.

## **PALEOSEISMIC PARAMETERS**

### **Earthquake Timing**

The timing of surface-faulting earthquakes reported in paleoseismic-source documents typically is constrained by either numerical or relative ages and in several instances by a combination of both. Depending on the number of ages available and their geologic context, the timing of surface faulting can be constrained in the best cases to within a few hundred years. More often, resolution of earthquake timing is less precise, in some instances tens of thousands of years or more. Because the WFZ is Utah’s most intensely studied Quaternary fault, and therefore has the greatest number of numerical ages, the timing of surface-faulting earthquakes on the six active central segments of the WFZ is better constrained, at least to the middle Holocene, than are earthquakes on other faults in Utah. Because earthquake timing is critical to determining RI and VSR, the Working Group made a careful review of information relevant to earthquake timing on Utah’s Quaternary faults (appendix).

### **Wasatch Fault Zone**

**McCalpin and Nishenko (1996):** Recognizing the variability inherent in the WFZ numerical-age dataset, McCalpin and Nishenko (1996) re-evaluated the 276 <sup>14</sup>C and TL ages then available for the five central segments of the WFZ having evidence for multiple Holocene surface-faulting earthquakes (BCS, WS, SLCS, PS, NS). Based on stratigraphic criteria, they identified 89 limiting ages (76 maximum and 13 minimum) as closely constraining the timing of surface faulting on those segments (see McCalpin and Nishenko [1996] table 1). They recalibrated the <sup>14</sup>C ages, using a single calibration dataset (CALIB v. 3.0; Stuiver and Reimer, 1993) while applying a consistent methodology for assigning carbon age span, carbon mean residence time, and other calibration parameters. The result was a set of consistently calibrated, closely limiting <sup>14</sup>C ages and associated TL ages for surface-faulting earthquakes on the central WFZ current for investigations done up to about 1995. McCalpin and Nishenko (1996) used the revised absolute ages to calculate weighted means for the timing of surface-faulting earthquakes on the five WFZ segments. The ± confidence limits reported for the weighted means (see McCalpin and Nishenko [1996] table 1) reflect cumulative laboratory uncertainty associated with the calibrated ages used to calculate the weighted means, but do not incorporate geologic uncertainty associated with

earthquake timing (James McCalpin, GEO-HAZ Consulting, verbal communication to Working Group, 2003).

With the exceptions noted below, McCalpin and Nishenko's (1996) revised <sup>14</sup>C and associated TL ages remain the best available numerical-age data for the WS and PS. On those segments, the Working Group re-determined surface-faulting timing by calculating the simple mean of the McCalpin and Nishenko (1996) closely limiting absolute ages for each earthquake (appendix). The means were then rounded to the nearest half-century. In nearly every instance, the results were within 100 years of the corresponding McCalpin and Nishenko (1996) weighted means. To better accommodate geologic uncertainty associated with earthquake timing, the Working Group revised the ± confidence limits assigned to each earthquake. The Working Group determined revised confidence limits by dividing the range between the youngest and oldest bounding age limits resulting from calibration of the closely limiting ages for each earthquake by 2, and rounding the result to the nearest half-century (table 5). The Working Group confidence limits are significantly broader than those of McCalpin and Nishenko (1996), and are thought to better incorporate both the aleatory and epistemic uncertainty associated with earthquake timing.

**Table 5. Example of determining earthquake timing and approximate 2-sigma confidence limits using earthquakes Y and Z, Brigham City segment, Wasatch fault zone.**

Limiting <sup>14</sup> C or TL age <sup>1</sup>	Earthquake	McCalpin and Nishenko (1996) Calibrated Ages <sup>1</sup>	McCalpin and Nishenko (1996) Weighted-mean Earthquake Timing <sup>1</sup>	Working Group Mean Earthquake Timing
1720±90	Z	1691(1412)1142	2125±104 cal yr B.P.	2100 <sup>2</sup> ±800 <sup>3</sup> cal yr B.P.
1.7 ±0.2, 2.1 ±0.3 (TL)	Z	1900±300		
2320±70	Z	2251(2020)1801		
2580±60	Z	2680(2513)2200		
2630±90	Z	2767(2571)2187		
3320±80	Y	3615(3344)3085	3434±142 cal yr B.P.	3450±300 cal yr B.P.
3430±70	Y	3687(3462)3166		
3430±60	Y	3700(3476)3261		

<sup>1</sup>McCalpin and Nishenko (1996) table 1; <sup>2</sup>(1412+1900+2020+2513+2571)/5 = 2083, rounded = 2100; <sup>3</sup>(2767-1142/2) = 813, rounded = 800; approximates 2-sigma variability and includes analytical and sample context uncertainties.

### **New paleoseismic trenching information:**

Trenching information on the timing of surface-faulting earthquakes obtained subsequent to McCalpin and Nishenko (1996) is available for the BCS and SLCS. McCalpin and Forman (2002) presented an updated interpretation of their trenching investigation on the BCS originally performed in 1992-93, and first reported in McCalpin and Forman (1993). Table 4 in McCalpin and Forman (2002) revises the  $^{14}\text{C}$  and TL ages both as reported in the original investigation and in McCalpin and Nishenko (1996). Differences in ages between McCalpin and Nishenko (1996) and McCalpin and Forman (2002) are related chiefly to older earthquakes (T, U, V). The timing of earthquakes U and V remains the same, but the  $\pm$  confidence limits are broader in McCalpin and Forman (2002). Event T is constrained by a single  $^{14}\text{C}$  age, which McCalpin and Nishenko (1996) reported in radiocarbon years, but which McCalpin and Forman (2002) calendar calibrated and then reported as a range ( $>14,800 \pm 1200$  cal yr B.P.,  $<17,100$  [16.8 ka; see table 4]) using the time of the Bonneville flood as the upper bound for the timing of event T. The Working Group broadened the  $\pm$  confidence limits for event U by using the new limiting ages reported in McCalpin and Forman (2002) and employing the same methodology described above (table 5) for the McCalpin and Nishenko (1996) ages.

Trenching by Black and others (1996) constrained the timing of the four youngest earthquakes (W, X, Y, Z) on the SLCS, and McCalpin (2002) identified three older earthquakes (T, U, V) on the basis of a retrodeformation analysis of his "megatrench" exposure at Little Cottonwood Canyon. The Working Group judged the results of these two new investigations credible, and combined the results of the two studies to create a composite surface-faulting chronology for the SLCS. The Working Group re-evaluated the Black and others (1996) earthquake  $\pm$  confidence limits as described above. The Working Group believes that the revised limits account for both the laboratory and geologic uncertainty associated with younger surface faulting on the SLCS, but timing of the

three older earthquakes can be constrained only to broad time intervals.

**Original data:** In two instances, the Working Group chose to adopt earthquake timing on the WS and PS as reported by the original investigators prior to the McCalpin and Nishenko (1996) re-evaluation. They include (1) the third-oldest (antepenultimate) earthquake on the PS as originally reported by Machette and others (1992), and (2) the MRE on the WS as reported by Swan and others (1981b) and Machette and others (1992); McCalpin and Nishenko (1996) discounted a late Holocene surface-faulting earthquake at about 0.5 ka on the WS. Additionally, the Working Group chose to include the LS in their deliberations and accepts the timing of the MRE as reported by Jackson (1991) and later confirmed by the UGS (Hylland and Machette, 2004; table 1, appendix).

**Nephi segment:** The NS exhibits evidence of multiple Holocene surface-faulting earthquakes, but earthquake timing on the NS is the least well understood of any of the central WFZ segments. Two paleoseismic-trenching investigations (Hanson and others, 1981; Jackson, 1991) produced conflicting sets of numerical ages for horizons critical to determining the surface-faulting history of the NS. McCalpin and Nishenko (1996) re-evaluated the ages used by the original investigators to define their surface-faulting chronologies, but did not consider the alternative ages, or comment regarding the suitability of the alternate ages to constrain surface faulting. Additionally, McCalpin and Nishenko (1996) used five previously unpublished  $^{14}\text{C}$  ages from the southern part of the PS to help constrain the timing of the MRE and second oldest (penultimate) event (PE) on the NS. The Working Group believes that in the absence of supporting paleoseismic information from the northernmost trace of the NS, it is premature to use  $^{14}\text{C}$  ages from the PS to determine the timing of surface faulting on the NS. Lacking new paleoseismic-trenching information to better define earthquake timing, the Working Group used the preferred surface-faulting chronologies of the

original investigators to establish a composite chronology for the NS, but acknowledges a high level of uncertainty regarding earthquake timing.

### **Other Quaternary Faults**

The timing of surface faulting generally is not as well constrained for Utah's other Quaternary faults. Reasons include: (1) fewer earthquake-limiting absolute ages are available, (2) many investigations were reconnaissance in nature and either lack numerical ages entirely, or the available ages only confine surface faulting to broad time intervals, and (3) the primary purpose of the study was not to determine earthquake timing.

A comprehensive reinterpretation and recalibration of numerical ages similar to that performed by McCalpin and Nishenko (1996) for the central WFZ segments has not been made for Utah's other Quaternary faults. The principal reasons for not doing so are that: (1) many studies lack information regarding the geologic context of the material dated, or on how the samples were collected, processed, and analyzed, and (2) where available ages are only sufficient to constrain earthquake timing to broad time intervals, variations of a few tens to hundreds of years resulting from recalibration are inconsequential. Those studies that contain sufficient information to permit a re-evaluation of their absolute ages were carefully scrutinized during the Working Group review process.

### **Recurrence Intervals**

Active faults generate repeated surface-faulting earthquakes through time, and the time span between those earthquakes is called the recurrence interval (RI). Recurrence interval is a fundamental descriptor of fault activity (McCalpin, 1996), and defining earthquake recurrence is a major goal of most paleoseismic-trenching investigations. A RI is

typically reported in one of two ways: (1) as the interval between two individual paleoearthquakes or (2) as an average RI encompassing several paleoearthquakes. Considerable variation is possible between individual interevent intervals on some faults. An average RI smoothes out individual interevent variations, resulting in a mean value that is useful for earthquake-hazard analysis. However, average recurrence, especially determined over a long time period, can mask large variations in individual recurrence, some of which may represent fundamental changes or large irregularity in fault behavior. For example, the average RI for the SOMFZ determined for five to seven earthquakes over a nearly 100-kyr period is 12 to 25 kyr (Olig and others, 2001). However, information on earthquake timing for the SOMFZ indicates individual interevent intervals may be as long as 46 kyr or as short as a few kyr. Similarly large variations in interevent intervals over long time periods are seen on some other Utah Quaternary faults, and are of particular concern on the WFZ, where evidence suggests that post-Bonneville (late Pleistocene/Holocene) and particularly mid- to late-Holocene RIs are significantly shorter and more regular than recurrence prior to or during Lake Bonneville time (Machette and others, 1992; McCalpin, 2002; McCalpin and Forman, 2002).

### **Wasatch Fault Zone**

Surface-faulting chronologies for the five central segments of the WFZ that have multiple Holocene surface-faulting earthquakes are relatively well constrained through the middle Holocene (appendix), and permit calculation of interevent intervals between paleoearthquake pairs (table 6). Additionally, longer surface-faulting chronologies on the BCS and SLCS define less well-constrained interevent intervals to the latest Pleistocene (Lake Bonneville and immediate post-Bonneville time).

**Table 6. Example of determining mean recurrence intervals and 2-sigma confidence limits for the Brigham City segment of the Wasatch fault zone.**

Earthquake	Timing	Interevent Recurrence Interval	Mean Recurrence Interval
Z	2100±800	Y-Z = 1350±900 <sup>1</sup> X-Y = 1200±600 W-X = 1300±600 V-W = 1500±1000 U-V = 1000±1800	W-Z = 1300 <sup>2</sup> ±200 <sup>3</sup>
Y	3450±300		
X	4650±500		
W	5950±250		U-Z = 1300 <sup>2</sup> ±400 <sup>3</sup>
V	7500±1000		
U	8500±1500		

<sup>1</sup>±confidence limits equal the square root of the sum of the squares of the individual ± confidence limits for each bracketing earthquake; <sup>2</sup>Weighted mean rounded to the nearest 100 years; <sup>3</sup>2-sigma standard deviation rounded to the nearest 100 years.

The Working Group determined mean RI for the five central WFZ segments by calculating the weighted mean of the individual interevent intervals (rounded to the nearest 100 years) and then calculating 2-sigma confidence limits for the interevent interval distribution. This method was not applicable to the LS, where scarp-profile evidence (Hylland and Machette, 2004) indicates the possibility of two surface-faulting earthquakes on the southern part of the LS in latest Pleistocene/Holocene time, although only one earthquake has been positively identified and its timing constrained on that segment.

After a careful review of the available information regarding earthquake timing, interevent interval lengths, and data variability for each segment, the Working Group assigned preferred Holocene RI estimates for each segment along with “approximate” 2-sigma (5<sup>th</sup> and 95<sup>th</sup> percentile) confidence limits (table 1, appendix). However, limited data restricted the Working Group’s preferred RI estimate for the LS to a broadly defined range.

**Other Quaternary Faults**

Few of the other Quaternary faults/fault sections considered by the Working Group have sufficient information on earthquake timing to permit calculation of even a single, well-constrained interevent interval. Typically, the timing of bracketing earthquakes is poorly constrained, and resulting interevent intervals are broad.

The Working Group evaluated the information on earthquake timing available for each fault/fault section, and again employing a consensus process, assigned a preferred RI with “approximate” 2-sigma confidence limits to each fault/fault section where the data permitted (table 1, appendix). However, because the data are limited, most RI confidence limits are broad to reflect high uncertainty. Additionally, the Working Group review showed that existing paleoseismic information for several faults/fault sections is insufficient to make even a broadly constrained RI estimate (table 1, appendix).

**Vertical Slip Rates**

Vertical slip (displacement) represents the vertical component of total dip slip on a fault. Vertical slip is always smaller than dip slip unless the fault is vertical, in which case vertical slip and dip slip are the same. Accurately calculating dip slip requires knowing the fault dip, which is generally poorly constrained for most Utah faults. Vertical slip rate (VSR) is calculated by normalizing net vertical displacement at a point on a fault over time (net vertical displacement/time), and is a second fundamental descriptor of fault activity (McCalpin, 1996). In a manner similar to RIs, VSRs typically are reported in one of two ways: (1) as the slip rate between two individual paleoearthquakes, or (2) as the average slip rate over a longer time period that encompasses slip from several to possibly hundreds of paleoearthquakes. In the first instance, the net vertical displacement from the more recent of the

two earthquakes is divided by the time interval between the earthquakes. In the second, cumulative net vertical displacement and time are required parameters, but knowing the number of earthquakes that produced the displacement is not necessary.

For a VSR to be well constrained, both the net vertical displacement and the time interval must be bracketed (closed) by surface-faulting earthquakes (Wong and Olig, 1998). A common source of uncertainty in paleoseismic-source documents reviewed by the Working Group was the use of open time intervals when calculating slip rates. Intervals open to the present include time that is not represented by corresponding displacement, and thus produce slip rates that are too small (too much time and not enough displacement). Intervals open to the past typically include displacement that is not fully represented by time, and thus result in slip rates that are too large (too much displacement and not enough time). Intervals open at both ends can produce slip rates that are either too small or too large depending on the ratio of time not accounted for in the past compared to extra time included since the most recent surface faulting. However, the greater the interval length and the more earthquakes it represents, generally the smaller is the effect of open-ended intervals.

Because net vertical displacement is an essential component of slip-rate calculations, and because net vertical displacement produced by a surface-faulting earthquake varies along strike of a fault, so does the VSR. Like the net vertical-displacement measurements from which they are derived, VSRs are point values that reflect the rate of vertical displacement at a particular location on a fault. Whether a slip rate is a maximum or some lesser amount depends on the nature of the corresponding net vertical-displacement measurement.

Well-constrained net vertical-displacement measurements are limited on the faults/fault sections considered by the Working Group; therefore, well-constrained VSRs are similarly limited. This is particularly true for faults/fault sections off the Wasatch Front where net vertical-displacement and slip-rate data may come from as

few as one or two locations on a fault/fault section that is tens of kilometers long.

The Working Group evaluated available information on earthquake timing and net vertical displacement for each fault/fault section under their review, and employed a consensus process to assign a preferred VSR with "approximate" 2-sigma confidence limits to each fault/fault section where the data permitted (table 1, appendix). However, because the data are limited, many of the Working Group's confidence limits are broad to reflect high uncertainty. Additionally, the Working Group review showed that existing paleoseismic information for several faults/fault sections is insufficient to make even broadly constrained VSR estimates. Special cases in that regard are the Joes Valley and Towanta Flat grabens, which have no measurable net vertical displacement across them and therefore may not be seismogenic structures.

## SUMMARY

The Utah Geological Survey convened the Utah Quaternary Fault Parameters Working Group, a panel of experts in paleoseismology and seismology, to critically review Utah's Quaternary fault paleoseismic-trenching data, and to establish consensus preferred RI and VSR estimates and confidence limits for those faults/fault sections where the data permit. The *Quaternary Fault and Fold Database and Map of Utah* (Black and others, 2003) indicates that 33 of Utah's 212 Quaternary faults or fault-related structures have paleoseismic-trenching data available for them. The six active, central segments of the WFZ, collocated with the most populous part of Utah's Wasatch Front, account for the greatest number of investigations and best quality paleoseismic data. However, even for those segments, well-constrained information on surface faulting generally extends only to the middle Holocene, with less reliable information to the latest Pleistocene for two segments, and new long-term information pending for a third segment. Paleoseismic-trenching data for Utah's other Quaternary faults are generally less abundant and

not as well constrained. Those data are typically limited to a single location along a fault/fault section, including many suspected segmented faults or faults/fault sections exhibiting other tectonic complexities. Numerical ages available to constrain the timing of paleoearthquakes on faults/fault sections off the Wasatch Front are commonly much less abundant, and several trenching investigations resulted in no numerical ages at all. Consequently, significant questions remain to be answered, including questions pertaining to some comparatively well-studied WFZ segments, to ensure that Utah's earthquake hazard is characterized to the minimum level necessary for accurate hazard evaluation.

Issues related to data uncertainty and adequacy weighed heavily upon the Working Group's deliberations. The combined result of limited data and data uncertainties for many faults prevented rigorous statistical analysis of most paleoseismic-trenching data or constraint of RI and VSR estimates within rigidly quantifiable bounds. Consequently, the Working Group relied on its collective experience and best professional judgment to determine consensus preferred RI and VSR estimates and confidence limits for the faults under review. For several faults, the data were too sparse or too uncertain to make meaningful estimates.

The preferred RI and VSR estimates presented in this report are typically bracketed by upper and lower bounds that represent the Working Group's best estimate of 2-sigma confidence limits for the estimated values. The confidence limits are approximations, and were not derived in a statistically rigorous manner. Instead, they again represent the Working Group's best collective judgment regarding the range over which recurrence and slip is expected to vary for a particular fault. They are intended to incorporate both epistemic and aleatory uncertainty, and to approximate 2-sigma (5<sup>th</sup> and 95<sup>th</sup> percentile) confidence limits. In a few instances, the available data were not sufficient to determine individual preferred RI or VSR values. In those cases, the Working Group's consensus estimates are reported as a range of values rather

than as a central value with associated confidence limits. In other instances, the trenching data were insufficient to allow the Working Group to make fault parameter estimates.

## **CONCLUSIONS**

The Utah Quaternary Fault Parameters Working Group has completed a comprehensive evaluation of the paleoseismic-trenching data available for Utah's Quaternary faults, and where data permitted determined preferred RI and VSR estimates with approximate 2-sigma confidence limits. Although not based on rigorous statistical analysis, the consensus values and confidence limits represent the best professional judgment of a panel of experts thoroughly familiar with Utah's paleoseismic data. Until superseded by information from new paleoseismic investigations, the Working Group's preferred RI and VSR estimates and associated confidence limits represent the best available information regarding surface-faulting activity for the faults/fault sections reviewed. These data can be considered as approximating average RI and VSR values and 2-sigma variability about those mean values.

With paleoseismic-trenching performed on only 16 percent of Utah's Quaternary faults, clearly much remains to be done to characterize Utah's earthquake hazard. Future paleoseismic investigations will undoubtedly result in new data that will refine some Working Group estimates, answer outstanding questions, and fill data gaps. The Working Group looks forward to the completion of those studies and the clarity they will bring to earthquake-hazard evaluation in Utah.

## **ACKNOWLEDGMENTS**

The Utah Geological Survey thanks the members of the Utah Quaternary Fault Parameters Working Group. Without their volunteer efforts, this study could not have been completed. The UGS also thanks Bill Black (Western GeoLogic, LLC),

Christopher DuRoss (University of Utah), and Kathryn Hanson (Geomatrix Consultants, Inc.) for providing information on fault studies that was not otherwise available to the Working Group.

## BIBLIOGRAPHY

- Anderson, R.E., 1980, The status of seismotectonic studies of southwestern Utah: U.S. Geological Survey Open-File Report 80-801, p. 519-547.
- Anderson, R.E., and Bucknam, R.C., 1979, Two areas of Holocene deformation in southwestern Utah: *Tectonophysics*, v. 52, p. 417-430.
- Anderson, L.W., and Miller, D.G., 1979, Quaternary fault map of Utah: Long Beach, California, Fugro, Inc., 35 p., scale 1:500,000.
- Arabasz, W.J., and Smith, R.B., 1979, The November 1971 earthquake swarm near Cedar City, Utah, *in* Arabasz, W.J., Smith, R.B., and Richins, W.D., editors, *Earthquake studies in Utah, 1850 to 1978*: Salt Lake City, University of Utah Seismograph Stations Special Publication, p. 423-432.
- Bacon, C.R., 1983, Eruptive history of Mount Mazama and Crater Lake caldera, Cascade Range, USA: *Journal of Volcanology and Geothermal Research*, v. 18, p. 57-115.
- Barnhard, T.P., and Dodge, R.L., 1988, Map of fault scarps formed on unconsolidated sediments, Tooele 1° x 2° quadrangle, northwestern Utah: U.S. Geological Survey Miscellaneous Field Studies Map MF-1990, scale 1:250,000.
- Bates, R.L., and Jackson, J.A., editors, 1987, *Glossary of geology* (3<sup>rd</sup> edition): Falls Church, Virginia, American Geological Institute, 788 p.
- Best, M.G., McKee, E.H., and Damon, P.E., 1980, Space-time-composition patterns of late Cenozoic mafic volcanism, southwestern Utah and adjoining areas: *American Journal of Science*, v. 280, p. 1035-1050.
- Black, B.D., Giraud, R.E., and Mayes, B.H., 2000, Paleoseismic investigation of the Clarkston, Junction Hills, and Wellsville faults, West Cache fault zone, Cache County, Utah: Utah Geological Survey Special Study 98, 23 p.
- Black, B.D., Hecker, S., Hylland, M.D., Christenson, G.E., and McDonald, G.N., 2003, Quaternary fault and fold database and map of Utah: Utah Geological Survey Map 193DM, scale 1:50,000, compact disk.
- Black, B.D., Lund, W.R., Schwartz, D.P., Gill, H.E., and Mayes, B.H., 1996, Paleoseismic investigation on the Salt Lake City segment of the Wasatch fault zone at the South Fork Dry Creek and Dry Gulch sites, Salt Lake County, Utah: Utah Geological Survey Special Study 92, 22 p.
- Brimhall, W.H., and Merritt, L.B., 1981, The geology of Utah Lake - Implications for resource management: Great Basin Naturalist Memoirs Number 5, p. 24-42, scale 1:250,000.
- Bucknam, R.C., 1978, Northwestern Utah seismotectonic studies, *in* Seiders, W., and Thompson, J., compilers, *Summaries of technical reports*, volume VII: Menlo Park, California, U.S. Geological Survey Office of Earthquake Studies, p. 64.
- Bucknam, R.C., and Anderson, R.E., 1979, Estimation of fault-scarp ages from a scarp-height-slope-angle relationship: *Geology*, v. 7, no. 1, p. 11-14.
- Bucknam, R.C., Crone, A.J., and Machette, M.N., 1989, Characteristics of active faults, *in* Jacobson, J.L., compiler, *National Earthquake Hazards Reduction Program, summaries of technical reports volume XXVIII*: U.S. Geological Survey Open-File Report 89-453, p. 117.
- Bull, W.B., and Pearthree, P.A., 1988, Frequency and size of Quaternary surface ruptures of the Pitaycachi fault, northern Sonora, Mexico: *Bulletin of the Seismological Society of America*, v. 78, p. 965-978.
- Coleman, S.M., 2001, Seismic-stratigraphic framework for drill cores and paleoclimate records in Bear Lake, Utah-Idaho: *EOS, American Geophysical Union Transactions*, v. 82, p. F755.
- Coleman, S.M., Kelts, K.R., and Dinter, D.A., 2002, Depositional history and neotectonics in Great Salt Lake, Utah, from high-resolution seismic

- stratigraphy: *Sedimentary Geology*, v. 148, p. 61-78.
- Crone, A.J., and Harding, S.T., 1984, Near-surface faulting associated with Holocene fault scarps, Wasatch fault zone, Utah - A preliminary report, *in* Hays, W.W., and Gori, P.L., editors, A workshop on "Evaluation of regional and urban earthquake hazards and risk in Utah": U.S. Geological Survey Open-File Report 84-763, p. 241-268.
- Crone, A.J., Machette, M.N., Bonilla, M.G., Lienkaemper, J.J., Pierce, K.L., Scott, W.E., and Bucknam, R.C., 1985, Characteristics of surface faulting accompanying the Borah Peak earthquake, central Idaho, *in* Stein, R.S., and Bucknam, R.C., editors and conveners, Proceedings of Workshop XXVIII on the Borah Peak, Idaho earthquake: U.S. Geological Survey Open-File Report 85-290, p. 43-58.
- Dames and Moore, 1978, Phase II - preliminary geotechnical studies, proposed power plant, lower Sevier River area, Utah: Los Angeles, unpublished consultant's report for Intermountain Power Project, job nos. 10629-00206 and 10629-003-06, 45 p., scale 1:24,000.
- deJong, A.F.M., Becker, B., and Mook, W.G., 1986, High-precision calibration of the radiocarbon time scale, 3930-3230 BC, *in* Stuiver, M., and Kra, R.S., editors, Radiocarbon calibration issue - Proceedings of the 12<sup>th</sup> International Radiocarbon Conference, Trondheim, Norway: *Radiocarbon*, v. 28, no. 2B, p. 939-942.
- dePolo, C.M., Clark, D.G., Slemmons, D.B., and Aymard, W.H., 1989, Historical Basin and Range Province surface faulting and fault segmentation, *in* Schwartz, D.P., and Sibson, R.H., editors, Fault segmentation and controls of rupture initiation and termination - Proceedings of conference XLV: U.S. Geological Survey Open-File Report 89-315, p. 131-162.
- Dinter, D.A., and Pechmann, J.C., 2000, Paleoseismology of the East Great Salt Lake fault: U.S. Geological Survey, National Earthquake Hazards Reduction Program Final Technical Report, award no. 98HQGR1013, 6 p.
- \_\_\_\_\_, 2004a, Segmentation and Holocene displacement history of the East Great Salt Lake fault: Salt Lake City, PowerPoint presentation to the 2004 Utah Earthquake Conference, 26 February 2004.
- \_\_\_\_\_, 2004b, Holocene segmentation and displacement history of the East Great Salt Lake fault, Utah [ext. abs.]: submitted to Proceedings of the Basin and Range Province Seismic Hazards Summit II, Reno, Nevada, May 16-19, 2004, 5 p.
- DuRoss, C.B., and Bruhn, R.L., 2003, Variations in the timing and pattern of rupturing along the Nephi segment of the Wasatch fault zone, Utah [abs]: *Geological Society of America Abstracts with Programs*, v. 35, no. 6, p. 581.
- Earth Sciences Associates, 1982, Phase I report, seismic safety investigation of eight SCS dams in southwestern Utah: Palo Alto, California, unpublished consultant's report for U.S. Soil Conservation Service, 2 volumes, variously paginated.
- Ertec Western, Inc., 1981, MX siting investigation, faults and lineaments in the MX siting region, Nevada and Utah: Long Beach, California, unpublished consultant's report no. E-TR-54 for U.S. Air Force, volume I, 77 p.; volume II, variously paginated, scale 1:250,000.
- Everitt, B.L., and Kaliser, B.N., 1980, Geology for assessment of seismic risk in the Tooele and Rush Valleys, Tooele County, Utah: Utah Geological and Mineral Survey Special Studies 51, 33 p.
- Foley, L.L., Martin, R.A., Jr., and Sullivan, J.T., 1986, Seismotectonic study for Joes Valley, Scofield, and Huntington North Dams, Emery County and Scofield Projects, Utah: Denver, U.S. Bureau of Reclamation Seismotectonic Report No. 86-7, 132 p., scale 1:60,000 and 1:155,000.
- Forman, S.L., Nelson, A.R., and McCalpin, J.P., 1991, Thermoluminescence dating of fault-scarp-derived colluvium - Deciphering the

- timing of paleoearthquakes on the Weber segment of the Wasatch fault zone, north-central Utah: *Journal of Geophysical Research*, v. 96, no. B1, p. 595-605.
- Gilbert, G.K., 1890, Lake Bonneville: U.S. Geological Survey Monograph 1, 438 p.
- Hanks, T.C., Bucknam, R.C., Lajoie, K.R., and Wallace, R.E., 1984, Modification of wave-cut and faulting-controlled landforms: *Journal of Geophysical Research*, v. 89, no. B7, p. 5771-5790.
- Hanson, K.L., Swan, F.H., III, and Schwartz, D.P., 1981, Study of earthquake recurrence intervals on the Wasatch fault, Utah: San Francisco, Woodward-Clyde Consultants, Sixth Semi-Annual Technical Report prepared for the U.S. Geological Survey, contract no. 14-08-0001-16827, 22 p.
- \_\_\_\_\_, 1982, Study of earthquake recurrence intervals on the Wasatch fault, Utah: San Francisco, Woodward-Clyde Consultants, Seventh Semi-Annual Technical Report prepared for the U.S. Geological Survey, contract no. 14-08-0001-19842, 26 p.
- Harty, K.M., Mulvey, W.E., and Machette, M.N., 1997, Surficial geologic map of the Nephi segment of the Wasatch fault zone, eastern Juab County, Utah: Utah Geological Survey Map 170, scale 1:50,000, 14 p. booklet.
- Hecker, S., 1993, Quaternary tectonics of Utah with emphasis on earthquake-hazard characterization: Utah Geological Survey Bulletin 127, 157 p., 2 plates, scale 1:500,000.
- Hecker, S., Harty, K.M., and Christenson, G.E., 1987, May 26, 1987, reconnaissance of late Quaternary fault along west side of Sanpete Valley: Utah Geological and Mineral Survey, unpublished memorandum, 2 p.
- Hecker, S., Kendrick, K.J., Ponti, D.J., and Hamilton, J.C., 1998, Fault map and database for Southern California - Long Beach 30'x60' quadrangle: U.S. Geological Survey Open-File Report 98-129, 27 p., 3 appendices.
- Hylland, M.D., and Machette, M.N., 2004, Part III – Interim surficial geologic map of the Levan segment of the Wasatch fault zone, Juab and Sanpete Counties, in Christenson, G.E., Ashland, F.X., Hylland, M.D., McDonald, G.N., and Case, B., Database compilation, coordination of earthquake-hazards mapping, and study of the Wasatch fault and earthquake-induced landslides, Wasatch Front, Utah: Utah Geological Survey Final Contract Report to the U.S. Geological Survey, contract no. 03HGAG0008, 30 p.
- Jackson, M.E., 1991, Paleoseismology of Utah, Volume 3 - The number and timing of Holocene paleoseismic events on the Nephi and Levan segments, Wasatch fault zone, Utah: Utah Geological Survey Special Studies 78, 23 p.
- Keaton, J.R., and Currey, D.R., 1989, Earthquake hazard evaluation of the West Valley fault zone in the Salt Lake City urban area, Utah: Salt Lake City, Dames and Moore, Final Technical Report for U.S. Geological Survey, contract no. 14-08-001-G1397, 69 p.; also published as Utah Geological Survey Contract Report 93-7, 1993.
- Keaton, J.R., Currey, D.R., and Olig, S.J., 1987, Paleoseismicity and earthquake hazards evaluation of the West Valley fault zone, Salt Lake City urban area, Utah: Salt Lake City, Dames and Moore, Final Technical Report for U.S. Geological Survey, contract no. 14-08-0001-22048, 55 p.; also published as Utah Geological Survey Contract Report 93-8, 1993.
- Korbay, S.R., and McCormick, W.V., 1999, Faults, lateral spreading, and liquefaction features, Salt Palace Convention Center, Salt Lake City [abs.]: Association of Engineering Geologists, 42<sup>nd</sup> Annual Meeting Program with Abstracts, p. 73.
- Linick, T.W., Long, A., Damon, P.E., and Ferguson, C.W., 1986, High-precision radiocarbon dating of bristlecone pine from 6554 to 5350 BC, in Stuiver, M., and Kra, R.S., editors, Radiocarbon calibration issue – Proceedings of the 12<sup>th</sup> International Radiocarbon Conference, Trondheim, Norway: Radiocarbon, v. 28, no. 2B, p. 943-953.
- Lund, W.R., 1992, New information on the timing of earthquakes on the Salt Lake City segment of the Wasatch fault zone - Implications for

- increased earthquake hazard along the central Wasatch Front: Utah Geological Survey, Wasatch Front Forum, v. 8, no. 3, p. 12-13.
- Lund, W.R., and Black, B.D., 1998, Paleoseismology of Utah, Volume 8 - Paleoseismic investigation at Rock Canyon, Provo segment, Wasatch fault zone, Utah County, Utah: Utah Geological Survey Special Study 93, 21 p.
- Lund, W.R., Black, B.D., and Schwartz, D.P., 1990, Late Holocene displacement on the Provo segment of the Wasatch fault zone at Rock Canyon, Utah County, Utah [abs.]: Geological Society of America Abstracts with Programs, v. 22, no. 6, p. 37.
- Lund, W.R., Hozik, M.J., and Hatfield, S.C., in preparation, Paleoseismic investigation of earthquake hazard and long-term movement history of the Hurricane fault in southwestern Utah: Utah Geological Survey.
- Lund, W.R., Pearthree, P.A., Amoroso, L., Hozik, M.J., and Hatfield, S.C., 2001, Paleoseismic investigation of earthquake hazard and long-term movement history of the Hurricane fault, southwestern Utah and northwestern Arizona: Utah Geological Survey (Salt Lake City) and Arizona Geological Survey (Tucson), Final Technical Report to the U.S. Geological Survey National Earthquake Hazard Reduction Program, award no. 99HQGR0026, 96 p, 3 appendices.
- Lund, W.R., Schwartz, D.P., Mulvey, W.E., Budding, K.E., and Black, B.D., 1991, Paleoseismology of Utah, Volume 1 - Fault behavior and earthquake recurrence on the Provo segment of the Wasatch fault zone at Mapleton, Utah County, Utah: Utah Geological and Mineral Survey Special Studies 75, 41 p.
- Machette, M.N., 1984, Preliminary investigation of late Quaternary slip rates along the southern part of the Wasatch fault zone, central Utah, *in* Hays, W.W., and Gori, P.L., editors, Proceedings of Conference XXVI, A workshop on "Evaluation of regional and urban earthquake hazards and risk in Utah": U.S. Geological Survey Open-File Report 84-763, p. 391-406.
- \_\_\_\_\_, 1988, American Fork Canyon, Utah – Holocene faulting, the Bonneville fan-delta complex, and evidence for the Keg Mountain oscillation, *in* Machette, M.N., editor, In the footsteps of G.K. Gilbert – Lake Bonneville and neotectonics of the eastern Basin and Range: Utah Geological and Mineral Survey Miscellaneous Publication 88-1, p. 89-95.
- \_\_\_\_\_, 1992, Surficial geologic map of the Wasatch fault zone, eastern Utah Valley, Utah County and parts of Salt Lake and Juab Counties, Utah: U.S. Geological Survey Miscellaneous Investigations Series Map I-2095, scale 1:50,000.
- Machette, M.N., and Lund, W.R., 1987, Trenching across the American Fork segment of the Wasatch fault zone, Utah [abs.]: Geological Society of America Abstracts with Programs, v. 19, no. 5, p. 317.
- Machette, M.N., Personius, S.F., and Nelson, A.R., 1992, Paleoseismology of the Wasatch fault zone - A summary of recent investigations, interpretations, and conclusions, *in* Gori, P.L., and Hays, W.W., editors, Assessment of regional earthquake hazards and risk along the Wasatch Front, Utah: U.S. Geological Survey Professional Paper 1500-A, p. A1-A71.
- Martin, R.A., Jr., Nelson, A.R., Weisser, R.R., and Sullivan, J.T., 1985, Seismotectonic study for Taskeech Dam and Reservoir site, Upalco Unit and Upper Stillwater Dam and Reservoir site, Bonneville Unit, Central Utah Project, Utah: Denver, U.S. Bureau of Reclamation Seismotectonic Report 85-2, 95 p.
- McCalpin, J.P., 1985, Quaternary fault history and earthquake potential of the Hansel Valley area, north-central Utah: Final Technical Report to the U.S. Geological Survey, Contract No. 14-08-001-21899, 37 p.
- \_\_\_\_\_, 1989, Surficial geologic map of the East Cache fault zone, Cache County, Utah: U.S. Geological Survey Miscellaneous Field Studies Map MF-2107, scale 1:50,000.
- \_\_\_\_\_, 1990, Latest Quaternary faulting in the northern Wasatch to Teton corridor (NWTC): Final

- Technical Report for U.S. Geological Survey, contract no. 14-08-001-G1395, 42 p.
- \_\_\_\_ 1993, Neotectonics of the northeastern Basin and Range margin, western USA, *in* Stewart, I., Vita-Finzi, C., and Owen, L., editors, Neotectonics and active faulting: Zeitschrift für Geomorphologie, Supplement Bd., p. 137-157.
- \_\_\_\_ 1994, Neotectonic deformation along the East Cache fault zone, Cache County, Utah: Utah Geological Survey Special Study 83, 37 p.
- \_\_\_\_ 1996, editor, Paleoseismology: New York, Academic Press, 586 p.
- \_\_\_\_ 2002, Post-Bonneville paleoearthquake chronology of the Salt Lake City segment, Wasatch fault zone, from the 1999 "Megatrench" site: Utah Geological Survey Miscellaneous Publication 02-7, 37 p.
- \_\_\_\_ 2003, Neotectonics of Bear Lake Valley, Utah and Idaho; a preliminary assessment: Utah Geological Survey Miscellaneous Publication 03-4, 43 p.
- McCalpin, J.P., and Forman, S.L., 1991, Late Quaternary faulting and thermoluminescence dating of the East Cache fault zone, north-central Utah: Bulletin of the Seismological Society of America, v. 81, no. 1, p. 139-161.
- \_\_\_\_ 1993, Assessing the paleoseismic activity of the Brigham City segment, Wasatch fault zone, Utah - Site of the next major earthquake on the Wasatch Front?, *in* Jacobson, M.L., compiler, Summaries of Technical Reports, v. XXXIV: U.S. Geological Survey Open-File Report 93-195, p. 485-489.
- \_\_\_\_ 2002, Post-Provo paleoearthquake chronology of the Brigham City segment, Wasatch fault zone, Utah: Utah Geological Survey Miscellaneous Publication 02-9, 46 p.
- McCalpin, J.P., Forman, S.L., and Lowe, M., 1994, Reevaluation of Holocene faulting at the Kaysville site, Weber segment of the Wasatch fault zone, Utah: Tectonics, v. 13, no. 1, p. 1-16.
- McCalpin, J.P., and Nelson, C.V., 2000, Long recurrence records from the Wasatch fault zone, Utah: U.S. Geological Survey, National Earthquake Hazards Reduction Program Final Technical Report, contract no. 99HQGR0058, 61 p.
- McCalpin, J.P., and Nishenko, S.P., 1996, Holocene paleoseismicity, temporal clustering, and probabilities of future large ( $M > 7$ ) earthquakes on the Wasatch fault zone: Journal of Geophysical Research, v. 101, no. B3, p. 6233-6253.
- McCalpin, J.P., Robison, R.M., and Garr, J.D., 1992, Neotectonics of the Hansel Valley-Pocatello Valley corridor, northern Utah and southern Idaho, *in* Gori, P.L., and Hays, W.W., editors, Assessment of regional earthquake hazards and risk along the Wasatch Front, Utah: U.S. Geological Survey Professional Paper 1500-G, p. G1-G18.
- Miller, D.M., and Schneyer, J.E., 1990, Geologic map of the Sunset Pass quadrangle, Box Elder County, Utah: Utah Geological and Mineral Survey Open-File Report 201, 32 p., scale 1:24,000.
- Nelson, A.R., 1988, The northern part of the Weber segment of the Wasatch fault zone near Ogden, Utah, *in* Machette, M.N., editor, In the footsteps of G.K. Gilbert - Lake Bonneville and neotectonics of the eastern Basin and Range Province, Guidebook for Field Trip Twelve: Utah Geological and Mineral Survey Miscellaneous Publication 88-1, p. 33-37.
- Nelson, A.R., Klauk, R.H., Lowe, M., and Garr, J.D., 1987, Holocene history of displacement on the Weber segment of the Wasatch fault zone at Ogden, northern Utah [abs.]: Geological Society of America Abstracts with Programs, v. 19, no. 5, p. 322.
- Nelson, A.R., and Martin, R.A., Jr., 1982, Seismotectonic study for Soldier Creek Dam, Central Utah Project: Denver, U.S. Bureau of Reclamation Seismotectonic Report 82-1, 115 p., scale 1:250,000.
- Nelson, A.R., and Personius, S.F., 1993, Surficial geologic map of the Weber segment, Wasatch fault zone, Weber and Davis Counties, Utah: U.S. Geological Survey Miscellaneous Investigations Series Map I-2199, 22 p. pamphlet, scale 1:50,000.

- Nelson, A.R., and Sullivan, J.T., 1992, Late Quaternary history of the James Peak fault, southernmost Cache Valley, north-central Utah, *in* Gori, P.L., and Hays, W.W., editors, Assessment of regional earthquake hazards and risk along the Wasatch Front, Utah: U.S. Geological Survey Professional Paper 1500-J, p. J1-J13.
- Nelson, A.R., and VanArsdale, R.B., 1986, Recurrent late Quaternary movement on the Strawberry normal fault, Basin and Range - Colorado Plateau transition zone, Utah: *Neotectonics*, v. 1, p. 7-37.
- Nelson, A.R., and Weisser, R.R., 1985, Quaternary faulting on Towanta Flat, northwestern Uinta Basin, Utah, *in* Picard, M.D., editor, Geology and energy resources, Uinta Basin of Utah: Utah Geological Association Publication 12, p. 147-158.
- North American Commission on Stratigraphic Nomenclature, 1983, North American stratigraphic code: American Association of Petroleum Geologists Bulletin, v. 67, no. 5, p. 841-875.
- Olig, S.S., Gorton, A.E., Black, B.D., and Forman, S.L., 2000, Evidence for young, large earthquakes on the Mercur fault - implications for segmentation and evolution of the Oquirrh-East Great Salt Lake fault zone, Wasatch Front, Utah [abs.]: Geological Society of America Abstracts with Programs, 2000 Annual Meeting, v. 32, no. 7, p. A-120.
- \_\_\_\_\_, 2001, Paleoseismology of the Mercur fault and segmentation of the Oquirrh - East Great Salt Lake fault zone, Utah: Oakland, California, URS Corporation, unpublished technical report for U.S. Geological Survey, award no. 98HQGR1036, variously paginated.
- Olig, S.S., Gorton, A.E., and Chadwell, L., 1999, Mapping and Quaternary fault scarp analysis of the Mercur and West Eagle Hill faults, Wasatch Front, Utah: Oakland, California, URS Greiner Woodward Clyde, National Earthquake Hazards Reduction Program Final Technical Report, award no. 1434-HQ-97-GR-03154, variously paginated, scale 1:48,000.
- Olig, S.S., Lund, W.R., Black, B.D., and Mayes, B.H., 1996, Paleoseismic investigation of the Oquirrh fault zone, Tooele County, Utah, *in* Lund, W.R., editor, Paleoseismology of Utah, Volume 6, The Oquirrh fault zone, Tooele County, Utah - Surficial geology and paleoseismicity: Utah Geological Survey Special Study 88, p. 22-64.
- Olig, S., McDonald, G., Black, B., DuRoss, C., and Lund, B., 2004, The Mapleton "Megatrench" - Deciphering 11,000 years of earthquake history on the Wasatch fault near Provo: Utah Geological Survey, Survey Notes, v. 36, no. 2, p. 4-6.
- Ostenaar, D., 1990, Late Holocene displacement history, Water Canyon site, Wasatch fault zone [abs.]: Geological Society of America Abstracts with Programs, v. 22, no. 6, p. 42.
- Oviatt, C.G., 1991, Quaternary geology of the Fish Springs Flat, Juab County, Utah: Utah Geological Survey Special Studies 77, 16 p.
- Oviatt, C.G., and Thompson, R.S., 2002, Recent developments in the study of Lake Bonneville since 1980, *in* Gwynn, J.W., editor, Great Salt Lake, an overview of change: Utah Department of Natural Resources Special Publication, p. 1-6.
- Pearson, G.W., and Stuiver, M., 1986, High-precision calibration of the radiocarbon time scale, 500-2500 BC, *in* Stuiver, M., and Kra, R.S., editors, Radiocarbon calibration issue - Proceedings of the 12<sup>th</sup> International Radiocarbon Conference, Trondheim, Norway: Radiocarbon, v. 28, no. 2B, p. 839-862.
- Pearthree, P.A., compiler, 1998, Quaternary fault data and map for Arizona: Arizona Geological Survey Open-File Report 98-24, scale 1:750,000, 122 p.
- Pechmann, J.C., Arabasz, W.J., and Nava, S.J., 1995, Seismology, *in* Christenson, G.E., editor, The September 2, 1992 M<sub>L</sub> 5.8 St. George earthquake, Washington County, Utah: Utah Geological Survey Circular 88, p.1.
- Personius, S.F., 1990, Surficial geologic map of the Brigham City segment and adjacent parts of the Weber and Collinston segments, Wasatch fault

- zone, Box Elder and Weber Counties, Utah: U.S. Geological Survey Miscellaneous Investigations Series Map I-1979, scale 1:50,000.
- \_\_\_\_ 1991, Paleoseismology of Utah, volume 2 - Paleoseismic analysis of the Wasatch fault zone at the Brigham City trench site, Brigham City, Utah, and Pole Patch trench site, Pleasant View, Utah: Utah Geological and Mineral Survey Special Studies 76, 39 p.
- Personius, S.F., and Scott, W.E., 1992, Surficial geology of the Salt Lake City segment and parts of adjacent segments of the Wasatch fault zone, Davis, Salt Lake, and Utah Counties, Utah: U.S. Geological Survey Miscellaneous Investigations Series Map I-2106, scale 1:50,000.
- Piety, L.A., and Vetter, U.R., 1999, Seismotectonic report for Flaming Gorge Dam, Colorado River Storage Project, northeastern Utah: Denver, Bureau of Reclamation Seismotectonic Report 98-2, 78 p.
- Robison, R.M., and Burr, T.N., 1991, Fault-rupture hazard analysis using trenching and borings - Warm Springs fault, Salt Lake City, Utah, *in* McCalpin, J.P., editor, Proceedings of the 27th Symposium on Engineering Geology and Geotechnical Engineering: Boise, Idaho Department of Transportation, p. 26-1 - 26-13.
- Schwartz, D.P., and Coppersmith, K.J., 1984, Fault behavior and characteristic earthquakes - Examples from the Wasatch and San Andreas fault zones: *Journal of Geophysical Research*, v. 89, no. B7, p. 5681-5698.
- Schwartz, D.P., Hanson, K.L., and Swan, F.H., III, 1983, Paleoseismic investigations along the Wasatch fault zone - An update, *in* Gurgel, K.D., editor, Geologic excursions in neotectonics and engineering geology in Utah: Utah Geological and Mineral Survey Special Studies 62, p. 45-48.
- Schwartz, D.P., and Lund, W.R., 1988, Paleoseismicity and earthquake recurrence at Little Cottonwood Canyon, Wasatch fault zone, Utah, *in* Machette, M.N., editor, In the footsteps of G.K. Gilbert - Lake Bonneville and neotectonics of the eastern Basin and Range Province, Guidebook for Field Trip Twelve: Utah Geological and Mineral Survey Miscellaneous Publication 88-1, p. 82-85.
- Scott, W.E., 1989, Temporal relations of lacustrine and glacial events at Little Cottonwood and Bells Canyons, *in* Machette, M.N., editor, In the footsteps of G.K. Gilbert - Lake Bonneville and neotectonics of the eastern Basin and Range Province, Guidebook for Field Trip Twelve: Utah Geological and Mineral Survey Miscellaneous Publication 88-1, p. 78-81.
- Simon, D.B., and Shlemon, R.J., 1999, The Holocene "Downtown Fault" in Salt Lake City, Utah [abs.]: Association of Engineering Geologists, 42<sup>nd</sup> Annual Meeting Program with Abstracts, p. 85.
- Skeen, R.C., 1975, A reflection seismic study of the subsurface structure and sediments of Bear Lake, Utah-Idaho: Salt Lake City, University of Utah, senior thesis, 25 p.
- Solomon, B.J., 1996, Surficial geology of the Oquirrh fault zone, Tooele County, Utah, *in* Lund, W.R., editor, Paleoseismology of Utah, Volume 6, The Oquirrh fault zone, Tooele County, Utah - Surficial geology and paleoseismicity: Utah Geological Survey Special Study 88, p. 1-17.
- \_\_\_\_ 1998, New evidence for the age of faulting on the West Valley fault zone: Utah Geological Survey, Survey Notes, v. 30, no. 3, p. 8 and 13.
- \_\_\_\_ 1999, Surficial geologic map of the West Cache fault zone and nearby faults, Box Elder and Cache Counties, Utah: Utah Geological Survey Map 172, scale 1:50,000, 21 p. pamphlet.
- Stenner, H.D., Crosby, C.J., Dawson, T.E., Amoroso, L., Pearthree, P.A., and Lund, W.R., 2003, Evidence for variable slip from the last three surface-rupturing earthquakes along the central Hurricane fault zone [abs.]: *Seismological Research Letters*, v. 74, no. 2, p. 238.
- Stenner, H.D., Lund, W.R., Pearthree, P.A., and Everitt, B.L., 1999, Paleoseismic investigation of the Hurricane fault, northwestern Arizona and southwestern Utah: Arizona Geological Survey Open-File Report 99-8, 137 p.

- Sterr, H.M., 1985, Rates of change and degradation of hill slopes formed in unconsolidated materials, a morphometric approach to dating Quaternary fault scarps in western Utah, USA: *Zeitschrift für Geomorphologie*, v. 29, no. 3, p. 315-333.
- Stewart, M.E., and Taylor, W.J., 1996, Structural analysis and fault segment boundary identification along the Hurricane fault in southwestern Utah: *Journal of Structural Geology*, v. 18, p. 1017-1029.
- Stuiver, M., and Reimer, P.J., 1993, Extended  $^{14}\text{C}$  database and revised CALIB 3.0  $^{14}\text{C}$  calibration program: *Radiocarbon*, v. 35, no. 1, p. 215-230.
- \_\_\_\_\_, 1998, University of Washington Quaternary Isotope Lab Radiocarbon Calibration Program Rev. 4.3: *Radiocarbon*, v. 35, p. 215-230.
- Stuiver, M., Reimer, P.J., Bard, E., Beck, J.W., Stuiver, M., Reimer, P.J., and Braziunas, T.F., 1998, Revised calibration dataset: *Radiocarbon* v. 40, p.1127-1151.
- Sullivan, J.T., Martin, R.A., and Foley, L.L., 1988a, Seismotectonic study for Jordanelle Dam, Bonneville Unit, Central Utah Project, Utah: Denver, U.S. Bureau of Reclamation Seismotectonic Report 88-6, 76 p., scale 1:24,000.
- Sullivan, J.T., and Nelson, A.R., 1992, Late Quaternary displacement on the Morgan fault, a back valley fault in the Wasatch Range of northeastern Utah, *in* Gori, P.L., and Hays, W.W., editors, Assessment of regional earthquake hazards and risk along the Wasatch Front: U.S. Geological Survey Professional Paper 1500-I, p. II-II19.
- Sullivan, J.T., Nelson, A.R., LaForge, R.C., Wood, C.K., and Hansen, R.A., 1988b, Central Utah regional seismotectonic study for USBR dams in the Wasatch Mountains: Denver, U.S. Bureau of Reclamation Seismotectonic Report 88-5, 269 p., scale 1:250,000.
- Swan, F.H., III, Hanson, K.L., Schwartz, D.P., and Knuepfer, P.L., 1981a, Study of earthquake recurrence intervals on the Wasatch fault, Utah - Little Cottonwood Canyon site: U.S. Geological Survey Open-File Report 81-450, 30 p.
- Swan, F.H., III, Schwartz, D.P., and Cluff, L.S., 1980, Recurrence of moderate to large magnitude earthquakes produced by surface faulting on the Wasatch fault zone, Utah: *Bulletin of the Seismological Society of America*, v. 70, no. 5, p. 1431-1462.
- Swan, F.H., III, Schwartz, D.P., Hanson, K.L., Knuepfer, P.L., and Cluff, L.S., 1981b, Study of earthquake recurrence intervals on the Wasatch fault at the Kaysville site, Utah: U.S. Geological Survey Open-File Report 81-228, 30 p.
- Threft, R.L., 1963, Geology of the Parowan Gap area, Iron County, Utah, *in* Heylman, E.B., editor, Guidebook to the geology of southwestern Utah: Intermountain Association of Petroleum Geologists, Twelfth Annual Field Conference, p. 136-145.
- Viveiros, J.J., 1986, Cenozoic tectonics of the Great Salt Lake from seismic reflection data: University of Utah, Salt Lake City, M.S. thesis, 99 p.
- Walter, H.G., 1934, Hansel Valley, Utah, earthquake: *The Compass of Sigma Gamma Epsilon*, v. 14, no. 4, p. 178-181.
- Wells, D.L., and Coppersmith, K.J., 1994, New empirical relationships among magnitude, rupture length, rupture width, rupture area, and surface displacement: *Bulletin of the Seismological Society of America*, v. 84, p. 974-1002.
- West, M.W., 1994, Paleoseismology of Utah, Volume 4 - Seismotectonics of north central Utah and southwestern Wyoming: Utah Geological Survey Special Study 82, 93 p.
- Wilson, E.A., Saugy, L., and Zimmermann, M.A., 1986, Cenozoic tectonics and sedimentation of the eastern Great Salt Lake area, Utah: *Bulletin de Société Géologique Française*, v. 2, no. 5, p. 777-782.
- Wong, I.G., and Olig, S.S., 1998, Seismic hazards in the Basin and Range Province - Perspectives from probabilistic analyses, *in* Lund, W.R., editor, Proceedings Volume, Basin and Range Seismic-Hazards Summit: Utah Geological

Survey Miscellaneous Publication 98-2, p. 110-127.

Wong, I., Silva, W., Olig, S., Thomas, P., Wright, D., Ashland, F., Gregor, N., Pechmann, J., Dober, M., Christenson, G., and Gerth, R., 2002, Earthquake scenario and probabilistic ground shaking maps for the Salt Lake City, Utah metropolitan area: Utah Geological Survey Miscellaneous Publication 02-5, 50 p., compact disk in back.

Working Group on California Earthquake Probabilities, 1988, Probabilities of large earthquakes occurring in California on the San Andreas fault: U.S. Geological Survey Open-File Report 88-398, 62 p.

—1990, Probabilities of large earthquakes in the San Francisco Bay region, California: U.S. Geological Survey Circular 1053, 51 p.

—1999, Earthquake probabilities in the San Francisco Bay region: 2000 to 2030 - A summary of findings: U.S. Geological Survey Open-File Report 99-517, 36 p.

Youngs, R.R., Swan, F.H., Power, M.S., Schwartz, D.P., and Green, R.K., 2000, Probabilistic analysis of earthquake ground shaking hazards along the Wasatch Front, Utah, *in* Gori, P.L., and Hays, W.W., editors, Assessment of regional earthquake hazards and risk along the Wasatch Front, Utah: U.S. Geological Survey Professional Paper 1500-M, p. M1-M67.

***APPENDIX***

***WORKING GROUP CONSENSUS***  
***EARTHQUAKE TIMING***  
***AND***  
***PREFERRED RECURRENCE-INTERVAL AND VERTICAL SLIP-RATE***  
***ESTIMATES***  
***WITH SUPPORTING INFORMATION***

Fault/Fault Section <sup>1</sup>	Length <sup>2</sup> (km)		Earthquake Timing <sup>3</sup>	Consensus Preferred Recurrence Interval <sup>4</sup>	Consensus Preferred Vertical Slip Rate <sup>5</sup>
	Straight Surface Line	Trace			
Wasatch fault zone Brigham City segment	35.5	40	Z 2100±800 cal yr B.P. Y 3450±300 cal yr B.P. X 4650±500 cal yr B.P. W 5950±250 cal yr B.P. V 7500±1000 cal yr B.P. U 8500±1500 cal yr B.P. T >14,800±1200, <17,000 cal yr B.P.	Three most recent (W to Z) interevent interval average recurrence: 1300 <sup>6</sup> ±200 <sup>7</sup> cal yr  Five most recent (U to Z) interevent interval average recurrence: 1300 <sup>6</sup> ±400 <sup>7</sup> cal yr  Working Group Preferred Recurrence Interval  500-1300-2800 yr	Personius (1990) BC Slip Rates: X-Y 0.6 –0.8-1.4 mm/yr W-X 1.4-1.9-3.1 mm/yr V-W 1.0-1.6-4.5 mm/yr  Longer term slip rates in Provo-age deposits range from 0.24 mm/yr near the north segment boundary to 1.36 mm/yr near Willard. Bonneville-age deposits at Willard Canyon record a single slip-rate of 1.5-1.6 mm/yr.  Working Group Preferred Vertical Slip Rate  0.6-1.4-4.5 mm/yr
Weber segment	56	61	Za 0.5±0.3 ka <sup>8</sup> (partial segment rupture?) Zb 950±450 cal yr B.P. <sup>8</sup> Y 3000±700 cal yr B.P. X 4500±700 cal yr B.P. W 6100±700 cal yr B.P.	Three most recent (W to Zb) interevent interval average recurrence: 1600 <sup>6</sup> ±600 <sup>7</sup> cal yr  Four most recent (W to Za) interevent interval average recurrence: 1100 <sup>6</sup> ±1400 <sup>7</sup> cal yr  Working Group Preferred Recurrence Interval  500-1400-2400 yr	Y-Zb 0.6-0.9-1.4 mm/yr X-Y 1.0-1.9-4.3 mm/yr W-X 0.6-0.9-1.6 mm/yr  Using an updated Lake Bonneville chronology and net-slip values from Nelson and Personius (1993) shows long-term slip rates as high as 2.0 mm/yr in Bonneville-phase deposits, and up to 1.3 mm/yr in Provo-phase deposits.  Working Group Preferred Vertical Slip Rate  0.6-1.2-4.3 mm/yr
Salt Lake City segment	39	46	Z 1300±650 cal yr B.P. Y 2450±550 cal yr B.P. X 3950±550 cal yr B.P.	Three most recent (W to Z) interevent interval average recurrence: 1300 <sup>6</sup> ±400 <sup>7</sup> cal yr	Swan and others (1981) reported 14.5+10/-3 meters of net slip across the WFZ on the crest of the Bells Canyon glacial moraine south of Little

Provo segment	59	69.5	<p>W 5300±750 cal yr B.P.  V ~7.5 ka (after 8.8-9.1 ka but before 5.1-5.3 ka)  U ~9 ka (shortly after 9.5-9.9 ka)  T ~17 ka  S (?) 17–20 ka</p> <p>Z 600±350 cal yr B.P.  Y 2850±650 cal yr B.P.  X 5300±300 cal yr B.P.</p>	<p>V-W and U-V intervals are each roughly 2 kyr; the T-U mean interevent interval is ~8 kyr, indicating surface-faulting quiescence during earliest Holocene and latest Pleistocene time (McCalpin, 2002).</p> <p>Working Group Preferred Recurrence Interval  500-<b>1300</b>-2400 yr</p> <p>Two most recent (X to Z) interevent interval average recurrence:  2400<sup>6</sup>±300<sup>7</sup> cal yr</p> <p>Working Group Preferred Recurrence Interval  1200-<b>2400</b>-3200 yr</p>	<p>Cottonwood Canyon. Scott (1989) reports the age of the moraine as 18-26 ka, resulting in a late Pleistocene slip rate of:  0.4-0.7-1.4 mm/yr</p> <p>Working Group Preferred Vertical Slip Rate  0.6-<b>1.2</b>-4.0 mm/yr</p> <p>Hobble Creek:  Post-Provo time  0.68-0.76-0.83 mm/yr  Post-Bonneville time  2.2-2.4-2.7 mm/yr  American Fork Canyon:  Post-Bonneville time  0.8-1.1-1.4 mm/yr  Spanish Fork Canyon:  Post-Provo time  0.18-0.19 mm/yr  East of Provo between Slate and Slide Canyons:  Post-Bonneville time  ≤ 1.1-1.2 mm/yr</p> <p>Working Group Preferred Vertical Slip Rate  0.6-<b>1.2</b>-3.0 mm/yr</p>
Nephi segment	37.5	42.5	<p>Z ≤1.0±0.4 ka  Y ~3.9±0.5 ka  X &gt;3.9±0.5 ka, &lt;5.3±0.7 ka</p>	<p>Two most recent (X to Z) interevent interval average recurrence:  ~2500<sup>6</sup>±2100<sup>7</sup> cal yr</p> <p>Working Group Preferred Recurrence Interval  1200-<b>2500</b>-4800 yr</p>	<p>North Creek (Schwartz and Coppersmith, 1984):  Middle Holocene 1.27-1.36±0.1 mm/yr  Harty and others (1997) middle Holocene slip-rate estimates:  North Creek 0.8-1.2 mm/yr  Willow Creek 0.7-1.0 mm/yr  Gardner Creek 0.5-0.7 mm/yr  Red Canyon 0.6-1.0 mm/yr</p>

Levan segment	25.5	30	Z $\leq 1000 \pm 150$ cal yr B.P. Y unknown but likely earliest Holocene to latest Pleistocene; partial segment rupture possible along southern portion of segment (Hylland and Machette, 2004).	Working Group Preferred Recurrence Interval  <b>&gt;3 and &lt;12 kyr<sup>9</sup></b>	Working Group Preferred Vertical Slip Rate  0.5-1.1-3.0 mm/yr  Working Group Preferred Vertical Slip Rate  <b>0.1-0.6 mm/yr<sup>9</sup></b>  Slip rate is based on the likelihood that an event Y (Hylland and Machette, 2004) occurred during early Holocene or latest Pleistocene time on the LS.
Joes Valley fault zone <sup>10</sup> East Joes Valley fault  West Joes Valley fault  Middle Mountain fault Bald Mountain faults (intragraben)	57  57  34	61  81  39	The JVfZ forms a long, narrow graben (JVG) on the Wasatch Plateau. The EJVF experienced a minimum of 4 earthquakes in 250 kyr; the WJVF and intragraben faults have each experienced a minimum of 2 earthquakes in the past ~30 kyr. Individual earthquake timing is not constrained.	Foley and others (1986) determined broad recurrence interval estimates of:  <u>Individual Fault Recurrence</u> EJVF <60 kyr (~250 ka record) WJVF 10-20 kyr (~30 ka record) MMF 10-15 kyr (~30 ka record)  Earthquake timing is constrained only within broad time intervals. Consequently, the Working Group's recurrence-interval estimate is intentionally broad to reflect high uncertainty.  Working Group Consensus Preferred Recurrence Interval  <b>5-10-50 kyr</b>	Foley and others (1986) report no net vertical slip across the JVG, and question the seismogenic capability of the JVfZ. Therefore, despite the presence of scarps on Quaternary deposits along the northern JVfZ, a fundamental question remains regarding the nature of the JVG, and the seismogenic capability of the JVfZ.  Lacking net vertical slip across the JVfZ, the Working Group recommends that: (1) the JVfZ be considered a single integrated structure, and (2) a consensus vertical slip rate not be reported for the JVfZ at this time.  <b>No estimate</b>
West Valley fault zone  Taylorsville fault	16  15	44  19	The WVfZ includes the subparallel Taylorsville fault (TF) and Granger fault (GF) and a zone of short, less well-defined	Keaton and others (1987) determined a mean recurrence of 1.8-2.2 kyr for the southern WVfZ. Keaton and Currey	Keaton and others (1987) determined the following vertical slip rates for the WVfZ: Taylorsville fault <12 kyr

Granger fault	16	25	<p>faults to the north.</p> <p>Based chiefly on geomorphic and drill-hole evidence, Keaton and others (1987) and Keaton and Currey (1989) report a minimum of 2 surface-faulting earthquakes in ~12 kyr on the TF and 5 earthquakes on the GF in the past 13 kyr, for a total of 6-7 earthquakes for the WVFZ as a whole; however, individual earthquake timing is not constrained.</p> <p>Solomon (1998) and unpublished UGS data show that the TF and GF MREs occurred shortly after 2.0-2.4 ka and 1.3-1.7 ka, respectively, which is similar to the timing of the two most recent surface-faulting earthquakes on the nearby SLCS of the WFZ.</p> <p>The similarity in timing between the earthquakes on the WVFZ and the SLCS raises questions regarding whether the WVFZ ruptures coseismically with the WFZ. However, until demonstrated otherwise, the Working Group considers the WVFZ independently seismogenic.</p>	<p>(1989) report a mean recurrence on the less well-defined northern part of the WVFZ of 6 to 11 kyr.</p> <p>Based on their review, the Working Group considers the available paleoseismic data insufficient to make a recurrence-interval estimate for the WVFZ.</p> <p><b>Insufficient data – no estimate possible.</b></p>	<p>0.1-0.2 mm/yr Granger fault 13 kyr 0.4-0.5 mm/yr WVFZ (entire) 13 kyr 0.5-0.6 mm/yr Granger fault 47±20 kyr 0.1-0.3 mm/yr Granger fault 60±20 kyr 0.02-0.04 mm/yr Granger fault 80±30 kyr 0.03-0.1 mm/yr Granger fault 140±10 kyr 0.01 mm/yr</p> <p>Slip-rate information for the WVFZ comes chiefly from geomorphic and drill-hole information and is broadly constrained. Therefore, the confidence limits for the WVFZ as a whole are intentionally broad to reflect high uncertainty:</p> <p>Working Group Preferred Vertical Slip Rate</p> <p>0.1-0.4-0.6 mm/yr</p>
West Cache fault zone	51	70 <sup>11</sup>	<p>The WCFZ consists of three east-dipping normal faults: the Clarkston (CF), Junction Hills (JHF), and Wellsville faults (WF). Each fault is a seismogenic segment of the WCFZ, and each has experienced Holocene surface faulting.</p>	<p>The timing of older earthquakes either could not be determined or could only be constrained within broad time intervals. Therefore, the Working Group's preferred recurrence-interval estimates for the CF, JHF, and WF are reported as ranges and are intentionally broad to reflect high uncertainty.</p> <p>Working Group Preferred Recurrence Intervals</p>	<p>The timing and displacement of older earthquakes either could not be determined or could only be constrained within broad time intervals. Therefore, confidence limits for the Working Group's slip-rate estimates for the CF, JHF, and WF are intentionally broad to reflect high uncertainty.</p> <p>Working Group Preferred Vertical Slip Rates</p>
Clarkston fault	?	35 <sup>11</sup>	<p>Z 3600-4000 cal yr B.P. No trench evidence of older earthquakes,</p>	<p><b>5-20 kyr<sup>9</sup></b></p>	<p>0.1-0.4-0.7 mm/yr</p>

Junction Hills fault	25	25	but geomorphic relations indicate a minimum of two earthquakes in post-Bonneville time. Z 8250-8650 cal yr B.P. Y > 22 ka	<b>10-25 kyr<sup>9</sup></b>	0.05- <b>0.1</b> -0.2 mm/yr
Wellsville fault	20	31	Z 4400-4800 cal yr B.P. Y 15 to 25 ka	<b>10-25 kyr<sup>9</sup></b>	0.05- <b>0.1</b> -0.2 mm/yr
East Cache fault zone central section	16	16	McCalpin (1989, 1994) subdivided the ECFZ into northern, central, and southern sections. The central section is the only section with geomorphic evidence of Holocene surface faulting, and is the only section for which paleoseismic trenching data are available.  Z 4.3-4.6 ka Y between 16.2 and 18 ka	Single interevent interval (Y-Z): minimum 11.6 kyr, maximum 13.7 kyr, average 12.7 kyr.  Evidence for a third earthquake (X) during the Bonneville transgression is equivocal. If a third earthquake did occur, the interval between events X and Y is likely ~4 kyr, which implies large variations in interevent interval length. Therefore, the confidence limits assigned to the Working Group's recurrence-interval estimate are intentionally broad to reflect high uncertainty:  Working Group Preferred Recurrence Interval  <b>4-10-15 kyr</b>	The minimum, maximum, and average Y-Z recurrence intervals, and an event Z displacement of 0.5-1.2 m (McCalpin, 1994), produce a slip-rate range of: 0.04-0.07-0.10 mm/yr  Possible large differences in interevent interval length would produce corresponding large variations in slip rate through time. Therefore, the confidence limits assigned to the Working Group's slip-rate estimate are intentionally broad to reflect high uncertainty:  Working Group Preferred Vertical Slip Rate  <b>0.04-0.2-0.4 mm/yr</b>
Hurricane fault zone Anderson Junction section	42	54	The Anderson Junction section (AJS) straddles the Utah/Arizona border and is one of 6 identified HFZ sections. Two trench sites, both in Arizona, provide evidence for 3 surface-faulting earthquakes; however, earthquake timing is only constrained to broad time intervals:  Z 5-10 ka Y >5-10 ka and <25-50 ka	Earthquake timing is poorly constrained on the AJS. The Working Group's recurrence-interval estimate is based largely on slip-rate information, and therefore, the confidence limits are intentionally broad to reflect high uncertainty:  Working Group Preferred Recurrence Interval	Scarp profiles (Stenner and others, 1999) indicate slip rates of 0.1-0.3 mm/yr in ~70-125 ka deposits, and 0.1-0.4 mm/yr in ~25-50 ka deposits. Displaced basalt flows (Lund and others, 2001) indicate that slip rates since the middle Quaternary are $\geq 0.45$ mm/yr, slowing to $\leq 0.2$ mm/yr sometime before 350 ka.  Because information on earthquake

			X >25-50 ka?	<b>5-50 kyr<sup>9</sup></b>	timing and displacement is limited, the Working Group's slip-rate estimate is based chiefly on information from scarp profiles and displaced basalt flows; confidence limits are intentionally broad to reflect high uncertainty:  Working Group Consensus Preferred Vertical Slip Rate  0.05- <b>0.2</b> -0.4 mm/yr
Great Salt Lake fault zone <sup>12</sup> Fremont Island segment	30		Z 3150+235/-211 cal yr B.P. Y 6412+209/-211 cal yr B.P. X <11,247 +605/-499 cal yr B.P.	Y-Z 3262+151/-184 yr X-Y <5015+587/-424 yr  Working Group Preferred Recurrence Interval  1.8- <b>4.2</b> -6.6 kyr	Working Group Preferred Vertical Slip Rate  0.3- <b>0.6</b> -1.6 mm/yr
Antelope Island segment	35		Z 586+201/-241 cal yr B.P. Y 6170+236/-234 cal yr B.P. X 9898+247/-302 cal yr B.P.	Y-Z 5584+219/-172 yr X-Y 3728+223/-285 yr  Working Group Preferred Recurrence Interval  1.8- <b>4.2</b> -6.6 kyr	Working Group Preferred Vertical Slip Rate  0.3- <b>0.6</b> -1.6 mm/yr
Oquirrh fault zone	21	22	Olig and others (1996) excavated trenches at two sites on the northern portion of the OFZ and found evidence for three surface-faulting earthquakes:  Z between 4800 and 7900 cal yr B.P. Y between 20,300 and 26,400 <sup>14</sup> C yr B.P. X > 26,400 <sup>14</sup> C yr B.P.  Olig and others (2001) believe that the OFZ ruptures coseismically with the	Single interevent interval (Y-Z): minimum 12.4 kyr, maximum 21.6 kyr, average 17.0 kyr.  Recurrence information is restricted to one poorly constrained interevent interval. Therefore, confidence limits for the Working Group's recurrence-interval estimate are intentionally broad to reflect high uncertainty:	The minimum, maximum, and average Y-Z recurrence intervals, and an event Z displacement of 2.0-2.7 m (Olig and others, 1996) produce a slip-rate range of 0.09-0.14-0.22 mm/yr.  Because information on recurrence and vertical net slip for the OFZ is restricted to a single, poorly constrained interevent interval, the confidence limits for the Working Group's slip-rate estimate are

			Southern Oquirrh Mountains fault zone to the south.	Working Group Preferred Recurrence Interval  5-20-50 kyr	intentionally broad to reflect high uncertainty:  Working Group Preferred Vertical Slip Rate  0.05-0.2-0.4 mm/yr
Southern Oquirrh Mountains fault zone (Mercur fault)	24	56	<p>Olig and others (1999) included the Mercur, West Eagle Hill, Soldier Canyon, and Lakes of Kilarney faults in the SOMFZ. Three trenches (east, central, and west) excavated across strands of the Mercur fault (MF) exposed evidence for 5 to 7 surface-faulting earthquakes since <math>92 \pm 14</math> ka</p> <p>Z shortly after <math>4.6 \pm 0.2</math> ka and well before <math>1.4 \pm 0.1</math> ka  Y between 20 and 50 ka  X shortly after <math>42 \pm 8</math> ka – may or may not correlate with earthquakes <math>V_C</math> (central trench) or <math>W_E</math> (east trench),  W shortly after <math>75 \pm 10</math> ka – may or may not correlate with earthquakes <math>V_C</math> and <math>W_E</math>, although event <math>V_C</math> is probably older  V around (shortly after?) <math>92 \pm 14</math> ka</p> <p>Olig and others (2001) consider these 5 earthquakes well established but poorly constrained. Uncertainty regarding the total number of earthquakes comes from difficulty correlating some earthquakes between trenches.</p>	<p>Olig and others (2001) determined a mean recurrence of 12 to 25 kyr based on 5 to 7 surface-faulting earthquakes between <math>92 \pm 14</math> and <math>4.6 \pm 0.2</math> ka. However, recurrence intervals between individual earthquakes could be as much as 46 kyr, or as short as a few kyr, suggesting order-of-magnitude variations in interevent intervals.</p> <p>Olig and others (2001) believe that the SOMFZ likely ruptures coseismically with the OFZ to the north, and the Working Group's recurrence-interval and slip-rate estimates are the same for both faults to reflect that possibility.</p> <p>Working Group Preferred Recurrence Interval  5-20-50 kyr</p>	<p>Based on the past 4 to 6 interevent intervals over <math>\sim 90</math> kyr, Olig and others (2001) determined average slip rates ranging from 0.09 to 0.14 mm/yr.</p> <p>The Working Group's slip-rate estimate reflects the Olig and others (2001) long-term average above; however, confidence limits have been increased to accommodate uncertainty resulting from possible large variations in slip through time:</p> <p>Working Group Preferred Vertical Slip Rate  0.05-0.2-0.4 mm/yr</p>
Eastern Bear Lake fault southern section	23	27	<p>McCalpin (2003) divided the EBLF into northern, central, and southern sections. He excavated two trenches on the southern section and determined the following composite earthquake timing:</p>	<p>McCalpin (2003) determined a long-term mean recurrence (5 interevent intervals) of 7.6 kyr. However, individual interevent intervals are highly variable, ranging from <math>\sim 2.9</math> kyr between earthquakes Y and Z to <math>\geq 10.2</math> kyr</p>	<p>McCalpin (2003) reports <math>\geq 22.1</math> m of net vertical displacement over the past 5 interevent intervals, producing an average vertical slip rate of <math>\geq 0.58</math> mm/yr. However, this slip rate may be affected by undetected antithetic faulting beneath</p>

			<p>Z &lt;2.1±0.2 ka, but &gt;0.6±0.08 ka  Y &gt;5.0±0.5 ka, but likely not much greater  X &lt;31±6 ka, but much &gt;15.2±0.8 ka  W &gt;31±6 ka, but &lt;39±3 ka  V &gt;31±6 ka, but &lt;39±3 ka  U &gt;39±3 ka, but likely not much greater</p> <p>The southern section is the only section for which paleoseismic trenching data are available.</p>	<p>between earthquakes X and Y.</p> <p>The confidence limits assigned to the Working Group's recurrence-interval estimate are intentionally broad to reflect uncertainty due to possible large variations in interevent interval length through time:</p> <p>Working Group Preferred Recurrence Interval</p> <p>3-8-15 kyr</p>	<p>Bear Lake or by unmeasured tectonic back-tilting. Additionally, slip rates for individual interevent intervals are highly variable, reflecting both variability in the length of time between earthquakes and in the net vertical slip per earthquake.</p> <p>The confidence limits assigned to the Working Group's slip-rate estimate are intentionally broad to reflect uncertainty associated with possible large variations in slip through time:</p> <p>Working Group Preferred Vertical Slip Rate</p> <p>0.2-0.6-1.6 mm/yr</p>
Bear River fault zone	35	93	<p>West (1994) excavated seven trenches, logged an irrigation ditch exposure, and measured 11 scarp profiles on the BRFZ. Results indicate a minimum of two surface-faulting earthquakes on the BRFZ, although a third earthquake is possible on some scarps. West concluded that the BRFZ is a young (new) normal fault resulting from geologically recent normal-slip reactivation on an underlying thrust fault</p> <p>Z 2370 ±1050 yr B.P.<sup>13</sup>  Y 4620±690 yr B.P.<sup>10</sup></p> <p>(These ages are on bulk organics and are calendar calibrated, but are not corrected for carbon mean residence time)</p>	<p>The Y-Z interevent interval is 2250 (+690/-1050) yrs. Event Z timing is 2370±1050 yr B.P., indicating that the elapsed time since the MRE exceeds the Y-Z interevent interval.</p> <p>The Working Group recognizes the likelihood of a young age for the BRFZ, but notes the possibility of an alternative fault-behavior model for the BRFZ, one of an old fault that produces large, infrequent earthquakes or earthquake clusters. Therefore, the Working Group's recurrence-interval estimate reflects both possibilities, and is reported as a broad range rather than as a preferred value with ~2-sigma confidence limits.</p> <p>Working Group Preferred Recurrence Interval</p> <p>1-100 kyr<sup>9</sup></p>	<p>Vertical slip-rate estimates for the Y-Z interevent interval range from 0.5-2.3 mm/yr depending on the scarp investigated and assumptions made about surface-faulting recurrence.</p> <p>The Working Group's slip-rate estimate reflects the possibility of two potential fault-behavior models, and therefore, the assigned confidence limits are appropriately broad.</p> <p>Working Group Preferred Vertical Slip Rate</p> <p>0.05-1.5-2.5 mm/yr</p>



				<p>reflect uncertainty associated with possible large variations in recurrence through time.</p> <p>Working Group Preferred Recurrence Interval</p> <p>10-50-100 kyr</p>	<p>Working Group Preferred Vertical Slip Rate</p> <p>0.01-0.03-0.07 mm/yr</p>
Towanta Flat graben <sup>10</sup>	5	16	<p>Nine short fault scarps on Towanta Flat bound a narrow, 5-km-long graben. Martin and others (1985) excavated three trenches and found evidence for at least three surface-faulting earthquakes. Based on soil-profile development on colluvial wedges, the earthquakes occurred within the past 250-500 ka, with no earthquakes younger than 130-150 ka.</p> <p>Z, Y, X &gt;130 ka, &lt;250-500 ka</p>	<p>Martin and others (1985) report a mean recurrence for surface faulting between 250-500 ka and 130-150 ka of 25 to 90 kyr, with no surface faulting since 130-150 ka.</p> <p>Because the timing of individual surface-faulting earthquakes is unknown, confidence limits assigned to the Working Group's recurrence-interval estimate are intentionally broad to reflect uncertainty associated with possible large variations in recurrence through time.</p> <p>Working Group Preferred Recurrence Interval</p> <p>25-50-200 kyr</p>	<p>Martin and others (1985) estimated maximum slip rates across individual TFG scarps ranging from 0.02 to 0.04 mm/yr, and Piety and Vetter (1999) estimate the maximum slip rate for the TFG faults is <math>\leq 0.09</math> mm/yr.</p> <p>However, Nelson and Weisser (1985) found no net vertical displacement across the graben as a whole, and question the seismogenic capability of the TFG. In the absence of any net vertical displacement across the graben, the Working Group is unable to make a slip-rate estimate for the TFG.</p> <p><b>Insufficient data – no estimate possible</b></p>
Bald Mountain Fault	2	2	<p>MRE &gt;130 ka based on soil-profile development on an unfaulted colluvial wedge and associated basin-fill deposits. No scarps on unconsolidated deposits.</p>	<p><b>Insufficient data – no estimate possible.</b></p>	<p><b>Insufficient data – no estimate possible.</b></p>
Strawberry fault	32	43	<p>Quaternary deposits are not displaced along the main SF. Two trenches across a subsidiary fault (1 of 4) on an alluvial fan 1.3 km west of the main SF indicate 2 to 3 surface-faulting earthquakes in the past 15-30 kyr, with the youngest earthquake occurring in the early to mid-Holocene</p>	<p>Nelson and VanArsdale (1986) report a mean recurrence of 5 to 15 kyr based on two or three earthquakes since 15 to 30 ka.</p> <p>Because paleoseismic data are poorly constrained and limited to a subsidiary</p>	<p>Nelson and VanArsdale (1986) report a slip rate for the trenched scarp of 0.04-0.17 mm/yr based on 1 to 2 m of displacement per earthquake. However, they assume the displacement recorded by the alluvial scarps represents only part of the total slip during the earthquakes</p>

			(minimum 1.5 ka). Estimates of earthquake timing are based on soil-profile development and older earthquakes are only constrained as >MRE and <15-30 ka.	<p>fault, the confidence limits assigned to the Working Group's recurrence-interval estimate are intentionally broad to reflect high uncertainty.</p> <p>Working Group Preferred Recurrence Interval</p> <p>5-15-25 kyr</p>	<p>that formed them.</p> <p>Because paleoseismic data are not well constrained and limited to a subsidiary fault, the confidence limits assigned to the Working Group's slip-rate estimate are intentionally broad to reflect the possibility of unrecognized slip on the main trace of the SF.</p> <p>Working Group Preferred Vertical Slip Rate</p> <p>0.03-0.1-0.3 mm/yr</p>
Hansel Valley fault	13	22	<p>Utah's only historical surface-faulting earthquake – 1934 M<sub>L</sub> 6.6 Hansel Valley earthquake occurred on this fault.</p> <p>McCalpin and others (1992) logged a gully exposure and interpreted surface faulting based on pluvial lake cycles. They argue for multiple earthquakes between 140 and 72 ka, no earthquakes between 72 and 58 ka, at least one earthquake between 58 and 26 ka, an earthquake around 15 to 14 ka, and possibly an earthquake at 13 ka. The actual timing and displacement of individual earthquakes is unknown.</p>	<p>McCalpin and others (1992) report wide variation in interevent intervals on the HVF. Time between earthquakes ranges from <math>\geq 32</math> kyr to possibly as little as 1-2 kyr, although the data supporting such a short recurrence interval are equivocal. Based on the limited information available, the confidence limits assigned to the Working Group's recurrence-interval estimate are intentionally broad to reflect uncertainty associated with possible large variations in recurrence through time.</p> <p>Working Group Preferred Recurrence Interval</p> <p>15-25-50 kyr</p>	<p>McCalpin (verbal communication to Working Group, 2003) re-evaluated his paleoseismic data for the HVF based on an estimated 1 to 4 m of displacement since ~17 ka. The Working Group adopts McCalpin's late Pleistocene/Holocene slip rate as their preferred slip-rate estimate for the HVF:</p> <p>Working Group Preferred Vertical Slip Rate</p> <p>0.06-0.1-0.2 mm/yr</p>
Hogsback fault southern section	39	103	West (1994) excavated a trench across a 2.5-m-high, uphill-facing scarp on the southern section of the HF in Utah. The trench did not expose evidence of faulting and no datable material was recovered.	<b>Insufficient data – no estimate possible.</b>	<b>Insufficient data – no estimate possible.</b>
North Promontory fault	26	27	No trench data are available. McCalpin	McCalpin and others (1992) proposed a	McCalpin (verbal communication to

			<p>and others (1992) believe that two large scarps along the main NPF represent multiple surface-faulting earthquakes, but evidence of recurrent movement is lacking. They believe faulting is latest Pleistocene or early Holocene (?) based on estimated ages of the displaced deposits and slope-angle versus scarp-height relations.</p> <p>A subsidiary fault in a road cut near the north end of the main fault shows evidence for a single, young (&lt;15 ka) surface-faulting earthquake in the past ~100 kyr. This fault's relation to the main NPF is unknown.</p>	<p>variety of possible mean recurrence values for the NPF based on assumed numbers of earthquakes and average displacements. However, both the number and timing of individual surface-faulting earthquakes remain unknown, and the Working Group is unable to make a meaningful recurrence-interval estimate for the NPF.</p> <p><b>Insufficient data – no estimate possible.</b></p>	<p>Working Group, 2003) re-evaluated his paleoseismic data for the NPF based on an estimated 8 m of displacement since ~17 ka. The Working Group adopts McCalpin's late Pleistocene/Holocene slip rate as their preferred slip-rate estimate for the NPF:</p> <p>Working Group Preferred Vertical Slip Rate</p> <p>0.1-0.2-0.5 mm/yr</p>
Sugarville area faults	4	13	<p>Eight trenches exposed liquefaction features and faults, but no evidence of individual surface-faulting earthquakes.</p> <p>Broad correlations with Lake Bonneville stratigraphy established fault timing. A short fault trace and <math>\geq 3.8</math> m of cumulative slip on one fault trace caused Dames and Moore (1978) to conclude that the displacement represents multiple small earthquakes.</p>	<p><b>Insufficient data – no estimate possible.</b></p>	<p><b>Insufficient data – no estimate possible.</b></p>
Washington fault zone northern section	36	43	<p>Individual earthquakes could not be identified; trenches excavated by Earth Sciences Associates (1982) documented displacement only.</p>	<p><b>Insufficient data – no estimate possible.</b></p>	<p><b>Insufficient data – no estimate possible.</b></p>
Fish Springs fault	30	20	<p>Single-event fault scarp</p> <p>Z ~2ka (maximum limiting age <math>2280 \pm 70^{14}\text{C yr B.P.}</math>)</p>	<p><b>Insufficient data – no estimate possible.</b></p>	<p><b>Insufficient data – no estimate possible.</b></p>

<sup>1</sup>"Section" refers to a portion of a fault defined on the basis of static geologic criteria (geomorphic or structural), but for which no evidence presently exists to show that its history of surface faulting is different from other adjacent parts of the fault. "Segment" refers to a portion of a fault, typically also defined on the basis of geomorphic or structural criteria, but for

which historical surface ruptures or paleoseismic data show that the history of surface faulting is different from other adjacent portions of the fault, and therefore that the seismogenic behavior of the segment is independent from that of the remainder of the fault.

<sup>2</sup> Straight line and surface trace lengths as determined from best available geologic mapping, surface trace length may or may not reflect total rupture length during the most recent surface-faulting earthquake.

<sup>3</sup> Earthquake timing for the WFZ rounded to the nearest 50 years; timing for remaining faults reported as published in paleoseismic source documents.

<sup>4</sup> Working Group consensus preferred recurrence-interval estimate (**bold**) and approximate 2-sigma confidence limits; see Consensus Process section in report text for a discussion of the methodology used to determine these values.

<sup>5</sup> Working Group consensus preferred vertical slip-rate estimate (**bold**) and approximate 2-sigma confidence limits; see section on Consensus Process in report text for a discussion of the process used to determine these values.

<sup>6</sup> Weighted mean rounded to the nearest 100 years.

<sup>7</sup> Two-sigma confidence limits rounded to the nearest 100 years.

<sup>8</sup> Earthquake timing reported in calendar corrected years (cal yr B.P.) where the data from the original study permit, and as kilo-annum ( $10^3$  years before present [ka]) where the available data do not permit calendar calibration; note that for both cal yr B.P. and ka, "present" refers to A.D. 1950 (North American Commission on Stratigraphic Nomenclature, 1983).

<sup>9</sup> Due to limited data, reported as a range rather than as a central value with approximate 2-sigma confidence limits.

<sup>10</sup> Seismogenic origin uncertain

<sup>11</sup> Length of WCFZ in Utah only; the CF extends northward into Idaho for several additional km.

<sup>12</sup> Information for the GSLFZ is derived from high-resolution geophysics and drilling information; there are no trench data.

<sup>13</sup> Calendar calibrated but no mean residence correction applied.

# ***ESTIMATING PREHISTORIC EARTHQUAKE MAGNITUDE FROM POINT MEASUREMENTS OF SURFACE RUPTURE***

Mark A. Hemphill-Haley\* and Ray J. Weldon, II

Department of Geological Sciences  
University of Oregon  
Eugene, OR 97403-1272

\*now at:  
Department of Geology  
Humboldt State University  
Arcata, CA 95521  
markhh@humboldt.edu

*This paper was previously published by the Seismological Society of America (BSSA, vol. 89, no 5, pp. 1264-1279, 1999)*

## **ABSTRACT**

We have developed a method for estimating the magnitude of prehistoric earthquakes using displacement data that usually can be collected from paleoseismic investigations. This method is necessary because essentially all current magnitude estimates for prehistoric events rely upon determining the total length of coseismic surface rupture, which is rarely measurable, or rely on segmentation scenarios, for which uncertainties cannot be quantified. While, surface-rupture length is a better predictor of magnitude than displacement for historic earthquakes, paleoseismic investigations are better at providing measurements of the amount of displacement at a site along a fault. Our method incorporates the variability in displacement observed in 14 modern surface faulting earthquakes, which allows a formal uncertainty in magnitude to be assigned to prehistoric ruptures. We show how multiple measurements along a preserved fraction of a rupture can be combined to reduce the uncertainty in the estimate of magnitude. Our analysis shows that uncertainty asymptotically approaches the natural variability of ruptures, so 5 to 10 displacement measurements are sufficient to characterize paleomagnitude. We conclude that sampling of scarps with lengths of even 10% of the original rupture can provide magnitude values that reasonably estimate the earthquake. Tests of the method, using randomly sampled data from the 1992  $M_w$  7.3 Landers and 1954  $M_s$  6.8 Dixie Valley earthquakes, provide close approximations of the actual magnitudes.

## **INTRODUCTION**

Most estimates of the magnitude of prehistoric earthquakes rely upon a measure of the length of the coseismic surface rupture (Wells and Coppersmith, 1994). This is because 1) most data for historic ruptures includes rupture length that can be compared and compiled to estimate magnitude (Schwartz and others, 1984); 2)

magnitude estimates are most reliably correlated to fault length in historic data sets (Wells and Coppersmith, 1994); 3) measurements of fault length are easily acquired using available geologic maps, seismicity plots or air photos; and 4) segmentation schemes can be used to break large

faults into rupture segments (e.g. Schwartz and Coppersmith, 1984).

However, rupture length is not a reliable parameter for estimating magnitudes of prehistoric earthquakes because: 1) rupture length estimates are based upon identification of often times subtle, fragile geomorphic features which are easily eroded or buried, especially along long-recurrence faults; 2) recent earthquakes have demonstrated that surface ruptures can integrate faults that were previously not known to be related (e.g. 1992 Landers Mw 7.3, Sieh and others, 1993); 3) studies have demonstrated the difficulties in assessing single event rupture segments on even the most active, mature faults with relatively short recurrence (Schwartz and Coppersmith, 1984, Machette and others, 1990, Machette and others, 1991, Fumal and others, 1993); and 4) segmentation schemes generally are not quantifiable in the sense that one can assign an uncertainty to the choice of a segment boundary. Often this latter factor is handled with "decision trees", where scenarios are weighted (e.g. Coppersmith and Youngs, 1986, Woodward-Clyde Consultants and others, 1992, Wong and others, 1993, Geomatrix Consultants, 1995), but this approach cannot result in true uncertainties because only a few possibilities are considered and weights are assessed by experience that is often shared by the experts who weight the scenarios.

Coseismic surface displacement is a better parameter for estimating prehistoric earthquake magnitude than surface rupture length because paleoseismic techniques are better at measuring amount of displacement at a site than assessing the extent of surface rupture. Also, commonly only a portion(s) of the scarp is preserved. Areas of the scarp where either displacement is low, erosion or deposition rates are high, or the fault is obscured in bedrock or in poorly consolidated deposits, such as playas, are susceptible to being discounted or missed during mapping. However, a fortuitously preserved rupture fragment retains measurable data on the displacement at one or more points.

To determine paleomagnitude one must relate two data sets: Measurements of

paleoearthquake slip and slip associated with modern events of known earthquake magnitude. Clearly, a single, fortuitously preserved portion of a scarp may not be representative of the entire rupture, so one must define uncertainty that formally includes the likelihood that a preserved portion reflects the mean displacement of the entire rupture. Our approach is to calculate a mean displacement for the entire surface rupture with formal uncertainties from preserved displacements. From these parameters we can estimate the magnitude of the paleoearthquake with an associated uncertainty by applying empirical relations between mean displacement and magnitude for modern earthquakes (e.g. Wells and Coppersmith, 1994).

To accomplish this we first evaluate displacement distributions for several historic earthquakes of known magnitude. Since the sample variability affects one's ability to estimate the displacement mean we must determine whether variability about the mean is independent of earthquake size. If, indeed, variability is independent of the magnitude then we can combine the displacement data for events of different magnitudes and, more importantly, draw inferences of magnitude from displacement data from paleoearthquakes of initially unknown magnitude. Also, we must understand how the number of samples collected and the fraction of the surface rupture sampled affect the mean displacement and uncertainties. So we develop an analytically derived model based on the combined earthquake data set using simple sample statistics that consider those two parameters. We then apply a Monte Carlo sampling algorithm across the data set to develop large-iteration, empirically based statistics that include uncertainty.

An underlying assumption of this method is that the distribution of measured displacements is similar between paleoevents and historic events. It is very likely that there are differences due to natural erosion and burial, and how a geologist samples historic versus prehistoric displacements. Also, we do not distinguish between different earthquake styles, which probably produces

slightly different displacement curves (e.g. Wells and Coppersmith, 1994). However, it is beyond the scope of this paper to address these second-order effects. Here we simply assume that a random sample of displacements from any prehistoric rupture is equivalent to one from a historic rupture.

## **HISTORIC EARTHQUAKE DATA AND DISPLACEMENT OBSERVATIONS**

For this initial evaluation of the technique we compiled displacement data for 14 historic earthquakes (Figure 1): 1857 ( $\sim M_w$  7.8) Fort Tejon, California along the southern San Andreas Fault (Sieh, 1978); 1931 ( $M$  8) Fu-yun, Mongolia (Baljinyam and others, 1993); 1939 ( $M$  7.9 – 8) Erzincan, Turkey (Barka, 1996); 1942 ( $M$  7.1) Niksar-Erbaa, Turkey (Barka, 1996); 1943 ( $M$  7.6) Tosya, Turkey (Barka, 1996); 1944 ( $M$  7.3) Bolu-Gerde, Turkey (Barka, 1996); 1952 ( $M_L$  7.2) Kern County, California (Stein and Thatcher, 1981), 1954 ( $M_s$  7.2) Fairview Peak, Nevada (Caskey and others, 1996); 1959 ( $M$  7.3) Hebgen Lake, Montana (Barrientos and others, 1987); 1968 ( $M_w$  6.6) Borrego Mountain, California (Clark, 1972, Wells and Coppersmith, 1994); 1983 ( $M_w$  6.9) Borah Peak, Idaho (Crone and others, 1985); 1987 ( $M_s$  6.6) Edgecumbe, New Zealand (Yeats and others, 1997); 1987 ( $M_w$  6.6) Superstition Hills, California (Rymer, 1989); and 1992 ( $M_w$  7.3) Landers, California (Sieh and others, 1993). We chose these data because they were the result of detailed, along-strike mapping that incorporated the entire range of surface displacements. They are not meant to be representative of all ruptures or styles, but a convenient data set to evaluate the

technique. We used published displacement data and, where tabular data were not available, digitized published displacement curves taking sample points at inflections.

The measured surface rupture lengths for the earthquakes ranged from about 14 km for Edgecumbe to almost 350 km for the Fort Tejon and Erzincan events. The mean displacements ranged from 0.15 m (Borrego Mountain, maximum displacement less than 1 m) to up to 4.9 m (Fort Tejon, reported maximum displacement of about 9 m) (Figure 1). We normalized the displacements for each event to its mean displacement in order to compare the variability of rupture among the 14 events and normalized by length to get the percentage of rupture length. These normalized ruptures have similarities: 1) a tail at each end, 2) several humps separated by low offset, 3) commonly, a larger hump close to the early part of the rupture, 4) maximum values that are about two times the mean, and 5) few values that are less than half the mean.

The combined normalized displacements for the 14 events as a function of percent rupture length shows that despite their magnitude range, there is a similar amount of variability in displacement for each of these events (Figure 2a). Since in most instances, the propagation direction for paleoearthquakes is not known, we have “folded” the displacement distribution in half so that the propagation direction does not affect the analysis (Figure 2b). The shape of the rupture can be characterized using the running mean of the combined distribution. In general, for the combined distribution, about 20% of the displacement rapidly ramps up, about 45% that shows a

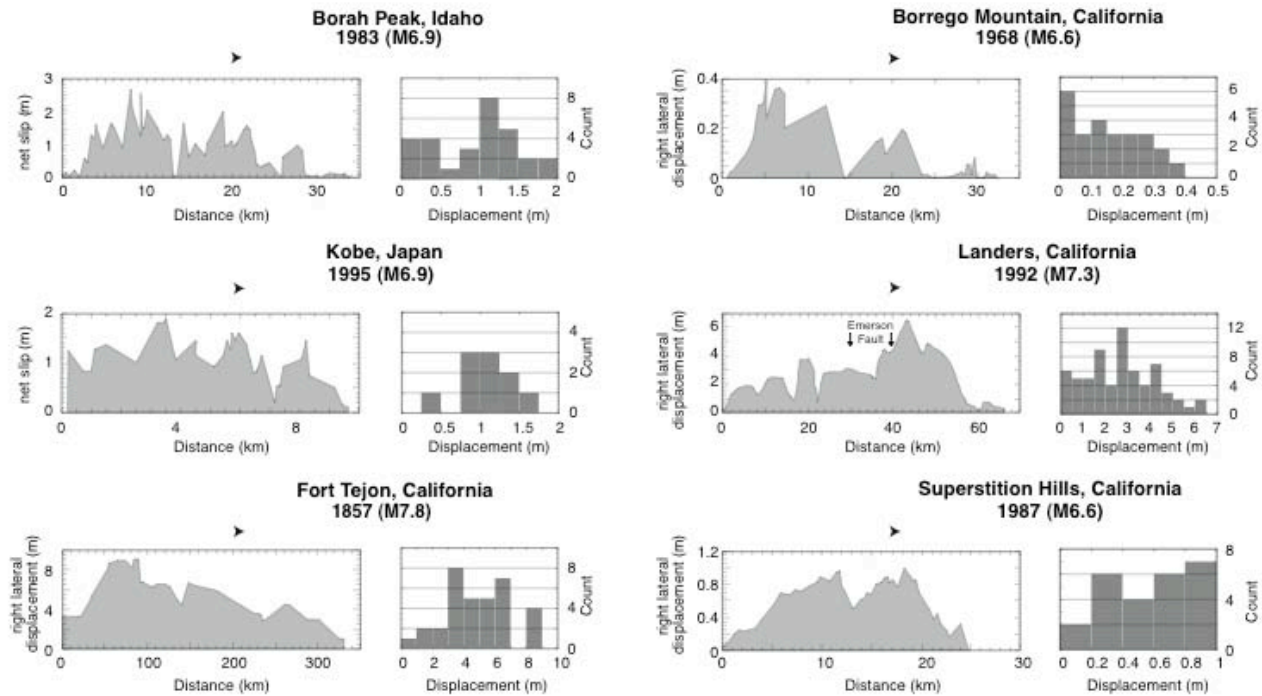


Figure 1 – Displacement distributions for six historic earthquakes (out of a total of 14 used in the analysis). For each earthquake the left figure depicts the measured displacement as a function of distance along the fault, the right is a displacement histogram. Rupture direction is indicated by arrow above the diagram.

relatively high slip plateau, and finally about 35% where the displacement gradually ramps down. Fractions near the ends provide displacement considerably below the data set mean while displacements along the approximately 50% central part of the fault will provide measurements above the data set mean. A histogram of the combined data (Figure 2c) shows that the displacements are distributed from 0 to 2 times the mean displacement with a tail at the larger displacements.

To better illustrate that displacement variability is independent of earthquake magnitude we constructed a probability plot of individual displacements (various line types) and for the normalized cumulative displacements (bold solid line) (Figure 3). There are no strongly disparate trends along any of the individual or the cumulative curves that would indicate that displacement variability is being affected by earthquake magnitude. Also, the nearly linear

shapes of the curves are an indication that the displacement data are approximately normally distributed.

## ANALYSIS OF DATA

To better understand the influence that the number of samples and the fraction of rupture sampled has on the estimate of the mean and its uncertainty, we construct both analytical and empirical sampling models. We first construct an analytical model assuming that the variability is normally distributed. We also construct and analyze synthetic ruptures with simple geometric displacement distributions to assess whether holes and peaks in displacement as well as the tapers at the rupture ends significantly influence the estimated mean. Finally, we develop empirical estimates of the mean and uncertainties about the mean by iterative sampling over the 14 event displacement data set.

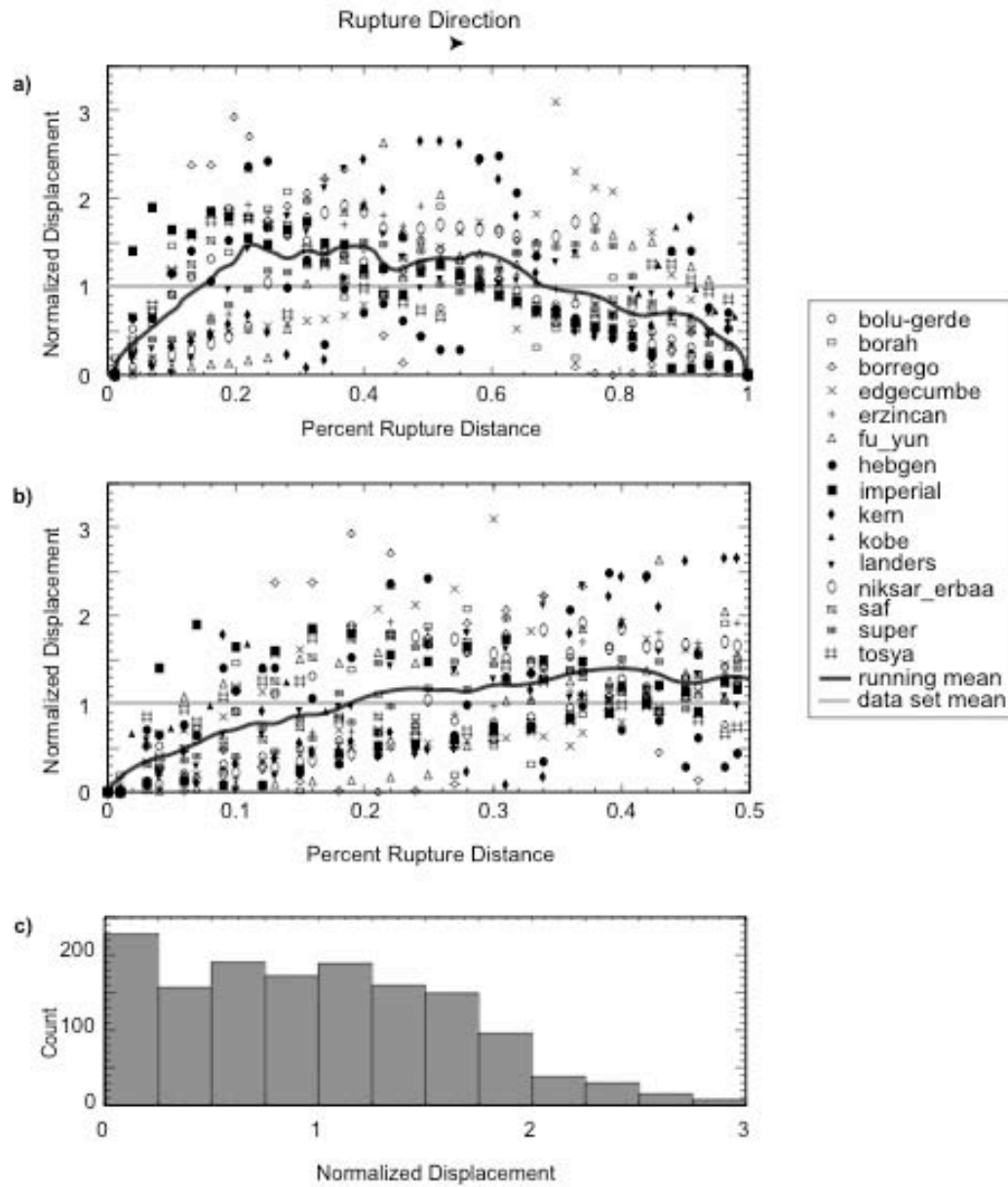


Figure 2 – Combined displacements from 14 historic surface-rupture earthquakes. A) Scatter plot of normalized displacements along percent rupture length. Rupture propagation direction is from left to right. Solid dark line depicts the running mean for the combined displacements. Solid light line depicts the normalized mean for the entire dataset. B) Scatter plot of normalized displacements along a “folded” percent rupture length. This is used when propagation direction is not known. C) Histogram of normalized displacements for the 14 event dataset.

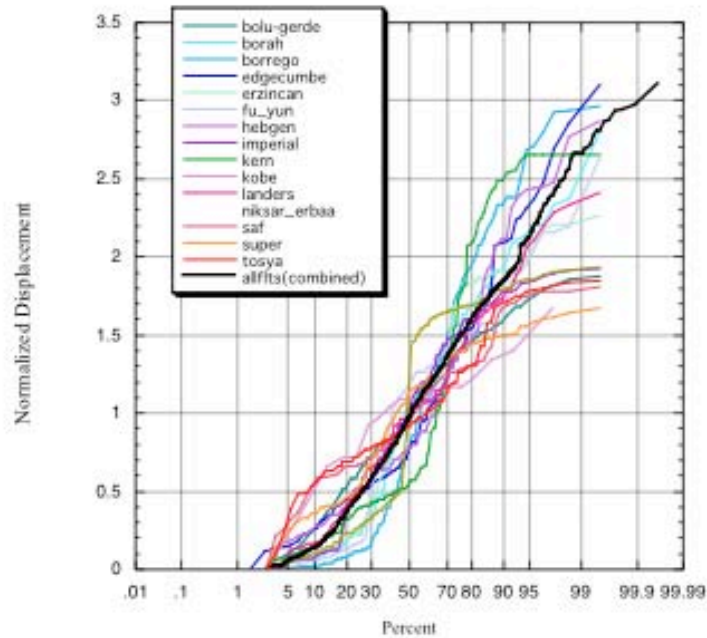


Figure 3 - Individual and cumulative probability plots for normalized displacement. The mean normalized displacement is 1. The cumulative curve (bold) is constructed using the combined displacements from the 14 rupture events. A more linear line indicates a more normal distribution.

The analytical model incorporates the effect of sample size and amount of rupture sampled on the estimate of mean displacement and uncertainty about that mean (Figure 4). We use:

$$\bar{x} \pm z^* \frac{s}{\sqrt{n}}$$

where  $\bar{x}$  is the sample mean,  $z^*$ , (the upper  $(1-C)/2$  critical value for the standard normal distribution) for a 95% confidence interval is 1.960, where  $C$  is the probability between the point  $z^*$  standard deviations below and above the mean,  $s$  is the sample standard deviation, and  $n$  is the sample number (Moore and McCabe, 1993 p.434-435).

The analytical model shows that uncertainties decrease with increases in sample size and amount of fault sampled. Figure 4 shows large uncertainties when sample size is less than 3

samples. The uncertainties decrease rapidly with a relatively small increase in sample size up to about 5 samples. The rate at which uncertainty decreases diminishes rapidly between 5 and 10 samples, so the ideal sample number is between 5 and 10. The four pairs of curves in Figure 4 depict varying amounts of the surface rupture sampled. The central, bold pair of curves representing the uncertainty when up to 100% of the surface rupture is sampled has the smallest uncertainty because the entire data set is sampled and includes the highest and lowest displacements. In contrast, the largest uncertainties occur when only small fractions of the rupture are sampled because the entire range of displacement likely will not be included. However, even in the case where only 10% rupture preservation occurs, the number of samples necessary to reduce the uncertainty to 50% about the mean is less than 10.

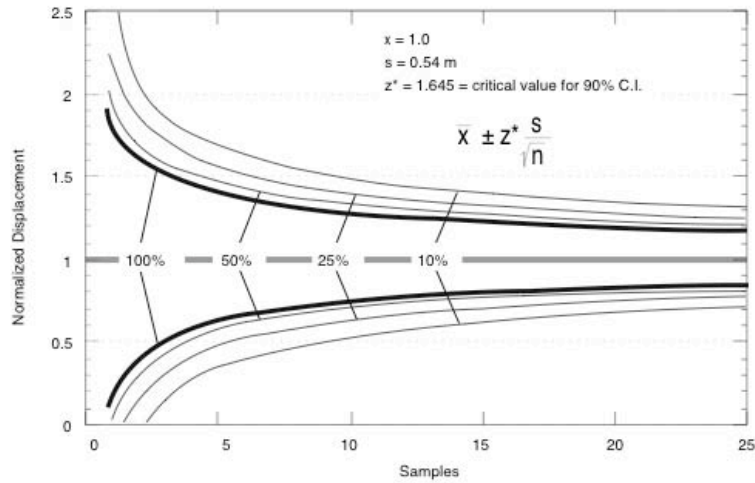


Figure 4 – Analytically derived curves depicting the 95% uncertainty about the normalized mean (bold horizontal line) for variations in two prominent sampling parameters, the number of samples collected and the amount of surface rupture sampled. Four fractions of the total surface rupture have been sampled to generate the four pairs of curves. The bold, inner curve represents the uncertainty about the mean when 100% of the original surface rupture is sampled. We calculated uncertainties using simple sampling statistics (Moore and McCabe, 1993).

To determine if real data are consistent with our simple analytical model we constructed empirical curves derived from large iteration random sampling using a Monte Carlo sampling algorithm (Hemphill-Haley, 1999). As with the analytical model we consider the effect of the number of samples and the fraction of the rupture sampled on the estimated mean and associated uncertainties. The algorithm randomly chooses the location of the portion of the rupture to be sampled and then the location of the samples within that sampling window. We conducted 1,000 iterations for each sample size selected with the window being changed during each iteration. We then calculated the mean, sample mode and 95% confidence limits for the 1,000 iterations.

We constructed the algorithm so the first data point chosen fixes the lower limit of the sampling position of the window for that group of samples. Subsequent samples, within that group, are randomly selected relative to the first point within the window. The algorithm does not allow the sampling window to extend beyond the ends of the rupture. We chose this sampling technique, of randomly dropping a finite length window on a fault, because all paleoseismic data are collected

from relatively small portions of actual ruptures, and we want to account for this source of error.

Our sampling technique, of randomly placing a finite length sampling window on a finite length fault (without allowing the ends to “hang-off”), slightly oversamples the middle portion of the fault and undersamples the tails (Figure 5). This yields a sample mean that is larger than the actual mean, lower uncertainty for moderate lengths of rupture sampled, and the distribution is centered on the mean (Figure 6a). As the sampled segment approaches 100%, the sampled mean approaches the true mean and the uncertainty grows because random samples include the rupture tails. While the approach of the sample mean toward the true mean is intuitive, the growth of the uncertainty may not be. One expects a more complete sample to have less uncertainty. However, in this case it doesn’t because a less complete sample lacks the variability of both of the tails and, thus, is a better estimator of mean displacement.

We have examined an alternative sampling method that allows the finite length sampling window to “hang-off” the ends of the surface

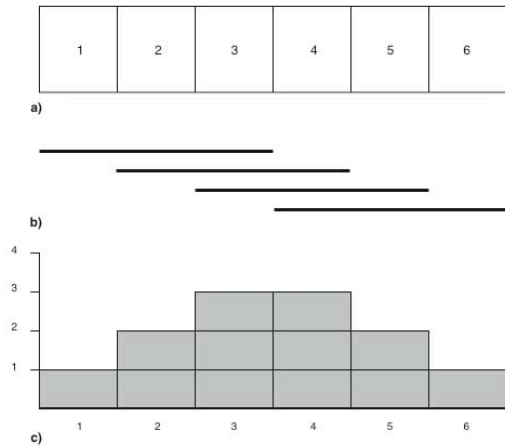


Figure 5 - An example of how the sampling algorithm tends to sample the middle part of a surface rupture more than the tails. a) Cartoon of a surface rupture 6 units in length, b) The bold horizontal lines depict four sample runs using a window that is 50% the width of the surface rupture. Each run begins one unit to the right of the previous one. c) A histogram of the fault units selected by the algorithm. The central segments are more likely to be sampled.

rupture. We do this by “folding” the displacement distributions at each end of the original distribution so the sampling window is allowed to extend beyond the end of the rupture and thus can sample the tails. This method produces a very asymmetric distribution and forces the mean to shift toward the smaller displacements (Figure 6b). Any sampling process that accounts for a finite fraction of the rupture will undersample the tails unless segments that extend past the ends of the rupture are up-weighted.

We feel that an actual geologist does not randomly sample a rupture but tends to sample the central part with the larger displacements, so we keep this aspect of the sampling technique, recognizing its apparent bias. If one does not wish to account for the fraction of the rupture the sample is taken from then one may simply use the 100% segment-length algorithm; it uniformly samples the entire rupture.

The large number of random samples collected for each run allows us to assume that the

Central Limit Theorem applies to the displacement data, and that the sampling distributions are normally distributed. We are then able to apply statistics that describe the variability of displacements about the normalized mean.

### ANALYSIS OF THE SYNTHETIC DATA SETS

Because preserved remnants of prehistoric ruptures span only a fraction of the original rupture it is critical to understand how displacement samples drawn from variably sized rupture remnants from different parts of the rupture vary from samples drawn from the entire rupture. Inspection of the six examples shown on Figure 1 indicates that the two greatest sources of possible deviation of a fraction of the rupture from mean results are: 1) the fact that displacement decreases near the ends of the rupture and 2) there are large “spikes” and “holes” where the displacement essentially doubles or decreases by about half,

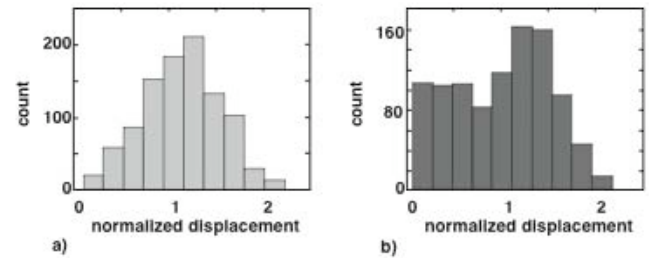


Figure 6 - Histograms representing the distribution of displacements acquired by using two sampling methods. a) Our preferred sampling method which prohibits a finite length sampling window from “hanging” beyond the rupture ends in order to more equally sample the lower displacement tails. This method results in a more normal distribution with the sampling mean centered about the normalized displacement mean. b) An alternative method which requires the displacement distribution to be “mirrored” at the end points and allows the sampling window to more evenly sample the ends. This results in a skewed distribution with the low displacement tails strongly influencing the sampling distribution.

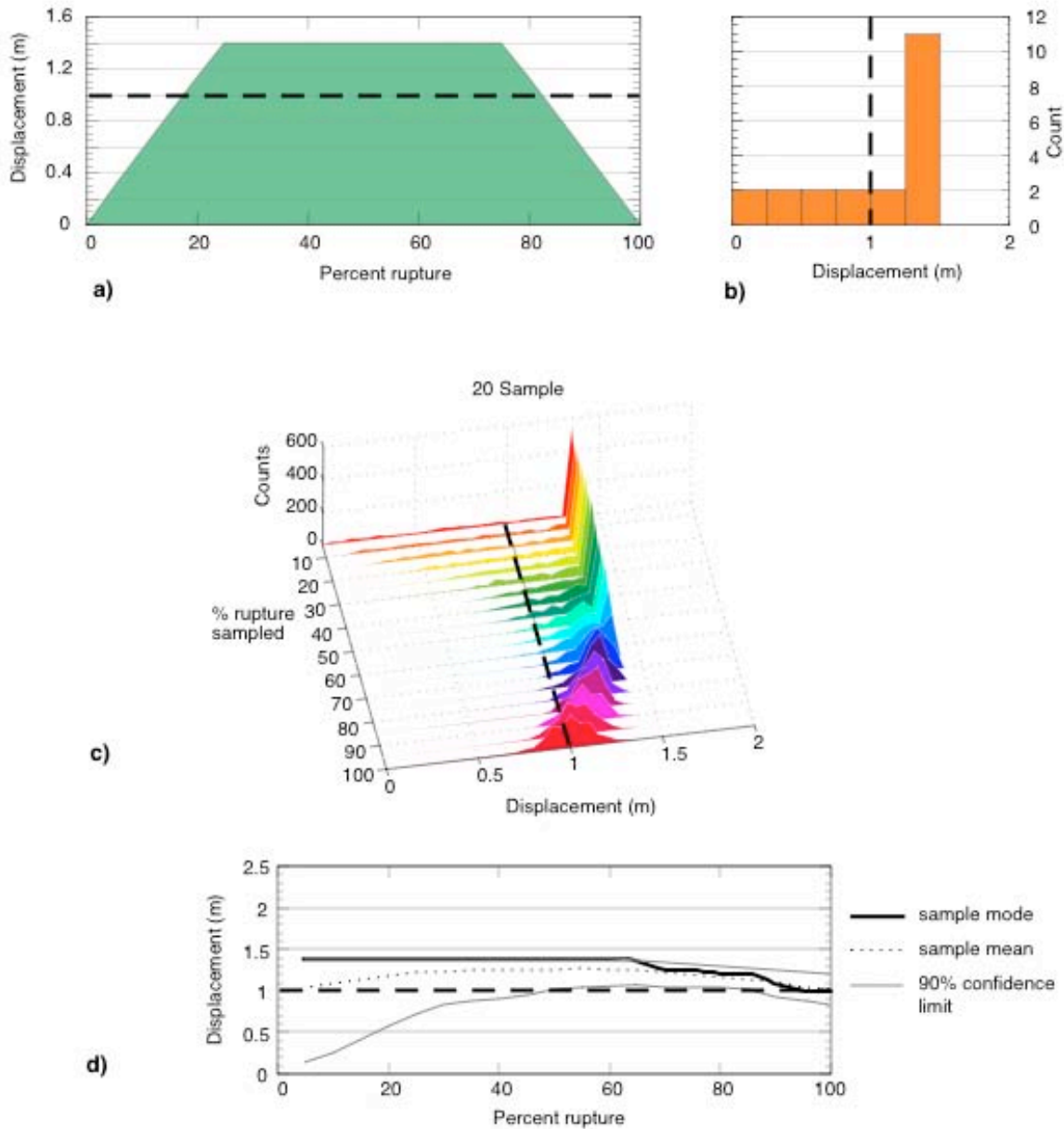


Figure 7 - Synthetic test 1. In each graph, the mean displacement for the actual rupture, 1 m, is shown as a bold, dashed line. a) Displacement distribution; b) Histogram of the sampled displacements; c) Probability density functions for 20 Monte Carlo runs (1000 iterations each) incremented by 5% increases in the amount of surface rupture sampled. This example shows the results when 20 samples are collected; d) Statistical results of the analyses when 20 samples collected.

respectively. To better understand and correct for these factors in the real data sets, we have created two simple synthetic ruptures to examine the impact of these attributes on the estimate of the mode, mean and variability taking into

consideration the number of samples collected and the fraction of rupture sampled

We constructed one synthetic rupture to assess the affect of the rupture taper near the ends (Figure 7). The rupture distribution has a plateau

that includes the maximum displacement and mode (Figures 7a and 7b). The sampling distributions for the incremented runs can be easily compared from the results of the Monte Carlo runs (Figure 7c). When a small fraction of the rupture is sampled, the plateau is most often represented, but the tails of the rupture are also sampled. The tails begin to affect the distribution again when the fraction of the rupture becomes so large that the full range of the displacements is likely to be included in each sample run. As the sampling fraction approaches the width of the entire rupture, the sampling distribution takes on a more normally distributed form.

The character of the sample mode, sample mean, and variability as a function of the amount of rupture sampled can be seen in Figure 7d. It is important to note that the sample “mode” is the most common mean result in the 1,000 runs, while the sample “mean” is the mean of 1,000 means produced by the sampling. For a small fraction of the rupture sampled (less than 20%), the sampling mode overestimates the population mean by 40% while the sampling mean overestimates the population mean by less than 20%. At the same time the uncertainties are asymmetric and large (about +40% and -90%). When the rupture fraction is 25% to 60%, the sample mode continues to oversample by 40% while the sample mean overestimates the true mean by about 20%. The upper 95% confidence limit remains at 40% greater than the true mean while the lower limit decreases dramatically. When 60% to 100% of the rupture is sampled, the sample mode, sample mean and the uncertainties converge toward the true mean of 1 m. When the entire fault can be sampled, the sample mode and sample mean are the same as the true mean, and the 95% confidence limits are  $\pm 20\%$  of the true mean.

The differences between the sample and actual statistics are due to the interaction of the fraction of rupture and the shape of the displacement. When the fraction of the fault

sampled is very small, the sample mean of many iterations approximates the actual mean because the tapered tails are sampled (Figure 7c). However, for this example, the displacement distribution is constructed so that the tails represent a small fraction of the rupture, while the maximum displacement is the most common measurement (Figure 7b) resulting in a sample mode that approximates the maximum displacement. As the size of the rupture fraction increases the tails are a smaller fraction of possible ruptures and the sample mode and mean are greater than the true mean. The uncertainties are dictated by the available range of displacements. In this synthetic case, the upper limit remains at about 1.4 m because of the 1.4 m plateau in displacement that has no variability. When the fraction sampled is greater than 60%, then some part of the tails are necessarily incorporated into the sampling statistics.

This analysis also shows why we choose the sample mode as the most reliable sampling statistic. When using a single iteration of several measurements to sample a rupture, the sampled mean will not approximate the true mean except where large fractions of the rupture are available (Figure 7d). Conversely, even when small fractions are sampled only once, the most common displacement of the entire rupture is most likely to be sampled.

The second synthetic rupture (Figure 8) illustrates the affect of “holes” and “peaks” in the displacement distribution on the sampling statistics. The form of the rupture consists of a plateau of high displacement with an intervening absence in displacement for about 20% of the total rupture (Figure 8a). The distribution has a maximum displacement of 1.25 m and a mean of 1 m (Figure 8b). Figures 8c and 8d show the results of the Monte Carlo sampling runs. When small fractions of the rupture are analyzed (less than 20% of the total rupture length) the maximum

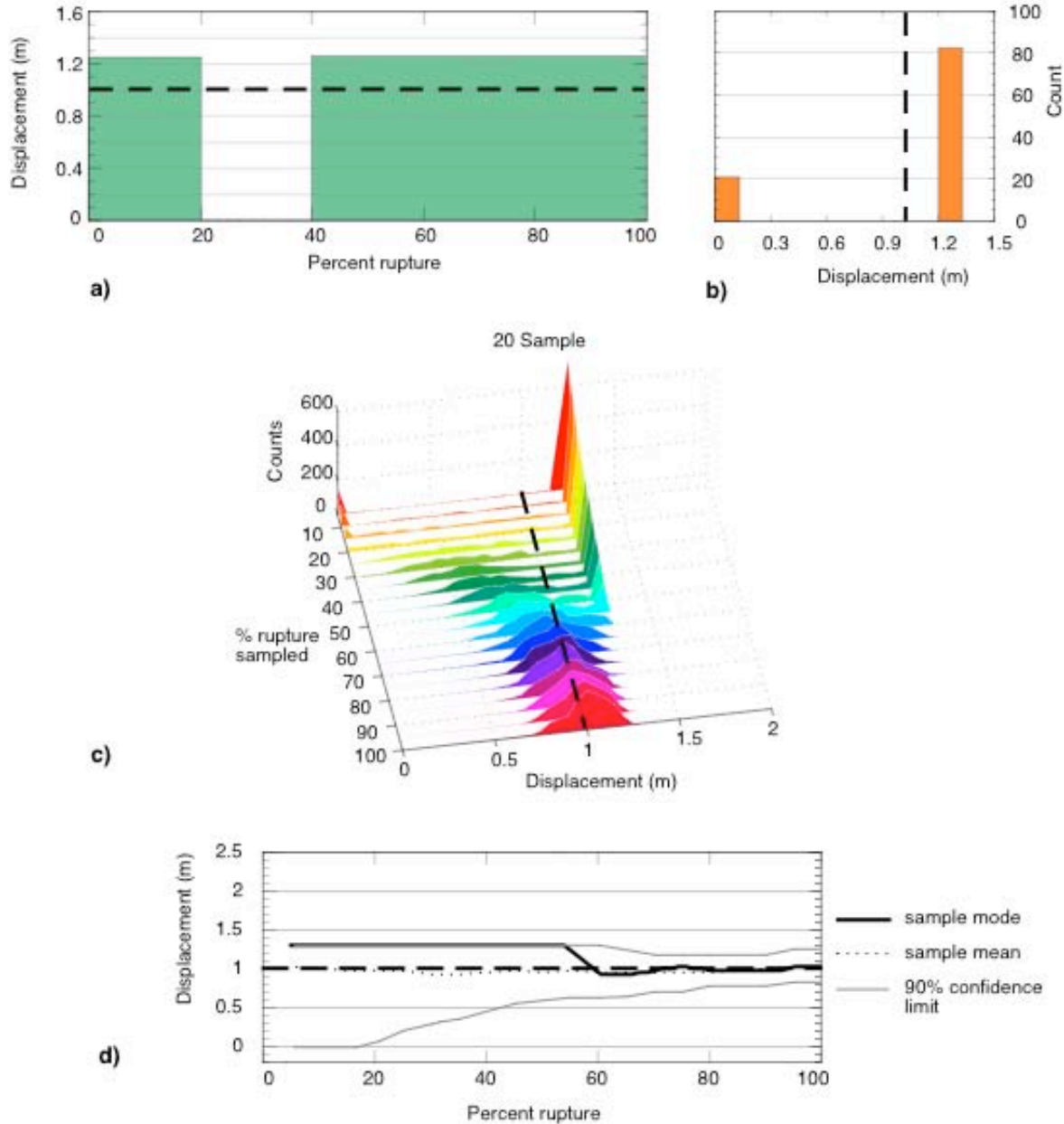


Figure 8 - Synthetic test 2. In each graph, the mean displacement for the actual rupture, 1m, is shown as a bold, dashed line. a) Displacement distribution; b) Histogram of the sampled displacements; c) Probability density functions for 20 Monte Carlo runs (1000 iterations each) incremented by 5% increases in the amount of surface rupture sampled. This example shows the results when 20 samples are collected; d) Statistical results of the analyses when 20 samples are collected.

displacement at 1.25 m is most often sampled (it is the most common displacement of the rupture). Also, some samples of the 0 m displacements are collected (Figure 8c). As larger fractions of the rupture are sampled the most likely displacement sampled is still the maximum displacement. As the

rupture fraction approaches 100% the distribution becomes more normal in form.

When very small portions of the rupture are sampled a large number of times, large, asymmetric

uncertainties occur (Figure 8d). When the rupture fraction is 5% of the total rupture the uncertainties span the entire displacement range from 1.25 to 0 m. The uncertainties about the true mean diminish rapidly until about 60% of the rupture is sampled. For this example, there is no contiguous portion of the rupture greater than 60% that does not include the full range of displacements. The effect of sample number on the sample statistics has not been included in this discussion; however, we conducted numerous runs across both synthetic distributions. The results were quite predictable with the uncertainties decreasing as the number of samples increase, similar to the effect shown in the analytically derived curves (Figure 4).

From the analysis of the synthetic displacements, we can see that several considerations must be made when analyzing a real earthquake data set: 1) a correction factor estimated from the sample mode, which accounts for the amount of rupture sampled will need to be applied to the sample mean to bring it to the population mean; and 2) uncertainties will have to incorporate three variables: a) the intrinsic variability of the rupture, b) the amount of rupture sampled, and c) the number of samples collected.

### **ANALYSIS OF THE HISTORIC EARTHQUAKE DATA SET**

Since the collection of displacement data from a prehistoric rupture can be viewed as a single iteration consisting of several samples from an underlying population like a modern rupture, the mean of those few samples is not comparable to the mean of the large iteration data set. It must be compared to the most likely small single-iteration run, which can be inferred by considering the sample mode of the large multi-iteration runs which serves as a proxy for mean. We have seen from the synthetic rupture analysis that the sample mode provides a consistent overestimate of the true mean for small numbers of samples and small

fractions of rupture sampled. As the number of samples and the size of the rupture fraction sampled increases, the mode more closely approximates the true mean. Thus, we calculated a combined sampling mode for the 14 historic events. The sample mode consistently overestimates the true mean by about 10% to 20% up to rupture fractions of about 75%, and then converges on the true mean.

We can also see that the location and magnitude of holes and peaks in a single displacement distribution affects the amount of uncertainty about the mean estimate. Since these variations in individual ruptures get smoothed in the global data set, we developed individual sampling curves for each historic event.

Two ruptures, from the 1968 (M6.6) Borrego Mountain and 1987 (M6.6) Superstition Hills earthquakes, shown in Figure 9, represent end member characteristics in displacement distribution. The Borrego Mountain rupture has a broad distribution of displacements about the mean (Figure 9a) with large holes and peaks in the displacement distribution (Figure 1). Conversely, displacements associated with the Superstition Hills rupture are more closely distributed about the mean value (Figure 9b), and the displacement distribution is relatively smooth with only a single dip in the rupture profile (Figure 1). The profile for the Superstition Hills rupture is quite similar to that of the first synthetic rupture (Figure 7). The irregular profile and preponderance of low displacements along the Borrego Mountain rupture cause the sample mode to vary about the true mean (Figure 9c). This behavior occurs when small fractions of the rupture are sampled. As the sampled rupture length approaches the true rupture length, the sample mode stabilizes and approaches the true mean. The sample mode for the Superstition Hills rupture almost always overestimates the true mean (Figure 9d) because there are virtually no holes in the displacement

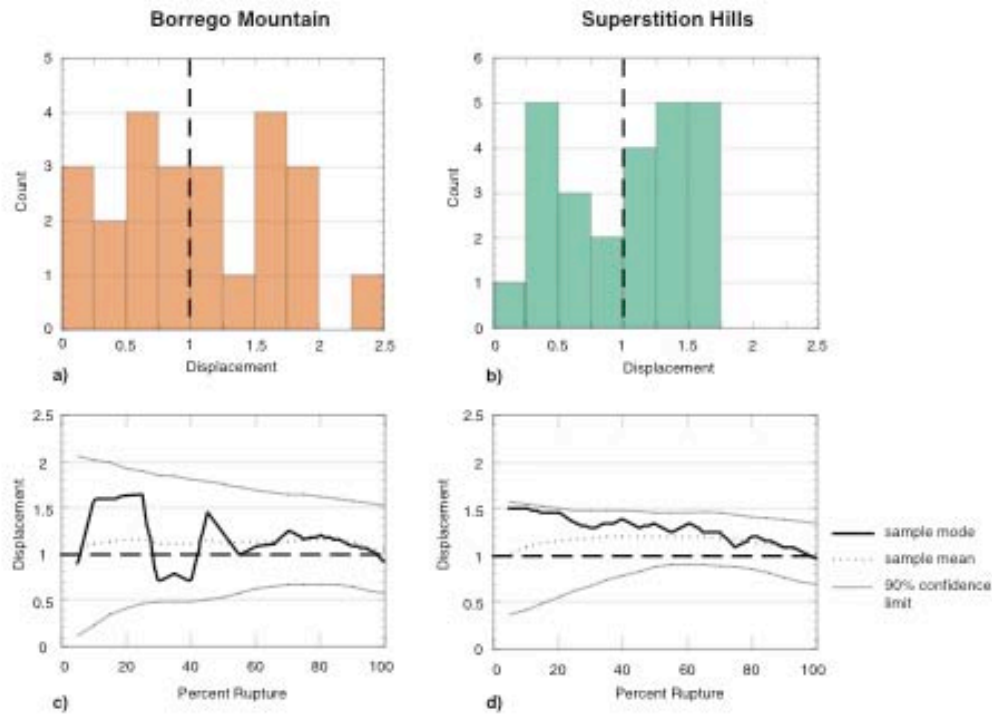


Figure 9 - Displacements for two example ruptures, Borrego Mountain and Superstition Hills (displacement profiles shown in Figure 1). Histograms of displacement distributions shown in a) and b). Results from Monte Carlo runs with incremented amounts of rupture analyzed are shown in c) and d).

Figure 9 - Displacements for two example ruptures, Borrego Mountain and Superstition Hills (displacement profiles shown in Figure 1). Histograms of displacement distributions shown in a) and b). Results from Monte Carlo runs with incremented amounts of rupture analyzed are shown in c) and d).

distribution and all low values are near the ends. The uncertainties about the means for both ruptures are dictated by the total range of displacements and the distribution of the displacements.

We calculated a composite mean uncertainty for the 14 historic ruptures to use for the global data set. The Monte Carlo sampling algorithm was modified so that an individual rupture is randomly sampled with each iteration. We avoided combining all of the displacements into a single file because the variability intrinsic to each rupture would tend to be smoothed. As with the synthetic tests, the spread of the distribution becomes narrower and more normally distributed as more of the rupture is sampled, because the true variability of the rupture can then be observed (Figure 10a). Consistent with results from the synthetic runs, the sampled mode and mean from

the combined data set overestimate the true mean by 10-15% for most fractions of the fault sampled (Figures 10b and c). This is due to the fact that we undersample the ends of the ruptures which have very small values. Zero and very small displacement portions of the rupture, although fractionally less important, contribute significantly to the actual mean. Once about 70% of the rupture is included in the evaluation the sample mean converges toward the actual rupture mean. The sample and rupture means are equal when 100% of the rupture is sampled.

So, when we have a small number of samples from actual field measurements that we compare with the global data set, model analyses show that the mean of those samples is likely to be 10-20% greater than the true mean. To derive a

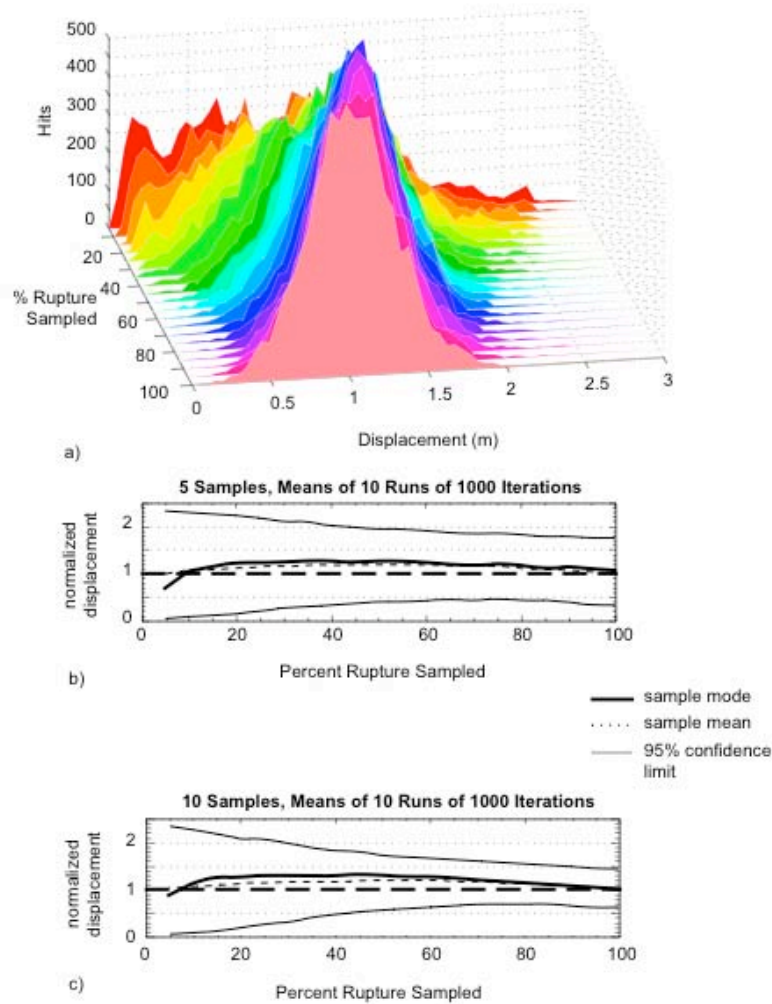


Figure 10 - Results from Monte Carlo runs using combined displacements of 14 historic ruptures (see Figure 1 for examples of individual rupture distributions). a) probability density functions for 20 Monte Carlo runs (1000 iterations each) incremented by 5% increases in the amount of surface rupture sampled. Five samples were randomly selected within each iteration. b) statistical results of 10 analyses when 5 samples collected. c) statistical results of 10 analyses when 10 samples collected.

magnitude for the event we correct for this overestimate. These values are then applied to empirical relation that describe earthquake magnitude as a function of mean displacement in order to calculate the magnitude and 95% confidence limits (Wells and Coppersmith (1994)):

$$M_w = 6.93 + 0.82 * \log (MD * CDS)$$

where MD is the mean displacement estimate and CDS is the combined displacement statistic (our correction factor).

### 1992 LANDERS AND 1954 DIXIE VALLEY EARTHQUAKES (EXAMPLES)

As a test of the point displacement method we estimated the magnitude of two historic earthquakes using their displacement data. We used the data from the 1992  $M_w$  7.3 Landers earthquake (Sieh and others, 1993) and the 1954  $M_s$  6.8 Dixie Valley earthquake (Caskey and others, 1996). We considered the Landers event because several faults, previously thought to rupture independently

(e.g. Wesnousky, 1986) were involved, and simply calculating magnitude from rupture length along each of these faults would not work. We chose the Dixie Valley earthquake because it is a well-documented event with essentially pure dip-slip displacement. The test involves varying both the amount of rupture available for sampling and the number of samples collected, and comparing our results with the known magnitudes. While the Landers displacement data are part of the combined data set used to develop the sampling statistics, the Dixie Valley data are not.

For both experiments we sample displacements from the entire surface rupture. Data points are assigned point numbers incremented from the beginning to the end of the rupture. We vary the number of samples (5 and 10) and also the amount of fault sampled. Based on the number of samples and the rupture fraction sampled (Table 1) the correction factor based on the global data set mode (used as a proxy for sample mean) is applied to the sample mean. These calculations result in an estimate of the mean displacement and 95% confidence limits about that mean for the entire rupture.

For the Landers earthquake rupture we also force the sampling routine to choose only within a small, fixed portion of the surface rupture. This test is analogous to evaluating one of the smaller, discontinuous faults prior to the 1992 Landers rupture. We selected the Emerson fault, of which a 5-km-long portion ruptured during the Landers event (Sieh and others, 1993, McGill and Rubin, 1994) (Figure 1, arrows show the location of the Emerson fault within the Landers rupture). The Emerson fault accounted for about 7% of the total rupture during the Landers event; the majority of the remaining rupture occurred along four other principal faults and intermontane cross-faults (Sowers and others, 1994). The Emerson Fault is located in a portion of coseismic surface faulting distribution containing

*Table 1*  
*Statistical parameters for use with varying sample analyses*

Number of Samples	Percent Fault Sampled	Upper Value (UVCDS)	Mode Value (MVCDS)	Lower Value (LVCDS)
<b>2</b>	10	0.08	0.99	2.35
	25	0.14	0.86	2.25
	50	0.29	0.74	2.17
	75	0.29	0.88	2.03
	100	0.12	1.07	1.94
<b>3</b>	10	0.09	0.89	2.31
	25	0.19	0.84	2.15
	50	0.4	0.74	1.98
	75	0.43	0.81	1.88
	100	0.27	0.96	1.77
<b>4</b>	10	0.09	0.99	2.32
	25	0.23	0.68	2.11
	50	0.45	0.67	1.92
	75	0.5	0.88	1.76
	100	0.36	1.05	1.69
<b>5</b>	10	0.09	0.97	2.31
	25	0.21	0.78	2.17
	50	0.42	0.74	1.95
	75	0.45	0.81	1.86
	100	0.3	0.97	1.73
<b>6</b>	10	0.1	0.94	2.23
	25	0.26	0.73	2.07
	50	0.51	0.73	1.83
	75	0.61	0.87	1.69
	100	0.47	1.03	1.54
<b>7</b>	10	0.1	0.93	2.23
	25	0.25	0.76	2.06
	50	0.54	0.71	1.81
	75	0.65	0.84	1.65
	100	0.5	0.99	1.5
<b>8</b>	10	0.1	0.88	2.23
	25	0.25	0.66	2.07
	50	0.55	0.65	1.78
	75	0.66	0.85	1.62
	100	0.52	1.03	1.46
<b>9</b>	10	0.1	0.89	2.25
	25	0.28	0.69	2.09
	50	0.55	0.69	1.76
	75	0.68	0.83	1.6
	100	0.56	1.01	1.43
<b>10</b>	10	0.1	0.85	2.26
	25	0.3	0.69	2.08
	50	0.56	0.71	1.75
	75	0.7	0.84	1.59
	100	0.59	1.02	1.42

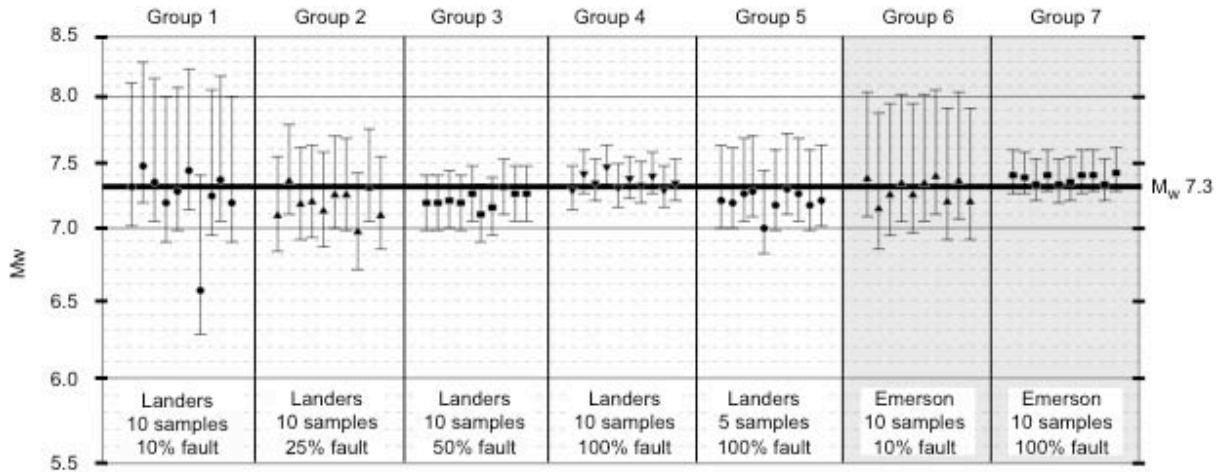


Figure 11 - Magnitude estimates for the  $M_w$  7.3 Landers earthquake (bold horizontal line). Each group represents 10 estimates derived individually from multiple samples chosen at random along a prescribed percentage of the fault. The last two groups represent estimates derived by evaluating only the Emerson fault which accounted for less than 10% of the total surface rupture for the Landers event. Error bars represent 95% confidence limits for the magnitude estimates.

some of the maximum displacements so it is also a test of whether the method overestimates the magnitude of the rupture.

Figure 11 presents seven groups of runs, representing variations in the sampling parameters, are presented. The first five analyses are of the entire Landers surface rupture while the last two groups are of the Emerson Fault portion of the rupture. The first four groups demonstrate the sensitivity of the method to the fraction of the surface rupture studied. There is greater variability of the magnitude value and associated error when the amount of the rupture sampled is small compared to the 100% evaluation. However, even when only 10% of the rupture was sampled the actual magnitude was captured within the 95% confidence limits every time. The uncertainties for such a small sampled portion of the rupture are relatively large with magnitude estimates for the entire group ranging from  $M_w$  6.3-8.3. The run that significantly underestimates the magnitude was located along a portion of the rupture with very small displacement.

As the amount of rupture sampled increases, the magnitude estimate converges on the true magnitude and the uncertainties decrease. When only five samples are collected (Group 5),

the correct magnitude is still estimated 100% of the time but with large uncertainties bounding the estimate.

The runs using only the Emerson Fault result in close estimates of the actual earthquake 100% of the time for both sampling window widths (Groups 6 and 7). This is probably because the displacement distribution that includes the Emerson Fault contains the true displacement mean for the entire Landers rupture. Obviously, if we had chosen instead to isolate the end points of the rupture for the analysis we would have underestimated the earthquake magnitude. However, it is unlikely that those parts of the scarp would be preserved significantly over thousands of years of interseismic weathering. Also, in practice, one would probably not conclude that displacements of up to 4.5 m were associated with only 5 km of rupture (as Group 7 would imply) so a smaller rupture fraction and associated larger uncertainties (such as Group 6) are most likely. The results also show that using displacement instead of rupture length is more appropriate in this instance. Without *a priori* knowledge of the true Landers rupture length a 5 km rupture length would have provided an estimate of  $M_w$  5.9, thus greatly underestimating the actual earthquake.

Results from the Dixie Valley earthquake are also promising (Figure 12). Calculation of the moment magnitude for the  $M_s$  6.8 Dixie Valley event provides an estimate of  $M_w$  6.9 based on geologic and seismologic data (Wells and Coppersmith, 1994, Caskey and others, 1996). Because our calculations result in an estimate of moment magnitude we compare them to the  $M_w$  6.9 value. Overall, the true magnitude is correctly estimated more than 97% of the time. The uncertainties about the mean estimate decrease with increased number of samples collected and amount of rupture evaluated.

### **DISCUSSION AND APPLICATION OF METHODOLOGY TO PALEOEARTHQUAKES**

Any investigator who intends to use this method should also consider several issues that may affect the results. For one, the uncertainties are based, in part, on an estimate of what fraction of the total surface rupture has been sampled. We can approximate this value simply based on the empirical relations between moment magnitude and mean and maximum displacement (Wells and Coppersmith, 1994). As in our example using the Emerson Fault portion of the Landers earthquake, it would be evident (even without *a priori* knowledge of the rupture distribution) that displacements on the order of 3 to 4 m would not be associated with a 5 km-long surface rupture. Instead, using the empirical relations of Wells and Coppersmith (1994) a surface rupture length of 70 to 80 km would be more likely and we would consider our samples to have been within a sampling segment of less than 10% of the total rupture (see Figure 12).

A potentially significant issue that we have not addressed in this analysis is whether degradation processes bias the intrinsic variability of the preserved rupture. Thus, do our estimates of the sampling mode, mean and associated uncertainties determined by comparison with modern ruptures need to be modified to take this into account? We are also interested in defining the types of features that might be preserved along a fault scarp that has various displacement magnitudes along its length. At first thought one might expect that the largest offsets will be preserved preferentially, however, since the largest offsets are relatively rare, preservation might favor the most common offsets (mode) as well. This will result in a slightly higher average offset than calculated from historic rupture. We speculate that the most common and relatively large offsets will be preserved the most, the largest offsets will be next because they are big, but uncommon, and small offsets will be the least preserved because they are small and uncommon.

For this analysis, we have attempted to eliminate bias from the sampling algorithms. However, geologic bias should serve to decrease the uncertainties when sampling a real fault scarp. A knowledgeable geologist is unlikely to sample portions of the scarp that have relatively small or even no displacements. Likewise, the rupture ends are less likely to be sampled while the middle portion of the rupture is more likely (i.e., geological sample means typically will overestimate the true mean but will have less variability). We do not present this method in an actual paleoseismic application because we have no way to verify the results.

This method can be easily applied to a paleoseismic study. A mean displacement could be calculated for some number of samples along a

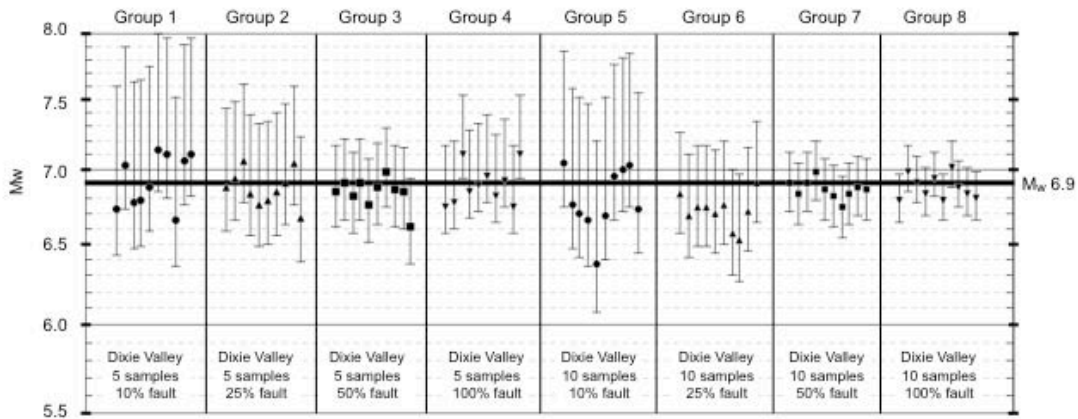


Figure 12 - Magnitude estimates for the Ms 6.8 (Mw 6.9) Dixie Valley earthquake (bold horizontal line). Each group represents 10 estimates derived individually from multiple samples chosen at random along a prescribed percentage of the fault. The first 4 groups used 5 randomly selected samples while the second 4 groups used 10 samples. Error bars represent 95% confidence limits for the magnitude estimates.

surface rupture (we would hesitate to use less than three to five measurements because of the extremely large uncertainties (Figure 4). The mean displacement (MD) is multiplied by the Mode Value Combined Displacement Statistic (MVCDS) from Table 1 that corresponds to both the number of samples collected and the estimated percent of the total rupture that was sampled. The estimate for percent of total rupture value can be approximated in instances where samples are collected from a portion of a discrete surface rupture or when comparison of displacement with apparent rupture length are in disagreement based on empirical relations (Wells and Coppersmith, 1994) as in the Emerson fault example above. From this calculation we derive the mean value of the magnitude estimate using the empirical relations of Wells and Coppersmith (1994) for mean displacement and  $M_w$ ;

$$M_w = 6.93 + 0.82 * \log (MD * MVCDS)$$

The 95% confidence limits about the mean estimate are calculated as follows. The maximum limit estimate is derived by dividing the MD by the Upper Value CDS (UVCDS) and multiplying the log of that value by the MVCDS:

$$M_w = 6.93 + 0.82 ( \log (MD / UVCDS) * MVCDS)$$

The lower limit estimate is calculated by dividing the MD by the Lower Value CDS (LVCDS) and multiplying the value by the MVCDS:

$$M_w = 6.93 + 0.82 ( \log (MD / LVCDS) * MVCDS)$$

We emphasize that measurements of displacement are required and not simply measurements of apparent displacement or scarp height. Although few samples are necessary to make an estimate, care should be taken to insure the quality of the data used.

## CONCLUSIONS

To date, the most widely used method for estimating magnitudes of paleoearthquakes has been to use the empirical relation between surface rupture length and moment magnitude. We propose that, for paleoearthquakes, a method that incorporates a few displacement samples, judiciously collected along a surface rupture, combined with globally-derived sampling statistics provided in this paper, is more suitable. This preliminary assessment of the method is promising

in that it provides a close approximation of the earthquake magnitude and allows one to quantify uncertainty based on the number of samples collected and the amount of rupture along which the samples were collected.

### ACKNOWLEDGMENTS

We thank Robert Witter, Robert Langridge, John Stimac and Miles Kenney for their discussions about this research. Journal reviews by Lisa Grant, Peter Knuepfer and Donald Wells greatly improved the manuscript. Research supported by the U.S. Geological Survey (USGS), Department of the Interior, under USGS award number (1434-HQ-97-GR-03020). The views and conclusions contained in this document are those of the authors and should not be interpreted as necessarily representing the official policies, either expressed or implied, of the U.S. Government.

### REFERENCES

- Baljinnyam, I., A. Bayasgalan, B.A. Borisov, A. Cisternas, M.G. Dem'yanovich, L. Ganbaatar, V.M. Kochetkov, R.A. Kurushin, P. Molnar and H. Philip, 1993, Ruptures of Major Earthquakes and Active Deformation in Mongolia and Its Surroundings: Geological Society of America, Memoir 181, 62p.
- Barka, A., 1996, Slip distribution along the North Anatolian fault associated with the large earthquakes of the period 1939 to 1967: Bulletin of the Seismological Society of America, v. 86, p. 1238-1254.
- Barrientos, S.E., R.S. Stein and S.N. Ward, 1987, Comparison of the 1959 Hebgen Lake, Montana and the 1983 Borah Peak, Idaho, earthquakes from geodetic observations: Bulletin Seismological Society of America, v. 77, p. 784-808.
- Caskey, S.J., S.G. Wesnousky, Z. Peizhen and D.B. Slemmons, 1996, Surface faulting of the 1954 Fairview Peak (Ms 7.2) and Dixie Valley (Ms 6.8) earthquakes, central Nevada: Bulletin Seismological Society of America, v. 86, p. 761-787.
- Clark, M.M., 1972, Surface rupture along the Coyote Creek fault, *in* The Borrego Mountain Earthquake of April 9, 1968: U.S. Geological Survey Professional Paper 787, p. 55-86.
- Coppersmith, K.J. and R.R. Youngs, 1986, Capturing uncertainty in probabilistic seismic hazard assessments within intraplate environments, *in* 3rd National Conference on Earthquake Engineering, p. 301-312.
- Crone, A.J., M.N. Machette, M.G. Bonilla, J.J. Lienkaemper, K.L. Pierce, W.E. Scott and R.C. Bucknam, 1985, Characteristics of surface faulting accompanying the Borah Peak earthquake, central Idaho: U.S. Geological Survey Open-File Report, 85-290, p. 43-58.
- Fumal, T.E., S.K. Pezzopane, R.J. Weldon II and D.P. Schwartz, 1993, A 100-year average recurrence interval for the San Andreas fault at Wrightwood, California: Science, v. 259, p. 199-203.
- Geomatrix Consultants, 1995, Seismic Design Mapping, State of Oregon: *for* Oregon Department of Transportation, Project No. 2442.
- Hemphill-Haley, M.A., 1999, Multi-scaled Analyses of Contemporary Crustal Deformation of North America, Ph.D., University of Oregon, Eugene, 237p.
- Machette, M.N., S.F. Personius and A.R. Nelson, 1990, Paleoseismology of the Wasatch Fault Zone: A Summary of Recent Investigations, Interpretations, and Conclusions: U.S. Geological Survey Professional Paper 1500-A, p. 72.
- Machette, M.N., S.F. Personius, A.R. Nelson, D.P. Schwartz and W.R. Lund, 1991, The Wasatch fault zone, Utah-segmentation and history of Holocene earthquakes, Journal of Structural Geology, v. 13, p. 137-149.
- McGill, S.F. and C.M. Rubin, 1994, Variability of surficial slip in the 1992 Landers earthquake; implications for studies of prehistoric ruptures, *in* Proceedings of the workshop on

- Paleoseismology, C. S. Prentice, D. P. Schwartz and R. S. Yeats (Editors), p. 118-120.
- Moore, D.S. and G.P. McCabe, 1993, Introduction to the Practice of Statistics, W.H. Freeman and Company, New York, 854 p.
- Rymer, M.J., 1989, Surface rupture in a fault stepover on the Superstition Hills Fault, California, in *Fault Segmentation and Controls of Rupture Initiation and Termination*, D. P. Schwartz and R. H. Sibson (Editors), Palm Springs, CA, p. 309-323.
- Schwartz, D.P. and K.J. Coppersmith, 1984, Fault behavior and characteristic earthquakes from the Wasatch and San Andreas faults: *Journal of Geophysical Research*, v. 89, p. 5681-5698.
- Schwartz, D.P., K.J. Coppersmith and F.H. Swan, III, 1984, Methods for estimating maximum earthquake magnitudes, *in* 8th World Conference on Earthquake Engineering, p. 279-285.
- Sieh, K., L. Jones, E. Hauksson, K. Hudnut, D. Eberhart-Phillips, T. Heaton, S. Hough, K. Hutton, H. Kanamori, A. Lilje, S. Lindvall, S.F. McGill, J. Mori, C. Rubin, J.A. Spotila, J. Stock, H.K. Thio, J. Treiman, B. Wernicke and J. Zachariassen, 1993, Near-field investigations of the Landers earthquake sequence, April to July 1992: *Science*, v. 260, p. 171-176.
- Sieh, K.E., 1978, Slip along the San Andreas fault associated with the great 1857 earthquake, *Bulletin Seismological Society of America*, v. 68, p. 1421-1448.
- Sowers, J.M., J.R. Unruh, W.R. Lettis and T.D. Rubin, 1994, Relationship of the Kickapoo Fault to the Johnson Valley and Homestead Valley faults, San Bernardino County, California: *Bulletin Seismological Society of America*, v. 84, p. 528-536.
- Stein, R.S. and W. Thatcher, 1981, Seismic and aseismic deformation associated with the 1952 Kern County, California, earthquake and relationship to the Quaternary history of the White Wolf fault: *Journal of Geophysical Research*, v. 86, p. 4913-4928.
- Wells, D.L. and K.J. Coppersmith, 1994, New empirical relation among magnitude, rupture length, rupture width, rupture area, and surface displacement: *Bulletin Seismological Society of America*, v. 84, p. 974-1002.
- Wesnousky, S.G., 1986, Earthquakes, Quaternary faults, and seismic hazard in California: *Journal of Geophysical Research*, v. 91, p. 12,587-12,631.
- Wong, I., M. Hemphill-Haley, T. Kolbe, G. Robert, J. Bott, H. Kanakari, K. Kelson, H. Colleen, J. Gardner, L. House, S. Reneau, D. Keller, W. Silva and C. Stark, 1993, A deterministic and probabilistic seismic hazard evaluation of the Los Alamos National Laboratory, *in* Fourth DOE Natural Phenomena Hazards Mitigation Conference.
- Woodward-Clyde Consultants, Geomatrix Consultants and Pacific Engineering and Analysis, 1992, Earthquake Ground Motion Evaluations for the Proposed New Production Reactor at the Idaho National Engineering Laboratory Volume 1: Deterministic Evaluation: U.S. Department of Energy, EGG-GEO-10304.
- Yeats, R.S., K. Sieh and C.R. Allen, 1997, *Geology of Earthquakes*, Oxford University Press, Oxford, 557p.

## ***PROBABILISTIC FAULT DISPLACEMENT HAZARD ANALYSIS: A CASE STUDY FROM SKULL VALLEY, UTAH***

Kathryn L. Hanson and Robert R. Youngs  
Geomatrix Consultants, Inc.  
2101 Webster, 12<sup>th</sup> Floor, Oakland, California 94612

Frank H. Swan  
Consulting Geologist  
240 Laidley Street, San Francisco, California 94131

### **ABSTRACT**

Probabilistic fault displacement hazard analysis (PFDHA) relates annual frequency of recurrence of surface faulting events to the size of the event. We present a case study for potential fault displacement hazard from distributed faulting in the hanging wall of a normal fault in the Basin and Range Province. The study focused on evaluating the hazard associated with secondary coseismic fault displacement in the hanging wall of a previously unrecognized fault, the East fault, in the central part of Skull Valley, Utah. The hazard analysis showed that the 2000-year return period displacement due to faulting at three sites representing different categories of locations within the area of concern is less than 0.1 cm, which is much lower than settlement displacements considered in the design of proposed facilities.

### **INTRODUCTION**

We integrated geologic and geophysical data in probabilistic analyses to evaluate surface-rupture hazard for a proposed interim storage facility for radioactive waste in Skull Valley, Utah (Figure 1). Results of this fault hazard study constrain the location, amount, and direction of ground movement expected during a single displacement event, and the event frequency or recurrence interval of surface-faulting events. A companion paper by Swan and others (this volume) describes new data on the location, geometry, and slip rate of late Quaternary faults in the site vicinity.

### **PFDHA METHODOLOGY**

The methodology used to evaluate fault displacement hazard was developed as part of the

seismic hazard assessment for the proposed nuclear waste repository at Yucca Mountain, Nevada (Civilian Radioactive Waste Management – Management and Operating Contractor (CRWMS M&O) (1998) and is analogous to the well-developed formulation for probabilistic evaluation due to earthquake strong ground shaking. Logic trees describe the significant input parameters, the uncertainties in the input parameters, and their related dependencies. A complete review of the methodology of conducting a Probabilistic Fault Displacement Hazard Analysis (PFDHA) is provided by (CRWMS M&O, 1998) and (Youngs and others, 2003).

The first step in developing hazard input data is to create a structural geologic model, or alternative models if needed, for the site region. The purpose of the model(s) is to help understand the faulting mechanisms and underlying causes of fault-related

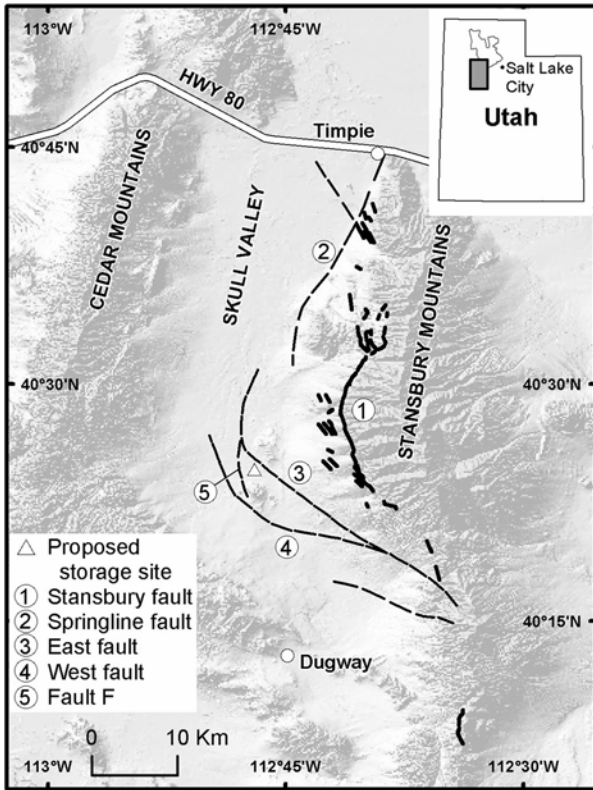


**Figure 1.** Location of known (solid lines) and inferred (dashed lines) active faults in the Skull Valley, Utah study area.

deformation. Besides constraining the movement direction, a geologic model also helps constrain estimates of slip-per-event and the likelihood of an event given the origin of faulting and current geologic environment. Developing an understanding of the different types of faulting and their driving forces also provides a framework for evaluating fault-related features where there are fewer data and/or it is not practical to do a site-specific analysis. Stratigraphic age control also is essential for developing information regarding the slip rate, and timing of past events. This information is necessary for calculating the recurrence estimates for potential future events.

### Basic Model

The PFDHA addresses how frequently displacement events occur and how large the displacements are in each event. The hazard can be

represented by a displacement hazard curve that is analogous to ground motion hazard curves (Figure 2). The curve relates the amount of displacement in a single event to how often displacements of that magnitude or larger occur (i.e., the frequency of exceeding a specified amount of displacement). Thus, the hazard curve is a plot of the frequency of events exceeding fault displacement value  $d$ , designated by  $\nu(d)$ . This frequency is computed by the expression:

$$\nu(d) = \lambda_{DE} \cdot P(D > d) \quad (1)$$

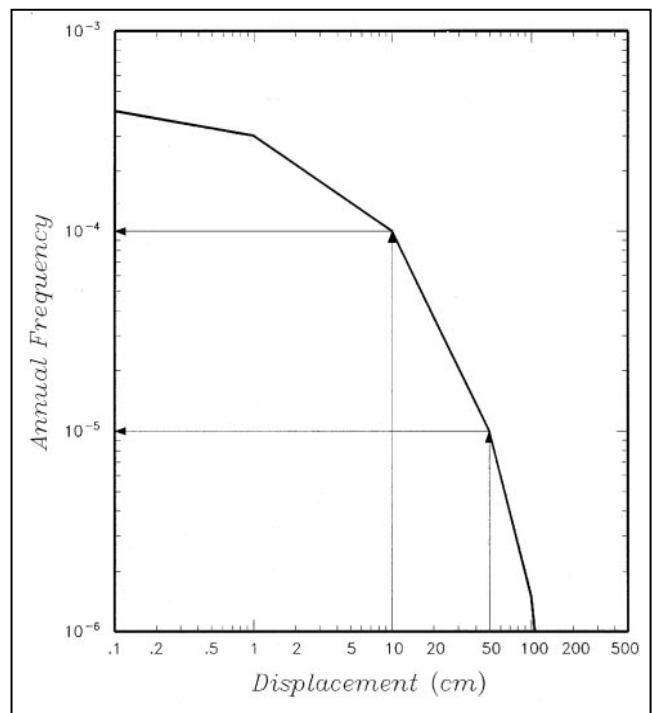


**Figure 2.** Example fault displacement hazard curve. The annual frequency of displacement events exceeding 10 cm is  $10^{-4}$  and the annual frequency of displacement events exceeding 50 cm is  $10^{-5}$ .

where  $\lambda_{DE}$  is the frequency at which displacement events occur on the feature (fault) located at the point of interest, and  $P(D > d)$  is the conditional probability that the displacement during a single event will exceed value  $d$ . When the events are infrequent and only characterized by an average rate of occurrence, then the probability that they occur within a specified

time period can be assessed by assuming that they correspond to a Poisson process.

### Estimation of Frequency of Displacement Events

Approaches for estimating the frequency of displacement events fall into two categories. The first, designated the *displacement approach*, provides an estimate of the frequency of displacement events directly from feature-specific or point-specific data. There are two techniques for direct estimation of

$D_E$ : the estimation of recurrence intervals and the use of slip rate. For the slip rate technique an estimate of the average slip per event is required

The second, designated the *earthquake approach*, involves relating the frequency of slip events to the frequency of earthquakes on various seismic sources. The earthquake approach utilizes earthquake recurrence models developed for ground shaking hazard assessments. The occurrence of an earthquake on a source may be associated with slip on the feature of interest. In the assessment of ground shaking hazard, it is assumed that every earthquake produces some level of ground shaking. However, surface faulting does not occur during every earthquake. Therefore, the frequency of displacement events is equal to the frequency of earthquakes times the probability that an individual earthquake will be associated with surface rupture. The methods used to evaluate this probability depend on whether one is considering principal or distributed faulting.

In this study, we focus on approaches used to evaluate distributed secondary faulting as the principal faults that would cause surface rupture are located to the east of the proposed facility site.

For distributed faulting, this probability expresses the likelihood that slip on an earthquake source some distance from the feature of interest will trigger slip locally. As described in (CRWMS M&O, 1998) and (Youngs and others, 2003), empirical data from historical earthquake ruptures in the western United States have been used to develop a logistic model that gives the probability of occurrence of distributed faulting on a feature located a

specified distance from an earthquake of a given magnitude.

### Conditional Probability of Exceedance

The conditional probability of exceedance,  $P(D > d)$  can be considered in two parts, the variability of slip from event to event, and the variability of slip along strike during a single event. The first part represents a distribution for the "size" of faulting events and is analogous to earthquake magnitude distribution models used in ground shaking hazard analysis. The second part represents the variation of the displacement from point-to-point along a rupture of a given size. This might be considered analogous to the lognormal distribution of peak ground motion about the median value predicted by an attenuation law for a specific magnitude and distance. A variety of approaches for evaluating the distribution of slip at a point in an individual event are discussed in Youngs and others (2003). The approaches differ depending on whether the earthquake or displacement approaches are being used for the assessment.

A single-step approach is used in the displacement approach. The method involves developing a distribution for  $D/D_{norm}$ , where  $D_{norm}$  is a representative measure of the amount of displacement at the location of interest. A logical choice for  $D_{norm}$  is the average displacement per event,  $\bar{D}_E$ . The distribution of  $D/\bar{D}_E$  represents the variability in displacement at a point in a single event about the average displacement over multiple events.

A two-step approach for assessing the conditional probability of exceedance is used to define the distribution of distributed displacement on a secondary fault in the earthquake approach. Based on empirical data for normal faults, estimates for the largest distributed displacements likely to occur on secondary faults can be expressed as a fraction of maximum displacement that occurs on the principal fault.

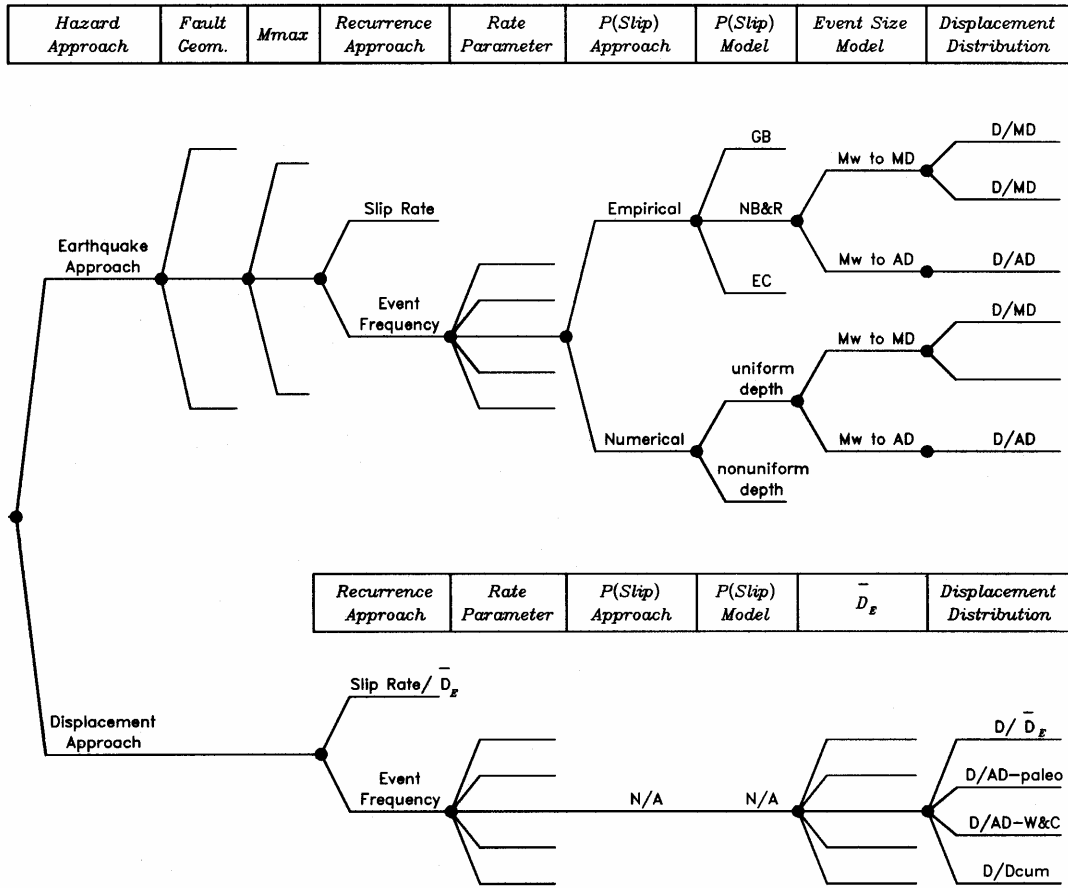


Figure 3. General logic tree showing alternative parameters required for the earthquake and displacement approaches.

### Treatment of Uncertainty

The formulation given by Equation (1) represents the randomness in the natural phenomena of fault displacement. The timing of a displacement event is considered a random phenomenon characterized by an average rate of occurrence. The size of an individual displacement event is random and is characterized by a specified probability distribution. In addition to the randomness in the phenomena, there is scientific uncertainty in the process of selecting the appropriate models and model parameters for the fault displacement hazard characterization. The logic tree methodology is utilized to characterize the uncertainty in the fault displacement probabilistic seismic hazard analysis (CRWS M&O, 1998; Youngs and others, 2003). An exam-

ple logic tree illustrating alternative models or input parameters needed to perform the analysis using both the earthquake and displacement approaches is shown in Figure 3.

### SKULL VALLEY, UTAH STUDY

In support of siting investigations for a proposed interim storage facility for radioactive waste, Geomatrix Consultants (1999) conducted seismic-hazard and fault-evaluation studies at a site in Skull Valley, Utah (Figure 4). Skull Valley is a structural basin bounded on the west and east by the Cedar Mountains and Stansbury Mountains, respectively. The site area is underlain by approximately 150 to 250 m of Quaternary and Tertiary basin fill that overlies Paleozoic bedrock. The Quaternary section

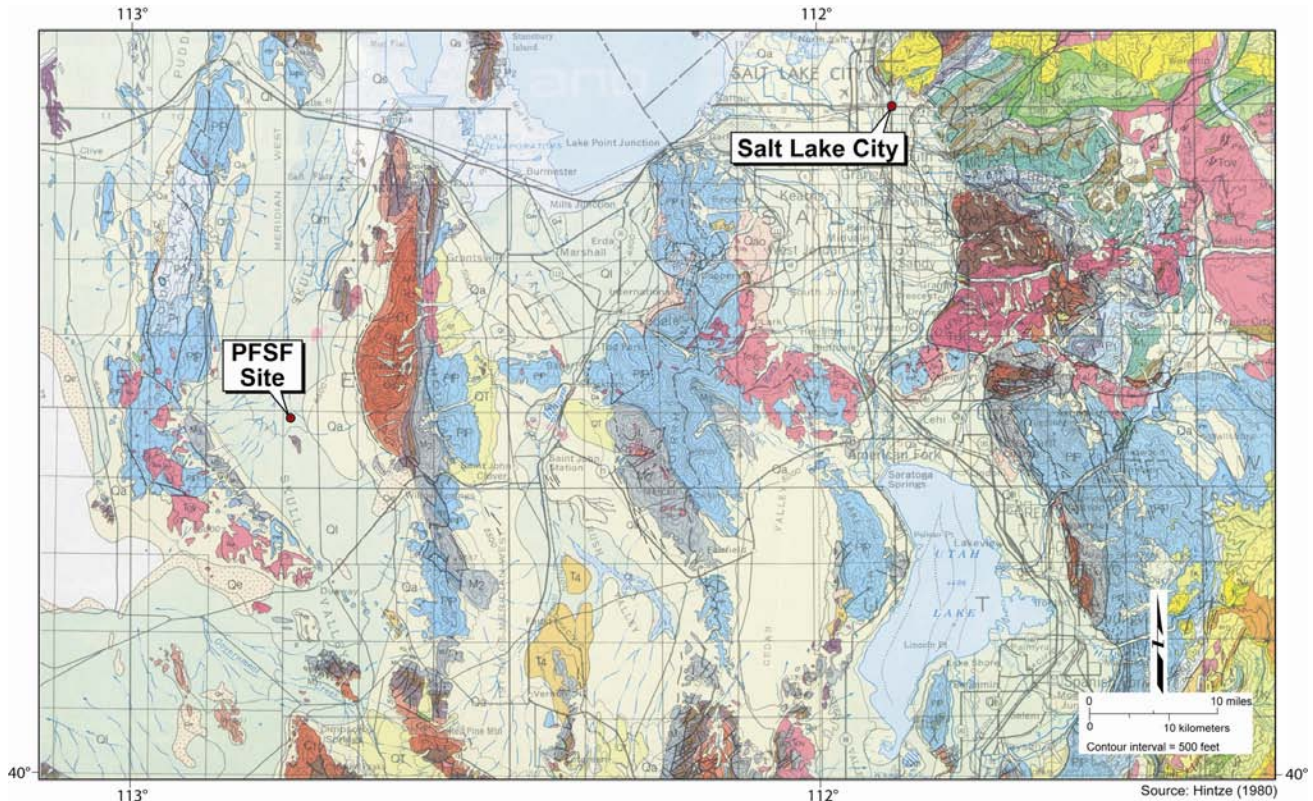


**Figure 4.** Regional geologic map showing the location of the PFSF Site in Skull Valley.

consists of a sequence of primarily lacustrine deposits representing a series of pluvial lake cycles with intertonguing subaerial sediments. Correlation of these deposits to a well established regional pluvial chronostratigraphy provides well-constrained ages for the late Quaternary deposits. (see Table 1 in Swan and others, this volume).

The Stansbury fault, which has a late Quaternary slip rate of  $0.37 \text{ mm} \pm 0.04 \text{ mm/yr}$ , lies 9 km east of the site along the western margin of the Stansbury Mountains (Figure 1) (Swan and others, this volume). Two previously unrecognized faults in central Skull Valley, which are informally referred to as the East and West faults, lie 0.9 km east and 2 km west of the site, respectively. The proposed storage area is in a postulated stepover zone between the East and West faults that is characterized by secondary distributed faulting. Characterization of the zone of distributed faulting between the East and West faults was of primary concern in assessing surface-rupture hazard at the proposed storage site.

Proprietary oil industry data, both gravity and seismic-reflection data (Line GSI-UT 34, Plate 1), constrain the locations of major faults in the valley adjacent to the site, including the East fault, West fault, and Fault F. Fault F, having a cumulative late Quaternary displacement of less than 2.38 m, is the largest of the intrablock faults within the zone of distributed faulting.

High-resolution seismic S-wave reflection surveys (Bay Geophysical lines as shown on Plate 1) and detailed surface and subsurface Quaternary studies provided data to evaluate the style, location, geometry, and slip rate of both primary faults (e.g., the East fault) and secondary distributed faulting in the vicinity of the proposed site (Plates 1 and 2). The seismic data image both west-dipping and east-dipping normal faults in the zone of distributed faulting (e.g., Plate 2 and Figure 5). The faults, which are labeled alphabetically from east to west, are subdivided into three categories based on recency of activity (Plate 1).

Two prominent reflectors that extend across the entire site are used to assess the recency and amounts of displacement for individual faults. Based on information from drilling and trenching, we interpret these reflectors as two unconformities (Figure 5). The younger Q<sub>p</sub> unconformity represents a period of subaerial exposure and erosion that occurred during an interpluvial period between approximately 130 ka and 32.5 ka. The age (<6 Ma to 160 ka) of the older Q/T unconformity, which represents the contact between Tertiary and Quaternary sediments is less well constrained and may vary at different locations across the site.

Within the boundaries of the proposed storage area, only one fault in the eastern part of the area (Fault D1) shows evidence for recent activity (post-Q<sub>p</sub> unconformity) (see inset map of detailed area on Plate 1). The other faults that underlie the proposed site (Faults E1, E2, and E3) do not appear to displace the Q/T unconformity. The total cumulative displacement across individual faults within the zone is small based on estimated displacements of the Q/T reflector across individual faults (Table 1).

### Fault Displacement Hazard Analysis

To quantify the hazard associated with coseismic fault displacement expected to occur within the zone of distributed faulting, we conducted a PFDHA. We calculated the hazard for three different conditions within the proposed storage area: (1) faults that appear to displace the Q<sub>p</sub> reflector (e.g., Faults D1 and F); (2) faults that appear to displace the Q/T reflector but do not extend to the Q<sub>p</sub> reflector (e.g., Fault C1); and (3) zones between the mapped Quaternary faults that may experience distributed faulting and/or movements on faults too small to map.

We employed both the earthquake approach and the displacement approach. The relative weights assigned to the two approaches are 0.63 for the displacement approach and 0.37 for the earthquake approach. These weights are consistent with the average weights assigned by the Yucca Mountain seismic source characterization expert teams (CRWMS

M&O, 1998). For the earthquake approach we used source characterization parameters developed for the ground motion hazard assessment (Geomatrix Consultants, 1999).

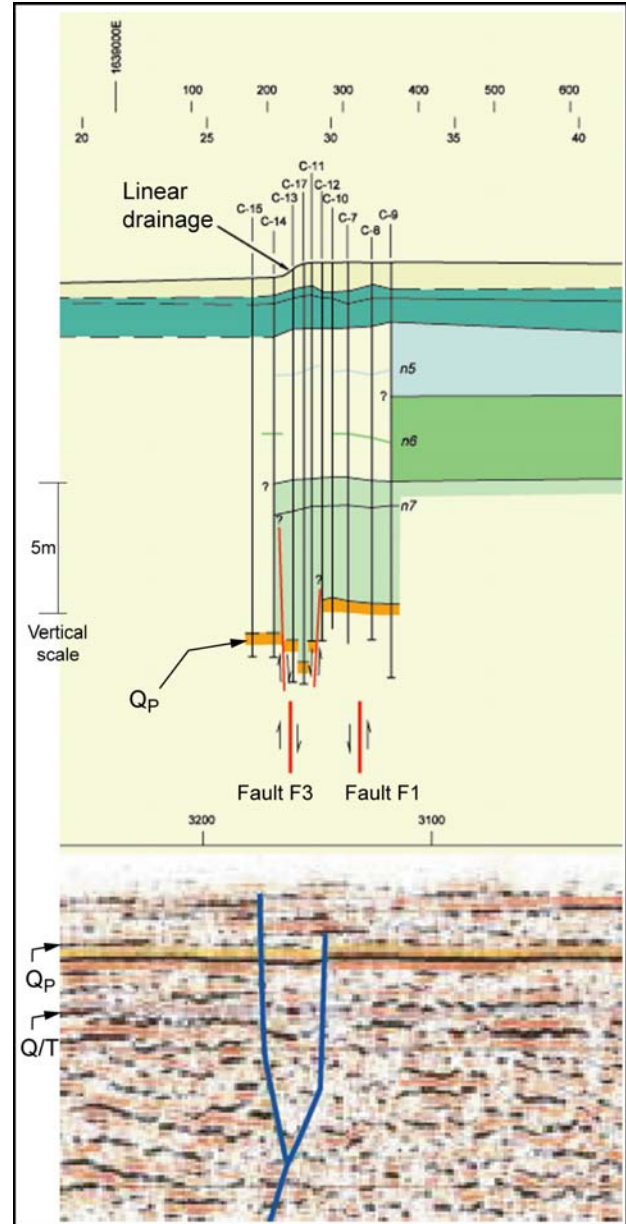


**Figure 5.** Examples of drilling and high-resolution s-wave seismic reflection data used to identify and characterize Quaternary faults. A more complete seismic section across the entire proposed storage area is shown on Plate 2.

**Table 1**  
 Summary of fault locations and displacements, Private Fuel Storage Facility  
 (Modified from Bay Geophysical Association, 1999)

Survey Line		Datum and Amount of Displacement				Sense of Slip		Fault Designation	Comments	
Line	Shot Point	Q/T (ms) <sup>1</sup>	Calculated Vertical Disp. (ft) <sup>2</sup>	Qp (ms) <sup>1</sup>	Calculated Vertical Disp. (ft) <sup>3</sup>	Down-to-the-East	Down-to-the-West			
<b>GSI</b>										
<b>UT-54</b>										
34	183	na		na		X		-	Unnamed fault pick. Upper part of section not imaged. "East Fault." Upper part of a section not imaged. Upper part of section not imaged Unnamed fault pick. Upper part of section not imaged. Upper part of section not imaged	
34	193	na		na			X	A		
34	227	na		na			X	F		
34	260	na		na		X		-		
34	280	na		na			X	West Fault		
<b>LINE C</b>										
C	357	4.3	2.4	N			X	C1	Fault appears to die out within the Salt Lake Group. Extends near surface.	
C	418	N		N				C2		
C	820	4.8	2.6	4.8	1.9		X	D1		
C	930	N		N				E2		
C	1027	N		N			X	E1		
C	1178			N			X	E3		
<b>LINE A</b>										
A	151	>10	>5.5	?				X	Uncertain of Qp pick SP 101-700 ?Qp and Q/T diverge on fault pick ?Qp and Q/T converge on fault pick Q/T reflector across faults is poorly defined. Displacement uncertain due to dip on Qp. Extends near surface. Poor data below Qp between faults B1 and B2. Questionable fault. Highest point on fault is at 121 ms. Possible flexure (change in dip) in Qp horizon. Highest point on fault is at 143 ms. Flexure in Q/T horizon; possible channels to west in Qp. Possible small flexure in Qp. Lateral uncertainty in location ~25 ft. Flexure in Qp horizon ? Highest point on fault is at 211 ms. Extends near surface. Extends near surface. Extends near surface. Extends near surface. Qp disrupted, but cannot tell amount of displacement.	
A	452	>7	>3.8	?			X	?A7 ?A6		
A	607	?		?				X		
A	761	?		12.7	5.1			X		
A	855			3.5	1.4			X		
A	907	?		2.3	0.9		X	A1 A2		
A	946	?		10.8	4.3			X		
A	1227	4.1?	2.3	2.7	1.1			X		
A	1450			≤2	<1		X	B2 B1		
A	1745	4.8	2.6	N				X		
A	1852	4.4	2.4	N				X		
A	2102	≤2.5		N						
A	2161	5.3	2.9	N				X		
A	2352	2.6	1.4	2.3				X		
A	2560	?						X		
A	2669	?						X		
A	2810	N					X?	E1 E3		
A	3138	<4	<2.2	5.5	2.2			X		
A	3168	<5	<2.8	3	1.2		X	F1 F3		
A	3304	<5	<2.8	4.5	1.8		X	F4		
A	3329	<5	<2.8	3.5	1.4			X		
A	3556	N						X		
A	3602	<2?					X	F2 G2		
A	3930	Y		Y			X	G1		
A	3904	Y		N				X		
<b>LINE D</b>										
D	197	3.2		3.6				X		Extends near surface. Unnamed questionable fault. Unnamed questionable fault.
D	330	2.8		3.7			X	F2 F3		
D	369	4.2		4.2				X		
D	828	?		?			X?	F1		
D	949	?		?			?	-		
D	1110	?		?				D1?		
<b>LINE B</b>										
B	283	≤5		N				X	Questionable displacement of Q/T. Questionable fault. No apparent displacement of Qp. Character change in Qp reflector; poor data to the west. Questionable fault. Data SW of shot point 1000 are very poor quality.	
B	327	≤5.7		N				X		
B	495	3		N				x		
B	766	?		N			?	?		
B	885	?		?			?	?		
B	1020	?		?			?	?		

<sup>1</sup> Two way travel time (ms). Y - Indicates that the unconformity is disrupted but the amount of offset is at or below the limit of resolution of the data (~0.6m); N - Indicates no detectable offset; ? - Indicates questionable displacement.

<sup>2</sup> Using interval Velocity = 1100 ft/sec.

<sup>3</sup> Using interval Velocity = 800 ft/sec. As noted in Table 3, the actual displacement appears to be 3 times the calculated value based on locations where displacements observed on seismic lines were measured between borings.

For analysis of displacement on a distributed rupture we use the curve of the distribution of displacement on a distributed rupture as a fraction of the maximum displacement on the principal rupture. This curve was developed from historical normal surface ruptures as either the 95<sup>th</sup> or 85<sup>th</sup> percentile of a gamma distribution of  $D_{distributed} / MD_{principal}$  (CRWMS M&O, 1998; Youngs and others, 2003).

For the displacement approach, the required parameters are the distribution for  $D/\bar{D}_E$ , and for each fault the average displacement per event and the fault slip rate. We utilized three alternative distributions for  $D/\bar{D}_E$  (DFS, SBKp, and SBKwc) that were developed during the Yucca Mountain project from analysis of paleoseismic data (CRWMS M&O, 1998) and gave them equal weight. The DFS distribution was developed by normalizing individual event displacements from a single trench location by their average and then pooling all of the data for trench sites containing three or more events. The SBKp distribution was developed by normalizing individual event displacements from a fault by the estimated average displacement for the fault over all events. The SBKwc distribution was developed by normalizing individual event displacements from a fault by the estimated average displacement for the fault based on the Wells and Coppersmith (1994) empirical relationship between average displacement and fault length.

We interpreted displacement and slip-rate data at specific locations from seismic data calibrated with drilling information. We estimated the average displacement per event for individual faults based on stratigraphic relationships inferred from drilling data that suggest multiple events. Based on these data, we developed slip-per-event distributions that characterize the overall uncertainty in these parameters (Table 2).

For example, across a graben formed by faults F1 and F3, displacement decreases upward within the Bonneville alloformation indicating that the cumulative displacement of the Qp unconformity was produced by multiple events (Figure 6). The average slip per event on the F faults is probably significantly less than the largest cumulative displacement

**Table 2**

*Distributions for average slip per event ( $\bar{D}_E$ ) and slip rate used in the displacement approach*

<b>Fault</b>	$\bar{D}_E$ (m) [weight]	<b>Slip rate (mm/yr)</b> [weight]
'F' faults	0.05 [0.1]	0.01 [0.1]
	0.3 [0.42]	0.02 [0.5]
	0.6 [0.43]	0.03 [0.3]
	0.9 [0.05]	0.04 [0.1]
'D' faults	0.1 [0.15]	Approach 1[0.8] post- 55 ± 5 ka
	0.2 [0.4]	0.01 [0.2]
	0.4 [0.4]	0.02 [0.3]
	0.7 [0.05]	0.03 [0.3]
		0.04 [0.2]
		Approach 2 [0.2] post 28 ka
		0.02[0.2]
		0.04 [0.3]
	0.06 [0.3]	
	0.08 [0.2]	
C1 and C2	0.02 [0.25]	0.001 [0.3]
	0.1[0.3]	0.005 [0.5]
	0.2 [0.3]	0.01 [0.1]
	0.4 [0.1]	0.02 [0.1]
	0.7 [0.05]	

reported on a single trace (1.4 m), which we interpret to have been produced by multiple events. We consider a displacement of 30 to 45 cm during a single event to be a likely value for the net slip during a single event (i.e., assuming the 0.9-m cumulative displacement across the F1/F3 graben was produced by at least 2 to 3 events). The average slip per event is probably greater than 5 cm. A 5 cm-average-slip event would suggest there have been more than 15 surface faulting events post-Qp and implies a recurrence interval of less than 3,000 to 4,000 years. Displacements on individual traces within a zone containing both down-on-the-west and down-on-the-east movements might be larger than the net slip across the zone. Given the overall uncertainty, a wide range of values is considered for the average slip per event on the F faults with the greatest weight assigned to values that are consistent with 2 or 3 events post-Qp. The range of values and probability

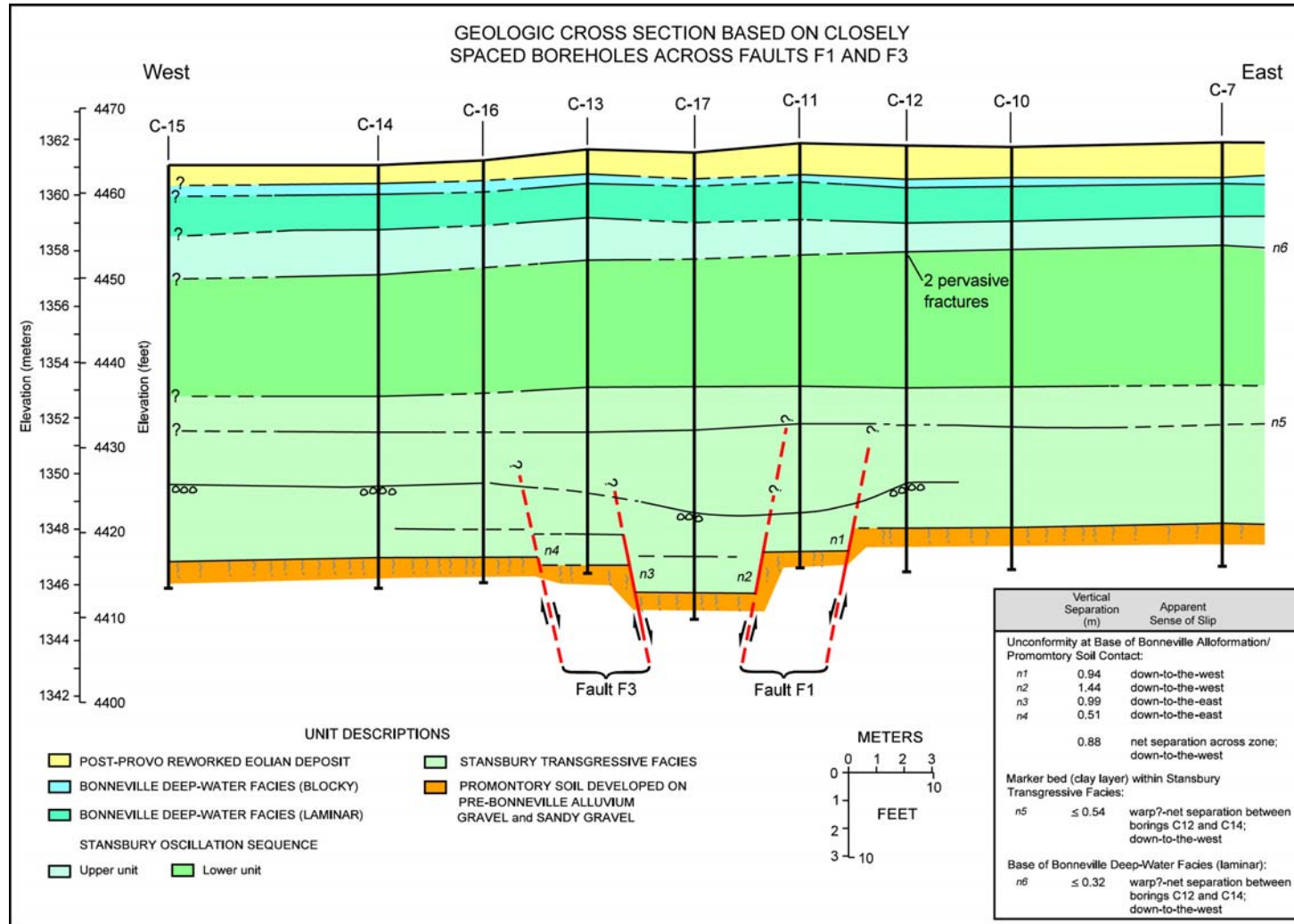


Figure 6. Geologic cross section based on tightly spaced boreholes across faults F1/F3

**Table 3**  
Displacement and fault slip rate estimates for 'D' faults

Location	Vertical Separation of Qp			Slip Rate (mm/year) <sup>6</sup>	
	Calculated Based on Seismic Profile (m) <sup>1</sup>	Adjusted Value (m) <sup>2</sup>	Measured Between Boreholes (m)		
1.) Seismic Line C:					
a)	Fault D1	0.6	1.7	--	0.032 +0.003
2.) Seismic Line A:					
a)	Fault D1	0.27	0.8	--	0.015 +0.001
b)	Fault D2	0 <sup>3</sup>	--	--	--
c)	Fault D3	0 <sup>3</sup>	---	--	--
3.) Seismic Line A:					
a)	Fault D1	--	--	0.7	0.013 +0.001
4.) Seismic Line D:					
a)	Fault D1	* <sup>4</sup>	<0.6 <sup>5</sup>	--	<0.012
5.) Seismic Line B:					
a)	Shotpoint 885 <sup>6</sup>	* <sup>4</sup>	<0.6 <sup>5</sup>	--	<0.012
	Shotpoint 1020 <sup>6</sup>	* <sup>4</sup>	<0.6 <sup>5</sup>	--	<0.012

<sup>1</sup> Source: Table 1 (Bay Geophysical Associates, 1999).

<sup>2</sup> Adjusted value is 3 times the calculated value based on locations where displacements observed on seismic lines were also measured between borings.

<sup>3</sup> No detectable offset of Qp reflector.

<sup>4</sup> Questionable displacement of Qp reflector; displacement not measureable.

<sup>5</sup> Assumes displacement is less than the 0.6 m (2.ft). limit of resolution of the survey.

<sup>6</sup> Upper bound rate post -55 ± 5 ka. Estimated age of Promontory soil based on age of 32.5 ka age of the base of the Bonneville alloformation at the site and estimated minimum time needed to form a stage 2+ carbonate soil (20 to 30 kyr).

weights used to characterize the F, D, and C faults in the probabilistic analysis are given in Table 2.

We estimate slip rate for individual faults based on interpretation of seismic data calibrated by drill-hole data. Comparison of displacements measured at several locations along a single fault trace illustrates along strike variability. An example of the 'D' faults data is shown in Table 3.

We considered a number of factors in developing distributions for slip rate on the larger more continuous secondary faults within the distributed zone of faulting in the vicinity of the proposed storage area (Table 2). In addition to uncertainties related to the age of the displaced datum and the amount of cumulative displacement, the slip-rate distributions also include uncertainties related to the limited sample size and the relation between the measured values at specific locations to the average value along the section of fault of concern.

The potential for displacement in areas between the mapped faults is very low, but this potential for small displacements is included in the displacement hazard analysis. The high-resolution seismic survey successfully imaged faults having very small (less than 0.6 m) cumulative displacement in the Promontory soil (i.e., the Qp reflector). We observed fractures in the Bonneville deep-water facies in several of the test pits and in Trench T-2 (locations of trenches and test pits are shown on Plate1). Careful mapping of the fractures in the trench shows that (1) the general north-south trend of the fractures is compatible with the regional pattern of east-west Basin and Range extension, (2) the fractures die out downward and do not cut the thin marker beds within underlying sandy Bonneville transgressive facies, and (3) there is no vertical displacement across most of the fractures indicating that the cumulative deformation during the past 15 to 20 ka is

very small. Sixty-four fractures were mapped in the 88-m-long trench. Only 11 had measurable displacement. The amount of displacement on the mapped fractures is listed in Table 4. The displacements ( $\leq 2.5$  cm) are all smaller than the amount of settlement considered in the design of the proposed storage facility.

**Table 4**

Summary of displacements on mapped fractures in Trench T-2

Number of fractures	Vertical Displacement	Percentage of Total
53	0	83 %
3	1.0 cm	5 %
6	2.0 cm	9 %
2	2.5 cm	3 %
Total 64		100 %

## Results

We conducted fault displacement hazard analyses for three locations: at Faults C1, D1, and the F faults (F1/F3 and F2/F4 graben) (labeled Faults C, D, and F on Figure 7). Figure 7 shows the fault displacement hazard results for the three locations. Each plot shows the mean hazard curve and 5<sup>th</sup> and 95<sup>th</sup> percentiles of the frequency of exceeding specific displacement values. The uncertainty in the hazard results is represented by the percentile curves, and the distribution is skewed, with the mean hazard lying near the 75<sup>th</sup> percentile of the distribution. This reflects the higher hazard estimated using the displacement approach versus the earthquake approach combined with the greater weight assigned to the displacement approach in the analysis. For comparison, the plots show the mean hazard results for the earthquake and displacement approaches for each site.

The displacement hazard curves display a characteristic shape that is different from that of a typical ground motion hazard curve. Typical ground motion hazard curves show a steeper slope at low ground motion levels rather than the relatively flat portion of the curve exhibited in the displacement hazard curves. In the earthquake approach, the pri-

mary contributors to displacement hazard are larger events occurring within a few kilometers of the site, due to the displacement hazard associated with distributed faulting. Therefore, the larger number of smaller and/or distant events that contribute to ground shaking hazard at low ground motion levels have no contribution to displacement hazard. The frequency of exceedance is limited by the frequency of large events occurring at or in the immediate vicinity of the site. In the displacement approach, the frequency of all displacement events occurring at the site is specified directly and the frequency of exceedance of a specific displacement value must be less than or equal to the frequency of displacement events.

In the earthquake approach, the hazard is dominated by contributions from the East fault with a minor contribution from the more distant Stansbury fault. The earthquake approach estimates are similar at all three sites and show a gradual decrease in frequency of exceedance as one moves away from the East fault (from Fault C to Fault F). The earthquake approach produces the most similar hazard as the displacement approach at Fault C and significantly lower hazard than the displacement approach at the other two sites.

The difference between the hazard results from the earthquake approach and the displacement approach demonstrate the value of obtaining site-specific data, especially in areas of distributed faulting. The empirical database for the amount of slip that occurs on secondary faults that move during distributed faulting is very limited (Youngs and others, 2003). The lower hazard from the earthquake approach calculated at all locations for this study suggests that this may be a limiting factor in the reliability of the earthquake approach. Alternatively, more similar results would be obtained from the two approaches if (1) earthquakes on the primary faults (the East and Stansbury faults) were larger or more frequent or (2) the frequency or average displacement estimated for individual faults in the displacement approach was overestimated.

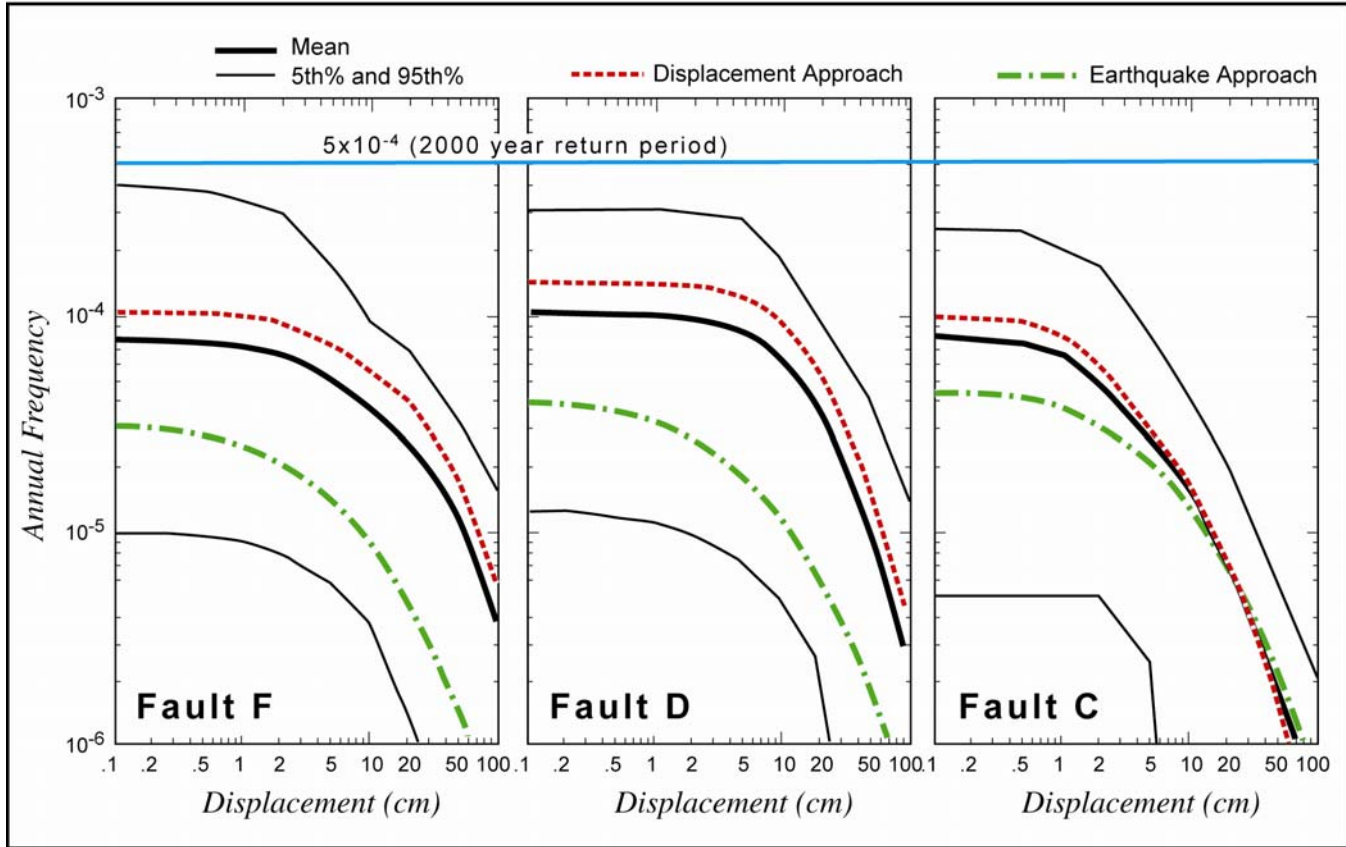


**Figure 7.** Effect of approach on mean displacement hazard

Based on the detailed fault characterization studies completed for this study, we do not favor this explanation. The objective of the detailed studies was to collect sufficient data to capture the range of uncertainty in the various parameters used in both approaches. The hazard results at the 5<sup>th</sup> and 95<sup>th</sup> percentiles capture the range of estimates for these parameters.

The well constrained displacement data on the F and D faults provide a useful basis for constraining the potential for displacement on other intrablock faults in the site vicinity. Fault F does not extend under the site and, therefore, does not pose a threat to the proposed storage area (Plate 1). This fault has larger Quaternary displacement than the other intrablock faults in the study area. Therefore, the potential for fault-rupture on the other faults is expected to be less than that of the F fault.

The design probability level for the proposed storage facility is  $5 \times 10^{-4}$  per year, which corre-

sponds to a 2000-year return period (Geomatrix Consultants, 1999). At these probability levels, even the 95<sup>th</sup> percentile displacement associated with locations on the largest intrablock faults in the zone of distributive faulting between the East and West faults are less than 0.1 cm (Figure 7), which is much lower than settlement displacements considered in the facility design. Therefore, despite the presence of recently active faults at the site, surface-fault rupture hazard does not pose a significant risk to the proposed facility.

## CONCLUSIONS

The case study presented in this paper highlights approaches developed to quantitatively assess fault displacement hazard. Key aspects of this study are the development of: 1) site-wide structural geologic characterization of the style and origin of active

faulting and fault-related deformation; 2) a late Quaternary stratigraphic model to evaluate the history, recency, and rate of fault activity; and 3) detailed characterizations of the faults most significant to potential facilities development.

The approaches used are tailored to fit the structural setting and site-specific data available. For sites proximal to active seismogenic normal faults, like the Skull Valley site, both the earthquake approach and displacement approach are appropriate and can be employed successfully to fully capture the range of uncertainty

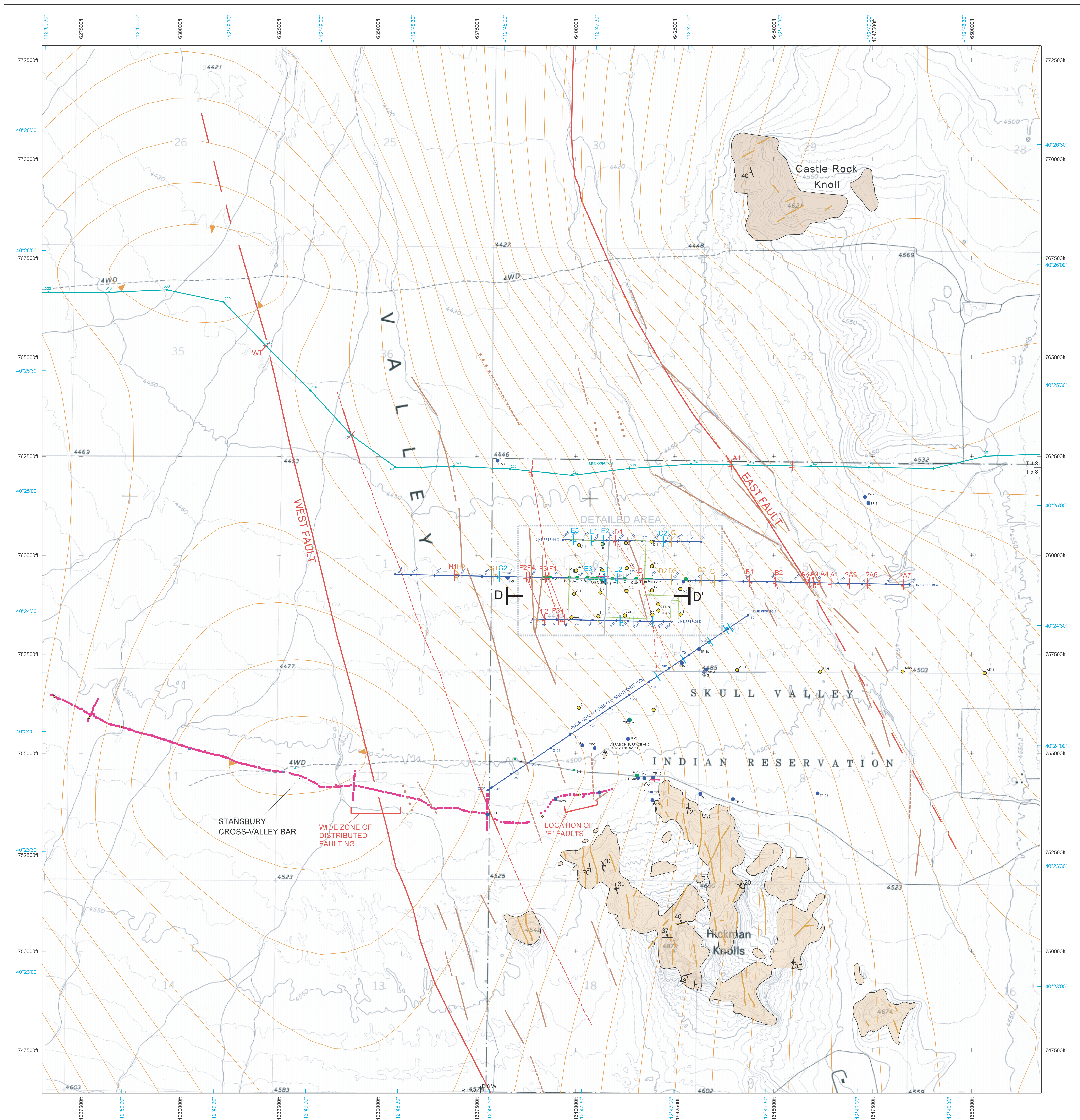
This study demonstrates that the presence of active faults may not preclude safe development of facilities. To evaluate risk associated with faulting, integrated hazard studies should be conducted during the early stages of development. PFDHA based on an understanding of the causative processes and limitation of the available data enables quantitative assessment of the location, magnitude, and recurrence of potential fault displacements.

### **ACKNOWLEDGMENTS**

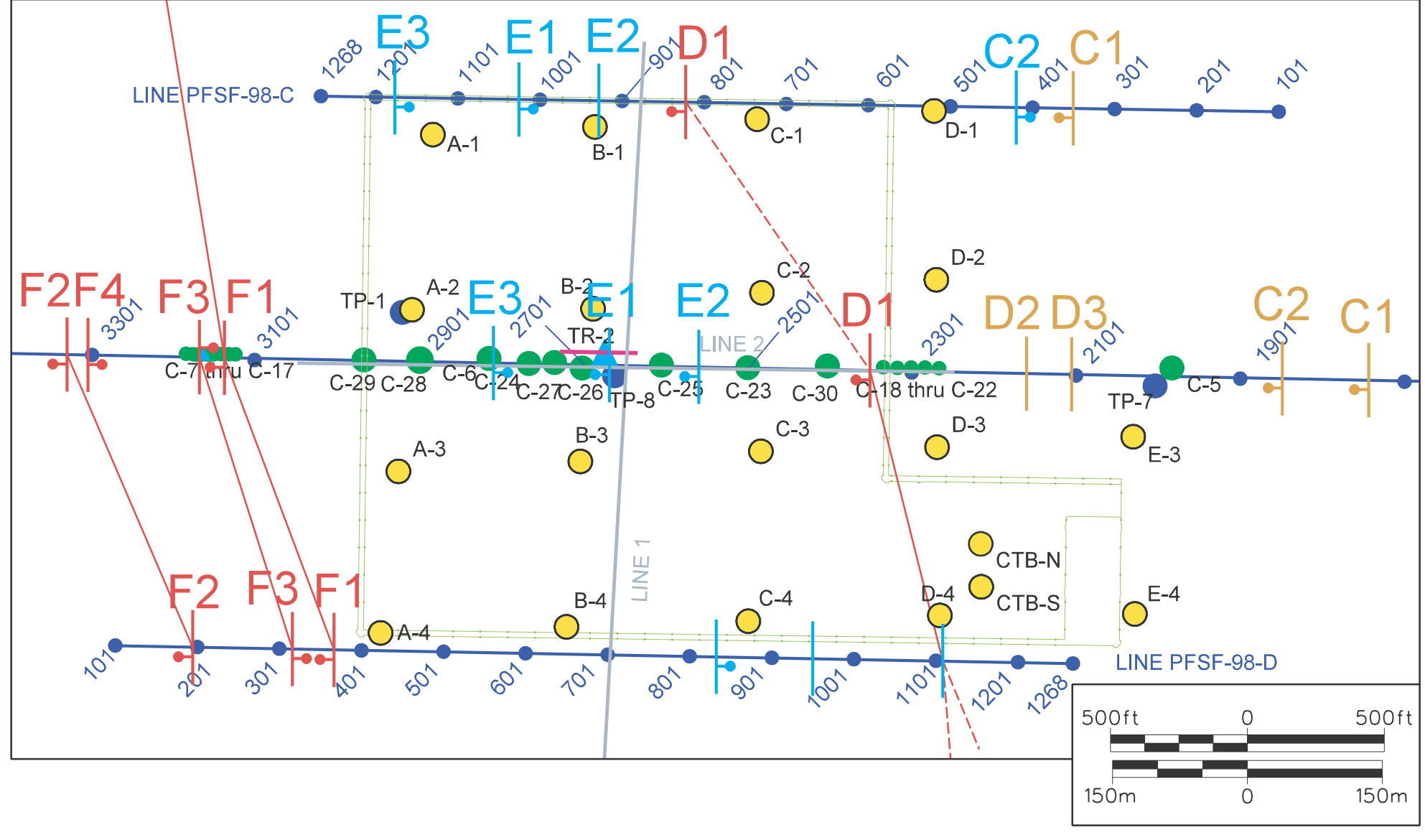
The authors wish to thank Private Fuel Storage, LLC for their support and permission to publish this summary of the PFDHA of the Skull Valley, Utah site. A special thanks to John Donnell, Project Director for PFSF-LLC, for his support throughout the project. Without the permission and cooperation of Chairman Leon Bear and the Skull Valley Band of the Goshute Indians, this study would not have been possible. We also would like to recognize Kevin Coppersmith, who provided technical oversight and review for the fault evaluation studies and seismic hazard assessments conducted by Geomatrix Consultants. Susan S. Olig and William R. Lund provided independent technical reviews of this paper. Support for the preparation of this paper was provided by Geomatrix Consultants Professional Development.

### **REFERENCES**

- Bay Geophysical Associates, 1999, High resolution seismic shear wave reflection profiling for the identification of faults at the Private Fuel Storage Facility Skull Valley, Utah: Report prepared for Stone & Webster Engineering Corporation, Englewood, Colorado, Bay Geophysical Project No. 98-024.
- Civilian Radioactive Waste Management System Management and Operating Contractor (CRWMS M&O), 1998, Probabilistic seismic hazard analyses for fault displacement and vibratory ground motion at Yucca Mountain, Nevada: Report prepared for U.S. Department of Energy, Milestone SP321M3, WBS No. 1.2.3.2.8.3.6, 3 Vols.
- Geomatrix Consultants, 1999, Fault evaluation study and seismic hazard assessment: unpublished report prepared for Private Fuel Storage, LLC, SWEC #0596602-18, GMX #4790.
- Hintze, L.F., (compiler), 1980, Geologic map of Utah: Utah Geological and Mineral Survey, Salt Lake City, Utah, scale 1:500,000.
- Moore, W.J., and Sorenson, M.L., 1979, Geologic map of the Tooele 1° x 2° Quadrangle, Utah: U.S. Geological Survey Miscellaneous Investigations Series Map I-1132, scale 1:100,000.
- Youngs, R. R., Arabasz, W. J., Anderson, R. E., Ramelli, A. R., Ake, J. P., Slemmons, D. B., McCalpin, J. P., Doser, D. I., Fridricdh, C. J., Swan, F. H., III, Rogers, A. M., Bruhn, R. L., Knuepfer, P. L. K., Smith, R. B., dePolo, C. M., O'Leary, D.W.O, Coppersmith, K. J., Pez-zopane, S. K., Schwartz, D. P., Whitney, J. W., Olig, S. S., and Toro, G. R., 2003, Probabilistic fault displacement hazard analysis (PFDHA)," *Earthquake Spectra*, v. 19, p. 191-219.



**DETAILED AREA:**



- EXPLANATION:**
- STONE AND WEBSTER BORING
  - STANSBURY BAR TOPOGRAPHIC PROFILE DATA POINT
  - GEOMATRIX TESTPIT
  - GEOMATRIX BORING
  - GEOMATRIX TRENCH
  - GRAVITY CONTOUR (1 mGal Interval - Based on proprietary data licenced from EDCON, Inc.)
  - BEDROCK OUTCROP- ORDOVICIAN CARBONATE (from Moore and Sorenson, 1979)
  - BEDROCK OUTCROP- MISSISSIPPIAN CARBONATE (from Moore and Sorenson, 1979)

- EXPLANATION (continued):**
- LINEAMENT IN BEDROCK
  - LINEAMENT IN QUATERNARY DEPOSITS
  - POST-Qp FAULT
  - ↘ 40 STRIKE AND DIP OF BEDDING
  - ↘ 30 STRIKE AND DIP OF PRIMARY DEPOSITIONAL LAYERING IN BRECCIA
  - ↘ 70 STRIKE AND DIP OF FAULT
  - ↘ 37 STRIKE AND DIP OF NORMAL FAULT
  - ↘ 20 STRIKE AND DIP OF EXTENSIONAL DUCTILE SHEAR ZONE
  - PROPOSED SITE BOUNDARY

- SEISMIC LINES:**
- GEOSPHERE MIDWEST
  - BAY GEOPHYSICS
  - LINE GSI-UT-34
- FAULT PICKS:**
- POST-Qp UNCONFORMITY DOWNTHROWN SIDE
  - POST-Q/T UNCONFORMITY
  - TERTIARY

- NOTES**
1. STATE PLANE PROJECTION - NAD27 UTAH CENTRAL ZONE
  2. USGS TOPOGRAPHIC BASE: 1:24,000 HICKMAN KNOLLS QUADRANGLE

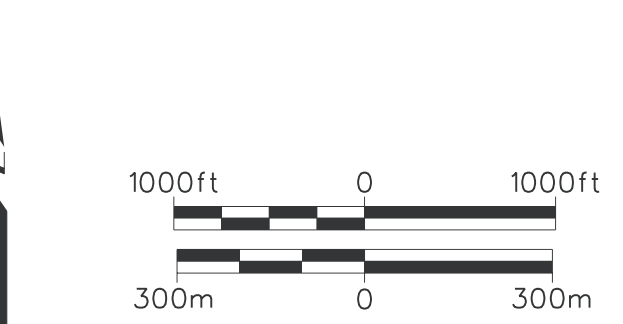
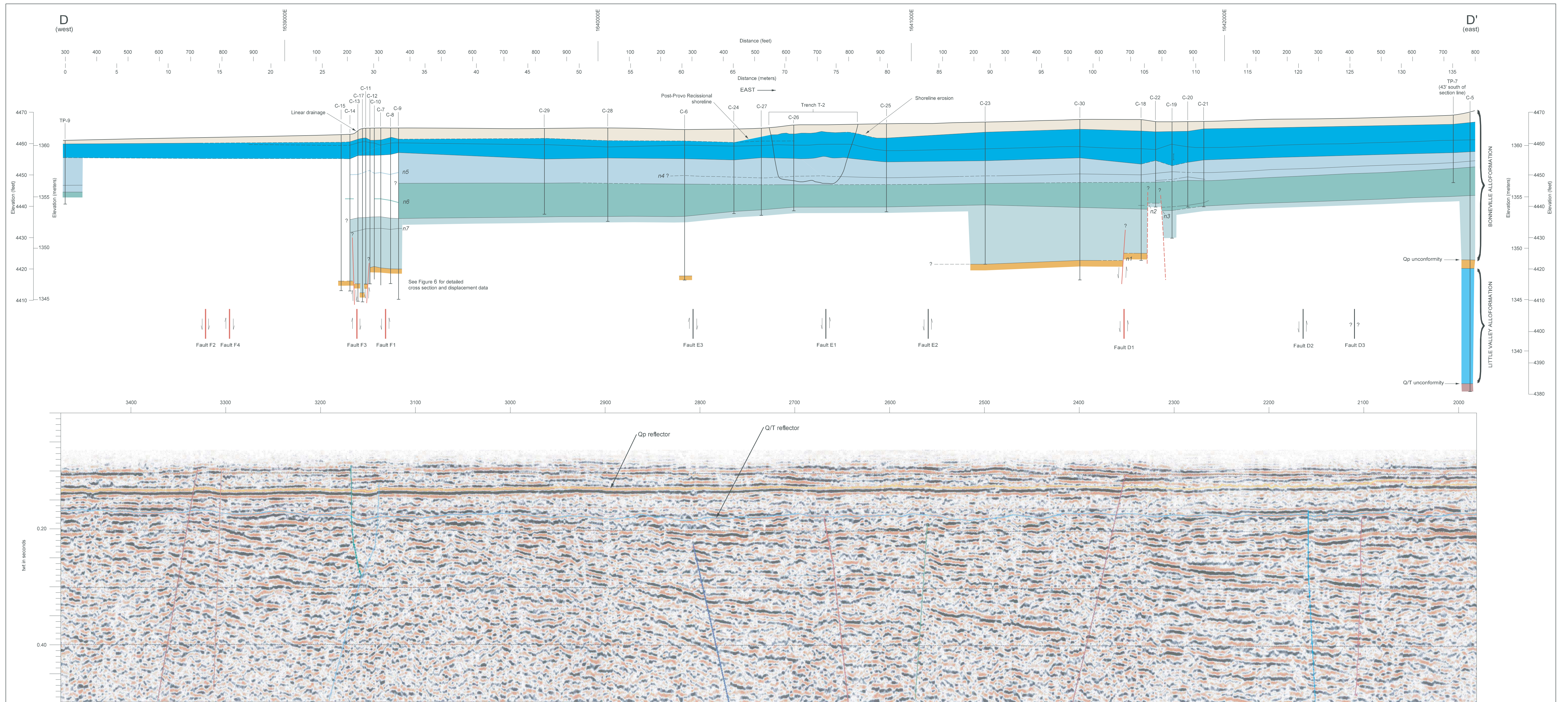


**PLATE 1**  
**PLAN MAP OF SITE INVESTIGATIONS**

*K. L. Hanson and others: Probabilistic Fault Displacement Hazard Analysis  
 A Case Study from Skull Valley, Utah  
 Basin and Range Province Seismic Hazards Summit II, 2004*



Source - Bay Geophysical Associates, Inc. (1999), Figure 20

**Unit Descriptions:**

POST- PROVO EOLIAN AND PLAYA DEPOSITS	PRE- BONNEVILLE DEPOSITS
<b>BONNEVILLE LACUSTRINE CYCLE DEPOSITS</b>	PROMONTORY SOIL DEVELOPED ON PRE - BONNEVILLE SUBAERIAL DEPOSITS (REWORKED, EOLIAN SAND RAMP AND ALLUVIUM)
PROVO (P) AND BONNEVILLE (B) DEEP - WATER FACIES	LITTLE VALLEY LACUSTRINE CYCLE DEPOSITS
POST-STANSBURY TRANSGRESSIVE FACIES OVERLYING STANSBURY REGRESSIVE AND SHORELINE FACIES	<b>TERTIARY</b>
STANSBURY DEEP - WATER FACIES (C=CHAROPHYTES PRESENT)	SALT LAKE GROUP
STANSBURY TRANSGRESSIVE FACIES	

Location of fault picks (seismic line PFSF-98-A); arrows show relative sense of slip; faults in red displace Qp unconformity

- Notes**
- n1 0.7 m (2.3 ft) down-to-the-west vertical separation of the Qp unconformity between C-30 and C-18.
  - n2 0.5 m (1.7 ft) down-on-the-west vertical separation of top of sand unit (Stansbury Transgressive Facies).
  - n3 ~0.66 m (2.2 ft) down-on-the-east vertical separation of top of sand unit (Stansbury Transgressive Facies).
  - n4 Contact was not identified in borings C-28 and C-29.
  - n5 Top of clayey silt marker bed.
  - n6 Top of clayey silt with abundant ostracodes.
  - n7 Thin (<2 cm) clay marker bed.
- Location of cross section, boreholes, testpits, and trench shown on Plate 1.

**PLATE 2**  
**CROSS-SECTION D-D' SHOWING STRATIGRAPHY INFERRED FROM BOREHOLE DATA ACROSS SITE**

*K. L. Hanson and others: Probabilistic Fault Displacement Hazard Analysis  
 A Case Study from Skull Valley, Utah  
 Basin and Range Province Seismic Hazards Summit II, 2004*

## ***A MULTIDISCIPLINARY APPROACH TO SEISMIC HAZARD IN THE RENO-CARSON METROPOLITAN REGION***

Feng Su, John G. Anderson, and Aasha Pancha  
Seismological Laboratory/ms174  
University of Nevada-Reno  
Reno, Nevada 89557  
Phone: 775-784-4975  
Fax: 775-784-4165  
feng@seismo.unr.edu

### **ABSTRACT**

In this study, we have conducted a multidisciplinary approach to seismic-hazard analysis in the Reno-Carson metropolitan region using geodetic, geological, and seismological inputs. The Reno-Carson region is the second most populous area in Nevada and lies in one of the most seismically active parts of the state. Rates of deformation in the region have very large uncertainties. Currently available geodetic, geological, and seismological data disagree significantly. To investigate the impact and uncertainty in hazard estimates resulting from these differences, we have developed a set of seismic source models based on independent geodetic, geological, and seismological inputs and calculated probabilistic seismic hazards for each of these models. We then compare these results with USGS National Seismic Hazard Map estimates (1996, 2002) for this region. Our results indicate that geodetic input predicts the highest hazard. For example, in downtown Reno at an annual occurrence rate of about 0.002/yr (1/500 yr), the USGS hazard curve shows a peak acceleration of about 0.33g, but our geodetic model predicts 0.43g, which is 30% higher than the USGS result.

### **INTRODUCTION**

The Reno-Carson metropolitan area is the second most populated region in Nevada. It lies in one of the most seismically active parts of the state. Thirteen earthquakes of magnitude 6 or greater have occurred in the region since 1850 (dePolo and others, 1997). While the region has been seismically active in historic time, recent seismicity has been low. The study region lies within the Basin and Range Province, which extends from the rigid Sierra Nevada block in the west to the Colorado Plateau in the east. Geodetic measurements show concentrated deformation at the eastern and western edges of the Basin and Range, with little deformation in between (Thatcher

and others, 1999). Part (about 25%) of the Pacific-North American relative plate motion is taken up by displacement and deformation in the Basin and Range Province. Along the western edge of the Basin and Range, geodesy shows a widening of the deformation zone from south to north (Figure 1). Motion west of about 118°W is approximately parallel to the Pacific Plate motion vector (Thatcher, 1999; Bennett and others, 2003; Hammond and Thatcher, 2004), suggesting coupling of the plate motion. The Sierra Nevada behaves as a block, and moves northwest at about 13 mm/yr. Motions east of the Sierra Nevada Range between 118° W and 120° W are approximately parallel to the motion of the Sierras (Thatcher and others, 1999). Relative motion,

oriented N37°W ± 2°W, between the Sierra Nevada Great Valley and central Great Basin regions occurs at a rate of 9.3 ± 0.2 mm/yr (Bennett *and others*, 2003). The greatest deformation takes place across a zone of conjugate strike-slip and normal faults, at a rate of 12.5 ± 0.15 mm/year between 119.1°W and 120.2°W. More recent data confirm this observation, with velocities west of 117.7°W increasing from ~1 mm/yr to ~12 mm/yr (Bennett *and others*, 2003; Hammond and Thatcher, 2004). This high velocity gradient implies high seismic risk, and increases the potential for more frequent damaging earthquakes. Other recent publications, such as Dixon and others (2000), Wernicke and others (2000), Cashman and Fontaine (2000), dePolo and others (2001), Svarc and others (2002), Oldow (2003), and Unruh and others (2003) also provide insight on deformation rates in the region. Geological slip rates are not well known for the study region, with many faults uncharacterized. The inferences from geodetic data suggest the greatest deformation rates compared to those from either seismicity or geology.

In this study, we have conducted a multidisciplinary approach to seismic-hazard analysis in the area using independent geodetic, geological, and seismological inputs. By comparing results from this wide range of independent models, we hope to better understand the uncertainties and the consequences of these uncertainties for the probabilistic seismic hazard of the area.

## METHOD

According to Gutenberg-Richter's frequency-magnitude relation, the number of seismic events with magnitude between  $M-dM/2$  and  $M+dM/2$  is given by  $n(M)dM$ , where  $n(M)=10^{a-bM}$ .

The moment rate  $\dot{M}_0$  is related to the earthquake-occurrence rate by

$$\dot{M}_0 = \int_{-\infty}^{\infty} M_0 n(M) dM = \int_{-\infty}^{\infty} M_0 10^{a-bM} dM \quad (1).$$

Using the moment-magnitude relation

$$M_0 = 10^{1.5M+c} \quad (2).$$

where  $c$  is a constant. This study uses  $c=16.095$  (cgs units) as defined by Hanks and Kanamori (1978).

Substitute (2) into (1), we obtain

$$\begin{aligned} \dot{M}_0 &= \int_{-\infty}^{\infty} 10^{1.5M+c+a-bM} dM = \int_{-\infty}^{\infty} 10^{a+c+(1.5-b)M} dM \\ &= \frac{10^{a+c}}{(1.5-b)\ln 10} 10^{(1.5-b)M} \Big|_{M_{\min}}^{M_{\max}} \end{aligned} \quad (3).$$

For  $b < 1.5$

$$\dot{M}_0 \approx \frac{10^{a+c+(1.5-b)M_{\max}}}{(1.5-b)\ln 10} \quad (4).$$

Equation (4) is the same as the result from Anderson (1979).

According to Ward (1994, 1998a, b) the minimum geodetic moment rate in a region can be estimated using the maximum eigenvalue of a 2-D strain-rate tensor, i.e., the principle surficial extension and contraction rates:

$$\dot{M}_0 = 2\mu A H_s \text{Max}(|\dot{\epsilon}_1|, |\dot{\epsilon}_2|) \quad (5).$$

where  $\dot{\epsilon}_1$  and  $\dot{\epsilon}_2$  are the principle surficial extension and contraction rates,  $A$  is the surface area and  $H_s$  is the seismogenic thickness of the region.

Assuming the  $b$  value and the maximum magnitude  $M_{\max}$  for the region, we can then estimate the  $a$  value for a given seismic-moment-rate distribution. The result is given by

$$10^a = \dot{M}_0 (1.5-b)\ln 10 / 10^{c+(1.5-b)M_{\max}} \quad (6).$$

## ANALYSIS AND RESULTS

Figure 2 shows the distribution of faults in Nevada and eastern California, with faults color coded by activity rate. These faults are used in the calculation of the USGS 2002 National Hazard Maps. Our focus area is outlined by the box. The orientation of the box is chosen so that it is consistent with the orientation of stresses in the region. From the figure we can see this area

contains some of the most active faults of the state, as shown by their color.

For the geodetic data, we have collected GPS data from the USGS at web site <http://quake.wr.usgs.gov/research/deformation/gps/auto/CL.html>, from Kreemer and others (2000, 2003), Blewitt and others (2002), Bennett and others (2003), and Blewitt and Coolbaugh (personal communication). In a recent work, Blewitt and others (2002) built a geodetic velocity database containing GPS, Satellite Laser Ranging and Very Long Baseline Interferometry data obtained across the Basin and Range from more than 42 studies. We have used their inverted strain-rate field data to obtain a geodetic-moment rate using Ward's approach (Equation 5). To compute probabilistic seismic hazard maps using geological and historical seismicity models, we have followed the method used by USGS in their National Seismic Hazard Map generation.

Figure 3 plots the calculated hazard curves from each of these different hazard models and compares them with the hazard curve from USGS National Hazard Maps for downtown Reno. We can see the hazard curve obtained from geology faults, historical seismicity, and GPS are all very different, with the GPS data giving the highest hazard estimation.

The current USGS maps use a hybrid of geological, geodetic, and seismic history data. The hazard curve from USGS National Hazard Maps is higher than the seismicity and geological estimates, but lower than that from geodesy alone. For example, at an annual occurrence rate of about 0.002/yr (1/500 yr), the USGS hazard curve shows a peak acceleration of about 0.33g, but our geodetic model predicts 0.43g, which is 30% higher than the USGS result. At an annual occurrence rate of about 0.0004/yr (1/2500 yr), the peak acceleration from the USGS model is about 0.60g, but from our geodetic model it is about 0.70g, which is about 17% higher than the USGS result.

We have also calculated the moment rate in this region based on geodetic, geological, and seismicity inputs. The moment rate is about  $0.83 \times 10^{25}$  dyne-cm/yr from seismicity and about  $0.37 \times 10^{25}$  dyne-

cm/yr from faults. Since our region is about 334 km long, this is equivalent to a through-going, strike-slip fault with a displacement rate of 2 mm/yr. The moment rate calculated based on maximum shear strain in this region is about  $2.7 \times 10^{25}$  dyne-cm/yr. So, according to GPS data, the relative shear in the region is much greater. We take this as an indication that so far, the geological mapping is not sufficiently complete to associate all of the plate motion with faults.

## DISCUSSION AND CONCLUSION

A challenge facing seismic-hazard assessment in the Reno-Carson area is the inconsistency among the seismic-moment rates estimated using geodetical, geological, and historical seismicity data. This inconsistency may be due to the lack of information regarding historical seismicity and paleoseismic data in this area. Under this hypothesis, GPS data has the advantage in that it can provide information on deformation within the network even if that activity occurs on faults that are unknown, too slowly slipping, or too deep to study by traditional methods. On the other hand, there are questions regarding how much the GPS data might be affected by transient behavior that follows past large earthquakes. Since geodesy, geology, and historical seismicity each provide a different view of the regional deformation, inconsistencies or consistencies among the results from different approaches will reveal new insights into the seismic hazard of this region. Based on present geodetic data, current seismic hazard for Reno may be underestimated.

The curves shown in Figure 3 present a preliminary result. Further studies will involve sensitivity tests. For instance, for the GPS data, there is the non-uniqueness and uncertainty involved with converting surface strain to a scalar-moment rate. Currently, there are several techniques for this in the literature. We have followed Ward's approach, which provides a minimum estimate of the geodetic-moment rate in the region. In addition, we have used an underdamped version of the

geodetic strain field. Further understanding of the geodetic data is required to identify where strain may be poorly predicted due to lack of station coverage.

## ACKNOWLEDGMENTS

We thank Dr. David Von Seggern and Bill Lund for their careful review and valuable comments. This work is supported by USGS grant 02HQGR0060.

## REFERENCES

- Anderson, J. G., 1979, Estimating the seismicity from geological structure for seismic-risk studies, *Bull. Seism. Soc. Am.*, 69, 135-158.
- Bennett, RA, Wernicke, BP, Niemi, NA, Friedrich, AM, Davis, JL, 2003, Contemporary strain rates in the northern Basin and Range province from GPS data, *Tectonics* 22, Is 2, Article 1008, 31 pg.
- Blewitt, G., Coolbaugh, M., Holt, W., Kreemer, C., Davis, J. and Bennett, R., 2002, Targeting of potential geothermal resources in the Great Basin from regional relationships between geodetic strain and geological structures, *Transactions Geothermal Resources Council*, Vol. 26, p. 523-526.
- Cashman, P. H. and Fontaine, S. A., 2000, Strain partitioning in the northern Walker Lane, western Nevada and northeastern California, *Tectonophysics* 326, 111-130.
- dePolo, C. M., J. G. Anderson, D. M. dePolo, and J. G. Price (1997). Earthquake occurrence in the Reno-Carson city urban Corridor, *Seismological Research Letters*, 68, p. 401-412.
- dePolo, C. M., A. R. Ramelli, R. H. Hess and J. G. Anderson, 2001, Reevaluation of pre-1900 earthquakes in western Nevada, Final Technical Report to NEHRP, Grant 99HQGR0083, Nevada Bureau of Mines and Geology, University of Nevada, Reno.
- Dixon, T. H., Miller, M., Farina, F., Wang, H., Johnson, D., (2000). Present-day motion of the Sierra Nevada block and some tectonic implications for the Basin and Range Province, North American Cordillera, *Tectonics*, vol.19, no.1, pp.1-24, Feb 2000.
- Hammond, W. C., and W. Thatcher (2004), Contemporary tectonic deformation of the Basin and Range province, western United States: 10 years of observation with the Global Positioning System, *J. Geophys. Res.*, in press.
- Hanks, T. C., and H. Kanamori, 1978, A Moment Magnitude Scale, *J. Geophys. Res.*, 84, 2348-2350.
- Kreemer, C., Haines, J., Holt, W. E., Blewitt, G. and D. Lavallee, 2000, On the determination of a global strain rate model, *Earth, Planets Space*, 52, 765-770.
- Kreemer, C., Holt, W. E. and J. Haines, 2003, An integrated global model of present-day plate motions and plate boundary deformation, *Geophys. J. Int.*, 154, 8-34.
- Oldow, JS, (2003). Active transtensional boundary zone between the western Great Basin and Sierra Nevada block, western US cordillera, *Geology* 31, 1033-1036.
- Svarc, JL; Savage, JC; Prescott, WH; Ramelli, AR., 2002, Strain accumulation and rotation in western Nevada, 1993-2000. *Journal Of Geophysical Research-Solid Earth*107 (B5): art. no.-2090.
- Thatcher, W., G. R. Foulger, B. R. Julian, J. Svarc, E Quilty and G. W. Bawden (1999). Present day deformation across the Basin and Range province, western United States, *Science* 283, 1714-1718.
- Unruh, J, Humphrey, J, Barron, A (2003). Transtensional model for the Sierra Nevada frontal fault system, eastern California, *Geology* 31, 327-330.
- Ward, S. N. (1994). A multidisciplinary approach to seismic hazard in Southern California, *Bull. Seism. Soc. Am.*, 84, 1293-1309.
- Ward, S. N. (1998a). On the consistency of earthquake moment rates, geological fault data,

and space geodetic strain: the United States, *Geophys. J. Int.*, 134, 172-186.

Ward, S. N. (1998b). On the consistency of earthquake moment rates, geological fault data, and space geodetic strain: Europe, *Geophys. J. Int.*, 135, 1011-1018.

Wernicke, B., A. Friedrich, N. A. Neimi, R. A. Bennett, J. L. Davis (2000). Dynamics of plate boundary fault systems from Basin and Range geodetic network (BARGEN) and geologic data, *GSA Today*, 10, No. 11, Nov. 2000, 1-7.

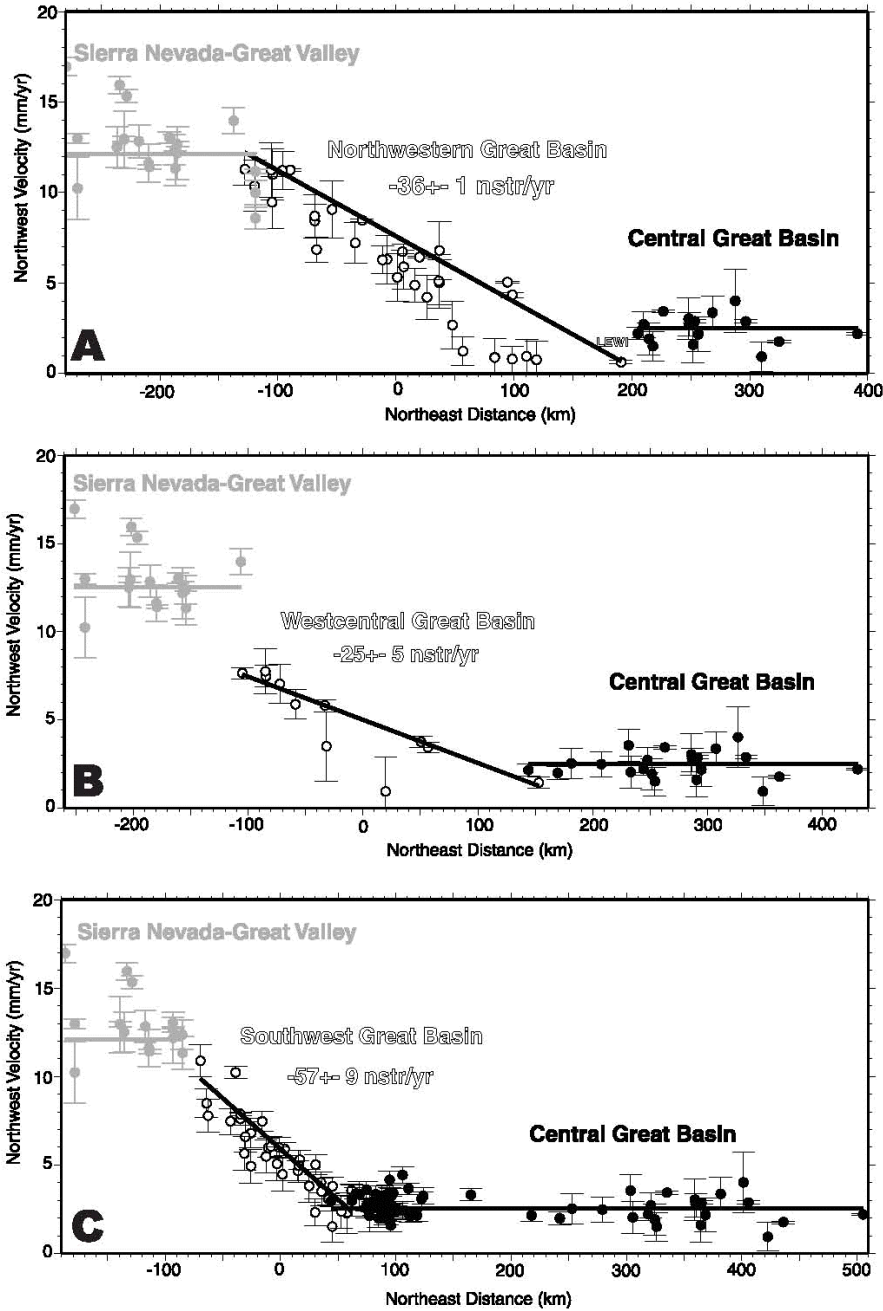


Figure 1: Reproduced from Figure 14 of Bennett and others (2003). (a)  $N37^{\circ}W$  components of velocity as a function of  $N53^{\circ}E$  distance for the Sierra Nevada Great Valley (gray circles), northwestern Great Basin (open circles), and central Great Basin (solid circles) domains. Velocities refer to the North America reference frame. Error bars represent 1 standard deviation. The lines show the block-strain model. Zero slopes indicate the region is not internally deforming. (b) Same as for figure 1a but for west central Great Basin domain. (c) Same as for figure 1a but for southwestern Great Basin domain.

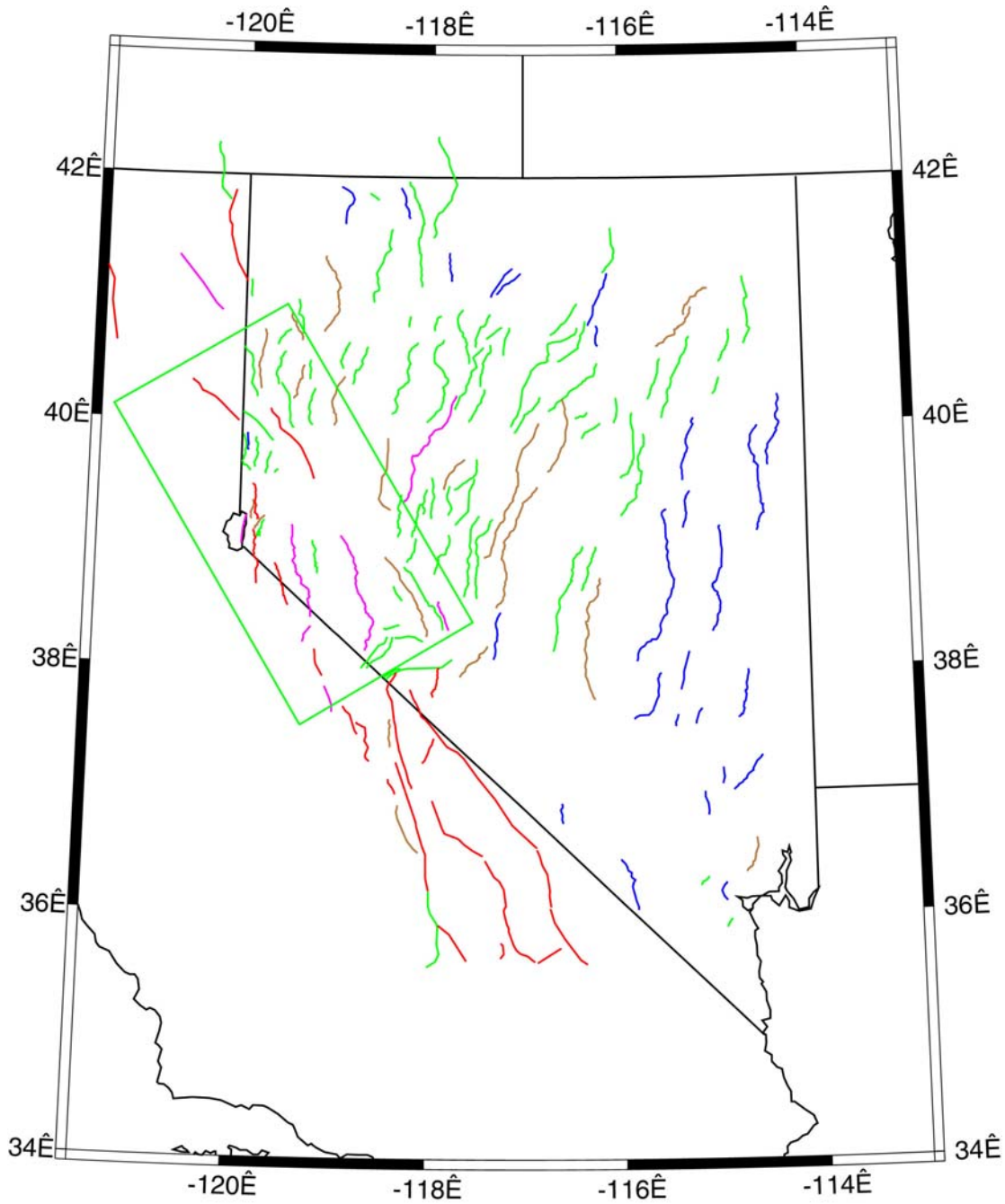


Figure 2: Map of faults in Nevada and eastern California used in the USGS 2002 hazard maps calculation. Faults are color coded by slip rate  $r$ . Red for  $r > 0.6$  mm/yr, Purple for  $0.3 < r < 0.6$  mm/yr; Brown for  $0.1 < r < 0.3$  mm/yr; Green for  $r = 0.1$  mm/yr and Blue for  $r < 0.1$  mm/yr. The box indicates our study region.

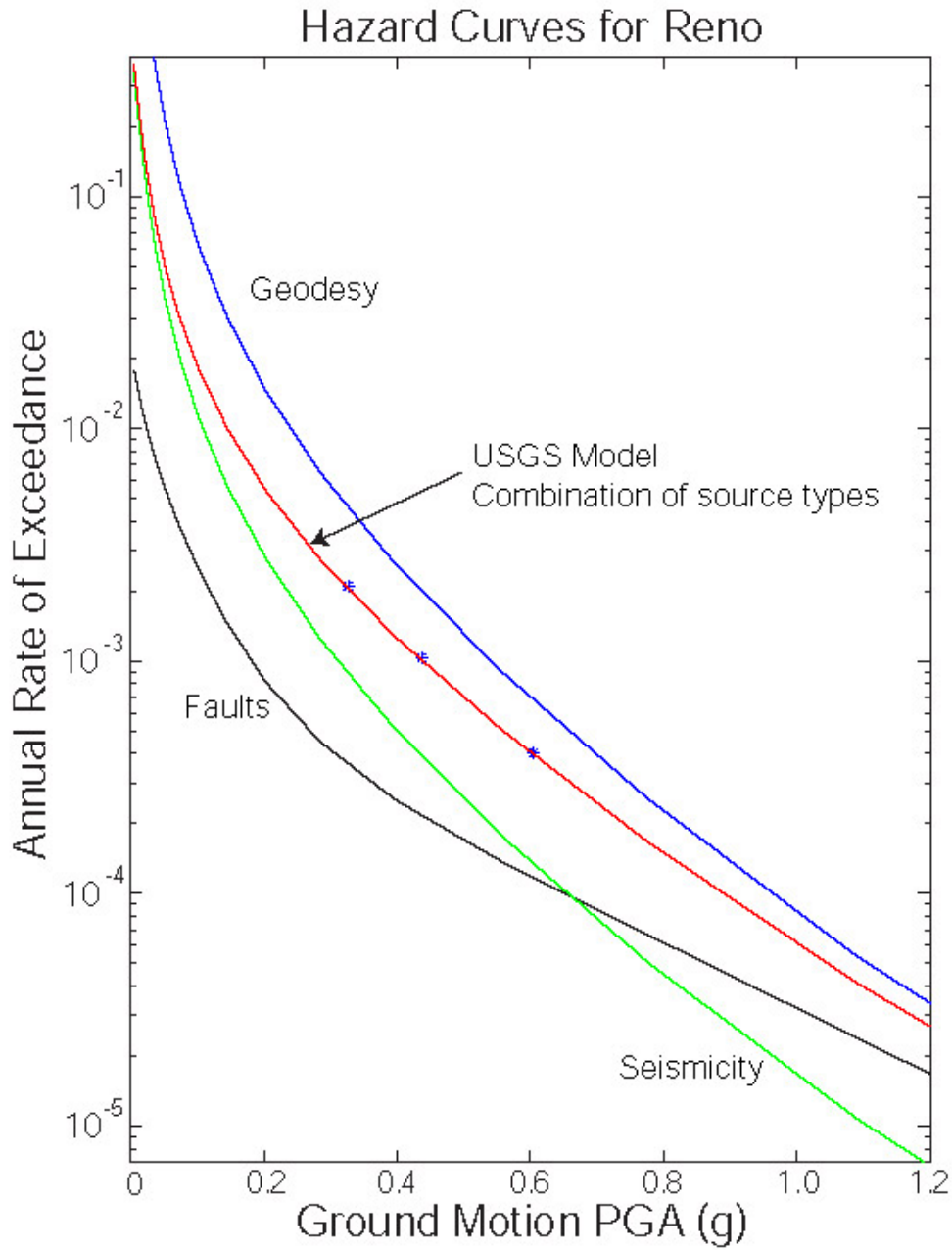


Figure 3: Plot of the seismic hazard curves we calculated in downtown Reno using different hazard models. The green line is calculated from seismicity. The black line is from faults, and blue line is from geodetic input. The red line is from USGS national hazard model.

## **ACTIVE TECTONICS OF THE NEPHI SEGMENT, WASATCH FAULT, UTAH**

Christopher B. DuRoss\* and Ronald L. Bruhn  
Department of Geology and Geophysics, University of Utah  
Salt Lake City, UT 84112

\**current address:* Utah Geological Survey, Salt Lake City, UT 84114

### **ABSTRACT**

The Nephi segment is the southernmost segment of the Wasatch fault known to have ruptured multiple times in the Holocene. The segment is divided into two fault strands separated by a step-over and connecting fault in bedrock: the 25-km-long Nephi strand and the 17-km-long Santaquin strand. In this study we have constrained the short- (Holocene) and long-term (Late Pleistocene) slip rates and history of paleoearthquakes on the Nephi segment by integrating the geometry and extent of surface faulting, fault-scarp diffusion modeling, and existing paleoseismic data.

The preferred rupture chronology, based on scarp-diffusion modeling and trench data, includes at least six paleoearthquakes on the Nephi segment since the latest Pleistocene (~12 ka). Two earthquakes ruptured the entire segment at 10-15 ka and ~5.2-7.0 ka, followed by four partial ruptures during the Holocene. The Nephi strand ruptured at ~3.9-4.0 ka and 1.0-1.4 ka, and the Santaquin strand ruptured at 2.0-3.0 ka and 0.4-0.6 ka.

Based on the preferred rupture scenario, the segment has ruptured with paleoearthquakes of magnitude 6.5 - 7.1 every 1.6 kyr since the mid-Holocene (~7 ka) and every 5.4 kyr from ~7 ka to the latest Pleistocene (~12 ka). The average recurrence interval is ~9.0 kyr from ~12-53 ka, using a mean vertical displacement per event of  $1.8 \pm 0.4$  m. The vertical slip rate for the Nephi segment, based on closed seismic cycles, is 0.5-0.7 mm/yr since the mid-Holocene (<7 ka), 0.3-0.4 mm/yr from the mid-Holocene to latest Pleistocene (~12 ka), and 0.2 mm/yr from the latest Pleistocene to Late Pleistocene (~53 ka).

The youngest ruptures on the Santaquin strand (mean event timing: ~0.5 and ~2.6 ka) may have been accompanied or triggered by faulting along the Provo segment to the north, evidenced by the moderate rupture lengths (southern 6.5 km of the 17-km-long Santaquin strand) and vertical displacements (1-2 m), and the similarity in the timing of those events with the youngest Provo segment events (~0.6 ka and ~2.8 ka). For the Nephi segment, the increased frequency of paleoearthquakes in the Holocene may indicate the temporal clustering of earthquakes and is important for assessing the seismic-hazard potential of the Wasatch fault. This study has helped resolve the timing of surface ruptures on the Nephi segment, and contributes to an understanding of Late Pleistocene to present spatial and temporal variability of paleoearthquakes on the Wasatch fault.

### **INTRODUCTION**

Fault ruptures are the surface expression of the dislocation or mechanical failure of rock along a fault plane at depth. Spatial patterns of surface faulting reflect the geometry of slip on the fault plane, and temporal patterns indicate the rate at

which stress accumulates to some critical level inducing rupture, or the behavior of the seismogenic cycle. Together, the spatial and temporal rupture trends have important implications for the segmentation of fault systems and recurrence of large slip events, or paleoearthquakes. Where the fault surface rupture displaces unconsolidated

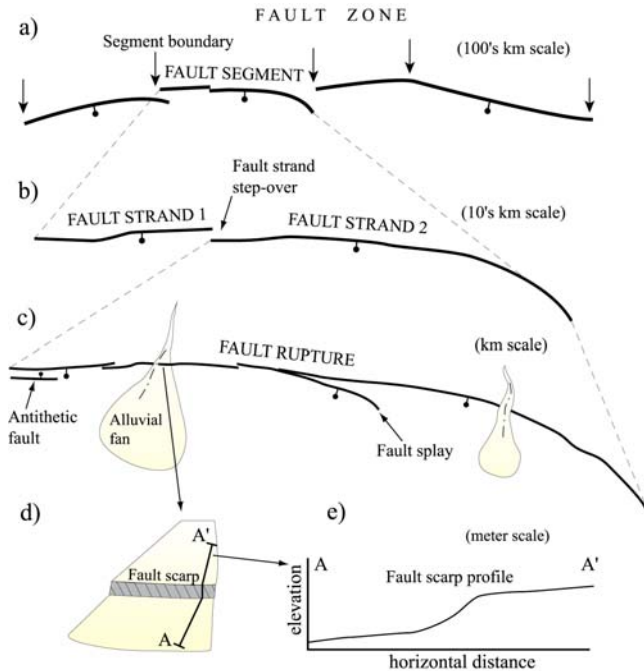


**Figure 1.** Schematic map traces of normal faults at various scales, indicating the scaling relations and descriptive terminology for a) a normal fault zone, consisting of individual fault segments and segment boundaries, b) two fault strands of an individual fault segment, c) surface ruptures along one of the fault strands, d) a fault scarp where the surface rupture displaces an alluvial-fan deposit, and e) a fault-scarp profile measured normal to the fault scarp.

surface deposits (e.g., alluvial-fan deposits), a fault scarp is formed (Figure 1). Fault trenches excavated normal to the scarp reveal the number, timing, and size of surface-faulting earthquakes at the site, but have a limited spatial and temporal window. Alternatively, along-strike observations of fault surface ruptures (e.g., Nelson and Personius, 1993) provide insight into the behavior and distribution of slip along the entire length of the fault, but are restricted in their ability to identify individual surface-faulting earthquakes. Thus, to identify and understand the complete rupture history of an active fault, including the spatial and temporal components, meter- to kilometer-scale rupture and scarp analyses must be used in concert with centimeter- to meter-scale fault-trench studies.

The Nephi segment of the Wasatch fault is an excellent example of a fault with sparse trench data and an extensive but underutilized record of latest Quaternary surface ruptures. The segment is one of

the most active segments of the Wasatch fault, with composite fault scarps (formed from multiple rupture events; Wallace, 1977) recording up to 27 m of vertical displacement over tens of thousands of years (Mattson and Bruhn, 2001). Despite the long record of earthquakes preserved along the fault trace, trench studies have identified only three broadly constrained Holocene paleoearthquakes on the southern part of the Nephi segment (Hanson and others, 1981; Jackson, 1991), supporting the need for regional morphologic scarp analyses.

In this study, we present geological observations from the Nephi segment, and characterize the extent, geometry, timing, displacement, and rate of slip of fault ruptures by analyzing scarps on Late Pleistocene and Holocene unconsolidated alluvium. Elucidating the pattern and timing of slip on the Nephi segment will lead to a more complete understanding of fault segmentation and earthquake recurrence at different scales in space and time, while allowing for a more accurate delineation of the fault and earthquake hazards along a major Basin and Range normal fault.

## Wasatch Fault

The Wasatch fault is a regionally extensive, segmented normal fault extending from southern Idaho to central Utah forming the physiographic boundary between the Middle Rocky Mountains and Colorado Plateau to the east, and the 750-km-wide northern Basin and Range Province to the west (subdivided into the west, central and east Great Basin sub-provinces; Bennett and others, 2003) (Figure 2). The fault accommodates approximately  $2.7 \pm 1.3$  mm/yr of east-west horizontal motion based on geodesy (Martinez and others, 1998), and  $\sim 1.0$  mm/yr of vertical motion based on fault trench studies (Machette and others, 1992), due to westward motion of the central Great Basin sub-province (2.8 mm/yr relative to the Colorado Plateau; Bennett and others, 2003; Figure 2). The fault consists of 10 individual segments (Figure 3), each capable of generating large magnitude earthquakes ( $M$  7-7.5) with accompanying surface faulting (Machette and others, 1992). The segments

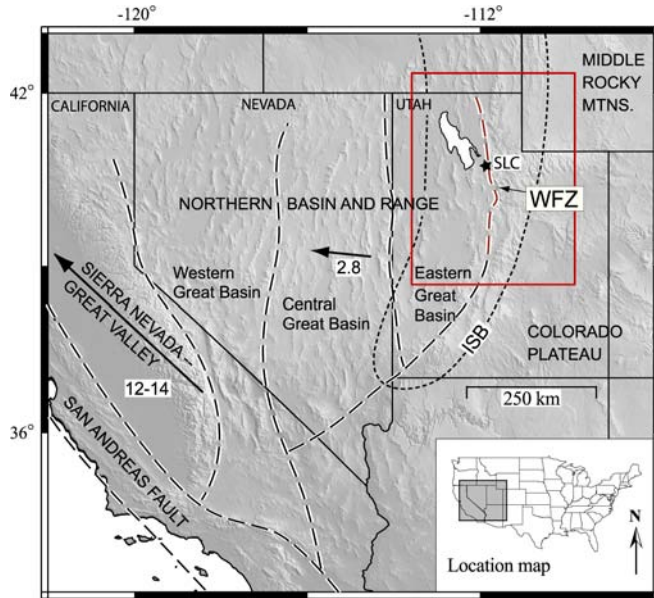


**Figure 2.** Physiographic and geodetic provinces of the southwestern United States. Provincial outlines (black and white long-dashed lines) from Bennett and others (2003). Arrows indicate horizontal velocity (mm/yr) and azimuth based on geodetic data (Bennett and others, 2003). WFZ - Wasatch fault zone. ISB - Intermountain seismic belt (Smith and Sbar, 1974). Box indicates location of Figure 3

are on average 33 km long (Machette and others, 1992), with segment boundaries based on the timing of Holocene surface ruptures, and the local and regional fault structure and surface rupture geometry (Swan and others, 1980; Schwartz and Coppersmith, 1984; Machette and others, 1991, 1992; Black and others, 2003). Only the five central segments, from north to south: Brigham City, Weber, Salt Lake City, Provo, Nephi, have evidence of multiple Holocene surface-faulting earthquakes (Schwartz and Coppersmith, 1984; Machette and others, 1991, 1992) (Figure 3). The five segments are on average 45 km long with paleoearthquakes having an average displacement of ~2 m and recurring every 1.2-2.6 ka during the Holocene (Schwartz and Coppersmith, 1984; Machette and others, 1991, 1992; McCalpin and Nishenko, 1996). The average vertical slip rate, based on up to five separate ruptures on each of the five segments since 7.5 ka ranges from 1.1-1.4 mm/yr (Machette and others, 1991, 1992; McCalpin and Nishenko, 1996; Friedrich and others, 2003;

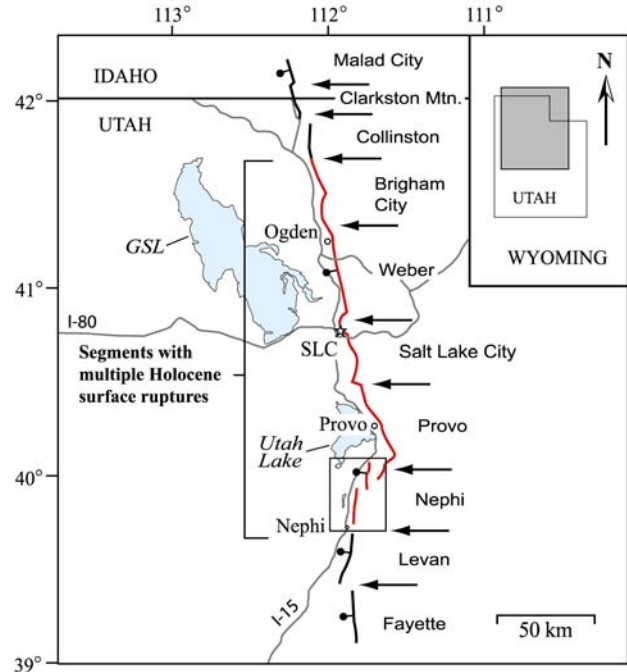


**Figure 3.** Segments of the Wasatch fault (heavy lines), after Machette and others (1992). Large arrows indicate segment boundary locations. GSL - Great Salt Lake. Box indicates location of Figure 4.

Lund, in press). In contrast, the long-term, Late Pleistocene to present slip rate is approximately 0.1-0.3 mm/yr, based on displaced sediments and geomorphic features associated with the Bonneville and Little Valley lake cycles and the Bull Lake glacial period (Scott and others, 1983; Oviatt and others, 1987, 1992; Machette and others, 1992; Hancock and others, 1999; Friedrich and others, 2003).

### Nephi Segment of the Wasatch Fault

The Nephi segment is an active segment of the Wasatch fault with multiple latest Quaternary surface ruptures displacing unconsolidated alluvial-fan and landslide deposits, and bedrock. Immediately northeast of the Nephi segment and separated by a 7.5-9 km right step (Figure 4), the 60-km-long trace of the Provo segment has evidence for three surface-faulting earthquakes since 5.5 ka (Lund and others, 1991; Machette and others, 1992; Lund and Black, 1998). The paleoearthquake activity of the Provo segment is

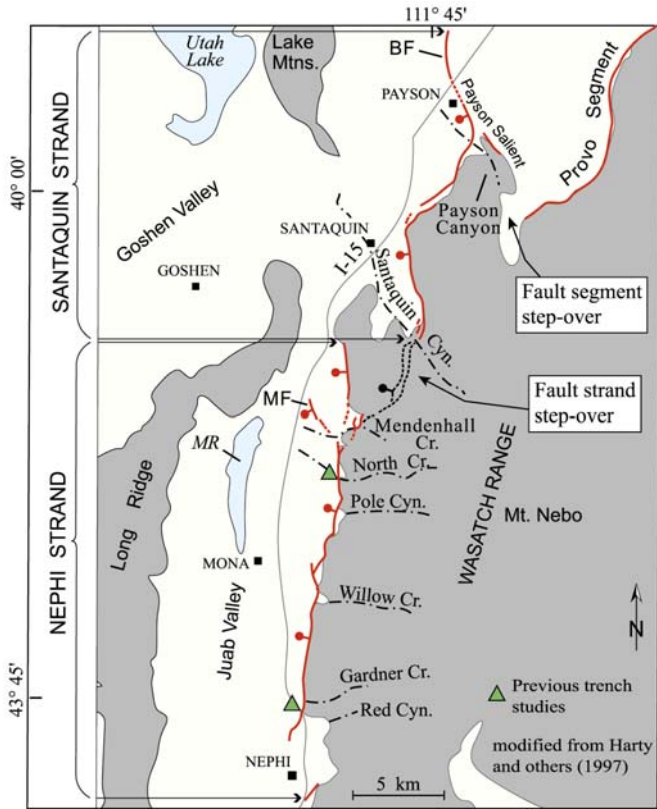


**Figure 4.** Nephi segment of the Wasatch fault, divided into the Nephi and Santaquin strands. Gray area represents mountainous regions; yellow indicates unconsolidated deposits. Dashed and dotted lines denote major drainages; red line is Wasatch fault with ball and bar on downthrown side. BF – Benjamin fault, MF – Mendenhall fault, MR – Mona Reservoir. Modified from Harty and others (1997).

significant as it potentially contributes to the loading of the Nephi segment (Chang, 1998; Chang and Smith, 2002). A 5-km-long gap in surface faulting (since the latest Pleistocene) separates the southern boundary of the Nephi segment from the Levan segment to the south (Hylland and Machette, 2004). The Levan segment is approximately 33 km long, with evidence for a 20-26-km-long Holocene rupture on the northern part of the segment (Jackson, 1991; Machette and others, 1992), and a possible earlier Holocene event with a minimum rupture length of 15 km on the southern part of the segment (Hylland and Machette, 2004).

The Nephi segment spans 42 km (straight-line distance, tip-to-tip), with fault displacement decreasing to zero north of Payson, and south of Nephi, Utah (Figure 4) (Machette, 1992). The

segment consists of two fault strands that are separated by a connecting fault in bedrock. The Santaquin strand is 17 km long, and includes the 3-6-km-long Benjamin fault to the north. To the south, the Nephi strand is 25 km long, and includes the ~3-km-long Mendenhall fault splay (Figure 4). The two strands correspond with the eastern and western strands of Machette and others (1992).

Diverse methods of investigation have generated various controls on the timing of the three most recent Holocene surface-faulting earthquakes to rupture the Nephi strand. The earthquake chronology is reported here to allow for a comparison with scarp-diffusion results (Table 1). Event timing is based on an analysis of fault-trench data (North Creek, Hanson and others, 1981, 1982; Red Canyon, Jackson, 1991), and radiocarbon results from Pole Canyon (Nephi strand, this study), which bracket the maximum timing of the youngest event. All radiocarbon ages are reported as calendar-calibrated (CALIB 4.4, Stuiver and Reimer, 1993) and soil residence time-corrected ages. The soil residence correction is the subtraction of the sample's estimated inherited age (at the time of burial) from the calendar-calibrated radiocarbon age, following the investigator's recommendation or an estimated 0.2 ka for bulk soil (Machette and others, 1992).

**Table 1.** Timing of the three most recent events on the Nephi strand of the Nephi segment based on fault-trench data.

Event:	Estimated timing:
Paleoearthquake 1	>0.4 ka, and <1.3 ka
Paleoearthquake 2	~3.9-4.0 ka
Paleoearthquake 3	>3.9 ka, and <5.0-5.5 ka

The timing of Paleoearthquake 1 is based on nine maximum limiting ages with a mean of  $1.3 \pm 0.2$  ka from the North Creek and Red Canyon trench sites and a natural exposure at Pole Canyon. A single radiocarbon age from the North Creek trench constrains the minimum timing of the event to  $0.4 \pm 0.1$  ka. McCalpin and Nishenko (1996) found a weighted mean value ( $\pm 2 \sigma$ ) of  $1.1 \pm 0.7$  ka, although the data set included two radiocarbon ages from the Water Canyon trench (Ostenaar, 1990) on

the Provo segment. Application of the Water Canyon trench data to the Nephi segment is not advisable due to the 17 km gap in paleoseismic data (which includes the poorly understood Santaquin strand) between the Water Canyon and North Creek trench sites. Based on fault-scarp morphology, Schwartz and Coppersmith (1984) favor the younger end of the most recent earthquake range (~0.3-0.5 ka), although an event timing of ~1.0 ka is also possible considering the youngest date to provide a maximum time constraint for the event. Lund (in press) indicates a preferred most recent event timing of  $<1.0 \pm 0.2$  ka, based on a review of available paleoseismic data for the Nephi segment.

The timing of Paleoequake 2 is constrained to a maximum of ~3.9 ka from material collected at Red Canyon, and minimum of 1.3-1.6 ka and 3.7-4.3 ka from five samples collected at North Creek. The younger ages may represent a better estimate of the minimum time constraint, based on a majority of younger age results, and a higher confidence placed in the analysis of charcoal vs. bulk soil (Jackson, 1991). However, all five dates constrain the age of a soil horizon above the second-event colluvial wedge, indicating possible contamination due to the incorporation of younger material. If valid, the younger dates may constrain the maximum time for the youngest event, whereas the older ages constrain the minimum time for the second event (Lund, personal communication, 2004). McCalpin and Nishenko (1996) determined a weighted mean event timing of  $3.8 \pm 0.2$  ka, using the minimum limiting age of 4.1 ka and the Water Canyon trench data, which is not suitable for the reasons stated in the discussion of the youngest event timing above. The estimated timing of Paleoequake 2 at ~3.9-4.0 ka reflects the maximum limiting age from Red Canyon and the minimum limiting ages from North Creek; however much uncertainty remains in the timing of the event due to the wide range of minimum limiting dates from North Creek. Lund (in press) reports a preferred timing of  $\sim 3.9 \pm 0.5$  ka for Paleoequake 2.

The time range for the oldest recognized paleoequake (3) on the southern part of the

Nephi segment is not well constrained by the paleoseismic data, which indicate a maximum limiting time between 3.6 and 14.6 ka. The younger date may constrain the timing of the second event (McCalpin and Nishenko, 1996), whereas the older date, based on thermoluminescence, may be erroneously old due to blocks of colluvial material not being reset in the formation of the third event wedge (Machette, personal communication, 2004). The age of an alluvial-fan deposit ( $5.2 \pm 0.3$  ka, Bucknam, 1978) at North Creek, which contains an abandoned terrace possibly related to the third event, is considered to be the best maximum-limiting time constraint for the third paleoequake (Machette, personal communication, 2004); however, a much older event timing is possible based on the age of the latest Pleistocene fan (which contains the third event) at Red Canyon (Jackson, 1991). Lund (in press) reports a preferred time-range of  $>3.9 \pm 0.5$  ka and  $<5.3 \pm 0.7$  ka for the third paleoequake.

## METHODS OF INVESTIGATION

### Fault Scarp Mapping and Surveying

We mapped and surveyed Late Pleistocene and Holocene single- and multiple-event fault scarps at 22 sites along the length of the Nephi segment (Figure 5), collecting over 70 fault scarp profiles (horizontal position and relative elevation) oriented normal to the scarp strike with a laser range finder. The profiles were extended a reasonable distance above and below the scarp to include near-fault surface tilt and disruption and to calculate the upper and lower far-field surface slopes (surface slope above and below the scarp face).

For each scarp profile we determined the vertical displacement, or net vertical tectonic displacement (Swan and others, 1980) using the far-field slopes and average slope on the steepest part of the scarp face (maximum slope angle). The vertical displacement across a scarp profile is the vertical separation of two geomorphic surfaces, measured at the midpoint of a line having a slope defined by the

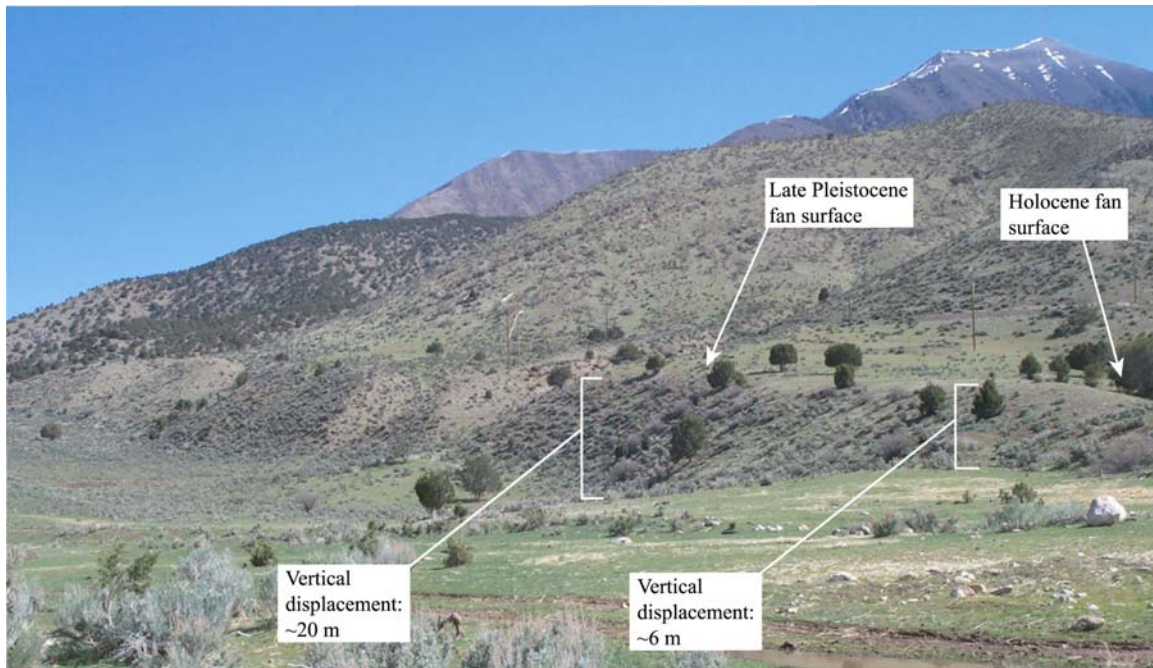


**Figure 5.** Fault scarps near Red Canyon on alluvial-fan surfaces of different ages, and having varying amounts of vertical displacement (after Mattson and Bruhn, 2001). View is to the northeast.

maximum scarp slope and endpoints which intersect the upper and lower far-field slope lines (Figure 6). Vertical displacement is a proxy for fault throw (vertical component of fault slip) for gently dipping surfaces displaced by steeply dipping fault ruptures (Caskey, 1995), although it is not directly correlated with throw due to potential variations in the orientation of the fault plane, surface rupture, or displaced geomorphic surfaces.

Determining the relative ages of different alluvial-fan surfaces is critical to investigate the number and relative ages of scarps on those surfaces. In this study we classified fault-scarp profiles according to the relative ages of the alluvial fan containing them, determined through an analysis of existing Quaternary geologic mapping (Harty and others, 1997) and a qualitative assessment of the fan morphology, aerial extent, cross-cutting relations with adjacent fans, pedogenic carbonate development, vertical stream incision, fault displacement, and relations to shorelines and sediments of the Bonneville lake cycle. Qualitative age ranges for the surfaces are broad (e.g., mid- to

late Holocene), reflecting much uncertainty in the actual ages due to poor absolute age control.

## Numerical Modeling of Fault Scarps

### Diffusion Models

Fault-scarp morphology is used to determine the relative timing of fault displacements (Wallace, 1977) and the timing of the most recent surface-faulting event (e.g., Bucknam and Anderson, 1979; Nash, 1980; Avouac, 1993; Arrowsmith and others, 1998). Morphological analyses of fault scarps use the diffusion equation to model the erosion of fault scarps over time, estimating the time of faulting for a single-event scarp (Hanks, 2000) or the time of initial scarp formation for composite scarps (Mattson and Bruhn, 2001). Diffusion-equation modeling of scarps is an efficient reconnaissance method, based on the premise that the rate of change in elevation of points on the scarp face is a function of the slope curvature and scarp diffusivity constant, which is a function of climate and material properties (Culling, 1963; Nash, 1980; Hanks and

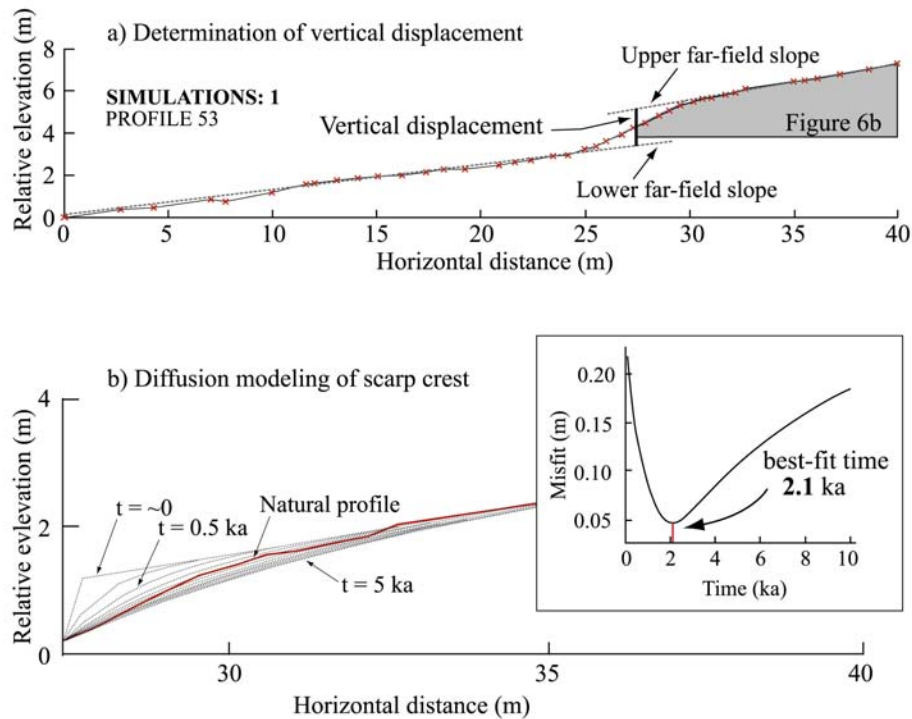


**Figure 6.** Scarp diffusion modeling, based on a) determination of the vertical displacement between upper and lower far-field slopes, and b) isolation of the scarp crest and comparison of the natural profile with synthetic profiles corresponding with specific time steps. The best-fit time, or scarp initiation time, is the time step associated with the synthetic profile having the lowest misfit (average standard deviation) between its points and the points of the natural profile.

others, 1984). Hanks and others (1984) found the product of scarp diffusivity and time to be dependent on scarp height or vertical displacement, which implies nonlinear transport processes.

In this study we used a nonlinear diffusion model (Equation 3, Andrews and Bucknam, 1987) to minimize the effect of vertical displacement on diffusivity. The model includes a nonlinear frictional sliding transport law, in which particles move as a function of weight, energy and velocity, the coefficient of friction, and the slope angle. The nonlinear transport model reduces to a linear transport model at small slope angles. The nonlinear diffusion model is based on the constant-slip-rate model of Mattson and Bruhn (2001), who calibrated their diffusion model with the Bonneville shoreline and known timing of earthquake ruptures from paleoseismic trench sites along the Wasatch and Mercur fault zones. The constant-slip-rate model approximates a multiple-event or composite

scarp by incrementally displacing and eroding an initially planar geomorphic surface at a constant rate through time (Mattson and Bruhn, 2001). We prefer the constant-slip-rate model as it is best applied to scarps younger than ~10 ka with an unknown rupture history.

In using the diffusion equation to model the erosion of scarps on unconsolidated material, we assumed that 1) diffusive processes (e.g., rain splash and soil creep) control sediment transport, 2) material from the scarp crest is transported to the base of the scarp (i.e., conservation of mass), 3) the surface ruptures at the same point in each event, and 4) scarp diffusivity is constant through time (Mattson and Bruhn, 2001). These assumptions are acceptable as a large scarp profile dataset accounts for variability in scarp erosion and vertical displacement, scarp mapping has revealed the surface rupture locations, and uncertainty in the diffusivity constant is considered during the

diffusion modeling. However, caution must be taken in interpreting the results as a potentially variable diffusivity constant (e.g., during the Pleistocene) and the possibility of unrecognized or completely eroded fault scarps may lead to erroneous results.

## Numerical Techniques

The constant-slip-rate, nonlinear diffusion model compares a suite of synthetically generated profiles with the observed, natural scarp profile. We only modeled the upper half of the natural profile (Figure 6) as the lower half is commonly subject to nondiffusive processes such as fan deposition, gullying, surface tilt, and graben formation. The shape of each synthetic profile corresponds to a discrete time since initiation of faulting on a geomorphic surface (Figure 6). The best-fit synthetic profile is defined as the one with minimal misfit between it and the natural profile. In this case, misfit is defined as the standard deviation between the elevation points along natural and synthetic profiles. The time at which surface displacement began on the best-fit synthetic profile is the modeled initiation of scarp formation, or the scarp initiation time.

We accounted for both geologic and instrumentation uncertainty in the diffusion modeling. A Monte Carlo simulation was achieved by running the constant-slip-rate diffusion model through numerous model simulations, with each simulation using a set of random input parameters (e.g., diffusivity) that individually are normally distributed about the preferred parameter value to account for instrumentation and geologic uncertainty. For example, scarp diffusivity varies slightly in each simulation, though when compared across all simulations it will have a mean value of  $2.8 \pm 0.8 \text{ m}^2/\text{ka}$ , which is the value calculated for the Nephi segment by Mattson and Bruhn (2001). Also, in each simulation, the locations (horizontal distance and elevation) of the individual scarp-profile points were allowed to “hover” around the actual, observed locations, using normally distributed random numbers with a mean equal to

the observed value and a standard deviation equal to the instrumentation error of  $\pm 0.05 \text{ m}$ .

Following each simulation, the vertical displacement, best-fit scarp initiation time and slip rate (vertical displacement divided by scarp initiation time) were logged (Figure 7). A typical solution involved 10,000 simulations for a single scarp profile, generating a mean scarp initiation time and mean slip rate ( $\pm 1 \sigma$ ). For a positively skewed distribution of scarp initiation times, we used a trimmed mean in place of the mean. The trimmed mean is the mean of the dataset with the outliers (upper and lower 5% of the data values) eliminated, effectively reducing the positive shift of the mean due to high-valued outliers. The slip-rate values are not reported here, as they are open-ended, incorporating the elapsed time since the most recent event.

## FAULT-SCARP ANALYSIS

### Fault Displacements

We profiled fault scarps on Late Pleistocene and Holocene alluvial fans of four different ages to determine the vertical displacement associated with surface ruptures on the Nephi segment. From oldest (~Late Pleistocene) to youngest (~late Holocene) the fan units include: Af3, Af2o, Af2y and Af1 (after Machette and others, 1992; Harty and others, 1997). Scarp displacement data are grouped according to the four alluvial-fan surfaces, with a fifth group representing single-event scarps due to the most recent surface-faulting earthquake (MRE) (Table 2). Most fault scarps on the Nephi and Santaquin strands indicate vertical displacement of less than 10 m, with a vertical error of  $\pm \sim 0.1 \text{ m}$ . The MRE scarps indicate vertical displacements of  $\sim 2 \text{ m}$ , with each successively older group (not including the Af3 scarps) having an additional  $\sim 2 \text{ m}$  of vertical displacement (i.e., MRE:  $\sim 2 \text{ m}$ , Af1:  $\sim 4 \text{ m}$ , Af2y:  $\sim 6 \text{ m}$ , Af2o:  $\sim 8 \text{ m}$ ) (Table 2). Exceptions include MRE scarps along the Santaquin strand which indicate displacement of  $\sim 1 \text{ m}$  in comparison to  $\sim 2 \text{ m}$  along the Nephi strand. Displacement is

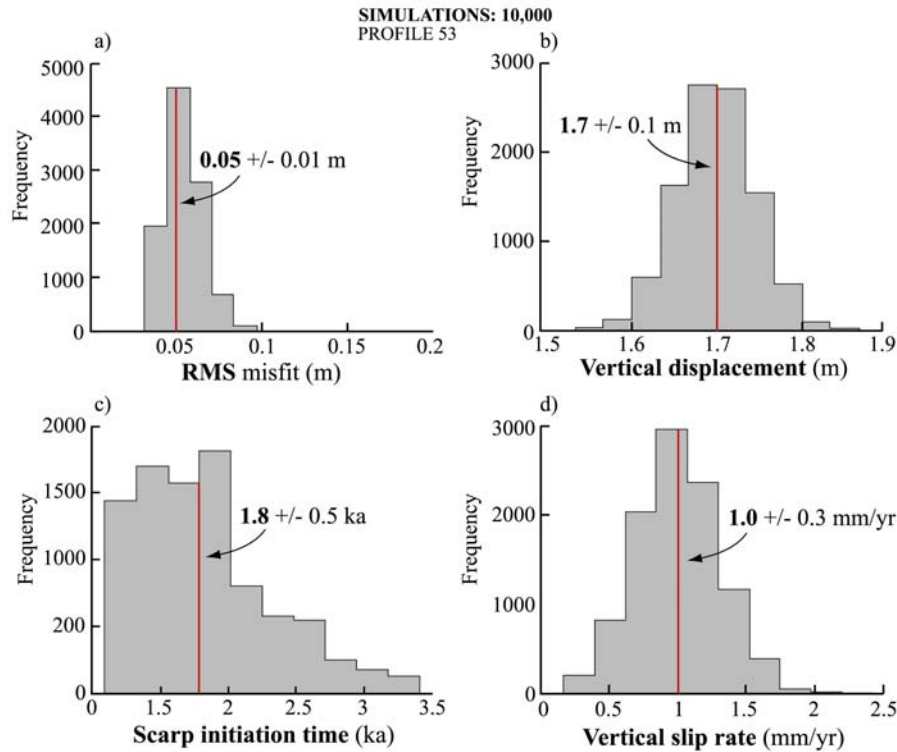


**Figure 7.** Diffusion modeling results from 10,000 simulations of 1 profile. a) Mean of diffusion model misfit values (standard deviation between synthetic and natural profile points), b) vertical displacement between upper and lower far-field slopes, c) trimmed scarp initiation time (upper and lower 5% of data discarded), and d) vertical slip rate. Vertical red line represents mean, or trimmed mean, for c). Values are mean  $\pm 1 \sigma$ .

greatest across the Bonneville shoreline (~10 m), landslide deposits (~11-22 m), and oldest alluvial fans (Af3: ~15-25 m), reflecting a long history of surface faulting during and since the Late Pleistocene.

Faulting is simple and continuous along the southern half of the Santaquin strand and the southern 3/4 of the Nephi strand (Figure 4). At the step-over between the strands the fault geometries are complex with multiple bifurcating faults and variable slip distributions (Figure 8). A relay fault connects the two fault strands and has no evidence for Late Pleistocene or younger slip. Fault displacement, based on fault scarps along the Nephi segment, varies along strike, though it generally decreases toward the fault ends and toward the fault strand step-over (Figure 9). Along the Nephi strand, scarps on successively older fan surfaces have greater cumulative vertical displacements, and

for each of the four youngest scarp groups (i.e., MRE-Af2o) the displacement is similar along strike; however slip decreases toward the strand step-over, especially along the Mendenhall fault. Sparse data on the displaced Af3 surfaces indicate a slight increase in displacement toward the south, although this is possibly the result of slightly older or younger Af3 surfaces having more or less cumulative displacement. On the Santaquin strand, scarps on the youngest fan surface (Af1, MRE) are limited to the southern 6.5 km of the segment, and for the youngest scarps, displacement is similar along strike. Sparse displacement data on the older surfaces suggest a similar pattern of slip, with a maximum toward the south, decreasing slightly toward the north.

## Numerical Analysis

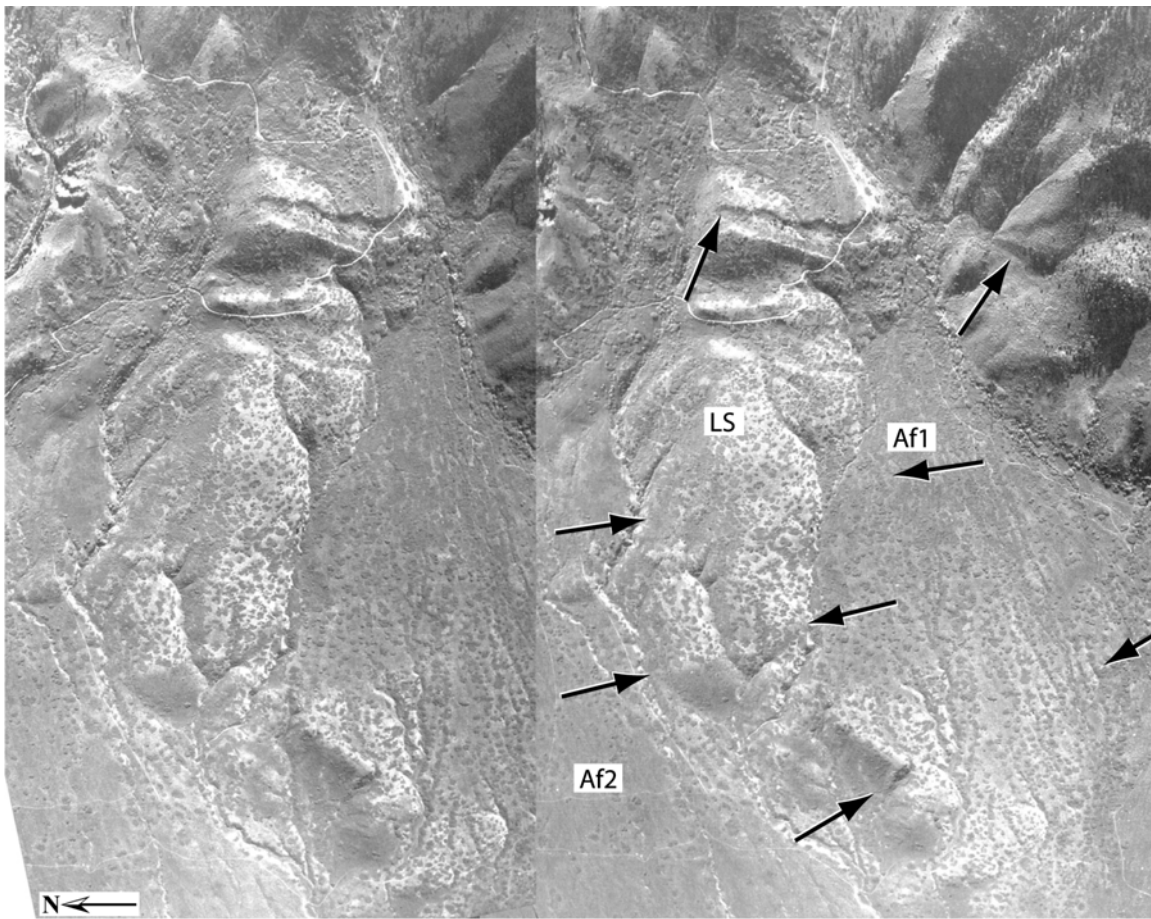


**Figure 8.** Stereo photographs of Wasatch fault scarps adjacent to Mendenhall Creek (Cluff and others, 1973). See figure 4 for location. LS – landslide deposit. Arrows indicate surface ruptures of the Wasatch fault. Scale is approximately 1:12,000.

Diffusion modeling of fault-scarp profiles constrains the time of scarp initiation for fault scarps cutting Quaternary deposits along the Nephi segment. We numerically modeled 38 scarp profiles using the constant-slip-rate diffusion model (Mattson and Bruhn, 2001) to determine the mean scarp initiation time ( $\pm 1 \sigma$ ) for scarps on 1) Late Pleistocene fans (Af3), 2) latest Pleistocene fans (Af2o), 3) mid-Holocene fans (Af2y), and 4) late Holocene fans (Af1), including the MRE (Table 2). The diffusion model misfit is a quantitative measure of the fit between the best-fit synthetic profile and the natural profile, where a lower value indicates a better fit. Misfit values are typically good, ranging between 0.07-0.5 m, and having the greatest resolution on the youngest event scarps (Table 2).

Fault scarps along the Nephi segment initiated between  $\sim 1$ -18 ka and  $\sim 45$ -60 ka. The lack of scarp initiation between  $\sim 18$ -45 ka does not indicate earthquake quiescence during that time, but rather that ruptures during that period occurred on already existing scarps. The mean scarp initiation times for scarps across late Holocene to latest Pleistocene fan deposits along the Nephi strand are  $1.4 \pm 0.5$  ka,  $4.0 \pm 1.5$  ka,  $7.0 \pm 1.4$  ka and  $11.4 \pm 1.9$  ka, respectively (Table 2). The mean scarp initiation times for similar fan deposits along the Santaquin strand are  $0.5 \pm 0.1$  ka,  $2.6 \pm 0.7$  ka and  $13.8 \pm 3.7$  ka (Table 2). Along the entire segment, scarps on Late Pleistocene fan surfaces initiated between 48-59 ka. We did not model scarps on mid-Holocene to latest Pleistocene fan alluvium (Af2y) along the

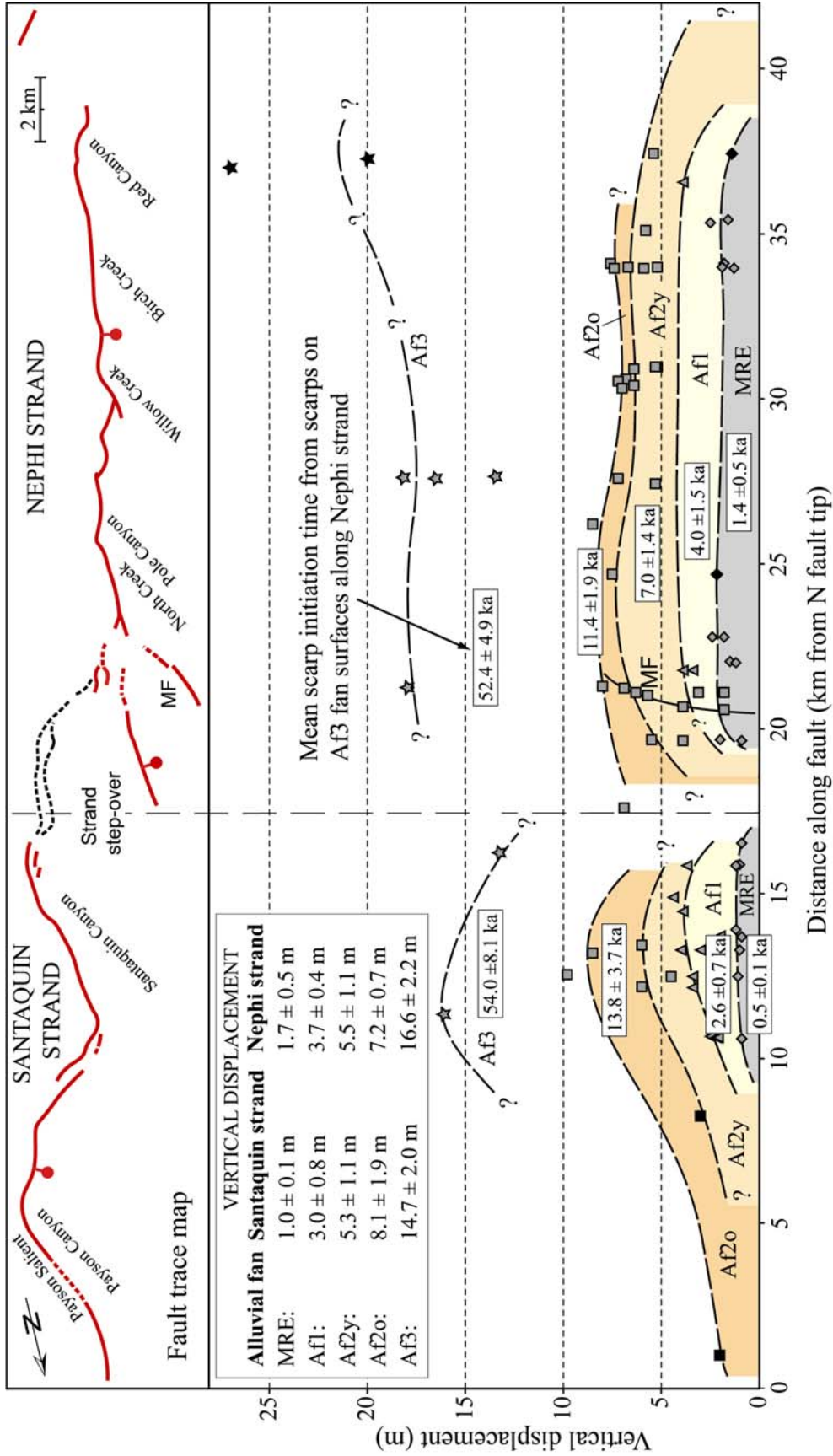


**Figure 9.** Distribution of vertical displacement along the Nephi segment from displaced alluvial-fan surfaces. Gray shapes (e.g., diamonds) and inset chart of vertical displacement data from scarp-profile surveying (this study), black from Hanson and others (1981), Jackson (1991), Machette, (1992), and Mattson and Bruhm (2001). Ages are mean scarp initiation times ( $\pm 1$  s) from scarp diffusion modeling (Table 2). MF - Mendenhall fault.

**Table 2.** Results of scarp-profile surveying and diffusion modeling of fault scarps on the Nephi segment.

Alluvial fan unit <sup>a</sup>	Vertical displacement <sup>b</sup> (m)	n <sup>c</sup>	Scarp initiation time <sup>d</sup> (ka)	Misfit <sup>e</sup> (m)	n <sup>f</sup>
MRE <sup>N</sup>	1.7 ± 0.5	11	1.4 ± 0.5	0.07	5
AF1 <sup>N</sup>	3.7 ± 0.4	2	4.0 ± 1.5	0.11	2
AF2y <sup>N</sup>	5.5 ± 1.1	22	7.0 ± 1.4	0.14	8
AF2o <sup>N</sup>	7.2 ± 0.7	6	11.4 ± 1.9	0.25	4
AF3 <sup>N</sup>	16.6 ± 2.2	4	52.4 ± 4.9	0.48	2
MRE <sup>S</sup>	1.0 ± 0.1	8	0.5 ± 0.1	0.07	5
AF1 <sup>S</sup>	3.0 ± 0.8	14	2.6 ± 0.7	0.09	7
AF2y <sup>S</sup>	5.3 ± 1.1	2	-	-	0
AF2o <sup>S</sup>	8.1 ± 1.9	3	13.8 ± 3.7	0.20	2
AF3 <sup>S</sup>	14.7 ± 2.0	2	54.0 ± 8.1	0.34	2

<sup>a</sup> Scarp profile classification by alluvial fan unit. <sup>N</sup> = Nephi strand, <sup>S</sup> = Santaquin strand.

<sup>b</sup> Mean vertical displacement value ± 1 standard deviation

<sup>c</sup> n is number of scarp profiles used for vertical displacement calculation

<sup>d</sup> Mean scarp initiation time ± 1 sigma, using constant-slip-rate diffusion model (Mattson and Bruhn, 2001)

<sup>e</sup> Misfit is mean diffusion model misfit (standard deviation between points on natural profile and best-fit synthetic profile).

<sup>f</sup> n is number of scarp profiles modeled to determine scarp initiation time and slip rate.

Santaquin strand due to limited fan exposures and nondiffusive scarp erosion (e.g. slumping).

## DISCUSSION

### Numerical Modeling

#### Timing of Scarp Initiation Versus Paleoseismic Data

The timing of scarp initiation calculated for scarps on surfaces of different ages and amounts of displacement provide evidence for the timing of individual rupture events and allow for a comparison with the paleoseismic-trench record. For example, two separate earthquakes may be identified by scarp analyses if one alluvial-fan surface records both ruptures, and a second,

younger fan surface, postdating the earlier rupture, only records the younger event. This model assumes a constant amount of displacement per fault rupture, and a significant period of time between paleoearthquakes during which alluvial fans develop. One potential problem is that an individual rupture may not be individually identified if no geomorphic surfaces predate the event and postdate an earlier event. This may occur if there are periods of little alluvial-fan deposition or if two ruptures occur close in time.

Displacement across the resulting composite scarp would be due to two rupture events, although only the timing of the older event would be estimated by diffusion modeling. As a result, the number of paleoearthquakes would be underestimated and the recurrence interval between events overestimated. Surface-faulting earthquakes on the Nephi segment have a constant amount of slip per event (Schwartz and Coppersmith, 1984) and are temporally spaced by thousands of years (McCalpin and Nishenko, 1996), and we are reasonably certain that the latest Pleistocene and younger ruptures have been individually identified.

### Fault-Rupture Scenarios

Vertical displacement data and information on the timing of scarp initiation from Nephi segment scarp profiles allow for two distinct rupture scenarios, including: 1) simultaneous rupturing of the two fault strands, and 2) synchronous and complete rupturing of both strands, followed by separate, partial ruptures on the fault strands (Table 3). These fault-rupture histories are based on geometric and morphometric analyses of fault scarps on alluvial-fan surfaces of four different ages and a constant amount of slip per event of ~2 m. Earthquake timing represents the mean scarp initiation times for the different alluvial-fan units (Tables 1, 2). Rupture scenario 2 is the preferred model as it honors the scarp profile and diffusion-modeling results and also the paleoseismic data. A third scenario, involving a long history of separate,

**Table 3.** Rupture scenarios for the Nephi segment, including rupture displacement, timing, and recurrence.

Rupture scenario <sup>a</sup>	Rupture event <sup>b</sup>	Displacement per event <sup>c</sup> (m)	Preferred event timing <sup>d</sup> (ka)	RI <sup>e</sup> (kyr), [SR] (mm/yr)
1	A <sup>N,S</sup>	1.4	1.0 ± 0.6	1.9 [0.7]
	B <sup>N,S</sup>	1.7	2.9 ± 1.0	4.1 [0.4]
	C <sup>N,S</sup>	2.4	7.0 ± 1.4	5.4 [0.4]
	D <sup>N,S</sup>	2.0	12.4 ± 2.5	
	Oldest <sup>N,S</sup>	-	53.2 ± 5.6	
2	Z <sup>N</sup>	1.7	1.4 ± 0.5	2.6 [0.7]
	Y <sup>N</sup>	2.0	4.0 ± 1.5	3.0 [0.7]
	X <sup>N,S</sup>	1.8	7.0 ± 1.4	5.4 [0.3]
	W <sup>N,S</sup>	2.0	12.4 ± 2.5	
	Oldest <sup>N,S</sup>	-	53.2 ± 5.6	
2	Z <sup>S</sup>	1.0	0.5 ± 0.1	2.1 [0.5]
	Y <sup>S</sup>	2.0	2.6 ± 0.7	4.4 [0.5]
	X <sup>N,S</sup>	1.8	7.0 ± 1.4	5.4 [0.3]
	W <sup>N,S</sup>	2.0	12.4 ± 2.5	
	Oldest <sup>N,S</sup>	-	53.2 ± 5.6	

<sup>a</sup> Rupture scenarios for the Nephi segment: 1) simultaneous rupturing of Nephi and Santaquin segments, 2) both complete and partial rupture of Nephi segment.

<sup>b</sup> N<sup>N</sup> = Nephi strand, S<sup>S</sup> = Santaquin strand, Events Y<sup>N</sup>, Y<sup>S</sup>, Z<sup>N</sup>, and Z<sup>S</sup> are partial ruptures of the Nephi segment.

<sup>c</sup> Average vertical displacement per individual rupture event based on scarp profile data.

<sup>d</sup> Preferred event timing is mean scarp initiation time (Table 2), averaged over all scarps for rupture scenario 1, or for scarps along only the Nephi or Santaquin strands for scenario 2.

<sup>e</sup> Recurrence interval (RI) = elapsed time between events, slip rate (SR) = average vertical displacement/RI, for the slip occurring after the time interval (e.g., SR (Z<sup>N</sup>) = 1.7 m/2.6 ka = 0.7 mm/yr).

asynchronous ruptures on the two fault strands is discussed and discounted in DuRoss (2004).

Rupture scenario 1 assumes that all ruptures identified on the Nephi and Santaquin strands occurred synchronously. The scenario includes four paleoearthquakes on the entire Nephi segment since the latest Pleistocene (Table 3). Oldest to youngest, Events D, C, and B have average vertical displacements per event of 1.7-2.4 m and occurred at ~12, ~7, and ~2.9 ka, respectively. The youngest event, A, ruptured the segment at 1.0 ka with an average of 1.4 m of displacement. The “oldest event” is estimated at 48-59 ka, based on the oldest fault scarps. The average vertical displacement per

paleoearthquake is 1.9 ± 0.4 m. The mean Holocene recurrence for Events A-C is 3.0 kyr, compared to a mid-Holocene to latest Pleistocene recurrence (Events C-D) of 5.4 kyr (Table 3).

The preferred rupture scenario 2 includes six ruptures of the Nephi segment since the latest Pleistocene (Figure 10, Table 3). Two events ruptured the entire Nephi segment (both Nephi and Santaquin strands simultaneously), and four younger events ruptured only one of the fault strands. The ruptures are, from oldest to youngest, Events W and X, rupturing the entire segment with an average vertical displacement of 1.8 and 2.0 m respectively. Event W ruptured at ~12 ka and Event X at ~7 ka (Table 3). Events Y<sup>N</sup>, Y<sup>S</sup>, Z<sup>N</sup> and Z<sup>S</sup> are partial ruptures of the Nephi segment at ~4 ka, ~2.6 ka, ~1.4 ka and ~0.5 ka, with average event displacements ranging from 1.0 to 2.0 m (Table 3). The “oldest event” is an average for the entire segment at 48-59 ka, based on the timing of scarp initiation for scarps on the oldest fan alluvium. The average vertical displacement per paleoearthquake is 1.8 ± 0.4 m. For scenario 2 the mean Holocene recurrence interval is 1.6 ka for the entire Nephi segment, 2.8 kyr for the Nephi strand, and 3.3 kyr for the Santaquin strand (Table 3). In comparison, the mid-Holocene to latest Pleistocene recurrence interval for the individual strands and the entire segment is 5.4 kyr.

Rupture scenario 2 includes events at ~1.4 ka and ~4 ka on the Nephi strand, commensurate with the maximum timing estimates of ~1.3 ka and ~3.9 ka for the youngest events, based on fault trenching. The rupture scenario also includes separate events at ~0.5 ka and ~2.6 ka on the Santaquin strand which do not fit the trench data. The two youngest events of scenario 1, at 1.0 ± 0.6 and 2.9 ± 1.0 ka, agree with the paleoseismic data (~1.3 and 3.9 ka) within one standard deviation, but do not account for the distribution of slip and diffusion modeling results for the Santaquin strand. Both scenarios combine the oldest two events, accounting for the increased vertical displacement along the segment. The estimated timing of the third event on the Nephi strand (X - scenario 2, C - scenario 1) is ~7 ka, as opposed to a maximum of 5.0-5.5 ka

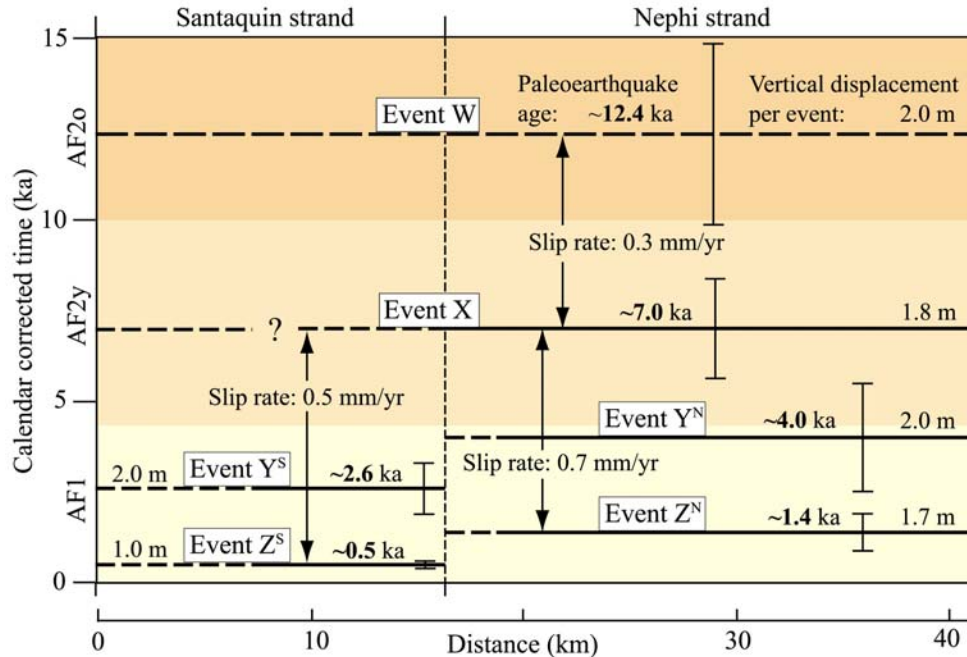


**Figure 10.** Paleoseismic timing vs. horizontal distance for the Nephi segment, for the preferred rupture scenario 2. Dashed lines indicate uncertainty in the extent of surface rupturing. Ages (with vertical error bars equal to  $\pm 1 \sigma$ ) are preferred event ages from rupture scenario 2 (Table 3).

estimated from fault trenching (North Creek site, Hanson and others, 1981).

The preferred paleoseismic chronology for the Nephi segment integrates the preferred rupture scenario (based on scarp displacement, geometry, and initiation data) with the existing paleoseismic-trench data (Table 4). The earthquake time ranges are qualitative estimates, based on diffusion model and fault-trench data uncertainties. Event  $Y^N$  is

**Table 4.** Preferred paleoseismic chronology for the Nephi segment based on the preferred rupture scenario and fault-trench data.

Event:	Preferred time range:
$Z^S$	0.4 – 0.6 ka (partial rupture – Santaquin strand)
$Z^N$	1.0 – 1.4 ka (partial rupture – Nephi strand)
$Y^S$	2.0 – 3.0 ka (partial rupture – Santaquin strand)
$Y^N$	~3.9 – 4.0 ka (partial rupture – Nephi strand)
X	~5.2 – 7.0 ka
W	~10 – 15 ka
$V_B$	>10 – 15 ka, and < 16.8 – 18 ka

based primarily on paleoseismic-trench data due to a paucity of scarps recording only the youngest two events on the Nephi strand. Event  $V_B$  is based on an additional ~2 m of displacement between Event

W and the timing of the Bonneville shoreline; however the event is speculative and is not used to determine final recurrence-interval or slip-rate estimates for the Nephi segment.

### Slip-Rate Estimates

Slip-rate estimates based on closed seismic cycles better approximate fault slip than the diffusion model constant-slip-rate solution, because the elapsed time since the youngest event is excluded. Slip rates for the rupture scenarios are equal to the vertical displacement due to a single paleoseismic event divided by the time, or recurrence interval between that event and an earlier event. For multiple earthquake cycles, we divided the average vertical displacement per event (excluding the oldest event) by the average recurrence interval between events (Tables 2, 3).

Rupture scenario 1 involves simultaneous rupturing of the Nephi and Santaquin strands in four events since the latest Pleistocene. The Holocene and latest Pleistocene to present slip rate averages 0.5 mm/yr. The Late Pleistocene to present slip rate is 0.3 mm/yr (Table 5).

**Table 5.** Closed seismic cycle slip rates for the Nephi segment

Rupture scenario <sup>a</sup>	Rupture events <sup>b</sup>	SR <sup>c</sup> (mm/yr)	Time range <sup>d</sup> (ka)	Epoch(s) <sup>e</sup>
1	A – C	0.5	1.0 – 7.0	LH – MH
	A – D	0.5	1.0 – 12.4	LH – LtP
	A – oldest	0.3	1.0 – 53.2	LH – LP
	C – D	0.4	7.0 – 12.4	MH – LtP
	C – oldest	0.2	12.4 – 53.2	LtP – LP
2 <sup>N</sup>	Z <sup>N</sup> – X	0.7	1.4 – 7.0	LH – MH
	Z <sup>N</sup> – W	0.5	1.4 – 12.4	LH – LtP
	Z <sup>N</sup> – oldest	0.3	1.4 – 53.2	LH – LP
2 <sup>S</sup>	Z <sup>S</sup> – X	0.5	0.5 – 7.0 (?)	LH – MH
	Z <sup>S</sup> – W	0.4	0.5 – 12.4	LH – LtP
	Z <sup>S</sup> – oldest	0.3	0.5 – 53.2	LH – LP
2 <sup>N, S</sup>	X – W	0.3	7.0 – 12.4	MH – LtP
	W – oldest	0.2	12.4 – 53.2	LtP – LP

<sup>a</sup> Rupture scenarios for the Nephi segment: see Table 3 for description.

<sup>b</sup> N = Nephi strand, S = Santaquin strand, see Table 3 for description.

<sup>c</sup> Slip rate (SR) = average displacement per event (not including the oldest event) divided by the average recurrence interval (Table 3).

<sup>d</sup> Time range over which the slip rate was calculated, based on preferred event ages from diffusion modeling (Table 3).

<sup>e</sup> LH – late Holocene, MH – mid-Holocene, LtP – latest Pleistocene, LP – Late Pleistocene.

Rupture scenario 2 considers multiple partial ruptures of the Nephi segment, which presents a problem in terms of fitting a single slip rate to the segment. Considering the individual fault strands, the Nephi strand slip rate averages 0.7 mm/yr during the Holocene, 0.5 mm/yr since the latest Pleistocene, and 0.3 mm/yr from the Late Pleistocene to late Holocene (Table 5). The Santaquin strand slip rate averages 0.5 mm/yr during the Holocene, 0.4 mm/yr since the latest Pleistocene, and 0.3 mm/yr since the Late Pleistocene (Table 5).

### Short-Term Versus Long-Term Slip Rates

For the Nephi segment, the Holocene slip rate ranges from 0.5-0.7 mm/yr, based on the last two closed seismic cycles (Table 5). In contrast, the mid-Holocene to latest Pleistocene (~7 ka to 10-15 ka) slip rate is approximately 0.3-0.4 mm/yr, and the latest Pleistocene to Late Pleistocene (10-15 ka

to 48-59 ka) slip rate is 0.2 mm/yr. Thus, the Holocene slip rate is 2.5-3.5 times greater than the Late Pleistocene slip rate, and is up to about two times greater than the latest Pleistocene slip rate. Furthermore, the mid-Holocene to Lake Bonneville (~7 ka to 16.8-18 ka) slip rate, based on an additional 1.9 m of slip occurring before event W on the Bonneville highstand shoreline, is 0.3-0.5 mm/yr. However, the rate estimate is open-ended, as an unknown amount of time elapsed between the formation of the shoreline and the oldest event (V<sub>B</sub>) to displace it.

The latest Pleistocene to Late Pleistocene slip rate (0.2 mm/yr) corresponds to a recurrence interval of ~9.0-9.5 kyr, using the average vertical displacement per event for the two rupture scenarios (1.8-1.9 m). In comparison, the average Holocene recurrence interval for the segment (including partial ruptures as separate events) ranges from 1.6 kyr (scenario 2) to 3.0 kyr (scenario 1).

These results indicate a low long-term slip rate along the length of the Nephi segment, similar to the slip rate calculated for the southernmost part of the Nephi strand by Machette (1984) and Mattson and Bruhn (2001). The apparent increase in slip rate with time, or decrease in slip rate with an increasing time window indicates either variable slip rates, the temporal clustering of large magnitude earthquakes, or a change in the rate of scarp erosion through time (Machette and others, 1991, 1992; Mattson and Bruhn, 2001).

The low slip-rate estimate for scarps on the oldest (Late Pleistocene) fan surfaces along the Nephi segment may be the effect of a cooler, wetter climate resulting in accelerated erosion of fault scarps (with a higher scarp diffusivity value). For the oldest (Af3) scarps to have a slip rate equivalent with the Holocene rates, a scarp diffusivity value 2.5-3.5 times the value calculated by Mattson and Bruhn (2001) is necessary; however a latest Pleistocene rather than Late Pleistocene timing of scarp initiation results. This does not agree with the subdued surface morphology and degree of pedogenic carbonate development (stage IV) indicative of a Late Pleistocene geomorphic surface (Machette, 1985). Although higher diffusivity values in the Late Pleistocene and nondiffusive processes controlling scarp erosion (e.g., slumping) can potentially lead to an erroneous timing of scarp initiation, the degree of soil carbonate development, relation to Lake Bonneville sediments and shorelines, and surface morphologies support the Late Pleistocene scarp initiation and thus the low long-term slip rates.

### **Potential for Earthquake Clustering**

On the Nephi segment, evidence exists for 1) temporally clustered paleoearthquakes and 2) ruptures occurring due to stress interaction with adjacent fault segments. Temporally clustered earthquakes on an individual fault have a recurrence time that is significantly shorter than the recurrence time between earthquakes in a previous or subsequent group (McCalpin and Nishenko, 1996). Stress triggering, or interaction, is another type of

clustered earthquake behavior where earthquakes are triggered by slip on a separate nearby or adjacent fault (Perkins, 1987; Cornell and others, 1993; Chang, 1998). Stress triggering may occur instantaneously (events are coseismic) or after a period of years to thousands of years (e.g., Pollitz and Sacks, 2002).

Paleoearthquakes on the Nephi segment may be temporally clustered, based on more frequent paleoearthquakes in the Holocene (every 1.6-3.0 ka) compared to the latest Pleistocene to Late Pleistocene (every ~9 ka). If ruptures are clustered, then the recurrence of paleoearthquakes in the Holocene represents a period of greater fault activity and the latest Pleistocene to Late Pleistocene a period of lesser activity. The transition from a quiescent to clustered period of fault rupturing is considered gradual, potentially occurring during the latest Pleistocene, based on the intermediate rates of slip and recurrence times.

The youngest paleoearthquakes on the Nephi segment may have occurred from stress interaction with either the Provo or Levan segments, based on similarity in the timing of events. The youngest paleoearthquakes on the Santaquin strand occurred at 0.4-0.6 ka and 2.0-3.0 ka, based on scarp morphology, compared to ruptures at a maximum of 0.6 ka and 2.8 ka on the Provo segment, based on fault-trench studies (Lund and others, 1991; Lund and Black, 1998). Also, the youngest event on the Nephi strand occurred between 1.0-1.4 ka based on fault scarp diffusion models and paleoseismic-trench data, which is similar to the most recent rupture of the Levan segment at ~1.0 ka (Jackson, 1991; Hylland and Machette, 2004).

Several fault studies indicate that temporally clustered earthquakes occur at a range of scales and in varied compressional, extensional, and strike-slip environments (e.g., Swan, 1988; Sieh and others, 1989; Marco and others, 1996; Dorsey and others, 1997; Rockwell and others, 2000). On the Wasatch fault, Holocene ruptures on the individual segments appear temporally clustered, based on low long-term slip-rate estimates (Machette and others, 1991, 1992). For example, six post-Lake Bonneville paleoearthquakes on the Salt Lake City segment

follow a period of relative quiescence, with only two events between ~9.5-9.9 ka and ~20 ka (McCalpin, 2002; Lund, in press). On the Brigham City segment, six events occurred in the past 8.5 ka, compared to only one event between 8.5 and ~17 ka (McCalpin and Forman, 2002; Lund, in press).

The six segments of the Wasatch fault with Holocene surface ruptures also may have experienced stress interaction, as all but one ruptured in a narrow time window between 0.6 and 1.5 ka (Machette and others, 1992; McCalpin and Nishenko, 1996). For the six segments, the recurrence time between the youngest events is approximately half of the mean recurrence time between the older mid-Holocene ruptures (Schwartz and Coppersmith, 1984; Machette and others, 1992; McCalpin and Nishenko, 1996).

### **Fault Segmentation**

Historic and prehistoric earthquake surface ruptures indicate that many fault zones consist of several independently rupturing fault segments (Schwartz and Coppersmith, 1984; Sibson, 1987, 1989; Machette and others, 1992), controlled by segment boundaries, which act as barriers to earthquake rupture propagation (Crone and Haller, 1991; dePolo and others, 1991). Segment boundaries develop as a result of complex variations in the geometry and structure of the fault zone (dePolo and others, 1991; Zhang and others, 1999), and are identified by the timing and pattern of surface faulting (Crone and Haller, 1991). Along-strike patterns of fault slip indicate how the fault rupture terminated. Convex-up or “rainbow” slip distributions suggest an abrupt increase in the complexity or physical strength of the fault zone (e.g., a segment boundary) that halts the rupture front over a relatively small distance (Ward, 1997). Conversely, concave-up or “dogtail” patterns identify a gradual termination of the rupture along-strike that reflects dissipation of rupture energy over a broader region (Ward, 1997). Evidence for the segmentation of ruptures on the Nephi segment suggests that 1) the Nephi and Santaquin fault strand step-over may impede small ruptures on the

individual strands, and 2) the segment boundary between the Provo segment and Santaquin strand (Payson Salient) acts as a one-way “valve,” impeding ruptures on the Nephi segment, and potentially allowing the transfer of slip from the Provo segment to the Santaquin strand.

### **Fault Strand Step-Over**

Changes in scarp morphology, complex rupture zones, and convex-up slip distributions are a good indication of the reduction or termination of slip at a strong rupture barrier (Schwartz and Coppersmith, 1984; Crone and Haller, 1991; Machette and others, 1991; Zhang and others, 1991; Ward, 1997). The 4.2-7 km wide fault strand step-over at Mendenhall Creek (Figure 4) is a structural boundary that impedes some ruptures but not others, evidenced by the timing and geometry of rupturing along the Nephi and Santaquin strands (Figure 11). Along both strands the youngest fault ruptures bifurcate and the vertical displacements decrease abruptly (rainbow slip distribution) toward the strand step-over (Figures 8, 9), indicating rupture impediment. The youngest two ruptures on each fault strand are morphologically and structurally distinct across the strand step-over. The youngest displacement on the Santaquin strand is limited to the southern half of the strand where 1.0 m of displacement occurred at ~0.4-0.6 ka; the youngest rupture on the Nephi strand occurred at ~1.0-1.4 ka with 1.7 m of displacement. Also, the next oldest event ruptured the Santaquin strand at ~2.0-3.0 ka, in contrast to the event on the Nephi strand at ~3.9-4.0 ka.

### **Payson Salient**

Basin-and-Range surface ruptures indicate that the size (e.g., width) of a fault discontinuity necessary to act as a segment boundary scales with the length of the fault surface rupture (Zhang and others, 1999). Empirical observations of strike-slip faults indicate that 1-5-km-wide discontinuities may or may not terminate ruptures, whereas discontinuities  $\geq 5$  km always arrested rupture propagation (Barka and Kadinsky-Cade, 1988). The

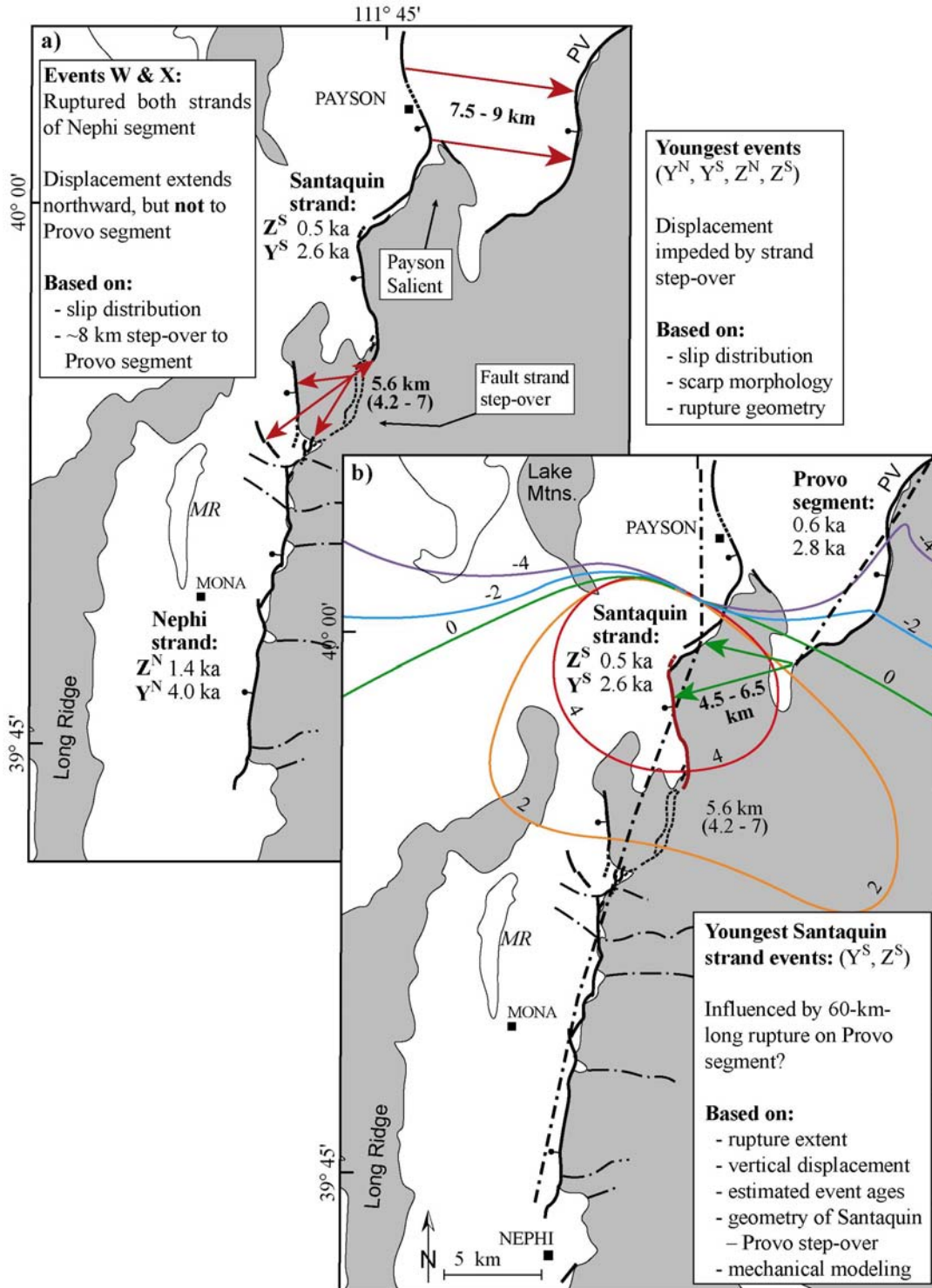


**Figure 11.** Controls on rupture propagation. *a)* Influence of fault strand step-over and Payson Salient on propagation of Nephi segment ruptures. Paleoseismic timing based on preferred rupture scenario. Red arrows indicate a complex fault zone capable of impeding rupture propagation. Northern 45 km of Provo segment not shown. *b)* Influence of Provo segment rupture on Santaquin strand. Contours are modeled Coulomb failure stress change (bars) at 10 km depth, for a 60-m-long, 2-m-slip event on the Provo segment (Chang, 1998, Chang and Smith, 2001). Heavy dashed-dotted line represents fault geometry used in mechanical model (Chang, 1998). Green arrows indicate width of fault step-over and proposed rupture propagation direction. Provo segment event ages from Lund and others (1991) and Lund and Black (1998).

Payson Salient, which separates the Santaquin strand and Provo segment, may allow the transfer of slip from the Provo segment to the Santaquin strand, and impede rupture propagation from the Nephi segment to the Provo segment.

The Santaquin strand may rupture due to coseismic stress interaction with paleoearthquakes along the Provo segment to the north. Provo segment ruptures propagating toward the fault's southern tip would need to transfer slip across a 4.5-6.5 km distance to rupture the Santaquin strand in Santaquin Canyon (Figure 11). Not coincidentally, the youngest two ruptures on the Santaquin strand are limited to Santaquin Canyon (~6.5 km long) (Figure 9) with paleoearthquake timing synchronous with the Provo segment events. The timing of the two Santaquin strand ruptures is estimated at ~0.5 ka and ~2.6 ka, in comparison to the two youngest events identified from Provo segment trenches at 0.6 ka and 2.8 ka (Lund and others, 1991; Lund and Black, 1998). Also, the youngest event on the Santaquin strand and the youngest event identified at the Water Canyon trench site (Ostenaa, 1990) on the southernmost part of the Provo segment have similar vertical displacements of ~1 m. Based on mechanical modeling, a 60-km-long rupture of the Provo segment would induce a Coulomb failure stress change of up to 4 bars at 10-km depth on the Nephi segment (Chang, 1998). More specifically, the greatest stress change is on the southern half of the Santaquin strand, decreasing to less than 2 bars along the Nephi strand (Figure 11).

Conversely, the Payson salient may be an effective barrier to ruptures propagated on the Nephi segment. Based on inferred concave-up (dogtail) slip distributions for the oldest events (U or V of rupture scenario 2), ruptures on the entire Nephi segment may gradually dissipate energy along the northern part of the Santaquin strand and Benjamin fault, rather than transfer slip to the Provo segment (Figure 11). Ruptures continuing northward toward the Benjamin fault may then be less likely to transfer slip across the 7.5-9 km distance from the northern part of the Santaquin strand to the Provo segment (Figure 11).

Furthermore, a 30 km rupture on the Nephi strand would create a Coulomb failure stress change of ~1.8 bars at 10 km depth on the southern part of the Provo segment (Chang, 1998), approximately half of the load induced on the Santaquin strand by a rupture on the Provo segment.

### Paleoearthquake Magnitude Estimates

Seismic-hazard analyses estimate the location and activity of potential seismic sources, and characterize the seismic energy that a fault could generate in both space and time (Schwartz and Coppersmith, 1986; McCalpin, 1996). For faults without historical ground ruptures (e.g., the Wasatch fault), hazards analyses are based on the location, number, and size of surface ruptures, and the development of fault segmentation and earthquake recurrence models (Schwartz and Coppersmith, 1984, 1986; McCalpin, 1996; McCalpin and Nishenko, 1996). In this discussion we quantify the seismic potential of the Nephi segment, using rupture parameter-magnitude regressions for normal, reverse and strike-slip faults (Wells and Coppersmith, 1994) to estimate paleoearthquake moment magnitudes ( $M_w$ ).

Events  $Z^S$  and  $Y^S$  of the preferred rupture scenario 2 ruptured the Santaquin strand at ~0.5 ka and ~2.6 ka with minimum rupture lengths of 6.5 km. Paleoearthquake magnitude estimates for Events  $Z^S$  and  $Y^S$  range from  $M_w 6.5 \pm 0.5$  to  $6.7 \pm 0.6$ , respectively (Table 6), and are very close to the lower bound necessary to generate a fault surface break (~ $M 6.5$ ), indicating a potential relation to events on the Provo segment. If the Provo segment and Santaquin strand rupture coseismically, then a 66.5-km-long rupture with a theoretical maximum displacement of 6.0 m (based on rupture length; Wells and Coppersmith, 1994) would generate an earthquake of  $M_w 7.2-7.3$  (Table 6). Events  $Z^N$  and  $Y^N$  ruptured the Nephi strand at ~1.4 ka and ~4.0 ka, with mean paleoearthquake magnitudes of  $M_w 6.9 \pm 0.3$ , based on minimum rupture lengths of 20.5 km, and the estimated average and maximum displacements (Table 6). The next oldest events, Event X and W ruptured the Nephi segment at ~7

**Table 6.** Paleoearthquake moment magnitude estimates determined from empirical regressions of fault rupture characteristics versus magnitude.

EQ <sup>a</sup>	L <sup>b</sup>	d <sup>c</sup>	D <sup>d</sup>	M <sub>1</sub> <sup>e</sup>	M <sub>2</sub> <sup>f</sup>	M <sub>3</sub> <sup>f</sup>	M <sub>4</sub> <sup>f</sup>	Mag <sup>g</sup>
Z <sup>S</sup>	6.5	1.0	2.0	6.2	6.0	6.9	6.9	6.5±0.5
Y <sup>S</sup>	6.5	2.0	4.0	6.4	6.0	7.2	7.1	6.7±0.6
Z <sup>N</sup>	20.5	1.7	3.8	6.7	6.6	7.1	7.1	6.9±0.3
Y <sup>N</sup>	20.5	2.0	4.0	6.8	6.6	7.2	7.1	6.9±0.3
X	33.5	1.8	3.8	6.9	6.8	7.1	7.1	7.0±0.2
W	40.0	2.0	3.8	7.0	6.9	7.2	7.1	7.1±0.1
A	27.0	1.4	2.8	6.7	6.7	7.0	7.0	6.9±0.2
B	27.0	1.7	3.8	6.8	6.7	7.1	7.1	6.9±0.2
C	33.5	2.4	3.8	7.0	6.8	7.2	7.2	7.1±0.1
D	40.0	2.0	3.8	7.0	6.9	7.2	7.1	7.1±0.1
Max	55.0	2.3	4.5	7.1	7.1	7.2	7.2	7.1±0.1
PV-SS	66.5	3.0	6.0	7.2	7.2	7.3	7.3	7.2±0.1

<sup>a</sup> EQ is rupture event (Table 3), <sup>N</sup> is Nephi strand, <sup>S</sup> is Santaquin strand, Max is maximum possible event, PV-SS is coseismic rupture of the Provo segment and Santaquin strand.

<sup>b</sup> L is straight line rupture length.

<sup>c</sup> d is average displacement, from fault scarp profiles.

<sup>d</sup> D is maximum displacement, ~twice d (Wells and Coppersmith, 1994).

<sup>e</sup> M is moment magnitude,  $M_1 = 0.66 \log(Mo) - 10.7$ , where  $Mo$  (seismic moment) =  $u d A$ ,  $u$  is shear modulus ( $3.3 \times 10^{11}$  dyne/cm<sup>2</sup>),  $A$  is fault rupture area (Hanks and Kanamori, 1979). Fault dip is 45°, and seismogenic depth is 15 km.

<sup>f</sup> M is moment magnitude,  $M_2 = 1.16 \log(L) + 5.08$ ,  $M_3 = 0.82 \log(d) + 6.93$ ,  $M_4 = 0.74 \log(D) + 6.69$  (Wells and Coppersmith, 1994).

<sup>g</sup> Mean paleoearthquake magnitude ± 1 standard deviation

ka and ~12.4 ka, with paleoearthquake magnitude estimates of  $M_w$  ~7.0-7.1, based on 33.5- to 40-km-long surface ruptures, respectively (Table 6).

The maximum moment magnitude estimate of 7.2 for Event W (Table 6) is a reasonable upper bound for a rupture of the entire Nephi segment. As a maximum potential event, the Nephi segment rupture may include the 5 km gap between the Nephi and Levan segments (Hylland and Machette, 2004), and continue north of Payson for an extra ~5-10 km, producing a 55-km-long rupture. Utilizing the surface rupture length and a theoretical maximum vertical displacement of 4.5 m (based on rupture length; Wells and Coppersmith, 1994), the earthquake moment magnitude estimate is  $M_w$  7.1-7.2 (Table 6).

## CONCLUSIONS

In this study we have completed both regional and local investigations of the Nephi segment of the Wasatch fault, using the geometry and structure of surface ruptures and the displacement and timing of initiation of fault scarps on alluvial fans of different ages to formulate a preferred rupture scenario and fault-segmentation model. Six to seven paleoearthquakes have ruptured the Nephi segment since the latest Pleistocene (~12 ka), including four partial ruptures of the segment during the Holocene. The two most recent earthquakes on the Santaquin strand may have accompanied or occurred due to stress interaction with events on the Provo segment to the north. This inference is based on the timing of the events, the geometry of the Nephi-Provo segment boundary, and the limited rupture lengths with moderate paleoearthquake magnitude estimates. Based on these results, indicating synchronicity between the Santaquin strand and Provo segment ruptures, the Santaquin strand may

rupture coseismically with the Provo segment rather than the Nephi segment.

Determining the correct rupture scenario is critical to assess Nephi segment seismic hazards, as partial-segment ruptures result in more frequent moderate-magnitude earthquakes, compared to whole-segment ruptures producing fewer large-magnitude events. For the preferred rupture scenario 2, a moment magnitude ( $M_w$ ) 6.5–7.1 event ruptured the Nephi segment every 1.6 ka in the Holocene, 5.4 ka during the latest Pleistocene, and ~9 ka from the latest to Late Pleistocene. In contrast, rupture scenario 1 predicts a  $M_w$  6.9–7.1 paleoearthquake every 3.0 ka in the Holocene, 5.4 ka during the latest Pleistocene, and ~9.5 ka during the latest to Late Pleistocene.

Based on the preferred earthquake scenario, the long-term (~12–53 ka) slip rate (0.2 mm/yr) is 2.5–3.5 times less than the Holocene rate (0.5–0.7 mm/yr), indicating that earthquakes may be temporally clustered in the Holocene; however the broadly constrained long-term record precludes a definitive conclusion. Thus, further investigation of the long-term (Late Pleistocene) seismic cycle is necessary to resolve issues related to earthquake clustering. Determining the long-term behavior of the segment, including the temporal length of potential clustered and quiescent periods is important to avoid over- or under-estimating the seismic hazards. Furthermore, continued paleoseismic work on the Nephi segment is necessary, and would serve to test the paleoearthquake chronology, provide additional data with which to re-calibrate the diffusion model parameters, and fill in the paleoseismic data gap between the southern part of the Nephi strand and the Provo segment.

Overall, this research complements the existing paleoseismic data for the Nephi segment by clarifying the geometry and evolution of the fault ruptures and helping resolve the short- and long-term behavior of the segment, including the Late Pleistocene rate of slip and latest Pleistocene rupture chronology. This study contributes to an understanding of the spatial and temporal variability and stress triggering-effect of Wasatch fault

ruptures, and the potential for temporally clustered moderate to large magnitude paleoearthquakes on the Nephi segment.

## ACKNOWLEDGMENTS

This research was supported by National Science Foundation Grant EAR-0207373. We thank Frank Brown and David Dinter (University of Utah) for early reviews of this work. Gary Christenson, William Lund (Utah Geological Survey), and Leif Tapanila (University of Utah) helped to improve this manuscript through constructive reviews and discussions. Thanks to Susan Olig (URS Corporation), Michael Machette (U.S. Geological Survey), Anke Friedrich (Universität Potsdam), Ann Mattson (University of Utah), and Michael Hylland (Utah Geological Survey) for contributing to many discussions of the Nephi segment. Riyad Ali-Adeeb, Christopher Busch, Eric Cline, Ben Davis, Chip DuRoss, Erika DuRoss, Joanie DuRoss, and Courtney Neuffer provided much hard work in the field.

## REFERENCES

- Andrews, D.J., and Bucknam, R.C., 1987, Fitting degradation of shoreline scarps by a nonlinear diffusion model: *Journal of Geophysical Research*, v. 92, no. B12, p. 12,857–12,867.
- Arrowsmith, J.R., Rhodes, D.D., and Pollard, D.D., 1998, Morphologic dating of scarps formed by repeated slip events along the San Andreas fault, Carrizo Plain, California: *Journal of Geophysical Research*, v. 103, p. 10,141–10,160.
- Avouac, J., 1993, Analysis of scarp profiles—evaluation of errors in morphologic dating: *Journal of Geophysical Research*, v. 98, no. B4, p. 6,745–6,754.
- Barka, A., and Kadinsky-Cade, K., 1988, Strike-slip fault geometry in Turkey and its influence on earthquake activity: *Tectonics*, v. 7, p. 663–684.
- Bennett, R.A., Wernicke, B.P., Niemi, N.A., Friedrich, A.M., and Davis, J.L., 2003,

- Contemporary strain rates in the northern Basin and Range province from GPS data: *Tectonics*, v. 22, no. 2, 29 p.
- Black, B.D., Lund, W.R., Schwartz, D.P., Gill, H.E., and Mayes, B.H., 2003, Paleoseismic investigation of the Salt Lake City segment of the Wasatch fault zone at the South Fork Dry Creek and Dry Gulch sites, Salt Lake County, Utah: Utah Geological Survey Special Study 92, 22 p.
- Bucknam, R.C., 1978, Northwestern Utah seismotectonics studies, *in* Seiders, W., and Thomson, J., compilers, *Summaries of Technical Reports*, v. VII: Menlo Park, California, U.S. Geological Survey Office of Earthquake Studies, p. 64.
- Bucknam, R.C., and Anderson, R.E., 1979, Estimation of fault–scarp ages from a scarp–height–slope–angle relationship: *Geology*, v. 7, p. 11–14.
- Caskey, S.J., 1995, Geometric relations of dip slip to a faulted ground surface—new nomograms for estimating components of fault displacement: *Journal of Structural Geology*, v. 17, no. 8, p. 1197–1202.
- Chang, W.L., 1998, Earthquake hazards on the Wasatch fault—tectonically induced flooding and stress triggering of earthquake [M.S. thesis]: Salt Lake City, University of Utah, 123 p.
- Chang, W.L., and Smith, R.B., 2002, Integrated seismic–hazard analysis of the Wasatch Front, Utah: *Bulletin of the Seismological Society of America*, v. 92, no. 5, p. 1904–1922.
- Cluff, L.S., Brogan, G.E., and Glass, C.E., 1973, Wasatch fault – southern portion, earthquake fault investigation and evaluation—a guide to land use planning for Utah Geological & Mineral Survey: Oakland, California, Woodward-Lundgren & Associates, Project G-12069A, 56 p.
- Cornell, C.A., Wu, S-C., Winterstein, S.R., Dietrich, J.H., and Simpson, R.W., 1993, Seismic hazard induced by mechanically interactive fault segments: *Bulletin of the Seismological Society of America*, v. 83, no. 2, p. 436–449.
- Crone, A.J., and Haller, K.M., 1991, Segmentation and the coseismic behavior of Basin and Range normal faults—examples from east–central Idaho and southwestern Montana, U.S.A.: *Journal of Structural Geology*, v. 13, p. 151–164.
- Culling, W.E.H., 1963, Soil creep and the development of hillside slopes: *Journal of Geology*, v. 71, p. 127–161.
- dePolo, C.M., Clark, D.G., Slemmons, D.B., Ramallie, A., 1991, Historical Basin and Range Province surface faulting and fault segmentation: *Journal of Structural Geology*, v. 13, p. 123–136.
- Dorsey, R.J., Umhoefer, P.J., and Falk, P.D., 1997, Earthquake clustering inferred from Pliocene Gilbert–type fan deltas in the Loreto basin, Baja California Sur, Mexico: *Geology*, v. 25, no. 8, p. 679–682.
- DuRoss, C.B., 2004, Spatial and temporal trends of surface rupturing on the Nephi segment of the Wasatch Fault, Utah—implications for fault segmentation and the recurrence of paleoearthquakes: Salt Lake City, University of Utah, M.S. Thesis, 120 p.
- Friedrich, A.M., Wernicke, B.P., Niemi, N.A., Bennett, R.A., and Davis, J.L., 2003, Comparison of geodetic and geologic data from the Wasatch region, Utah, and implications for the spectral character of Earth deformation at periods of 10 to 10 million years: *Journal of Geophysical Research*, v. 108, no. B4, p. 1–23.
- Hancock, G.S., Anderson, R.S., Chadwick, O.A., and Finkel, R.C., 1999, Dating fluvial terraces with (super 10) Be and (super 26) Al profiles; application to the Wind River, Wyoming, U.S.A.: *Geological Society of America, Abstracts with Programs*, v. 31, no. 7, p. 55.
- Hanks, T.C., 2000, The age of scarplike landforms from diffusion–equation analysis, *in* *Quaternary geochronology—methods and applications*, Noller, J.S., Sowers, J.M., and Lettis, W.R., editors, American Geophysical Union reference shelf, v. 4: Washington, D.C., American Geophysical Union, p. 313–338.
- Hanks, T.C., Bucknam, R.C., Lajoie, K.R., and Wallace, R.E., 1984, Modification of wave–cut

- and faulting controlled landforms: *Journal of Geophysical Research*, v. 89, p. 5571-5790.
- Hanks, T.C., and Kanamori, H., 1979, A moment magnitude scale: *Journal of Geophysical Research*, v. 84, no. B5, p. 2348-2350.
- Hanson, K.L., Swan, F.H., and Schwartz, D.P., 1981, Study of earthquake recurrence intervals on the Wasatch fault, Utah: San Francisco, California, Woodward-Clyde Consultants, Sixth-annual technical report prepared for U.S. Geological Survey under contract No. 14-08-0001-19115, 22 p.
- 1982, Study of earthquake recurrence intervals on the Wasatch fault, Utah: San Francisco, California, Woodward-Clyde Consultants, Seventh-annual technical report prepared for U.S. Geological Survey under contract No. 14-08-0001-19842, 10 p.
- Harty, K.M., Mulvey, W.E., and Machette, M.N., 1997, Surficial geologic map of the Nephi segment of the Wasatch fault zone, eastern Juab County, Utah: Utah Geological Survey Map 170, scale 1:50,000.
- Hylland, M.D., and Machette, M.N., 2004, Interim surficial geologic map of the Levan segment of the Wasatch fault zone, Juab and Sanpete Counties, Utah, *in* Christenson, G.E., Ashland, F.X., Hylland, M.D., McDonald, G.N., and Case, B., Database compilation, coordination of earthquake-hazards mapping, and study of the Wasatch fault and earthquake-induced landslides, Wasatch Front, Utah: U.S. Geological Survey, National Earthquake Hazards Reduction Program Final Technical Report, award no. 03HQAG0008, variously paginated, map scale 1:50,000.
- Jackson, M., 1991, Number and timing of Holocene paleoseismic events on the Nephi and Levan segments, Wasatch fault zone, Utah: Utah Geological Survey Special Studies, v. 78, 23 p.
- Lund, W.R., in press, Utah Quaternary Fault Parameter Working Group review of Utah paleoseismic-trenching data and determination of consensus recurrence-interval and vertical slip-rate estimates: U.S. Geological Survey, National Earthquake Hazards Reduction Program Final Technical Report, Contract No. 03HQGR0033, variously paginated.
- Lund, W.R., and Black, B.D., 1998, Paleoseismic investigation at Rock Canyon, Provo segment, Wasatch fault zone, Utah County, Utah: Utah Geological Survey Special Study 93, 21 p.
- Lund, W.R., Schwartz, D.P., Mulvey, W.E., Budding, K.E., and Black, B.D., 1991, Fault behavior and earthquake recurrence on the Provo segment of the Wasatch fault zone, at Mapleton, Utah County, Utah: Utah Geological Survey Special Study 75, 41 p.
- Machette, M.N., 1984, Preliminary investigations of late Quaternary slip rates along the southern part of the Wasatch fault zone, central Utah, *in* Hayes, W.W., and Gori, T.L., editors, Proceedings of Conference XXVI, A Workshop "Evaluation of Regional and Urban Earthquake Hazards and Risk in Utah": U.S. Geological Survey Open-File Report 84-763, p. 391-406.
- 1985, Calcic soils of the southwestern United States: Geological Society of America Special Paper 203, 21 p.
- 1992, Surficial geologic map of the Wasatch fault zone, eastern part of Utah Valley, Utah County and parts of Salt Lake and Juab Counties, Utah: U.S. Geological Survey Miscellaneous Investigations Series Map I-2095, scale 1:50,000.
- Machette, M.N., Personius, S.F., and Nelson, A.R., 1991, The Wasatch fault zone, Utah – segmentation and history of Holocene earthquakes: *Journal of Structural Geology*, v. 13, no. 2, p. 137-149.
- 1992, Paleoseismology of the Wasatch fault zone—A summary of recent investigations, interpretations, and conclusions: U.S. Geological Survey Professional Paper 1500—A—J, p. A1-A59.
- Marco, S., Stein, M., Agnon, A., and Ron, H., 1996, Long-term earthquake clustering—a 50,000 year paleoseismic record in the Dead Sea graben: *Journal of Geophysical Research* v. 101, p. 6179-6192.
- Martinez, L.J., Meertens, C.M., and Smith, R.B., 1998, Rapid deformation rates along the

- Wasatch fault zone, Utah, from first GPS measurements with implications for earthquake hazard: *Geophysical Research Letters*, v. 25, no. 4, p. 567-570.
- Mattson, A., and Bruhn, R.L., 2001, Fault slip rates and initiation age based on diffusion equation modeling—Wasatch fault zone and eastern Great Basin: *Journal of Geophysical Research*, v. 106, no. B7, p. 13,739-13,750.
- McCalpin, J.P., 1996, Application of paleoseismic data to seismic hazard assessment and neotectonics research, *in* McCalpin, J.P., editor, *Paleoseismology*: Academic Press, San Diego, California, p. 439-493.
- 2002, Post-Bonneville paleoearthquake chronology of the Salt Lake City segment, Wasatch fault zone, from the 1999 “megatrench” site: Utah Geological Survey Miscellaneous Publications 02-7, 37 p.
- McCalpin, J.P., and Forman, S.L., 2002, Post-Provo paleoearthquake chronology of the Brigham City segment, Wasatch fault zone, Utah: Utah Geological Survey Miscellaneous Publication 02-9, 46 p.
- McCalpin, J.P., and Nishenko, S.P., 1996, Holocene paleoseismicity, temporal clustering, and probabilities of future large ( $M > 7$ ) earthquakes on the Wasatch fault zone, Utah: *Journal of Geophysical Research*, B, Solid Earth and Planets, v. 101, no. 3, p. 6233-6253.
- Nash, D.B., 1980, Morphologic dating of degraded normal fault scarps: *Journal of Geology*, v. 88, p. 353-360.
- Nelson, A.R., and Personius, S.F., 1993, Surficial geologic map of the Weber segment, Wasatch fault zone, Weber and Davis Counties, Utah: U.S. Geological Survey Miscellaneous Investigations Series Map I-2199, 22. p. pamphlet, scale 1:50,000.
- Ostenaar, D., 1990, Late Holocene displacement history, Water Canyon site, Wasatch fault zone: *Geological Society of America Abstracts with Programs*, v. 22, p. 42.
- Oviatt, C.G., Currey, D.R., and Sack, D., 1992, Radiocarbon chronology of Lake Bonneville, eastern Great Basin, USA: *Palaeogeography, Palaeoclimatology, Palaeoecology*, v. 99, p. 225-241.
- Oviatt, C.G., McCoy, W.D., and Reider, R.G., 1987, Evidence for a shallow early or middle Wisconsin-age lake in the Bonneville basin, Utah: *Quaternary Research*, v. 27, p. 248-262.
- Perkins, D.M., 1987, Contagious fault rupture, probabilistic hazard, and contagion observability, *in* Crone, A.J., and Omdahl, E.M., editors, *Proceedings of Conference XXXIX, Directions in Paleoseismology*: U.S. Geological Survey Open-File Report 87-673, p. 428-437.
- Pollitz F.F., and Sacks, I.S., 2002, Stress triggering of the 1999 Hector Mine earthquake by transient deformation following the 1992 Landers earthquake: *Bulletin of the Seismological Society of America*, v. 92, p. 1487-1496.
- Rockwell, T.K., Lindvall, S., Herzberg, M., Murback, D., Dawson, T., and Berger, G., 2000, Paleoseismology of the Johnson Valley, Kickapoo, and Homestead Valley faults—clustering of earthquakes in the Eastern California Shear Zone: *Bulletin of the Seismological Society of America*, v. 90, p. 1200-1236.
- Schwartz, D.P., and Coppersmith, K.J., 1984, Fault behavior and characteristic earthquakes—Examples from the Wasatch and San Andreas fault zones: *Journal of Geophysical Research*, v. 89, no. 7, p. 5681-5698.
- 1986, Seismic hazards, new trends in analysis using geologic data, *in* Wallace, R.E., editor, *Active tectonics*: Washington, D.C., National Academic Press, p. 215-230.
- Scott, W.E., McCoy, W.D., Shroba, R.R., and Rubin, M., 1983, Reinterpretation of the exposed record of the last two cycles of Lake Bonneville, western United States: *Quaternary Research*, v. 20, no. 3, p. 261-285.
- Sibson, R.H., 1987, Effects of fault heterogeneity on rupture propagation, *in* Crone, A.J., and Omdahl, E.M., editors, *Proceedings of Conference XXXIX, Directions in Paleoseismology*: U.S. Geological Survey Open-File Report 87-673, p. 362-373.

- Sibson, R.H., 1989, Earthquake faulting as a structural process: *Journal of Structural Geology*, v. 11, p. 1-14.
- Sieh, K., Stuiver, M., and Brillinger, D., 1989, A more precise chronology of earthquakes produced by the San Andreas fault in southern California: *Journal of Geophysical Research*, v. 94, no. 1, p. 603-623.
- Smith, R.B., and Sbar, M.L., 1974, Contemporary tectonics and seismicity of the western United States with emphasis on the Intermountain seismic belt: *Geological Society of America Bulletin*, v. 85, p. 1205-1218.
- Stuiver, M., and Reimer, P.J., 1993, Extended <sup>14</sup>C database and revised CALIB radiocarbon calibration program: *Radiocarbon*, v. 35, p. 215-230.
- Swan, F.H., 1988, Temporal clustering of paleoseismic events on the Oued Fodda fault, Algeria: *Geology*, v. 16, p. 1092-1095.
- Swan, F.H., Schwartz, D.P., and Cluff, L.S., 1980, Recurrence of moderate to large magnitude earthquakes produced by surface faulting on the Wasatch fault zone, Utah: *Bulletin of the Seismological Society of America*, v. 70, no. 5, p. 1431-1462.
- Wallace, R.E., 1977, Profiles and ages of young fault scarps, north-central Nevada: *Geological Society of America Bulletin*, v. 88, p. 1267-1281.
- Ward, S.N., 1997, Dogtails versus rainbows—synthetic earthquake rupture models as an aid in interpreting geologic data: *Bulletin of the Seismological Society of America*, v. 87, no. 6, p. 1422-1441.
- Wells, D.L., and Coppersmith, K.J., 1994, New empirical relationships among magnitude, rupture length, rupture width, rupture area, and surface displacement: *Bulletin of the Seismological Society of America*, v. 84, no. 4, p. 974-1002.
- Zhang, P., Fengying, M., Slemmons, D.B., 1999, Rupture terminations and size of segment boundaries from historical earthquake ruptures in the Basin and Range Province: *Tectonophysics*, v. 308, p. 37-52.
- Zhang, P., Slemmons, D.B., and Mao, F., 1991, Geometric pattern, rupture termination and fault segmentation of the Dixie Valley – Pleasant Valley active normal fault system, Nevada, U.S.A.: *Journal of Structural Geology*, v. 13, p. 165-176.

# ***A STRAIGHTFORWARD WAY OF NAMING PALEOEARTHQUAKES***

Craig M. dePolo  
Nevada Bureau of Mines and Geology  
University of Nevada, Reno, NV 89557

## **ABSTRACT**

Use a simpler scheme for naming paleoearthquakes. Current schemes involve using letters backwards or using Latin words in a dead ended system. Paleoearthquakes can be more straightforwardly named by numbering them backwards from the beginning of the historical record, which is the reference frame. The most recent earthquake would be Paleoequake 1 (PE1), the second event back would be Paleoequake 2 (PE2), and so forth.

## **INTRODUCTION**

Current approaches to identify paleoearthquakes are cumbersome, non-intuitive, and difficult to communicate, especially to non-earthquake scientists and lay people. A simpler method that numbers events is more straightforward, more easily communicated, and is commonly used by default in discussions and presentations.

The most common ways to name paleoearthquakes, such as those identified in trenching studies, are to assign them letters starting with the end of the alphabet, or to give the most recent three events some specific terms. In the first approach, the “z” event is the most recent paleoevent, “y” is the next oldest, and so forth. I find this confusing, especially when the earthquake chronology extends backwards for several events.

The second approach starts clearly with the term “the most recent event,” although it occasionally has to be referenced to the prehistorical record to distinguish it from the most recent historical event. The second event back is termed the “penultimate” event, a Latin word that means, “second last” or the “last but one,” and is intended to mean the earthquake that came before the most recent event. Although there is a bit of a learning period for newcomers, paleoearthquake geologists smoothly use these terms as lingo. The third event back is

given the name the “antepenultimate” event, or the “last but two.” This system breaks down seriously at the forth-event back, the “pre-antepenultimate” event, and the fifth-event back, the “pre-pre-antepenultimate event,” or perhaps we should substitute “the last but four.” Earthquake geologists commonly refer to these terms by their acronyms, MRE, PE, APE, and pre-APE in conversation. The terms penultimate and antepenultimate are perceived as quintessential scientific jargon by non-earthquake scientists, and they are commonly surprised we have such complicated jargon for such a simple notion.

## **A STRAIGHTFORWARD APPROACH**

A straightforward way to name paleoearthquakes is to number them backwards, using the same reference frame that we naturally use to refer to these events. The first event back would be Paleoequake 1 (PE1), the second event back would be Paleoequake 2 (PE2), and so forth (figure 1). Sweet! This approach is intuitively easy to use, and is readily communicated to others, including those not familiar with paleoearthquake jargon. For example, PE6 is the sixth event back. The terms are efficient and effective to use, especially their acronyms; for example, the scarp generated by PE2, or scarp-derived colluvium from

PE2 overlying PE3 fractures. The datum for this approach is the beginning of the historical record. It expands open ended back in time, in the direction of new discoveries. Thus, paleoearthquake chronologies using this system are easily built on when older events are identified. Historical earthquakes are usually given site names, so there is not a large need for a parallel naming system; if there was, however, the same datum would be advocated, the beginning of the historical record, and the event numbers would increase with time into the open-ended future, and be labeled Historical Earthquake 1 (HE1), Historical Earthquake 2 (HE2), and so forth (figure 1).

## **CONCLUSIONS**

The term “most recent event” is simple, eloquent, and is easily communicated, and I do not advocate abandoning it. The most recent event is synonymous with Paleoearthquake 1. I do advocate, however, that this simpler, numbered approach to naming paleoearthquakes is superior to approaches currently used, and should replace them.

## **ACKNOWLEDGMENTS**

I would like to thank Gary Christenson, Bill Lund, and Dick Meeuwig for helpful suggestions that improved the text.

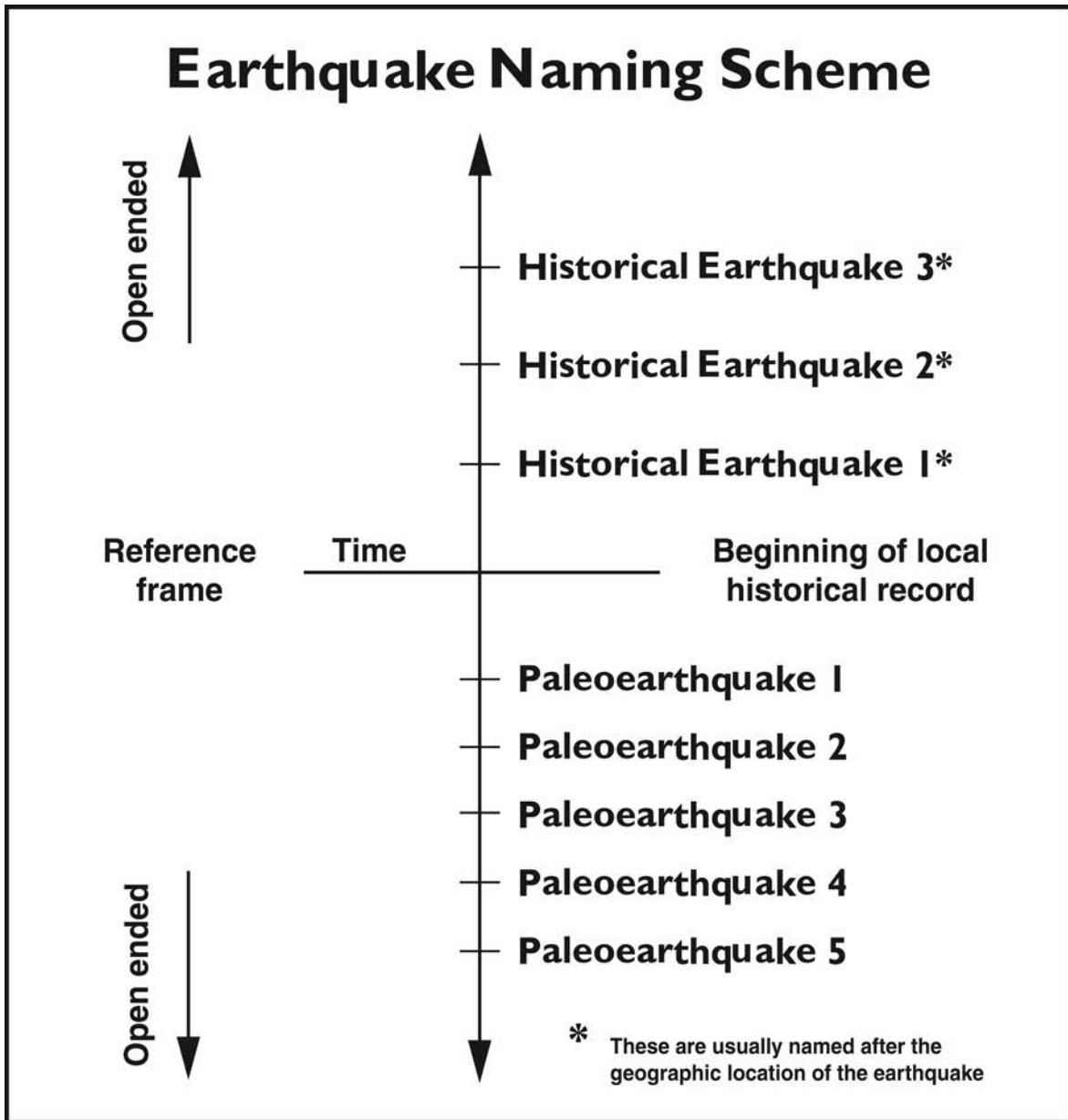


Figure 1. Earthquake naming scheme presented in time.

# ***SHAKEMAP AS A TOOL FOR UNDERSTANDING EARTHQUAKE HAZARD IN NEVADA***

Glenn Biasi  
University of Nevada Reno  
Nevada Seismological Laboratory, MS-174,  
Reno, NV 89557  
and  
Kent Lindquist  
Lindquist Consulting  
Fairbanks, AK 99701

## **ABSTRACT**

ShakeMap is a mapping and display tool developed by the United States Geological Survey for displaying measured and predicted strong ground shaking. This paper reports on the implementation of ShakeMap in the real-time seismic network operations of the Nevada Seismological Laboratory at the University of Nevada Reno. The Nevada Seismological Laboratory was the first network to integrate ShakeMap into the Antelope Real-Time System, a seismic network acquisition and operations package written by Boulder Real-Time Technologies. The Advanced National Seismic System initiative has provided over 35 new strong-motion recorders for the populated regions of Nevada, so ShakeMaps can now be constructed for both the Las Vegas and Reno-Carson City areas. ShakeMaps are designed to help emergency responders decide where to direct resources in the period shortly following a damaging earthquake, to guide engineers in post-earthquake response, and as a resource for loss estimators that need to evaluate how significant the earthquake may be in economic and social costs. ShakeMaps are also useful for generating scenario earthquakes to assess potential impact of slip on known or suspected faults. We demonstrate this capability by presenting scenario earthquakes on three discrete faults identified in the USGS National Seismic Hazards Mapping Project as being the most significant for seismic hazard in Reno.

## **INTRODUCTION**

The U. S. Geological Survey (USGS) developed ShakeMap as a tool to synthesize recorded and predicted strong ground motions and to present them in map views useful for emergency response, loss evaluation, and public information (Wald and others, 1999b). ShakeMaps are being made by regional seismic networks in California,

Utah, and the Pacific Northwest, typically within minutes after  $M \sim 3.5$  and larger earthquakes (<http://earthquake.usgs.gov/shakemap>). This paper discusses the recent implementation of a real-time ShakeMap capability at the Nevada Seismological Laboratory (NSL), and presents potential applications of ShakeMap for understanding earthquake hazards in western Nevada.

## SHAKEMAP - AN OVERVIEW

A ShakeMap is initiated when automatic network software determines that an earthquake larger than some threshold magnitude has occurred in the coverage area. A data retrieval process is then initiated that predicts S-wave arrival times at strong-motion stations and retrieves peak ground motion amplitudes in a window around the predicted arrivals. On-scale velocity recordings are used in the Nevada implementation to supplement strong-motion station coverage and improve regional coverage.

### How It Works

A brief description of how ShakeMap works will facilitate understanding of its map products. The core of ShakeMap, a routine called *grind*, determines the ground motions that are actually contoured and presented in final maps. *Grind* begins by using a reported earthquake magnitude and location to predict ground motions at hypothetical rock sites on a grid of pseudostations throughout the coverage area. The spacing of this prediction grid is configurable, but a spacing of 10 to 30 km is typical. Rock-site ground motions are predicted using empirical attenuation regressions. When a grid point falls near an instrumented strong-motion site, the station location is used instead. Measured peak ground motions are corrected for site conditions, if known, to give the corresponding equivalent rock ground motions at the site. Measurements are then compared to the predictions, and the entire map may be shifted upward or downward to adjust for any small systematic bias. This correction can compensate to some degree for a biased estimate of earthquake magnitude. A sanity check can be applied, where if an individual measurement strongly disagrees with the prediction, the station value can be overridden by the prediction. The grid of predicted pseudostation and measurement sites is then contoured to a surface of rock ground motions. These surfaces are then

resampled at a finer grid spacing, and the finer grid is projected through a gridded map of local site conditions to produce a grid of surface ground motions. The grids of surface ground motions are then handed off to mapping utilities that contour them and develop final maps of ground motions and derivative products such as Mercalli Intensity.

Because of the nature and number of interacting parameters, results are most stable in well-instrumented areas. Significant errors in location or magnitude can lead to poor maps or in extreme cases, no maps at all. Consequently, configuration of ShakeMap for reliable automatic operation requires adjustments and regular attention, and unreviewed maps should be viewed with this in mind.

Region-specific attenuation regressions are readily accommodated by implementing them as modules meeting the necessary interface requirements. NSL uses Pankow and Pechman (2004) for large earthquakes, and a generic regression for earthquakes of  $M < 5.3$ . The Pankow and Pechman (2004) relations modified relations of Spudich and others (1999), which were developed for use in extensional tectonic regimes. Other standard regressions, such as those of Boore and others (1997), are available in the standard ShakeMap distribution. As of this writing, no earthquakes of adequate magnitude near strong-motion instrumentation have occurred by which to compare Nevada accelerations to those predicted by the Pankow and Pechman (2004) regression.

### Unique to Nevada: ShakeMap Integration with the Antelope Real-Time System

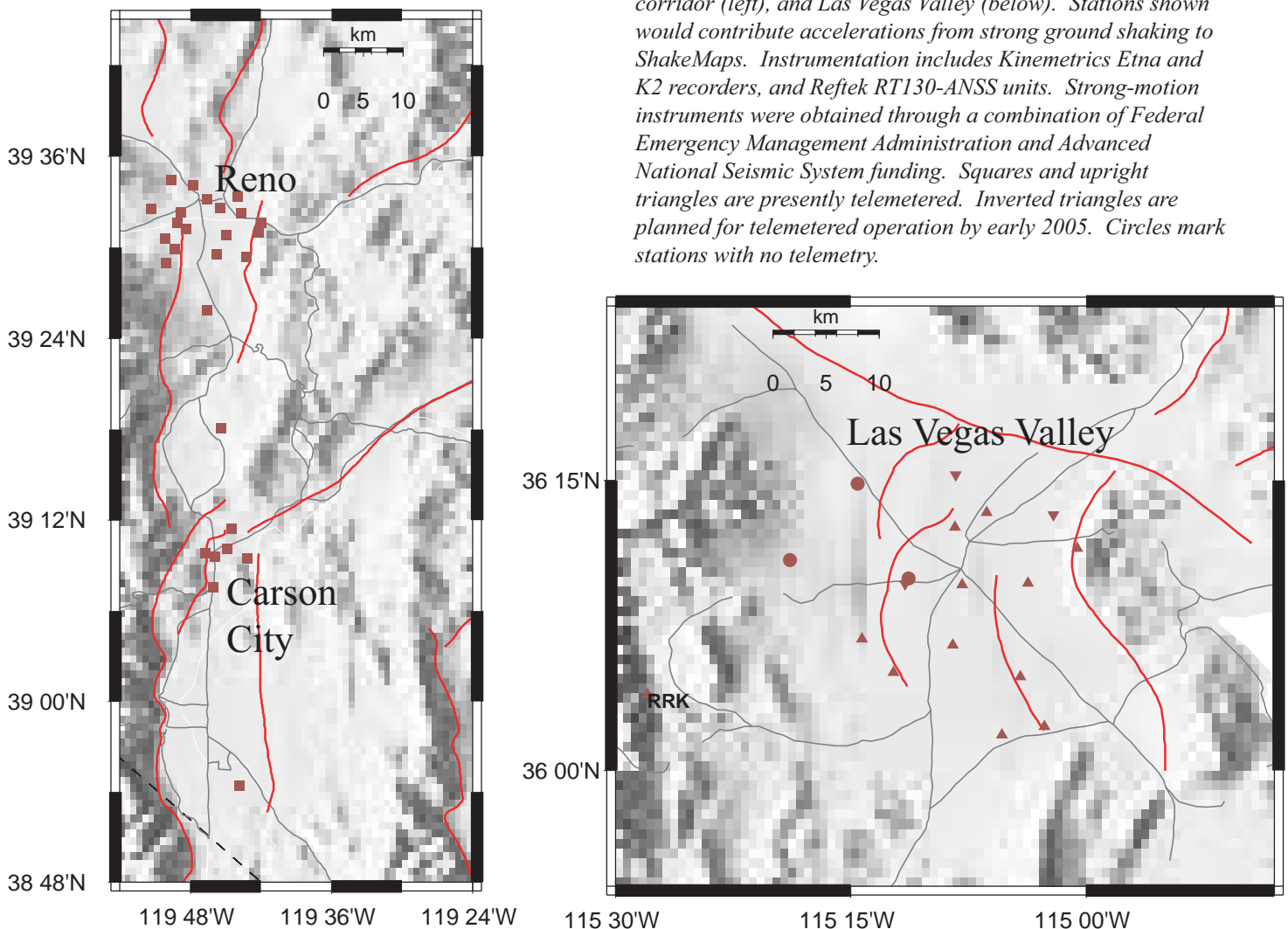
The University of Nevada Reno implementation of ShakeMap was the first to be integrated with the Antelope Real-Time System software. Antelope is a commercial seismic network acquisition and processing product developed by Boulder Real-Time Technologies in Boulder, Colorado ([www.brtt.com](http://www.brtt.com)). The Antelope

Real-Time System integrates modules including datalogger control, data input and archiving, automatic arrival detection, picking, association, event location, web and mail notification, and data exchange with other networks. A full suite of integrated post-processing tools is also included. Antelope strengths include a high level of software and systems engineering and a fully integrated, easy-to-use database. The database model enables uniform access to the data in both real-time and post-processing environments. Antelope comes with an extensive set of application programmer interfaces (API's), so that one can access real-time or archive databases and data from a variety of

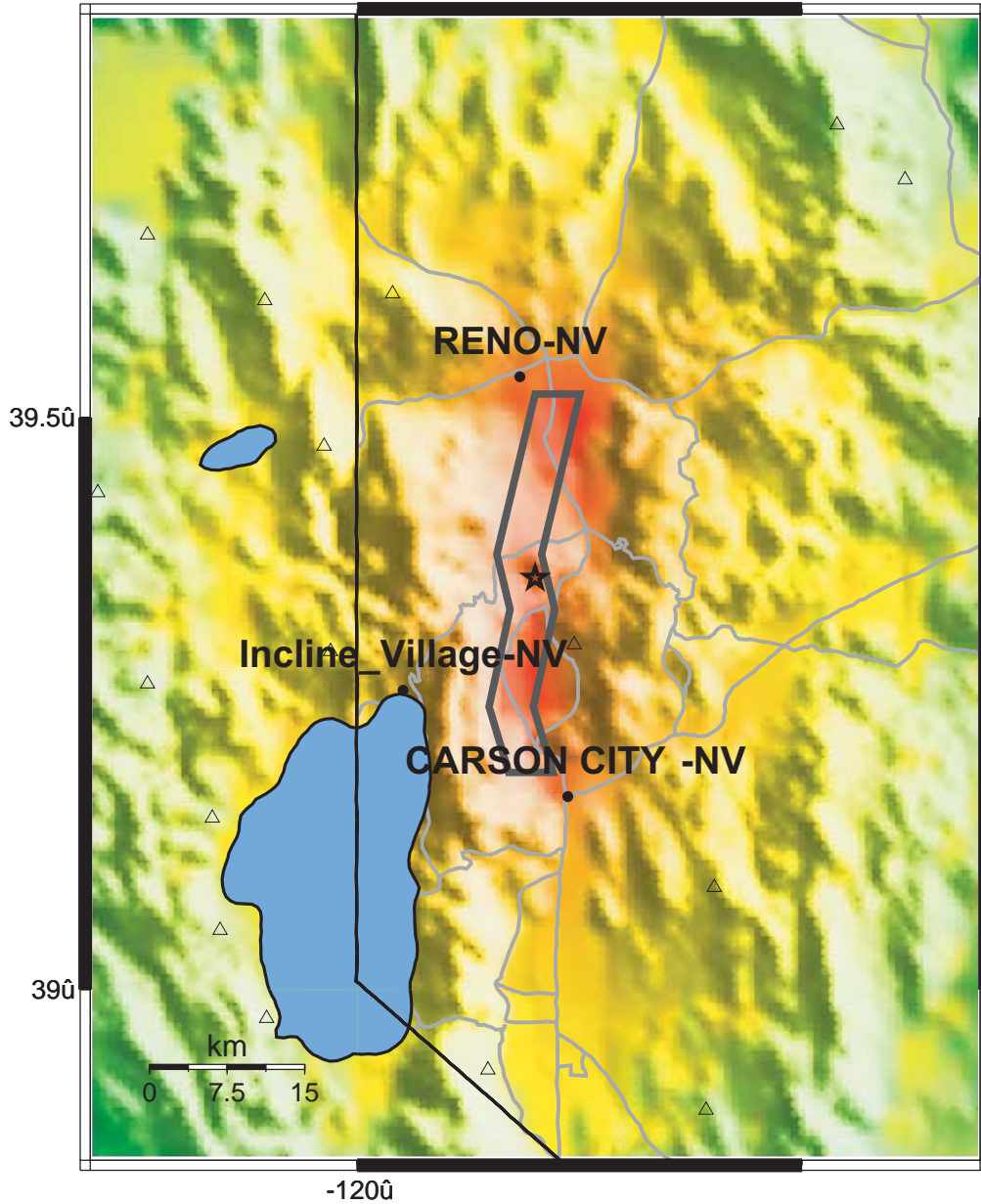
high-level programming languages including C, Perl, Tcl/Tk, Fortran, Java, and Matlab. This facilitates research and new application development. Antelope is being used by the Earthscope US Array program ([www.earthscope.org](http://www.earthscope.org)) to integrate their backbone and 400 element transportable array now being deployed in the western United States. The Antelope APIs greatly facilitated ShakeMap implementation in Nevada.

The integration of ShakeMap with Antelope was implemented in Perl. Two main code pieces were developed, an event selection and queuing module and a data retrieval and formatting module.

*Figure 1. Strong-motion station maps for the Reno-Carson corridor (left), and Las Vegas Valley (below). Stations shown would contribute accelerations from strong ground shaking to ShakeMaps. Instrumentation includes Kinemetrics Etna and K2 recorders, and Reftek RT130-ANSS units. Strong-motion instruments were obtained through a combination of Federal Emergency Management Administration and Advanced National Seismic System funding. Squares and upright triangles are presently telemetered. Inverted triangles are planned for telemetered operation by early 2005. Circles mark stations with no telemetry.*



Scenario Date: Sun May 16, 2004 12:00:00 PM GST M 6.7 N39.36 W119.80 Depth: 10.0km



PLANNING SCENARIO ONLY -- PROCESSED: Wed Mar 31, 2004 10:55:53 PM GST

PERCEIVED SHAKING	Not felt	Weak	Light	Moderate	Strong	Very strong	Severe	Violent	Extreme
POTENTIAL DAMAGE	none	none	none	Very light	Light	Moderate	Moderate/Heavy	Heavy	Very Heavy
PEAK ACC. (%g)	<.17	.17-1.4	1.4-3.9	3.9-9.2	9.2-18	18-34	34-65	65-124	>124
PEAK VEL. (cm/s)	<0.1	0.1-1.1	1.1-3.4	3.4-8.1	8.1-16	16-31	31-60	60-116	>116
INSTRUMENTAL INTENSITY	I	II-III	IV	V	VI	VII	VIII	IX	X+

Figure 2. Mercalli Intensity ShakeMap for a scenario involving an M6.7 earthquake on the Mount Rose fault system. Rupture on this fault accounts for 54% of the 2% in 50 year hazard for Reno - by far the largest single contributor.

The event selection and queuing module takes in events generated by the automatic system, screens candidates on magnitude and location criteria, and on finding one or more suitable, begins a broader database retrieval. The data retrieval module is more extensive, as it reads waveform segments from disk, corrects them to actual ground motion amplitudes, and extracts peak ground motion parameters. It also computes derivative products such as peak velocity and pseudo-acceleration peaks

at three periods. Finally it produces the formatted XML file of station parameters that ShakeMap actually uses as input. The Antelope ShakeMap utilities are available from the Antelope contributed-code repository at <http://www.indiana.edu/~aug>.

**Data Sources in Nevada**

The USGS Advanced National Seismic

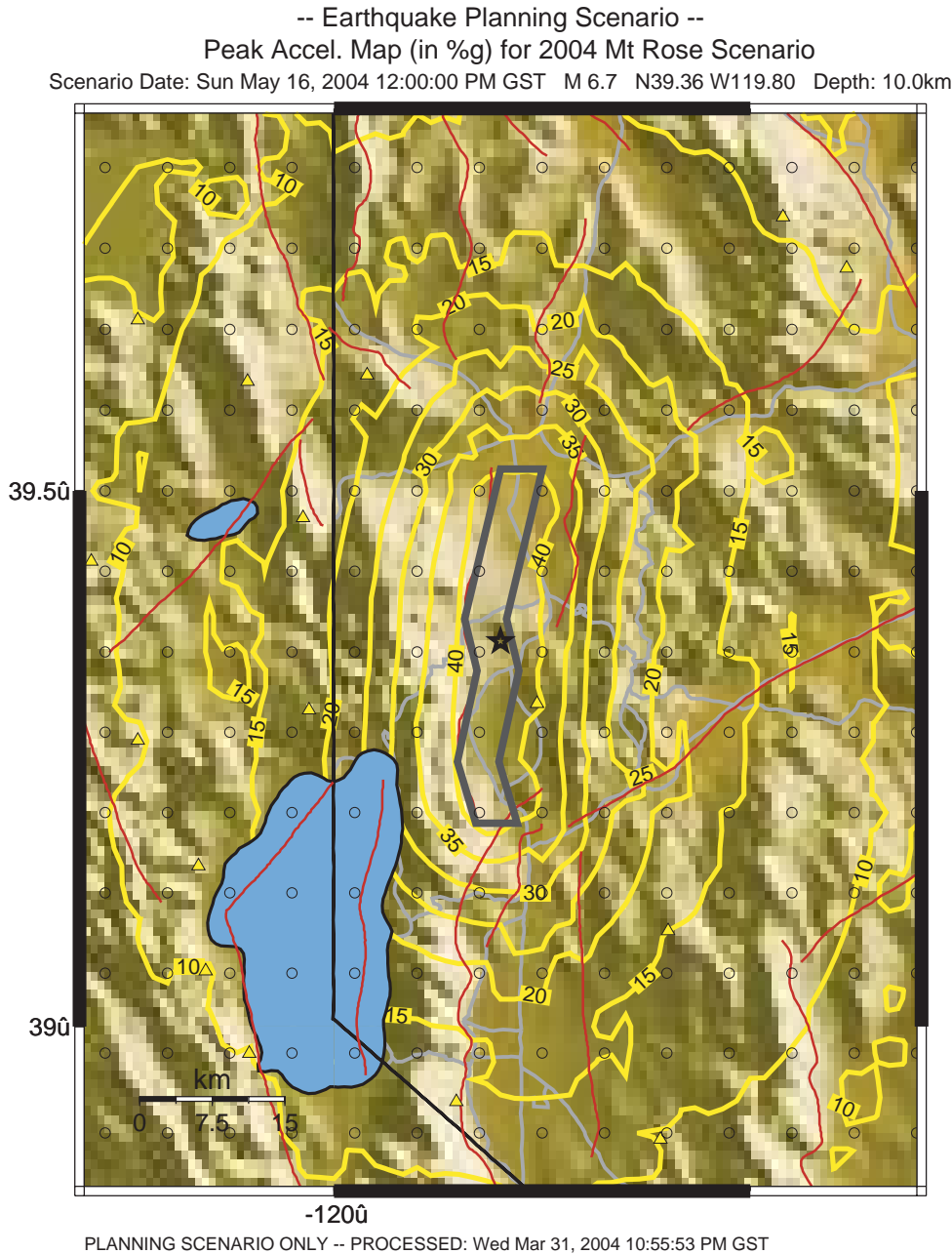
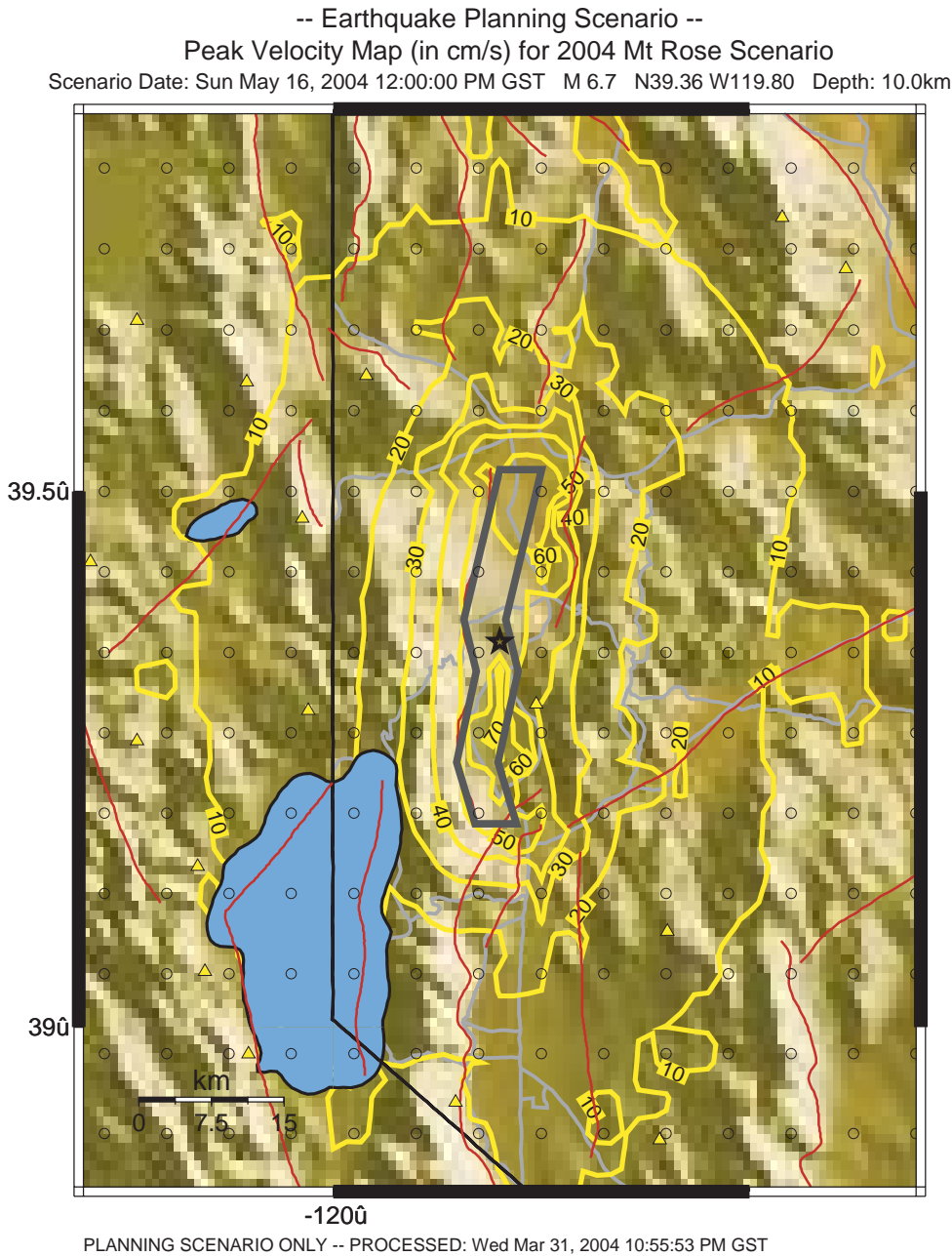


Figure 3. Peak ground acceleration ShakeMap for the scenario Mount Rose earthquake. Peak accelerations in excess of 0.4 g are predicted for portions of the hanging wall above and east of the rupture area, where river sediments are generally thicker, finer, and younger than to the west (Scott and others, 2004b).

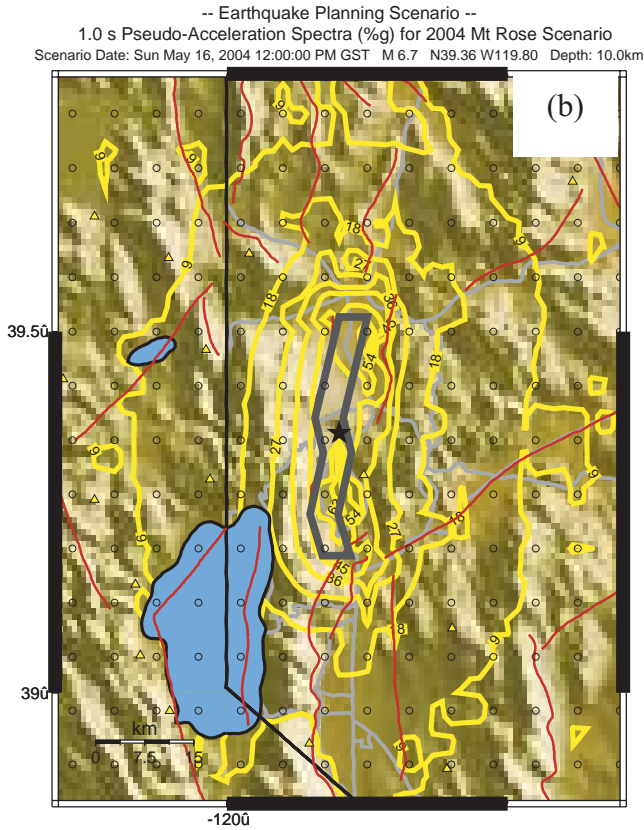
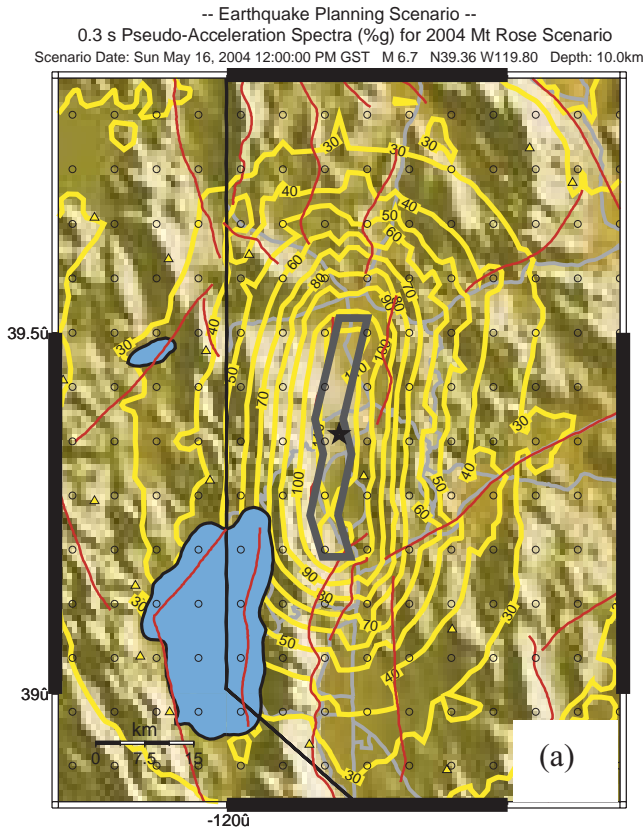
System (ANSS) initiative has provided significant new instrumentation (figure 1) and development funding to regional seismic networks, especially in the western United States where seismic risk is concentrated. In Nevada the ANSS program has provided 35 new accelerographs and related support to enable several existing strong-motion stations to be integrated into the real-time data stream coming into NSL. Figure 1 shows that coverage is divided between the Reno-Carson City urban corridor and

the Las Vegas Valley, commensurate with the hazard. Using the informal standard of having at least ten contributing stations, NSL is able to make instrumental ShakeMaps for the urban areas in which the vast majority of Nevadans live.

Strong-motion station telemetry includes a mixture of methods, including direct radio links, semi-private internet via Virtual Private Networking, IP over analog microwave, and shared public internet. NSL does not presently use dial-up



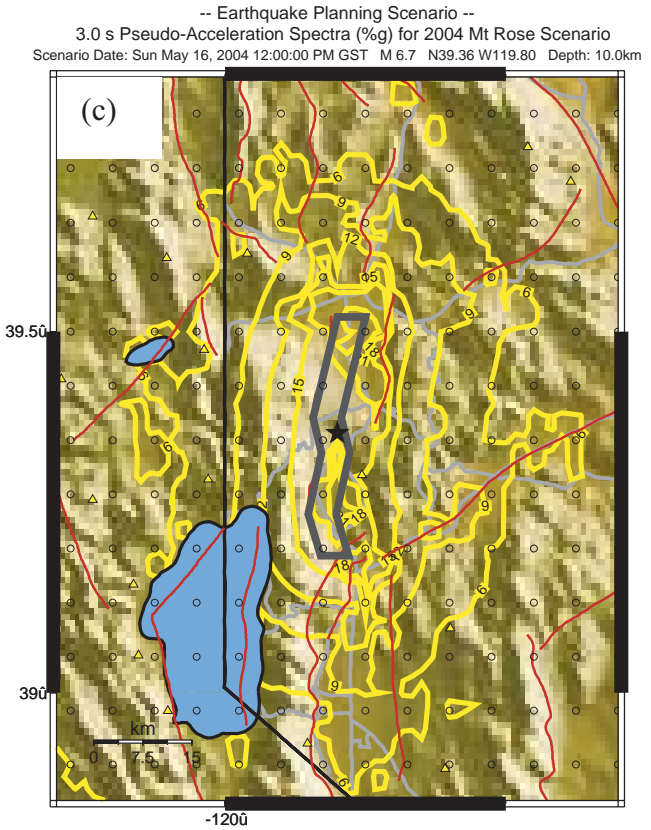
*Figure 4. Peak ground velocity ShakeMap for the Mount Rose scenario rupture. Contour interval is 10 cm/sec. Peak velocities are predicted to exceed 60 cm/sec in much of the valley. The Reno-Tahoe International Airport is near the north end of the scenario rupture in the region of peak predicted velocities.*

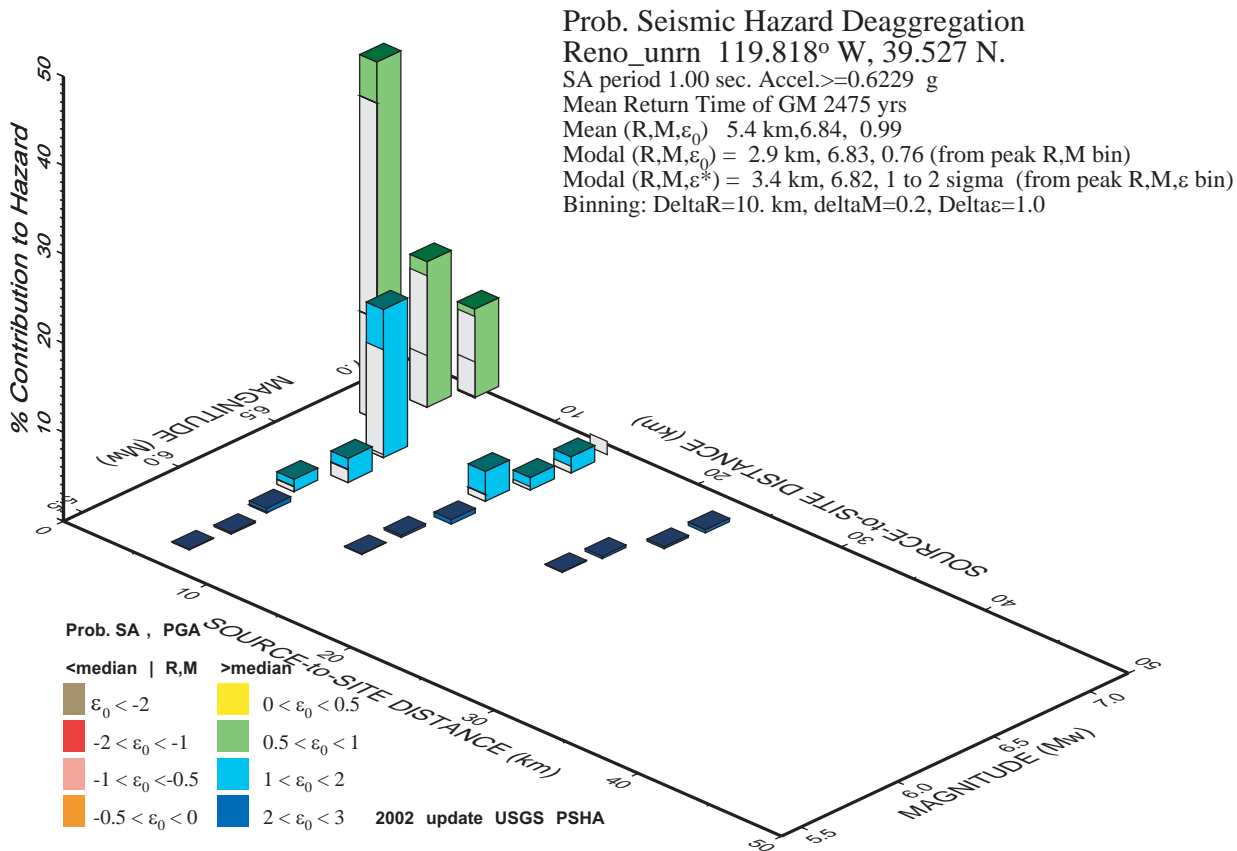


as a data retrieval method. Continuous data have the great advantage of providing data from moderate earthquakes that often do not trigger the station, but never-the-less are recorded at a good signal-to-noise level. Moderate earthquake recordings are valuable for site effect studies and as some assurance that the instrument will function well when a larger earthquake happens. Beside their uses for Nevada, northern Nevada strong-motion instruments also contribute to ShakeMaps in easternmost California, including earthquakes in the Truckee-Tahoe area.

### SHAKEMAP AS A PLANNING AND PREDICTION TOOL

Figure 5. Pseudo-acceleration maps for (a) 0.3 s, (b) 1.0 s, and (c) 3.0 s periods for a M6.7 scenario earthquake on the Mount Rose fault in western Nevada. Pseudo-acceleration provides an assessment of damage potential for structures of various heights. In this case accelerations are predicted to exceed 1.1 g locally at 3.3 Hz.





**GMT** Mar 20 17:29 Distance (R), magnitude (M), epsilon (E0,E) deaggregation for a site on rock with average vs=760m/s top 30 m.  
 Bins with lt 0.05% contrib. omitted

Figure 6. Hazard deaggregation for a point in downtown Reno using USGS National Seismic Hazards Mapping Project on-line tools. Hazards are identified for the 2% in 50 year level. Three discrete faults contribute 1% or more, the Mount Rose fault system (tallest bars, shortest distance), the North Peavine fault (~8 km) and the Spanish Springs fault (~12 km). The several hazard bars for each fault reflect the contribution of possible magnitudes to the total hazard.

The forward prediction facilities that enable ShakeMap to estimate ground-shaking at pseudo-stations for an actual event make it useful as a tool for evaluating the effects of scenario earthquakes. Figure 2 illustrates a scenario intensity map involving a "characteristic" rupture of the Mount Rose fault, a range-bounding, east-dipping normal fault that extends from the northern Carson Valley to near downtown Reno. The fault geometry, likely magnitude, and length were taken from the USGS National Seismic Hazards Mapping Project database. ShakeMap in automatic mode uses a point source at the earthquake hypocenter, but with

analyst input, can use a finite-length source such as the one shown. The map-view width of the fault reflects the horizontal extent of the dip of the fault. Thus a vertical fault would be displayed as a line. Ground motions are estimated from the least distance to the surface trace of the fault.

Figure 2 shows that the scenario Mount Rose characteristic event could produce Intensity VIII shaking throughout the Reno and north Carson areas. The Instrumental Mercalli Intensities are determined from a regression against peak ground acceleration and peak ground velocity values as described in Wald and others (1999a).

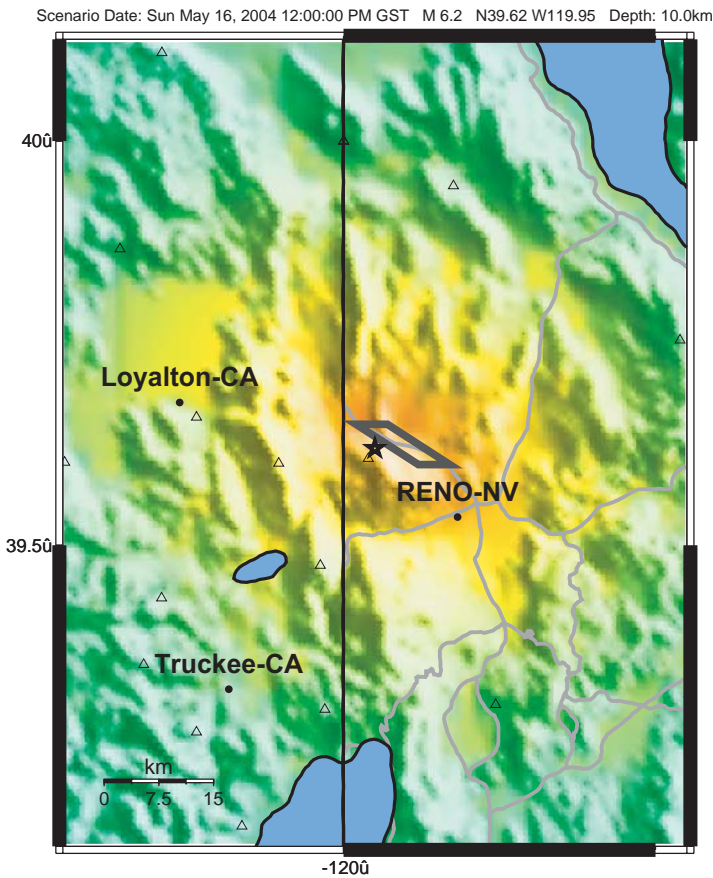
Amplification effects are predicted throughout the valley areas, especially in the hanging-wall region in and east of Reno. At least light damage can be predicted for the majority of the region shown.

Figure 3 shows predicted peak ground accelerations for the Mount Rose fault scenario event. Horizontal peak accelerations are predicted

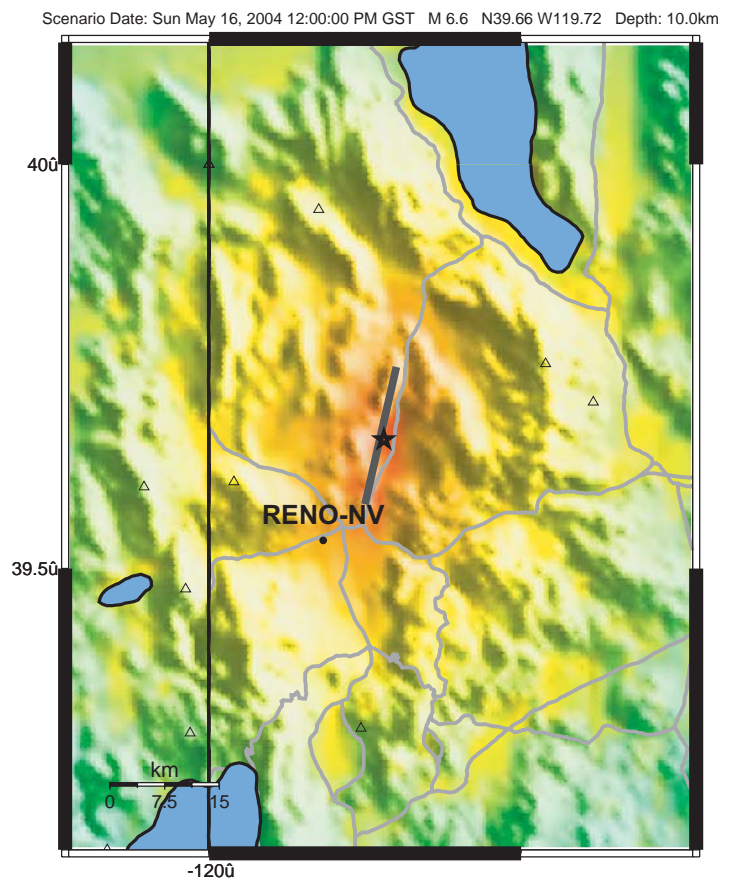
Figure 7. Scenario characteristic rupture of the North Peavine fault. The scenario assumes a rupture length of 10 km, and a moment magnitude of 6.2. Ramelli and others (2004) recently excavated the North Peavine fault and found Holocene ground ruptures with offsets consistent with the scenario magnitude. Accelerations in Reno could exceed 0.20 g for much of the downtown region for this scenario rupture.

to reach over 40% of gravity for much of the hanging-wall region of the rupture - in this case the most populated portion of the valley. Figure 4 shows the corresponding ground velocities, which are predicted to locally exceed 70 cm/sec. Ground motions of this magnitude pose a serious hazard to life and property. dePolo and others (1997)

Figure 8. Scenario Spanish Springs fault rupture assuming a rupture length of 18 km and a scenario magnitude of 6.6. This fault is a minor contributor to hazard in downtown Reno, but runs through one of the fastest growing regions of northern Nevada. Peak accelerations associated with this scenario reach 0.4 g near the fault.



PERCEIVED SHAKING	Not felt	Weak	Light	Moderate	Strong	Very strong	Severe	Violent	Extreme
POTENTIAL DAMAGE	none	none	none	Very light	Light	Moderate	Moderate/Heavy	Heavy	Very Heavy
PEAK ACC. (%g)	<.17	.17-1.4	1.4-3.9	3.9-9.2	9.2-18	18-34	34-65	65-124	>124
PEAK VEL. (cm/s)	<0.1	0.1-1.1	1.1-3.4	3.4-8.1	8.1-16	16-31	31-60	60-116	>116
INSTRUMENTAL INTENSITY	I	II-III	IV	V	VI	VII	VIII	IX	X+



PERCEIVED SHAKING	Not felt	Weak	Light	Moderate	Strong	Very strong	Severe	Violent	Extreme
POTENTIAL DAMAGE	none	none	none	Very light	Light	Moderate	Moderate/Heavy	Heavy	Very Heavy
PEAK ACC. (%g)	<.17	.17-1.4	1.4-3.9	3.9-9.2	9.2-18	18-34	34-65	65-124	>124
PEAK VEL. (cm/s)	<0.1	0.1-1.1	1.1-3.4	3.4-8.1	8.1-16	16-31	31-60	60-116	>116
INSTRUMENTAL INTENSITY	I	II-III	IV	V	VI	VII	VIII	IX	X+

developed a ground-shaking scenario for the Reno area based on a similar earthquake, and showed that it would present a significant hazard, especially to the city's unreinforced masonry buildings. Since the majority of the region's emergency responders live in the region that could see damaging levels of shaking, preparation for such an event should consider potential difficulties in mounting an emergency response.

While not shown here, the ShakeMap program also generates files formatted for input into HAZUS. When ground shaking such as in figure 3 is overlain on coverages of building density and fragility, reasonable estimates of the scope of damage and cost can be developed. While the integration is still in work at UNR, similar connections of ShakeMap and HAZUS in California are exercised routinely by the California Office of Emergency Services. In a related vein, GIS tools have been developed for California users to allow individual stakeholders such as power companies to integrate structural fragilities in real-time; these tools will eventually be available from regional seismic networks that produce ShakeMaps. The application, called ShakeCast, is designed as a client to be run by users that pulls in ShakeMaps from a central server in a format useful for overlay and rapid damage assessment.

ShakeMap also supports quick-look engineering assessments of possible damage. Figure 5 shows pseudo-acceleration spectra from the M6.7 Mount Rose fault scenario for three free periods. Pseudo-acceleration estimates used in making ShakeMaps are calculated from ground motion regression relations such as Pankow and Pechmann (2004) or Boore and others (1997). Physically, the pseudo-acceleration time series is the convolution of a one-degree-of-freedom harmonic oscillator with an input acceleration. The pseudo-accelerations thus provide a quick-look assessment of the demand in multi-story structures with commensurate free periods. In this example at

3.0 seconds, pseudo-acceleration spectra are less than 20% g, but reach to over 110% g at 0.3 seconds. The latter period is relevant to much of the mid-rise construction in Reno.

### **ShakeMap in Seismic-Hazard Analysis**

The above examples consider the seismic potential of a single fault. Seismic-hazard analysis methodologies, however, require that all faults capable of contributing to the hazard be included in the analysis. The USGS National Seismic Hazards Mapping Project provides the capability to do probabilistic seismic hazard deaggregations for specific points. To illustrate how ShakeMap might contribute to the seismic-hazard assessment process, we deaggregated the hazard (figure 6) for a point just west of downtown Reno. Three faults contribute more than ~1% to the 2% in 50 years (2475 year return period) hazard: the Mount Rose fault zone, the North Peavine Mountain fault, and the Spanish Springs Valley fault. By far the largest contributor (54% of the total) comes from the Mount Rose fault zone. Within the present understanding of relative fault activity, the Mount Rose fault rupture scenario is the most severe likely event in the long-term future for the Reno-Carson City urban corridor.

Earthquakes on each fault were run as scenario events assuming characteristic magnitudes in ShakeMap (figures 3, 7, 8). ShakeMaps provide a visual context of the respective hazards that is not readily apparent from the deaggregated hazard plots. Figures 7 and 8 from, respectively, the North Peavine Mountain and Spanish Springs faults, are greater hazards for communities north and northeast of Reno, but still contribute predicted accelerations near downtown Reno of about 0.25 g. While not changing the hazard, per se, ShakeMaps do allow the hazard to be better understood by engineers and stakeholders.

Scenario evaluations of shaking for seismic-hazard analysis highlight the need for more detailed

site characterization in urban valleys. Probabilities of ground motion and predicted amplifications presently depend on limited field estimates based on gravity and local seismic investigations. Some progress in this area is being made (Scott and others, 2004a, 2004b), but much work remains to characterize basin response with any real confidence.

### Conclusion

ShakeMap has become an integral part of the NSL real-time seismic network operations. Strong-motion station coverage realized through ANSS funding and support will constrain estimates of strong shaking in the urbanized areas of Nevada where seismic risk is greatest. Real-time telemetry of acceleration data allows recording of smaller earthquakes that are no hazard to people but are useful for characterization of site amplification and instrument sensitivity. Integration around Antelope data acquisition and analysis software means that data are available from a database in a uniform and easily accessed manner.

The ShakeMap scenario capability is useful as a tool for visualizing seismic hazard from known or hypothesized faults. When applied to known faults, scenario shaking maps facilitate understanding of and planning for what could happen should such an earthquake actually occur. When applied to hypothesized faults, the social consequences can be assessed, and the value of further study evaluated. In both cases, interacting with ShakeMaps can develop familiarity and confidence in the mapping products should a strong earthquake hit in Nevada.

### References

- Boore, D.M., Joyner, W.B., and Fumal, T.E., 1997, Equations for estimating horizontal response spectra and peak acceleration from western North American earthquakes: A summary of recent work: *Seismological Research Letters* v. 86, p. 128-153.
- dePolo, C.M., Anderson, J.G., dePolo, D.M., and Price, J.G., 1997, Earthquake occurrence in the Reno-Carson City urban corridor: *Seismological Research Letters*, v. 68, p. 401-412.
- Pankow, K.L., and Pechman, J.C., 2004, The SEA99 ground-motion predictive relations for extensional tectonic regimes: Revisions and a new peak ground velocity relation: *Bulletin of the Seismological Society of America*, v. 94, p. 341-348.
- Ramelli, A.R., Bell, J.W., and dePolo, C.M., 2004, Peavine Peak fault: Another piece of the Walker Lane puzzle [abs.]: *Western States Seismic Policy Council Basin and Range Province Seismic Hazards Summit II, Program and Abstracts*, p. 126-128.
- Scott, J.B., Clark, M., Rennie, T., Pancha, A., Park, H., Purvance, M., Biasi, G., Anoooshehpour, A., and Louie, J.N., 2004a, Evaluation of an earthquake mapping model for Reno, Nevada [abs.]: *Western States Seismic Policy Council Basin and Range Province Seismic Hazards Summit II, Program and Abstracts*, p. 129-134.
- Scott, J.B., Clark, M., Rennie, T., Pancha, A., Park, H., and Louie, J.N., 2004b, A shallow shear-wave velocity transect across the Reno, Nevada area basin: *Bulletin of the Seismological Society of America*, v. 94, to appear in December.
- Spudich, P., Joyner, W.B., Lindh, A.G., Boore, D.M., Margaris, B.M., and Fletcher, J.B., 1999, SEA99: A revised ground motion prediction relation for use in extensional tectonic regimes: *Bulletin of the Seismological Society of America*, v. 89, p. 1156-1170.
- Wald, D.J., Quitoriano, V., Heaton, T.H., and Kanamori, H., 1999a, Relationships between peak ground acceleration, peak ground velocity, and Modified Mercalli intensity in

California: *Earthquake Spectra*, v. 15, p. 557-564.

Wald, D.J., Quitoriano, V., Heaton, T.H., Kanamori, H., Scrivner, C.W., and Worden, C.B., 1999b, TriNet "ShakeMaps": rapid generation of peak ground motion and intensity maps for earthquakes in southern California: *Earthquake Spectra*, v. 15, p. 537-555.

### **Acknowledgments**

Support from the National Earthquake Hazard Reduction Program through Cooperative Agreements 1HQAG0009 and 04HQAG0004, the Department of Energy through the Cooperative Agreement with the University and Community College System of Nevada for ShakeMaps around Yucca Mountain, and the State of Nevada are gratefully acknowledged. Kris Pankow and Bill Lund provided helpful and constructive reviews.

# ***PATTERN AND TIMING OF FAULTING IN THE CENTRAL NEVADA SEISMIC BELT AND IMPLICATIONS FOR SEISMIC HAZARDS OF THE WESTERN BASIN AND RANGE PROVINCE***

John W. Bell<sup>1</sup>, S. John Caskey<sup>2</sup>, and Alan R. Ramelli<sup>1</sup>

<sup>1</sup> Nevada Bureau of Mines and Geology, University of Nevada, Reno NV 89557

<sup>2</sup> Department of Geosciences, San Francisco State University, San Francisco, CA 94132

## **ABSTRACT**

The central Nevada seismic belt (CNSB) is a concentration of historical (1915-1932-1954) surface faulting in the western Basin and Range Province, forming a linear, nearly continuous 300-km-long rupture zone. In this study, we have integrated previous results with new paleoseismic and exploratory trenching data from the historical zones to look for evidence of older, similar belt-like patterns or elevated slip rates that could indicate whether the CNSB is a zone of focused, long-term crustal strain, and hence a persistent zone of elevated seismic hazard. Conversely, the lack of evidence for long-term belt-like behavior in the CNSB would have implications bearing on the seismic hazard presented by other late Quaternary faults in the western Nevada region.

The data show that the continuous rupture belt produced by the seven earthquakes occurring between 1915 and 1954 is unique in the available paleoseismic record. At the 1954 Fairview Peak fault, the lack of prehistorical faulting in deposits containing the Wilson Creek bed 19 tephra eliminates the possibility of an identical seismic belt in the past 35.4 ky. Our studies also show that the faults have net slip rates ranging from a low of 0.09 mm/yr on the Fairview Peak fault to a high of 0.7 mm/yr on the 1932 Cedar Mountain fault. These are considered moderate to low rates similar to most late Quaternary faults in the western Basin and Range Province, which have slip rates between 0.1-1.0 mm/yr. In contrast, it is significant to note that the highest slip-rate faults (>1 mm/yr) known in the region-- the Genoa, Honey Lake, and Pyramid Lake faults (Figure 1)--have not ruptured historically. Such faults illustrate that high slip rate cannot be the sole determining factor in forecasting seismic hazard.

Based on these results, we reach several conclusions regarding the longer term (~Holocene) behavior of the CNSB and the western Nevada region. Although paleoseismic data preclude an older identical rupture belt among the historical zones, consideration of associated Holocene faults within the greater CNSB region indicates that several similar, but not identical, belt-like rupture patterns are plausible during the past 13 ky. Although long-term strain (represented by density of young faults) does appear to increase from east to west into the CNSB, the slip-rate data demonstrate that the CNSB is not a belt of concentrated or elevated crustal strain compared with areas that extend west to the Sierra Nevada. The increase in the distribution of Holocene fault activity from east to west into the CNSB is consistent with a marked increase in the 1992-2002 GPS velocity field at the latitude of the 1954 rupture sequence. The contemporary strain measured by GPS across the CNSB (2.20-3.13 mm/yr) is significantly greater than the long-term geologic extension rate (0.59-1.17 mm/yr), indicating that the CNSB may continue to be a zone of elevated near-term seismic hazard.

We further conclude that the results of our study of fault behavior in the CNSB best support the belt migration model proposed by Wallace (1987) for the western Basin and Range Province in which temporal tectonic pulses are believed to migrate regionally, activating different belt-like combinations of late Quaternary faults in an as-yet unknown pattern of migration. Together with the evidence indicating that the highest slip-rate faults in the region have not been historically active, the migration model introduces uncertainties into estimating seismic hazard and suggests that probabilistic seismic hazard models that utilize moment rate as a determining hazard factor may need to incorporate these variables.

## **BACKGROUND AND PURPOSE OF STUDY**

The central Nevada seismic belt (CNSB) is a concentration of historical medium- to large-magnitude (M 6.4-7.7) earthquake activity between 1915 and 1954 that produced a linear, nearly continuous zone of surface faulting more than 300 km in length (Figure 1). Including the eastern California shear zone and the 1872 Owens Valley event, the combined historical rupture zone is more than 600 km in length with only two fault segments that did rupture: the White Mountains and Stillwater seismic gaps. This continuity of surface rupturing is unprecedented in the historical record of the Basin and Range Province. Although linear in extent, the CNSB does not mark the trace of a single, through-going fault system. Rather surface ruptures occurred along a series of individual faults distributed among numerous similar late Quaternary faults in the western Basin and Range region.

The contemporary seismotectonics of the western Basin and Range Province are related to a broad zone of diffuse, northwest-directed, right-lateral shear occurring between the Sierra Nevada microplate and the central part of the Basin and Range Province (cf., Thatcher and others, 1999). Portions of the CNSB lie within the Walker Lane belt (WLB), a 700-km-long zone of late Cenozoic, northwest-trending, strike-slip faulting that disrupts the more characteristic pattern of northeast-striking normal faulting of the central Basin and Range Province (Figure 1). Right-lateral shear within

the WLB has long been thought to represent San Andreas-style motion within the Basin and Range Province (Gianella and Callaghan, 1934).

During the past decade, several sets of space-based geodetic data demonstrated that contemporary northwest-directed shear strain across the Sierra Nevada-Basin and Range transition zone is on the order of 11-13 mm/yr (Thatcher and others, 1999; Wernicke and others, 2000; Bennett and others, 2003; Hammond and Thatcher, 2004). Continuous and campaign GPS data collected since 1992 suggest that some of this regional strain is localized across the CNSB, where as much as 3-3.5 mm/yr of differential strain may be occurring (Hammond and Thatcher, 2004; R. Bennett, 2004, written commun.).

This historical, belt-like clustering of earthquakes and accompanying surface faulting are also unusual in that recurrence intervals on these and similar Basin and Range Province faults have been estimated to be on the order of thousands to tens of thousands of years (Wallace, 1984). To explain this pulse of historical activity, Wallace (1987) proposed a model in which belt-like, temporal clusters of fault activity migrate about the Basin and Range Province over time. He postulated that such belt-like migration would occur in some unknown and unpredictable pattern and would involve faults with variable recurrence and slip rates.

The CNSB provides a unique historical data set for better understanding the longer term seismotectonic behavior of the Basin and

Range Province. The historical rupture patterns and slip data together with paleoseismic information for the faults can demonstrate whether the CNSB has been (or still is) a zone of long-term, elevated seismicity or just a temporal pulse of activity as suggested by Wallace (1987). Combined with the provisional observations that these faults are similar to most other faults in the western Basin and Range Province, knowledge of the pattern and timing of surface faulting events within the CNSB can provide additional insights into the behavior of seismogenic faults and to the characterization of seismic hazard.

In this study, we have compiled paleoseismic data for faults within the 1915-1932-1954 portion of the CNSB based on new trenching data in combination with previously published results. We examined both historical and associated prehistorical faults to search for evidence of prior belt-like behavior. We determined net geologic slip directions at each fault site to closely estimate geologic slip rates for comparison with contemporary geodetic rates. The principal area of focus is the region of the 1954 sequence where three Rainbow Mountain events occurred in July and August 1954, followed by the Fairview Peak-Dixie Valley sequence in December (Figure 2). This portion of the CNSB is crossed by the U.S. Geological Survey (USGS) highway 50 GPS line, which provides the opportunity to closely compare contemporary geodetic rates with longer-term geologic slip rates of faults crossed by the line.

This paper summarizes the detailed results presented in Bell and others (2004) and

Caskey and others (2004), with an emphasis on the relevant highlights related to seismic hazard in the western Basin and Range.

## **SUMMARY OF PALEOSEISMIC DATA**

We have combined results of previous studies from the 1915 Pleasant Valley zone (Anderson and Machette, 2003), the 1932 Cedar Mountain zone (Bell and others, 1999), and the 1954 Dixie Valley zone (Bell and Katzer, 1990) with new paleoseismic data from the 1954 Rainbow Mountain zone and the 1954 Fairview Peak zone. In addition we examined the paleoseismic histories of several structurally associated faults: the Sand Springs-La Plata Canyon fault, the West Stillwater fault, and the Stillwater seismic gap. Collectively, these faults form the paleoseismic data set that we use to assess the pattern and timing of faulting in the CNSB.

New exploratory trenches were excavated at six locations (Figure 2) and additional structural-stratigraphic data were developed from surficial mapping in the Stillwater seismic gap. A combination of radiocarbon dating and tephrochronology was used to constrain the ages of events, with regional stratigraphic controls provided by the late Quaternary histories of pluvial Lake Lahontan (Morrison, 1991) and Lake Dixie (Thompson and Burke, 1973). Table 1 summarizes the timing of events for each of the fault zones.

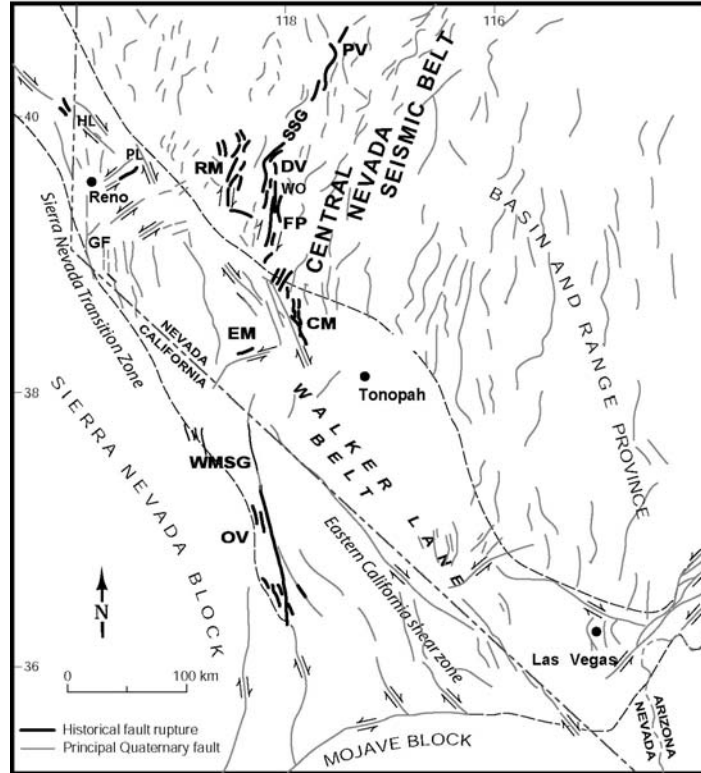


Figure 1. Principal structural-tectonic features of the western Basin and Range region showing major Quaternary fault traces (light black lines), historical surface fault traces (heavy black lines), and the location of the central Nevada seismic belt. The historical events include: 1872 Owens Valley (OV), 1903 Wonder (WO), 1915 Pleasant Valley (PV), 1932 Cedar Mountain (CM), 1934 Excelsior Mountain (EM), 1954 Rainbow Mountain-Stillwater (RM), 1954 Fairview Peak (FP), and 1954 Dixie Valley (DV). The only two sections in the sequence of faulting between Owens Valley and Pleasant Valley that have not historically ruptured are the White Mountains seismic gap (WMSG) and the Stillwater seismic gap (SSG). Other principal faults include: Genoa fault (GF), Pyramid Lake fault (PL), and the Honey Lake fault (HL). The dashed line delineates the Walker Lane belt.

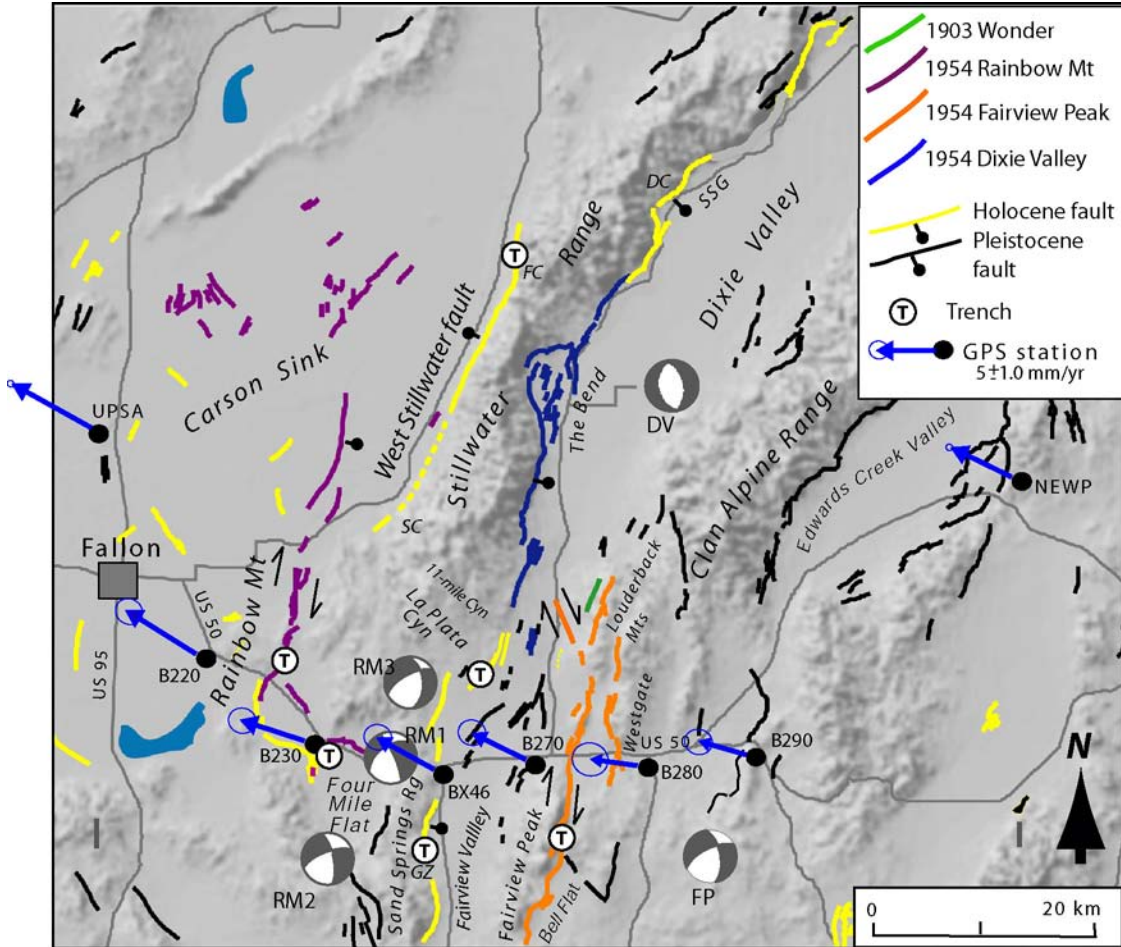


Figure 2. Map of historical and Quaternary faults in the 1954 Rainbow Mountain-Fairview Peak-Dixie Valley region, location of trench sites, and earthquake mechanisms marking the epicentral locations for the Rainbow Mountain-Stillwater (RM1, RM2, RM3), Fairview Peak (FP), and Dixie Valley (DV) events (from Doser, 1986). Campaign GPS velocity data along US 50 (stations B220-B290) are from Hammond and Thatcher (2004) and the continuous velocity data (NEWP-UPSA) from Bennett and others (2003). Site locations discussed in text: GZ Canyon (GZ), Dixie Comstock (DC), Shirrtail Canyon (SC), and Fondaway Canyon (FC). Fault map modified from Bell (1984) and Dohrenwend and others (1996).

*Table 1. Summary of ages of most recent event (MRE) and penultimate event (PE) for faults in the central Nevada seismic belt.*

<u>Fault zone</u>	<u>MRE</u>	<u>PE</u>	<u>Reference</u>
1915 Pleasant Valley	historical	6.9 ka to 15-18 ka	Anderson and Machette (2003)
1932 Cedar Mountain	historical	4 ka	Bell and others (1999)
1954 Fairview Peak	historical	35.4 ka to >100 ka	This study
1954 Dixie Valley	historical	2.0-2.5 ka	This study
1954 Rainbow Mt	historical	6.3-9.9 ka	Caskey and others (2004)
1954 Fourmile Flat	historical	<0.5-1.5 ka	Caskey and others (2004)
Sand Springs fault at Sand Springs Rg	0.5-9.3 ka	>10.5-11.7 ka	This study
Sand Springs fault at La Plata Cyn	0.5-3.4 ka	7.3-13.3 ka	This study
Stillwater seismic gap	2.0-2.5 ka	>10.5-11.7 ka	This study; Lutz and others (2003)
West Stillwater	5.6-6.9 ka	>13.0 ka	This study

### **EVIDENCE FOR PRIOR BELT-LIKE PATTERNS**

A synthesis of new and previous paleoseismic studies demonstrates that the historical rupture zones and the associated Holocene fault zones each have different slip histories. Based on a space-time distribution of paleoearthquakes within these fault zones (Figure 3), it is evident that the 300-km-long, nearly continuous rupture pattern produced by the 1915-1932-1954 sequence is unprecedented in the available paleoseismic record. Most importantly, the number and timing of events in each of the zones preclude the possibility of an identical belt during the late Quaternary. The most convincing evidence supporting this conclusion comes from the Fairview Peak fault where we can demonstrate that no other faulting events have occurred since deposition of the 35.4 ka Wilson Creek tephra bed. In addition, the ages of the penultimate events in each of the historical zones are diverse, ruling out the possibility of a similar rupture belt during the last prehistorical ruptures.

Historical ruptures occurred on only a few of the late Quaternary faults in the greater

CNSB region (Figure 2). Considering the possibility of other similar, but not identical belts, we examined and compared the slip histories of the historical zones with the associated Holocene fault zones. We found that if the Sand Springs-La Plata fault zone is substituted for the Fairview Peak fault, several plausible belt-like scenarios are possible: 2-4 ka, 6-9 ka, and 10-13 ka. None of these possible rupture patterns would fully duplicate the historical pattern, however, and each would require one or more seismic gaps.

### **GEOLOGIC SLIP RATES**

We have determined geologic slip rates for the four principal faults of the 1954 rupture zone that are crossed by the US highway 50 GPS transect: the Fairview Peak, Sand Springs-La Plata Canyon, Fourmile Flat, and Rainbow Mountain faults (Figure 2). We used vertical slip rates, fault dip measurements, and instrumental and geologic slip azimuths to calculate net slip vectors and slip rates, an approach we consider preferable to using site-specific slip indicators such as the rake of slickenlines.

Net slip and net slip rates were determined from vertical slip and rates measured at each of the trenching sites, and from the plunge of the net slip vector. The net slip rates were converted into extensional slip rates in the direction of the GPS vector in order to directly compare the geodetic and geologic rates (Table 2).

The slip-rate data indicate that these are not high-slip rate (>1 mm/yr) faults, but are instead considered moderate- to low-slip rate structures (cf. Slemmons and dePolo, 1986). These faults also do not exhibit elevated slip rates relative to other Basin and Range faults. Despite their varied slip histories, the CNSB faults have similar late Quaternary slip rates in the range of ~0.1 mm/yr (Fairview Peak) to 0.7 mm/yr (Cedar Mountain). The most recent compilation of geologic slip rates for the western Basin and Range Province (U.S. Geological Survey, 2003) shows that most faults in the region between the CNSB and the Sierra Nevada have slip rates in the range 0.2-1.0 mm/yr.

### **COMPARISON OF GEOLOGIC AND GEODETIC SLIP RATES**

Several sets of GPS data are available for the CNSB between Rainbow Mountain and Fairview Peak. For this study we compared the geologic data with the most recent campaign data reported by Hammond and Thatcher (2004). Their study reports velocity data between 1992-2002 for six stations crossing the CNSB (stations B220 to B290, Figure 2).

Our comparison indicates that geologic extension rates determined using our preferred slip azimuth approach are significantly lower than the horizontal GPS velocity rates (Table 2). The largest differences are on the order of a factor of four to five. For the four principal faults crossed by the US 50 line, the total extensional slip rate resolved along a 321° GPS azimuth is 0.59-0.69 mm/yr compared to the

velocity gradient of 3.13 mm/yr between stations B220-B290.

Such discrepancies between geologic and geodetic strain rates have previously been attributed to several possible causes: post-seismic (transient) relaxation, temporal variations in geologic rates, and incompleteness of the geologic record. The location and paleoseismic histories of faults in the greater CNSB region are well known, precluding the likelihood that undetected, high-slip-rate faults can account for the difference. Most current models attribute the difference at least in part to post-seismic transient effects (Hetland and Hager, 2003; Hammond and Thatcher, 2004). An additional possibility that should be considered, however, is that the elevated contemporary rates may be the result of accelerating strain in advance of another earthquake in the CNSB region. Such a possibility is supported by recent synthetic aperture radar interferometry (InSAR) studies that show regional uplift on the order of 1-3 mm/yr occurring throughout the CNSB between Fairview Peak and Pleasant Valley (Gourmelen and Amelung, 2003).

We also find that although the geologic extension rates are considerably lower than the geodetic rates, the overall pattern of Holocene faulting appears to be consistent with increasing GPS strain rates, which begin to accelerate at about the latitude of the CNSB. The area extending from the CNSB west to the Sierra Nevada generally contains a larger number of Holocene faults than the area to the east. This fault density is well displayed on the most recent fault compilation for the Basin and Range Province (U.S. Geological Survey, 2003), and it is a pattern first noted in the early CNSB studies by Wallace (1984; 1987).

### **IMPLICATIONS FOR SEISMIC HAZARDS**

Our principal conclusion indicating that the

CNSB is unique in the available paleoseismic record has several implications for characterizing seismic hazards in the western Basin and Range Province. Our findings support the belt-migration model of Wallace (1984, 1987), which proposed that the CNSB is illustrative of belt-like patterns of fault activity that move about the region in an as-yet unknown pattern. Such a model would indicate that similar belts may develop in the future, which could activate other faults with diverse slip histories and low- to moderate-slip rates, i.e., other ordinary Basin and Range faults.

Most seismic-hazard models incorporate geologic slip rates in the form of geologic moment rates as a matter of convention in calculating probabilistic ground motion levels (cf., Frankel and others, 1996). This means that higher slip-rate faults will produce relatively higher probabilistic hazard compared to lower slip-rate faults.

As we have found in this study, however, the lower slip rates faults have been the most historically active, while the highest slip rate faults, such as the Genoa fault (Ramelli and others, 1996) have not been historically active. This suggests that geologic slip rate should not be a principal determining factor in estimating hazard in the Basin and Range Province.

These observations pose a dilemma for modeling seismic hazard because of the many moderate- to low-slip-rate faults in the western Nevada region (USGS, 2003). While high-slip-rate faults should arguably be considered significant seismogenic sources, the lower slip-rate faults clearly have higher potential hazard than currently incorporated in most models.

Further implications for seismic-hazard modeling are derived from the discrepancies that are observed between the geologic and geodetic strain rates. Elevated contemporary geodetic rates are suggestive of elevated crustal strain that may be precursory to earthquakes. To account for such occurrences, the National Seismic Hazard Maps initially

included an areal shear zone along the Sierra Nevada-Basin and Range Transition where geodetic data suggested higher geodetic strain was occurring compared to the geologic fault rates (Figure 4; Frankel and others, 1996). This areal shear zone consisted of a set of fictitious faults, which were assigned a collective shear rate of 4 mm/yr. The most recent revision of the National Seismic Hazard Maps (Frankel and others, 2002) further includes an areal shear for the CNSB, where a shear rate of 2 mm/yr has been applied to the probabilistic model. This addition was made after consideration of the elevated GPS gradients measured across the belt. The results of our study, which show that the geodetic rates are significantly higher than the long-term geologic rates, clearly support this addition to the maps.

## CONCLUSIONS

Paleoseismic investigations that we have conducted in the central Nevada seismic belt indicate that this historical combination of fault ruptures is unprecedented in the available paleoseismic record for the Basin and Range Province. A comparison of the space-time histories of the historical rupture zones indicates that while the faults have similar slip rates, they exhibit diverse slip histories, with no evidence of an identical rupture belt during the past 35.4 kyr. The paleoseismic data further demonstrate that the CNSB is not a zone of long-term, elevated geologic strain that could explain the occurrence and location of the belt. The faults have moderate to low slip rates similar to most other typical faults of the western Basin and Range Province. These results provide evidence supporting the belt migration proposed by Wallace (1984, 1987) where the CNSB is a temporal belt of activity. In this model, similar belts may become active within the Basin and Range Province in an as-

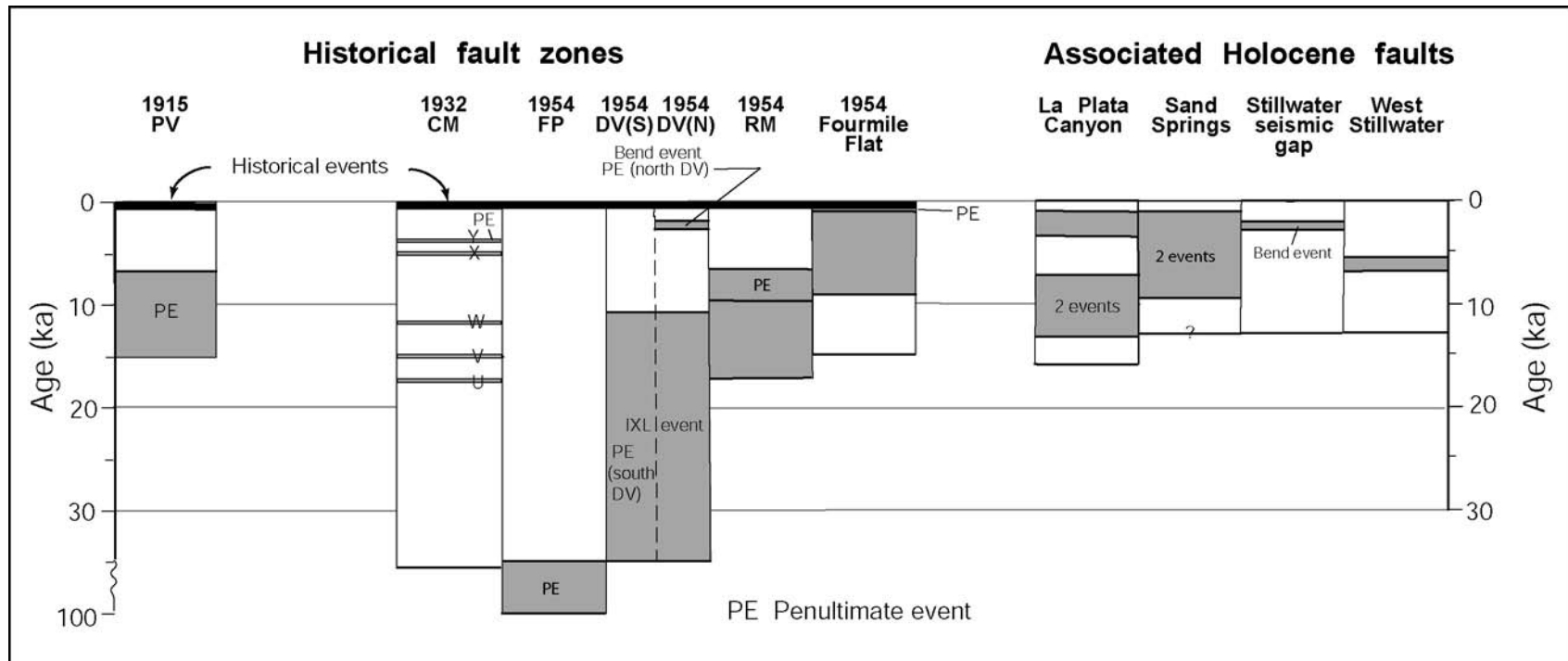


Figure 3. Simplified space-time diagram showing age constraints for events on historical and associated Holocene faults in the CNSB. Ages of events are determined from radiocarbon dating, tephrochronology, and dated shorelines of pluvial Lakes Lahontan and Dixie. Data from previous studies were obtained from the following: 1915 Pleasant Valley (Anderson and Machette, 2003); 1932 Cedar Mountain (Bell and others, 1999); 1954 Dixie Valley (Bell and Katzer, 1990). Detailed listing of the numerical age constraints are in Bell and others (2004) and Caskey and others (2004).

Table 2. Net slip rates (NSR) and extensional slip rates (ESR) for faults in the Rainbow Mountain to Fairview Peak transect. The extensional slip rate is resolved on the GPS azimuth for comparison of geodetic and geologic rates.

<b><u>Fault</u></b>	<b><u>NSR (mm/yr)</u></b>	<b><u>ESR (mm/yr)</u></b>	<b><u>ESR on 321° GPS Az</u></b>
<b>Rainbow Mt</b>	<b>0.20±0.02- 0.25±0.04</b>	<b>0.11±0.02- 0.13±0.04</b>	<b>0.11±0.02- 0.13±0.04</b>
<b>Fourmile Flat</b>	<b>0.40±0.01</b>	<b>0.20±0.01</b>	<b>0.20±0.01</b>
<b>Fairview Peak</b>	<b>0.09-0.22±0.03</b>	<b>0.05 - 0.13±0.03</b>	<b>0.05 - 0.13±0.03</b>
<b>Sand Springs- La Plata</b>	<b>0.50±0.01</b>	<b>0.23±0.08</b>	<b>0.23±0.08</b>
<b><i>Cumulative extensional geologic slip rate on GPS Az</i></b>			<b><i>0.59±0.14- 0.69±0.16</i></b>
<b><i>GPS rate (Hammond and Thatcher, 2004)</i></b>			<b><i>3.13±1.88</i></b>

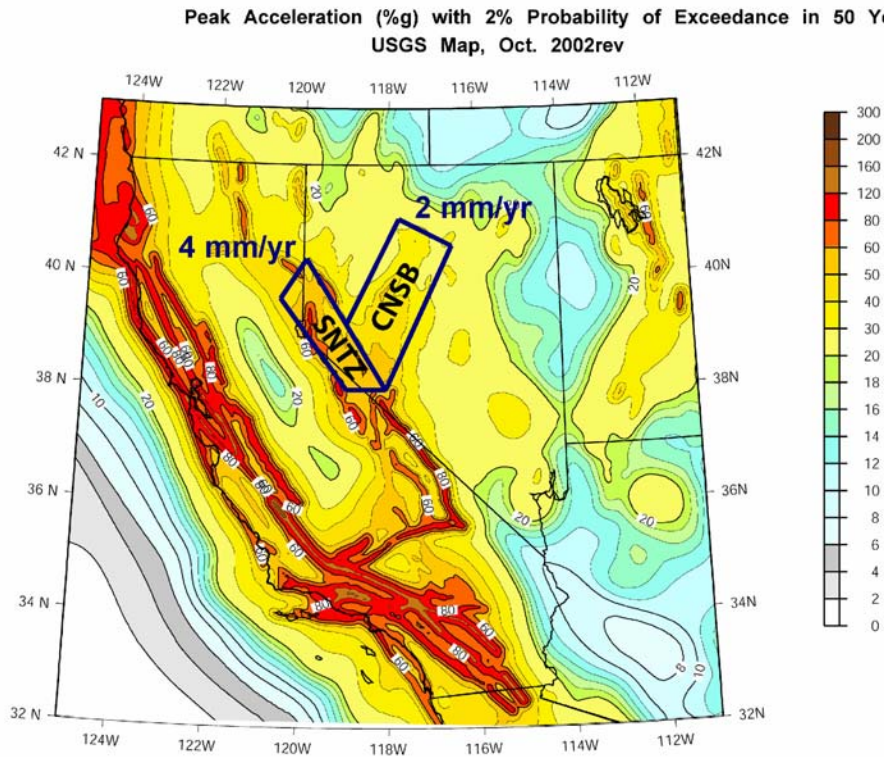


Figure 4. National Seismic Hazard Map for the Nevada-California region showing peak ground acceleration (2% PGA) in 50 years (Frankel and others, 2002). An areal shear with a shear rate of 4 mm/yr was added to the 1996 maps for the Sierra Nevada-Basin and Range Transition zone, and an areal shear zone with a shear rate of 2 mm/yr was added to the 2002 maps for the CNSB.

yet unknown pattern of activation.

This pattern of fault behavior together with evidence showing that the geologic slip rates are significantly lower than the contemporary geodetic strain (GPS) rates suggests that fault slip rate (geologic moment rate) should not be a principal determining criterion for estimating probabilistic seismic hazard.

### ACKNOWLEDGMENTS

This study was supported by U.S. Geological Survey National Earthquake Hazard Reduction Grants 1434-HQ-97-GR-03164, 1434-HQ-98-GR-00016, and 00HQGR0022 and Department of Energy Grant DE-FG07-98ID13620.

### REFERENCES

- Anderson, R.E., and Machette, M.N., compilers, 2003, Fault number 1136a-d, Pleasant Valley fault zone, *in* Quaternary fault and fold database of the United States, ver. 1.0: U.S. Geological Survey Open-File Report 03-417, <http://qfaults.cr.usgs.gov>.
- Bell, J.W., 1984, Quaternary fault map of Nevada—Reno sheet: Nevada Bureau of Mines and Geology Map 79, scale 1:250,000.
- Bell, J.W., and Katzer, T., 1990, Timing of late Quaternary faulting in the 1954 Dixie Valley earthquake area, central Nevada: *Geology*, v. 18, p. 622-625.
- Bell, J.W., dePolo, C.M., Ramelli, A.R., Sarna-Wojcicki, A.M., and Meyer, C.E., 1999, Surface faulting and paleoseismic history of the 1932 Cedar Mountain earthquake area, west-central Nevada, and implications for modern tectonics of the Walker Lane: *Geological Society of America Bulletin*, v. 111, p. 791-807.
- Bell, J.W., Caskey, S.J., Ramelli, A.R., Guerrieri, L., 2004, Pattern and timing of faulting in the central Nevada seismic belt and paleoseismic evidence for prior belt-like behavior: *Bulletin of the Seismological Society of America*, v. 94, no. 4, p. 1229-1254.
- Bennett, R.A., Wernicke, B.P., Niemi, N.A., and Friedrich, A.M., 2003, Contemporary strain rates in the northern Basin and Range Province from GPS data: *Tectonics*, v. 22, no. 2, 1008, doi:10.1029/2001TC001355, 2003.
- Caskey, S.J., Bell, J.W., Wesnousky, S.G., and Ramelli, A.R., 2004, Historic surface faulting and paleoseismicity in the area of the 1954 Rainbow Mountain-Stillwater earthquake sequence, central Nevada: *Bulletin of the Seismological Society of America*, v. 94, no. 4, p.1255-1275.
- Dohrenwend, J.C., Schell, B.A., Menges, C.M., Moring, B.C., and McKittrick, M.A., 1996, Reconnaissance photogeologic map of young (Quaternary and late Tertiary) faults in Nevada: Nevada Bureau of Mines and Geology Open-file Report 96-2, scale: 1,000,000.
- Doser, D., 1986, Earthquake processes in the Rainbow Mountain-Fairview Peak-Dixie Valley, Nevada region 1954-1959: *Journal of Geophysical Research*, v. 91, p. 12,572-12,586.
- Frankel, A., Mueller, C., Barnhard, T., Perkins, D., Leyendecker, E.V., Dickman, N., Hanson, S., and Hopper, M., 1996, National seismic hazard maps: Documentation June 1996: U.S. Geological Survey Open-File Report 96-532, 71 p.
- Frankel, A.D., Peterson, M.D., Mueller, C.S., Haller, K.M., Wheeler, R.L., Leyendecker, E.V., Wesson, R.L., Harmsen, S.C., Cramer, C.H., Perkins, D.M., and Rukstales, K.S., 2002, Documentation for

- the 2002 update of the National seismic hazard maps: U.S. Geological Survey Open-File Report 02-420, 33 p.
- Gianella, V.P., and Callaghan, E., 1934, The earthquake of December 20, 1932, at Cedar Mountain, Nevada, and its bearing on the genesis of Basin Range structure: *Journal of Geology*, v. 42, p. 1-22.
- Gourmelen, N., and Amelung, F., 2003, Anomalous crustal deformation in the central Nevada seismic belt detected by InSAR: *Eos Transactions of the American Geophysical Union*, v. 84 (46), Abstract G31B-0170.
- Hammond, W.C., and Thatcher, W., 2004, Contemporary tectonic deformation of the Basin and Range Province, western United States: 10 years of observation with the Global Positioning System: *Journal of Geophysical Research*, v. 109, n. B8, B08403, doi: 10.1029/2003JB002746, 2004.
- Hetland, E.A., and Hager, B.H., 2003, Postseismic relaxation across the central Nevada seismic belt: *Journal of Geophysical Research*, v. 108, no. B8, 2394, doi:10.1029/2002JB002257, 2003.
- Lutz, S.J., Caskey, S.J., Johnson, S.D., 2003, Geyserite, faulted sinter terraces, and other fossil hot spring deposits, northern Dixie Valley fault system, Nevada, *in* S. Foster, ed., 2003 Field Trip Guidebook: Nevada Petroleum Society, p. 75-89.
- Morrison, R.B., 1991, Quaternary stratigraphic, hydrologic and climatic history of the Great Basin, with emphasis on Lakes Lahontan, Bonneville, and Tecopa, *in* R.L. Morrison, ed., *Quaternary nonglacial geology, Conterminous U.S.*: Geological Society of America, *The Geology of North America*, v. K-2, p. 283-320.
- Ramelli, A.R., Bell, J.W., dePolo, C.M., and Yount, J.C., 1996, Large-magnitude, late Holocene earthquakes on the Genoa fault, west-central Nevada and eastern California: *Bulletin of the Seismological Society of America*, v. 89, p. 1458-1472.
- Slemmons, D.B., and dePolo, C.M., 1986, Evaluation of active faulting and associated hazards, *in* *Active tectonics*: Washington, D.C., National Academy Press, National Research Council, Panel on Active Tectonics, p. 45-62.
- Thatcher, W., Foulger, G.R., Julian, B.R., Svarc, J., Quilty, E., and Bawden, G.W., 1999, Present day deformation across the Basin and Range Province, western United States: *Science*, v. 283, p. 1714-1718.
- Thompson, G.A., and Burke, D.B., 1973, Rate and direction of spreading in Dixie Valley, Basin and Range Province, Nevada: *Geological Society of America Bulletin*, v. 84, p. 627-632.
- U.S. Geological Survey, 2003, Quaternary fault and fold database of the United States, ver. 1.0: U.S. Geological Survey Open-File Report 03-417, <http://qfaults.cr.usgs.gov>.
- Wallace, R. E., 1984, Patterns and timing of late Quaternary faulting in the Great Basin Province and relation to some regional tectonic features: *Journal of Geophysical Research*, v. 89, p. 5,763-5,769.
- Wallace, R.E., 1987, Grouping and migration of surface faulting and variations in slip rates on faults in the Great Basin Province: *Bulletin of the Seismological Society of America*, v. 77, p. 868-876.
- Wernicke, B., Friedrich, A.M., Niemi, N.A., Bennett, R.A., and Davis, J.L., 2000, Dynamics of plate boundary fault systems from Basin and Range geodetic network (BARGEN) and geologic data: *GSA Today*, v. 10, p. 1-7.

## ***PALEOSEISMIC INVESTIGATION OF THE CANYON FERRY FAULT, WEST-CENTRAL MONTANA***

Larry W. Anderson  
Lucille A. Piety

U.S. Bureau of Reclamation, Seismotectonics and Geophysics Group, Box 25007, D-8330  
Denver, CO 80225

Susan S. Olig  
URS Corporation, 1333 Broadway, Suite 800, Oakland, CA 94612

Steven L. Forman  
Department of Earth and Environmental Sciences, University of Illinois, 845 W. Taylor St.,  
Chicago, IL 60607

### **ABSTRACT**

The 48-km-long Canyon Ferry fault bounds the west side of the Big Belt Mountains, approximately 30 km east of Helena, Montana. The fault is a major, down-to-the-west structure bounding the northern Townsend Basin. Although the fault has significant late Cenozoic displacement, like many faults in Montana and the northern Basin and Range, the late Quaternary activity of the fault is poorly documented. Based on aerial photograph interpretation, reconnaissance surficial geologic mapping, and scarp profiling, the late Quaternary Canyon Ferry fault can be characterized by rupture lengths of at least 40 km. The possibility also exists that the Toston fault, immediately south of the Canyon Ferry fault, may be part of this system which would indicate that total rupture lengths of over 60 km may be possible.

A paleoseismic trench excavated at the G/T Ranch near the central portion of the Canyon Ferry fault provides important information on the slip rate, recurrence, and slip per event for the fault. Age data are from eleven infrared stimulated luminescence (IRSL) analyses on fine-grained deposits (primarily loess) collected from the trench. At the trench site, total dip-slip displacement of approximately 9 m occurred over a 55 kyr period between about 68 ka and 13 ka. These data indicate a long-term late-Quaternary slip rate of 0.13 mm/yr for the fault. Interestingly, based on about 5 m of dip slip in the past 21 kyr, the rate is 0.24 mm/yr. More importantly, stratigraphic relations and the numerical ages provide strong evidence for seismic clustering of events. At least two, and probably three, surface-rupturing events occurred between about 21 ka and 13 ka indicating a short-term rate of 0.56 mm/yr. No surface rupturing events have occurred since about 13 ka. Thus, recurrence intervals for the Canyon Ferry fault could be as long or longer than 13 kyr or as short as a few thousand years.

## INTRODUCTION

The Canyon Ferry fault is a recurrently active,

late Quaternary, range-bounding normal fault at the western base of the Big Belt Mountains in west-central Montana (Figure 1). The fault is about

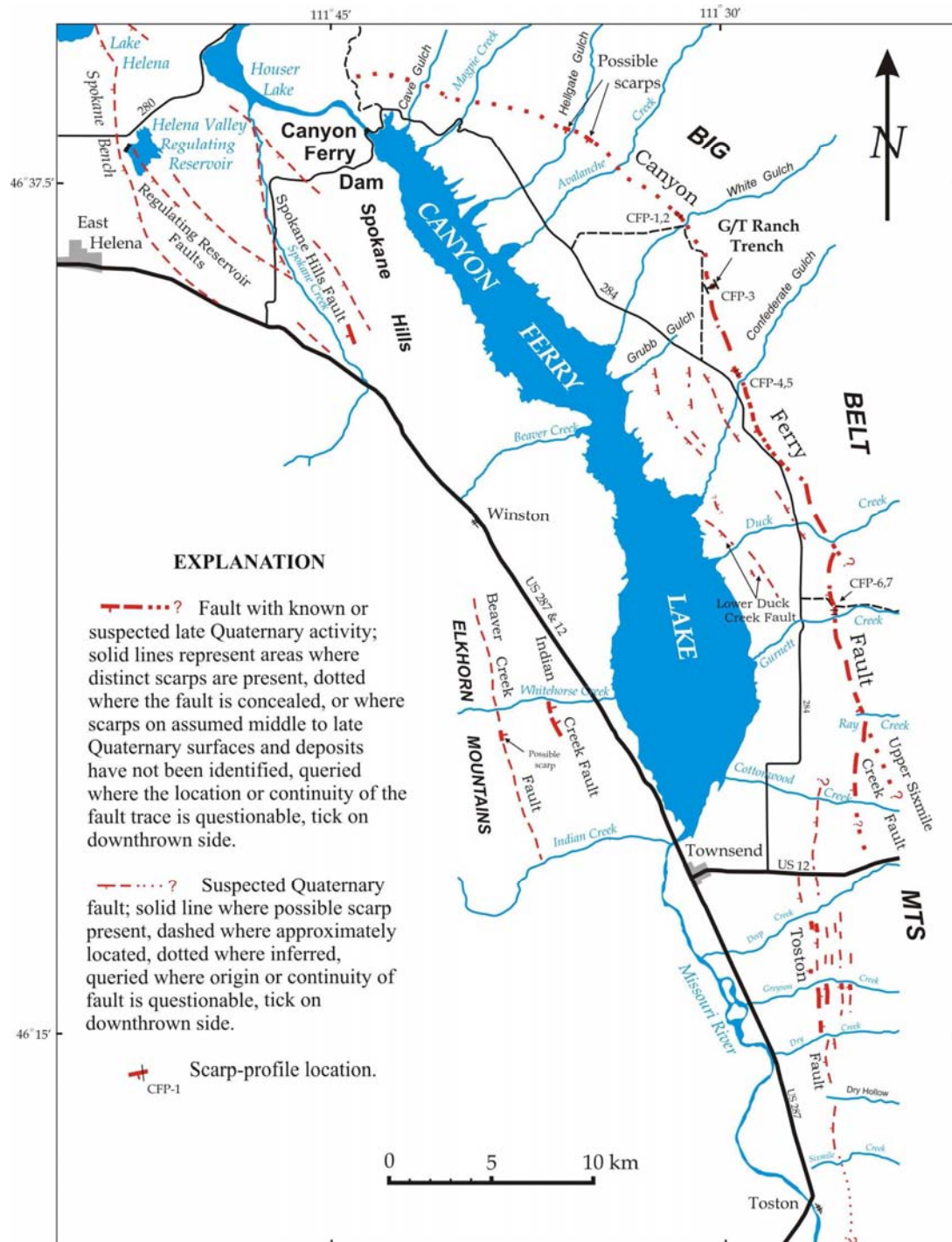


Figure 1. Quaternary fault map of the Canyon Ferry Lake area (modified from Stickney and others, 2000)

30 km east of the capital city of Helena, the location of several **M** 6 earthquakes in 1935. Pardee (1925, 1950) first discussed evidence for a young structure along the front of the Big Belt Mountains, but a young fault (or faults) was not actually identified by name until the work of Johns and others (1982), who called it the Canyon Ferry-Duck Creek fault. Mertie and others (1951) did not show a range-bounding fault (not even as concealed or inferred) along the west flank of the Big Belt Mountains, while Nelson (1963) showed only a northwest-striking fault offsetting Tertiary deposits against Precambrian rocks at the mouths of Duck and Gurnett Creeks. Nelson also mapped this fault north of Duck Creek as a concealed structure. Witkind (1975) identified a late Cenozoic range-bounding fault or faults along the west side of the Big Belt Mountains based in part on the work of Pardee (1925) and the mapping of Nelson (1963). Both Davis and others (1963) and Kinoshita and others (1964), based on geophysical data, show a major range-bounding structure along the west side of the Big Belt Mountains.

Stickney and Bartholomew (1987) were the first to document late Quaternary displacement along the Big Belt Mountains range front and to call the fault the Canyon Ferry fault. They estimated that the Canyon Ferry fault had a total length of 70 km but an active length of only 6 km. This 6-km-long "active length" was further identified as the "Confederate Gulch scarp" on the basis of reported 1- to 2-m-high scarps on pre-Holocene to post-Pinedale deposits and 15- to 20-m-high scarps on Pinedale to post-Bull Lake deposits near the mouth of Confederate Gulch. In a further comment, they added that Holocene/late Pleistocene alluvial fans cross the fault trace with no apparent displacement.

Recent state-wide compilations of Quaternary faults by Stickney and others (2000) and Haller and others (2000) show and describe the Canyon Ferry fault as consisting of two sections with a total length of about 36 km. What Haller and others (2000) describe as the 18- to 20-km-long northern section extends from Cave Gulch on the north, south to

about to 3 km north of Confederate Gulch (Figure 1). Based on range-front morphology, they suggest Quaternary activity for this section but they indicate that no scarps on late Quaternary deposits have been reported. Their 18-km-long southern section of the fault extends from 3 km north of Confederate Gulch to 2 km south of Gurnett Creek. This section includes the scarps reported by Stickney and Bartholomew (1987) at Confederate Gulch, as well as reported scarps at the mouths of Duck and Gurnett Creeks. Stickney and others (2000) and Haller and others (2000) did not extend the fault along the range front south of Gurnett Creek or include it in their compilation "based on the absence of evidence suggesting Quaternary movement." However, Wong and others (1999) characterized three features south of Gurnett Creek as possible seismic sources in their study for Toston Dam. All of these features could be part of the Canyon Ferry fault. Gorton and Olig (1999) identified the first feature as the Toston fault, while they named the second the Upper Sixmile Creek fault (Figure 1). The third feature is a southeast continuation of the Canyon Ferry fault originally termed the Ray Creek and Deep Creek sections by Johns and others (1982).

As part of a probabilistic seismic hazard study for Canyon Ferry Dam (Anderson and LaForge, 2003), assessment of the Canyon Ferry fault began in 2001. The assessment consisted of a review of aerial photographs (generally at a scale of 1:40,000), a geologic field reconnaissance of the entire Canyon Ferry-Toston fault area, and measurement in the field of scarp profiles at four separate sites along the Canyon Ferry fault (Profiles CFP-1 through CFP-7; Figure 1). Measurement of these profiles followed the methodology and the terminology of Bucknam and Anderson (1979) and Hanks and others (1984). The scarp profiles clearly indicate that repeated late Quaternary surface-faulting earthquakes are associated with the Canyon Ferry fault as older surfaces are consistently displaced more than younger surfaces. In June 2002, we excavated a 62-m-long trench across the Canyon

Ferry fault at the G/T Ranch (Figure 1). This trench not only provided definitive evidence for multiple late Quaternary surface-rupturing earthquakes, but also provided important information regarding fault slip rates, recurrent surface-rupturing earthquakes, and Quaternary stratigraphy of the Canyon Ferry area.

The results of our studies indicate that the late-Quaternary Canyon Ferry fault is a much longer, potentially more active late-Quaternary feature than previously thought. We found evidence suggestive of late-Quaternary surface faulting from Hellgate Gulch on the north to Cottonwood Creek on the south, and definitive evidence for recurrent late-Quaternary faulting from White Gulch on the north to Little Cottonwood Creek on the south. The previously identified Lower Duck Creek fault appears to be part of a series of relatively short, intrabasin faults related to a major change in strike of the Canyon Ferry fault. Finally, our studies also suggest that the Toston fault could be the southern continuation of the Canyon Ferry fault, which would indicate that surface rupture lengths of over 60 km are possible.

## **GEOLOGIC OVERVIEW**

As defined in this paper, the Canyon Ferry fault extends from about Oregon Gulch (just northwest of Cave Gulch) southward to Cottonwood Creek, an along-strike distance of 48 km (Figure 1). For about 8 km, from Oregon Gulch to southeast of Magpie Creek, the fault forms the west-northwest-striking contact between Precambrian and Paleozoic bedrock and Tertiary basin-fill deposits. The fault contact is typically marked by an abrupt to gradual break in slope between steeply dipping bedrock and gently dipping basin-fill deposits. The Tertiary deposits appear to be little deformed adjacent to the fault (i.e., no obvious backtilting and dips are low, typically about 10°). We did not identify obvious scarps, although in a few places (one to the south of Cave Gulch) short troughs are present that could be grabens; however, these features could be erosional in origin as they are very short and discontinuous.

Near Little Hellgate Gulch (between Magpie and Hellgate Gulch), a broad alluvial fan extends from Highway 264, east to the range front with no obvious break in slope or scarp in the area of the fault.

From Hellgate Gulch south to White Gulch, the geomorphic character of the range front changes considerably and the overall strike of the Canyon Ferry fault changes from west-northwest to northwest. In this area, the range front of the Big Belt Mountains is quite steep and exhibits possible triangular facets. However, much of the range front bedrock in this area is steeply dipping, resistant limestone which suggests at least some of the relief and steepness is a function of bedrock lithology. In addition, instead of Tertiary basin-fill deposits in direct contact with bedrock, broad Quaternary alluvial fans mark the downthrown (west or hanging wall) side of the fault. In several locations, such as at the mouths of Avalanche Creek and White Gulch, the fan surfaces near the mountain front are nearly flat suggesting rotation of the fans into the fault (Figure 2). The heights of these fans above their respective creeks (30-50 m) suggest that these alluvial fans are not latest-Pleistocene features. More likely, they are either "Bull Lake" or "pre-Bull Lake" in age.

Suspected scarps on steep colluvium or bedrock also are present immediately south of Hellgate Gulch and a northwest-striking scarp is present north of White Gulch (Figure 1). We measured two scarp profiles (CFP-1 and 2; Table 1) at the White Gulch site, on what may be a "Bull Lake"-age fan surface. The possibility exists that these scarps are fluvial in origin (or are tectonic and subsequently fluvially modified); however, scarp heights and surface displacement measurements are consistent with those at locations where the scarps are clearly tectonic.

We observed fairly continuous scarps along the northwest-striking range front from Spring Creek (1 km south of White Gulch), south to Confederate Gulch. At one site in particular on the G/T Ranch, a prominent northwest-trending scarp is present (Figure 3). This 13.4-m-high scarp displaces the

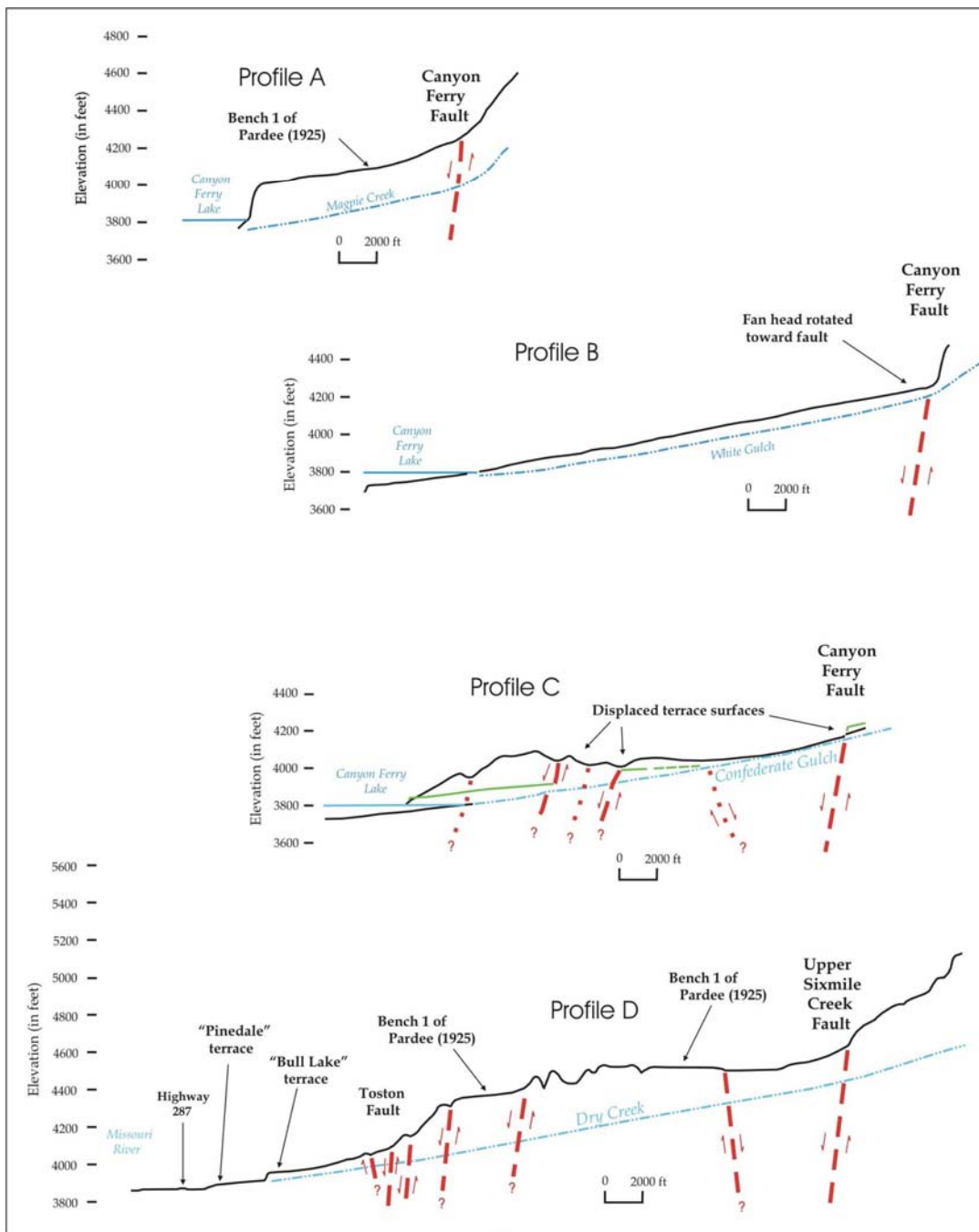


**Figure 2.** Topographic profiles constructed from U.S. Geological Survey 7 1/2' quadrangles showing locations of major know and suspected quaternary faults in the Canyon Ferry area. Green line on Profile C is displaced terrace of possible "Bull Lake age." Locations of profiles correspond to identified creeks or gulches shown on Figure 1.

apex of a somewhat isolated, younger alluvial fan that appears to overlie the upper portions of the much larger, older ("pre-Bull Lake?") fan that

issued primarily from Avalanche and White Gulches (Figure 1). The measured surface displacement across this scarp is 6.4 m (CFP-3;

Table 1).

Scarps, primarily at the range front at the bedrock-colluvium contact are continuous from the G/T Ranch site south to Confederate Gulch. On the north side of Confederate Gulch, the fault displaces

a broad alluvial fan or terrace surface (Figure 4). We measured two profiles, CFP-4 and 5 (Figure 1, Table 1), across the low scarp on this surface originally reported by Stickney and Bartholomew (1987). The alluvial-fan or terrace surface displaced

Table 1. Scarp-profile data

Profile	Scarp Height	Surface Offset	Maximum scarp slope angle
	<i>m</i>	<i>m</i>	<i>degree</i>
CFP-1	8.85	4.6	23
CFP-2	11.1	6.5	26
CFP-3	13.4	6.4	16
CFP-4	2.8	1.5	14
CFP-5	1.6	1.0	11
CFP-6	11.4	8.1	19
CFP-7	3.0-5.2 (disturbed)	2.4	16



Figure 3. View of the G/T Ranch trench site looking northeast. Scarp is approximately 13 m high.

by the scarp is about 6.5 to 8 m above the current creek bed. The fan surface is bouldery and in the area of the scarp has been partially disturbed or modified by cultural activities (irrigation ditches, old roads, trails, and pits). Given these uncertainties and possible modifications, the two profiles suggest that the scarp is less than 3 m high. Measured surface displacements are 1.0 (CFP-5) and 1.5 m (CFP-4). Maximum scarp-slope angles are  $11^{\circ}$  and  $14^{\circ}$ , respectively. CFP-4 is at what appears to be the highest portion of the scarp. A possible bevel exists near the crest of CFP-4, but none is present on CFP-5. Based on our ground reconnaissance, the possible bevel on CFP-4 appears to be a local effect, and given the surface displacement values ( $< 2$  m), this scarp likely represents a single surface faulting event. At this location, Confederate Creek is deeply entrenched and no lower terraces are present. The fan surface displaced by the Canyon Ferry fault is probably, at a maximum, latest Pleistocene (10 to  $< 40$  ka) because of its height above the creek (6.5 to 8 m), lack of lower terraces, and degree of soil

development (including stage II carbonate development on granitic clasts). However, Confederate Gulch upstream of the site was extensively mined in the 1800s and it is unclear how much this activity affected the channel morphology (i.e., width, depth, and preservation of younger terraces) of Confederate Gulch.

On the south side of Confederate Gulch is the “15- to 20-m-high scarp” reported by Stickney and Bartholomew (1987). The scarp truncates an inset terrace that is about 20-25 m above Confederate Gulch. The scarp is highly modified (the road up Confederate Gulch crosses the scarp obliquely and several pits and irrigation ditches also cross the scarp). Based on the height above Confederate Gulch, the minimum age of the terrace is probably Bull Lake equivalent ( $> 130$  ka). However, the 15-20 m scarp height is likely a minimum displacement estimate because the correlative surface on the downthrown side of the scarp is buried. We speculate that the uncertainty in the measurement is at least 5 m.



*Figure 4. View looking south along the scarp on the north side of Confederate Gulch, near the site of profile CFP-4. Scarp is approximately 1.5 m high (Ms. Olig for scale).*

From Confederate Gulch south to Gurnett Creek, scarps at the base of bedrock slopes are common although the range front is quite low. However, access is difficult in this area because most land is private and several irrigation ditches cross or parallel the scarps. A prominent 2-m-high scarp crosses a terrace surface at the mouth of Duck Creek; we did not profile this scarp because it is on private land and the surface of the fan may be disturbed. South of Duck Creek, the Canyon Ferry fault appears to splay into two faults, one trending south-southeast and the other trending south. The eastern, northwest-striking splay apparently separates Precambrian rocks on the east from Tertiary deposits on the west (Nelson, 1963). The western, north-striking splay separates Tertiary deposits from Quaternary alluvial fans. From Duck Creek south for 1 km, obvious scarps are not present. But from this point (1 km south of Duck Creek) south to Gurnett Creek, a prominent west-facing scarp is present and the overall trend of the fault is north.

We measured two profiles (CFP-6 and 7, Table 1) across different age surfaces displaced by the scarp at Gurnett Creek (Figure 1). Profile CFP-6 is across the highest part of the scarp, approximately 300 m north of the creek. This 11-m-high scarp appears similar to the scarp on the south side of Confederate Gulch and the fan/terrace surface that is displaced may be roughly correlative in age because it is about 20-30 m above the creek. A surface displacement of 8.1 m was measured on CFP-6. The second profile, CFP-7, is where a 3- to 5.2-m-high scarp cuts across a lower, inset terrace, immediately north of Gurnett Creek (the site is disturbed by an irrigation ditch). This lower, inset terrace is about 13 m above the present creek, nearly twice as high above the creek as the lower fan surface at Confederate Gulch. Profile CFP-7 shows a maximum surface displacement of 2.4 m and a maximum scarp angle of  $16^\circ$ . The surface displacement of 2.4 m suggests that this scarp probably represents one, but possibly two, surface-rupturing earthquakes. Based on the height above the creek, this low terrace is probably latest

Pleistocene (10 to < 40 ka), but it could be older.

South of Gurnett Creek, scarps on low fan surfaces are present at the mouths of Dry and Ray Creeks. At Ray Creek, several northwest-striking lineaments trend to the southeast. These lineaments probably correspond to the Upper Sixmile Creek fault of Wong and others (1999). However, the north-striking sharp break in slope continues south to about Cottonwood Creek. An apparent graben on the north side of Cottonwood Creek displaces a high surface (Bench 1 or 2? of Pardee, 1925). On the south side of Cottonwood Creek, a 20-25 m high terrace does not appear to be displaced. Although this may mark the southern end of the late Quaternary rupture on the Canyon Ferry fault, the northern end of the Toston fault is only 2 km to the west.

Our reconnaissance studies found evidence for probable late Quaternary surface rupture associated with the Canyon Ferry fault from roughly Hellgate Gulch on the north, to about Cottonwood Gulch on the south, a distance of 40 km. Northwest of Hellgate Gulch, no definitive evidence of late Quaternary surface rupture exists. Perhaps the fault in this area is not optimally oriented for the current stress regime because of its more westerly trend. It may also be that because this is the northern end of the fault, displacement is decreasing and slip per event is less and evidence of surface faulting is not preserved.

We used aerial photograph interpretation and construction of topographic profiles to identify several suspected fault scarps just west of the main Canyon Ferry fault, particularly between Grubb Gulch on the north and Gurnett Creek on the south (Figure 1). These subdued east- and west-facing scarps include the feature referred to as the lower Duck Creek fault (Haller and others, 2000; Stickney and others, 2000) and appear responsible for the series of low rounded hills in this area and the disruption and truncation of some of the inset fluvial terraces along Confederate Creek (Figure 2). The subdued appearance of the scarps may be due to the abundant loess in this area. We believe these faults are secondary faults, related to the change in

strike of the Canyon Ferry fault. As discussed previously, from about Duck Creek on the north to Cottonwood Creek on the south, the Canyon Ferry fault strikes nearly due north. However, at about Duck Creek, the fault changes to a more northwesterly strike, with the fault becoming increasingly more westerly striking to the north (northeast of Canyon Ferry Dam the fault strikes almost due west). In a simple extensional model, this abrupt change in strike could produce a zone of compression in the area of the inter-basin faults. Hence, the faults and low hills (horsts) west of the Canyon Ferry fault in the area of Confederate Gulch.

### **G/T RANCH TRENCH**

We excavated and logged a 62-m-long paleoseismic trench on the G/T Ranch (formally the Gravelly Ranch) in June 2002 at the site of scarp profile CFP-3 (Figures 1 and 3). This site was selected for study because it displays definitive evidence for multiple late Quaternary faulting events, Quaternary deposits are clearly present, access is excellent, and the site is grassland and undisturbed.

The G/T Ranch trench revealed a sequence of faulted alluvial-fan deposits, slope colluvium, fault-scarp colluvium, and eolian deposits (Figure 5). Several strands of the Canyon Ferry fault are present in the trench, with one strand displacing all but the upper-most soil and colluvial horizons. We collected eleven samples from the trench for infrared stimulated luminescence (IRSL) dating (Table 2) in an attempt to better constrain the age of the deposits and to decipher the faulting history at this site.

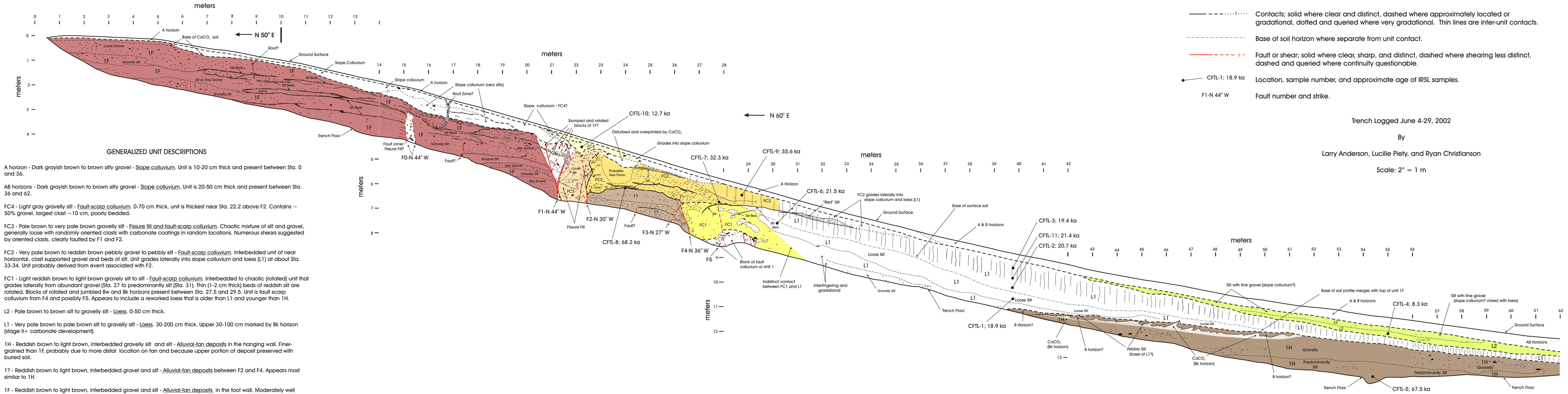
### **Stratigraphy**

Exposed in the G/T Ranch trench are alluvial-fan deposits, loess, scarp-derived colluvium, and slope colluvium. Alluvial-fan deposits, interpreted to be primarily debris flows, are the oldest deposits

in the trench. This mapping unit, designated unit 1 (1F east of station 21, 1? between stations 22 and 27, and 1H west of station 39), consists of beds of generally clast-supported, fine to medium gravel (debris-flow deposits), alternating and interfingering with parallel beds of light brown silt (mudflow deposits). The clasts in the gravel beds are predominantly (60-80 %) Spokane Shale (Precambrian Belt Series), with smaller amounts (20-40 %) of possible Empire Shale (also Precambrian Belt Series). The clasts of Spokane Shale impart a reddish brown color to most of the unit. The upper portion (1-2 m) of 1F appears to be stripped or eroded because of the poor degree of soil development. The silt beds appear to be mudflow deposits because of crude laminations in many of the beds, although their color (light brown) and fine-grained, well-sorted texture suggest they may have originally been eolian (loess?).

In the bottom of the west end of the trench (station 39 to 62) is unit 1H (Figure 6). We interpret this unit to be the uppermost, now-buried, portion of the faulted alluvial-fan deposit observed on the footwall. Unit 1H is very similar to unit 1F, except that it is generally finer grained. The finer texture is likely due to the more distal location of the deposit and to the preservation of the upper part of the unit, which includes a fine-grained soil. Both unit 1H and 1F appear to be locally derived debris-flow and mudflow deposits that originated in drainages immediately east of the trench site. Sample CFTL-5 from the lowest exposed portion of unit 1H (Figure 5 and 6) yielded an IRSL age of 67.5 ka (Table 2). Between unit 1F and 1H (stations 21 to 33), is a complex zone of various colluvial units (designated FC1 thru FC4), older loess, and a block of alluvial-fan material very similar in appearance to unit 1H and 1F shown on the trench log as unit 1? (Figure 5). Sample CFTL-8 collected from near the top of this unit (Figure 5) yielded an IRSL age of 68.2 ka (Table 2) indicating that this deposit is a block of unit 1 material.

A well-developed buried soil (Bt-Bk horizons, stage II+ carbonate) is present on unit 1H but not on



GENERALIZED UNIT DESCRIPTIONS

- A horizon - Dark grayish brown to brown silty gravel - Slope colluvium. Unit is 10-20 cm thick and present between Sta. 0 and 36.
- AB horizons - Dark grayish brown to brown silty gravel - Slope colluvium. Unit is 20-50 cm thick and present between Sta. 36 and 62.
- FC4 - Light gray gravelly silt - Fault-scarp colluvium. 0-70 cm thick, unit is thickest near Sta. 22.2 above F2. Contains ~ 50% gravel, largest clast ~10 cm, poorly bedded.
- FC3 - Pale brown to very pale brown gravelly silt - Fissure fill and fault-scarp colluvium. Chaotic mixture of silt and gravel, generally loose with randomly oriented clasts with carbonate coatings in random locations. Numerous shears suggested by oriented clasts, clearly faulted by F1 and F2.
- FC2 - Very pale brown to reddish brown pebbly gravel to pebbly silt - Fault-scarp colluvium. Interbedded unit of near horizontal, clast supported gravel and beds of silt. Unit grades laterally into slope colluvium and loess (L1) at about Sta. 33-34. Unit probably derived from event associated with F2.
- FC1 - Light reddish brown to light brown gravelly silt to silt - Fault-scarp colluvium. Interbedded to chaotic (rotated) unit that grades laterally from abundant gravel (Sta. 27 to predominantly silt (Sta. 31). Thin (1-2 cm thick) beds of reddish silt are rotated. Blocks of rotated and jumbled Bw and Bk horizons present between Sta. 27.5 and 29.5. Unit is fault scarp colluvium from F4 and possibly F5. Appears to include a reworked loess that is older than L1 and younger than 1H.
- L2 - Pale brown to brown silt to gravelly silt - Loess. 0-50 cm thick.
- L1 - Very pale brown to pale brown silt to gravelly silt - Loess. 30-200 cm thick. Upper 30-100 cm marked by Bk horizon (stage II+ carbonate development).
- 1H - Reddish brown to light brown, interbedded gravelly silt and silt - Alluvial-fan deposits in the hanging wall. Finer-grained than 1F, probably due to more distal location on fan and because upper portion of deposit preserved with buried soil.
- 17 - Reddish brown to light brown, interbedded gravel and silt - Alluvial-fan deposits between F2 and F4. Appears most similar to 1H.
- 1F - Reddish brown to light brown, interbedded gravel and silt - Alluvial-fan deposits in the foot wall. Moderately well bedded, moderately well stratified deposit of fine gravel and some coarse sand, some clast supported (debris-flow facies), interbedded with beds of gravelly silt to silt (mudflow facies). Gravel clasts predominately Spokane Shale which imparts the reddish color to the unit. Unit appears rotated between Sta. 10 and 21, upper portion of unit (Sta. 0-6) probably stripped.

EXPLANATION

- · · · · · Contacts; solid where clear and distinct, dashed where approximately located or gradational, dotted and queried where very gradational. Thin lines are inter-unit contacts.
- · · · · · Base of soil horizon where separate from unit contact.
- · · · · · Fault or shear; solid where clear, sharp, and distinct, dashed where shearing less distinct, dashed and queried where continuity questionable.
- CFTL-1; 18.9 ka Location, sample number, and approximate age of IRSL samples.
- F1-N 44° W Fault number and strike.

Trench Logged June 4-29, 2002

By

Larry Anderson, Lucille Piety, and Ryan Christianson

Scale: 2" = 1 m

Figure 5. Log of the G/T Ranch trench across the Canyon Ferry fault.

unit 1F (apparently due to erosion). The upper soil horizon boundaries are wavy, which suggests flowage that we believe may be due to permafrost action. The degree of soil development on unit 1H indicates a considerable amount of time between the deposition of unit 1H and the deposition of the overlying unit L1. Unit L1 consists of over 2 m of medium- to fine-grained silt (Figure 7). Unit L1 is loess, apparently derived from late Pleistocene outwash deposits in the floodplain of the Missouri River. Unit L1 consists of at least three sub-units: a basal, slightly gravelly silt; an intermediate horizon of very loose silt with essentially no pebbles or gravel clasts; and an upper unit of moderately hard

silt (hardness due to overprinting by soil formation; stage II Bk horizon) with some fine gravel. We collected five samples from unit L1 for IRSL dating (CFTL-1, 2, 3, 6, and 11; Table 2). These samples yielded ages of 18.9 to 21.5 ka, with four of the five ages clustering around 21 ka. Although at first glance these ages do not appear entirely stratigraphically consistent (see Figure 5), within their 1- $\sigma$  error bounds all the ages overlap. Thus, unit L1 is late Pleistocene loess deposited during the main Pinedale glaciation, probably about 21 ka.

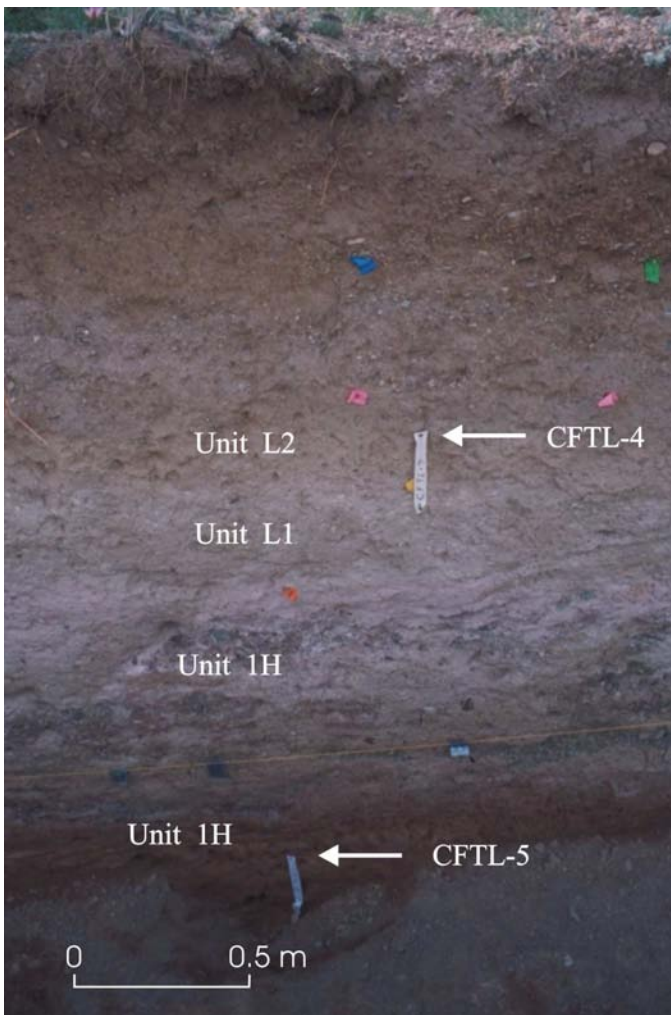


**Figure 6. Photograph of the G.T Ranch trench, stations 55-56, showing the locations of samples CFGL-5 in unit 1H and sample CFTL-4 in unit L2.**

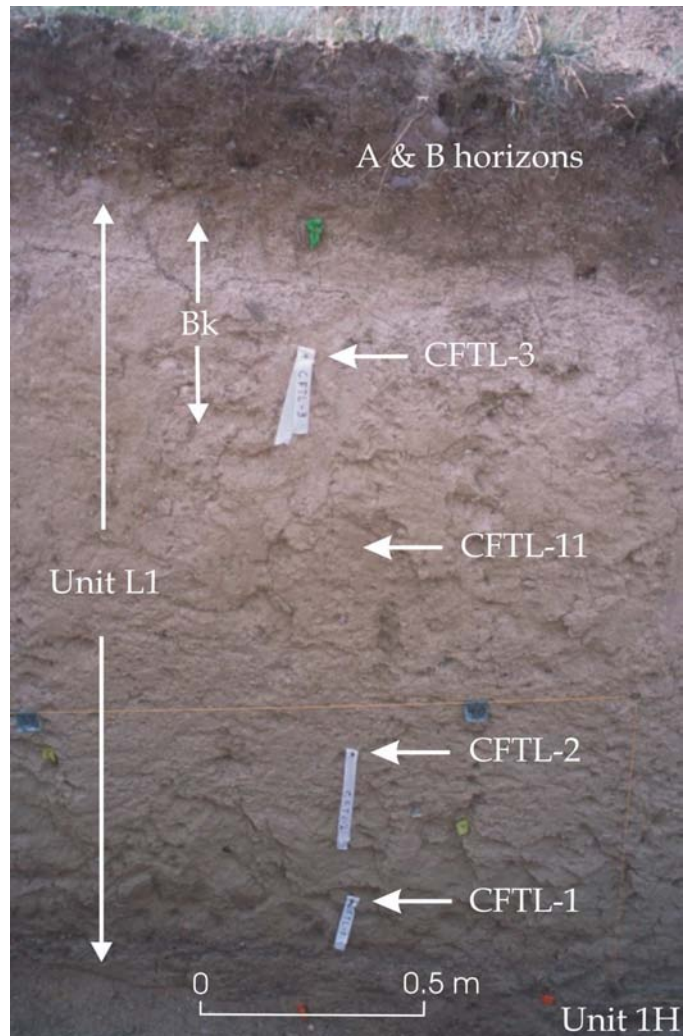


**Figure 7. Photograph of the G.T Ranch trench, station 40, showing unit L1 and the locations of samples CFTL-3, 2, and 1 (upper to lower, respectively)**

Four fault-derived colluvial units are present in the G/T Ranch trench, between stations 20 and 30 (Figure 5). FC1 is a 1.5-m-thick, gravelly silt. This

Table 2. Infrared stimulated luminescence ages, G/T Ranch trench

Field #	Lab #	Equivalent Dose	U	Th	K20	Moisture	Dose Rate	IRSL age
		Gy	ppm	ppm	%	%	Gy/ky	yr
CFTL-1	UIC1032	75.42 ± 0.24	4.4 ± 0.1	11.3 ± 0.1	2.54 ± 0.02	25 ± 10	4.00 ± 0.16	18,860 ± 2010
CFTL-2	UIC1023	85.08 ± 0.31	3.3 ± 0.1	10.8 ± 0.1	2.51 ± 0.02	15 ± 5	4.22 ± 0.17	20,660 ± 1490
CFTL-3	UIC1020	78.13 ± 0.24	2.6 ± 0.1	9.6 ± 0.1	2.25 ± 0.02	10 ± 3	4.02 ± 0.16	19,440 ± 1170
CFTL-4	UIC1030	38.94 ± 0.17	3.2 ± 0.1	11.9 ± 0.1	2.85 ± 0.03	10 ± 3	2.69 ± 0.12	8,330 ± 510
CFTL-5	UIC1033	331.85 ± 0.90	4.0 ± 0.1	12.6 ± 0.1	3.00 ± 0.02	20 ± 5	2.70 ± 0.12	67,540 ± 4800
CFTL-6	UIC1001	95.52 ± 0.30	2.8 ± 0.1	10.9 ± 0.1	2.47 ± 0.02	10 ± 3	4.30 ± 0.18	21,520 ± 1300
CFTL-7	UIC1021	170.40 ± 0.56	3.3 ± 0.1	12.0 ± 0.1	3.09 ± 0.02	10 ± 3	5.30 ± 0.21	32,340 ± 1960
CFTL-8	UIC1022	382.77 ± 1.89	3.6 ± 0.1	12.5 ± 0.1	3.01 ± 0.02	10 ± 3	5.61 ± 0.22	68,210 ± 4070
CFTL-9	UIC1018	174.33 ± 0.83	3.1 ± 0.1	10.7 ± 0.1	2.84 ± 0.02	10 ± 3	4.89 ± 0.20	35,640 ± 2800
CFTL-10	UIC1031	57.21 ± 0.21	3.0 ± 0.1	11.0 ± 0.1	2.43 ± 0.02	10 ± 3	4.51 ± 0.18	12,690 ± 750
CFTL-11	UIC1034	90.46 ± 0.41	2.9 ± 0.1	11.5 ± 0.1	2.40 ± 0.02	10 ± 3	4.23 ± 0.17	21,390 ± 1280

Note: All errors are at 1 sigma

unit consists of jumbled or rotated blocks of silt mixed with apparent blocks of soil material (carbonate-cemented silt horizons, Figure 8). Unit FC2 overlies both FC1 and loess L1, and is texturally distinct from FC1. It consists of interbedded pebbly gravel to pebbly silt, which is almost identical in appearance to unit 1 (Figure 9). No buried soil separates FC1 from FC2. We collected two samples from unit FC2 for IRSL dating. These samples, CFTL-7 and CFTL-9 (Figure 5; Table 2), produced inverted ages of 32.3 and 35.6 ka, respectively. We believe these ages are anomalously old and do not represent the time of

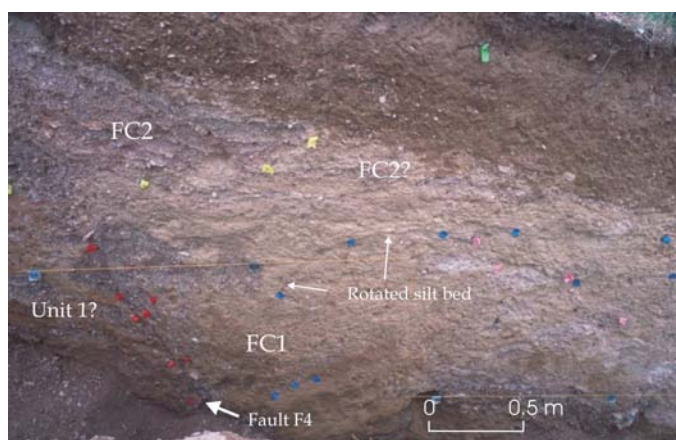


Figure 8. Photograph of the G.T Ranch trench, stations 26 to 29, showing fault F4.

deposition of unit FC2 because the material's luminescence was not completely reset when it was rapidly transported and re-deposited. We base this conclusion on: (1) the similarity of the material to unit 1 (it was originally very difficult to differentiate the FC2 colluvium from unit 1); and, (2) these ages are considerably greater than the five consistent ages for the underlying loess (unit L1).

Colluvial unit FC3 is a gravely silt interpreted to be a fissure fill (Figure 10). Overlying FC3 and FC2 is colluvial unit FC4 (Figure 11). FC4 consists of gravelly silt, and again, no soil separates FC4 from FC3 and FC2. An IRSL sample (CFTL-10; Table 2) from FC4 yielded an age of 12.7 ka. This age is stratigraphically consistent with ages from unit L1 (approximately 21 ka) and observations from areas north and south of the trench regarding the age of last surface rupture on the Canyon Ferry fault.

Overlying units 1F, 1H, L1, FC2, and FC3 are thin deposits of slope colluvium and the surface soil. In addition, a second thin loess unit (L2) overlies L1 in the west portion of the trench (stations 43 to 62; Figure 5). A sample (CFTL-4) of this loess yielded an age of 8.3 ka (Table 2) which indicates it is early Holocene.

## Interpretation of the G/T Ranch Trench

The stratigraphy exposed in the G/T Ranch trench provides clear evidence for multiple late Quaternary surface-rupturing earthquakes on the Canyon Ferry fault. Total displacement is at least 8 m, but probably 9 m, since deposition of the alluvial-fan deposits (units 1F, 1H, and 1?). At least 3, and probably the past 4, surface-faulting events are recorded in the trench stratigraphy (units FC1 thru FC4). The following discussion outlines our interpretation of the stratigraphic relations exposed in the trench.

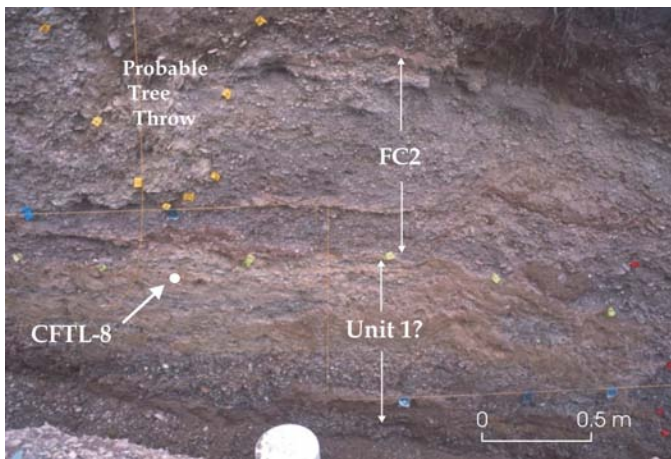


**Figure 9.** Photograph of the G/T Ranch trench, stations 24 to 26, showing colluvial wedge FD2 overlying unit 1?. Note color and texture similarities between unit 1? and FC2.

The first geologic event recorded in the trench is the deposition of the alluvial-fan deposits (units 1F, 1H, and 1?). Following stabilization of the alluvial-fan surface, the soil, now buried and preserved on 1H, formed. As discussed previously, the degree of soil development indicates a significant amount of time separated stabilization of unit 1 and deposition of unit L1. This interpretation is confirmed by the IRSL ages from the two units.

The earliest faulting event recognized probably occurred on F0. It appears to be contemporaneous with deposition of unit 1, because the uppermost portion of 1F overlies the fault and is unfaulted. An early event(s) also occurred at F3 and/or F4. This earlier event(s) may have initially produced the block of unit 1 (unit 1?; Figure 5) as well as an

unnamed unit beneath FC1 between stations 22 and 29. The last of these events was followed by deposition of an older loess-rich colluvial deposit (stations 26 to 31, mapped as unit FC1) for which we have no numerical ages. This older loess was probably deposited against an existing scarp and a moderate carbonate soil developed on it.

The oldest recognized faulting event with distinct stratigraphic evidence occurred on fault F4. This event (*Event W*) displaced the older loess unit (broke up the associated soil with the gravelly carbonate material; Figures 5 and 8) incorporating it into and producing unit FC1. It is possible a later event is responsible for the folding of the silt beds observed near the top of the unit, but direct evidence for fault displacement is difficult to find. *Event W* (or events) slightly predates deposition of most of the loose, unweathered loess of unit L1 because no soil separates the older loess and the loose loess and the contact between the two units is indistinct and gradational.

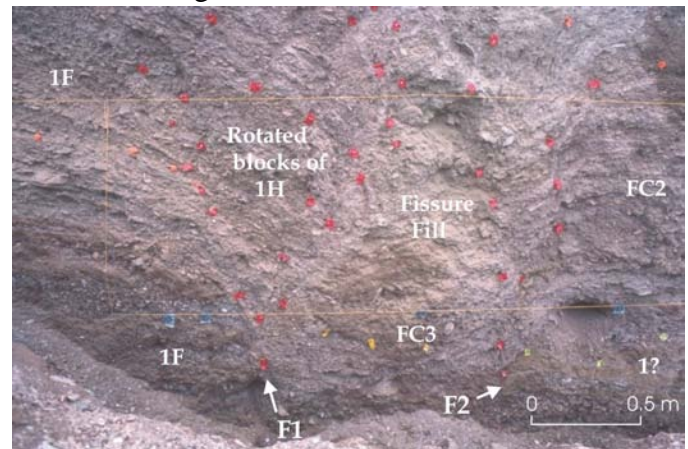


**Figure 10.** Photograph of G/T Ranch trench, stations 20 to 23, showing fault F1 and lower portion of fissure fill (unit FC3)

The next event (*Event X*) is associated with either fault F1 or F2, or both. This event shed colluvium, unit FC2 (Figures 5 and 9), over unit 1? and the loose loess of unit L1. Based on the thickness of unit FC2 (~1.5 m), displacement from this event could have been nearly 3 m. As discussed previously, samples CFTL-7 and CFTL-9 (Figure 5; Table 2), produced inverted ages of 32.3 and 35.6 ka, respectively. We believe these ages are

anomalously old and do not represent the time of deposition of unit FC2.

A soil, represented by stage II carbonate morphology, then formed on units FC2 and L1. The fact that no buried soil is present on FC1 and that a stage II carbonate soil is present on both units L1 and FC2, indicates that the event that produced unit FC2 occurred soon after deposition of unit L1 ceased.

The next faulting event, *Event Y*, produced a fissure fill (unit FC3) between stations 21 and 23 (Figures 5 and 10). This event also may have produced some of the folding in unit 1F between stations 15 and 21, but the amount of net-vertical displacement from this event, at this site, was apparently small. This event may also have produced the small displacement observed at the base of unit FC2 near station 26 on fault F4. *Event Y* clearly post-dates development of the soil on units FC2 and L1.

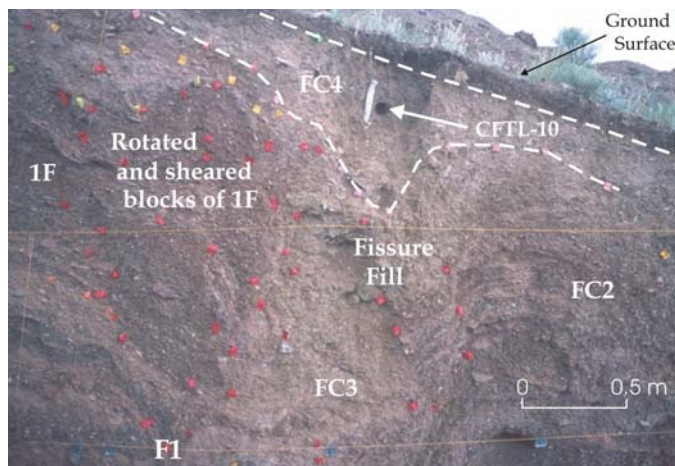


**Figure 11.** Photograph of the G/T Ranch trench, stations 20 to 23, showing the upper portion of the fissure fill (FC3), fault colluvium (FC4), and location of sample CDFL-10.

The last faulting event recognized in the trench, *Event Z*, occurred primarily on fault F2 and produced colluvial unit FC4 (Figures 5 and 11). This event could have folded unit 1F, faulted and fractured the fissure fill (unit FC3), and produced limited displacement on fault F1. Displacement from this event was small, probably only about 0.5

m or less. It also occurred very soon after *Event Y*, as no soil separates colluvial units FC3 and FC4. The possibility exists that the event was associated with an aftershock from *Event Y*; however, the numerical age of 12.7 ka on unit FC4 (sample CFTL-10; Table 2) provides a minimum age for this most-recent faulting event exposed in the trench. Unlike the IRSL ages for unit FC2, we believe that this age is correct because: (1) the colluvium is much finer grained than that associated with FC2; (2) the age is in agreement with the geomorphic expression of the fault to the north and south of the trench site; and, (3) it is stratigraphically consistent with the other IRSL ages and with soil relations in the trench.

### Discussion - Slip Rate and Recurrence

The G/T Ranch trench provides important information regarding the Quaternary history of the Canyon Ferry fault. Most importantly, we estimate approximately 9 m of dip slip displacement (8 m minimum) on the fault at the G/T Ranch site since about 68 ka (Figure 12). Also, the fault displays strong evidence for seismic clustering of events. Over half of the total estimated dip slip (5 m), representing at least two and possibly 3 events, occurred between about 21 ka and 13 ka. No surface rupturing events have occurred in about the last 13 kyr.

The age of the alluvial-fan deposits represented by unit 1 is constrained by the two IRSL ages of 67.5 and 68.2 ka (samples CFTL-5 and 8). For this analysis, this yields an age of about  $68 \pm 4$  ka for unit 1. This age, in conjunction with the dip-slip displacement of  $9 \pm 1$  m that occurred since deposition of unit 1, but before about  $13 \pm 1$  ka (the age of the last surface-faulting event), indicates that the maximum late Quaternary slip rate for the Canyon Ferry fault at the G/T Ranch site is about 0.13 mm/yr (Figure 13).

Displacement resulting from the past two or three, post-loess faulting events is a minimum of about 5 m ( $\pm 0.5$  m). This value, measured at fault

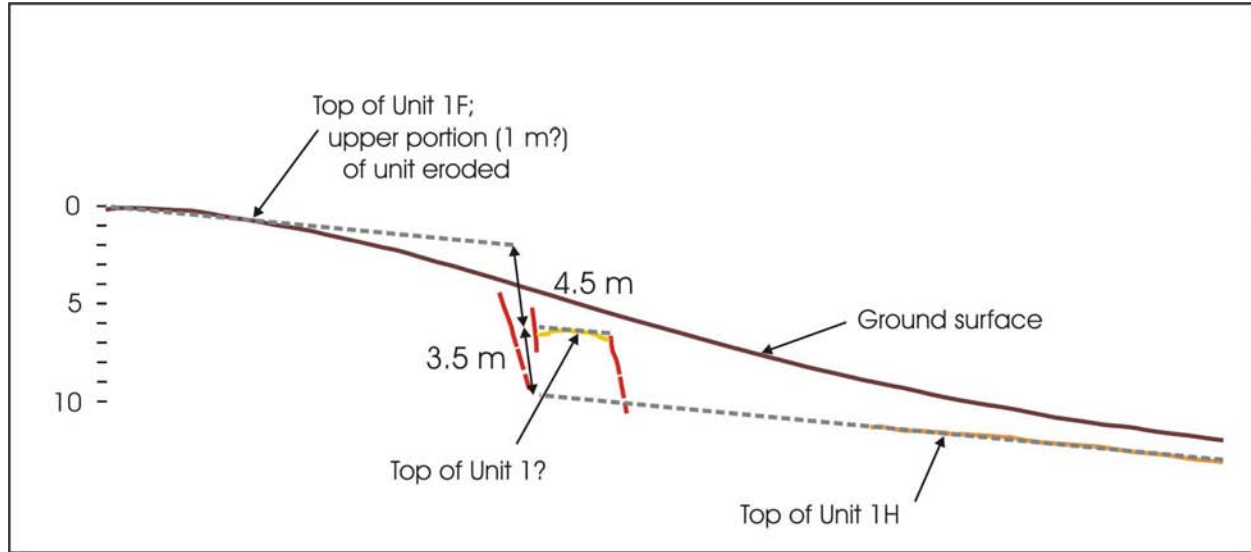


**Figure 12.** Diagram showing amount of dip slip associated with Canyon Ferry fault at the G/T Ranch trench site. Slip is measured assuming  $75^\circ$ -dipping fault plane. Displacement value (8 m total) is considered a minimum value as upper (~1 m) portion of unit 1F is eroded. Horizontal scale is the same as the vertical scale and is in meters. Diagram modified from Figure 5.

F1 from the top of unit 1? to the projection of the top of unit 1F (Figure 12), assumes that most of the stripping and erosion of the top of unit 1F occurred contemporaneously with these events. We believe this is a reasonable interpretation because the apparent volume of material eroded from unit 1F between stations 10 and 20, appears to be roughly equivalent to that represented by colluvial wedge units FC2, FC3, and FC4. The 5 m ( $5 \pm 0.5$  m used in calculations) of dip-slip displacement since deposition of unit L1 ( $21 \pm 2$  ka) indicates a maximum latest Quaternary slip rate of between 0.20 to 0.29 mm/yr, or about 0.24 mm/yr, a rate considerably higher than that of the long-term late Quaternary slip rate. In addition, most of this slip ( $4.5 \pm 0.5$  m; *Events X and Y*) occurred in only about 8 kyr. This yields a short-term maximum slip rate of about 0.56 mm/yr (range between 0.36 and 0.91 mm/yr). This observation, plus the lack of faulting events since about 13 ka, shows that the Canyon Ferry fault has strong indications of clustering of surface-rupturing earthquakes. Thus, the recurrence of surface-rupturing earthquakes on the Canyon Ferry fault can be as long or longer than 13 ka or as short as a few thousand years.

Finally, the trench exposure indicates about 9 m

of total dip-slip displacement since about 68 ka. This is considerably more than was estimated from the scarp profile (CFP-3), which indicates only about 6 m of total displacement. The discrepancy between the scarp-profile data and the trench data is apparently due to the greater than 2 m of loess present on the downthrown side of fault, as well as the apparent erosion of soil material from the top of unit 1H).

## CONCLUSIONS

Based on our reconnaissance geologic mapping, scarp profiling, and excavation of a paleoseismic trench, the Canyon Ferry fault is longer and more active than previously thought. Evidence for recurrent late Quaternary surface-rupturing earthquakes associated with the fault extends for a distance of at least 40 km, from Hellgate Gulch on the north to Cottonwood Creek on the south (Figure 1). In addition, late Quaternary activity could continue southward for another 20 km and include the Toston fault. Additional investigations are needed to resolve whether the Toston fault has ruptured coseismically with the Canyon Ferry fault.

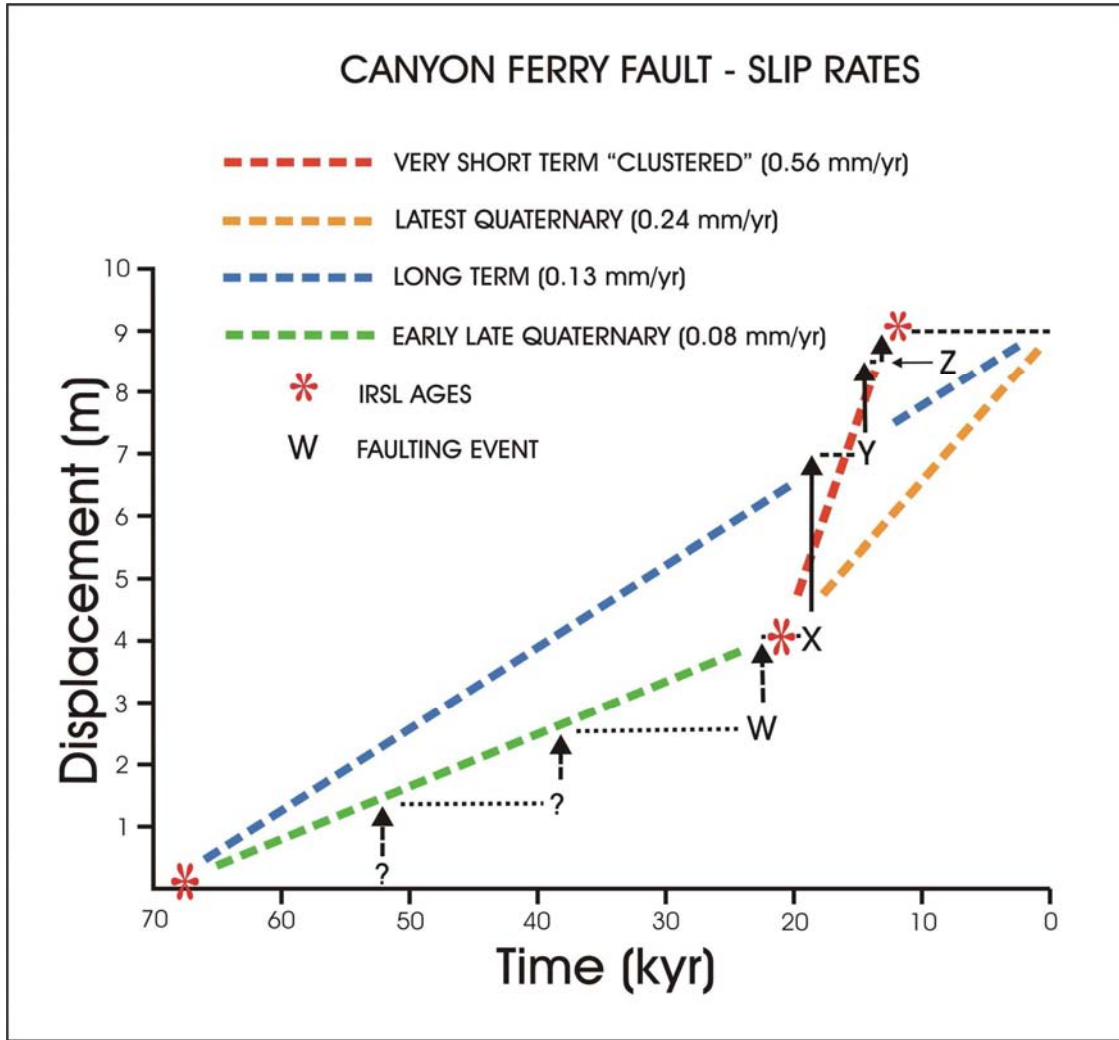


Figure 13. Diagram showing displacement verses time and range of slip rates for the Canyon Ferry fault at the G/T Ranch trench site. Vertical arrows indicate amount of displacement per event (dashed where no actual data on individual event). Dashed horizontal lines represent inter-event time. Slip rates are preferred or mean values, and do not show full range of uncertainties in ages and/or amount of displacement.

The most-recent surface-rupturing earthquake on the Canyon Ferry fault occurred about  $13 \pm 1$  ka. This is indicated by information from the G/T Ranch trench and supported by observations from other sites along the fault where no obvious evidence for Holocene rupture exists. The amount of displacement per event is not well constrained and could vary considerably between sites along the fault. At least one event (*Event X*) at the G/T Ranch trench may have produced up to 3 m of displacement, whereas scarp data from the Confederate Gulch site (3 km to the south) indicate

0.8 to 1.5 m of displacement from what was probably the most recent event at that site. In addition, there may be variability in earthquake magnitude between events.

Data obtained from the G/T Ranch trench indicate a long-term slip rate of about 0.13 mm/yr for the Canyon Ferry fault. However, there are strong indications of seismic clustering, which could indicate a short-term slip rate of nearly 1.0 mm/yr. These data also indicate that recurrence intervals for the fault could be greater than 13 ka or as short as a few thousand years.

## ACKNOWLEDGMENTS

Study of the Canyon Ferry fault was conducted as part of a probabilistic seismic hazard analysis for Canyon Ferry Dam, supported by the Dam Safety Office of the Bureau of Reclamation, Denver, Colorado. The assistance and support of the Canyon Ferry Field Office and the Montana Area Office, Bureau of Reclamation is greatly appreciated. Special thanks and appreciation go to Mr. Dave Graytak of the G/T Ranch who provided access to the ranch and allowed us to excavate the trench across the Canyon Ferry fault. Our thanks to Kathy Haller for her timely review of this paper and Kenneth Mahrer for his patient and helpful editing and formatting.

## References

- Anderson, L.W., and LaForge, R.C., 2003, Seismotectonic study for Canyon Ferry Dam, Missouri River Basin Project, Montana: U.S. Department of the Interior, Bureau of Reclamation, Seismotectonic Report 2003-1, Denver, Colorado, 70 p.
- Bucknam, R.C., and Anderson, R.E., 1979, Estimation of fault-scarp ages from a scarp-height-slope-angle relationship: *Geology*, v. 7, p. 11-14.
- Davis, W.E., Kinoshita, W.T., and Smedes, H.W., 1963, Bouguer gravity, aeromagnetic, and generalized geologic map of east Helena and Canyon Ferry quadrangles and part of the Diamond City quadrangle, Lewis and Clark, Broadwater, and Jefferson Counties, Montana: U.S. Geological Survey Geophysical Investigations Map-444, scale 1:62,500.
- Gorton, A.E., and Olig, S.S., 1999, The new Toston fault - Implications for basin evolution and seismic hazards in western Montana: *Geological Society of America Abstracts with Programs*, v. 31, no. 4, p. A-14.
- Haller, K.M., Dart, R.L., Machette, M.N., and Stickney, M.C., 2000, Data for Quaternary faults in western Montana: Montana Bureau of Mines and Geology Open-file Report 411, 241 p.
- Hanks, T.C., Bucknam, R.C., Lajoie, K.R., and Wallace, R.E., 1984, Modification of wave-cut and faulting controlled landforms: *Journal of Geophysical Research*, v. 89, p. 5771-5790.
- Johns, W.M., Straw, W.T., Bergantino, R.N., Dresser, H.W., Hendrix, T.E., McClernan H.G., Palmquist, J.C., and Schmidt, C.J., 1982, Neotectonic features of southern Montana east of 112° 30' west longitude: Montana Bureau of Mines and Geology Open-file Report 91, 79 p.
- Kinoshita, W.T., Davis, W.E., Smedes, H.W., and Nelson, W.H., 1964, Bouguer gravity, aeromagnetic, and generalized geologic map of Townsend and Duck Creek Pass quadrangles, Broadwater County, Montana: U.S. Geological Survey Geophysical Investigations Map-439, scale 1:62,500.
- Mertie, J.B., Jr., Fischer, R.P., and Hobbs, S.W., 1951, Geology of the Canyon Ferry quadrangle, Montana: U.S. Geological Survey Bulletin 972, 97 p, 2 pls., scale 1:48,000.
- Nelson, W.H., 1963, Geology of the Duck Creek Pass quadrangle, Montana: U.S. Geological Survey Bulletin 1121-J, 56 p, 1 pl., scale 1:62,500.
- Pardee, J.T., 1925, Geology and ground-water resources of the Townsend Valley, Montana: U.S. Geological Survey Water-Supply Paper 539, 61 p.
- Pardee, J.T., 1950, Late Cenozoic block faulting in western Montana: *Geological Society of America Bulletin*, v. 61, p. 359-406.
- Stickney, M.C., and Bartholomew, M.J., 1987, Seismicity and late Quaternary faulting of the northern Basin and Range Province, Montana and Idaho: *Bulletin of the Seismological Society of America*, v. 77, no. 5, p. 1602-1625.

- Stickney, M.C., Haller, K.M., and Machette, M.N.,  
2000, Quaternary faults and seismicity in  
western Montana: Montana Bureau of Mines  
and Geology Special Publication No. 114, 1  
pl., scale 1:750,000
- Witkind, I.J., 1975, Preliminary map showing  
known and suspected active faults in Montana:  
U.S. Geological Survey Open-file Report 75-  
285, scale 1:500,000.
- Wong, I.G., Olig, S.S., Gorton, A.E., and Naugler,  
W.E., 1999, Seismotectonic evaluation of the  
Broadwater Power Project, Toston Dam,  
Montana: Report prepared for Montana  
Department of Natural resources and  
Conservation by URS Greiner Woodward  
Clyde Federal Services, Oakland, California.

# ***ISSUES IN EVALUATING GROUND MOTION HAZARD IN THE BASIN AND RANGE PROVINCE***

Ivan G. Wong

Seismic Hazards Group, URS Corporation, 1333 Broadway, Suite 800, Oakland, CA 94612

## **ABSTRACT**

An improved understanding of the active faults and seismicity in the Basin and Range Province coupled with increasing population and urbanization in areas located in fault-bounded basins highlight the need to better quantify seismic hazards. However, due principally to a lack of both strong motion recordings of large earthquakes ( $M \geq 6.5$ ) and the resulting strong ground motion research, there are numerous issues that challenge our ability to accurately predict strong ground shaking in the province, including those associated with ground-motion attenuation, near-fault effects (e.g., directivity), and near-surface and basin amplification. Future research efforts need to focus on these issues and hopefully, with significant increases in the number of strong motion stations, relevant data will become available to improve ground motion prediction in the Basin and Range Province.

## **INTRODUCTION**

Assessing earthquake ground motion hazard in the Basin and Range Province has been based largely on the assumption that ground shaking in the province behaves in the same manner as it does in California. This situation has arisen due to a lack of strong motion data in the Basin and Range Province where the few recordings that exist are primarily for moment magnitude ( $M$ )  $< 6$  earthquakes. No large Basin and Range Province earthquake ( $M \geq 6.5$ ) has been recorded at distances less than 80 km. Of course, only two large Basin and Range significant earthquakes have occurred in modern times: the 1959  $M$  7.3 Hebgen Lake, Montana, and the 1983  $M$  6.8 Borah Peak, Idaho, earthquakes. This lack of data poses a challenge to understanding and evaluating seismic hazards in the Basin and Range Province because large ground motions are of the greatest engineering relevance. Reflecting this situation, there are no empirical attenuation relationships specific to the Basin and Range Province. In addition to the need to characterize ground-motion attenuation, because the large population centers in the province (e.g., Salt Lake City and the Wasatch Front, Las Vegas,

Albuquerque, and Reno-Carson City) are located in fault-bounded sedimentary basins (Figure 1), near-fault effects, and near-surface and basin site amplification also need to be considered when estimating ground motions. The following is a brief overview of the significant ground motion issues associated with evaluating seismic hazards in the Basin and Range Province.

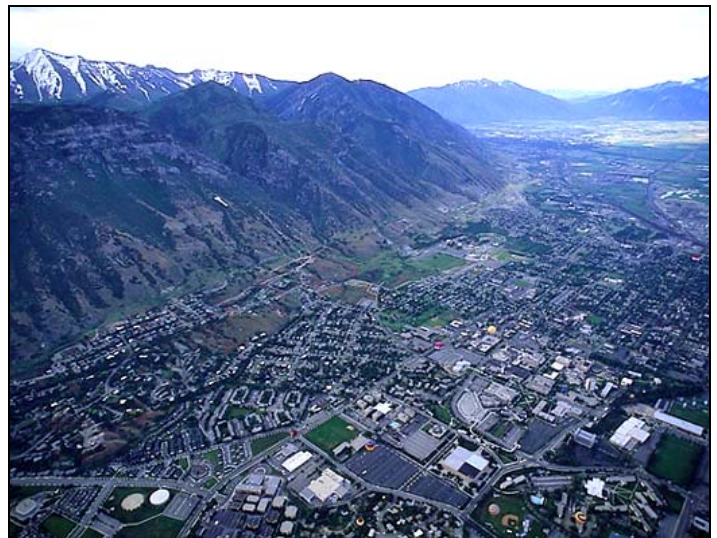


*Figure 1. A view along the Wasatch Front, which is located adjacent to and on the hanging wall of the Wasatch fault.*

## ATTENUATION

In the past decade, efforts to characterize ground shaking in the Basin and Range Province have benefited from comprehensive seismic hazard studies of U.S. Department of Energy facilities including the Idaho National Engineering and Environmental Laboratory in eastern Idaho, Los Alamos National Laboratory in northern New Mexico, and Yucca Mountain, Nevada (Wong and others, 1996a, 1996b; Stepp and others, 2001). As part of these efforts, the first attenuation relationships for the Basin and Range Province and other extensional environments were developed based largely on strong motion data from outside the province (Spudich and others, 1997, 1999) or numerical ground-motion modeling (Wong and others, 1996a). In the probabilistic seismic hazard analysis of Yucca Mountain, seven ground-motion

experts developed attenuation relationships for the Yucca Mountain region (southern Basin and Range Province) (Stepp and others, 2001). Most recently, Pankow and Pechmann (2004a) have revised the rock relationship of Spudich and others (1999).

These relationships, in general, suggest that for a given magnitude and distance, ground motions are about 20% lower in extensional regimes compared to California (Figure 2). Studies of precarious rocks (Brune, 2000) also suggest that ground motions in extensional tectonic regimes are lower. Although this is an extremely significant observation, it has yet to be confirmed by large magnitude Basin and Range Province strong motion data. A key question is what is the cause of these lower ground motions. One explanation offered to date is that stress drops for earthquakes in the Basin and Range Province are lower than for events in compressional tectonic

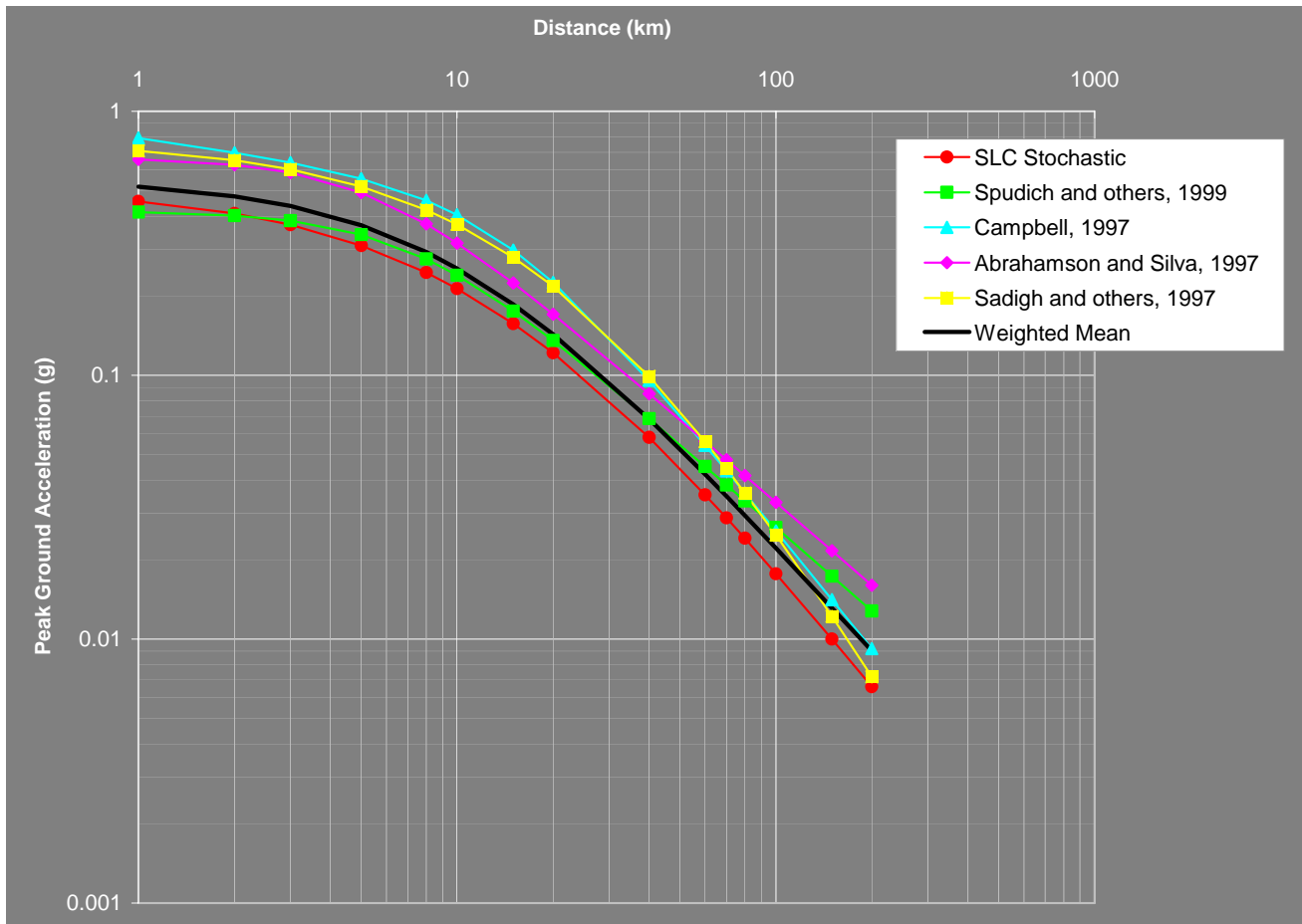


Figure 2. Comparison of some rock attenuation relationships for  $M$  7.0 and peak horizontal acceleration. The Abrahamson and Silva (1997) relationship is modified for extensional faulting and the Salt Lake City (SLC) stochastic relationship is based on numerical modeling from Wong and others (2002a).

regimes like coastal California. Limited analyses of the small Basin and Range strong motion database suggest a 10% decrease in stress drop relative to California earthquakes (e.g., Becker and Abrahamson, 1997). Physical modeling also indicates that normal faults near the surface must be weak and therefore cannot store much strain energy (Brune and Anooshehpour, 1999). This condition would also result in lower ground motions than for example, strike-slip faults in compressional settings.

Studies to date, also indicate that  $Q$  in the Basin and Range Province is higher (lower damping) than in California, but not as high as in the central and eastern U.S. This difference, however, would result in higher ground motions than in California. In addition to the effects of ground-motion attenuation, crustal structure effects on ground motions (e.g., "Moho reflection") have not been evaluated in the Basin and Range Province.

The Pacific Earthquake Engineering Research (PEER) Center's Next Generation of Attenuation (NGA) Project is expected to be completed in the fall of 2004. The product of this research will be new sets of attenuation relationships including ones for normal faulting. Unfortunately, the NGA strong-motion database for these new attenuation relationships is still devoid of large Basin and Range earthquake data.

### NEAR-FIELD EFFECTS

Potential near-field effects such as hanging wall/footwall effects and rupture directivity on normal faults need to be evaluated. Although theoretically these effects are expected to occur in areas such as along the Wasatch fault (Figure 1; Wong and others, 2002a, 2002b), and in the Rio Grande rift (Wong and others, 2004a), strong-motion data to corroborate their existence in extensional regimes are almost nonexistent. Directivity has been observed primarily from strike-slip and reverse faults (Somerville and others, 1997). The issue is whether directivity effects differ for normal faults. In the 1983 Borah Peak earthquake, rupture began at the southern end of the fault based on slip inversions (Richins and others, 1987; Mendoza and Hartzell, 1988) and appears to have proceeded up dip and to the north. Observations

of any directivity were, however, lacking due to the absence of strong-motion data and man-made structures in the vicinity of the fault. Fling, the long-period effect on ground motions due to the static displacement of the fault, is currently being investigated as part of the PEER NGA Project. An unanswered question is whether fling impacts engineering design.

### NEAR-SURFACE SITE RESPONSE

Dramatic effects on man-made structures due to site amplification have occurred worldwide in recent well-recorded large earthquakes such as the 1985  $M$  7.9 Michocan, Mexico, 1994  $M$  6.7 Kobe, Japan, and 2001  $M$  7.6 Chi Chi, Taiwan earthquakes. In the Basin and Range Province, populated basins abound and thus near-surface site amplification will be a significant if not controlling factor in future earthquake ground shaking at levels of engineering relevance. Near-surface site amplification can be estimated through the calculation of amplification factors based on *in situ* shear-wave velocity ( $V_S$ ) data and nonlinear dynamic material properties. If available, depth to rock information is valuable because amplification is strongly dependent upon the thickness of the underlying soil and unconsolidated sediments (Wong and others, 2002a). Empirical amplification factors are preferred, but they have only been estimated for low-strain ground motions in a few areas in the province (e.g., Pankow and Pechmann, 2004b). Based on the  $V_S$  data and surficial geology, site-response categories can be defined, and strain- and depth-dependent amplification factors calculated (Figure 3). The 1D equivalent-linear approach is the most widely used technique (e.g., SHAKE) to calculate amplification factors.

With the possible exception of portions of the Salt Lake Valley, adequate local and regional databases of  $V_S$  are lacking in the urban areas of the Basin and Range Province. Current shear modulus reduction and damping curves are for generic soil types and may not be representative of some deposits found in the province such as glacial till. The identification and characterization of site response units is well underway in the Salt Lake City area (Figure 4) and is

just beginning in the Reno-Carson City and Las Vegas areas. Efforts in these areas and elsewhere in the province need to be intensified.

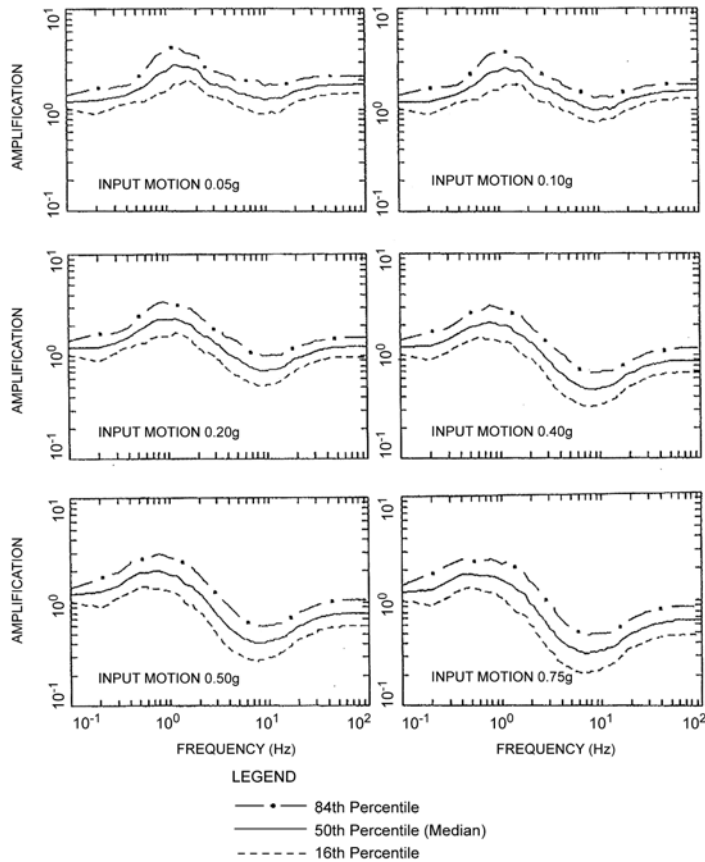


Figure 3. Example of strain-dependent amplification factors for lacustrine-alluvial silts and clays for the Salt Lake Valley (Wong and others, 2002a).

Kappa, the near-surface parameter, which describes the attenuation in the upper 1 km of the crust (Silva and Darragh, 1995), has received little research attention in the western U.S., and even less in the Basin and Range Province. The low kappa value used in the seismic hazard evaluation of Yucca Mountain (0.0186 sec) northwest of Las Vegas has highlighted the importance of this parameter (Stepp and others, 2001). The average kappa of western U.S. strong-motion sites is about 0.03 to 0.04 sec (Silva and Darragh, 1995), and these values are implicit in western U.S. attenuation relationships. Assessments of kappa at sites where there may be significant deviations from this average range, particularly at low kappa values (higher ground motions), need to be

made to accurately predict high-frequency ground motions.

## BASIN EFFECTS

For many large urban areas in the Basin and Range Province, 2D and 3D long-period basin effects ( $\geq 1$  sec) may be significant. As for the other previously discussed effects on strong ground shaking, the empirical data are lacking. The alternative to characterizing basin effects is numerical modeling. A few studies have been conducted, for example, in the Salt Lake Valley (Olsen and others, 1995) and in the Las Vegas Valley (Su and others, 1998). The presence of shallow basins may not necessarily result in amplification of engineering relevance. There is a significant need for models that characterize basin geometry and depth, velocities, and distribution of unconsolidated and semi-consolidated sediments in the Basin and Range Province. The role of the interface between the unconsolidated and semi-consolidated sediments in amplification also needs to be evaluated. Although efforts have been ongoing in the Salt Lake Basin, insufficient studies have been performed elsewhere along the Wasatch Front, in the Rio Grande rift, and other urbanized basins, to estimate long-period basin effects on ground motions. An additional important challenge is how to incorporate basin effects into probabilistic hazard maps given that such effects are earthquake-dependent.

## SUMMARY

The acquisition of strong-motion data from a large magnitude earthquake awaits the next such event in the Basin and Range Province. In the meantime, research efforts need to be increased to address the issues described in this paper, and more instruments need to be deployed to increase the likelihood of recording data.

In recently developed ground shaking hazard maps for the central Wasatch Front, Utah (including the Salt Lake City area; Figure 5), the Albuquerque-Santa Fe, New Mexico, corridor, and western Montana (Wong and others, 2002a; 2002b; 2004a; 2004b), we relied extensively on stochastic numerical ground-motion

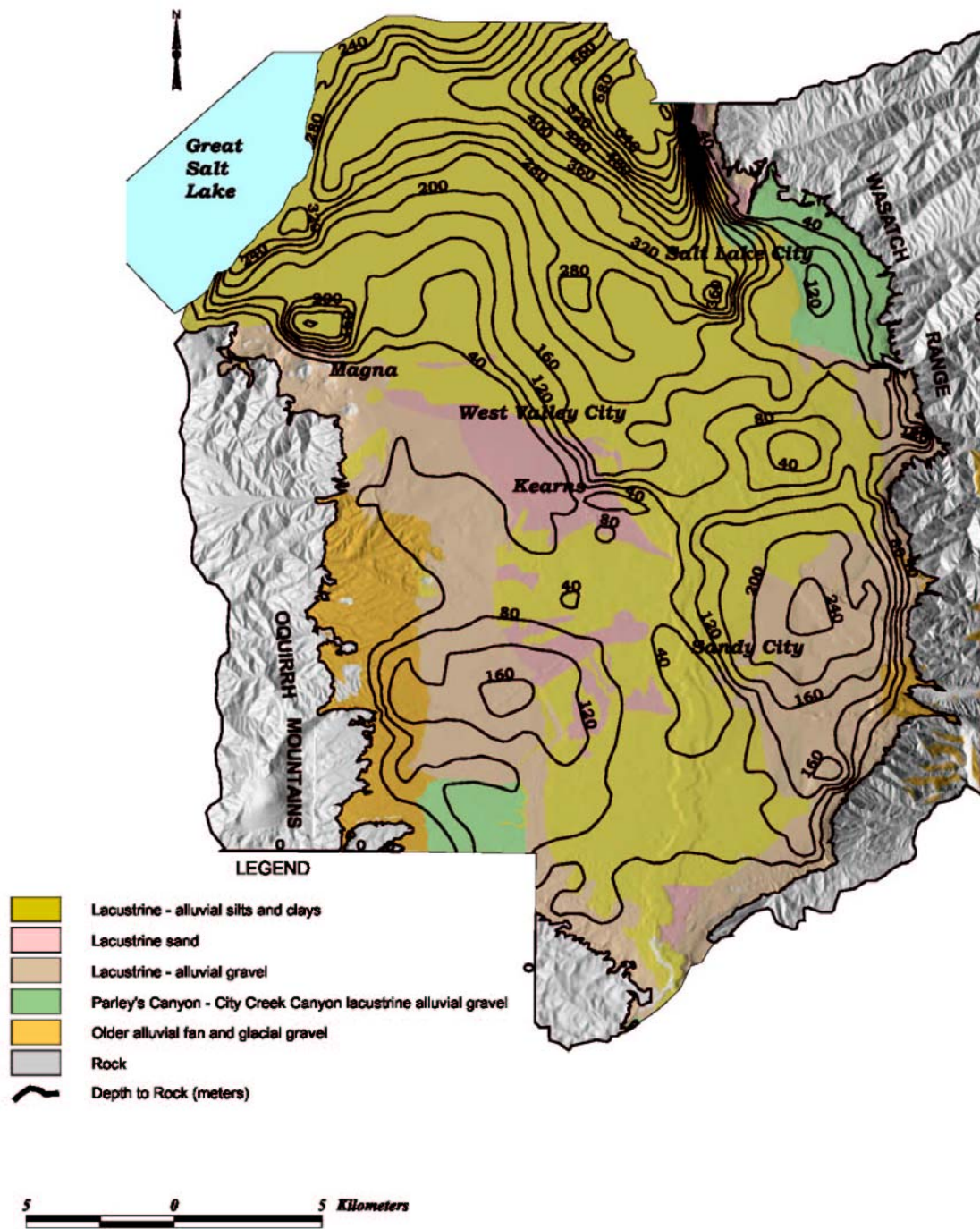


Figure 4. Site-response units and depth of Quaternary sediments in Salt Lake Valley (Wong and others, 2002a)

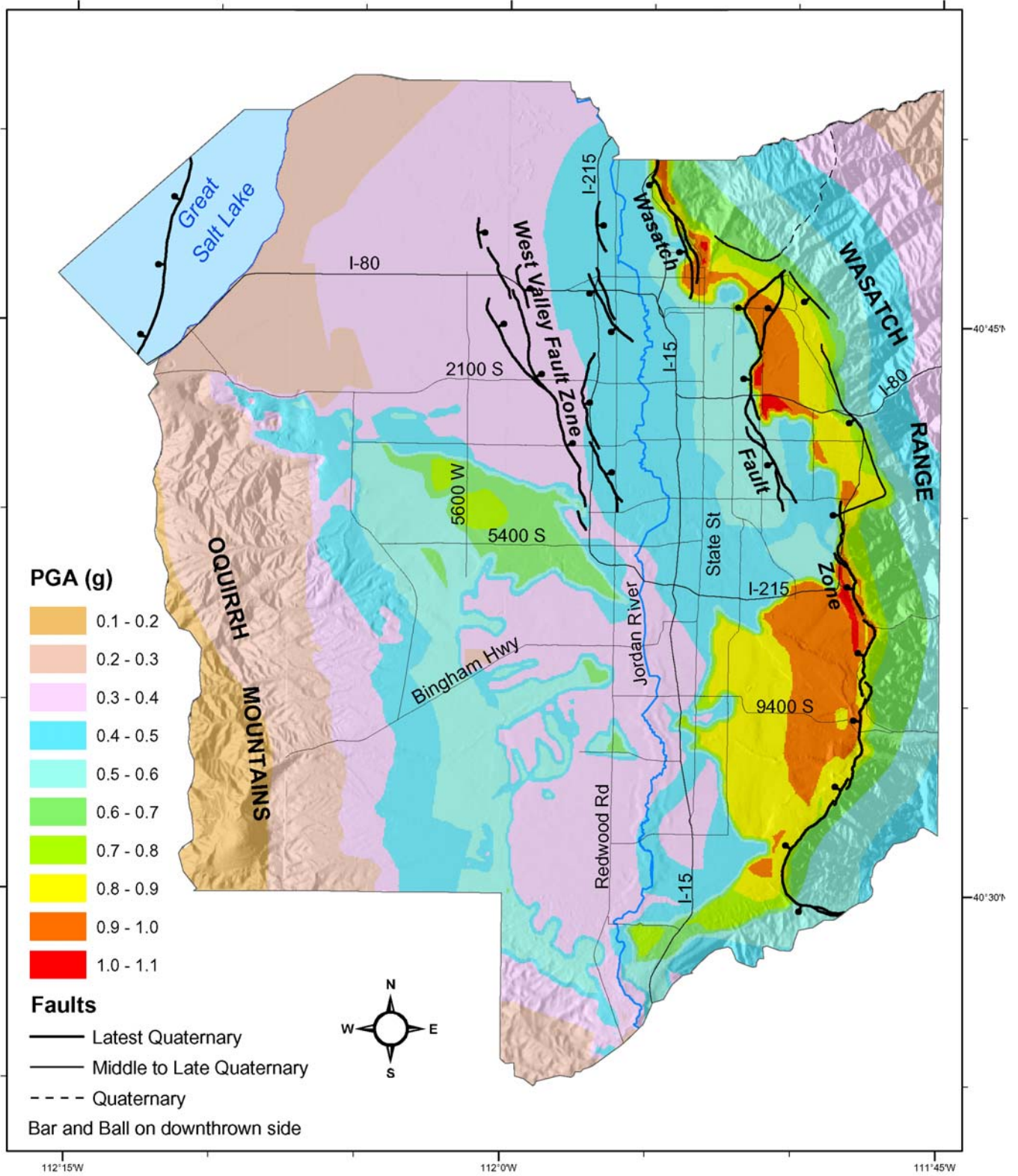


Figure 5. Salt Lake City segment, Wasatch fault  $M$  7.0 earthquake scenario, peak horizontal acceleration (g) at the ground surface (Wong and others, 2002a)

modeling to address most of the above issues. For example, we used point-source and finite-fault simulations combined with empirical attenuation relationships to estimate scenario and probabilistic ground motions. The normal faulting finite-fault simulations include rupture directivity, hanging wall/footwall effects, region-specific  $Q$ , and  $\kappa$ . Basin effects were not, however, addressed. Admittedly, the inputs required for the numerical modeling are not well constrained, again emphasizing the need for empirical data.

Coordinated and concerted efforts along the Wasatch Front by the Utah Ground Shaking Working Group are underway to fill gaps in the data required to accurately predict ground shaking in the region (Figure 5). Similar U.S. Geological Survey, state, and university-coordinated efforts to address earthquake ground-shaking hazard need to be undertaken in other populated areas of the Basin and Range Province.

## **ACKNOWLEDGMENTS**

This paper summarizes the introductory presentation for the “Ground Motion in the Basin and Range Province” session in the BRSBS II. My thanks to Craig dePolo for his leadership in the Summit and to the speakers Bob Darragh, Ken Campbell, Rob Graves, Paul Somerville, and Jim Brune. This paper benefited from reviews by Susan Olig, Jim Pechmann, and Bill Lund. My thanks to Melinda Lee for her assistance in the preparation of this paper.

## **REFERENCES**

- Abrahamson, N.A., and Silva, W.J., 1997, Empirical response spectral attenuation relations for shallow crustal earthquakes: *Seismological Research Letters*, v. 68, p. 94-127.
- Becker, A.M., and Abrahamson, N.A., 1997, Stress drops in normal faulting earthquakes [abs.]: *Seismological Research Letters*, v. 68, p. 322.
- Brune, J.N., 2000, Precarious rock evidence for low ground shaking on the footwall of major normal faults: *Bulletin of the Seismological Society of America*, v. 90, p. 1107-1112.
- Brune, J.N., and Anoushehpour, A., 1999, Dynamic geometrical effects on strong ground motion in a normal fault model: *Journal of Geophysical Research*, v. 104, p. 809-815.
- Campbell, K.W., 1997, Empirical near-source attenuation relationships for horizontal and vertical components of peak ground acceleration, peak ground velocity, and pseudo-absolute acceleration response spectra: *Seismological Research Letters*, v. 68, p. 154-179.
- Mendoza, C., and Hartzell, S.H., 1988, Inversion of slip distribution using teleseismic P waveforms: North Palm Springs, Borah Peak and Michoacan earthquakes: *Bulletin of the Seismological Society of America*, v. 78, p. 1092-1111.
- Olsen, K.B., Pechmann, J.C., and Schuster, G.T., 1995, Simulation of 3-D elastic wave propagation in the Salt Lake Basin: *Bulletin of the Seismological Society of America*, v. 85, p. 1688-1710.
- Pankow, K.L. and Pechmann, J.C., 2004a, The SEA99 ground-motion predictive relations for extensional regimes: Revisions and a new peak ground velocity relation: *Bulletin of the Seismological Society of America*, v. 94, p. 341-348.
- Pankow, K.L. and Pechmann, J.C., 2004b, Determination of low-strain site amplification factors in the Salt Lake Valley, Utah using ANSS data: *Proceedings, Basin and Range Seismic Hazards Summit II* (this volume).
- Richins, W.D., Pechmann, J.C., Smith, R.B., Langer, C.J., Goter, S.K., Zollweg, J.E., and King, J.J., 1987, The 1983 Borah Peak, Idaho, earthquake and its aftershocks: *Bulletin of the Seismological Society of America*, v. 77, p. 694-723.
- Sadigh, K., Chang, C.-Y., Egan, J.A., Makdisi, F., and Youngs, R.R., 1997, Attenuation relationships for shallow crustal earthquakes based on California strong motion data: *Seismological Research Letters*, v. 68, p. 180-189.
- Silva, W.J., and Darragh, R.B., 1995, Engineering characterization of strong ground motion recorded at rock sites: Electric Power Research Institute, EPRI TR-102262.
- Somerville, P.G., Smith, N.F., Graves, R.W., and Abrahamson, N.A., 1997, Modification of empirical strong ground-motion attenuation

- relations to include the amplitude and duration effects of rupture directivity: *Seismological Research Letters*, v. 68, p. 199-222.
- Spudich, P., Fletcher, J.B., Hellweg, M., Boatwright, J., Sullivan, C., Joyner, W.B., Hanks, T.C., Boore, D.M., McGarr, A., Baker, L.M., and Lindh, A.G., 1997, SEA96 – A new predictive relation for earthquake ground motions in extensional tectonic regimes: *Seismological Research Letters*, v. 68, p. 190-198.
- Spudich, P., Joyner, W.B., Lindh, A.G., Boore, D.M., Margaris, B.M., and Fletcher, J.B., 1999, SEA99 – A revised ground motion prediction relation for use in extensional tectonic regimes: *Bulletin of the Seismological Society of America*, v. 89, p. 1156-1170.
- Stepp, J.C., Wong, I., Whitney, J., Quittmeyer, R., Abrahamson, N., Coppersmith, K., Toro, G., Youngs, R., Savy, J., Sullivan, T., and Yucca Mountain PSHA Project Members, 2001, Probabilistic seismic hazard analyses for ground motions and fault displacement at Yucca Mountain, Nevada: *Earthquake Spectra*, v. 17, p.113-151.
- Su, F., Anderson, J.G., Der Ni, S., and Zeng, Y., 1998, Effect of site amplification and basin response on strong motion in Las Vegas, Nevada: *Earthquake Spectra*, v. 14, p. 357-376.
- Wong, I., Kelson, K., Olig, S., Bott, J., Green, R., Kolbe, T., Hemphill-Haley, M., Gardner, J., Reneau, S., and Silva, W., 1996b, Earthquake potential and ground shaking hazard at the Los Alamos National Laboratory, *in* Goff, F., Kues, B., Rogers, M.A., McFadden, L.D., and Gardner J. (eds.), *The Jemez Mountains Region*, New Mexico Geological Society Guidebook 47, p. 143-151.
- Wong, I., Olig, S., Dober, M., Silva, W., Wright, D., Thomas, P., Gregor, N., Sanford, A., Lin, K-W., and Love, D., 2004a, Earthquake scenario and probabilistic ground-shaking hazard maps for the Albuquerque-Belen-Santa Fe, New Mexico corridor: *New Mexico Geology*, v. 26, p. 3-33.
- Wong, I., Olig, S., Dober, M., Wright, D., Nemser, E., Lageson, D., Silva, W., Stickney, M., Lemieux, M., and Anderson, L., 2004b, Probabilistic earthquake hazard maps for the State of Montana: Montana Bureau of Mines and Geology (in preparation).
- Wong, I., Silva, W., Gregor, N., Wright, D., Ashland, F., McDonald, G., Olig, S., Christenson, G., and Solomon, B., 2002b, Earthquake scenario ground shaking maps for the central Wasatch Front, Utah: 7th U.S. National Conference on Earthquake Engineering Proceedings (CD ROM).
- Wong, I., Silva, W., Olig, S., Thomas, P., Wright, D., Ashland, F., Gregor, N., Pechmann, J., Dober, M., Christenson, G., and Gerth, R., 2002a, Earthquake scenario and probabilistic ground shaking maps for the Salt Lake City metropolitan area, Utah: Utah Geological Survey Miscellaneous Publication MP-02-5, 50 p.
- Wong, I.G., Silva, W.J., Youngs, R.R., and Stark, C.L., 1996a, Numerical earthquake ground motion modeling and its use in microzonation, Proceedings, 11th World Conference on Earthquake Engineering: Pergamon (CD-ROM).

## **POSTERS**

### **MAGNITUDE AND RUPTURE LENGTH ESTIMATES FROM POINT MEASUREMENTS OF DISPLACEMENT**

by Glenn Biasi, University of Nevada, Reno Seismological Laboratory, and Ray J. Weldon II,  
University of Oregon Department of Geological Sciences

### **MIOCENE AND YOUNGER FAULTS IN IDAHO**

compiled by Roy M. Breckenridge, Reed S. Lewis, Guy W. Adema, and Daniel W. Weisz

### **MIOCENE AND YOUNGER FAULTS IN IDAHO AND EARTHQUAKES IN IDAHO 1872—2000**

compiled by Roy M. Breckenridge, Reed S. Lewis, Guy W. Adema, and Daniel W. Weisz, Idaho Geological Survey

### **GUIDELINES FOR EVALUATING SURFACE-FAULT-RUPTURE HAZARDS IN UTAH**

by Gary E. Christenson, Utah Geological Survey; L. Darlene Batatian, Salt Lake County Geologist;  
Craig V Nelson, Western GeoLogic

### **INTEGRATION OF GEOLOGIC AND GEODETIC DATA INTO KINEMATIC MODELS OF CONTEMPORARY STRAIN IN THE PACIFIC NORTHWEST AND ACROSS THE CASCADIA SUBDUCTION ZONE**

by Mark Hemphill-Haley, Department of Geology, Humboldt State University, and Gene Humphreys,  
Department of Geological Sciences, University of Oregon

### **QUATERNARY FAULT AND FOLD DATABASE AND MAP OF UTAH**

by Michael D. Hylland, Utah Geological Survey

### **CRITIQUE AND USE OF HISTORICAL METHODOLOGY IN SEISMIC HAZARDS ANALYSIS OF EARTHQUAKES IN THE BASIN AND RANGE: EXPANDING THE HISTORICAL CATALOG AND THE SEARCH FOR TRIGGERED (?) EVENTS FROM THE SAN ANDREAS FAULT**

by Dawn C. Martindale, Department of History, Utah State University, and James P. Evans,  
Department of Geology, Utah State University

### **HORSTS AND GRABENS OF COLORADO'S HIGH PLAINS**

by Vince Matthews and Matthew L. Morgan, Colorado Geological Survey

### **ACTIVE TECTONICS AND STRAIN PARTITIONING IN THE NORTHERN INTERMOUNTAIN SEISMIC BELT**

by Michael C. Stickney, Montana Bureau of Mines and Geology, and David R. Lageson,  
Department of Earth Sciences, Montana State University

### **DIGITAL TRENCH WALL LOGGING: APPLYING MORPHOLOGICAL IMAGE PROCESSING TECHNIQUES TO TRENCH WALL STRATIGRAPHY – WASATCH FAULT 2003 TRENCH AT MAPLETON, UTAH**

by Julie B. Willis, Chaiwoot Boonyasiriwat, Gerald T. Schuster, and Christopher B. DuRoss, University of Utah

# Magnitude and Rupture Length Estimates From Point Measurements of Displacement

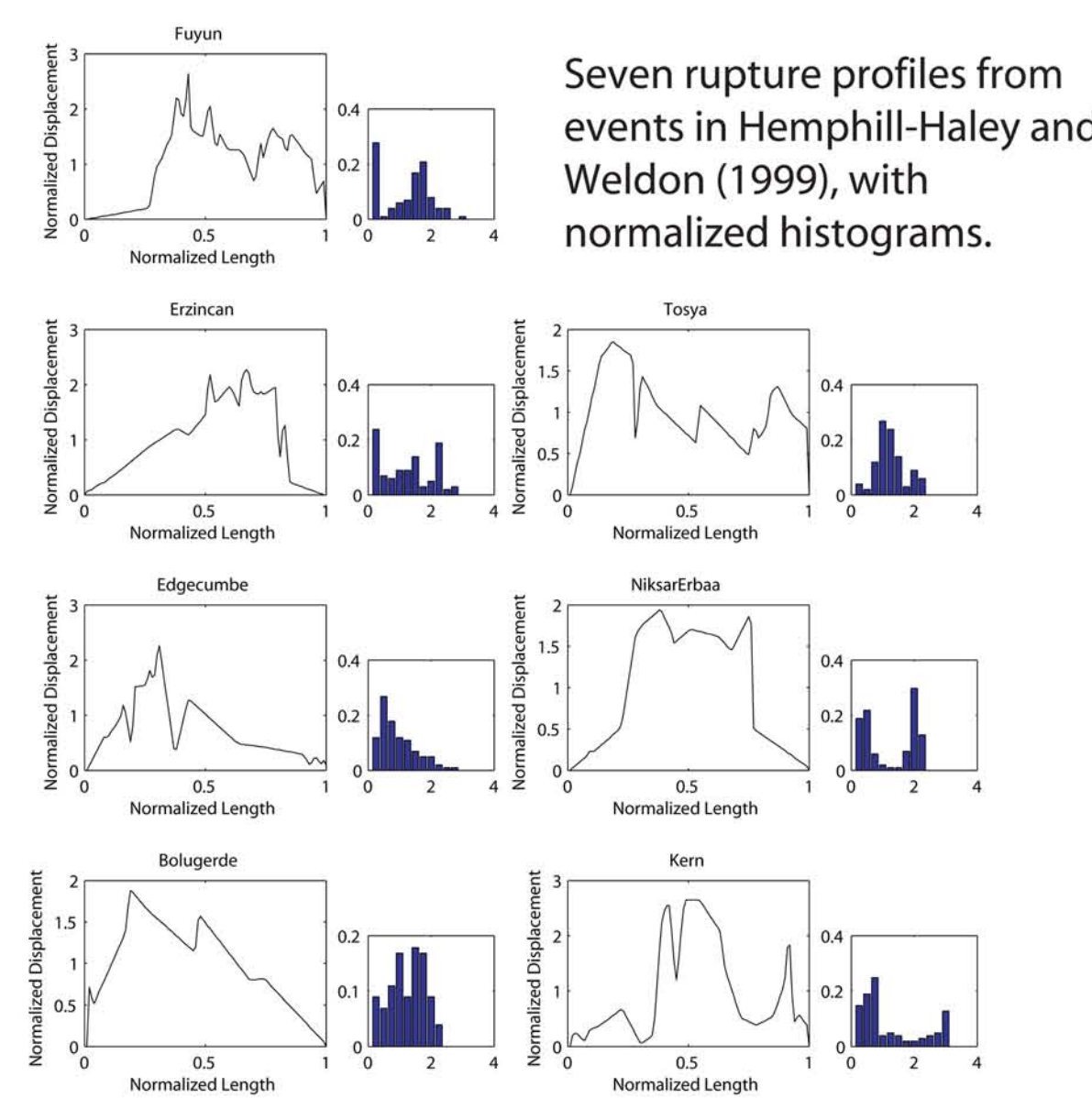
Glenn Biasi<sup>1</sup> and Ray J. Weldon II<sup>2</sup>

<sup>1</sup>University of Nevada Reno Seismological Laboratory, Reno, NV 89557, glenn@seismo.unr.edu

<sup>2</sup>University of Oregon Dept. of Geological Sciences, Eugene, OR 97403, ray@newberry.uoregon.edu

The Basic Problem: Displacement estimates in trenches may not be representative of the rupture. One might sample a peak of what is actually a small rupture or a low spot in a large event. Assuming  $d_{obs}=d_{ave}$  is a big leap. This makes paleomagnitude and rupture length estimates from observed displacements very uncertain. We show that quantitative magnitude and length estimates are possible that respect the intrinsic variability of ground ruptures.

## Mapped Ruptures Are Unpredictable



Seven rupture profiles from events in Hemphill-Haley and Weldon (1999), with normalized histograms.

## Bayesian Inversion When No Magnitude Distribution Is Available

The basic concept in a Bayesian inversion is to modify an initial opinion about likely magnitudes with the information that a displacement has been observed. The least informative prior model for  $p(M)$  is a uniform distribution on all reasonable magnitudes (any magnitude is as likely as another among those capable of producing ground rupture).

$$P(M|d) = P(M)P(d|M)/P(d)$$

$$P(d) = \sum P(d|M_i)P(M_i)$$

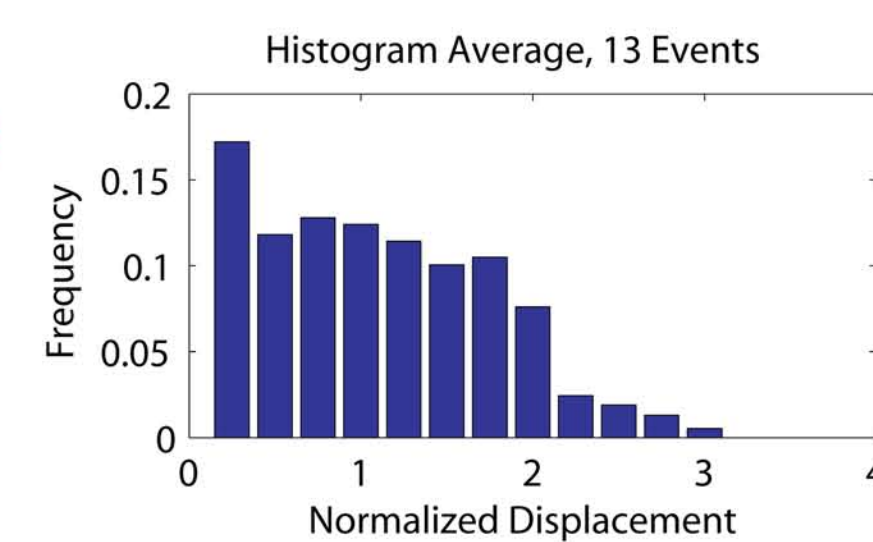
Since some magnitude earthquake must have caused the observed ground rupture, considering all possible magnitudes will include the likely ones. Results are shown in the left column at right for observed displacements from 1 to 6 meters. Declines in  $p(M|d)$  with increasing magnitude indicate small displacements (e.g.,  $d=2$  m) are unlikely for largest events because larger displacements are expected.

## Given Mw, Regressions Also Give Length

$p(M|d)$  is converted to  $P(L|d)$  by use of a regression relating surface rupture length  $L$  to magnitude  $M$ .

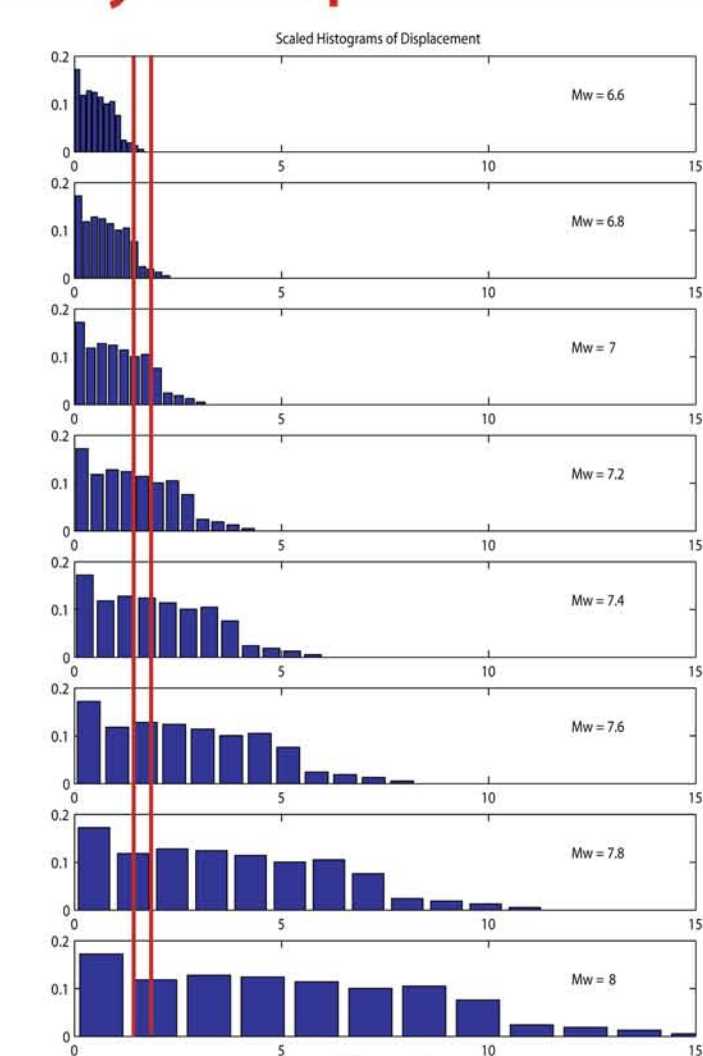
## Bayesian Inversion of Rupture Variability Requires a Magnitude Distribution Model.

Three magnitude distribution models ( $P(M)$ ) were considered (Below). The distribution is used as a priori information. Complete paleoseismic records combined with the slip rate constrain the preferred choice for the southern San Andreas fault. The detailed shape of the average displacement model is unknown.  $p(M|d)$  distributions are shown below for the Gutenberg-Richter  $p(M)$  distribution and far right for the Average Displacement model. The two models differ most for the smallest observed displacements. The GR displacement forces  $p(M|d)$  weight to smaller events since it includes 10x as many ways to explain a 1-m displacement as a 6.8 as a M7.8. Peaks in  $p(M|d)$  are thus biased 0.2 to 0.3 units smaller than inferred from M-Avg Displacement regressions.



Normalizing by Length and Average Displacement Keeps Variability Without Constraining Order (right).

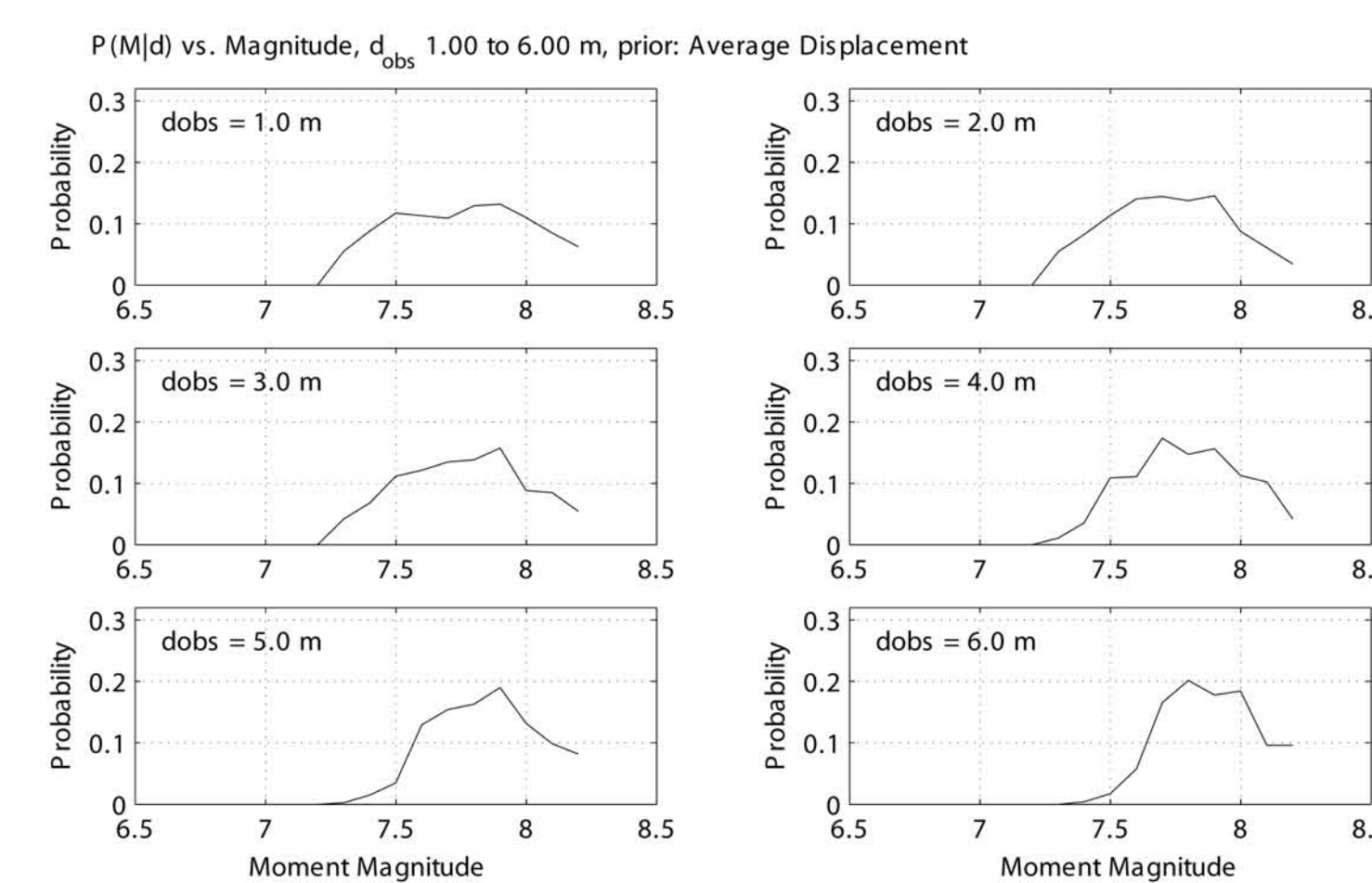
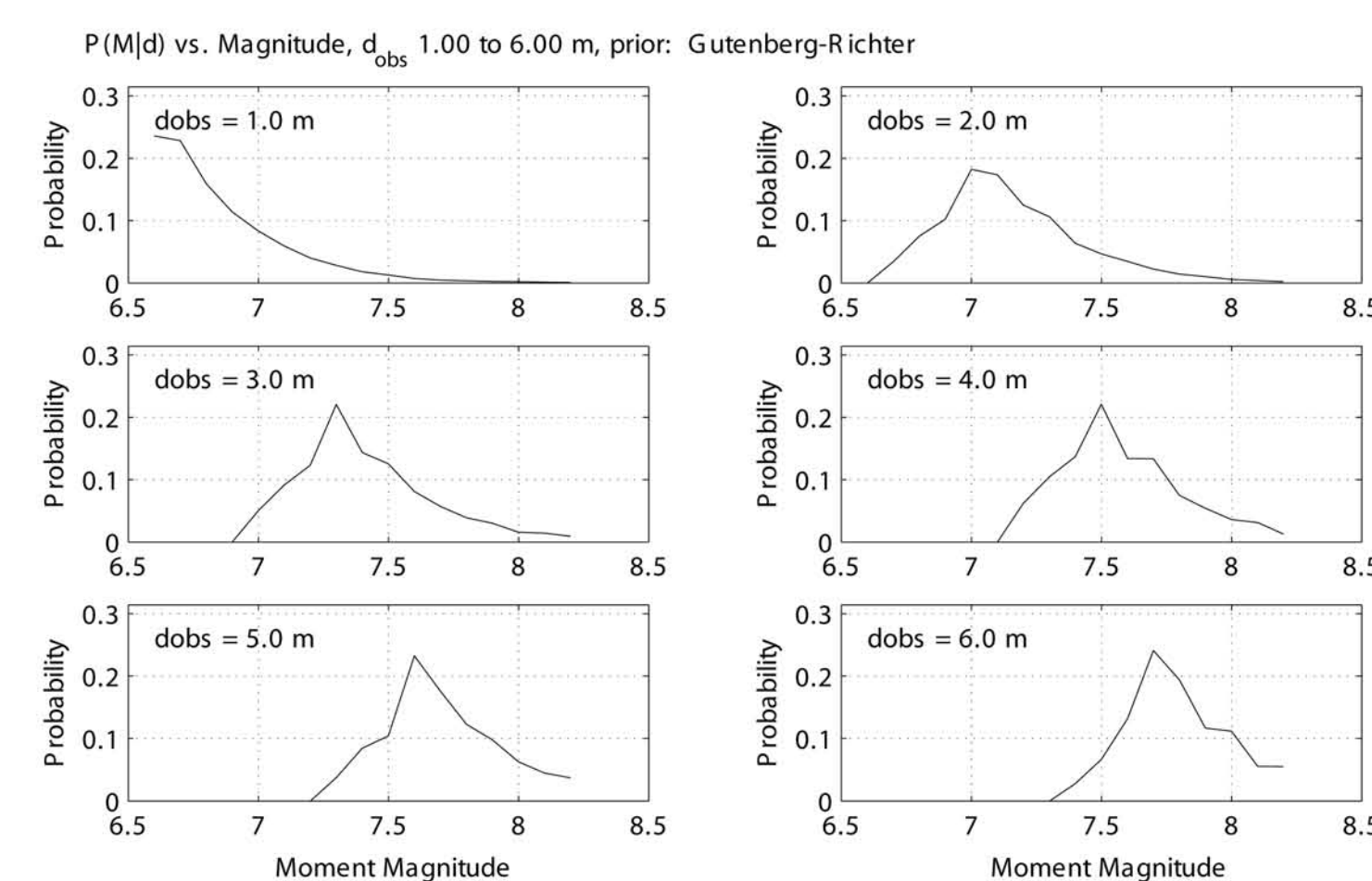
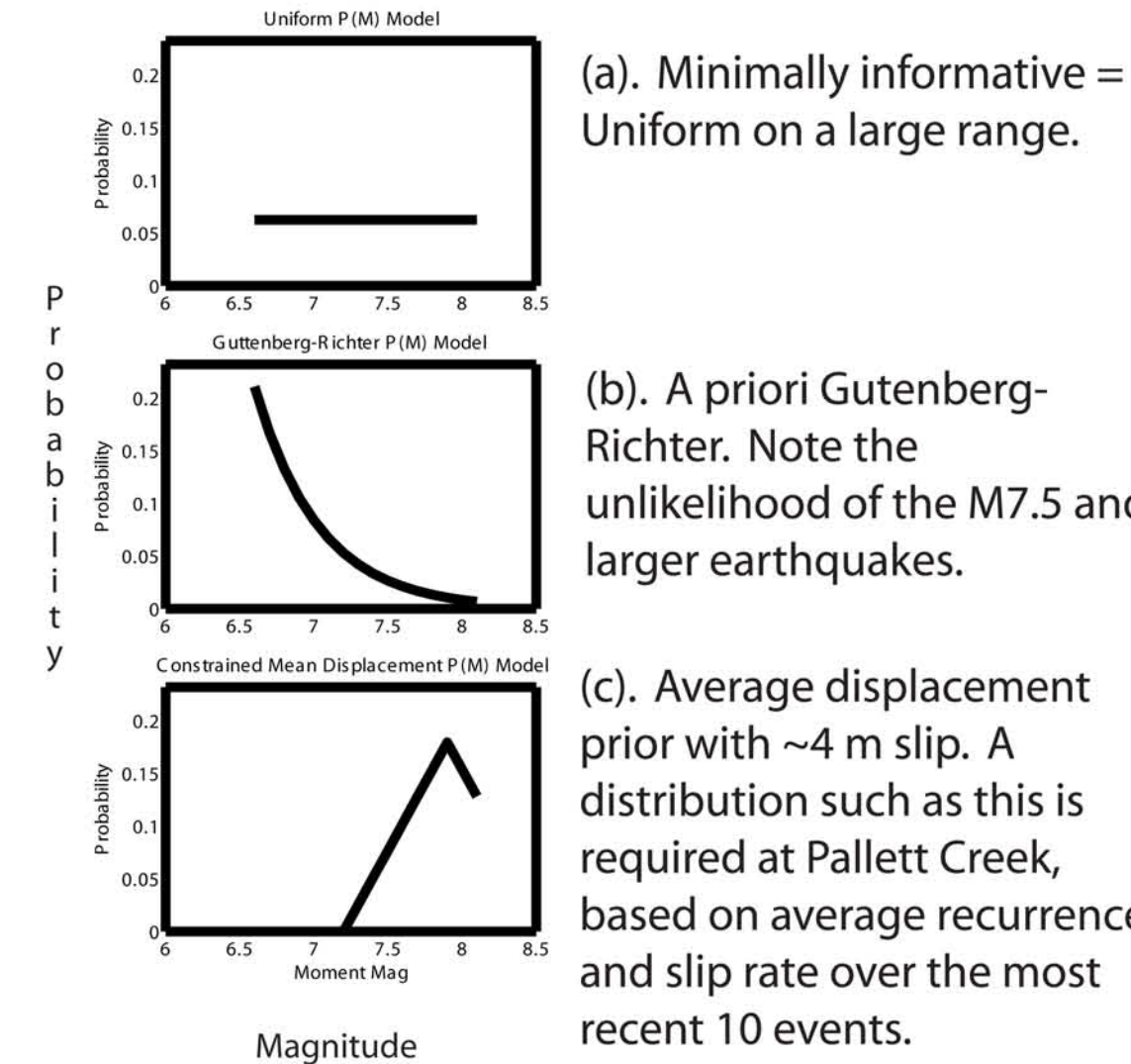
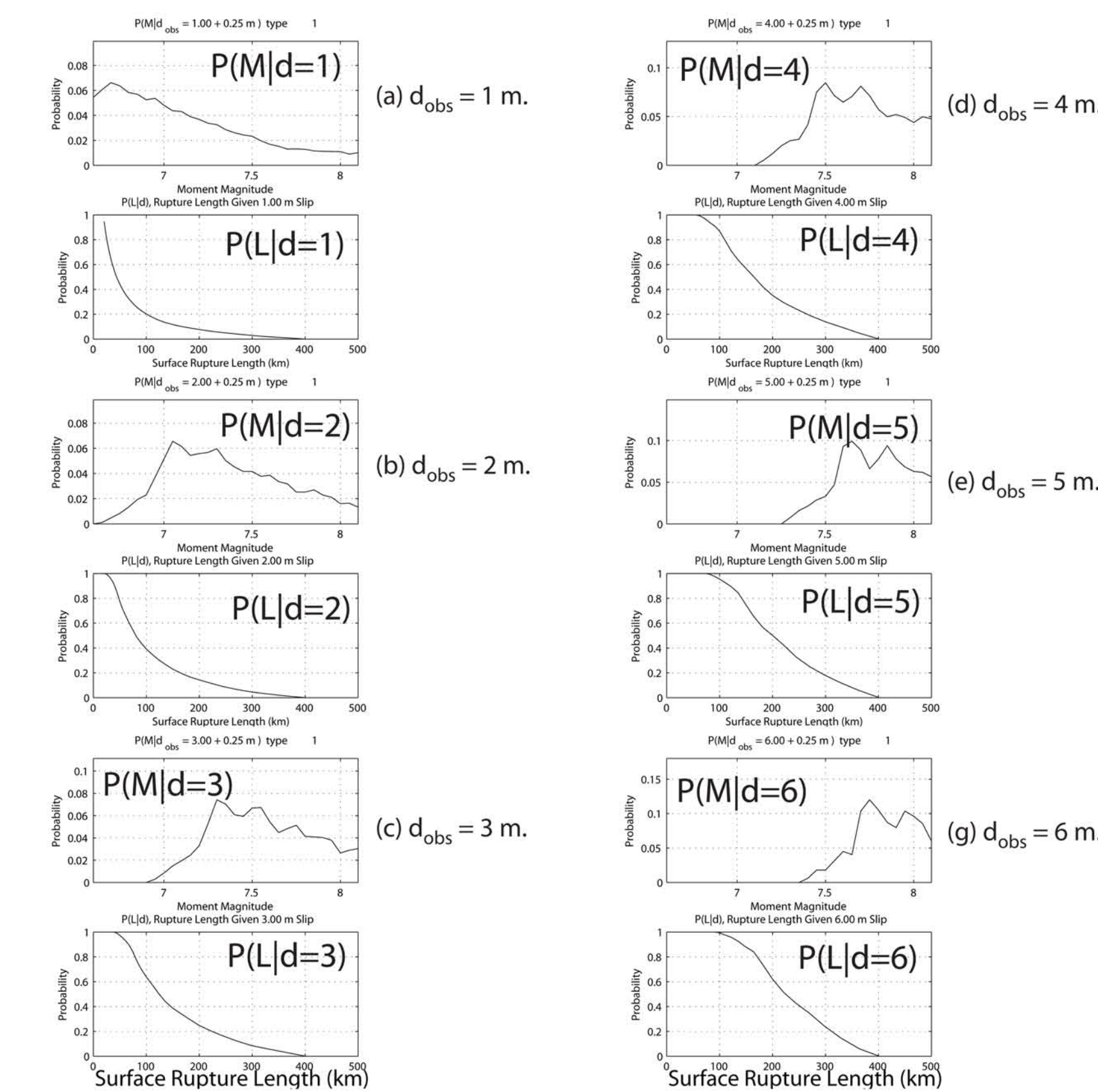
## Scaling the Normalized Histogram Predicts Variability of Displacement for a Given Mw



$P(d|M)$

When the normalized histogram is scaled by AD (see regressions) the predicted displacement histogram is obtained. Thus, given magnitude one has  $P(d|M)$ , the probability distribution to be inverted by Bayes Theorem.

Inputs:  $Mw=5.16 + 1.12 \log(SRL)$  SRL = surface rupture length  
 $\log(AD) = -6.32 + 0.90 Mw$  AD = average surface displacement

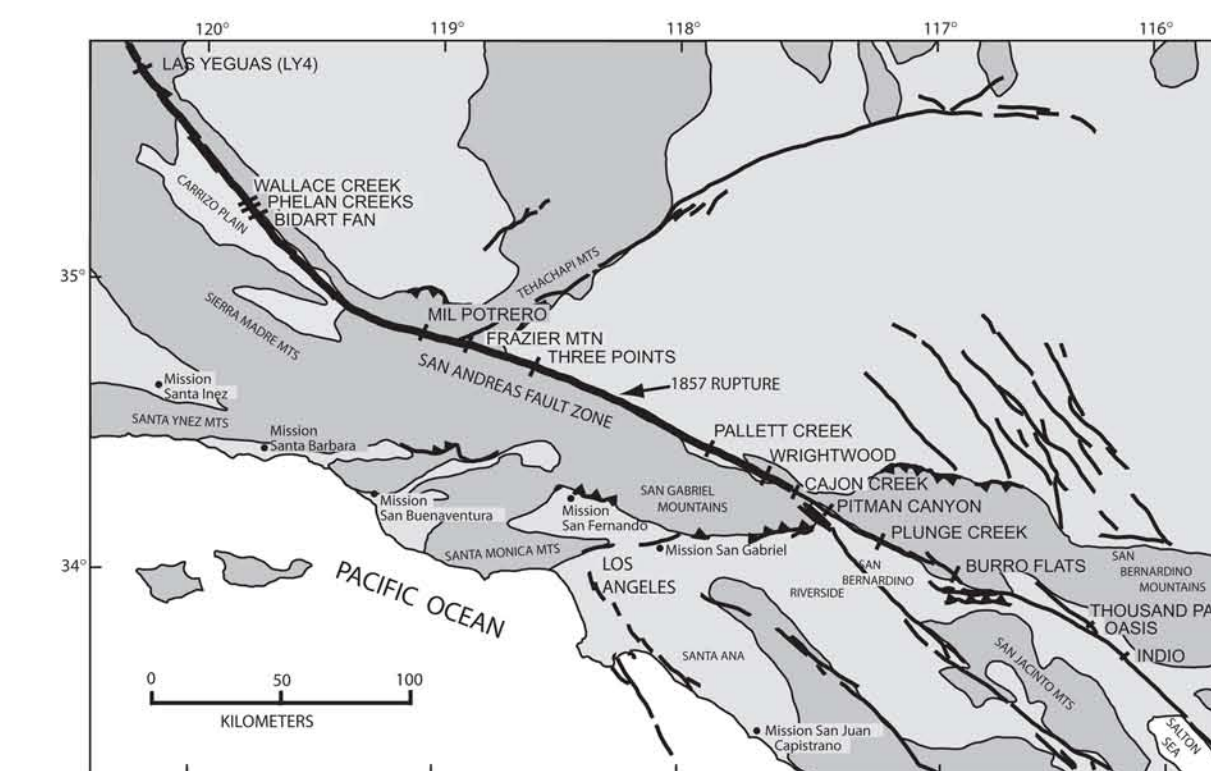


## Rupture Length and Magnitude Given Observed Displacement: The Bayesian Inversion Result

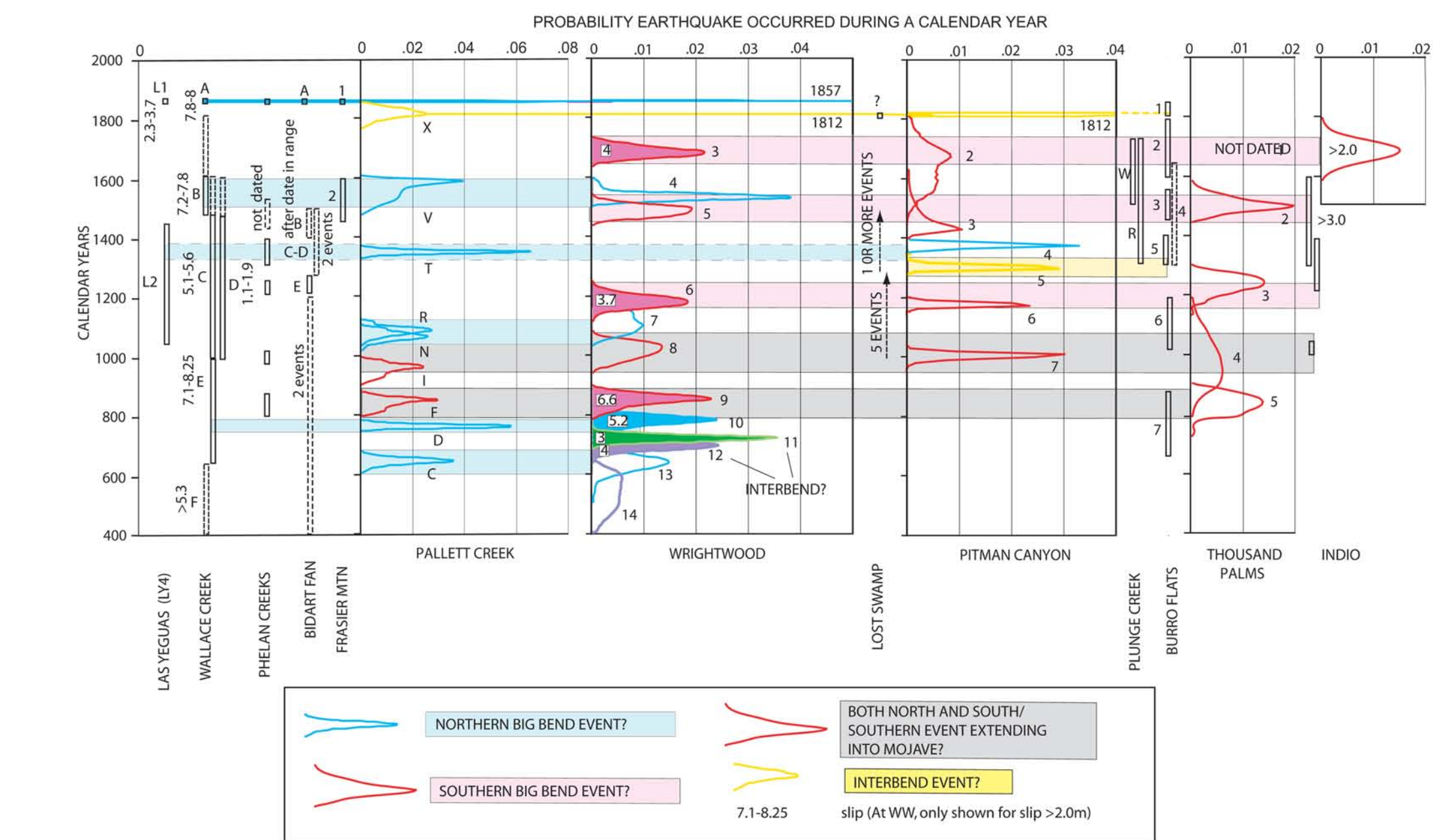
The plots at left provide magnitude and rupture length given point estimates of slip,  $p(M|d)$  and  $P(L|d)$ , respectively.  $P(L|d)$  shows how far one may expect seismic rupture to extend and with what probability. For example,  $d_{obs}=4$  m at Wrightwood on the southern San Andreas fault (see map below) is almost certain to extend 80 km, meaning that event is sure to have ruptured either at Pitman Canyon or Pallett Creek, and possibly both. Rupture over 160 km is expected at 50% and 200 km at ~33%.  $P(L|d)$  provides a quantitative basis for event correlation among neighboring paleoseismic sites.  $p(M|d)$  gives a basis to estimate  $Mw$  and  $P(Mw)$  from as little as one paleoseismic slip measurement. A uniform distribution  $p(M)$  distribution is assumed in this example. Irregularities in the shape of  $p(M|d)$  reflect the fine scale structure of  $p(d|M)$ .

## Implications for Correlation of Rupture Evidence Between Trenches

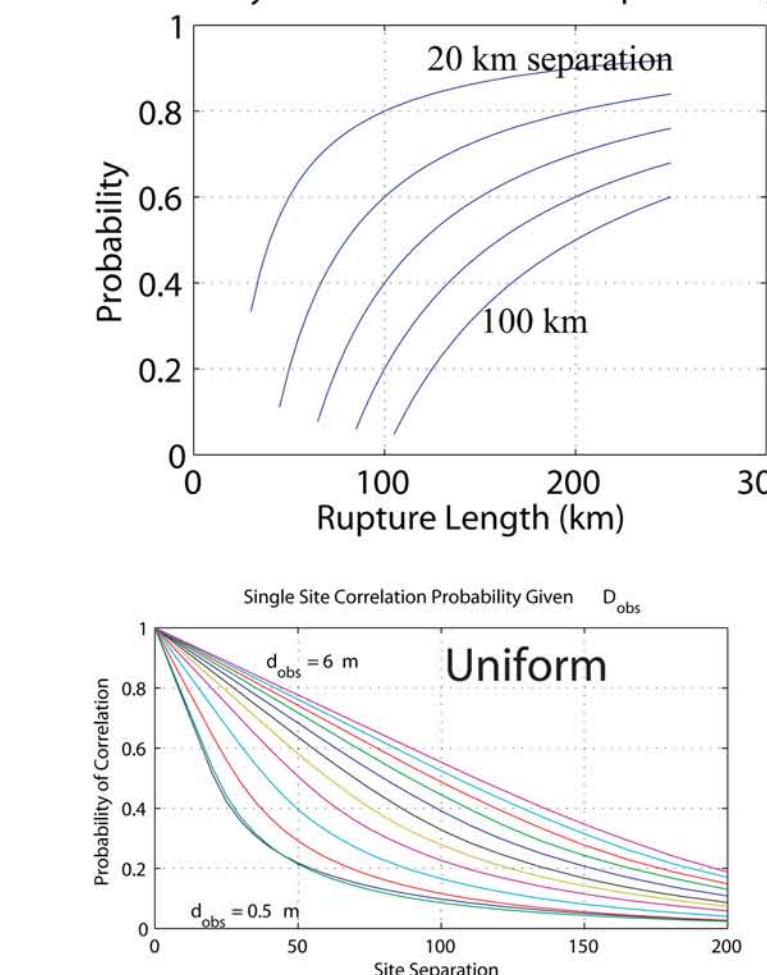
With  $p(L|d)$  one can quantify probabilities of correlation between trenches. Dating evidence for SAF sites (below) is shown above-right. Dating uncertainty makes correlation difficult. With measured displacements per event, the figures at right give the probability of observing that rupture at any distance from the measurement. At Wrightwood displacements are estimated for the most recent 14 events. These displacements give a physical basis for building rupture scenarios.



Site	Latitude	Longitude	Paleoseismic Site	Site Pair	Separation (km)
WLC	35.2714	-119.8278	Wallace Creek	WLC-BDF	6
BDF	35.2371	-119.7771	Bidart Fan	BDF-FRM	92.6
FRM	34.8122	-118.9019	Frazier Mtn.	FRM-PAL	101
PAL	34.4553	-117.8872	Pallett Creek	PAL-WWD	22.2
WWD	34.3703	-117.6678	Wrightwood	WWD-LOS	22
LOS	34.2700	-117.4606	Lost Swamp	LOS-PIT	3.4
PIT	34.2522	-117.4306	Pitman Canyon	PIT-PLC	30.9
PLC	34.1158	-117.1375	Plunge Creek	PLC-BFL	28.4
BFL	34.0022	-116.8614	Burro Flats	BFL-THP	51.9
THP	33.9197	-116.3075	Thousand Palms		

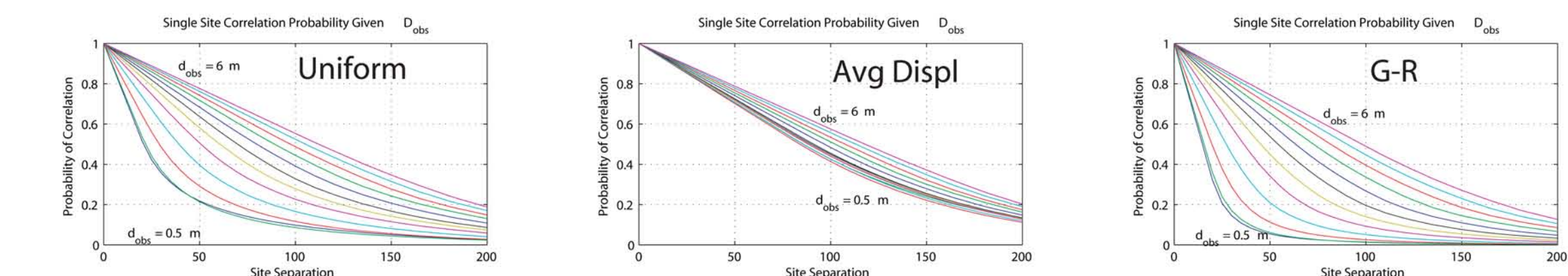


Probability of Correlation Given Rupture Length



## Length and the Assumption of Random Trench Placement Give a Probability of Spanning to Adjacent Sites

(Left) Sampling at random within the normalized histogram and trenching at a random location within a rupture are equivalent procedures. Given a random location within the rupture and the rupture length, probabilities of correlation are known. By combining  $P(corr|L)$  with  $P(L|d)$  (above left), probabilities of correlation given an observed displacement are computed (below).



Correlation Given a Displacement Observation. (Above) Probability that a rupture will be observed at some distance given a paleoseismically observed rupture displacement at a point. Uniform, Average Displacement, and Gutenberg-Richter (G-R) distributions of magnitude on the fault are shown. The G-R has the largest fraction of small events capable of producing ground rupture, and thus the shortest likely rupture length. Short likely ruptures translate to lowest probabilities of correlation for a given observed displacement. Forcing the sum of slips to the geologic average (A-D model) leads to probabilities that even small  $d_{obs}$  have long likely ruptures. Pallett Creek (10 events since A.D. 650, ~32 mm/yr) requires such a model. The G-R model average displacement is too small to produce a record such as Pallett Creek or Wrightwood.

## Conclusions

Rupture displacements provide a physical basis for earthquake magnitude and rupture length estimates.

Along-strike variability in rupture has made these estimates highly uncertain.

Bayesian inversion that includes the variability of rupture gives probability relationships between point displacement observations, earthquake magnitude and rupture length. Thus given  $d_{obs}$ , one can quantify the probability that it was caused by an earthquake of any given magnitude. This makes  $p(M|d)$  and  $p(L|d)$  suitable for quantitative logic-tree and PSHA applications.

Rupture length estimates from  $d_{obs}$  provide quantitative probabilities of correlation for ruptures at neighboring paleoseismic sites.

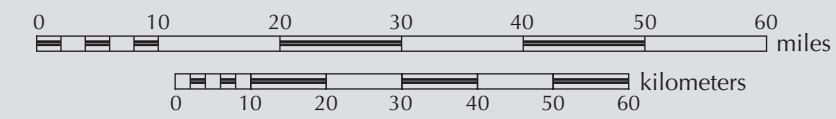
Correlation probabilities depend on the distribution model for magnitudes. The Gutenberg-Richter magnitude distribution predicts too many small displacement ruptures to match the paleoseismic record. Completeness and the approximate date of the oldest event are strong constraints on the magnitude distribution.

Support of the Southern California Earthquake Center is gratefully acknowledged.

# MIOCENE AND YOUNGER FAULTS IN IDAHO

Compiled by  
Roy M. Breckenridge, Reed S. Lewis,  
Guy W. Adema, and Daniel W. Weisz  
2003

Digital Cartography by  
Loudon R. Stanford and Jane S. Freed  
Funded in part by grants from the Idaho Bureau of Disaster Services



Scale 1:1,000,000

Lambert conformal conic projection based on standard parallels 33° and 45°, 1927 North American datum.

Shaded relief from U.S. Geological Survey's national elevation data (NED), 30 meter; 2x vertical exaggeration; sun angle of 30°; NW azimuth.

Geographic names and locations, streams, and roads from 1976 U.S. Geological Survey's 1:500,000 topographic map of Idaho.

## INTRODUCTION

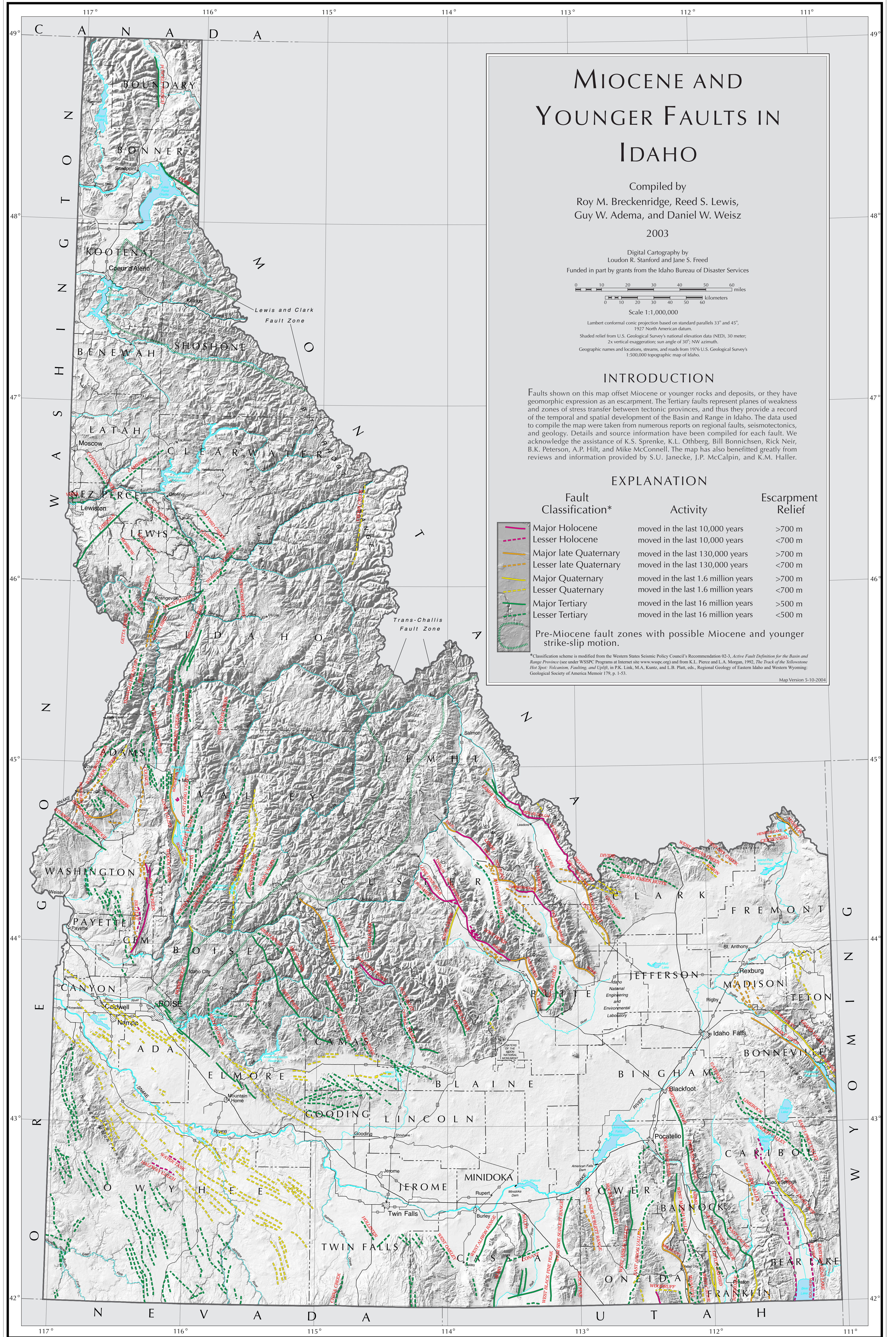
Faults shown on this map offset Miocene or younger rocks and deposits, or they have geomorphic expression as an escarpment. The Tertiary faults represent planes of weakness and zones of stress transfer between tectonic provinces, and thus they provide a record of the temporal and spatial development of the Basin and Range in Idaho. The data used to compile the map were taken from numerous reports on regional faults, seismotectonics, and geology. Details and source information have been compiled for each fault. We acknowledge the assistance of K.S. Sprenke, K.L. Othberg, Bill Bonnichsen, Rick Neir, B.K. Peterson, A.P. Hilt, and Mike McConnell. The map has also benefitted greatly from reviews and information provided by S.U. Janecke, J.P. McCalpin, and K.M. Haller.

## EXPLANATION

Fault Classification*	Activity	Escarpment Relief
Major Holocene	moved in the last 10,000 years	>700 m
Lesser Holocene	moved in the last 10,000 years	<700 m
Major late Quaternary	moved in the last 130,000 years	>700 m
Lesser late Quaternary	moved in the last 130,000 years	<700 m
Major Quaternary	moved in the last 1.6 million years	>700 m
Lesser Quaternary	moved in the last 1.6 million years	<700 m
Major Tertiary	moved in the last 16 million years	>500 m
Lesser Tertiary	moved in the last 16 million years	<500 m
Pre-Miocene fault zones with possible Miocene and younger strike-slip motion.		

\*Classification scheme is modified from the Western States Seismic Policy Council's Recommendation 02-3, *Active Fault Definition for the Basin and Range Province* (see under WSSPC Programs at Internet site www.wsspc.org) and from K.L. Pierce and L.A. Morgan, 1992, *The Track of the Yellowstone Hot Spot: Volcanism, Faulting, and Uplift*, in P.K. Link, M.A. Kuntz, and L.B. Platt, eds., *Regional Geology of Eastern Idaho and Western Wyoming*; Geological Society of America Memoir 179, p. 1-53.

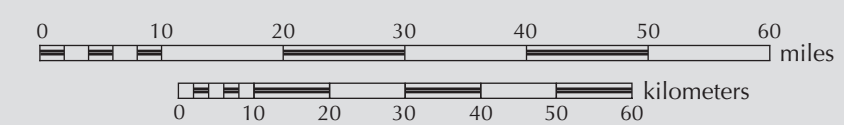
Map Version 5-10-2004



# MIOCENE AND YOUNGER FAULTS IN IDAHO AND EARTHQUAKES IN IDAHO 1872—2000

Compiled by  
Roy M. Breckenridge, Reed S. Lewis,  
Guy W. Adema, and Daniel W. Weisz  
2003

Digital Cartography by  
Loudon R. Stanford and Jane S. Freed  
Funded in part by grants from the Idaho Bureau of Disaster Services



Scale 1:1,000,000

Lambert conformal conic projection based on standard parallels 33° and 45°,  
1927 North American datum.  
Shaded relief from U.S. Geological Survey's national elevation data (NED), 30 meter;  
2x vertical exaggeration; sun angle of 30°; NW azimuth.  
Geographic names and locations, streams, and roads from 1976 U.S. Geological Survey's  
1:500,000 topographic map of Idaho.

## INTRODUCTION

Faults shown on this map offset Miocene or younger rocks and deposits, or they have geomorphic expression as an escarpment. The Tertiary faults represent planes of weakness and zones of stress transfer between tectonic provinces, and thus they provide a record of the temporal and spatial development of the Basin and Range in Idaho. The data used to compile the map were taken from numerous reports on regional faults, seismotectonics, and geology. Details and source information have been compiled for each fault. We acknowledge the assistance of K.S. Sprenke, K.L. Othberg, Bill Bonnicksen, Rick Neir, B.K. Peterson, A.P. Hill, and Mike McConnell. The map has also benefited greatly from reviews and information provided by S.U. Janecke, J.P. McCalpin, and K.M. Haller.

## EXPLANATION

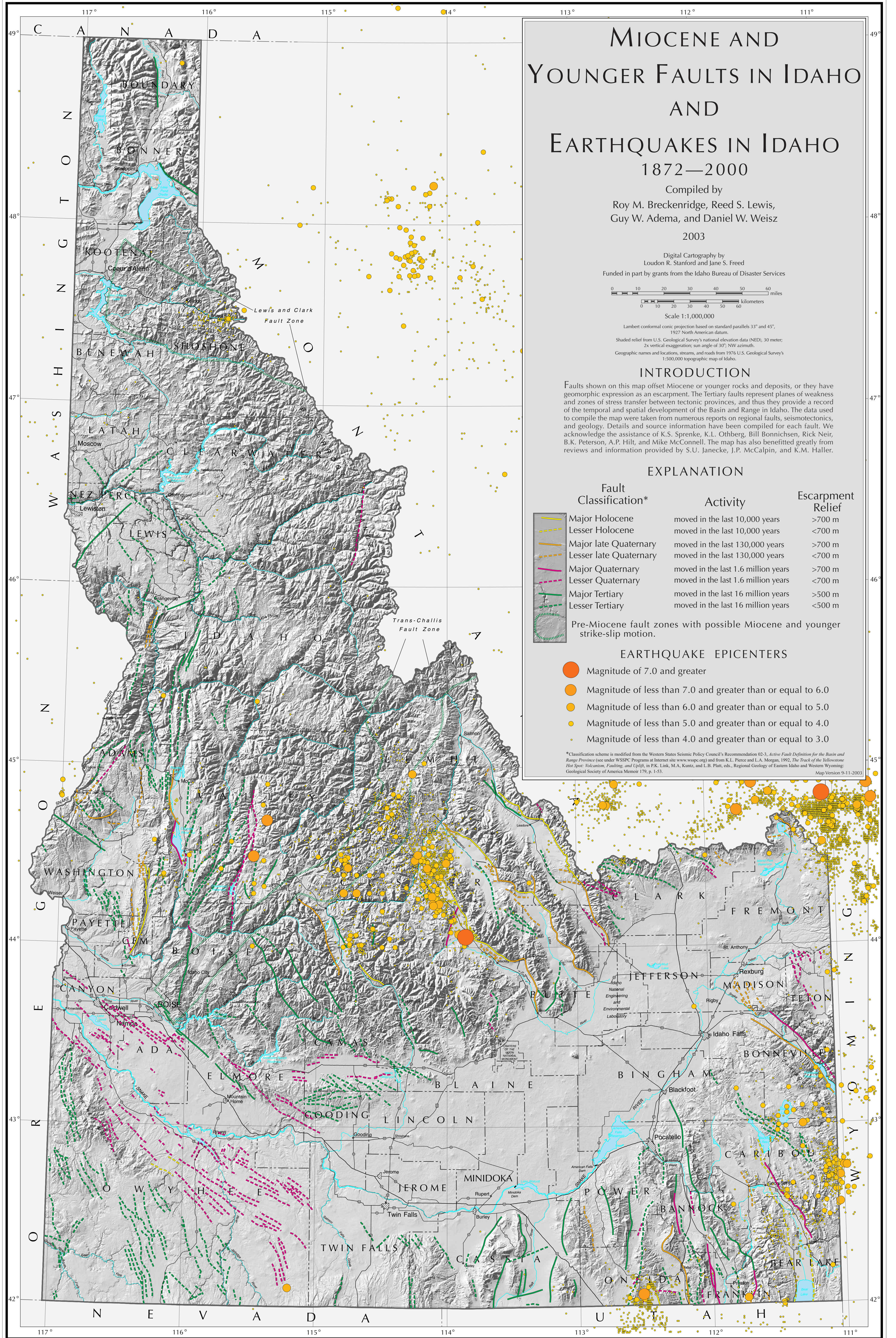
Fault Classification*	Activity	Escarpment Relief
Major Holocene	moved in the last 10,000 years	>700 m
Lesser Holocene	moved in the last 10,000 years	<700 m
Major late Quaternary	moved in the last 130,000 years	>700 m
Lesser late Quaternary	moved in the last 130,000 years	<700 m
Major Quaternary	moved in the last 1.6 million years	>700 m
Lesser Quaternary	moved in the last 1.6 million years	<700 m
Major Tertiary	moved in the last 16 million years	>500 m
Lesser Tertiary	moved in the last 16 million years	<500 m

Pre-Miocene fault zones with possible Miocene and younger strike-slip motion.

## EARTHQUAKE EPICENTERS

- Magnitude of 7.0 and greater
- Magnitude of less than 7.0 and greater than or equal to 6.0
- Magnitude of less than 6.0 and greater than or equal to 5.0
- Magnitude of less than 5.0 and greater than or equal to 4.0
- Magnitude of less than 4.0 and greater than or equal to 3.0

\*Classification scheme is modified from the Western States Seismic Policy Council's Recommendation 02-3, *Active Fault Definition for the Basin and Range Province* (see under WSSPC Programs at Internet site [www.wsspc.org](http://www.wsspc.org)) and from K.L. Pierce and L.A. Morgan, 1992, *The Track of the Yellowstone Hot Spot: Volcanism, Faulting, and Uplift*, in P.K. Link, M.A. Kuntz, and L.B. Platt, eds., *Regional Geology of Eastern Idaho and Western Wyoming*; Geological Society of America Memoir 179, p. 1-55. Map Version 9-11-2003



# GUIDELINES FOR EVALUATING SURFACE-FAULT-RUPTURE HAZARDS IN UTAH

Gary E. Christenson, Utah Geological Survey, L. Darlene Batatian, Salt Lake County Geologist, Craig V Nelson, Western GeoLogic



Determine  
FAULT ACTIVITY CLASS  
(time of most recent event)

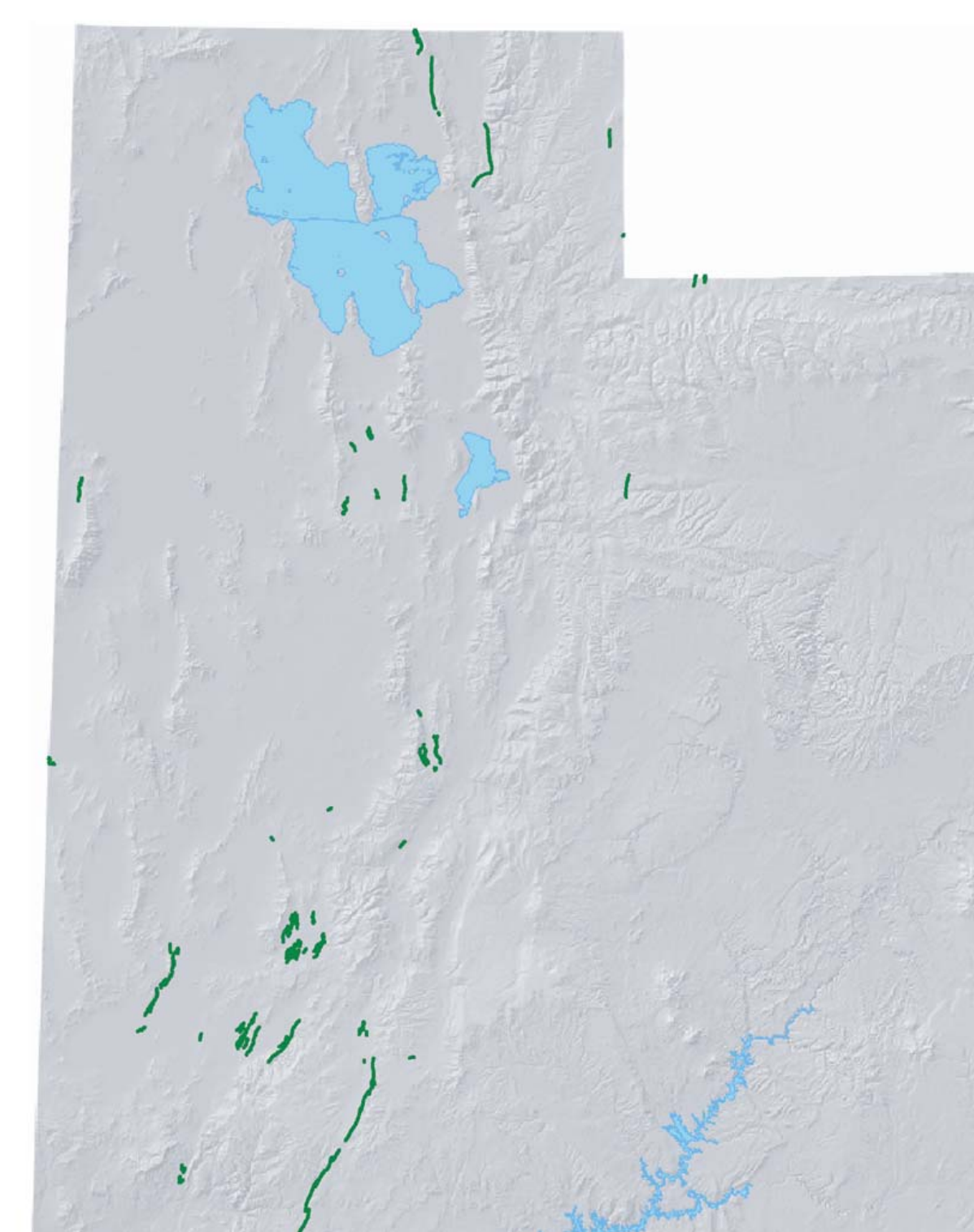
Define  
WIDTH OF FAULT-ZONE  
SPECIAL STUDY AREAS

Perform Investigation and Determine  
SETBACKS

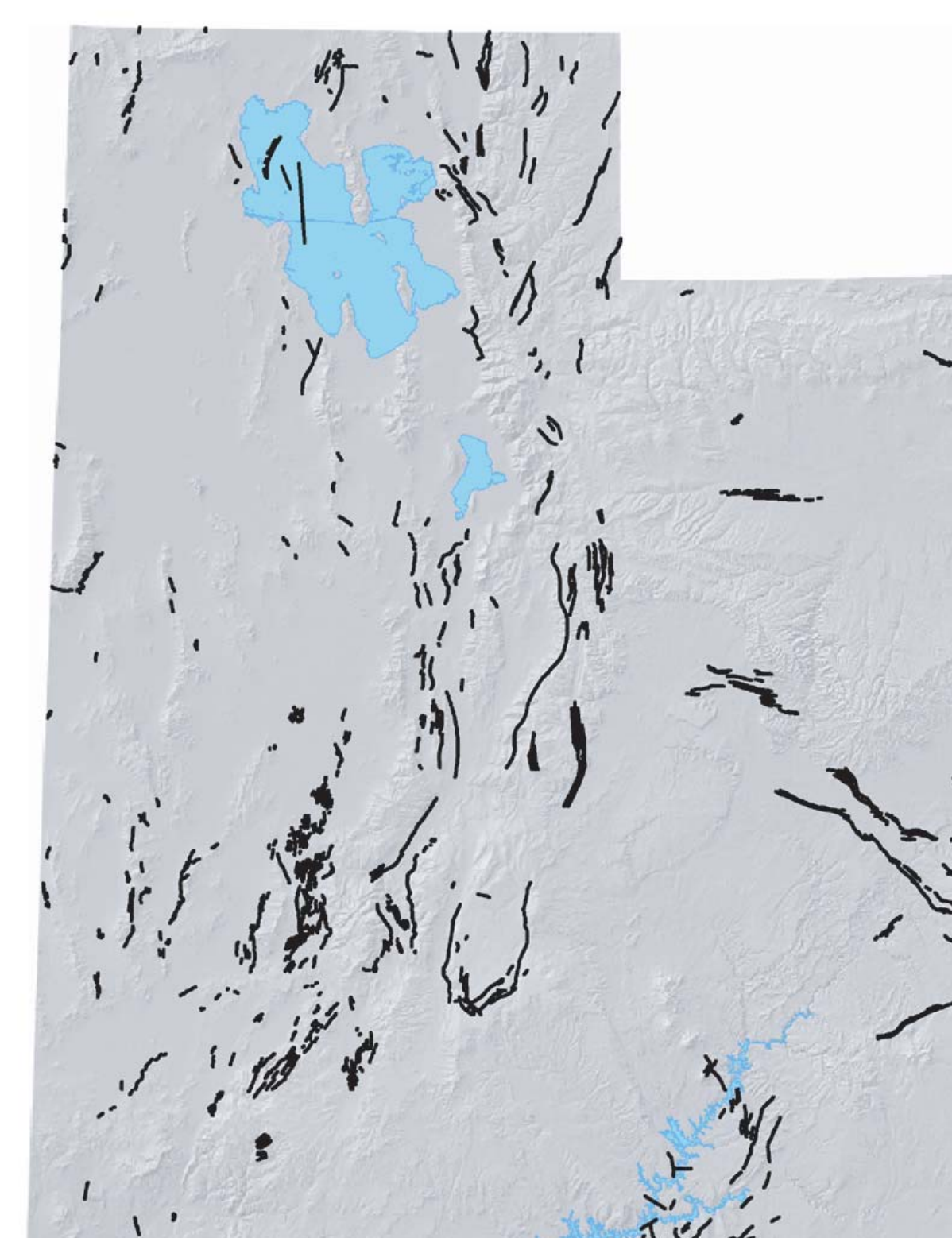
Holocene /  
Post-Bonneville  
( $<10,000$  yrs)



Late Quaternary  
( $<130,000$  yrs)



Quaternary  
( $<1.6$  my)



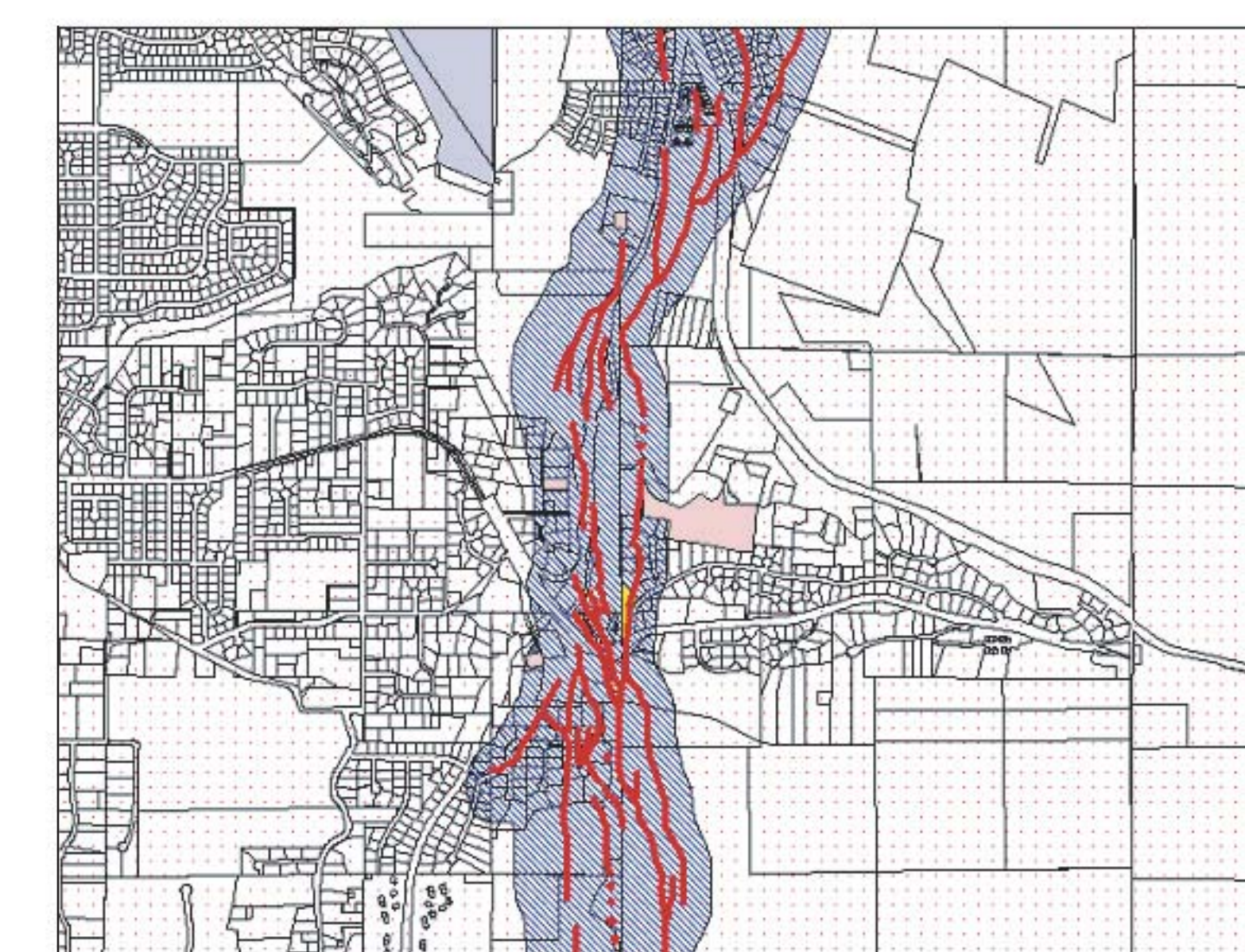
The time of most recent event (MRE) used to determine the fault activity class (shown on maps above) is taken from the *Quaternary Fault and Fold Database and Map of Utah*. Where poorly understood, the MRE must be determined by site-specific studies. Recommendations for surface-fault-rupture hazard studies and setbacks are based on the fault activity class as shown in the **Study and Setback Recommendations** table at right.

## Well-Defined Fault

250 feet - upthrown side; 500 feet - downthrown side

Salt Lake County, 1995, Surface Fault Rupture and Liquefaction Potential Special Study Area Map, Salt Lake County Planning and Development Services Division.

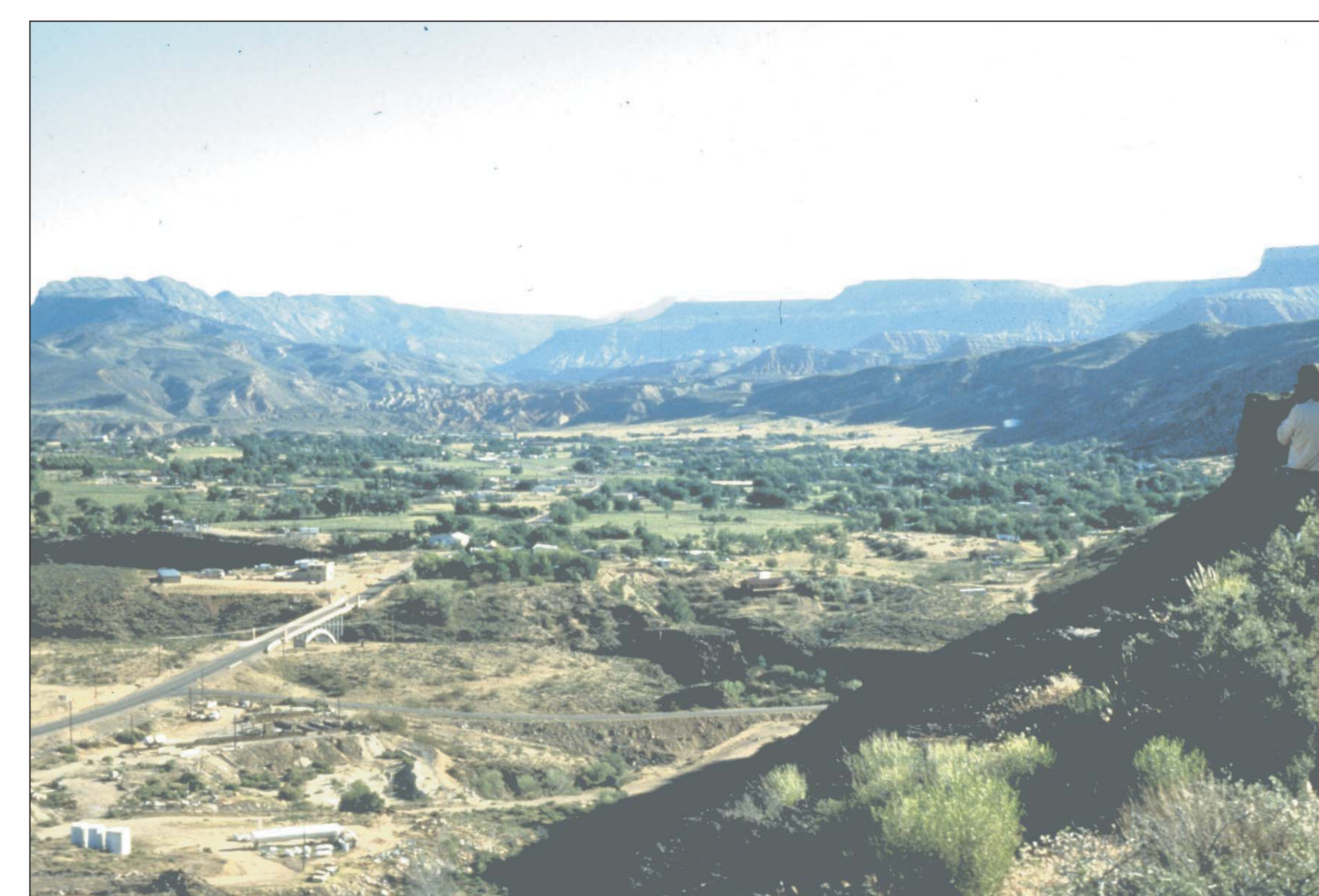
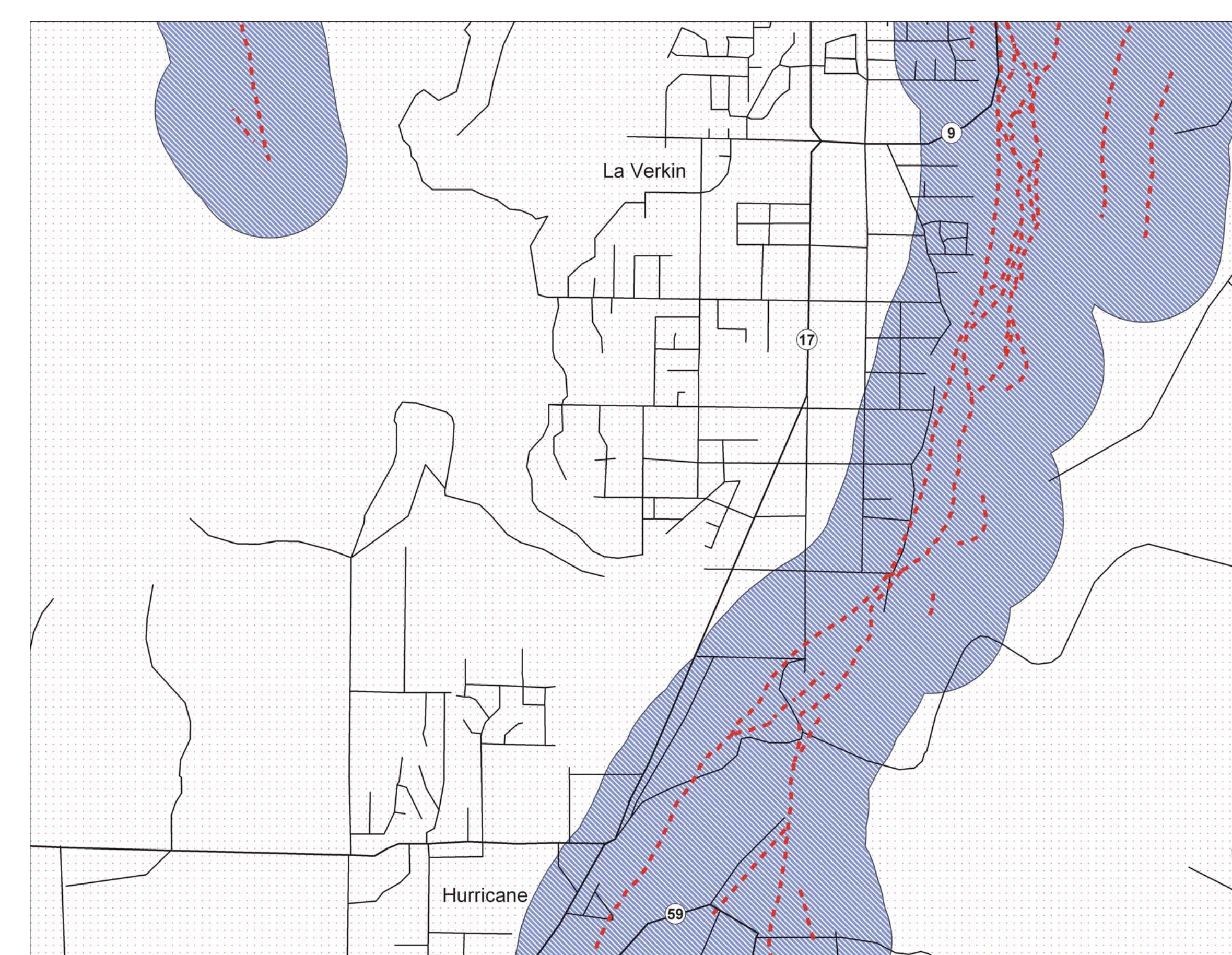
- Blue shaded area = Surface Fault Rupture Special Study Area
- Red Line = Wasatch fault trace
- Pink Areas = Sites where fault studies have been conducted



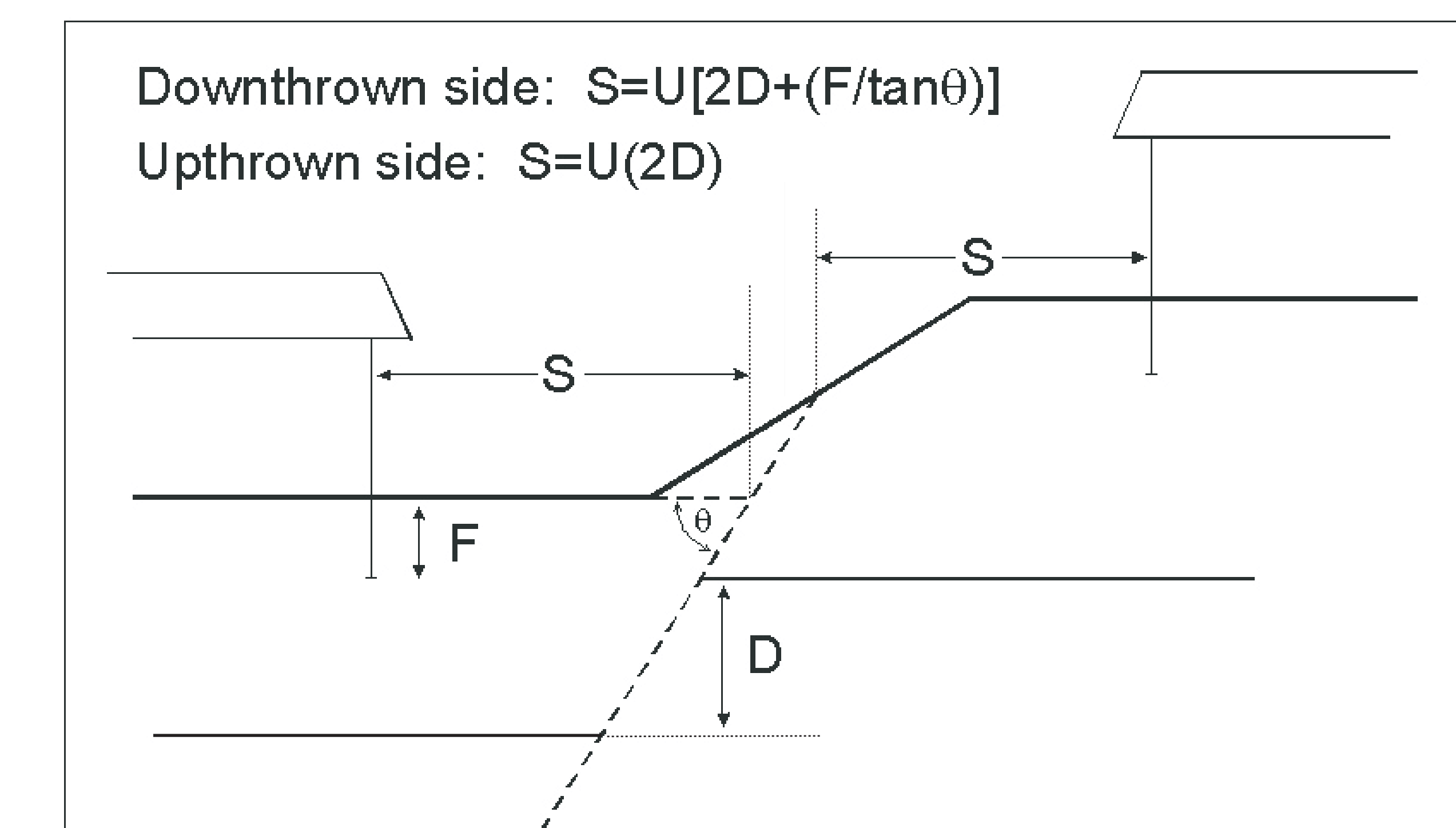
Special-study area map and oblique aerial view to the east of the Wasatch fault zone at the mouth of Little Cottonwood Canyon in Salt Lake County.

## Buried or Approximately Located Fault

1,000 feet on either side



Special-study area map and view to the north of the Hurricane fault where the Virgin River emerges from the Hurricane Cliffs near Hurricane in southwestern Utah.



where:

- S = Setback area, within which buildings are not permitted.
- U = Criticality factor, based on the IBC building occupancy class (below).
- D = Expected fault displacement per event (use the maximum vertical displacement measured for past events or, if not measurable, estimated based on paleoseismic data). Along main traces where displacement is not measurable, a maximum estimated single-event displacement should be used.
- F = Maximum depth of footing or subgrade portion of the building.
- $\theta$  = Dip of the fault (degrees).

Formulas and schematic diagram showing variables used to determine setbacks.

Damage caused by surface faulting in the 1959 Hebgen Lake, Montana earthquake (photo by Irving Witkind, USGS).



## STUDY AND SETBACK RECOMMENDATIONS

IBC building occupancy class	Study and setback recommendations <sup>1</sup> Fault activity class H LQ Q	Criticality <sup>2</sup>	U <sup>3</sup>	Minimum setback <sup>4</sup>
A. Assembly	R P O	2	2.5	25 feet
B. Business	R P O	3	2.0	20 feet
E. Educational	R R R <sup>2</sup>	1	3.0	50 feet
F. Factory/Industrial	R P O	3	2.0	20 feet
H. High hazard	R R R <sup>2</sup>	1	3.0	50 feet
I. Institutional	R R R <sup>2</sup>	1	3.0	50 feet
M. Mercantile	R P O	3	2.0	20 feet
R. Residential (R-1, R-2, R-3 [ $>10$ dwelling units], R-4)	R P O	3	2.0	20 feet
R-3. Residential (R-3 [ $\leq 10$ dwelling units])	R P O	4	1.5	15 feet
S. Storage	O O O	-	-	-
U. Utility and misc.	O O O	-	-	-

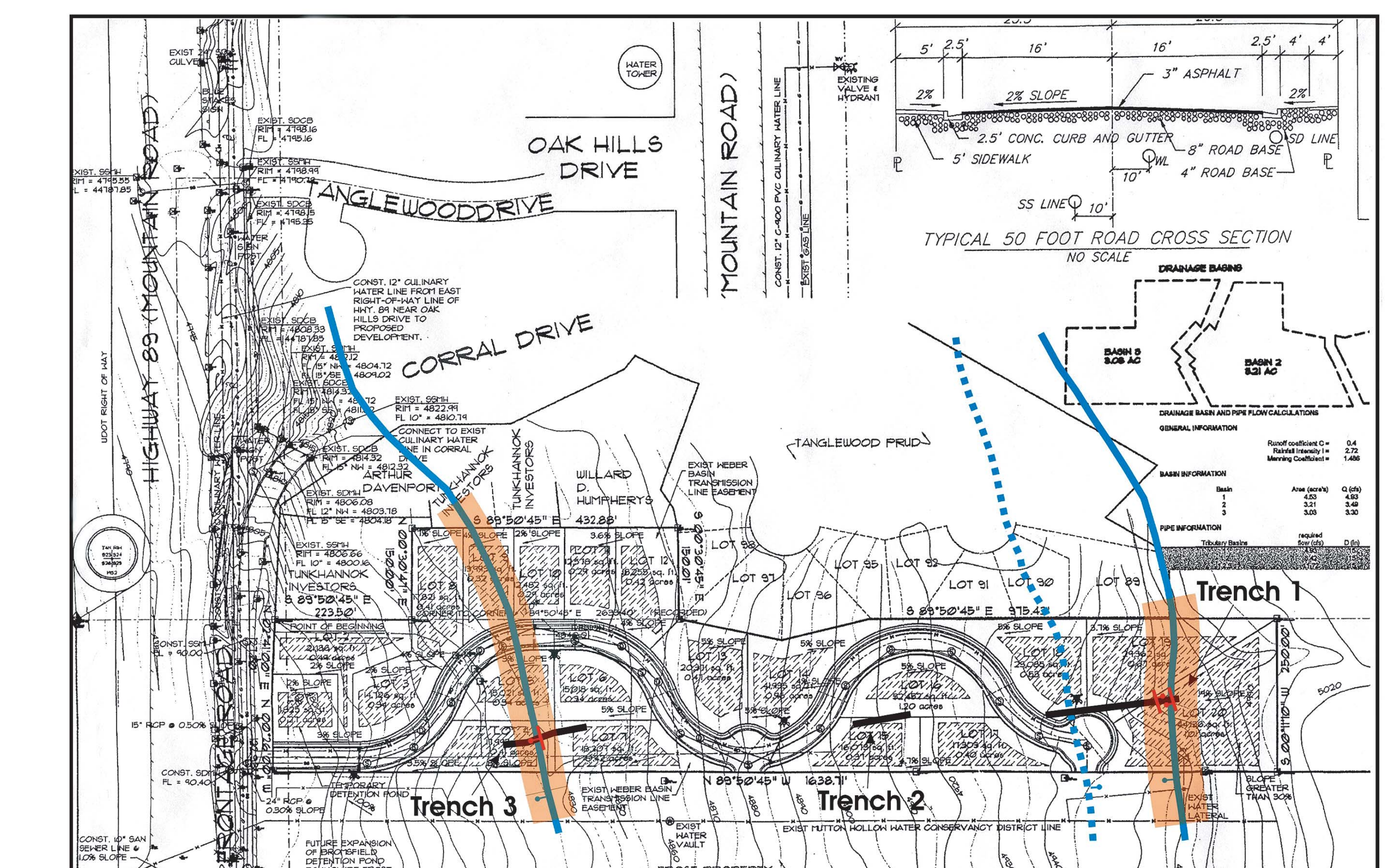
<sup>1</sup> Fault activity class (H-Holocene, LQ-Late Quaternary, Q-Quaternary); study and setback or other risk-reduction measure: R – recommended; P - considered prudent but decision should be based on risk assessment; O – optional but need not be required by local government based on the low likelihood of surface rupture. Appropriate disclosure is recommended in all cases.

<sup>2</sup> Study recommended; setback or other risk-reduction measure considered prudent but decision should be based on risk assessment; appropriate disclosure is recommended.

<sup>3</sup> Criticality is a factor based on relative importance and risk posed by a building; lower numbers indicate more critical facilities. Criticality is included in setback equations by the factor U. U is inversely proportional to criticality to increase setbacks for more critical facilities.

<sup>4</sup> Use the greater of this minimum or the calculated setback.

Prepare  
FINAL SITE MAP



- Blue line with bar and ball on downthrown side (dotted where trenching found no evidence of mapped fault)
- Red line with bar and ball on upthrown side (dotted where trenching found no evidence of mapped fault)
- Actual location of faults from trenching evidence
- Recommended Setback Zones (no building pads)

Scale: 1 inch = 200 feet

Example of a site-specific map by Craig V Nelson for a subdivision in Layton, Utah, showing trench locations, faults, and setbacks defining non-buildable area.

# INTEGRATION OF GEOLOGIC AND GEODETIC DATA INTO KINEMATIC MODELS OF CONTEMPORARY STRAIN IN THE PACIFIC NORTHWEST AND ACROSS THE CASCADIA SUBDUCTION ZONE

Mark Hemphill-Haley, Department of Geology, Humboldt State University, mark@humboldt.edu  
 Gene Humphreys, Department of Geological Sciences, University of Oregon, gene@newberry.uoregon.edu

## INTRODUCTION

### Abstract

Penetrative dextral shear combined with gravitational collapse-driven extension provide complex but coherent patterns of deformation within the interior of the western United States. We model geologic, neotectonic and GPS geodesic data to infer the western North America velocity and deformation field. Geologic observations indicate a 12 mm/yr of margin-parallel shear (with respect to stable North America) is located east of the Sierra Nevada and 3-5 mm/yr of northeast-directed extension occurs in the central Basin and Range.

Our goal has been to resolve the horizontal velocity field and strain rate tensor within western North America and specifically in the Pacific Northwest. We use finite element modeling of deformation to incorporate available neotectonic and geodesic data. A finite element mesh divides the elements in which material properties are assigned, with properties chosen to produce desired deformation behavior. For instance, blocks are made rigid and deformation zones are weak. Block motion is then prescribed, and the resulting velocity field is compared to GPS velocities. The deformation field is then compared to principal strain indicators. We adjust material strength and applied velocities in an attempt to eliminate conflicts between the modeled and observed fields. This modeling, though done with finite elements, is kinematic in nature. That is, we use finite element modeling to produce velocity and strain fields that are consistent with observations. We do not attempt to model the actual forces or rheologies active in the Earth. Finite elements are a means of producing relatively smooth fields (in this kinematic modeling, the modeled velocity field can be viewed as the weighted least squares best velocity field consistent with the prescribed velocities (Heem and Humphreys, 1999).

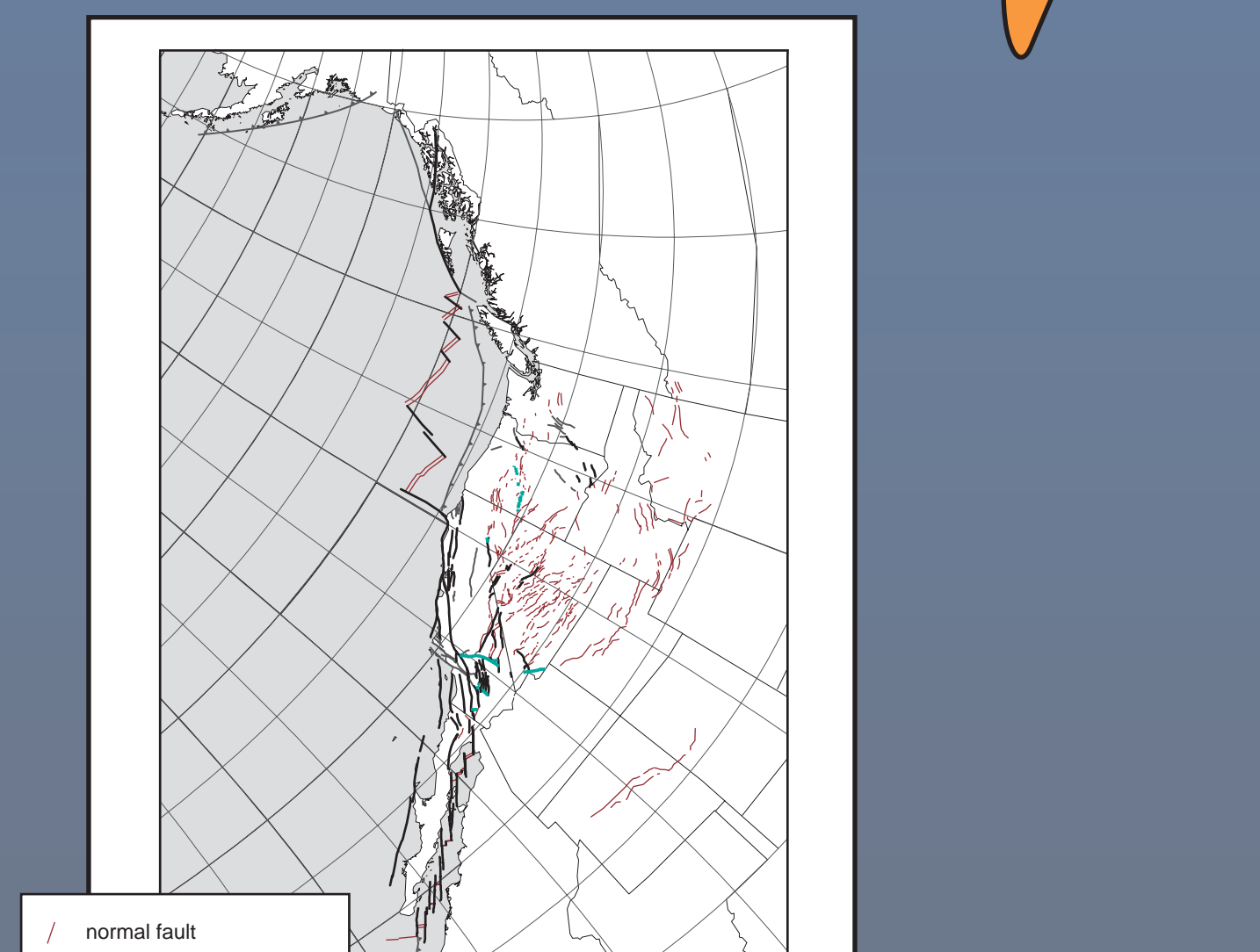
To summarize the results of our modeling, broadly distributed strain occurs throughout the region with transform rates being much greater and largely concentrated near margin while gravitational collapse drives extension and deformation of the interior. The Oregon Coast Range block is rotating rapidly clockwise with a pole of rotation in south-central Washington consistent with a model proposed by Wells et al. (1998). This accommodates both the northern motion of the Coast Ranges into the Olympic Mountains and Basin and Range extension in such a way that North America strain rate diminishes to the north and is very slight in Canada. It also increases subduction velocities, especially in Oregon. Eastern California shear zone strain "fans" broadly over the Pacific Northwest with several mm/yr of strain rate occurring in the Klamath Mountain region. This unexpected result finds support directly in the GPS velocity field; comparison of the velocity of a station at Quincy with that of Yreka shows a transfer of Eastern California shear zone strain to the northern California coast, reducing the strain required in Oregon and Washington.

The results also indicate that our current modeling is inadequate in some regions, and is substantially unconstrained throughout much of the Pacific Northwest. In particular, a prevalence of strike-slip deformation in the Great Basin results from a N-S contraction field that is too great. This problem may simply result from moving station (NAD 83) (Petersen) in Canada at about 1 mm/yr to the northeast instead of 2-3 mm/yr consistent with recent observations. This slower velocity may prevent northwest Washington and northern Idaho from "springing out of the way" of the northwest-directed Basin and Range extension.

An additional result of our kinematic modeling is the determination of subduction velocity, which requires knowledge of the Coast Ranges and Juan de Fuca velocities. Older estimates used NVEL-derived Juan de Fuca-North America velocities. The Coast Range is in motion relative to North America, and importantly relative to the subduction zone. Juan de Fuca velocity estimates have uncertainties related to dependency on the Pacific plate velocity which is being refined, and appears to be several mm/yr more westerly than previously assumed (Lottalis et al., 1999) (Dillon and Dixon, 1999; Humphreys and Weston, 1994), which reduces subduction velocities.

Finally, the Cascadia subduction zone serves as the outlet (inflow) for both transform and gravitational collapse-driven deformation and the expansion of North America. Conversely, the transform prevents collapse from being accommodated in California. The result, over time, is that the expansion of the western U.S. has been restricted toward the Pacific Northwest as the transform margin has expanded and the length of the subduction zone has decreased.

### Distribution of Western US Cenozoic Faults



### Gravitational Collapse

Continental collapse is superimposed over transform deformation. The figure above shows the geoid over a portion of western North America. If we let the geoid serve as a proxy for potential energy then the pattern of strain associated with PE can be observed. Note that at PE highs extension is dominant while at PE lows contraction prevails. Margin-related transform deformation also can be seen.

The figure below shows the transform deformation field, consisting of the San Andreas system and an interior system, the ECSZ, which is the result of shear penetration. Most of the ~1 cm/yr of dextral shear along the ECSZ must get back to the transform margin within the span of the CSZ.



The difficulty arises in trying to discern the contribution of either form of deformation in areas where they clearly overlap (purple), for example, in the western Basin and Range.

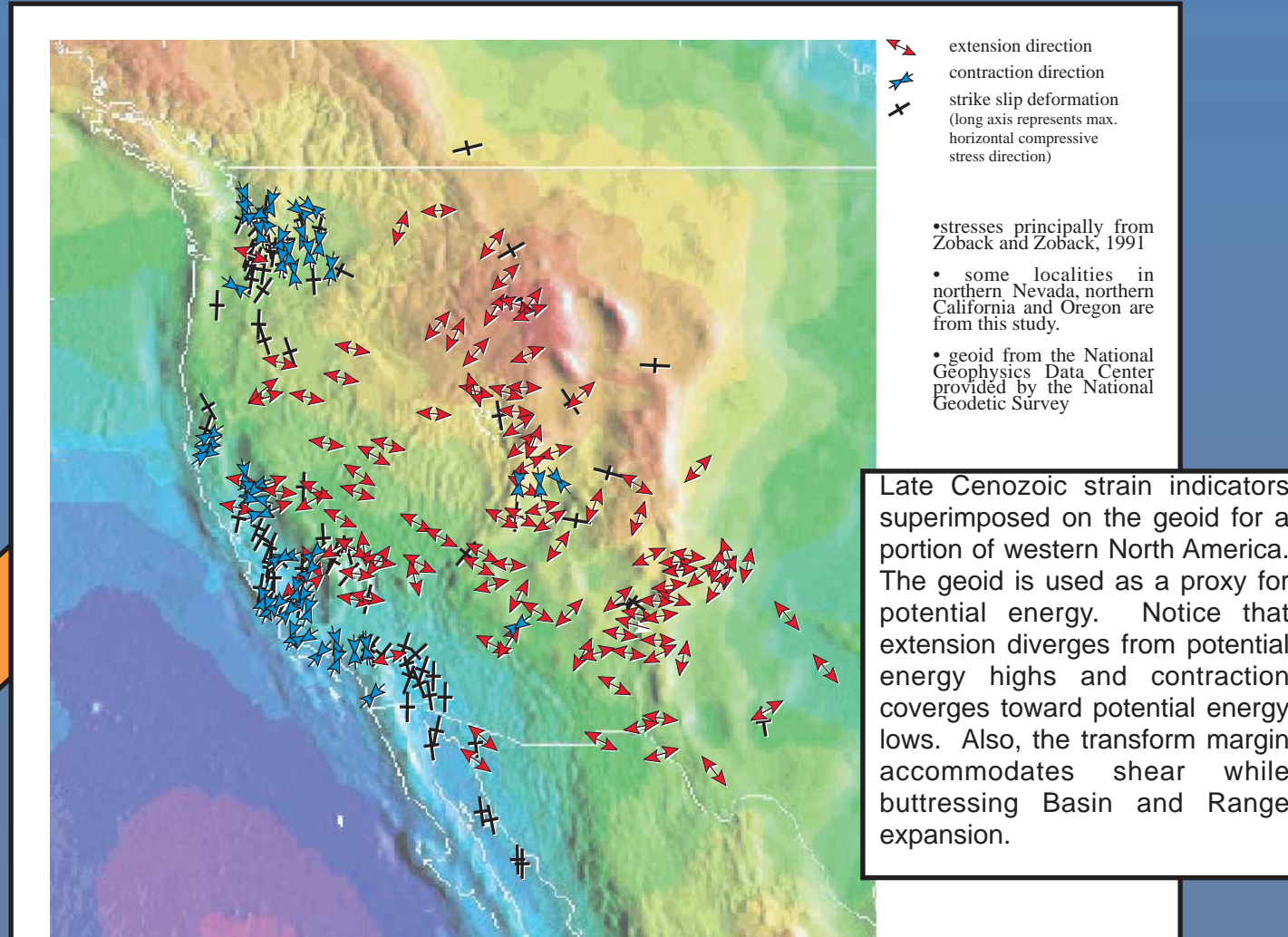
### Motivation/Questions

We attempt to describe the Cenozoic deformation of the western US by developing kinematic models. This is aided by the use of finite element modeling which provides internal consistency within the model space.

Questions that have been addressed in this modeling effort (not all results are shown in this poster):

- Can the Pacific Plate motion be resolved by observing the deformation along the transform margin?
- What is the Sierra Nevada motion relative to stable North America?
- Where does the ~1cm/yr of dextral shear of the Eastern California Shear Zone (ECSZ) go north of the Sierra Nevada within the Pacific Northwest?
- What is the motion of the OR-WA Coast Ranges? (which may be in response to both the internal deformation of the continent as well as the CSZ).
- What portion of the WUS deformation is the result of gravitational collapse versus transform shear penetration?
- Can the deformation field be modeled (using independent constraints) so that geodesic velocities are adequately resolved?

### Potential Energy and Strain

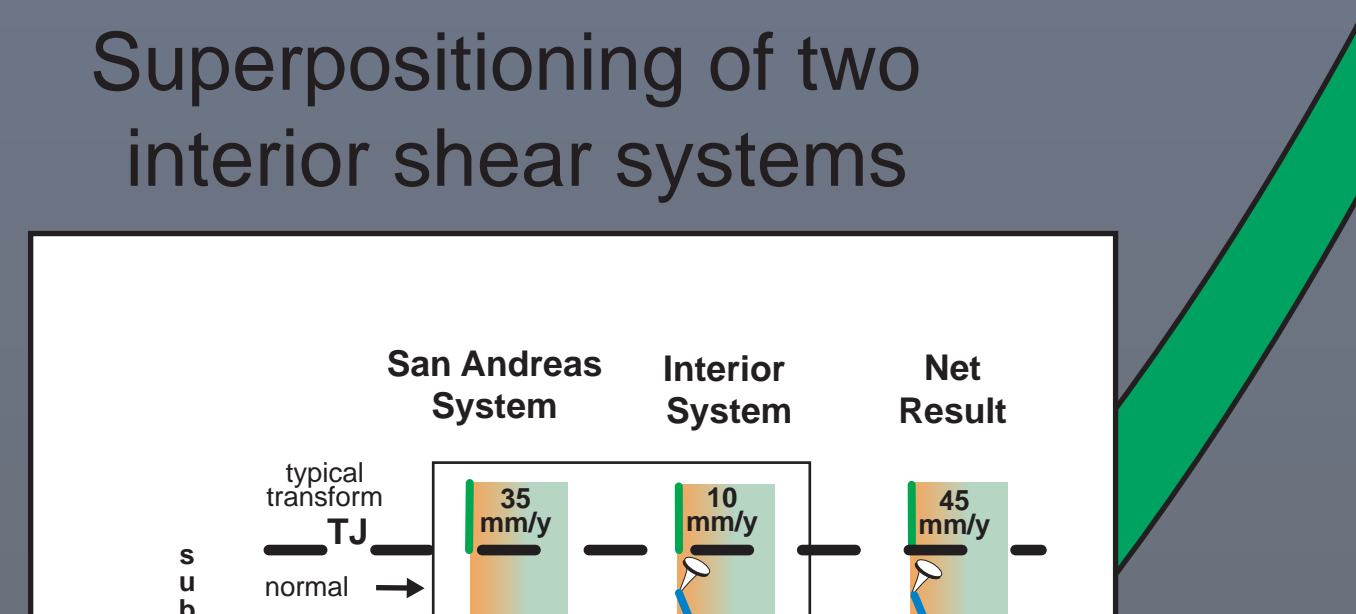


### Shear Penetration

The deformation field within the western US results from gravitational collapse-driven poloidal deformation (orange) and transform margin-driven toroidal deformation (green). In the far interior of the WUS, gravitational collapse is dominantly responsible for the contemporary deformation while along the margin, the transform processes dominate.

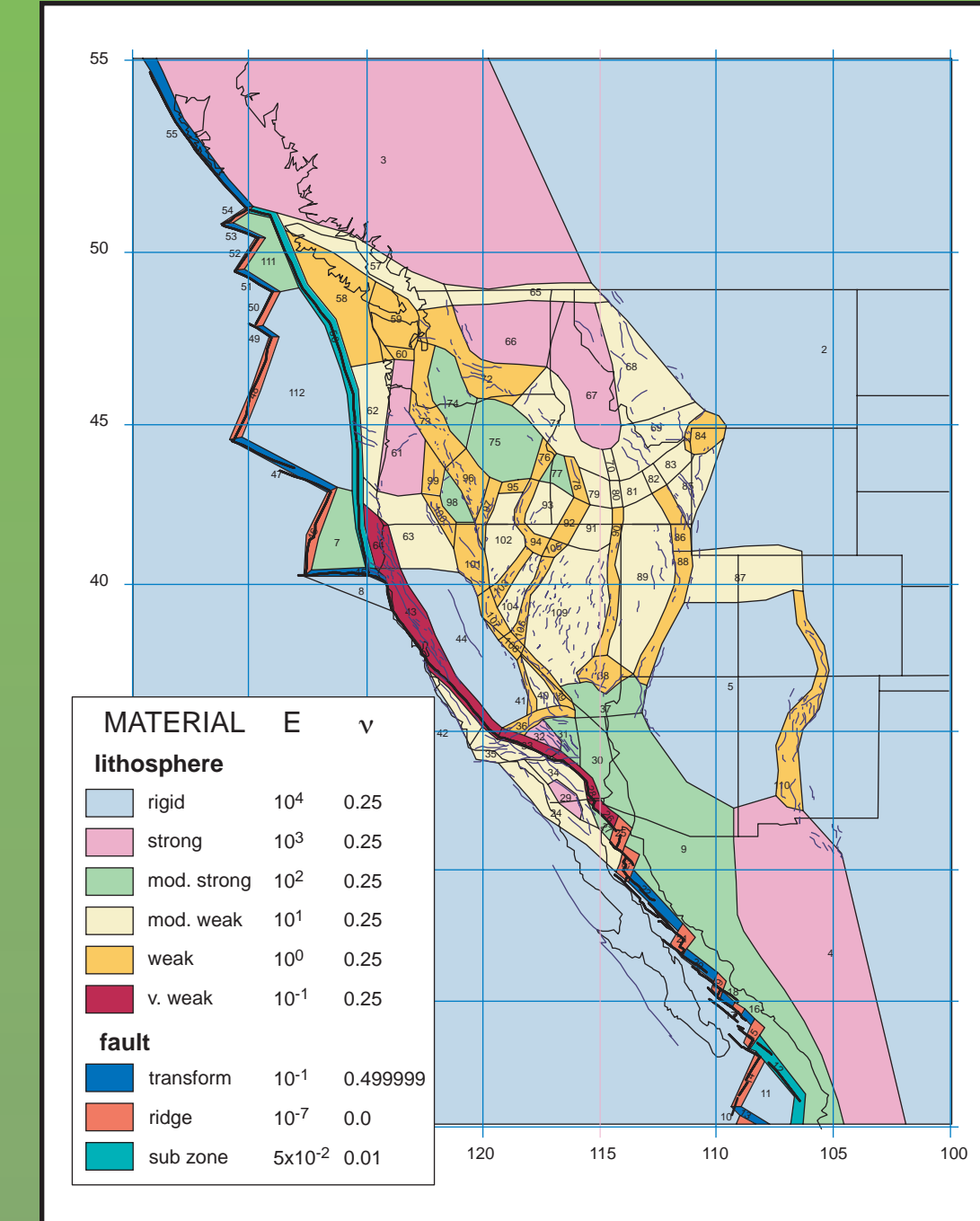
The difficulty arises in trying to discern the contribution of either form of deformation in areas where they clearly overlap (purple), for example, in the western Basin and Range.

### Superpositioning of two interior shear systems



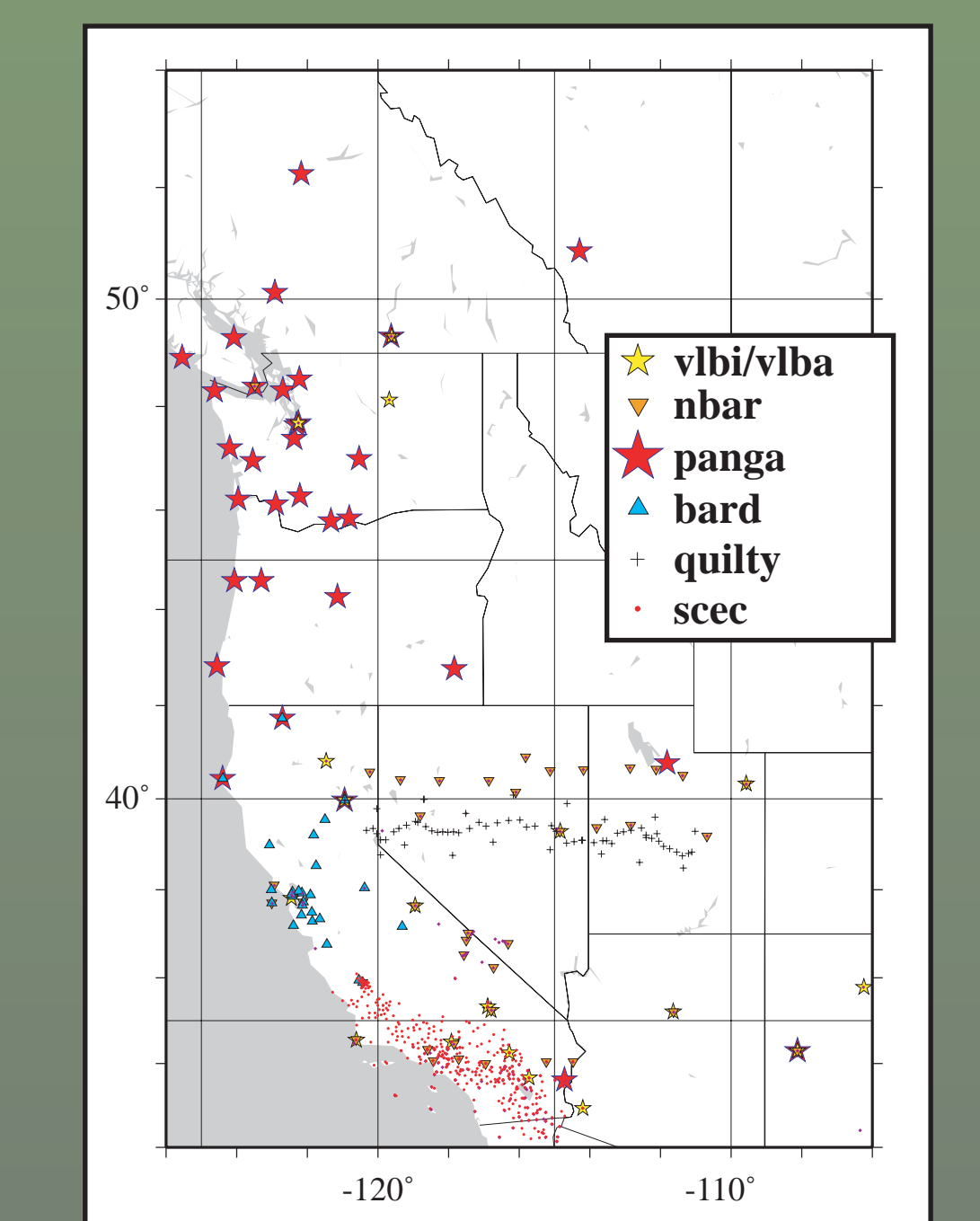
The difficulty arises in trying to discern the contribution of either form of deformation in areas where they clearly overlap (purple), for example, in the western Basin and Range.

## FINITE ELEMENT MODELING METHOD



### FINITE ELEMENT MESH

The mesh consists of 13083 "Tri-a-3" elements and 6009 nodes. The mesh is constructed over the geometric surfaces. This allows for freedom to vary mesh/nodal density. Element density is greatest in areas of a) high fault density and/or b) anticipated large strain variations. Element density is lowest in areas where strain variation is anticipated to be minimal (see Pacific Plate).



### COMBINED GEODETIC REFERENCE ARRAY

The finite element models are compared to this array which consists of components of seven regional geodesic arrays. The error ellipses represent 1 sigma limits for the velocity estimates.

### GEOMETRIC SURFACES AND MATERIAL PROPERTIES

The models shown here are kinematic. We attempt to reproduce observed deformation rates and styles by varying specific model parameters.

We construct geometric surfaces that depict zones and areas of deformation and of stability.

We vary the elasticity using Young's Modulus (E) and the compressibility using Poisson's Ratio ( $\nu$ ) for individual surfaces.

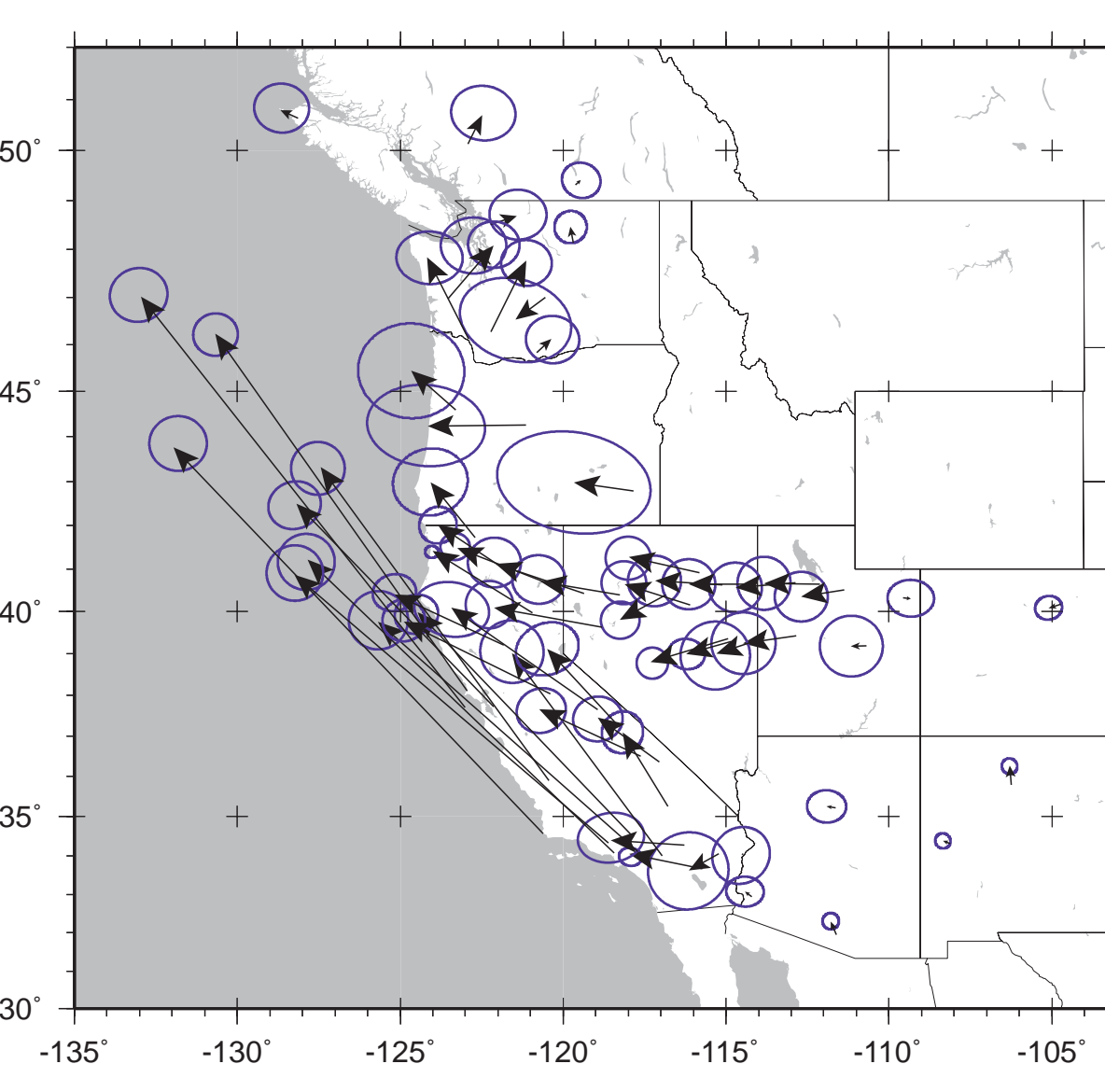
We also apply velocities to the surfaces. Rigid body rotations are calculated about an Euler pole.

### COMPARISON OF MODEL VELOCITIES WITH OBSERVED VELOCITIES

We verify individual model runs by comparing the nodal velocities with observed geodesic and geologic rates. Data from six regional geodesic arrays were used for verification.

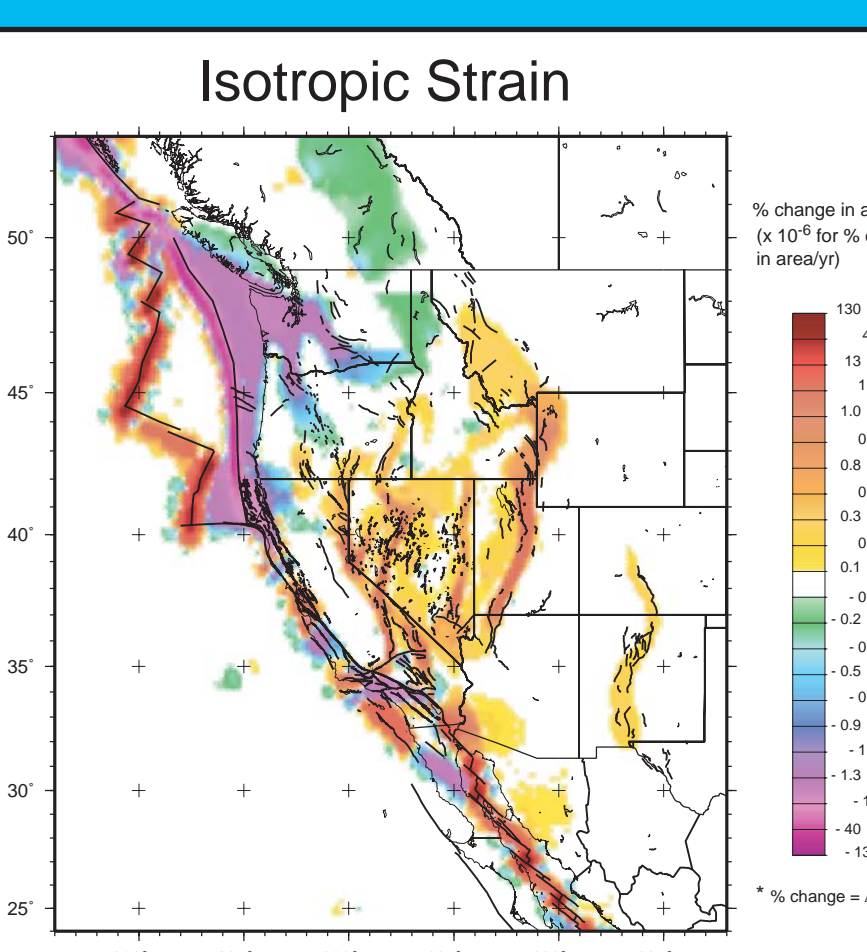
Rarely were separate array velocities reported with respect to a common reference point. Therefore, we have rotated individual arrays into a "foundation" group of stations using least squares minimization.

The entire collected array was then rotated to compensate for a possible systematic rotation error.

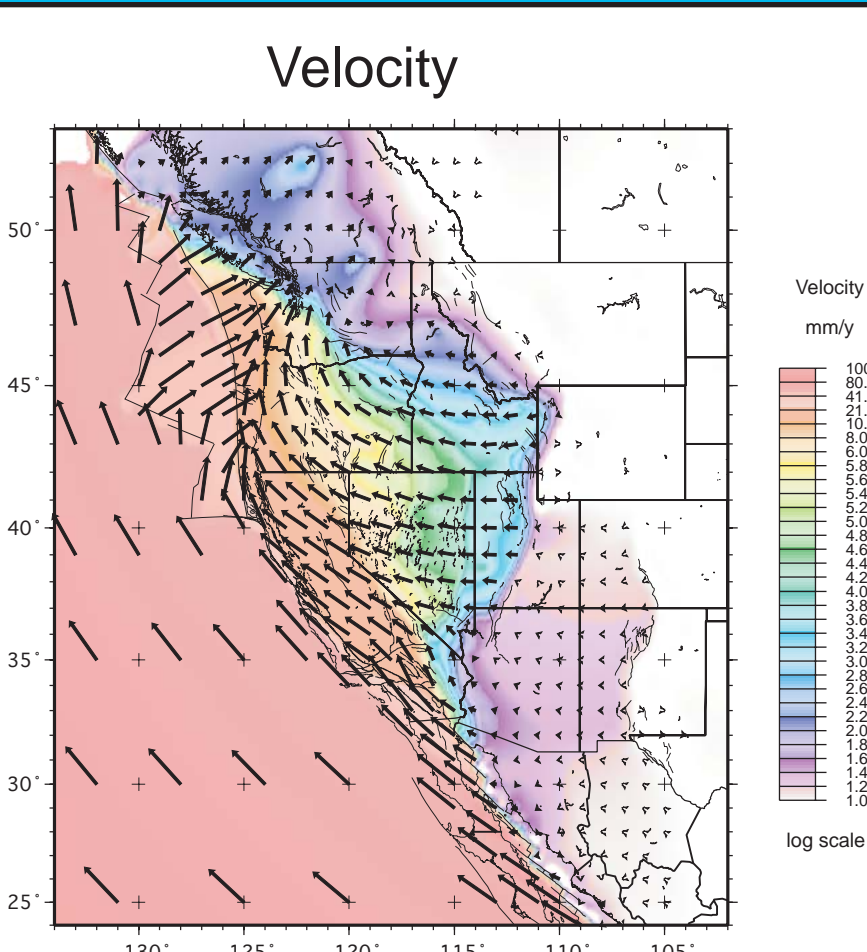


## MODELING RESULTS

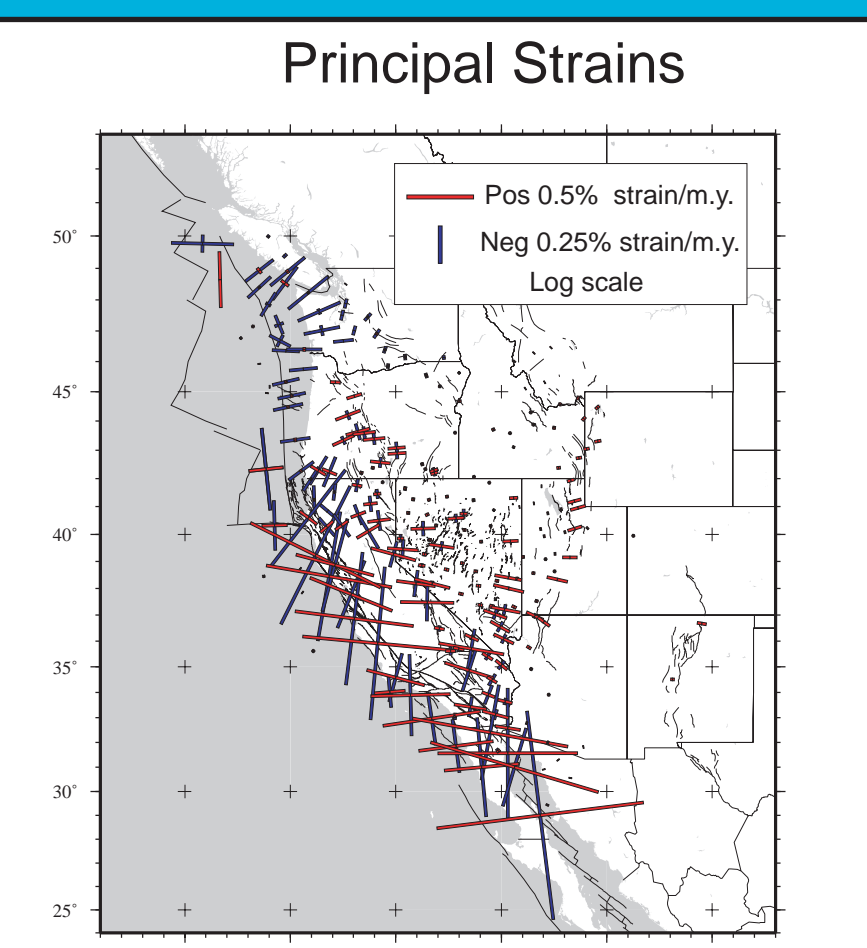
### Entire WUS Model



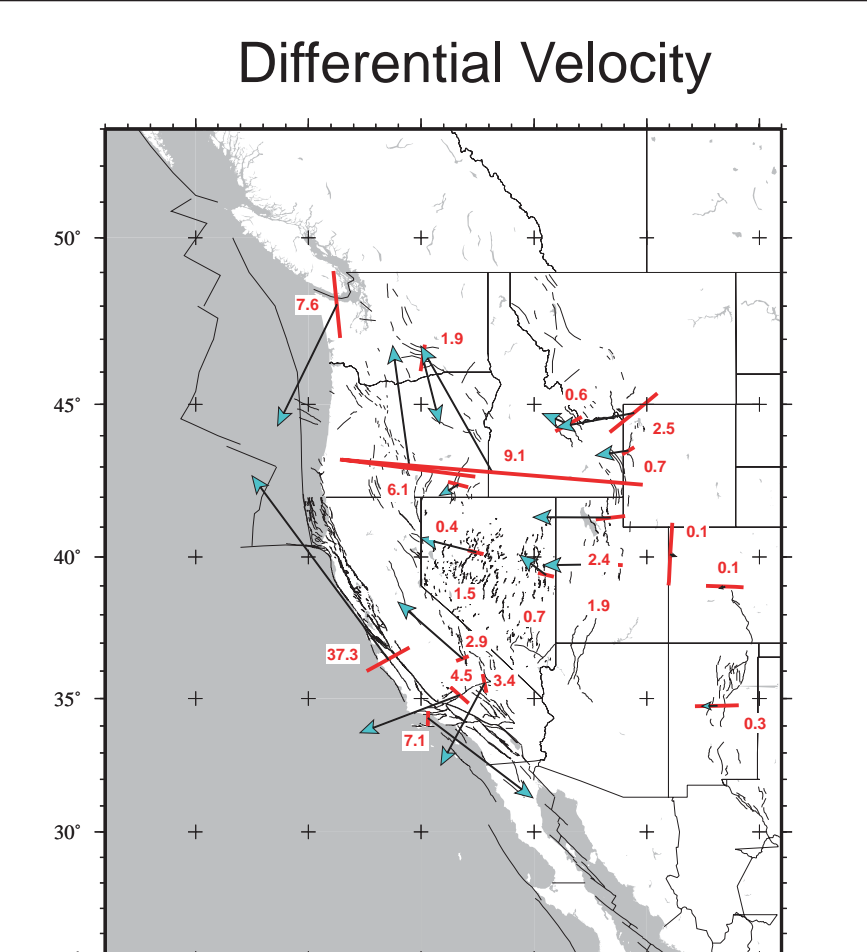
• Directs area change (non-directional)  
 • Dilatation and Contraction  
 • Interior CWW dominated by dilatation  
 • PNW, CSZ and Klamath Mtns. dominated by contraction



• Velocities are relative to stable North America  
 • Margin normal vectors in eastern Great Basin reflect dominance of gravity-driven collapse  
 • Vectors from basins in central NV and western ID  
 • Anomalous of Sierra Nevada vectors nearly parallel Pacific plate due to shear penetration  
 • Cores depict contours of velocity  
 • Arrows depict particle velocities  
 • Interior velocities largely normal to transform margin  
 • Interior velocities largely normal to transform margin

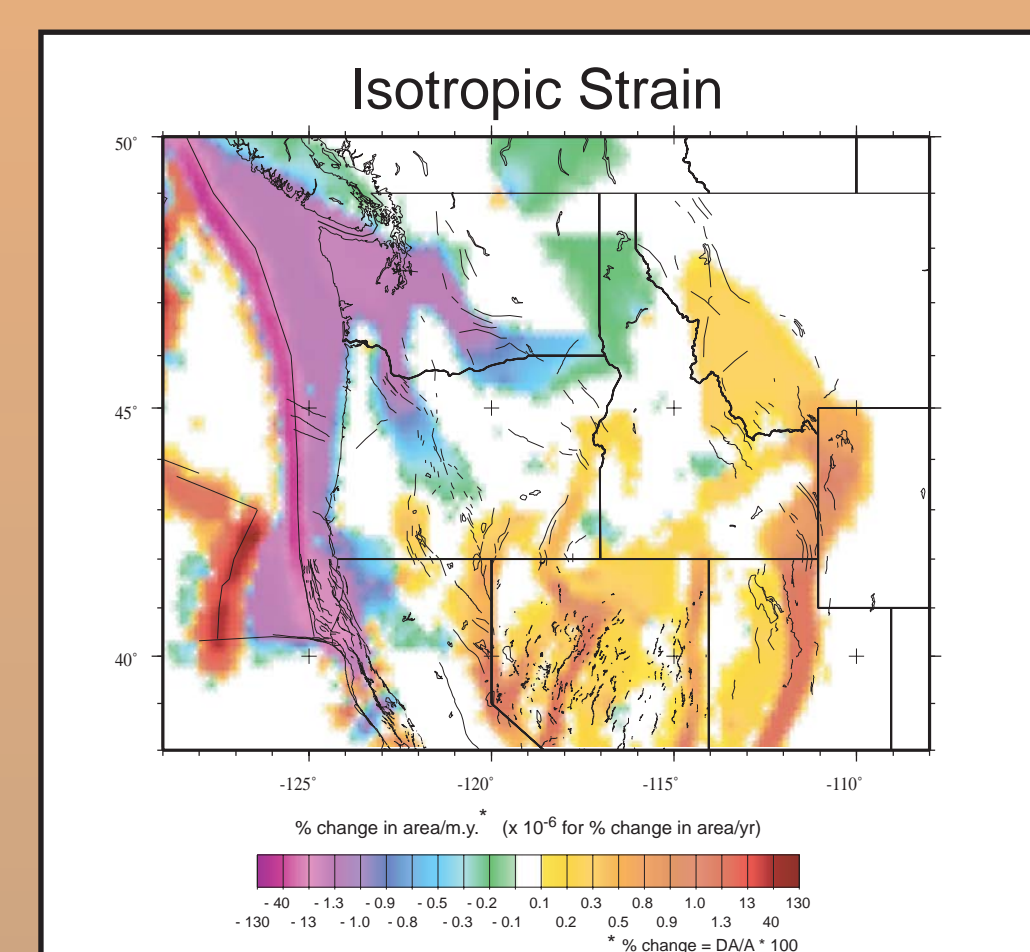


• Extensional  $\pm 1$  in Great Basin rotated clockwise from E-W  
 • Large contractional  $\pm 1$  in Olympics and Puget Sound and within Cordillera  
 • Cordillera rotated clockwise from N-S  
 • Olympic Mtns. have contractional  $\pm 1$  axes that are -NE and -E-W and NW-SE

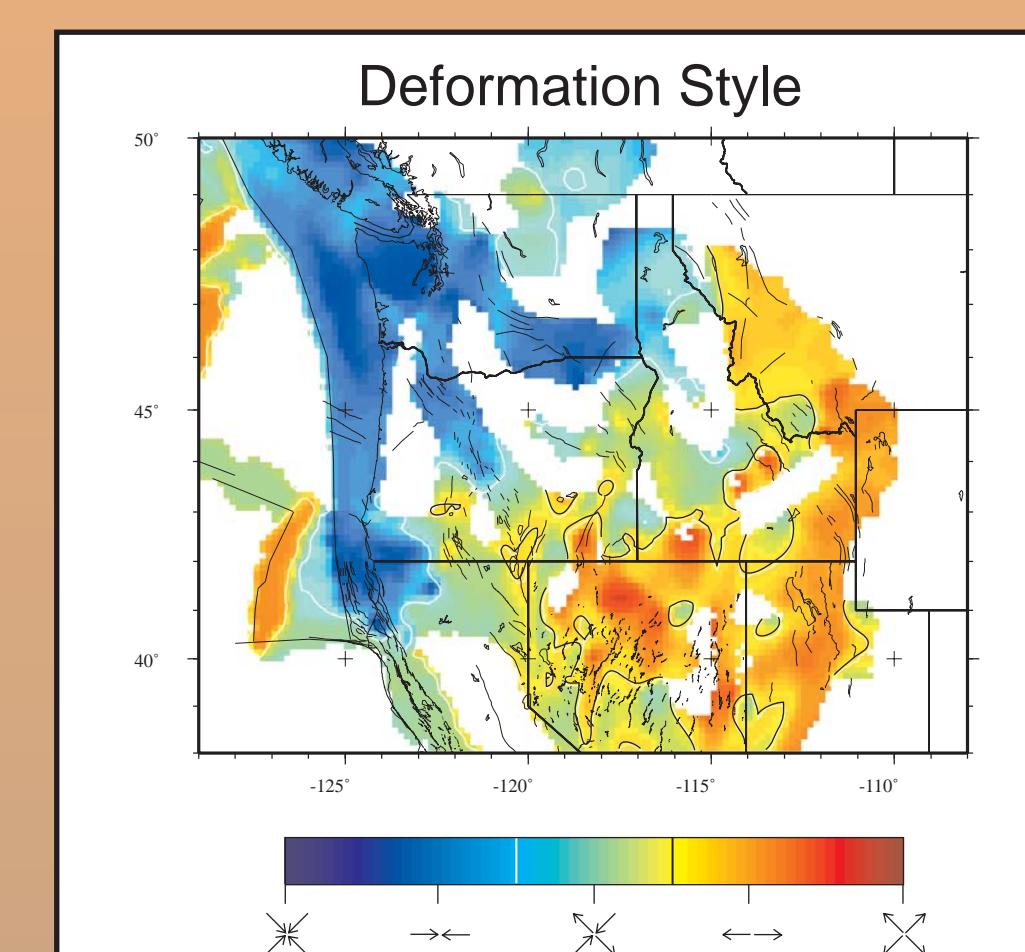


• Differential velocities across several select faults or features  
 • Velocities can be viewed as slip rates (mm/yr)  
 • End points of red lines correspond to measured nodes  
 • FEM-derived velocity tangential to subzone  
 • Arrows indicate velocity of W with E or N with S nodes.

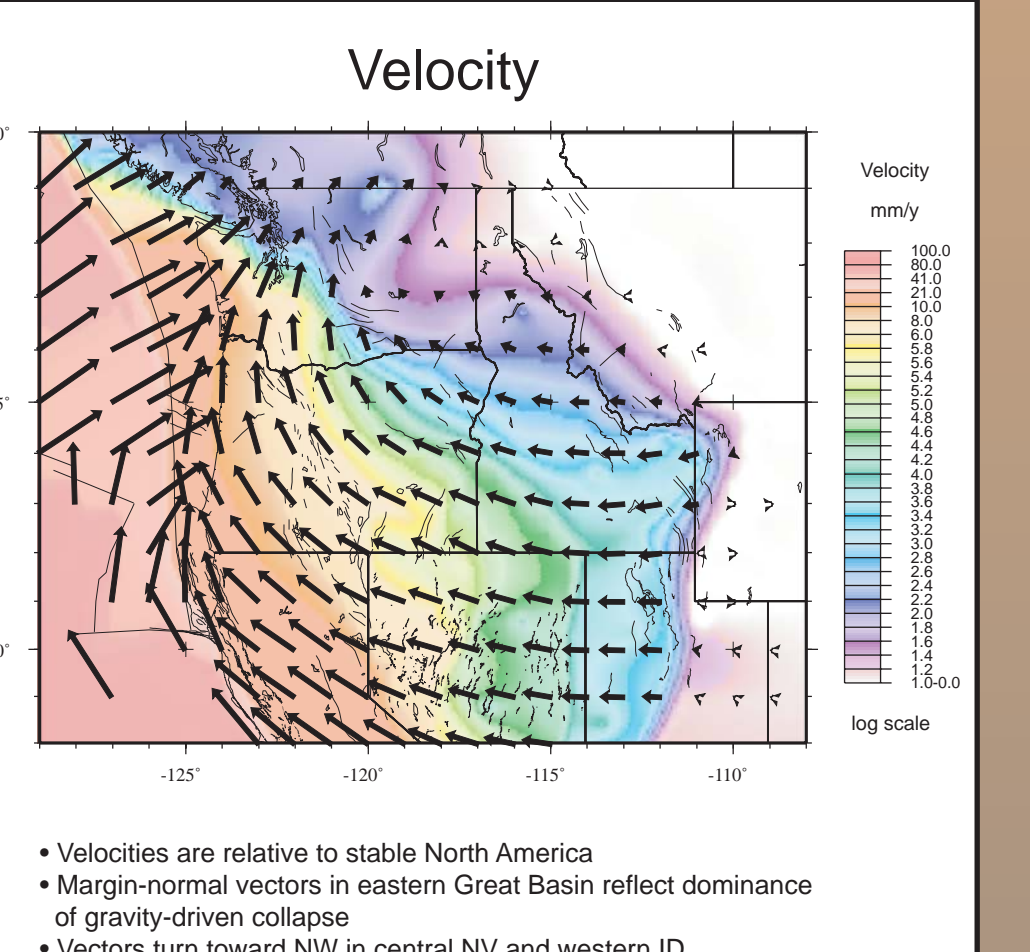
### Pacific Northwest



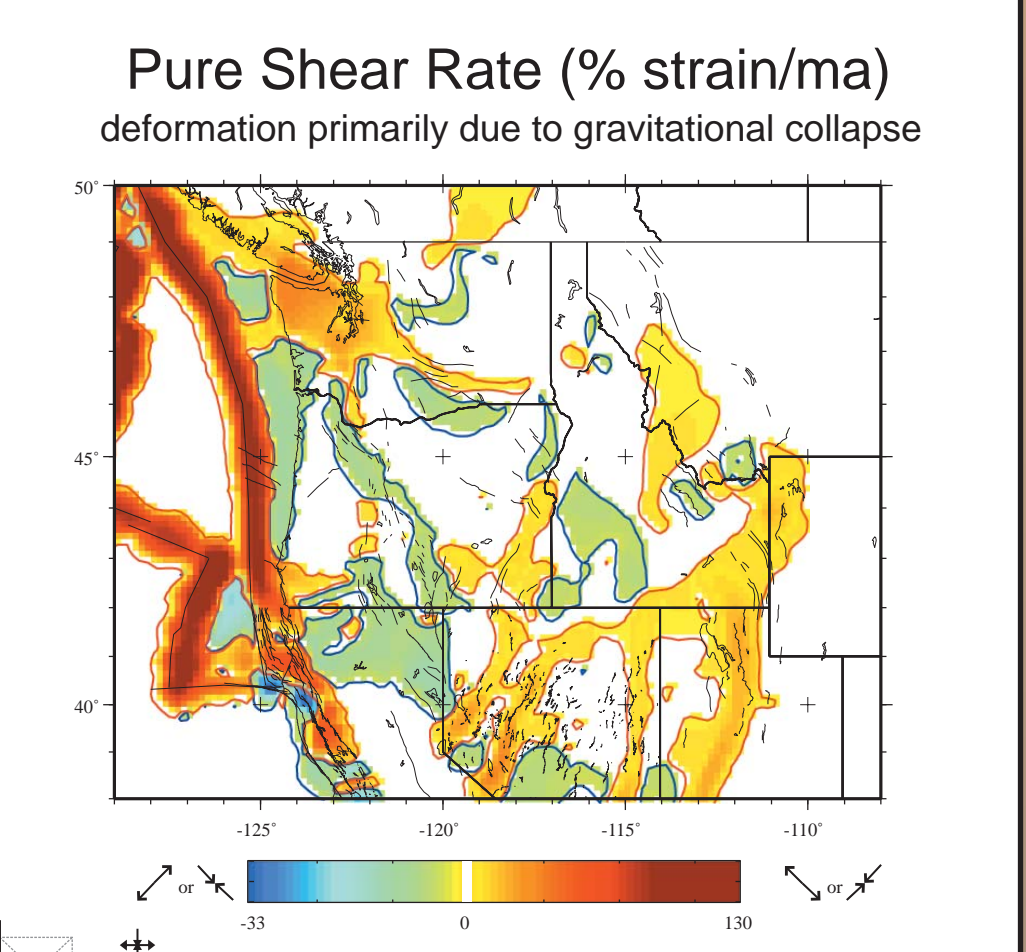
• Isotropic (non-directional) area change  
 • Margins that are strong are within the Great Basin, ECSZ and Tolovana/SRP and Cordillera de Fuca ridges  
 • Interior of Cordillera in the Puget Sound, Olympic Mtns., Yakima Fold Belt, Klamath Mtns. and California North Coast  
 • These areas are primarily the result of gravity-driven processes



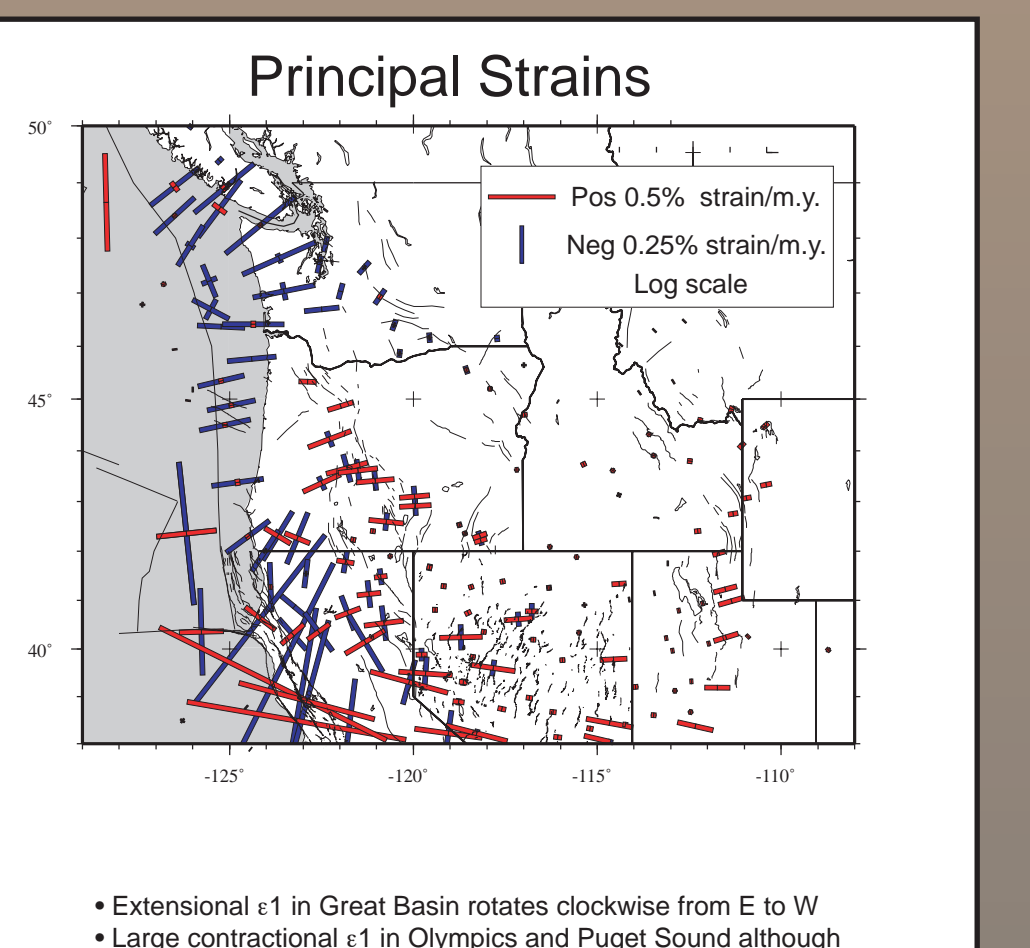
• Normal faulting is localized in the Great Basin  
 • Transition with SAF, ECSZ, Molokai, and Southern OR  
 • Transition with OWS, and portions of N. Cascades  
 • Reverse faulting and folding within the Klamath Mtns., Olympic Mtns. and CSZ



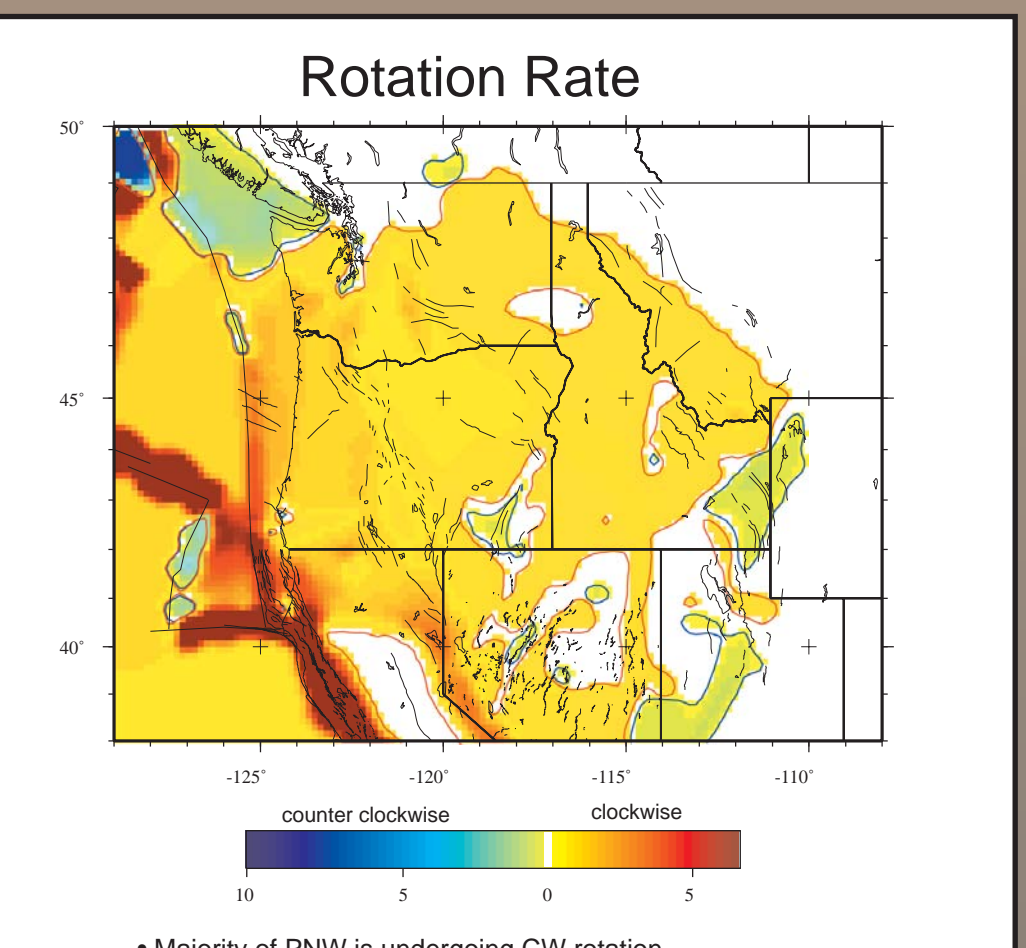
• Pure shear is largely related to gravitational processes (there is no rotation)  
 • Greatest amounts of pure shear are at the CSZ, MTA, MOR's and Olympic Mtns.



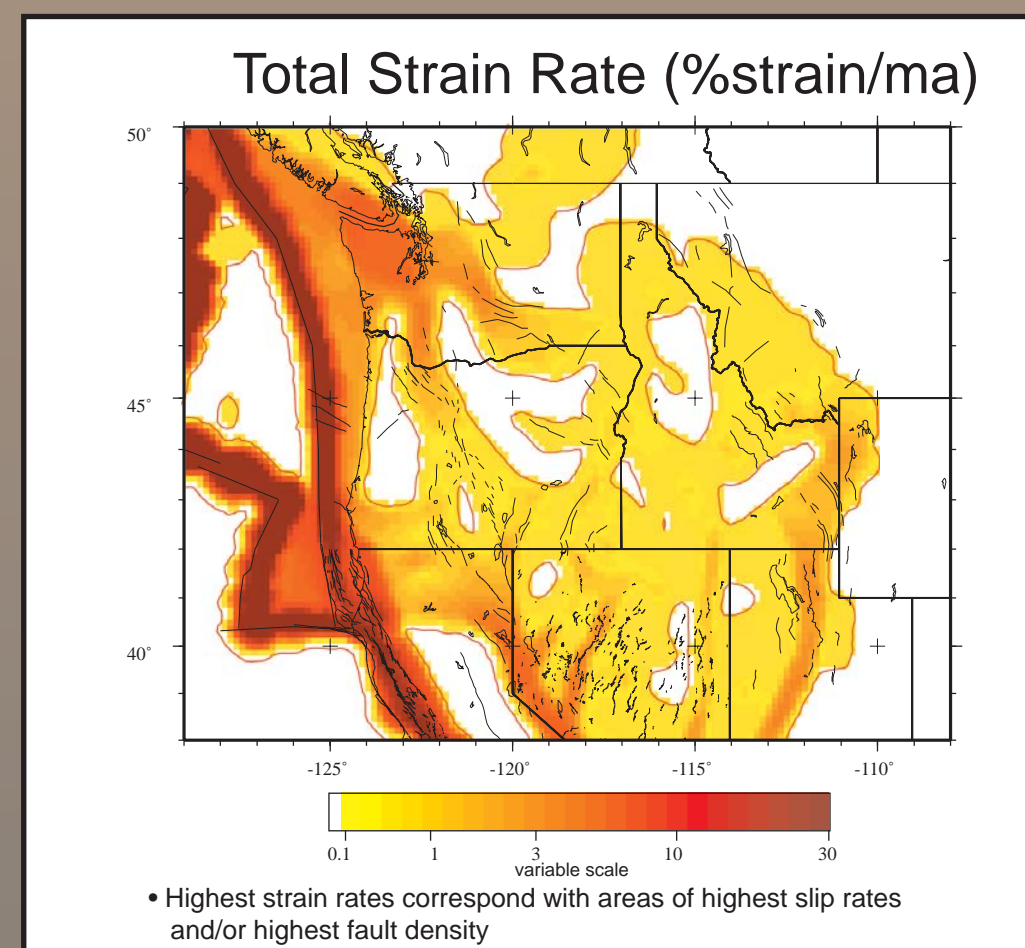
• Simple shear is primarily derived from transform-related forces  
 • Greatest amounts of simple shear is along the plate margin  
 • Dextral shear localized through ECSZ, and Cascadia backarc



• Extensional  $\pm 1$  in Great Basin rotated clockwise from E-W  
 • Large contractional  $\pm 1$  in Olympics and Puget Sound and within Cordillera  
 • Cordillera rotated clockwise from N-S  
 • Olympic Mtns. have contractional  $\pm 1$  axes that are -NE and -E-W and NW-SE

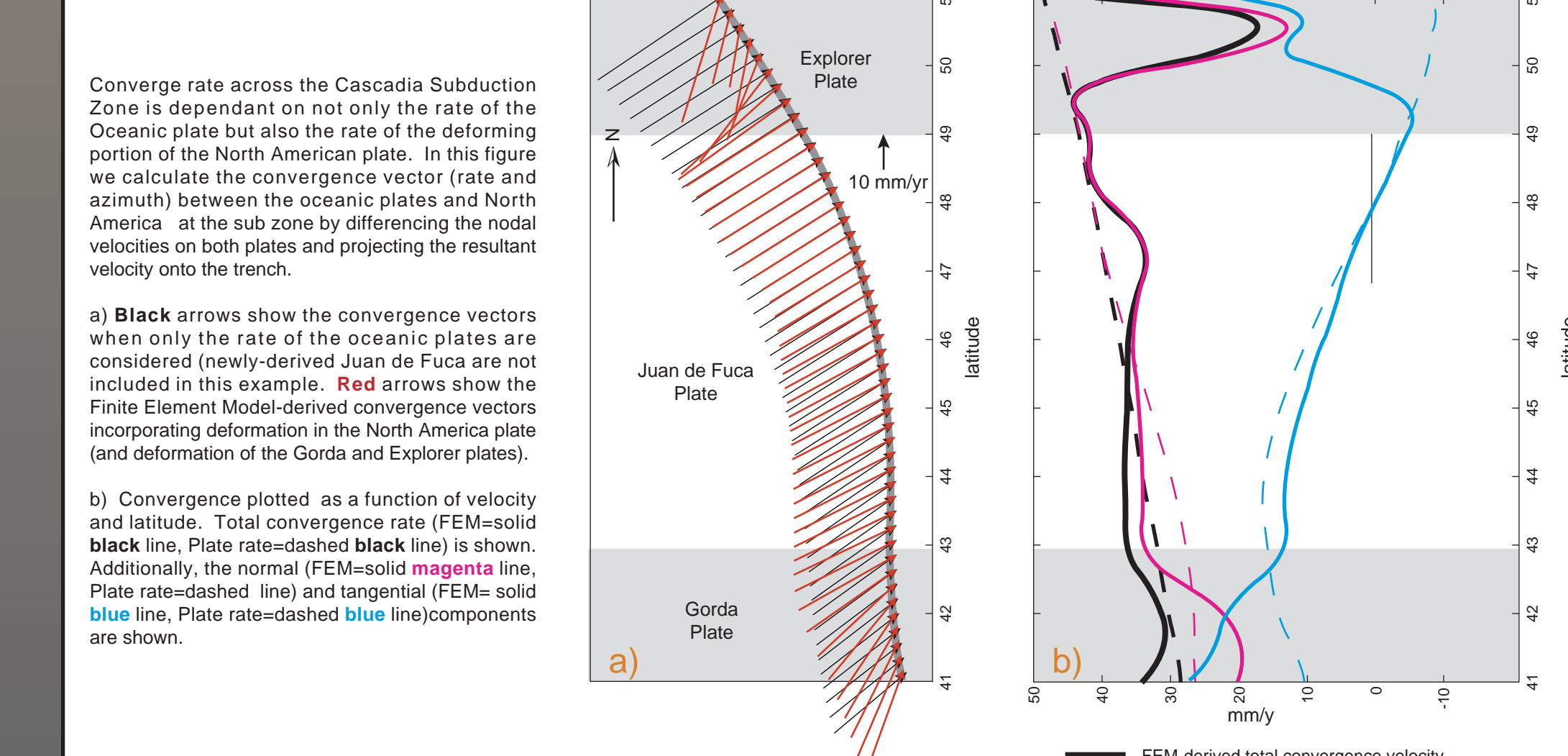


• Majority of PNW is undergoing CWW rotation  
 • Areas undergoing CWW rotation include the area south of the SRP, southern Washington, and Vancouver Island (V)  
 • The Sierra Nevada is not rotating appreciably



• Highest strain rates associated with areas of highest dip rates and/or highest fault density  
 • High strain rates occur within the Cordillera and Explorer plates but not the Juan de Fuca plate  
 • Underlying areas include the OR-WA Coast Range, Sierra Nevada, SRP, Idaho Batholith, Columbia Plateau and Canadian Rockies

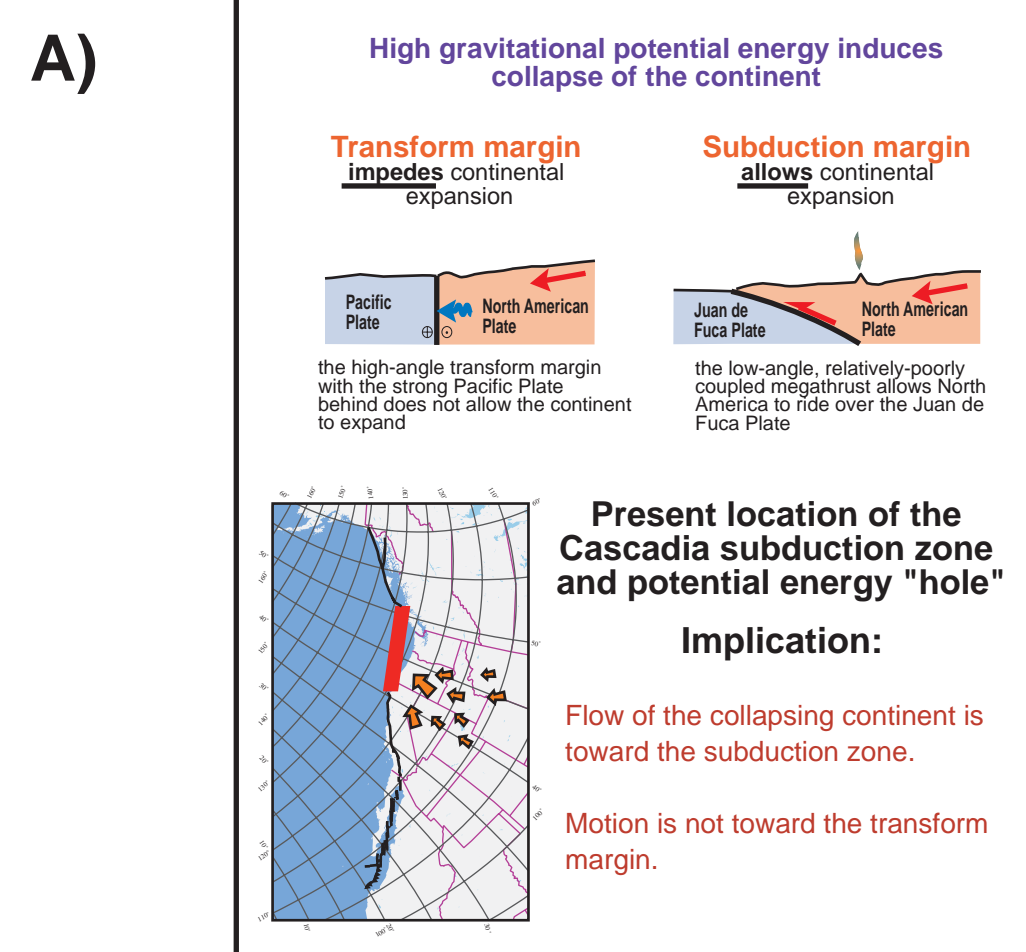
### How does a deforming North American plate affect the CSZ Convergence Velocity?



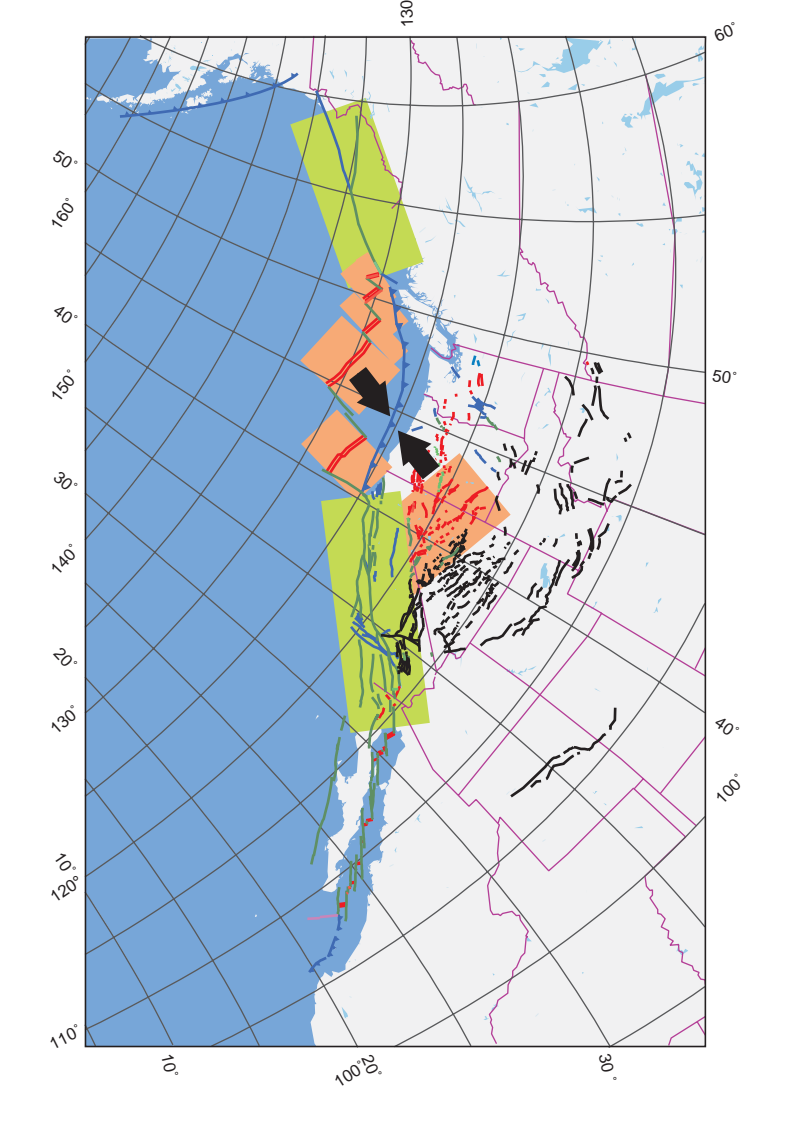
• FEM-derived total convergence velocity  
 • Plate rate-derived convergence velocity  
 • FEM-derived velocity normal to subzone  
 • Plate rate-derived velocity normal to subzone  
 • FEM-derived velocity tangential to subzone  
 • Plate rate-derived velocity tangential to subzone

## CONCLUSIONS

- Finite element modeling can be used to construct kinematic models of WUS deformation.
- Sierra Nevada motion relative to stable North America has less rotation than commonly thought.
- A significant fraction of the ~1 cm/yr of deformation of the ECSZ passes through the Klamath Mountains (approximately 3 to 5 mm/yr).
- Northern Basin and Range expansion is accompanied by clockwise rotation of the WA-OR Coast Range. The Coast Ranges are also translating northward at about 7 mm/yr. This motion may be induced by the tangential component of convergence along the CSZ and by "pushing" by the Sierra Nevada from the south.
- Transform boundary conditions, especially as a result of shear penetration, are accommodated by deformation extending as far east as central NV and as far north as northwest WA.
- Gravitational collapse of the high-standing, post-Laramide interior is responsible for a significant amount of contemporary deformation, especially in the northern Basin and Range.
- The western margin of North America is comprised of two large transform faults (San Andreas and Queen Charlotte) that impede the gravitationally-driven westward expansion of the weak interior. Conversely, the Cascadia subduction zone is a poorly-coupled, low-angle interface which is easily over-run by the expanding continent. Deformation within the interior is directed toward this "outlet" (Figure A).



- A pull-apart geometry results from a right-step in the dextral-slip San Andreas and Queen Charlotte transform fault (Figure B). Within this step, the Juan de Fuca ridge serves as an extensional northwest limb of the pull-apart structure, the Basin and Range serves as an extensional southeast limb and the Cascadia subduction zone is embedded within the pull-apart structure. The pull-apart structure may also allow expansion of the continent to occur and allow the interior dextral shear to step back to the margin.



### Acknowledgements

This research was funded largely by grants from the US Geological Survey National Earthquake Hazards Reduction Program and the National Science Foundation. We thank Megan Miller and the PANGA array for Pacific Northwest geodesic data. We also thank other sources of geodesic data including the BARD array, UNAVCO and the USGS.



# Horsts and Grabens of Colorado's High Plains

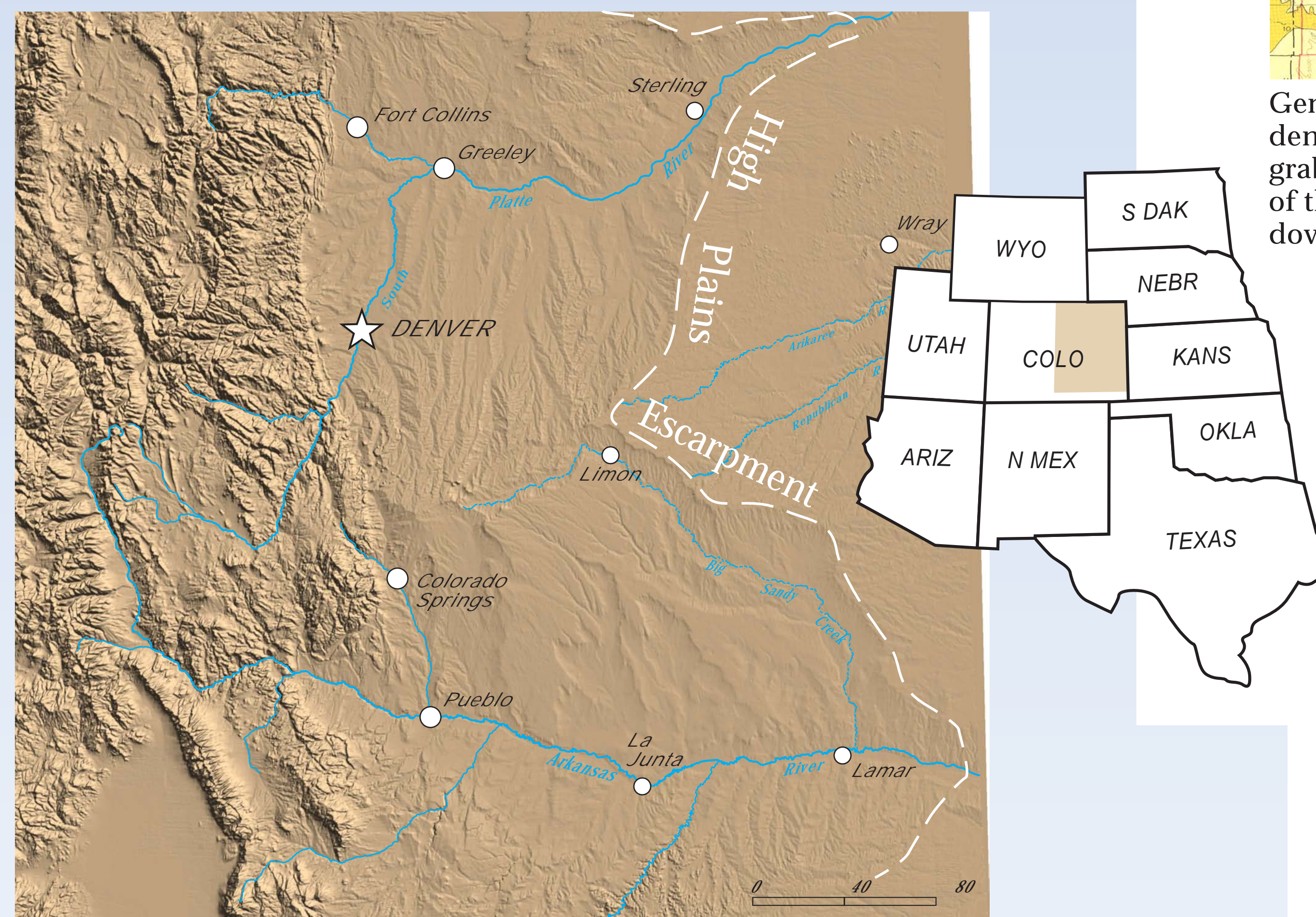
Vince Matthews and Matthew L. Morgan, Colorado Geological Survey

1313 Sherman St., Rm. 715, Denver, CO 80203

The prevalent view of Neogene deformation in the Great Plains contends that it is limited to gentle, eastward tilting during uplift of the Southern Rocky Mountains. This deformation is commonly characterized as a broad up-warping of the whole region. Documentation of brittle, Neogene and Quaternary deformation in the Colorado Rockies on discrete faults with displacements of thousands of meters (Widmann and others, 2002), raised the question of whether the accompanying deformation in the Great Plains was also accomplished by faulting. Several lines of evidence suggest that Neogene faulting may be an important deformational component in the Great Plains. This evidence includes geomorphic highs and lows bounded by linear scarps, subsurface offset of the Cretaceous strata, and striking differences in stream incision.

Examination of a 100-meter-resolution, shaded digital elevation model of eastern Colorado reveals a 40-kilometer-wide topographic depression thought to be a graben. A 150-kilometer-long scarp forms the west side of the "graben". The scarp profile varies by location, but is generally between 20 and 30 meters high. This scarp cuts the Mio-Pliocene Ogallala Formation and perhaps Quaternary deposits. The linearity of the scarp, apparent offset of stream channels, and a left-stepping, en echelon pattern suggest the possibility of left-lateral displacement as much as 1.5 kilometers.

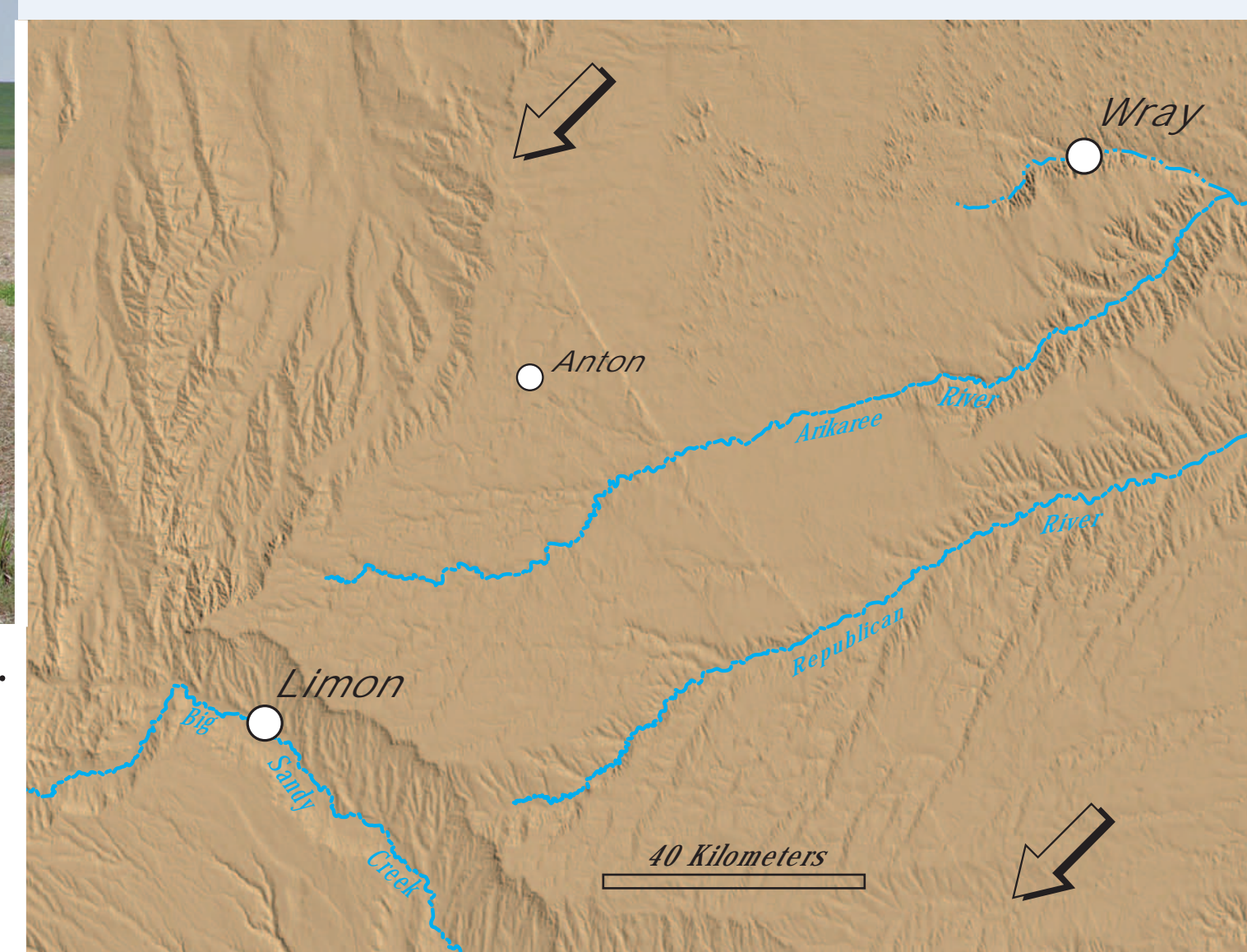
Geomorphic, geologic, and GIS analyses of the Colorado High Plains revealed additional horst and graben structures occurring over wide areas farther to the east. These features may have significance for groundwater production, earthquake hazard, and hydrocarbon accumulation.



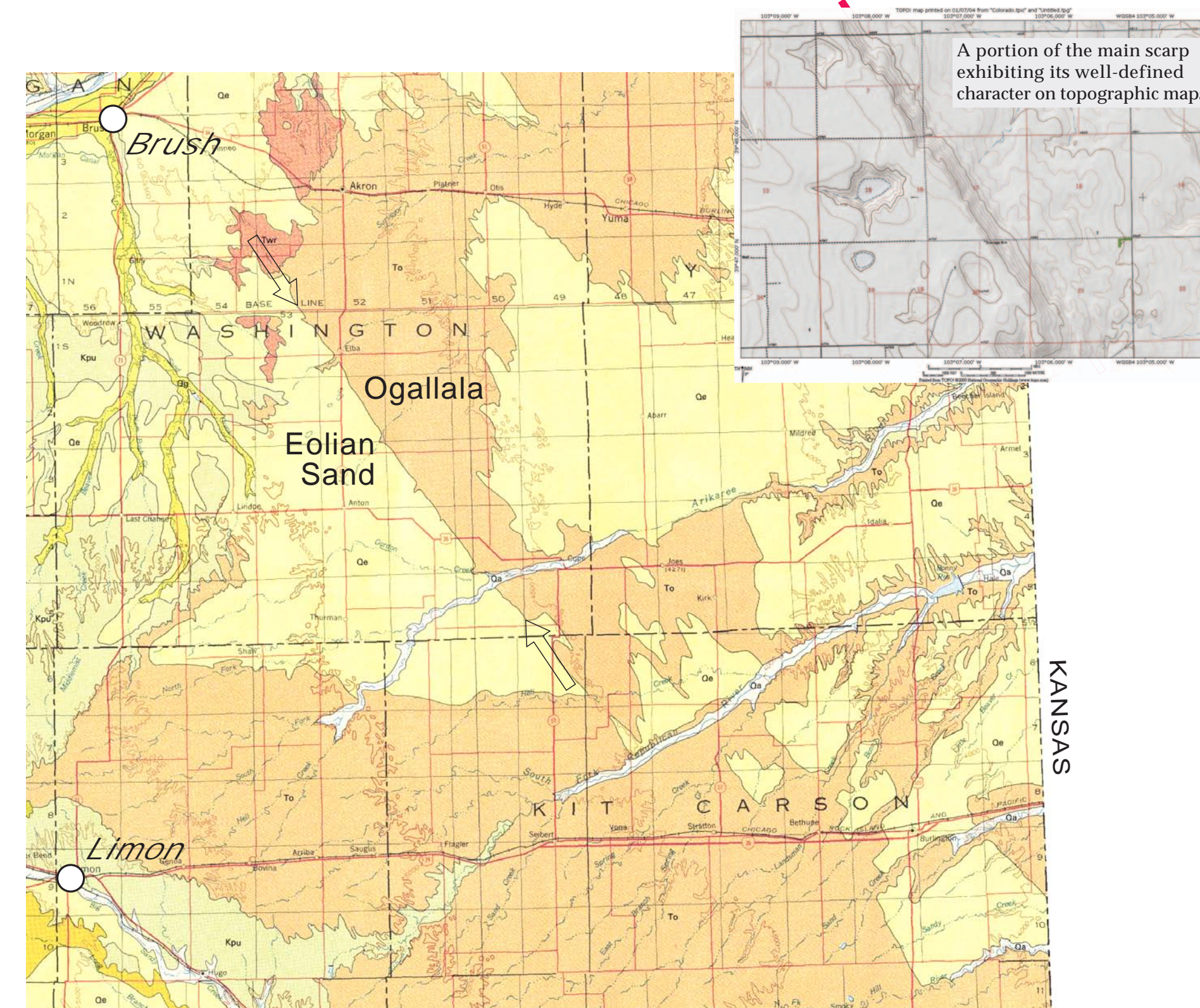
Shaded relief digital elevation model of eastern Colorado showing the High Plains Escarpment in relation to major cities and rivers.



Photograph looking west toward scarp. Scarp height is 20-30 meters. Surface displacement is 20-30 meters above low-lying area in foreground.



Detailed digital elevation model of the High Plains escarpment. Arrows bracket the 150-km-long scarp that forms the western edge of a graben.



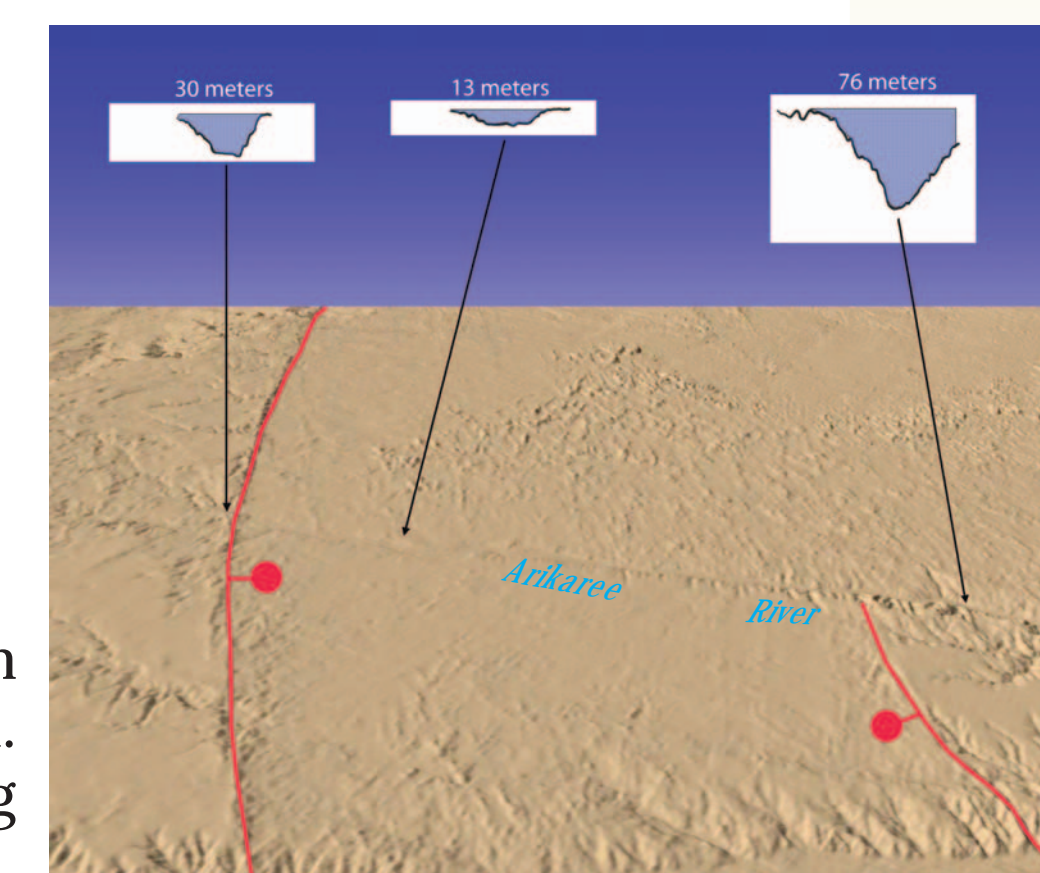
Generalized geologic map of east-central Colorado. Arrows denote the location of the scarp on the west side of the graben. Eolian sand (Qe) is mapped on the upthrown side of the scarp and Ogallala Formation (To) is mapped on the downthrown side. Map from Tweto (1979).



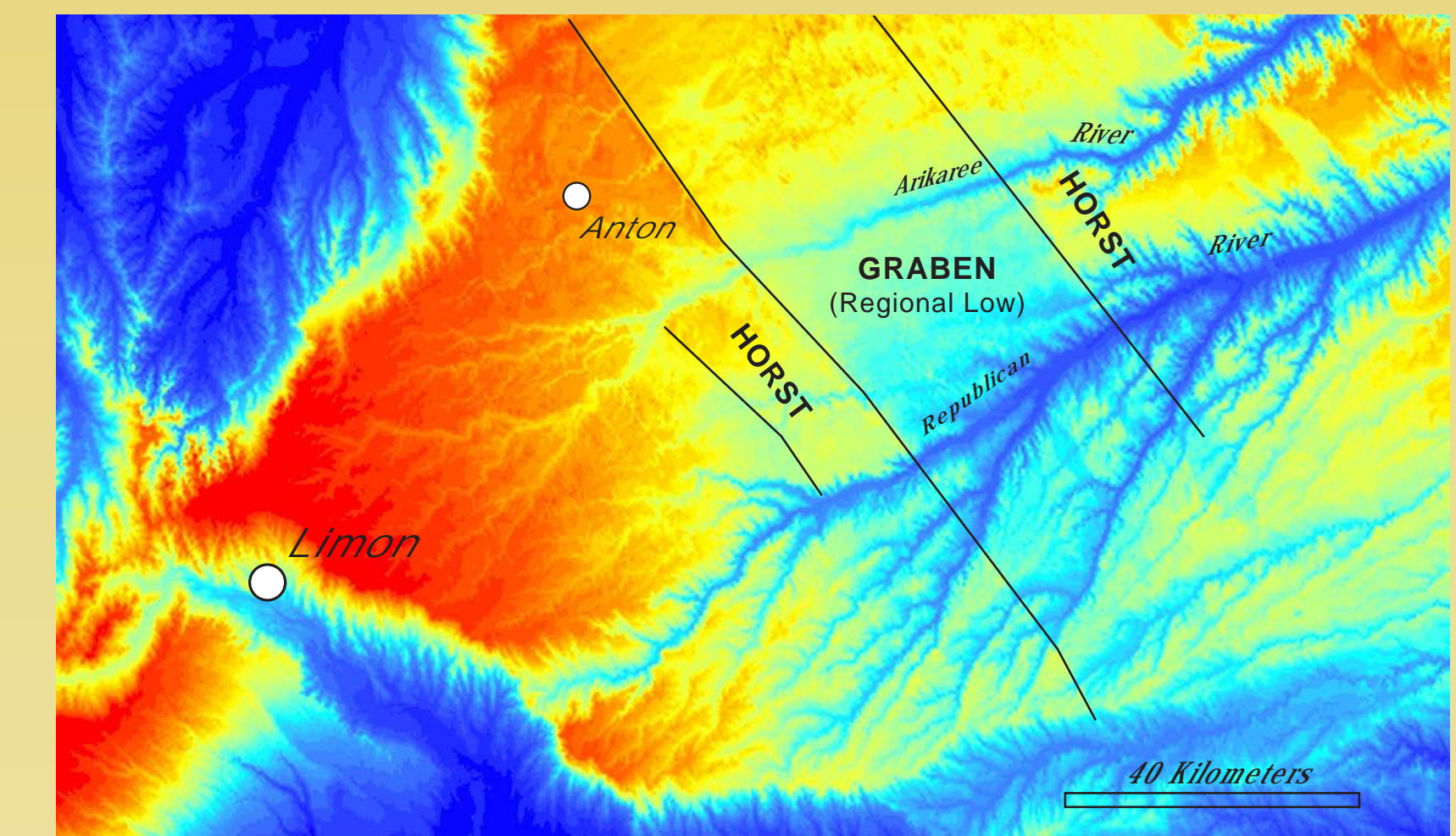
Westward view into the graben from top of east scarp.



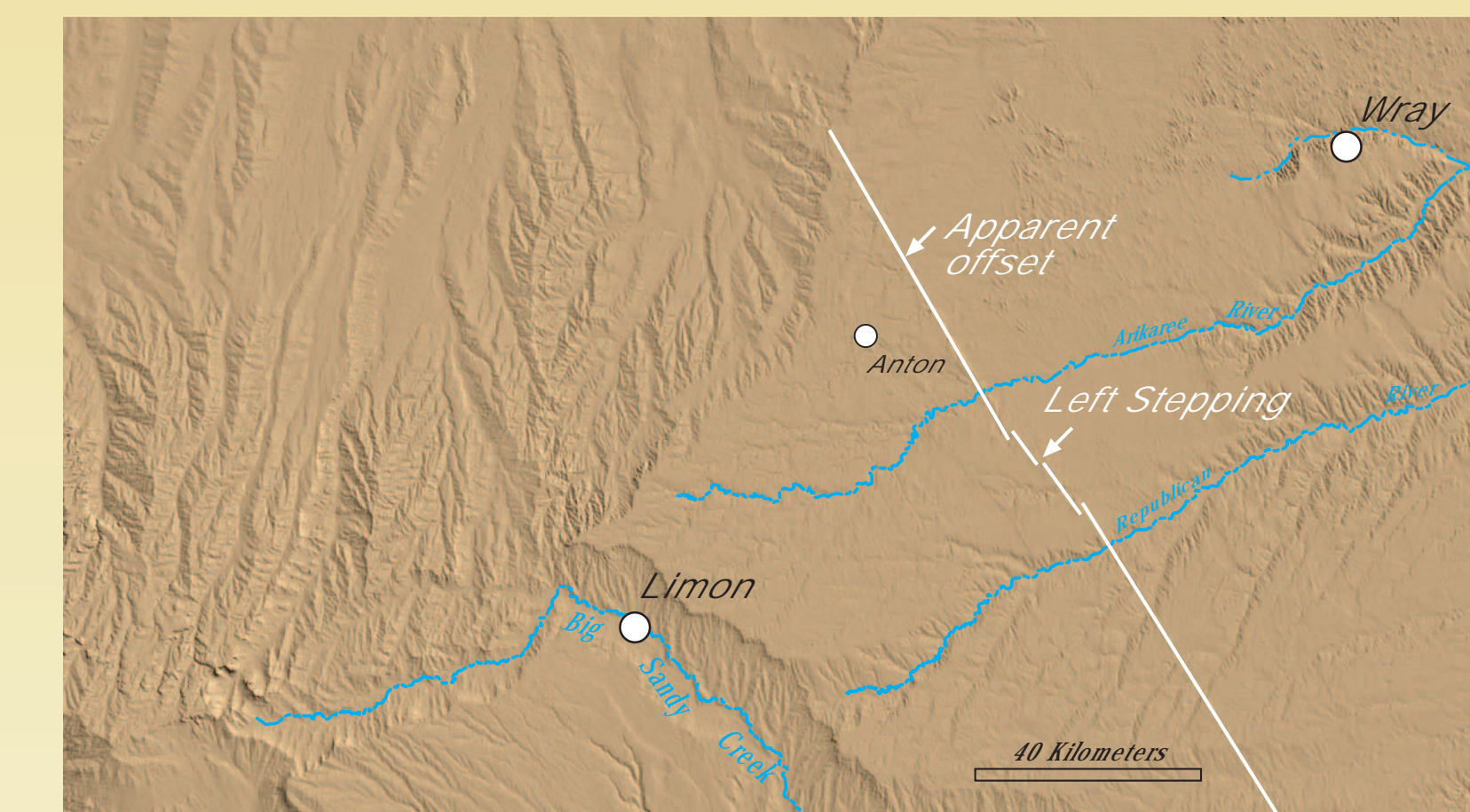
Oblique view looking northwest along strike of the 150-km-long scarp. Note difference in stream incision across the scarp.



Streams are more deeply incised on upthrown blocks than in the graben. The Arikaree River may be aggrading in the graben.



First-order trend surface residual map showing at least two sets of horst and graben structures. Areas with slopes higher than the regional slope are depicted as shades of red, and areas with slopes lower than the regional slope are shaded blue.



Several characteristics of the 150-km-long scarp suggest possible left-lateral displacement.

- Linearity of scarp
- Left-stepping en echelon pattern
- Apparent left-lateral offset of streams.



Several streams that cross the western scarp appear to be offset in a left-lateral sense. The apparent horizontal offset is approximately 1.5 km.

## References

- Tweto, Ogden, 1979. Geologic map of Colorado: U.S. Geological Survey Special Geologic Map, scale 1:500,000.
- Widmann, B. L., Kirkham, R. M., Morgan, M. L., and Rogers, W. P., with contributions by Crone, A. J., Personius, S. F., and Kelson, K. L., and GIS and Web design by Morgan, K. S., Pattyn, G. R., and Phillips, R. C., 2002. Colorado Late Cenozoic Fault and Fold Database and Internet Map Server: Colorado Geological Survey Information Series 60a, <http://geosurvey.state.co.us/pubs/ceno>



# Critique and Use of Historical Methodology in Seismic Hazards Analysis of Earthquakes in the Basin and Range: Expanding the Historical Catalog, and the Search for Triggered (?) Events from the San Andreas Fault

Dawn C. Martindale, Dept. of History, Utah State University, Logan, UT 84322  
James P. Evans, Dept. of Geology, Utah State University, Logan, UT 84322-4505

## The Abstract

In recent years the use of historical methodology introduced and integrated into seismic studies of the Basin and Range has resulted in two outcomes. The first consists primarily of crucial analytical updates of moderate large earthquakes leading to increased understanding in the nature of shaking. The second result includes the location of new earthquakes previously not listed in earthquake catalogs and scholarly publications, with possible reference to triggered events from the San Andreas Fault.

We examine single event records that convey information addressing displacement, damage and other distinct attributes of shaking for large Western United States earthquakes. A prime example of the use of this methodology is our reexamination of the 1884 Bear Lake, Utah earthquake. Original estimates state the 1884 event to encompass roughly 15,600 km<sup>2</sup> and an MMI intensity range between IV and VIII. Utilizing historical research methods, including examining additional newspapers, personal journals, local photographs, archival collections, and historical-society documents new estimates of the initial and subsequent shocks surfaced. Intensity range increased to between two and ten and the felt area expanded to encompass roughly 44,200 km<sup>2</sup>. A more intriguing result included the relocation of the inferred epicenter from the southeast location of Bear Lake to the northwest side near Paris and Liberty, Idaho. This places the earthquake on an antithetic normal fault in the hanging wall of the east-dipping Bear Lake fault.

Other interesting data included direction, length and time of the initial and subsequent shocks. During the reanalysis of the Bear Lake earthquake primary sources also led to the discovery of six additional earthquakes in Utah not previously listed in catalogs. Application of similar methodology is currently being utilized to update the nineteenth-century earthquake catalogs and further understand the seismic hazard threat in Utah.

We use similar methodology to reexamine the 1857 Fort Tejon, California earthquake. We have found 150 additional felt reports beyond the ones listed by previous scholars. Similar results to those of Bear Lake are anticipated as initial analysis is being processed. We also infer that earthquakes in Beaver, Utah, February 1857 and Western Nevada, September 1857 may be related to large aftershocks or the main rupture of the Ft. Tejon event. Both shocks are currently under review, using historical methodology, to further understand the relationship and relevance to the 1857 event and the nature of triggered events in the Basin and Range area.

Methods and techniques used by historians, specifically an extensive review of archival and historical society materials, along with a historiography of previous work, serve a crucial role in assisting seismologists in further understanding the significance and implications of seismic events in the pre-instrument era.

## Introduction

Historical seismicity of the eastern Basin and Range - Rocky Mountain region area includes numerous events of M 4-6.5. Most of these earthquakes are interpreted as slip on moderately west-dipping normal faults, formed in response to the modern east-west extension of the region (Bjarnasson and Pechman, 1989; Zoback, 1989).

In this poster, we review results of three efforts

1. The 1884 Bear Lake Earthquake in SE Idaho/NE Utah
2. Updating the Utah catalog
3. Reevaluation of the 1857 Ft. Tejon earthquake on the San Andreas fault

The 1884 Bear Lake event is the largest earthquake reported for the period 1850-1902 for the Utah region. Its antiquity precludes seismographic analyses, and the reports of the location, damage, and the number of aftershocks indicate that it can provide insight into the nature of ground shaking and damage possible from moderate earthquakes in the region.

The 1884 Bear Lake earthquake was assigned a magnitude of 6.3 and was located at 42° N, 111° 16' W (Arabasz et al., 1979) based on interpretations of newspaper accounts and catalogs of the era (Williams and Tapper, 1953; Cook and Smith, 1967), and the proximity to the steep eastern range-front of the Bear Lake valley.

## Methods

Martindale (2001) conducted a rigorous historical analysis of the earthquake which encompassed reviewing newspaper accounts, maps, church archive collections, and personal diaries at 13 archives and libraries in Utah, Idaho, and Wyoming.

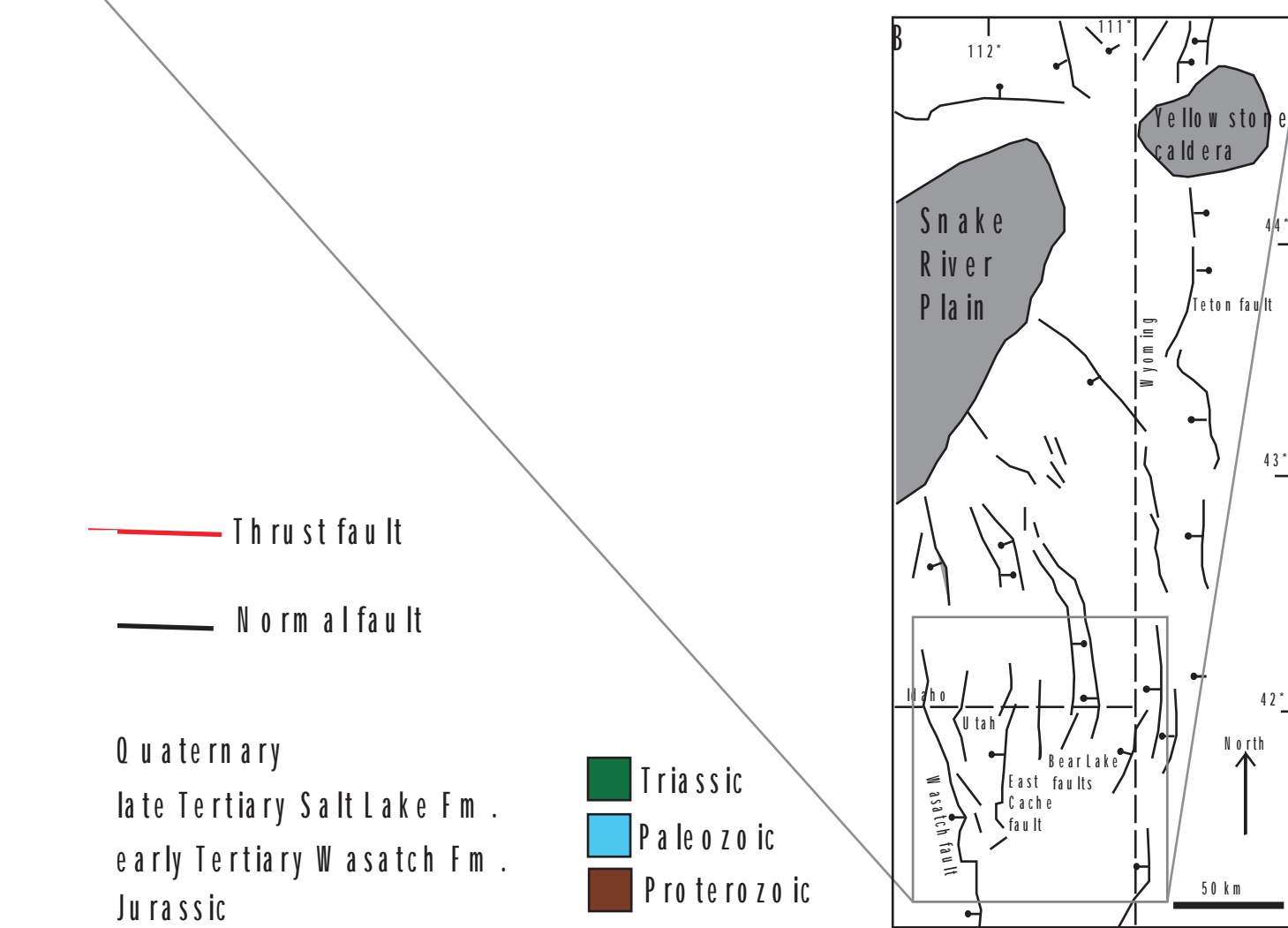
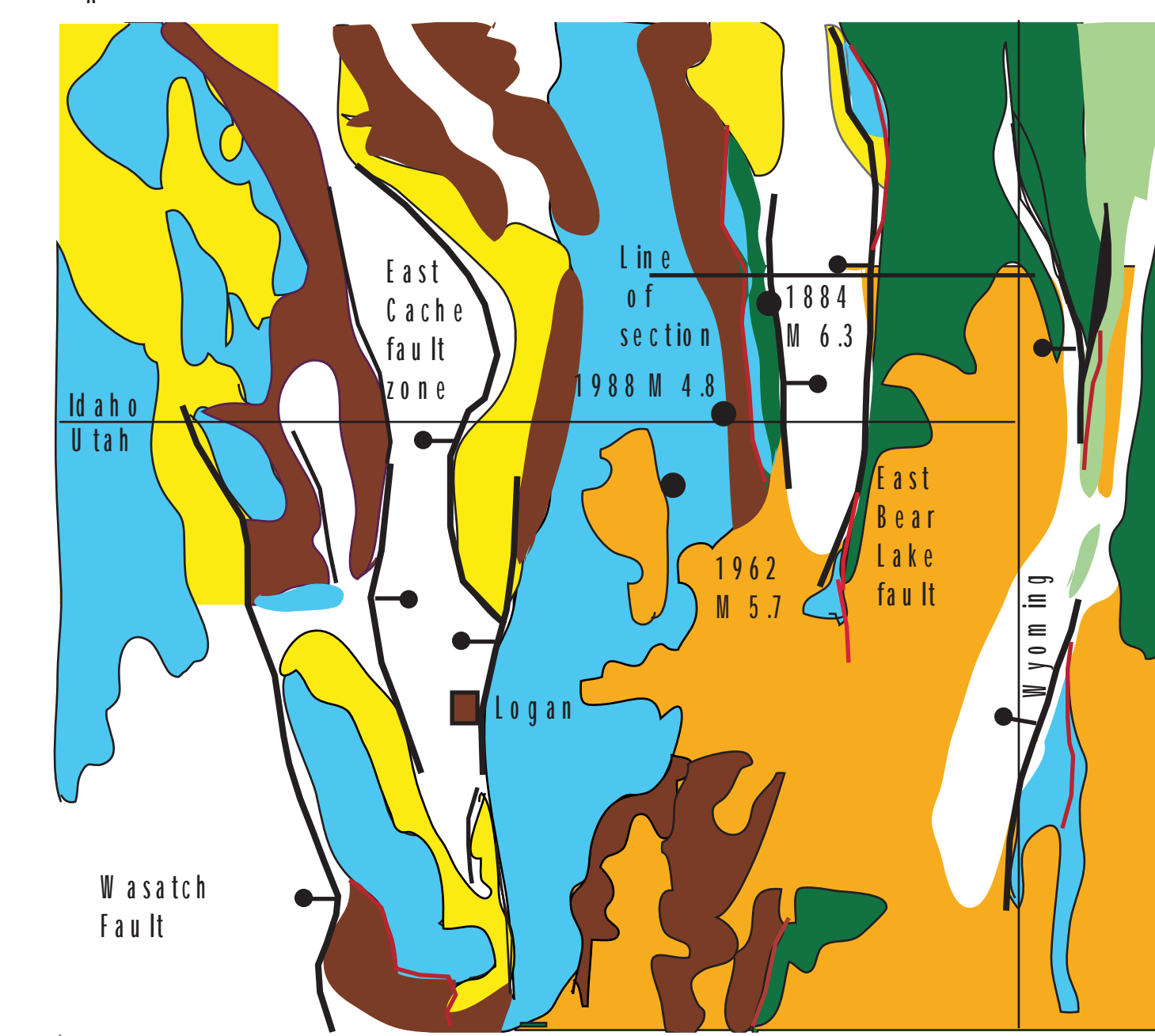
We combine the results with geological analysis of the region to determine the likely epicenter location for the earthquake.

## Geologic Setting of area

The Intermontian Seismic Belt is a northeast-trending region of diffuse, moderate seismicity between the Wasatch Fault, Utah and the Teton Mountains, Wyoming (Fig. 1, inset). The region consists of north-trending valleys bounded on one or both sides by active normal faults.

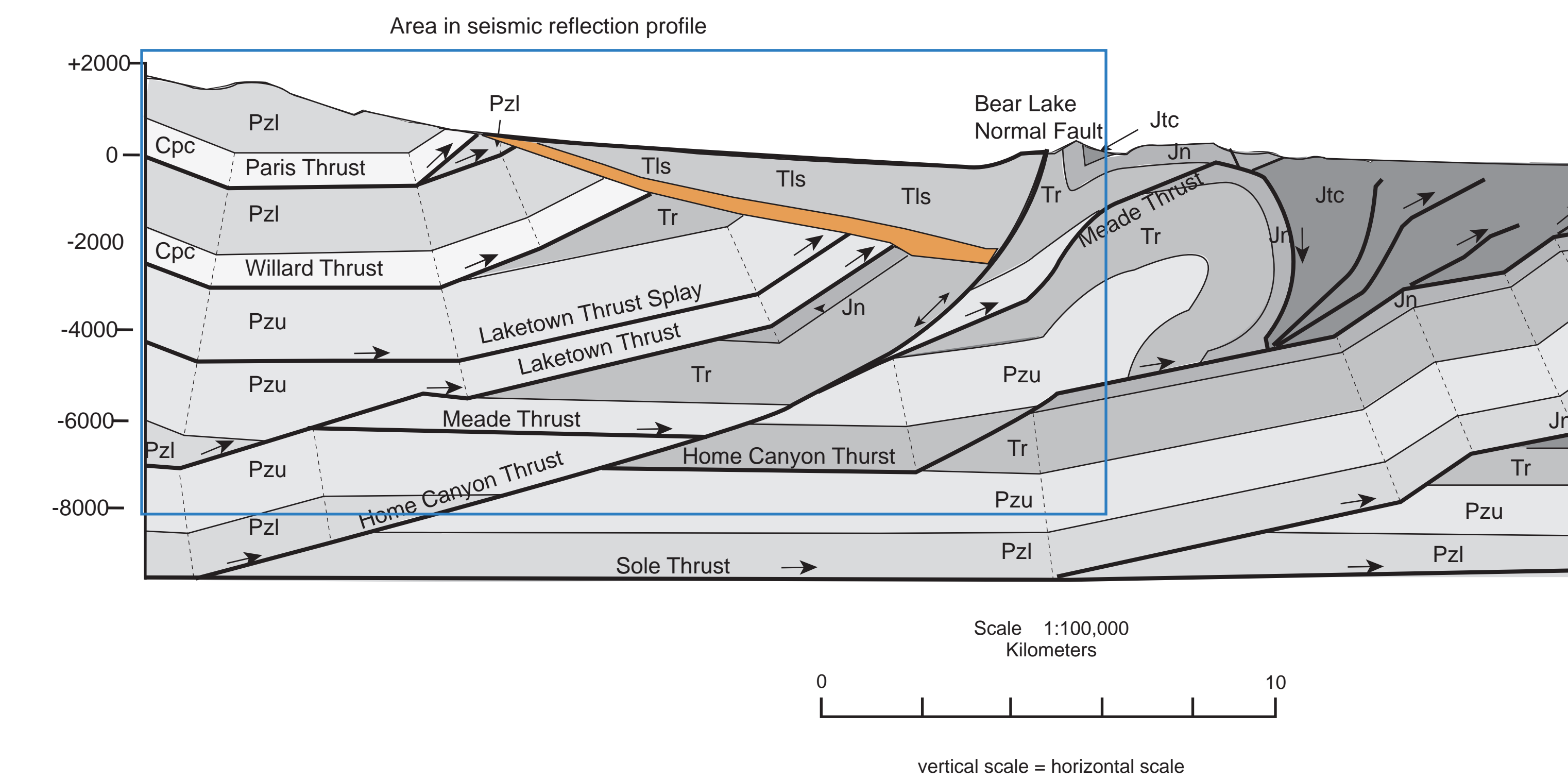
The normal faults cut Precambrian through Cretaceous rocks that were thrust eastward during the Cretaceous in the Sevier fold and thrust belt development

## The 1884 BearLake Idaho/Utah earthquake



## Summary of Historical analysis

- The Bear Lake earthquake occurred at approximate 01:50 am (local time) in the morning of 10 November 1884.
- 75 felt reports at 19 sites were recorded over a region in excess of 70,000 km<sup>2</sup>
- Mercalli magnitude intensity reports indicate intensities from III to VIII
- Shaking duration of the event ranged from ten to thirty seconds
- the direction to depend on the location of the site.
- No reports of liquefaction, sand blows, fissures or ground displacement were documented.
- The number of aftershocks range from two to twenty one, with the highest number reported for Liberty and Paris, Idaho, northwest of Bear Lake
- Descriptions of ground shaking include the rocking of a moving train, dislodging and rolling of stacked logs at a sawmill, loud roaring sounds, lights similar to lightning, people thrown from their beds, abundant damage to masonry, and milk spilled from creamer pans.
- The only multiple reports of Intensity VII or greater shaking come from Liberty and Paris, Idaho. Intensities fall off steeply with distance from these towns, and this area also had the largest number of aftershocks.



## Geologic interpretation of the earthquake

The geologic structure of the epicentral region are based on unpublished seismic reflection data, surface geologic mapping, some deep drill hole data, and construction of balanced cross sections of the region

The geology of the study area is characterized by contractional structures formed during the development of the Cretaceous Sevier fold and thrust belt (Armstrong and Oriol, 1965; Dixon, 1982). Tertiary extension of the easternmost Basin and Range is related to the location of ramps in the underlying thrusts (Royce et al., 1975; Arabasz and Julander, 1986; West, 1993).

- No surface ruptures were reported for the 1884 earthquake
- Robertson (1978) recognized fault scarps on both sides of the valley, including an 8 m high scarp on the west side of the Bear Lake valley
- McCalpin (1993) trenched both the east and west Bear Lake faults and found that M>7 earthquakes occurred on the faults 2.1 ka and 5.9-6.5 ka, respectively.
- The traces of these faults are 6-15 km north of the location of the interpreted seismic section of and thus the West Bear Lake fault zone may be a set of steeply dipping synthetic faults.

- The dominant normal fault in the area is the East Bear Lake fault, a listric normal fault that soles into the Home Canyon thrust (Kendrick (1994) and Coogan and Royce (1990) interpret the Bear Lake fault to cut out the Meade thrust.
- The Bear Lake normal fault has 3.8-3.9 km of slip. The Bear Lake fault has a large radius of curvature, dipping 70° at the surface, and gradually reaching a dip of 20° at a depth of 6 km below sea level
- Numerous small-displacement faults were interpreted to cut reflectors that represent the Paleozoic and Proterozoic rocks in the hanging wall of the Bear Lake normal fault. These small offset faults (throws of ~40-100 m) may represent extensional strain in the hanging wall of the normal fault.

## Analysis of the Utah Catalog

Year	Month	Location	Mag	Intensity	Dist. (km)	St. Miles
1884	October 10	Bear Lake	6.3	VI-VIII	1500	930
1884	December 1	Highway	VI	VI	1500	930
1884	August 26	Paria	VI	VI	1500	930
1884	October 10	Bear Lake	6.3	VI-VIII	1500	930
1884	November 10	Bear Lake	6.3	VI-VIII	1500	930
1884	December 1	Highway	VI	VI	1500	930
1884	August 26	Paria	VI	VI	1500	930
1884	October 10	Bear Lake	6.3	VI-VIII	1500	930
1884	November 10	Bear Lake	6.3	VI-VIII	1500	930
1884	December 1	Highway	VI	VI	1500	930
1884	August 26	Paria	VI	VI	1500	930
1884	October 10	Bear Lake	6.3	VI-VIII	1500	930
1884	November 10	Bear Lake	6.3	VI-VIII	1500	930
1884	December 1	Highway	VI	VI	1500	930
1884	August 26	Paria	VI	VI	1500	930
1884	October 10	Bear Lake	6.3	VI-VIII	1500	930
1884	November 10	Bear Lake	6.3	VI-VIII	1500	930
1884	December 1	Highway	VI	VI	1500	930
1884	August 26	Paria	VI	VI	1500	930
1884	October 10	Bear Lake	6.3	VI-VIII	1500	930
1884	November 10	Bear Lake	6.3	VI-VIII	1500	930
1884	December 1	Highway	VI	VI	1500	930
1884	August 26	Paria	VI	VI	1500	930
1884	October 10	Bear Lake	6.3	VI-VIII	1500	930
1884	November 10	Bear Lake	6.3	VI-VIII	1500	930
1884	December 1	Highway	VI	VI	1500	930
1884	August 26	Paria	VI	VI	1500	930
1884	October 10	Bear Lake	6.3	VI-VIII	1500	930
1884	November 10	Bear Lake	6.3	VI-VIII	1500	930
1884	December 1	Highway	VI	VI	1500	930
1884	August 26	Paria	VI	VI	1500	930
1884	October 10	Bear Lake	6.3	VI-VIII	1500	930
1884	November 10	Bear Lake	6.3	VI-VIII	1500	930
1884	December 1	Highway	VI	VI	1500	930
1884	August 26	Paria	VI	VI	1500	930
1884	October 10	Bear Lake	6.3	VI-VIII	1500	930
1884	November 10	Bear Lake	6.3	VI-VIII	1500	930
1884	December 1	Highway	VI	VI	1500	930
1884	August 26	Paria	VI	VI	1500	930
1884	October 10	Bear Lake	6.3	VI-VIII	1500	930
1884	November 10	Bear Lake	6.3	VI-VIII	1500	930
1884	December 1	Highway	VI	VI	1500	930
1884	August 26	Paria	VI	VI	1500	930
1884	October 10	Bear Lake	6.3	VI-VIII	1500	930
1884	November 10	Bear Lake	6.3	VI-VIII	1500	930
1884	December 1	Highway	VI	VI	1500	930
1884	August 26	Paria	VI	VI	1500	930
1884	October 10	Bear Lake	6.3	VI-VIII	1500	930
1884	November 10	Bear Lake	6.3	VI-VIII	1500	930
1884	December 1	Highway	VI	VI	1500	930
1884	August 26	Paria	VI	VI	1500	930
1884	October 10	Bear Lake	6.3	VI-VIII	1500	930
1884	November 10	Bear Lake	6.3	VI-VIII	1500	930
1884	December 1	Highway	VI	VI	1500	930
1884	August 26	Paria	VI	VI	1500	930
1884	October 10	Bear Lake	6.3	VI-VIII	1500	930
1884	November 10	Bear Lake	6.3	VI-VIII	1500	930
1884	December 1	Highway	VI	VI	1500	930
1884	August 26	Paria	VI	VI	1500	930
1884	October 10	Bear Lake	6.3	VI-VIII	1500	930
1884	November 10	Bear Lake	6.3	VI-VIII	1500	930
1884	December 1	Highway	VI	VI	1500	930
1884	August 26	Paria	VI	VI	1500	930
1884	October 10	Bear Lake	6.3	VI-VIII	1500	930
1884	November 10	Bear Lake	6.3	VI-VIII	1500	930
1884	December 1	Highway	VI	VI	1500	930
1884	August 26	Paria	VI	VI	1500	930
1884	October 10	Bear Lake	6.3	VI-VIII	1500	930
1884	November 10	Bear Lake	6.3	VI-VIII	1500	930
1884	December 1	Highway	VI	VI	1500	930
1884	August 26	Paria	VI	VI	1500	930
1884	October 10	Bear Lake	6.3	VI-VIII	1500	930
1884	November 10	Bear Lake	6.3	VI-VIII	1500	930
1884	December 1	Highway	VI	VI	1500	930
1884	August 26	Paria	VI	VI	1500	930
1884	October 10	Bear Lake	6.3	VI-VIII	1500	930
1884	November 10	Bear Lake	6.3	VI-VIII	1500	930
1884	December 1	Highway	VI	VI	1500	930
1884	August 26	Paria	VI	VI	1500	930
1884	October 10	Bear Lake	6.3	VI-VIII	1500	930
1884	November 10	Bear Lake	6.3	VI-VIII	1500	930
1884	December 1	Highway	VI	VI	1500	930
1884	August 26	Paria	VI	VI	1500	930
1884	October 10	Bear Lake	6.3	VI-VIII	1500	930
1884	November 10	Bear Lake	6.3	VI-VIII	1500	930
1884	December 1	Highway	VI	VI	1500	930
1884	August 26	Paria	VI	VI	1500	930
1884	October 10	Bear Lake	6.3	VI-VIII	1500	930
1884	November 10	Bear Lake	6.3	VI-VIII	1500	930
1884	December 1	Highway	VI	VI	1500	930
1884	August 26	Paria	VI	VI	1500	930
1884	October 10	Bear Lake	6.3	VI-VIII	1500	930
1884	November 10	Bear Lake	6.3	VI-VIII	1500	930
1884	December 1	Highway	VI	VI	1500	930
1884	August 26	Paria	VI	VI	1500	930
1884	October 10	Bear Lake	6.3	VI-VIII	1500	930
1884	November 10	Bear Lake	6.3	VI-VIII	1500	930
1884	December 1	Highway	VI	VI	1500	930
1884	August 26	Paria	VI	VI	1500	930
1884	October 10	Bear Lake	6.3	VI-VIII	1500	930
1884	November 10	Bear Lake	6.3	VI-VIII	1500	930
1884	December 1	Highway	VI	VI	1500	930
1884	August 26	Paria	VI	VI	1500	930
1884	October 10	Bear Lake	6.3	VI-VIII	1500	930
1884	November 10	Bear Lake	6.3	VI-VIII	1500	930
1884	December 1	Highway	VI	VI	1500	930
1884	August 26	Paria	VI	VI	1500	930
1884	October 10	Bear Lake	6.3	VI-VIII	1500	930
1884	November 10	Bear Lake	6.3	VI-VIII	1500	930
1884	December 1	Highway	VI	VI	1500	930
1884	August 26	Paria	VI	VI	1500	930
1884	October 10	Bear Lake	6.3	VI-VIII	1500	930
1884	November 10	Bear Lake	6.3	VI-VIII	1500	930
1884	December 1	Highway	VI	VI	1500	930
1884	August 26	Paria	VI	VI	1500	930
1884	October 10	Bear Lake	6.3	VI-VIII	1500	930
1884	November 10	Bear Lake	6.3	VI-VIII	1500	930
1884	December 1	Highway	VI	VI	1500	930
1884	August 26	Paria	VI	VI	1500	930
1884	October 10	Bear Lake	6.3	VI-VIII	1500	930
1884	November 10	Bear Lake	6.3	VI-VIII	1500	930
1884	December 1	Highway	VI	VI	1500	930
1884	August 26	Paria	VI	VI	1500	930
1884	October 10	Bear Lake	6.3	VI-VIII	1500	930
1884	November 10	Bear Lake	6.3	VI-VIII	1500	930
1884	December 1	Highway	VI	VI	1500	930
1884	August 26	Paria	VI	VI	1500	930
1884	October 10	Bear Lake	6.3	VI-VIII	1500	930

# Active Tectonics and Strain Partitioning in the Northern Intermountain Seismic Belt

## Abstract

We determined fault plane solutions for 82 earthquakes that have occurred since 1982 in northwest and west-central Montana using P-wave first motions recorded by the Montana seismograph network. We included four older fault plane solutions in our analysis. Thirty-six percent of the focal mechanisms showed strike-slip offset, 34 percent showed normal offset, and 29 percent showed oblique offset. A single event in northern Idaho showed oblique reverse slip.

All but four normal-faulting earthquakes occurred north of the Lewis and Clark zone (LCZ) in the vicinity of the Mission and Swan faults, and near the southern tip of the South Fork Flathead fault. They also occurred well away from mapped Quaternary faults. North of the LCZ, the preponderance of normal mechanisms have northerly trending nodal planes subparallel to mapped Quaternary faults. However, hypocenter positions and nodal plane orientations suggest that only one normal mechanism event is consistent with slip on the Mission fault. Strike-slip earthquakes are widely distributed throughout the northernmost Intermountain Seismic Belt; many are near mapped Quaternary normal faults. A linear cluster of epicenters trending east-southeast from the southern tip of the Ovando fault includes four strike-slip mechanisms having nodal planes subparallel to the trend, indicating right-lateral slip at depth along this LCZ fault. The westerly trending nodal planes from strike-slip events within the LCZ consistently indicate right-lateral slip.

T-axis orientations for 50 percent of the fault plane solutions trend east-west  $\pm 15^\circ$ ; another 30 percent trend N  $45^\circ$  E-S  $45^\circ$  W  $\pm 15^\circ$ , which is the average Basin and Range extension direction observed in southwest Montana. Seventy-seven percent of the P-axes trend N  $15^\circ$  W-S  $15^\circ$  E  $\pm 30^\circ$ . Normal and strike-slip fault plane solutions with east-west to northeast-southwest T-axes indicate that the regional stress field is favorably oriented to produce slip on normal faults in northwest Montana. Where these faults terminate southward into the LCZ, right-lateral slip on older west-northwest-trending faults is expected. We believe that low-slip-rate, right-lateral strike-slip faults exist in the LCZ but surface expressions have not yet been identified in forested regions with glacial cover.

Our model of regional extension places the northern limit of the Basin and Range province at the north end of the Flathead Valley. Southward, the northern Rockies are extending westward in five quasi-coherent crustal domains bounded by right-lateral, strike-slip, and oblique-slip accommodation and transfer zones, with each south-side domain translating further west than those to the north. The LCZ represents the northernmost trending east-southeast zone. This model predicts a horizontal velocity field (westward extension accompanied by clockwise rotation) for the region between the Snake River Plain and northwest Montana.

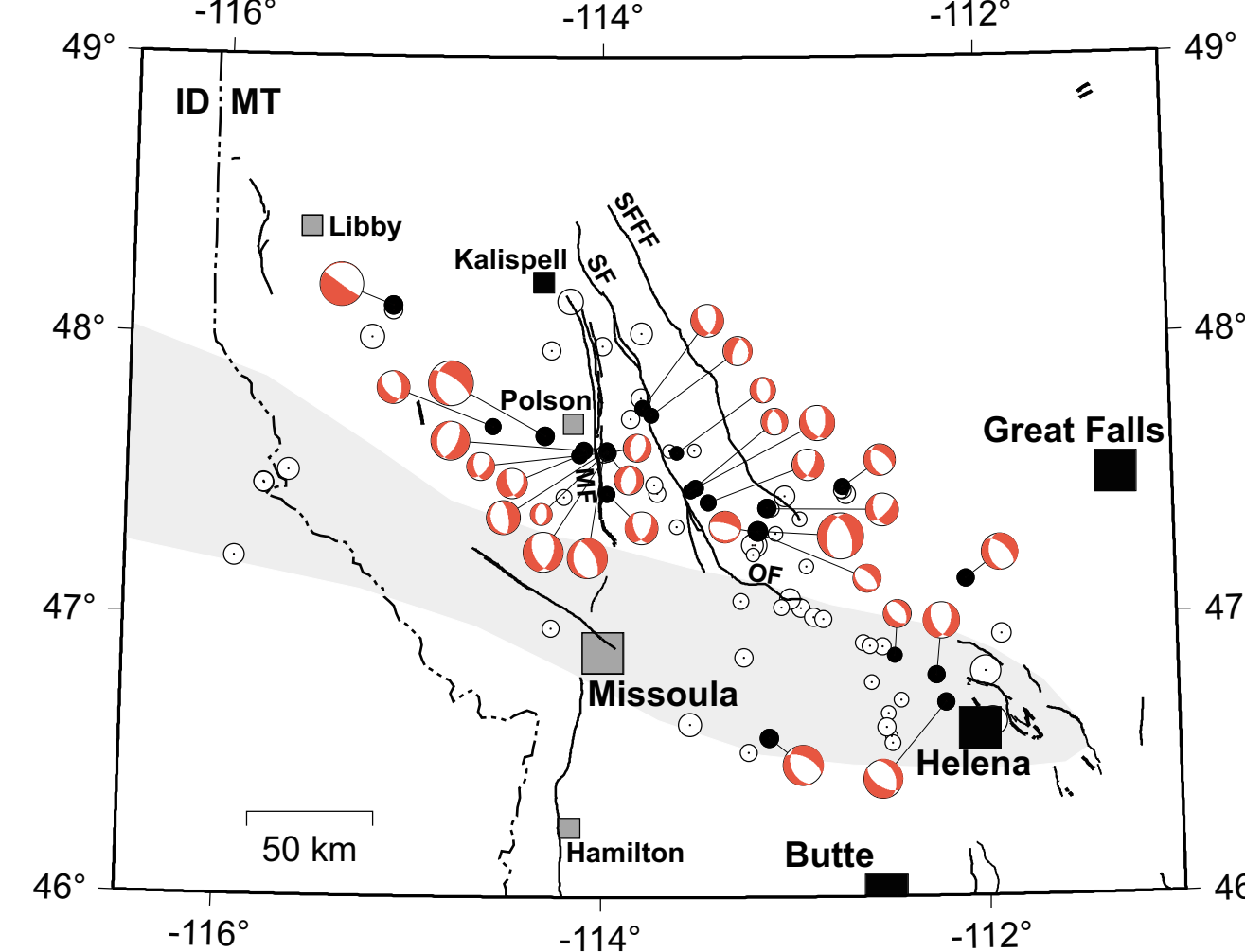
## Discussion

Recent seismicologic data suggest that dextral slip occurs within the Lewis and Clark zone (LCZ), primarily in the eastern half between Helena and Missoula. However, very few of the faults that make up the LCZ have recognized late Quaternary faulting in the eastern LCZ may result from the dearth of field studies focusing on young faulting in the LCZ, low slip rates along these faults, glacial cover, and heavily forested regions. Also, low slip-rate strike-slip faults are probably more difficult to identify than low-slip-rate normal faults. In any case, we believe that our present understanding of the seismicogenic potential of LCZ faults may significantly underestimate the potential for moderate- to large-magnitude earthquakes in west-central Montana.

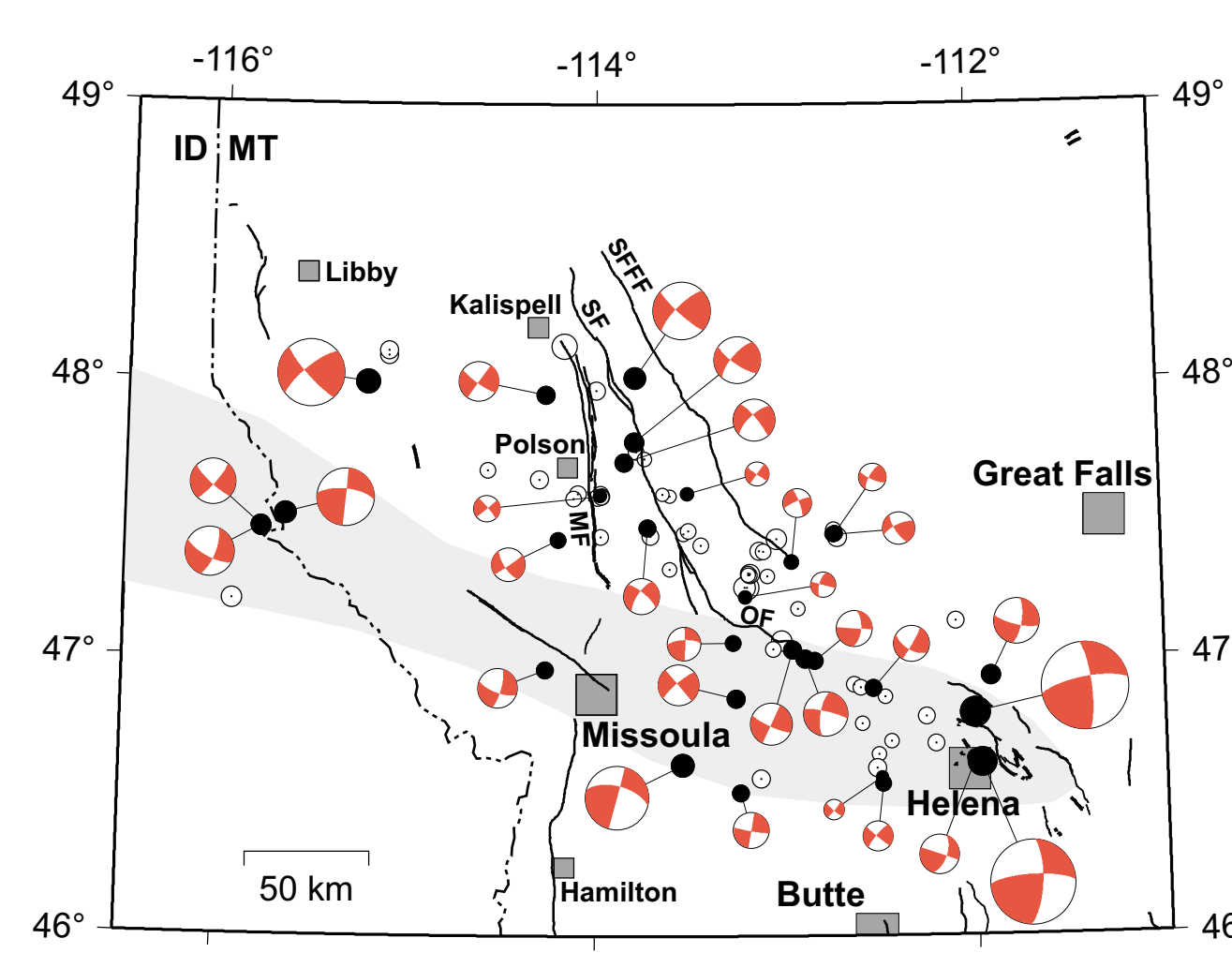
In the Intermountain seismic belt north of the LCZ, seismicologic data reveal the occurrence of both strike-slip and normal faulting. The normal faulting mechanisms indicate an east-west extensional stress field that is favorably oriented to produce future slip on the major range-bounding normal faults in northwest Montana. Despite this favorably oriented stress field, the southern part of the Mission fault—the only major range-bounding fault in northwest Montana with demonstrated Holocene slip—is conspicuously devoid of recent seismicity. The adjacent southern portion of the Swan fault also exhibits a low level of seismicity. Although late Quaternary faulting has not been identified along the southern Swan fault, a steep, linear range front with well-developed facets suggests that it may be active.

Michael C. Stickney  
Montana Bureau of Mines and Geology  
Montana Tech of the University of Montana  
Butte, MT 59701  
E-mail: mstickney@mtech.edu

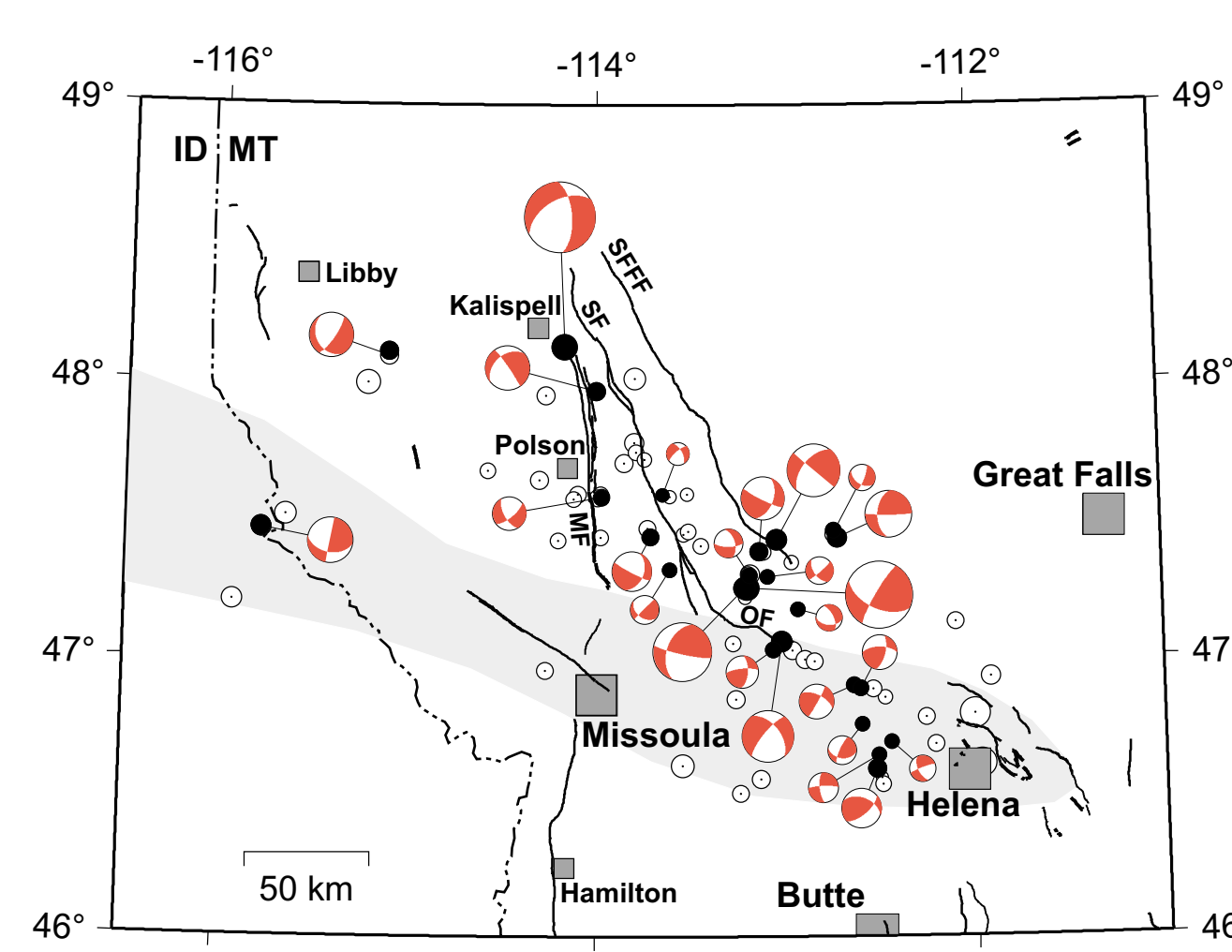
David R. Lageson  
Department of Earth Sciences  
Montana State University  
Bozeman, MT 59717  
E-mail: lageson@montana.edu



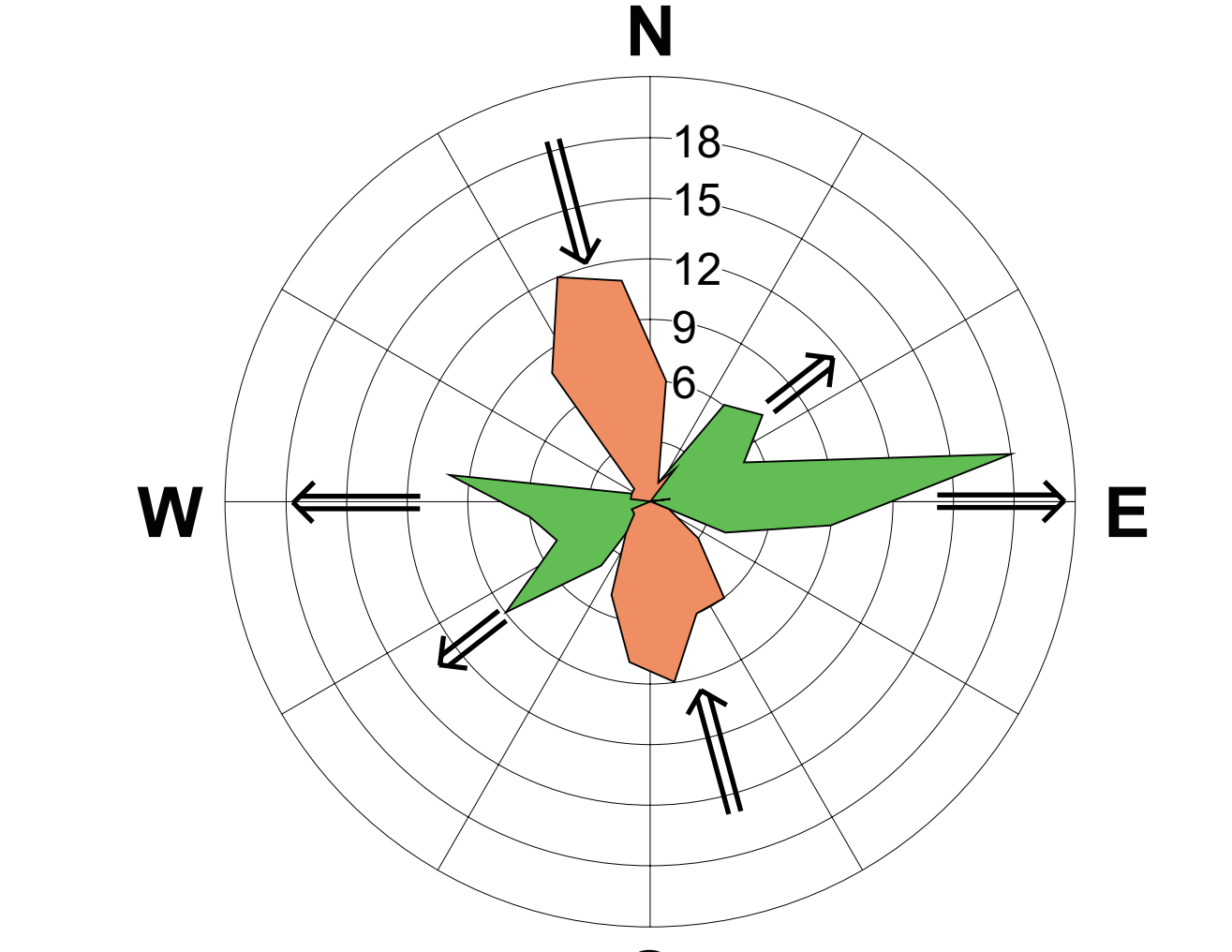
Earthquakes with normal slip mechanisms (black circles), open circles are epicenters with other mechanisms. Fault plane solutions are lower hemisphere projections plotted to earthquake magnitude, with compressional quadrants shaded. Light gray shading shows the extent of the Lewis and Clark zone. Line segments show Quaternary faults, bold segments near Helena and southern Mission faults show faults with recent Quaternary offset. **BD**, Grand Staircase-Escalante National Monument; **DF**, Snake River Plain; **DFP**, South Fork Flathead fault; **DFR**, Snake River Plain; **DFR**, Snake River Plain; **DFR**, Snake River Plain.



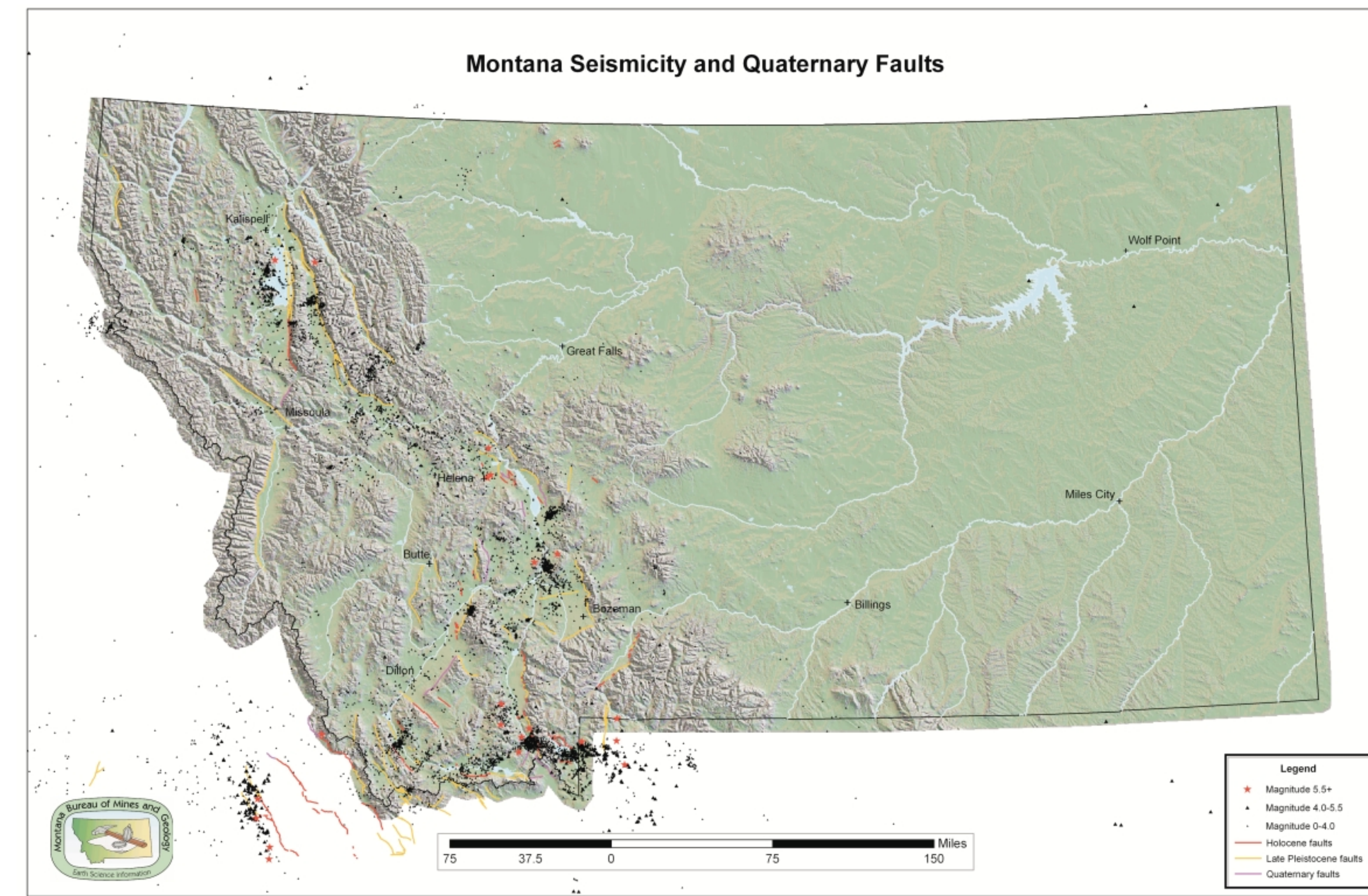
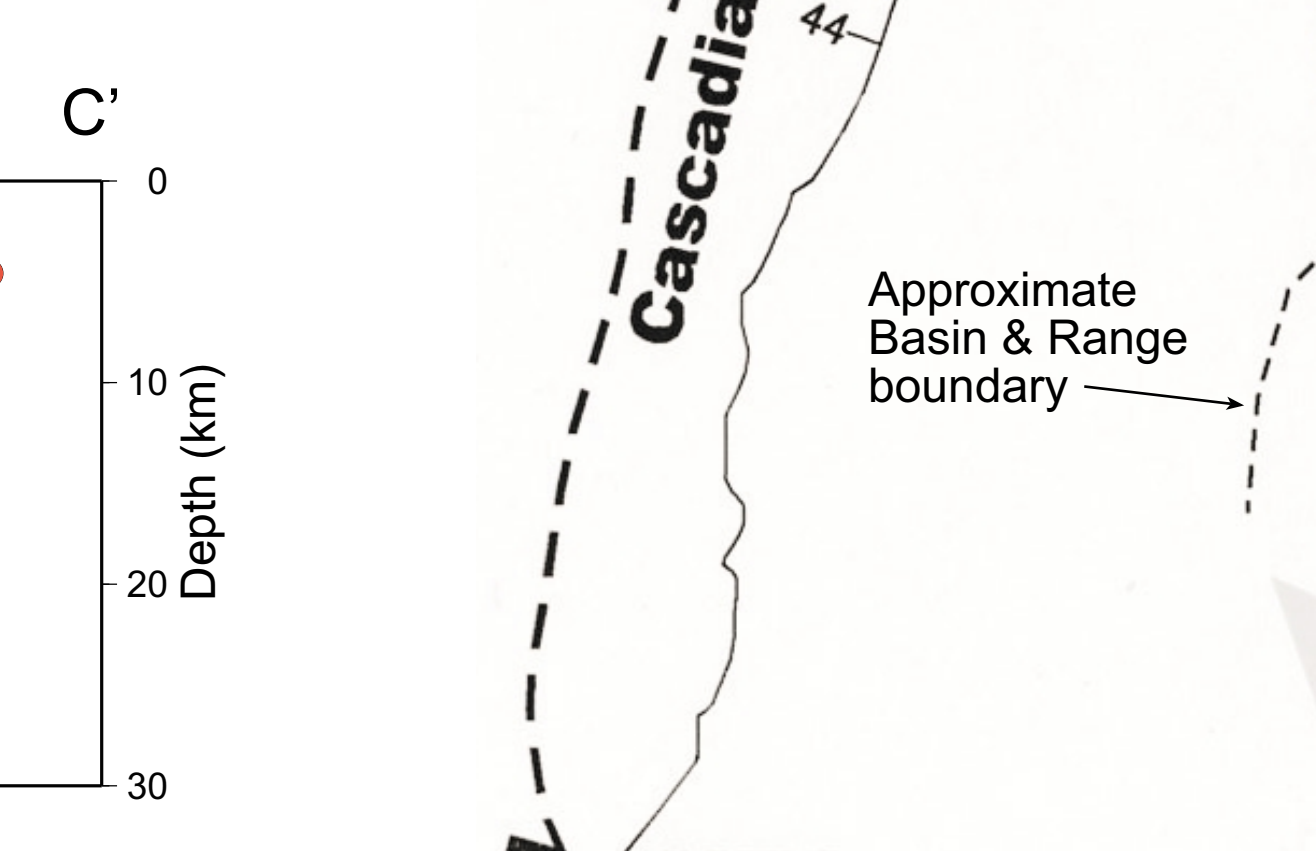
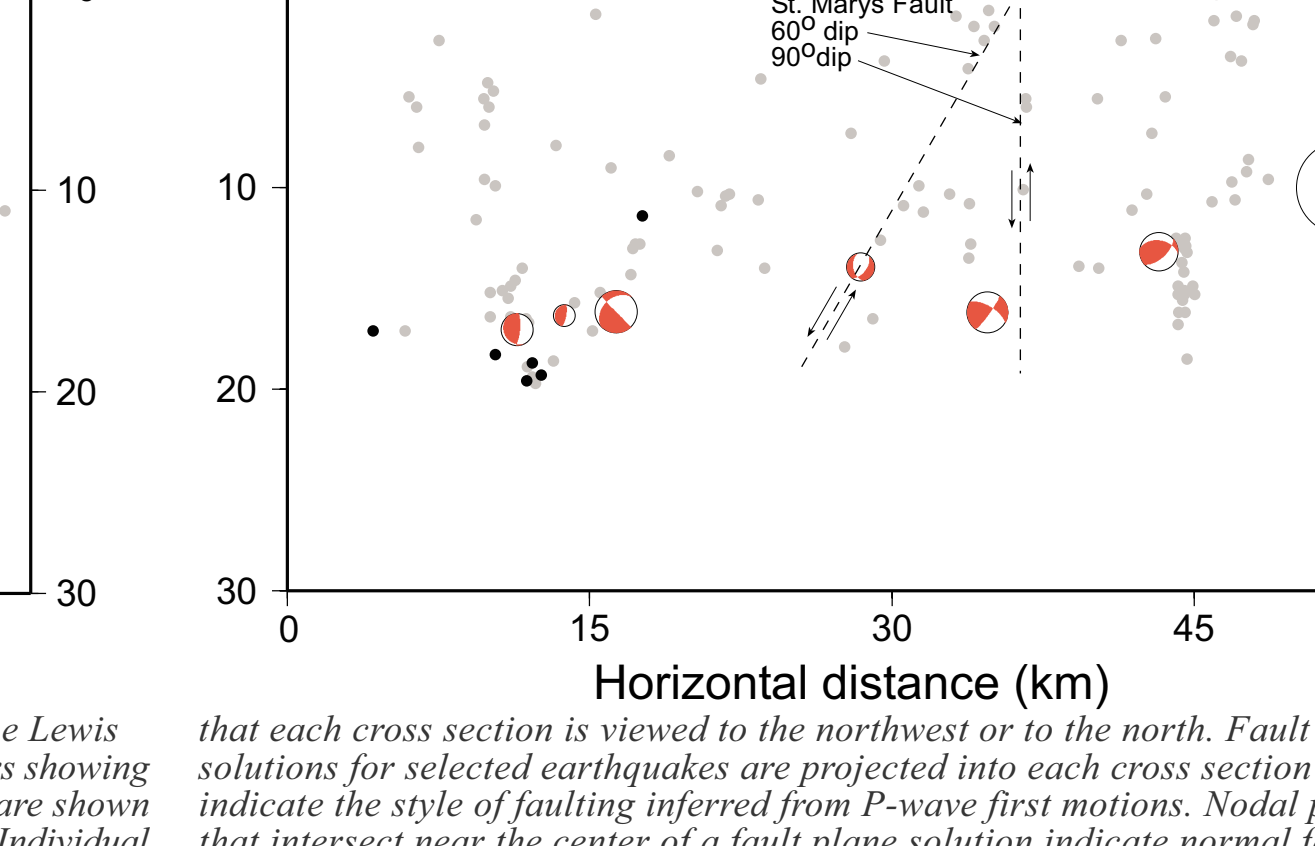
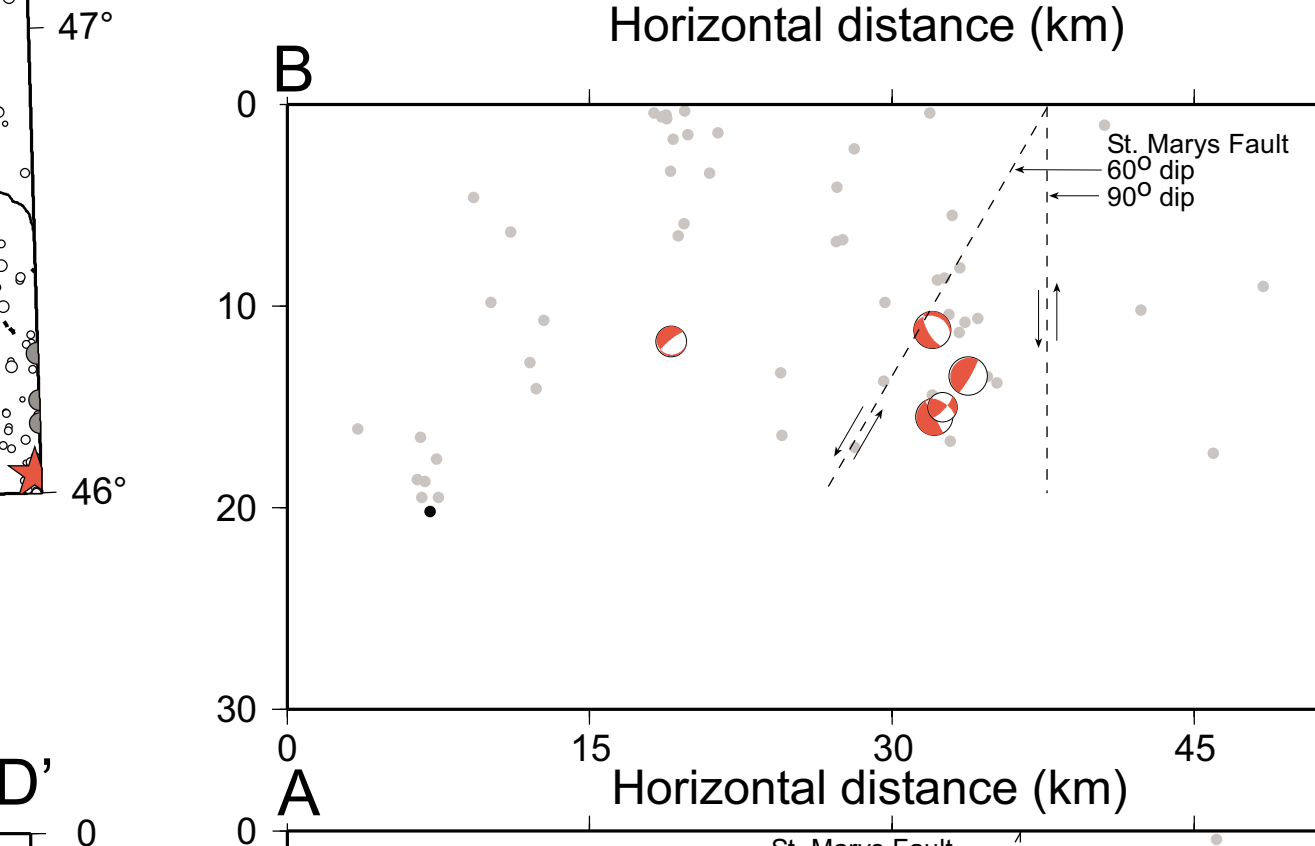
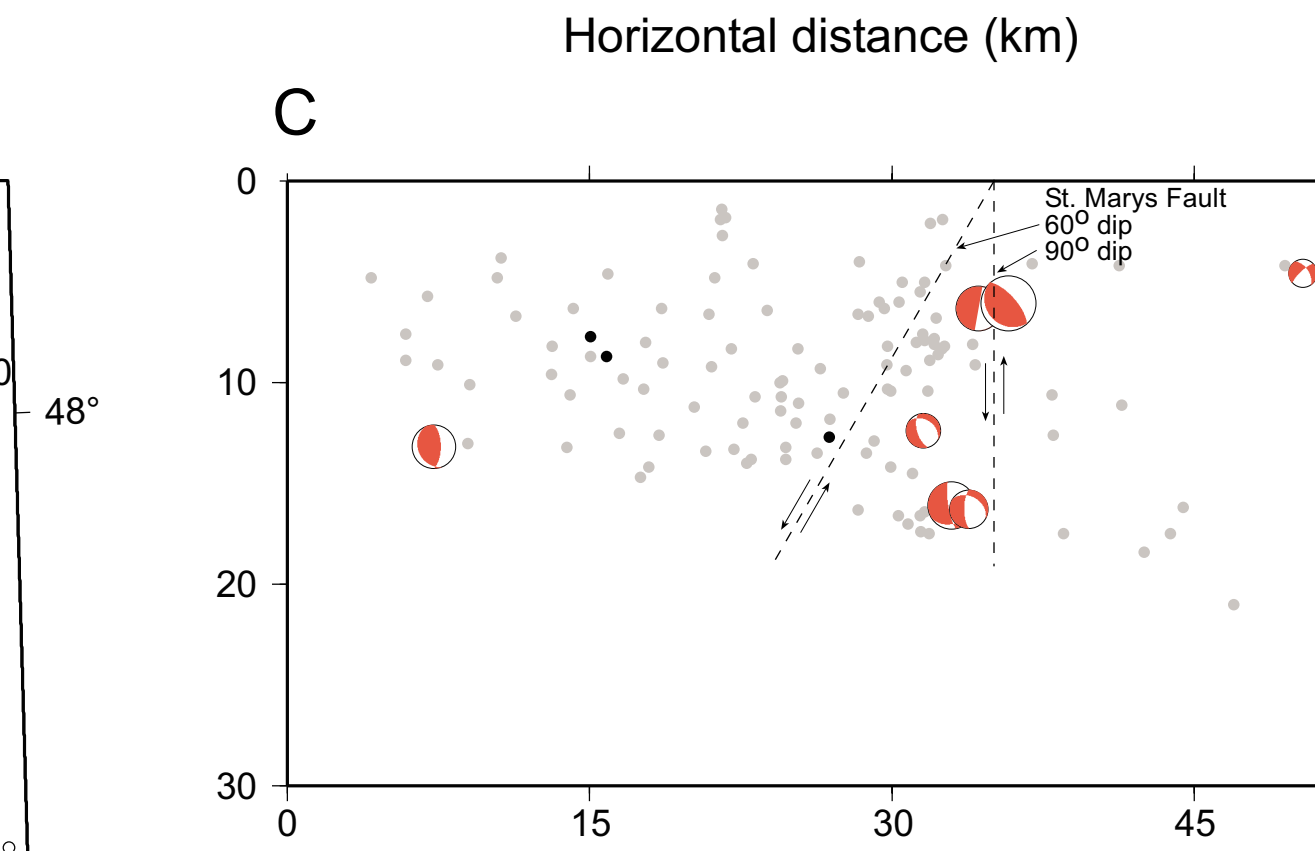
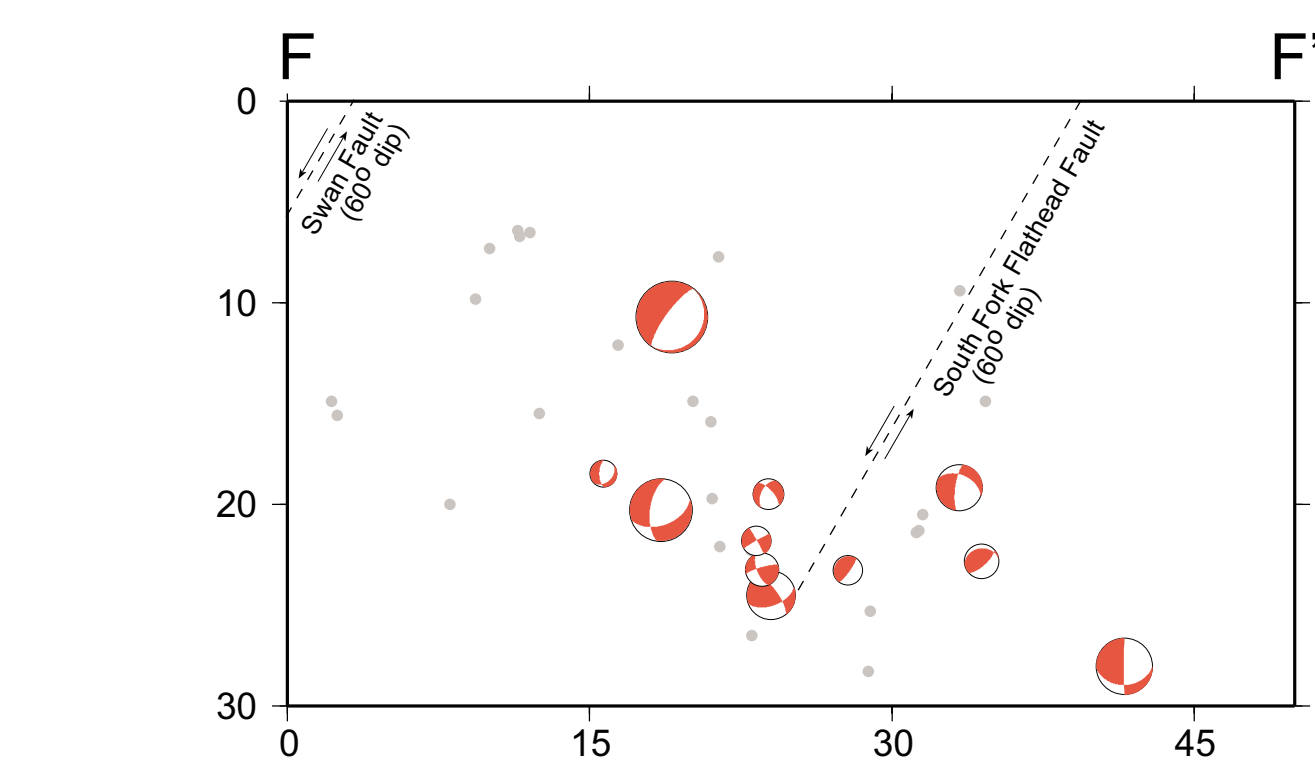
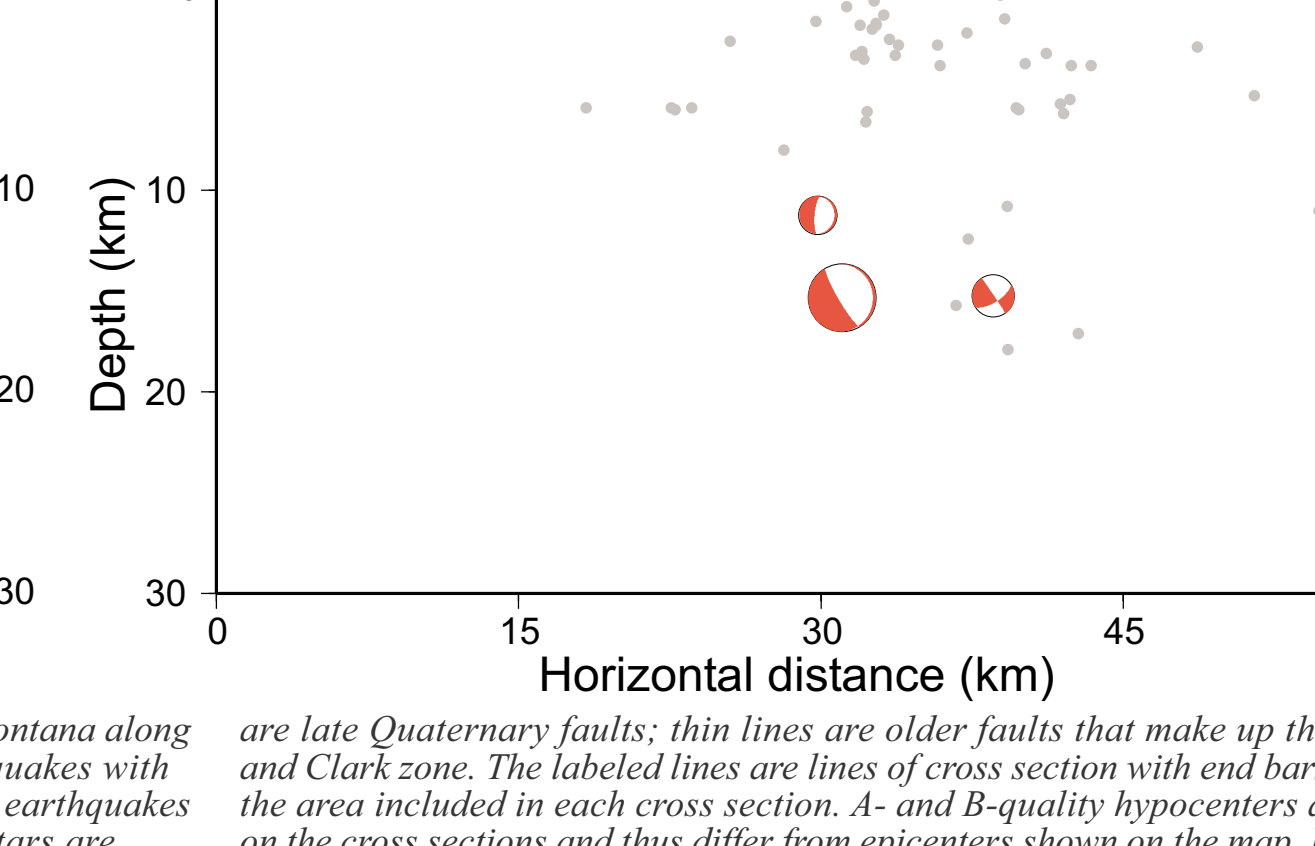
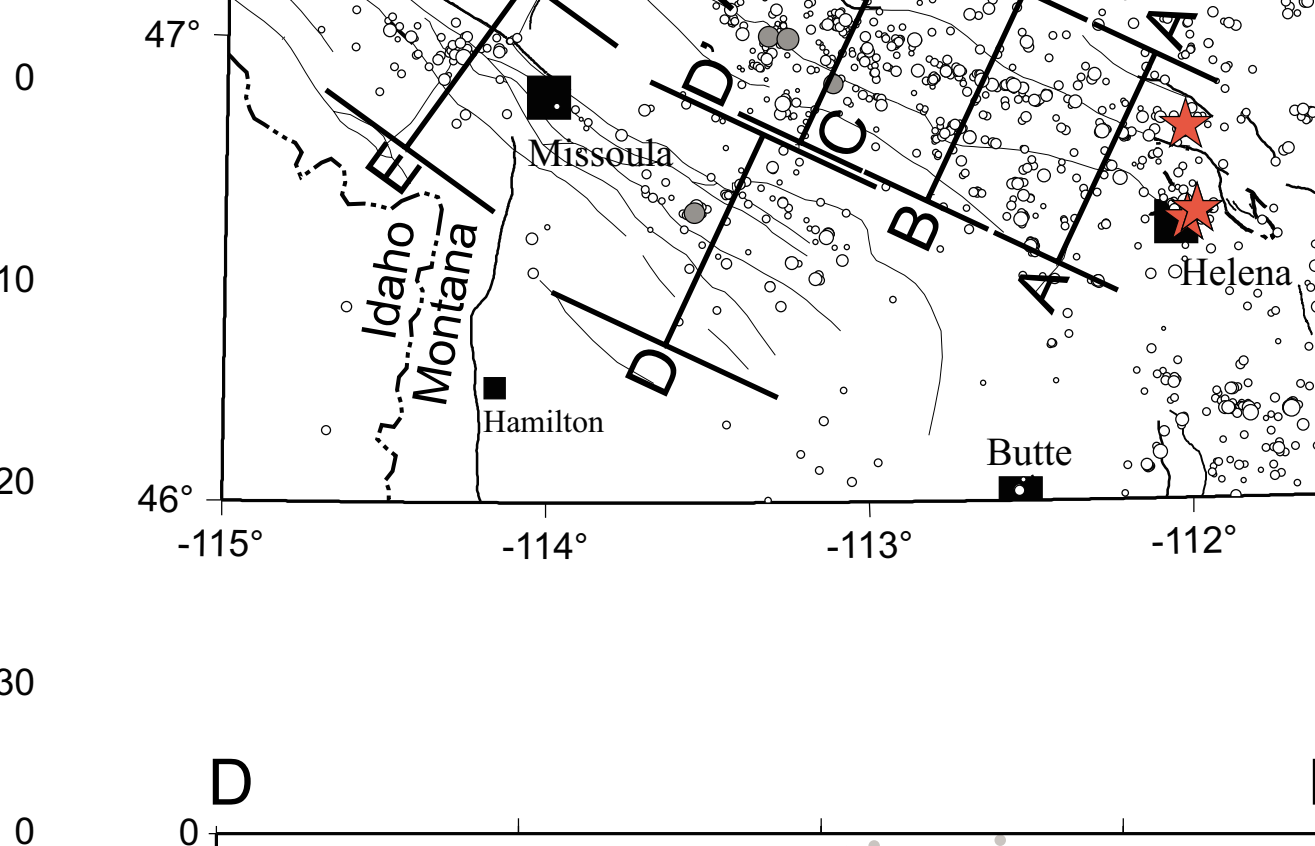
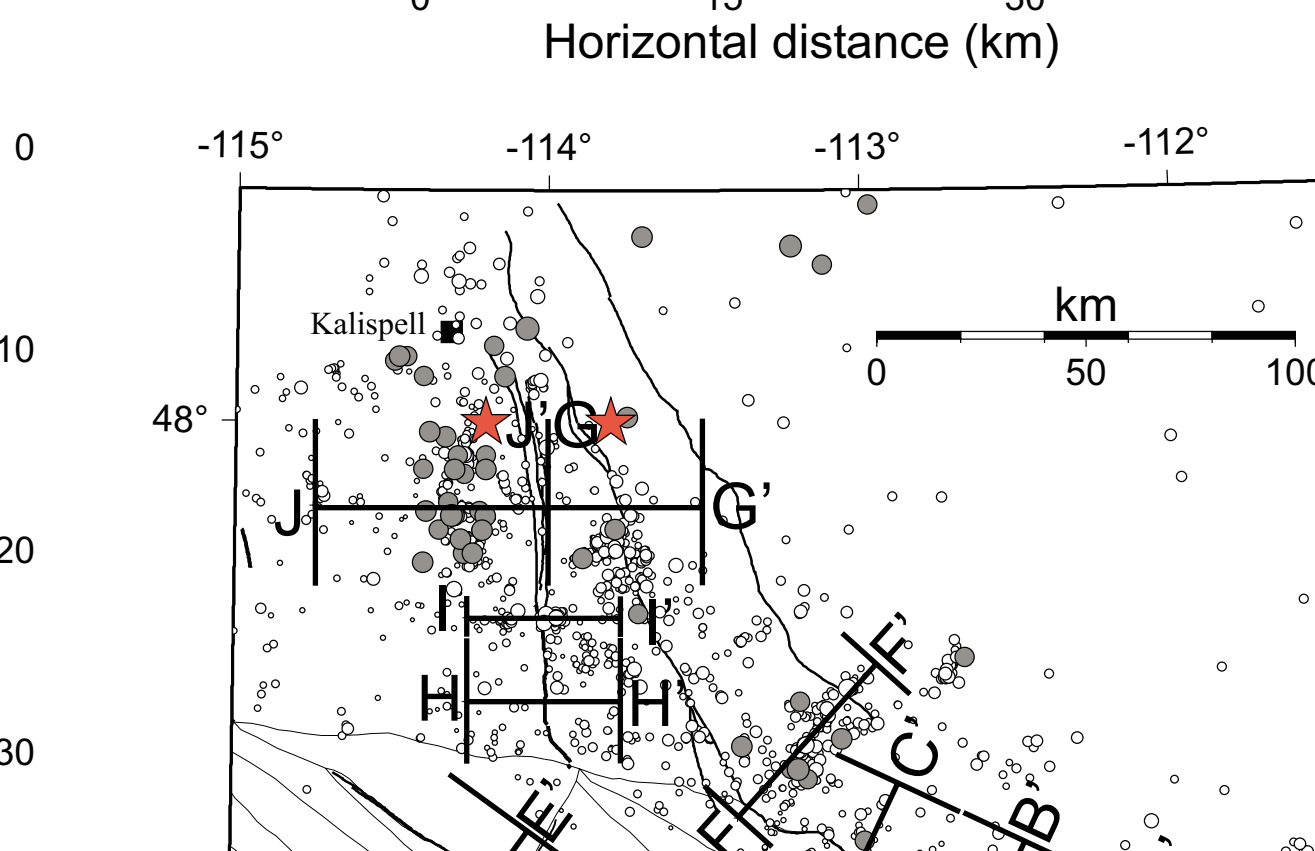
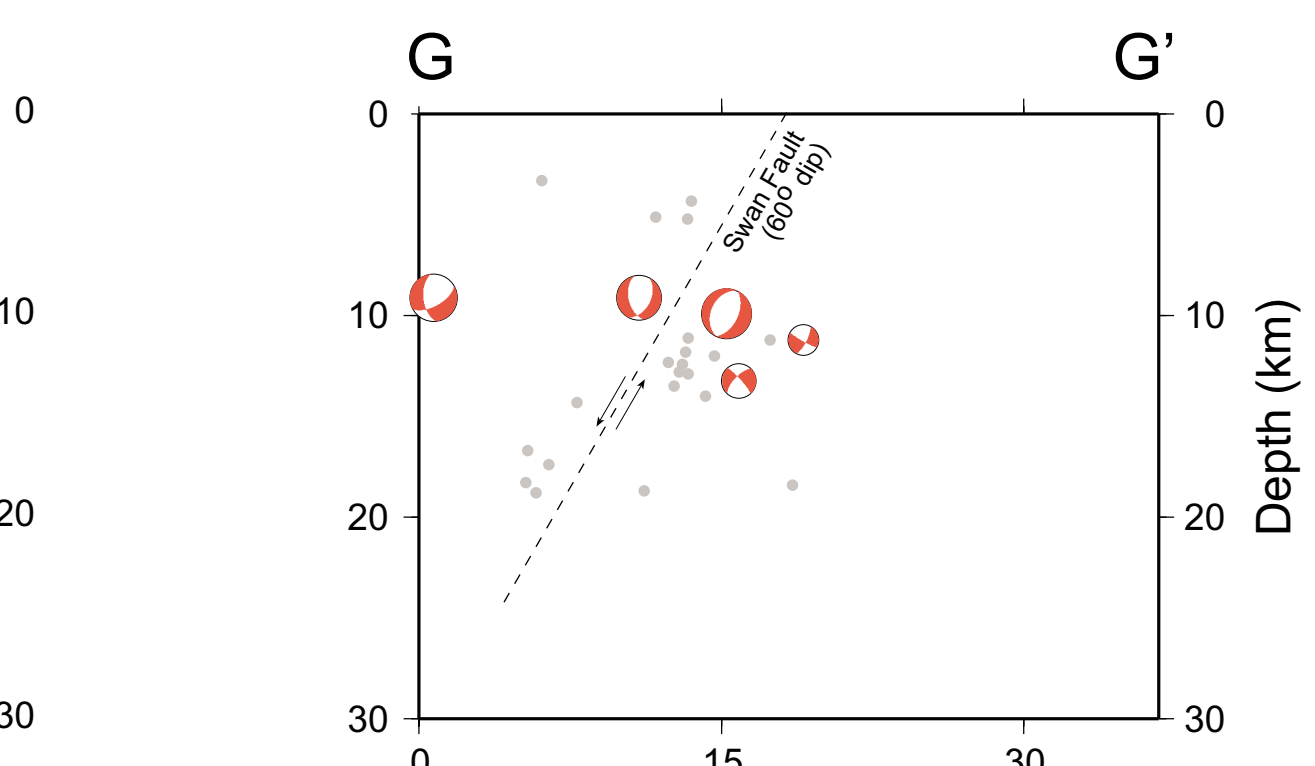
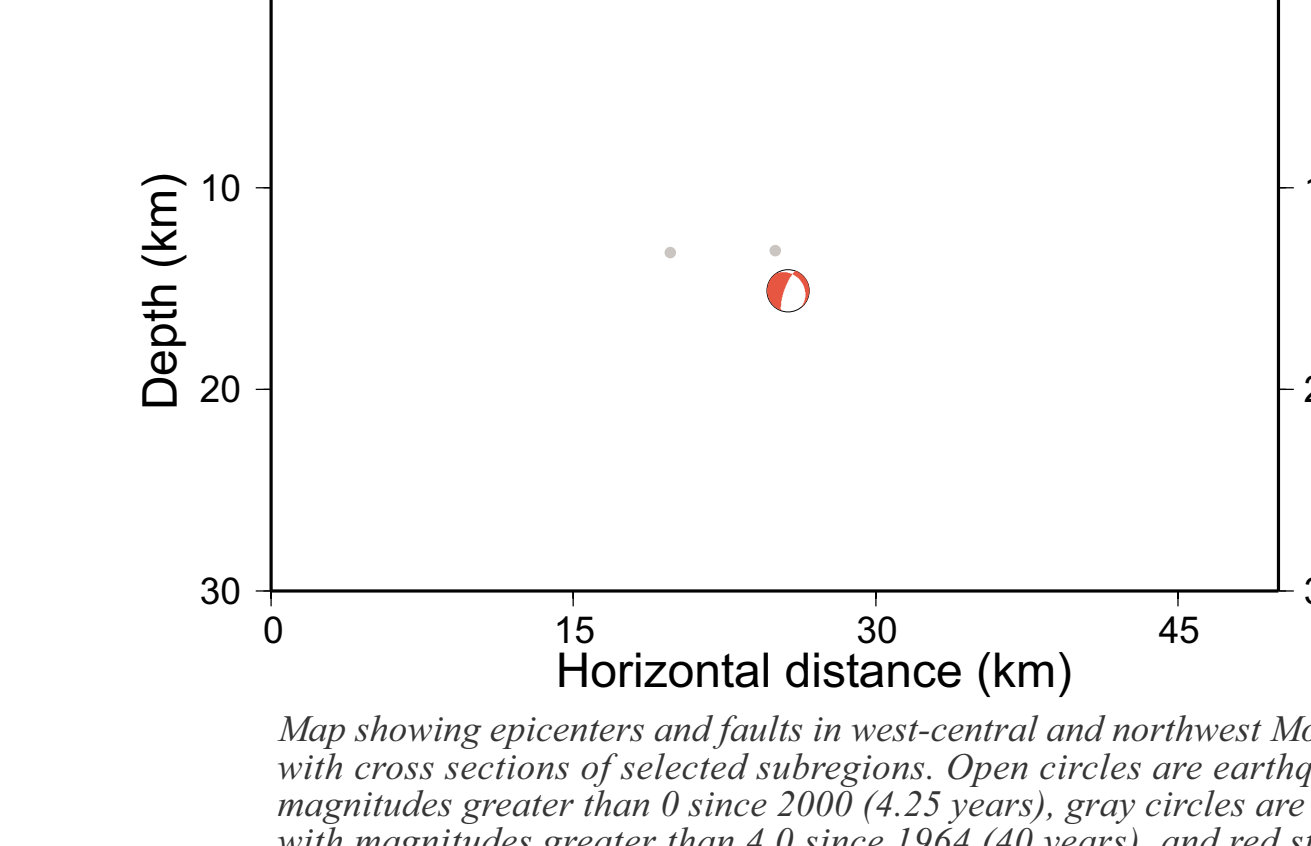
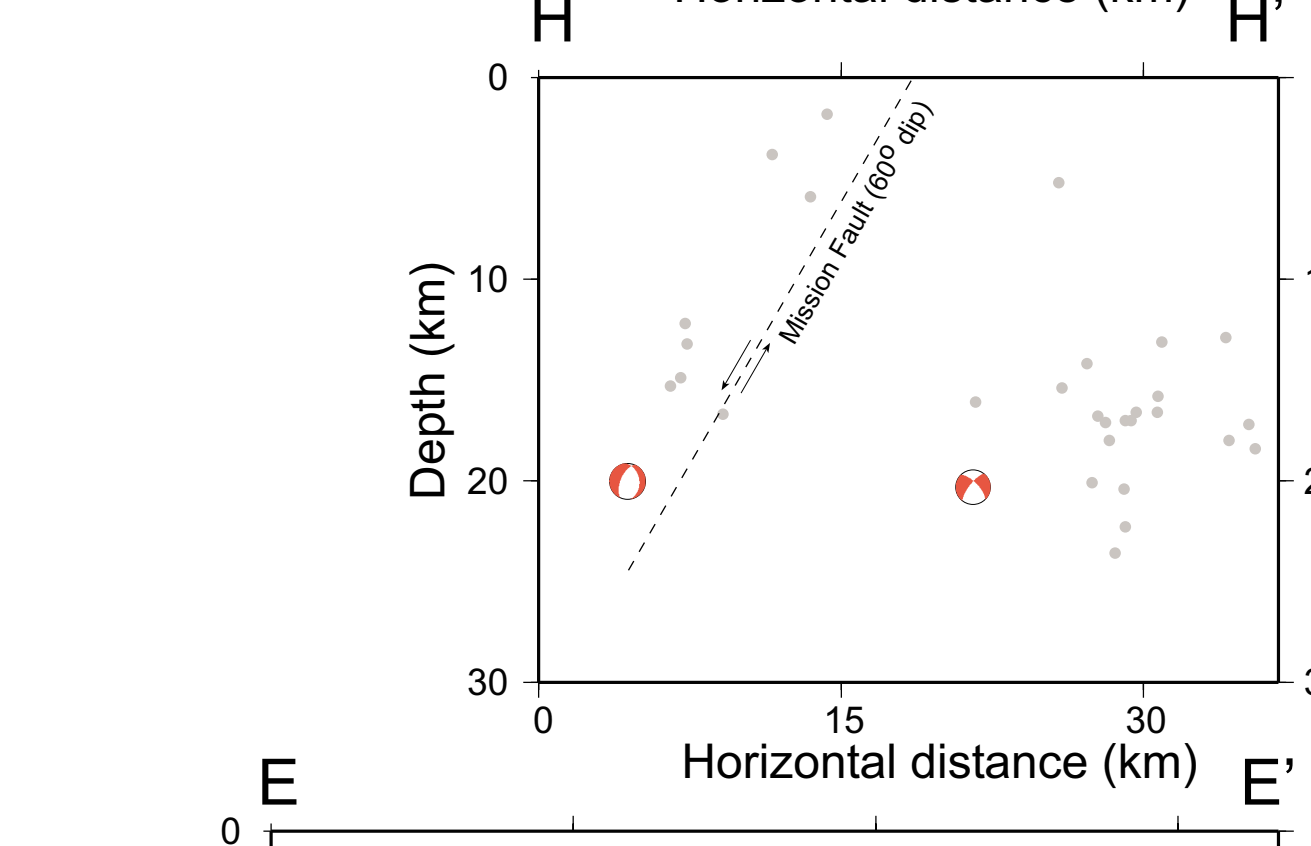
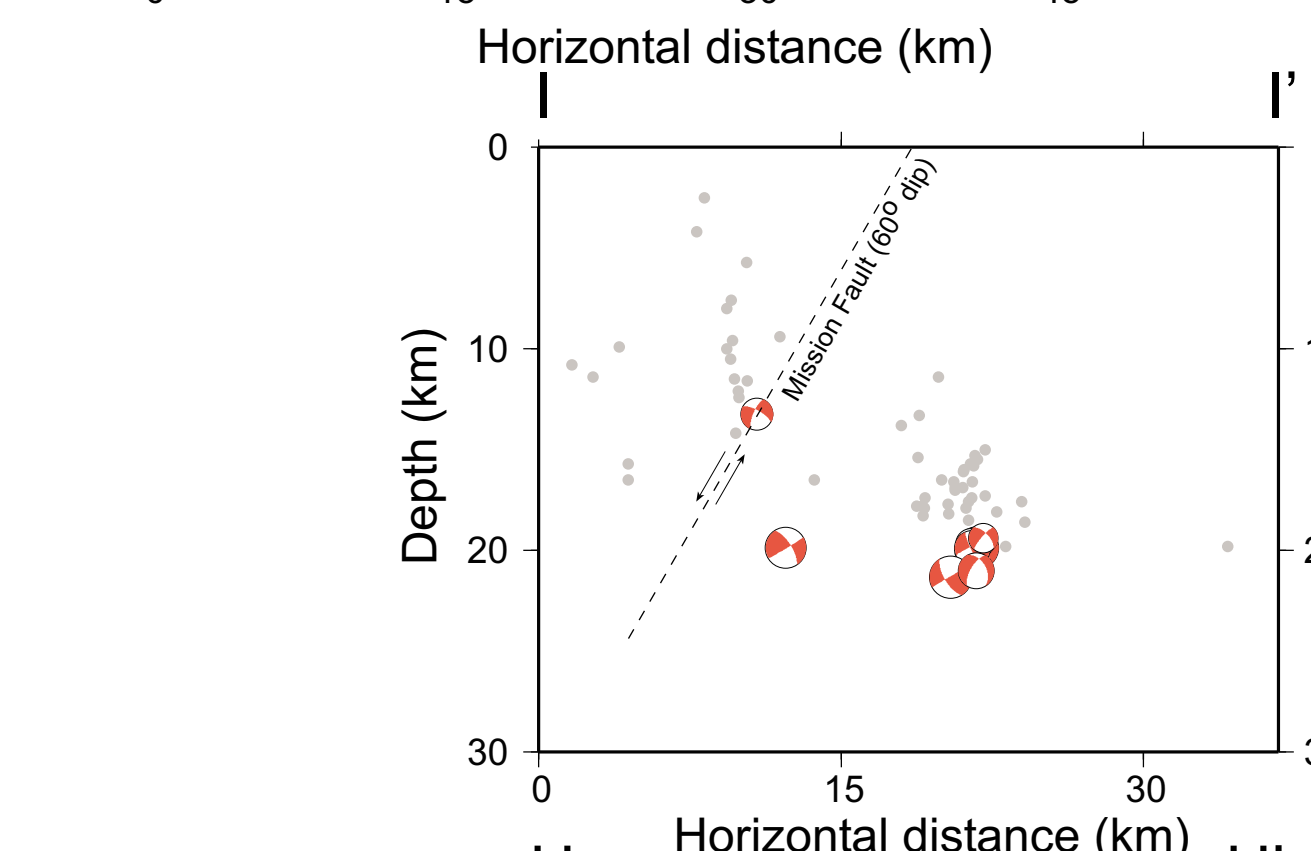
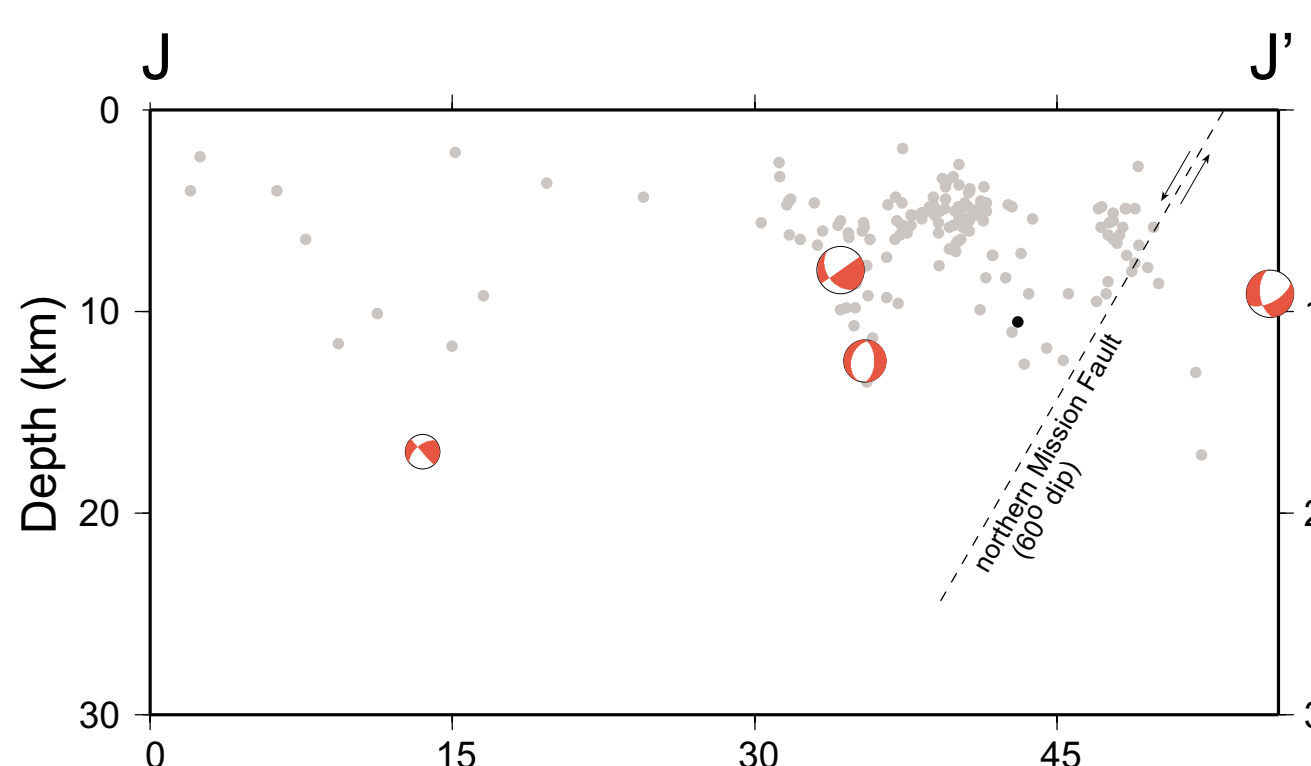
Earthquakes with strike-slip mechanisms. Other features are the same as in previous figure.



Earthquakes with oblique-slip mechanisms. Other features are the same as in previous figure.



T-axis (green) and P-axis (red) orientations for 86 fault plane solutions in northwestern and west-central Montana. Radial units are the number of P-axis orientations per 25 degrees, inner arrow shows dominant extension and compression directions.



Seismicity in western Montana generally coincides with regions traversed by Quaternary faults. However, very few of the faults that make up the LCZ have recognized late Quaternary faulting in the eastern LCZ may result from the dearth of field studies focusing on young faulting in the LCZ, low slip rates along these faults, glacial cover, and heavily forested regions. Also, low slip-rate strike-slip faults are probably more difficult to identify than low-slip-rate normal faults. In any case, we believe that our present understanding of the seismicogenic potential of LCZ faults may significantly underestimate the potential for moderate- to large-magnitude earthquakes in west-central Montana.

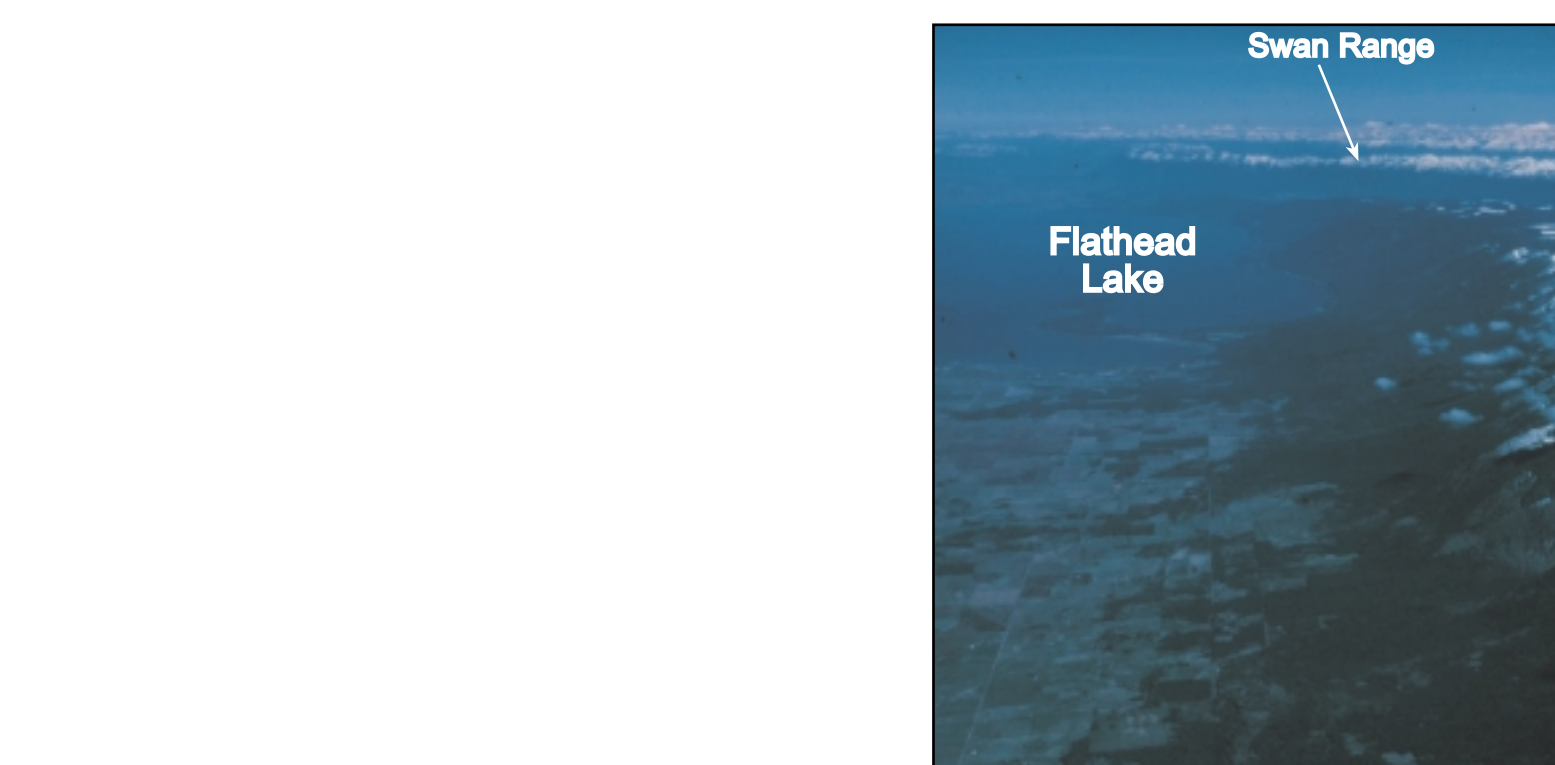
The northern Intermountain Seismic Belt seems to deflect westward at the latitude of Helena, where it intersects the Lewis and Clark fault zone before extending into northwestern Montana north of Missoula.



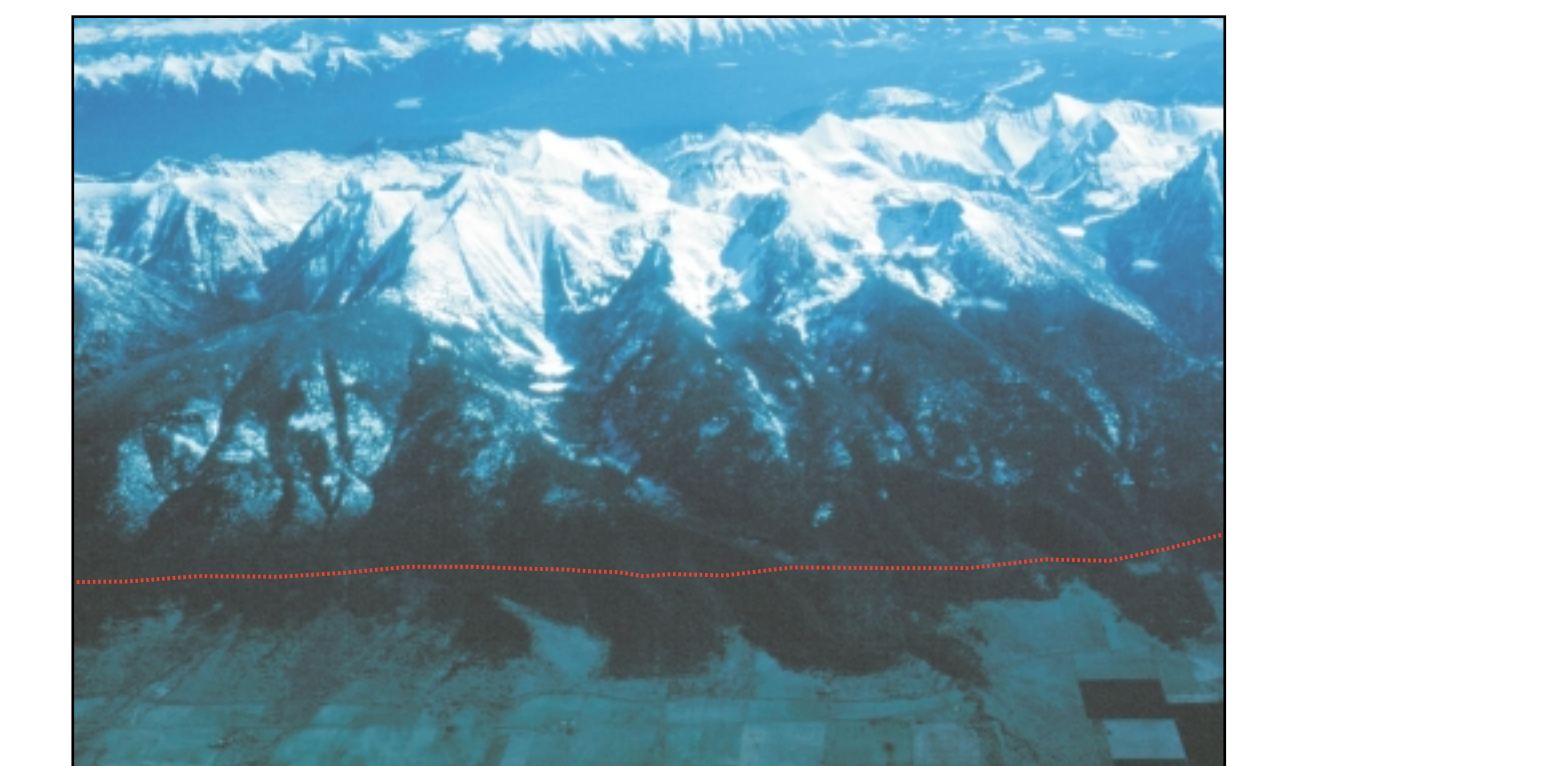
Southern Swan Range viewed to the NNW. The range front bands eastward as it approaches the northernmost faults of the Lewis and Clark zone. The Swan fault trends along the overstepped range front and passes through the saddle where the smaller fault-block ridge meets the main range front.



Southern Swan Range viewed to the NNW just to the north of the photo above. The overstepped range front just south of Flathead Lake is dissected and heavily forested. Field evidence for late Quaternary faulting has not yet been identified along this fault.



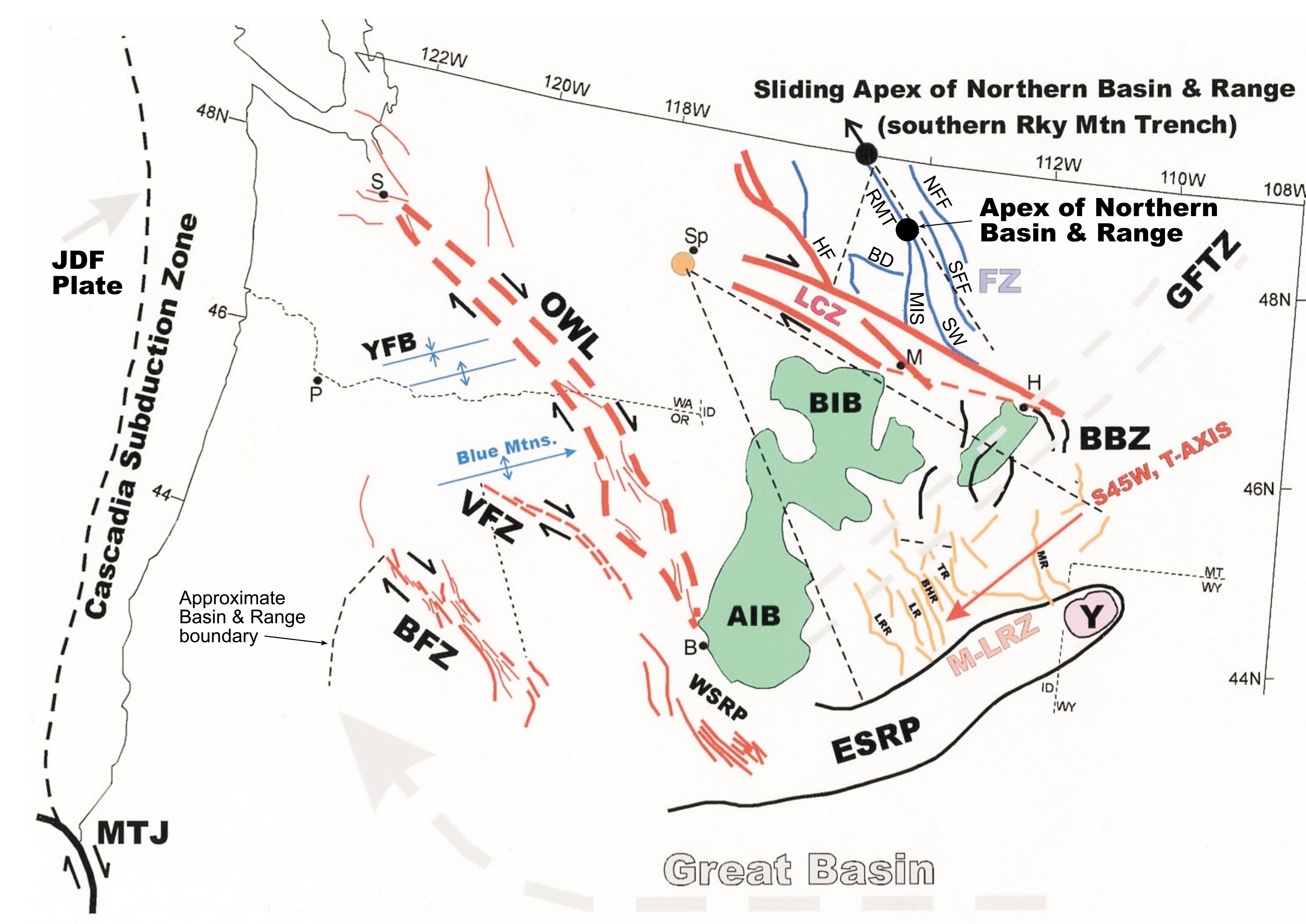
View north along the northern part of the Mission Range. Notice how the range elevation decreases northward. Holocene faulting is limited to the southern third of the range front (shown below).



View to the east of part of the southern Mission Range. The red dashed line marks the approximate location of the Mission fault, which last ruptured in a M7.5 earthquake approximately 7700 years ago. The Mission fault scarp is up to 7 m high and records multiple late Quaternary faulting events. The Swan Range is visible in the background.



View to the east of the southern Mission Range. Note the rapid decrease in the height of the range crest where it bends eastward just before intersecting the northernmost fault of the Lewis and Clark zone. Near its southern tip where the Mission fault trends southward, late Quaternary events reveal equal amounts of normal and dextral late Quaternary offset. To the north, where the fault trends due north, pure normal displacement is observed.



Kinematic model for contemporary extension of the Northern Rocky Mountains and Pacific Northwest. **BC** divide the northern Intermountain Seismic Belt into five major seismicogenic zones: 1) FZ, Flathead zone; 2) LCZ, Lewis and Clark zone; 3) BBZ, Big Belt zone; 4) AIB, Intermountain Seismic Belt; 5) ESRR, Snake River Plain. **YFB**, Yaltonia fold belt; **OWL**, Olympic-Wallowa lineament; **VFZ**, Vase fault zone; **BFZ**, Brothers fault zone; **JDF**, Juan de Fuca plate; **MTJ**, Mendocino triple junction; **CBC**, Helena; **M**, Missoula; **Sp**, Spokane; **B**, Boise; **S**, Seattle; and **P**, Portland.

## Discussion (continued)

Well-determined hypocenters in the foot-wall block of the southern Swan fault and in the vicinity of the southern Swan fault extend to depths at least 25 km below the surface. These earthquakes occur at depths 10 km deeper than typical seismicity elsewhere in the Intermountain seismic belt, suggesting the potential for proportionally larger earthquakes at a given surface rupture length.

## Regional Kinematic Model

We place the north end of the "structural" Basin and Range Province at the north end of the Flathead Valley where seismicity of the northern Intermountain seismic belt falls off dramatically. Between this northern apex of the Basin and Range and the eastern Snake River Plain, we subdivide the northern Rockies into five major extensional domains.

1) The Flathead zone lies north of the LCZ. All the major late Tertiary-Quaternary range-bounding normal faults within this region converge northward to an apex or pole in the northern Flathead Valley (southern Rocky Mountain Trench), about which they appear to "fan" in a clockwise sense with greater displacement southward. Numerous normal and strike-slip fault plane solutions throughout the Flathead zone demonstrate east-west extension consistent with future slip along these large normal faults.

2) East-west extension north of the LCZ is apparently transferred to right-lateral strike-slip faults within the eastern LCZ. The prevalence of strike-slip faulting within the LCZ suggests that it accommodates differential extension occurring north and south of the LCZ. Fault plane solutions within the LCZ show a slight counterclockwise rotation of the T-axes compared to T-axis orientation in the Flathead zone to the north. The LCZ appears to partition extensional strain across the region and, because it has a finite width and distinctive structural expression, is herein defined as a separate extensional domain. Areas south of the LCZ are extending westward relative to those to the north.

3) The Big Belt zone lies south of the LCZ and is characterized by north-south-trending range-bounding normal faults and valleys. The Big Belt zone includes the Boulder batholith and is undergoing east-west extension. 4) The Madison-Lost River zone is characterized by northwest-striking, highly segmented, range-front normal faults in southwest Montana and east-central Idaho. The Madison-Lost River zone is extending southwest, possibly rotating about a pole near Spokane, and that the Big Belt and Flathead zones are extending westward. Overall, the northern Rockies are extending westward in a clockwise rotating arc, subparallel to and segmented by the major transverse accommodation zones. The Idaho batholith, like the Sierra Nevada batholith (Bennett and others, 1999), may be moving west-northwest as a coherent, relatively rigid crustal block. As a guess, the horizontal velocity field may decrease from ~3 mm/year just north of the Snake River Plain to < 1 mm/year in the Flathead zone.

## Conclusions

Fault plane solutions indicate that seismicity along the northern Intermountain seismic belt in west-central and northwest Montana results from movement on strike-slip and normal faults in response to an east-west-oriented extensional stress field. Most earthquakes with normal faulting mechanisms occur north of the LCZ, while strike-slip and oblique-normal slip events occur both within and north of the LCZ. The vast majority of recent earthquakes do not correlate with mapped Quaternary faults. Unrecognized active strike-slip faults probably exist within the eastern half of the LCZ and the southern Swan fault is probably active. Well-determined hypocenters at depths of 25 km near the southern Mission and southern Swan faults imply a greater seismicogenic thickness than elsewhere in the Basin and Range Province. Future surface-rupturing earthquakes on these faults may be proportionally greater than earthquakes from equally long ruptures in other parts of the Basin and Range Province.

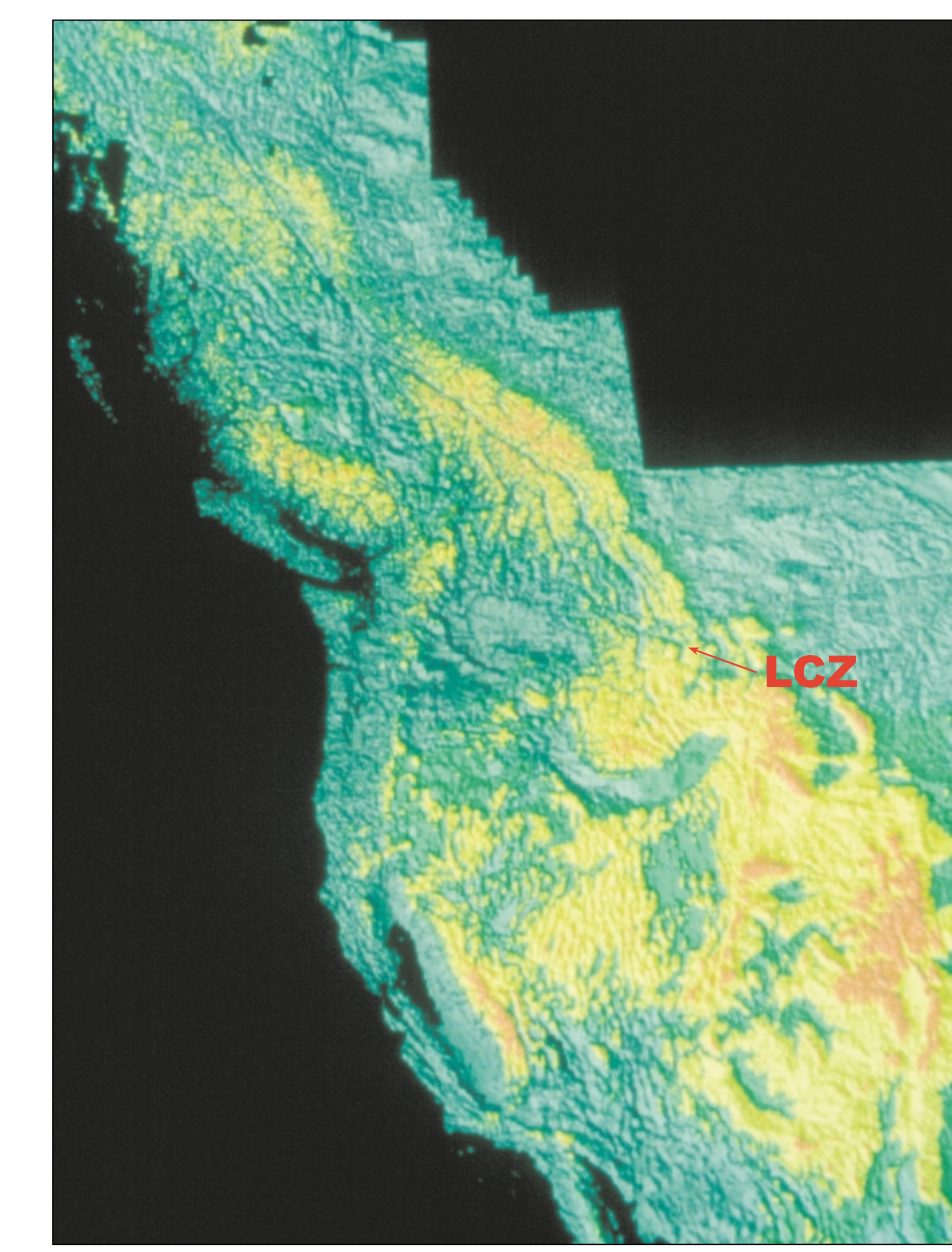
## References Cited

Anders, M.H., Geissman, J.W., Piety, L.A., and Sullivan, J.T., 1989, Parabolic distribution of circum-eastern Snake River Plain seismicity and latest Quaternary faulting: migratory pattern and association with the Yellowstone hot spot. *Journal of Geophysical Research*, v. 94, p. 1589-1962.  
Bennett, R.A., Davis, J.L., and Vermicke, B.P., 1999, Present-day pattern of Cordilleran deformation in the western United States. *Geology* v. 27, p. 371-374.  
Mann, G.M., and Meyer, C.E., 1993, Late Cenozoic structure and correlations to seismicity along the Olympic-Wallowa lineament, northwest United States. *Geological Society of America Bulletin*, v. 105, p. 853-871.  
Stickney, M.C., and Bartholomew, M.J., 1987, Seismicity and late Quaternary faulting of the northern Basin and Range Province, Montana and Idaho. *Seismological Society of America Bulletin*, v. 77, p. 1602-1625.  
Thatcher, W., Foulger, G.R., Julian, B.R., Svare, J., Quilty, E., and Bawden, G.W., 1999, Present-day deformation across the Basin and Range Province, western United States. *Science*, v. 283, p. 1714-1718.

5) The Idaho batholith, lying west of the Big Belt Valley where seismicity of the northern Intermountain seismic belt falls off dramatically. Between this northern apex of the Basin and Range and the eastern Snake River Plain, we subdivide the northern Rockies into five major extensional domains.

From north to south, the LCZ, Olympic-Wallowa lineament, Vale and Brothers fault zones have partitioned extension across the northern Basin and Range province, along with a host of smaller northeast-trending accommodation zones and transfer faults (Mann and Meyer, 1993). Each zone involves varying amounts of right-lateral strike-slip and right-oblique offset, with south-side blocks moving westward relative to north-side blocks. Consequently, these zones have partitioned extensional strain into ever-smaller domains of crustal extension in a northward direction, eventually terminating the structural Basin and Range in the northern Flathead Valley.

Recent continuous GPS and very long baseline interferometry geodetic studies south of the Snake River Plain have documented a westward and northward horizontal velocity field for the western U.S., partitioned by major belts of seismicity (Bennett and others, 1999; Thatcher and others, 1999). This type of research is in its infancy in the northern Basin and Range and few results are available. If the horizontal velocity field reflects the orientation of major Tertiary-Quaternary fault systems, as seems to be the case south of the Snake River Plain, then we could predict as a first-order approximation that the Madison-Lost River zone is extending southwest, possibly rotating about a pole near Spokane, and that the Big Belt and Flathead zones are extending westward. Overall, the northern Rockies are extending westward in a clockwise rotating arc, subparallel to and segmented by the major transverse accommodation zones. The Idaho batholith, like the Sierra Nevada batholith (Bennett and others, 1999), may be moving west-northwest as a coherent, relatively rigid crustal block. As a guess, the horizontal velocity field may decrease from ~3 mm/year just north of the Snake River Plain to < 1 mm/year in the Flathead zone.



Digital elevation model of western North America showing the relationship of the Lewis and Clark zone (LCZ) to surrounding tectonic elements.

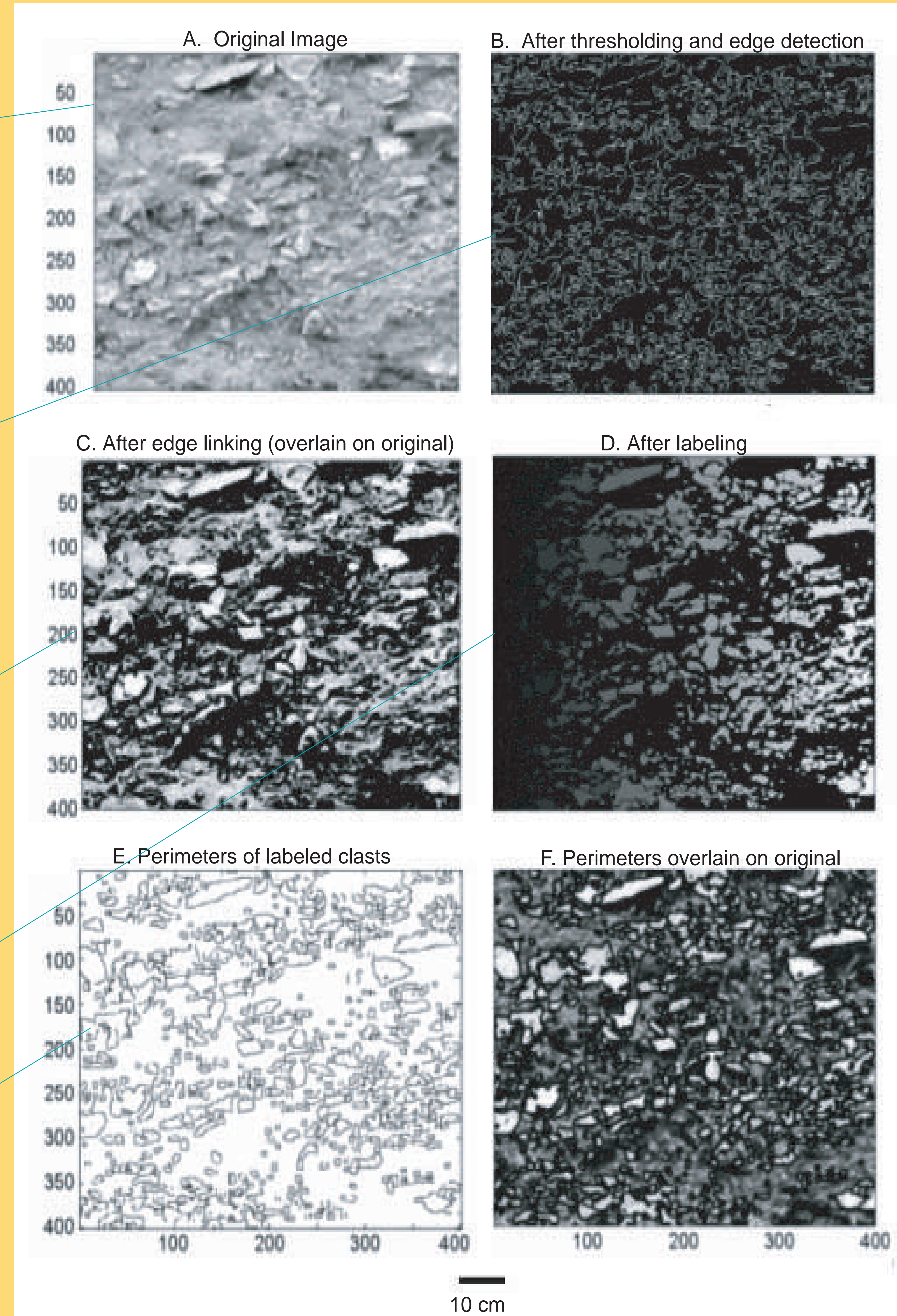
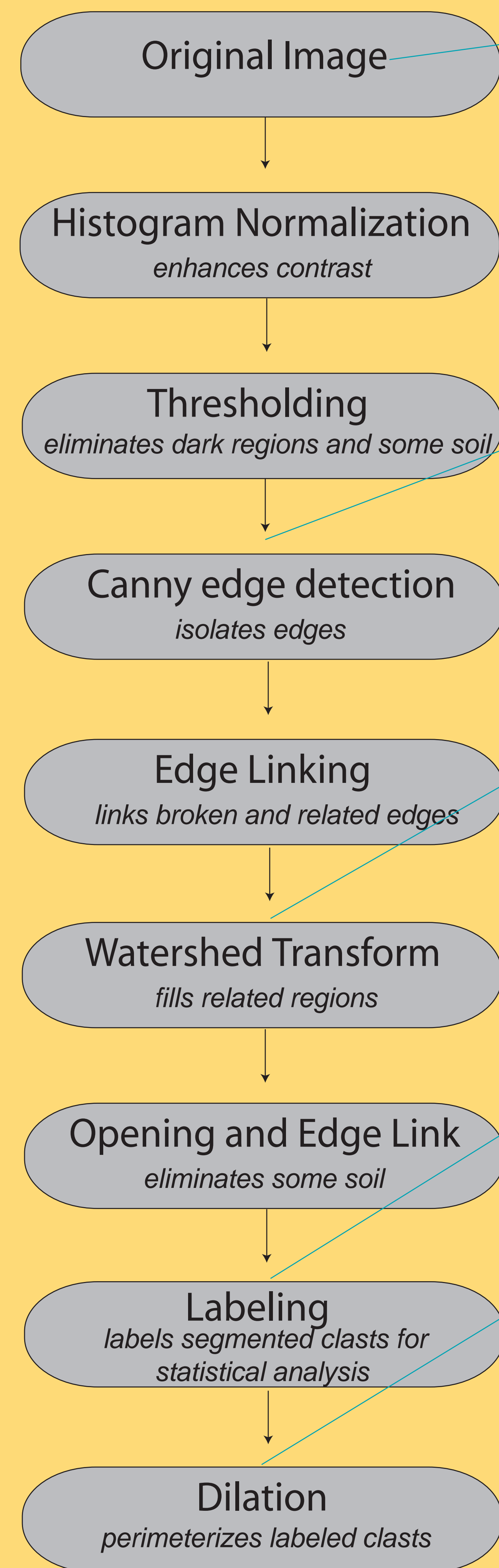
# Digital trench wall logging: Applying morphological image processing techniques to trench wall stratigraphy

Wasatch fault 2003 trench at Mapleton Utah

Julie B. Willis, Chaiwoot Boonyasiriwat, Gerald T. Schuster, Christopher B. DuRoss  
University of Utah

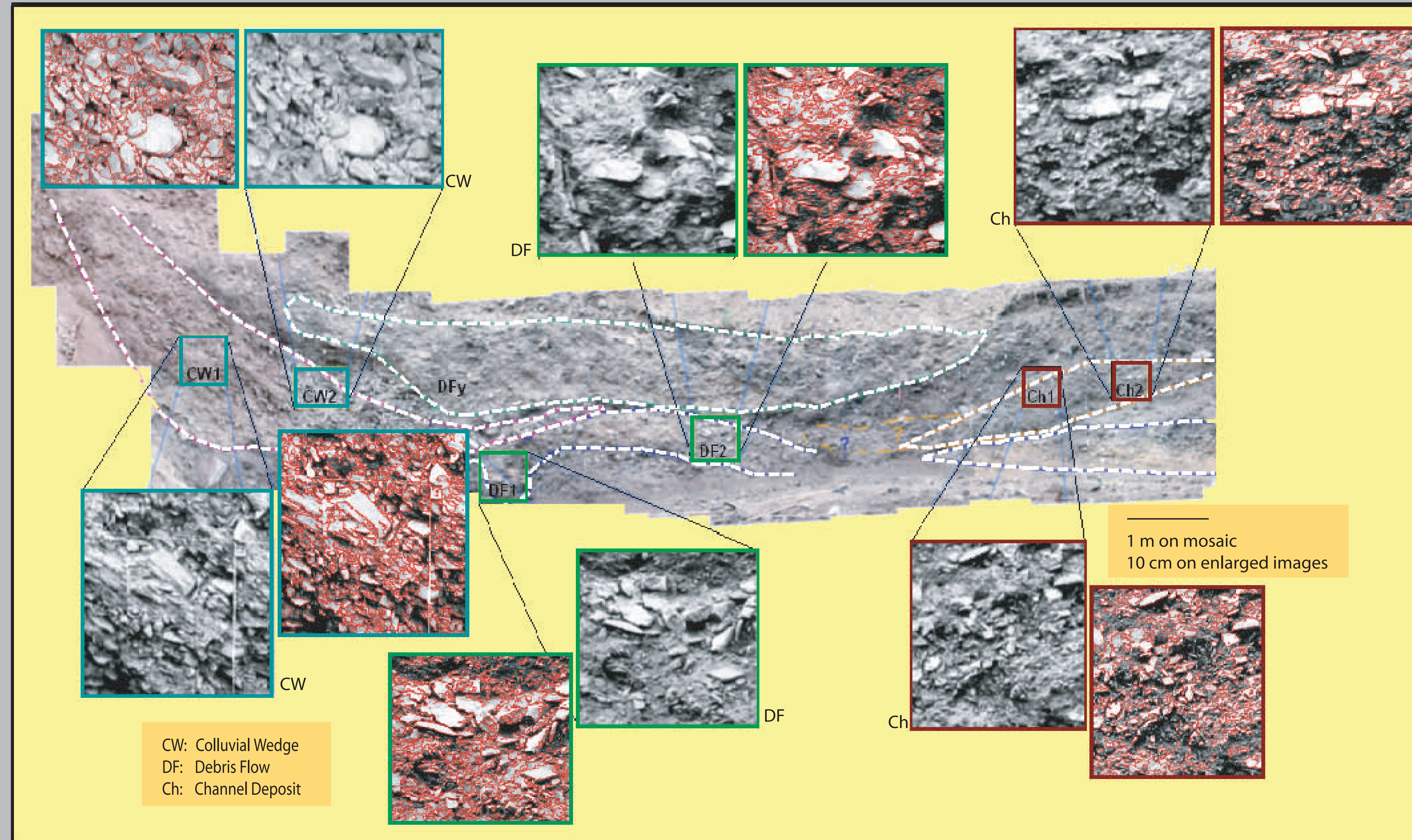
Traditionally trench walls are hand logged to separate clasts exposed in the walls from matrix fill. Hand logging is subject to human error and does not lend itself readily to statistical analysis of the sediments. We developed an algorithm of morphological image processing techniques that autonomously separates clast from matrix and generated dimensional and orientation statistics for the separated clasts. The algorithm was developed and tested using digital photos of a section of Level 1 of a 2003 trench across the Wasatch fault near Mapleton, Utah. The algorithm uses MatLabTM software with the image processing add-on.

## Processing Flowchart

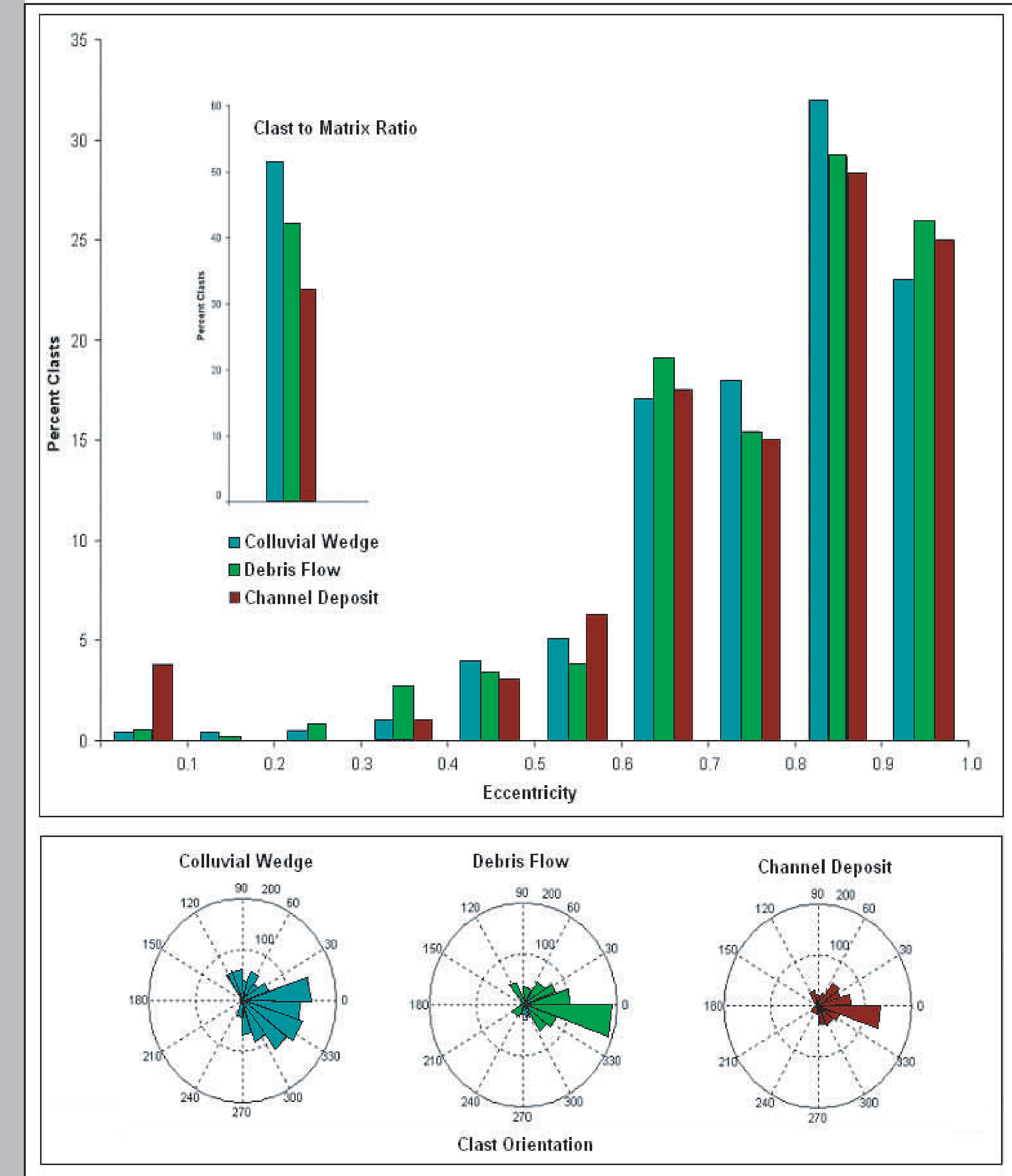


Flowchart and selected images that illustrate the morphological clast segmentation algorithm. The numbers are pixels. How well do you think the algorithm separated clasts from matrix?

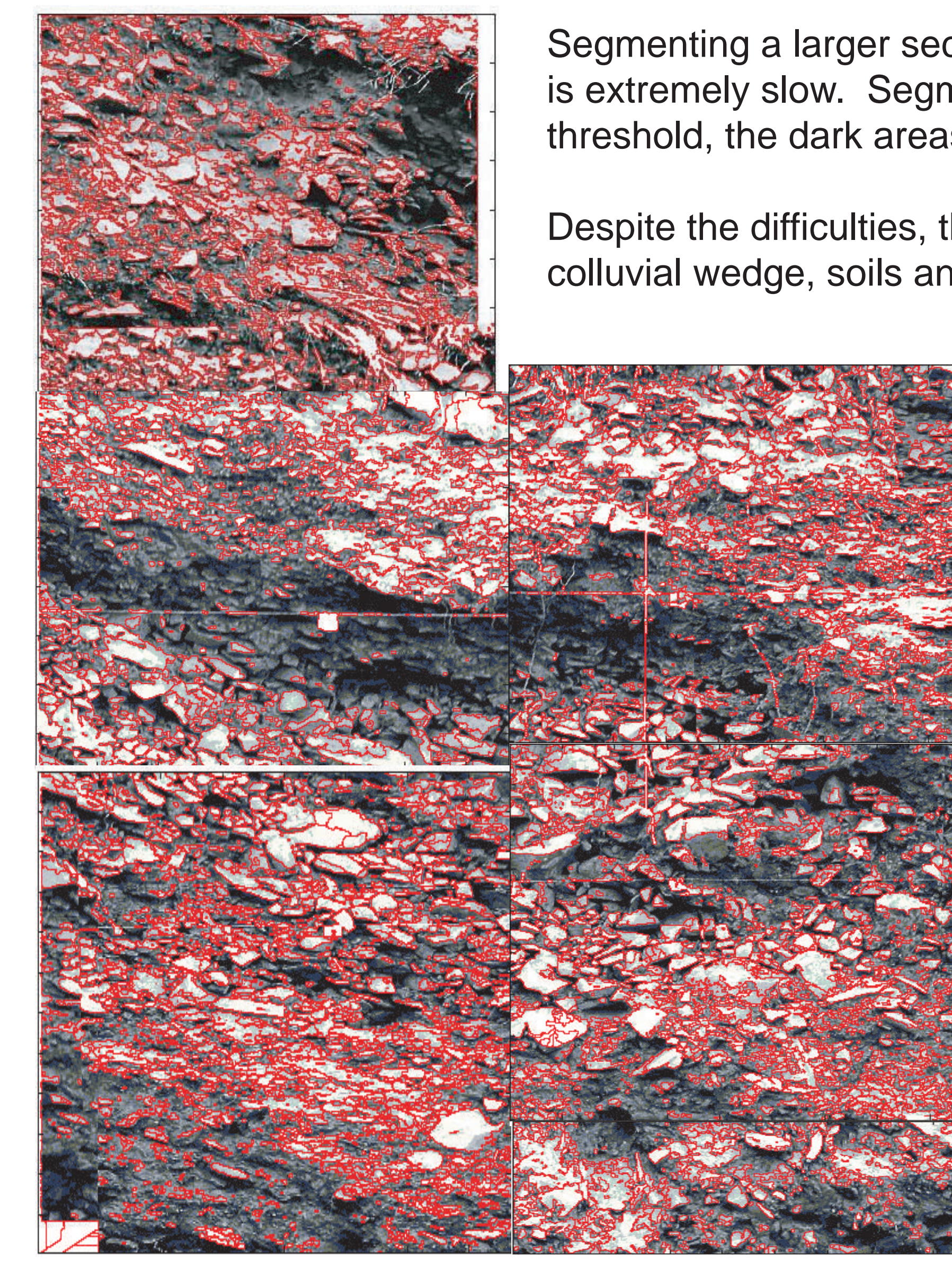
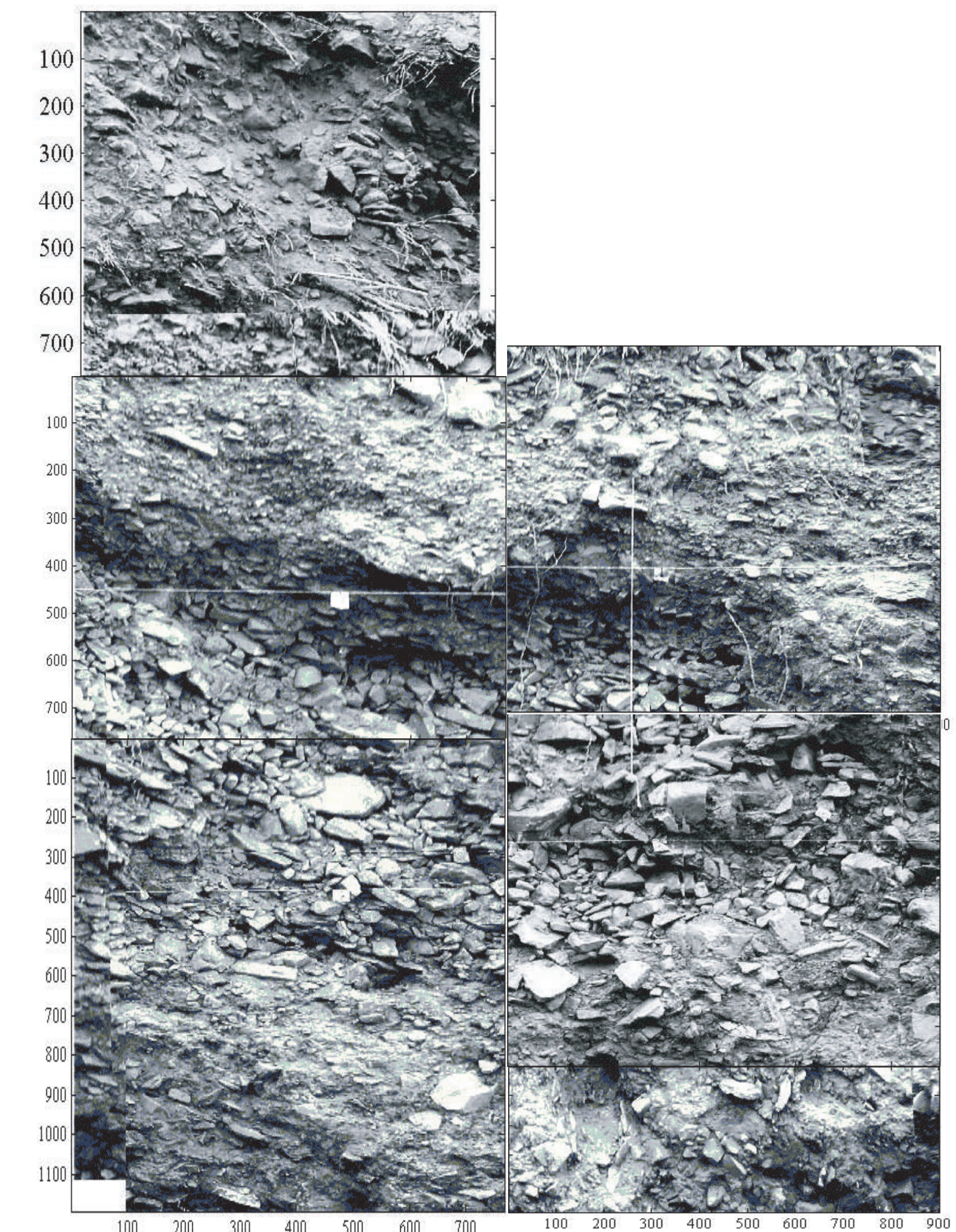
Eccentricity, orientation, size, ratio of clasts to matrix, and other statistics can be calculated quickly for segmented clasts.



Statistics were calculated for the outlined regions of the Mapleton, Utah 2003 megatrench across the Wasatch fault (Level 1, Sections 1 to 10).



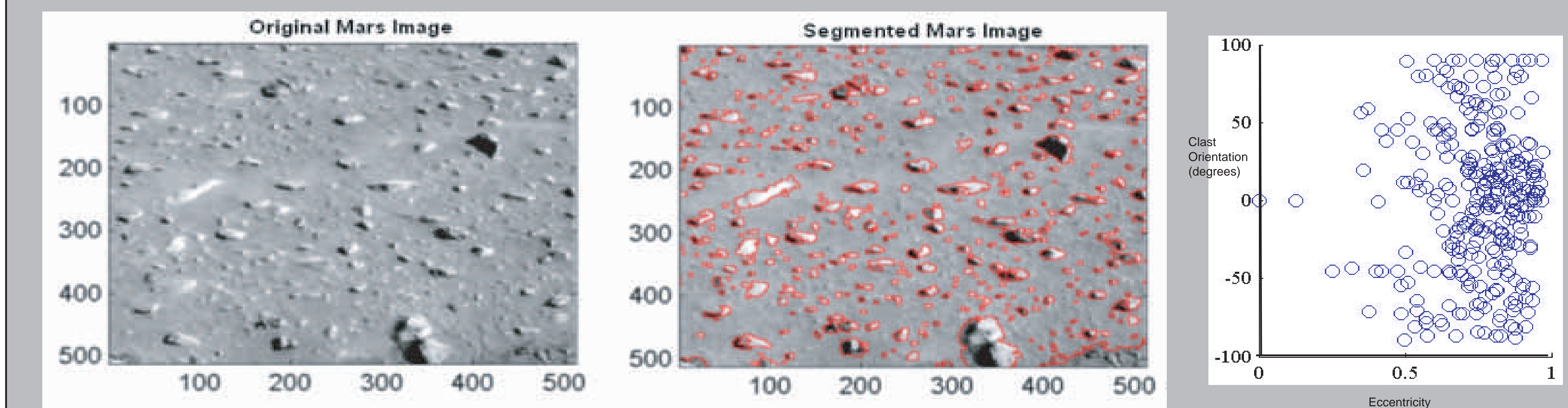
2938 clasts analyzed. Clasts less than 0.3 cm<sup>2</sup> were eliminated before analysis. Standard deviation eccentricity: 0.16 (colluvial wedge), 0.15 (debris flow), 0.20 (channel deposit). Standard deviation orientation: 48.6 (colluvial wedge), 39.0 (debris flow), 40.2 (channel deposit). Standard deviation area: 14.3 (colluvial wedge), 17.3 (debris flow), 28.4 (channel deposit).



Segmenting a larger section of the Mapleton Utah trench met with marginal success. Processing images larger than 1000 x 1000 is extremely slow. Segmentation of larger images was not only slow, but it was less accurate. Images that contain both very light and very dark areas were difficult to threshold, the dark areas were not segmented or the light areas were grossly over-segmented.

Despite the difficulties, the segmented clasts show fabric and general size of clasts within a section; lines based on segmentation show possible location of colluvial wedge, soils and debris flow. The optimal size of an image for processing is 400 pixels by 400 pixels. In the trench that is about 40 x 40 cm.

Other applications for the technique are abundant. Applications we've thought of include segmenting rocks in landslides on earth and Mars, mapping and statistically analyzing glacier crevasses, stream braiding density, down-borehole images, and the surface of Mars as shown below. What ideas do you have for using segmentation and statistical analysis?



## EXTENDED ABSTRACTS

SEGMENTATION AND HOLOCENE DISPLACEMENT HISTORY OF THE GREAT SALT LAKE FAULT, UTAH *by David A. Dinter and James C. Pechmann, University of Utah Department of Geology and Geophysics*

DIGITAL TRENCH WALL LOGGING: APPLYING MORPHOLOGICAL IMAGE PROCESSING TECHNIQUES TO TRENCH WALL STRATIGRAPHY *by Julie B. Willis<sup>1</sup>, Chaiwoot Boonyasiriwat<sup>2</sup>, Gerard T. Schuster<sup>1</sup>, and Christopher B. DuRoss<sup>1</sup>*

*(<sup>1</sup>University of Utah, Department of Geology and Geophysics, <sup>2</sup>University of Utah, Department of Computational Engineering and Science)*

## ***SEGMENTATION AND HOLOCENE DISPLACEMENT HISTORY OF THE GREAT SALT LAKE FAULT, UTAH***

David A. Dinter and James C. Pechmann  
University of Utah Department of Geology and Geophysics  
135 South 1460 East, Rm. 719 WBB, Salt Lake City, UT 84112-0111  
E-mail: [dadinter@mines.utah.edu](mailto:dadinter@mines.utah.edu) and [pechmann@seis.utah.edu](mailto:pechmann@seis.utah.edu)

The Great Salt Lake fault (GSLF) is an active, segmented, west-dipping normal fault submerged beneath the Great Salt Lake 10-30 km west of the Ogden-Salt Lake City metropolitan area and 30-65 km west of the Wasatch fault (Fig. 1). A discontinuous topographic high defined from north to south by the Promontory Mountains and Fremont and Antelope Islands marks the footwall of the GSLF. The north and south main basins of the Great Salt Lake, which contain up to 4000 meters of Neogene sediment, lie to the west in its hanging wall. Using Geopulse and Chirp high-resolution seismic reflection profiling, we mapped the active traces of the GSLF and auxiliary faults south of Promontory Point and imaged hanging-wall tectonostratigraphic geometries indicative of six Holocene surface-rupturing earthquakes. We cored the seismic event horizons, dated them by radiocarbon methods, and calculated the average recurrence interval of large earthquakes from the dates obtained.

A neotectonic map constructed from 40 seismic profiles crossing the GSLF and some 20 additional lines crossing the basin to the west delineates two major normal fault segments south of Promontory Point, separated by a 1-2-km left step west of northern Antelope Island (Fig. 1). The southern (Antelope) segment is 35 km long (straight line, tip-to-tip) and has a prominent lakebed scarp with up to 3.6 m relief. It bends sharply to the southwest near its southern terminus, where displacement is apparently transferred to the Oquirrh fault zone. The Fremont segment is 30 km long and has no lakebed scarp along most of its length. Active traces of one or more additional segments to the north, submerged beneath the north arm of the lake west of the Promontory Peninsula, have not yet been fully profiled or mapped. Normal fault empirical relationships for both rupture length and rupture area predict maximum event magnitudes ( $M_w$ ) of 6.9 for the Antelope segment and 6.8 for the Fremont segment (Wells and Coppersmith, 1994, BSSA, v. 84, 974-1002). The maximum net vertical tectonic displacement of  $5.5 +0.5/-0.8$  m associated with the most recent Antelope segment earthquake is consistent with a magnitude ( $M_w$ ) as great as 7.1.

Surface ruptures of GSLF segments produce tectonic event horizons in hanging-wall deposits within ~1 kilometer of the main fault trace that are recognizable on high-resolution seismic reflection profiles. Tectonostratigraphic geometries imaged in post-Bonneville (post-13.5 ka) hanging-wall deposits include coseismic bedding rotations and stratigraphically limited subsidiary faults, and displacement-related onlap surfaces and angular unconformities (Figs. 2 and 3). These features delineate event horizons associated with the three most recent earthquakes each on the Antelope and Fremont segments.

To obtain material for radiocarbon dating, continuous cores were collected from hanging wall deposits near the center of each fault segment using a hydraulic-assisted piston corer deployed from a

barge. Five of the six recognized event horizons occur within Holocene clastic lacustrine sediment, from which was separated nonwood charcoal presumed to derive primarily from grass and brush fires on slopes and in valleys surrounding the Great Salt Lake. The sixth event horizon, the earliest imaged on the Fremont segment, falls within a 12-meter-thick pre-Holocene salt and sapropel unit. A maximum date for this event was obtained from charcoal contained in clastic deposits immediately beneath the salt interval. The radiocarbon dates are summarized in Table 1. Our results indicate single-segment recurrence intervals ranging from 3260 (+150/-180) to 5580 (+220/-170) years on the Antelope and Fremont segments of the Great Salt Lake fault, with a mean single-segment recurrence interval of  $4200 \pm 1400$  years.

**Table 1.** Earthquake recurrence intervals, Great Salt Lake fault

Earthquake pairs	Dates of occurrence (terrestrially calibrated <sup>1</sup> , residence- corrected <sup>2</sup> calendar yr BP <sup>3</sup> ) <sup>4</sup>	Recurrence interval (yr) <sup>4</sup>
<b>Antelope Island segment (<math>M_w[\max]^5 \leq 7.1 \pm 0.4</math>)</b>		
EH-A3	586 +201/-241	5584 +219/-172
EH-A2	6170 +236/-234	
EH-A2	6170 +236/-234	3728 +223/-285
EH-A1	9898 +247/-302	
<b>Fremont Island segment (<math>M_w[\max]^5 = 6.8 \pm 0.3</math>)</b>		
EH-F3	3150 +235/-211	3262 +151/-184
EH-F2	6412 +209/-211	
EH-F2	6412 +209/-211	< 5015 +587/-424
EH-F1	< 11,427 +605/-449	
<b>Average single-segment recurrence interval<sup>6</sup> = <math>4200 \pm 1400</math> years</b>		

1 - Raw <sup>14</sup>C years were converted to calendar years using Stuiver et al. (1998) terrestrial calibration (CALIB v. 4.3).

2 - Correction for carbon residence time in provenance area prior to deposition = -321 +191/-171 cal yr, the difference between the terrestrially calibrated <sup>14</sup>C date of Mazama ash interval at Site GSL00-3 (= 7994 +170/-128 cal yr BP) and terrestrial calibration (= 7673 +113/-86 cal yr BP) of published Mazama <sup>14</sup>C age (= 6845 ± 50 <sup>14</sup>C yr BP; Bacon, 1983, JVGR, v. 18, 57-115).

3 - Calendar years before 1950.

4 - Errors shown are 2 sigma.

5 - Errors shown are 1 sigma

6 - The mean, with 2 sigma error bars, for the three closed recurrence intervals

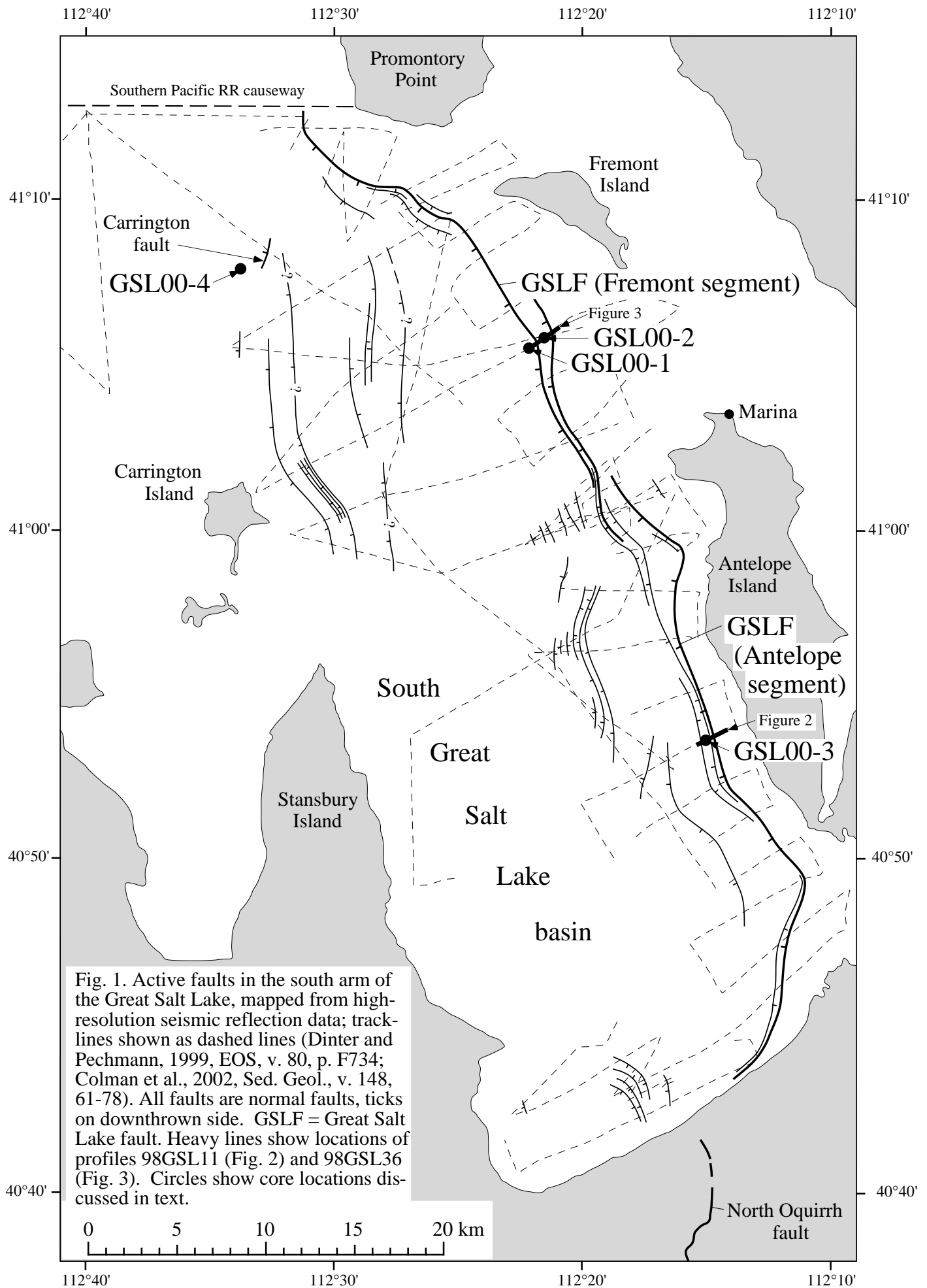
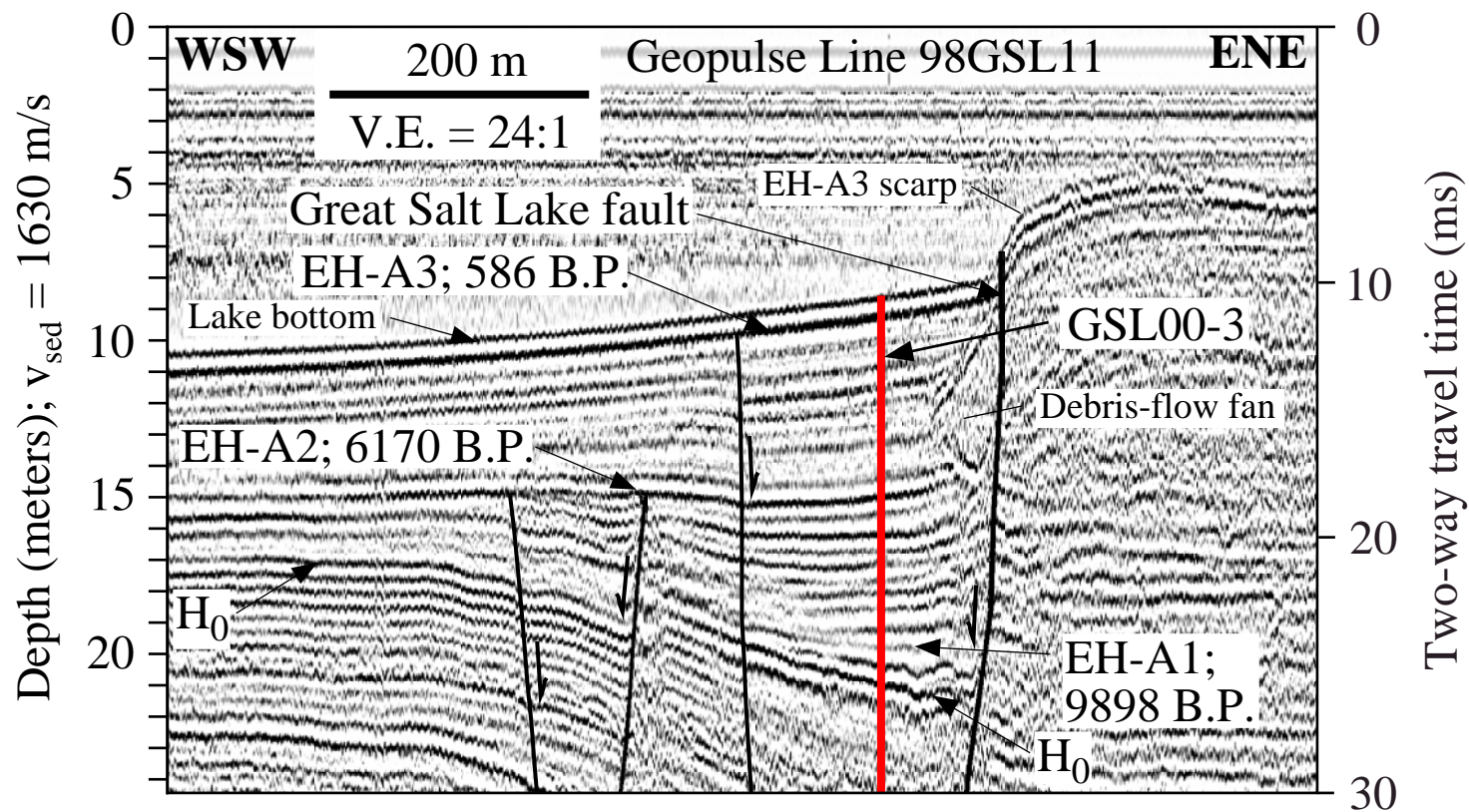
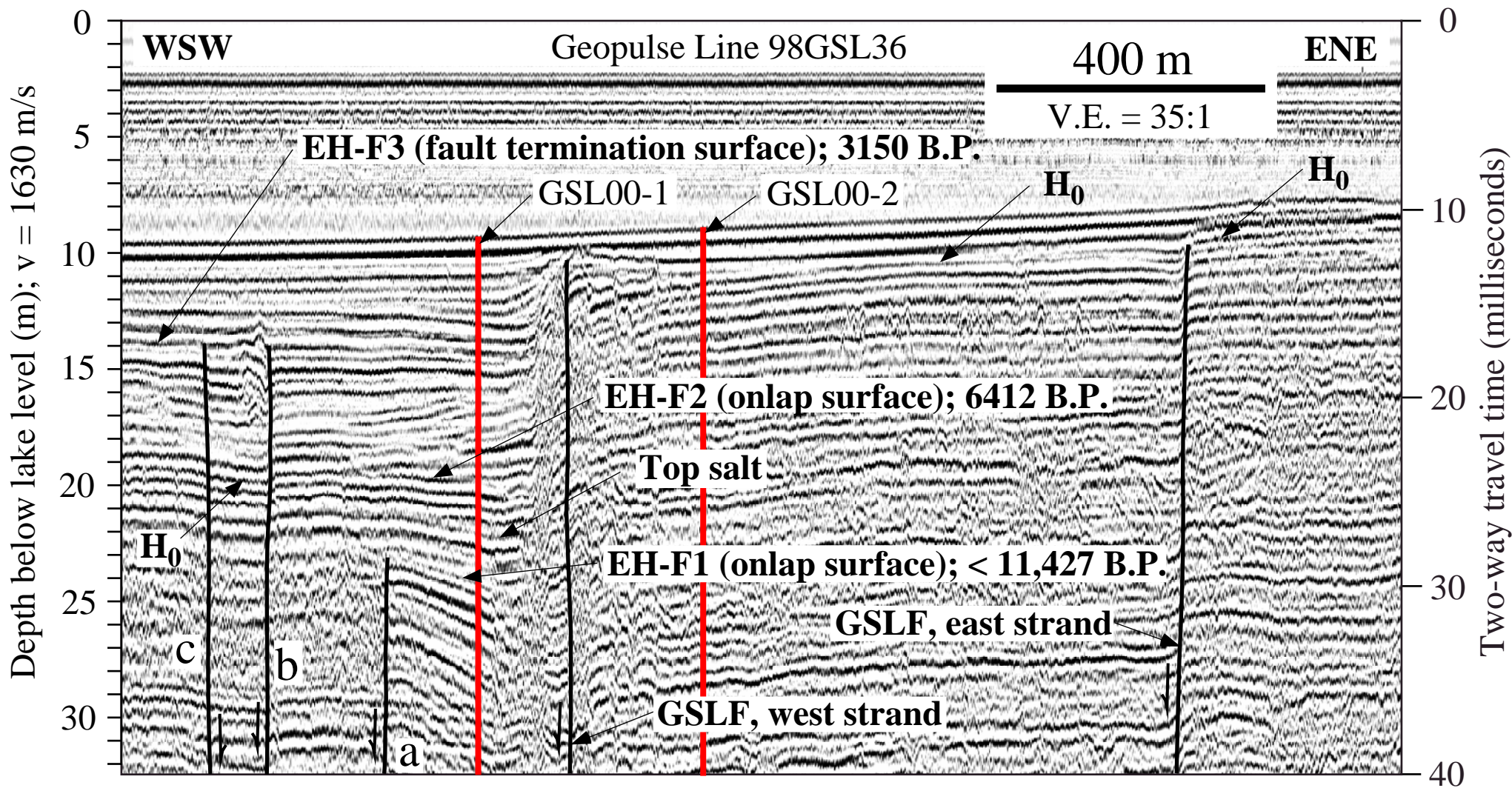


Fig. 1. Active faults in the south arm of the Great Salt Lake, mapped from high-resolution seismic reflection data; track-lines shown as dashed lines (Dinter and Pechmann, 1999, EOS, v. 80, p. F734; Colman et al., 2002, Sed. Geol., v. 148, 61-78). All faults are normal faults, ticks on downthrown side. GSLF = Great Salt Lake fault. Heavy lines show locations of profiles 98GSL11 (Fig. 2) and 98GSL36 (Fig. 3). Circles show core locations discussed in text.



**Fig. 2.** Geopulse Line 98GSL11, showing earthquake event horizons for the three most recent surface-rupturing events on Antelope Island segment of Great Salt Lake fault, and location of core site GSL00-3. Event ages shown are terrestrial-calibration calendar years B.P. (before 1950), corrected for carbon residence time in depositional provenance. (See Table 1 footnotes). See Fig. 1 for location of profile.



**Fig. 3.** Geopulse Line 98GSL36, showing earthquake event horizons for the three most recent surface-rupturing events on Fremont Island segment of Great Salt Lake fault, and locations of core sites GSL00-1 and GSL00-2. Event ages shown are terrestrial-calibration calendar years B.P. (before 1950), corrected for carbon residence time in depositional provenance. (See Table 1 footnotes). See Fig. 1 for location of profile.

**DIGITAL TRENCH WALL LOGGING:  
APPLYING MORPHOLOGICAL IMAGE PROCESSING TECHNIQUES  
TO TRENCH WALL STRATIGRAPHY**

Julie B. Willis<sup>1</sup>, Chaiwoot Boonyasiriwat<sup>2</sup>, Gerard T. Schuster<sup>1</sup>, Christopher B. DuRoss<sup>1</sup>

<sup>1</sup>University of Utah, Department of Geology and Geophysics

<sup>2</sup>University of Utah, Department of Computational Engineering and Science

E-mail: jwillis@mines.utah.edu

Traditionally, the walls of trenches dug across active faults are hand logged to separate clasts exposed in the trench walls from the matrix fill. Such logging is subject to human error and does not lend itself readily to statistical analyses of the sedimentary packages identified in the trench walls. Here we propose an algorithm to produce a digital log of trench wall sediments that autonomously separates clasts from the matrix and generates dimensional and orientation statistics for the separated clasts. The algorithm was developed and tested using digital photos of a section of the upper level of the Mapleton, Utah 'mega-trench,' which was cut across the Wasatch fault in 2003 (Figure 1).

The algorithm consists of a linked sequence of fundamental image processing techniques: histogram normalization, thresholding, edge detection, edge linking, watershed transform, opening, and dilation (Figure 2). The algorithm successfully segmented 2900 clasts from each other and from the matrix in a colluvial wedge, a debris flow and a channel deposit previously identified in the trench wall. Accuracy varied between 70% and 95%, depending on the contrast between the clasts and between the clasts and the matrix in the digital photo. The algorithm was also applied to a higher contrast and less complex image of a Mars surface with 100% accuracy (Figure 3). Further optimization of the algorithm can be achieved with minimal user-controlled reclassification prior to the final labeling step.

After executing the algorithm, each classified clast is a labeled watershed region from which the eccentricity, area, perimeter, axes lengths, and orientation among other parameters quickly can be calculated. Statistical comparisons of our minimal data set (4 m<sup>2</sup>) indicate that three measures, the clast-to-matrix ratio, clast eccentricity, and clast orientation potentially may be used to statistically differentiate colluvial wedges, debris flows and channel deposits exposed in trench walls (Figure 4). For the data set, the clast to matrix ratio is 9 to 18 % greater in the colluvial wedge than in the debris flow and channel deposit respectively. Clasts in the channel deposit have a slightly greater tendency towards roundness than clasts in the colluvial wedge and debris flow. In the colluvial wedge 73% of clasts have a planar preferred orientation greater than  $\pm 20^\circ$  (with 24% of these clasts oriented coincident with a fault dip of  $\sim 60^\circ$ ), while only  $60 \pm 3\%$  of clasts in the debris flow and channel deposit have a planar preferred orientation greater than  $\pm 20^\circ$ . These latter clasts also have no preferred orientation coincident with the dip of the fault. Future work on additional trench wall images will help determine whether measurements of clast eccentricity, clast orientation and the clast-to-matrix ratio can be used to definitively categorize trench wall stratigraphy.

The proposed algorithm is not restricted to clast segmentation and trench wall stratigraphy. Other suggested applications include analyzing landslides, stream braiding patterns, downhole digital images of boreholes, joint patterns, and planetary surfaces (Figure 3).

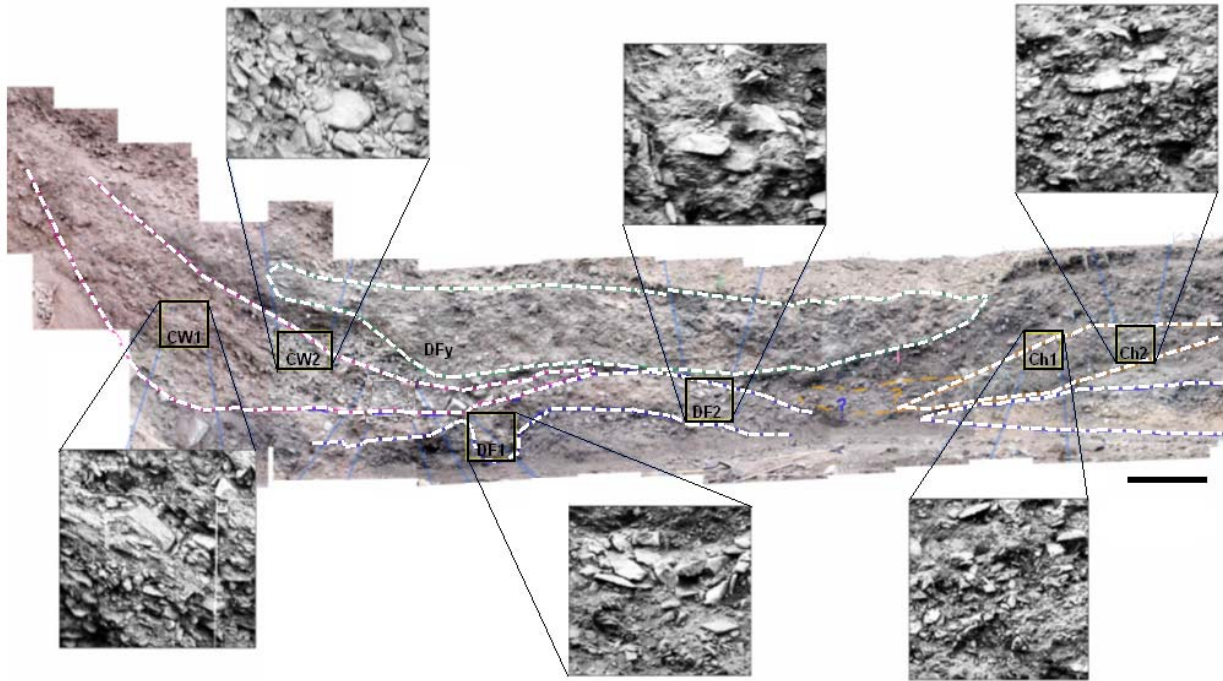


Figure 1. Digital photo mosaic of a section of the upper level of the 2003 Mapleton trench wall. An optimized sequence of morphological image processing techniques was used to separate clasts from matrix in each enlarged image. The resulting digital log of the enlarged image could then be statistically analyzed. Dashed lines separate previously determined stratigraphic units: CW = colluvial wedge; DF = debris flow; DFy = younger debris flow; Ch = channel deposits. Bar represents 1 m on the mosaic and 10 cm on the enlarged images. Photos courtesy Utah Geological Survey.

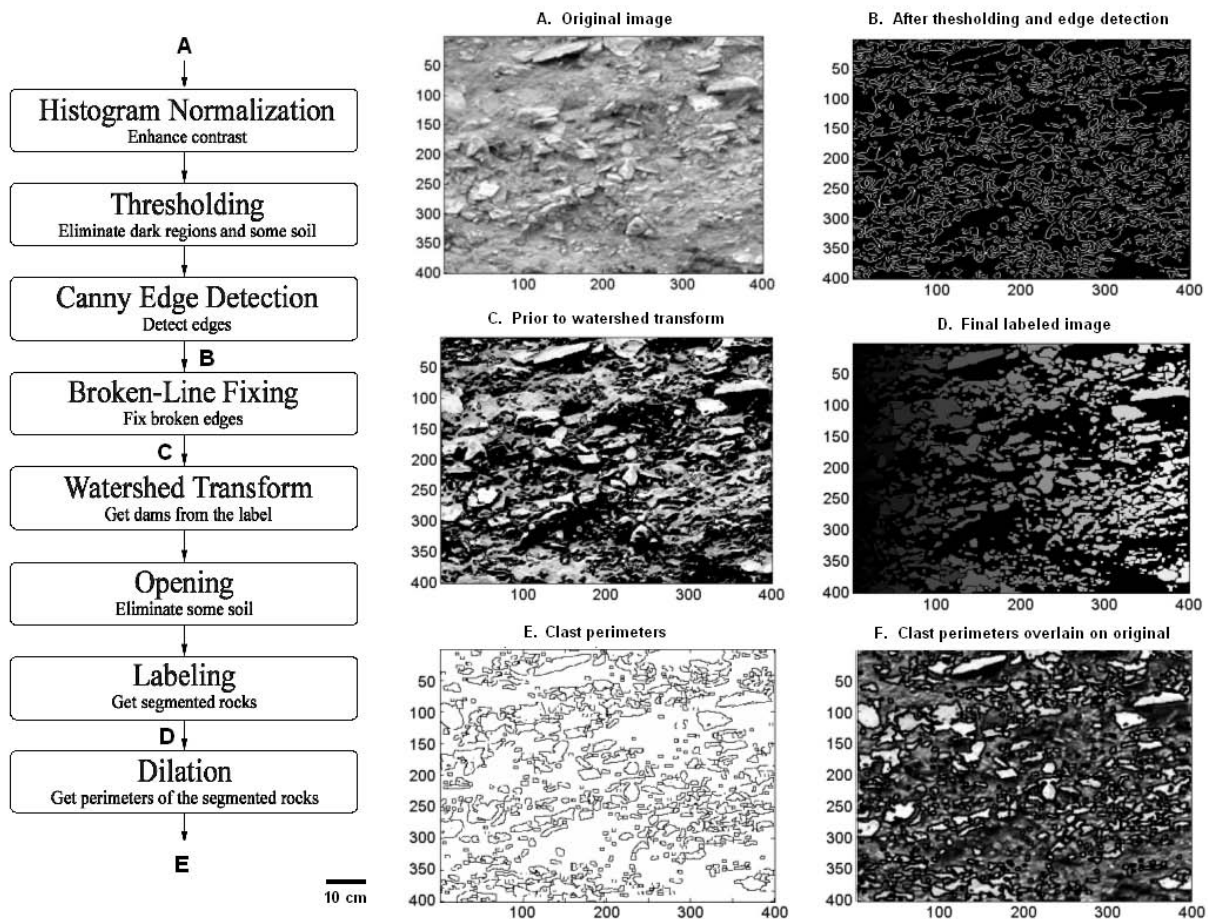


Figure 2. Flowchart and selected images illustrating the morphological clast segmentation algorithm. The original image is Ch1 from Figure 1. Letters on algorithm refer to images. The algorithm correctly separated 90% of the clasts from each other and from the background matrix. About 10% of the clasts were oversegmented. About 20% of the matrix was classified as small clasts ( $<0.3 \text{ cm}^2$ ), which were eliminated in the statistical analysis. Figure E is the digital log.

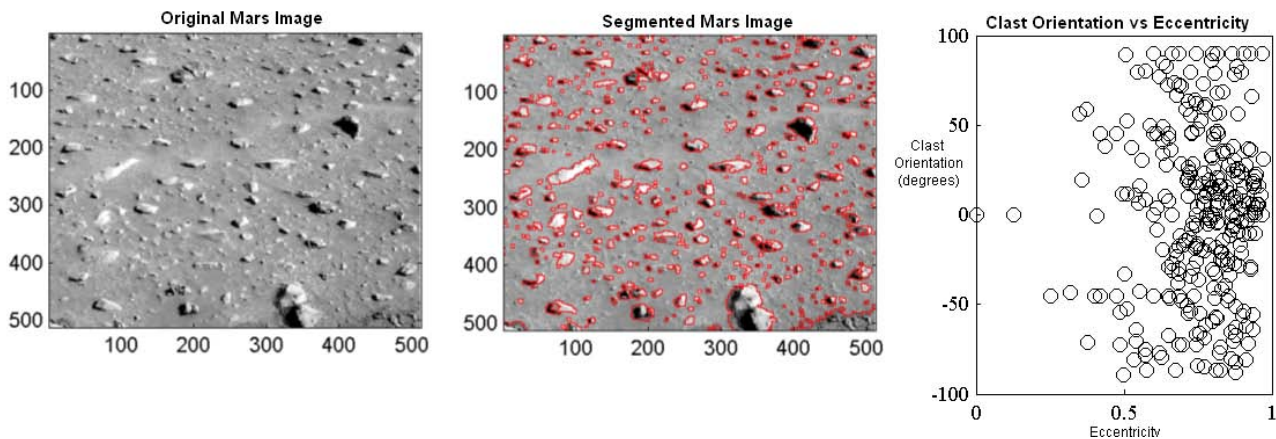


Figure 3. Segmentation of rocks exposed on a Mars surface. Plot shows example statistics that quickly can be calculated for each segmented and labeled rock. Other statistics that can be calculated include centroid, perimeter, area, and lengths of major and minor axes.

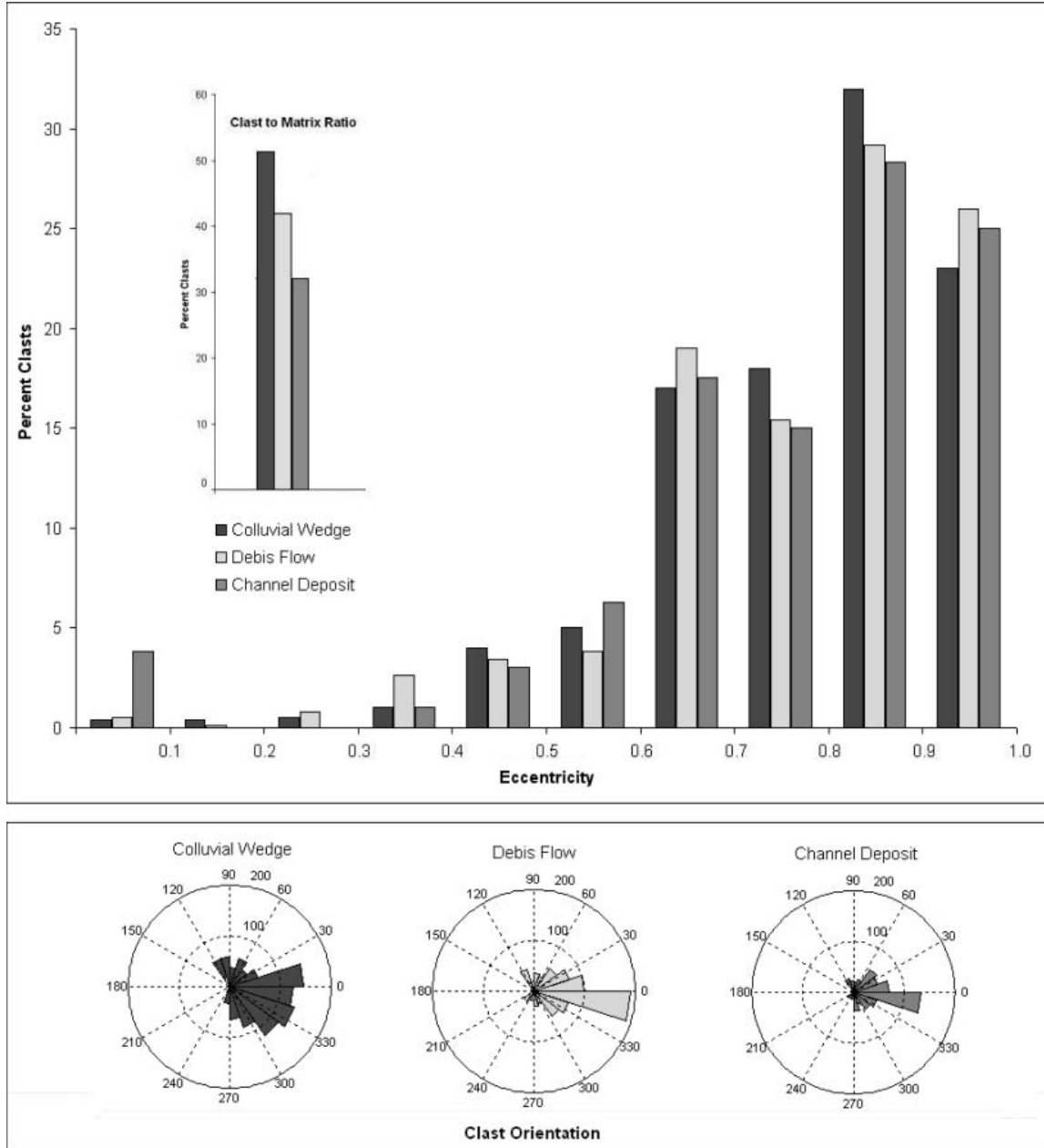


Figure 4. Comparison of data generated using 4 m<sup>2</sup> of segmented images from the 2003 Mapleton, Utah trench walls. The images were previously identified as colluvial wedge, debris flow or channel deposit. Noticeable differences between the percent clasts, the eccentricity, and the clast orientation may prove to be statistically important if they persist after processing additional trench wall images. Clasts less than 0.3 cm<sup>2</sup> were considered oversegmented matrix and were eliminated from the analyses. Standard deviation eccentricity: 0.16 (colluvial wedge), 0.15 (debris flow), 0.20 (channel deposit). Standard deviation orientation: 48.6 (colluvial wedge), 39.0 (debris flow), 40.2 (channel deposit). Standard deviation area: 14.3 (colluvial wedge), 17.3 (debris flow), 28.4 (channel deposit).

RELATED PUBLICATIONS from  
UTAH GEOLOGICAL SURVEY

Quaternary fault and fold database and map of Utah, by Bill D. Black, Suzanne Hecker, Michael D. Hylland, Gary E. Christenson, and Greg N. McDonald, CD-ROM [CD contains GIS data), scale 1:500,000, ISBN 1-55791-593-8, 2/03, Map 193DM **\$24.95**

Earthquake-hazards scenario for a M7 earthquake on the Salt Lake City segment of the Wasatch fault zone, Utah, by Barry J. Solomon, Neil Storey, Ivan Wong, Walter Silva, Nick Gregor, Douglas Wright, and Greg McDonald, CD (59 p., 6 pl. scale 1:250,000), 5/04, ISBN 1-55791-704-3, SS-111DM **\$24.95** [CD contains GIS data]

Proceedings volume, Basin and Range Province Seismic-Hazards Summit, edited by William R. Lund, 204 p., 12/98, MP-98-2 **\$16.00**

Earthquake scenario and probabilistic ground shaking maps for the Salt Lake City, Utah, metropolitan area, by Ivan Wong, Walter Silva, Susan Olig, Patricia Thomas, Douglas Wright, Francis Ashland, Nick Gregor, James Pechmann, Mark Dober, Gary Christenson, and Robyn Gerth, 50 p. + CD-ROM, ISBN 1-55791-666-7, MP-02-5 **\$25.00**

Guidelines for evaluating surface-fault-rupture hazards in Utah, by Gary E. Christenson, L. Darlene Batatian, and Craig V Nelson, 14 p., 8/03, MP-03-6 **\$5.50**

Geologic evaluation and hazard potential of liquefaction-induced landslides along the Wasatch Front, Utah, by Kimm M. Harty and Mike Lowe, 40 p., 16 pl., ISBN 1-55791-687-X, 3/03, SS-104 **\$12.95**

Paleoseismology of Utah Volume 10: Post-Bonneville paleoearthquake chronology of the Salt Lake City segment, Wasatch fault zone, from the 1999 "megatrench" site, by James P. McCalpin, 5/02, 37 p., ISBN 1-55791-670-5, MP-02-7 **\$15.95**

Site-response characterization for implementing *SHAKEMAP* in northern Utah, by Francis X. Ashland, 10 p., 2 pl., 10/01, RI-248 **\$9.50**